UNIVERSITY OF CALIFORNIA,
IRVINE

Understanding the Steric and Electronic Factors that Stabilize Th(III), Th(II), and U(II) Complexes

DISSERTATION

submitted in partial satisfaction of the requirements
for the degree of

DOCTOR OF PHILOSOPHY

in Chemistry

by

Justin C. Wedal

Dissertation Committee:
Professor William J. Evans, Chair
Professor Filipp Furche
Professor Jenny Y. Yang

2022

DEDICATION

To those who pushed me by telling me it would not work.

TABLE OF CONTENTS

LIST OF FIGURES

Page

LIST OF SCHEMES

LIST OF TABLES

LIST OF COMPOUNDS

Molecular Formula	Number
[K(crypt)][$(C_5Me_5)_2U^{III}(CH_2SiMe_2NSiMe_3–\kappa C,\kappa N)$]	**4.1**
[K(crypt)(THF)][$(C_5Me_5)U^{III}(NR_2)(CH_2SiMe_2NSiMe_3–\kappa C,\kappa N)$]	**4.2**
$(C_5Me_5)_2U(OAr')$	**5.1-U**
$(C_5Me_5)_2Ce(OAr')$	**5.1-Ce**
$(C_5Me_4H)_2U(OAr')$	**5.2**
$(C_5Me_5)_2U(OAr*)$	**5.3**
$(C_5Me_4H)_2U(OAr*)$	**5.4**
$(C_5Me_5)_2U(CHR_2)$	**5.5**
$(C_5Me_5)_2U(C_5H_5)$	**5.6**
$(C_5Me_5)_2U(C_5Me_4H)$	**5.7**
$(C_5Me_5)_2U(\kappa^2–O,O'–O_2C–C_5Me_4H)$	**5.8**
$(C_5Me_5)_2U(NR_2)$	**5.9**
$(C_5Me_5)U(NR_2)_2$	**5.10**
$(C_5Me_5)_2U^{V}I(=NSiMe_3)$	**7.1**
$(C_5Me_5)_2UI(THF)$	**8.1**
$\{[K(OEt_2)_2][(C_5Me_5)_2U(\mu–I)(\mu_3–I)]\}_2$	**8.2**
$[K(18\text{-crown-}6)][(C_5Me_5)_2U(\mu–I)_2]$	**8.3**
$[K(2.2.2\text{-cryptand})][(C_5Me_5)_2UI_2]$	**8.4**
$[Li(THF)_4][(C_5Me_5)_2UI_2]$	**8.5**
$[Li(THF)_3][(C_5Me_5)_2UI(\mu–I)]$	**8.6**
$\{[K(18\text{-crown-}6)]_2(\mu–\text{toluene})\}\{[C_5H_3(SiMe_3)_2]_2UI(\mu–I)\}_2$	**8.7**
$[(C_5Me_5)U]_3(\mu_3–I)_2(\mu–I)_3I(THF)_2$	**8.8**
$(\eta^5\text{-}C_5Ph_5)UI_2(THF)_2$	**9.1**
$[Na(THF)_3][\eta^5\text{-}C_5Ph_5]$	**9.2**
$[K(18\text{-crown-}6)(THF)_2][C_5Ph_5]$	**9.3**
Dark blue solution formed by reaction of Cp'_3ThBr with KC_8 in THF at −35 °C	**A**
$(Me_3tach)_2LnI_3$	**13.1-Ln**
$[(Me_3tach)_2NdI_2][I]$	**13.2-Nd**
$(Me_3tach)_2LaCl_3$	**13.3-La**
$(Me_3tach)YCl_3(THF)_2$,	**13.4-Y**
$\{[(Me_3tach)La(\mu–OH)(\mu–OTf)]_2(\mu–OTf)_2\}_2$	**13.5-La**
$[HMe_3tach][(Me_3tach)_2La(OTf)_4]$	**13.6-La**
$(Me_3tach)_2SmI_2(THF)$	**13.7-Sm**
$(Me_3tacn)LaI_3(THF)$	**13.8-La**
$(Me_3tacn)YCl_3$	**13.9-Y**
$(Me_3tacn)SmI_2(THF)$	**13.10**
$(Me_3tach)_2UI_3$	**14.1**
$(Me_3tach)UI_3(py)_2$	**14.2**

$(Me_3tacn)UI_3(THF)$	**14.3**
$[BiI(THF)(\mu–I)_2]_n$	**15.1**
$(Me_3tach)_2BiI_3$	**15.2**
$[(Me_3tach)_2BiI_2][(Me_3tach)BiI_4]$	**15.3**
$[(Me_3tach)_2BiI_2]_3[Bi_2I_9][I][HMe_3tach]\cdot THF$	**15.4**
$(Me_3tach)BiI_3(py)_2$	**15.5**
$(Me_3tach)BiCl_3(py)_2$	**15.6**
$(Me_3tacn)BiI_3$	**15.7**
$[(C_5Me_5)_2Y(\mu\text{-}2\text{-}CNC_6H_4O\text{-}\kappa C\text{:}\kappa O)]_2$	**B.1**
$\{[(C_5Me_5)_2Y(\mu\text{-}2\text{-}CNC_6H_4O\text{-}\kappa C\text{:}\kappa O)]_2\}^{1-}$	**B.2**
$[Cp^{An}Y(\mu–Cl)]_2$	**C.1**
$Cp^{An}YCl(THF)$	**C.2**
$Cp^{An}Y(C_3H_5)(THF)$	**C.3**
$[Cp^{An}Y(\mu\text{-}H)(THF)]_2$	**C.4**
$[(\mu–Cp^{An})Y(\mu–H)]_2$	**C.5**
$[K(crypt)][(\mu–CpAn)Y(\mu–H)]_2$	**C.6**
$U(BH_4)_3(THF)_2$	**D.1**
$U(BH_4)_2I(THF)_2$	**D.2**
$U(H_3BCMe_2CHMe_2)_3(THF)_x$	**D.3**
$[U(H_3BCMe_2CHMe_2)_2(THF)_2(u–I)]_2$	**D.4**
$(C_5Me_5)_2U(BH_4)(THF)$	**D.5**
$(C_5Me_5)U(BH_4)_2(THF)_2$	**D.6**
$[K(crypt)][(C_5Me_5)_2U(BH_4)_2]$	**D.7**

ACKNOWLEDGEMENTS

To begin, I would like to thank my advisor Bill Evans for everything he has done for me over the past five years. I have learned so much from him, both in and out of the lab, that I will carry with me for the rest of my career. The first time I sat down with Bill, I told him I wanted to make new compounds. That was it. I was lucky to have an advisor that let me pursue such an experience. I will forever appreciate Bill letting me work with him, to chase after my interests and to make any compound I could imagine, as long as it was from commercially available ligand.

I want to thank the members of the Evans lab that I have worked alongside during my tenure in Reines. I would like to specifically mention Dr. Samuel Moehring who made my first three years easier, and Lauren Anderson-Sanchez, Will Moore, and Dr. Cary Stennett who made my last year enjoyable. I've also had the opportunity to work alongside two fantastic ungraduated students Michael Trinh and Gabriella Godinho, who have probably taught me more than I taught them.

I would also like to thank Filipp Furche and his group who helped me learn density functional theory and how it can be applied as a synthetic chemist. Filipp has acted as a second advisor to me during my PhD which has been invaluable. Professors Jenny Yang, A. S. Borovik, and their groups have also been a significant help for me, whether it was discussing electrochemistry, EPR, or just chemistry in general.

I want to recognize the scientific collaborators I have worked with, including Dr. Joe Ziller and his immeasurable help with crystallography; Dr. Jeff Barlow and Professor Jenny Yang for their insight into (spectro)electrochemistry; Nathalia Cajiao and Professor Mike Neidig at the University of Rochester for low-temperature spectroscopy; Jesse Murillo and Andy Gaunt at Los Alamos National Lab for taking the chemistry I developed at UCI with uranium and applying it to

Np and Pu; and David Villareal, Wen Fu, and Dave Britt at UC Davis and Wayne Lukens at Lawrence Berkeley National Lab for their help with collecting and interpreting the wild EPR spectra I collected. I also want to acknowledge my coauthors on various publications that I have not yet mentioned, including Megan Dumas, Dan Huh, Tener "TJ" Jenkins, Austin Ryan, Cory Windorff, and the groups at Florida State and Los Alamos.

Portions of the content in Chapters 2, 4, 5, and Appendix B are reproduced with permission from the American Chemical Society journals *Inorganic Chemistry* (Chapters 2 and 5) and *Organometallics* (Chapter 4 and Appendix B). Portions of Chapters 3, 10, 11, and 12 are reproduced with permission from the Royal Society of Chemistry journals *Chemical Science* (Chapter 3), *Dalton Transactions* (Chapters 10 and 12) and *Chemical Communications* (Chapter 11). Portions of Chapter 8 are reproduced with permission from the Taylor & Francis Online journal *Journal of Coordination Chemistry*. Portions of Chapter 9 are reproduced with permission from the CSIRO Publishing journal *Australian Journal of Chemistry*.

Finally, I would like to thank my friends for putting up with and supporting me for this duration. In alphabetical order, I want to give a big shoutout to Carly (Carl), Chuck (Chuckles), Leah (Leah Sal), Maddy, Meghen (Mom), Tanner, Taylor (TThane), and Tyler (Tyty). I would also like to thank my parents for their constant support. Finally, I want to thank Kirsten (Kiki) for her love, support, help, guidance, and everything else that cannot be covered in words. Kirsten made graduate school easier, more fun, and an overall a better experience that would not have happened otherwise.

VITA
JUSTIN C. WEDAL

Education and Research Experience

University of California-Irvine, Irvine, CA

M.Sc. Chemistry **January 2022**

Ph.D. Chemistry. Advisor: Professor William J. Evans **May 2022**

Synthesis, characterization, reactivity, and theoretical analysis of low-valent thorium(III), thorium(II), and uranium(II) complexes. Collaborative studies with Professor Filipp Furche performing DFT analysis of compounds synthesized in the Evans lab

University of Wisconsin-La Crosse, La Crosse, WI **September 2013- May 2017**

B. Sc., with Honors Chemistry and Physics. Advisor: Professor Kendric J. Nelson

Synthesis and characterization of transition metal complexes as precursors for molecular materials and extended chain structures

Publications

13. "Expanding Bismuth Trihalide Coordination Chemistry with Trimethyltriazacyclohexane and Trimethyltriazacyclononane" **Justin C. Wedal**, Joseph W. Ziller, and William J. Evans *Inorganic Chemistry*, submitted.

12. "Synthesis and Reduction of Heteroleptic Bis(cyclopentadienyl) Uranium(III) Complexes" **Justin C. Wedal**, Joseph W. Ziller, Filipp Furche, and William J. Evans *Inorganic Chemistry*, *in press*. DOI: 10.1021/acs.inorgchem.2c00322.

11. "Anion-Included Disproportionation of Th(III) Complexes to Form Th(II) and Th(IV) Products" **Justin C. Wedal**, Nathalia Cajiao, Michael L. Neidig, and William J. Evans *Chemical Communications* **2022**, *58*, 5289-5921, DOI: 10.1039/D2CC01272C. Selected as a HOT Article of 2022.

10. "Exploring the Use of Pentaphenylcyclopentadienyl Ligand in Reductive f-Block Chemistry. The Crystal Structure of $(C_5Ph_5)UI_2(THF)_2$" **Justin C. Wedal**, Joseph W. Ziller, and William J. Evans *Australian Journal of Chemistry* **2022**, *in press*. DOI: 10.1071/CH21318. Invited issue for Glen Deacon.

9. "Isolation and Characterization of a Californium Metallocene" Conrad A. P. Goodwin, Jing Su, Lauren M. Stevens, Frankie D. White, Nickolas H. Anderson, John D. Auxier II, Thomas E. Albrecht-Schönzart, Enrique R. Batista, Sasha F. Briscoe, Justin N. Cross, William J. Evans, Alyssa N. Gaiser, Andrew J. Gaunt, Michael R. James, Michael T. Janicke, Tener F. Jenkins, Zachary R. Jones, Stosh A. Kozimor, Brian L. Scott, Joseph. M. Sperling, **Justin C. Wedal**,

Cory J. Windorff, Ping Yang, and Joseph W. Ziller *Nature* **2021**, 599, 421-424. DOI: 10.1038/s41586-021-04027-8.

8. "A Rare-Earth Metal Retrospective to Stimulate All Fields" **Justin C. Wedal** and William J. Evans *Journal of the American Chemical Society* **2021**, *143*, 18354-18367. DOI: 10.1021/jacs.1c08288.

7. "DFT Analysis of the Importance of Coordination Geometry for $5f^3 6d^1$ vs $5f^4$ Electron Configurations in U(II) Complexes" **Justin C. Wedal**, Filipp Furche, and William J. Evans *Inorganic Chemistry* **2021**, *60*, 16316-16325. DOI: 10.1021/acs.inorgchem.1c02161.

6. "Evaluating Electrochemical Accessibility of $4f^n 5d^1$ and $4f^{n+1}$ Ln(II) Ions in $(C_5H_4SiMe_3)_3Ln$ and $(C_5Me_4H)_3Ln$ Complexes" Michael T. Trinh, **Justin C. Wedal**, and William J. Evans *Dalton Transactions* **2021**, *50*, 14384-14389. DOI: 10.1039/D1DT02427B.

5. "Electrochemistry of Tris(cyclopentadienyl) Actinide Complexes in the +2, +3, and +4 Oxidation State" **Justin C. Wedal**, Jeffrey M. Barlow, Joseph W. Ziller, Jenny Y. Yang, and William J. Evans *Chemical Science* **2021**, *12*, 8501. DOI: 10.1039/D1SC01906F.

4. "Synthesis of a 2-Isocyanophenolate Ligand, $[2\text{-}CNC_6H_4O]^{1-}$, by Ring-Opening of Benzoxazole with Rare-Earth Metal Complexes" Megan T. Dumas, Tener F. Jenkins, **Justin C. Wedal**, Joseph W. Ziller, Fillip Furche, and William J. Evans *Organometallics* **2021**, *40*, 735. DOI: 10.1021/acs.organomet.1c00002.

3. "Structural Variations in Cyclopentadienyl Uranium(III) Iodide Complexes" **Justin C. Wedal**, Cory J. Windorff, Austin J. Ryan, Joseph W. Ziller, and William J. Evans *Journal of Coordination Chemistry* **2020**, *74*, 74-91. DOI: 10.1080/00958972.2020.1856824. Invited issue for Jerry L. Atwood.

2. "C–H Bond Activation via U(II) in the Reduction of Heteroleptic Bis(trimethylsilyl)amide Uranium Complexes" **Justin C. Wedal,** Samuel Bekoe, Joseph W. Ziller, Filipp Furche, and William J. Evans *Organometallics* **2020**, *39*, 3425. DOI: 10.1021/acs.organomet.0c00496.

1. "In Search of Tris(trimethylsilyl)cyclopentadienyl Thorium" **Justin C. Wedal,** Samuel Bekoe, Joseph W. Ziller, Filipp Furche, and William J. Evans *Dalton Transactions* **2019**, *48*, 16633. DOI: 10.1039/C9DT03674A.

Selected Presentations

"Disproportionation of Th(III) Complexes to Form Th(II) and Th(IV) Complexes by addition of simple salts" *American Chemical Society National Meeting*, San Diego, CA, March 2022.

"Synthesis and Reduction Studies of Heteroleptic Bis(cyclopentadienyl) Uranium(III) Complexes" *American Chemical Society National Meeting*, virtual, August 2021. *Chair of session.*

"Disproportionation of Th(III) Complexes to Form Th(II) and Th(IV) Complexes by Addition of Simple Salts" *Angular Momentum f-element seminar series*, virtual, July 2021.

Outreach and Mentorship

LEAPS Outreach program at UC-Irvine **2017-2022**
UCI Mentoring Excellence Program **2021**
UCI Competitive Edge Peer Mentor **2021**

Undergraduate Mentoring

Worked with Michael Trinh for two years.
Worked with Gabriella Godinho for one year.

UCI Teaching Assistant **2017-2020**

Laboratory Courses: General Chemistry (1LC, 1LD), Organic Chemistry (51LB, 51LC), and Inorganic Chemistry (107L)
Lecture Courses: Upper-division Inorganic Chemistry (127), Graduate Inorganic Chemistry (215), and Graduate Organometallic Chemistry (216)

Selected Awards

Edward K. C. Lee Award for Most Outstanding Graduate Student, **2022**
UCI Most Promising Future Faculty Award, *Honorable Mention* **2022**
UCI Dissertation Fellowship **2022**
US Dept of Energy Office of Isotope R&D and Production Pacifichem Bursary **2021**
UCI Chemistry Department Travel Grant, **2020**
Associated Graduate Students Travel Grant, **2020, 2021, 2022**
UW-La Crosse Alpha Phi "Mr. Chemistry" **2016**
UW-La Crosse Outstanding Student in Inorganic Chemistry **2016**

ABSTRACT OF THE DISSERTATION

Understanding the Steric and Electronic Factors that Stabilize

Th(III), Th(II), and U(II) Complexes

Justin C. Wedal

Doctor of Philosophy in Chemistry

University of California, Irvine, 2022

Professor William J. Evans, Chair

This dissertation describes synthetic, structural, spectroscopic, reactivity, and theoretical investigations into the factors that stabilize thorium and uranium compounds in the low oxidation states +2 and +3. Extensions of the actinide work to rare-earth metals and bismuth are also included. The importance of understanding this aspect of actinide metal chemistry is described in Chapter 1. Chapter 2 describes a theoretical study using density functional theory (DFT) on U(II) complexes analyzing how the local coordination geometry around the uranium center influences the electronic configuration. U(II) species with planar coordination geometries favor $5f^3 6d^1$ electron configurations, while non-planer geometries appear to favor $5f^4$ configurations. Chapter 3 describes electrochemical determination of the Th(IV)/Th(III), Th(III)/Th(II), and U(III)/U(II) reduction potentials in tris(cyclopentadienyl) complexes with complementary spectroelectrochemical measurements. It was found that the reduction potentials trend with ligand donation strength. In addition, the study revealed that the Th(IV)/Th(III) and Th(III)/Th(II)

reduction potentials were quite similar which led to the synthesis of Th(II) compounds directly from Th(IV) precursors.

Chapters 4–6 detail reduction studies of heteroleptic U(III) complexes to prepare new U(II) compounds and understand how to stabilize this low oxidation state. Within these Chapters are UV-visible and EPR spectroscopic studies and DFT calculations on newly synthesized compounds to probe the electronic structure of the U(II) species. The heteroleptic species appear less stable than the homoleptic analogs despite having similar steric properties and reduction potentials.

Chapter 7 describes the reaction of U(III) compounds with organoazides which led to the observation of a U(V) intermediate and a new mechanistic proposal for the formation of U(VI) imides. Such an intermediate had not been observed in this type of reaction and the results redefine the mechanism for the reduction of azides by uranium compounds. Chapters 8 and 9 are crystallographic studies on U(III) compounds containing cyclopentadienyl and iodide ligands, showing the many structural variations that can exist with simple organoactinide compositions.

Chapters 10 and 11 describe the synthesis of new Th(III) compounds with the $C_5H_4SiMe_3$ (Cp′) and $C_5H_3(SiMe_3)_2$ (Cp″) ligands and a new disproportionation route to Th(II) complexes that was discovered. Chapter 10 describes extensive efforts to characterize the elusive Cp'_3Th. In Chapter 11, reactions of Cp''_3Th with simple salts are described that lead to formation of Th(II) complexes by disproportionation. An unusual reduction of benzene by "$[Cp''_3ThMe]^{1-}$" is also reported. Chapter 12 extends the electrochemistry method described in Chapter 3 to the Cp'_3Ln series and some $(C_5Me_4H)_3Ln$ compounds. It was found that the reduction potentials for the Cp'_3Ln series were found to be practically identical across the Ln series (excluding Eu, Sm, Tm, and Yb). The remaining Chapters describe the coordination chemistry of the underutilized

nitrogen heterocycles trimethyltriazacyclohexane and trimethyltriazacyclononane with the rare-earth metals (Chapter 13), the actinide metals (Chapter 14), and bismuth (Chapter 15).

Appendix A describes attempts to form Th(II) complexes by reduction of C_5Me_4H-ligated Th(III) complexes. Appendix B describes DFT studies on a bimetallic yttrium system with benzoxazole-derived ligands. Appendices C and D summarize work with the bimetallic $(Cp^{An}YH)_2$ system [Cp^{An} = $(C_5H_3SiMe_3)_2SiMe_2$] and uranium borohydride coordination chemistry, respectively. Appendix E summarizes DFT studies on various complexes not yet mentioned in other sections of this dissertation. Finally, Appendix F contains a chronological list of crystal structures obtained throughout this work.

Chapter 1:

Introduction

The Actinide Metals. The study of the actinide (An) metals expanded during the Manhattan project and applications now range from nuclear energy and weaponry, targeted isotope therapy, natural gas small-molecule reactivity, theoretical bonding and covalency investigations, and even catalysis.[1–10] All of these applications are driven by fundamental studies which allow for a detailed understanding of the properties of these elements and in turn can improve the current technology.

The electronic structure of the actinides is different than most of the periodic table, Figure 1.1. It is unlike the transition metals, where the *n*d orbitals form strong covalent interactions with ligand orbitals that leads to small molecule transformation and catalysis. Nor is it like the 4f orbitals of the lanthanides (Ln) where the 4f electrons can be considered buried within the [Xe] core which leads to mostly ionic lanthanide-element interactions.[11] Instead, the valence 5f orbitals extend a small distance beyond the [Rn] core, Figure 1.2.[11] While most actinide-ligand interactions are ionic in nature, the extension of the 5f orbitals could allow for covalent bonding to occur.

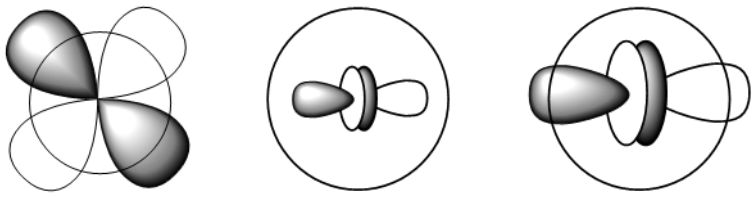

Figure 1.1: Qualitative representation of the 5d (left), 4f (middle), and 5f (right) orbitals depicting their radial extension beyond the core electron density, which is represented by the circles.

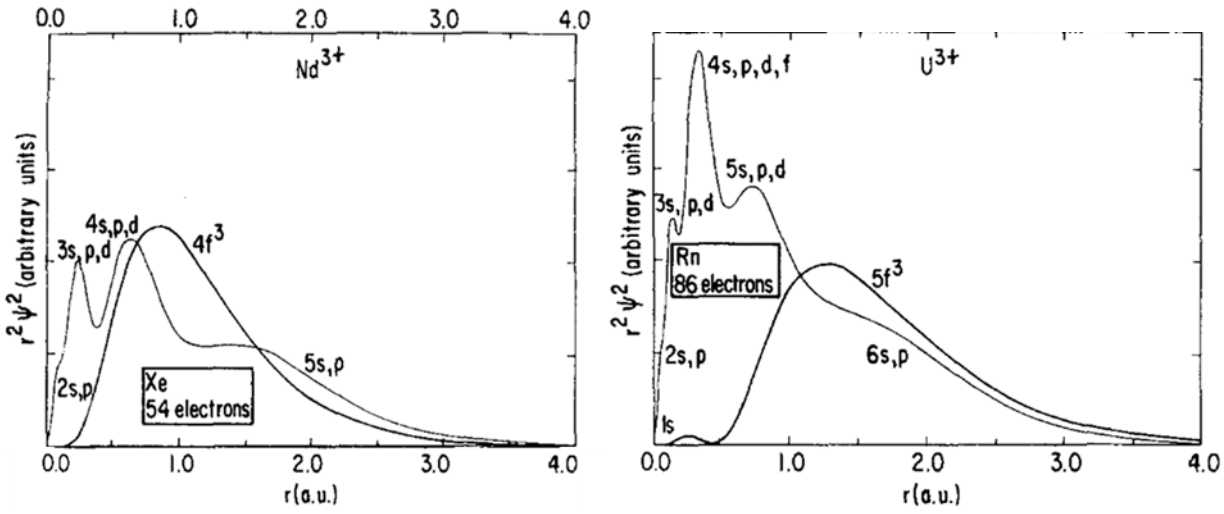

Figure 1.2:[11] (left) Plot of Hartree-Fock radial wave functions for Nd(III) showing how the 4f orbitals are buried in the [Xe] core; (right) Plot of Hartree-Fock radial wave functions for U(III) showing the minimal extension of the 5f orbitals beyond the [Rn] core electrons.

Available Oxidation States. The availability of oxidation states is variable across the actinide series. The later actinides, Am–Lr, are found in either the +3 or +2 oxidation state[8] like the lanthanides. The first element in the series, actinium, has only been observed in the +3 oxidation state[10] and the +4 oxidation state dominates thorium chemistry. However, U–Pu have many more oxidation states available. Many examples of U(III), U(IV), U(V), and U(VI) have been reported.[12–14] Additionally, the oxidation state range of neptunium and plutonium spans the +3 to +7 states.[8] The oxidation state diversity, or lack thereof for some actinide elements, can be explained by the gas-phase and thermochemical data, that shows the energy needed to access Th(III), Th(II), U(II), Np(II), and Pu(II) is so large and the reduction potentials are so negative that there would be no reasonable way to isolate compounds in those oxidation states.[15–17]

Since thorium and uranium have low radioactivity and high natural abundance, investigation of the chemistry of the actinide elements is dominated by compounds with these two elements. The $5f^0$ Th(IV) ion is a closed-shell system and, except for reactions that start with Th

metal, thorium starting materials exist as Th(IV). In 1986, Lappert reported the first example of Th(III) compound, Cp''_3Th [$Cp'' = C_5H_3(SiMe_3)_2$], via NaK alloy reduction of a Th(IV) starting material, eq 1.1.[18–20]

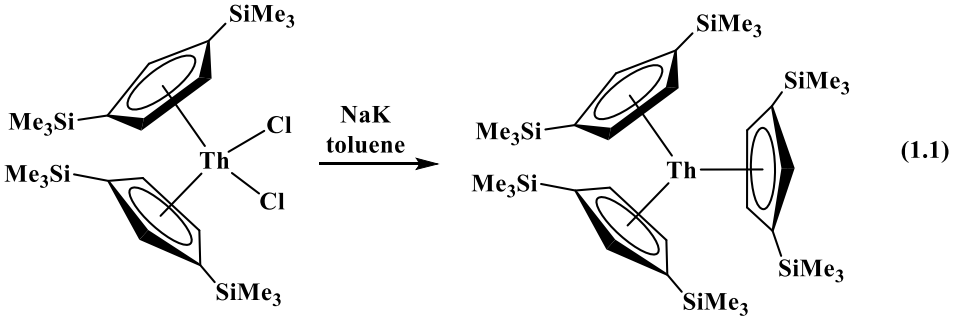

(1.1)

Since NaK has a reduction potential of roughly −2.9 V vs NHE, this result is in contrast to the calculated Th(IV)/Th(III) reduction potentials at the time, which ranged from −3.0 to −3.82 V vs NHE.[15–17,21,22] Since then, many more Th(III) compounds have been reported, although almost all contain bulky cyclopentadienyl or cyclooctatetraenyl ligands.[23–26]

Compounds of U(III) are much more common than Th(III) and most contain bulky aromatic ligands. The tris(cyclopentadienyl) ligand environment, $(C_5R_5)_3U$, (R = H, alkyl, aryl) is particularly common and allows for facile steric and electronic tuning of the complexes. Many lanthanide analogs, $(C_5R_5)_3Ln$,[27] exist and the chemistry of the lanthanides and early actinides can be directly compared. In 2008, Lappert reported that the reduction of Cp''_3La formed $[Cp''_3La]^{1-}$, the first example of La(II), eq 1.2. This system was analogous to the Th(IV)/Th)(III) system in eq 1.1 and was extended to Ce.[28]

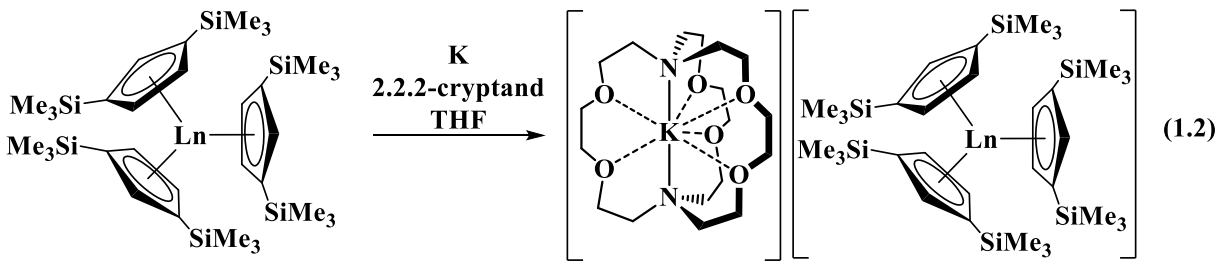

(1.2)

Ln = La, Ce

Based on these results, similar reduction chemistry was investigated with the smaller ligand Cp′ (Cp′ = $C_5H_4SiMe_3$) and molecular examples of Ln(II) in $[Cp'_3Ln]^{1-}$ were isolated, eq 1.3[29–34]

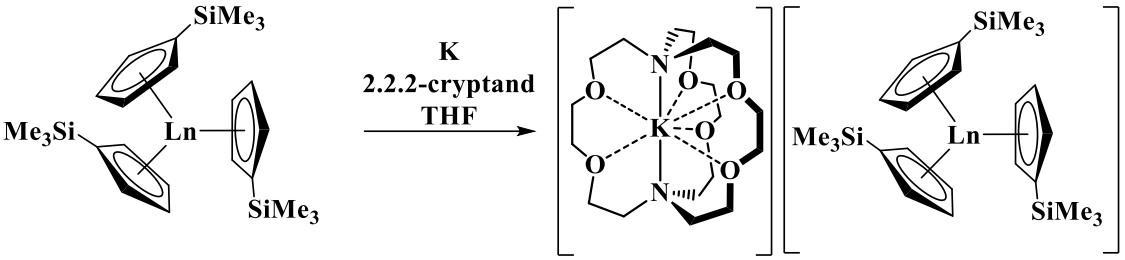

(1.3)

Ln = Y, La-Nd, Sm-Lu

To compare the lanthanides with U, the reduction of Cp'_3U was also investigated and $[Cp'_3U]^{1-}$, the first molecular example of U(II), was isolated.[35] Subsequently, the reduction of Cp''_3U, analogous to the Th, La, and Ce results in eq 1.1-1.3, was performed and $[Cp''_3U]^{1-}$ was indeed formed, eq 1.4.[36] This chemistry was extended to Th, Np, and Pu and the first molecular examples of those elements in the +2 oxidation state were discovered, eq 1.4.[37–39]

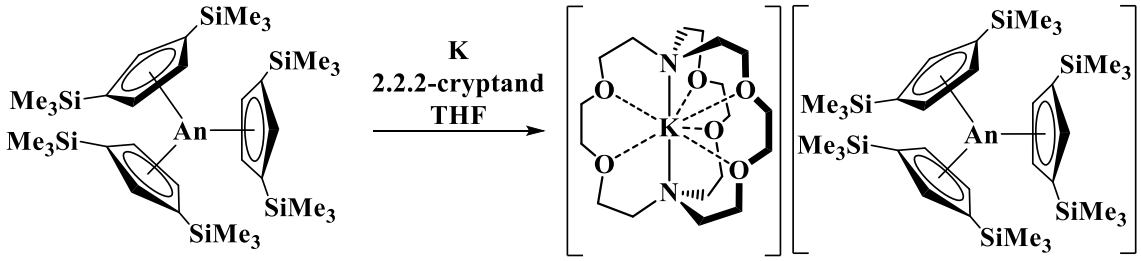

(1.4)

An = Th, U, Np, Pu

Evidently, there was something unique about the $(C_5R_5)_3M$ compounds since this ligand geometry was found to stabilize Ln(II), Th(III), Th(II), U(II), Np(II), and Pu(II), all of which were expected to be too reactive to isolate. It is worth noting that $[Cp'_3Np]^{1-}$ was likely also synthesized, but X-ray diffraction data could not be obtained due to the high radioactivity and decomposition.[40]

The Electronic Structure of $[(C_5R_5)_3An]^{1-}$ Compounds. Based on crystallographic, spectroscopic, magnetic, and theoretical studies, the ground state electronic configurations for U(II) and Np(II) compounds were predominantly $5f^n6d^1$ in character (n = 3 for U, 4 for Np) and

Th had a $5f^0 6d^2$ configuration where the 6d orbital is best described as a $6dz^2$-like orbital with 7s mixing.[35,36,38] The Pu(II) complex was best described as having a $5f^6$ electron configuration, but a $5f^5 6d^1$ configuration was close in energy such that this compound may have a multiconfigurational ground state.[37]

Qualitative MO diagrams for $[AnO_2]^{m+}$ show the 5f orbital manifold decreases in energy across the actinide series while 6d remain relatively constant, Figure 1.3.[41] However, the observed

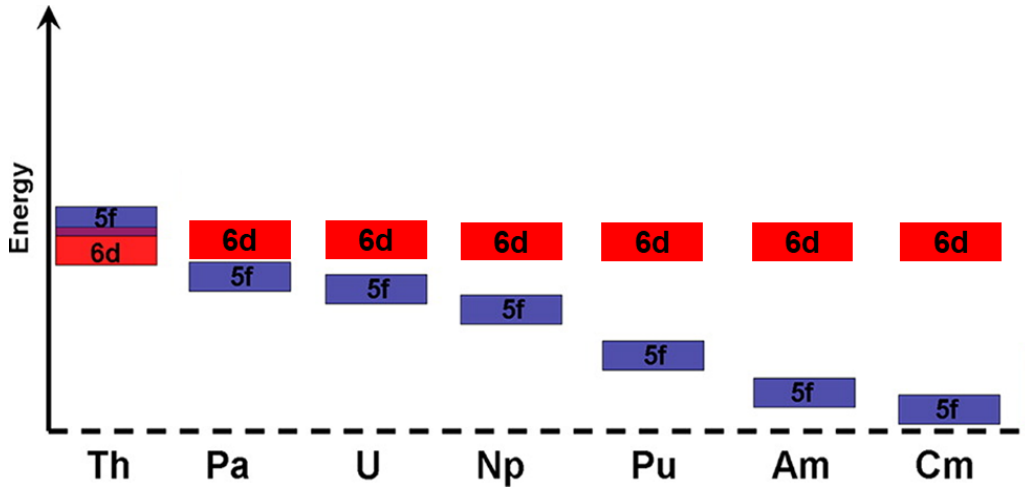

Figure 1.3: Qualitative plot of the 5f and 6d atomic orbital energy for the early actinides.[41] It should be noted this plot is extremely dependent on the oxidation state and ligand environment of the actinide ion.

$5f^n 6d1$ configuration is enforced by the $(C_5R_5)_3M$ geometry. Within this geometry, the $6dz^2$ orbital is non-bonding and the other four 6d orbitals are antibonding in character due to π symmetry interactions with the C_5R_5 ligand orbitals.[42–44] Evidently, the $6dz^2$ orbital becomes low enough in energy such that it is comparable to the 5f manifold. Reduction of the $5f^n$ complex leads to population of the $6dz^2$-like orbital instead of a 5f orbital. The Th(II) compound is unique since it is a diamagnetic, $6d^2$ configuration.[39] Thorium is at the beginning of the actinide series where the

6d orbitals are lower in energy than the 5f orbitals. As a result, the 6d orbitals are the valence orbitals and only $6d^1$ Th(III) compounds have been isolated. The same analysis holds for the Ln(II) compounds, as they form $4f^n5d^1$ configurations,[29] except for Ln = Eu, Sm, Tm, and Yb which form $4f^n$ configurations due to the quantum mechanical stabilization of half-filled or filled 4f manifold. Nd(II) and Dy(II) are unique where both $4f^n$ and $4f^n5d^1$ configurations have been observed depending on the ligand environment.[32,45–47]

Like the lanthanides, U(II) compounds have been observed with two different electron configurations. $5f^36d^1$ configurations were found for $[Cp'_3U]^{1-}$,[35] $[Cp''_3U]^{1-}$,[36,48] $[(C_5Me_4H)_3U]^{1-}$,[49] $[U(NR_2)_3]^{1-}$ (R = $SiMe_3$),[49] and $(C_5{}^iPr_5)_2U$[50] while $5f^4$ configurations were found for $\{[(^{Ad,Me}ArO)_3mes]U\}^{1-}$,[51] $U(NHAr^{iPr6})_2$,[52] and {U[(*N*-2,6-di-isopropylphenyl)pivalamido]$_2$}$^{1-}$.[53]

Testing our Current Understanding. The studies described in this Dissertation aim to explore and expand our knowledge of the electronic and steric properties that lead to stable, low-valent thorium and uranium compounds. These studies also help to expand and challenge the fundamental understanding of the actinide elements that are crucial to the current nuclear age.

It should be noted that some of the results presented in the following Chapters were relatively straightforward studies built on the previous results. However, some of the results had little to no literature precedent but were developed based on a series of what we deem "What If?" questions.[54] These questions are rooted in the idea of challenging the currently accepted body of knowledge, in this case on the non-aqueous reductive chemistry of the actinides. Examples of these types of questions have already been discussed.[54]

For example, the discovery of $[Cp'_3Ln]^{1-}$ was initially intended as a study on Cp''_3Ln. Since KCp′ is a synthetic precursor to KCp″,[55] it was proposed to use the smaller ligand and

investigate its reduction chemistry, even though it was widely assumed that the large ligand Cp″ was necessary for kinetic stabilization of the Ln(II) ion.[56–58] The question "What if we used the smaller Cp′ ligand?" proved to be crucial in isolating Ln(II) complexes of the entire Ln series.

In a broader sense, the existence of $4f^n5d^1$ Ln(II) ions was contrary to the chemical beliefs at the time. Many organometallic chemists considered the rare-earth elements boring and lacking diverse chemistry with their core-like f^n electronic configurations.[59–61] It turns out that there is rich chemistry to be developed. The reactivity pathways are unique compared to transition metals and provide novel and unprecedented transformations.[7,62–67]

Given this background, there are many questions in actinide chemistry that remain to be answered. For example, what ligand environment will stabilize a $5f^1$ Th(III) ion? Can An(I) and An(0) compounds be isolated?[68] Can metal-based reduction be coupled with alkyl-like reactivity across an An–R bond?[69] Do $5f^36d^1$ U(II) compounds react differently than $5f^4$ U(II) compounds? Can oxidative addition and reductive elimination be performed at an actinide center to perform catalysis like what is observed for transition metals?[70–72] These are only a few questions that can be developed based on expanding low-valent actinide chemistry. While these exact questions have not been directly addressed in this dissertation, hopefully the following content will provide fundamental information to help advance these areas in the future.

References

(1) Liddle, S. T. The Renaissance of Non-Aqueous Uranium Chemistry. *Angew. Chem. Int. Ed.* **2015**, *54*, 8604–8641, DOI: 10.1002/anie.201412168.

(2) Jones, M. B.; Gaunt, A. J. Recent Developments in Synthesis and Structural Chemistry of Nonaqueous Actinide Complexes. *Chem. Rev.* **2013**, *113*, 1137–1198, DOI: 10.1021/cr300198m.

(3) Wigeland, R. A.; Bauer, T. H.; Fanning, T. H.; Morris, E. E. Separations and Transmutation Criteria to Improve Utilization of a Geologic Repository. *Nucl. Technol.* **2006**, *154*, 95–106, DOI: 10.13182/NT06-3.

(4) Choppin, G. R. Actinide Speciation in the Environment. *Radiochim. Acta* **2003**, *91*, 645–650, DOI: 10.1524/ract.91.11.645.23469.

(5) Fox, A. R.; Bart, S. C.; Meyer, K.; Cummins, C. C. Towards Uranium Catalysts. *Nature* **2008**, *455*, 341–349, DOI: 10.1038/nature07372.

(6) Liu, H.; Ghatak, T.; Eisen, M. S. Organoactinides in Catalytic Transformations: Scope, Mechanisms and Quo Vadis. *Chem. Commun.* **2017**, *53*, 11278–11297, DOI: 10.1039/c7cc04415a.

(7) Halter, D. P.; Heinemann, F. W.; Bachmann, J.; Meyer, K. Uranium-Mediated Electrocatalytic Dihydrogen Production from Water. *Nature* **2016**, *530*, 317–321, DOI: 10.1038/nature16530.

(8) *The Chemistry of the Transactinide Elements*, 4th ed.; Morss, L. R., Edelstein, N. M., Fuger, J., Katz, J. J., Eds.; Springer: Dordrecht, **2010**.

(9) Monreal, M. J.; Diaconescu, P. L. The Riches of Uranium. *Nat. Chem.* **2010**, *2*, 424, DOI: 10.1038/nchem.642.

(10) Ferrier, M. G.; Stein, B. W.; Batista, E. R.; Berg, J. M.; Birnbaum, E. R.; Engle, J. W.; John, K. D.; Kozimor, S. A.; Lezama Pacheco, J. S.; Redman, L. N. Synthesis and Characterization of the Actinium Aquo Ion. *ACS Cent. Sci.* **2017**, *3*, 176–185, DOI: 10.1021/acscentsci.6b00356.

(11) Crosswhite, H. M.; Crosswhite, H.; Carnall, W. T.; Paszek, A. P. Spectrum Analysis of U^{3+}:$LaCl_3$. *J. Chem. Phys.* **1980**, *72*, 5103–5117, DOI: 10.1063/1.439742.

(12) Evans, W. J.; Kozimor, S. A. Expanding the Chemistry of U^{3+} Reducing Agents. *Coord. Chem. Rev.* **2006**, *250*, 911–935, DOI: 10.1016/j.ccr.2006.01.017.

(13) Edelmann, F. T. Lanthanides and Actinides: Annual Survey of Their Organometallic Chemistry Covering the Year 2017. *Coord. Chem. Rev.* **2018**, *370*, 129–223, DOI: 10.1016/j.ccr.2018.05.013.

(14) La Pierre, H. S.; Meyer, K. Activation of Small Molecules by Molecular Uranium Complexes. *Prog. Inorg. Chem.* **2014**, *58*, 303–416, DOI: 10.1002/9781118792797.ch05.

(15) Bratsch, S. G.; Lagowski, J. J. Actinide Thermodynamic Predictions. 3. Thermodynamics of Compounds and Aquo-Ions of the 2+, 3+, and 4+ Oxidation States and Standard Electrode Potentials at 298.15 K. *J. Phys. Chem.* **1986**, *90*, 307–312, DOI: 10.1021/j100274a021.

(16) Nugent, L. J.; Baybarz, R. D.; Burnett, J. L.; Ryan, J. L. Electron-Transfer and f-d Absorption Bands of Some Lanthanide and Actinide Complexes and the Standard (II—III) Oxidation Potential for Each Member of the Lanthanide and Actinide Series. *J. Phys. Chem.* **1973**, *77*, 1528–1539, DOI: 10.1021/j100631a011.

(17) Ionova, G.; Madic, C.; Guillaumont, R. About the Existence of Th(III) in Aqueous Solution. *Polyhedron* **1991**, *17*, 1991–1995.

(18) Blake, P. C.; Lappert, M. F.; Atwood, J. L.; Zhang, H. The Synthesis and Characterisation, Including X-Ray Diffraction Study, of [Th{η-$C_5H_3(SiMe_3)_2$}$_3$]; the First Thorium(III) Crystal Structure. *J. Chem. Soc., Chem. Commun.* **1986**, *453*, 1148–1149, DOI: 10.1039/C39860001148.

(19) Kot, W. K.; Shalimoff, G. V.; Edelstein, N. M.; Edelman, M. A.; Lappert, M. F. [Th^{III}{η^5-$C_5H_3(SiMe_3)_2$}$_3$], an Actinide Compound with a $6d^1$ Ground State. *J. Am. Chem. Soc.* **1988**,

110, 986–987, DOI: 10.1021/ja00211a059.

(20) Blake, P. C.; Edelstein, N. M.; Hitchcock, P. B.; Kot, W. K.; Lappert, M. F.; Shalimoff, G. V.; Tian, S. Synthesis, Properties and Structures of the Tris(Cyclopentadienyl)-Thorium(III) Complexes [Th{η^5-$C_5H_3(SiMe_2R)_2$-1,3}$_3$] (R = Me or ^{t}Bu). *J. Organomet. Chem.* **2001**, *636*, 124–129, DOI: 10.1016/S0022-328X(01)00860-9.

(21) Morss, L. R. Comparative Thermochemical and Oxidation-Reduction Properties of Lanthanides and Actinides. In *Handbook on the Physics and Chemistry of Rare Earths*; Gschneider Jr., K. A., Eyring, L., Choppin, G. R., Lander, G. H., Eds.; Elsevier Science: Amsterdam, 1994; pp 239–291.

(22) Mikheev, N. B. Lower Oxidation States of Lanthanides and Actinides. *Inorg. Chim. Acta* **1984**, *94*, 241–248, DOI: 10.1016/S0020-1693(00)87451-4.

(23) Ortu, F.; Formanuik, A.; Innes, J. R.; Mills, D. P. New Vistas in the Molecualr Chemistry of Thorium: Low Oxidation State Complexes. *Dalton Trans.* **2016**, *45*, 7537–7549, DOI: 10.1039/c6dt01111j.

(24) Formanuik, A.; Ariciu, A.-M.; Ortu, F.; Beekmeyer, R.; Kerridge, A.; Tuna, F.; McInnes, E. J. L.; Mills, D. P. Actinide Covalency Measured by Pulsed Electron Paramagnetic Resonance Spectroscopy. *Nat. Chem.* **2017**, *9*, 578–583, DOI: 10.1038/nchem.2692.

(25) Altman, A. B.; Brown, A. C.; Rao, G.; Lohrey, T. D.; Britt, R. D.; Maron, L.; Minasian, S. G.; Shuh, D. K.; Arnold, J. Chemical Structure and Bonding in a Thorium(III)-Aluminum Heterobimetallic Complex. *Chem. Sci.* **2018**, *9*, 4317–4324, DOI: 10.1039/c8sc01260a.

(26) Huh, D. N.; Roy, S.; Ziller, J. W.; Furche, F.; Evans, W. J. Isolation of a Square-Planar Th(III) Complex: Synthesis and Structure of [Th$(OC_6H_2{}^tBu_2$-2,6-Me-4$)_4]^{1-}$. *J. Am. Chem. Soc.* **2019**, *141*, 12458–12463, DOI: 10.1021/jacs.9b04399.

(27) Schumann, H.; Meese-Marktscheffel, J. A.; Esser, L. Synthesis, Structure, and Reactivity of Organometallic π-Complexes of the Rare Earths in the Oxidation State Ln^{3+} with Aromatic Ligands. *Chem. Rev.* **1995**, *95*, 865–986, DOI: 10.1021/cr00036a004.

(28) Hitchcock, P. B.; Lappert, M. F.; Maron, L.; Protchenko, A. V. Lanthanum Does Form Stable Molecular Compounds in the +2 Oxidation State. *Angew. Chem. Int. Ed.* **2008**, *47*, 1488–1491, DOI: 10.1002/anie.200704887.

(29) Woen, D. H.; Evans, W. J. Expanding the +2 Oxidation State of the Rare-Earth Metals, Uranium, and Thorium in Molecular Complexes. In *Handbook on the Physics and Chemistry of Rare Earths*; Bünzli, J.-C., Pecharsky, V. K., Eds.; Elsevier B.V., **2016**; pp 1–57, DOI: 10.1016/bs.hpcre.2016.08.002.

(30) MacDonald, M. R.; Bates, J. E.; Ziller, J. W.; Furche, F.; Evans, W. J. Completing the Series of +2 Ions for the Lanthanide Elements: Synthesis of Molecular Complexes of Pr^{2+}, Gd^{2+}, Tb^{2+}, and Lu^{2+}. *J. Am. Chem. Soc.* **2013**, *135*, 9857–9868, DOI: 10.1021/ja403753j.

(31) MacDonald, M. R.; Bates, J. E.; Fieser, M. E.; Ziller, J. W.; Furche, F.; Evans, W. J. Expanding Rare-Earth Oxidation State Chemistry to Molecular Complexes of Holmium(II) and Erbium(II). *J. Am. Chem. Soc.* **2012**, *134*, 8420–8423, DOI: 10.1021/ja303357w.

(32) Fieser, M. E.; MacDonald, M. R.; Krull, B. T.; Bates, J. E.; Ziller, J. W.; Furche, F.; Evans, W. J. Structural, Spectroscopic, and Theoretical Comparison of Traditional vs Recently Discovered Ln^{2+} Ions in the [K(2.2.2-Cryptand)][$(C_5H_4SiMe_3)_3Ln$] Complexes: The Variable Nature of Dy^{2+} and Nd^{2+}. *J. Am. Chem. Soc.* **2015**, *137*, 369–382, DOI: 10.1021/ja510831n.

(33) MacDonald, M. R.; Ziller, J. W.; Evans, W. J. Synthesis of a Crystalline Molecular Complex of Y^{2+}, [(18-Crown-6)K][$(C_5H_4SiMe_3)_3Y$]. *J. Am. Chem. Soc.* **2011**, *133*, 15914–15917,

DOI: 10.1021/ja207151y.

(34) Palumbo, C. T.; Darago, L. E.; Windor, C. J.; Ziller, J. W.; Evans, W. J.; Windorff, C. J.; Ziller, J. W.; Evans, W. J. Trimethylsilyl versus Bis(Trimethylsilyl) Substitution in Tris(Cyclopentadienyl) Complexes of La, Ce, and Pr: Comparison of Structure, Magnetic Properties, and Reactivity. *Organometallics* **2018**, *37*, 900–905, DOI: 10.1021/acs.organomet.7b00881.

(35) MacDonald, M. R.; Fieser, M. E.; Bates, J. E.; Ziller, J. W.; Furche, F.; Evans, W. J. Identification of the +2 Oxidation State for Uranium in a Crystalline Molecular Complex, [K(2.2.2-Cryptand)][$(C_5H_4SiMe_3)_3U$]. *J. Am. Chem. Soc.* **2013**, *135*, 13310–13313, DOI: 10.1021/ja406791t.

(36) Windorff, C. J.; MacDonald, M. R.; Meihaus, K. R.; Ziller, J. W.; Long, J. R.; Evans, W. J. Expanding the Chemistry of Molecular U^{2+} Complexes: Synthesis, Characterization, and Reactivity of the $\{[C_5H_3(SiMe_3)_2]_3U\}^-$ Anion. *Chem. Eur. J.* **2016**, *22*, 772–782, DOI: 10.1002/chem.201503583.

(37) Windorff, C. J.; Chen, G. P.; Cross, J. N.; Evans, W. J.; Furche, F.; Gaunt, A. J.; Janicke, M. T.; Kozimor, S. A.; Scott, B. L. Identification of the Formal +2 Oxidation State of Plutonium: Synthesis and Characterization of $\{Pu^{II}[C_5H_3(SiMe_3)_2]_3\}^-$. *J. Am. Chem. Soc.* **2017**, *139*, 3970–3973, DOI: 10.1021/jacs.7b00706.

(38) Su, J.; Windorff, C. J.; Batista, E. R.; Evans, W. J.; Gaunt, A. J.; Janicke, M. T.; Kozimor, S. A.; Scott, B. L.; Woen, D. H.; Yang, P. Identification of the Formal +2 Oxidation State of Neptunium: Synthesis and Structural Characterization of $\{Np^{II}[C_5H_3(SiMe_3)_2]_3\}^{1-}$. *J. Am. Chem. Soc.* **2018**, *140*, 7425–7428, DOI: 10.1021/jacs.8b03907.

(39) Langeslay, R. R.; Fieser, M. E.; Ziller, J. W.; Furche, F.; Evans, W. J. Synthesis, Structure,

and Reactivity of Crystalline Molecular Complexes of the $\{[C_5H_3(SiMe_3)_2]_3Th\}^{1-}$ Anion Containing Thorium in the Formal +2 Oxidation State. *Chem. Sci.* **2015**, *6*, 517–521, DOI: 10.1039/C4SC03033H.

(40) Arnold, P. L.; Dutkiewicz, M. S.; Walter, O. Organometallic Neptunium Chemistry. *Chem. Rev.* **2017**, *117*, 11460–11475, DOI: 10.1021/acs.chemrev.7b00192.

(41) Wen, X. D.; Martin, R. L.; Henderson, T. M.; Scuseria, G. E. Density Functional Theory Studies of the Electronic Structure of Solid State Actinide Oxides. *Chem. Rev.* **2013**, *113*, 1063–1096, DOI: 10.1021/cr300374y.

(42) Lauher, J. W.; Hoffmann, R. Structure and Chemistry of Bis(Cyclopentadienyl)-ML_n Complexes. *J. Am. Chem. Soc.* **1976**, *98*, 1729–1742, DOI: 10.1021/ja00423a017.

(43) Bursten, B. E.; Rhodes, L. F.; Strittmatter, R. J. Bonding in Tris(η^5-Cyclopentadienyl) Actinide Complexes. 2. On the Ground Electronic Configurations of "Base-Free" Cp_3An Complexes (An = Th, Pa, U, Np, Pu). *J. Am. Chem. Soc.* **1989**, *111*, 2756–2758, DOI: 10.1021/ja00190a002.

(44) Strittmatter, R. J.; Bursten, B. E. Bonding in Tris(η^5-Cyclopentadienyl) Actinide Complexes. 5. A Comparison of the Bonding in Np, Pu, and Transplutonium Compounds with That in Lanthanide Compounds and a Transition-Metal Analogue. *J. Am. Chem. Soc.* **1991**, *113*, 552–559, DOI: 10.1021/ja00002a024.

(45) Bochkarev, M. N.; Fedushkin, I. L.; Dechert, S.; Fagin, A. A.; Schumann, H. $[NdI_2(THF)_5]$, the First Crystallographically Authenticated Neodymium(II) Complex. *Angew. Chem. Int. Ed.* **2001**, *40*, 3176–3178, DOI: 10.1002/1521-3773(20010903)40:17<3176::AID-ANIE3176>3.0.CO;2-Y.

(46) Bochkarev, M. N. Molecular Compounds of "New" Divalent Lanthanides. *Coord. Chem.*

Rev. **2004**, *248*, 835–851, DOI: 10.1016/j.ccr.2004.04.004.

(47) Jenkins, T. F.; Woen, D. H.; Mohanam, L. N.; Ziller, J. W.; Furche, F.; Evans, W. J. Tetramethylcyclopentadienyl Ligands Allow Isolation of Ln(II) Ions across the Lanthanide Series in [K(2.2.2-Cryptand)][$(C_5Me_4H)_3Ln$] Complexes. *Organometallics* **2018**, *37*, 3863–3873, DOI: 10.1021/acs.organomet.8b00557.

(48) Huh, D. N.; Ziller, J. W.; Evans, W. J. Chelate-Free Synthesis of the U(II) Complex, $[(C_5H_3(SiMe_3)_2)_3U]^{1-}$, Using Li and Cs Reductants and Comparative Studies of La(II) and Ce(II) Analogs. *Inorg. Chem.* **2018**, *57*, 11809–11814, DOI: 10.1021/acs.inorgchem.8b01966.

(49) Ryan, A. J.; Angadol, M. A.; Ziller, J. W.; Evans, W. J. Isolation of U(II) Compounds Using Strong Donor Ligands, C_5Me_4H and $N(SiMe_3)_2$, Including a Three-Coordinate U(II) Complex. *Chem. Commun.* **2019**, *55*, 2325–2327, DOI: 10.1039/C8CC08767A.

(50) Guo, F. S.; Tsoureas, N.; Huang, G. Z.; Tong, M. L.; Mansikkamäki, A.; Layfield, R. A. Isolation of a Perfectly Linear Uranium(II) Metallocene. *Angew. Chem. Int. Ed.* **2020**, *59*, 2299–2303, DOI: 10.1002/anie.201912663.

(51) La Pierre, H. S.; Scheurer, A.; Heinemann, F. W.; Hieringer, W.; Meyer, K. Synthesis and Characterization of a Uranium(II) Monoarene Complex Supported by δ Backbonding. *Angew. Chem. Int. Ed.* **2014**, *53*, 7158–7162, DOI: 10.1002/anie.201402050.

(52) Billow, B. S.; Livesay, B. N.; Mokhtarzadeh, C. C.; Mccracken, J.; Shores, M. P.; Boncella, J. M.; Odom, A. L. Synthesis and Characterization of a Neutral U(II) Arene Sandwich Complex. *J. Am. Chem. Soc.* **2018**, *140*, 17369–17373, DOI: 10.1021/jacs.8b10888.

(53) Straub, M. D.; Ouellette, E. T.; Boreen, M. A.; Britt, R. D.; Chakarawet, K.; Douair, I.; Gould, C. A.; Maron, L.; Del Rosal, I.; Villarreal, D.; Minasian, S. G.; Arnold, J. A

Uranium(II) Arene Complex That Acts as a Uranium(I) Synthon. *J. Am. Chem. Soc.* **2021**, *143*, 19748–19760, DOI: 10.1021/jacs.1c07854.

(54) Wedal, J. C.; Evans, W. J. A Rare-Earth Metal Retrospective to Stimulate All Fields. *J. Am. Chem. Soc.* **2021**, *143*, 18354–18367, DOI: 10.1021/jacs.1c08288.

(55) Peterson, J. K.; MacDonald, M. R.; Ziller, J. W.; Evans, W. J. Synthetic Aspects of $(C_5H_4SiMe_3)_3Ln$ Rare-Earth Chemistry: Formation of $(C_5H_4SiMe_3)_3Lu$ via $[(C_5H_4SiMe_3)_2Ln]^+$ Metallocene Precursors. *Organometallics* **2013**, *32*, 2625–2631, DOI: 10.1021/om400116d.

(56) Cassani, M. C.; Duncalf, D. J.; Lappert, M. F. The First Example of a Crystalline Subvalent Organolanthanum Complex: $[K([18]Crown-6)-(\eta^2-C_6H_6)_2][(LaCp^{tt}_2)_2(\mu-\eta^6:\eta^6-C_6H_6)]\bullet 2C_6H_6$ ($Cp^{tt} = \eta^5-C_5H_3Bu^t_2$-1,3). *J. Am. Chem. Soc.* **1998**, *120*, 12958–12959, DOI: 10.1021/ja980377t.

(57) Gun'ko, Y. K.; Hitchcock, P. B.; Lappert, M. F. Activation of a CO Bond by Reaction of a Tris(Cyclopentadienyl)Lanthanide Complex with an Alkali Metal in Dimethoxyethane (DME); Crystal Structures of $[Nd\{\eta-C_5H_3(SiMe_3)_2$-1,3$\}_2(\mu-OMe)_2Li(DME)]$ and $[\{Ce(\eta-C_5H_3{}^tBu_2$-1,3$)_2(\mu-OMe)_2]$. *J. Organomet. Chem.* **1995**, *499*, 213–219, DOI: 10.1016/0022-328X(95)00330-S.

(58) Cassani, M. C.; Lappert, M. F.; Laschi, F. First Identification by EPR Spectra of Lanthanum(II) Organometallic Intermediates (and $E_{1/2}$ for $La^{3+} \rightarrow La^{2+}$) in the C-O Bond Activation of Dimethoxyethane. *Chem. Commun.* **1997**, *2*, 1563–1564, DOI: 10.1039/a702493b.

(59) Pimentel, G. C.; Spratley, R. D. Understanding Chemistry; Holden-Day: San Fransisco, CA, **1971**.

(60) Hart, F. A.; Laming, F. P. Some O-Phenanthroline Complexes of Yttrium and the Lanthanides. In *Proc. Chem. Soc. London*; **1963**; p 107, DOI: 10.1039/PS9630000101.

(61) Collman, J. P.; Hegedus, L. S.; Norton, J. R.; Finke, R. G. *Principles and Applications of Organotransition Metal Chemistry*; University Science Books: Mill Valley, CA, **1987**.

(62) Castro-Rodriguez, I.; Nakai, H.; Zakharov, L. N.; Rheingold, A. L.; Meyer, K. A Linear, O-Coordinated η^1-CO_2 Bound to Uranium. *Science* **2004**, *305*, 1757–1759, DOI: 10.1126/science.1102602.

(63) Evans, W. J.; Kozimor, S. A.; Ziller, J. W. Molecular Octa-Uranium Rings with Alternating Nitride and Azide Bridges. *Science* **2005**, *309*, 1835–1838, DOI: 10.1126/science.1116168.

(64) Summerscales, O. T.; Cloke, F. G. N.; Hitchcock, P. B.; Green, J. C.; Hazari, N. Reductive Cyclotrimerization of Carbon Monoxide to the Deltate Dianion by an Organometallic Uranium Complex. *Science* **2006**, *311*, 829–831, DOI: 10.1126/science.1121784.

(65) Hayton, T. W.; Boncella, J. M.; Scott, B. L.; Palmer, P. D.; Batista, E. R.; Jeffrey Hay, P. Sythesis of Imido Analogs of the Uranyl Ion. *Science* **2005**, *310*, 1941–1943, DOI: 10.1126/science.1120069.

(66) Falcone, M.; Chatelain, L.; Scopelliti, R.; Živković, I.; Mazzanti, M. Nitrogen Reduction and Functionalization by a Multimetallic Uranium Nitride Complex. *Nature* **2017**, *547*, 332–335, DOI: 10.1038/nature23279.

(67) Halter, D. P.; Heinemann, F. W.; Maron, L.; Meyer, K. The Role of Uranium–Arene Bonding in H_2O Reduction Catalysis. *Nat. Chem.* **2018**, *10*, 259–267, DOI: 10.1038/nchem.2899.

(68) Cloke, F. G. N. Zero Oxidation State Compounds of Scandium, Yttrium, and the

Lanthanides. *Chem. Soc. Rev.* **1993**, *22*, 17–24, DOI: 10.1039/CS9932200017.

(69) Evans, W. J.; Davis, B. L. Chemistry of Tris (Pentamethylcyclopentadienyl) f-Element Complexes, $(C_5Me_5)_3M$. *Chem. Rev.* **2002**, *102*, 2119–2136, DOI: 10.1021/cr010298r.

(70) Lu, E.; Liddle, S. T. Uranium-Mediated Oxidative Addition and Reductive Elimination. *Dalton Trans.* **2015**, *44*, 12924–12941, DOI: 10.1039/C5DT00608B.

(71) Gardner, B. M.; Kefalidis, C. E.; Lu, E.; Patel, D.; McInnes, E. J. L.; Tuna, F.; Wooles, A. J.; Maron, L.; Liddle, S. T. Evidence for Single Metal Two Electron Oxidative Addition and Reductive Elimination at Uranium. *Nat. Commun.* **2017**, *8*, 1898, DOI: 10.1038/s41467-017-01363-0.

(72) Finke, R. G.; Keenan, S. R.; Schiraldi, D. A.; Watson, P. L. Organolanthanide and Organoactinide Oxidative Additions Exhibiting Enhanced Reactivity. 3. Products and Stoichiometries for the Addition of Alkyl and Aryl Halides to $(C_5Me_5)_2Yb^{II}\cdot OEt_2$ and Evidence for Facile, Inner-Sphere $(C_5Me_5)_2Yb^{III}R$ and $(C_5Me_5)_2Yb^{III}X$ + RX"Yb^{III} Grignard" Reactions. *Organometallics* **1986**, *5*, 598–601, DOI: 10.1021/om00134a039.

Chapter 2:

Density Functional Theory Analysis of the Importance of Coordination Geometry for $5f^36d^1$ vs $5f^4$ Electron Configurations in U(II) Complexes

Introduction[†]

The discovery that the +2 oxidation state is accessible to uranium in $[K(crypt)][Cp'_3U]$[1] raised the question of what other coordination environments could support the U(II) ion. The unique $5f^36d^1$ electron configuration was rationalized for this complex by the pseudo-D_3 symmetry of the tris(cyclopentadienyl) ligand environment[2–5] and density functional theory (DFT) calculations were consistent with this view. As other U(II) complexes were reported,[6–10] it was noted that the U(II) complexes with trigonal or planar geometries had $5f^36d^1$ configurations, while others with a non-planar and arene-tether had $5f^4$ configurations.

The study in this Chapter was initiated to better understand how the electronic structure of new U(II) complexes is affected by ligand geometries and was performed with the guidance of Professor Filipp Furche. Eleven total U(II) compounds with various coordination geometries including trigonal planar, square planar, linear, tetrahedral, and octahedral were analyzed. The results are compared with known U(II) complexes[1,2,15] and related Ln(II) compounds.[10,20-22,24,25,47] Note that within this study, the term planar refers to the primary coordination sphere of the uranium complex, considering the donor atom of a monohaptic ligand or the centroid of a ring system.

The theoretical compounds chosen for this study were selected because they are derived from known U(IV) or U(III) compounds that could serve as reasonable experimental precursors for the theoretical U(II) complexes. Hence, there is a realistic possibility that the results reported

[†] Portions of this Chapter have been published: Wedal, J. C.; Furche, F.; Evans, W. J. Density Functional Theory Analysis of the Importance of Coordination Geometry for $5f^36d^1$ versus $5f^4$ Electron Configurations in U(II) Complexes *Inorg. Chem.* **2021**, *60*, 16316.

here could be verified experimentally. This study should be considered a targeted screening effort aiming to guide future synthetic, as well as more refined theoretical, efforts to probe how the ligand geometry affects the electronic structure of low-valent f-block complexes.

Computational Details

All calculations were completed at the density functional level of theory using the TPSSh hybrid meta-generalized gradient density functional[11] with Grimme's D3 dispersion correction[12,13] and the resolution of the identity (RI-J) approximation.[14] Scalar relativistic small-core effective core potentials (ECPs)[15] with def-TZVP basis set[16] were used for uranium while the polarized split-valence basis sets def2-SV(P)[16] were used for the other atoms. Quadrature grids of size m4 were used.[17] Structure optimizations were initiated from the crystal structure coordinates or DFT-optimized coordinates of $[Li(THF)_4][Cp''_3U]$,[8] $[K(crypt)][Cp^{tet}_3U]$,[7] $[K(crypt)][U(NR_2)_3]$,[7] $U(NHAr^{iPr6})_2$,[9] $U(CHR_2)_3$,[18] $[Th(OAr')_4]^{1-}$,[19] $(C_8H_8)_2U$,[20] $U(\eta^4\text{–bnz}')_4$,[21] and $U(H_3BH)_3(THF)_3$[22] at convergence thresholds of 10^{-4} a.u. and energy convergence of at least 10^{-7} a.u. No point-group symmetry constraints were applied. The continuum solvation model COSMO[23] was used for anionic species with a dielectric constant $\varepsilon = 7.52$ for THF,[24] except for the uranocene compound in which a dielectric constant of $\varepsilon = \infty$ was employed to guarantee a bound ground state. Ground state geometries were confirmed by the lack of imaginary frequencies in the vibrational spectrum.[25] Various spin states were analyzed for these U(II) compounds and the highest spin value (S = 2, quintet state) was always energetically favored. Representative energies for the singlet, triplet, and quintet states of $[Cp''_3U]^{1-}$ and $[Cp^{tet}_3U]^{1-}$ are given in Table 2.1. The $\langle S^2 \rangle$ values for all U(II) compounds in this study were between 6.006–6.024, indicating a negligible amount of spin contamination in the quintet ground states [expected $S(S+1) = 6$ for $S = 2$ system, see Table 2.2].

Table 2.1: Spin state energies for $[Cp''_3U]^{1-}$ and $[Cp^{tet}_3U]^{1-}$

	$[Cp''_3U]^{1-}$		
	$S = 0$	$S = 1$	$S = 2$
Energy (eV)	−95466.4618	−95468.2517	−956468.4328
	$[Cp^{tet}_3U]^{1-}$		
	$S = 0$	$S = 1$	$S = 2$
Energy (eV)	−41594.3117	−41595.4866	−41597.5773

Time-dependent DFT (TDDFT) calculations[26] were carried out on the optimized structures with the same functional and basis sets described above. An additional diffuse *p* primitive was added to the def-TZVP basis set for uranium by downward extrapolation. This addition to the basis set has been shown to be essential for accurate simulation of d to p transitions in similar U(II) and Ln(II) compounds.[27–29] TDDFT calculations on $[U(NR_2)_3]^{1-}$ and $[Cp^{tet}_3U]^{1-}$ without this basis set extrapolation lacked transitions at lower energy seen in the experimental spectra. Electronic absorption spectra were simulated using Gaussian line profiles centered on the oscillator energy. The transitions are summarized and complete details can be found in the SI. Electronic configurations were assigned by inspection of the molecular orbitals using VMD[30] and Mulliken population analysis. All calculations were performed with TURBOMOLE version 7.4.1.[31,32]

One main goal of this study was to analyze changes in the electronic structure as a function of ligand geometry. Further computational studies, such as multiconfiguration character, inclusion of spin-orbit coupling, and larger basis sets, could certainly be performed. The present methods were chosen since they have been shown to accurately predict the electronic structure for many low-valent f element compounds[1,10,15-27,36,50,52,54] and are a compromise between accuracy and computational cost.

Table 2.2: $<S^2>$ values of compounds in this study

	$<S^2>$
$[Cp''_3U]^{1-}$	6.010
$[Cp^{tet}_3U]^{1-}$	6.012
$[U(NR_2)_3]^{1-}$ in C_1	6.008
$[U(NR_2)_3]^{1-}$ in C_3	6.008
$[U(NR_2)_3]^{1-}$ in D_3	6.006
$U(NHAr^{iPr6})_2$	6.012
$[U(CHR_2)_3]^{1-}$	6.009
$[U(H_3BH)_3]^{1-}$	6.007
$[U(OAr')_4]^{2-}$ in C_2	6.009
$[C_8H_8)U]^{2-}$	6.024
$[U(bnz')_4]^{2-}$	6.024
$U(H_3BH)_3(THF)_3$	4.838
$[U(H_3BH)_3(THF)_3]^{1-}$	6.006
$[U(crypt)]^{2+}$	6.005
$U(crypt)(OMe)_2$	6.005

Results

Previously Synthesized U(II) Compounds. Initially, the electronic structures of known U(II) complexes were investigated, including three trigonal U(II) compounds, $[Cp''_3U]^{1-}$,[6,8] $[Cp^{tet}_3U]^{1-}$,[7] and $[U(NR_2)_3]^{1-}$,[7] and the arene-tethered complex, $(NHAr^{iPr6})_2U$,[9] Scheme 2.1.

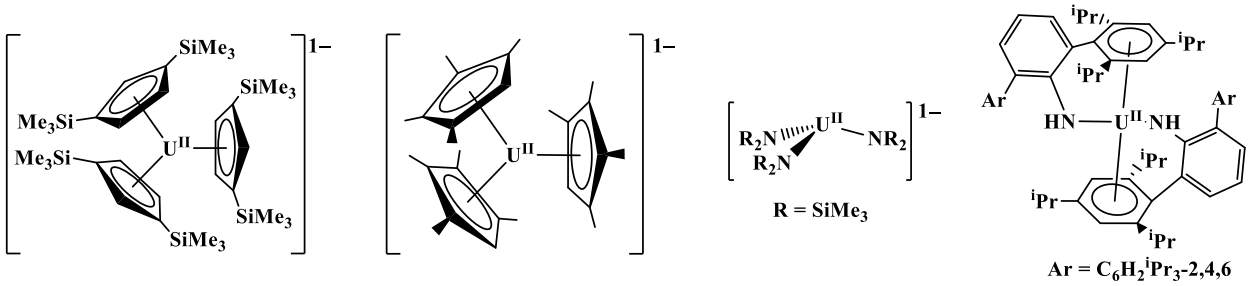

Scheme 2.1: Molecular structures of $[Cp''_3U]^{1-}$, $[Cp^{tet}_3U]^{1-}$, $[U(NR_2)_3]^{1-}$, and $(NHAr^{iPr6})_2U$.

The first three tris(ligand) complexes have been assigned a $5f^36d^1$ electron configuration based on the UV-visible spectroscopy, magnetic data, structural data, and analogy to the lanthanide compounds.[28,29,33] The arene-tethered complex $(NHAr^{iPr6})_2U$ was described as a $5f^4$ configuration based on X-ray distances and spectroscopic evidence.

$[Cp''_3U]^{1-}$. Geometry optimizations of $[Cp''_3U]^{1-}$ resulted in a ground state where the highest occupied molecular orbital (HOMO) had significant $6dz^2$-like character, Figure 2.1. This orbital is essentially non-bonding with respect to the cyclopentadienyl ligands. The next three highest occupied orbitals were 5f orbitals, yielding an overall electron configuration best described as $5f^3 6d^1$. This electronic configuration is in agreement with the spectroscopic assignment in the literature[6] as well as previous studies on $[Cp''_3Ln]^{1-}$ [33,34] and other tris(cyclopentadienyl) f-block complexes.[3,29,33–39]

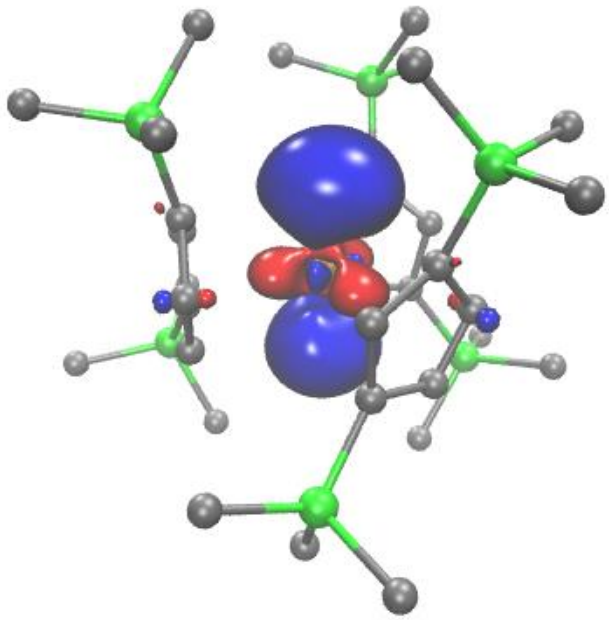

Figure 2.1: Calculated HOMO of $[Cp''_3U]^{1-}$, plotted with a contour value of 0.05. Hydrogen atoms are omitted for clarity. Calculated orbital energy $\varepsilon = -1.453$ eV.

The simulated UV-visible spectrum of $[Cp''_3U]^{1-}$ is shown along with the experimental spectrum in Figure 2.2. The transitions between 1000–550 nm are metal-based with 6d to 5f character. In addition, three transitions are calculated to occur from occupied 5f into 7p orbitals at 577 nm, one transition occurs from the occupied 6d orbital into the 7s orbital at 514 nm, and three transitions from occupied 5f to the 7s orbital at 422 nm. Below 500 nm, the transitions are

mostly metal-to-ligand in character, from occupied 5f and 6d orbitals into unoccupied π orbitals on the Cp″ rings.

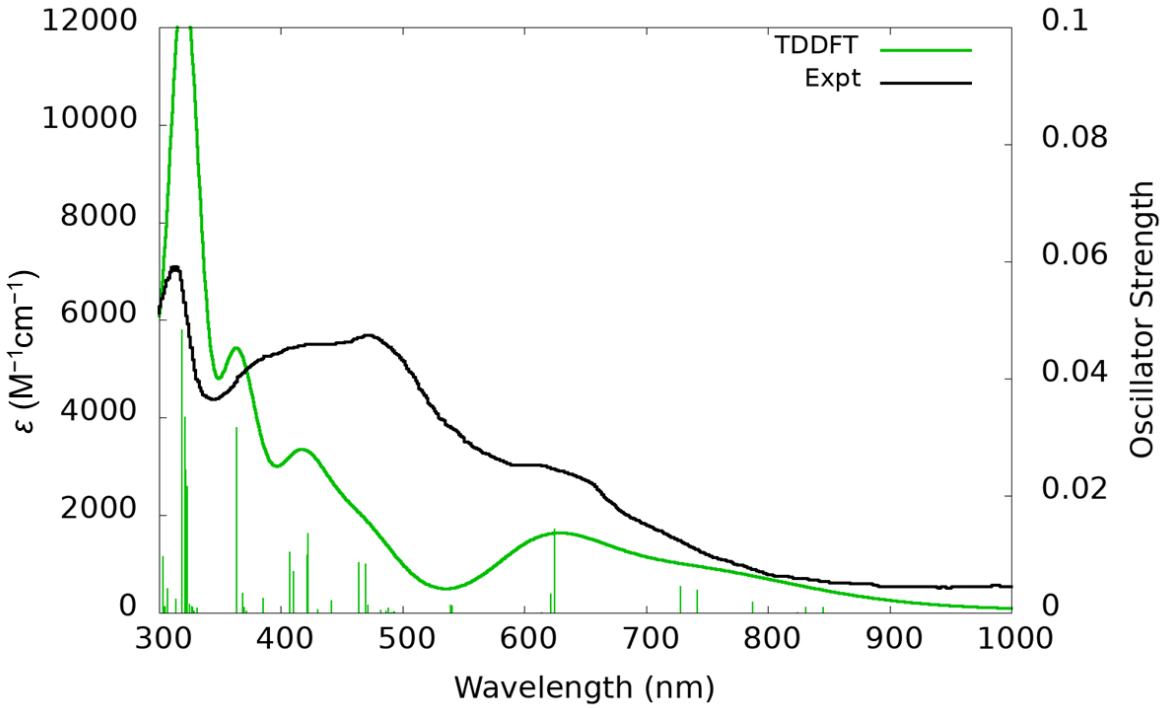

Figure 2.2: Experimental[6] (black) and simulated (green) UV-visible spectrum of $[Cp''_3U]^{1-}$. A Gaussian line broadening of 0.15 eV was applied and the computed excitation spectrum was empirically blue shifted by 0.40 eV.

Table 2.4. Electronic excitation summary for $[Cp''_3U]^{1-}$. Oscillator strengths are reported in the length gauge. Only the dominant contributions to the overall excitation are reported. 191a is the $6dz^2$-like HOMO. The assignment "π" is the π system of the Cp″ rings.

Wavelength (nm)	Oscillator Strength	Dominant contributions			Assignment
		Occupied	Virtual	% weight	
1055	0.002	191a	197a	41.3	6d-5f
976	0.004	190a	192a	22.7	5f-5f/7p/6d
952	0.004	190a	197a	19.5	5f-5f
782	0.014	191a	197a	30.8	6d-5f
778	0.003	191a	196a	54.5	6d-5f/7p

778	0.003	191a	195a	73.8	6d-7p/5f
655	0.001	190a	200a	39.6	5f-5f/π
653	0.001	189a	200a	42.2	5f-5f/π
556	0.001	191a	200a	48.0	6d-5f/π
554	0.008	191a	199a	65.1	6d-5f/π
545	0.009	191a	201a	57.9	6d-5f/π
514	0.002	191a	198a	90.1	6d-7s
489	0.014	190a	199a	37.7	5f-5f/π
488	0.010	190a	201a	35.1	5f-5f/π
473	0.007	188a	199a	75.1	5f-5f/π
469	0.010	188a	201a	44.7	5f-5f/π
440	0.002	190a	199a	27.5	5f-5f/π
420	0.001	188a	198a	60.3	5f-7s
418	0.003	191a	202a	59.0	6d-π
412	0.032	191a	203a	89.1	6d-π
412	0.031	191a	204a	88.6	6d-π
370	0.001	191a	207a	25.3	6d-5f/π
366	0.001	190a	204a	32.7	5f-π
366	0.001	190a	203a	23.0	5f-π
363	0.001	190a	201a	41.1	5f-π
363	0.001	188a	204a	26.7	5f-π
360	0.019	188a	202a	31.1	5f-π
360	0.021	188a	203a	23.9	5f-π
360	0.010	191a	205a	40.1	6d-π
359	0.024	191a	206a	50.0	6d-π
359	0.033	188a	204a	36.6	5f-π
355	0.048	191a	208a	57.8	6d-5f/π
349	0.002	188a	202a	26.3	5f-π
341	0.004	187b	188b	86.1	π-6d/π
338	0.001	191a	209a	93.8	6d-π
338	0.001	191a	210a	94.4	6d-π
336	0.010	191a	201a	63.7	6d-5f/π
327	0.001	187a	192a	43.8	5f-5f/7p/6d
325	0.002	187a	193a	22.9	5f-7p/5f
323	0.006	189a	207a	56.8	5f-5f/π
323	0.006	190a	207a	39.5	5f-5f/π
321	0.011	191a	212a	80.6	6d-π
316	0.008	191a	214a	34.2	6d-π
316	0.008	191a	213a	35.7	6d-π

312	0.002	190a	206a	51.1	5f-π
312	0.003	189a	206a	40.7	5f-π
311	0.001	189a	205a	29.6	5f-π
310	0.002	188a	205a	65.7	5f-π
310	0.002	188a	206a	63.5	5f-π
308	0.001	190a	208a	27.8	5f-5f/π
308	0.001	191a	216a	35.2	6d-7p/π
304	0.013	188a	208a	43.8	5f-5f/π
304	0.049	186b	188b	59.0	π-6d/π
304	0.001	187b	189b	26.6	π-7p
303	0.001	187b	190b	22.8	π-7p
300	0.001	191a	218a	47.9	6d-π

$[Cp^{tet}_3U]^{1-}$. Calculations on $[Cp^{tet}_3U]^{1-}$ also resulted in a $5f^36d^1$ ground state electronic configuration. The HOMO was found to have $6dz^2$-like character, Figure 2.3, like that of $[Cp''_3U]^{1-}$ above.

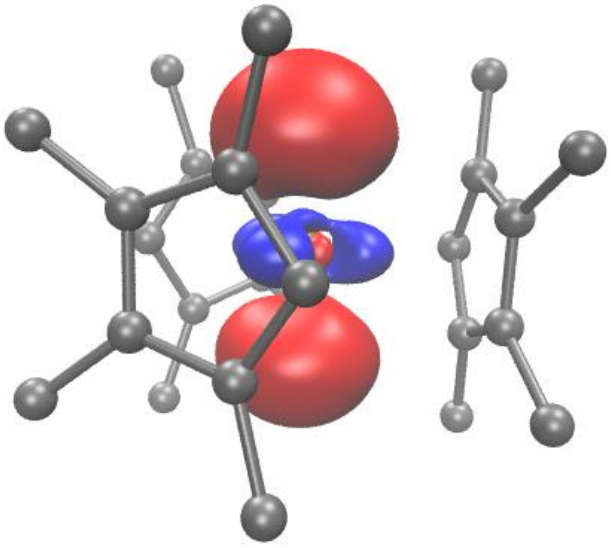

Figure 2.3: Calculated HOMO of $[Cp^{tet}_3U]^{1-}$, plotted with a contour value of 0.05. Hydrogen atoms are omitted for clarity. Calculated orbital energy $\varepsilon = -1.069$ eV.

The simulated UV-visible spectrum along with the experimental spectrum is shown in Figure 2.4. The broad absorption around 800 nm assigned as a 6d to 7p transition. Additional

transitions with 6d to 5f character are also observed in this region. The experimental spectrum is similar to that of $[(C_5Me_5)_2U(NR_2)]^{1-}$ and $[(C_5Me_5)U(NR_2)_2]^{1-}$, which featured broad absorptions centered at 750 nm and 684 nm, respectively, that were assigned as 6d to 7p transitions (see Chapter 4).[27] These features are different than those observed for $[Cp'_3U]^{1-}$[1] and $[Cp''_3U]^{1-}$, Figure 2.2, which feature mostly 6d to π/5f and π to 6d/5f transitions at higher energy.[1] The calculated spectrum for $[Cp^{tet}_3U]^{1-}$ is also similar to the $[Cp^{tet}_3Ln]^{1-}$ lanthanide analogs in which a 5d to 6p absorption dominates within the visible region.[29]

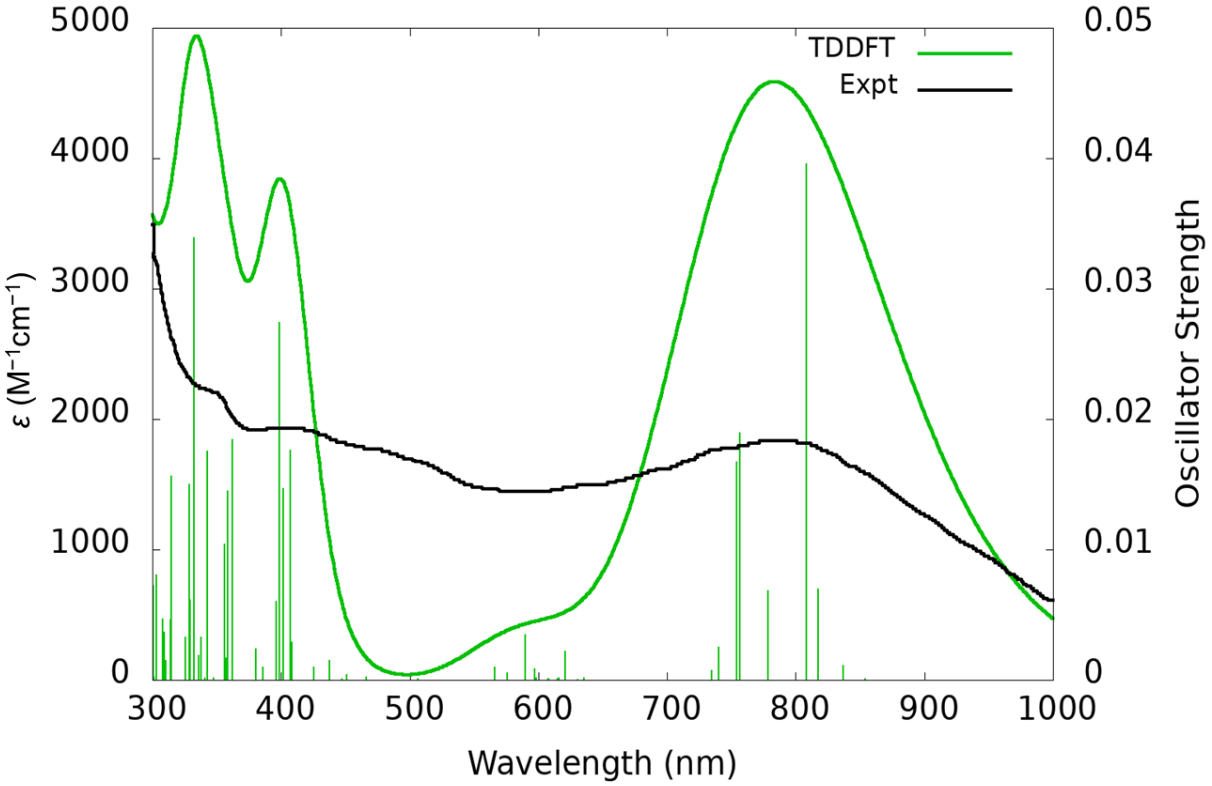

Figure 2.4: Experimental[7] (black) and simulated (green) UV-visible spectrum of $[Cp^{tet}_3U]^{1-}$. A Gaussian line broadening of 0.15 eV was applied and the computed excitation spectrum was empirically blue shifted by 0.40 eV and scaled by a factor of 0.5 to ease comparison with the experimental spectrum.

Table 2.5. Electronic excitation summary for $[Cp^{tet}_3U]^{1-}$. Oscillator strengths are reported in the length gauge. Only the dominant contributions to the overall excitation are reported. 119a is the $6dz^2$-like HOMO. The assignment "π" is the π system of the Cp^{tet} rings.

Wavelength (nm)	Oscillator Strength	Dominant contributions			Assignment
		Occupied	Virtual	% weight	
1080	0.001	119a	121a	73.9	6d-5f
993	0.004	117a	120a	36.7	5f-5f
964	0.004	116a	121a	17.9	5f-5f
954	0.004	116a	122a	19.6	5f-7p
766	0.044	119a	122a	70.2	6d-7p
699	0.001	118a	127a	34.0	5f-5f
695	0.001	116a	127a	33.9	5f-5f
605	0.003	119a	123a	96.6	6d-7s
574	0.063	119a	124a	87.4	6d-5f
538	0.014	119a	127a	81.1	6d-5f
505	0.003	119a	128a	24.5	6d-5f
501	0.001	118a	124a	25.3	5f-5f
493	0.004	116a	124a	13.5	5f-5f
487	0.007	117a	128a	23.9	5f-π
485	0.001	116a	124a	28.9	5f-5f
475	0.044	119a	125a	38.2	6d-7p
469	0.067	119a	129a	40.0	6d-7p
462	0.040	116a	129a	27.8	5f-π
456	0.006	119a	128a	32.8	6d-π
453	0.002	116a	128a	22.0	5f-π
451	0.003	118a	129a	18.1	5f-π
441	0.001	117a	129a	22.3	5f-π
418	0.006	117a	125a	38.0	5f-7p
415	0.006	118a	125a	29.5	5f-7p
413	0.002	116a	125a	62.5	5f-7p
411	0.011	117a	126a	40.4	5f-7p
403	0.001	116a	126a	50.2	5f-7p
399	0.002	119a	130a	73.5	6d-π
396	0.003	119a	131a	65.4	6d-π
387	0.010	119a	132a	91.7	6d-π
366	0.007	118a	130a	62.5	5f-π

363	0.011	118a	131a	58.6	5f-π
361	0.013	116a	130a	23.6	5f-π
360	0.007	116a	131a	31.6	5f-π
358	0.005	116a	130a	46.2	5f-π
352	0.005	118a	132a	78.4	5f-π
351	0.005	117a	132a	79.0	5f-π
348	0.006	116a	132a	76.4	5f-π
343	0.009	117a	133a	52.6	5f-π
341	0.007	116a	133a	42.7	5f-π
334	0.004	119a	134a	84.2	6d-π
333	0.005	119a	135a	87.0	5f-π
330	0.002	116a	133a	29.8	5f-π
327	0.010	114b	116b	72.2	π -6d
322	0.001	115a	120a	77.8	5f-5f
317	0.016	119a	136a	92.3	6d-π
309	0.001	119a	138a	93.8	6d-π
304	0.001	113b	116b	27.9	π-6d
303	0.001	117a	134a	49.4	5f-π
299	0.001	116a	135a	52.6	5f-π

$[U(NR_2)_3]^{1-}$. The optimized structure of $[U(NR_2)_3]^{1-}$ resulted in a C_1 symmetric ground state. C_3- and D_3-symmetric structures were found to be 1.6 and 4.2 kcal/mol higher in energy. However, the D_3-symmetric structure was a transition state with a single imaginary frequency of 10.62 cm^{-1}. It is possible the D_3-symmetric structure is in fact a ground state and the single imaginary mode is an artifact of the calculation, but this fact does not affect the remaining analysis. For the C_1- and C_3-symmetric structures, Mulliken population analyses revealed the HOMO was roughly half 6d and half 5f character, Figure 2.5, while the HOMO−3 of the D_3-symmetric structure was purely $6dz^2$ with 7s admixture, Figure 2.5 and Table 2.6.

Table 2.6: Orbital energies and MPA occupations for C_1-, C_3-, and D_3-symmetrical structures of $[U(NR_2)_3]^{1-}$.

		C_1 symmetry		
	Orbital	Energy (eV)	MPA Occupation numbers	Orbital assignment
LUMO	153a,α	−0.007	52% 7p, 43% 5f	7p
HOMO	152a,α	−1.689	49% 5f, 35% 6d	$6dz^2$
HOMO−1	151a,α	−1.808	40% 5f, 17% 6d, 35% 7s	5f
HOMO−2	150a,α	−1.886	93% 5f	5f
HOMO−3	149a,α	−1.888	94% 5f	5f
		C_3 symmetry		
	Orbital	Energy (eV)	MPA Occupation numbers	Orbital assignment
LUMO	51a,β	−0.071	54% 7s, 26% 7p, 22% 6d	7p
HOMO	52a,α	−1.594	64% 5f, 26% 6d	$6dz^2$
HOMO−1	100e,α	−1.663	94% 5f	5f
HOMO−2	99e,α	−1.663	94% 5f	5f
HOMO−3	51a,α	−1.812	27% 5f, 22% 6d, 35% 7s	5f
		D_3 symmetry		
	Orbital	Energy (eV)	MPA Occupation numbers	Orbital assignment
LUMO	27a1,β	0.273	83% 7s, 22% 6d	$6dz^2$
HOMO	25a2,α	−1.449	95% 5f	5f
HOMO−1, HOMO−2	50e,α	−1.537	96% 5f	5f
HOMO−3	27a1,α	−1.586	44% 6d, 62% 7s	$6dz^2$

All three geometries (C_1, C_3, and D_3) are likely to be accessible in solution due to the small energy difference. In fact, $[K(crypt)][U(NR_2)_3]$ crystallizes in the *R*32 space group with D_3-molecular symmetry.[7] The lanthanide analog $[Gd(NR_2)_3]^{1-}$ was previously analyzed by DFT and assigned as a $4f^7 5d^1$ configuration in a D_3-symmetric ground state.[28] Based on the present theoretical results and the structural and spectroscopic data,[7] a $5f^3 6d^1$ configuration is assigned to $[U(NR_2)_3]^{1-}$ although this assignment is based on a single-electron approximation. The present calculations suggest that the overall configuration and amount of orbital mixing can possibly be controlled by small geometrical changes.

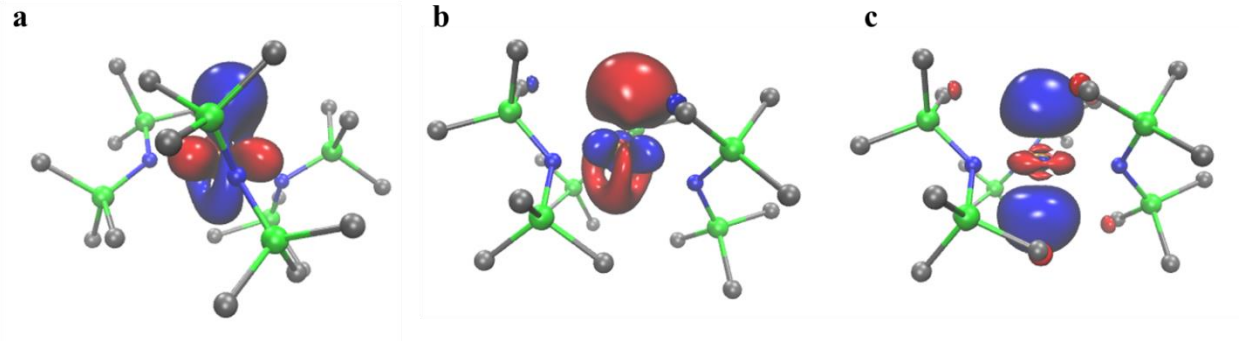

Figure 2.5: (a) HOMO, (b) HOMO−1, and (c) HOMO−3 of the C_1-, C_3- and D_3-symmetric structures of $[U(NR_2)_3]^{1-}$, plotted with a contour value of 0.05. Hydrogen atoms are omitted for clarity. Calculated orbital energies $\varepsilon = -1.689$, $\varepsilon = -1.594$, $\varepsilon = -1.449$ eV, respectively.

The simulated electronic absorption spectrum for the C_1-symmetric state of $[U(NR_2)_3]^{1-}$ is shown in Figure 2.6 along with the experimental spectrum. The lack of defining features in the experimental spectrum is consistent with the fact that electronic transitions were found to occur over the entire UV-visible region. Transitions at wavelengths greater than 400 nm were metal-based, while transitions at wavelengths shorter than 400 nm were found to be metal-to-ligand charge transfers. Strong transitions attributed to 6d to 7p transitions were found at 670 nm and 5f to 7p transitions were found between 650–600 nm. Transitions from 6d to 7s were found at 480 nm. Other transitions between 1000–400 nm were 6d to 5f, 5f to 6d, and 5f to 5f in character. Further details can be found in Table 2.4.

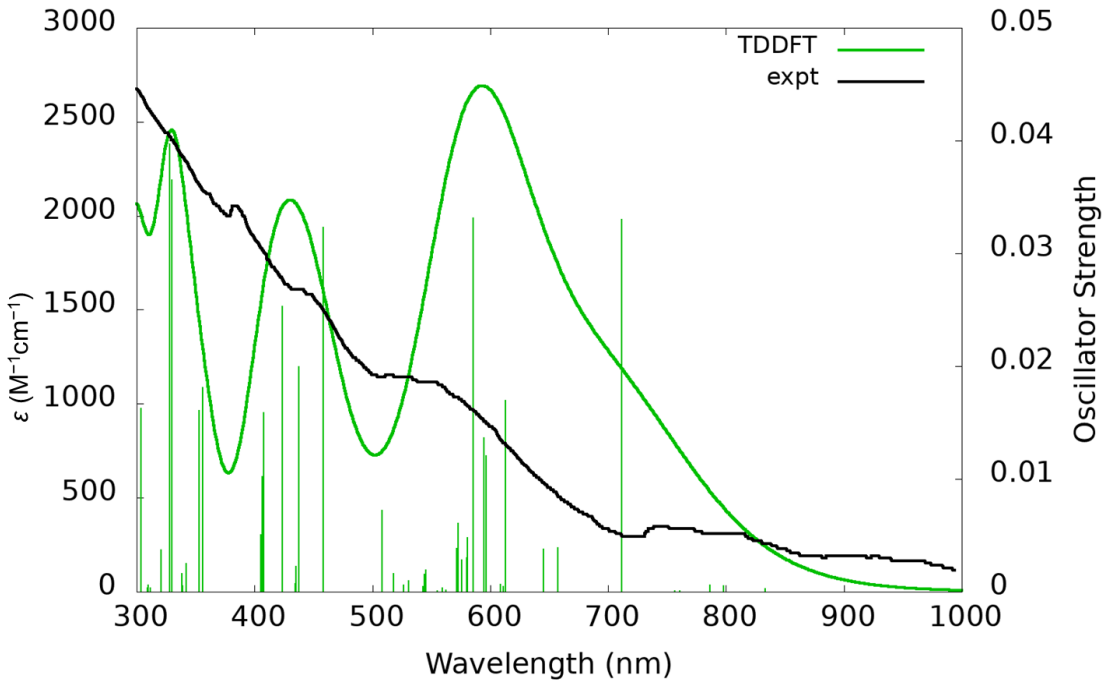

Figure 2.6: Experimental[7] (black) and simulated (green) UV-visible spectrum of $[U(NR_2)_3]^{1-}$ computed in C_1 symmetry. A Gaussian line broadening of 0.15 eV was applied and the computed excitation spectrum was empirically blue shifted by 0.40 eV and scaled by a factor of 0.15 to ease comparison with the experimental spectrum.

Table 2.4. Electronic excitation summary for $[U(NR_2)_3]^{1-}$ computed in C_1 symmetry. Oscillator strengths are reported in the length gauge. Only the dominant contributions to the overall excitation are reported. 152a is the HOMO.

Wavelength (nm)	Oscillator Strength	Dominant contributions			Assignment
		Occupied	Virtual	% weight	
916	0.001	152	157	14.9	6d-6d/5f
901	0.001	152	158	17.8	6d-6d/5f
803	0.033	152	153	26.3	6d-7p
735	0.004	152	157	24.4	6d-6d/5f
720	0.004	152	158	24.0	6d-6d/5f

680	0.017	152	153	60.3	6d-7p
675	0.001	152	155	32.2	6d-7p
660	0.012	152	155	40.4	6d-7p
658	0.014	152	154	34.6	6d-7p
647	0.033	151	153	60.1	5f-7p
641	0.005	150	153	26.8	5f-7p
640	0.003	149	153	17.7	5f-7p
634	0.003	149	160	11.9	5f-5f/6d
634	0.006	150	153	34.8	5f-7p
629	0.004	149	153	47.9	5f-7p
598	0.002	150	154	30.9	5f-7p
597	0.002	150	155	35.7	5f-7p
580	0.001	151	159	36.8	5f-5f
575	0.001	151	160	45.2	5f-5f/6d
565	0.002	151	161	41.9	5f-5f/6d
554	0.007	152	156	13.2	6d-5f/7p
495	0.032	152	162	72.3	6d-7s
471	0.020	151	162	60.5	5f-7s
468	0.002	150	162	44.2	5f-7s
467	0.001	149	162	48.1	5f-7s
454	0.025	152	163	65.3	6d-7p/5f
436	0.016	151	163	39.9	5f-7p/5f
435	0.010	149	163	27.3	5f-7p/5f
434	0.005	149	163	24.6	5f-7p/5f
378	0.018	152	164	71.5	6d-ligand
374	0.016	152	165	72.5	6d-ligand
362	0.002	150	164	75.9	5f-ligand
358	0.002	149	165	84.4	5f-ligand
348	0.036	151	164	66.4	5f-ligand
346	0.040	151	165	72.0	5f-ligand
338	0.004	152	166	95.9	6d-ligand
326	0.001	150	166	91.9	5f-ligand
320	0.016	152	168	59.5	6d-ligand
319	0.012	152	167	64.8	6d-ligand
310	0.021	151	167	41.6	5f-ligand
310	0.024	151	168	58.4	5f-ligand
309	0.002	152	169	39.7	6d-ligand
304	0.001	150	168	56.4	5f-ligand
304	0.001	150	167	43.9	5f-ligand

303	0.001	149	168	36.7	5f-ligand
300	0.001	151	170	67.0	5f-ligand
296	0.007	152	171	88.5	6d-ligand

$(NHAr^{iPr6})_2U$. The arene-tethered complex was found to have a $5f^4$ electron configuration by our DFT analysis, in agreement with the reported assignment.[9] The optimized ground state structure was found to have C_2 symmetry, consistent with the solid state structure. The HOMO of $(NHAr^{iPr6})_2U$ is shown in Figure 2.7. The 5f orbitals on uranium have an interaction with the arene π system, much like what was observed by Meyer and coworkers for $5f^4$ [K(crypt)]{[(^{Ad,Me}ArO)$_3$mes]U}.[10] Thus, the 5f-arene interaction may be important in stabilizing the $5f^4$ electronic configuration.

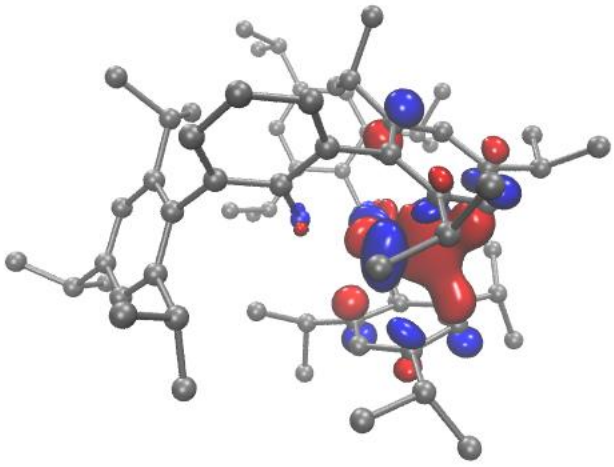

Figure 2.7: HOMO of $(NHAr^{iPr6})_2U$, plotted with a contour value of 0.05. Hydrogen atoms are omitted for clarity. Calculated orbital energy $\varepsilon = -3.132$ eV.

Model U(II) systems. The above results, in addition to the study on heteroleptic uranium systems,[27] provide further evidence that the ligand geometry around the uranium center has a direct impact on the electron configuration. It appears that planar geometries yield $5f^36d^1$ electron configurations for U(II) complexes, while less planar or complexes with arene interactions, like those found in [K(crypt)]{[(^{Ad,Me}ArO)$_3$mes]U}[10] and $(NHAr^{iPr6})_2U$,[9] yield $5f^4$ electron

configurations. Described below are DFT studies on seven model U(II) compounds in trigonal planar, square planar, linear, tetrahedral, and octahedral ligand environments. Each complex is derived from known U(III) or U(IV) compounds.

$[U(CHR_2)_3]^{1-}$, $[U(H_3BH)_3]^{1-}$, and $[U(OAr')_4]^{2-}$. Initially, three hypothetical homoleptic complexes were investigated, Scheme 2.2. $[U(CHR_2)_3]^{1-}$ (R = $SiMe_3$) was examined because the $[CHR_2]^{1-}$ ligand is the alkyl analog of the $[NR_2]^{1-}$ ligand used to form the known $[K(crypt)][U(NR_2)_3]$.[7] Geometry optimizations of $[U(CHR_2)_3]^{1-}$ afforded a pyramidalized C_1-symmetric ground state that is similar to the structure of $[U(NR_2)_3]^{1-}$ discussed above.

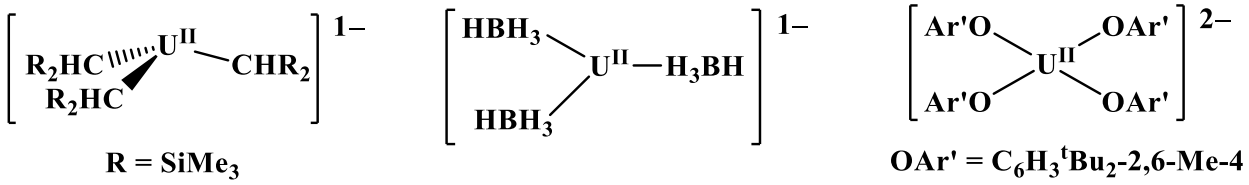

Scheme 2.2: Molecular structures of $[U(CHR_2)_3]^{1-}$, $[U(H_3BH)_3]^{1-}$, and $[U(OAr')_4]^{2-}$.

The electronic configuration was found to be $5f^36d^1$, with a $6dz^2$-like HOMO, Figure 2.8 (left). Electron density was observed on the $SiMe_3$ moieties which was previously observed for $[(C_5Me_5)_2U(NR_2)]^{1-}$ and $[(C_5Me_5)U(NR_2)_2]^{1-}$.[27] This suggests that reduction of $U(CHR_2)_3$ may ultimately form a cyclometallated product such as $[U(CHR_2)_2(CH_2SiMe_2CHR\text{-}\kappa C,\kappa C)]^{1-}$.[27]

Geometry optimizations of $[U(H_3BH)_3]^{1-}$ yielded a $5f^36d^1$ electronic ground state, with population of a $6dz^2$-like orbital, Figure 2.8. Each tetrahedral $(BH_4)^{1-}$ ligand had three hydrides coordinated to the uranium center. To a first approximation, the $(BH_4)^{1-}$ ligand is similar to a cyclopentadienide $(C_5R_5)^{1-}$ ligand in that both are monoanions with three electron pairs available for coordination. It is therefore not too surprising that the electron configuration of $[U(H_3BH)_3]^{1-}$ is identical to that of the tris(cyclopentadienyl) U(II) complexes $(Cp'_3U)^{1-}$, $(Cp''_3U)^{1-}$, and

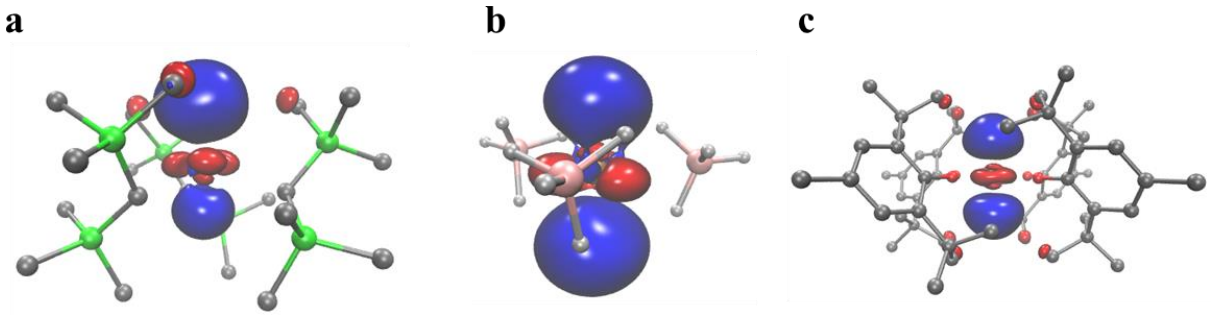

Figure 2.8: (a) HOMO of $[U(CHR_2)_3]^{1-}$, (b) HOMO of $[U(H_3BH)_3]^{1-}$, and (c) HOMO of $[U(OAr')_4]^{2-}$, plotted with a contour value of 0.05. Hydrogen atoms, except those attached to boron, are omitted for clarity. Calculated orbital energies $\varepsilon = -1.596$, $\varepsilon = -2.352$, $\varepsilon = -0.394$ eV, respectively.

$(Cp^{tet}_3U)^{1-}$. From these results along with those of $[(C_5Me_5)_2U(NR_2)]^{1-}$ and $[(C_5Me_5)U(NR_2)_2]^{1-}$,[15] it appears that the identity of the donor atom in trigonal complexes does not affect the electron configuration.

In addition to the homoleptic tris(alkyl) and tris(borohydride) complexes, the tetrakis(aryloxide) environment was investigated. The Th(III) compound $[Th(OAr')_4]^{1-}$ (OAr′ = $C_6H_2{}^tBu_2$-2,6-Me-4) was recently synthesized and found to be square-planar.[19] The U(II) analog, $[U(OAr')_4]^{2-}$, was analyzed in C_1, C_2, and C_4 symmetry. The optimized ground state geometry was square-planar and had C_2 symmetry. The C_1- and C_4-symmetric square planar structures were local minima only 0.16 kcal/mol and 0.14 kcal/mol higher in energy than the C_2-symmetric structure, respectively, which is within the expected error margins of the electronic structure methods used here. The ground-state of $[U(OAr')_4]^{2-}$ was found to have a $5f^36d^1$ electron configuration, again populating a $6dz^2$-like orbital, Figure 2.8. This suggests that planarity about the metal center can lead to f^nd^1 configurations even as the number of ligands is varied from three

to four. The U(III) compound $\{K[U(OAr)_4]\}_n$ (OAr = OC_6H_3-^{t}Bu$_2$-2,6) has been previously reported and adopts a tetrahedral geometry around the uranium center.[40]

$[(C_8H_8)_2U]^{2-}$. The U(II) complex formed by two-electron reduction of bis(cyclooctatetraenyl)uranium, uranocene, Figure 2.9, was also studied. The ground state configuration of the dianionic, U(II) species $[(C_8H_8)_2U]^{2-}$ was found to be $5f^36d^1$ in D_{8h} symmetry. Various lower-symmetry structures were analyzed and all converged to the D_{8h}-symmetric local minimum. The HOMO appears to be a non-bonding, $6dz^2$ orbital, Figure 2.9. Previously, similar theoretical analysis on the linear U(II) species $(C_5{}^i Pr_5)_2U$[41] found a $5f^36d^1$ electron configuration without π interactions in the $6dz^2$-like orbital.[41,42] The U(III) complex, $[(C_8H_8)_2U]^{1-}$, has a $5f^3$ configuration, with a $6dz^2$-like LUMO that is evidently populated upon addition of another electron to form $[(C_8H_8)_2U]^{2-}$.

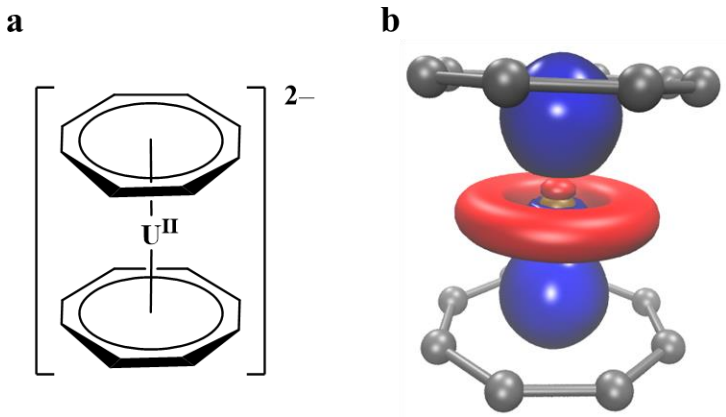

Figure 2.9: (a) Molecular structure and (b) HOMO of $[(C_8H_8)_2U]^{2-}$, plotted with a contour value of 0.05. Hydrogen atoms are omitted for clarity. Calculated orbital energy $\varepsilon = -0.390$ eV.

$[U(bnz')_4]^{2-}$, $[U(H_3BH)_3(THF)_3]^{1-}$, and the U-in-(2.2.2-cryptand) System. The tetrahedral geometry for U(II) was examined starting with the previously reported U(IV) complex, $U(\eta^4$-bnz′$)_4$ (bnz′ = CH_2-C_6H_4-^{t}Bu-4).[21] DFT analysis of the monoanionic complex $[U(bnz')_4]^{1-}$ revealed a tetrahedral structure with a $5f^3$ configuration for the U(III) center. However, the ground

state for the dianionic species, $[U(bnz')_4]^{2-}$, was found to have three electrons localized on the uranium atom and one electron delocalized in the π system of the benzyl ligands, Figure 2.10. This is formally a U(III) complex with a ligand radical. The energy of the π system of the benzyl ligands is clearly close to the energy of the 5f orbitals, as the LUMO was predominantly localized in the π system of the benzyl ligands while the LUMO+1, LUMO+2, and LUMO+3 had significantly more 5f character. The calculations were also performed with an infinite dielectric constant within the COSMO model, but the only change was the overall lowering of all orbital energies. The resulting electronic configuration was still $5f^3$ with a ligand radical.

The benzyl π system in $[U(bnz')_4]^{2-}$ is not in the correct spatial orientation to interact with the 5f orbitals, in contrast to $(NHAr^{iPr6})_2U$ and $[K(crypt)]\{[(^{Ad,Me}ArO)_3mes]U\}^2$ where the π system of the arene anchor was found to interact with the 5f orbitals on uranium, Figure 2.7. It can be concluded that the 5f manifold is lower in energy than the 6d orbitals as there was not an orbital with significant 6d character close to the HOMO-LUMO gap. In the present calculations, the ligands are best described as η^3-bnz′ based on their Δ and Δ' values[38,53] in each of the three geometry-optimized structures $U(bnz')_4$, $[U(bnz')_4]^{1-}$, and $[U(bnz')_4]^{2-}$.

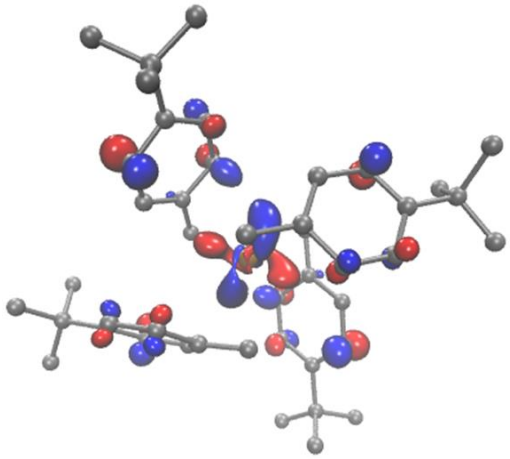

Figure 2.10: HOMO of $[U(bnz')_4]^{2-}$, plotted with a contour value of 0.05. Hydrogen atoms are omitted for clarity. Calculated orbital energy $\varepsilon = -0.128$ eV.

An octahedral complex was also investigated. Initially, the crystal structure of $U(H_3BH)_3(THF)_3$ was used as a starting point and the electronic configuration was found to be $5f^3$, as expected for a U(III) ion. The structure maintained an octahedral geometry. The four lowest unoccupied orbitals (LUMO through LUMO+3) were all 5f in character, Figure 2.11. Addition of one electron and subsequent re-optimization of $[U(H_3BH)_3(THF)_3]^{1-}$ resulted in a structure that had three BH_4 units in a much more planar arrangement around the uranium atom than in the neutral complex and three THF molecules further from the uranium center at distances of 2.667–2.681 Å, Figure 2.11. For comparison, the crystal structure of $U(H_3BH)_3(THF)_3$ has U–O distances of 2.54(1)–2.579(8) Å.[39] Excluding the THF molecules, the geometry around the uranium atom in $[U(H_3BH)_3(THF)_3]^{1-}$ was practically identical to $[U(H_3BH)_3]^{1-}$ discussed above. The resulting $5f^36d^1$ electron configuration with a $6dz^2$-like HOMO, Figure 2.11, was the same as $[U(H_3BH)_3]^{1-}$. The calculations predict that reduction of $U(H_3BH)_3(THF)_3$ would likely result in dissociation of THF and formation of $[U(H_3BH)_3]^{1-}$. This suggests that an octahedral environment around the uranium center does not effectively lower any 6d orbitals enough to be comparable in energy to the 5f orbitals.

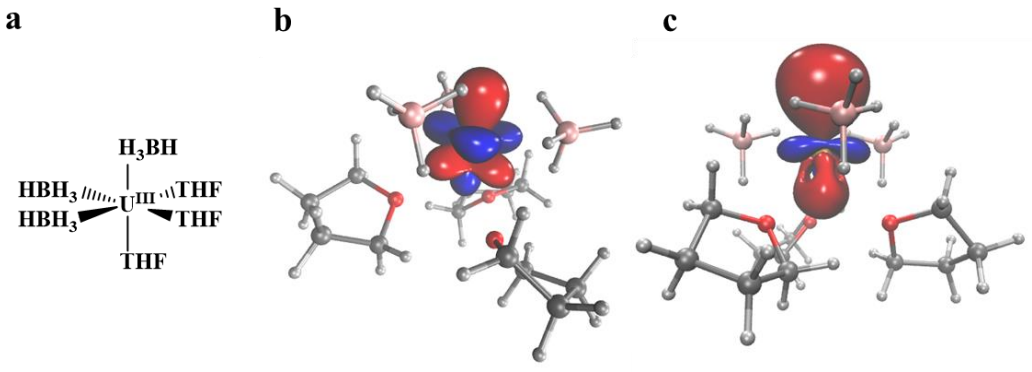

Figure 2.11: (a) Molecular structure of $U(H_3BH)_3(THF)_3$, (b) calculated 5f LUMO of $U(H_3BH)_3(THF)_3$, and (c) $6dz^2$-like HOMO of $[U(H_3BH)_3(THF)_3]^{1-}$. Calculated orbital energies ε = −0.600 and −0.928 eV, respectively.

The 2.2.2-cryptand (crypt) ligand system was also investigated since it surrounds the metal center in a somewhat symmetrical way such that all 6d orbitals should have similar energy. Recently, the compounds Ln(crypt)$(OTf)_2$ (Ln = Nd, Sm; OTf = O_3SCF_3) were reported and were assigned $4f^4$ and $4f^6$ configurations, respectively.[54] The spherical ligand environment of the cryptand does not appear to split the 5d orbitals strongly enough to allow population of a $5dz^2$ orbital in the Ln complexes. To determine if the cryptand system would impart similar chemistry for uranium, the structures of $[U(crypt)]^{2+}$ and U(crypt)$(OMe)_2$ were optimized. The triflate anions were replaced with methoxides, as geometry optimizations on U(crypt)$(OTf)_2$ led to triflate dissociation.

Contrary to the Nd and Sm systems, calculations on $[U(crypt)]^{2+}$ are consistent with a $5f^36d^1$ ground state with a $6dz^2$-like HOMO, Figure 2.12. The optimized structure had space between the arms of the cryptand ligand in which no donor atoms are located. It is in this space that the $6dz^2$-like orbital is located. However, the ground state of U(crypt)$(OMe)_2$ had a HOMO with significantly less 6d character, Figure 2.12. The HOMO of U(crypt)$(OMe)_2$ is still metal-centered, but it is predominantly 7p in character by Mulliken population analysis (44% 7p, 36% 7s, 10% 6d). The OMe ligands bind to the uranium center in the space between cryptand arms. Thus, the 6d orbital that is populated in $[U(crypt)]^{2+}$ is clearly higher in energy in U(crypt)$(OMe)_2$.

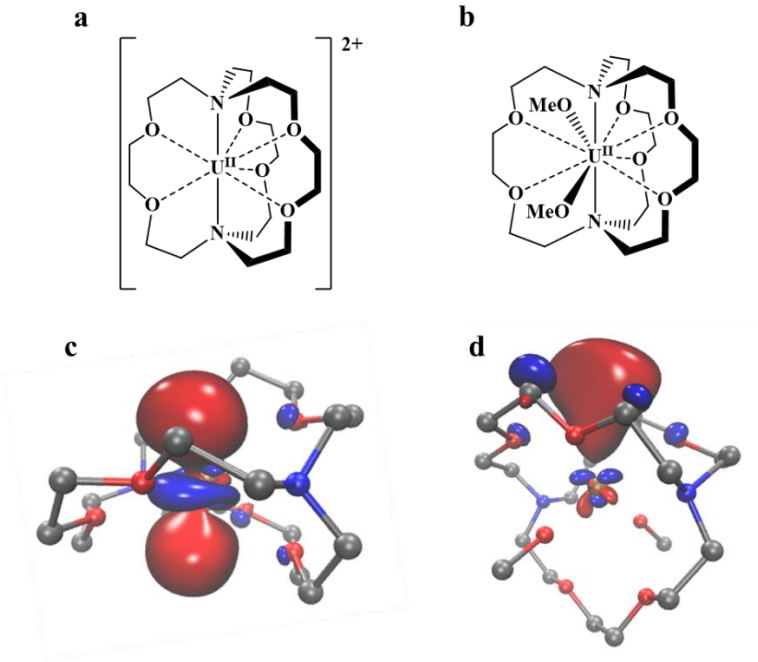

Figure 2.12: Molecular structures of (a) $[U(crypt)]^{2+}$ and (b) $U(crypt)(OMe)_2$ (top right). HOMO of (c) $[U(crypt)]^{2+}$ and (d) $U(crypt)(OMe)_2$, plotted with a contour value of 0.05. Hydrogen atoms are omitted for clarity. Calculated orbital energies $\varepsilon = -7.811$ and -0.596 eV, respectively.

Discussion

$5f^36d^1$ U(II). The calculated electronic structures of $[Cp''_3U]^{1-}$,[6,8] $[Cp^{tet}_3U]^{1-}$,[7] $[U(H_3BH)_3]^{1-}$, and $[U(OAr')_4]^{2-}$ were all found to have $5f^36d^1$ ground-state electron configurations with population of a $6dz^2$-like orbital. These results are consistent with other previously characterized U(II) species $[Cp'_3U]^{1-}$,[1] $(C_5Me_5)_2U(NR_2)]^{1-}$,[27] and $[(C_5Me_5)U(NR_2)_2]^{1-}$.[27] In each of these cases, the planar ligand environment leads to one low-lying $6dz^2$-like orbital which is similar in energy to the 5f orbitals. The identity of the ligands and donor atoms seems less important than the geometry of the coordination environment. Clearly, planar complexes favor $5f^36d^1$. In addition, the trigonal pyramidal complexes $[U(NR_2)_3]^{1-}$ [7] and $[U(CHR_2)_3]^{1-}$ also have $5f^36d^1$ ground-state electron configurations with population of a $6dz^2$-like orbital. Hence, even in these pyramidal structures the $5f^36d^1$ is lowest in energy.

The $5f^3 6d^1$ electronic configuration in $[Cp'_3U]^{1-}$, eq 1, could be rationalized[1] based on the d-orbital splitting of the tris(cyclopentadienyl) ligand framework.[4] Simple crystal field splitting would not put the $6dz^2$ orbital lowest for all of the above complexes, but inclusion of 7s orbital mixing with $6dz^2$ could explain how the $6dz^2$-like orbital is comparable in energy to the 5f orbitals. Indeed 7s character was observed in most of the $6dz^2$-like orbitals, see SI. Another possible explanation involves π donation from the lone pairs of the donor atom which could destabilize the d orbitals with the appropriate symmetry.[55-57]

The uranocene dianion, $[(C_8H_8)_2U]^{2-}$ was also found to have a $5f^3 6d^1$ ground-state electron configurations with population of a $6dz^2$-like orbital. This result is similar to that of another parallel-plane metallocene, $(C_5{}^iPr_5)_2U$.[41,42] These compounds differ in ground state from the arene complexes discussed in the next section.

$5f^4$ U(II). The arene-tethered U(II) complex $(NHAr^{iPr6})_2U$ was found to have a $5f^4$ electron configuration. In this case, the 5f orbitals have an interaction with the π system of the arene ring as was found in the $5f^4$ U(II) complex [K(crypt)]{[(^{Ad,Me}ArO)$_3$mes]U}. In these two complexes, the arene rings have the correct spatial orientation to interact with the 5f orbitals, whereas the arene rings in the benzyl complex $[U(bnz')_4]^{2-}$ do not interact with the 5f orbitals, despite the calculated energy similarity. For $[U(bnz')_4]^{2-}$, this leads to reduction of the arene rings instead of formation of U(II).

It is unclear whether the arene interaction is a requirement to stabilize the $5f^4$ electron configuration. In the case of $U(H_3BH)_3(THF)_3$, which has no π system available to interact with the 5f manifold, the four lowest unoccupied orbitals are still 5f orbitals, which suggests that reduction within a pseudo-octahedral environment would also favor a $5f^4$ electron configuration. The synthesis of a U(II) complex within a spherical ligand environment that does not have π

systems is a reasonable target that will help further determine how the deviation from planarity affects the electron configuration.

The U(II)-in-(2.2.2-cryptand) system. The calculations on $[U(crypt)]^{2+}$ differ from those above in that they do not match calculations on the lanthanide analogs.[43] Additionally, the predicted ground state changes whether additional ligands are present or not. For $[U(crypt)]^{2+}$, a $5f^3 6d^1$ ground state with $6dz^2$-like HOMO is predicted. However, inclusion of two OMe groups binding to the uranium center directly affects the $6dz^2$ orbital energy and the resulting HOMO of $U(crypt)(OMe)_2$ was found to be predominantly 7p in character. The orbital shape and location are suggestive of a Rydberg state, and indeed the inclusion of a *p* primitive to the uranium basis functions helps to more accurately describe 6d to 7p electronic transitions.[27–29] The present calculations suggest that binding additional ligands to the U(II) center within the crypt ligand framework could directly change the electron configuration. In contrast, calculations on both $[Nd(crypt)]^{2+}$ and $Nd(crypt)(OTf)_2$ indicate $4f^4$ ground state configurations.[43] The ramifications of this difference are under investigation.

Overall Charge of the U(II) Complexes. Most of the U(II) complexes that have been experimentally synthesized are anions. This raises the question of the importance of overall charge of the complex. On a simplistic basis, it makes sense for electropositive metals like uranium that are typically surrounded with anionic ligands that reduction of the oxidation state of the metal will require the overall complex to be an anion. In addition, for large metals like uranium, more than two ligands are typically needed to sterically saturate the coordination sphere. However, since formation of anion complexes gives the benefit of the lattice energy of forming a salt, it is possible that this factor is important in isolating these complexes.

Conclusion

Electronic structure calculations on four known and seven hypothetical U(II) complexes predict that with planar symmetry, $5f^3 6d^1$ electron configurations are the expected ground state regardless of the nature of the ligand, donor atoms, or number of ligands. If the symmetry of the complex does not place a 6d orbital comparable in energy to the 5f manifold, the $5f^4$ Aufbau configuration could become the ground state. In some complexes like those of crypt and borohydride, additional ligation effects the orbital energies and may change the overall electronic configuration. This study provides information to guide synthetic efforts and suggests how to change the electronic configuration of low-valent uranium complexes. These results may be transferrable to other low-valent f-block compounds.

References

(1) MacDonald, M. R.; Fieser, M. E.; Bates, J. E.; Ziller, J. W.; Furche, F.; Evans, W. J. Identification of the +2 Oxidation State for Uranium in a Crystalline Molecular Complex, [K(2.2.2-Cryptand)][(C5H4SiMe3)3U]. *J. Am. Chem. Soc.* **2013**, *135*, 13310–13313, DOI: 10.1021/ja406791t.

(2) Evans, W. J. Tutorial on the Role of Cyclopentadienyl Ligands in the Discovery of Molecular Complexes of the Rare-Earth and Actinide Metals in New Oxidation States. *Organometallics* **2016**, *35*, 3088–3100, DOI: 10.1021/acs.organomet.6b00466.

(3) Fieser, M. E.; MacDonald, M. R.; Krull, B. T.; Bates, J. E.; Ziller, J. W.; Furche, F.; Evans, W. J. Structural, Spectroscopic, and Theoretical Comparison of Traditional vs Recently Discovered Ln^{2+} Ions in the [K(2.2.2-Cryptand)][$(C_5H_4SiMe_3)_3Ln$] Complexes: The Variable Nature of Dy^{2+} and Nd^{2+}. *J. Am. Chem. Soc.* **2015**, *137*, 369–382, DOI: 10.1021/ja510831n.

(4) Lauher, J. W.; Hoffmann, R. Structure and Chemistry of Bis(Cyclopentadienyl)-ML_n Complexes. *J. Am. Chem. Soc.* **1976**, *98*, 1729–1742, DOI: 10.1021/ja00423a017.

(5) Pepper, M.; Bursten, B. E. The Electronic Structure of Actinide-Containing Molecules: A Challenge to Applied Quantum Chemistry. *Chem. Rev.* **1991**, *91*, 719–741, DOI: 10.1021/cr00005a005.

(6) Windorff, C. J.; MacDonald, M. R.; Meihaus, K. R.; Ziller, J. W.; Long, J. R.; Evans, W. J. Expanding the Chemistry of Molecular U^{2+} Complexes: Synthesis, Characterization, and Reactivity of the $\{[C_5H_3(SiMe_3)_2]_3U\}^-$ Anion. *Chem. Eur. J.* **2016**, *22*, 772–782, DOI: 10.1002/chem.201503583.

(7) Ryan, A. J.; Angadol, M. A.; Ziller, J. W.; Evans, W. J. Isolation of U(II) Compounds Using Strong Donor Ligands, C_5Me_4H and $N(SiMe_3)_2$, Including a Three-Coordinate U(II) Complex. *Chem. Commun.* **2019**, *55*, 2325–2327, DOI: 10.1039/C8CC08767A.

(8) Huh, D. N.; Ziller, J. W.; Evans, W. J. Chelate-Free Synthesis of the U(II) Complex, $[(C_5H_3(SiMe_3)_2)_3U]^{1-}$, Using Li and Cs Reductants and Comparative Studies of La(II) and Ce(II) Analogs. *Inorg. Chem.* **2018**, *57*, 11809–11814, DOI: 10.1021/acs.inorgchem.8b01966.

(9) Billow, B. S.; Livesay, B. N.; Mokhtarzadeh, C. C.; Mccracken, J.; Shores, M. P.; Boncella, J. M.; Odom, A. L. Synthesis and Characterization of a Neutral U(II) Arene Sandwich Complex. *J. Am. Chem. Soc.* **2018**, *140*, 17369–17373, DOI: 10.1021/jacs.8b10888.

(10) La Pierre, H. S.; Scheurer, A.; Heinemann, F. W.; Hieringer, W.; Meyer, K. Synthesis and Characterization of a Uranium(II) Monoarene Complex Supported by δ Backbonding. *Angew. Chem. Int. Ed.* **2014**, *53*, 7158–7162, DOI: 10.1002/anie.201402050.

(11) Staroverov, V. N.; Scuseria, G. E.; Tao, J.; Perdew, J. P. Comparative Assessment of a New Nonempirical Density Functional: Molecules and Hydrogen-Bonded Complexes. *J. Chem. Phys.* **2003**, *119*, 12129–12137, DOI: 10.1063/1.1626543.

(12) Grimme, S.; Antony, J.; Ehrlich, S.; Krieg, H. A Consistent and Accurate Ab Initio Parametrization of Density Functional Dispersion Correction (DFT-D) for the 94 Elements H-Pu. *J. Chem. Phys.* **2010**, *132*, 154104, DOI: 10.1063/1.3382344.

(13) Grimme, S. Semiempirical GGA-Type Density Functional Constructed with a Long-Range Dispersion Correction. *J. Comput. Chem.* **2006**, *27*, 1787–1799, DOI: 10.1002/jcc.20495.

(14) Weigend, F.; Köhn, A.; Hättig, C. Efficient Use of the Correlation Consistent Basis Sets in Resolution of the Identity MP2 Calculations. *J. Chem. Phys.* **2002**, *116*, 3175–3183, DOI: 10.1063/1.1445115.

(15) Küchle, W.; Dolg, M.; Stoll, H.; Preuss, H. Energy-Adjusted Pseudopotentials for the Actinides. Parameter Sets and Test Calculations for Thorium and Thorium Monoxide. *J. Chem. Phys.* **1994**, *100*, 7535–7542, DOI: 10.1063/1.466847.

(16) Weigend, F.; Ahlrichs, R. Balanced Basis Sets of Split Valence, Triple Zeta Valence and Quadruple Zeta Valence Quality for H to Rn: Design and Assessment of Accuracy. *Phys. Chem. Chem. Phys.* **2005**, *7*, 3297–3305, DOI: 10.1039/b508541a.

(17) Treutler, O.; Ahlrichs, R. Efficient Molecular Numerical Integration Schemes. *J. Chem. Phys.* **1995**, *102*, 346–354, DOI: 10.1063/1.469408.

(18) Van Der Sluys, W. G.; Burns, C. J.; Sattelberger, A. P. First Example of a Neutral Homoleptic Uranium Alkyl. Synthesis, Properties, and Structure of U[CH($SiMe_3$)$_2$]=. *Organometallics* **1989**, *8*, 855–857, DOI: 10.1021/om00105a051.

(19) Huh, D. N.; Roy, S.; Ziller, J. W.; Furche, F.; Evans, W. J. Isolation of a Square-Planar Th(III) Complex: Synthesis and Structure of $[Th(OC_6H_2{}^tBu_2\text{-}2,6\text{-}Me\text{-}4)_4]^{1-}$. *J. Am. Chem. Soc.* **2019**, *141*, 12458–12463, DOI: 10.1021/jacs.9b04399.

(20) Zalkin, A.; Raymond, K. N. Structure of Di-π.-Cyclooctatetraeneuranium (Uranocene). *J. Am. Chem. Soc.* **1969**, *91*, 5667–5668, DOI: 10.1021/ja01048a055.

(21) Johnson, S. A.; Kiernicki, J. J.; Fanwick, P. E.; Bart, S. C. New Benzylpotassium Reagents and Their Utility for the Synthesis of Homoleptic Uranium(IV) Benzyl Derivatives. *Organometallics* **2015**, *34*, 2889–2895, DOI: 10.1021/acs.organomet.5b00212.

(22) Mannig, D.; Noth, H. Metal Boranates and Boranatometallates. 13. Preparation and Molecular Structure of Uranium(III) Tetrahydridoborate-3-Tetrahydrofuran. *Z. Anorg. Allg. Chem.* **1986**, *543*, 66, DOI: 10.1002/zaac.19865431208.

(23) Schäfer, A.; Klamt, A.; Sattel, D.; Lohrenz, J. C. W.; Eckert, F. COSMO Implementation in TURBOMOLE: Extension of an Efficient Quantum Chemical Code towards Liquid Systems. *Phys. Chem. Chem. Phys.* **2000**, *2*, 2187–2193, DOI: 10.1039/b000184h.

(24) In *CRC Handbook of Chemistry and Physics*; Haynes, W. M., Lide, D. R., Bruno, T. J., Eds.; CRC Press, 2016; pp 943–950.

(25) Deglmann, P.; Furche, F.; Ahlrichs, R. An Efficient Implementation of Second Analytical Derivatives for Density Functional Methods. *Chem. Phys. Lett.* **2002**, *362*, 511–518, DOI: 10.1016/S0009-2614(02)01084-9.

(26) Bates, J. E.; Furche, F. Harnessing the Meta-Generalized Gradient Approximation for Time-Dependent Density Functional Theory. *J. Chem. Phys.* **2012**, *137*, 164105, DOI: 10.1063/1.4759080.

(27) Wedal, J. C.; Bekoe, S.; Ziller, J. W.; Furche, F.; Evans, W. J. C–H Bond Activation via U(II) in the Reduction of Heteroleptic Bis(Trimethylsilyl)Amide U(III) Complexes. *Organometallics* **2020**, *39*, 3425–3432, DOI: 10.1021/acs.organomet.0c00496.

(28) Ryan, A. J.; Darago, L. E.; Balasubramani, S. G.; Chen, G. P.; Ziller, J. W.; Furche, F.; Long, J. R.; Evans, W. J. Synthesis , Structure , and Magnetism of Tris(Amide) $[Ln\{N(SiMe_3)_2\}_3]^{1-}$ Complexes of the Non-Traditional +2 Lanthanide Ions. *Chem. Eur. J.* **2018**, *24*, 7702–7709, DOI: 10.1002/chem.201800610.

(29) Jenkins, T. F.; Woen, D. H.; Mohanam, L. N.; Ziller, J. W.; Furche, F.; Evans, W. J. Tetramethylcyclopentadienyl Ligands Allow Isolation of Ln(II) Ions across the Lanthanide Series in [K(2.2.2-Cryptand)][$(C_5Me_4H)_3Ln$] Complexes. *Organometallics* **2018**, *37*, 3863–3873, DOI: 10.1021/acs.organomet.8b00557.

(30) Humphrey, W.; Dalke, A.; Schulten, K. VMD: Visual Molecular Dynamics. *J. Mol. Graph.* **1996**, *14*, 33–38.

(31) Balasubramani, S. G.; Chen, G. P.; Coriani, S.; Diedenhofen, M.; Frank, M. S.; Franzke, Y. J.; Furche, F.; Grotjahn, R.; Harding, M. E.; Hättig, C.; Hellweg, A.; Helmich-Paris, B.; Holzer, C.; Huniar, U.; Kaupp, M.; Marefat Khah, A.; Karbalaei Khani, S.; Müller, T.; Mack, F.; Nguyen, B. D.; Parker, S. M.; Perlt, E.; Rappoport, D.; Reiter, K.; Roy, S.; Rückert, M.; Schmitz, G.; Sierka, M.; Tapavicza, E.; Tew, D. P.; van Wüllen, C.; Voora, V. K.; Weigend, F.; Wodyński, A.; Yu, J. M. TURBOMOLE: Modular Program Suite for Ab Initio Quantum-Chemical and Condensed-Matter Simulations. *J. Chem. Phys.* **2020**, *152*, 184107, DOI: 10.1063/5.0004635.

(32) TURBOMOLE V7.4.1. a development of University of Karlsruhe and Forschungszentrum Karlsruhe GmbH, since 2007; available from http://www.turbomole.com

(33) Hitchcock, P. B.; Lappert, M. F.; Maron, L.; Protchenko, A. V. Lanthanum Does Form Stable Molecular Compounds in the +2 Oxidation State. *Angew. Chem. Int. Ed.* **2008**, *47*, 1488–1491, DOI: 10.1002/anie.200704887.

(34) Corbey, J. F.; Woen, D. H.; Palumbo, C. T.; Fieser, M. E.; Ziller, J. W.; Furche, F.; Evans, W. J. Ligand Effects in the Synthesis of Ln^{2+} Complexes by Reduction of Tris(Cyclopentadienyl) Precursors Including C–H Bond Activation of an Indenyl Anion. *Organometallics* **2015**, *34*, 3909–3921, DOI: 10.1021/acs.organomet.5b00500.

(35) MacDonald, M. R.; Bates, J. E.; Ziller, J. W.; Furche, F.; Evans, W. J. Completing the Series of +2 Ions for the Lanthanide Elements: Synthesis of Molecular Complexes of Pr^{2+}, Gd^{2+}, Tb^{2+}, and Lu^{2+}. *J. Am. Chem. Soc.* **2013**, *135*, 9857–9868, DOI: 10.1021/ja403753j.

(36) MacDonald, M. R.; Bates, J. E.; Fieser, M. E.; Ziller, J. W.; Furche, F.; Evans, W. J. Expanding Rare-Earth Oxidation State Chemistry to Molecular Complexes of Holmium(II) and Erbium(II). *J. Am. Chem. Soc.* **2012**, *134*, 8420–8423, DOI: 10.1021/ja303357w.

(37) Kot, W. K.; Shalimoff, G. V.; Edelstein, N. M.; Edelman, M. A.; Lappert, M. F. [$Th^{III}\{\eta^5$-$C_5H_3(SiMe_3)_2\}_3$], an Actinide Compound with a $6d^1$ Ground State. *J. Am. Chem. Soc.* **1988**, *110*, 986–987, DOI: 10.1021/ja00211a059.

(38) Siladke, N. A.; Webster, C. L.; Walensky, J. R.; Takase, M. K.; Ziller, J. W.; Grant, D. J.; Gagliardi, L.; Evans, W. J. Actinide Metallocene Hydride Chemistry: C–H Activation in Tetramethylcyclopentadienyl Ligands to Form [μ-η^5-$C_5Me_3H(CH_2)$-κC]$^{2-}$ Tuck-over Ligands in a Tetrathorium Octahydride Complex. *Organometallics* **2013**, *32*, 6522–6531, DOI: 10.1021/om4008482.

(39) Langeslay, R. R.; Chen, G. P.; Windorff, C. J.; Chan, A. K.; Ziller, J. W.; Furche, F.; Evans, W. J. Synthesis, Structure, and Reactivity of the Sterically Crowded Th^{3+} Complex $(C_5Me_5)_3Th$ Including Formation of the Thorium Carbonyl, $[(C_5Me_5)_3Th(CO)][BPh_4]$. *J. Am. Chem. Soc.* **2017**, *139*, 3387–3398, DOI: 10.1021/jacs.6b10826.

(40) Mansell, S. M.; Kaltsoyannis, N.; Arnold, P. L. Small Molecule Activation by Uranium Tris(Aryloxides): Experimental and Computational Studies of Binding of N_2, Coupling of CO, and Deoxygenation Insertion of CO_2 under Ambient Conditions. *J. Am. Chem. Soc.* **2011**, *133*, 9036–9051, DOI: 10.1021/ja2019492.

(41) Yu, J. M.; Furche, F. Theoretical Study of Divalent Bis(Pentaisopropylcyclopentadienyl) Actinocenes. *Inorg. Chem.* **2019**, *58*, 16004–16010, DOI: 10.1021/acs.inorgchem.9b02505.

(42) Guo, F. S.; Tsoureas, N.; Huang, G. Z.; Tong, M. L.; Mansikkamäki, A.; Layfield, R. A. Isolation of a Perfectly Linear Uranium(II) Metallocene. *Angew. Chem. Int. Ed.* **2020**, *59*, 2299–2303, DOI: 10.1002/anie.201912663.

(43) Huh, D. N.; Ciccone, S. R.; Bekoe, S.; Roy, S.; Ziller, J. W.; Furche, F.; Evans, W. J. Synthesis of Ln^{II}-in-Cryptand Complexes by Chemical Reduction of Ln^{III}-in-Cryptand Precursors: Isolation of a Nd^{II}-in-Cryptand Complex. *Angew. Chem. Int. Ed.* **2020**, *59*, 16141–16146, DOI: 10.1002/anie.202006393.

Chapter 3:

Electrochemical Studies of Tris(cyclopentadienyl) Thorium and Uranium Complexes in the +2, +3, and +4 Oxidation States

Introduction[†]

Electrochemical studies on actinide complexes have primarily involved higher oxidation states, i.e. +4, +5 and +6,[1–4] in part due to the high reactivity of the +2 and +3 metal ions. Even +3 and +4 metal complexes can react with supporting electrolytes. For example, Inman and Cloke found problems studying $(C_5Me_5)Th^{IV}[C_8H_6(SiMe_2{}^tBu)_2]Cl$ using $[^nBu_4N][PF_6]$ as supporting electrolyte[5] as well as with $Cp''_3Th^{IV}Cl$ using $[^nBu_4N][B(C_6F_5)_4]$ as supporting electrolyte.[6]

Before the results reported in this Chapter were obtained, electrochemical data had been reported on only two U(II) systems.[7,8] Meyer and coworkers identified the U(III)/U(II) couple in $[(^{Ad,Me}ArO)_3mes]U^{III}$ at −2.495 V vs $Fc^{+/0}$,[7] which guided synthetic efforts and allowed isolation of $[K(crypt)]\{[(^{Ad,Me}ArO)_3mes]U^{II}\}$.[9] Layfield and coworkers reported the U(III)/U(II) couple of $(C_5{}^iPr_5)_2U^{II}$ to be −2.33 V vs $Fc^{+/0}$.[8] Analogous studies on Th(III) and Th(II) complexes and on the tris(cyclopentadienyl) systems that led to the first molecular examples of U(II) were absent.

This chapter reports the electrochemistry of a variety of tris(cyclopentadienyl) uranium and thorium complexes using Cp″, Cp′, and Cp^{tet} ligands, a topic chosen due to the importance of the tris(cyclopentadienyl) ligand set in the development of low oxidation state actinide chemistry,[11,12] This study also led to the first reported electrochemical measurements on isolated Th(II) complexes.[13] Also included in this chapter are spectroelectrochemical studies on the Th(II) compounds that led to the discovery of new synthetic routes to Th(II) compounds. The results are

[†] Portions of this Chapter have been published: Wedal, J. C.; Barlow, J. M.; Ziller, J. W.; Yang, J. Y.; Evans, W. J. Electrochemical studies of tris(cyclopentadienyl)thorium and uranium complexes in the +2, +3, and +4 oxidation states. *Chem. Sci.* **2021**, *12*, 8501-8511. DOI: 10.1039/D1SC01906F.

compared with cyclopentadienyl ligand effects previously examined electrochemically with titanium and zirconium complexes[14] and with rare-earth metal reaction chemistry.[15–17]

Results

Electrochemical Protocol. All data were collected in THF using 100 mM [^{n}Bu$_4$N][BPh$_4$] or 200 mM [^{n}Bu$_4$N][PF$_6$] supporting electrolyte concentrations. Both [^{n}Bu$_4$N][BPh$_4$] and [^{n}Bu$_4$N][PF$_6$] were recrystallized three times prior to use. The low polarity of THF leads to large internal resistance in the electrochemical cell with peak separations over 200 mV often observed.[6,7] Unless specifically stated, all potentials are referenced to the ferrocenium/ferrocene couple with $(C_5Me_5)_2Fe$ as an internal standard. All electrochemical data were collected with a glassy carbon disc working electrode, platinum wire counter electrode, and silver wire pseudo-reference electrode. All scans were recorded in the cathodic direction except for the isolated U(II) and Th(II) compounds which were recorded in the anodic direction.

Uranium Complexes. Initially, U(III) complexes known to undergo chemical reduction and oxidation were examined to determine if both the U(IV)/U(III) and U(III)/U(II) redox events could be observed electrochemically. Indeed, both redox couples were observed in the voltammograms for the U(III) complexes Cp′$_3$U^{III},[18] Cp″$_3$U^{III},[19] and Cp$^{tet}_3$U^{III},[19] and for the isolated U(II) complexes [K(crown)(THF)$_2$][Cp″$_3$U^{II}] (crown = 18-crown-6)[20] and [K(crypt)][Cp′$_3$U^{II}].[21] These values are summarized in Tables 3.1 and 3.2 and highlights are described in the following paragraphs.

Cp″. With the bis(trimethylsilyl)cyclopentadienyl ligand, redox couples assigned to U(IV)/U(III) and U(III)/U(II) are observed at −0.94 V and −2.73 V, respectively, for Cp″$_3$U^{III}, Figure 3.1. In comparison, the isolated U(II) complex [K(crown)(THF)$_2$][Cp″$_3$U^{II}][20] displays two redox events at −0.73 V and −2.71 V, Figure 3.2. The $E_{1/2}$ values for the U(III)/U(II) couple are

nearly identical in both systems and the event centered at −2.71 V only appears when scanning anodically for [K(crypt)][Cp''_3U^{II}], which supports the assignment as the U(III)/U(II) couple.

Table 3.1: Reduction potentials assigned to U(IV)/U(III) couples in this study and the literature.

	E_{PA} (V)	E_{PC} (V)	U(IV)/U(III) $E_{1/2}$ (V)	ΔE_{pp} $(C_5Me_5)_2Fe$ (V)
Cp''_3U^{III}	−1.04	−0.83	−0.94 [a]	0.20
Cp'_3U^{III}	−1.33	−1.20	−1.26 [b]	0.36
$Cp^{tet}_3U^{III}$	−1.54	−1.39	−1.46 [a]	0.12
[K(crown)$(THF)_2$][Cp''_3U^{II}]	−1.09	−0.37	−0.73 [a]	0.15
[K(crypt)][Cp'_3U^{II}]	−1.45	−1.12	−1.28 [a]	0.57
$Cp'_3U^{IV}Cl$			−1.83 [22,c]	
$(C_5H_5)_3U^{IV}Cl$			−1.87 [22,23,c]	
$(C_5MeH_4)_3U^{IV}Cl$			−1.88 [22,c]	
$(C_5{}^tBuH_4)_3U^{IV}Cl$			−1.93 [22,c]	

a: 100 mM [^{n}Bu$_4$N][BPh_4] / THF
b: 50 mM [^{n}Bu$_4$N][BPh_4]/ THF
c: 130 mM [^{n}Bu$_4$N][PF_6]/ THF

Table 3.2: Reduction potentials assigned to U(III)/U(II) couples in this study and the literature.

	E_{PA} (V)	E_{PC} (V)	U(III)/U(II) $E_{1/2}$ (V)	ΔE_{pp} $(C_5Me_5)_2Fe$ (V)
Cp''_3U^{III}	−2.79	−2.67	−2.73 [a]	0.20
Cp'_3U^{III}	−2.43	−2.08	−2.26 [b]	0.36
$Cp^{tet}_3U^{III}$	−3.18	−3.04	−3.11 [a]	0.12
[K(crown)$(THF)_2$][Cp''_3U^{II}]	−2.77	−2.65	−2.71 [a]	0.15
[K(crypt)][Cp'_3U^{II}]	−2.50	−2.03	−2.27 [b]	0.57
$[(^{Ad,Me}ArO)_3mes]U^{III}$			−2.495 [7,c]	
$(C_5{}^iPr_5)_2U^{II}$			−2.33 [8,c]	

a: 100 mM [^{n}Bu$_4$N][BPh_4]/ THF
b: 50 mM [^{n}Bu$_4$N][BPh_4]THF
c: 60 mM [^{n}Bu$_4$N][BPh_4]/ THF

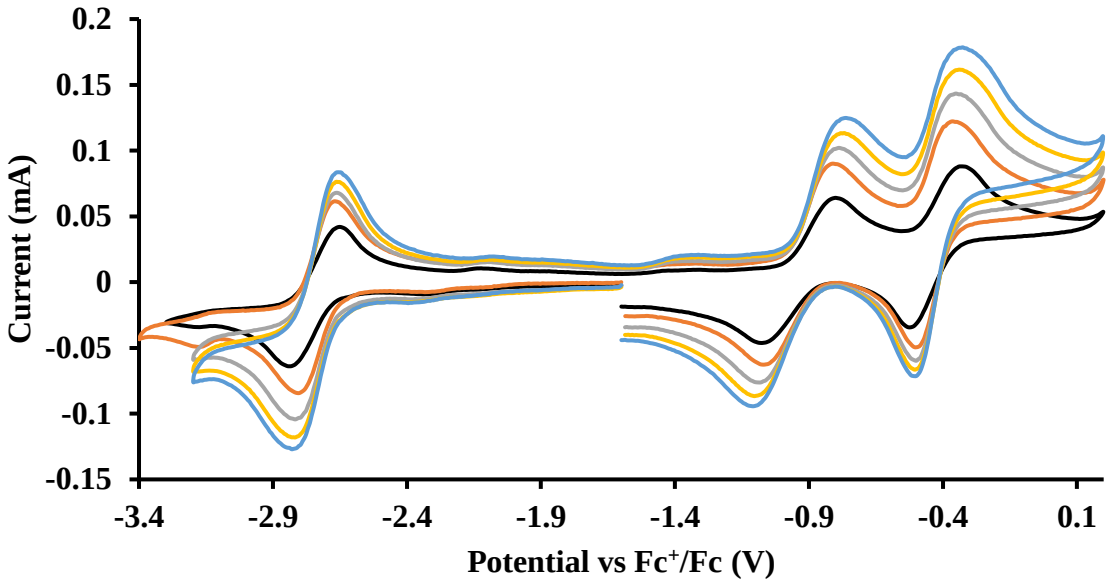

Figure 3.1: Voltammogram of 4.6 mM Cp''_3U at ν = 200 (black), 400 (orange), 600 (grey), 800 (yellow) and 1000 (blue) mV/s in 100 mM $TBABPh_4$ / THF. The event centered at −0.495 V is due to internal standard $(C_5Me_5)_2Fe^{II}$.

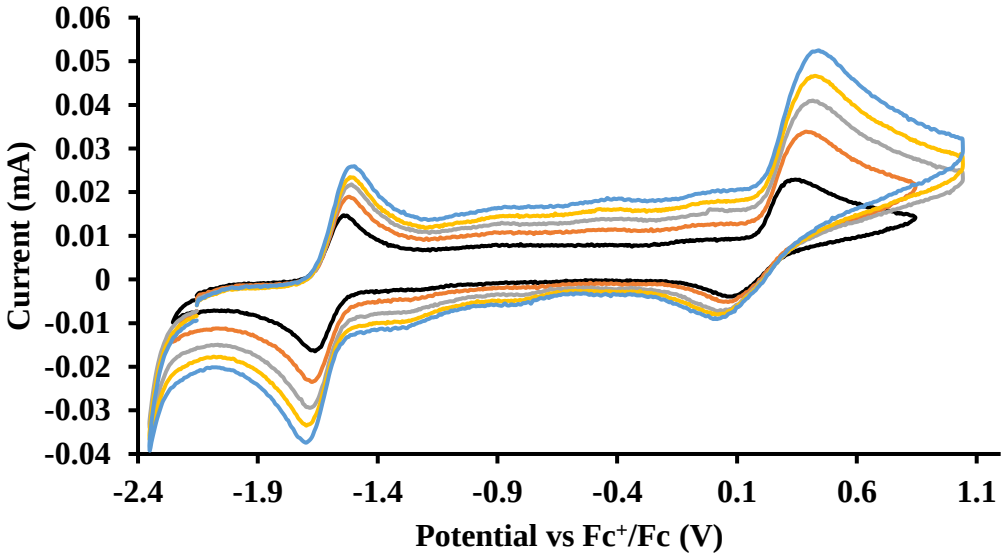

Figure 3.2: Voltammogram of 3.0 mM $[K(crown)(THF)_2][Cp''_3U]$ at ν = 200 (black), 400 (orange), 600 (grey), 800 (yellow) and 1000 (blue) mV/s in 100 mM $TBABPh_4$ / THF.

Cp′. Similar reproducible data were obtained with the mono(trimethylsilyl)cyclopentadienyl ligand with U(IV)/U(III) and U(III)/U(II) couples at −1.26 V and −2.26 V, respectively, for Cp'_3U^{III}, Figure 3.3. Likewise, the U(IV)/U(III) and U(III)/U(II) couples were observed at −1.28 V and −2.27 V for the U(II) complex $[K(crypt)][Cp'_3U^{II}]$, Figure 3.4. These data were obtained with 50 mM $[^nBu_4N][BPh_4]$ because decomposition occurred at higher electrolyte concentrations. The event at −2.27 V for $[K(crypt)][Cp'_3U^{II}]$ only appears when scanning anodically. The −2.27 V $E_{1/2}$ value for $[K(crypt)][Cp'_3U^{II}]$ was less negative than the −2.71 V value for $[K(crypt)][Cp''_3U^{II}]$, but it is similar to the two previously reported U(III)/U(II) couples for $[(^{Ad,Me}ArO)_3mes]U^{III}$ and $(C_5{}^iPr_5)_2U^{II}$.[7,8] The minor unassigned events at about −1.9 V in Figure 3.3 attest to the complexity of the system. They were observed across multiple runs and do not disappear after repeated recrystallization of substrate and electrolyte.

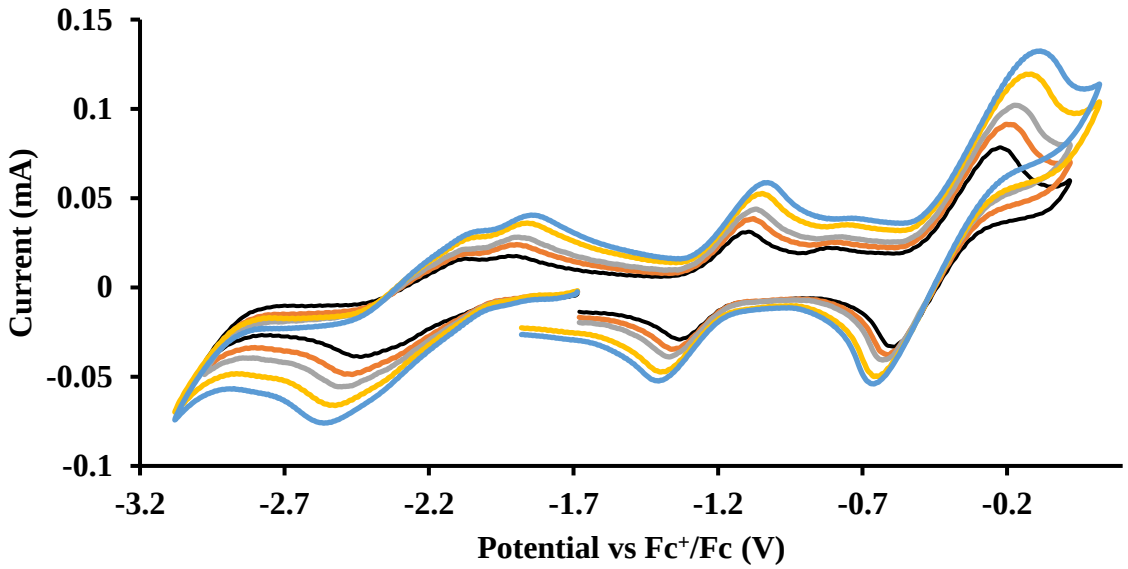

Figure 3.3: Voltammogram of 11 mM Cp'_3U at v = 200 (black), 400 (orange), 600 (grey), 800 (yellow) and 1000 (blue) mV/s in 50 mM $TBABPh_4$ / THF. The event centered at −0.495 V is due to internal standard $(C_5Me_5)_2Fe^{II}$.

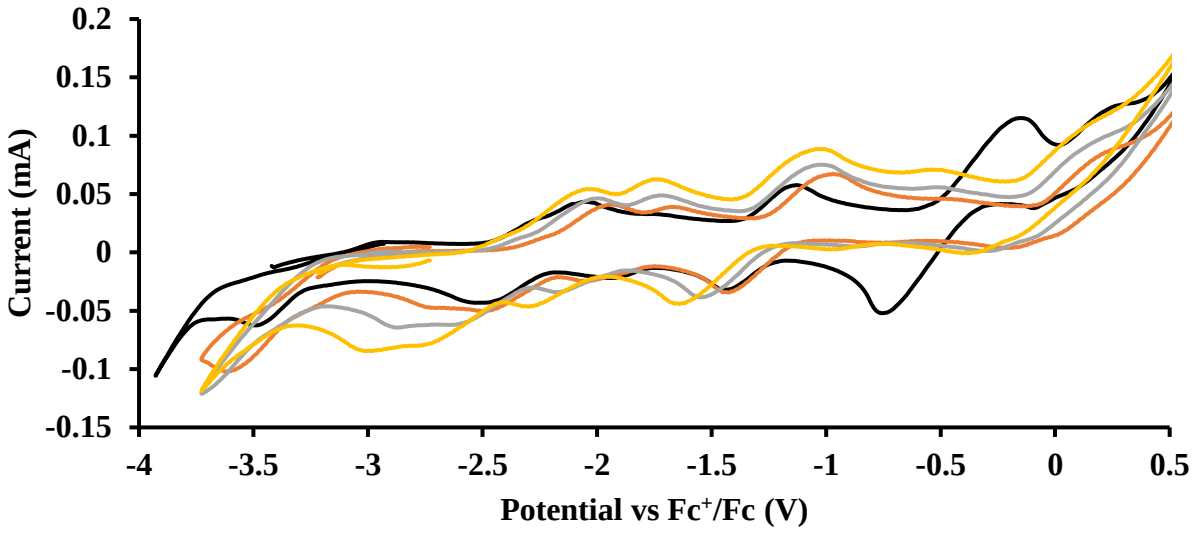

Figure 3.4: Voltammogram of 7.7 mM [K(crypt)][Cp′$_3$U] at ν = 200 (black), 400 (orange), 600 (grey), and 1000 (yellow) mV/s in 100 mM TBABPh$_4$ / THF. The peak centered at −0.495 V is due to internal standard $(C_5Me_5)_2Fe$.

Cp^{tet}. With the tetramethylcyclopentadienyl ligand, the U(IV)/U(III) and U(III)/U(II) couples in Cp$^{tet}_3$U^{III} were more negative than in Cp″$_3$U^{III} and Cp′$_3$U^{III}: −1.46 V and −3.11 V, Figure 3.5. However, data could not be obtained from the isolated U(II) compound [K(crypt)][Cp$^{tet}_3$U^{II}] because contact with the supporting electrolyte led to immediate decomposition. The voltammogram obtained from the resulting solution displayed at least five redox events, Figure 3.6. This reactivity is consistent with the more strongly reducing nature of the Cp^{tet} complexes as shown by the data in Tables 3.1 and 3.2. A third, minor event at −1.7 V was present and cannot be assigned with confidence.

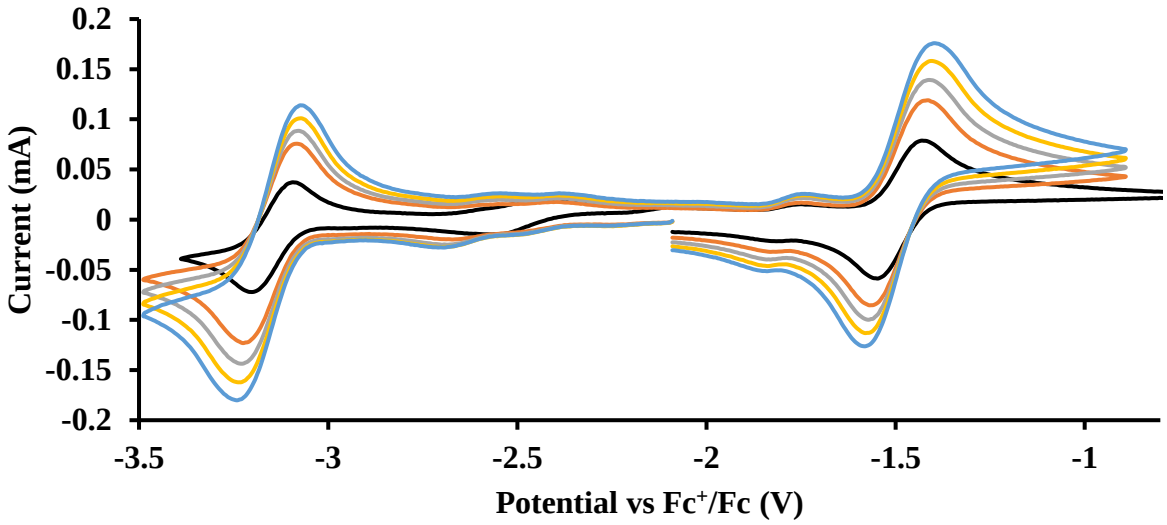

Figure 3.5: Voltammogram of 7.2 mM Cp^{tet}_3U at ν = 200 (black), 400 (orange), 600 (grey), 800 (yellow) and 1000 (blue) mV/s in 100 mM $TBABPh_4$ / THF.

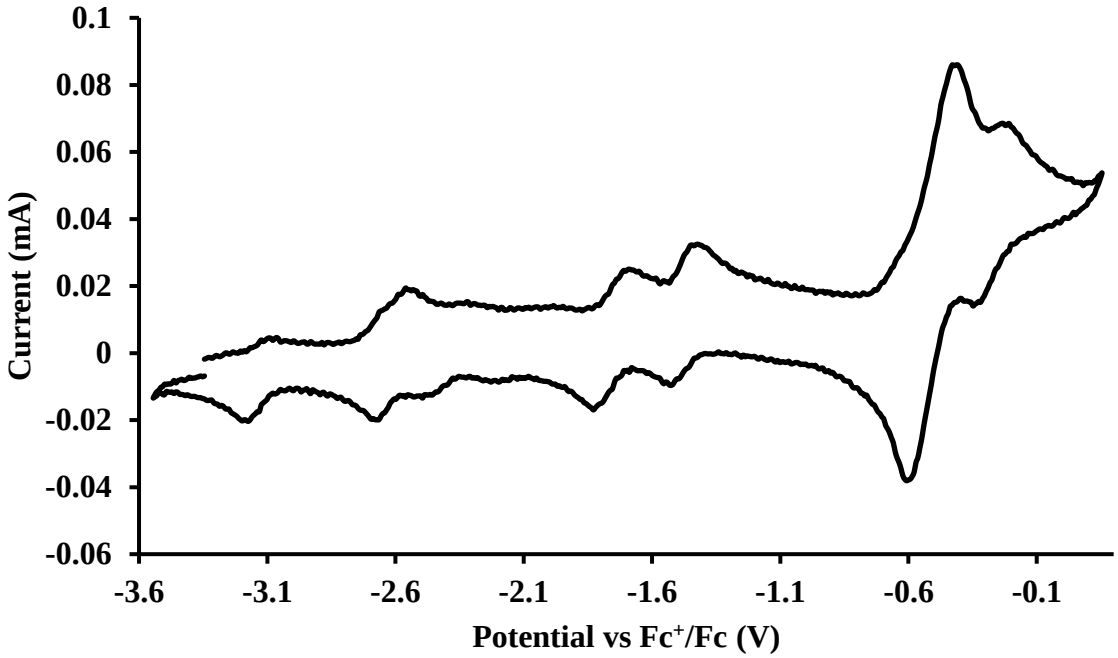

Figure 3.6: Voltammogram of [K(crypt)][Cp^{tet}_3U] at ν = 200 mV/s in 100 mM $TBABPh_4$ / THF. The event centered at −0.495 V is due to internal standard $(C_5Me_5)_2Fe^{II}$.

Thorium Complexes. Electrochemical data were collected on all the thorium compounds in this study using both [^{n}Bu$_4$N][PF$_6$] and [^{n}Bu$_4$N][BPh$_4$] despite multiple reports that electrochemical data on organothorium complexes are difficult to obtain using [^{n}Bu$_4$N][PF$_6$].[2,5,6,24–26] Since the voltammograms do not differ drastically between electrolytes, only the data using [^{n}Bu$_4$N][BPh$_4$], Table 3.3, are discussed below. Data with [^{n}Bu$_4$N][PF$_6$] are in Table 3.4.

Table 3.3: Reduction potentials (V) of tris(cyclopentadienyl) thorium complexes with 100 mM [^{n}Bu$_4$N][BPh$_4$] supporting electrolyte.

	Th(IV)/Th(III)			Th(III)/Th(II)			
	E_{PC}	E_{PA}	$E_{1/2}$	E_{PC}	E_{PA}	$E_{1/2}$	ΔE_{pp} Fc
Cp″$_3$Th^{IV}Br	−3.00	−2.77	−2.89				0.14
Cp″$_3$Th^{IV}Cl	−3.04	−2.81	−2.93				0.22
Cp′$_3$Th^{IV}Cl	−3.38	−2.90	−3.14				0.16
Cp′$_3$Th^{IV}Br	−3.17						
Cp$^{tet}_3$Th^{IV}Br	−3.48	−3.19	−3.34				0.18
Cp″$_3$Th^{III}				−2.92	−2.78	−2.85	0.19
Cp$^{tet}_3$Th^{III}				−3.33	−3.23	−3.28	0.16
[K(crown)(THF)$_2$][Cp″$_3$Th^{II}]				−2.89	−2.79	−2.84	0.09
[K(crypt)][Cp″$_3$Th^{II}]				−2.90	−2.81	−2.85	0.09

Table 3.4: Reduction potentials (V) of tris(cyclopentadienyl) thorium complexes with 200 mM [^{n}Bu$_4$N][PF$_6$] supporting electrolyte

	Th(IV)/Th(III)			Th(III)/Th(II)			
	E_{PC}	E_{PA}	$E_{1/2}$	E_{PC}	E_{PA}	$E_{1/2}$	ΔE_{pp} Fc
Cp″$_3$Th^{IV}Br	−2.99	−2.73	−2.86				0.17
Cp′$_3$Th^{IV}Cl	−3.39	−2.70	−3.04				0.14
Cp$^{tet}_3$Th^{IV}Br	−3.29	−3.20	−3.24				0.13
Cp″$_3$Th^{III}				−2.94	−2.73	−2.84	0.18
Cp$^{tet}_3$Th^{III}				−3.28	−3.22	−3.25	0.15
[K(crown)(THF)$_2$][Cp″$_3$Th^{II}]				−2.89	−2.73	−2.81	0.13
[K(crypt)][Cp″$_3$Th^{II}]				−2.88	−2.75	−2.82	0.06

Thorium(IV) Complexes. Cp″. Initially, $Cp''_3Th^{IV}Cl$ was examined to compare with the values previously reported by Cloke et al.[6] The cyclic voltammogram of $Cp''_3Th^{IV}Cl$ under our conditions shows the Th(IV)/Th(III) couple at −2.93 V, Figure 3.7, which is close to the value of −2.96 V reported for $Cp''_3Th^{IV}Cl$ and Cp''_3Th^{III}.[6] Similarly, the cyclic voltammogram of $Cp''_3Th^{IV}Br$[13] shows a Th(IV)/Th(III) redox couple at −2.89 V, Figure 3.8. This suggests that the identity of halide does not significantly affect the reduction potential in this system. This is also consistent with bulk synthetic studies that show that Cp''_3Th^{III} can be synthesized from both $Cp''_3Th^{IV}Cl$ and $Cp''_3Th^{IV}Br$.[13,27,28]

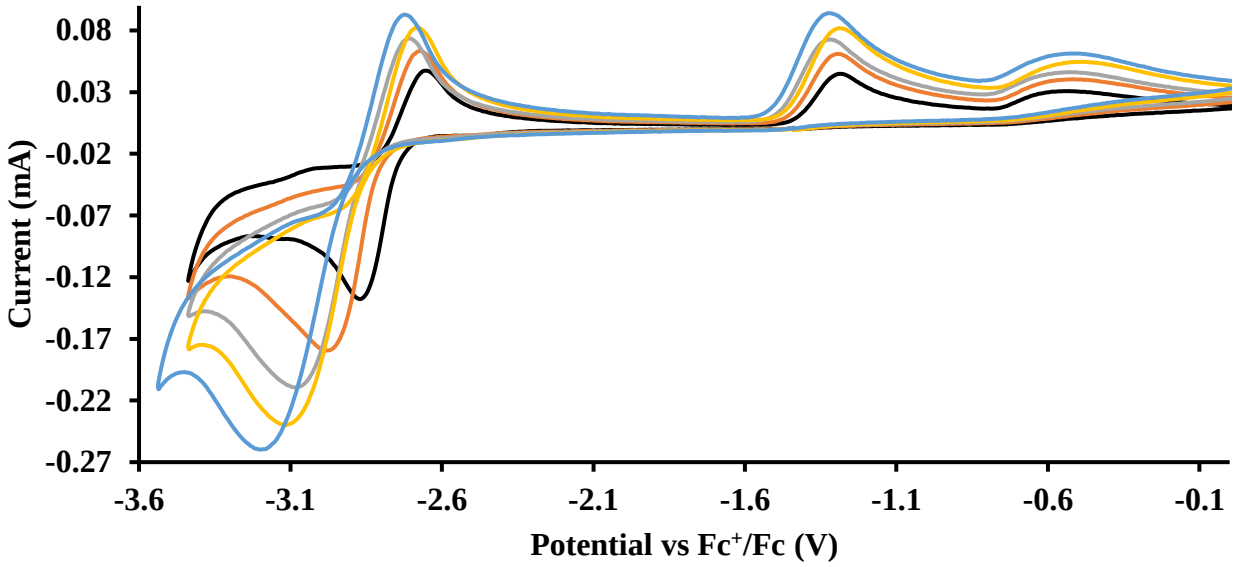

Figure 3.7: Voltammogram of 12 mM Cp''_3ThCl at ν = 200 (black), 400 (orange), 600 (grey), 800 (yellow) and 1000 (blue) mV/s in 100 mM $TBABPh_4$ / THF.

Cp′ and Cp^{tet}. $Cp'_3Th^{IV}Cl$[29] and $Cp^{tet}{}_3Th^{IV}Br$[30] were also examined as each these complexes can be chemically reduced to form tris(cyclopentadienyl) Th(III) species.[30,31] The cyclic voltammogram of $Cp'_3Th^{IV}Cl$,[29] Figure 3.9, exhibited a cathodic event at −3.14 V that is 0.21 V more negative than that of $Cp''_3Th^{IV}Cl$. Similarly, the voltammogram of $Cp'_3Th^{IV}Br$ had a

cathodic event at −3.17 V, Figure 3.10. This event was determined to be a one electron process by comparing the current passed to that of the internal standard.

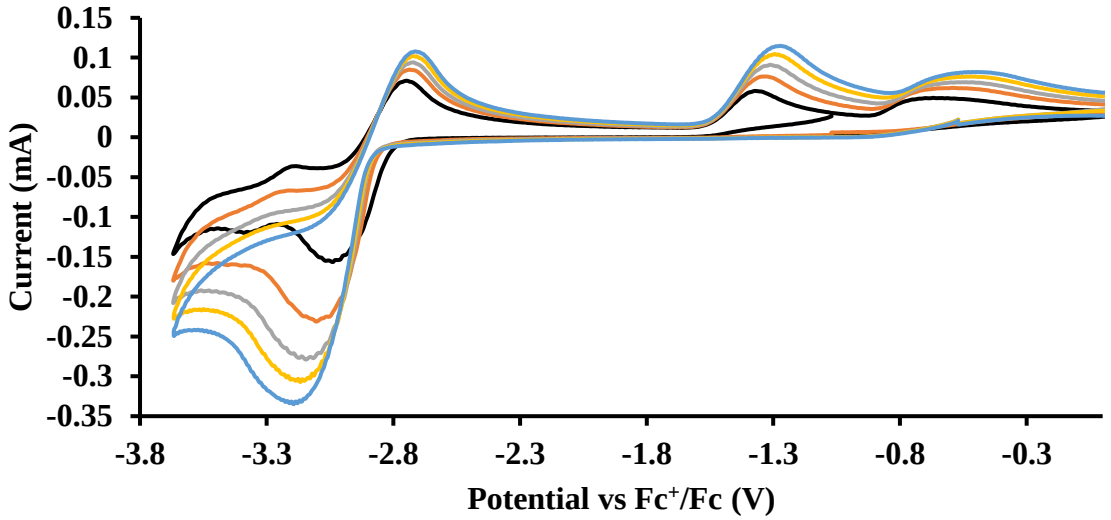

Figure 3.8: Voltammogram of 7.4 mM Cp″$_3$ThBr at v = 200 (black), 400 (orange), 600 (grey), 800 (yellow) and 1000 (blue) mV/s in 100 mM TBABPh$_4$ / THF.

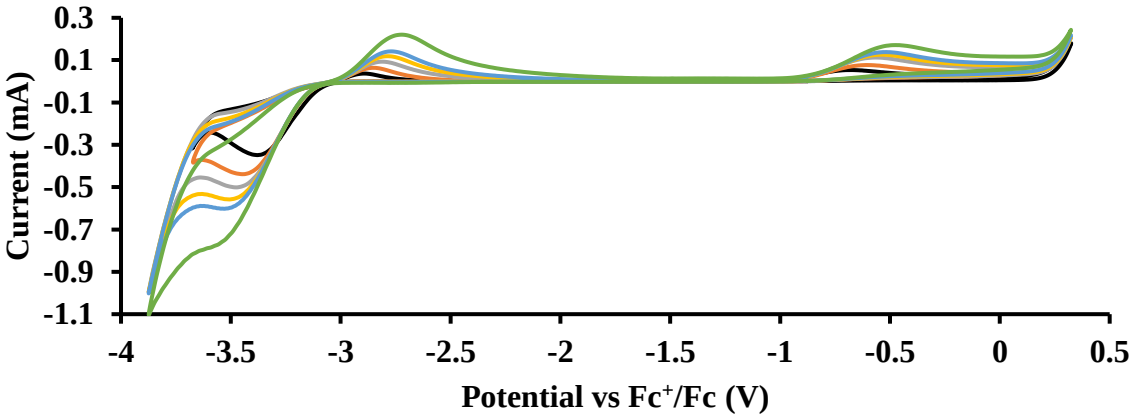

Figure 3.9: Voltammogram of 14 mM Cp′$_3$ThCl at v = 200 (black), 400 (orange), 600 (grey), 800 (yellow), 1000 (blue), and 2000 (green) mV/s in 100 mM TBABPh$_4$ / THF.

The voltammogram of $Cp^{tet}{}_3Th^{IV}Br$ had a cathodic event at −3.48 V, Figure 3.11. The events in the voltammograms of $Cp'_3Th^{IV}Br$ and $Cp^{tet}{}_3Th^{IV}Br$ are practically irreversible even at scan rates up to 2000 mV/s. These results, along with the uranium studies above in Table 3.1, clearly show that the reduction potential of the actinide complex trends with the electron donation strength of the ligand in the order of $Cp^{tet} > Cp' > Cp''$.

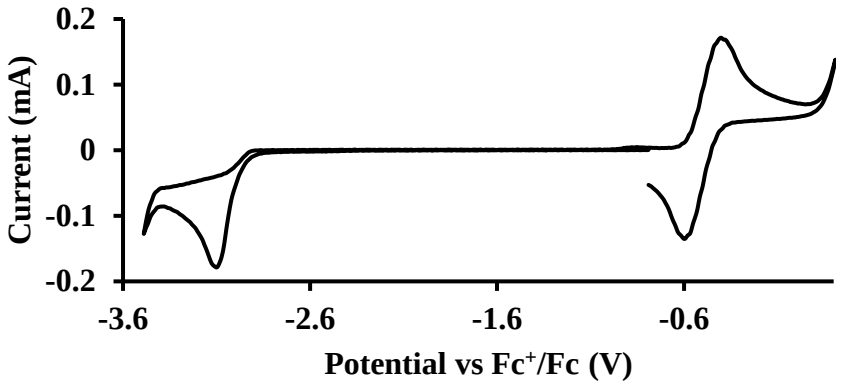

Figure 3.10: Voltammogram of 15 mM $Cp'_3Th^{IV}Br$ and 14.6 mM $(C_5Me_5)_2Fe$ in 100 mM $TBABPh_4$ / THF. The ratio of current passed for $Cp'_3Th^{IV}Br$ to $(C_5Me_5)_2Fe$ is 0.77, suggesting a one-electron process is occurring for $Cp'_3Th^{IV}Br$.

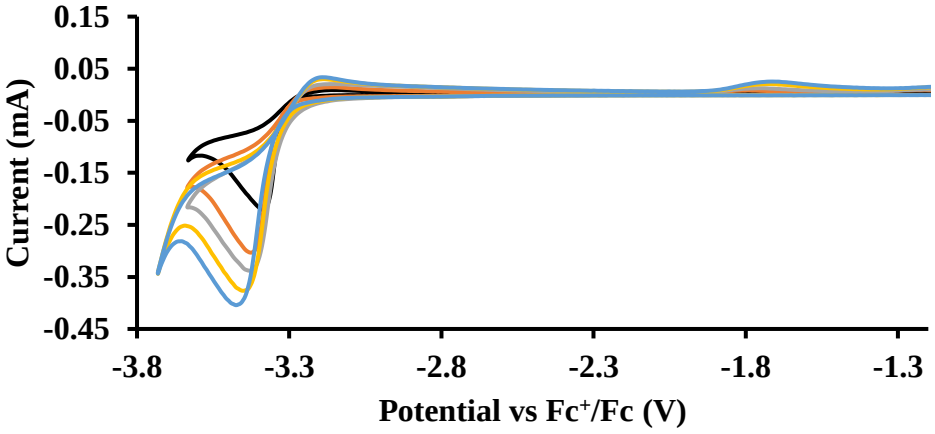

Figure 3.11: Voltammogram of 22 mM $Cp^{tet}{}_3ThBr$ at ν = 200 (black), 400 (orange), 600 (grey), 800 (yellow) and 1000 (blue) mV/s in 100 mM $TBABPh_4$ / THF.

In addition to the Th(IV)/Th(III) couple, the voltammograms of the Th(IV) compounds showed an irreversible anodic process that could be a cyclopentadienide oxidation, based on the electrochemical data collected on the cyclopentadienyl salts, KCp′, KCp″, and KCp^{tet}, Figure 3.12. These irreversible anodic events were not found in the uranium systems. This difference in Th and U electrochemistry has been previously observed.[2,6,32,33] Clearly, the Lewis acidity of the metal influences the potential for these cyclopentadienide oxidations. Cyclopentadienyl rings bound to K^+, $[K(chelate)]^+$, or An^{n+} could have different oxidation potentials as evidenced by the differing voltammograms of KCp″, [K(crown)][Cp″], and [K(crypt)][Cp″], Figure 3.13.

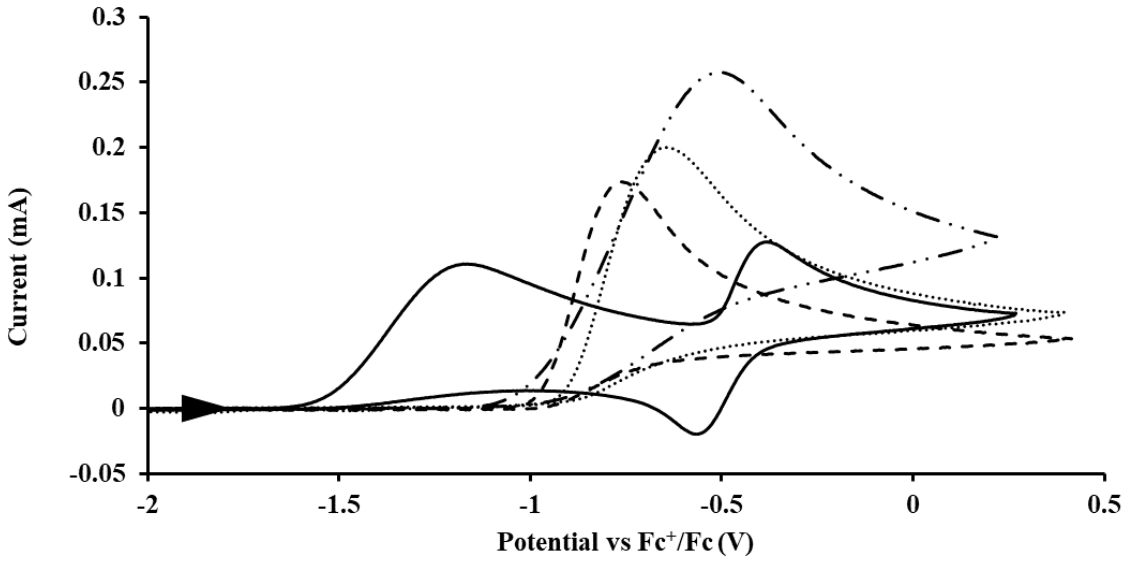

Figure 3.12: Voltammogram of KCp^{tet} (solid, 15 mM), KCp″ (dashed, 17 mM), KCp′ (dotted, 14 mM), and KCp (dotted dash, 22 mM) at ν = 200 mV/s in 200 mM [^{n}Bu$_4$N][PF$_6$] / THF. The event centered at −0.495 V in the voltammogram of KCp^{tet} is due to internal standard $(C_5Me_5)_2Fe^{II}$.

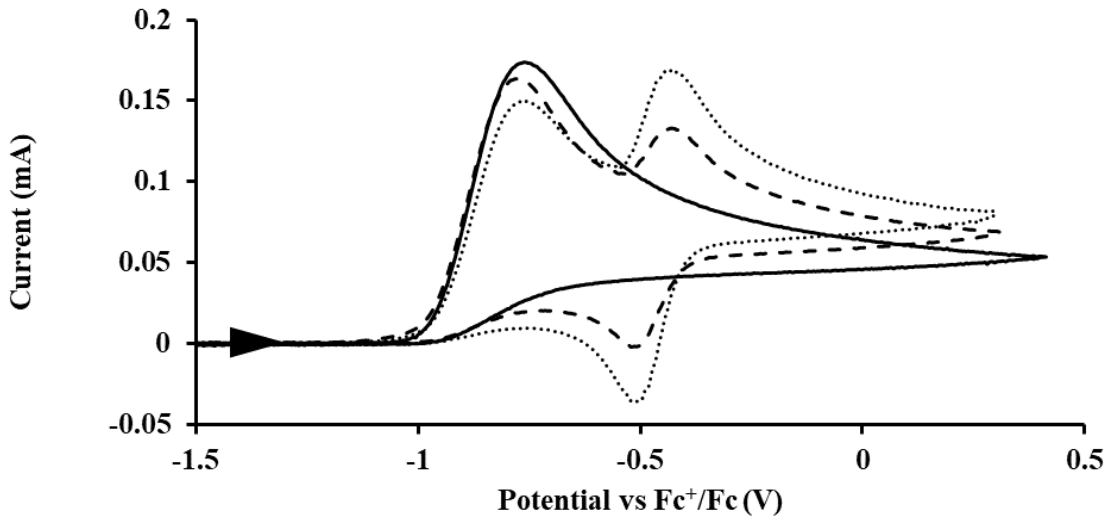

Figure 3.13: Voltammogram of 17 mM KCp″ (solid), [K(crown)][Cp″] (dashed), and [K(crypt)][Cp″] (dotted) at 200 mV/s in 200 mM [^{n}Bu$_4$N][PF$_6$] / THF. The event centered at −0.495 V is due to internal standard $(C_5Me_5)_2Fe^{II}$.

Table 3.5: Peak anodic potentials for potassium cyclopentadienide salts with 200 mM [^{n}Bu$_4$N][PF$_6$] supporting electrolyte

	E_{PA} (V)
KCp^{tet}	−1.17
KCp	−0.50
KCp′	−0.63
KCp″	−0.71
[K(crown)][Cp″]	−0.76
[K(crypt)][Cp″]	−0.77

Th(III) Complexes. Cp″. There are fewer Th(III) options to study since there are only four crystallographically-characterized tris(cyclopentadienyl) Th(III) complexes, Cp''_3Th^{III},[27,28] $Cp^{tet}_3Th^{III}$,[30] $(C_5{}^{t}Bu_2H_3)_3Th^{III}$,[34] and $(C_5Me_5)_3Th^{III}$.[35] Other Th(III) compounds have been isolated with different ligand environments,[36–40] but our initial attempts to collect electrochemical data on $(C_5Me_5)_2Th^{III}[{}^{i}PrNC(Me)N{}^{i}Pr]$[39] led to immediate decomposition. Inman and Cloke found that

scanning anodically on Cp''_3Th^{III} gave a process at −2.96 V that matched the reduction of $Cp''_3Th^{IV}Cl$ described above and established the Th(IV)/Th(III) couple.[6] In comparison, in our hands, scanning cathodically on Cp''_3Th^{III} showed a voltammogram with a redox process centered at −2.85 V, Figure 3.14. A second cathodic event appears after the first cycle at −2.29 V, or when scanning anodically from the open circuit potential. The event at −2.29 V was also observed by Cloke and was attributed to a ligand-based event.

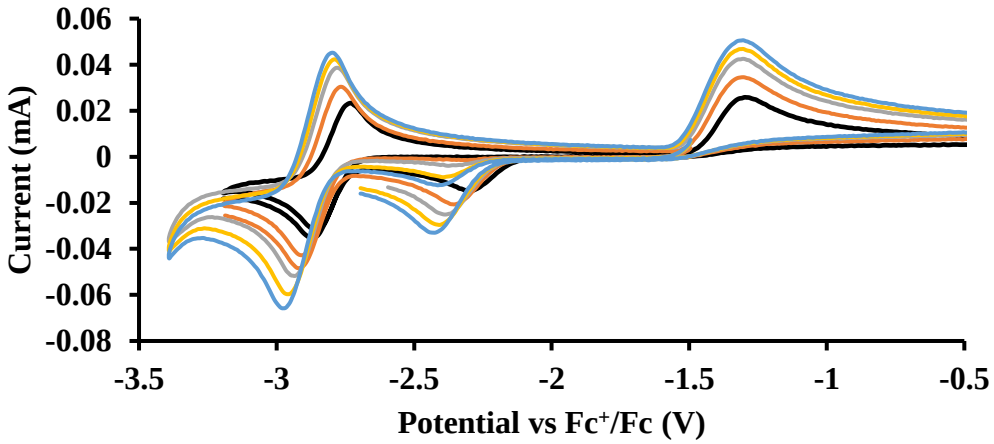

Figure 3.14: Voltammogram of 4.9 mM Cp''_3Th at v = 200 (black), 400 (orange), 600 (grey), 800 (yellow) and 1000 (blue) mV/s in 100 mM $TBABPh_4$ / THF.

Cp′ and Cp^{tet}. Since Cp'_3Th^{III} has only been generated *in situ* (see Chapter 9),[31] it was not studied under the present conditions. The voltammogram of $Cp^{tet}{}_3Th^{III}$ at v = 200 mV/s displays only a cathodic event, but at $v \geq 400$ mV/s, a return oxidation appears and the Th(III)/Th(II) redox couple is centered at −3.28 V, Figure 3.15. This value matches the trend observed for the uranium systems in that Cp^{tet} complexes of thorium are more difficult to reduce than the silyl-cyclopentadienyl analogs. An anodic event at −1.87 V is present and is attributed to a Cp^{tet}-based process.

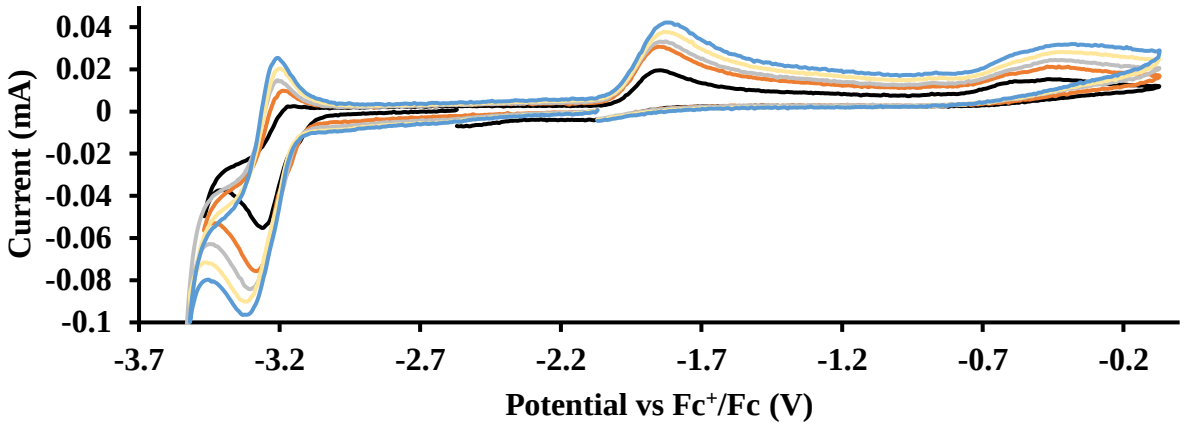

Figure 3.15: Voltammogram of 6.7 mM $Cp^{tet}{}_3Th$ at ν = 200 (black), 400 (orange), 600 (grey), 800 (yellow) and 1000 (blue) mV/s in 100 mM $TBABPh_4$ / THF.

Th(II) Complexes. The only isolated Th(II) compounds $[K(crown)(THF)_2][Cp''_3Th^{II}]$ and $[K(crypt)][Cp''_3Th^{II}]$ exhibited nearly identical voltammograms. Scanning anodically, $[K(crown)(THF)_2][Cp''_3Th^{II}]$ showed a redox process centered at −2.84 V, which is assigned as the Th(III)/Th(II) redox couple, and a second irreversible anodic event at −1.38 V, attributed to ligand-based oxidation, Figure 3.16. The voltammogram of this Th(II) compound was practically identical over 5 cycles. $[K(crypt)][Cp''_3Th^{II}]$ similarly showed a reversible event centered at −2.85 V and a second anodic event at −1.43 V.

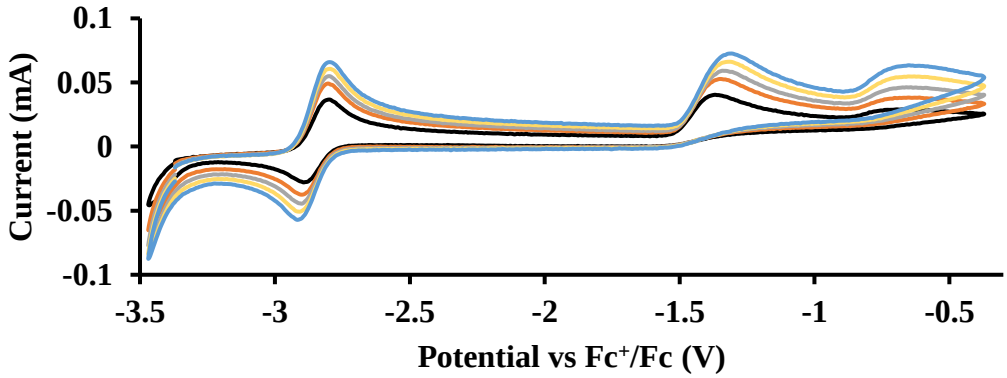

Figure 3.16: Voltammogram of 4.6 mM $[K(crown)(THF)_2][Cp''_3Th]$ at ν = 200 (black), 400 (orange), 600 (grey), 800 (yellow) and 1000 (blue) mV/s in 100 mM $TBABPh_4$ / THF.

Thorium Spectroelectrochemistry. The data on isolated $[Cp''_3Th^{II}]^{1-}$ complexes suggested that the Th(III)/Th(II) redox process occurs at about the same potential as the Th(IV)/Th(III) potential of $Cp''_3Th^{IV}Br$. To investigate this further, spectroelectrochemical UV-visible measurements were obtained with the aid of Jeff Barlow and Jenny Yang. A potential of −2.90 V was applied to a solution of $Cp''_3Th^{IV}Br$ in 200 mM $[^nBu_4N][PF_6]$ / THF and the UV-visible spectrum was recorded approximately every 5 seconds during electrolysis. The formation of Cp''_3Th^{III} is clearly shown by the growth of four bands at roughly 360, 500, 580, and 680 nm, Figure 3.17, which correspond to the absorption spectrum of Cp''_3Th^{III}.[27,28] No further reduction to the $[Cp''_3Th^{II}]^{1-}$ was observed,[13] although it cannot be entirely ruled out as the absorbance spectrum reached the maximum of the detector.

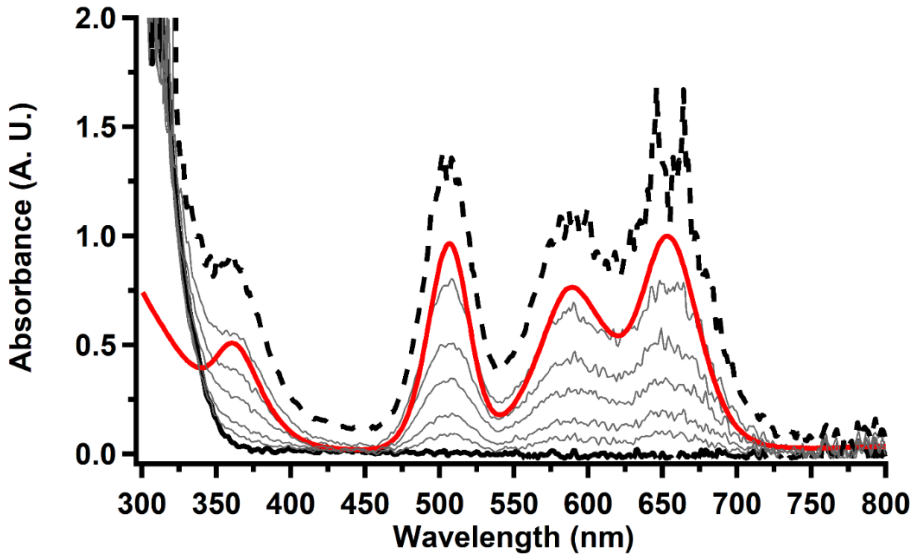

Figure 3.17: UV-visible spectrum of $Cp''_3Th^{IV}Br$ (black, solid) converting to Cp''_3Th^{III} (black, dashed) during electrolysis at −2.90 V with a starting concentration of 7.0 mM in 200 mM $[^nBu_4N][PF_6]$ / THF. The growth of four bands at 365, 510, 590, and 655 nm is indicative of Cp''_3Th^{III} (red).[34]

Electrolysis of a solution of Cp''_3Th^{III} in 200 mM [^{n}Bu$_4$N][PF$_6$] / THF at −2.90 V shows clean conversion to the Th(II) species $[Cp''_3Th^{II}]^{1-}$,[13] as indicated by the growth of the large absorption at 650 nm and the concomitant decrease in absorptions at 360, 500, 580, and 680 nm, Figure 3.18. Although the absorption spectrum of Cp''_3Th^{III} had disappeared, the absorption at 650 nm, indicative of Th(II),[2] decreased in intensity as the electrolysis continued. The Th(II) species appears to be unstable under the electrolysis conditions.

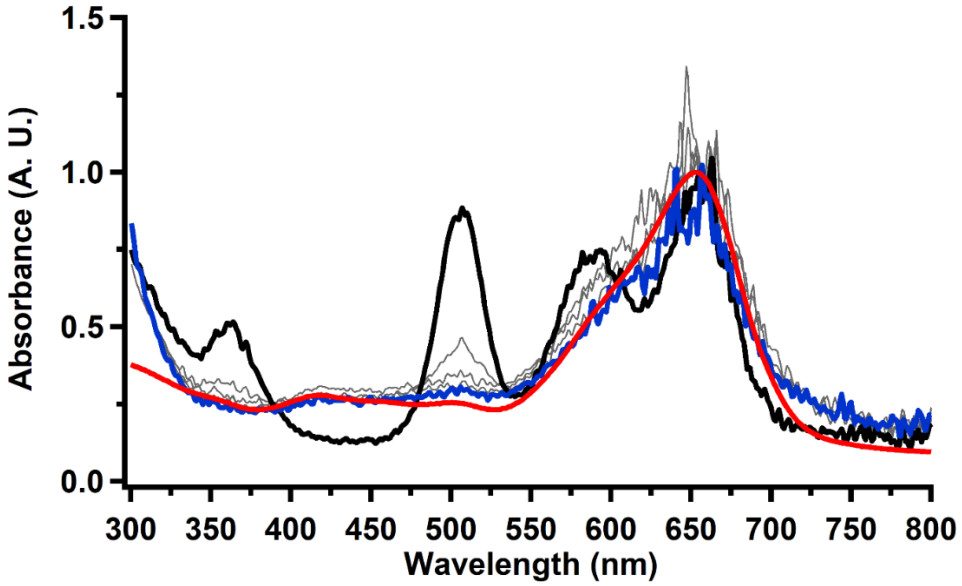

Figure 3.18: UV-visible spectrum of Cp''_3Th^{III} (black) converting to $[Cp''_3Th^{II}]^{1-}$ (blue) during electrolysis at −2.90 V with a starting concentration of 1.1 mM in 200 mM [^{n}Bu$_4$N][PF$_6$] / THF. The growth of the band at 650 nm is indicative of $[Cp''_3Th^{II}]^{1-}$ (red).[2]

Chemical Synthesis of Th(II) Complexes from Th(IV) Precursors. The similarity of the Th(IV)/Th(III) couple in $Cp''_3Th^{IV}Br$ and Th(III)/Th(II) couple in $[Cp''_3Th^{II}]^{1-}$ suggested that Th(IV) compounds could be used as the precursors to Th(II) compounds as well as the known Th(III) precursor, Cp''_3Th^{III}. Indeed, reaction of 2.2 equivalents of KC_8 to a THF solution of $Cp''_3Th^{IV}Cl$ and crown afforded [K(crown)(THF)$_2$][Cp''_3Th^{II}] in 50% crystalline yield, with a significant amount of Cp''_3Th^{III} as a byproduct. Previously, Lappert reported that prolonged

stirring of a solution of $Cp''_3Th^{IV}Cl$ over excess NaK alloy developed a green color,[28] which was later confirmed to be the color of Th(II).[13]

Th(IV) to Th(II) conversion was also studied with $Cp''_3Th^{IV}Br$. Reaction of $Cp''_3Th^{IV}Br$ with 2 equivalents of KC_8 in THF generated a dark green solution characteristic of Th(II) within 5 minutes, as did reaction of $Cp''_3Th^{IV}Br$ with excess Na and with excess Li. The UV-visible spectra of these solutions have a strong absorption at 650 nm, identical to the previously reported spectra of $[K(crypt)][Cp''_3Th^{II}]$ and $[K(crown)(THF)_2][Cp''_3Th^{II}]$,[13] but the spectra also show a non-negligible amount of Cp''_3Th^{III}.[28] Formation of the Th(III) complex is reasonable based on the fact that $[Na(\kappa^6\text{-crown})(\kappa^2\text{-crown})][Cp''_3Th^{II}]$ (see below) reacts with $Cp''_3Th^{IV}Br$ in THF to immediately form Cp''_3Th^{III} in near quantitative yield.

These results show that a chelating agent is not necessary for the chemical synthesis of Th(II) species in solution. However, the chelating agent appears necessary for efficient separation of the Th(II) product from the Th(III) starting material, as analytically pure samples of $[M(THF)_x][Cp''_3Th^{II}]$ (M = Li, Na, K) were not isolated even though it is possible to isolate chelate-free examples of $[Cp''_3U^{II}]^{1-}$.[41] Further support for the importance of alkali metal chelates is that addition of 18-crown-6 to the reaction of $Cp''_3Th^{IV}Br$ and excess Na provided X-ray quality crystals that were identified as $[Na(\kappa^6\text{-crown})(\kappa^2\text{-crown})][Cp''_3Th^{II}]$, only the third reported crystal structure of a Th(II) complex, Scheme 3.1, Figure 3.19.

Similarly, the reaction of Cp''_3Th^{III}, Rb, and crypt in THF afforded dichroic blue/red crystals of $[Rb(crypt)][Cp''_3Th^{II}]$, isolated in 61% crystalline yield and identified by X-ray crystallography, Scheme 3.1, Figure 3.20. In addition, the reaction of Cp''_3Th^{III}, Cs, and crypt afforded dark blue/red crystals of $[Cs(crypt)][Cp''_3Th^{II}]$ in 54% crystalline yield, Scheme 3.1, Figure 3.20. The $[Rb(crypt)]^{1+}$ and $[Cs(crypt)]^{1+}$ compounds are isomorphous with the

[K(crypt)]$^{1+}$ anlog[2] and can be easily separated from Cp″$_3$Th^{III} starting material, which was difficult without

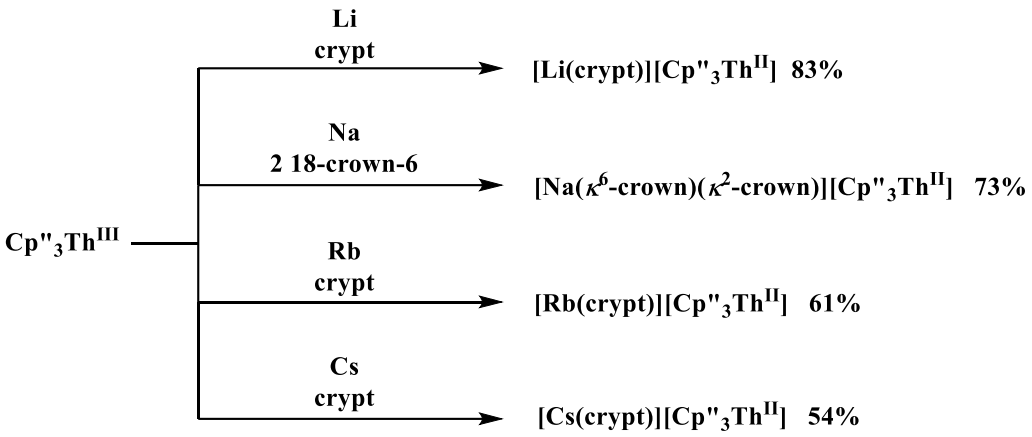

Scheme 3.1: Synthesis of new Th(II) compounds.

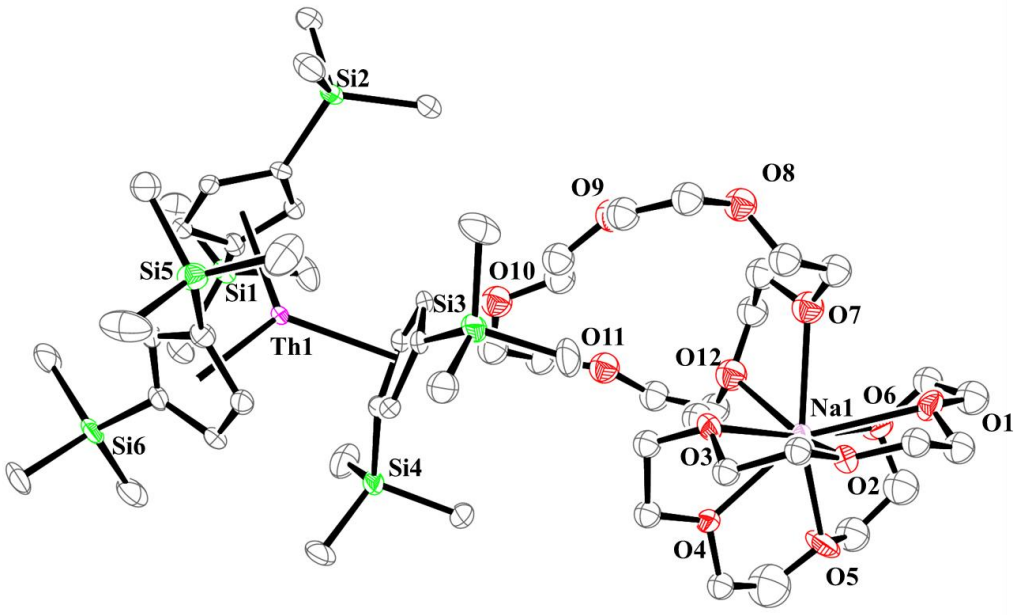

Figure 3.19: Thermal ellipsoid plot of [Na(κ^6–crown)(κ^2–crown)][Cp″$_3$Th^{II}] plotted at the 35% probability level. Hydrogen atoms and disorder in the κ^2-crown unit have been removed for clarity.

the use of a chelate. The reaction of Cp''_3Th^{III} with Li and crypt formed dark blue-green needles of $[Li(crypt)][Cp''_3Th^{II}]$ in 83% yield, but the crystals were not suitable for X-ray diffraction, Scheme 3.1.

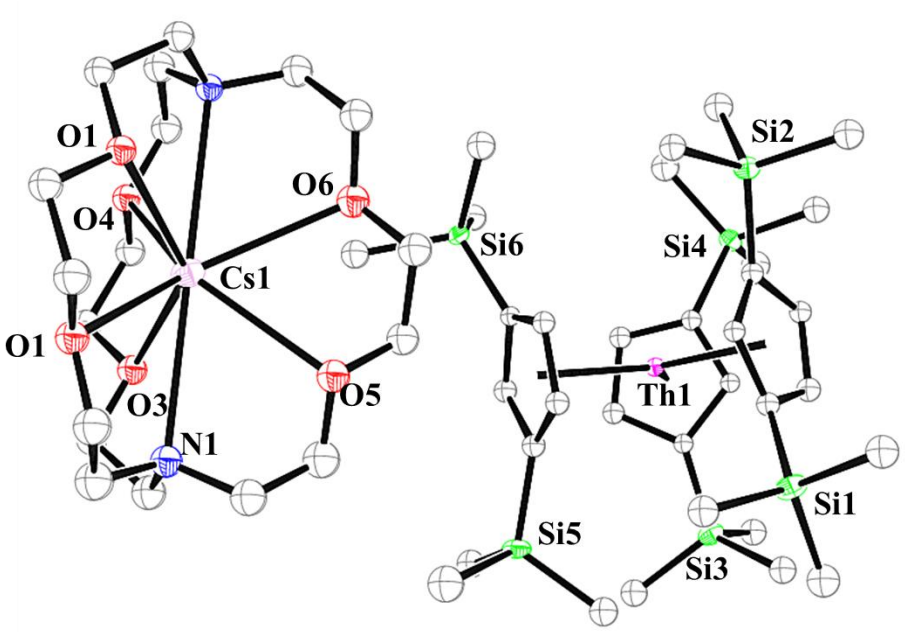

Figure 3.20: Thermal ellipsoid plot of $[Cs(crypt)][Cp''_3Th^{II}]$ plotted at the 50% probability level. Hydrogen atoms have been removed for clarity.

Since the reaction chemistry and the spectroelectrochemistry suggested that the Th(II) complexes were generated from a Th(IV) precursor through a Th(III) intermediate, reactions with the two-electron reductant Ba were studied. The Ba(II)/Ba(0) reduction potential is nearly identical to that of K(I)/K(0).[42] Surprisingly, prolonged stirring of a THF solution of $Cp''_3Th^{IV}Br$ and excess Ba afforded *only* Cp''_3Th^{III}. When chelates were added, the reaction of $Cp''_3Th^{IV}Br$ and crown or $Cp''_3Th^{IV}Br$ and crypt over excess Ba formed Cp''_3Th^{III} *and then* the dark green color of Th(II) with UV-Visible spectra consistent with $[Cp''_3Th^{II}]^{1-}$. Addition of elemental Hg did not appear to affect the rate of formation of the Th(II) species. These results, coupled with the

spectroelectrochemical measurements, strongly suggest that the Th(IV)/Th(II) redox couple is not observed experimentally in these systems and that instead two one-electron processes occur.

Discussion

An(IV)/An(III) Processes. The trends observed in the U(IV)/U(III) and Th(IV)/Th(III) redox couples in Tables 3.1–3.3 indicate that Cp^{tet} is more electron donating than Cp′, which is more electron donating than Cp″. This follows the electron-donating ability of the ligands previously found in studies of $(C_5R_5)_2Zr(CO)_2$ complexes[14] and yttrium compounds.[15,17] For the zirconium complexes, the CO stretching frequency and the reduction potentials were analyzed to determine electron-donation strength of the cyclopentadienyl ligand. Generally in these An(IV)/An(III) studies, the thorium complexes showed less reversible processes than the uranium compounds. In the $Cp''_3Th^{IV}Br$ case, UV-visible spectroelectrochemistry measurements show that this compound is reduced under electrochemical conditions to Cp''_3Th^{III}, which requires loss of Br^{1-} and geometric reorganization. In the $Cp'_3Th^{IV}Br$ case, density functional theory calculations are available that show that the putative initial reduction product, $[Cp'_3Th^{III}Br]^{1-}$, would be unstable with respect to Cp'_3Th^{III} and Br^{1-}.[31] These results are consistent with the electrochemical irreversibility of the system.

An(III)/An(II) Processes. The −2.26 V value for Cp'_3U^{III} matches well with the two other U(III)/U(II) couples have been assigned via electrochemistry, $[(^{Ad,Me}ArO)_3mes]U^{III}$ at −2.495 V[7] and $(C_5{}^iPr_5)_2U^{II}$ at −2.33 V,[8] even though $[Cp'_3U^{II}]^{1-}$ and $(C_5{}^iPr_5)_2U^{II}$ have been assigned $5f^36d^1$ electron configurations[8,21] while $\{[(^{Ad,Me}ArO)_3mes]U^{II}\}^{1-}$ is best described as $5f^4$.[9] The −2.73 V reduction potential for Cp''_3U^{III} is unexpectedly more reducing than those of these other three complexes. This is also unusual in that solutions of $[Cp''_3U^{II}]^{1-}$ have longer lifetimes than solutions of $[Cp'_3U^{II}]^{1-}$.[20] The U(III)/U(II) reduction potential for $Cp^{tet}{}_3U^{III}$ was determined to be −3.11 V,

which is the most negative reduction potential for these compounds and matches the trend observed for the An(IV)/An(III) couples.

Th(II) complexes were investigated for the first time via electrochemistry and the $E_{1/2}$ values for the Th(III)/Th(II) couple observed in the isolated Th(II) compounds matched the value observed in Cp''_3Th^{III}. Surprisingly, the Th(IV)/Th(III) couple of $Cp''_3Th^{IV}Br$ appears to be about the same as the value for the Th(III)/Th(II) couple of $[Cp''_3Th^{II}]^{1-}$. This result was tested chemically and it was found that reduction of Th(IV) with excess reducing agent would form Th(II) compounds directly with KC_8, Na, Li, and Ba both with and without the use of a chelating agent. Blue Cp''_3Th^{III} is observed as an intermediate in these reactions which indicates formation of the Th(II) products arises from two one-electron reductions. Furthermore, the $E_{1/2}$ values for Th(III)/Th(II) match the expected trend compared to uranium based on previously calculated An(III)/An(II) reduction potentials.[48-50]

The thorium electrochemistry was also unusual in that electrochemical data-were obtained using $[^nBu_4N][PF_6]$ as supporting electrolyte on isolated Th(IV), Th(III), and Th(II) compounds. This electrolyte has proven to be more reactive than $[^nBu_4N][BPh_4]$ with some complexes[2,6] and it may have been expected that Th(II) would react with it. The fact that the Th(III)/Th(II) reduction potentials vary slightly depending on the specific electrolyte highlights the fact the reduction potentials of these systems are very sensitive to experimental conditions.

Conclusion

Electrochemical data on three series of tris(cyclopentadienyl) An(IV), An(III), and An(II) (An = Th, U) complexes, including the first data on Th(II) complexes, complimented by UV-visible spectroelectrochemical measurements, show a correlation between reduction potential and the electron-donating ability of the cyclopentadienyl ring. The studies indicate that Th(III) is a

stronger reductant than U(III), but the reduction potential of U(II) is similar to that of Th(II). Two unexpected results should stimulate further studies. The U(III)/U(II) reduction potential of Cp'_3U^{III} is similar to the two previously reported U(III)/U(II) values, but it is significantly less negative than the Cp″ analog. The reduction potentials of Th(IV)/Th(III) and Th(III)/Th(II) couples are sufficiently similar that Th(II) complexes can be made directly from Th(IV) precursors without the need to isolate the Th(III) intermediate.

Experimental Details

All syntheses and manipulations were conducted under an Ar atmosphere with rigorous exclusion of air and water using standard glovebox and vacuum line techniques. Solvents were sparged with UHP argon and dried by passage through columns containing Q-5 and molecular sieves prior to use. Deuterated NMR solvents were dried over NaK alloy, degassed by three freeze-pump-thaw cycles, and vacuum transferred prior to use. NMR spectra were recorded on an AVANCE600 MHz spectrometer at 298 K and referenced to residual proteo-solvent resonances. Cp'_3U,[21] [K(crypt)][Cp'_3U],[21] Cp''_3U,[20] [K(crown)$(THF)_2$][Cp''_3U],[20] Cp^{tet}_3U,[43] $U(NR_2)_3$,[44] Cp''_3ThBr,[28] Cp'_3ThCl,[45] Cp^{tet}_3ThBr,[30] Cp''_3Th,[27,28] Cp^{tet}_3Th,[30] [K(crown)$(THF)_2$][Cp''_3Th],[13] [K(crypt)][Cp''_3Th],[13] KCp^{tet},[43] KCp′,[46] and KCp″[46] were synthesized according to literature procedures. 18-crown-6 (Alfa Aesar) was sublimed at 30 °C at 10^{-5} Torr before use. 2.2.2-cryptand (Aldrich) was dried under vacuum at 10^{-5} Torr before use. Electrochemical grade (>99%) [^{n}Bu$_4$N][BPh_4] (Sigma) and electrochemical grade (>99.9%) [^{n}Bu$_4$N][PF_6] (Sigma) were recrystallized from acetone three times and dried at 80 °C and 10^{-5} Torr overnight before use. $(C_5Me_5)_2Fe$ was purified by sublimation before use.

All actinide compounds were purified by recrystallization and dried before data collection. Electrochemical measurements were collected with a freshly made THF solution of supporting

electrolyte with a glassy carbon working electrode, platinum wire counter electrode, and silver wire pseudo-reference electrode with a Princeton Applied Research PARSTAT 2273 Advanced Electrochemical System and referenced with internal standard $(C_5Me_5)_2Fe$. Internal resistance was measured for each solution and resistance was manually compensated by approximately 90% of the measured value. All scans were measured in the cathodic direction except for the isolated U(II) and Th(II) complexes and KC_5R_5 compounds which were measured in the anodic direction. UV-visible spectroelectrochemical measurements were made using a Pine Instruments UV-visible kit with a Pt working and counter electrode and Ag wire pseudo-reference and an Agilent Cary 60 UV-visible spectrophotometer fitted with an Agilent fiber optic coupler connected to an Ocean Optics CUV 1 cm cuvette holder inside the glovebox. UV-visible measurements were made using an Agilent Cary 60 spectrophotometer in THF in a 1 mm cuvette.

Although the highest purity of commercially available $[^nBu_4N][BPh_4]$ was used, it reacted with some actinide compounds. The Th(IV) compounds $Cp'_3Th^{IV}Cl$[29] and $Cp^{tet}_3Th^{IV}Br$[30] showed no noticeable decomposition while in the presence of this material, but purple $Cp^{tet}_3Th^{III}$ [30] immediately decomposed to a yellow solution and brown $Cp^{tet}_3U^{III}$ [19] turned orange when added to commercial $[^nBu_4N][BPh_4]$ in THF. Hence, multiple recrystallizations of the commercial electrolyte were required until no reaction was observed with the actinide complexes and reproducible data were obtained. Fresh electrolyte solutions were made immediately before data collection, as small amounts of precipitate formed if the electrolyte solution sat for an extended period of time, even overnight. These samples caused decomposition with some actinide samples upon mixing. Small events were present in the voltammograms of Cp'_3U and Cp^{tet}_3U that are attributed to either decomposition or impurities in the sample, despite recrystallization immediately prior to data collection. These events were present across multiple runs with different

batches of material. The solubility limit of [^{n}Bu$_4$N][BPh$_4$] in THF was roughly 100 mM which is the concentration used for most experiments. Exceptions are Cp′$_3$U^{III} and [K(crypt)][Cp′$_3$U^{II}] in which 50 mM concentrations were used since the compounds appeared to decompose in higher concentration solutions. [^{n}Bu$_4$N][PF$_6$] was used at a concentration of 200 mM to determine if peak separations would be smaller than 100–200 mV. They were not.

General Electrochemistry Procedure. Inside the glovebox, a stock electrolyte solution was freshly prepared in THF. Between 1–2 mL of this solution was transferred to a 20 mL scintillation vial and a voltammogram of this solution was collected to verify the electrolyte solution was free of impurities. Roughly 10–15 mg of actinide compound was dissolved in the same electrolyte solution to yield approximately a 5 mM solution. Electrodes were placed into the vial and the vial was left open to the box atmosphere during data collection. The internal resistance was measured and cyclic voltammetry experiments were recorded. Decamethylferrocene, (C$_5$Me$_5$)$_2$Fe was added to the same solution following all data collection, and a single scan was recorded to measure the internal standard redox event.

Synthesis of [Li(crypt)][Cp″$_3$Th]. Cp″$_3$Th (50 mg, 0.058 mmol) and crypt (23 mg, 0.061 mmol) were dissolved in THF (1 mL) and transferred to a vial containing a Li smear (~5 mg) and placed in the freezer at −35 °C overnight. The inky blue/green solution was filtered and dried under vacuum. The solids were dissolved in Et$_2$O (3 mL) and layered under hexane at −35 °C. Dark blue needles grew overnight (60 mg, 83%). ^{1}H NMR (THF-d_8): δ 5.10 (s, 9H, C$_5$*H*$_3$R$_2$), 3.66 (m, 11H, crypt), 3.57 (m, 14H, crypt) (overlapping with THF), 2.68 (m, 11H, crypt), 0.60 ppm (s, 42H, Si*Me*$_3$). ^{13}C (THF-d_8): δ 119.5 (C$_5$*H*$_3$R$_2$), 114.6 (C$_5$*H*$_3$R$_2$), 113.0 (C$_5$*H*$_3$R$_2$), 71.2 (crypt), 69.2 (crypt), 54.6 (crypt), 1.5 ppm (Si*Me*$_3$). ^{7}Li NMR (THF-d_8): δ −1.19 ppm. IR: 2943m, 2881m, 1233s, 1168s, 1071s, 910s, 820s, 743s, 675s cm^{-1}. UV-visible (THF): 657 nm (15,000

$M^{-1}cm^{-1}$). Anal Calcd for $C_{51}H_{99}N_2O_6Si_6ThLi$: C 49.25, H 8.02, N 2.25. Found: C 43.76, H 7.09, N 1.68. Low values were observed across multiple runs and suggests incomplete combustion which has been problematic for high silicon-containing actinide species. [13,20,21,28,47] The calculated C:H:N ratio of $C_{51}H_{98.5}N_{1.5}$ is close to the expected value.

Synthesis of [Na(crown)$_2$][Cp″$_3$Th]. Cp″$_3$Th (48 mg, 0.056 mmol) and 18-crown-6 (28 mg, 0.11 mmol) were dissolved in THF (1 mL) and transferred into a vial containing a Na (22 mg, 0.96 mmol) smear along the wall. The vial was placed in the freezer at −35 °C overnight. The inky blue/green solution was filtered and dried under vacuum. The solids were dissolved in Et_2O (3 mL) and layered under hexane at −35 °C. Dark blue crystals suitable for X-ray diffraction grew overnight (58 mg, 73%). ^{1}H NMR (THF-d_8): δ 4.42 (s, 9H, $C_5H_3R_2$), 3.58 (s, 35H, OCH_2CH_2O) 0.18 ppm (s, 54H, SiMe_3). ^{13}C (THF-d_8): δ 120.07 ($C_5H_3R_2$), 115.33 ($C_5H_3R_2$), 114.22 ($C_5H_3R_2$), 70.64 (OCH_2CH_2O), 1.76 ppm (SiMe_3). IR: 2943m, 2886m 1352m, 1233s, 1169s, 1105s, 1072s, 965m, 910s, 822s, 783s, 742m, 673m cm^{-1}. UV-visible (THF): 658 nm (12,000 $M^{-1}cm^{-1}$). Anal Calcd for $C_{57}H_{111}O_{12}Si_6ThNa$: C 48.48, H 7.92. Found: C 44.23, H 6.87. Low values were observed across multiple runs and suggests incomplete combustion which has been problematic for high silicon-containing actinide species.[13,20,21,28,47] The calculated C:H ratio was $C_{57}H_{105.5}$. The combustion values are suggestive of bulk formulation as [Na(crown)$(THF)_x$][Cp″$_3$Th] but crystallization repeatedly afforded single crystals of [Na(crown)$_2$][Cp″$_3$Th].

Synthesis of [Rb(crypt)][Cp″$_3$Th]. As above, Cp″$_3$Th (50 mg, 0.058 mmol) and crypt (22 mg, 0.058 mmol) were reacted with a Rb (14 mg, 0.16 mmol) smear at −35 °C. Dark blue/red dichroic crystals were grown overnight from Et_2O/hexane at −35 °C (47 mg, 61%). ^{1}H NMR (THF-d_8): δ 4.84 (s, 9H, $C_5H_3R_2$), 3.54 (s, 14H, OCH_2CH_2O), 3.49 (m, 13H, crypt), 2.51 (m, 15H, crypt), 0.44 ppm (s, 53H, SiMe_3). ^{13}C (THF-d_8): δ 120.4 ($C_5H_3R_2$), 114.9 ($C_5H_3R_2$), 111.9

($C_5H_3R_2$), 71.3 (crypt), 68.4 (crypt), 54.9 (crypt), 2.2 ppm ($SiMe_3$). ^{29}Si NMR (THF-d_8): δ −15.69 ppm ($SiMe_3$). UV-visible (THF): 656 nm (19,000 $M^{-1}cm^{-1}$). IR: 2944m, 2884m, 2810m, 1352m, 1296m, 1233s, 1171s, 1102s, 1070s, 947s, 909s, 818s, 782m, 742s, 674s cm^{-1}. Anal Calcd for $C_{51}H_{99}N_2O_6Si_6ThRb$: C 46.32, H 7.55, N 2.12. Found: C 43.80, H 7.20, N 2.53. Low C values were observed across multiple runs and suggests incomplete combustion or carbide formation which has been problematic for high silicon-containing actinide species.[13,20,21,28,47] The calculated C:H:N ratio of $C_{51}H_{99.9}N_{2.5}$ is close to the expected value.

Synthesis of [Cs(crypt)][Cp″$_3$Th]. As above, Cp″$_3$Th (52 mg, 0.060 mmol) and crypt (22 mg, 0.058 mmol) were reacted with a Cs (10 mg, 0.075 mmol) smear at −35 °C. Dark blue/red dichroic crystals were grown overnight from Et_2O/hexane at −35 °C (43 mg, 54%). ^{1}H NMR (THF-d_8): δ 5.51 (s, 9H, $C_5H_3R_2$), 3.57 (m, 18H, OCH_2CH_2O) (overlapping with THF), 3.50 (m, 7H, crypt), 2.54 (m, 9H, crypt), 0.87 ppm (s, 37H, $SiMe_3$). ^{13}C (THF-d_8): δ 121.9 ($C_5H_3R_2$), 117.0 ($C_5H_3R_2$), 115.2 ($C_5H_3R_2$), 71.4 (OCH_2CH_2O), 68.3 (crypt), 54.6 (crypt), 1.5 ppm ($SiMe_3$). ^{29}Si NMR (THF-d_8): δ −14.88 ppm ($SiMe_3$). ^{133}Cs NMR (THF-d_8): δ 20 ppm (br, $\nu_{1/2}$ = 3600 Hz). UV-visible (THF): 658 nm (14,000 $M^{-1}cm^{-1}$). IR: 2944m, 2884m, 2809m, 1349m, 1295m, 1233s, 1171s, 1098s, 1064s, 942m, 909s, 817s, 782m, 742s, 674s cm^{-1}. Anal Calcd for $C_{51}H_{99}N_2O_6Si_6ThCs$: C 44.72, H 7.28, N 2.05. Found: C 40.81, H 6.59, N 1.57. Low values were observed across multiple runs and suggests incomplete combustion which has been problematic for high silicon-containing actinide species.[13,20,21,28,47] The calculated C:H:N ratio of $C_{51}H_{98.1}N_{1.7}$ is close to the expected value.

Synthesis of [K(crown)(THF)$_2$][Cp″$_3$Th] from Cp″$_3$ThCl. Cp″$_3$ThCl (77 mg, 0.093 mmol) and 18-crown-6 (24 mg, 0.091 mmol) were dissolved in THF (3 mL). Pre-cooled KC_8 (31 mg, 0.229 mmol) was added and the reaction was stirred for approximately 5 minutes. The initially

colorless solution turned bright blue, followed by the change to inky blue/green. Black solids were removed via centrifugation and the solution was dried under vacuum. The product was extracted in Et_2O, filtered, and dried. The solids were washed with hexane to remove Cp''_3Th and dried. Dark blue crystals of $[K(crown)(THF)_2][Cp''_3Th]$[13] were grown overnight from Et_2O/hexane at −35 °C (58 mg, 50%).

Reaction of Cp''_3ThBr with Ba. Cp''_3ThBr (47 mg, 0.054 mmol) was dissolved in THF (3 mL). Freshly shaved Ba powder (excess) was added and the solution was stirred vigorously. After approximately four hours of stirring, the solution began to turn blue. No further color changes were observed after an additional 5 hours of stirring. Cp''_3Th was identified by UV-visible spectroscopy.[27,28]

Reaction of Cp''_3Th with Ba. Cp''_3Th (26 mg, 0.030 mmol) was dissolved in THF (3 mL). Freshly shaved Ba powder (excess) was added and the solution was placed in the freezer overnight. The solution was stirred vigorously for approximately two hours of stirring at which point the solution began to turn dark blue/green. The solution was dried and the solids were washed with hexane to remove Cp''_3Th. The remaining solids were extracted into THF and the presence of $[Cp''_3Th]^{1-}$ was confirmed by UV-visible spectroscopy.

Reaction of Cp''_3ThBr with Ba and crown. Cp''_3ThBr (42 mg, 0.048 mmol) and crown (13 mg, 0.049 mmol) were dissolved in THF (3 mL). Freshly shaved Ba powder (excess) was added and the solution was stirred vigorously. After approximately 10 minutes of stirring, the solution began to turn blue. The solution was placed in the freezer overnight and maintained the dark blue color of Cp''_3Th. The solution was stirred again at which point a dark blue/green color developed. The solution was stirred for one hour and the presence of $[Cp''_3Th]^{1-}$ was confirmed by UV-Visible spectroscopy.

Synthesis of [K(crown)][Cp″]. In a J-Young NMR tube, 18-crown-6 (8.7 mg, 0.033 mmol) was added to a solution of KCp″ (8.2 mg, 0.033 mmol) in THF-d_8 (1 mL). The solution was mixed by inversion multiple times before the spectrum was collected. ^{1}H spectroscopy showed quantitative conversion to [K(crown)][Cp″]. ^{1}H NMR (THF-d_8): δ 6.10 (s, 1H, $C_5H_3(SiMe_3)_2$), 5.95 (m, 2H, $C_5H_3(SiMe_3)_2$), 3.51 (s, 24H, O–CH_2CH_2–O), 0.06 ppm (s, 18H, SiMe_3). Cf. KCp″ ^{1}H NMR (THF-d_8): δ6.09 (s, 1H, $C_5H_3(SiMe_3)_2$), 6.00 (m, 2H, $C_5H_3(SiMe_3)_2$), 0.07 ppm (s, 18H, SiMe_3).

Crystallographic Details

Table 3.6: Crystal data and structure refinement for [Na(crown)$_2$][Cp″$_3$Th], [Rb(crypt)][Cp″$_3$Th], and [Cs(crypt)][Cp″$_3$Th].

	[Na(crown)$_2$][Cp″$_3$Th]	[Rb(crypt)][Cp″$_3$Th]	[Cs(crypt)][Cp″$_3$Th]
Identification code	Jcw35	Nrr6	Jcw48
Empirical formula	C_{57} H_{111} Na O_{12} Si_6 Th	C_{51} H_{99} N_2 O_6 Rb Si_6 Th	C_{51} H_{99} Cs N_2 O_6 Si_6 Th
Formula weight	1412.02	1322.37	1369.81
Temperature (K)	133(2)	88(2)	133(2)
Wavelength (Å)	0.71073	0.71073	0.71073
Crystal system	Triclinic	Triclinic	Triclinic
Space group	$P\bar{1}$	$P\bar{1}$	$P\bar{1}$
a (Å)	13.8938(13)	12.1971(13)	12.1953(8)
b (Å)	14.4588(13)	12,7473(13)	12.7501(8)
c (Å)	18.3420(17)	22.242(2)	22.2212(14)
α (°)	74.4602(14)	100.6648(130	100.6711(10)
β (°)	84.1350(14)	104.4725(13)	104.3758(9)
γ (°)	83.5214(14)	95.7340(13)	95.7421(10)
Volume (Å^3)	3517.3(6)	3251.6(6)	3250.2(4)
Z	2	2	2
Calc. Density (mg/m^3)	1.333	1.351	1.400
Absorption coefficient (mm^{-1})	2.280	3.189	2.998

F(000)	1468	1356	1392
Crystal color	Red	Blue	Blue
Crystal size (mm^3)	0.289 x 0.258 x 0.153	0.435 x 0.316 x 0.296	0.182 x 0.110 x 0.082
θ range for data collection (°)	1.156 to 25.350	1.645 to 29.044	1.645 to 28.322
Index ranges	$-16 \le h \le 16$, $-17 \le k \le 17$, $-22 \le l \le 22$	$-16 \le h \le 16$, $-17 \le k \le 17$, $-30 \le l \le 30$	$-16 \le h \le 16$, $-17 \le k \le 17$, $-29 \le l \le 29$
Reflections collected	39152	40057	43962
Independent reflections	12873	15844	16125
Completeness to θ = 25.500°	100.0	99.9	100.0
Absorption correction	Semi-empirical from equivalents	Semi-empirical from equivalents	Semi-empirical from equivalents
Max. and min. transmission	0.6465 and 0.5424	0.4085 and 0.2845	0.6471 and 0.5186
Refinement method	Full-matrix least-squares on F^2	Full-matrix least-squares on F^2	Full-matrix least-squares on F^2
Data / restraints / parameters	12873 / 36 / 598	15844 / 0 / 622	16125 / 0 / 622
Goodness-of-fit on F^2	1.044	1.019	1.024
Final R indices [$I>2\sigma(I)$ = 10983 data]	R1 = 0.0479, wR2 = 0.1153	R1 = 0.0212, wR2 = 0.0462	R1 = 0.0382, wR2 = 0.0809
R indices (all data)	R1 = 0.0608, wR2 = 0.1218	R1 = 0.0256, wR2 = 0.0475	R1 = 0.0556, wR2 = 0.0866
Data cutoff (Å)	0.80	0.73	0.75
Largest diff. peak and hole	2.464 and -2.311	1.117 and -0.690	1.613 and -2.543

X-ray Data Collection, Structure Solution and Refinement for $[Na(crown)_2][Cp''_3Th]$.

A red crystal of approximate dimensions 0.153 x 0.258 x 0.289 mm was mounted in a cryoloop and transferred to a Bruker SMART APEX II diffractometer. The APEX2[53] program package was used to determine the unit-cell parameters and for data collection (30 sec/frame scan

time). The raw frame data was processed using SAINT[54] and SADABS[55] to yield the reflection data file. Subsequent calculations were carried out using the SHELXTL[56] program package. There were no systematic absences nor any diffraction symmetry other than the Friedel condition. The centrosymmetric triclinic space group $P\bar{1}$ was assigned and later determined to be correct.

The structure was solved by direct methods and refined on F^2 by full-matrix least-squares techniques. The analytical scattering factors[57] for neutral atoms were used throughout the analysis. Hydrogen atoms were included using a riding model. Disordered atoms were included using multiple components, partial site-occupancy-factors, thermal (EADP) and geometric restraints (DFIX).[56]

Least-squares analysis yielded wR2 = 0.1218 and Goof = 1.044 for 598 variables refined against 12873 data (0.80 Å), R1 = 0.0479 for those 10989 data with $I > 2.0\sigma(I)$.

Table 3.7: Bond lengths [Å] and angles [°] for $[Na(crown)_2][Cp''_3Th]$.

Th(1)-Cnt1	2.527	Th(1)-C(23)	2.826(6)
Th(1)-Cnt2	2.521	Th(1)-C(5)	2.826(6)
Th(1)-Cnt3	2.531	Th(1)-C(27)	2.832(5)
Th(1)-C(13)	2.754(6)	Si(1)-C(1)	1.849(7)
Th(1)-C(2)	2.757(6)	Si(1)-C(7)	1.866(9)
Th(1)-C(24)	2.761(6)	Si(1)-C(6)	1.881(8)
Th(1)-C(25)	2.785(6)	Si(1)-C(8)	1.882(8)
Th(1)-C(12)	2.796(6)	Si(2)-C(3)	1.837(7)
Th(1)-C(14)	2.798(6)	Si(2)-C(11)	1.861(7)
Th(1)-C(3)	2.800(6)	Si(2)-C(9)	1.863(9)
Th(1)-C(4)	2.807(6)	Si(2)-C(10)	1.877(8)
Th(1)-C(16)	2.813(6)	Si(3)-C(12)	1.847(7)
Th(1)-C(15)	2.816(6)	Si(3)-C(17)	1.865(9)
Th(1)-C(1)	2.818(6)	Si(3)-C(19)	1.866(8)
Th(1)-C(26)	2.818(6)	Si(3)-C(18)	1.875(8)

Si(4)-C(14)	1.839(6)	Na(1)-O(3)	2.617(6)
Si(4)-C(20)	1.861(8)	Na(1)-O(5)	2.652(6)
Si(4)-C(22)	1.879(7)	O(1)-C(34)	1.414(8)
Si(4)-C(21)	1.882(9)	O(1)-C(45)	1.421(8)
Si(5)-C(23)	1.846(6)	O(2)-C(35)	1.410(8)
Si(5)-C(28)	1.871(7)	O(2)-C(36)	1.412(8)
Si(5)-C(30)	1.872(7)	O(3)-C(38)	1.344(11)
Si(5)-C(29)	1.879(7)	O(3)-C(37)	1.415(14)
Si(6)-C(25)	1.848(6)	O(4)-C(39)	1.403(11)
Si(6)-C(33)	1.861(7)	O(4)-C(40)	1.410(9)
Si(6)-C(32)	1.869(7)	O(5)-C(42)	1.398(9)
Si(6)-C(31)	1.883(8)	O(5)-C(41)	1.427(10)
C(1)-C(2)	1.419(9)	O(6)-C(44)	1.414(8)
C(1)-C(5)	1.431(9)	O(6)-C(43)	1.417(8)
C(2)-C(3)	1.438(9)	C(34)-C(35)	1.512(10)
C(3)-C(4)	1.434(9)	C(36)-C(37)	1.452(14)
C(4)-C(5)	1.383(9)	C(38)-C(39)	1.403(13)
C(12)-C(16)	1.423(9)	C(40)-C(41)	1.494(12)
C(12)-C(13)	1.433(8)	C(42)-C(43)	1.488(10)
C(13)-C(14)	1.426(9)	C(44)-C(45)	1.498(9)
C(14)-C(15)	1.423(9)	O(7)-C(57)	1.401(9)
C(15)-C(16)	1.390(9)	O(7)-C(46)	1.409(9)
C(23)-C(24)	1.421(9)	O(8)-C(47)	1.417(9)
C(23)-C(27)	1.426(8)	O(8)-C(48)	1.419(9)
C(24)-C(25)	1.447(8)	O(9)-C(50)	1.405(9)
C(25)-C(26)	1.424(8)	O(9)-C(49)	1.417(9)
C(26)-C(27)	1.388(9)	O(10)-C(52)	1.403(9)
Na(1)-O(12)	2.429(13)	O(10)-C(51)	1.403(9)
Na(1)-O(6)	2.519(5)	O(11)-C(54)	1.375(9)
Na(1)-O(2)	2.520(5)	O(11)-C(53)	1.402(9)
Na(1)-O(7B)	2.541(19)	O(12)-C(56)	1.407(9)
Na(1)-O(7)	2.579(13)	O(12)-C(55)	1.419(9)
Na(1)-O(4)	2.583(5)	C(46)-C(47)	1.492(9)
Na(1)-O(1)	2.589(5)	C(48)-C(49)	1.438(9)
Na(1)-O(12B)	2.593(19)	C(50)-C(51)	1.470(9)

C(52)-C(53)	1.470(9)	C(13)-Th(1)-C(14)	29.77(19)
C(54)-C(55)	1.466(9)	C(2)-Th(1)-C(14)	132.55(18)
C(56)-C(57)	1.500(9)	C(24)-Th(1)-C(14)	100.00(18)
O(7B)-C(57B)	1.410(10)	C(25)-Th(1)-C(14)	103.92(19)
O(7B)-C(46B)	1.422(10)	C(12)-Th(1)-C(14)	49.89(18)
O(8B)-C(47B)	1.436(10)	C(13)-Th(1)-C(3)	100.29(19)
O(8B)-C(48B)	1.445(9)	C(2)-Th(1)-C(3)	29.98(18)
O(9B)-C(50B)	1.441(10)	C(24)-Th(1)-C(3)	134.49(18)
O(9B)-C(49B)	1.457(9)	C(25)-Th(1)-C(3)	126.04(18)
O(10B)-C(52B)	1.412(9)	C(12)-Th(1)-C(3)	101.4(2)
O(10B)-C(51B)	1.433(9)	C(14)-Th(1)-C(3)	125.06(19)
O(11B)-C(54B)	1.357(9)	C(13)-Th(1)-C(4)	73.42(19)
O(11B)-C(53B)	1.419(9)	C(2)-Th(1)-C(4)	47.72(18)
O(12B)-C(56B)	1.416(10)	C(24)-Th(1)-C(4)	164.05(18)
O(12B)-C(55B)	1.417(10)	C(25)-Th(1)-C(4)	146.59(17)
C(46B)-C(47B)	1.494(10)	C(12)-Th(1)-C(4)	84.08(19)
C(48B)-C(49B)	1.490(10)	C(14)-Th(1)-C(4)	95.60(19)
C(50B)-C(51B)	1.505(10)	C(3)-Th(1)-C(4)	29.63(18)
C(52B)-C(53B)	1.496(10)	C(13)-Th(1)-C(16)	47.83(18)
C(54B)-C(55B)	1.474(10)	C(2)-Th(1)-C(16)	158.3(2)
C(56B)-C(57B)	1.515(10)	C(24)-Th(1)-C(16)	75.38(18)
		C(25)-Th(1)-C(16)	99.76(18)
Cnt1-Th(1)-Cnt2	120.0	C(12)-Th(1)-C(16)	29.39(19)
Cnt1-Th(1)-Cnt3	120.1	C(14)-Th(1)-C(16)	48.49(17)
Cnt2-Th(1)-Cnt3	119.9	C(3)-Th(1)-C(16)	128.39(19)
C(13)-Th(1)-C(2)	119.76(19)	C(4)-Th(1)-C(16)	113.43(19)
C(13)-Th(1)-C(24)	119.82(18)	C(13)-Th(1)-C(15)	47.7(2)
C(2)-Th(1)-C(24)	120.39(18)	C(2)-Th(1)-C(15)	161.57(18)
C(13)-Th(1)-C(25)	132.53(19)	C(24)-Th(1)-C(15)	73.37(18)
C(2)-Th(1)-C(25)	100.30(18)	C(25)-Th(1)-C(15)	86.64(18)
C(24)-Th(1)-C(25)	30.25(17)	C(12)-Th(1)-C(15)	48.4(2)
C(13)-Th(1)-C(12)	29.91(17)	C(14)-Th(1)-C(15)	29.36(18)
C(2)-Th(1)-C(12)	129.99(19)	C(3)-Th(1)-C(15)	147.32(19)
C(24)-Th(1)-C(12)	103.46(18)	C(4)-Th(1)-C(15)	120.96(19)
C(25)-Th(1)-C(12)	129.15(19)	C(16)-Th(1)-C(15)	28.59(18)

C(13)-Th(1)-C(1)	103.48(18)	C(24)-Th(1)-C(5)	156.24(18)
C(2)-Th(1)-C(1)	29.48(18)	C(25)-Th(1)-C(5)	125.99(17)
C(24)-Th(1)-C(1)	128.61(18)	C(12)-Th(1)-C(5)	97.81(18)
C(25)-Th(1)-C(1)	99.60(18)	C(14)-Th(1)-C(5)	85.61(18)
C(12)-Th(1)-C(1)	127.16(18)	C(3)-Th(1)-C(5)	48.52(18)
C(14)-Th(1)-C(1)	105.69(18)	C(4)-Th(1)-C(5)	28.42(18)
C(3)-Th(1)-C(1)	49.97(19)	C(16)-Th(1)-C(5)	123.16(18)
C(4)-Th(1)-C(1)	48.42(19)	C(15)-Th(1)-C(5)	114.96(18)
C(16)-Th(1)-C(1)	151.05(18)	C(1)-Th(1)-C(5)	29.38(18)
C(15)-Th(1)-C(1)	132.80(18)	C(26)-Th(1)-C(5)	112.05(17)
C(13)-Th(1)-C(26)	161.63(19)	C(23)-Th(1)-C(5)	151.34(18)
C(2)-Th(1)-C(26)	73.76(18)	C(13)-Th(1)-C(27)	158.50(17)
C(24)-Th(1)-C(26)	47.90(17)	C(2)-Th(1)-C(27)	76.00(17)
C(25)-Th(1)-C(26)	29.44(17)	C(24)-Th(1)-C(27)	47.63(17)
C(12)-Th(1)-C(26)	150.04(18)	C(25)-Th(1)-C(27)	48.46(18)
C(14)-Th(1)-C(26)	132.04(19)	C(12)-Th(1)-C(27)	129.01(17)
C(3)-Th(1)-C(26)	96.87(18)	C(14)-Th(1)-C(27)	147.58(18)
C(4)-Th(1)-C(26)	121.46(17)	C(3)-Th(1)-C(27)	87.30(18)
C(16)-Th(1)-C(26)	123.27(18)	C(4)-Th(1)-C(27)	116.82(18)
C(15)-Th(1)-C(26)	115.73(18)	C(16)-Th(1)-C(27)	112.13(17)
C(1)-Th(1)-C(26)	82.68(17)	C(15)-Th(1)-C(27)	120.21(17)
C(13)-Th(1)-C(23)	130.38(17)	C(1)-Th(1)-C(27)	96.81(17)
C(2)-Th(1)-C(23)	103.93(18)	C(26)-Th(1)-C(27)	28.43(17)
C(24)-Th(1)-C(23)	29.43(18)	C(23)-Th(1)-C(27)	29.19(16)
C(25)-Th(1)-C(23)	49.76(17)	C(5)-Th(1)-C(27)	123.00(17)
C(12)-Th(1)-C(23)	103.23(17)	C(1)-Si(1)-C(7)	111.8(3)
C(14)-Th(1)-C(23)	122.89(18)	C(1)-Si(1)-C(6)	108.5(4)
C(3)-Th(1)-C(23)	107.53(18)	C(7)-Si(1)-C(6)	108.5(4)
C(4)-Th(1)-C(23)	135.54(19)	C(1)-Si(1)-C(8)	111.9(3)
C(16)-Th(1)-C(23)	83.00(17)	C(7)-Si(1)-C(8)	111.3(4)
C(15)-Th(1)-C(23)	93.61(18)	C(6)-Si(1)-C(8)	104.4(4)
C(1)-Th(1)-C(23)	125.93(17)	C(3)-Si(2)-C(11)	110.4(3)
C(26)-Th(1)-C(23)	48.13(17)	C(3)-Si(2)-C(9)	115.2(3)
C(13)-Th(1)-C(5)	75.48(18)	C(11)-Si(2)-C(9)	108.6(4)
C(2)-Th(1)-C(5)	47.42(18)	C(3)-Si(2)-C(10)	108.2(3)

C(11)-Si(2)-C(10)	105.8(4)	C(4)-C(3)-C(2)	103.3(6)
C(9)-Si(2)-C(10)	108.2(5)	C(4)-C(3)-Si(2)	129.0(5)
C(12)-Si(3)-C(17)	107.8(4)	C(2)-C(3)-Si(2)	124.3(5)
C(12)-Si(3)-C(19)	112.1(3)	C(4)-C(3)-Th(1)	75.5(4)
C(17)-Si(3)-C(19)	106.2(4)	C(2)-C(3)-Th(1)	73.4(3)
C(12)-Si(3)-C(18)	112.6(3)	Si(2)-C(3)-Th(1)	131.4(3)
C(17)-Si(3)-C(18)	106.9(4)	C(5)-C(4)-C(3)	110.3(6)
C(19)-Si(3)-C(18)	110.9(4)	C(5)-C(4)-Th(1)	76.5(4)
C(14)-Si(4)-C(20)	112.7(3)	C(3)-C(4)-Th(1)	74.9(3)
C(14)-Si(4)-C(22)	106.5(3)	C(4)-C(5)-C(1)	110.1(6)
C(20)-Si(4)-C(22)	107.0(4)	C(4)-C(5)-Th(1)	75.0(3)
C(14)-Si(4)-C(21)	112.6(3)	C(1)-C(5)-Th(1)	75.0(3)
C(20)-Si(4)-C(21)	110.6(5)	C(16)-C(12)-C(13)	104.5(6)
C(22)-Si(4)-C(21)	106.9(4)	C(16)-C(12)-Si(3)	125.4(5)
C(23)-Si(5)-C(28)	110.9(3)	C(13)-C(12)-Si(3)	125.4(5)
C(23)-Si(5)-C(30)	113.2(3)	C(16)-C(12)-Th(1)	76.0(3)
C(28)-Si(5)-C(30)	111.0(3)	C(13)-C(12)-Th(1)	73.4(3)
C(23)-Si(5)-C(29)	108.2(3)	Si(3)-C(12)-Th(1)	134.4(3)
C(28)-Si(5)-C(29)	108.3(4)	C(14)-C(13)-C(12)	111.2(6)
C(30)-Si(5)-C(29)	105.0(3)	C(14)-C(13)-Th(1)	76.8(3)
C(25)-Si(6)-C(33)	117.5(3)	C(12)-C(13)-Th(1)	76.7(3)
C(25)-Si(6)-C(32)	108.7(3)	C(15)-C(14)-C(13)	104.5(5)
C(33)-Si(6)-C(32)	109.5(3)	C(15)-C(14)-Si(4)	125.9(5)
C(25)-Si(6)-C(31)	108.1(3)	C(13)-C(14)-Si(4)	124.5(5)
C(33)-Si(6)-C(31)	105.3(4)	C(15)-C(14)-Th(1)	76.0(3)
C(32)-Si(6)-C(31)	107.3(4)	C(13)-C(14)-Th(1)	73.4(3)
C(2)-C(1)-C(5)	104.0(5)	Si(4)-C(14)-Th(1)	135.0(3)
C(2)-C(1)-Si(1)	126.1(5)	C(16)-C(15)-C(14)	110.0(6)
C(5)-C(1)-Si(1)	127.1(5)	C(16)-C(15)-Th(1)	75.6(3)
C(2)-C(1)-Th(1)	72.9(3)	C(14)-C(15)-Th(1)	74.6(3)
C(5)-C(1)-Th(1)	75.6(3)	C(15)-C(16)-C(12)	109.8(6)
Si(1)-C(1)-Th(1)	130.6(3)	C(15)-C(16)-Th(1)	75.8(3)
C(1)-C(2)-C(3)	112.3(5)	C(12)-C(16)-Th(1)	74.6(3)
C(1)-C(2)-Th(1)	77.6(3)	C(24)-C(23)-C(27)	105.1(5)
C(3)-C(2)-Th(1)	76.7(3)	C(24)-C(23)-Si(5)	125.2(4)

C(27)-C(23)-Si(5)	125.7(5)	O(7B)-Na(1)-O(1)	89.6(4)
C(24)-C(23)-Th(1)	72.8(3)	O(7)-Na(1)-O(1)	83.4(3)
C(27)-C(23)-Th(1)	75.6(3)	O(4)-Na(1)-O(1)	169.57(19)
Si(5)-C(23)-Th(1)	133.9(3)	O(6)-Na(1)-O(12B)	148.1(4)
C(23)-C(24)-C(25)	110.8(5)	O(2)-Na(1)-O(12B)	76.8(3)
C(23)-C(24)-Th(1)	77.8(3)	O(7B)-Na(1)-O(12B)	66.0(5)
C(25)-C(24)-Th(1)	75.8(3)	O(4)-Na(1)-O(12B)	84.7(4)
C(26)-C(25)-C(24)	104.2(5)	O(1)-Na(1)-O(12B)	85.9(4)
C(26)-C(25)-Si(6)	129.3(4)	O(12)-Na(1)-O(3)	101.7(3)
C(24)-C(25)-Si(6)	122.2(4)	O(6)-Na(1)-O(3)	106.8(2)
C(26)-C(25)-Th(1)	76.6(3)	O(2)-Na(1)-O(3)	62.85(17)
C(24)-C(25)-Th(1)	74.0(3)	O(7B)-Na(1)-O(3)	144.0(4)
Si(6)-C(25)-Th(1)	132.2(3)	O(7)-Na(1)-O(3)	151.6(3)
C(27)-C(26)-C(25)	110.1(5)	O(4)-Na(1)-O(3)	62.88(18)
C(27)-C(26)-Th(1)	76.3(3)	O(1)-Na(1)-O(3)	123.42(18)
C(25)-C(26)-Th(1)	74.0(3)	O(12B)-Na(1)-O(3)	99.5(4)
C(26)-C(27)-C(23)	109.8(5)	O(12)-Na(1)-O(5)	124.0(3)
C(26)-C(27)-Th(1)	75.2(3)	O(6)-Na(1)-O(5)	62.89(16)
C(23)-C(27)-Th(1)	75.2(3)	O(2)-Na(1)-O(5)	150.22(18)
O(12)-Na(1)-O(6)	149.4(3)	O(7B)-Na(1)-O(5)	73.3(4)
O(12)-Na(1)-O(2)	83.8(3)	O(7)-Na(1)-O(5)	72.5(3)
O(6)-Na(1)-O(2)	99.38(17)	O(4)-Na(1)-O(5)	63.88(18)
O(6)-Na(1)-O(7B)	99.9(3)	O(1)-Na(1)-O(5)	120.20(18)
O(2)-Na(1)-O(7B)	135.8(4)	O(12B)-Na(1)-O(5)	131.2(4)
O(12)-Na(1)-O(7)	65.6(3)	O(3)-Na(1)-O(5)	97.9(2)
O(6)-Na(1)-O(7)	92.7(3)	C(34)-O(1)-C(45)	113.1(5)
O(2)-Na(1)-O(7)	135.1(3)	C(34)-O(1)-Na(1)	106.6(4)
O(12)-Na(1)-O(4)	79.8(3)	C(45)-O(1)-Na(1)	109.7(4)
O(6)-Na(1)-O(4)	123.22(19)	C(35)-O(2)-C(36)	114.6(5)
O(2)-Na(1)-O(4)	118.0(2)	C(35)-O(2)-Na(1)	121.8(4)
O(7B)-Na(1)-O(4)	82.5(4)	C(36)-O(2)-Na(1)	120.6(4)
O(7)-Na(1)-O(4)	89.2(3)	C(38)-O(3)-C(37)	106.2(9)
O(12)-Na(1)-O(1)	90.4(3)	C(38)-O(3)-Na(1)	116.0(5)
O(6)-Na(1)-O(1)	64.70(16)	C(37)-O(3)-Na(1)	118.4(7)
O(2)-Na(1)-O(1)	63.96(16)	C(39)-O(4)-C(40)	112.1(7)

C(39)-O(4)-Na(1)	113.9(5)	O(8)-C(48)-C(49)	106.0(11)
C(40)-O(4)-Na(1)	110.4(5)	O(9)-C(49)-C(48)	128.5(11)
C(42)-O(5)-C(41)	113.7(6)	O(9)-C(50)-C(51)	113.1(10)
C(42)-O(5)-Na(1)	110.3(4)	O(10)-C(51)-C(50)	105.8(9)
C(41)-O(5)-Na(1)	117.7(5)	O(10)-C(52)-C(53)	126.0(11)
C(44)-O(6)-C(43)	112.1(5)	O(11)-C(53)-C(52)	117.0(11)
C(44)-O(6)-Na(1)	118.0(4)	O(11)-C(54)-C(55)	119.8(11)
C(43)-O(6)-Na(1)	121.3(4)	O(12)-C(55)-C(54)	120.9(12)
O(1)-C(34)-C(35)	113.1(6)	O(12)-C(56)-C(57)	107.9(13)
O(2)-C(35)-C(34)	107.6(6)	O(7)-C(57)-C(56)	109.0(12)
O(2)-C(36)-C(37)	112.3(8)	C(57B)-O(7B)-C(46B)	113.3(17)
O(3)-C(37)-C(36)	111.2(10)	C(57B)-O(7B)-Na(1)	115.3(15)
O(3)-C(38)-C(39)	112.5(9)	C(46B)-O(7B)-Na(1)	123.4(14)
O(4)-C(39)-C(38)	111.8(9)	C(47B)-O(8B)-C(48B)	120.4(15)
O(4)-C(40)-C(41)	113.0(7)	C(50B)-O(9B)-C(49B)	104.8(13)
O(5)-C(41)-C(40)	108.2(7)	C(52B)-O(10B)-C(51B)	137.1(15)
O(5)-C(42)-C(43)	108.9(6)	C(54B)-O(11B)-C(53B)	111.5(15)
O(6)-C(43)-C(42)	108.6(6)	C(56B)-O(12B)-C(55B)	108.2(16)
O(6)-C(44)-C(45)	108.8(6)	C(56B)-O(12B)-Na(1)	107.4(14)
O(1)-C(45)-C(44)	107.2(5)	C(55B)-O(12B)-Na(1)	115.5(14)
C(57)-O(7)-C(46)	116.2(12)	O(7B)-C(46B)-C(47B)	113.3(17)
C(57)-O(7)-Na(1)	114.2(10)	O(8B)-C(47B)-C(46B)	109.7(16)
C(46)-O(7)-Na(1)	125.6(10)	O(8B)-C(48B)-C(49B)	123.3(17)
C(47)-O(8)-C(48)	107.4(10)	O(9B)-C(49B)-C(48B)	119.1(16)
C(50)-O(9)-C(49)	111.3(10)	O(9B)-C(50B)-C(51B)	104.4(12)
C(52)-O(10)-C(51)	116.8(10)	O(10B)-C(51B)-C(50B)	109.7(13)
C(54)-O(11)-C(53)	132.5(10)	O(10B)-C(52B)-C(53B)	112.3(16)
C(56)-O(12)-C(55)	111.4(11)	O(11B)-C(53B)-C(52B)	113.7(15)
C(56)-O(12)-Na(1)	114.9(9)	O(11B)-C(54B)-C(55B)	118.6(16)
C(55)-O(12)-Na(1)	115.2(9)	O(12B)-C(55B)-C(54B)	113.4(17)
O(7)-C(46)-C(47)	114.2(12)	O(12B)-C(56B)-C(57B)	108(2)
O(8)-C(47)-C(46)	109.0(11)	O(7B)-C(57B)-C(56B)	108.2(18)

X-ray Data Collection, Structure Solution and Refinement for [Rb(crypt)][Cp″$_3$Th].

A blue crystal of approximate dimensions 0.296 x 0.316 x 0.435 mm was mounted in a cryoloop and transferred to a Bruker SMART APEX II diffractometer. The APEX2[53] program package was used to determine the unit-cell parameters and for data collection (10 sec/frame scan time). The raw frame data was processed using SAINT[54] and SADABS[55] to yield the reflection data file. Subsequent calculations were carried out using the SHELXTL[56] program package. There were no systematic absences nor any diffraction symmetry other than the Friedel condition. The centrosymmetric triclinic space group $P\bar{1}$ was assigned and later determined to be correct.

The structure was solved by direct methods and refined on F^2 by full-matrix least-squares techniques. The analytical scattering factors[57] for neutral atoms were used throughout the analysis. Hydrogen atoms were included using a riding model.

Least-squares analysis yielded wR2 = 0.0475 and Goof = 1.019 for 622 variables refined against 15844 data (0.73 Å), R1 = 0.0212 for those 14524 data with I > 2.0σ(I).

Table 3.8: Bond lengths [Å] and angles [°] for [Rb(crypt)][Cp″$_3$Th].

Th(1)-Cnt1	2.536	Th(1)-C(4)	2.8567(19)
Th(1)-Cnt2	2.509	Th(1)-C(23)	2.860(2)
Th(1)-Cnt3	2.522	Si(1)-C(1)	1.848(2)
Th(1)-C(13)	2.739(2)	Si(1)-C(8)	1.868(2)
Th(1)-C(25)	2.7453(19)	Si(1)-C(7)	1.873(2)
Th(1)-C(24)	2.7556(19)	Si(1)-C(6)	1.886(2)
Th(1)-C(2)	2.7607(19)	Si(2)-C(3)	1.849(2)
Th(1)-C(12)	2.770(2)	Si(2)-C(9)	1.868(2)
Th(1)-C(1)	2.7774(19)	Si(2)-C(11)	1.877(2)
Th(1)-C(26)	2.7825(19)	Si(2)-C(10)	1.885(2)
Th(1)-C(16)	2.8029(19)	Si(3)-C(12)	1.842(2)
Th(1)-C(14)	2.8087(19)	Si(3)-C(19)	1.873(2)
Th(1)-C(5)	2.8139(19)	Si(3)-C(18)	1.874(2)
Th(1)-C(15)	2.8208(19)	Si(3)-C(17)	1.880(2)
Th(1)-C(3)	2.8502(19)	Si(4)-C(14)	1.850(2)
Th(1)-C(27)	2.853(2)	Si(4)-C(20)	1.869(2)

Si(4)-C(21)	1.870(2)	O(2)-C(38)	1.425(3)
Si(4)-C(22)	1.880(2)	O(2)-C(37)	1.428(3)
Si(5)-C(23)	1.852(2)	O(3)-C(41)	1.421(3)
Si(5)-C(30)	1.867(2)	O(3)-C(42)	1.430(3)
Si(5)-C(29)	1.870(2)	O(4)-C(43)	1.423(3)
Si(5)-C(28)	1.882(2)	O(4)-C(44)	1.430(3)
Si(6)-C(25)	1.848(2)	O(5)-C(47)	1.427(2)
Si(6)-C(32)	1.869(2)	O(5)-C(48)	1.428(2)
Si(6)-C(33)	1.875(2)	O(6)-C(50)	1.423(3)
Si(6)-C(31)	1.878(2)	O(6)-C(49)	1.432(3)
C(1)-C(5)	1.439(3)	N(1)-C(34)	1.469(3)
C(1)-C(2)	1.440(3)	N(1)-C(40)	1.473(3)
C(2)-C(3)	1.432(3)	N(1)-C(46)	1.479(3)
C(3)-C(4)	1.426(3)	N(2)-C(51)	1.468(3)
C(4)-C(5)	1.401(3)	N(2)-C(39)	1.475(3)
C(12)-C(16)	1.437(3)	N(2)-C(45)	1.480(3)
C(12)-C(13)	1.447(3)	C(34)-C(35)	1.505(3)
C(13)-C(14)	1.434(3)	C(36)-C(37)	1.496(3)
C(14)-C(15)	1.430(3)	C(38)-C(39)	1.490(4)
C(15)-C(16)	1.401(3)	C(40)-C(41)	1.511(3)
C(23)-C(27)	1.426(3)	C(42)-C(43)	1.506(3)
C(23)-C(24)	1.431(3)	C(44)-C(45)	1.506(3)
C(24)-C(25)	1.439(3)	C(46)-C(47)	1.505(3)
C(25)-C(26)	1.443(3)	C(48)-C(49)	1.497(3)
C(26)-C(27)	1.401(3)	C(50)-C(51)	1.514(3)
Rb(1)-O(1)	2.8662(15)		
Rb(1)-O(2)	2.8717(15)	Cnt1-Th(1)-Cnt2	122.7
Rb(1)-O(5)	2.8743(14)	Cnt1-Th(1)-Cnt3	119.7
Rb(1)-O(6)	2.8822(15)	Cnt2-Th(1)-Cnt3	117.6
Rb(1)-O(3)	2.8890(15)	C(13)-Th(1)-C(25)	132.68(6)
Rb(1)-O(4)	2.8918(15)	C(13)-Th(1)-C(24)	118.07(6)
Rb(1)-N(1)	3.0535(17)	C(25)-Th(1)-C(24)	30.32(6)
Rb(1)-N(2)	3.0564(19)	C(13)-Th(1)-C(2)	121.78(6)
O(1)-C(35)	1.424(3)	C(25)-Th(1)-C(2)	100.74(6)
O(1)-C(36)	1.434(3)	C(24)-Th(1)-C(2)	120.05(6)

C(13)-Th(1)-C(12)	30.46(6)	C(1)-Th(1)-C(5)	29.82(6)
C(25)-Th(1)-C(12)	125.95(6)	C(26)-Th(1)-C(5)	121.20(6)
C(24)-Th(1)-C(12)	99.49(6)	C(16)-Th(1)-C(5)	117.63(6)
C(2)-Th(1)-C(12)	131.61(6)	C(14)-Th(1)-C(5)	93.26(6)
C(13)-Th(1)-C(1)	98.38(6)	C(13)-Th(1)-C(15)	48.20(6)
C(25)-Th(1)-C(1)	128.26(6)	C(25)-Th(1)-C(15)	85.26(6)
C(24)-Th(1)-C(1)	136.88(6)	C(24)-Th(1)-C(15)	72.33(6)
C(2)-Th(1)-C(1)	30.13(6)	C(2)-Th(1)-C(15)	163.26(6)
C(12)-Th(1)-C(1)	101.64(6)	C(12)-Th(1)-C(15)	49.05(6)
C(13)-Th(1)-C(26)	162.92(6)	C(1)-Th(1)-C(15)	146.42(6)
C(25)-Th(1)-C(26)	30.24(6)	C(26)-Th(1)-C(15)	115.13(6)
C(24)-Th(1)-C(26)	48.36(6)	C(16)-Th(1)-C(15)	28.86(6)
C(2)-Th(1)-C(26)	73.21(6)	C(14)-Th(1)-C(15)	29.42(6)
C(12)-Th(1)-C(26)	145.89(6)	C(5)-Th(1)-C(15)	120.65(6)
C(1)-Th(1)-C(26)	98.43(6)	C(13)-Th(1)-C(3)	109.19(6)
C(13)-Th(1)-C(16)	48.53(6)	C(25)-Th(1)-C(3)	97.55(6)
C(25)-Th(1)-C(16)	96.17(6)	C(24)-Th(1)-C(3)	126.30(6)
C(24)-Th(1)-C(16)	71.67(6)	C(2)-Th(1)-C(3)	29.52(5)
C(2)-Th(1)-C(16)	159.86(6)	C(12)-Th(1)-C(3)	133.89(6)
C(12)-Th(1)-C(16)	29.87(6)	C(1)-Th(1)-C(3)	49.73(6)
C(1)-Th(1)-C(16)	129.99(6)	C(26)-Th(1)-C(3)	79.79(6)
C(26)-Th(1)-C(16)	120.00(6)	C(16)-Th(1)-C(3)	156.80(6)
C(13)-Th(1)-C(14)	29.92(6)	C(14)-Th(1)-C(3)	109.28(6)
C(25)-Th(1)-C(14)	104.82(6)	C(5)-Th(1)-C(3)	48.17(6)
C(24)-Th(1)-C(14)	100.12(6)	C(15)-Th(1)-C(3)	134.68(6)
C(2)-Th(1)-C(14)	134.53(6)	C(13)-Th(1)-C(27)	154.35(6)
C(12)-Th(1)-C(14)	50.36(6)	C(25)-Th(1)-C(27)	49.12(6)
C(1)-Th(1)-C(14)	122.26(6)	C(24)-Th(1)-C(27)	47.64(6)
C(26)-Th(1)-C(14)	134.01(6)	C(2)-Th(1)-C(27)	75.44(6)
C(16)-Th(1)-C(14)	48.79(6)	C(12)-Th(1)-C(27)	124.05(6)
C(13)-Th(1)-C(5)	73.75(6)	C(1)-Th(1)-C(27)	89.64(6)
C(25)-Th(1)-C(5)	145.41(6)	C(26)-Th(1)-C(27)	28.76(6)
C(24)-Th(1)-C(5)	166.59(6)	C(16)-Th(1)-C(27)	108.51(6)
C(2)-Th(1)-C(5)	48.14(6)	C(14)-Th(1)-C(27)	147.75(6)
C(12)-Th(1)-C(5)	88.29(6)	C(5)-Th(1)-C(27)	118.97(6)

C(15)-Th(1)-C(27)	119.18(6)	C(3)-Si(2)-C(9)	111.74(10)
C(3)-Th(1)-C(27)	94.61(6)	C(3)-Si(2)-C(11)	114.91(9)
C(13)-Th(1)-C(4)	80.63(6)	C(9)-Si(2)-C(11)	111.04(10)
C(25)-Th(1)-C(4)	122.02(6)	C(3)-Si(2)-C(10)	106.88(10)
C(24)-Th(1)-C(4)	152.34(6)	C(9)-Si(2)-C(10)	108.62(12)
C(2)-Th(1)-C(4)	47.63(6)	C(11)-Si(2)-C(10)	103.03(11)
C(12)-Th(1)-C(4)	105.39(6)	C(12)-Si(3)-C(19)	107.34(10)
C(1)-Th(1)-C(4)	48.65(6)	C(12)-Si(3)-C(18)	114.96(10)
C(26)-Th(1)-C(4)	108.58(6)	C(19)-Si(3)-C(18)	111.38(10)
C(16)-Th(1)-C(4)	129.09(6)	C(12)-Si(3)-C(17)	109.78(10)
C(14)-Th(1)-C(4)	86.90(6)	C(19)-Si(3)-C(17)	106.66(12)
C(5)-Th(1)-C(4)	28.60(6)	C(18)-Si(3)-C(17)	106.43(11)
C(15)-Th(1)-C(4)	116.04(6)	C(14)-Si(4)-C(20)	110.80(10)
C(3)-Th(1)-C(4)	28.93(6)	C(14)-Si(4)-C(21)	114.44(9)
C(27)-Th(1)-C(4)	121.70(6)	C(20)-Si(4)-C(21)	108.68(11)
C(13)-Th(1)-C(23)	127.02(6)	C(14)-Si(4)-C(22)	107.51(9)
C(25)-Th(1)-C(23)	50.02(6)	C(20)-Si(4)-C(22)	107.34(11)
C(24)-Th(1)-C(23)	29.44(5)	C(21)-Si(4)-C(22)	107.80(10)
C(2)-Th(1)-C(23)	103.04(6)	C(23)-Si(5)-C(30)	112.94(10)
C(12)-Th(1)-C(23)	98.57(6)	C(23)-Si(5)-C(29)	113.14(10)
C(1)-Th(1)-C(23)	109.80(6)	C(30)-Si(5)-C(29)	110.06(11)
C(26)-Th(1)-C(23)	48.32(6)	C(23)-Si(5)-C(28)	106.83(10)
C(16)-Th(1)-C(23)	79.64(6)	C(30)-Si(5)-C(28)	105.97(11)
C(14)-Th(1)-C(23)	122.22(6)	C(29)-Si(5)-C(28)	107.44(11)
C(5)-Th(1)-C(23)	138.83(6)	C(25)-Si(6)-C(32)	117.87(10)
C(15)-Th(1)-C(23)	92.81(6)	C(25)-Si(6)-C(33)	109.48(10)
C(3)-Th(1)-C(23)	123.39(6)	C(32)-Si(6)-C(33)	106.61(10)
C(27)-Th(1)-C(23)	28.91(5)	C(25)-Si(6)-C(31)	106.99(10)
C(4)-Th(1)-C(23)	150.35(6)	C(32)-Si(6)-C(31)	107.11(11)
C(1)-Si(1)-C(8)	110.90(10)	C(33)-Si(6)-C(31)	108.47(10)
C(1)-Si(1)-C(7)	112.46(10)	C(5)-C(1)-C(2)	104.38(17)
C(8)-Si(1)-C(7)	112.23(11)	C(5)-C(1)-Si(1)	127.10(15)
C(1)-Si(1)-C(6)	108.11(10)	C(2)-C(1)-Si(1)	124.23(15)
C(8)-Si(1)-C(6)	106.35(11)	C(5)-C(1)-Th(1)	76.50(11)
C(7)-Si(1)-C(6)	106.42(10)	C(2)-C(1)-Th(1)	74.29(10)

Si(1)-C(1)-Th(1)	132.21(9)	C(15)-C(16)-Th(1)	76.28(11)
C(3)-C(2)-C(1)	111.03(17)	C(12)-C(16)-Th(1)	73.82(11)
C(3)-C(2)-Th(1)	78.71(11)	C(27)-C(23)-C(24)	105.04(17)
C(1)-C(2)-Th(1)	75.58(11)	C(27)-C(23)-Si(5)	126.28(15)
C(4)-C(3)-C(2)	105.17(17)	C(24)-C(23)-Si(5)	123.24(14)
C(4)-C(3)-Si(2)	126.10(15)	C(27)-C(23)-Th(1)	75.26(11)
C(2)-C(3)-Si(2)	124.74(15)	C(24)-C(23)-Th(1)	71.24(11)
C(4)-C(3)-Th(1)	75.79(11)	Si(5)-C(23)-Th(1)	138.55(10)
C(2)-C(3)-Th(1)	71.77(10)	C(23)-C(24)-C(25)	111.52(17)
Si(2)-C(3)-Th(1)	134.76(9)	C(23)-C(24)-Th(1)	79.32(11)
C(5)-C(4)-C(3)	109.74(17)	C(25)-C(24)-Th(1)	74.44(11)
C(5)-C(4)-Th(1)	74.01(11)	C(24)-C(25)-C(26)	103.87(17)
C(3)-C(4)-Th(1)	75.28(11)	C(24)-C(25)-Si(6)	122.62(14)
C(4)-C(5)-C(1)	109.69(17)	C(26)-C(25)-Si(6)	129.28(15)
C(4)-C(5)-Th(1)	77.40(11)	C(24)-C(25)-Th(1)	75.24(11)
C(1)-C(5)-Th(1)	73.69(11)	C(26)-C(25)-Th(1)	76.30(11)
C(16)-C(12)-C(13)	104.37(16)	Si(6)-C(25)-Th(1)	131.11(9)
C(16)-C(12)-Si(3)	127.27(15)	C(27)-C(26)-C(25)	109.94(17)
C(13)-C(12)-Si(3)	126.14(15)	C(27)-C(26)-Th(1)	78.40(11)
C(16)-C(12)-Th(1)	76.32(11)	C(25)-C(26)-Th(1)	73.45(11)
C(13)-C(12)-Th(1)	73.56(11)	C(26)-C(27)-C(23)	109.63(17)
Si(3)-C(12)-Th(1)	127.91(9)	C(26)-C(27)-Th(1)	72.84(11)
C(14)-C(13)-C(12)	110.98(17)	C(23)-C(27)-Th(1)	75.83(11)
C(14)-C(13)-Th(1)	77.75(11)	O(1)-Rb(1)-O(2)	61.10(4)
C(12)-C(13)-Th(1)	75.98(11)	O(1)-Rb(1)-O(5)	95.33(4)
C(15)-C(14)-C(13)	104.98(17)	O(2)-Rb(1)-O(5)	117.99(4)
C(15)-C(14)-Si(4)	125.52(15)	O(1)-Rb(1)-O(6)	135.12(4)
C(13)-C(14)-Si(4)	126.21(15)	O(2)-Rb(1)-O(6)	95.55(4)
C(15)-C(14)-Th(1)	75.76(11)	O(5)-Rb(1)-O(6)	60.48(4)
C(13)-C(14)-Th(1)	72.34(11)	O(1)-Rb(1)-O(3)	96.57(4)
Si(4)-C(14)-Th(1)	132.60(9)	O(2)-Rb(1)-O(3)	136.43(4)
C(16)-C(15)-C(14)	109.90(17)	O(5)-Rb(1)-O(3)	99.82(4)
C(16)-C(15)-Th(1)	74.86(11)	O(6)-Rb(1)-O(3)	122.98(4)
C(14)-C(15)-Th(1)	74.82(11)	O(1)-Rb(1)-O(4)	120.16(4)
C(15)-C(16)-C(12)	109.77(17)	O(2)-Rb(1)-O(4)	97.57(4)

O(5)-Rb(1)-O(4)	139.35(4)	C(34)-N(1)-C(46)	110.20(17)
O(6)-Rb(1)-O(4)	99.32(4)	C(40)-N(1)-C(46)	109.25(17)
O(3)-Rb(1)-O(4)	59.79(4)	C(34)-N(1)-Rb(1)	109.23(12)
O(1)-Rb(1)-N(1)	59.84(5)	C(40)-N(1)-Rb(1)	109.09(12)
O(2)-Rb(1)-N(1)	120.20(5)	C(46)-N(1)-Rb(1)	108.61(12)
O(5)-Rb(1)-N(1)	60.40(4)	C(51)-N(2)-C(39)	110.90(19)
O(6)-Rb(1)-N(1)	120.02(5)	C(51)-N(2)-C(45)	110.51(19)
O(3)-Rb(1)-N(1)	59.96(4)	C(39)-N(2)-C(45)	109.86(19)
O(4)-Rb(1)-N(1)	119.09(4)	C(51)-N(2)-Rb(1)	108.43(13)
O(1)-Rb(1)-N(2)	120.45(5)	C(39)-N(2)-Rb(1)	108.67(13)
O(2)-Rb(1)-N(2)	60.17(5)	C(45)-N(2)-Rb(1)	108.40(13)
O(5)-Rb(1)-N(2)	119.91(5)	N(1)-C(34)-C(35)	113.95(18)
O(6)-Rb(1)-N(2)	60.19(5)	O(1)-C(35)-C(34)	108.94(18)
O(3)-Rb(1)-N(2)	119.48(5)	O(1)-C(35)-Rb(1)	44.03(9)
O(4)-Rb(1)-N(2)	60.36(5)	C(34)-C(35)-Rb(1)	81.67(12)
N(1)-Rb(1)-N(2)	179.43(5)	O(1)-C(36)-C(37)	108.68(18)
C(35)-O(1)-C(36)	112.31(17)	O(1)-C(36)-Rb(1)	46.58(9)
C(35)-O(1)-Rb(1)	115.76(12)	C(37)-C(36)-Rb(1)	76.80(12)
C(36)-O(1)-Rb(1)	112.11(12)	O(2)-C(37)-C(36)	109.94(17)
C(38)-O(2)-C(37)	111.11(17)	O(2)-C(37)-Rb(1)	48.15(9)
C(38)-O(2)-Rb(1)	114.71(13)	C(36)-C(37)-Rb(1)	79.47(12)
C(37)-O(2)-Rb(1)	110.12(12)	O(2)-C(38)-C(39)	109.77(19)
C(41)-O(3)-C(42)	111.21(16)	O(2)-C(38)-Rb(1)	44.81(10)
C(41)-O(3)-Rb(1)	115.91(12)	C(39)-C(38)-Rb(1)	82.10(13)
C(42)-O(3)-Rb(1)	112.69(12)	N(2)-C(39)-C(38)	114.5(2)
C(43)-O(4)-C(44)	111.87(17)	N(1)-C(40)-C(41)	114.17(18)
C(43)-O(4)-Rb(1)	113.56(12)	O(3)-C(41)-C(40)	109.26(17)
C(44)-O(4)-Rb(1)	114.19(12)	O(3)-C(41)-Rb(1)	44.07(9)
C(47)-O(5)-C(48)	111.66(16)	C(40)-C(41)-Rb(1)	80.80(11)
C(47)-O(5)-Rb(1)	112.71(11)	O(3)-C(42)-C(43)	109.13(17)
C(48)-O(5)-Rb(1)	113.69(11)	O(3)-C(42)-Rb(1)	46.33(9)
C(50)-O(6)-C(49)	111.15(17)	C(43)-C(42)-Rb(1)	78.73(12)
C(50)-O(6)-Rb(1)	115.59(13)	O(4)-C(43)-C(42)	109.05(18)
C(49)-O(6)-Rb(1)	110.58(12)	O(4)-C(43)-Rb(1)	45.79(9)
C(34)-N(1)-C(40)	110.42(17)	C(42)-C(43)-Rb(1)	77.73(12)

O(4)-C(44)-C(45)	108.91(19)	O(5)-C(48)-Rb(1)	45.54(9)
O(4)-C(44)-Rb(1)	45.25(9)	C(49)-C(48)-Rb(1)	76.49(12)
C(45)-C(44)-Rb(1)	81.38(12)	O(6)-C(49)-C(48)	109.76(18)
N(2)-C(45)-C(44)	114.33(19)	O(6)-C(49)-Rb(1)	47.82(9)
N(1)-C(46)-C(47)	113.85(17)	C(48)-C(49)-Rb(1)	79.96(12)
O(5)-C(47)-C(46)	108.76(16)	O(6)-C(50)-C(51)	109.36(18)
O(5)-C(47)-Rb(1)	46.26(9)	O(6)-C(50)-Rb(1)	44.25(10)
C(46)-C(47)-Rb(1)	83.05(11)	C(51)-C(50)-Rb(1)	80.64(12)
O(5)-C(48)-C(49)	109.25(18)	N(2)-C(51)-C(50)	113.90(19)

X-ray Data Collection, Structure Solution and Refinement for [Cs(crypt)][Cp″$_3$Th].

A blue crystal of approximate dimensions 0.082 x 0.110 x 0.182 mm was mounted in a cryoloop and transferred to a Bruker SMART APEX II diffractometer. The APEX2[53] program package was used to determine the unit-cell parameters and for data collection (120 sec/frame scan time). The raw frame data was processed using SAINT[54] and SADABS[55] to yield the reflection data file. Subsequent calculations were carried out using the SHELXTL[56] program package. There were no systematic absences nor any diffraction symmetry other than the Friedel condition. The centrosymmetric triclinic space group $P\bar{1}$ was assigned and later determined to be correct.

The structure was solved by direct methods and refined on F^2 by full-matrix least-squares techniques. The analytical scattering factors[57] for neutral atoms were used throughout the analysis. Hydrogen atoms were included using a riding model.

Least-squares analysis yielded wR2 = 0.0866 and Goof = 1.024 for 622 variables refined against 16125 data (0.75 Å), R1 = 0.0382 for those 13147 data with I > 2.0σ(I).

Table 3.9: Bond lengths [Å] and angles [°] for [Cs(crypt)][Cp″$_3$Th].

Th(1)-Cnt1	2.534	Th(1)-C(24)	2.731(4)
Th(1)-Cnt2	2.522	Th(1)-C(12)	2.749(4)
Th(1)-Cnt3	2.507	Th(1)-C(13)	2.756(4)

Th(1)-C(2)	2.759(4)	Si(6)-C(31)	1.870(5)
Th(1)-C(25)	2.769(4)	C(1)-C(5)	1.424(6)
Th(1)-C(3)	2.776(4)	C(1)-C(2)	1.425(6)
Th(1)-C(16)	2.782(4)	C(2)-C(3)	1.438(6)
Th(1)-C(26)	2.795(4)	C(3)-C(4)	1.439(6)
Th(1)-C(23)	2.804(4)	C(4)-C(5)	1.398(6)
Th(1)-C(4)	2.807(4)	C(12)-C(16)	1.438(6)
Th(1)-C(27)	2.816(4)	C(12)-C(13)	1.440(6)
Th(1)-C(15)	2.843(4)	C(13)-C(14)	1.421(6)
Th(1)-C(1)	2.848(4)	C(14)-C(15)	1.423(6)
Th(1)-C(5)	2.853(4)	C(15)-C(16)	1.389(6)
Th(1)-C(14)	2.854(4)	C(23)-C(27)	1.418(6)
Si(1)-C(1)	1.844(4)	C(23)-C(24)	1.432(6)
Si(1)-C(8)	1.867(5)	C(24)-C(25)	1.435(6)
Si(1)-C(7)	1.872(5)	C(25)-C(26)	1.433(6)
Si(1)-C(6)	1.887(5)	C(26)-C(27)	1.392(6)
Si(2)-C(3)	1.843(4)	Cs(1)-O(6)	2.931(3)
Si(2)-C(9)	1.860(5)	Cs(1)-O(5)	2.933(3)
Si(2)-C(10)	1.866(5)	Cs(1)-O(1)	2.933(3)
Si(2)-C(11)	1.880(5)	Cs(1)-O(2)	2.941(3)
Si(3)-C(12)	1.846(4)	Cs(1)-O(3)	2.942(3)
Si(3)-C(19)	1.867(5)	Cs(1)-O(4)	2.947(3)
Si(3)-C(17)	1.873(5)	Cs(1)-N(2)	3.073(4)
Si(3)-C(18)	1.876(5)	Cs(1)-N(1)	3.073(4)
Si(4)-C(14)	1.851(4)	O(1)-C(35)	1.414(5)
Si(4)-C(22)	1.866(5)	O(1)-C(36)	1.426(5)
Si(4)-C(20)	1.868(5)	O(2)-C(37)	1.426(6)
Si(4)-C(21)	1.887(5)	O(2)-C(38)	1.429(6)
Si(5)-C(23)	1.847(4)	O(3)-C(42)	1.420(5)
Si(5)-C(28)	1.853(5)	O(3)-C(41)	1.421(6)
Si(5)-C(29)	1.862(5)	O(4)-C(44)	1.418(6)
Si(5)-C(30)	1.883(5)	O(4)-C(43)	1.427(6)
Si(6)-C(25)	1.837(5)	O(5)-C(47)	1.421(6)
Si(6)-C(33)	1.862(5)	O(5)-C(48)	1.431(6)
Si(6)-C(32)	1.865(5)	O(6)-C(49)	1.425(6)

O(6)-C(50)	1.426(6)	C(24)-Th(1)-C(16)	162.80(12)
N(1)-C(34)	1.469(6)	C(12)-Th(1)-C(16)	30.15(12)
N(1)-C(46)	1.471(6)	C(13)-Th(1)-C(16)	48.30(12)
N(1)-C(40)	1.474(6)	C(2)-Th(1)-C(16)	73.40(12)
N(2)-C(39)	1.473(7)	C(25)-Th(1)-C(16)	145.92(13)
N(2)-C(51)	1.475(7)	C(3)-Th(1)-C(16)	98.59(12)
N(2)-C(45)	1.476(6)	C(24)-Th(1)-C(26)	48.13(13)
C(34)-C(35)	1.515(7)	C(12)-Th(1)-C(26)	96.27(13)
C(36)-C(37)	1.501(7)	C(13)-Th(1)-C(26)	71.84(13)
C(38)-C(39)	1.514(7)	C(2)-Th(1)-C(26)	159.78(13)
C(40)-C(41)	1.508(7)	C(25)-Th(1)-C(26)	29.85(12)
C(42)-C(43)	1.501(7)	C(3)-Th(1)-C(26)	129.90(13)
C(44)-C(45)	1.502(7)	C(16)-Th(1)-C(26)	120.12(12)
C(46)-C(47)	1.508(7)	C(24)-Th(1)-C(23)	29.96(12)
C(48)-C(49)	1.490(8)	C(12)-Th(1)-C(23)	104.84(12)
C(50)-C(51)	1.497(8)	C(13)-Th(1)-C(23)	100.12(12)
		C(2)-Th(1)-C(23)	134.52(12)
Cnt1-Th(1)-Cnt2	119.7	C(25)-Th(1)-C(23)	50.35(12)
Cnt1-Th(1)-Cnt3	122.7	C(3)-Th(1)-C(23)	122.23(12)
Cnt2-Th(1)-Cnt3	117.6	C(16)-Th(1)-C(23)	133.93(12)
C(24)-Th(1)-C(12)	132.66(12)	C(26)-Th(1)-C(23)	48.49(12)
C(24)-Th(1)-C(13)	117.94(12)	C(24)-Th(1)-C(4)	73.85(12)
C(12)-Th(1)-C(13)	30.33(12)	C(12)-Th(1)-C(4)	145.38(12)
C(24)-Th(1)-C(2)	121.81(13)	C(13)-Th(1)-C(4)	166.64(12)
C(12)-Th(1)-C(2)	100.86(13)	C(2)-Th(1)-C(4)	48.05(12)
C(13)-Th(1)-C(2)	120.14(13)	C(25)-Th(1)-C(4)	88.25(13)
C(24)-Th(1)-C(25)	30.24(13)	C(3)-Th(1)-C(4)	29.87(12)
C(12)-Th(1)-C(25)	126.02(13)	C(16)-Th(1)-C(4)	121.28(12)
C(13)-Th(1)-C(25)	99.55(13)	C(26)-Th(1)-C(4)	117.51(13)
C(2)-Th(1)-C(25)	131.41(13)	C(23)-Th(1)-C(4)	93.21(12)
C(24)-Th(1)-C(3)	98.37(12)	C(24)-Th(1)-C(27)	47.97(12)
C(12)-Th(1)-C(3)	128.34(13)	C(12)-Th(1)-C(27)	85.41(12)
C(13)-Th(1)-C(3)	136.89(12)	C(13)-Th(1)-C(27)	72.52(12)
C(2)-Th(1)-C(3)	30.11(13)	C(2)-Th(1)-C(27)	163.09(12)
C(25)-Th(1)-C(3)	101.48(13)	C(25)-Th(1)-C(27)	49.06(12)

C(3)-Th(1)-C(27)	146.21(12)	C(26)-Th(1)-C(5)	128.95(12)
C(16)-Th(1)-C(27)	115.19(12)	C(23)-Th(1)-C(5)	86.98(12)
C(26)-Th(1)-C(27)	28.73(12)	C(4)-Th(1)-C(5)	28.59(12)
C(23)-Th(1)-C(27)	29.22(12)	C(27)-Th(1)-C(5)	115.91(12)
C(4)-Th(1)-C(27)	120.43(12)	C(15)-Th(1)-C(5)	121.64(12)
C(24)-Th(1)-C(15)	154.28(13)	C(1)-Th(1)-C(5)	28.93(12)
C(12)-Th(1)-C(15)	48.83(12)	C(24)-Th(1)-C(14)	126.84(13)
C(13)-Th(1)-C(15)	47.46(12)	C(12)-Th(1)-C(14)	49.87(12)
C(2)-Th(1)-C(15)	75.59(12)	C(13)-Th(1)-C(14)	29.28(12)
C(25)-Th(1)-C(15)	124.23(13)	C(2)-Th(1)-C(14)	103.15(12)
C(3)-Th(1)-C(15)	89.87(12)	C(25)-Th(1)-C(14)	98.67(13)
C(16)-Th(1)-C(15)	28.57(12)	C(3)-Th(1)-C(14)	109.92(12)
C(26)-Th(1)-C(15)	108.78(12)	C(16)-Th(1)-C(14)	48.25(13)
C(23)-Th(1)-C(15)	147.57(12)	C(26)-Th(1)-C(14)	79.88(12)
C(4)-Th(1)-C(15)	119.20(12)	C(23)-Th(1)-C(14)	122.13(12)
C(27)-Th(1)-C(15)	119.24(12)	C(4)-Th(1)-C(14)	139.06(12)
C(24)-Th(1)-C(1)	109.50(12)	C(27)-Th(1)-C(14)	92.92(12)
C(12)-Th(1)-C(1)	97.55(12)	C(15)-Th(1)-C(14)	28.92(12)
C(13)-Th(1)-C(1)	126.27(12)	C(1)-Th(1)-C(14)	123.25(12)
C(2)-Th(1)-C(1)	29.39(12)	C(5)-Th(1)-C(14)	150.32(12)
C(25)-Th(1)-C(1)	133.90(13)	C(1)-Si(1)-C(8)	115.2(2)
C(3)-Th(1)-C(1)	49.70(12)	C(1)-Si(1)-C(7)	111.6(2)
C(16)-Th(1)-C(1)	79.73(12)	C(8)-Si(1)-C(7)	110.8(2)
C(26)-Th(1)-C(1)	156.69(12)	C(1)-Si(1)-C(6)	106.6(2)
C(23)-Th(1)-C(1)	109.48(12)	C(8)-Si(1)-C(6)	102.7(2)
C(4)-Th(1)-C(1)	48.11(12)	C(7)-Si(1)-C(6)	109.3(2)
C(27)-Th(1)-C(1)	134.72(12)	C(3)-Si(2)-C(9)	112.4(2)
C(15)-Th(1)-C(1)	94.44(12)	C(3)-Si(2)-C(10)	110.8(2)
C(24)-Th(1)-C(5)	80.91(12)	C(9)-Si(2)-C(10)	112.7(2)
C(12)-Th(1)-C(5)	121.91(12)	C(3)-Si(2)-C(11)	108.2(2)
C(13)-Th(1)-C(5)	152.24(13)	C(9)-Si(2)-C(11)	105.8(2)
C(2)-Th(1)-C(5)	47.54(12)	C(10)-Si(2)-C(11)	106.6(2)
C(25)-Th(1)-C(5)	105.45(13)	C(12)-Si(3)-C(19)	117.8(2)
C(3)-Th(1)-C(5)	48.73(12)	C(12)-Si(3)-C(17)	106.6(2)
C(16)-Th(1)-C(5)	108.50(12)	C(19)-Si(3)-C(17)	107.2(2)

C(12)-Si(3)-C(18)	109.5(2)	Si(2)-C(3)-Th(1)	132.5(2)
C(19)-Si(3)-C(18)	106.8(2)	C(5)-C(4)-C(3)	109.9(4)
C(17)-Si(3)-C(18)	108.7(2)	C(5)-C(4)-Th(1)	77.5(2)
C(14)-Si(4)-C(22)	113.0(2)	C(3)-C(4)-Th(1)	73.9(2)
C(14)-Si(4)-C(20)	113.2(2)	C(4)-C(5)-C(1)	109.5(4)
C(22)-Si(4)-C(20)	110.0(3)	C(4)-C(5)-Th(1)	73.9(2)
C(14)-Si(4)-C(21)	106.7(2)	C(1)-C(5)-Th(1)	75.3(2)
C(22)-Si(4)-C(21)	106.0(2)	C(16)-C(12)-C(13)	103.8(4)
C(20)-Si(4)-C(21)	107.5(3)	C(16)-C(12)-Si(3)	129.6(3)
C(23)-Si(5)-C(28)	114.9(2)	C(13)-C(12)-Si(3)	122.6(3)
C(23)-Si(5)-C(29)	110.7(2)	C(16)-C(12)-Th(1)	76.2(2)
C(28)-Si(5)-C(29)	109.1(2)	C(13)-C(12)-Th(1)	75.1(2)
C(23)-Si(5)-C(30)	107.5(2)	Si(3)-C(12)-Th(1)	130.75(19)
C(28)-Si(5)-C(30)	107.4(2)	C(14)-C(13)-C(12)	111.4(4)
C(29)-Si(5)-C(30)	106.8(2)	C(14)-C(13)-Th(1)	79.2(2)
C(25)-Si(6)-C(33)	115.2(2)	C(12)-C(13)-Th(1)	74.5(2)
C(25)-Si(6)-C(32)	107.3(2)	C(13)-C(14)-C(15)	104.9(4)
C(33)-Si(6)-C(32)	111.0(2)	C(13)-C(14)-Si(4)	123.3(3)
C(25)-Si(6)-C(31)	109.9(2)	C(15)-C(14)-Si(4)	126.2(3)
C(33)-Si(6)-C(31)	106.4(2)	C(13)-C(14)-Th(1)	71.6(2)
C(32)-Si(6)-C(31)	106.7(3)	C(15)-C(14)-Th(1)	75.1(2)
C(5)-C(1)-C(2)	105.2(4)	Si(4)-C(14)-Th(1)	138.6(2)
C(5)-C(1)-Si(1)	125.8(3)	C(16)-C(15)-C(14)	110.1(4)
C(2)-C(1)-Si(1)	124.9(3)	C(16)-C(15)-Th(1)	73.3(2)
C(5)-C(1)-Th(1)	75.7(2)	C(14)-C(15)-Th(1)	76.0(2)
C(2)-C(1)-Th(1)	71.8(2)	C(15)-C(16)-C(12)	109.8(4)
Si(1)-C(1)-Th(1)	134.8(2)	C(15)-C(16)-Th(1)	78.2(2)
C(1)-C(2)-C(3)	111.4(4)	C(12)-C(16)-Th(1)	73.7(2)
C(1)-C(2)-Th(1)	78.8(2)	C(27)-C(23)-C(24)	104.7(4)
C(3)-C(2)-Th(1)	75.6(2)	C(27)-C(23)-Si(5)	125.6(3)
C(2)-C(3)-C(4)	104.0(4)	C(24)-C(23)-Si(5)	126.4(3)
C(2)-C(3)-Si(2)	124.2(3)	C(27)-C(23)-Th(1)	75.9(2)
C(4)-C(3)-Si(2)	127.4(3)	C(24)-C(23)-Th(1)	72.2(2)
C(2)-C(3)-Th(1)	74.3(2)	Si(5)-C(23)-Th(1)	132.6(2)
C(4)-C(3)-Th(1)	76.3(2)	C(23)-C(24)-C(25)	111.6(4)

C(23)-C(24)-Th(1)	77.8(2)	O(6)-Cs(1)-N(1)	119.77(10)
C(25)-C(24)-Th(1)	76.3(2)	O(5)-Cs(1)-N(1)	59.81(10)
C(26)-C(25)-C(24)	103.6(4)	O(1)-Cs(1)-N(1)	60.35(9)
C(26)-C(25)-Si(6)	127.4(3)	O(2)-Cs(1)-N(1)	119.75(10)
C(24)-C(25)-Si(6)	126.8(3)	O(3)-Cs(1)-N(1)	60.28(9)
C(26)-C(25)-Th(1)	76.1(2)	O(4)-Cs(1)-N(1)	119.22(9)
C(24)-C(25)-Th(1)	73.4(2)	N(2)-Cs(1)-N(1)	179.80(11)
Si(6)-C(25)-Th(1)	127.8(2)	C(35)-O(1)-C(36)	112.5(3)
C(27)-C(26)-C(25)	110.3(4)	C(35)-O(1)-Cs(1)	110.0(2)
C(27)-C(26)-Th(1)	76.5(2)	C(36)-O(1)-Cs(1)	111.6(3)
C(25)-C(26)-Th(1)	74.1(2)	C(37)-O(2)-C(38)	111.7(4)
C(26)-C(27)-C(23)	109.8(4)	C(37)-O(2)-Cs(1)	108.7(3)
C(26)-C(27)-Th(1)	74.8(2)	C(38)-O(2)-Cs(1)	112.3(3)
C(23)-C(27)-Th(1)	74.9(2)	C(42)-O(3)-C(41)	112.3(4)
O(6)-Cs(1)-O(5)	60.88(10)	C(42)-O(3)-Cs(1)	110.8(3)
O(6)-Cs(1)-O(1)	117.03(9)	C(41)-O(3)-Cs(1)	112.9(3)
O(5)-Cs(1)-O(1)	95.39(9)	C(44)-O(4)-C(43)	112.8(4)
O(6)-Cs(1)-O(2)	95.79(9)	C(44)-O(4)-Cs(1)	110.5(3)
O(5)-Cs(1)-O(2)	135.79(9)	C(43)-O(4)-Cs(1)	111.3(3)
O(1)-Cs(1)-O(2)	60.38(9)	C(47)-O(5)-C(48)	113.1(4)
O(6)-Cs(1)-O(3)	137.09(9)	C(47)-O(5)-Cs(1)	113.1(3)
O(5)-Cs(1)-O(3)	96.65(9)	C(48)-O(5)-Cs(1)	110.0(3)
O(1)-Cs(1)-O(3)	100.03(9)	C(49)-O(6)-C(50)	111.6(4)
O(2)-Cs(1)-O(3)	122.23(9)	C(49)-O(6)-Cs(1)	108.2(3)
O(6)-Cs(1)-O(4)	97.59(9)	C(50)-O(6)-Cs(1)	112.0(3)
O(5)-Cs(1)-O(4)	119.05(9)	C(34)-N(1)-C(46)	110.3(4)
O(1)-Cs(1)-O(4)	140.46(9)	C(34)-N(1)-C(40)	110.0(4)
O(2)-Cs(1)-O(4)	99.77(9)	C(46)-N(1)-C(40)	110.5(4)
O(3)-Cs(1)-O(4)	59.79(9)	C(34)-N(1)-Cs(1)	108.5(3)
O(6)-Cs(1)-N(2)	60.24(11)	C(46)-N(1)-Cs(1)	109.1(3)
O(5)-Cs(1)-N(2)	120.16(11)	C(40)-N(1)-Cs(1)	108.3(3)
O(1)-Cs(1)-N(2)	119.84(10)	C(39)-N(2)-C(51)	111.0(4)
O(2)-Cs(1)-N(2)	60.42(11)	C(39)-N(2)-C(45)	110.6(4)
O(3)-Cs(1)-N(2)	119.56(10)	C(51)-N(2)-C(45)	110.6(4)
O(4)-Cs(1)-N(2)	60.60(10)	C(39)-N(2)-Cs(1)	108.3(3)

C(51)-N(2)-Cs(1)	108.6(3)	C(43)-C(42)-Cs(1)	79.0(2)
C(45)-N(2)-Cs(1)	107.6(3)	O(4)-C(43)-C(42)	109.3(4)
N(1)-C(34)-C(35)	114.0(4)	O(4)-C(43)-Cs(1)	47.7(2)
N(1)-C(34)-Cs(1)	50.0(2)	C(42)-C(43)-Cs(1)	77.6(2)
C(35)-C(34)-Cs(1)	73.3(2)	O(4)-C(44)-C(45)	109.7(4)
O(1)-C(35)-C(34)	109.5(4)	O(4)-C(44)-Cs(1)	48.4(2)
O(1)-C(35)-Cs(1)	48.72(19)	C(45)-C(44)-Cs(1)	82.2(3)
C(34)-C(35)-Cs(1)	83.4(3)	N(2)-C(45)-C(44)	114.9(4)
O(1)-C(36)-C(37)	109.6(4)	N(2)-C(45)-Cs(1)	50.6(2)
O(1)-C(36)-Cs(1)	47.4(2)	C(44)-C(45)-Cs(1)	74.7(3)
C(37)-C(36)-Cs(1)	76.6(3)	N(1)-C(46)-C(47)	114.2(4)
O(2)-C(37)-C(36)	109.9(4)	N(1)-C(46)-Cs(1)	49.6(2)
O(2)-C(37)-Cs(1)	49.6(2)	C(47)-C(46)-Cs(1)	75.1(3)
C(36)-C(37)-Cs(1)	79.9(3)	O(5)-C(47)-C(46)	109.3(4)
O(2)-C(38)-C(39)	110.0(4)	O(5)-C(47)-Cs(1)	46.4(2)
O(2)-C(38)-Cs(1)	46.9(2)	C(46)-C(47)-Cs(1)	81.8(3)
C(39)-C(38)-Cs(1)	81.3(3)	O(5)-C(48)-C(49)	109.1(4)
N(2)-C(39)-C(38)	113.8(4)	O(5)-C(48)-Cs(1)	48.6(2)
N(2)-C(39)-Cs(1)	50.1(2)	C(49)-C(48)-Cs(1)	76.8(3)
C(38)-C(39)-Cs(1)	75.5(3)	O(6)-C(49)-C(48)	110.5(4)
N(1)-C(40)-C(41)	114.8(4)	O(6)-C(49)-Cs(1)	50.0(2)
N(1)-C(40)-Cs(1)	50.1(2)	C(48)-C(49)-Cs(1)	79.7(3)
C(41)-C(40)-Cs(1)	75.8(3)	O(6)-C(50)-C(51)	110.0(4)
O(3)-C(41)-C(40)	109.9(4)	O(6)-C(50)-Cs(1)	47.2(2)
O(3)-C(41)-Cs(1)	46.6(2)	C(51)-C(50)-Cs(1)	82.3(3)
C(40)-C(41)-Cs(1)	81.1(3)	N(2)-C(51)-C(50)	114.8(4)
O(3)-C(42)-C(43)	109.7(4)	N(2)-C(51)-Cs(1)	49.9(2)
O(3)-C(42)-Cs(1)	48.2(2)	C(50)-C(51)-Cs(1)	74.7(3)

References

(1) Jantunen, K. C.; Burns, C. J.; Castro-Rodriguez, I.; Da Re, R. E.; Golden, J. T.; Morris, D. E.; Scott, B. L.; Taw, F. L.; Kiplinger, J. L. Thorium(IV) and Uranium(IV) Ketimide Complexes Prepared by Nitrile Insertion into Actinide-Alkyl and -Aryl Bonds.

Organometallics **2004**, *23*, 4682–4692, DOI: 10.1021/om0343824.

(2) Morris, D. E.; Da Re, R. E.; Jantunen, K. C.; Castro-Rodriguez, I.; Kiplinger, J. L. Trends in Electronic Structure and Redox Energetics for Early-Actinide Pentamethylcyclopentadienyl Complexes. *Organometallics* **2004**, *23*, 5142–5153, DOI: 10.1021/om049634v.

(3) Schelter, E. J.; Veauthier, J. M.; Thompson, J. D.; Scott, B. L.; John, K. D.; Morris, D. E.; Kiplinger, J. L. 4f-5f Heterotrimetallic Complexes Exhibiting Electrochemical and Magnetic Communication. *J. Am. Chem. Soc.* **2006**, *128*, 2198–2199, DOI: 10.1021/ja057808+.

(4) Erickson, K. A.; Kagan, B. D.; Scott, B. L.; Morris, D. E.; Kiplinger, J. L. Revisiting the Bis(Dimethylamido) Metallocene Complexes of Thorium and Uranium: Improved Syntheses, Structure, Spectroscopy, and Redox Energetics of $(C_5Me_5)_2An(NMe_2)_2$ (An = Th, U). *Dalton Trans.* **2017**, *46*, 11208–11213, DOI: 10.1039/C7DT02373A.

(5) Button, Z. E.; Higgins, J. A.; Suvova, M.; Cloke, F. G. N.; Roe, S. M. Mixed Sandwich Thorium Complexes Incorporating Bis(Tri-Isopropylsilyl)Cyclooctatetraenyl and Pentamethylcyclopentadienyl Ligands: Synthesis, Structure and Reactivity. *Dalton Trans.* **2015**, *44*, 2588–2596, DOI: 10.1039/c4dt02362e.

(6) Inman, C. J.; Cloke, F. G. N. The Experimental Determination of Th(IV)/Th(III) Redox Potentials in Organometallic Thorium Complexes. *Dalton Trans.* **2019**, *48*, 10782–10784, DOI: 10.1039/c9dt01553a.

(7) La Pierre, H. S.; Kameo, H.; Halter, D. P.; Heinemann, F. W.; Meyer, K. Coordination and Redox Isomerization in the Reduction of a Uranium(III) Monoarene Complex. *Angew. Chem. Int. Ed.* **2014**, *53*, 7154–7157, DOI: 10.1002/anie.201402048.

(8) Guo, F. S.; Tsoureas, N.; Huang, G. Z.; Tong, M. L.; Mansikkamäki, A.; Layfield, R. A. Isolation of a Perfectly Linear Uranium(II) Metallocene. *Angew. Chem. Int. Ed.* **2020**, *59*, 2299–2303, DOI: 10.1002/anie.201912663.

(9) La Pierre, H. S.; Scheurer, A.; Heinemann, F. W.; Hieringer, W.; Meyer, K. Synthesis and Characterization of a Uranium(II) Monoarene Complex Supported by δ Backbonding. *Angew. Chem. Int. Ed.* **2014**, *53*, 7158–7162, DOI: 10.1002/anie.201402050.

(10) Hlina, J. A.; Pankhurst, J. R.; Kaltsoyannis, N.; Arnold, P. L. Metal-Metal Bonding in Uranium-Group 10 Complexes. *J. Am. Chem. Soc.* **2016**, *138*, 3333–3345, DOI: 10.1021/jacs.5b10698.

(11) Evans, W. J. Tutorial on the Role of Cyclopentadienyl Ligands in the Discovery of Molecular Complexes of the Rare-Earth and Actinide Metals in New Oxidation States. *Organometallics* **2016**, *35*, 3088–3100, DOI: 10.1021/acs.organomet.6b00466.

(12) Woen, D. H.; Evans, W. J. Expanding the +2 Oxidation State of the Rare-Earth Metals, Uranium, and Thorium in Molecular Complexes. In *Handbook on the Physics and Chemistry of Rare Earths*; Bünzli, J.-C., Pecharsky, V. K., Eds.; Elsevier B.V., 2016; pp 1–57, DOI: 10.1016/bs.hpcre.2016.08.002.

(13) Langeslay, R. R.; Fieser, M. E.; Ziller, J. W.; Furche, F.; Evans, W. J. Synthesis, Structure, and Reactivity of Crystalline Molecular Complexes of the $\{[C_5H_3(SiMe_3)_2]_3Th\}^{1-}$ Anion Containing Thorium in the Formal +2 Oxidation State. *Chem. Sci.* **2015**, *6*, 517–521, DOI: 10.1039/C4SC03033H.

(14) Zachmanoglou, C. E.; Docrat, A.; Bridgewater, B. M.; Parkin, G.; Brandow, C. G.; Bercaw, J. E.; Jardine, C. N.; Lyall, M.; Green, J. C.; Keister, J. B. The Electronic Influence of Ring Substituents and Ansa Bridges in Zirconocene Complexes as Probed by Infrared

Spectroscopic, Electrochemical, and Computational Studies. *J. Am. Chem. Soc.* **2002**, *124*, 9525–9546, DOI: 10.1021/ja020236y.

(15) Corbey, J. F.; Woen, D. H.; Palumbo, C. T.; Fieser, M. E.; Ziller, J. W.; Furche, F.; Evans, W. J. Ligand Effects in the Synthesis of Ln^{2+} Complexes by Reduction of Tris(Cyclopentadienyl) Precursors Including C–H Bond Activation of an Indenyl Anion. *Organometallics* **2015**, *34*, 3909–3921, DOI: 10.1021/acs.organomet.5b00500.

(16) Moehring, S. A.; Beltran-Leiva, M.; Paez-Hernandez, D.; Arratia-Perez, R.; Ziller, J. W.; Evans, W. J. Rare-Earth Metal (II) Aryloxides: Structure, Synthesis, and EPR Spectroscopy of [K(2.2.2-Cryptand)][$Sc(OC_6H_2{}^tBu_2$-2,6-Me-4)$_3$]. *Chem. Eur. J.* **2018**, *24*, 18059–18067, DOI: 10.1002/chem.201803807.

(17) Moehring, S. A.; Evans, W. J. Evaluating Electron Transfer Reactivity of Rare-Earth Metal(II) Complexes Using EPR Spectroscopy. *Organometallics* **2020**, *39*, 1187–1194, DOI: 10.1021/acs.organomet.9b00837.

(18) Brennan, J. G.; Andersen, R. A.; Zalkin, A. Chemistry of Trivalent Uranium Metallocenes: Electron-Transfer Reactions with Carbon Disulfide. Formation of [$(RC_5H_4)_3U]_2[\mu$-η^1,η^1-CS_2]. *Inorg. Chem.* **1986**, *25*, 1756–1760, DOI: 10.1021/ic00231a007.

(19) del Mar Conejo, M.; Parry, J. S.; Carmona, E.; Schultz, M.; Brennann, J. G.; Beshouri, S. M.; Andersen, R. A.; Rogers, R. D.; Coles, S.; Hursthouse, M. B. Carbon Monoxide and Isocyanide Complexes of Trivalent Uranium Metallocenes. *Chem. Eur. J.* **1999**, *5*, 3000–3009, DOI: 10.1002/(SICI)1521-3765(19991001)5:10<3000::AID-CHEM3000>3.0.CO;2-Q.

(20) Windorff, C. J.; MacDonald, M. R.; Meihaus, K. R.; Ziller, J. W.; Long, J. R.; Evans, W. J. Expanding the Chemistry of Molecular U^{2+} Complexes: Synthesis, Characterization, and

Reactivity of the $\{[C_5H_3(SiMe_3)_2]_3U\}^-$ Anion. *Chem. Eur. J.* **2016**, *22*, 772–782, DOI: 10.1002/chem.201503583.

(21) MacDonald, M. R.; Fieser, M. E.; Bates, J. E.; Ziller, J. W.; Furche, F.; Evans, W. J. Identification of the +2 Oxidation State for Uranium in a Crystalline Molecular Complex, [K(2.2.2-Cryptand)][$(C_5H_4SiMe_3)_3U$]. *J. Am. Chem. Soc.* **2013**, *135*, 13310–13313, DOI: 10.1021/ja406791t.

(22) Clappe, C.; Leveugle, D.; Hauchard, D.; Durand, G. Electrochemical Studies of Tricyclopentadienyl Uranium IV Chloride Complexes: $(^RCp)_3UCl$ ($^RCp = RC_5H_4$ with R = H; Me: CH_3; ^{t}Bu: $(CH_3)_3C$); TMS: $(CH_3)_3Si$). *J. Electroanal. Chem.* **1998**, *448*, 95–103, DOI: 10.1016/S0022-0728(98)00029-1.

(23) Hauchard, D.; Cassir, M.; Chivot, J.; Ephritikhine, M. Electrochemical Study of Uranium(IV) and Uranium(IV) Organometallic Compounds in Tetrahydrofuran by Means of Conventional Microelectrodes and Ultramicroelectrodes. Part I. Application to the Na(Hg) Reduction of Cp_3UCl (Cp = η-C_5H_5). *J. Electroanal. Chem.* **1991**, *313*, 227–241, DOI: 10.1016/0022-0728(91)85182-O.

(24) Finke, R. G.; Gaughan, G.; Voegeli, R. Organoactinide Electrochemistry. A Cyclic Voltammetric and Coulometric Study of $(C_5Me_5)_2UCl_2$, $[(C_5Me_5)_2UCl_2\cdot THF]^-Na^+$, $(C_5Me_5)_2UCl\cdot THF$ and $(C_5Me_5)_2ThCl_2$. *J. Organomet. Chem.* **1982**, *229*, 179–184, DOI: 10.1016/S0022-328X(00)90280-8.

(25) Watson, P. L.; Tulip, T. H.; Williams, I. Defluorination of Perfluoroolefins by Divalent Lanthanoid Reagents: Activating Carbon-Fluorine Bonds. *Organometallics* **1990**, *9*, 1999–2009, DOI: 10.1021/om00157a006.

(26) Maury, O.; Ephritikhine, M.; Nierlich, M.; Lance, M.; Samuel, E. Chloride Ion Transfer

during the U(IV)/U(III) Reduction of UCl_4 in Tetrahydrofuran (THF), Studied by Cyclic Voltammetry; Synthesis and Molecular Structure of $[NBu_4][UCl_5(THF)]$. *Inorg. Chim. Acta* **1998**, *279*, 210–216, DOI: 10.1016/S0020-1693(98)00126-1.

(27) Blake, P. C.; Lappert, M. F.; Atwood, J. L.; Zhang, H. The Synthesis and Characterisation, Including X-Ray Diffraction Study, of $[Th\{\eta\text{-}C_5H_3(SiMe_3)_2\}_3]$; the First Thorium(III) Crystal Structure. *J. Chem. Soc., Chem. Commun.* **1986**, *453*, 1148–1149, DOI: 10.1039/C39860001148.

(28) Blake, P. C.; Edelstein, N. M.; Hitchcock, P. B.; Kot, W. K.; Lappert, M. F.; Shalimoff, G. V.; Tian, S. Synthesis, Properties and Structures of the Tris(Cyclopentadienyl)Thorium(III) Complexes $[Th\{\eta^5\text{-}C_5H_3(SiMe_2R)_2\text{-}1,3\}_3]$ (R = Me or ^{t}Bu). *J. Organomet. Chem.* **2001**, *636*, 124–129, DOI: 10.1016/S0022-328X(01)00860-9.

(29) Windorff, C. J.; MacDonald, M. R.; Ziller, J. W.; Evans, W. J. Trimethylsilylcyclopentadienyl (Cp′) Uranium Chemistry: Synthetic and Structural Studies of Cp'_4U and Cp'_3UX (X = Cl, I, Me). *Z. Anorg. Allg. Chem.* **2017**, *643*, 2011–2018, DOI: 10.1002/zaac.201700323.

(30) Siladke, N. A.; Webster, C. L.; Walensky, J. R.; Takase, M. K.; Ziller, J. W.; Grant, D. J.; Gagliardi, L.; Evans, W. J. Actinide Metallocene Hydride Chemistry: C–H Activation in Tetramethylcyclopentadienyl Ligands to Form $[\mu\text{-}\eta^5\text{-}C_5Me_3H(CH_2)\text{-}\kappa C]^{2-}$ Tuck-over Ligands in a Tetrathorium Octahydride Complex. *Organometallics* **2013**, *32*, 6522–6531, DOI: 10.1021/om4008482.

(31) Wedal, J. C.; Bekoe, S.; Ziller, J. W.; Furche, F.; Evans, W. J. In Search of Tris(Trimethylsilylcyclopentadienyl) Thorium. *Dalton Trans.* **2019**, *48*, 16633–16640, DOI: 10.1039/C9DT03674A.

(32) Kuehl, C. J.; Da Re, R. E.; Scott, B. L.; Morris, D. E.; John, K. D. Toward New Paradigms in Mixed-Valency: Ytterbocene–Terpyridine Charge-Transfer Complexes. *Chem. Commun.* **2003**, *3*, 2336–2337, DOI: 10.1039/B306484K.

(33) Da Re, R. E.; Kuehl, C. J.; Brown, M. G.; Rocha, R. C.; Bauer, E. D.; John, K. D.; Morris, D. E.; Shreve, A. P.; Sarrao, J. L. Electrochemical and Spectroscopic Characterization of the Novel Charge-Transfer Ground State in Diimine Complexes of Ytterbocene. *Inorg. Chem.* **2003**, *42*, 5551–5559, DOI: 10.1021/ic030069i.

(34) Formanuik, A.; Ariciu, A.-M.; Ortu, F.; Beekmeyer, R.; Kerridge, A.; Tuna, F.; McInnes, E. J. L.; Mills, D. P. Actinide Covalency Measured by Pulsed Electron Paramagnetic Resonance Spectroscopy. *Nat. Chem.* **2017**, *9*, 578–583, DOI: 10.1038/nchem.2692.

(35) Langeslay, R. R.; Chen, G. P.; Windorff, C. J.; Chan, A. K.; Ziller, J. W.; Furche, F.; Evans, W. J. Synthesis, Structure, and Reactivity of the Sterically Crowded Th^{3+} Complex $(C_5Me_5)_3Th$ Including Formation of the Thorium Carbonyl, $[(C_5Me_5)_3Th(CO)][BPh_4]$. *J. Am. Chem. Soc.* **2017**, *139*, 3387–3398, DOI: 10.1021/jacs.6b10826.

(36) Altman, A. B.; Brown, A. C.; Rao, G.; Lohrey, T. D.; Britt, R. D.; Maron, L.; Minasian, S. G.; Shuh, D. K.; Arnold, J. Chemical Structure and Bonding in a Thorium(III)-Aluminum Heterobimetallic Complex. *Chem. Sci.* **2018**, *9*, 4317–4324, DOI: 10.1039/c8sc01260a.

(37) Huh, D. N.; Roy, S.; Ziller, J. W.; Furche, F.; Evans, W. J. Isolation of a Square-Planar Th(III) Complex: Synthesis and Structure of $[Th(OC_6H_2{}^tBu_2\text{-}2,6\text{-}Me\text{-}4)_4]^{1-}$. *J. Am. Chem. Soc.* **2019**, *141*, 12458–12463, DOI: 10.1021/jacs.9b04399.

(38) Parry, J. S.; Cloke, F. G. N.; Coles, S. J.; Hursthouse, M. B. Synthesis and Characterization of the First Sandwich Complex of Trivalent Thorium : A Structural Comparison with the Uranium Analogue. *J. Am. Chem. Soc.* **1999**, *121*, 6867–6871, DOI: 10.1021/ja9903633.

(39) Walensky, J. R.; Martin, R. L.; Ziller, J. W.; Evans, W. J. Importance of Energy Level Matching for Bonding in Th^{3+}-Am^{3+} Actinide Metallocene Amidinates, $(C_5Me_5)_2[^iPrNC(Me)N^iPr]An$. *Inorg. Chem.* **2010**, *49*, 10007–10012, DOI: 10.1021/ic1013285.

(40) Langeslay, R. R.; Fieser, M. E.; Ziller, J. W.; Furche, F.; Evans, W. J. Expanding Thorium Hydride Chemistry Through Th^{2+}, Including the Synthesis of a Mixed-Valent Th^{4+}/Th^{3+} Hydride Complex. *J. Am. Chem. Soc.* **2016**, *138*, 4036–4045, DOI: 10.1021/jacs.5b11508.

(41) Huh, D. N.; Ziller, J. W.; Evans, W. J. Chelate-Free Synthesis of the U(II) Complex, $[(C_5H_3(SiMe_3)_2)_3U]^{1-}$, Using Li and Cs Reductants and Comparative Studies of La(II) and Ce(II) Analogs. *Inorg. Chem.* **2018**, *57*, 11809–11814, DOI: 10.1021/acs.inorgchem.8b01966.

(42) In *CRC Handbook of Chemistry and Physics*; Haynes, W. M., Lide, D. R., Bruno, T. J., Eds.; CRC Press, 2016; pp 943–950.

(43) Evans, W. J.; Kozimor, S. A.; Ziller, J. W.; Fagin, A. A.; Bochkarev, M. N. Facile Syntheses of Unsolvated UI_3 and Tetramethylcyclopentadienyl Uranium Halides. *Inorg. Chem.* **2005**, *44*, 3993–4000, DOI: 10.1021/ic0482685.

(44) Andersen, R. A. Tris((Hexamethyldisilyl)Amido)Uranium (III): Preparation and Coordination Chemistry. *Inorg. Chem.* **1979**, *18*, 1507–1509, DOI: 10.1021/ic50196a021.

(45) Weydert, M.; Brennan, J. G.; Andersen, R. A.; Bergman, R. G. Reactions of Uranium(IV) Tertiary Alkyl Bond: Facile Ligand-Assisted Reduction and Insertion of Ethylene and Carbon Monoxide. *Organometallics* **1995**, *14*, 3942–3951, DOI: 10.1021/om00008a046.

(46) Peterson, J. K.; MacDonald, M. R.; Ziller, J. W.; Evans, W. J. Synthetic Aspects of $(C_5H_4SiMe_3)_3Ln$ Rare-Earth Chemistry: Formation of $(C_5H_4SiMe_3)_3Lu$ via

[$(C_5H_4SiMe_3)_2Ln]^+$ Metallocene Precursors. *Organometallics* **2013**, *32*, 2625–2631, DOI: 10.1021/om400116d.

(47) Hitchcock, P. B.; Lappert, M. F.; Maron, L.; Protchenko, A. V. Lanthanum Does Form Stable Molecular Compounds in the +2 Oxidation State. *Angew. Chem. Int. Ed.* **2008**, *47*, 1488–1491, DOI: 10.1002/anie.200704887.

Chapter 4:

C–H Bond Activation via U(II) in the Reduction of Heteroleptic Bis(Trimethylsilyl)amide U(III) Complexes

Introduction[†]

Following the original report of the synthesis of [K(crypt)][Cp′$_3$U^{II}][1] described in the Introduction, U(II) was subsequently identified by X-ray diffraction in eight ligand environments via reduction of a U(III) precursor.[2–8] Two different electron configurations were observed, and based on the results in Chapter 2, it appeared the local coordination geometry around the uranium center can explain the resulting configuration.

Reduction of $(C_5Me_5)_3U^{III}$ [9,10] was reported since this sterically crowded tris(pentamethylcyclopentadienyl) complex reacts with THF,[10] the common solvent for alkali metal reductions. An option to make U(II) complexes with C_5Me_5 ancillary ligands is to reduce heteroleptic $(C_5Me_5)_nU^{III}X_{3-n}$ complexes (X = anion; n = 1,2) that are stable to THF. However, reduction of heteroleptic rare earth and actinide complexes is an underdeveloped area in general.[11]

In this Chapter, the reductive chemistry of the heteroleptic pentamethylcyclopentadienyl amide complexes $(C_5Me_5)_2U^{III}(NR_2)$[12,13] and $(C_5Me_5)U^{III}(NR_2)_2$[14] (R = SiMe$_3$) is described in efforts to synthesize U(II) complexes with C_5Me_5 ancillary ligands. Surprisingly, this led to C–H bond activation chemistry that could be an important aspect of U(II) reactivity.

[†] Portions of this Chapter have been published: Wedal, J. C.; Bekoe, S.; Ziller, J. W.; Furche, F.; Evans, W. J. C–H Bond Activation via U(II) in the Reduction of Heteroleptic Bis(Trimethylsilyl)Amide U(III) Complexes. *Organometallics* **2020**, *39*, 3425–3432, DOI: 10.1021/acs.organomet.0c00496.

Results

Reduction of $(C_5Me_5)_2U^{III}(NR_2)$. Reaction of excess KC_8 with $(C_5Me_5)_2U^{III}(NR_2)$ in the presence of 2.2.2-cryptand (crypt) in THF at −35 °C generates a dark blue solution as is commonly observed in reactions forming U(II) compounds.[1–3] The UV-visible spectrum of this solution shows a broad absorption at 750 nm (ε = 4000 $M^{-1}cm^{-1}$), Figure 4.1. This absorption band compares well with the observed spectrum for $[(C_5Me_4H)_3U^{II}]^{1-}$, which had a broad absorption band at 790 nm (ε = 1800 $M^{-1}cm^{-1}$). In comparison, $(C_5Me_5)_2U^{III}(NR_2)$ shows only weak absorptions ($\varepsilon \leq 250$ $M^{-1}cm^{-1}$) in the visible region, Figure 4.2. The relatively large molar attenuation coefficient supports the $5f^36d^1$ electronic assignment, which has been assigned for $[Cp'_3U^{II}]^{1-}$,[1] $[Cp''_3U^{II}]^{1-}$,[2] $[(C_5Me_4H)_3U^{II}]^{1-}$,[5] $[U^{II}(NR_2)_3]^{1-}$,[3] and $(C_5{}^iPr_5)_2U^{II}$.[8] Other U(II) compounds, $[K(crypt)]\{[(^{Ad,Me}ArO)_3mes]U^{II}\}$[4] and $U^{II}(NHAr^{iPr6})_2$,[5] have weak (ε < 1000 $M^{-1}cm^{-1}$) electronic transitions in the visible region and were described as having $5f^4$ electron configurations.

The dark blue solution generated by reduction of $(C_5Me_5)_2U^{III}(NR_2)$ was layered under hexane at −35 °C for crystallization, but after two hours, the solution had changed to a red-brown color. Overnight, dark brown crystals formed and were identified by X-ray diffraction as the cyclometallated U(III) product $[K(crypt)][(C_5Me_5)_2U^{III}(CH_2SiMe_2NSiMe_3{-}\kappa C,\kappa N)]$, **4.1**, Figure 4.4, in 97% yield, in which a C–H bond of the silylamide had been activated by the uranium center. Activation of this ligand to form cyclometallated products has been observed previously,[15–21] although most often the mechanism of the cyclometallation occurs via deprotonation with a source of $(NR_2)^{1-}$. However, here it is possible that the C–H bond is activated by the U(II) center with concomitant formation of H_2 due to the high isolated yield of **4.1**. This activation pathway has been observed in the $U^{III}(Tren^R)$ examples under photolytic conditions.[22] Indeed, when the

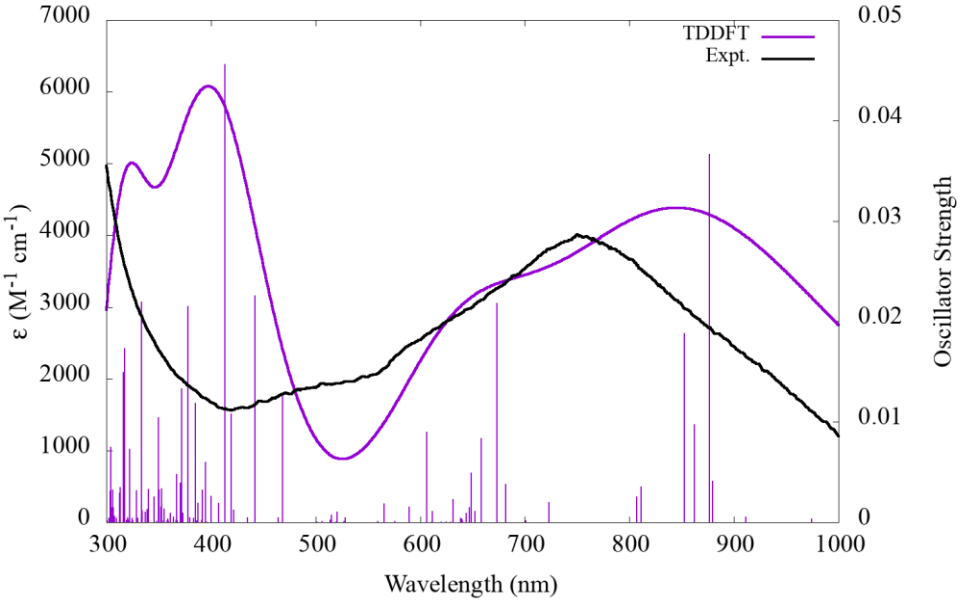

Figure 4.1: UV-visible spectrum of the reaction product of $(C_5Me_5)_2U^{III}(NR_2)$ with KC_8 in the presence of crypt in THF (black) and the theoretical UV-visible spectrum of $[(C_5Me_5)_2U^{II}(NR_2)]^{1-}$ (violet) with computed TDDFT oscillator strengths shown as vertical lines. A Gaussian line broadening of 0.20 eV was applied and the computed excitation energies were empirically blue-shifted by 0.2 eV. The computed intensities were scaled by a factor 0.4 to ease comparison with the experimental spectrum.

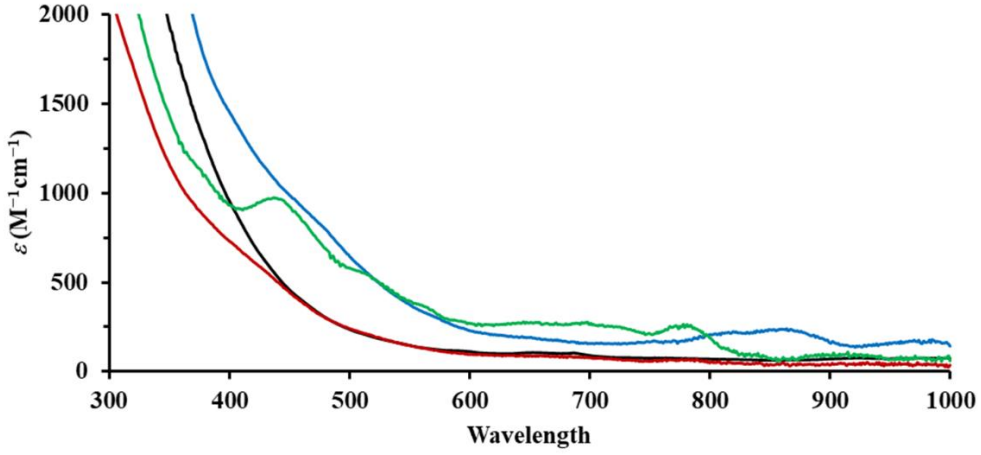

Figure 4.2: UV-visible spectrum of $(C_5Me_5)_2U^{III}(NR_2)$ (black), $(C_5Me_5)U^{III}(NR_2)_2$ (red), **4.1** (blue), and **4.2** (green).

conversion of $(C_5Me_5)_2U(NR_2)$ to **2.1** was followed by ^1H NMR spectroscopy in THF-d_8 in a J-Young tube, a peak at δ 4.53 attributable to H_2 formation[23] was observed, Figure 4.3.

Compound **4.1** crystallizes in the $P\bar{1}$ space group. The $[K(crypt)]^{1+}$ cation is well-separated from the metallocene unit. The uranium center was disordered across two positions. The data were modelled with 91% occupancy at U1 above the plane that is created by the two (C_5Me_5) centroids and nitrogen donor atom and 9% at U2 below the plane. For the predominant component of the crystal, the 2.354(5) Å U1–N1 and 2.558(6) Å U1–C21 distances and the 99.4(2)° U1–N1–Si1 and 102.0(3) N1–Si1–C21(CH_2) angles are all consistent with a cyclometallated product. In comparison, the U1–N1–Si2 angle is 131.2(3)° and N1–Si2–C(Me) angles are 111.6(3)°, 113.9(3)°, and 114.0(3)°. The bond distances in **4.1** are compared to those in the previously-characterized U(IV) analog, $(C_5Me_5)_2U^{IV}(CH_2SiMe_2NSiMe_3{-}\kappa C,\kappa N)$,[24] in Table 2.1. The 2.354(5) Å U–N1 distance in **4.1** is longer than the U–N distance in the U(IV) analog, 2.221(8) Å which is consistent with the larger ionic radius of U(III) compared to U(IV).[25] However, the U–(C_5Me_5 ring centroid) and U–CH_2 distances are similar.

The disordered locations of U1 and U2 differ by 0.576 Å which leads to a significant change in the bond distances. For example, the 2.959 Å U2–C21 distance is much longer than the 2.558(6) Å U1–C21 bond length. The former distance is too long for a U2–C21 single bond which raises the possibility that the crystal contains 9% of a disordered U(II) anion, $[(C_5Me_5)_2U^{II}(NR_2)]^{1-}$ at the U2 site. The dark color of the crystals also could suggest the presence of U(II), even in very low amounts due to the large ε values of U(II).[1–3] However, there was no disorder in the rest of the crystal structure that would suggest a U(II) compound exists within the crystal.

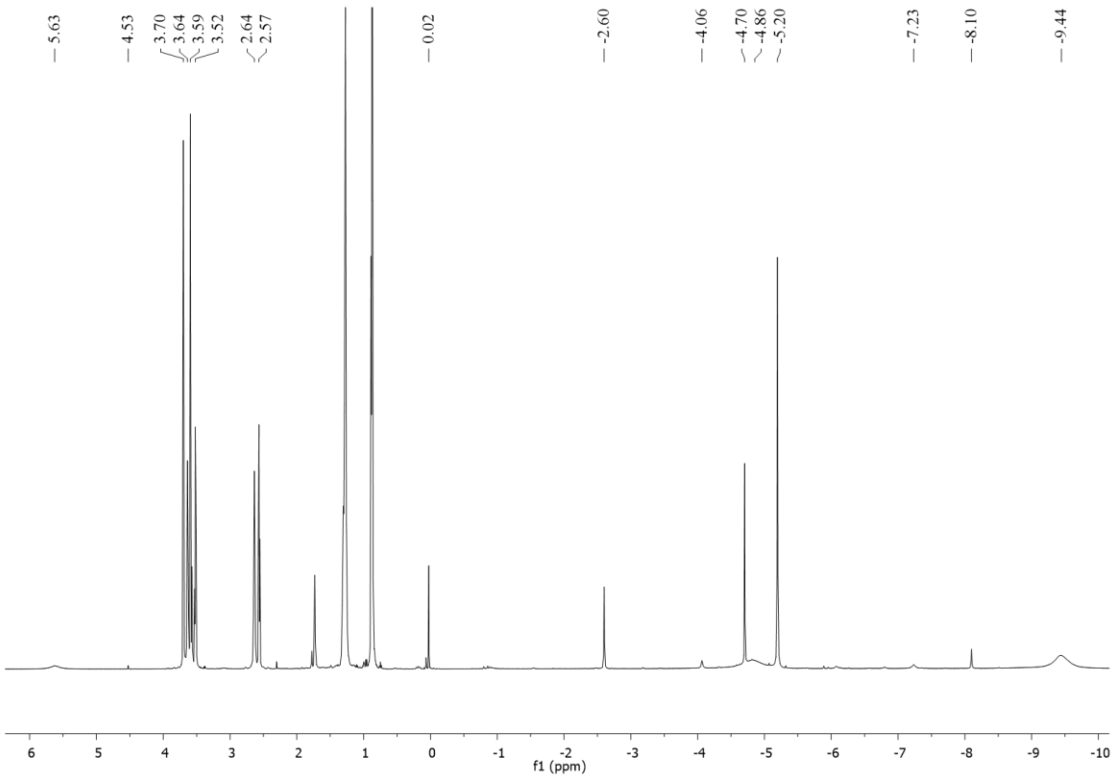

Figure 4.3: ^{1}H NMR in THF-d_8 spectrum 30 min after passing a $(C_5Me_5)_2U(NR_2)$ / crypt solution through a KC_8 column into a J-Young tube. The peak at δ 4.53 is attributed to H_2 formation. The peak at δ 0.02 does not match HNR_2, which appears at δ 0.05 in THF-d_8.

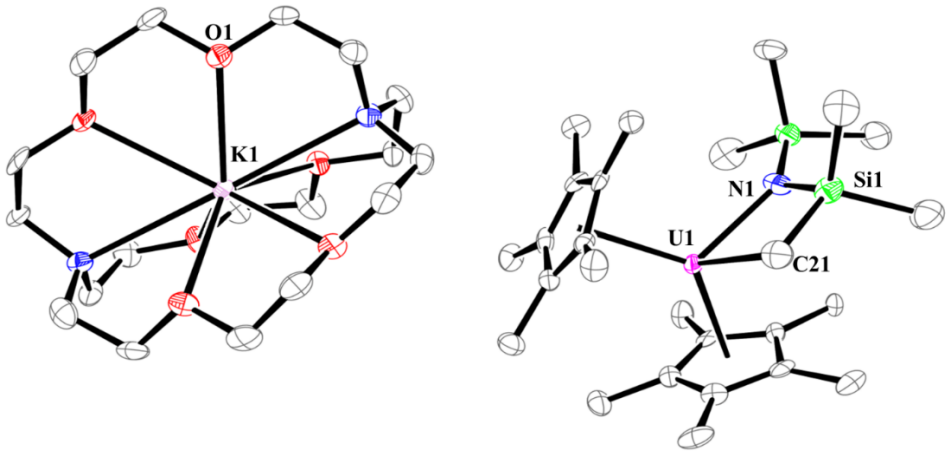

Figure 4.4: Thermal ellipsoid plot of $[K(crypt)][(C_5Me_5)_2U^{III}(CH_2SiMe_2NSiMe_3–\kappa C,\kappa N)]$, **4.1**, with selective atom labelling. Ellipsoids are drawn at the 50% probability level. Hydrogen atoms and disorder in the U center have been omitted for clarity.

Table 4.1: Selected bond lengths (Å) and angles (°) for [K(crypt)][$(C_5Me_5)_2U^{III}(CH_2SiMe_2NSiMe_3–\kappa C,\kappa N)$], **4.1,** $(C_5Me_5)_2U^{IV}(CH_2SiMe_2NSiMe_3–\kappa C,\kappa N)$,[24] and [K(crypt)(THF)][$(C_5Me_5)U^{III}(NR_2)(CH_2SiMe_2NSiMe_3–\kappa C,\kappa N)$], **4.2.** For **4.1** and **4.2**, only values involving U1 are given. Cnt is the C_5Me_5 ring centroid.

	4.1	$(C_5Me_5)_2U^{IV}(CH_2SiMe_2NSiMe_3–\kappa C,\kappa N)$	**4.2**
U–cnt	2.559, 2.584	2.608	2.533
U–N1	2.354(5)	2.221(8)	2.363(4)
U–N2			2.399(4)
U–CH_2	2.558(6)	2.52(2)	2.500(5)
Cnt–U–cnt	132.5	138.20	
Cnt–U–N1	114.6, 109.8	109.28	119.5
Cnt–U–N2			123.3
N1–U–N2			114.1(1)
U–N1–Si1	99.4(2)	100.7(4)	96.0(2)
U–N1–Si2	131.2(3)		114.4(2)
U–CH_2–Si1	89.3(3)	86.6(7)	88.9(2)
N1–Si1–CH_2	102.0(3)	102.2(8)	103.9(2)

Electronic Structure Calculations on $[(C_5Me_5)_2U^{II}(NR_2)]^{1-}$. In collaboration with Sam Bekoe and Filipp Furche, the viability of a U(II) complex like $[(C_5Me_5)_2U^{II}(NR_2)]^{1-}$ as the initial reduction product was probed with geometry optimization calculations using the TPSSh hybrid meta-generalized gradient density functional approximation.[26] Scalar relativistic effective core potentials (ECPs)[27] with the def-TZVP basis set[28] were used for uranium and polarized split-valence basis sets def2-SV(P)[27] were used for other atoms. All calculations were completed with TURBOMOLE v7.4.1.[28] The solvent optimized ground state structure suggests a $5f^36d^1$ configuration with the highest occupied molecular orbital, HOMO resembling a $6dz^2$ orbital, Figure 4.5, and the first three diffused lowest unoccupied molecular orbitals (LUMO) indicating mixing of 7p of U with bound p-type Rydberg states, Figure 4.6. This ground state provides good modeling of the UV-visible spectrum by time-dependent DFT (TDDFT) calculations as shown in

Figure 4.1. All absorptions between 1000–300 nm originate from either the 5f or 6d orbitals on the uranium center. The bands between 1000–450 nm are predominantly 6d/5f to 7p and 6d to 5f transitions. Bands between 450–300 nm arise from metal to ligand charge transfer (MLCT) transitions. Further computational details can be found in Table 4.6.

These results are analogous to previous observations for $[Cp'_3U^{II}]^{1-}$.[1] In $[Cp'_3U^{II}]^{1-}$, the trigonal arrangement (pseudo-D_3 symmetry) of the ligands allows the $6dz^2$ orbital to be similar in energy to the 5f shell. This has been observed in the lanthanide series $[Cp'_3Ln]^{1-}$.[29–32] The ligand field of the heteroleptic complex, $[(C_5Me_5)_2U^{II}(NR_2)]^{1-}$, also allows population of the $6dz^2$ orbital upon reduction.

While most of the electron density resides on the U center, there is a small amount that resides on two amide methyl groups, Figure 4.5. This electron density is in a σ^* C–H antibonding orbital. Hence, population of this orbital could lead to activation of the C–H bond to form **4.1**, Scheme 4.1. There is no comparable electron density on the methyl groups in the HOMO of $(C_5Me_5)_2U^{III}(NR_2)$: the three highest occupied orbitals for the neutral compound are purely 5f orbitals with essentially no contribution from the ligands, Figure 4.6. The calculated LUMO of $(C_5Me_5)_2U^{III}(NR_2)$, Figure 4.7, was similar to the HOMO of $[(C_5Me_5)_2U^{II}(NR_2)]^{1-}$, with electron density on the methyl groups.

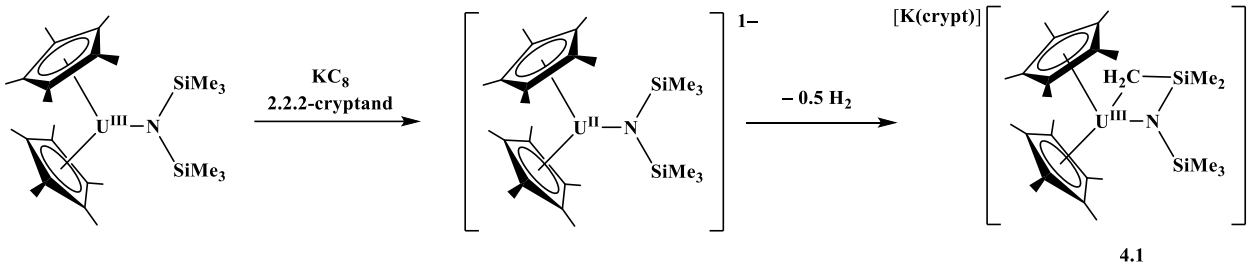

4.1

Scheme 4.1: Possible route to **4.1** via a U(II) complex.

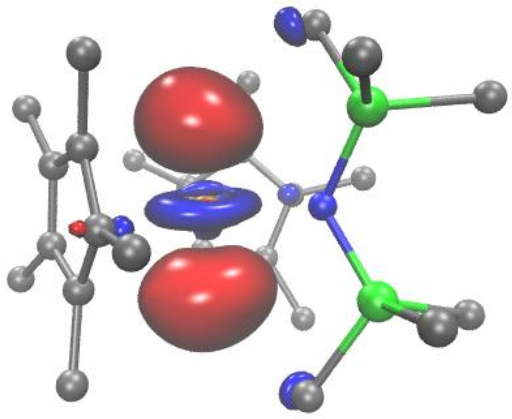

Figure 4.5: Calculated 6dz^2-like HOMO of $[(C_5Me_5)_2U^{II}(NR_2)]^{1-}$, plotted with a contour value of 0.05 with hydrogen atoms omitted for clarity.

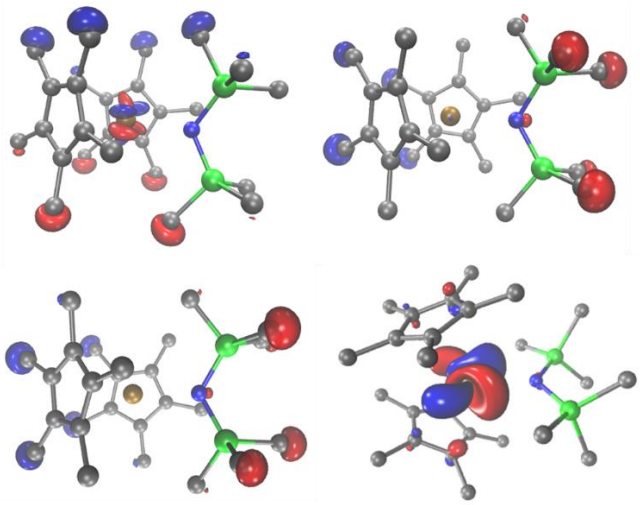

Figure 4.6: (From left to right) LUMO +1 (contour value of 0.02), LUMO +2 (contour value of 0.02), LUMO +3 (contour value of 0.02), and LUMO +8 (contour value of 0.05) of $[(C_5Me_5)_2U(NR_2)]^{1-}$, with hydrogen atoms excluded for clarity.

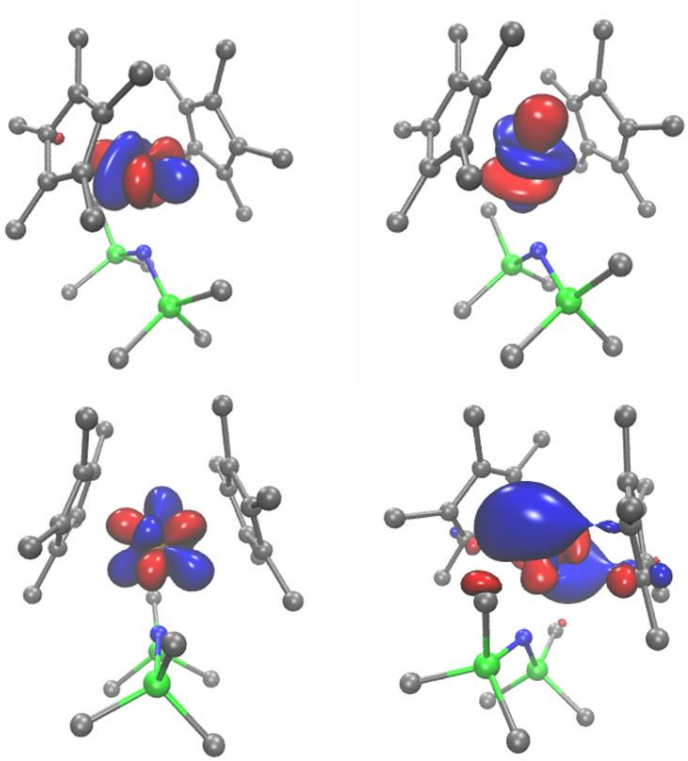

Figure 4.7: (from left to right) HOMO −2, HOMO −1, HOMO, LUMO of $(C_5Me_5)_2U^{III}(NR_2)$, plotted with contour value of 0.05. Hydrogen atoms have been omitted for clarity.

Reduction of $(C_5Me_5)U^{III}(NR_2)_2$. In a reduction reaction identical to that described above, the bis(amide) complex, $(C_5Me_5)U^{III}(NR_2)_2$, was reduced with KC_8 in THF at −35 °C in the presence of crypt. This generated a dark blue solution analogous to the above reaction, suggestive of the formation of a U(II) species. However, by the time the UV-visible spectrum of this solution could be collected (within ~60 s), the color had changed to brown and the observed spectrum was nearly identical to the product ultimately isolated from this reaction, $[K(crypt)(THF)][(C_5Me_5)U^{III}(NR_2)(CH_2SiMe_2NSiMe_3–\kappa C,\kappa N)]$, **4.2**. A spectrum of the dark solution ultimately was collected by executing all manipulations at −78 °C in a cold well in the glovebox and by keeping the cuvette submerged in a dry ice/isopropanol bath during transfer. The spectrum had a broad feature at 684 nm, Figure 4.8, with an estimated attenuation coefficient ε =

1300 $M^{-1}cm^{-1}$. This value is likely an underestimation because it assumes quantitative conversion with no decomposition and it was collected through an isopropanol film.

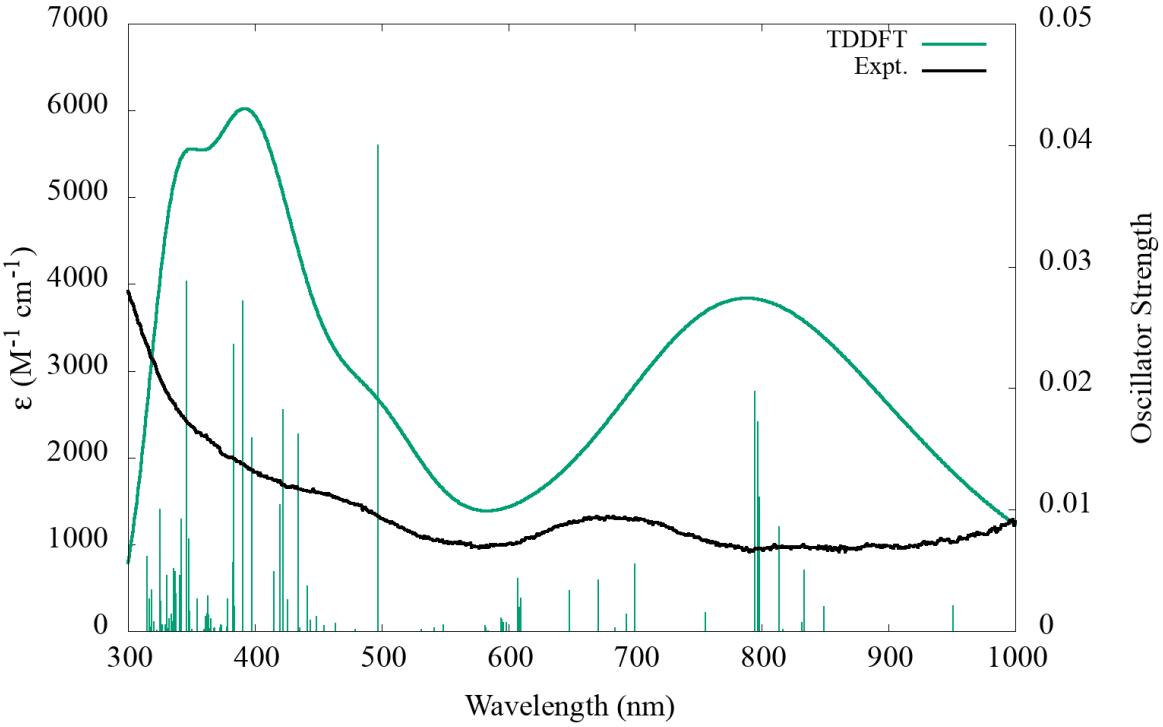

Figure 4.8: UV-visible spectrum of the reaction product of $(C_5Me_5)U^{III}(NR_2)_2$ with KC_8 in the presence of crypt in THF, collected through an isopropanol film (black) and theoretical UV-visible spectrum of $[(C_5Me_5)U^{II}(NR_2)_2]^{1-}$ with computed TDDFT oscillator strengths shown as vertical lines. A Gaussian line broadening of 0.20 eV was applied and the computed excitation energies were empirically blue-shifted by 0.2 eV. The computed intensities were scaled by a factor 0.4.

The reaction solution was layered under hexane at −35 °C and black crystals suitable for X-ray diffraction deposited at the bottom of the vial overnight. These were identified as the cyclometallated product **2** isolated in 82% yield as shown in Figure 4.9. A possible route to **4.2** through a U(II) intermediate, similar to that in Scheme 4.1, is shown in Scheme 4.2.

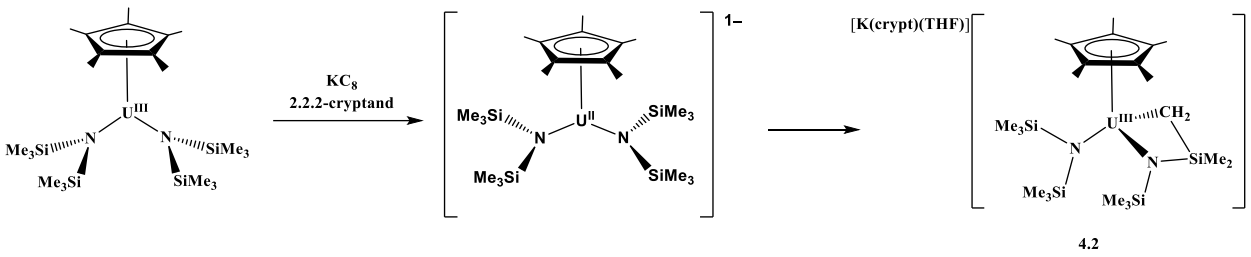

Scheme 4.2: Possible route to **4.2** via initial reduction to a U(II) complex.

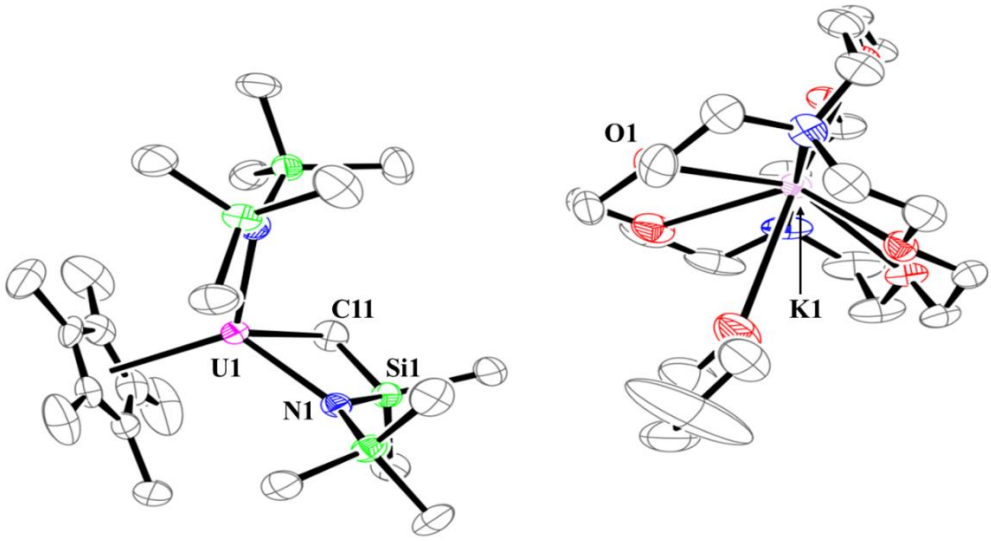

Figure 4.9: Thermal ellipsoid plot of [K(crypt)(THF)][(C_5Me_5)U^{III}(NR_2)($CH_2SiMe_2NSiMe_3$–$\kappa C,\kappa N$)], **4.2** with selective atom labelling. Ellipsoids are drawn at the 50% probability level and hydrogen atoms have been omitted for clarity.

Compound **4.2** crystallizes in the $P2_1/c$ space group as a distinct ion pair like compound **4.1**. The potassium is encapsulated by crypt, but also binds one molecule of THF in the solid state. This cation has been observed in complexes of the type [K(crypt)(THF)]{[($C_5Me_4H)_2Ln^{III}$(THF)]$_2$(μ-η^2:η^2–N_2)} (Ln = Gd, Tb, Dy).[33]

As in **4.1**, the uranium center in **4.2** is disordered over two positions. In this case, there is 96% occupancy at U1 above the plane created by the C_5Me_5 ring centroid and the two nitrogen donor atoms and 4% occupancy at U2 below this plane. As in **4.1**, these two centers are separated by a large distance, 0.586 Å, which leads to different bond lengths and the possibility that the 4%

component is a U(II) species that has not yet converted to the cyclometallate. However, no other crystallographic evidence was observed that would suggest the presence of a U(II) species. As with **4.1**, the dark color of the crystals could suggest the presence of a U(II) species in low concentration. However, compound **4.2** forms a brown solution when dissolved, as expected for a U(III) species.

Selected bond distances and angles in **4.2** are shown in Table 2.1. Considering the difference in formal coordination numbers of **4.1** vs **4.2**, i.e. 8 vs 6, the bond distances are quite similar. The 2.500(5) Å U1–C11 distance in **4.2** is slightly shorter than that in **4.1** and the U1–N1 distance of the metallated amide ligand is equivalent to that in **4.1**. The 2.533 Å U–(C_5Me_5 ring centroid) distance is not far from the 2.559 and 2.584 Å analogs in **4.1**. As expected for a cyclometallated amide ligand, the 96.0(2)° U1–N1–Si1 angle in **2.2** is much smaller than the other U–N–Si angles in the molecule, 114.4(2)°, 123.4(2)°, and 137.6(2)°.

Electronic Structure Calculations on $[(C_5Me_5)U^{II}(NR_2)_2]^{1-}$. In collaboration with Sam Bekoe and Filipp Furche, geometry optimization calculations on $[(C_5Me_5)U^{II}(NR_2)_2]^{1-}$ were carried out at the density functional level of theory in an identical manner as described above for $[(C_5Me_5)_2U^{II}(NR_2)]^{1-}$. An electronic structure consistent with a U ground state configuration of $5f^36d^1$ was found with the HOMO again resembling a $6dz^2$ orbital, Figure 4.10. The calculations showed that even in the mono-cyclopentadienyl heteroleptic complex $(C_5Me_5)U^{II}(NR_2)_2$, the $6dz^2$ orbital is energetically accessible upon reduction.

As in $[(C_5Me_5)_2U^{II}(NR_2)]^{1-}$, most of the electron density resides on the uranium, but there exists some electron density that resides on two of the methyl groups of the amide ligand. As with $[(C_5Me_5)_2U^{II}(NR_2)]^{1-}$, this orbital is a σ^* C–H antibonding orbital that could be responsible for the activation of the C–H bond to form **4.2**. Also paralleling the $(C_5Me_5)_2U^{III}(NR_2)$ system, the three

highest occupied orbitals of $(C_5Me_5)U^{III}(NR_2)_2$ are almost purely 5f in character, Figure 4.11, with no electron density on the methyl groups. In contrast to the $(C_5Me_5)_2U^{III}(NR_2)$ system, the calculated LUMO of $(C_5Me_5)U^{III}(NR_2)_2$ is a 5f orbital with contribution from the π system of the C_5Me_5 ligand, Figure 4.11, and not a $6dz^2$ orbital.

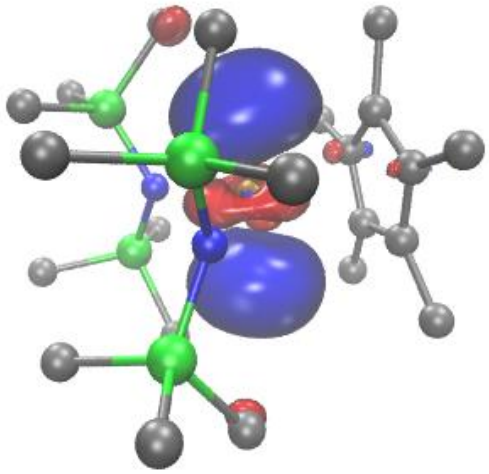

Figure 4.10: Calculated $6dz^2$-like HOMO of $[(C_5Me_5)U^{II}(NR_2)_2]^{1-}$, plotted with a contour value of 0.05 with hydrogen atoms omitted for clarity.

The simulated TDDFT UV-visible spectrum of $[(C_5Me_5)U^{II}(NR_2)_2]^{1-}$, Figure 4.7, is similar to that of $[(C_5Me_5)_2U^{II}(NR_2)]^{1-}$, Figure 4.1. The bands between 1000–300 nm originate predominantly from excitations out of the 6d and some 5f orbitals on the uranium center, Figure 4.8. The bands between 1000–450 nm are predominantly 6d to 7p transitions, whereas the higher-energy absorptions between 450–300 nm arise from metal to ligand charge transfer (MLCT) transitions. Compared to the UV-visible spectrum of $[(C_5Me_5)_2U^{II}(NR_2)]^{1-}$, the relatively intense transitions at ~800 nm are blue-shifted by about ~100 nm, while the intense transition at 497 nm is red-shifted by ~100 nm compared to the transition in $[(C_5Me_5)_2U^{II}(NR_2)]^{1-}$. Complete details can be found in Table 4.7.

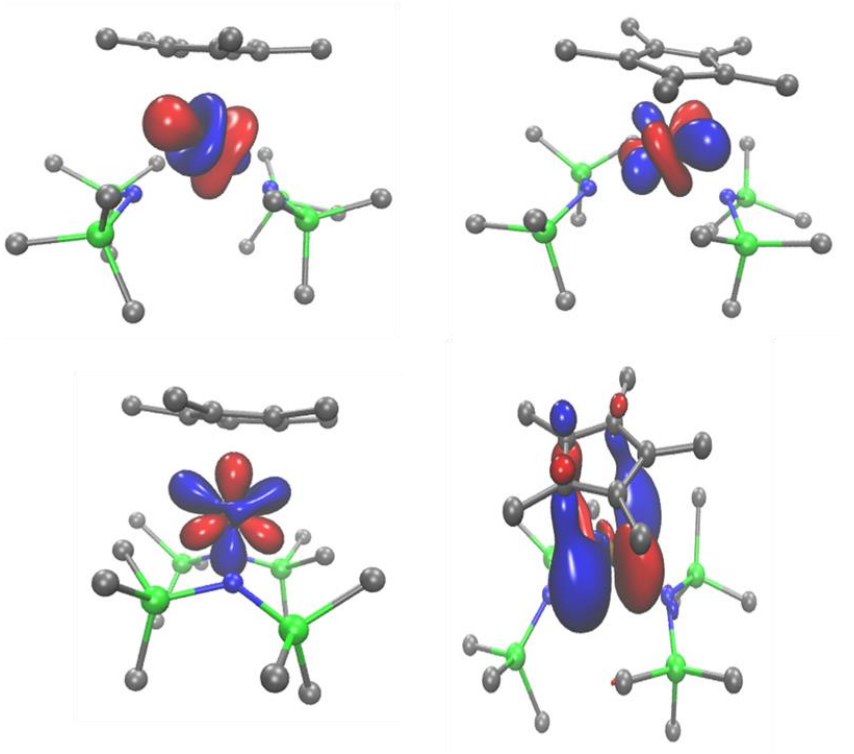

Figure 4.11: (From left to right) HOMO−2, HOMO−1, HOMO, LUMO of $(C_5Me_5)U(NR_2)_2$, plotted with a contour value of 0.05. Hydrogen atoms have been omitted for clarity.

Discussion

Reduction of the heteroleptic complexes $(C_5Me_5)_2U^{III}(NR_2)$ and $(C_5Me_5)U^{III}(NR_2)_2$ generates dark solutions with UV-visible spectral properties consistent with $[(C_5Me_5)_2U^{II}(NR_2)]^{1-}$ and $[(C_5Me_5)U^{II}(NR_2)_2]^{1-}$, respectively, based on TDDFT calculations. Although the reactions initially appear to form U(II) species, these products are thermally unstable even at −35 °C. The isolated products of these reductions are not U(II) species, but instead the cyclometallated compounds [K(crypt)][$(C_5Me_5)_2U^{III}(CH_2SiMe_2NSiMe_3$–*κC,κN*)], **4.1**, and [K(crypt)][$(C_5Me_5)U^{III}(NR_2)(CH_2SiMe_2NSiMe_3$–*κC,κN*), **4.2**. Hence, the goal of making a pentamethylcyclopentadienyl U(II) complex, which is difficult with the homoleptic $(C_5Me_5)_3U^{III}$ due to its high reactivity,[9] was complicated by the C–H bond activation reactivity of the

bis(trimethylsilyl) amide ligand. C–H bond activation has been previously observed in reduction of [(^{Ad,Me}ArO)$_3$mes]U^{III},[4,34] and is often observed in higher-valent uranium chemistry.[35–43]

Interestingly, the DFT calculations on the U(II) complexes showed some electron density in the HOMO on the C–H bonds of the silylamide groups that could facilitate the observed metallation. In addition to the [(^{Ad,Me}ArO)$_3$mes]U^{III} system[4,34] cited above, examples of C–H bond activation with Ln(II) complexes also have been reported previously. These include the metallated tert-butyl group in [(C$_5$H$_2$^{t}Bu$_3$)(η^5–C$_3$H$_2$^{t}Bu$_2$CMe$_2$CH$_2$–κC)Nd^{III}(μ–I)K(18-crown-6)], obtained from a Nd(II) reaction[44] and {[C$_5$H$_3$(SiMe$_3$)$_2$]$_2$Y(μ–H)}$_2$ formed in the reduction of [C$_5$H$_3$(SiMe$_3$)$_2$]$_2$Y,[45] the unusual (C$_9$H$_6$)$^{2–}$ indenyl dianion in a Dy(II) reduction,[11] the isolation of hydrides, [((^{Ad,Me}ArO)$_3$mes)Ln^{III}H]$^{1–}$ (Ln = Gd, Dy, Er, Y) from reactions designed to generate Ln(II) compounds,[46–48] and reduction of the (C$_5$Me$_5$)$_2$Y(NR$_2$) system that forms a mixture of Y(II) and Y(III) products analogous to the present U compound **4.1**.[49]

The DFT calculations also are consistent with 5f^{3}6d^1 configurations for U(II) in [(C$_5$Me$_5$)U^{II}(NR$_2$)$_2$]$^{1–}$ and [(C$_5$Me$_5$)$_2$U^{II}(NR$_2$)]$^{1–}$, as previously observed for the homoleptic, pseudo-D_3 symmetric tris(cyclopentadienyl) and tris(amide) species.[1–3] In the homoleptic lanthanide and actinide complexes, it has been well established by simple molecular orbital theory, dating back to Hoffmann's classic 1976 bent metallocene paper,[50] that dz^2 is the d-orbital lowest energetically.[1,29–32,50–53] Despite the lowered symmetry in [(C$_5$Me$_5$)$_2$U^{II}(NR$_2$)]$^{1–}$ and [(C$_5$Me$_5$)U^{II}(NR$_2$)$_2$]$^{1–}$, the HOMO still has 6dz^2-like character. The ordering of the d manifold in [(C$_5$Me$_5$)$_2$U^{II}(NR$_2$)]$^{1–}$ is necessarily the same as that in the bent metallocene, [(C$_5$H$_5$)$_2$TiH]$^{1+}$, described in Hoffmann's paper,[50] with the 6dz^2 orbital lowest in energy followed by the 6dxy orbital (LUMO+8), Figure 4.6.

Similarly, the d orbital ordering in the mono(cyclopentadienyl) bis(amide) $[(C_5Me_5)U^{II}(NR_2)_2]^{1-}$ matches the 1976 molecular orbital calculations of Mingos on the platinum borane, $[B_{11}H_{11}]Pt(PH_3)_2$, which has either $5dz^2$ or 5dxy lowest, depending on the orientation of the $Pt(PR_3)_2$ fragment.[54] The frontier orbitals for the $[B_{11}H_{11}]^{2-}$ fragment are nearly identical to those of the cyclopentadienide which allows this comparison to be made.[55,56] These calculations show that heteroleptic complexes with the proper ligands in a trigonal planar geometry will have a d orbital ordering with dz^2 lowest.

The color of the dark solution generated upon reduction of the mono(cyclopentadienyl) complex, $(C_5Me_5)U^{III}(NR_2)_2$, fades much faster than the reduction product of bis(cyclopentadienyl) $(C_5Me_5)_2U^{III}(NR_2)$. This could be related to the fact that close interactions between the uranium center and two methyl groups of the amide ligand have been observed in the solid state structure of $(C_5Me_5)U^{III}(NR_2)_2$,[14] which were not seen in $(C_5Me_5)_2U^{III}(NR_2)$. This interaction was not observed in the DFT-optimized structure of $[(C_5Me_5)U(NR_2)_2]^{1-}$. The putative "$[(C_5Me_5)U^{II}(NR_2)_2]^{1-}$" could also have enhanced reactivity simply because it has twice the number of C–H bonds that can be activated or that the amide ligand is a stronger donor than the C_5Me_5 ligand. However, the U(II) ion has previously been isolated in $[K(crypt)][U^{II}(NR_2)_3]$ under similar reduction conditions as **4.1** and **4.2**,[5] so it is not clear how the number of available bonds and ligand donor strength affects the C–H activation pathway.

The lower stability of "$[(C_5Me_5)U^{II}(NR_2)_2]^{1-}$" is also consistent its smaller degree of steric saturation of the metal center, 82.7% compared to 85.7% for "$[(C_5Me_5)_2U^{II}(NR_2)]^{1-}$", as measured by the Solid-G method of Guzei[57,58] using the structures determined for these species by DFT calculations, Table 2.2.[59] However, these G values are in the range of the isolable compounds **4.1** and **4.2**, so steric factors are also not the only ones involved in the stability in this case.

Table 4.2: *G*-parameters for U compounds. Structures for $[(C_5Me_5)_2U^{II}(NR_2)]^{1-}$ and $[(C_5Me_5)U^{II}(NR_2)_2]^{1-}$ are taken from DFT optimized geometries.

	Guzei *G*-parameter
$(C_5Me_5)_2U^{IV}(CH_2SiMe_2NSiMe_3\text{–}\kappa N,\kappa C)$[24]	91.3
$(C_5Me_5)_2U^{III}(NR_2)$[13]	85.9
$[(C_5Me_5)_2U^{II}(NR_2)]^{1-}$	85.7
4.1	85.7
$(C_5Me_5)U^{III}(NR_2)_2$[14]	88.9
$[(C_5Me_5)U^{II}(NR_2)_2]^{1-}$	82.7
4.2	82.7

Conclusion

Reduction of the heteroleptic uranium complexes $(C_5Me_5)_2U^{III}(NR_2)$ and $(C_5Me_5)U^{III}(NR_2)_2$ with KC_8 generates dark solutions that appear to contain U(II) complexes based on UV-visible spectroscopy and DFT analysis. Calculations on possible U(II) reduction products, $[(C_5Me_5)_2U^{II}(NR_2)]^{1-}$ and $[(C_5Me_5)U^{II}(NR_2)_2]^{1-}$, indicate $5f^36d^1$ electronic configurations with a $6dz^2$-like HOMO, similar to those found for previously isolated homoleptic tris(cyclopentadienyl) and tris(amide) complexes, despite the lowered symmetry of the heteroleptic species. However, the proposed U(II) species are not stable with respect to C–H bond activation in the amide ligands, and the cyclometallated products $[K(crypt)][(C_5Me_5)_2U^{III}(CH_2SiMe_2NSiMe_3\text{–}\kappa C,\kappa N)]$, **4.1**, and $[K(crypt)][(C_5Me_5)U^{III}(NR_2)(CH_2SiMe_2NSiMe_3\text{–}\kappa C,\kappa N)$, **4.2**, were isolated and characterized by X-ray crystallography. If C–H activation is a common reaction of U(II) species, ligands with accessible C–H bonds may not be innocent ancillary ligands in low-valent uranium chemistry.

Experimental

All syntheses and manipulations were conducted under an Ar atmosphere with rigorous exclusion of air and water using standard glovebox techniques. Solvents were sparged with UHP

argon and dried by passage through columns containing Q-5 and molecular sieves prior to use. Deuterated NMR solvent were dried over NaK alloy, degassed by three freeze-pump-thaw cycles, and vacuum transferred prior to use. ^{1}H and ^{29}Si{^{1}H} NMR spectra were collected at room temperature on an AVANCE600 MHZ spectrometer. UV-visible spectra were collected on a Varian Cary 50 Scan UV-visible spectrophotometer in 1 mm quartz cuvette. Infrared spectra were collected as compressed solids on an Agilent Cary 630 ATR-FTIR. Elemental analyses were conducted on a PerkinElmer 2400 Series II CHNS elemental analyzer. $(C_5Me_5)_2U(NR_2)$,[13] $(C_5Me_5)U(NR_2)_2$,[14] and KC_8[60] were synthesized following literature procedures. 2.2.2-cryptand (crypt) (Aldrich) was dried under 10^{-5} Torr for 12 h before use.

Synthesis of 4.1. $(C_5Me_5)_2U(NR_2)$ (44 mg, 0.066 mmol) and crypt (25 mg, 0.066 mmol) were dissolved in THF (1 mL) in a vial and chilled to −35 °C. In a separate vial, hexane (18 mL) was chilled −35 °C. A pipet was packed with KC_8 (~20 mg, excess) to form a KC_8 reduction column and also chilled to −35 °C. The solution of $(C_5Me_5)_2U(NR_2)$ and crypt was passed through the KC_8 column to form a dark blue/black solution. This solution was immediately filtered and layered under the chilled hexane and placed in the freezer at −35 °C. Overnight, dark brown X-ray quality crystals of **4.1** deposited (70 mg, 97%). Due to the low symmetry and paramagnetism of **4.1**, the ^{1}H NMR spectra could not be confidently assigned. ^{29}Si{^{1}H} (THF-d_8): δ 5.08, −44.63 ppm. IR: 2881s, 2844s, 2716sh, 1476m, 1442m, 1354s, 1295m, 1259m, 1231s, 1173w, 1102s, 1078m, 1007m, 980m, 949s, 830m, 749m, 706m, 652m cm^{-1}. Anal Calcd for $C_{44}H_{83}KN_3O_6Si_2U$: C 48.78, H 7.72, N 3.88. Found: C 46.57, H 7.47, N 3.31. Incomplete combustion and low C values were found across multiple samples, but the experimental C:H:N ratio of $C_{44}H_{84}N_{2.7}$ is close to the expected value.[61–66]

Synthesis of 4.2. In a similar synthesis as above, **(**C_5Me_5)U(NR_2)$_2$ (53 mg, 0.076 mmol), crypt (29 mg, 0.077 mmol) and KC_8 (excess) were reacted to form a dark brown solution. Layering this solution under chilled hexane overnight yielded black X-ray quality crystals of **4.2** (74 mg, 82%). Due to the low symmetry and paramagnetism of **4.2**, the ^{1}H NMR spectra could not be confidently assigned. ^{29}Si{^{1}H} (THF-d_8): δ 302.55 ppm. IR: 2944m, 2881m, 1476m, 1443m, 1354s, 1294m, 1235s, 1101s, 949s, 820s, 751m, 659m cm^{-1}. Anal Calcd for $C_{40}H_{86}KN_4O_6Si_4U$: C 43.34, H 7.82, N 5.05. Found: C 39.28, H 7.02, N 4.00. Incomplete combustion and low C values were found across multiple samples, but the experimental C:H:N ratio of $C_{40}H_{85.2}N_{3.6}$ is close to the expected value.[61–66]

Crystallographic Data

X-ray Data Collection, Structure Solution and Refinement for 4.1. A black crystal of approximate dimensions 0.109 x 0.165 x 0.183 mm was mounted in a cryoloop and transferred to a Bruker SMART APEX II diffractometer. The APEX2[67] program package and the CELL_NOW[68] were used to determine the unit-cell parameters. Data was collected using a 120 sec/frame scan time. The raw frame data was processed using SAINT[69] and TWINABS[70] to yield the reflection data file (HKLF5 format).[70] Subsequent calculations were carried out using the SHELXTL[71] program. There were no systematic absences nor any diffraction symmetry other than the Friedel condition. The centrosymmetric triclinic space group $P\bar{1}$ was assigned and later determined to be correct.

The structure was solved by direct methods and refined on F^2 by full-matrix least-squares techniques. The analytical scattering factors[72] for neutral atoms were used throughout the analysis. Hydrogen atoms were included using a riding model. The uranium atom was disordered (0.91/0.09) and included using multiple components and partial site-occupancy-factors.

Least-squares analysis yielded wR2 = 0.0910 and Goof = 1.054 for 539 variables refined against 10446 data (0.80 Å), R1 = 0.0445 for those 9263 with I > 2.0σ(I). The structure was refined as a two-component twin, BASF[71] = 0.1749.

Table 4.3. Crystal data and structure refinement for **4.1** and **4.2**.

	4.1	**4.2**
Identification code	jcw27	jcw30
Empirical formula	C_{44} H_{83} K N_3 O_6 Si_2 U	C_{44} H_{94} K N_4 O_7 Si_4 U
Formula weight	1083.44	1180.72
Temperature (K)	133(2)	93(2)
Wavelength (Å)	0.71073	0.71073
Crystal system	Triclinic	Monoclinic
Space group	$P\bar{1}$	$P2_1/c$
a (Å)	9.2058(9)	11.1961(7)
b (Å)	16.3697(16)	29.3529(18)
c (Å)	16.9560(16)	17.8199(11)
α (°)	93.4572(17)	90
β (°)	92.9995(17)	93.8794(11)
γ (°)	90.7046(16)	90
Volume (Å^3)	2546.8(4)	5842.9(6)
Z	2	4
Calculated density (mg/m^3)	1.413	1.342
Absorption Coefficient (mm^{-1})	3.360	2.975
F(000)	1110	2436
Crystal color	Black	Black
Crystal size (mm^3)	0.183 x 0.165 x 0.109	0.280 x 0.183 x 0.168
θ range for data collection (°)	1.205 to 26.372	1.339 to 26.372
Index ranges	$-11 \le h \le 11$, $-20 \le k \le 20$, $0 \le l \le 21$	$-13 \le h \le 13$, $-36 \le k \le 36$, $-22 \le l \le 22$
Reflections collected	10446	70405
Completeness to θ = 25.500°	100.0%	100.0%
Absorption correction	Semi-empirical from equivalents	Semi-empirical from equivalents
Max. and min. transmission	0.4311 and 0.3086	0.7457 and 0.5874
Refinement method	Full-matrix least-squares on F^2	Full-matrix least-squares on F^2
Data / restraints / parameters	10446 / 0 / 539	11941 / 0 574
Goodness-of-fit on F^2	1.054	1.022
Final R indices [I>2σ(I)]	R1 = 0.0445, wR2 = 0.0869	R1 = 0.0400, wR2 = 0.0804
R indices (all data)	R1 = 0.0556, wR2 = 0.0910	R1 = 0.0645, wR2 = 0.0891
Data cutoff (Å)	0.80	0.80
Largest diff. peak and hole (e.A^{-3})	1.367 and −1.314	1.283 and −0.701

Table 4.4. Bond lengths [Å] and angles [°] for **4.1**.

U(1)-Cnt1	2.559	C(12)-C(13)	1.407(8)
U(1)-Cnt2	2.584	C(12)-C(17)	1.490(8)
U(1)-N(1)	2.354(5)	C(13)-C(14)	1.401(8)
U(1)-C(21)	2.558(6)	C(13)-C(18)	1.516(7)
U(1)-C(4)	2.793(5)	C(14)-C(15)	1.419(7)
U(1)-C(12)	2.798(5)	C(14)-C(19)	1.508(8)
U(1)-C(5)	2.810(5)	C(15)-C(20)	1.494(7)
U(1)-C(3)	2.826(5)	K(1)-O(6)	2.789(4)
U(1)-C(11)	2.830(5)	K(1)-O(3)	2.790(4)
U(1)-C(1)	2.846(5)	K(1)-O(2)	2.818(4)
U(1)-C(13)	2.854(5)	K(1)-O(1)	2.820(4)
U(1)-C(2)	2.871(5)	K(1)-O(4)	2.853(4)
U(1)-C(14)	2.881(5)	K(1)-O(5)	2.854(4)
U(1)-C(15)	2.881(5)	K(1)-N(2)	3.028(4)
Si(1)-N(1)	1.733(5)	K(1)-N(3)	3.045(5)
Si(1)-C(21)	1.856(7)	O(1)-C(29)	1.426(7)
Si(1)-C(23)	1.888(6)	O(1)-C(28)	1.438(6)
Si(1)-C(22)	1.891(7)	O(2)-C(30)	1.424(7)
Si(2)-N(1)	1.676(5)	O(2)-C(31)	1.428(6)
Si(2)-C(24)	1.871(6)	O(3)-C(35)	1.412(7)
Si(2)-C(25)	1.878(7)	O(3)-C(34)	1.424(7)
Si(2)-C(26)	1.887(7)	O(4)-C(36)	1.421(8)
C(1)-C(2)	1.415(7)	O(4)-C(37)	1.429(8)
C(1)-C(5)	1.417(7)	O(5)-C(40)	1.418(7)
C(1)-C(6)	1.507(8)	O(5)-C(41)	1.427(7)
C(2)-C(3)	1.415(8)	O(6)-C(42)	1.417(7)
C(2)-C(7)	1.508(8)	O(6)-C(43)	1.430(7)
C(3)-C(4)	1.427(8)	N(2)-C(33)	1.466(7)
C(3)-C(8)	1.510(7)	N(2)-C(27)	1.467(7)
C(4)-C(5)	1.414(7)	N(2)-C(39)	1.475(7)
C(4)-C(9)	1.504(8)	N(3)-C(44)	1.457(8)
C(5)-C(10)	1.505(7)	N(3)-C(38)	1.467(7)
C(11)-C(12)	1.410(8)	N(3)-C(32)	1.473(7)
C(11)-C(15)	1.419(8)	C(27)-C(28)	1.498(8)
C(11)-C(16)	1.504(7)	C(29)-C(30)	1.488(8)

C(31)-C(32)	1.495(9)	C(4)-U(1)-C(1)	48.02(15)
C(33)-C(34)	1.508(8)	C(12)-U(1)-C(1)	109.98(16)
C(35)-C(36)	1.493(10)	C(5)-U(1)-C(1)	29.00(15)
C(37)-C(38)	1.502(9)	C(3)-U(1)-C(1)	47.64(15)
C(39)-C(40)	1.512(9)	C(11)-U(1)-C(1)	133.20(16)
C(41)-C(42)	1.487(8)	N(1)-U(1)-C(13)	130.95(16)
C(43)-C(44)	1.497(8)	C(21)-U(1)-C(13)	124.88(19)
		C(4)-U(1)-C(13)	115.36(15)
Cnt1-U(1)-N(1)	114.6	C(12)-U(1)-C(13)	28.80(16)
Cnt1-U(1)-C(21)	101.9	C(5)-U(1)-C(13)	133.18(15)
Cnt2-U(1)-N(1)	109.8	C(3)-U(1)-C(13)	87.86(15)
Cnt2-U(1)-C(21)	109.1	C(11)-U(1)-C(13)	47.24(14)
Cnt1-U(1)-Cnt2	132.5	C(1)-U(1)-C(13)	112.31(15)
N(1)-U(1)-C(21)	69.1(2)	N(1)-U(1)-C(2)	139.08(15)
N(1)-U(1)-C(4)	95.02(16)	C(21)-U(1)-C(2)	105.07(18)
C(21)-U(1)-C(4)	111.55(18)	C(4)-U(1)-C(2)	47.87(16)
N(1)-U(1)-C(12)	126.60(16)	C(12)-U(1)-C(2)	93.94(15)
C(21)-U(1)-C(12)	96.09(19)	C(5)-U(1)-C(2)	47.55(15)
C(4)-U(1)-C(12)	136.64(16)	C(3)-U(1)-C(2)	28.76(15)
N(1)-U(1)-C(5)	91.92(15)	C(11)-U(1)-C(2)	122.63(16)
C(21)-U(1)-C(5)	83.26(18)	C(1)-U(1)-C(2)	28.65(14)
C(4)-U(1)-C(5)	29.24(15)	C(13)-U(1)-C(2)	86.71(15)
C(12)-U(1)-C(5)	138.65(16)	N(1)-U(1)-C(14)	104.05(16)
N(1)-U(1)-C(3)	122.92(16)	C(21)-U(1)-C(14)	130.72(18)
C(21)-U(1)-C(3)	126.85(18)	C(4)-U(1)-C(14)	117.70(15)
C(4)-U(1)-C(3)	29.42(15)	C(12)-U(1)-C(14)	47.32(16)
C(12)-U(1)-C(3)	107.23(15)	C(5)-U(1)-C(14)	145.67(14)
C(5)-U(1)-C(3)	48.01(14)	C(3)-U(1)-C(14)	98.59(15)
N(1)-U(1)-C(11)	97.61(16)	C(11)-U(1)-C(14)	47.23(15)
C(21)-U(1)-C(11)	84.32(18)	C(1)-U(1)-C(14)	136.89(15)
C(4)-U(1)-C(11)	162.54(15)	C(13)-U(1)-C(14)	28.28(16)
C(12)-U(1)-C(11)	29.00(16)	C(2)-U(1)-C(14)	108.61(15)
C(5)-U(1)-C(11)	160.50(16)	N(1)-U(1)-C(15)	85.31(15)
C(3)-U(1)-C(11)	134.35(15)	C(21)-U(1)-C(15)	104.03(17)
N(1)-U(1)-C(1)	116.60(15)	C(4)-U(1)-C(15)	142.02(15)
C(21)-U(1)-C(1)	79.74(18)	C(12)-U(1)-C(15)	47.49(16)

C(5)-U(1)-C(15)	170.61(15)	C(3)-C(2)-U(1)	73.8(3)
C(3)-U(1)-C(15)	127.08(14)	C(7)-C(2)-U(1)	125.0(3)
C(11)-U(1)-C(15)	28.75(16)	C(2)-C(3)-C(4)	108.0(4)
C(1)-U(1)-C(15)	157.12(16)	C(2)-C(3)-C(8)	127.7(5)
C(13)-U(1)-C(15)	46.87(15)	C(4)-C(3)-C(8)	124.1(5)
C(2)-U(1)-C(15)	133.55(14)	C(2)-C(3)-U(1)	77.4(3)
C(14)-U(1)-C(15)	28.52(14)	C(4)-C(3)-U(1)	74.0(3)
N(1)-Si(1)-C(21)	102.0(3)	C(8)-C(3)-U(1)	118.9(3)
N(1)-Si(1)-C(23)	112.5(3)	C(5)-C(4)-C(3)	107.6(5)
C(21)-Si(1)-C(23)	112.6(3)	C(5)-C(4)-C(9)	125.0(5)
N(1)-Si(1)-C(22)	111.6(3)	C(3)-C(4)-C(9)	127.0(5)
C(21)-Si(1)-C(22)	115.8(3)	C(5)-C(4)-U(1)	76.0(3)
C(23)-Si(1)-C(22)	102.7(3)	C(3)-C(4)-U(1)	76.6(3)
N(1)-Si(1)-U(1)	47.67(16)	C(9)-C(4)-U(1)	119.7(3)
C(21)-Si(1)-U(1)	54.5(2)	C(4)-C(5)-C(1)	108.3(5)
C(23)-Si(1)-U(1)	124.4(2)	C(4)-C(5)-C(10)	125.1(5)
C(22)-Si(1)-U(1)	132.5(2)	C(1)-C(5)-C(10)	126.3(5)
N(1)-Si(2)-C(24)	114.0(3)	C(4)-C(5)-U(1)	74.7(3)
N(1)-Si(2)-C(25)	113.9(3)	C(1)-C(5)-U(1)	76.9(3)
C(24)-Si(2)-C(25)	105.7(3)	C(10)-C(5)-U(1)	119.2(3)
N(1)-Si(2)-C(26)	111.6(3)	C(12)-C(11)-C(15)	108.0(4)
C(24)-Si(2)-C(26)	105.2(3)	C(12)-C(11)-C(16)	126.2(5)
C(25)-Si(2)-C(26)	105.6(3)	C(15)-C(11)-C(16)	125.5(5)
Si(2)-N(1)-Si(1)	129.4(3)	C(12)-C(11)-U(1)	74.2(3)
Si(2)-N(1)-U(1)	131.2(3)	C(15)-C(11)-U(1)	77.6(3)
Si(1)-N(1)-U(1)	99.4(2)	C(16)-C(11)-U(1)	119.9(3)
C(2)-C(1)-C(5)	108.0(5)	C(13)-C(12)-C(11)	107.9(5)
C(2)-C(1)-C(6)	124.6(5)	C(13)-C(12)-C(17)	126.7(5)
C(5)-C(1)-C(6)	127.0(5)	C(11)-C(12)-C(17)	125.3(5)
C(2)-C(1)-U(1)	76.7(3)	C(13)-C(12)-U(1)	77.8(3)
C(5)-C(1)-U(1)	74.1(3)	C(11)-C(12)-U(1)	76.8(3)
C(6)-C(1)-U(1)	120.8(4)	C(17)-C(12)-U(1)	114.1(4)
C(1)-C(2)-C(3)	108.1(5)	C(14)-C(13)-C(12)	108.6(5)
C(1)-C(2)-C(7)	124.5(5)	C(14)-C(13)-C(18)	126.0(5)
C(3)-C(2)-C(7)	126.7(5)	C(12)-C(13)-C(18)	124.7(5)
C(1)-C(2)-U(1)	74.7(3)	C(14)-C(13)-U(1)	76.9(3)

C(12)-C(13)-U(1)	73.4(3)	O(6)-K(1)-N(3)	60.33(12)
C(18)-C(13)-U(1)	123.3(4)	O(3)-K(1)-N(3)	119.51(12)
C(13)-C(14)-C(15)	108.0(5)	O(2)-K(1)-N(3)	60.01(12)
C(13)-C(14)-C(19)	126.2(5)	O(1)-K(1)-N(3)	119.57(12)
C(15)-C(14)-C(19)	125.5(5)	O(4)-K(1)-N(3)	59.94(12)
C(13)-C(14)-U(1)	74.8(3)	O(5)-K(1)-N(3)	120.07(12)
C(15)-C(14)-U(1)	75.7(3)	N(2)-K(1)-N(3)	179.15(13)
C(19)-C(14)-U(1)	120.3(3)	C(29)-O(1)-C(28)	111.1(4)
C(11)-C(15)-C(14)	107.5(5)	C(29)-O(1)-K(1)	114.8(3)
C(11)-C(15)-C(20)	125.3(5)	C(28)-O(1)-K(1)	116.8(3)
C(14)-C(15)-C(20)	126.8(5)	C(30)-O(2)-C(31)	111.5(4)
C(11)-C(15)-U(1)	73.7(3)	C(30)-O(2)-K(1)	114.3(3)
C(14)-C(15)-U(1)	75.7(3)	C(31)-O(2)-K(1)	117.9(3)
C(20)-C(15)-U(1)	121.9(3)	C(35)-O(3)-C(34)	111.6(5)
Si(1)-C(21)-U(1)	89.3(3)	C(35)-O(3)-K(1)	117.2(3)
O(6)-K(1)-O(3)	123.88(12)	C(34)-O(3)-K(1)	120.0(3)
O(6)-K(1)-O(2)	99.42(12)	C(36)-O(4)-C(37)	110.9(5)
O(3)-K(1)-O(2)	130.54(12)	C(36)-O(4)-K(1)	112.4(3)
O(6)-K(1)-O(1)	137.37(12)	C(37)-O(4)-K(1)	115.5(3)
O(3)-K(1)-O(1)	94.35(12)	C(40)-O(5)-C(41)	111.1(4)
O(2)-K(1)-O(1)	59.98(11)	C(40)-O(5)-K(1)	115.3(3)
O(6)-K(1)-O(4)	98.11(12)	C(41)-O(5)-K(1)	111.3(3)
O(3)-K(1)-O(4)	59.91(11)	C(42)-O(6)-C(43)	112.2(4)
O(2)-K(1)-O(4)	94.31(12)	C(42)-O(6)-K(1)	116.7(3)
O(1)-K(1)-O(4)	118.90(13)	C(43)-O(6)-K(1)	116.7(3)
O(6)-K(1)-O(5)	60.24(11)	C(33)-N(2)-C(27)	110.1(5)
O(3)-K(1)-O(5)	99.17(11)	C(33)-N(2)-C(39)	110.0(4)
O(2)-K(1)-O(5)	124.53(12)	C(27)-N(2)-C(39)	109.7(4)
O(1)-K(1)-O(5)	99.00(11)	C(33)-N(2)-K(1)	108.8(3)
O(4)-K(1)-O(5)	136.49(13)	C(27)-N(2)-K(1)	109.8(3)
O(6)-K(1)-N(2)	120.52(12)	C(39)-N(2)-K(1)	108.5(3)
O(3)-K(1)-N(2)	60.09(12)	C(44)-N(3)-C(38)	110.8(5)
O(2)-K(1)-N(2)	119.57(12)	C(44)-N(3)-C(32)	110.2(5)
O(1)-K(1)-N(2)	59.92(12)	C(38)-N(3)-C(32)	109.5(4)
O(4)-K(1)-N(2)	119.58(12)	C(44)-N(3)-K(1)	108.5(3)
O(5)-K(1)-N(2)	60.78(12)	C(38)-N(3)-K(1)	109.5(3)

C(32)-N(3)-K(1)	108.4(3)	O(4)-C(36)-C(35)	109.5(6)
N(2)-C(27)-C(28)	113.8(5)	O(4)-C(37)-C(38)	109.1(5)
O(1)-C(28)-C(27)	108.4(4)	N(3)-C(38)-C(37)	113.8(5)
O(1)-C(29)-C(30)	108.6(5)	N(2)-C(39)-C(40)	113.8(5)
O(2)-C(30)-C(29)	109.0(5)	O(5)-C(40)-C(39)	109.7(4)
O(2)-C(31)-C(32)	109.0(4)	O(5)-C(41)-C(42)	109.1(5)
N(3)-C(32)-C(31)	113.5(5)	O(6)-C(42)-C(41)	109.6(5)
N(2)-C(33)-C(34)	114.1(5)	O(6)-C(43)-C(44)	109.2(5)
O(3)-C(34)-C(33)	109.0(5)	N(3)-C(44)-C(43)	114.1(5)
O(3)-C(35)-C(36)	109.0(6)		

X-ray Data Collection, Structure Solution and Refinement for 4.2. A black crystal of approximate dimensions 0.168 x 0.183 x 0.280 mm was mounted in a cryoloop and transferred to a Bruker SMART APEX II diffractometer. The APEX2[67] program package was used to determine the unit-cell parameters and for data collection with 30 sec/frame scan time. The raw frame data was processed using SAINT[69] and SADABS[73] to yield the reflection data file. Subsequent calculations were carried out using the SHELXTL[71] program. The diffraction symmetry was 2/*m* and the systematic absences were consistent with the monoclinic space group $P2_1/c$ that was later determined to be correct.

The structure was solved by direct methods and refined on F^2 by full-matrix least-squares techniques. The analytical scattering factors[72] for neutral atoms were used throughout the analysis. Hydrogen atoms were included using a riding model. The uranium atom and C(41) were disordered and included using multiple components with partial site-occupancy-factors.

Least-squares analysis yielded wR2 = 0.0891 and Goof = 1.022 for 574 variables refined against 11941 data (0.80 Å), R1 = 0.0400 for those 8996 data with $I > 2.0\sigma(I)$.

Table 4.5. Bond lengths [Å] and angles [°] for **4.2**.

U(1)-Cnt	2.533	U(1)-N(1)	2.363(4)

U(1)-N(2)	2.399(4)	K(1)-O(1)	2.838(3)
U(1)-C(11)	2.500(5)	K(1)-O(4)	2.883(3)
U(1)-C(5)	2.784(4)	K(1)-O(3)	2.915(3)
U(1)-C(4)	2.789(4)	K(1)-N(3)	3.007(4)
U(1)-C(3)	2.802(5)	K(1)-N(4)	3.038(4)
U(1)-C(1)	2.813(5)	K(1)-O(7)	3.314(4)
U(1)-C(2)	2.813(5)	O(1)-C(35)	1.417(6)
Si(1)-N(1)	1.744(4)	O(1)-C(34)	1.433(6)
Si(1)-C(11)	1.850(5)	O(2)-C(37)	1.406(7)
Si(1)-C(12)	1.867(5)	O(2)-C(36)	1.429(7)
Si(1)-C(13)	1.879(5)	O(3)-C(29)	1.416(5)
Si(2)-N(2)	1.714(4)	O(3)-C(28)	1.422(5)
Si(2)-C(18)	1.871(5)	O(4)-C(30)	1.421(5)
Si(2)-C(19)	1.876(5)	O(4)-C(31)	1.428(5)
Si(2)-C(17)	1.883(6)	O(5)-C(23)	1.411(6)
Si(3)-N(2)	1.699(4)	O(5)-C(44)	1.420(6)
Si(3)-C(21)	1.867(6)	O(6)-C(25)	1.419(6)
Si(3)-C(20)	1.880(5)	O(6)-C(24)	1.427(6)
Si(3)-C(22)	1.886(5)	O(7)-C(42)	1.408(7)
Si(4)-N(1)	1.687(4)	O(7)-C(39)	1.426(7)
Si(4)-C(16)	1.865(5)	N(3)-C(26)	1.459(8)
Si(4)-C(14)	1.887(5)	N(3)-C(38)	1.473(8)
Si(4)-C(15)	1.890(6)	N(3)-C(27)	1.489(6)
C(1)-C(2)	1.393(7)	N(4)-C(43)	1.463(6)
C(1)-C(5)	1.406(7)	N(4)-C(33)	1.464(6)
C(1)-C(6)	1.511(7)	N(4)-C(32)	1.470(6)
C(2)-C(3)	1.409(7)	C(23)-C(24)	1.493(7)
C(2)-C(7)	1.523(7)	C(25)-C(26)	1.511(8)
C(3)-C(4)	1.397(7)	C(27)-C(28)	1.498(7)
C(3)-C(8)	1.509(8)	C(29)-C(30)	1.488(6)
C(4)-C(5)	1.408(7)	C(31)-C(32)	1.492(7)
C(4)-C(9)	1.523(7)	C(33)-C(34)	1.491(8)
C(5)-C(10)	1.499(7)	C(35)-C(36)	1.474(8)
K(1)-O(2)	2.757(3)	C(37)-C(38)	1.486(9)
K(1)-O(5)	2.796(3)	C(39)-C(40)	1.467(9)
K(1)-O(6)	2.812(3)	C(40)-C(41)	1.48(2)

C(40)-C(41B)	1.619(12)	N(1)-Si(1)-C(11)	103.9(2)
C(41)-C(42)	1.45(2)	N(1)-Si(1)-C(12)	112.6(2)
C(41B)-C(42)	1.474(11)	C(11)-Si(1)-C(12)	110.4(2)
C(43)-C(44)	1.500(7)	N(1)-Si(1)-C(13)	110.7(2)
		C(11)-Si(1)-C(13)	113.1(2)
Cnt-U(1)-N(1)	119.5	C(12)-Si(1)-C(13)	106.3(2)
Cnt-U(1)-N(2)	123.3	N(1)-Si(1)-U(1)	49.71(12)
Cnt-U(1)-C(21)	111.5	C(11)-Si(1)-U(1)	54.21(15)
N(1)-U(1)-N(2)	114.09(12)	C(12)-Si(1)-U(1)	125.12(17)
N(1)-U(1)-C(11)	71.12(14)	C(13)-Si(1)-U(1)	128.48(16)
N(2)-U(1)-C(11)	101.77(15)	N(2)-Si(2)-C(18)	109.5(2)
N(1)-U(1)-C(5)	108.41(13)	N(2)-Si(2)-C(19)	115.0(2)
N(2)-U(1)-C(5)	119.20(13)	C(18)-Si(2)-C(19)	104.3(3)
C(11)-U(1)-C(5)	132.61(16)	N(2)-Si(2)-C(17)	113.2(2)
N(1)-U(1)-C(4)	137.61(14)	C(18)-Si(2)-C(17)	106.9(3)
N(2)-U(1)-C(4)	98.90(13)	C(19)-Si(2)-C(17)	107.3(3)
C(11)-U(1)-C(4)	128.79(16)	N(2)-Si(3)-C(21)	112.3(2)
C(5)-U(1)-C(4)	29.26(14)	N(2)-Si(3)-C(20)	112.9(2)
N(1)-U(1)-C(3)	138.94(14)	C(21)-Si(3)-C(20)	105.3(3)
N(2)-U(1)-C(3)	106.95(14)	N(2)-Si(3)-C(22)	113.6(2)
C(11)-U(1)-C(3)	99.89(16)	C(21)-Si(3)-C(22)	106.5(3)
C(5)-U(1)-C(3)	48.14(14)	C(20)-Si(3)-C(22)	105.6(3)
C(4)-U(1)-C(3)	28.95(15)	N(1)-Si(4)-C(16)	112.0(2)
N(1)-U(1)-C(1)	94.60(13)	N(1)-Si(4)-C(14)	114.6(2)
N(2)-U(1)-C(1)	146.18(13)	C(16)-Si(4)-C(14)	104.2(2)
C(11)-U(1)-C(1)	104.34(16)	N(1)-Si(4)-C(15)	111.8(2)
C(5)-U(1)-C(1)	29.10(14)	C(16)-Si(4)-C(15)	107.5(2)
C(4)-U(1)-C(1)	47.61(14)	C(14)-Si(4)-C(15)	106.3(3)
C(3)-U(1)-C(1)	47.56(15)	Si(4)-N(1)-Si(1)	125.7(2)
N(1)-U(1)-C(2)	110.10(15)	Si(4)-N(1)-U(1)	137.64(19)
N(2)-U(1)-C(2)	135.37(15)	Si(1)-N(1)-U(1)	96.04(16)
C(11)-U(1)-C(2)	86.49(16)	Si(3)-N(2)-Si(2)	122.0(2)
C(5)-U(1)-C(2)	47.99(14)	Si(3)-N(2)-U(1)	123.4(2)
C(4)-U(1)-C(2)	47.73(14)	Si(2)-N(2)-U(1)	114.38(19)
C(3)-U(1)-C(2)	29.06(15)	C(2)-C(1)-C(5)	108.8(4)
C(1)-U(1)-C(2)	28.67(15)	C(2)-C(1)-C(6)	126.3(5)

C(5)-C(1)-C(6)	124.8(6)	O(5)-K(1)-O(4)	93.35(9)
C(2)-C(1)-U(1)	75.7(3)	O(6)-K(1)-O(4)	114.58(10)
C(5)-C(1)-U(1)	74.3(3)	O(1)-K(1)-O(4)	94.56(10)
C(6)-C(1)-U(1)	116.9(3)	O(2)-K(1)-O(3)	95.16(10)
C(1)-C(2)-C(3)	107.8(4)	O(5)-K(1)-O(3)	131.63(10)
C(1)-C(2)-C(7)	125.7(6)	O(6)-K(1)-O(3)	93.26(10)
C(3)-C(2)-C(7)	126.2(6)	O(1)-K(1)-O(3)	117.14(10)
C(1)-C(2)-U(1)	75.6(3)	O(4)-K(1)-O(3)	58.65(8)
C(3)-C(2)-U(1)	75.0(3)	O(2)-K(1)-N(3)	60.94(13)
C(7)-C(2)-U(1)	120.6(3)	O(5)-K(1)-N(3)	121.66(12)
C(4)-C(3)-C(2)	107.8(5)	O(6)-K(1)-N(3)	60.90(11)
C(4)-C(3)-C(8)	126.4(6)	O(1)-K(1)-N(3)	121.28(13)
C(2)-C(3)-C(8)	125.6(6)	O(4)-K(1)-N(3)	117.19(10)
C(4)-C(3)-U(1)	75.0(3)	O(3)-K(1)-N(3)	59.25(10)
C(2)-C(3)-U(1)	75.9(3)	O(2)-K(1)-N(4)	120.73(12)
C(8)-C(3)-U(1)	119.1(4)	O(5)-K(1)-N(4)	60.12(11)
C(3)-C(4)-C(5)	108.6(4)	O(6)-K(1)-N(4)	120.30(11)
C(3)-C(4)-C(9)	125.7(5)	O(1)-K(1)-N(4)	59.84(10)
C(5)-C(4)-C(9)	125.6(5)	O(4)-K(1)-N(4)	59.36(10)
C(3)-C(4)-U(1)	76.0(3)	O(3)-K(1)-N(4)	117.27(10)
C(5)-C(4)-U(1)	75.2(3)	N(3)-K(1)-N(4)	176.52(11)
C(9)-C(4)-U(1)	116.8(3)	O(2)-K(1)-O(7)	63.67(10)
C(1)-C(5)-C(4)	106.9(4)	O(5)-K(1)-O(7)	65.69(9)
C(1)-C(5)-C(10)	125.4(5)	O(6)-K(1)-O(7)	70.94(10)
C(4)-C(5)-C(10)	127.0(5)	O(1)-K(1)-O(7)	75.49(11)
C(1)-C(5)-U(1)	76.6(3)	O(4)-K(1)-O(7)	153.39(10)
C(4)-C(5)-U(1)	75.6(3)	O(3)-K(1)-O(7)	147.77(10)
C(10)-C(5)-U(1)	121.4(3)	N(3)-K(1)-O(7)	88.64(11)
Si(1)-C(11)-U(1)	88.90(18)	N(4)-K(1)-O(7)	94.85(11)
O(2)-K(1)-O(5)	129.22(10)	C(35)-O(1)-C(34)	111.5(4)
O(2)-K(1)-O(6)	104.30(11)	C(35)-O(1)-K(1)	110.8(3)
O(5)-K(1)-O(6)	61.33(10)	C(34)-O(1)-K(1)	115.1(3)
O(2)-K(1)-O(1)	61.36(12)	C(37)-O(2)-C(36)	112.2(5)
O(5)-K(1)-O(1)	102.46(10)	C(37)-O(2)-K(1)	120.6(3)
O(6)-K(1)-O(1)	146.34(10)	C(36)-O(2)-K(1)	114.8(3)
O(2)-K(1)-O(4)	133.04(10)	C(29)-O(3)-C(28)	110.6(3)

C(29)-O(3)-K(1)	113.4(2)	C(32)-N(4)-K(1)	110.2(3)
C(28)-O(3)-K(1)	117.4(3)	O(5)-C(23)-C(24)	109.7(4)
C(30)-O(4)-C(31)	111.4(4)	O(6)-C(24)-C(23)	108.7(4)
C(30)-O(4)-K(1)	115.6(2)	O(6)-C(25)-C(26)	108.8(4)
C(31)-O(4)-K(1)	117.3(3)	N(3)-C(26)-C(25)	113.8(5)
C(23)-O(5)-C(44)	112.1(4)	N(3)-C(27)-C(28)	113.4(4)
C(23)-O(5)-K(1)	112.6(3)	O(3)-C(28)-C(27)	108.7(4)
C(44)-O(5)-K(1)	119.9(3)	O(3)-C(29)-C(30)	109.0(4)
C(25)-O(6)-C(24)	111.3(4)	O(4)-C(30)-C(29)	109.6(4)
C(25)-O(6)-K(1)	113.8(3)	O(4)-C(31)-C(32)	109.2(4)
C(24)-O(6)-K(1)	112.5(3)	N(4)-C(32)-C(31)	114.2(4)
C(42)-O(7)-C(39)	106.6(5)	N(4)-C(33)-C(34)	113.1(5)
C(42)-O(7)-K(1)	122.6(4)	O(1)-C(34)-C(33)	109.3(4)
C(39)-O(7)-K(1)	129.6(4)	O(1)-C(35)-C(36)	109.8(4)
C(26)-N(3)-C(38)	112.1(5)	O(2)-C(36)-C(35)	110.0(4)
C(26)-N(3)-C(27)	109.7(5)	O(2)-C(37)-C(38)	109.2(5)
C(38)-N(3)-C(27)	108.9(4)	N(3)-C(38)-C(37)	115.9(5)
C(26)-N(3)-K(1)	108.9(3)	O(7)-C(39)-C(40)	110.0(6)
C(38)-N(3)-K(1)	106.2(3)	C(39)-C(40)-C(41)	99.2(10)
		C(39)-C(40)-C(41B)	98.5(6)
C(27)-N(3)-K(1)	110.9(3)	C(42)-C(41)-C(40)	105.5(14)
C(43)-N(4)-C(33)	109.9(4)	C(42)-C(41B)-C(40)	97.9(7)
C(43)-N(4)-C(32)	110.4(4)	O(7)-C(42)-C(41)	102.9(10)
C(33)-N(4)-C(32)	109.0(4)	O(7)-C(42)-C(41B)	108.0(6)
C(43)-N(4)-K(1)	107.5(3)	N(4)-C(43)-C(44)	113.4(4)
C(33)-N(4)-K(1)	109.9(3)	O(5)-C(44)-C(43)	109.8(4)

Computational Details

Theoretical calculations on $[(C_5Me_5)_2U(NR_2)]^{1-}$ and $[(C_5Me_5)U(NR_2)_2]^{1-}$ were carried out at the density functional level of theory using the TPSSh[26] functional with Grimme's D3 dispersion correction[74,75] in C_1 symmetry. Scalar relativistic effective core potentials (ECPs)[27] with the def-TZVP[76] basis set were used for U and polarized split-valence basis sets with diffuse functions def2-SV(P)[77] were used for the other atoms. Quadrature grids of size 4 were used throughout.[78]

The continuum solvation model COSMO[79] was included to model solvent effects with a dielectric constant of 7.52[80] and a refractive index of 1.3 for THF. Geometry optimizations were computed starting from X-ray structures with geometry convergence thresholds of 10^{-4} a.u. and energy convergence of 10^{-8} a.u. Ground state geometries were confirmed by the lack of imaginary frequencies in the vibrational spectrum. Time dependent density functional theory (TDDFT) calculations of vertical excitations and oscillator strengths were carried out on the solvent-optimized structures of $[(C_5Me_5)_2U(NR_2)]^{1-}$ and $[(C_5Me_5)U(NR_2)_2]^{1-}$ using def2-SVPD[81] basis sets for the ligands and def-TZVP basis set for U. An additional diffuse *p* primitive (Gaussian exponent 0.91577408313 x 10^{-2}) was added to the U basis set by downward extrapolation. Diffuse p augmentation is essential for accurate computational modeling of d to p excitations in similar f-element compounds with trigonal ligand fields.[82] UV-Vis spectra were simulated using Gaussian line profiles with a root mean-square width of 0.20 eV, and excitation energies were empirically shifted by 0.2 eV to account for systematic errors inherent in the functional, basis sets, and solvation model. Molecular orbitals and electronic transitions and states were analyzed with VMD[83] and Mulliken population analysis (MPA). All computations were completed using the TURBOMOLE program suite, Version V7.4.1.[84,85]

$[(C_5Me_5)_2U(NR_2)]^{1-}$. The solvent optimized structure of $[(C_5Me_5)_2U(NR_2)]^{1-}$ resulted in a C_1 symmetric minimum, a quintet (S = 2) state with $5f^36d^1$ occupation. Molecular orbital plots and population analysis revealed a highest occupied molecular orbital with $6dz^2$-like character. The structure is in qualitative agreement with the X-ray data with the U–N distance being ~0.06 Å longer, consistent with the experimental observed increase in bond distance upon reduction of U(III) to U(II). The average distance of U to the closest C in the amide methyl groups is 3.744 Å, approximately 1 Å larger than would be expected to form a bond. The average distance of U to the

corresponding closest H on the amide methyl groups is 3.256 Å, outside the typical M–H bond distance for any considerable interaction.

$(C_5Me_5)_2U(NR_2)$. Structure optimization of the neutral compound $(C_5Me_5)_2U(NR_2)$ resulted in a triplet (S = 3/2), C_1-symmetric ground state. The three highest occupied orbitals are almost pure 5f orbitals. The calculated LUMO was a 6dz2-like orbital with contribution from the C_5Me_5 π system. There was electron density observed on the methyl groups of the silylamide ligand, similar to what was found for U(II) species above.

$[(C_5Me_5)U(NR_2)_2]^{1-}$. Structure optimization of $[(C_5Me_5)U(NR_2)_2]^{1-}$ also resulted in a in a C_1 symmetric minimum, a quintet (S = 2) state with $5f^36d^1$ occupation. Molecular orbital plots and population analysis revealed a highest occupied molecular orbital with $6dz^2$-like character. The structure is in qualitative agreement with the X-ray data with the average U-N distance being ~0.2 pm shorter. The average distances of U to the closest C in the amide methyl groups are 3.699 and 3.757 Å with their corresponding closest H being 3.337 and 3.220 Å away from the U center.

Table 4.6: Electronic excitation summary for $[(C_5Me_5)_2U(NR_2)]^{1-}$ computed using the TPSSh functional with the def2-SVPD basis set for ligand atoms. All excitations computed are single excitations involving alpha spin to alpha spin transitions. Oscillator strengths are reported in the length gauge. Only transitions above 10% contribution to the overall excitation are listed.

Wavelength (nm)	Oscillator Strength (len)	Dominant Contributions			Assignment
		Occupied	Virtual	% weight	
876.5	0.037	138a	140a	25.0	$6d_z^2 \rightarrow 7p_z$
		138a	148a	23.0	$6d_z^2 \rightarrow 5f_{yz}^2$
		136a	142a	15.5	$5f_{z(x^2-y^2)} \rightarrow 7p_z+6d_{yz}+f$
		137a	148a	15.5	$5f_{y(y^2-3x^2)} \rightarrow 5f_{yz}^2$
852.5	0.019	138a	141a	97.1	$6d_z^2 \rightarrow 7p_x$
673.2	0.022	138a	144a	60.4	$6d_z^2 \rightarrow 7p_z+6d_{yz}+f$

			142a	22.8	$6d_z^2 \rightarrow 7p_z + 6d_{yz} + f$
605.0	0.010	138a	150a	43.9	$6d_z^2 \rightarrow 5f_{x(x^2-3y^2)}$
			149a	22.9	$6d_z^2 \rightarrow 5f_{z(x^2-y^2)} + 5f_z^3$
		137a	149a	16.5	$5f_{y(y^2-3x^2)} \rightarrow 5f_{z(x^2-y^2)} + 5f_z^3$
442.0	0.023	138a	144a	91.4	$6d_z^2 \rightarrow 7p_z + 6d_{yz} + f$
413.4	0.046	138a	158a	70.0	$6d_z^2 \rightarrow$ ligand
			156a	20.4	$6d_z^2 \rightarrow 7p_z +$ ligand
378.0	0.021	136a	162a	21.8	$5f_{z(x^2-y^2)} \rightarrow$ ligand
			154a	18.8	$5f_{z(x^2-y^2)} \rightarrow 5f_{y(y^2-3x^2)} + 5f_z^3$
			160a	16.3	$5f_{z(x^2-y^2)} \rightarrow 7p_y + 5f_z^3$
333.3	0.022	138a	169a	66.5	$6d_z^2 \rightarrow 7p_x + 5f_{xz}^2$
			168a	13.1	$6d_z^2 \rightarrow 7p_x + 5f_{y(y^2-3x^2)}$

$(C_5Me_5)U(NR_2)_2$. Structure optimization of the neutral compound $(C_5Me_5)U(NR_2)_2$ resulted in a triplet (S = 3/2), C_1-symmetric ground state. The three highest occupied orbitals are almost pure 5f orbitals. The calculated LUMO was a 5f orbital with contribution from the C_5Me_5 π system. There was no observed electron density on the methyl groups of the silylamide ligand, unlike what was found for the U(II) species above.

Table 4.7: Electronic excitation summary for $[(C_5Me_5)U(NR_2)_2]^{1-}$ computed using the TPSSh functional with the def2-SVPD basis set for ligand atoms. All excitations computed are single excitations involving alpha spin to alpha spin transitions. Oscillator strengths are reported in the length gauge.

Wavelength (nm)	Oscillator Strength (len)	Dominant Contributions			Assignment
		Occupied	Virtual	% weight	
796.6	0.017	145a	148a	71.3	$6d_z^2 \rightarrow 7p_z$
		145a	147a	19.4	$6d_z^2 \rightarrow 7p_x$
794.6	0.020	145a	147a	40.9	$6d_z^2 \rightarrow 7p_x$
			152a	23.0	$6d_z^2 \rightarrow 5f_{z(x^2-y^2)}$
			148a	10.3	$6d_z^2 \rightarrow 7p_z$
607.7	0.004	144a	148a	87.3	$5f_{y(y^2-3x^2)} \rightarrow 7p_z$
497.2	0.040	145a	156a	67.7	$6d_z^2 \rightarrow 6d_{x^2-y^2}$
			160a	17.2	$6d_z^2 \rightarrow$ ligand

390.4	0.027	145a	163a	71.1	$6d_z^2 \rightarrow$ ligand
			162a	15.0	$6d_z^2 \rightarrow 7p_z$+ligand
383.5	0.023	145a	166a	57.3	$6d_z^2 \rightarrow$ ligand
		144a	155a	13.9	$5f_{y(y^2-3x^2)} \rightarrow 6d_{xy}$
346.0	0.029	145a	172a	48.9	$6d_z^2 \rightarrow$ ligand
		143a	162a	9.4	$5f_{x(x^2-3y^2)} \rightarrow$ ligand

References

(1) MacDonald, M. R.; Fieser, M. E.; Bates, J. E.; Ziller, J. W.; Furche, F.; Evans, W. J. Identification of the +2 Oxidation State for Uranium in a Crystalline Molecular Complex, [K(2.2.2-Cryptand)][$(C_5H_4SiMe_3)_3U$]. *J. Am. Chem. Soc.* **2013**, *135*, 13310–13313, DOI: 10.1021/ja406791t.

(2) Windorff, C. J.; MacDonald, M. R.; Meihaus, K. R.; Ziller, J. W.; Long, J. R.; Evans, W. J. Expanding the Chemistry of Molecular U^{2+} Complexes: Synthesis, Characterization, and Reactivity of the $\{[C_5H_3(SiMe_3)_2]_3U\}^-$ Anion. *Chem. Eur. J.* **2016**, *22*, 772–782, DOI: 10.1002/chem.201503583.

(3) Ryan, A. J.; Angadol, M. A.; Ziller, J. W.; Evans, W. J. Isolation of U(II) Compounds Using Strong Donor Ligands, C_5Me_4H and $N(SiMe_3)_2$, Including a Three-Coordinate U(II) Complex. *Chem. Commun.* **2019**, *55*, 2325–2327, DOI: 10.1039/C8CC08767A.

(4) La Pierre, H. S.; Scheurer, A.; Heinemann, F. W.; Hieringer, W.; Meyer, K. Synthesis and Characterization of a Uranium(II) Monoarene Complex Supported by δ Backbonding. *Angew. Chemie Int. Ed.* **2014**, *53*, 7158–7162, DOI: 10.1002/anie.201402050.

(5) Billow, B. S.; Livesay, B. N.; Mokhtarzadeh, C. C.; Mccracken, J.; Shores, M. P.; Boncella, J. M.; Odom, A. L. Synthesis and Characterization of a Neutral U(II) Arene Sandwich Complex. *J. Am. Chem. Soc.* **2018**, *140*, 17369–17373, DOI: 10.1021/jacs.8b10888.

(6) Straub, M. D.; Ouellette, E. T.; Boreen, M. A.; Britt, R. D.; Chakarawet, K.; Douair, I.;

Gould, C. A.; Maron, L.; Del Rosal, I.; Villarreal, D.; Minasian, S. G.; Arnold, J. A Uranium(II) Arene Complex That Acts as a Uranium(I) Synthon. *J. Am. Chem. Soc.* **2021**, *143*, 19748–19760, DOI: 10.1021/jacs.1c07854.

(7) Huh, D. N.; Ziller, J. W.; Evans, W. J. Chelate-Free Synthesis of the U(II) Complex, $[(C_5H_3(SiMe_3)_2)_3U]^{1-}$, Using Li and Cs Reductants and Comparative Studies of La(II) and Ce(II) Analogs. *Inorg. Chem.* **2018**, *57*, 11809–11814, DOI: 10.1021/acs.inorgchem.8b01966.

(8) Guo, F. S.; Tsoureas, N.; Huang, G. Z.; Tong, M. L.; Mansikkamäki, A.; Layfield, R. A. Isolation of a Perfectly Linear Uranium(II) Metallocene. *Angew. Chem. Int. Ed.* **2020**, *59*, 2299–2303, DOI: 10.1002/anie.201912663.

(9) Evans, W. J.; Forrestal, K. J.; Ziller, J. W. Activity of $[Sm(C_5Me_5)_3]$ in Ethylene Polymerization and Synthesis of$[U(C_5Me_5)_3]$, the First Tris(Pentamethylcyclopentadienyl) 5f-Element Complex. *Angew. Chem. Int. Ed.* **1997**, *36*, 774–776, DOI: 10.1002/anie.199707741.

(10) Evans, W. J.; Davis, B. L. Chemistry of Tris (Pentamethylcyclopentadienyl) f-Element Complexes, $(C_5Me_5)_3M$. *Chem. Rev.* **2002**, *102*, 2119–2136, DOI: 10.1021/cr010298r.

(11) Corbey, J. F.; Woen, D. H.; Palumbo, C. T.; Fieser, M. E.; Ziller, J. W.; Furche, F.; Evans, W. J. Ligand Effects in the Synthesis of Ln^{2+} Complexes by Reduction of Tris(Cyclopentadienyl) Precursors Including C–H Bond Activation of an Indenyl Anion. *Organometallics* **2015**, *34*, 3909–3921, DOI: 10.1021/acs.organomet.5b00500.

(12) Fagan, P. J.; Manriquez, J. M.; Marks, T. J.; Day, C. S.; Day, V. W.; Vollmer, S. H.; Day, V. W. Synthesis and Properties of a New Class of Highly Reactive Trivalent Actinide Organometallic Compounds. Derivatives of

Bis(Pentamethylcyclopentadienyl)Uranium(III). *Organometallics* **1982**, *1*, 170–180, DOI: 10.1021/om00061a028.

(13) Evans, W. J.; Nyce, G. W.; Forrestal, K. J.; Ziller, J. W. Multiple Syntheses of $(C_5Me_5)_3U$. *Organometallics* **2002**, *21*, 1050–1055, DOI: 10.1021/om010831t.

(14) Avens, L. R.; Burns, C. J.; Butcher, R. J.; Clark, D. L.; Gordon, J. C.; Schake, A. R.; Scott, B. L.; Watkin, J. G.; Zwick, B. D. Mono(Pentamethylcyclopentadienyl)Uranium(III) Complexes: Synthesis, Properties, and X-Ray Structures of $(\eta\text{-}C_5Me_5)UI_2(THF)_3$, $(\eta\text{-}C_5Me_5)UI_2(Py)_3$, and $(\eta\text{-}C_5Me_5)U[N(SiMe_3)_2]_2$. *Organometallics* **2000**, *19*, 451–457, DOI: 10.1021/om990718r.

(15) Simpson, S. J.; Turner, H. W.; Andersen, R. A. Preparation and Hydrogen-Deuterium Exchange of Alkyl and Hydride Bis(Trimethylsilyl)Amido Derivatives of the Actinide Elements. *Inorg. Chem.* **1981**, *20*, 2991–2995, DOI: 10.1021/ic50223a047.

(16) Fortier, S.; Kaltsoyannis, N.; Wu, G.; Hayton, T. W. Probing the Reactivity and Electronic Structure of a Uranium(V) Terminal Oxo Complex. *J. Am. Chem. Soc.* **2011**, *133*, 14224–14227, DOI: 10.1021/ja206083p.

(17) Fortier, S.; Wu, G.; Hayton, T. W. Synthesis of a Nitrido-Substituted Analogue of the Uranyl Ion, [N═U═O]+. *J. Am. Chem. Soc.* **2010**, *132*, 6888–6889, DOI: 10.1021/ja101567h.

(18) Hervé, A.; Bouzidi, Y.; Berthet, J.-C.; Belkhiri, L.; Thuéry, P.; Boucekkine, A.; Ephritikhine, M. U^{III}–CN versus U^{IV}–NC Coordination in Tris(Silylamide) Complexes. *Inorg. Chem.* **2015**, *54*, 2474–2490, DOI: 10.1021/acs.inorgchem.5b00034.

(19) Dormond, A.; Aziz, A.; Bouadili, E.; Moise, C. Reactivity of the Actinoid-Carbon o Bond: Reaction of $[(Me_3Si)_2N]_2MCH_2Si(Me)_2NSiMe_3$ with Acidic Hydrogen, Ready C-H

Activation. *J. Chem. Soc. Chem. Commun.* **1985**, *26*, 914–916.

(20) Staun, S. L.; Sergentu, D. C.; Wu, G.; Autschbach, J.; Hayton, T. W. Use of ^{15}N NMR Spectroscopy to Probe Covalency in a Thorium Nitride. *Chem. Sci.* **2019**, *10*, 6431–6436, DOI: 10.1039/c9sc01960j.

(21) Trnka, T. M.; Bonanno, J. B.; Bridgewater, B. M.; Parkin, G. Bis(Permethylindenyl) Complexes of Thorium: Synthesis, Structure, and Reactivity. *Organometallics* **2001**, *20*, 3255–3264, DOI: 10.1021/om010233e.

(22) Rookes, T. M.; Wildman, E. P.; Balázs, G.; Gardner, B. M.; Wooles, A. J.; Gregson, M.; Tuna, F.; Scheer, M.; Liddle, S. T. Actinide–Pnictide (An−Pn) Bonds Spanning Non-Metal, Metalloid, and Metal Combinations (An = U, Th; Pn = P, As, Sb, Bi). *Angew. Chem. Int. Ed.* **2018**, *57*, 1332–1336, DOI: 10.1002/anie.201711824.

(23) Fulmer, G. R.; Miller, A. J. M.; Sherden, N. H.; Gottlieb, H. E.; Nudelman, A.; Stoltz, B. M.; Bercaw, J. E.; Goldberg, K. I. NMR Chemical Shifts of Trace Impurities: Common Laboratory Solvents, Organics, and Gases in Deuterated Solvents Relevant to the Organometallic Chemist. *Organometallics* **2010**, *29*, 2176–2179, DOI: 10.1021/om100106e.

(24) Graves, C. R.; Schelter, E. J.; Cantat, T.; Scott, B. L.; Kiplinger, J. L. A Mild Protocol to Generate Uranium(IV) Mixed-Ligand Metallocene Complexes Using Copper(I) Iodide. *Organometallics* **2008**, *27*, 5371–5378, DOI: 10.1021/om800622g.

(25) Shannon, R. D. Revised Effective Ionic Radii and Systematic Studies of Interatomic Distances in Halides and Chalcogenides. *Acta Crystallogr. Sect. A* **1976**, *32*, 751–767, DOI: 10.1107/S0567739476001551.

(26) Staroverov, V. N.; Scuseria, G. E.; Tao, J.; Perdew, J. P. Comparative Assessment of a New

Nonempirical Density Functional: Molecules and Hydrogen-Bonded Complexes. *J. Chem. Phys.* **2003**, *119*, 12129–12137, DOI: 10.1063/1.1626543.

(27) Küchle, W.; Dolg, M.; Stoll, H.; Preuss, H. Energy-Adjusted Pseudopotentials for the Actinides. Parameter Sets and Test Calculations for Thorium and Thorium Monoxide. *J. Chem. Phys.* **1994**, *100*, 7535–7542, DOI: 10.1063/1.466847.

(28) Cao, X.; Dolg, M. Segmented Contraction Scheme for Small-Core Actinide Pseudopotential Basis Sets. *J. Mol. Struct.* **2004**, *673*, 203–209, DOI: 10.1016/j.theochem.2003.12.015.

(29) MacDonald, M. R.; Bates, J. E.; Fieser, M. E.; Ziller, J. W.; Furche, F.; Evans, W. J. Expanding Rare-Earth Oxidation State Chemistry to Molecular Complexes of Holmium(II) and Erbium(II). *J. Am. Chem. Soc.* **2012**, *134*, 8420–8423, DOI: 10.1021/ja303357w.

(30) Fieser, M. E.; MacDonald, M. R.; Krull, B. T.; Bates, J. E.; Ziller, J. W.; Furche, F.; Evans, W. J. Structural, Spectroscopic, and Theoretical Comparison of Traditional vs Recently Discovered Ln^{2+} Ions in the [K(2.2.2-Cryptand)][$(C_5H_4SiMe_3)_3Ln$] Complexes: The Variable Nature of Dy^{2+} and Nd^{2+}. *J. Am. Chem. Soc.* **2015**, *137*, 369–382, DOI: 10.1021/ja510831n.

(31) MacDonald, M. R.; Bates, J. E.; Ziller, J. W.; Furche, F.; Evans, W. J. Completing the Series of +2 Ions for the Lanthanide Elements: Synthesis of Molecular Complexes of Pr^{2+}, Gd^{2+}, Tb^{2+}, and Lu^{2+}. *J. Am. Chem. Soc.* **2013**, *135*, 9857–9868, DOI: 10.1021/ja403753j.

(32) MacDonald, M. R.; Ziller, J. W.; Evans, W. J. Synthesis of a Crystalline Molecular Complex of Y^{2+}, [(18-Crown-6)K][$(C_5H_4SiMe_3)_3Y$]. *J. Am. Chem. Soc.* **2011**, *133*, 15914–15917, DOI: 10.1021/ja207151y.

(33) Demir, S.; Gonzalez, M. I.; Darago, L. E.; Evans, W. J.; Long, J. R. Giant Coercivity and High Magnetic Blocking Temperatures for N_2^{3-} Radical-Bridged Dilanthanide Complexes

upon Ligand Dissociation. *Nat. Commun.* **2017**, *8*, 2144, DOI: 10.1038/s41467-017-01553-w.

(34) La Pierre, H. S.; Kameo, H.; Halter, D. P.; Heinemann, F. W.; Meyer, K. Coordination and Redox Isomerization in the Reduction of a Uranium(III) Monoarene Complex. *Angew. Chem. Int. Ed.* **2014**, *53*, 7154–7157, DOI: 10.1002/anie.201402048.

(35) Turner, H. W.; Simpson, S. J.; Andersen, R. A. Hydrido[Tris(Hexamethyldisilyiamido)]Thorium(IV) Anduranium(IV). *J. Am. Chem. Soc.* **1979**, *101*, 2782, DOI: 10.1021/ja00504a072.

(36) Simpson, S. J.; Turner, H. W.; Andersen, R. A. Hydrogen-Deuterium Exchange: Perdeuteriohydridotris(Hexamethyldisilylamido)Thorium(IV) and-Uranium(IV). *J. Am. Chem. Soc.* **1979**, *101*, 7728–7729, DOI: 10.1021/ja00520a023.

(37) Arnold, P. L.; Mansell, S. M.; Maron, L.; McKay, D. Spontaneous Reduction and C-H Borylation of Arenes Mediated by Uranium(III) Disproportionation. *Nat. Chem.* **2012**, *4*, 668–674, DOI: 10.1038/nchem.1392.

(38) Monreal, M. J.; Khan, S.; Diaconescu, P. L. Beyond C–H Activation with Uranium: A Cascade of Reactions Mediated by a Uranium Dialkyl Complex. *Angew. Chem. Int. Ed.* **2009**, *48*, 8352–8355, DOI: 10.1002/anie.200903270.

(39) Pool, J. A.; Scott, B. L.; Kiplinger, J. L. A New Mode of Reactivity for Pyridine N -Oxide: C−H Activation with Uranium(IV) and Thorium(IV) Bis(Alkyl) Complexes. *J. Am. Chem. Soc.* **2005**, *127*, 1338–1339, DOI: 10.1021/ja044153o.

(40) Lam, O. P.; Feng, P. L.; Heinemann, F. W.; O'Connor, J. M.; Meyer, K. Charge-Separation in Uranium Diazomethane Complexes Leading to C−H Activation and Chemical Transformation. *J. Am. Chem. Soc.* **2008**, *130*, 2806–2816, DOI: 10.1021/ja0766472.

(41) Thomson, R. K.; Cantat, T.; Scott, B. L.; Morris, D. E.; Batista, E. R.; Kiplinger, J. L. Uranium Azide Photolysis Results in C–H Bond Activation and Provides Evidence for a Terminal Uranium Nitride. *Nat. Chem.* **2010**, *2*, 723–729, DOI: 10.1038/nchem.705.

(42) King, D. M.; Tuna, F.; McInnes, E. J. L.; McMaster, J.; Lewis, W.; Blake, A. J.; Liddle, S. T. Isolation and Characterization of a Uranium(VI)–Nitride Triple Bond. *Nat. Chem.* **2013**, *5*, 482–488, DOI: 10.1038/nchem.1642.

(43) Yadav, M.; Metta-Magaña, A.; Fortier, S. Intra- and Intermolecular Interception of a Photochemically Generated Terminal Uranium Nitride. *Chem. Sci.* **2020**, *11*, 2381–2387, DOI: 10.1039/C9SC05992J.

(44) Jaroschik, F.; Nief, F.; Le Goff, X.-F.; Ricard, L. Isolation of Stable Organodysprosium(II) Complexes by Chemical Reduction of Dysprosium(III) Precursors. *Organometallics* **2007**, *26*, 1123–1125, DOI: 10.1021/om0700213.

(45) Coles, M. P.; Hitchcock, P. B.; Lappert, M. F.; Protchenko, A. V. Syntheses and Structures of the Crystalline, Highly Crowded 1,3-Bis(Trimethylsilyl)Cyclopentadienyls [MCp″$_3$] (M = Y, Er, Yb), [PbCp″$_2$], [{YCp″$_2$(μ-OH)}$_2$], [(ScCp″$_2$)$_2$(μ-η^2:η^2-C$_2$H$_4$)], [YbCp″$_2$Cl(μ-Cl)K(18-Crown-6)], and [{KCp″}$_\infty$]. *Organometallics* **2012**, *31*, 2682–2690, DOI: 10.1021/om2009364.

(46) Fieser, M. E.; Palumbo, C. T.; La Pierre, H. S.; Halter, D. P.; Voora, V. K.; Ziller, J. W.; Furche, F.; Meyer, K.; Evans, W. J. Comparisons of Lanthanide/Actinide +2 Ions in a Tris(Aryloxide)Arene Coordination Environment. *Chem. Sci.* **2017**, *8*, 7424–7433, DOI: 10.1039/C7SC02337E.

(47) Palumbo, C. T.; Halter, D. P.; Voora, V. K.; Chen, G. P.; Ziller, J. W.; Gembicky, M.; Rheingold, A. L.; Furche, F.; Meyer, K.; Evans, W. J. Using Diamagnetic Yttrium and

Lanthanum Complexes to Explore Ligand Reduction and C–H Bond Activation in a Tris(Aryloxide)Mesitylene Ligand System. *Inorg. Chem.* **2018**, *57*, 12876–12884, DOI: 10.1021/acs.inorgchem.8b02053.

(48) Palumbo, C. T.; Halter, D. P.; Voora, V. K.; Chen, G. P.; Chan, A. K.; Fieser, M. E.; Ziller, J. W.; Hieringer, W.; Furche, F.; Meyer, K.; Evans, W. J. Metal versus Ligand Reduction in Ln^{3+} Complexes of a Mesitylene-Anchored Tris(Aryloxide) Ligand. *Inorg. Chem.* **2018**, *57*, 2823–2833, DOI: 10.1021/acs.inorgchem.7b03236.

(49) Jenkins, T. F.; Bekoe, S.; Ziller, J. W.; Furche, F.; Evans, W. J. Synthesis of a Heteroleptic Pentamethylcyclopentadienyl Yttrium(II) Complex, [K(2.2.2-Cryptand)]{$(C_5Me_5)_2Y^{II}[N(SiMe_3)_2]$}, and Its C–H Bond Activated Y(III) Derivative. *Organometallics* **2021**, *40*, 3917–3925, DOI: 10.1021/acs.organomet.1c00482.

(50) Lauher, J. W.; Hoffmann, R. Structure and Chemistry of Bis(Cyclopentadienyl)-ML_n Complexes. *J. Am. Chem. Soc.* **1976**, *98*, 1729–1742, DOI: 10.1021/ja00423a017.

(51) Pepper, M.; Bursten, B. E. The Electronic Structure of Actinide-Containing Molecules: A Challenge to Applied Quantum Chemistry. *Chem. Rev.* **1991**, *91*, 719–741, DOI: 10.1021/cr00005a005.

(52) Bursten, B. E.; Rhodes, L. F.; Strittmatter, R. J. Bonding in Tris(η^5-Cyclopentadienyl) Actinide Complexes. 2. On the Ground Electronic Configurations of "Base-Free" Cp_3An Complexes (An = Th, Pa, U, Np, Pu). *J. Am. Chem. Soc.* **1989**, *111*, 2756–2758, DOI: 10.1021/ja00190a002.

(53) Langeslay, R. R.; Fieser, M. E.; Ziller, J. W.; Furche, F.; Evans, W. J. Synthesis, Structure, and Reactivity of Crystalline Molecular Complexes of the $\{[C_5H_3(SiMe_3)_2]_3Th\}^{1-}$ Anion Containing Thorium in the Formal +2 Oxidation State. *Chem. Sci.* **2015**, *6*, 517–521, DOI:

10.1039/C4SC03033H.

(54) Mingos, D. M. P. Molecular-Orbital Studies on Carbametallaboranes. Part 1. Icosahedral Carbaplatinaborane Polyhedra. *J. Chem. Soc. Dalt. Trans.* **1976**, 602–610.

(55) Hawthorne, M. F.; Young, D. C.; Andrews, T. D.; Howe, D. V.; Pilling, R. L.; Pitts, A. D.; Reintjes, M.; Warren, L. F.; Wegner, P. A. π-Dicarbollyl Derivatives of the Transition Metals. Metallocene Analogs. *J. Am. Chem. Soc.* **1968**, *90*, 879–896, DOI: 10.1021/ja01006a008.

(56) Moore, E. B.; Lohr, L. L.; Lipscomb, W. N. Molecular Orbitals in Some Boron Compounds. *J. Chem. Phys.* **1961**, *35*, 1329–1334.

(57) Guzei, I. A.; Wendt, M. Solid-G. Madison, WI 2004.

(58) Guzei, I. A.; Wendt, M. An Improved Method for the Computation of Ligand Steric Effects Based on Solid Angles. *Dalt. Trans.* **2006**, No. 33, 3991, DOI: 10.1039/b605102b.

(59) Moehring, S. A.; Beltran-Leiva, M.; Paez-Hernandez, D.; Arratia-Perez, R.; Ziller, J. W.; Evans, W. J. Rare-Earth Metal (II) Aryloxides: Structure, Synthesis, and EPR Spectroscopy of [K(2.2.2-Cryptand)][Sc($OC_6H_2{}^tBu_2$-2,6-Me-4)$_3$]. *Chem. Eur. J.* **2018**, *24*, 18059–18067, DOI: 10.1002/chem.201803807.

(60) Bergbreiter, D. E.; Killough, J. M. Reactions of Potassium-Graphite. *J. Am. Chem. Soc.* **1978**, *100*, 2126–2134, DOI: 10.1021/ja00475a025.

(61) Blake, P. C.; Edelstein, N. M.; Hitchcock, P. B.; Kot, W. K.; Lappert, M. F.; Shalimoff, G. V.; Tian, S. Synthesis, Properties and Structures of the Tris(Cyclopentadienyl)Thorium(III) Complexes [Th{η^5-$C_5H_3(SiMe_2R)_2$-1,3}$_3$] (R=Me or ^{t}Bu). *J. Organomet. Chem.* **2001**, *636*, 124–129, DOI: 10.1016/S0022-328X(01)00860-9.

(62) Langeslay, R. R.; Fieser, M. E.; Ziller, J. W.; Furche, F.; Evans, W. J. Expanding Thorium

Hydride Chemistry Through Th^{2+}, Including the Synthesis of a Mixed-Valent Th^{4+}/Th^{3+} Hydride Complex. *J. Am. Chem. Soc.* **2016**, *138*, 4036–4045, DOI: 10.1021/jacs.5b11508.

(63) Liu, J.; Seed, J. A.; Formanuik, A.; Ortu, F.; Wooles, A. J.; Mills, D. P.; Liddle, S. T. Thorium(IV) Alkyl Synthesis from a Thorium(III) Cyclopentadienyl Complex and an N-Heterocyclic Olefin. *J. Organomet. Chem.* **2018**, *857*, 75–79, DOI: 10.1016/j.jorganchem.2017.08.015.

(64) Gaunt, A. J.; Scott, B. L.; Neu, M. P. U(IV) Chalcogenolates Synthesized via Oxidation of Uranium Metal by Dichalcogenides. *Inorg. Chem.* **2006**, *45*, 7401–7407, DOI: 10.1021/ic060560k.

(65) Mansell, S. M.; Kaltsoyannis, N.; Arnold, P. L. Small Molecule Activation by Uranium Tris(Aryloxides): Experimental and Computational Studies of Binding of N_2, Coupling of CO, and Deoxygenation Insertion of CO_2 under Ambient Conditions. *J. Am. Chem. Soc.* **2011**, *133*, 9036–9051, DOI: 10.1021/ja2019492.

(66) Wedal, J. C.; Bekoe, S.; Ziller, J. W.; Furche, F.; Evans, W. J. In Search of Tris(Trimethylsilylcyclopentadienyl) Thorium. *Dalton Trans.* **2019**, *48*, 16633–16640, DOI: 10.1039/C9DT03674A.

(67) APEX2. Bruker AXS, Inc: Madison, WI 2014.

(68) Sheldrick, G. M. CELL_NOW. Bruker AXS, Inc: Madison, WI 2008.

(69) SAINT. Bruker AXS, Inc: Madison, WI 2013.

(70) Sheldrick, G. M. TWINABS. Bruker AXS, Inc: Madison, WI 2012.

(71) Sheldrick, G. M. SHELXTL. Bruker AXS, Inc: Madison, WI 2014.

(72) *International Tables for Crystallography*; Kluwer Academic Publishers: Dordrecht, 1992.

(73) Sheldrick, G. M. SADABS. Bruker AXS, Inc: Madison, WI 2014.

(74) Grimme, S. Semiempirical GGA-Type Density Functional Constructed with a Long-Range Dispersion Correction. *J. Comput. Chem.* **2006**, *27*, 1787–1799, DOI: 10.1002/jcc.20495.

(75) Grimme, S.; Antony, J.; Ehrlich, S.; Krieg, H. A Consistent and Accurate Ab Initio Parametrization of Density Functional Dispersion Correction (DFT-D) for the 94 Elements H-Pu. *J. Chem. Phys.* **2010**, *132*, 154104, DOI: 10.1063/1.3382344.

(76) Weigend, F.; Ahlrichs, R. Balanced Basis Sets of Split Valence, Triple Zeta Valence and Quadruple Zeta Valence Quality for H to Rn: Design and Assessment of Accuracy. *Phys. Chem. Chem. Phys.* **2005**, *7*, 3297–3305, DOI: 10.1039/b508541a.

(77) Schäfer, A.; Horn, H.; Ahlrichs, R. Fully Optimized Contracted Gaussian Basis Sets for Atoms Li to Kr. *J. Chem. Phys.* **1992**, *97*, 2571–2577.

(78) Treutler, O.; Ahlrichs, R. Efficient Molecular Numerical Integration Schemes. *J. Chem. Phys.* **1995**, *102*, 346–354, DOI: 10.1063/1.469408.

(79) Schäfer, A.; Klamt, A.; Sattel, D.; Lohrenz, J. C. W.; Eckert, F. COSMO Implementation in TURBOMOLE: Extension of an Efficient Quantum Chemical Code towards Liquid Systems. *Phys. Chem. Chem. Phys.* **2000**, *2*, 2187–2193, DOI: 10.1039/b000184h.

(80) In *CRC Handbook of Chemistry and Physics*; Haynes, W. M., Lide, D. R., Bruno, T. J., Eds.; CRC Press, 2016; pp 943–950.

(81) Rappoport, D.; Furche, F. Property-Optimized Gaussian Basis Sets for Molecular Response Calculations. *J. Chem. Phys.* **2010**, *133*, 0–11, DOI: 10.1063/1.3484283.

(82) Ryan, A. J.; Darago, L. E.; Balasubramani, S. G.; Chen, G. P.; Ziller, J. W.; Furche, F.; Long, J. R.; Evans, W. J. Synthesis, Structure, and Magnetism of Tris(Amide) $[Ln\{N(SiMe_3)_2\}_3]^{1-}$ Complexes of the Non-Traditional +2 Lanthanide Ions. *Chem. Eur. J.* **2018**, *24*, 7702–7709, DOI: 10.1002/chem.201800610.

(83) Humphrey, W.; Dalke, A.; Schulten, K. VMD: Visual Molecular Dynamics. *J. Mol. Graph.* **1996**, *14*, 33–38.

(84) TURBOMOLE V7.4.1. University of Karlsruhe and Forschungszentrum Karlsruhe GmbH.

(85) Balasubramani, S. G.; Chen, G. P.; Coriani, S.; Diedenhofen, M.; Frank, M. S.; Franzke, Y. J.; Furche, F.; Grotjahn, R.; Harding, M. E.; Hättig, C.; Hellweg, A.; Helmich-Paris, B.; Holzer, C.; Huniar, U.; Kaupp, M.; Marefat Khah, A.; Karbalaei Khani, S.; Müller, T.; Mack, F.; Nguyen, B. D.; Parker, S. M.; Perlt, E.; Rappoport, D.; Reiter, K.; Roy, S.; Rückert, M.; Schmitz, G.; Sierka, M.; Tapavicza, E.; Tew, D. P.; van Wüllen, C.; Voora, V. K.; Weigend, F.; Wodyński, A.; Yu, J. M. TURBOMOLE: Modular Program Suite for Ab Initio Quantum-Chemical and Condensed-Matter Simulations. *J. Chem. Phys.* **2020**, *152*, 184107, DOI: 10.1063/5.0004635.

Chapter 5:

Synthesis and Reduction of Heteroleptic Bis(cyclopentadienyl) Uranium(III) Complexes

Introduction[†]

The previous Chapter reported reduction studies of the heteroleptic bis- and mono-(cyclopentadienyl) complexes, $(C_5Me_5)_2U(NR_2)$ and $(C_5Me_5)U(NR_2)_2$. The putative U(II) products had $5f^36d^1$ configurations, but were unstable with respect to C–H bond activation reactivity of the bis(trimethylsilyl)amide ligands.[1]

It was therefore desirable to explore reduction of other heteroleptic U(III) cyclopentadienyl complexes that had functional groups other than amide ligands to circumvent ligand activation as a decomposition pathway for U(II) compounds. It was also of interest to explore other heteroleptic systems to further understand the electronic impact of the ligands and their coordination geometry on the stability and the electronic structure of the U(II) ion. One additional desirable aspect of heteroleptic $[(C_5Me_5)_2U^{II}(A)]^{1-}$ compounds in which A is an alkyl group is that this could provide the basis for coupling of metal-based electron transfer with alkyl-like reactivity at the U–C bond.

Surprisingly, relatively few fully characterized heteroleptic U(III) metallocenes were in the literature except for halides.[2–11] This Chapter reports new synthetic and crystallographic data on this class of complexes. Electrochemical data were collected on six heteroleptic U(III) complexes to examine them as precursors for reduction to U(II). The suitability for forming U(II) compounds chemically was also evaluated. Density functional theory (DFT) and solid-G[12] analysis were employed to evaluate the electronic and steric properties of the expected products.

[†] Portions of this Chapter have been published: Wedal, J. C.; Ziller, J. W.; Furche, F.; Evans, W. J. Synthesis and Reduction of Heteroleptic Bis(cyclopentadienyl) Uranium(III) Complexes *Inorg. Chem.* **2022**, DOI: 10.1021/acs.inorgchem.2c00322.

Results

Synthesis of Bis(cyclopentadienyl)uranium(aryloxide) Complexes. $(C_5Me_5)_2U(OAr')$, 5.1-U ($OAr' = OC_6H_2{}^tBu_2$-2,6-Me-4). Reaction of $(C_5Me_5)_2UI(THF)$[13] with KOAr′ in THF, followed by extraction into hexane, afforded $(C_5Me_5)_2U(OAr')$, **5.1-U**, as a dark brown solid in 76% yield, eq 5.1. The ^1H NMR spectrum of **5.1-U** in C_6D_6 displays a broad signal at −8.69 ppm for the C_5Me_5 ligand, and three signals at −3.40, −8.80, and −20.54 ppm for the methyl group, aromatic hydrogens, and *tert*-butyl group, respectively. NMR shifts for all compounds included in this report are summarized in Table 5.1.

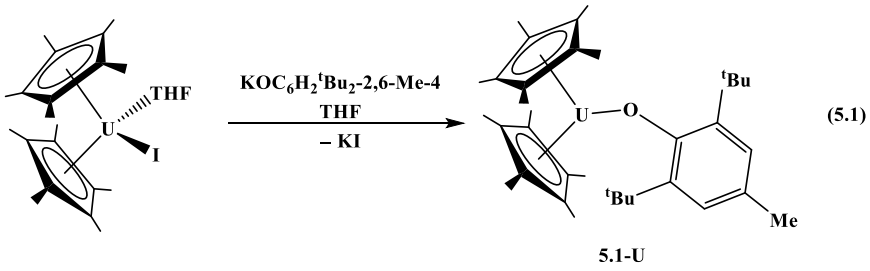

(5.1)

5.1-U

Brown crystals of **5.1-U** suitable for X-ray diffraction were grown by a slow evaporation of a pentane solution at −35 °C, Figure 5.1. Compound **5.1-U** crystallized in the *Cmc*2_1 space group with two independent molecules in the asymmetric unit. One molecule had a U–O–C bond angle of 166.0(5)° and the other had a much more acute U–O–C bond angle of 115.7(5)°. However, the corresponding U–O distances of 2.201(6) and 2.225(6) Å, respectively, are similar. It is well established that M–O–R angles do not necessarily correlate with M–O distances[14–19] and this provides another excellent example with the two variants in the same crystal. The U–O distances in **5.1-U** are in the range of other U(III) aryloxide compounds: 2.144(8) A in $[(C_5Me_5)(OAr')U]_2(C_6H_6)$;[20] 2.229(2), 2.253(2), and 2.256(2) Å in $[(ArO)_3tacn]U$;[21] 2.242(2) Å in (trans-calix[2]benzene[2]pyrrolide)U(OAr);[22] 2.136(6), 2.154(6), and 2.168(7), and 2.169(7) Å in $[U(OAr)]_2(C_7H_8)$;[23] 2.151(3), 2.175(3), and 2.177(3) Å in $U(OC_6H_2Ad_2$-2,6-Me-4$)_3$;[24] 2.161(2),

2.165(2), and 2.166(2) Å in $U(OAr)_3$[25] (OAr = $OC_6H_3{}^tBu_2$-2,6). The metrical data of all compounds included in this study are summarized in Table 5.2.

Table 5.1: ^1H NMR shifts (δ, ppm) of compounds in this study (OAr′ = O-C_6H_2-$^tBu_2$-2,6-Me-4, OAr* = O-C_6H_2-Ad_2-2,6-^{t}Bu-4, R = $SiMe_3$)

	C_5Me_5	C_5Me_4H	aryl CH	Me	^{t}Bu	Ad	Other
$(C_5Me_5)_2U(OAr')$, **5.1-U**[a]	−8.69		8.80	3.40	−20.54		
$(C_5Me_5)_2Ce(OAr')$, **5.1-Ce**[a]	2.71		8.46	3.37	−6.97		
$(C_5Me_4H)_2UI(THF)$[b]		18.93, −20.69					
$(C_5Me_4H)_2U(OAr')$, **5.2**[a]		−1.57, −27.38	8.45	2.64	−17.55		
$(C_5Me_5)_2U(OAr*)$, **5.3**[a]	−8.74		13.76		4.00	1.80, −9.74, −12.34, −15.72, −17.94	
$(C_5Me_4H)_2U(OAr*)$, **5.4**[a]		−17.84	15.29		4.61	−11.05, −16.70, −18.89	−8.19, −8.85 (C_5Me_4-H or Ad)
$(C_5Me_5)_2U(CHR_2)$, **5.5**[a,3]	−5.56						−22.8 ($SiMe_3$)
$(C_5Me_5)_2U(C_5H_5)$, **5.6**[a]	−4.42						−23.04 (C_5H_5)
$(C_5Me_5)_2U(C_5Me_4H)$, **5.7**[a]	−3.87						
$(C_5Me_5)_2U(\kappa^2$–*O,O′*–O_2C–$C_5Me_4H)$, **5.8**[a]	13.12, 0.29	4.89, 4.01					

a: C_6D_6
b: THF-d_8

The U–cnt (cnt = C_5Me_5 ring centroid) distances in **5.1-U** were in the range of 2.498 to 2.560 Å, and the cnt–U–cnt angles were 131.4 and 135.2°. These values are within the common range for bent metallocenes containing the $(C_5Me_5)_2U^{III}$ fragment.[6,26] The metrical data of the

metallocene components of all of the compounds included in this report are not unusual for the bent metallocene motif. These data are included in Table 5.12 and will not be discussed further.

$(C_5Me_5)_2Ce(OAr')$, 5.1-Ce. To determine the influence of the 5f orbitals on the structure of **5.1-U**, the synthesis of the 4f cerium analog **5.1-Ce**, was attempted because Ce^{3+} has a similar six-coordinate ionic radius to U^{3+}.[27] The cerium complex was prepared by the salt metathesis route of eq 5.2. Dark pink crystals of **5.1-Ce** suitable for X-ray diffraction were isolated from a

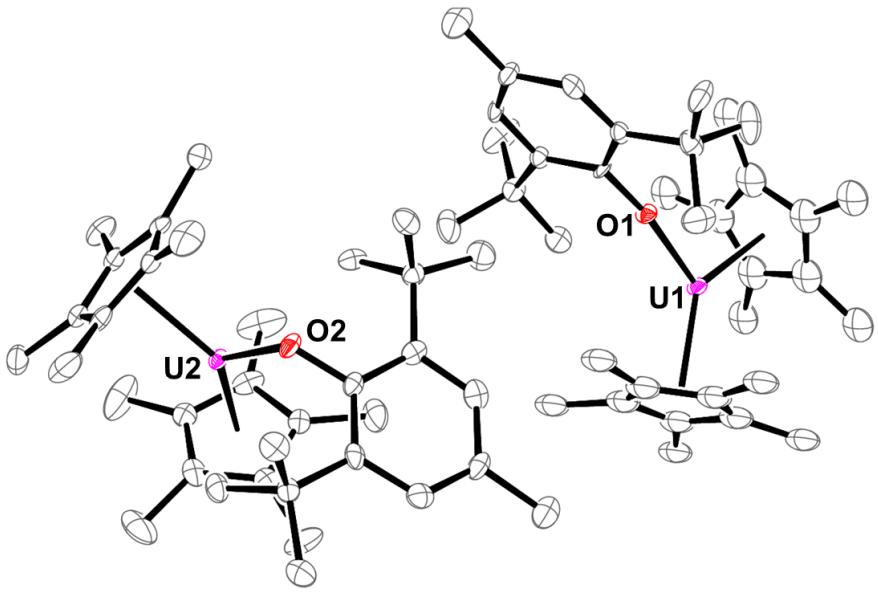

Figure 5.1: Molecular structure of **5.1-U** with selective atom labelling. Ellipsoids are drawn at the 50% probability level. Disordered C_5Me_5 rings and hydrogen atoms have been omitted for clarity. **5.1-U** and **5.1-Ce** are isomorphous.

Table 5.2: Selected distances (Å) and angles (°) for compounds **5.1-M**, **5.2**, and **5.5** (OAr′ = O-C_6H_2-^{t}Bu$_2$-2,6-Me-4, R = SiMe$_3$).

	M–cnt	M–O, M–C	Cnt–M–cnt	Cnt–M–O, Cnt–M–C	M–O–C_{ipso}
$(C_5Me_5)_2U(OAr')$, **5.1-U**	2.498, 2.502, 2.560	2.201(6), 2.225(6)	131.4, 135.2	114.1, 128.6	115.7(5), 166.0(5)
$(C_5Me_5)_2Ce(OAr')$, **5.1-Ce**	2.525, 2.531, 2.585	2.213(3), 2.246(3)	131.5, 135.3	96.2, 114.1, 128.5	115.4(3), 166.5(3)
$(C_5Me_4H)_2U(OAr')$, **5.2**	2.517, 2.549, 2.472, 2.511	2.268(4), 2.269(4)	124.2, 126.2	112.7, 99.7, 100.2, 133.6	159.5(4) 111.5(3)
$(C_5Me_5)_2U(CHR_2)$, **5.5**	2.505, 2.547	2.502(7)	133.9	109.3, 111.6	

concentrated hexane solution at −35 °C, following reaction of bright yellow $(C_5Me_5)_2Ce(\mu$–$Cl)_2K(THF)_2$[28,29] with KOAr′ in THF at 60 °C. The resonances in the ^{1}H NMR spectrum of **5.1-Ce** are shifted significantly from **5.1-U**, Table 5.1. For example, the C_5Me_5 resonance in **5.1-Ce** is 2.71 ppm while it occurs at −8.69 ppm in **5.1-U**.

5.1-Ce is isomorphous with **5.1-U** and has two distinct molecules in the asymmetric unit with Ce–O–C angles of 115.4(3)° and 166.5(3)° and corresponding Ce–O distances of 2.246(3) and 2.213(3) Å, respectively. These distances are very close to the U–O distances in **5.1-U** which is consistent with the similar six-coordinate Shannon ionic radii of U(III) and Ce(III), 1.025 Å and 1.01 Å.[27]

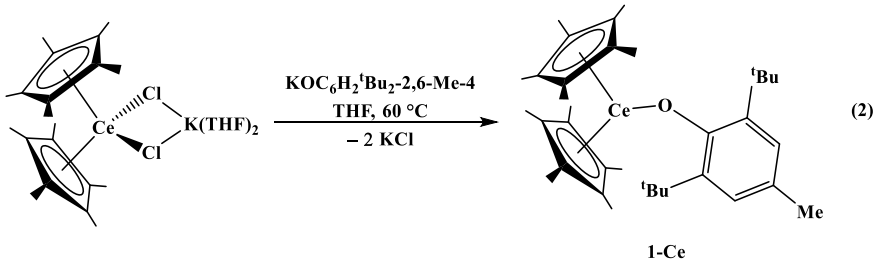

$(C_5Me_4H)_2U(OAr')$, 5.2. A tetramethylcyclopentadienyl analog of **5.1-U** was prepared to compare the effect of the ancillary cyclopentadienyl ligand on structure. Following the synthesis of **5.1-U**, reaction of UI_3 with 2 equivalents of KC_5Me_4H in THF afforded dark green needles of $(C_5Me_4H)_2UI(THF)$ in 63% yield, eq 5.3. $(C_5Me_4H)_2UI(THF)$ adopts a bent metallocene motif analogous to $(C_5Me_5)_2UI(THF)$,[6,13] Figure 5.2, but the crystals obtained were not of high enough quality to discuss metrical parameters.

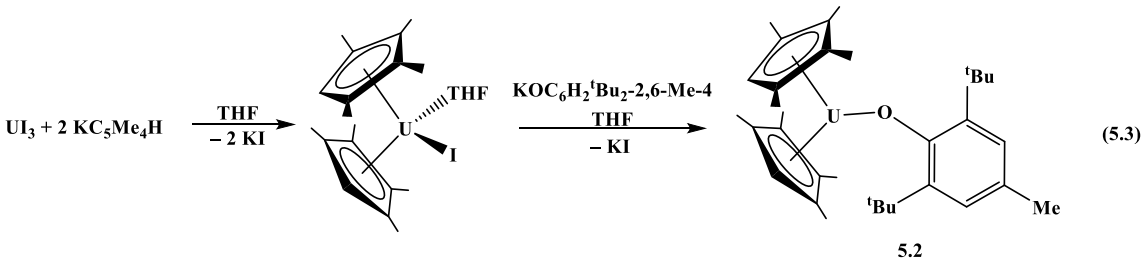

(5.3)

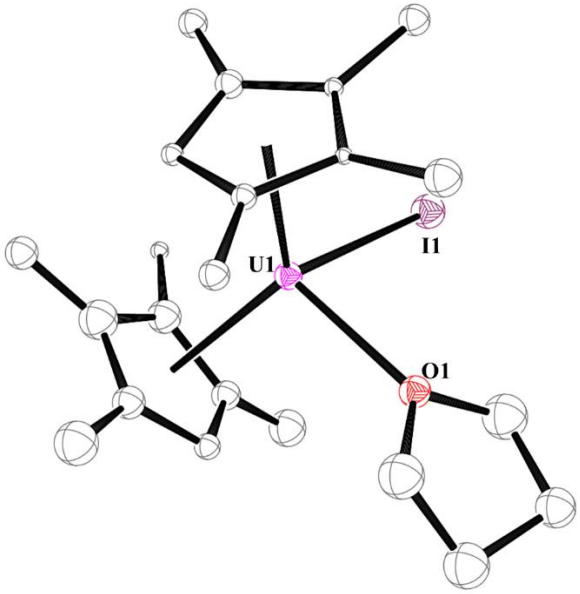

Figure 5.2: Connectivity plot of $(C_5Me_4H)_2UI(THF)$ with selective atom labelling. Hydrogen atoms are omitted for clarity.

Reaction of $(C_5Me_4H)_2UI(THF)$ with KOAr′, followed by crystallization from hexane, afforded **5.2** as a dark brown solid in 62% yield, eq 5.3. Compound **5.2** had two resonances in the ^1H NMR spectrum in C_6D_6 at −1.57 and −27.38 ppm that are assigned to the C_5Me_4H methyl

groups and one resonance at −15.02 ppm for the C_5Me_4H ring proton. Additional resonances at 8.45, 2.64, and −17.38 ppm are assigned to the ring protons, methyl group, and *tert*-butyl groups, respectively, of the OAr′ ligand. Hence, the ^{1}H NMR spectrum of **2** had resonances analogous to those of **5.1-U**, but the shifts were substantially different, Table 5.1. The ^{1}H NMR resonances of the OAr′ ligand in **5.2** are significantly different than those in **5.1-U**, Table 5.2. For example, the aromatic C–H resonance in**5. 1-U** occurs at −8.80 ppm while the analogous resonance in **5.2** occurs at +8.45 ppm. The two C_5Me_4H methyl resonances are significantly split at −1.57 and −27.38 ppm compared to the single methyl resonance of **5.1-U** at −8.69 ppm. This appears to be a general trend, further exemplified by $(C_5Me_4H)_3U$[30] with resonances at 7.4 and −35.5 ppm and $(C_5Me_5)_3U$ at −0.93 ppm.[31]

An X-ray diffraction study on **5.2** revealed a structure different from that of **5.1-U** in that one of the two metallocene units in the unit cell was a THF adduct. Compound **5.2** crystallizes in the $P\bar{1}$ space group with $(C_5Me_4H)_2U(OAr')$, $(C_5Me_4H)_2U(OAr')(THF)$, and a molecule of hexane in the asymmetric unit. The two molecules had significantly different U–O–C_{ipso} angles, as in **5.1-U**: 110.98 in $(C_5Me_4H)_2U(OAr')$ and 158.92° in $(C_5Me_4H)_2U(OAr')(THF)$, Figure 5.3. THF was not observed in the ^{1}H NMR spectrum of **5.2** and was most likely introduced during crystallization. The U–cnt distances of the $(C_5Me_4H)_2U(OAr')$ molecule were 2.472 and 2.511 Å while the U–cnt distances were 2.517 and 2.549 Å for the $(C_5Me_4H)_2U(OAr')(THF)$ molecule.

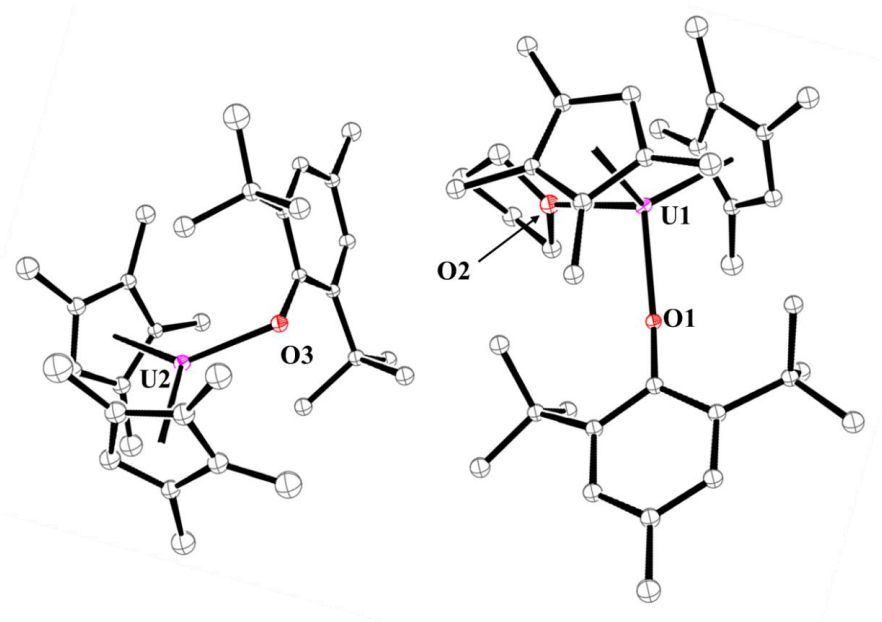

Figure 5.3: Molecular structure of **5.2** and co-crystallized $(C_5Me_4H)_2U(OAr')(THF)$, with ellipsoids drawn at the 50% probability level. Hydrogen atoms have been omitted for clarity.

$(C_5Me_5)_2U(OAr^*)$, 5.3 ($OAr^* = OC_6H_2Ad_2$-2,6-^{t}Bu-4). A complex similar to **5.1-U** which has adamantyl instead of *tert*-butyl groups in the 2,6-positions, $(C_5Me_5)_2U(OAr^*)$, **5.3**, was synthesized as shown for**5. 1-U** in eq 5.1. Green/brown solids of **5.3** were isolated in 51% yield after extraction with hexane and removal of HOAr* by crystallization of HOAr* from THF. The formation of phenol in KOAr* reactions has been observed previously in the case of the lanthanides.[32,33] The C_5Me_5 ligand in compound **5.3** resonates at −8.74 ppm, which is similar to compound **5.1-U** and other $(C_5Me_5)U^{III}$ metallocenes.[3] Peaks at 13.76 and 4.00 ppm are assigned to the aromatic hydrogen and *tert*-butyl group, respectively. Five peaks at 1.80, −9.74, −12.34, −15.72, and −17.94 ppm were observed for the adamantyl groups, where one set of methylene protons are inequivalent presumably due to the close contact with the metal center. Unfortunately, single crystals of **5.3** suitable for X-ray diffraction were not obtained.

$(C_5Me_4H)_2U(OAr^*)$, 5.4. Reaction of $(C_5Me_4H)_2UI(THF)$ (see above) with KOAr* in THF, a synthesis similar to that of **5. 2** in eq 5.3, afforded brown solids of $(C_5Me_4H)_2U(OAr^*)$,

5.4, in 62% yield. The ^{1}H NMR spectrum of **5.4** had resonances at 15.29 and 4.61 ppm, that are assigned to the aromatic and *tert*-butyl groups, respectively. Other resonances at −11.05, −16.70, and −18.89 ppm are assigned to the adamantyl groups. The aryl C–H and *tert*-butyl resonances for the aryloxide moieties are similar in **5.3** and **5.4**, but the adamantyl resonances are over a much broader range in **5.3**, Table 5.1. The direct comparison is made difficult since four other resonances at −8.19, −8.85, and −17.84 ppm integrate to twelve protons and can be assigned to either the C_5Me_4H methyl groups or adamantyl groups. The resonance at −17.84 ppm is likely due to C_5Me_4H, based on the chemical shifts of compound **5.2**. In general, the resonances of compounds **5.1-U** and **5.2** are similar as are the resonances in **5.3** and **5.4**, but the chemical shifts in **5.1-U** and **5.3** are not comparable. Brown crystals could be grown from concentrated hexane solutions at −35 °C but were not of high enough quality for X-ray diffraction.

$(C_5Me_5)_2U[CH(SiMe_3)_2]$, 5.5.[3] For a comparison with our previous studies on $(C_5Me_5)_2U[N(SiMe_3)_2]$, the alkyl analog $(C_5Me_5)_2U[CH(SiMe_3)_2]$, **5.5**, was synthesized from $(C_5Me_5)_2UI(THF)$ and $KCH(SiMe_3)_2$ in Et_2O in 87% yield in a variation of a previously reported synthesis,[3] eq 5.4. It was necessary to use the alkyl-potassium reagent since the reaction of $(C_5Me_5)_2UI(THF)$ and $LiCH(SiMe_3)_2$ in our hands did not form **5.5**,[6] although the La, Nd, and Lu analogs can be synthesized using the lithium reagent.[28] Brown crystals of **5.5** suitable for X-ray diffraction were grown from a concentrated hexane solution at −35 °C, Figure 5.4.

The structure of **5.5** was solved as a multi-component twin and displays disorder in both C_5Me_5 rings and both $SiMe_3$ arms of the alkyl ligand. The structure is isomorphous with that of $(C_5Me_5)_2Nd[CH(SiMe_3)_2]$, [28] The alkyl group is not attached to uranium symmetrically. Instead, one $SiMe_3$ group is oriented toward the metal with a 97.3(4)° U–C(21)—Si(1) angle more acute than the 151.5(6)° U–C(21)—Si(2) angle. This puts the C(22) methyl group closer to the uranium

than any other silyl methyl moieties. This structural motif was also found in $(C_5Me_5)_2Nd[CH(SiMe_3)_2]$ and $(C_5Me_5)_2U[N(SiMe_3)_2]$ and was described as a M…C interaction. The 2.502(7) Å U–C(alkyl) distance in **5.5** is similar to the 2.51(1) Å Nd–C and 2.535(5) Å Ce–C distances in $(C_5Me_5)_2Ln[CH(SiMe_3)_2]$, when the difference in ionic radius is considered.[27] The U–C distance in **5.5** is shorter than the 2.352(4) Å U–N distance in $(C_5Me_5)_2U[N(SiMe_3)_2]$.[2]

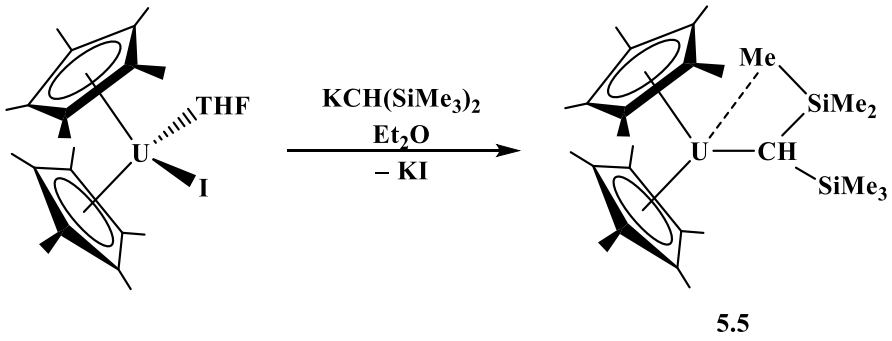

(5.4)

5.5

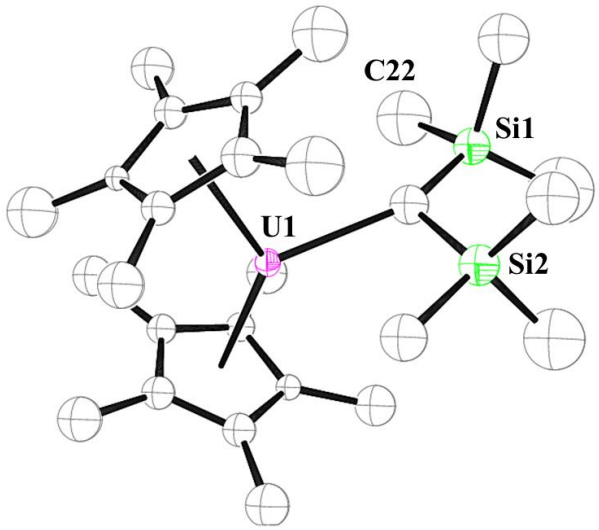

Figure 5.4: Molecular structure of **5.5** with ellipsoids drawn at the 50% probability level. Hydrogen and disordered atoms have been omitted for clarity.

$(C_5Me_5)_2U(C_5H_5)$, 5.6. The reaction between $(C_5Me_5)_2UI(THF)$ and NaC_5H_5 *in toluene* generated $(C_5Me_5)_2U(C_5H_5)$, **5.6**, as a brown solid in 76% yield, eq 5.6. Compound**5. 6** can also be synthesized using KC_5H_5 in toluene, but using THF as a solvent produces multiple products and **5.6** was not formed, as assessed by ^1H NMR spectroscopy. The analogous samarium

compound was previously synthesized from $(C_5Me_5)_2Sm$ or $(C_5Me_5)_2Sm(THF)_2$ and C_5H_6,[34] while the $(C_5Me_5)_2Ln(C_5H_5)$ complexes for Ln = La, Nd, Sm were synthesized from $(C_5H_5)_3Ln$ and $(C_5Me_5)_2Ca$.[35] The ^1H NMR spectrum of **5.6** in C_6D_6 had two broad resonances at −4.42 and −23.04 ppm for the C_5Me_5 and C_5H_5 ligand, respectively. Brown crystals could be grown from a slow evaporation of a hexane or pentane solution at −35 °C but were not of high enough quality for X-ray diffraction.

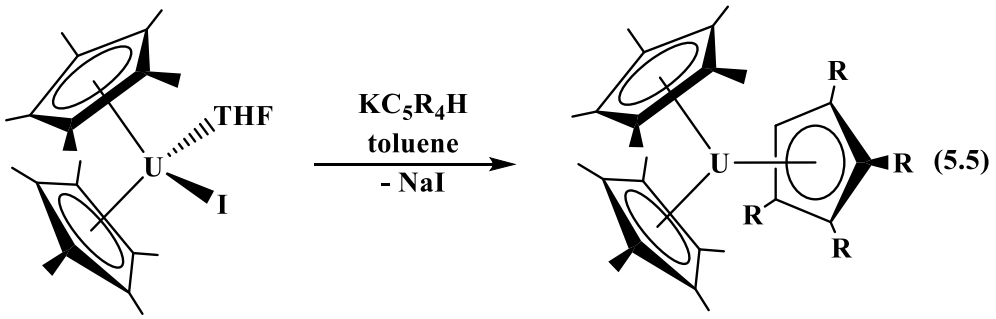

$(C_5Me_5)_2U(C_5Me_4H)$, 5.7. An analog of **5.6** with a larger cyclopentadienyl ligand, $(C_5Me_5)_2U(C_5Me_4H)$, **5.7**, was synthesized from $(C_5Me_5)_2UI(THF)$ and KC_5Me_4H in toluene and isolated as a brown solid in 57% yield, eq 5.5. Brown crystals of **5.7** could be grown from a concentrated solution of Et_2O at −35 °C or from slow evaporation of a hexane or pentane solution at −35 °C. The X-ray diffraction data on **5.7** were not high enough quality to report, but showed a tris(η^5-cyclopentadienyl) structure around the metal. The substituents on each ring could not be precisely determined from the data. The ^1H NMR spectrum of **5.7** in C_6D_6 at 298K had a single, broad peak at −3.87 ppm attributed to the C_5Me_5 resonance while the resonances for the C_5Me_4H ligand were not observed.

Previously, the Ln = Y and Lu compounds $(\eta^5\text{-}C_5Me_5)_2Ln(\eta^3\text{-}C_5Me_4H)$ were synthesized from $[(C_5Me_5)_2Ln][BPh_4]$ and KC_5Me_4H.[36] These compounds exhibited an extra absorption in

their UV-visible spectra compared to their homoleptic analogs that were photoactive. The UV-visible spectrum of **5.7** in THF displayed weak absorptions in the visible region and did not display any unusual bands that could allow for photoreduction as was observed for the rare-earth metal analogs.[37] This is most likely because the C_5Me_4H ring binds as η^5–C_5Me_4H and not η^3–C_5Me_4H, which was analyzed as the source of the photochemistry in the rare-earth metal compounds. Complex **5.7** could be considered quite crowded and a candidate for sterically induced reduction (SIR). However, it does not react with THF to form the ring-opened products common in SIR chemistry.[38] Moreover, $(C_5Me_5)_2U(C_5Me_4H)Me$ and $(C_5Me_5)_2U(C_5Me_4H)Cl$ can be synthesized[39] showing that $(C_5Me_5)_2U(C_5Me_4H)$ is not at the steric limit.

A second route to compound **5.7** was investigated starting from $(C_5Me_5)_2U(\mu\text{–}Ph)_2BPh_2$.[2] A new route to this tetraphenylborate precursor was explored that proved to be more efficient than the literature method.[20] $(C_5Me_5)_2U[CH(SiMe_3)_2]$, **5.5**, reacts with $[HNEt_3][BPh_4]$ in benzene to form $(C_5Me_5)_2U(\mu\text{–}Ph)_2BPh_2$ in 44% yield, eq 5.6.

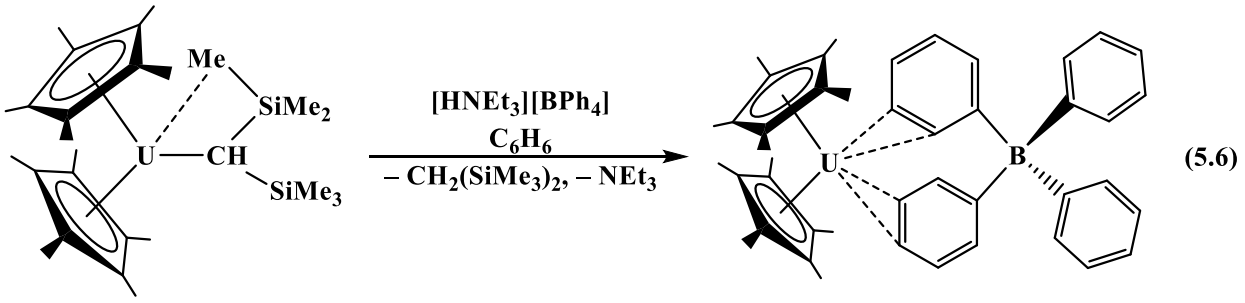

5.5 **(5.6)**

The reaction of $(C_5Me_5)_2U(\mu\text{–}Ph)_2BPh_2$ with KC_5Me_4H in benzene afforded compound **5.7** in 58% yield, eq 5.7.

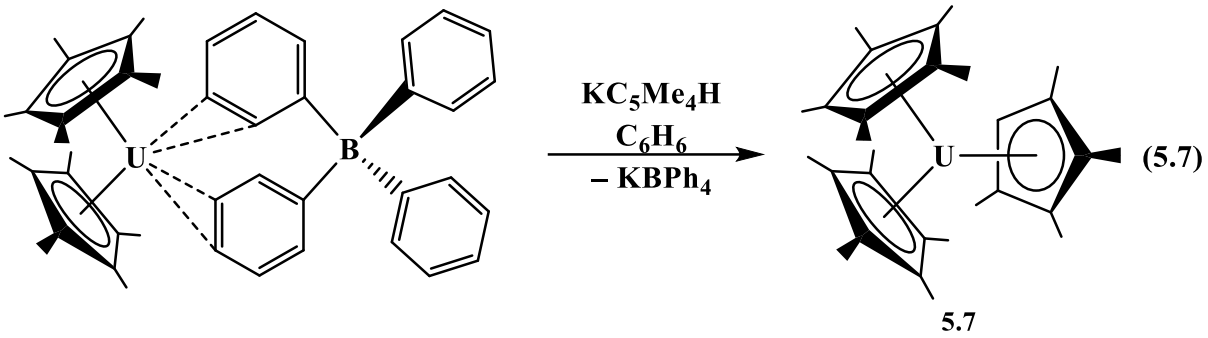

Further evidence on the composition of **5.7** was obtained by reacting it with CO_2. Complex **5.7** reacts with CO_2 to form a dark red solution, from which the insertion product $(C_5Me_5)_2U(\kappa^2$–*O,O′*–O_2C–$C_5Me_4H)$, **5.8**, was isolated in 38% yield as dark red microcrystals, eq 5.8. The ^1H NMR spectrum contained resonances at 13.12 and 0.29 ppm assigned to two magnetically inequivalent C_5Me_5 rings and resonances at 4.89 and 4.01 ppm for the methyl groups of C_5Me_4H. A broad, intense absorption in the infrared spectrum at 1432 cm^{-1} was observed, characteristic of the carboxylate moiety.[40–42]

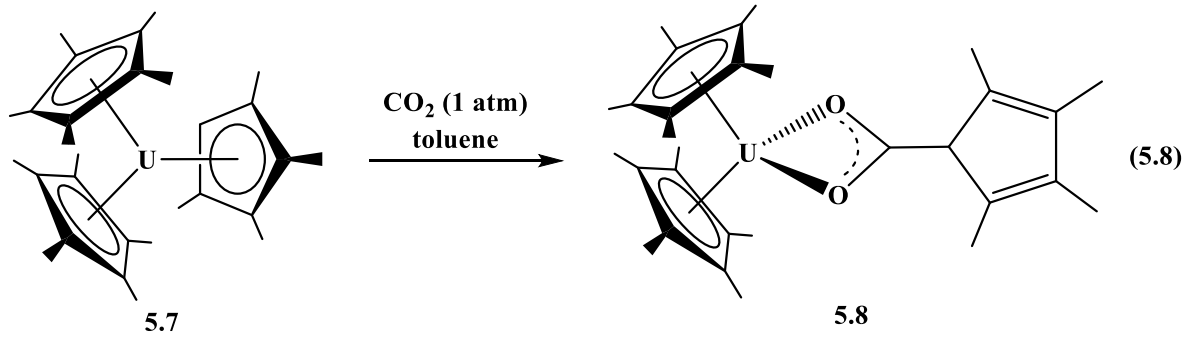

Electrochemistry. Electrochemical data on U(III) compounds have been reported only sporadically.[43–45] This may be due to the reactivity of U(III) compounds with common electrolytes such as $[^nBu_4N][PF_6]$.[46,47] Moreover, most of the investigations have reported just the U(IV)/U(III) redox couple. The first electrochemical reports on U(III)/U(II) couples involved $[(^{Ad,Me}ArO)_3mes]U$ (−2.495 V vs Fc^+/Fc)[11] and $(C_5{}^iPr_5)_2U$ (−2.33 V vs Fc^+/Fc)[6] [Fc = $(C_5H_5)_2Fe$]. Chapter 3 reported electrochemical measurements on a series of tris(cyclopentadienyl) uranium

complexes, $(C_5R_5)_3U$, and the U(III)/U(II) reduction potentials for Cp''_3U, Cp'_3U, and $(C_5Me_4H)_3U$ were found to be −2.79 V, −2.43 V, and −3.11 V, respectively.[44]

Before the electrochemistry of the new heteroleptic systems was examined, electrochemical studies were conducted on $(C_5Me_5)_2U(NR_2)$,[2] **5.9**, and $(C_5Me_5)U(NR_2)]_2$[13], **5.10**, since these two compounds were previously shown to form U(II) complexes.[1] Electrochemical data on all the compounds in this study were collected with a 100 mM $[^nBu_4N][BPh_4]$ supporting electrolyte in THF. The voltammogram of **5.9** is shown in Figure 5.5 (see Figure 5.11 for data on **5.10**). Two events, centered at −3.22 V and −1.29 V vs Fc^+/Fc, are assigned to the U(III)/U(II) and U(IV)/U(III) couples, respectively. A minor event centered at −2.50 V was present and cannot be confidently assigned. Another minor anodic process was observed at −1.58 V that could be a ligand-based event.[44,46]

To determine if the other U(III) compounds reported here were good candidates for reduction to U(II) species, the voltammograms of compounds $(C_5Me_5)_2U(OAr')$, **5.1-U**, $(C_5Me_5)_2U(OAr^*)$, **5.2**, **(**$C_5Me_4H)_2U(OAr')$, **5.3**, $(C_5Me_4H)_2U(OAr^*)$, **5.4**, $(C_5Me_5)_2U[CH(SiMe_3)_2]$, **5.5**, and $(C_5Me_5)_2U(C_5Me_4H)$, **5.7**, were collected in THF with 100 mM $[^nBu_4N][BPh_4]$ as the supporting electrolyte. Both the U(IV)/U(III) and U(III)/U(II) couples were observed in the voltammograms of all compounds except for $(C_5Me_5)_2U(C_5H_5)$, **5.6**, which displayed multiple events suggestive of decomposition or ligand rearrangement during data collection. The results are compiled in Tables 5.3 and 5.4 along with some literature values, arranged in order of decreasing U(III)/U(II) and U(IV)/U(II) reduction potentials, respectively. The full sets of electrochemical measurements can be found in Figures 5.9-5.14.

Table 5.3: U(III)/U(II) Reduction potentials of some compounds in this study and previously reported compounds in order of decreasing reduction potential (R = $SiMe_3$)

	E_{PC} (V)	E_{PA} (V)	$E_{1/2}$ U(III)/U(II)
$(C_5{}^iPr_5)_2U$			−2.33[48,a]
$[(^{Ad,Me}ArO)_3mes]U$	−2.586	−2.405	−2.495[11]
$[C_5H_3(SiMe_3)_2]_3U$	−2.79	−2.67	−2.73[44]
$(C_5Me_5)_2U(C_5Me_4H)$, **5.7**	−3.15	−2.98	−3.07
$(C_5Me_4H)_3U$	−3.18	−3.04	−3.11[44]
$(C_5Me_5)_2U(OAr^*)$, **5.3**	−3.23	−3.04	−3.14
$(C_5Me_5)_2U[CH(SiMe_3)_2]$, **5.5**	−3.21	−3.09	−3.15
$(C_5Me_5)_2U(OAr')$, **5.1-U**	−3.40	−3.06	−3.23
$(C_5Me_5)_2U(NR_2)$, **5.9**	−3.30	−3.23	−3.27
$(C_5Me_5)U(NR_2)_2$, **5.10**	−3.36	−3.27	−3.32

a: E_{PC} and E_{PA} values not reported

Table 5.4: U(IV)/U(III) Reduction potentials of some compounds in this study and previously reported compounds in order of decreasing reduction potential (R = $SiMe_3$)

	E_{PC} (V)	E_{PA} (V)	$E_{1/2}$ U(IV)/U(III)
$[C_5H_3(SiMe_3)_2]_3U$	−1.04	−0.83	−0.94[44]
$(C_5Me_5)_2U[CH(SiMe_3)_2]$, **5.5**	−1.26	−1.12	−1.19
$(C_5Me_5)_2U(OAr^*)$, **5.3**	−1.31	−1.18	−1.25
$(C_5Me_5)_2U(OAr')$, **5.1-U**	−1.44	−1.10	−1.27
$(C_5Me_5)_2U(NR_2)$, **5.9**	−1.39	−1.18	−1.29
$(C_5Me_5)U(NR_2)_2$, **5.10**	−1.42	−1.23	−1.33
$(C_5Me_5)_2U(C_5Me_4H)$, **5.7**	−1.44	−1.31	−1.38
$(C_5Me_4H)_3U$	−1.54	−1.39	−1.46[44]

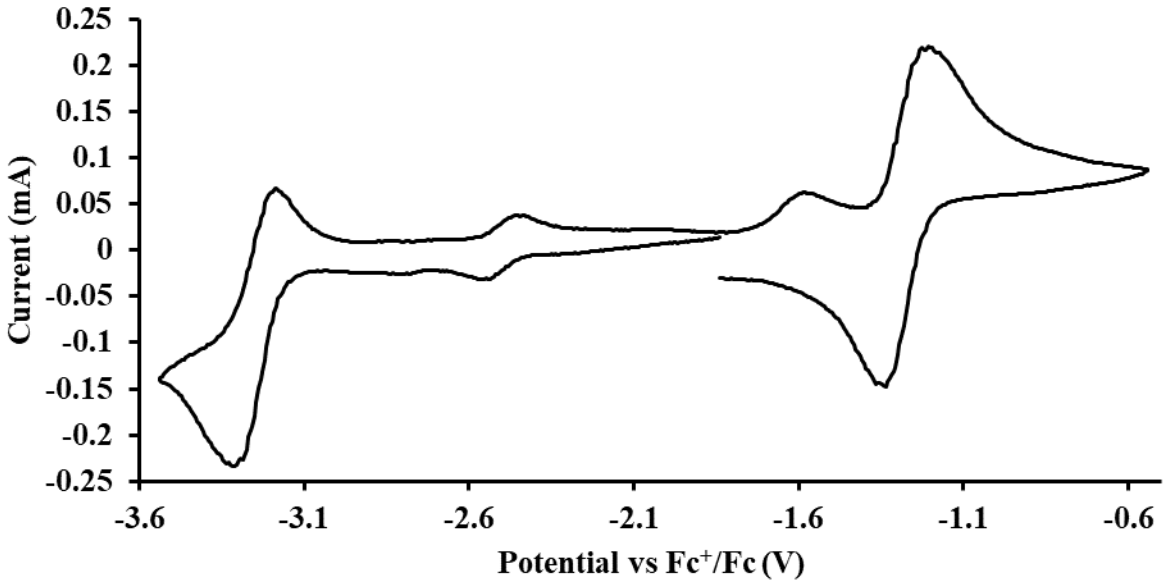

Figure 5.5: Voltammogram of 16 mM $(C_5Me_5)_2U(NR_2)$, **5.9**, at v = 200 mV/s in 100 mM $[^nBu_4N][BPh_4]$ / THF (R = $SiMe_3$). The events centered at −3.22 V and −1.29 V are assigned to the U(III)/U(II) and U(IV)/U(III) couples, respectively. The other two events cannot be assigned with confidence.

As shown in Tables 5.3 and 5.4, the U(III)/U(II) reduction potential for these heteroleptic compounds spans the relatively narrow range of −3.07 V to −3.32 V which corresponds to an energy difference of 5.8 kcal/mol (24 kJ/mol). In general, the U(IV)/U(III) reduction potentials follow a similar trend as for the U(III)/U(II) reduction potentials and span an even narrower range of −1.19 V to −1.38 V. It is interesting to note that the trend in U(III)/U(II) reduction potential is not identical to the U(IV)/U(III) reduction potential. For example, $(C_5Me_5)_2U(C_5Me_4H)$, **5.7**, has the least negative U(IV)/U(III) reduction potential of the compounds tabulated, but the most negative U(III)/U(II) reduction potential. It has been observed that reduction potentials for cyclopentadienyl complexes are sensitive to the specific system[49] and the present results should be used carefully. Nevertheless, this set of compounds further shows that the U(III)/U(II) reduction

potential can be observed with appropriate experimental conditions and electrochemistry can be used to guide the synthesis of U(II) complexes.

Chemical Reduction Attempts. Chemical reduction of **5.1-U, 5.3,** and **5.5-5.7** in THF at −78 °C with KC_8 in the presence of 2.2.2-cryptand generated dark blue solutions, suggestive of $5f^36d^1$ U(II) species[1,50–52] in all cases. However, in each case the blue color quickly faded, and all attempts to isolate and crystallographically characterize the putative U(II) species have so far been unsuccessful. The dark blue color of solutions generated by reduction of **5.1-U**, **5.5**, and **5.7** appeared to last the longest, but even in these cases, useful UV-visible spectra were not obtained. The color change is ambiguous and could indicate the presence of $[K(crypt)][e^-]$.[53] However, EPR studies on frozen solutions immediately following reaction with KC_8 do *not* show a sharp feature attributable to electride.[54,55] These spectra are discussed in Chapter 6.

Multiple attempts were made to collect the UV-visible spectra of the putative U(II) compounds generated by reduction of **5.1-U** and **5.2-5.7** both at −78 °C through a dry ice/isopropanol film and at −35 °C inside the glovebox. Although spectra of reduction products from **5.9** and **5.10** were obtainable as previously reported,[1,56] the reduced heteroleptic products in the present study were too unstable to provide useful optical spectra. A reduction was also examined at −90 °C using $(C_5Me_5)_2U(CHR_2)$, **5.5**, because its solutions appeared to last longer, but even at this temperature, clean UV-visible spectra were not observed (see Figure 5.8).

Electronic Structure Calculations. Electronic structure calculations were performed to evaluate the possibility that the dark blue solutions formed on reduction were viable U(II) complexes. Calculations were performed on the bis(pentamethylcyclopentadienyl) uranium(III) species **5.1-U** and **5.5-5.7** and their one-electron reduced U(II) analogs using the TPSSh hybrid meta-generalized gradient density functional approximation.[57] The continuum solvation model

COSMO[58] with a dielectric constant $\varepsilon = 7.52$ for THF[59] was used for the anionic U(II) compounds. Time dependent DFT calculations of vertical excitations and oscillator strengths[60] were carried out with an additional diffuse *p* primitive added to the uranium basis set by downward extrapolation which is necessary for accurate modelling of d to p transitions.[1,61] All computations were completed using TURBOMOLE V7.4.1.[62,63] See the methods section for complete details.

The electronic ground states for $[(C_5Me_5)_2U(OAr')]^{1-}$, $\{(C_5Me_5)_2U[CH(SiMe_3)_2\}^{1-}$, $[(C_5Me_5)_2U(C_5H_5)]^{1-}$, and $[(C_5Me_5)_2U(C_5Me_4H)]^{1-}$ are consistent with $5f^3 6d^1$ configurations. The ground-state structure of $[(C_5Me_5)_2U(OAr')]^{1-}$ was found to have a 145.5° U–O–C angle, in between the 110.98° and 158.92° angles found in the solid state structure of the neutral species $(C_5Me_5)_2U(OAr')$, **5.1-U**. For comparison, the neutral species **5.1-U** was also optimized and the ground state structure had a U–O–C angle of 119.3° indicating that, in the absence of crystal packing forces, a bent orientation is preferred. The calculated 2.233 Å U–O distance in $(C_5Me_5)_2U(OAr')$ is close to the 2.201(6) and 2.225(6) Å values in the two different molecules in the unit cell of the structure. The highest occupied molecular orbital (HOMO) of $[(C_5Me_5)_2U(OAr')]^{1-}$ is a non-bonding, $6dz^2$-like orbital, Figure 5.6. This electronic configuration is consistent with previous results[1] on $[(C_5Me_5)_2U(NR_2)]^{1-}$ and $(Cp'_3U)^{1-}$.[50] Clearly, a $6dz^2$-like orbital is energetically accessible upon reduction within the trigonal framework of $[(C_5Me_5)_2U(A)]^{1-}$.[64]

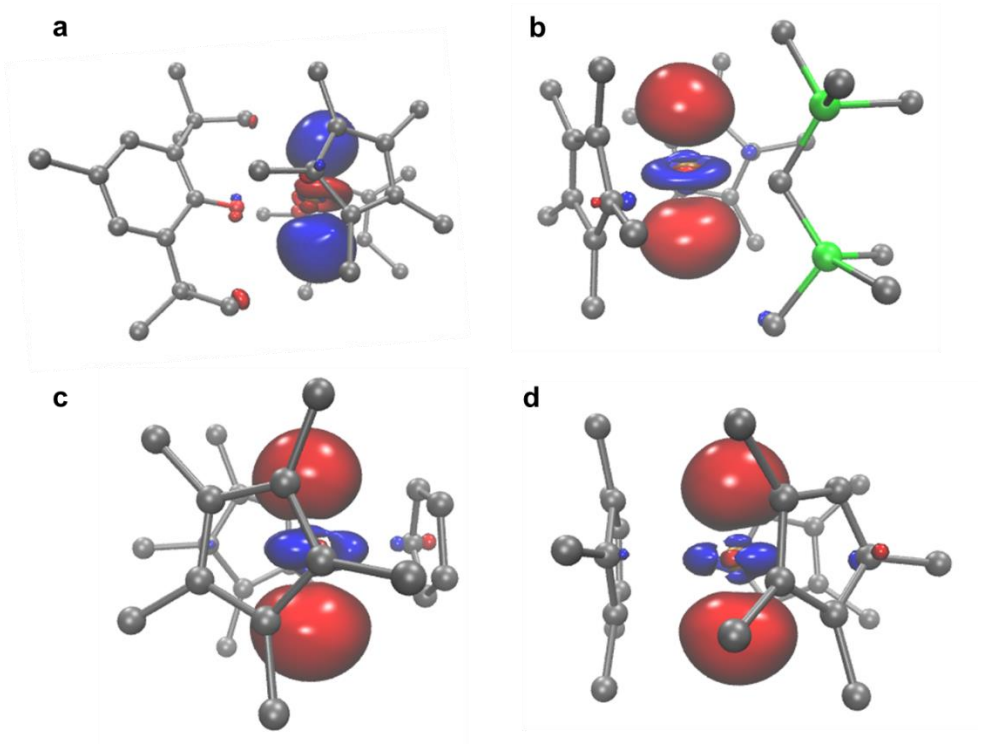

Figure 5.6: HOMO of (a) $[(C_5Me_5)_2U(OAr')]^{1-}$, (b) $[(C_5Me_5)_2U(CHR_2)]^{1-}$, (c) $[(C_5Me_5)_2U(C_5H_5)]^{1-}$, and (d) $[(C_5Me_5)_2U(C_5Me_4H)]^{1-}$, plotted with a contour value of 0.05. Hydrogen atoms have been removed for clarity.

Discussion

The number of heteroleptic $(C_5Me_4R)_2U(A)$ complexes (R = Me, H; A = anion) was increased by the synthesis of $(C_5Me_5)_2U(OAr')$, **5.1-U**, $(C_5Me_4H)_2U(OAr')$,**5. 2**, $(C_5Me_5)_2U(OAr^*)$, **5.3**, $(C_5Me_4H)_2U(OAr^*)$, **5.4**, $(C_5Me_5)_2U(C_5H_5)$, **5.6**, $(C_5Me_5)_2U(C_5Me_4H)$, **5.7**, and $(C_5Me_5)_2U(\kappa^2\text{–}O,O'\text{–}O_2C\text{–}C_5Me_4H)$, **5.8**. Compounds **5.1-5.7** were synthesized via salt-metathesis routes from $(C_5Me_4R)_2UI(THF)$ starting materials and the corresponding (alkali-metal)(anion) salt. Complex **5.7** was also synthesized from $(C_5Me_5)_2U(\mu\text{–}Ph)_2BPh_2$, which was generated by an improved method, eq 5.7. The newly developed synthesis of $(C_5Me_5)_2U(\mu\text{–}Ph)_2BPh_2$ is more efficient as it begins with UI_3 and only requires three steps, while the previous route involves four steps starting from UCl_4.[12]

Previously known $(C_5Me_5)_2U[CH(SiMe_3)_2]$, **5.5**,[3] was structurally characterized for the first time. It was found to have the alkyl group bound asymmetrically to allow a close contact of one methyl group with the uranium as also found with isomorphous Nd and Ce complexes. The aryloxides **5.1-U** and **5. 2** were structurally unusual in that they displayed two different U–O–C angles in each crystal structure as did the cerium analog, $(C_5Me_5)_2Ce(OAr')$, **5.1-Ce**. The isomorphous nature of the U and Ce complexes indicates that the angle is not affected by 5f vs 4f orbital properties. DFT studies on $(C_5Me_5)_2U(OAr')$, **5.1-U**, predicted a U–O–C angle of 119.3° in between the 110.98° and 158.92° angles found in the solid-state structure. Although a bent structure may be preferred, the energy surface between bent and linear M–O–C angles in these metallocene aryloxides must be shallow such that crystal packing effects give the two disparate angles.

Electrochemical analysis of the U(III)/U(II) couple in the $(C_5Me_5)_2U(A)$ complexes showed a potential range between −3.07 V to −3.32 V. These values are more negative than the reduction potentials reported for $(C_5{}^iPr_5)_2U$[48] and $[(^{Ad,Me}ArO)_3mes]U$,[43] but are similar to −3.11 V couple of the homoleptic, tris(cyclopentadienyl) complex $(C_5Me_4H)_3U$.[44] The relatively small range suggests that the electron donation strength of the ligand does not play a significant role in determining the reduction potential in this series of complexes.

Chemical reduction of the heteroleptic uranium compounds **5.1-U**, **5.3**, and **5.5-5.7** generated dark blue solutions, but no U(II) compounds could be crystallographically characterized. Although these heteroleptic complexes are electrochemically similar to $(C_5Me_5)_2U(NR_2)$, **5.9**,[40] they are no better precursors to isolable U(II) products. DFT analysis of four targeted $[(C_5Me_5)_2U(A)]^{1-}$ complexes indicates that formation of complexes of U(II) with a $5f^36d^1$ electron configuration is reasonable, as found in isolated $[K(crypt)][Cp'_3U]$, $[Li(THF)_4][Cp''_3U]$,[65]

{[(THF)$_2$Cs(μ–η^5:η^5–Cp″)$_2$Cp″U}$_n$,[65] and [K(crypt)][(C_5Me_4H)$_3$U].[52] The $5f^3 6d^1$ electron configuration appears to be the common ground state for these tris(ligand) complexes.[64]

The HOMO-LUMO energy gap for U(II) complexes does not appear to be a great indicator for stability either. Unstable heteroleptic U(II) species have HOMO-LUMO energy gaps both larger and smaller than those of isolable U(II) complexes, Table 5.5.

Table 5.5. Calculated HOMO and LUMO energies of U(II) compounds

	HOMO (eV)	LUMO (eV)	Δ*E* (eV)	Total Energy (eV)
[(C_5Me_5)$_2$U(CHR_2)]$^{1-}$	−1.188	0.565	1.753	−57513.6250630
[(C_5Me_5)$_2$U(C_5H_5)]$^{1-}$	−1.133	0.466	1.599	−39458.9918878
[(C_5Me_5)$_2$U(C_5Me_4H)]$^{1-}$	−1.112	0.560	1.672	−43734.8807130
[(C_5Me_5)$_2$U(OAr′)]$^{1-}$	−0.928	0.588	1.516	−52164.037525
[Cp″$_3$U]$^{1-}$ [40,32]	−1.453	0.092	1.545	−95468.4964571
[(C_5Me_4H)$_3$U]$^{1-}$ [32,41]	−1.069	0.555	1.624	−41597.5772726
[U(NR_2)$_3$]$^{1-}$ [32,41]	−1.689	−0.007	1.696	−84245.4330163
[(C_5Me_5)$_2$U(NR_2)]$^{1-}$ [28]	−1.061	0.669	1.730	−57951.8944421
[(C_5Me_5)U(NR_2)$_2$]$^{1-}$ [28]	−1.263	0.310	1.573	−71098.4936726
{[(^{Ad,Me}ArO)$_3$mes]U}$^{1-}$ [42]	−1.602	−1.414	0.188	[a]
(NHAr^{iPr6})$_2$U [28,43]	−3.132	−1.869	1.263	[a]

a: Value not reported

Furthermore, there is no correlation between the measured U(III)/U(II) $E_{1/2}$ values from Table 5.3 with the calculated HOMO-LUMO energy gap of the U(II) compound, the HOMO-LUMO energy gap of the U(III) compound, or the calculated U(II) HOMO energy, Figures 5.15–5.17. The energy difference between the U(III) and U(II) compound does correlate well with the measured reduction potentials, Table 5.6 and Figure 5.7, where the larger energy difference correlates with a more negative reduction potential.

Table 5.6. Calculated HOMO and LUMO energies and measured U(III)/U(II) $E_{1/2}$ of U(III) compounds

	HOMO (eV)	LUMO (eV)	Δ*E* (eV)	Total energy (eV)	Measured $E_{1/2}$ (V)
$(C_5Me_5)_2U(CHR_2)$	−3.234	−1.108	2.126	−57512.2391927	−3.15
$(C_5Me_5)_2U(C_5Me_4H)$	−3.126	−1.377	1.749	−43733.4485022	−3.07
$(C_5Me_5)_2U(OAr')$	−3.166	−0.978	2.188	−52162.7951511	−3.23
Cp''_3U[40,32]	−3.528	−1.814	1.714	−95466.7519212	−2.73
$(C_5Me_4H)_3U$[32,41]	−3.026	−1.267	1.759	-41597.5772726	−3.11
$(C_5Me_5)_2U(NR_2)$[28]	−3.020	−1.010	2.010	−57950.6278114	−3.27
$(C_5Me_5)U(NR_2)_2$ [28]	−3.132	−0.805	2.327	−71097.3322362	−3.32

The energy difference between the two compounds determined by DFT methods can approximate the ionization potential or electron affinity of the species, which can explain why the reduction potentials are correlated with such a value.

The low stability of the dark blue reduction products was also evaluated in terms of steric saturation. This has been shown to be an important factor in the stabilization of other low oxidation state f element complexes.[33,50,66] The steric factors of the ligands can be analyzed using the method of Guzei,[12,67] where the *G* parameter (as a percent) denotes the coverage of the metal center by the ligands.[32] A larger *G* parameter indicates a more sterically crowded metal center. As shown in Table 5.7, the *G* parameter for the U(II) compounds fall within the range of 81.5 to 85.7%. The isolable U(II) compound $[(C_5Me_4H)_3U]^{1-}$ has a *G* parameter of 82.0% and a U(III)/U(II) reduction potential of −3.11 V,[44] while the putative U(II) compound $[(C_5Me_5)_2U(C_5Me_4H)]^{1-}$ compound has a *G* parameter of 81.7% and an $E_{1/2}$ of −3.07 V, but cannot be isolated.

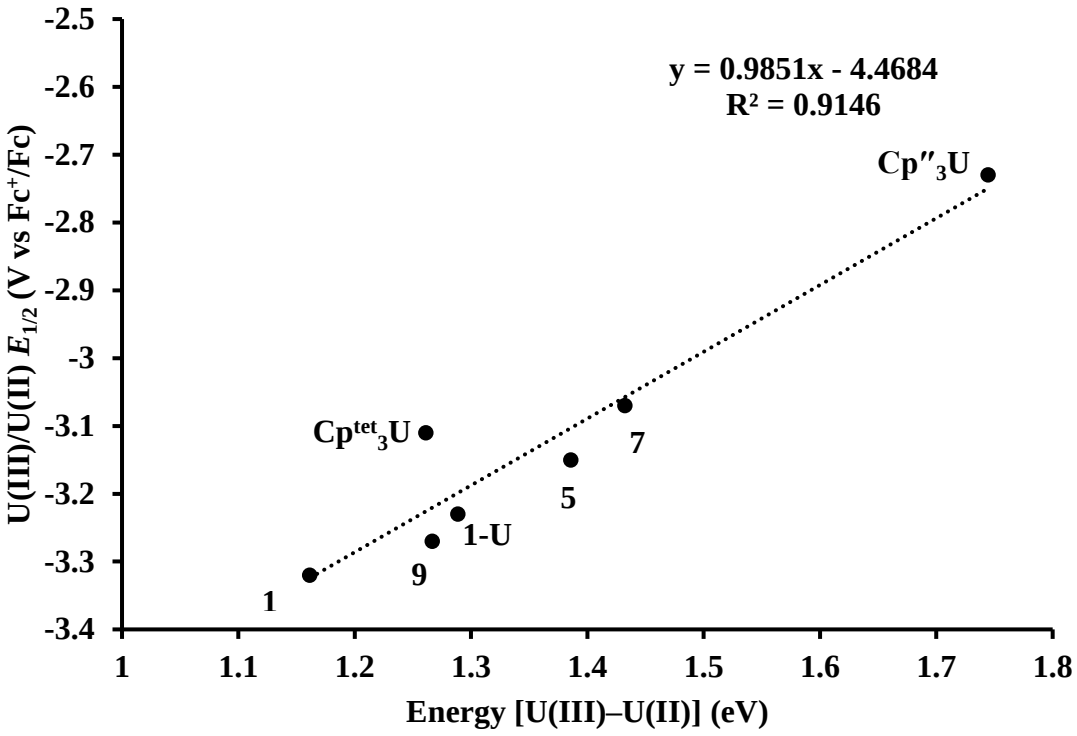

Figure 5.7: Plot of measured U(III)/U(II) $E_{1/2}$ vs the calculated energy difference between U(III) and U(II) compounds.

Since ligand redistribution is possible for these heteroleptic species and not for the more stable homoleptic complexes, this could be a point of difference for the $(C_5Me_5)_2UA$ reduction products. While we do not see evidence for ligand rearrangement in the $(C_5Me_5)_2UA$ compounds based on NMR studies, Table 5.1, ligand rearrangement cannot be ruled out for the U(II) compounds to form species such as $[(C_5Me_5)_xUA_{3-x}]^{1-}$ (x = 1, 2, 3). However, the high G values for these complexes suggest that the usual driving force of steric saturation is not operable here, Table 5.7. In addition, the difficulty of forming the sterically crowded $(C_5Me_5)_3U$[31,38] argues against ligand redistribution.

Table 5.7: Calculated *G* Parameters. R= $SiMe_3$

	G Parameter (%)
$(C_5Me_5)_2U(CHR_2)$, **5.5**	89.2,[a] 87.3 [b]
$(C_5Me_5)_2U(C_5H_5)$, **5.6**	82.4[a]
$(C_5Me_5)_2U(C_5Me_4H)$, **5. 7**	82.9[a]
$(C_5Me_5)_2U(OAr')$, **5.1-U**	86.9,[a,b] 89.8,[b,c]
$(C_5Me_4H)_2U(OAr')$, **5.2**	87.6[b]
$(C_5Me_4H)_3U$	83.7[b]
$[(C_5Me_5)_2U(CHR)_2]^{1-}$	84.7[d]
$[(C_5Me_5)_2U(C_5H_5)]^{1-}$	81.5[d]
$[(C_5Me_5)_2U(C_5Me_4H)]^{1-}$	81.7[d]
$[(C_5Me_5)_2U(OAr')]^{1-}$	85.7[c,d]
$(C_5Me_5)U(NR_2)_2$, **5.10**	89.5[b,13]
$(C_5Me_5)_2U(NR_2)$, **5.9**	85.9[b,2]
"$[(C_5Me_5)_2U(NR_2)]^{1-}$"	85.7[d,1]
"$[(C_5Me_5)U(NR_2)_2]^{1-}$"	82.7[d,1]
$[(C_5Me_4H)_3U]^{1-}$	82.0[d,52]

a: linear U–O–C structure
b: Value computed from solid-state structure
c: bent U–O–C structure
d: Value computed from DFT-optimized structure

The fact that reduction products from $(C_5Me_5)_2U(C_5H_5)$, **5.6**, and $(C_5Me_5)_2U(C_5Me_4H)$, **5.7**, could not be isolated is particularly surprising considering that crystal structures of other tris(cyclopentadienyl) U(II) complexes $[Cp'_3U]^{1-}$,[50] $[Cp''_3U]^{1-}$,[65] and $[(C_5Me_4H)_3U]^{1-}$ [52] are known.

From the present results, it appears that heteroleptic U(II) compounds, at least those within the $(C_5Me_5)_2UA$ ligand environment, are less stable than homoleptic tris(cyclopentadienyl) U(II) compounds such as $[Cp'_3U]^{1-}$, $[Cp''_3U]^{1-}$, and $[Cp^{tet}_3U]^{1-}$. Clearly, neither steric saturation, orbital energy, nor reduction potential alone can explain the relative instability of these U(II) compounds. Although the decomposition products for the compounds reported in this Chapter were not able to be determined, previous reduction studies on $(C_5Me_5)_2U(NR_2)$ and $(C_5Me_5)U(NR_2)_2$ showed C–H activation by the U(II) center as a facile decomposition route which be occurring in the

$[(C_5Me_5)_2UA]^{1-}$ compounds.[10] Under photolytic conditions, $(Tren^R)U$ ($Tren^R = N(CH_2CH_2NR)_3$) also decomposes via C–H bond activation to form cyclometallated species.[71] Furthermore, C–H activation by U(II) has been observed in the $[(^{Ad,Me}ArO)_3mes]U$ system[43] and with $[K(crypt)][U(NR_2)_3]$.[52,68] The previous results suggest that C–H activation is a likely decomposition route for U(II) compounds, even for those without the $N(SiMe_3)_2$ ligand.

Conclusion

The range of fully characterized heteroleptic $(C_5Me_4R)_2U(A)$ (R = Me, H; A = anion) complexes has been expanded by salt metathesis syntheses from $(C_5Me_4R)_2UI(THF)$ and the corresponding alkali-metal salt of anion A. The solid-state structures of $(C_5Me_5)_2U(OAr')$, $(C_5Me_5)_2Ce(OAr')$, and $(C_5Me_4H)_2U(OAr')$ indicate that conformations with both linear and bent M–O–C angles are accessible in these systems. U(III)/U(II) reduction potentials were determined for these heteroleptic species by cyclic voltammetry and were found to vary only slightly as the ligands changed. Chemical reduction generated dark blue solutions characteristic of $5f^36d^1$ U(II) compounds as established by DFT analysis. Despite the similar reduction potentials and steric saturation of these systems, none of the heteroleptic U(II) species were stable enough for isolation and crystallographic characterization.

Experimental Details

All syntheses and manipulations described below were conducted with rigorous exclusion of air and water using standard glovebox and vacuum line techniques. Solvents were sparged with UHP argon and dried by passage through columns containing Q-5 and molecular sieves prior to use. Deuterated NMR solvents were dried over NaK alloy, degassed by three freeze-pump-thaw cycles, and vacuum transferred before use. ^1H NMR spectra were recorded on either a CRYO500 MHz or AVANCE600 MHz at 298 K and referenced to residual protio-solvent resonances. UV-

visible spectra were collected at 298 K using a Varian Cary 50 Scan UV-visible spectrophotometer in a 1 mm cuvette for Methods A and B. Method C used an 8453 Agilent UV-visible spectrometer equipped with an Unisoku Unispeks cryostat in a 1 cm cuvette; red Play-Doh was placed around the cuvette to minimize moisture collection in the cryostat. Infrared spectra were recorded as compressed solids on an Agilent Cary 630 ATR-FTIR. Electrochemistry were collected in THF with 100 mM [^{n}Bu$_4$N][BPh$_4$] supporting electrolyte with a glassy carbon working electrode, platinum wire counter electrode, and silver wire pseudoreference electrode with decamethylferrocene as an internal reference (−0.495 V vs Fc^{+}/Fc under these conditions).[44]

2.2.2-Cryptand (crypt) (Aldrich) was used as received. KN(SiMe$_3$)$_2$ (Aldrich) was dissolved in minimal toluene and the solution was centrifuged to remove a yellow oil. The solution was then dried to yield a white solid of KN(SiMe$_3$)$_2$. HOAr′ (Aldrich) were sublimed prior to use. Electrochemical grade [^{n}Bu$_4$N][BPh$_4$] (Sigma) was recrystallized three times from acetone and dried under 10^{-7} Torr at 80 °C before use.

KCH(SiMe$_3$)$_2$,[69] LiCH(SiMe$_3$)$_2$,[70] UI$_3$,[71] Cp*$_2$U(NPh$_2$)(THF),[5] NaCp,[72] KC$_5$Me$_4$H,[73] UOAr$_3$,[74] (C$_5$Me$_5$)$_2$UI(THF),[13] (C$_5$Me$_5$)$_2$U(NR$_2$),[2] (C$_5$Me$_5$)U(NR$_2$)$_2$,[13] and KC$_8$[75] were synthesized following literature procedures. KOAr′ was synthesized following an adaptation from literature route using KN(SiMe$_3$)$_2$ and HOAr′ in toluene.[76] KC$_5$Me$_5$ and KOAr* were synthesized from KN(SiMe$_3$)$_2$ and HC$_5$Me$_5$ (Sigma) or HOAr*,[77] respectively, in toluene.

Synthesis of (C$_5$Me$_5$)$_2$U(OAr′), 5.1-U. (C$_5$Me$_5$)$_2$UI(THF) (80 mg, 0.11 mmol) was dissolved in toluene (7 mL) to give a dark green solution. KOAr′ (29 mg, 0.11 mmol) was added as a solid and the solution was stirred overnight. Brown solids were removed via centrifugation and the solution was filtered and dried under vacuum. Hexane (7 mL) was added and the solution was filtered and dried to afford **5.1-U** as a red-brown solid (73 mg, 76%). The solids were

sometimes contaminated with HOAr′ which can be removed by crystallization of **5.1-U** from pentane. Brown X-ray quality crystals were grown by slow evaporation of a pentane solution at −35 °C. ^{1}H NMR (C_6D_6): δ 8.80 (s, 2 H, Ar), 3.40 (s, 3 H, Me), −8.69 (s, 30 H, $C_5\mathit{Me}_5$), −20.54 ppm (s, 18 H, ^{t}Bu). IR: 2896s, 2846s, 1438s, 1358m, 1306m, 1243s, 1116w, 1053m, 1018m, 878w, 821m, 721m, 659w cm^{-1}. Anal Calcd for $C_{35}H_{53}OU$: C, 57.76; H, 7.34. Found: C, 55.16; H, 7.17. Low C values were found across multiple runs and suggests incomplete combustion or carbide formation. The observed C:H ratio of $C_{35}H_{54.2}$ is close to the calculated value.

Synthesis of $(C_5Me_5)_2Ce(OAr')$, 5.1-Ce. In a Schlenk flask with a grease-free Teflon stopcock, $(C_5Me_5)_2Ce(\mu\text{–}Cl)_2K(THF)_2$ (130 mg, 0.196 mmol) and KOAr′ (51 mg, 0.197 mmol) were dissolved in THF (30 mL) to form a bright yellow solution. The flask was attached a vacuum line and heated to 60 °C and allowed to stir overnight. As the reaction progressed, the solution became dark orange in color. The flask was cooled to room temperature and the solvent was removed under vacuum. The flask was brought into a glovebox and the product was extracted into hexane to afford a deep red/purple solution. The solvent was removed under vacuum to yield 1-Ce as a dark pink solid (82 mg, 85%). Dark pink crystals suitable for X-ray crystallography were grown from a concentrated hexane solution at −35 °C. ^{1}H NMR (C_6D_6): δ 8.46 (s, 2H, Ar), 3.37 (s, 3H, Me), 2.71 (s, 30H, $C_5\mathit{Me}_5$), −6.97 ppm (s, 18H, ^{t}Bu). ^{13}C NMR (C_6D_6): 163.2, 151.1, 36.17, 22.08, 5.36 ppm. IR: 2957m, 2902m, 2854m, 1418s, 1380m, 1356w, 1256s, 1236s, 1118m, 1063m, 1020m, 945m, 862m, 824s, 803s, 774w cm^{-1}. Anal Calcd for $C_{35}H_{53}OCe$: C, 66.74; H, 8.48. Found: C, 66.44; H, 8.86.

Synthesis of $(C_5Me_4H)_2UI(THF)$. UI_3 (105 mg, 0.170 mmol) and KC_5Me_4H (54 mg, 0.337 mmol) were dissolved in THF (15 mL) to form a green solution and stirred overnight. Solvent was removed under vacuum and the product was extracted into toluene (15 mL). Solids

were removed via centrifugation and the solvent was removed to yield a green/brown solid. THF (5 mL) was added to dissolve all the material, then solvent was removed under vacuum to afford dark green solids of $(C_5Me_4H)_2UI(THF)$ (73 mg, 63%). Dark green X-ray quality crystals were grown by layering a concentrated THF solution with hexane at −35 °C. The data provided connectivity of the molecule but were not of high enough quality to discuss metrical parameters. ^{1}H NMR (THF-d_8): δ 18.93 (br s, 6H, C_5Me_4H), −20.69 (br s, 6H, C_5Me_4H) ppm. IR: 2893s, 2854s, 1438m, 1380s, 1321w, 1005s, 851m, 768s cm^{-1}. Anal Calcd for $C_{22}H_{34}OIU$: C, 38.89; H, 5.04. Found: C, 37.75; H, 5.56. Found: C, 39.45; H, 5.72.

$(C_5Me_4H)_2UOAr'$, 5.2. $(C_5Me_4H)_2UI(THF)$ (82 mg, 0.12 mmol) and KOAr′ (31 mg, 0.12 mmol) were dissolved in THF (5 mL) to form a green solution. The solution was stirred overnight at which point it had turned brown. Solvent was removed under vacuum and the product was extracted into hexane (10 mL). White solids were removed via centrifugation and the solvent was removed under vacuum to afford **7** as a green/brown solid (62 mg, 73%). In some instances, $(C_5Me_4H)_3U$ was observed in the ^{1}H NMR[30] which can be removed by crystallization from a concentrated toluene solution at −35 °C. ^{1}H NMR (C_6D_6): δ 8.45 (s, 2H, Ar), 2.64 (s, 3H, Me), −1.57 (s, 6H, C_5Me_4H), −15.02 (s, 2H, C_5Me_4H), −17.55 (s, 18H, ^{t}Bu), −27.38 ppm (s, 6H, C_5Me_4H). IR: 2899s, 2854s, 1419s, 1381m, 1244s, 1019m, 770s cm^{-1}. Anal Calcd for $C_{33}H_{49}OU$: C, 56.64; H, 7.06. Found: C, 53.21; H, 5.97. Incomplete combustion was observed across multiple runs. The calculated ratio was $C_{33}H_{43.8}$.

Synthesis of $(C_5Me_5)_2UOAr^*$, 5.3. $(C_5Me_5)_2UI(THF)$ (80 mg, 0.11 mmol) was dissolved in toluene (7 mL) to give a dark green solution. KOAr* (52 mg, 0.11 mmol) was added as a solid and the solution was stirred overnight. White solids were removed via centrifugation and the solution was filtered and dried under vacuum. Hexane (7 mL) was added, the solution was filtered

and dried to afford a brown solid. The solids were washed with cold (−35 °C) pentane (1 mL) to remove HOAr* and dried to yield **5.3** as a brown solid (53 mg, 51%). ^{1}H NMR (C_6D_6): δ 13.76 (s, 2H, Ar), 4.00 (s, 9H, ^{t}Bu), 1.80 (s, 6H, Ad), −8.74 (s, 30 H, C_5Me_5), −9.74 (d, 6 H, Ad), −12.34 (d, 6 H, Ad), −15.72 (s, 12 H, Ad), −17.94 ppm (s, 6 H, Ad). IR: 2959m, 2871m, 2813m, 1566m, 1512s, 1352s, 1294m, 1257w, 1130m, 1099s, 1075m, 948s, 930m, 751m cm^{-1}. Anal Calcd for $C_{50}H_{71}OU$: C, 64.84; H, 7.73. Found: C, 56.26; H, 6.63. Found: C, 52.43; H, 6.24. Low C and H values were found across multiple runs and suggest incomplete combustion. The observed C:H ratios of $C_{50}H_{70.2}$ and $C_{50}H_{70.9}$ are close to the calculated value.

Synthesis of $(C_5Me_4H)_2UOAr^*$, 5.4. $(C_5Me_4H)_2UI(THF)$ (55 mg, 0.081 mmol) and KOAr* (37mg, 0.081 mmol) were dissolved in THF (5 mL) to form a green solution. The solution was stirred overnight at which point it had turned brown. Solvent was removed under vacuum and the product was extracted into toluene (10 mL). White solids were removed via centrifugation and the solvent was removed under vacuum. The solids were dissolved in a minimal amount of THF and placed in the freezer overnight at −35 °C to crystallize HOAr*. The mother liquor was decanted, and solvent was removed under vacuum to afford **5.4** as a green/brown solid (45 mg, 62%). In some instances, $(C_5Me_4H)_3U$ was observed in the ^{1}H NMR[30] which can be removed by crystallization from a concentrated toluene solution at −35 °C. ^{1}H NMR (C_6D_6): δ 15.29 (2H, Ar), 4.61 (s, 9H, ^{t}Bu), −8.19 (s, 12H, Ad or C_5Me_4H), −8.85 (12H, Ad or C_5Me_4H), −11.05 (s, 6H, Ad), −16.70 (s, 6H, Ad), −17.84 (s, 12H, C_5Me_4H), −18.89 (s, 6H, Ad). IR: 2899s, 2847s, 1445m, 1359w, 1278w, 1241m, 1101w, 873w, 838m, 773m cm^{-1}. Anal Calcd for $C_{48}H_{67}OU$: C, 64.19; H, 7.52. Found: C, 60.79; H, 7.79. Found: C, 60.32; H, 7.53. Found: C, 55.14; H, 7.34. Low C values were observed across multiple runs and suggests formation of carbide species.

Synthesis of $(C_5Me_5)_2U[CH(SiMe_3)_2]$, 5.5. $(C_5Me_5)_2UI(THF)$ (50 mg, 0.071 mmol) was dissolved in Et_2O (5 mL) to give a dark green solution. $KCH(SiMe_3)_2$ (14 mg, 0.071 mmol) was added as a solid and the solution was stirred overnight. White solids were removed via centrifugation and the solution was filtered and dried under vacuum. Hexane (5 mL) was added and the solution was filtered and dried to afford a brown solid (41 mg, 87%), identified as **5.5** by ^{1}H NMR spectroscopy.[3] Brown X-ray quality crystals were grown from a concentrated hexane solution at −35 °C and provided connectivity of the molecule.

Synthesis of $(C_5Me_5)_2U(C_5H_5)$, 5.6. $(C_5Me_5)_2UI(THF)$ (50 mg, 0.071 mmol) was dissolved in toluene (5 mL) to give a dark green solution. $Na(C_5H_5)$ (6.2 mg, 0.071 mmol) was added as a solid and the solution was stirred overnight. White solids were removed via centrifugation and the solution was filtered and dried under vacuum to afford a dark brown/green solid (31 mg, 76%). Brown crystals could be grown by slow evaporation of a pentane solution at −35 °C but were not high enough quality for X-ray diffraction. ^{1}H NMR (C_6D_6): δ −4.42 (s, 30 H, C_5Me_5), −23.04 ppm (s, 5 H, C_5H_5). IR: 2900m, 2851m, 1434s, 1375s, 1243m, 1079w, 1012s, 902m, 755s cm^{-1}. Anal Calcd for $C_{25}H_{35}U$: C, 52.35; H, 6.15. Found: C, 42.25; H, 4.98. Found: C, 41.52; H, 4.89. Low C and H values were found across multiple runs and suggest incomplete combustion. The observed C:H ratio of $C_{25}H_{35.1}$ in both cases is identical to the calculated value.

Synthesis of $(C_5Me_5)_2U(C_5Me_4H)$, 5.7. $(C_5Me_5)_2UI(THF)$ (50 mg, 0.071 mmol) was dissolved in toluene (5 mL) to give a dark green solution. KC_5Me_4H (11 mg, 0.071 mmol) was added as a solid and the solution was stirred overnight. Brown solids were removed via centrifugation and the solution was filtered and dried under vacuum. Hexane (5 mL) was added, the solution was filtered and dried to afford a brown/red solid (25 mg, 57%). Dark brown crystals could be grown from a concentrated Et_2O solution at −35 °C or by slow evaporation of a pentane

solution at −35 °C. The X-ray data provided connectivity but were not high enough quality to discuss metrical parameters. ^{1}H NMR (C_6D_6): δ −3.87 ppm (s, 30 H, C_5Me_5). The C_5Me_4H resonances could not be identified. IR: 2987s, 2848s, 1436s, 1377m, 1244m, 1017m, 879m, 832w, 771m, 660m cm^{-1}. Anal Calcd for $C_{29}H_{43}U$: C, 55.32; H, 6.88. Found: C, 47.09; H, 6.35. Found: C, 46.57; H, 6.15. Low C values were observed across multiple runs and suggests formation of carbide species. The observed C:H ratio of $C_{29}H_{46.6}$ and $C_{29}H_{45.6}$ is close to the calculated value.

Synthesis of $(C_5Me_5)_2U(\mu\text{–}Ph)_2BPh_2$ from 5.5. $(C_5Me_5)_2U(CHR_2)$, **5.5**, (72 mg, 0.11 mmol) was dissolved in benzene (5 mL) to form a brown solution. $[HNEt_3][BPh_4]$ (45 mg, 0.11 mmol) was added and the brown slurry was stirred overnight. White solids were removed via centrifugation and the solvent was removed under vacuum. The solids were washed with hexane and dried under vacuum to yield light brown solids of $(C_5Me_5)_2U(\mu\text{–}Ph)_2BPh_2$, identified by ^{1}H NMR spectroscopy (39 mg, 44%).[2]

Synthesis of $(C_5Me_5)_2U(C_5Me_4H)$, 5.7, from $(C_5Me_5)_2U(\mu\text{–}Ph)_2BPh_2$. KC_5Me_4H (5 mg, 0.03 mmol) was added to a brown solution of $(C_5Me_5)_2U(\mu\text{–}Ph)_2BPh_2$ (25 mg, 0.030 mmol) in benzene (5 mL) and was allowed to stir overnight. Solvent was removed under vacuum. The product was extracted into hexane (5 mL) and green solids were removed via filtration. The solvent was removed under vacuum to yield **5.7** as a brown solid and identified by ^{1}H NMR spectroscopy (11 mg, 58%).

$(C_5Me_5)_2U(\kappa^2\text{–}O,O'\text{-}O_2CC_5Me_4H)$, 5.8. In a Schlenk flask with a grease-free Teflon stopcock, $(C_5Me_5)_2U(C_5Me_4H)$, **5.7**, (66 mg, 0.11 mmol) was dissolved in toluene (5 mL) to form a brown solution. The flask was attached to a vacuum line and the solution was degassed by one freeze-pump-thaw cycle. CO_2 (1 atm) was introduced to the flask and the brown solution turned

red/brown as the solution was stirred for 30 min. The remaining CO_2 was removed and the flask was brought into a glovebox. Solvent was removed under vacuum and the product was extracted into hexane (5 mL) and placed in the freezer at −35 °C. Red crystals of **5.8** formed overnight (27 mg, 38%). ^{1}H NMR (C_6D_6): δ 13.12 (s, 15H, C_5Me_5), 4.89 (s, 6H, C_5Me_4H), 4.01 (s, 6H, C_5Me_4H), 0.29 (s, 15H, C_5Me_5). IR: 2902s, 2855s, 1432s, 1376s, 1258w, 1077m, 1019m, 883w, 788w, 725s, 694m cm^{-1}. Anal Calcd for $C_{30}H_{43}O_2U$: C, 53.49; H, 6.43. Found: C, 49.15; H, 6.43. Found: C, 48.09; H, 6.12. Found: C, 48.57; H, 6.10. Low C values were observed across multiple runs and suggests formation of carbide species.

General Method for UV-Visible measurements

Method A. Approximately 10–15 mg of the U(III) compound of interest and one equivalent of crypt was dissolved in approximately 1 mL of THF in a vial and chilled to −35 °C. A cuvette with a greaseless Teflon stopcock, a pipet filter packed with KC_8, two empty pipets, and an empty vial were also chilled to −35 °C. After a few hours, the uranium and crypt solution was passed through the KC_8 filter into the cold receiving vial or directly into the cuvette. The cuvette was sealed and brought quickly to the spectrometer. Scans were taken sequentially until the spectrum did not change. Using Et_2O as a solvent yielded no better results.

Method B. The samples were prepared as described above in Method A, except the spectra were collected inside the glovebox via a fiber-optic cable coupler attachment to the spectrophotometer. The solutions were passed directly through the KC_8 filter pipet immediately into the pre-chilled cuvette and spectra were collected. These resulting spectra were similar to those from Method A.

Method C. A 1 cm cuvette, equipped with a greaseless Teflon stopcock and side arm, was charged with **5** (5 mg), crypt (3 mg), and KC_8 (~5 mg) and a stir bar. The stopcock was closed

and the side arm was sealed with a septum. The cuvette was placed in the sample holder cryostat and chilled to −90 °C for 15 minutes. Then, THF pre-cooled at −78 °C was syringed into the side arm and the stopcock was opened to allow the THF to mix and reaction to take place. Spectra were collected every 2 seconds until the spectrum did not change.

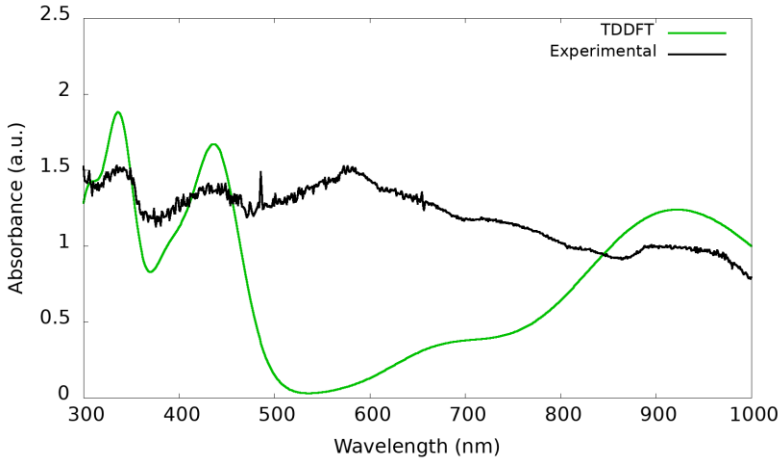

Figure 5.8: UV-visible spectra collected from the reduction of **5** (black) collected at −90 °C using Method C described above. Simulated UV-visible spectrum of $[(C_5Me_5)_2U(CHR_2)]^{1-}$ (green) with a Gaussian line broadening of 0.15 eV.

General Method for Electrochemistry

Inside the glovebox, a stock electrolyte solution was freshly prepared in THF. Between 1–2 mL of this solution was transferred to a 20 mL scintillation vial and a voltammogram of this solution was collected to verify the electrolyte solution was free of impurities. Roughly 10-300 mg of U(III) compound was dissolved in the same electrolyte solution to yield approximately a 10 mM solution. Electrodes were placed into the vial and the vial was left open to the box atmosphere during data collection. The internal resistance was measured, and cyclic voltammetry experiments were recorded. $(C_5Me_5)_2Fe$ was added to the same solution following all data collection, and a single scan was recorded to measure the internal standard redox event. All scans were in the cathodic direction.

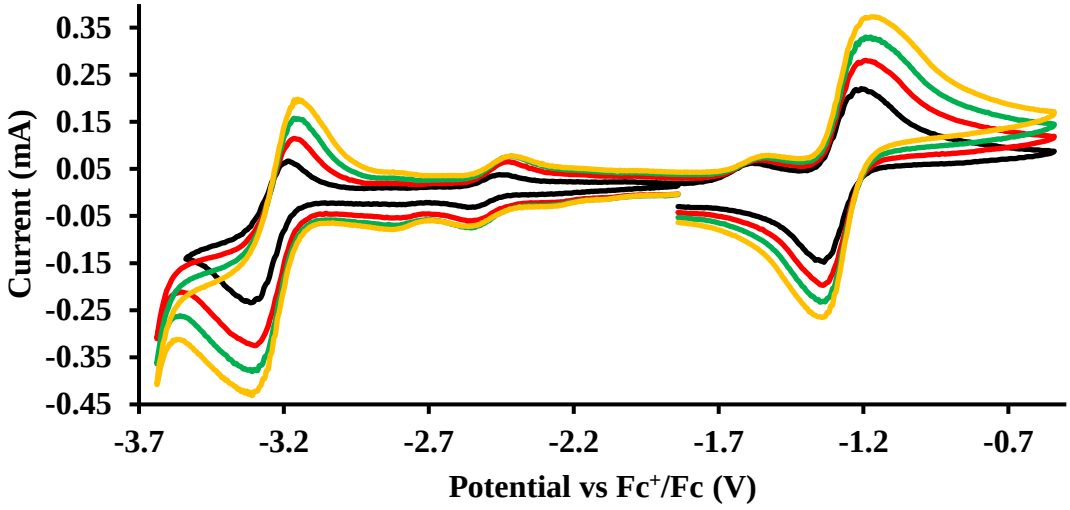

Figure 5.9. Voltammogram of $(C_5Me_5)_2U(NR_2)$, **5.9**, at 200 (black), 400 (red), 600 (green), and 800 (orange) mV/s in THF. The event centered at −2.53 is likely due to decomposition or an impurity.

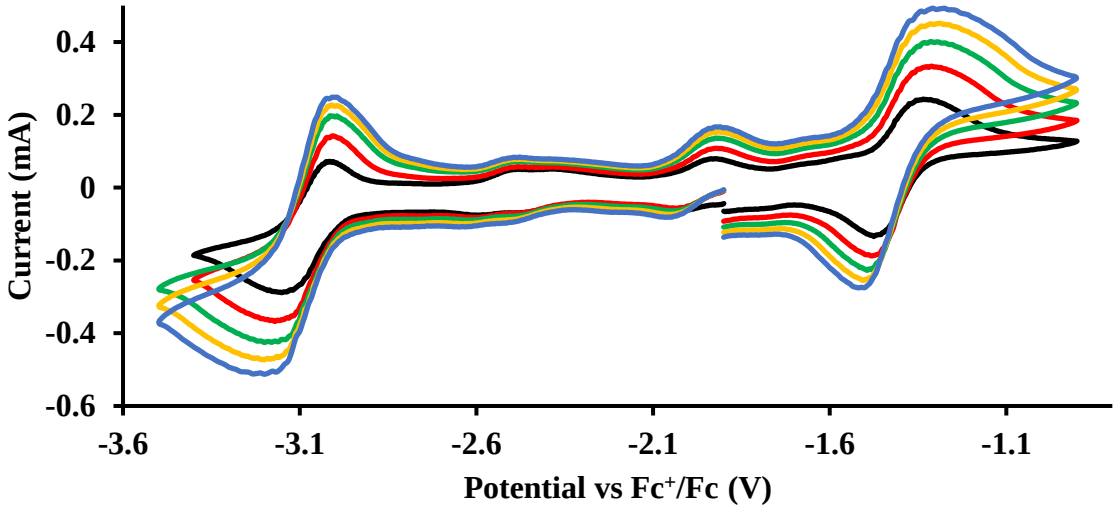

Figure 5.10. Voltammogram of $(C_5Me_5)_2U(C_5Me_4H)$, **5.7**, at 200 (black), 400 (red), 600 (green), 800 (orange), and 1000 (blue) mV/s in THF. The anodic event at −1.98 V is likely due to decomposition or an impurity.

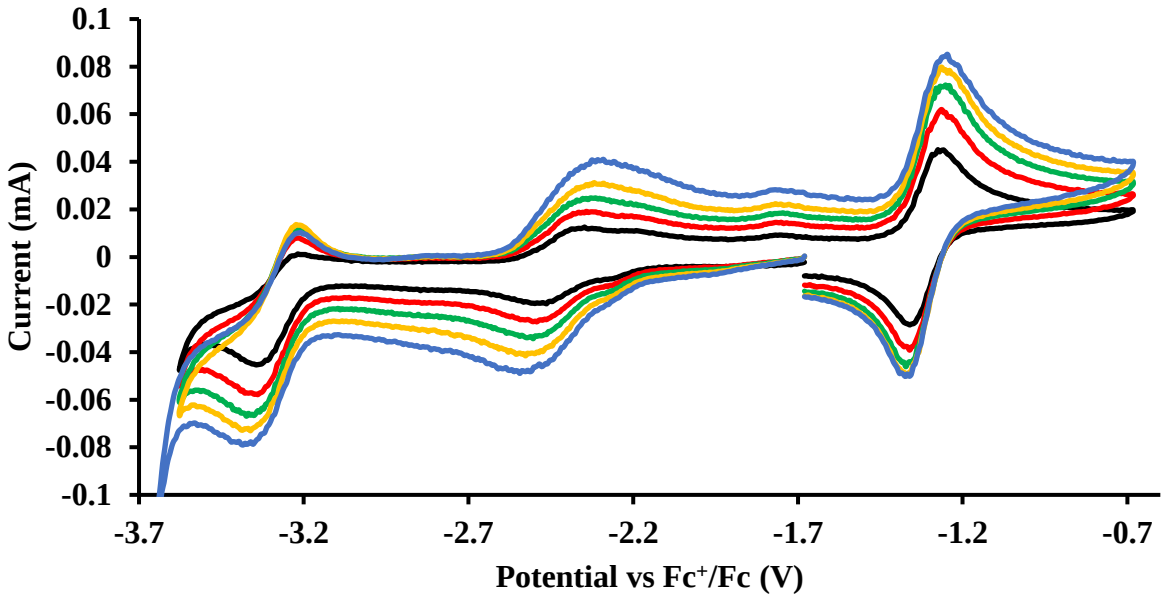

Figure 5.11. Voltammogram of $(C_5Me_5)U(NR_2)_2$, **5.10**, at 200 (black), 400 (red), 600 (green), 800 (orange), and 1000 (blue) mV/s in THF. The event centered at −2.45 is likely due to decomposition or an impurity.

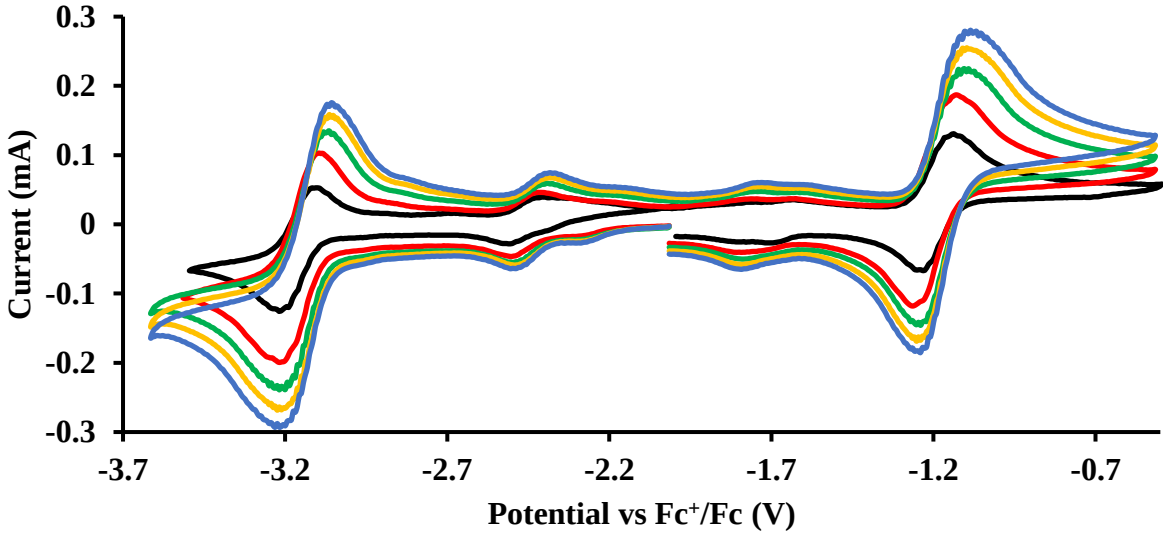

Figure 5.12. Voltammogram of $(C_5Me_5)_2U(CHR_2)$, **5.5**, at 200 (black), 400 (red), 600 (green), 800 (orange), and 1000 (blue) mV/s in THF. The event centered at −2.45 is likely due to decomposition or an impurity.

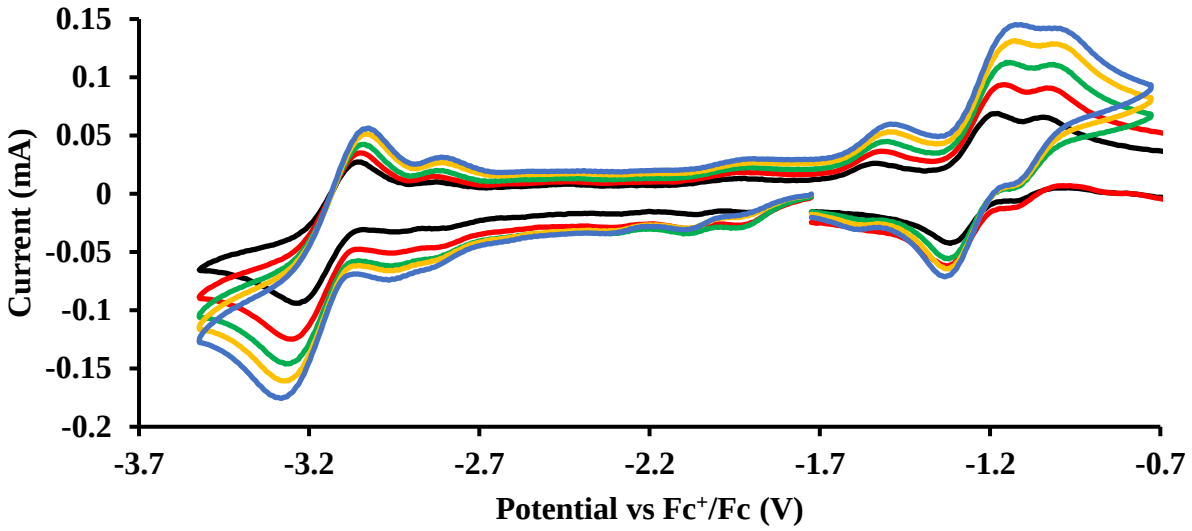

Figure 5.13. Voltammogram of $(C_5Me_5)_2U(OAr^*)$, **5.3**, at 200 (black), 400 (red), 600 (green), 800 (orange), and 1000 (blue) mV/s in THF.

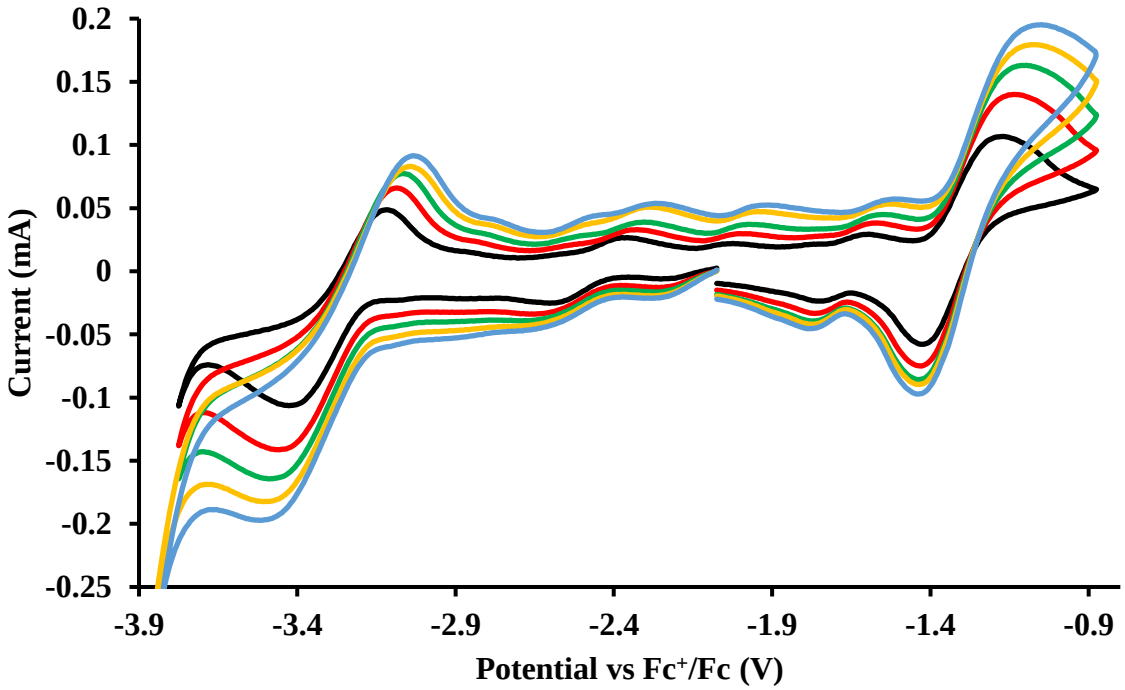

Figure 5.14. Voltammogram of $(C_5Me_5)_2U(OAr')$, **5.1-U**, at 200 (black), 400 (red), 600 (green), 800 (orange), and 1000 (blue) mV/s in THF.

Electronic Structure Calculations

Electronic structure calculations were performed on bis(pentamethylcyclopentadienyl) uranium species using the TPSSh hybrid meta-generalized gradient density functional approximation[57] with Grimme's D3 dispersion correction[78] and the resolution of the identity (RI-J) approximation.[79] Scalar relativistic effective core-potentials (ECPs)[80] with polarized triple-ζ basis sets def-TZVP[81] were used for uranium and split-valence basis sets with polarization on non-hydrogen atoms def2-SV(P)[82] were used for other atoms. Quadrature grids of size m4 were used throughout.[83] The continuum solvation model COSMO[58] with a dielectric constant $\varepsilon = 7.52$ for THF[59] was used for the anionic U(II) compounds. Geometry optimizations of the putative U(II) species were computed starting from the X-ray structure of the U(III) analog with a geometry convergence threshold of 10^{-4} a.u. and energy convergence of at least 10^{-7} a.u. and confirmed to be ground state geometries by lack of imaginary frequencies in the vibrational spectrum.[84] Time dependent DFT calculations of vertical excitations and oscillator strengths[60] were carried out with identical basis sets as described above, with an added primitive p function to the def-TZVP basis set on uranium which is necessary for accurate modelling of d to p transitions.[1,61] UV-visible spectra were simulated using Gaussian line profiles with a root mean-square width of 0.15 eV. Molecular orbitals were analyzed with VMD[85] and Mulliken population analysis. All computations were completed using TURBOMOLE V7.4.1.[62,63]

Time-dependent DFT calculations on all four compounds analyzed revealed broad, intense transitions centered between 700–900 nm, Figure S24, that could explain the observed dark blue colors as was previously observed for $[(C_5Me_4H)_3U]^{1-}$,[64] $[(C_5Me_5)_2U(NR_2)]^{1-}$,[1] and $[(C_5Me_5)U(NR_2)_2]^{1-}$.[1] These are predominantly 6d to 7p transitions. Electronic transitions at

higher energy are attributed to metal-to-ligand charge transfer. Complete details can be found in Tables 5.8–5.11.

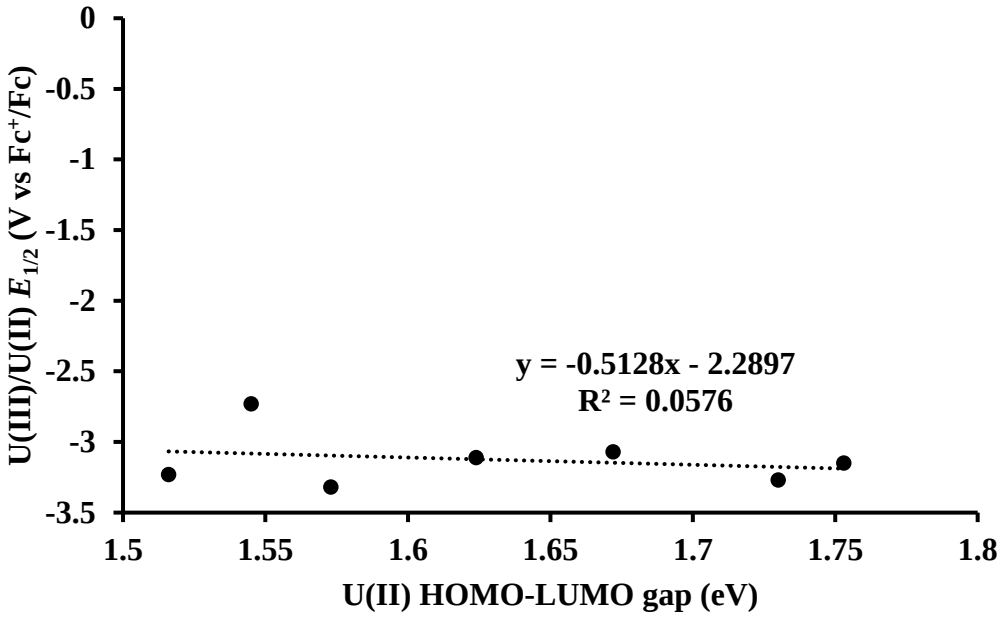

Figure 5.15: Plot of U(III)/U(II) $E_{1/2}$ vs U(II) HOMO-LUMO gap.

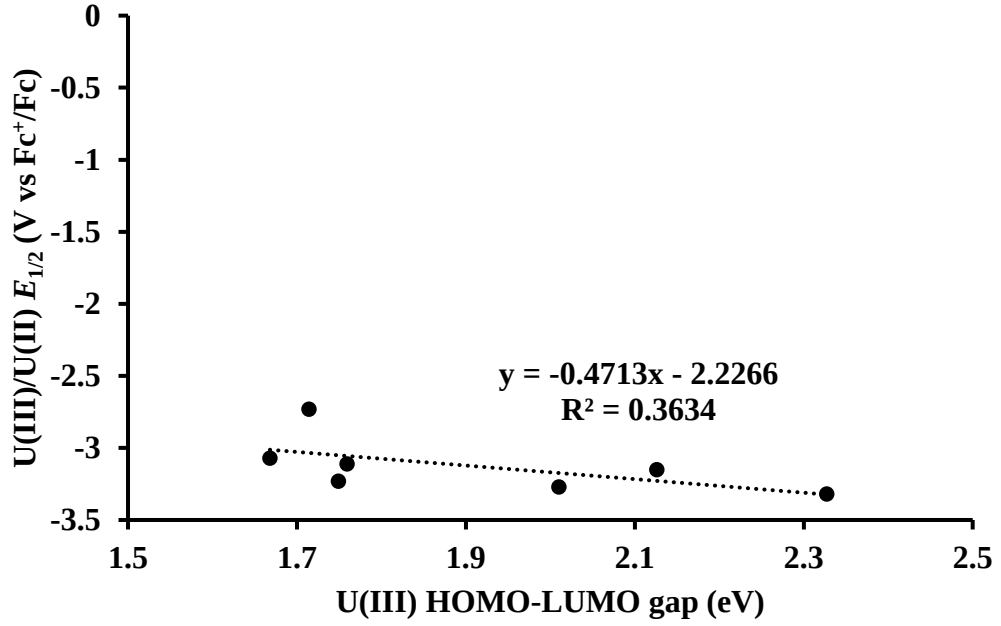

Figure 5.16: Plot of U(III)/U(II) $E_{1/2}$ vs U(III) HOMO-LUMO gap.

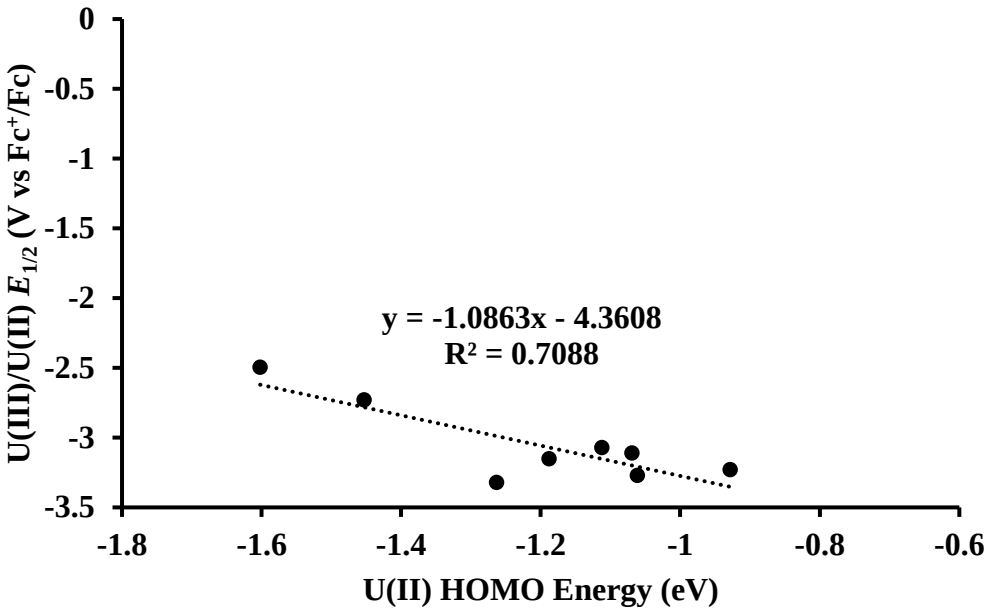

Figure 5.17: Plot of U(III)/U(II) $E_{1/2}$ vs U(II) HOMO energy

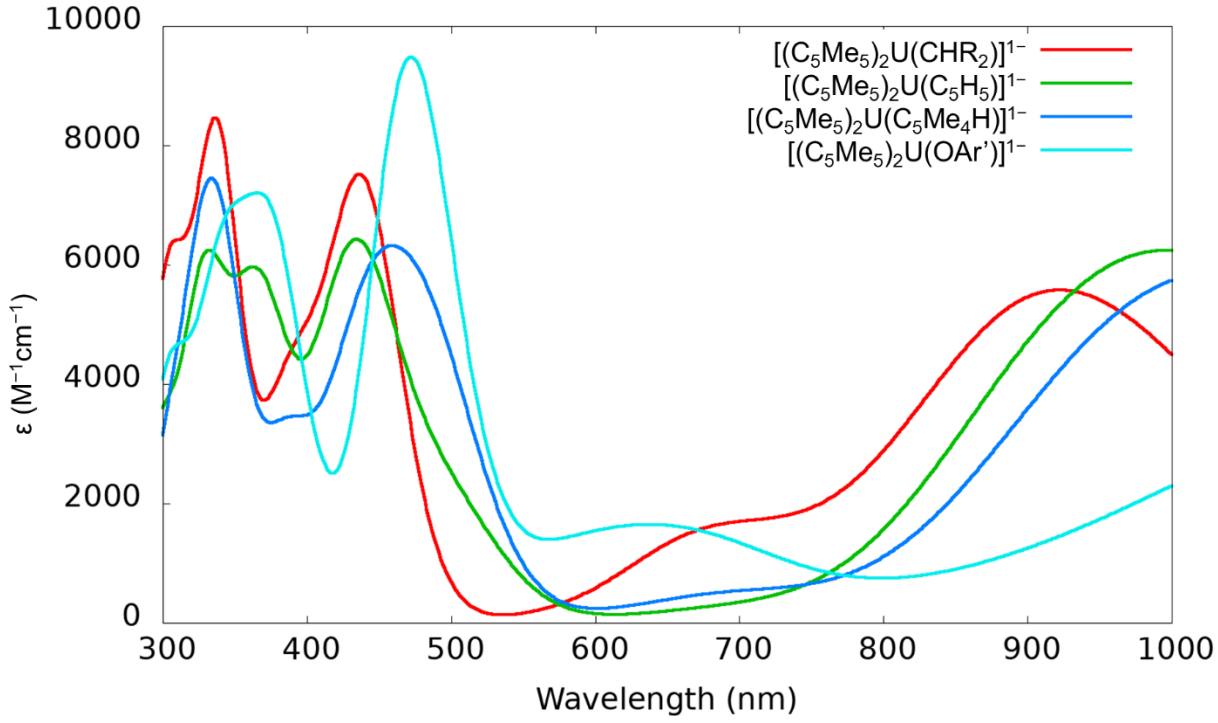

Figure 5.18. Simulated UV-visible spectrum of $[(C_5Me_5)_2U(CHR_2)]^{1-}$ (red), $[(C_5Me_5)_2U(C_5H_5)]^{1-}$ (green), $[(C_5Me_5)_2U(C_5Me_4H)]^{1-}$ (blue), and $[(C_5Me_5)_2U(OAr')]^{1-}$ (cyan). A Gaussian line broadening of 0.15 eV was applied.

Table 5.8. Electronic excitation summary for $[(C_5Me_5)_2U(CHR_2)]^{1-}$. Oscillator strengths are reported in the length gauge. Only the dominant contributions to the overall excitation and only excitations with oscillator strengths above 0.001 are reported. 138a is the $6dz^2$-like HOMO and 136a, 137a, and 138a are 5f orbitals. The assignment "π" is the π system of the C_5Me_5 rings with contributions from the CHR_2 ligand.

Wavelength (nm)	Oscillator Strength	Dominant contribution			Assignment
		Occupied	Virtual	% weight	
943	0.039	138	144	36.4	6d-5f
913	0.008	138	140	84.3	6d-7p
911	0.009	138	141	27.2	6d-7p
905	0.015	138	141	59.7	6d-7p
805	0.003	135	146	35.6	5f-5f
757	0.003	138	145	48.8	6d-5f
745	0.001	135	142	35.4	5f-6d
733	0.001	138	146	69.9	6d-5f
698	0.007	138	145	28.4	6d-5f
693	0.001	137	14	29.6	5f-6d
664	0.003	136	139	63.7	5f-7p
663	0.001	137	141	89.6	5f-7p
662	0.003	136	140	78.5	5f-7p
658	0.002	136	141	94.3	5f-7p
581	0.002	138	147	93.1	6d-7s
445	0.046	138	148	61.1	6d-π
436	0.046	138	149	60.4	6d-7p
402	0.029	136	148	75.6	5f-π
386	0.001	135	148	59.4	5f-π
384	0.025	137	150	54.2	5f-π
381	0.001	136	150	50.3	5f-π
378	0.002	135	150	45.6	5f-π
376	0.002	137	149	69.4	5f-7p
363	0.004	138	152	86.8	6d-π
356	0.001	137	151	79.9	5f-π
351	0.001	138	153	78.9	6d-π
346	0.014	135	151	81.3	5f-π

344	0.009	138	154	73.2	6d-π
343	0.006	136	151	75.7	5f-π
338	0.050	138	155	48.3	6d-π
333	0.017	138	157	58.9	6d-π
330	0.005	134	142	67.7	5f-6d
328	0.004	138	155	35.7	6d-π
323	0.001	133	142	26.7	5f-6d

Table 5.9. Electronic excitation summary for $[(C_5Me_5)_2U(C_5H_5)]^{1-}$. Oscillator strengths are reported in the length gauge. Only the dominant contributions to the overall excitation and only excitations with oscillator strengths above 0.001 are reported. 111a is the $6dz^2$-like HOMO and 108a, 109a, and 110a are 5f orbitals. The assignment "π" is the π system of the C_5H_5 rings.

Wavelength (nm)	Oscillator Strength	Dominant contribution			Assignment
		Occupied	Virtual	% weight	
1016	0.005	109a	115a	23.8	5f-5f
981	0.006	108a	116a	20.3	5f-5f
969	0.015	111a	112a	28.0	6d-7p
933	0.014	111a	113a	87.2	6d-7p
899	0.012	111a	114a	98.8	6d-7p
789	0.003	111a	117a	69.7	6d-5f
695	0.001	108a	113a	47.6	5f-7p
631	0.001	111a	118a	88.1	6d-7s
525	0.001	109a	118a	70.6	5f-7s
517	0.003	108a	118a	73.4	5f-7s
503	0.015	111a	120a	75.7	6d-π
480	0.004	109a	120a	53.1	5f-π
476	0.001	111a	121a	25.0	6d-π
461	0.015	108a	120a	46.2	5f-π
453	0.008	110a	120a	40.4	5f-π
447	0.003	110a	121a	31.3	5f-π
437	0.032	111a	122a	31.8	6d-π
431	0.010	111a	122a	30.3	6d-π
427	0.001	109a	121a	28.7	5f-π
419	0.027	111a	123a	62.1	6d-π

395	0.012	111a	124a	83.8	6d-π
384	0.001	110a	122a	28.9	5f-π
381	0.001	110a	123a	40.0	5f-π
379	0.008	109a	122a	21.2	5f-π
374	0.013	108a	123a	58.7	5f-π
374	0.002	108a	122a	20.4	5f-π
371	0.009	111a	125a	80.6	6d-π
367	0.012	111a	126a	88.4	6d-π
363	0.001	110a	124a	40.9	5f-π
360	0.006	109a	124a	32.2	5f-π
356	0.014	108a	124aa	52.1	5f-π
349	0.007	111a	127a	42.5	6d-π
347	0.007	111a	127	47.3	6d-π
337	0.001	109a	126a	67.4	5f-π
335	0.001	110a	125a	35.3	5f-π
334	0.001	107a	112a	46.8	π-7p
333	0.004	106b	108b	27.9	π-π

Table 5.10. Electronic excitation summary for $[(C_5Me_5)_2U(C_5Me_4H)]^{1-}$. Oscillator strengths are reported in the length gauge. Only the dominant contributions to the overall excitation and only excitations with oscillator strengths above 0.001 are reported. 127a is the $6dz^2$-like HOMO and 124a, 125a, and 126a are 5f orbitals. The assignment "π" is the π system of the C_5Me_5/C_5Me_4H rings.

Wavelength (nm)	Oscillator Strength	Dominant contributions			Assignment
		Occupied	Virtual	% weight	
1108	0.007	127a	131a	68.6	6d-5f
1090	0.002	127a	132a	73.7	6d-5f
1067	0.047	127a	128a	82.5	6d-7p
1004	0.003	125a	131a	12.2	5f-5f
956	0.003	127a	132a	11.4	6d-5f
961	0.002	124a	133a	46.1	5f-5f
948	0.013	127a	129a	76.1	6d-7p
933	0.010	127a	130a	73.1	6d-7p

800	0.002	127a	133a	80.1	6d-5f
743	0.001	126a	135a	46.2	5f-5f
709	0.001	124a	128a	79.1	5f-7p
687	0.002	124a	129a	91.1	5f-7p
680	0.002	124a	130a	91.1	5f-7p
614	0.001	127a	134a	80.3	6d-7s
509	0.001	125a	134a	74.2	5f-7s
503	0.024	127a	136a	65	6d-5f/π
488	0.004	127a	137a	46.5	6d-5f/π
478	0.024	127a	138a	26.7	6d-5f/π
461	0.012	127a	137a	22.9	6d-5f/π
460	0.014	127a	138a	25.3	6d-5f/π
437	0.025	127a	139a	70.7	6d-5f/π
433	0.020	127a	140a	64.4	6d-5f/π
409	0.001	126a	136a	21.9	5f-5f/π
403	0.008	124a	136a	45.3	5f-5f/π
394	0.002	126a	139a	39.7	5f-5f/π
391	0.001	125a	138a	28.4	5f-5f/π
386	0.013	124a	139a	38.9	5f-5f/π
384	0.012	124a	140a	37.2	5f-5f/π
380	0.005	124a	140a	25.1	5f-5f/π
356	0.001	123b	127b	35.2	π-7s
353	0.014	127a	143a	68.5	6d-π
352	0.005	123a	128a	70.2	π-7p
346	0.010	127a	144a	72	6d-π
346	0.002	123a	129a	40.8	π-7p
344	0.001	123b	125b	64.9	π-7p
342	0.008	126a	141a	67.6	5f-π
342	0.004	125a	141a	34.1	5f-π
342	0.010	125a	141a	44.4	5f-π
341	0.001	123b	127b	33.8	π-7s
339	0.003	123a	132a	41.7	π-5f
338	0.003	126a	142a	86.6	5f-π
337	0.002	125a	142a	75.5	5f-π
331	0.007	122b	127b	40.7	π-7s
330	0.023	127a	145a	73.5	6d-π
327	0.002	124a	142a	77.1	5f-π
325	0.001	122a	128a	91.5	π-7p
325	0.022	127a	146a	74.9	6d-π

322	0.001	122b	124b	89.4	π-7p

Table 5.11. Electronic excitation summary for $[(C_5Me_5)_2U(OAr')]^{1-}$. Oscillator strengths are reported in the length gauge. Only the dominant contributions to the overall excitation and only excitations with oscillator strengths above 0.001 are reported. 127a is the $6dz^2$-like HOMO and 124a, 125a, and 126a are 5f orbitals. The assignment "π" is the π system of the C_5Me_5 rings with contribution from the OAr′ ligand.

Wavelength (nm)	Oscillator Strength	Dominant contributions			Assignment
		Occupied	Virtual	% weight	
1137	0.009	154a	155a	36.9	6d-7p
1136	0.009	154a	157a	98.5	6d-7p
995	0.003	154a	158a	50.7	6d-pi
934	0.001	154a	160a	31.5	6d-5f/π
925	0.004	154a	162a	15.2	6d-5f
902	0.001	151a	162a	29.9	5f-5f
819	0.002	151a	164a	35.6	5f-5f
720	0.001	153a	155a	62.8	5f-7p
719	0.003	154a	164a	57.7	6d-5f
708	0.001	153a	157a	97.7	5f-7p
675	0.001	152a	157a	88.2	5f-7p
673	0.002	151a	155a	77.5	5f-7p
673	0.002	152a	156a	85.1	5f-7p
671	0.005	154a	163a	37.4	6d-7s
630	0.004	154a	165a	58.0	6d-5f/π
593	0.010	153a	159a	24.5	5f-5f/π
588	0.001	151a	159a	26.0	5f-5f/π
570	0.001	152a	159a	22.2	5f-5f/π
555	0.001	153a	165a	30.8	5f-5f/π
534	0.001	152a	165a	30.8	5f-5f/π
528	0.004	151a	160a	17.9	5f-5f/π
488	0.009	153a	163a	41.3	5f-7s
480	0.058	154a	166a	81.9	6d-7p/π
468	0.002	151a	163a	31.6	5f-7s

464	0.060	154a	167a	87.9	6d-π
438	0.003	154a	168a	91.9	6d-π
409	0.001	154a	169a	78.1	6d-7p/π
406	0.002	153a	167a	52.4	5f-π
397	0.019	152a	167a	49.7	5f-π
384	0.001	151a	167a	30.6	5f-π
379	0.003	154a	170a	37.5	6d-π
378	0.033	153a	168a	44.7	5f-π
375	0.014	153a	166a	23.6	5f-7p/π
371	0.009	154a	171a	84.5	6d-π
370	0.003	152a	168a	58.5	5f-π
369	0.001	152a	166a	31.0	5f-7p/π
367	0.001	151a	166a	32.5	5f-7p/π
366	0.005	154a	172a	54.0	6d-π
363	0.001	151a	168a	46.8	5f-π
352	0.026	154a	173a	69.5	6d-π
350	0.002	153	169a	37.6	5f-7p/π
349	0.004	154a	174a	61.6	6d-π
344	0.018	154a	175a	58.3	6d-7p/π
338	0.017	151a	169a	55.8	5f-7p/π
333	0.005	154a	176a	66.1	6d-π
332	0.010	152a	169a	47.2	5f-7p/π
330	0.002	154a	177a	64.0	6d-π
322	0.011	150b	151b	36.6	π-7p
320	0.001	150b	151b	38.4	π-7p
319	0.001	153a	170a	41.9	5f-π
315	0.003	150b	153b	46.0	π-7p
315	0.005	150b	153b	44.8	π-7p
313	0.002	152a	170a	41.0	5f-π
311	0.001	150a	155a	41.6	π-7p
310	0.004	154a	179a	69.1	6d-π

Table 5.12: Crystal data and structure refinement for **5.1-M**, **5.2**, and **5.5**.

	5.1-U	**5.1-Ce**	**5.2**	**5.5**
Identification code	jcw51	jcw67	jcw74	jcw50
Empirical formula	$C_{35}H_{53}OU$	$C_{35}H_{53}OCe$	$[C_{37}H_{57}O_2U]$ $[C_{33}H_{49}OU]$ $\cdot ½(C_6H_{14})$	$C_{27}H_{49}Si_2U$

Formula weight	727.80	629.89	1514.69	667.87
Temperature (K)	133(2)	133(2)	93(2)	133(2)
Wavelength (Å)	0.71073	0.71073	0.71073	0.71073
Crystal system	Orthorhombic	Orthorhombic	Triclinic	Monoclinic
Space group	$Cmc2_1$	$Cmc2_1$	P-1	$P2_1/n$
a (Å)	14.6962(12)	14.7118(10)	10.1439(17)	11.0237(8)
b (Å)	17.3369(15)	17.3650(12)	18.262(3)	23.4044(17)
c (Å)	24.750(2)	24.7819(17)	19.588(3)	11.6386(9)
α (°)	90	90	106.125(3)	90
β (°)	90	90	100.743(3)	1102.8982(12)
γ (°)	90	90	98.801(3)	90
Volume ($Å^3$)	6306.1(9)	6331.0(8)	3343.2(10)	2927.0(4)
Z	8	8	2	4
Density (mg/m^3)	1.533	1.322	1.505	1.516
Absorption coefficient (mm^{-1})	5.172	1.462	4.882	5.639
F(000)	2904	2632	1518	1324
Crystal color	brown	pink	black	brown
Crystal size	0.342x0.128x0.119	0.501x0.285x0.224	0.402x0.173x0.119	0.213x0.149x0.138
Theta range for data collection (°)	1.646 to 31.117	1.643 to 30.583	1.869 to 27.103	1.740 to 28.281
Index ranges	$-20 \leq h \leq 20$, $-23 \leq k \leq 24$, $-35 \leq l \leq 35$	$-21 \leq h \leq 20$, $-24 \leq k \leq 23$, $-34 \leq l \leq 34$	$-13 \leq h \leq 12$, $-23 \leq k \leq 22$, $0 \leq l \leq 25$	$-14 \leq h \leq 14$, $0 \leq k \leq 31$, $0 \leq l \leq 15$
Independent Reflections collected	9829	9752	15120	7274
Completeness to theta = 25.242°	100.0	100.0	99.6	100.0
Absorption correction	Semi-empirical from equivalents	Semi-empirical from equivalents	Semi-empirical from equivalents	Semi-empirical from equivalents
Max. and min. transmission	0.4335 and 0.3410	0.7461 and 0.6173	0.2673 and 0.1423	0.2657 and 0.1827
Refinement method	Full-matrix least-squares on F^2	Full-matrix least-squares on F^2	Full-matrix least-squares on F^2	Full-matrix least-squares on F^2

Data / restraints / parameters	9829 / 1 / 420	9752 / 1 / 473	15120 / 0 / 736	7274 / 0 / 189
Goodness-of-fit on F^2	1.001	1.024	1.061	1.049
Final R indices [I>2sigma(I)]	R1 = 0.0326, wR2 = 0.0613	R1 = 0.0248, wR2 = 0.0547	R1 = 0.0417, wR2 = 0.1015	R1 = 0.0429, wR2 = 0.1012
R indices (all data)	R1 = 0.0411, wR2 = 0.0638	R1 = 0.0266, wR2 = 0.0555	R1 = 0.0570, wR2 = 0.1090	R1 = 0.0583, wR2 = 0.1092
Data cutoff (Å)	0.69	0.70	0.78	0.75
Absolute structure parameter	0.019(5)	0.009(7)	N/A	N/A
Largest diff. peak and hole ($eÅ^3$)	2.008 and −1.521	0.530 and −0.920	2.559 and −1.514	1.761 and −1.362

X-ray Data Collection, Structure Solution and Refinement for 1-U.

A brown crystal of approximate dimensions 0.119 x 0.128 x 0.342 mm was mounted in a cryoloop and transferred to a Bruker SMART APEX II diffractometer system. The APEX2[86] program package was used to determine the unit-cell parameters and for data collection (20 sec/frame scan time). The raw frame data was processed using SAINT[87] and SADABS[88] to yield the reflection data file. Subsequent calculations were carried out using the SHELXTL[89] program package. The diffraction symmetry was *mmm* and the systematic absences were consistent with the orthorhombic space group $Cmc2_1$ which was later determined to be correct.

The structure was phased using the coordinates of the cerium analog and refined on F^2 by full-matrix least-squares techniques. The analytical scattering factors[90] for neutral atoms were used throughout the analysis. Hydrogen atoms were included using a riding model. There were two molecules of the formula-unit present; each was located on a mirror plane. One pentamethylcyclopentadienyl ligand was modeled as a 50:50 disorder.

Least-squares analysis yielded wR2 = 0.0638 and Goof = 1.001 for 420 variables refined against 9829 data (0.69 Å), R1 = 0.0326 for those 8848 data with I > 2.0σ(I). The absolute structure was assigned by refinement of the Flack parameter.[91]

Table 5.13. Bond lengths [Å] and angles [°] for **5.1-U**.

U(1)-Cnt1	2.498	C(1B)-C(5B)	1.389(18)
U(1)-O(1)	2.201(6)	C(1B)-C(6B)	1.512(19)
U(1)-C(4)	2.717(12)	C(2B)-C(3B)	1.422(19)
U(1)-C(4)#1	2.717(12)	C(2B)-C(7B)	1.55(2)
U(1)-C(5)	2.733(11)	C(3B)-C(4B)	1.45(2)
U(1)-C(5)#1	2.733(11)	C(3B)-C(8B)	1.51(2)
U(1)-C(1B)#1	2.744(11)	C(4B)-C(5B)	1.40(2)
U(1)-C(1B)	2.744(11)	C(4B)-C(9B)	1.51(2)
U(1)-C(4B)#1	2.762(14)	C(5B)-C(10B)	1.48(2)
U(1)-C(4B)	2.762(14)	C(11)-C(16)	1.400(11)
U(1)-C(5B)#1	2.773(12)	C(11)-C(12)	1.431(11)
U(1)-C(5B)	2.773(12)	C(12)-C(13)	1.371(12)
U(1)-C(1)#1	2.779(12)	C(12)-C(17)	1.547(11)
U(1)-C(1)	2.779(12)	C(13)-C(14)	1.401(12)
U(1)-C(3)	2.785(13)	C(14)-C(15)	1.362(11)
U(1)-C(3)#1	2.785(13)	C(14)-C(20)	1.499(13)
U(1)-C(3B)	2.796(13)	C(15)-C(16)	1.397(11)
U(1)-C(3B)#1	2.796(13)	C(16)-C(21)	1.532(11)
U(1)-C(2B)#1	2.811(13)	C(17)-C(18)#1	1.516(8)
U(1)-C(2B)	2.811(13)	C(17)-C(18)	1.516(8)
U(1)-C(2)#1	2.832(12)	C(17)-C(19)	1.546(13)
U(1)-C(2)	2.832(12)	C(21)-C(22)	1.539(9)
O(1)-C(11)	1.361(10)	C(21)-C(22)#1	1.539(9)
C(1)-C(5)	1.403(16)	C(21)-C(23)	1.556(13)
C(1)-C(2)	1.413(18)	U(2)-Cnt2	2.560
C(1)-C(6)	1.48(2)	U(2)-Cnt2	2.502
C(2)-C(3)	1.413(19)	U(2)-O(2)	2.225(6)
C(2)-C(7)	1.499(17)	U(2)-C(29)#2	2.755(6)
C(3)-C(4)	1.441(19)	U(2)-C(29)	2.755(5)
C(3)-C(8)	1.50(2)	U(2)-C(28)#2	2.782(6)
C(4)-C(5)	1.43(2)	U(2)-C(28)	2.783(6)
C(4)-C(9)	1.49(2)	U(2)-C(25)	2.801(6)
C(5)-C(10)	1.51(2)	U(2)-C(25)#2	2.801(6)
C(1B)-C(2B)	1.381(18)	U(2)-C(27)	2.816(9)

U(2)-C(24)	2.840(9)
U(2)-C(26)#2	2.848(6)
U(2)-C(26)	2.848(6)
O(2)-C(36)	1.368(10)
C(24)-C(25)#2	1.411(9)
C(24)-C(25)	1.411(9)
C(24)-C(30)	1.511(14)
C(25)-C(26)	1.409(8)
C(25)-C(31)	1.517(10)
C(26)-C(26)#2	1.425(12)
C(26)-C(32)	1.498(9)
C(27)-C(28)#2	1.420(8)
C(27)-C(28)	1.420(8)
C(27)-C(33)	1.498(13)
C(28)-C(29)	1.424(8)
C(28)-C(34)	1.503(9)
C(29)-C(29)#2	1.415(12)
C(29)-C(35)	1.500(9)
C(36)-C(37)	1.405(7)
C(36)-C(37)#2	1.405(7)
C(37)-C(38)	1.397(8)
C(37)-C(40)	1.542(9)
C(38)-C(39)	1.386(8)
C(39)-C(38)#2	1.386(8)
C(39)-C(44)	1.535(13)
C(40)-C(41)	1.532(9)
C(40)-C(42)	1.535(8)
C(40)-C(43)	1.544(8)

O(1)-U(1)-Cnt1	114.1
Cnt1-U(1)-Cnt1#1	131.4
O(1)-U(1)-C(4)	102.3(3)
O(1)-U(1)-C(4)#1	102.3(3)
C(4)-U(1)-C(4)#1	117.7(6)
O(1)-U(1)-C(5)	86.6(3)
C(4)-U(1)-C(5)	30.4(4)
C(4)#1-U(1)-C(5)	147.5(5)
O(1)-U(1)-C(5)#1	86.6(3)
C(4)-U(1)-C(5)#1	147.5(5)
C(4)#1-U(1)-C(5)#1	30.4(4)
C(5)-U(1)-C(5)#1	171.4(6)
O(1)-U(1)-C(1B)#1	117.5(3)
O(1)-U(1)-C(1B)	117.5(3)
C(1B)#1-U(1)-C(1B)	107.0(5)
O(1)-U(1)-C(4B)#1	95.8(3)
C(1B)#1-U(1)-C(4B)#1	48.2(4)
C(1B)-U(1)-C(4B)#1	146.4(4)
O(1)-U(1)-C(4B)	95.8(3)
C(1B)#1-U(1)-C(4B)	146.4(4)
C(1B)-U(1)-C(4B)	48.2(4)
C(4B)#1-U(1)-C(4B)	137.7(7)
O(1)-U(1)-C(5B)#1	92.7(3)
C(1B)#1-U(1)-C(5B)#1	29.2(4)
C(1B)-U(1)-C(5B)#1	135.5(5)
C(4B)#1-U(1)-C(5B)#1	29.4(4)
C(4B)-U(1)-C(5B)#1	165.8(4)
O(1)-U(1)-C(5B)	92.7(3)
C(1B)#1-U(1)-C(5B)	135.5(5)
C(1B)-U(1)-C(5B)	29.2(4)
C(4B)#1-U(1)-C(5B)	165.8(4)
C(4B)-U(1)-C(5B)	29.4(4)
C(5B)#1-U(1)-C(5B)	161.3(7)
O(1)-U(1)-C(1)#1	102.9(3)
C(4)-U(1)-C(1)#1	153.9(4)
C(4)#1-U(1)-C(1)#1	49.6(4)
C(5)-U(1)-C(1)#1	158.6(5)
C(5)#1-U(1)-C(1)#1	29.5(3)
O(1)-U(1)-C(1)	102.9(3)
C(4)-U(1)-C(1)	49.6(4)
C(4)#1-U(1)-C(1)	153.9(4)
C(5)-U(1)-C(1)	29.5(3)
C(5)#1-U(1)-C(1)	158.6(5)
C(1)#1-U(1)-C(1)	129.2(6)
O(1)-U(1)-C(3)	132.3(3)
C(4)-U(1)-C(3)	30.3(4)
C(4)#1-U(1)-C(3)	107.5(4)
C(5)-U(1)-C(3)	49.3(4)
C(5)#1-U(1)-C(3)	134.8(4)
C(1)#1-U(1)-C(3)	124.8(4)
C(1)-U(1)-C(3)	48.9(4)

O(1)-U(1)-C(3)#1	132.3(3)	C(3B)#1-U(1)-C(2B)	91.4(4)
C(4)-U(1)-C(3)#1	107.5(4)	C(2B)#1-U(1)-C(2B)	78.8(6)
C(4)#1-U(1)-C(3)#1	30.3(4)	O(1)-U(1)-C(2)#1	131.6(3)
C(5)-U(1)-C(3)#1	134.8(4)	C(4)-U(1)-C(2)#1	124.8(4)
C(5)#1-U(1)-C(3)#1	49.3(4)	C(4)#1-U(1)-C(2)#1	48.9(4)
C(1)#1-U(1)-C(3)#1	48.9(4)	C(5)-U(1)-C(2)#1	139.9(4)
C(1)-U(1)-C(3)#1	124.8(4)	C(5)#1-U(1)-C(2)#1	48.2(4)
C(3)-U(1)-C(3)#1	85.7(5)	C(1)#1-U(1)-C(2)#1	29.2(4)
O(1)-U(1)-C(3B)	124.2(3)	C(1)-U(1)-C(2)#1	115.1(4)
C(1B)#1-U(1)-C(3B)	118.0(4)	C(3)-U(1)-C(2)#1	95.9(4)
C(1B)-U(1)-C(3B)	48.2(4)	C(3)#1-U(1)-C(2)#1	29.1(4)
C(4B)#1-U(1)-C(3B)	116.9(4)	O(1)-U(1)-C(2)	131.6(3)
C(4B)-U(1)-C(3B)	30.2(4)	C(4)-U(1)-C(2)	48.9(4)
C(5B)#1-U(1)-C(3B)	137.5(4)	C(4)#1-U(1)-C(2)	124.8(4)
C(5B)-U(1)-C(3B)	49.0(4)	C(5)-U(1)-C(2)	48.2(4)
O(1)-U(1)-C(3B)#1	124.2(3)	C(5)#1-U(1)-C(2)	139.9(4)
C(1B)#1-U(1)-C(3B)#1	48.2(4)	C(1)#1-U(1)-C(2)	115.1(4)
C(1B)-U(1)-C(3B)#1	118.0(4)	C(1)-U(1)-C(2)	29.2(4)
C(4B)#1-U(1)-C(3B)#1	30.2(4)	C(3)-U(1)-C(2)	29.1(4)
C(4B)-U(1)-C(3B)#1	116.9(4)	C(3)#1-U(1)-C(2)	95.9(4)
C(5B)#1-U(1)-C(3B)#1	49.0(4)	C(2)#1-U(1)-C(2)	91.7(5)
C(5B)-U(1)-C(3B)#1	137.5(4)	C(11)-O(1)-U(1)	166.0(5)
C(3B)-U(1)-C(3B)#1	89.8(5)	C(5)-C(1)-C(2)	107.7(11)
O(1)-U(1)-C(2B)#1	140.6(3)	C(5)-C(1)-C(6)	127.8(15)
C(1B)#1-U(1)-C(2B)#1	28.8(4)	C(2)-C(1)-C(6)	123.4(14)
C(1B)-U(1)-C(2B)#1	98.3(4)	C(5)-C(1)-U(1)	73.4(7)
C(4B)#1-U(1)-C(2B)#1	48.7(4)	C(2)-C(1)-U(1)	77.5(7)
C(4B)-U(1)-C(2B)#1	121.5(4)	C(6)-C(1)-U(1)	124.6(10)
C(5B)#1-U(1)-C(2B)#1	48.2(4)	C(3)-C(2)-C(1)	109.1(11)
C(5B)-U(1)-C(2B)#1	125.9(4)	C(3)-C(2)-C(7)	126.7(16)
C(3B)-U(1)-C(2B)#1	91.4(4)	C(1)-C(2)-C(7)	123.9(15)
C(3B)#1-U(1)-C(2B)#1	29.4(4)	C(3)-C(2)-U(1)	73.6(7)
O(1)-U(1)-C(2B)	140.6(3)	C(1)-C(2)-U(1)	73.3(7)
C(1B)#1-U(1)-C(2B)	98.3(4)	C(7)-C(2)-U(1)	125.0(8)
C(1B)-U(1)-C(2B)	28.8(4)	C(2)-C(3)-C(4)	107.4(12)
C(4B)#1-U(1)-C(2B)	121.5(4)	C(2)-C(3)-C(8)	130.4(16)
C(4B)-U(1)-C(2B)	48.7(4)	C(4)-C(3)-C(8)	121.0(16)
C(5B)#1-U(1)-C(2B)	125.9(4)	C(2)-C(3)-U(1)	77.3(7)
C(5B)-U(1)-C(2B)	48.2(4)	C(4)-C(3)-U(1)	72.2(7)
C(3B)-U(1)-C(2B)	29.4(4)	C(8)-C(3)-U(1)	125.3(10)

C(5)-C(4)-C(3)	106.6(11)	C(4B)-C(5B)-U(1)	74.8(8)
C(5)-C(4)-C(9)	126.1(15)	C(10B)-C(5B)-U(1)	117.8(11)
C(3)-C(4)-C(9)	127.2(17)	O(1)-C(11)-C(16)	120.7(7)
C(5)-C(4)-U(1)	75.4(7)	O(1)-C(11)-C(12)	119.3(7)
C(3)-C(4)-U(1)	77.4(7)	C(16)-C(11)-C(12)	120.0(7)
C(9)-C(4)-U(1)	115.1(11)	C(13)-C(12)-C(11)	118.1(7)
C(1)-C(5)-C(4)	109.1(11)	C(13)-C(12)-C(17)	119.2(7)
C(1)-C(5)-C(10)	124.5(17)	C(11)-C(12)-C(17)	122.7(7)
C(4)-C(5)-C(10)	126.2(16)	C(12)-C(13)-C(14)	123.5(7)
C(1)-C(5)-U(1)	77.1(7)	C(15)-C(14)-C(13)	116.4(8)
C(4)-C(5)-U(1)	74.2(7)	C(15)-C(14)-C(20)	122.0(8)
C(10)-C(5)-U(1)	118.6(10)	C(13)-C(14)-C(20)	121.6(8)
C(2B)-C(1B)-C(5B)	110.9(11)	C(14)-C(15)-C(16)	124.5(8)
C(2B)-C(1B)-C(6B)	126.7(15)	C(15)-C(16)-C(11)	117.6(7)
C(5B)-C(1B)-C(6B)	122.0(16)	C(15)-C(16)-C(21)	114.2(7)
C(2B)-C(1B)-U(1)	78.3(7)	C(11)-C(16)-C(21)	128.2(7)
C(5B)-C(1B)-U(1)	76.6(7)	C(18)#1-C(17)-C(18)	111.2(8)
C(6B)-C(1B)-U(1)	118.5(9)	C(18)#1-C(17)-C(19)	106.2(5)
C(1B)-C(2B)-C(3B)	107.7(11)	C(18)-C(17)-C(19)	106.2(5)
C(1B)-C(2B)-C(7B)	122.3(15)	C(18)#1-C(17)-C(12)	110.2(5)
C(3B)-C(2B)-C(7B)	129.6(15)	C(18)-C(17)-C(12)	110.2(5)
C(1B)-C(2B)-U(1)	72.9(7)	C(19)-C(17)-C(12)	112.8(7)
C(3B)-C(2B)-U(1)	74.7(7)	C(16)-C(21)-C(22)	109.7(5)
C(7B)-C(2B)-U(1)	123.6(9)	C(16)-C(21)-C(22)#1	109.7(5)
C(2B)-C(3B)-C(4B)	106.2(12)	C(22)-C(21)-C(22)#1	109.0(9)
C(2B)-C(3B)-C(8B)	123.8(16)	C(16)-C(21)-C(23)	117.2(7)
C(4B)-C(3B)-C(8B)	129.3(17)	C(22)-C(21)-C(23)	105.5(5)
C(2B)-C(3B)-U(1)	75.9(7)	C(22)#1-C(21)-C(23)	105.5(5)
C(4B)-C(3B)-U(1)	73.6(7)	O(2)-U(2)-Cnt2	128.6
C(8B)-C(3B)-U(1)	123.9(11)	O(2)-U(2)-Cnt3	96.2
C(5B)-C(4B)-C(3B)	108.1(12)	Cnt2-U(2)-Cnt3	135.2
C(5B)-C(4B)-C(9B)	133.1(19)	O(2)-U(2)-C(29)#2	116.8(2)
C(3B)-C(4B)-C(9B)	117.9(18)	O(2)-U(2)-C(29)	116.8(2)
C(5B)-C(4B)-U(1)	75.7(7)	C(29)#2-U(2)-C(29)	29.8(2)
C(3B)-C(4B)-U(1)	76.2(8)	O(2)-U(2)-C(28)#2	87.93(19)
C(9B)-C(4B)-U(1)	122.8(11)	C(29)#2-U(2)-C(28)#2	29.79(18)
C(1B)-C(5B)-C(4B)	107.1(12)	C(29)-U(2)-C(28)#2	48.98(17)
C(1B)-C(5B)-C(10B)	132(2)	O(2)-U(2)-C(28)	87.93(19)
C(4B)-C(5B)-C(10B)	121.3(19)	C(29)#2-U(2)-C(28)	48.98(17)
C(1B)-C(5B)-U(1)	74.2(7)	C(29)-U(2)-C(28)	29.79(18)

C(28)#2-U(2)-C(28)	48.7(3)	C(28)-U(2)-C(26)	162.29(18)
O(2)-U(2)-C(25)	131.88(18)	C(25)-U(2)-C(26)	28.87(17)
C(29)#2-U(2)-C(25)	97.43(17)	C(25)#2-U(2)-C(26)	47.71(17)
C(29)-U(2)-C(25)	109.71(18)	C(27)-U(2)-C(26)	165.45(13)
C(28)#2-U(2)-C(25)	115.21(18)	C(24)-U(2)-C(26)	47.6(2)
C(28)-U(2)-C(25)	139.45(18)	C(26)#2-U(2)-C(26)	29.0(3)
O(2)-U(2)-C(25)#2	131.88(19)	C(36)-O(2)-U(2)	115.7(5)
C(29)#2-U(2)-C(25)#2	109.71(18)	C(25)#2-C(24)-C(25)	107.1(8)
C(29)-U(2)-C(25)#2	97.43(17)	C(25)#2-C(24)-C(30)	126.2(4)
C(28)#2-U(2)-C(25)#2	139.45(18)	C(25)-C(24)-C(30)	126.2(4)
C(28)-U(2)-C(25)#2	115.21(18)	C(25)#2-C(24)-U(2)	74.0(4)
C(25)-U(2)-C(25)#2	47.8(3)	C(25)-C(24)-U(2)	74.0(4)
O(2)-U(2)-C(27)	70.7(2)	C(30)-C(24)-U(2)	123.9(7)
C(29)#2-U(2)-C(27)	48.8(2)	C(26)-C(25)-C(24)	108.9(6)
C(29)-U(2)-C(27)	48.8(2)	C(26)-C(25)-C(31)	125.0(7)
C(28)#2-U(2)-C(27)	29.39(16)	C(24)-C(25)-C(31)	125.2(7)
C(28)-U(2)-C(27)	29.39(16)	C(26)-C(25)-U(2)	77.4(3)
C(25)-U(2)-C(27)	144.10(18)	C(24)-C(25)-U(2)	77.0(4)
C(25)#2-U(2)-C(27)	144.10(18)	C(31)-C(25)-U(2)	120.5(4)
O(2)-U(2)-C(24)	153.7(2)	C(25)-C(26)-C(26)#2	107.4(4)
C(29)#2-U(2)-C(24)	88.5(2)	C(25)-C(26)-C(32)	127.5(6)
C(29)-U(2)-C(24)	88.5(2)	C(26)#2-C(26)-C(32)	124.0(4)
C(28)#2-U(2)-C(24)	115.8(2)	C(25)-C(26)-U(2)	73.7(3)
C(28)-U(2)-C(24)	115.8(2)	C(26)#2-C(26)-U(2)	75.51(12)
C(25)-U(2)-C(24)	28.95(17)	C(32)-C(26)-U(2)	125.6(4)
C(25)#2-U(2)-C(24)	28.95(17)	C(28)#2-C(27)-C(28)	107.6(8)
C(27)-U(2)-C(24)	135.5(3)	C(28)#2-C(27)-C(33)	126.1(4)
O(2)-U(2)-C(26)#2	107.32(19)	C(28)-C(27)-C(33)	126.1(4)
C(29)#2-U(2)-C(26)#2	135.86(17)	C(28)#2-C(27)-U(2)	74.0(4)
C(29)-U(2)-C(26)#2	126.10(17)	C(28)-C(27)-U(2)	74.0(4)
C(28)#2-U(2)-C(26)#2	162.29(18)	C(33)-C(27)-U(2)	121.5(6)
C(28)-U(2)-C(26)#2	138.28(18)	C(27)-C(28)-C(29)	108.2(6)
C(25)-U(2)-C(26)#2	47.71(17)	C(27)-C(28)-C(34)	125.9(6)
C(25)#2-U(2)-C(26)#2	28.88(17)	C(29)-C(28)-C(34)	125.0(6)
C(27)-U(2)-C(26)#2	165.45(13)	C(27)-C(28)-U(2)	76.6(4)
C(24)-U(2)-C(26)#2	47.6(2)	C(29)-C(28)-U(2)	74.0(3)
O(2)-U(2)-C(26)	107.32(19)	C(34)-C(28)-U(2)	123.8(4)
C(29)#2-U(2)-C(26)	126.10(17)	C(29)#2-C(29)-C(28)	108.0(4)
C(29)-U(2)-C(26)	135.86(17)	C(29)#2-C(29)-C(35)	127.8(4)
C(28)#2-U(2)-C(26)	138.28(18)	C(28)-C(29)-C(35)	123.6(6)

C(29)#2-C(29)-U(2)	75.12(12)	C(38)#2-C(39)-C(38)	119.2(8)
C(28)-C(29)-U(2)	76.2(3)	C(38)#2-C(39)-C(44)	120.4(4)
C(35)-C(29)-U(2)	122.1(4)	C(38)-C(39)-C(44)	120.4(4)
O(2)-C(36)-C(37)	118.8(4)	C(41)-C(40)-C(42)	107.5(5)
O(2)-C(36)-C(37)#2	118.8(4)	C(41)-C(40)-C(37)	112.0(5)
C(37)-C(36)-C(37)#2	122.3(8)	C(42)-C(40)-C(37)	109.5(5)
C(38)-C(37)-C(36)	117.3(6)	C(41)-C(40)-C(43)	106.4(5)
C(38)-C(37)-C(40)	120.9(5)	C(42)-C(40)-C(43)	108.2(5)
C(36)-C(37)-C(40)	121.7(5)	C(37)-C(40)-C(43)	112.9(5)
C(39)-C(38)-C(37)	121.8(6)		

Symmetry transformations used to generate equivalent atoms:
#1 -x-1,y,z #2 -x,y,z

X-ray Data Collection, Structure Solution and Refinement for 1-Ce.

A pink crystal of approximate dimensions 0.224 x 0.285 x 0.501 mm was mounted in a cryoloop and transferred to a Bruker SMART APEX II diffractometer system. The APEX2[86] program package was used to determine the unit-cell parameters and for data collection (10 sec/frame scan time). The raw frame data was processed using SAINT[87] and SADABS[88] to yield the reflection data file. Subsequent calculations were carried out using the SHELXTL[89] program package. The diffraction symmetry was *mmm* and the systematic absences were consistent with the orthorhombic space group $Cmc2_1$ which was later determined to be correct.

The structure was solved by direct methods and refined on F^2 by full-matrix least-squares techniques. The analytical scattering factors[90] for neutral atoms were used throughout the analysis. Hydrogen atoms were included using a riding model. There were two molecules of the formula-unit present; each was located on a mirror plane. One pentamethylcyclopentadienyl ligand was modeled as a 50:50 disorder.

Least-squares analysis yielded wR2 = 0.0555 and Goof = 1.024 for 473 variables refined against 9752 data (0.70 Å), R1 = 0.0248 for those 9376 data with I > 2.0σ(I). The absolute structure was assigned by refinement of the Flack parameter.[91]

Table 5.14. Bond lengths [Å] and angles [°] for **5.1-Ce**.

Ce(1)-Cnt1	2.531	C(1B)-C(2B)	1.394(14)
Ce(1)-O(1)	2.213(3)	C(1B)-C(5B)	1.403(14)
Ce(1)-C(4)#1	2.75(2)	C(1B)-C(6B)	1.516(12)
Ce(1)-C(4)	2.75(2)	C(2B)-C(3B)	1.413(14)
Ce(1)-C(5)	2.766(12)	C(2B)-C(7B)	1.536(12)
Ce(1)-C(5)#1	2.766(12)	C(3B)-C(4B)	1.44(3)
Ce(1)-C(1B)#1	2.781(7)	C(3B)-C(8B)	1.49(2)
Ce(1)-C(1B)	2.781(7)	C(4B)-C(5B)	1.374(18)
Ce(1)-C(5B)	2.784(11)	C(4B)-C(9B)	1.53(2)
Ce(1)-C(5B)#1	2.784(11)	C(5B)-C(10B)	1.484(13)
Ce(1)-C(4B)	2.79(2)	C(11)-C(16)	1.412(6)
Ce(1)-C(4B)#1	2.79(2)	C(11)-C(12)	1.437(6)
Ce(1)-C(3)#1	2.802(16)	C(12)-C(13)	1.384(6)
Ce(1)-C(3)	2.802(16)	C(12)-C(17)	1.544(6)
Ce(1)-C(1)#1	2.812(9)	C(13)-C(14)	1.389(6)
Ce(1)-C(1)	2.812(9)	C(14)-C(15)	1.383(6)
Ce(1)-C(2B)	2.823(8)	C(14)-C(20)	1.503(7)
Ce(1)-C(2B)#1	2.823(8)	C(15)-C(16)	1.404(6)
Ce(1)-C(3B)	2.841(18)	C(16)-C(21)	1.538(6)
Ce(1)-C(3B)#1	2.841(18)	C(17)-C(18)#1	1.526(4)
Ce(1)-C(2)	2.854(9)	C(17)-C(18)	1.527(4)
Ce(1)-C(2)#1	2.854(9)	C(17)-C(19)	1.533(7)
O(1)-C(11)	1.347(5)	C(21)-C(23)	1.542(6)
C(1)-C(5)	1.397(13)	C(21)-C(22)#1	1.547(5)
C(1)-C(2)	1.408(14)	C(21)-C(22)	1.547(5)
C(1)-C(6)	1.505(13)	Ce(2)-Cnt2	2.585
C(2)-C(3)	1.418(15)	Ce(2)-Cnt3	2.525
C(2)-C(7)	1.505(11)	Ce(2)-O(2)	2.246(3)
C(3)-C(4)	1.45(3)	Ce(2)-C(29)#2	2.776(3)
C(3)-C(8)	1.520(16)	Ce(2)-C(29)	2.776(3)
C(4)-C(5)	1.387(17)	Ce(2)-C(28)	2.802(3)
C(4)-C(9)	1.47(2)	Ce(2)-C(28)#2	2.802(3)
C(5)-C(10)	1.517(17)	Ce(2)-C(25)	2.834(3)

Ce(2)-C(25)#2	2.834(3)
Ce(2)-C(27)	2.838(5)
Ce(2)-C(24)	2.838(5)
Ce(2)-C(26)	2.873(3)
Ce(2)-C(26)#2	2.873(3)
Ce(2)-C(36)	3.078(4)
O(2)-C(36)	1.351(5)
C(24)-C(25)	1.410(5)
C(24)-C(25)#2	1.410(5)
C(24)-C(30)	1.511(7)
C(25)-C(26)	1.417(5)
C(25)-C(31)	1.504(5)
C(26)-C(26)#2	1.409(7)
C(26)-C(32)	1.507(5)
C(27)-C(28)	1.419(4)
C(27)-C(28)#2	1.419(4)
C(27)-C(33)	1.493(7)
C(28)-C(29)	1.418(5)
C(28)-C(34)	1.498(5)
C(29)-C(29)#2	1.418(7)
C(29)-C(35)	1.505(5)
C(36)-C(37)	1.418(4)
C(36)-C(37)#2	1.418(4)
C(37)-C(38)	1.400(4)
C(37)-C(40)	1.543(5)
C(38)-C(39)	1.385(4)
C(39)-C(38)#2	1.385(4)
C(39)-C(44)	1.526(7)
C(40)-C(41)	1.533(5)
C(40)-C(42)	1.535(4)
C(40)-C(43)	1.543(4)

Cnt1-Ce(1)-O(1)	114.1
Cnt1-Ce(1)-Cnt1#1	131.5
O(1)-Ce(1)-C(4)#1	102.3(5)
O(1)-Ce(1)-C(4)	102.3(5)
C(4)#1-Ce(1)-C(4)	118.4(6)
O(1)-Ce(1)-C(5)	87.2(3)
C(4)#1-Ce(1)-C(5)	147.1(6)
C(4)-Ce(1)-C(5)	29.1(4)
O(1)-Ce(1)-C(5)#1	87.2(3)
C(4)#1-Ce(1)-C(5)#1	29.1(4)
C(4)-Ce(1)-C(5)#1	147.1(6)
C(5)-Ce(1)-C(5)#1	171.3(6)
O(1)-Ce(1)-C(1B)#1	116.6(4)
O(1)-Ce(1)-C(1B)	116.6(4)
C(1B)#1-Ce(1)-C(1B)	108.2(6)
O(1)-Ce(1)-C(5B)	92.5(3)
C(1B)#1-Ce(1)-C(5B)	136.9(6)
C(1B)-Ce(1)-C(5B)	29.2(3)
O(1)-Ce(1)-C(5B)#1	92.5(3)
C(1B)#1-Ce(1)-C(5B)#1	29.2(3)
C(1B)-Ce(1)-C(5B)#1	136.9(6)
C(5B)-Ce(1)-C(5B)#1	163.4(8)
O(1)-Ce(1)-C(4B)	97.3(4)
C(1B)#1-Ce(1)-C(4B)	145.7(5)
C(1B)-Ce(1)-C(4B)	47.1(4)
C(5B)-Ce(1)-C(4B)	28.5(3)
C(5B)#1-Ce(1)-C(4B)	164.2(5)
O(1)-Ce(1)-C(4B)#1	97.3(4)
C(1B)#1-Ce(1)-C(4B)#1	47.1(4)
C(1B)-Ce(1)-C(4B)#1	145.7(5)
C(5B)-Ce(1)-C(4B)#1	164.2(5)
C(5B)#1-Ce(1)-C(4B)#1	28.5(3)
C(4B)-Ce(1)-C(4B)#1	136.9(7)
O(1)-Ce(1)-C(3)#1	132.0(3)
C(4)#1-Ce(1)-C(3)#1	30.3(6)
C(4)-Ce(1)-C(3)#1	108.9(4)
C(5)-Ce(1)-C(3)#1	134.8(5)
C(5)#1-Ce(1)-C(3)#1	47.7(4)
O(1)-Ce(1)-C(3)	132.0(3)
C(4)#1-Ce(1)-C(3)	108.9(4)
C(4)-Ce(1)-C(3)	30.3(6)
C(5)-Ce(1)-C(3)	47.7(4)
C(5)#1-Ce(1)-C(3)	134.8(5)
C(3)#1-Ce(1)-C(3)	87.5(6)
O(1)-Ce(1)-C(1)#1	102.4(3)
C(4)#1-Ce(1)-C(1)#1	48.7(4)
C(4)-Ce(1)-C(1)#1	154.3(5)
C(5)-Ce(1)-C(1)#1	159.6(6)

C(5)#1-Ce(1)-C(1)#1	29.0(3)	C(4B)-Ce(1)-C(3B)#1	115.7(5)
C(3)#1-Ce(1)-C(1)#1	47.6(3)	C(4B)#1-Ce(1)-C(3B)#1	29.6(6)
C(3)-Ce(1)-C(1)#1	125.6(4)	C(2B)-Ce(1)-C(3B)#1	91.2(4)
O(1)-Ce(1)-C(1)	102.4(3)	C(2B)#1-Ce(1)-C(3B)#1	28.9(3)
C(4)#1-Ce(1)-C(1)	154.3(5)	C(3B)-Ce(1)-C(3B)#1	89.0(9)
C(4)-Ce(1)-C(1)	48.7(4)	O(1)-Ce(1)-C(2)	130.9(3)
C(5)-Ce(1)-C(1)	29.0(3)	C(4)#1-Ce(1)-C(2)	125.8(6)
C(5)#1-Ce(1)-C(1)	159.6(6)	C(4)-Ce(1)-C(2)	49.2(5)
C(3)#1-Ce(1)-C(1)	125.6(4)	C(5)-Ce(1)-C(2)	47.7(3)
C(3)-Ce(1)-C(1)	47.6(3)	C(5)#1-Ce(1)-C(2)	139.8(4)
C(1)#1-Ce(1)-C(1)	130.7(7)	C(3)#1-Ce(1)-C(2)	97.0(4)
O(1)-Ce(1)-C(2B)	140.1(2)	C(3)-Ce(1)-C(2)	29.0(3)
C(1B)#1-Ce(1)-C(2B)	99.2(4)	C(1)#1-Ce(1)-C(2)	115.7(5)
C(1B)-Ce(1)-C(2B)	28.8(3)	C(1)-Ce(1)-C(2)	28.8(3)
C(5B)-Ce(1)-C(2B)	47.8(3)	O(1)-Ce(1)-C(2)#1	130.9(3)
C(5B)#1-Ce(1)-C(2B)	126.5(4)	C(4)#1-Ce(1)-C(2)#1	49.2(5)
C(4B)-Ce(1)-C(2B)	47.1(4)	C(4)-Ce(1)-C(2)#1	125.8(6)
C(4B)#1-Ce(1)-C(2B)	120.7(5)	C(5)-Ce(1)-C(2)#1	139.8(4)
O(1)-Ce(1)-C(2B)#1	140.1(2)	C(5)#1-Ce(1)-C(2)#1	47.7(3)
C(1B)#1-Ce(1)-C(2B)#1	28.8(3)	C(3)#1-Ce(1)-C(2)#1	29.0(3)
C(1B)-Ce(1)-C(2B)#1	99.2(4)	C(3)-Ce(1)-C(2)#1	97.0(4)
C(5B)-Ce(1)-C(2B)#1	126.5(4)	C(1)#1-Ce(1)-C(2)#1	28.8(3)
C(5B)#1-Ce(1)-C(2B)#1	47.8(3)	C(1)-Ce(1)-C(2)#1	115.7(4)
C(4B)-Ce(1)-C(2B)#1	120.7(5)	C(2)-Ce(1)-C(2)#1	92.2(5)
C(4B)#1-Ce(1)-C(2B)#1	47.1(4)	C(11)-O(1)-Ce(1)	166.5(3)
C(2B)-Ce(1)-C(2B)#1	79.6(4)	C(5)-C(1)-C(2)	108.2(11)
O(1)-Ce(1)-C(3B)	125.2(5)	C(5)-C(1)-C(6)	129.5(15)
C(1B)#1-Ce(1)-C(3B)	117.9(5)	C(2)-C(1)-C(6)	121.5(14)
C(1B)-Ce(1)-C(3B)	48.1(4)	C(5)-C(1)-Ce(1)	73.7(7)
C(5B)-Ce(1)-C(3B)	48.7(4)	C(2)-C(1)-Ce(1)	77.3(5)
C(5B)#1-Ce(1)-C(3B)	136.6(5)	C(6)-C(1)-Ce(1)	123.1(6)
C(4B)-Ce(1)-C(3B)	29.6(6)	C(1)-C(2)-C(3)	106.7(10)
C(4B)#1-Ce(1)-C(3B)	115.7(5)	C(1)-C(2)-C(7)	126.4(14)
C(2B)-Ce(1)-C(3B)	28.9(3)	C(3)-C(2)-C(7)	126.4(15)
C(2B)#1-Ce(1)-C(3B)	91.2(4)	C(1)-C(2)-Ce(1)	74.0(5)
O(1)-Ce(1)-C(3B)#1	125.2(5)	C(3)-C(2)-Ce(1)	73.5(7)
C(1B)#1-Ce(1)-C(3B)#1	48.1(4)	C(7)-C(2)-Ce(1)	124.8(6)
C(1B)-Ce(1)-C(3B)#1	117.9(5)	C(2)-C(3)-C(4)	109.0(12)
C(5B)-Ce(1)-C(3B)#1	136.6(5)	C(2)-C(3)-C(8)	129.0(14)
C(5B)#1-Ce(1)-C(3B)#1	48.7(4)	C(4)-C(3)-C(8)	121.3(13)

C(2)-C(3)-Ce(1)	77.5(7)	C(4B)-C(5B)-C(10B)	126.4(18)
C(4)-C(3)-Ce(1)	73.0(10)	C(1B)-C(5B)-C(10B)	126.7(18)
C(8)-C(3)-Ce(1)	123.2(9)	C(4B)-C(5B)-Ce(1)	76.0(9)
C(5)-C(4)-C(3)	104.9(16)	C(1B)-C(5B)-Ce(1)	75.3(5)
C(5)-C(4)-C(9)	128(2)	C(10B)-C(5B)-Ce(1)	119.3(7)
C(3)-C(4)-C(9)	126.8(15)	O(1)-C(11)-C(16)	121.1(4)
C(5)-C(4)-Ce(1)	76.0(10)	O(1)-C(11)-C(12)	119.8(4)
C(3)-C(4)-Ce(1)	76.7(11)	C(16)-C(11)-C(12)	119.1(4)
C(9)-C(4)-Ce(1)	114.9(11)	C(13)-C(12)-C(11)	118.8(4)
C(4)-C(5)-C(1)	111.1(18)	C(13)-C(12)-C(17)	119.3(4)
C(4)-C(5)-C(10)	126.6(17)	C(11)-C(12)-C(17)	121.9(4)
C(1)-C(5)-C(10)	122.2(15)	C(12)-C(13)-C(14)	123.2(4)
C(4)-C(5)-Ce(1)	74.9(11)	C(15)-C(14)-C(13)	116.9(4)
C(1)-C(5)-Ce(1)	77.3(6)	C(15)-C(14)-C(20)	121.3(4)
C(10)-C(5)-Ce(1)	117.6(8)	C(13)-C(14)-C(20)	121.7(4)
C(2B)-C(1B)-C(5B)	108.8(9)	C(14)-C(15)-C(16)	123.7(4)
C(2B)-C(1B)-C(6B)	124.6(14)	C(15)-C(16)-C(11)	118.2(4)
C(5B)-C(1B)-C(6B)	126.5(16)	C(15)-C(16)-C(21)	114.0(4)
C(2B)-C(1B)-Ce(1)	77.3(5)	C(11)-C(16)-C(21)	127.8(4)
C(5B)-C(1B)-Ce(1)	75.5(6)	C(18)#1-C(17)-C(18)	110.4(4)
C(6B)-C(1B)-Ce(1)	117.2(5)	C(18)#1-C(17)-C(19)	106.2(3)
C(1B)-C(2B)-C(3B)	109.6(12)	C(18)-C(17)-C(19)	106.2(3)
C(1B)-C(2B)-C(7B)	125.1(13)	C(18)#1-C(17)-C(12)	110.5(2)
C(3B)-C(2B)-C(7B)	124.9(16)	C(18)-C(17)-C(12)	110.5(2)
C(1B)-C(2B)-Ce(1)	73.9(5)	C(19)-C(17)-C(12)	112.9(4)
C(3B)-C(2B)-Ce(1)	76.3(8)	C(16)-C(21)-C(23)	116.9(4)
C(7B)-C(2B)-Ce(1)	122.6(5)	C(16)-C(21)-C(22)#1	109.0(3)
C(2B)-C(3B)-C(4B)	103.9(13)	C(23)-C(21)-C(22)#1	106.4(3)
C(2B)-C(3B)-C(8B)	128(2)	C(16)-C(21)-C(22)	109.0(3)
C(4B)-C(3B)-C(8B)	127.5(16)	C(23)-C(21)-C(22)	106.4(3)
C(2B)-C(3B)-Ce(1)	74.9(8)	C(22)#1-C(21)-C(22)	108.9(5)
C(4B)-C(3B)-Ce(1)	73.3(11)	Cnt2-Ce(2)-O(2)	128.5
C(8B)-C(3B)-Ce(1)	123.7(10)	Cnt3-Ce(2)-O(2)	96.2
C(5B)-C(4B)-C(3B)	111.1(15)	Cnt2-Ce(2)-Cnt3	135.3
C(5B)-C(4B)-C(9B)	126.0(17)	O(2)-Ce(2)-C(29)#2	116.55(10)
C(3B)-C(4B)-C(9B)	122.2(15)	O(2)-Ce(2)-C(29)	116.55(10)
C(5B)-C(4B)-Ce(1)	75.5(9)	C(29)#2-Ce(2)-C(29)	29.60(13)
C(3B)-C(4B)-Ce(1)	77.2(10)	O(2)-Ce(2)-C(28)	88.01(10)
C(9B)-C(4B)-Ce(1)	122.3(11)	C(29)#2-Ce(2)-C(28)	48.53(9)
C(4B)-C(5B)-C(1B)	106.6(12)	C(29)-Ce(2)-C(28)	29.45(9)

O(2)-Ce(2)-C(28)#2	88.01(10)	C(29)#2-Ce(2)-C(26)#2	135.96(9)
C(29)#2-Ce(2)-C(28)#2	29.45(9)	C(29)-Ce(2)-C(26)#2	126.41(9)
C(29)-Ce(2)-C(28)#2	48.52(9)	C(28)-Ce(2)-C(26)#2	138.70(10)
C(28)-Ce(2)-C(28)#2	48.18(13)	C(28)#2-Ce(2)-C(26)#2	162.08(10)
O(2)-Ce(2)-C(25)	131.84(10)	C(25)-Ce(2)-C(26)#2	47.20(10)
C(29)#2-Ce(2)-C(25)	97.85(9)	C(25)#2-Ce(2)-C(26)#2	28.74(9)
C(29)-Ce(2)-C(25)	110.01(10)	C(27)-Ce(2)-C(26)#2	165.76(7)
C(28)-Ce(2)-C(25)	139.41(10)	C(24)-Ce(2)-C(26)#2	47.25(11)
C(28)#2-Ce(2)-C(25)	115.53(9)	C(26)-Ce(2)-C(26)#2	28.39(14)
O(2)-Ce(2)-C(25)#2	131.84(10)	O(2)-Ce(2)-C(36)	23.37(11)
C(29)#2-Ce(2)-C(25)#2	110.01(10)	C(29)#2-Ce(2)-C(36)	138.62(10)
C(29)-Ce(2)-C(25)#2	97.85(9)	C(29)-Ce(2)-C(36)	138.62(10)
C(28)-Ce(2)-C(25)#2	115.53(10)	C(28)-Ce(2)-C(36)	109.26(10)
C(28)#2-Ce(2)-C(25)#2	139.41(10)	C(28)#2-Ce(2)-C(36)	109.27(10)
C(25)-Ce(2)-C(25)#2	47.44(15)	C(25)-Ce(2)-C(36)	111.32(10)
O(2)-Ce(2)-C(27)	70.92(12)	C(25)#2-Ce(2)-C(36)	111.32(10)
C(29)#2-Ce(2)-C(27)	48.39(11)	C(27)-Ce(2)-C(36)	94.29(12)
C(29)-Ce(2)-C(27)	48.38(11)	C(24)-Ce(2)-C(36)	130.22(12)
C(28)-Ce(2)-C(27)	29.13(9)	C(26)-Ce(2)-C(36)	84.82(10)
C(28)#2-Ce(2)-C(27)	29.13(9)	C(26)#2-Ce(2)-C(36)	84.82(10)
C(25)-Ce(2)-C(27)	144.16(10)	C(36)-O(2)-Ce(2)	115.4(3)
C(25)#2-Ce(2)-C(27)	144.16(10)	C(25)-C(24)-C(25)#2	107.9(4)
O(2)-Ce(2)-C(24)	153.59(12)	C(25)-C(24)-C(30)	125.6(2)
C(29)#2-Ce(2)-C(24)	88.92(11)	C(25)#2-C(24)-C(30)	125.6(2)
C(29)-Ce(2)-C(24)	88.92(11)	C(25)-C(24)-Ce(2)	75.4(2)
C(28)-Ce(2)-C(24)	115.91(11)	C(25)#2-C(24)-Ce(2)	75.4(2)
C(28)#2-Ce(2)-C(24)	115.91(11)	C(30)-C(24)-Ce(2)	124.3(3)
C(25)-Ce(2)-C(24)	28.79(9)	C(24)-C(25)-C(26)	108.1(3)
C(25)#2-Ce(2)-C(24)	28.79(9)	C(24)-C(25)-C(31)	125.6(4)
C(27)-Ce(2)-C(24)	135.49(13)	C(26)-C(25)-C(31)	125.7(4)
O(2)-Ce(2)-C(26)	107.46(10)	C(24)-C(25)-Ce(2)	75.8(2)
C(29)#2-Ce(2)-C(26)	126.41(9)	C(26)-C(25)-Ce(2)	77.18(18)
C(29)-Ce(2)-C(26)	135.96(9)	C(31)-C(25)-Ce(2)	120.0(2)
C(28)-Ce(2)-C(26)	162.08(10)	C(26)#2-C(26)-C(25)	107.9(2)
C(28)#2-Ce(2)-C(26)	138.70(10)	C(26)#2-C(26)-C(32)	124.4(2)
C(25)-Ce(2)-C(26)	28.74(9)	C(25)-C(26)-C(32)	126.7(3)
C(25)#2-Ce(2)-C(26)	47.19(10)	C(26)#2-C(26)-Ce(2)	75.80(7)
C(27)-Ce(2)-C(26)	165.76(7)	C(25)-C(26)-Ce(2)	74.08(18)
C(24)-Ce(2)-C(26)	47.25(11)	C(32)-C(26)-Ce(2)	125.0(2)
O(2)-Ce(2)-C(26)#2	107.46(10)	C(28)-C(27)-C(28)#2	107.4(4)

C(28)-C(27)-C(33)	126.2(2)	O(2)-C(36)-C(37)#2	119.4(2)
C(28)#2-C(27)-C(33)	126.2(2)	C(37)-C(36)-C(37)#2	121.3(4)
C(28)-C(27)-Ce(2)	74.0(2)	O(2)-C(36)-Ce(2)	41.24(19)
C(28)#2-C(27)-Ce(2)	74.0(2)	C(37)-C(36)-Ce(2)	111.2(2)
C(33)-C(27)-Ce(2)	121.2(3)	C(37)#2-C(36)-Ce(2)	111.2(2)
C(29)-C(28)-C(27)	108.4(3)	C(38)-C(37)-C(36)	117.6(3)
C(29)-C(28)-C(34)	125.1(3)	C(38)-C(37)-C(40)	121.0(3)
C(27)-C(28)-C(34)	125.7(3)	C(36)-C(37)-C(40)	121.4(3)
C(29)-C(28)-Ce(2)	74.27(17)	C(39)-C(38)-C(37)	122.3(3)
C(27)-C(28)-Ce(2)	76.9(2)	C(38)-C(39)-C(38)#2	118.9(4)
C(34)-C(28)-Ce(2)	122.7(2)	C(38)-C(39)-C(44)	120.6(2)
C(28)-C(29)-C(29)#2	107.84(19)	C(38)#2-C(39)-C(44)	120.6(2)
C(28)-C(29)-C(35)	123.6(3)	C(41)-C(40)-C(42)	107.6(3)
C(29)#2-C(29)-C(35)	128.0(2)	C(41)-C(40)-C(43)	106.4(3)
C(28)-C(29)-Ce(2)	76.28(18)	C(42)-C(40)-C(43)	107.8(3)
C(29)#2-C(29)-Ce(2)	75.20(7)	C(41)-C(40)-C(37)	112.1(3)
C(35)-C(29)-Ce(2)	121.2(2)	C(42)-C(40)-C(37)	109.6(3)
O(2)-C(36)-C(37)	119.4(2)	C(43)-C(40)-C(37)	113.1(3)

Symmetry transformations used to generate equivalent atoms:

#1 -x+3,y,z #2 -x+2,y,z

X-ray Data Collection, Structure Solution and Refinement for 5.2.

A black crystal of approximate dimensions 0.119 x 0.173 x 0.402 mm was mounted in a cryoloop and transferred to a Bruker SMART APEX II diffractometer system. The APEX2[86] program package and the CELL_NOW[92] were used to determine the unit-cell parameters. Data was collected using a 30 sec/frame scan time. The raw frame data was processed using SAINT[87] and TWINABS[93] to yield the reflection data file (HKLF5 format).[93] Subsequent calculations were carried out using the SHELXTL[89] program package. There were no systematic absences nor any diffraction symmetry other than the Friedel condition. The centrosymmetric triclinic space group $P\bar{1}$ was assigned and later determined to be correct.

The structure was solved by direct methods and refined on F^2 by full-matrix least-squares techniques. The analytical scattering factors for neutral atoms were used throughout the analysis. Hydrogen atoms were included using a riding model. There were two different independent molecules and one-half molecule of *n*-hexane solvent present.

Least-squares analysis yielded wR2 = 0.1090 and Goof = 1.061 for 736 variables refined against 15120 data (0.78 Å), R1 = 0.0417 for those 12344 with $I > 2.0\sigma(I)$. The structure was refined as a three-component twin (BASF values 0.37652, 0.04644).

Table 5.15: Bond lengths [Å] and angles [°] for **5.2**.

U(1)-Cnt1	2.517	C(10)-C(11)	1.414(8)
U(1)-Cnt2	2.549	C(10)-C(15)	1.525(8)
U(1)-O(1)	2.268(4)	C(11)-C(12)	1.430(8)
U(1)-O(2)	2.562(4)	C(11)-C(16)	1.509(8)
U(1)-C(5)	2.728(5)	C(12)-C(13)	1.413(8)
U(1)-C(1)	2.775(6)	C(12)-C(17)	1.525(8)
U(1)-C(14)	2.788(6)	C(13)-C(14)	1.413(8)
U(1)-C(10)	2.790(6)	C(13)-C(18)	1.503(8)
U(1)-C(4)	2.792(6)	C(19)-C(24)	1.427(8)
U(1)-C(11)	2.814(6)	C(19)-C(20)	1.433(8)
U(1)-C(2)	2.823(7)	C(20)-C(21)	1.395(8)
U(1)-C(3)	2.825(6)	C(20)-C(25)	1.552(8)
U(1)-C(13)	2.838(6)	C(21)-C(22)	1.386(9)
U(1)-C(12)	2.862(6)	C(22)-C(23)	1.400(9)
O(1)-C(19)	1.356(7)	C(22)-C(29)	1.510(9)
O(2)-C(34)	1.466(8)	C(23)-C(24)	1.393(9)
O(2)-C(37)	1.475(7)	C(24)-C(30)	1.544(9)
C(1)-C(5)	1.397(8)	C(25)-C(28)	1.535(8)
C(1)-C(2)	1.427(9)	C(25)-C(27)	1.547(8)
C(1)-C(6)	1.517(9)	C(25)-C(26)	1.547(8)
C(2)-C(3)	1.413(9)	C(30)-C(31)	1.543(8)
C(2)-C(7)	1.509(9)	C(30)-C(32)	1.548(8)
C(3)-C(4)	1.419(9)	C(30)-C(33)	1.549(9)
C(3)-C(8)	1.513(8)	C(34)-C(35)	1.464(10)
C(4)-C(5)	1.406(8)	C(35)-C(36)	1.513(9)
C(4)-C(9)	1.500(8)	C(36)-C(37)	1.522(9)
C(10)-C(14)	1.406(9)	U(2)-Cnt3	2.472

U(2)-Cnt4	2.511	C(61)-C(67)	1.545(8)
U(2)-O(3)	2.269(4)	C(62)-C(64)	1.526(9)
U(2)-C(42)	2.697(6)	C(62)-C(65)	1.533(8)
U(2)-C(41)	2.717(7)	C(62)-C(63)	1.565(8)
U(2)-C(38)	2.743(6)	C(67)-C(69)	1.530(9)
U(2)-C(51)	2.759(6)	C(67)-C(70)	1.533(9)
U(2)-C(47)	2.774(6)	C(67)-C(68)	1.539(9)
U(2)-C(50)	2.775(6)	C(71)-C(72)	1.535(9)
U(2)-C(40)	2.789(7)	C(72)-C(73)	1.520(9)
U(2)-C(39)	2.795(7)	C(73)-C(73)#1	1.517(12)
U(2)-C(49)	2.802(6)		
U(2)-C(48)	2.816(6)	Cnt1-U(1)-O(1)	112.7
U(2)-C(56)	3.037(6)	Cnt1-U(1)-O(2)	112.3
O(3)-C(56)	1.352(7)	Cnt2-U(1)-O(1)	99.7
C(38)-C(42)	1.400(9)	Cnt2-U(1)-O(2)	103.9
C(38)-C(39)	1.429(9)	Cnt1-U(1)-Cnt2	124.2
C(38)-C(43)	1.499(9)	O(1)-U(1)-O(2)	99.16(14)
C(39)-C(40)	1.422(9)	O(1)-U(1)-C(5)	90.76(16)
C(39)-C(44)	1.491(10)	O(2)-U(1)-C(5)	117.65(16)
C(40)-C(41)	1.417(10)	O(1)-U(1)-C(1)	91.83(16)
C(40)-C(45)	1.520(10)	O(2)-U(1)-C(1)	88.51(16)
C(41)-C(42)	1.389(9)	C(5)-U(1)-C(1)	29.41(17)
C(41)-C(46)	1.537(10)	O(1)-U(1)-C(14)	130.66(17)
C(47)-C(51)	1.415(9)	O(2)-U(1)-C(14)	112.10(15)
C(47)-C(48)	1.423(9)	C(5)-U(1)-C(14)	105.96(17)
C(47)-C(52)	1.509(8)	C(1)-U(1)-C(14)	124.85(18)
C(48)-C(49)	1.417(8)	O(1)-U(1)-C(10)	101.66(17)
C(48)-C(53)	1.510(8)	O(2)-U(1)-C(10)	129.48(15)
C(49)-C(50)	1.408(9)	C(5)-U(1)-C(10)	107.57(18)
C(49)-C(54)	1.503(8)	C(1)-U(1)-C(10)	135.68(17)
C(50)-C(51)	1.416(9)	C(14)-U(1)-C(10)	29.19(18)
C(50)-C(55)	1.501(9)	O(1)-U(1)-C(4)	116.80(17)
C(56)-C(61)	1.421(8)	O(2)-U(1)-C(4)	121.62(16)
C(56)-C(57)	1.426(8)	C(5)-U(1)-C(4)	29.48(17)
C(57)-C(58)	1.401(8)	C(1)-U(1)-C(4)	48.81(17)
C(57)-C(62)	1.546(8)	C(14)-U(1)-C(4)	78.20(17)
C(58)-C(59)	1.387(8)	C(10)-U(1)-C(4)	88.04(17)
C(59)-C(60)	1.380(8)	O(1)-U(1)-C(11)	86.92(16)
C(59)-C(66)	1.516(8)	O(2)-U(1)-C(11)	108.56(15)
C(60)-C(61)	1.396(8)	C(5)-U(1)-C(11)	133.48(18)

C(1)-U(1)-C(11)	162.88(18)	C(3)-U(1)-C(12)	117.20(17)
C(14)-U(1)-C(11)	47.97(17)	C(13)-U(1)-C(12)	28.70(16)
C(10)-U(1)-C(11)	29.24(17)	C(19)-O(1)-U(1)	159.5(4)
C(4)-U(1)-C(11)	117.27(17)	C(34)-O(2)-C(37)	107.8(5)
O(1)-U(1)-C(2)	119.34(16)	C(34)-O(2)-U(1)	129.4(4)
O(2)-U(1)-C(2)	74.71(16)	C(37)-O(2)-U(1)	121.7(3)
C(5)-U(1)-C(2)	48.10(18)	C(5)-C(1)-C(2)	106.5(5)
C(1)-U(1)-C(2)	29.52(17)	C(5)-C(1)-C(6)	126.6(6)
C(14)-U(1)-C(2)	105.53(18)	C(2)-C(1)-C(6)	126.7(6)
C(10)-U(1)-C(2)	129.12(18)	C(5)-C(1)-U(1)	73.4(3)
C(4)-U(1)-C(2)	48.17(18)	C(2)-C(1)-U(1)	77.1(3)
C(11)-U(1)-C(2)	153.16(18)	C(6)-C(1)-U(1)	119.2(4)
O(1)-U(1)-C(3)	137.88(16)	C(3)-C(2)-C(1)	108.3(6)
O(2)-U(1)-C(3)	94.05(17)	C(3)-C(2)-C(7)	124.4(6)
C(5)-U(1)-C(3)	48.19(18)	C(1)-C(2)-C(7)	126.5(6)
C(1)-U(1)-C(3)	48.55(18)	C(3)-C(2)-U(1)	75.6(4)
C(14)-U(1)-C(3)	78.35(18)	C(1)-C(2)-U(1)	73.4(4)
C(10)-U(1)-C(3)	100.13(18)	C(7)-C(2)-U(1)	125.1(4)
C(4)-U(1)-C(3)	29.26(18)	C(2)-C(3)-C(4)	108.0(5)
C(11)-U(1)-C(3)	126.11(18)	C(2)-C(3)-C(8)	124.5(6)
C(2)-U(1)-C(3)	28.99(18)	C(4)-C(3)-C(8)	126.5(6)
O(1)-U(1)-C(13)	132.32(16)	C(2)-C(3)-U(1)	75.5(3)
O(2)-U(1)-C(13)	84.42(15)	C(4)-C(3)-U(1)	74.1(3)
C(5)-U(1)-C(13)	129.64(18)	C(8)-C(3)-U(1)	125.3(4)
C(1)-U(1)-C(13)	135.85(18)	C(5)-C(4)-C(3)	106.9(5)
C(14)-U(1)-C(13)	29.06(17)	C(5)-C(4)-C(9)	126.5(6)
C(10)-U(1)-C(13)	48.21(18)	C(3)-C(4)-C(9)	126.1(6)
C(4)-U(1)-C(13)	100.16(18)	C(5)-C(4)-U(1)	72.7(3)
C(11)-U(1)-C(13)	48.10(18)	C(3)-C(4)-U(1)	76.6(3)
C(2)-U(1)-C(13)	107.53(18)	C(9)-C(4)-U(1)	122.6(4)
C(3)-U(1)-C(13)	88.50(17)	C(1)-C(5)-C(4)	110.3(5)
O(1)-U(1)-C(12)	104.13(16)	C(1)-C(5)-U(1)	77.2(3)
O(2)-U(1)-C(12)	82.54(15)	C(4)-C(5)-U(1)	77.8(3)
C(5)-U(1)-C(12)	153.01(17)	C(14)-C(10)-C(11)	107.7(5)
C(1)-U(1)-C(12)	162.73(18)	C(14)-C(10)-C(15)	125.1(6)
C(14)-U(1)-C(12)	47.44(16)	C(11)-C(10)-C(15)	126.0(6)
C(10)-U(1)-C(12)	47.89(17)	C(14)-C(10)-U(1)	75.4(3)
C(4)-U(1)-C(12)	125.47(17)	C(11)-C(10)-U(1)	76.4(3)
C(11)-U(1)-C(12)	29.17(17)	C(15)-C(10)-U(1)	124.1(4)
C(2)-U(1)-C(12)	133.22(18)	C(10)-C(11)-C(12)	107.5(5)

C(10)-C(11)-C(16)	125.4(6)	C(31)-C(30)-C(24)	113.3(5)
C(12)-C(11)-C(16)	127.0(5)	C(31)-C(30)-C(32)	105.0(5)
C(10)-C(11)-U(1)	74.4(3)	C(24)-C(30)-C(32)	112.3(5)
C(12)-C(11)-U(1)	77.3(3)	C(31)-C(30)-C(33)	107.2(5)
C(16)-C(11)-U(1)	116.3(4)	C(24)-C(30)-C(33)	107.7(5)
C(13)-C(12)-C(11)	108.2(5)	C(32)-C(30)-C(33)	111.3(5)
C(13)-C(12)-C(17)	125.2(5)	C(35)-C(34)-O(2)	106.9(5)
C(11)-C(12)-C(17)	126.1(5)	C(34)-C(35)-C(36)	105.0(5)
C(13)-C(12)-U(1)	74.7(3)	C(35)-C(36)-C(37)	102.0(5)
C(11)-C(12)-U(1)	73.6(3)	O(2)-C(37)-C(36)	106.0(5)
C(17)-C(12)-U(1)	124.3(4)	Cnt3-U(2)-O(3)	100.2
C(14)-C(13)-C(12)	107.2(5)	Cnt4-U(2)-O(3)	133.6
C(14)-C(13)-C(18)	125.2(5)	Cnt3-U(2)-Cnt4	126.2
C(12)-C(13)-C(18)	127.0(5)	O(3)-U(2)-C(42)	125.93(18)
C(14)-C(13)-U(1)	73.5(3)	O(3)-U(2)-C(41)	107.25(19)
C(12)-C(13)-U(1)	76.6(3)	C(42)-U(2)-C(41)	29.7(2)
C(18)-C(13)-U(1)	122.7(4)	O(3)-U(2)-C(38)	107.23(17)
C(10)-C(14)-C(13)	109.3(5)	C(42)-U(2)-C(38)	29.82(19)
C(10)-C(14)-U(1)	75.5(3)	C(41)-U(2)-C(38)	49.83(19)
C(13)-C(14)-U(1)	77.4(3)	O(3)-U(2)-C(51)	159.01(17)
O(1)-C(19)-C(24)	120.5(5)	C(42)-U(2)-C(51)	74.8(2)
O(1)-C(19)-C(20)	121.7(5)	C(41)-U(2)-C(51)	89.8(2)
C(24)-C(19)-C(20)	117.8(5)	C(38)-U(2)-C(51)	93.0(2)
C(21)-C(20)-C(19)	119.0(6)	O(3)-U(2)-C(47)	138.70(18)
C(21)-C(20)-C(25)	119.6(5)	C(42)-U(2)-C(47)	90.1(2)
C(19)-C(20)-C(25)	121.3(5)	C(41)-U(2)-C(47)	113.7(2)
C(22)-C(21)-C(20)	123.3(6)	C(38)-U(2)-C(47)	95.13(19)
C(21)-C(22)-C(23)	116.9(6)	C(51)-U(2)-C(47)	29.6(2)
C(21)-C(22)-C(29)	121.3(6)	O(3)-U(2)-C(50)	133.13(17)
C(23)-C(22)-C(29)	121.7(6)	C(42)-U(2)-C(50)	93.4(2)
C(24)-C(23)-C(22)	122.8(6)	C(41)-U(2)-C(50)	95.4(2)
C(23)-C(24)-C(19)	119.3(5)	C(38)-U(2)-C(50)	118.6(2)
C(23)-C(24)-C(30)	118.6(5)	C(51)-U(2)-C(50)	29.64(18)
C(19)-C(24)-C(30)	121.8(6)	C(47)-U(2)-C(50)	49.00(19)
C(28)-C(25)-C(27)	106.2(5)	O(3)-U(2)-C(40)	79.59(18)
C(28)-C(25)-C(26)	112.3(5)	C(42)-U(2)-C(40)	48.4(2)
C(27)-C(25)-C(26)	106.7(5)	C(41)-U(2)-C(40)	29.8(2)
C(28)-C(25)-C(20)	111.2(5)	C(38)-U(2)-C(40)	49.17(19)
C(27)-C(25)-C(20)	112.6(5)	C(51)-U(2)-C(40)	119.1(2)
C(26)-C(25)-C(20)	107.8(5)	C(47)-U(2)-C(40)	138.5(2)

C(50)-U(2)-C(40)	123.3(2)	C(42)-C(38)-C(39)	106.2(6)
O(3)-U(2)-C(39)	79.45(17)	C(42)-C(38)-C(43)	127.5(6)
C(42)-U(2)-C(39)	48.6(2)	C(39)-C(38)-C(43)	126.0(6)
C(41)-U(2)-C(39)	49.3(2)	C(42)-C(38)-U(2)	73.3(4)
C(38)-U(2)-C(39)	29.88(19)	C(39)-C(38)-U(2)	77.1(4)
C(51)-U(2)-C(39)	121.47(19)	C(43)-C(38)-U(2)	119.8(5)
C(47)-U(2)-C(39)	124.16(19)	C(40)-C(39)-C(38)	107.7(6)
C(50)-U(2)-C(39)	141.5(2)	C(40)-C(39)-C(44)	124.9(6)
C(40)-U(2)-C(39)	29.5(2)	C(38)-C(39)-C(44)	127.1(6)
O(3)-U(2)-C(49)	110.72(16)	C(40)-C(39)-U(2)	75.0(4)
C(42)-U(2)-C(49)	121.31(19)	C(38)-C(39)-U(2)	73.0(4)
C(41)-U(2)-C(49)	123.8(2)	C(44)-C(39)-U(2)	122.5(5)
C(38)-U(2)-C(49)	140.79(18)	C(41)-C(40)-C(39)	108.2(6)
C(51)-U(2)-C(49)	48.41(18)	C(41)-C(40)-C(45)	127.8(7)
C(47)-U(2)-C(49)	48.69(17)	C(39)-C(40)-C(45)	123.8(7)
C(50)-U(2)-C(49)	29.25(18)	C(41)-C(40)-U(2)	72.3(4)
C(40)-U(2)-C(49)	148.4(2)	C(39)-C(40)-U(2)	75.5(4)
C(39)-U(2)-C(49)	169.77(18)	C(45)-C(40)-U(2)	121.4(5)
O(3)-U(2)-C(48)	113.24(16)	C(42)-C(41)-C(40)	106.7(6)
C(42)-U(2)-C(48)	119.09(19)	C(42)-C(41)-C(46)	127.5(7)
C(41)-U(2)-C(48)	138.1(2)	C(40)-C(41)-C(46)	125.6(7)
C(38)-U(2)-C(48)	122.71(18)	C(42)-C(41)-U(2)	74.3(4)
C(51)-U(2)-C(48)	48.37(18)	C(40)-C(41)-U(2)	77.9(4)
C(47)-U(2)-C(48)	29.49(18)	C(46)-C(41)-U(2)	117.3(5)
C(50)-U(2)-C(48)	48.37(18)	C(41)-C(42)-C(38)	111.1(6)
C(40)-U(2)-C(48)	167.16(19)	C(41)-C(42)-U(2)	75.9(4)
C(39)-U(2)-C(48)	148.40(18)	C(38)-C(42)-U(2)	76.9(4)
C(49)-U(2)-C(48)	29.22(16)	C(51)-C(47)-C(48)	107.2(5)
O(3)-U(2)-C(56)	24.46(15)	C(51)-C(47)-C(52)	126.0(6)
C(42)-U(2)-C(56)	150.32(19)	C(48)-C(47)-C(52)	126.7(6)
C(41)-U(2)-C(56)	127.85(19)	C(51)-C(47)-U(2)	74.6(4)
C(38)-U(2)-C(56)	129.38(18)	C(48)-C(47)-U(2)	76.9(4)
C(51)-U(2)-C(56)	134.65(18)	C(52)-C(47)-U(2)	118.2(4)
C(47)-U(2)-C(56)	117.86(18)	C(49)-C(48)-C(47)	108.0(5)
C(50)-U(2)-C(56)	112.04(18)	C(49)-C(48)-C(53)	125.8(6)
C(40)-U(2)-C(56)	102.82(18)	C(47)-C(48)-C(53)	125.4(6)
C(39)-U(2)-C(56)	103.42(18)	C(49)-C(48)-U(2)	74.8(4)
C(49)-U(2)-C(56)	86.80(17)	C(47)-C(48)-U(2)	73.6(4)
C(48)-U(2)-C(56)	89.94(17)	C(53)-C(48)-U(2)	125.1(4)
C(56)-O(3)-U(2)	111.5(3)	C(50)-C(49)-C(48)	108.3(5)

C(50)-C(49)-C(54)	126.8(5)	C(59)-C(58)-C(57)	122.1(6)
C(48)-C(49)-C(54)	124.0(6)	C(60)-C(59)-C(58)	118.9(6)
C(50)-C(49)-U(2)	74.3(4)	C(60)-C(59)-C(66)	120.8(5)
C(48)-C(49)-U(2)	75.9(4)	C(58)-C(59)-C(66)	120.1(6)
C(54)-C(49)-U(2)	124.4(4)	C(59)-C(60)-C(61)	122.6(6)
C(49)-C(50)-C(51)	107.7(5)	C(60)-C(61)-C(56)	118.0(5)
C(49)-C(50)-C(55)	126.5(6)	C(60)-C(61)-C(67)	121.4(5)
C(51)-C(50)-C(55)	125.2(6)	C(56)-C(61)-C(67)	120.5(6)
C(49)-C(50)-U(2)	76.4(3)	C(64)-C(62)-C(65)	108.6(5)
C(51)-C(50)-U(2)	74.6(3)	C(64)-C(62)-C(57)	108.3(5)
C(55)-C(50)-U(2)	121.8(5)	C(65)-C(62)-C(57)	111.4(5)
C(47)-C(51)-C(50)	108.7(6)	C(64)-C(62)-C(63)	108.8(5)
C(47)-C(51)-U(2)	75.8(4)	C(65)-C(62)-C(63)	107.0(5)
C(50)-C(51)-U(2)	75.8(3)	C(57)-C(62)-C(63)	112.7(5)
O(3)-C(56)-C(61)	119.9(5)	C(69)-C(67)-C(70)	109.9(6)
O(3)-C(56)-C(57)	119.7(5)	C(69)-C(67)-C(68)	107.0(5)
C(61)-C(56)-C(57)	120.4(6)	C(70)-C(67)-C(68)	106.3(6)
O(3)-C(56)-U(2)	44.0(2)	C(69)-C(67)-C(61)	113.1(5)
C(61)-C(56)-U(2)	112.0(4)	C(70)-C(67)-C(61)	108.5(5)
C(57)-C(56)-U(2)	109.8(4)	C(68)-C(67)-C(61)	111.9(6)
C(58)-C(57)-C(56)	117.9(5)	C(73)-C(72)-C(71)	113.4(6)
C(58)-C(57)-C(62)	121.2(5)	C(73)#1-C(73)-C(72)	112.7(7)
C(56)-C(57)-C(62)	120.6(5)		

Symmetry transformations used to generate equivalent atoms: #1 -x+2,-y,-z+2

X-ray Data Collection, Structure Solution and Refinement for 5.5.

A brown crystal of approximate dimensions 0.138 x 0.149 x 0.213 mm was mounted in a cryoloop and transferred to a Bruker SMART APEX II diffractometer system. The APEX2[86] program package and the CELL_NOW[92] were used to determine the unit-cell parameters. Data was collected using a 45 sec/frame scan time. The raw frame data was processed using SAINT[87] and TWINABS[93] to yield the reflection data file (HKLF 5 format).[93] Subsequent calculations were carried out using the SHELXTL[89] program package. The diffraction symmetry was 2/*m* and the

systematic absences were consistent with the monoclinic space group $P2_1/n$ that was later determined to be correct.

The structure was solved by direct methods and refined on F^2 by full-matrix least-squares techniques. The analytical scattering factors[90] for neutral atoms were used throughout the analysis. Hydrogen atoms were included using a riding model. The hydrogen atom associated with carbon C(21) could not be located or placed in a reasonable fixed location so was not included in the refinement. Several atoms were disordered and included using multiple components, partial site-occupancy-factors, geometric and displacement constraints.

Least-squares analysis yielded wR2 = 0.1092 and Goof = 1.049 for 189 variables refined against 7274 data (0.75Å), R1 = 0.0429 for those 6048 with $I > 2.0\sigma(I)$. The structure was refined as a two-component twin, BASF[89] = 0.39.

Table 5.16: Bond lengths [Å] and angles [°] for **5.5**.

U(1)-Cnt1	2.505	U(1)-C(13B)	2.843(7)
U(1)-Cnt2	2.547	U(1)-C(11B)	2.870(7)
U(1)-C(21)	2.502(7)	U(1)-C(12B)	2.872(7)
U(1)-C(4B)	2.680(7)	U(1)-C(1)	2.884(7)
U(1)-C(2B)	2.696(6)	U(1)-C(5)	2.884(7)
U(1)-C(3B)	2.712(7)	U(1)-Si(1)	3.286(2)
U(1)-C(5B)	2.724(7)	Si(1)-C(21)	1.835(9)
U(1)-C(13)	2.737(7)	Si(1)-C(24)	1.88(2)
U(1)-C(12)	2.756(7)	Si(1)-C(23)	1.864(10)
U(1)-C(1B)	2.777(7)	Si(1)-C(22)	1.894(11)
U(1)-C(14)	2.788(7)	Si(1)-C(24B)	1.90(2)
U(1)-C(3)	2.805(7)	C(21)-Si(2)	1.778(14)
U(1)-C(11)	2.818(7)	C(21)-Si(2B)	1.896(14)
U(1)-C(14B)	2.824(7)	Si(2)-C(26)	1.81(4)
U(1)-C(2)	2.835(7)	Si(2)-C(25)	1.86(3)
U(1)-C(4)	2.835(6)	Si(2)-C(27)	1.90(3)
U(1)-C(15)	2.837(7)	Si(2B)-C(27B)	1.81(3)
U(1)-C(22)	2.844(9)	Si(2B)-C(26B)	1.86(3)
U(1)-C(15B)	2.841(7)	Si(2B)-C(25B)	1.93(4)

C(1)-C(5)	1.403(4)		
C(1)-C(2)	1.403(4)	Cnt1-U(1)-C(21)	109.3
C(1)-C(6)	1.492(4)	Cnt2-U(1)-C(21)	111.6
C(2)-C(3)	1.403(4)	Cnt1-U(1)-Cnt2	133.9
C(2)-C(7)	1.492(4)	C(21)-U(1)-C(4B)	137.8(3)
C(3)-C(4)	1.404(4)	C(21)-U(1)-C(2B)	89.1(3)
C(3)-C(8)	1.492(4)	C(4B)-U(1)-C(2B)	50.89(16)
C(4)-C(5)	1.403(4)	C(21)-U(1)-C(3B)	115.3(3)
C(4)-C(9)	1.491(4)	C(4B)-U(1)-C(3B)	33.26(11)
C(5)-C(10)	1.493(4)	C(2B)-U(1)-C(3B)	29.59(10)
C(1B)-C(5B)	1.371(4)	C(21)-U(1)-C(5B)	113.7(3)
C(1B)-C(2B)	1.381(4)	C(4B)-U(1)-C(5B)	31.34(10)
C(1B)-C(6B)	1.499(4)	C(2B)-U(1)-C(5B)	47.74(15)
C(2B)-C(3B)	1.381(4)	C(3B)-U(1)-C(5B)	50.93(16)
C(2B)-C(7B)	1.513(4)	C(21)-U(1)-C(13)	94.5(3)
C(3B)-C(8B)	1.467(4)	C(21)-U(1)-C(12)	90.2(3)
C(3B)-C(4B)	1.543(4)	C(13)-U(1)-C(12)	29.88(10)
C(4B)-C(9B)	1.457(4)	C(21)-U(1)-C(1B)	87.8(3)
C(4B)-C(5B)	1.460(4)	C(4B)-U(1)-C(1B)	51.16(16)
C(5B)-C(10B)	1.532(4)	C(2B)-U(1)-C(1B)	29.18(9)
C(11)-C(15)	1.416(4)	C(3B)-U(1)-C(1B)	50.21(15)
C(11)-C(12)	1.416(4)	C(5B)-U(1)-C(1B)	28.84(9)
C(11)-C(16)	1.506(4)	C(21)-U(1)-C(14)	123.1(3)
C(12)-C(13)	1.416(4)	C(13)-U(1)-C(14)	29.68(10)
C(12)-C(17)	1.505(4)	C(12)-U(1)-C(14)	48.81(16)
C(13)-C(14)	1.416(4)	C(21)-U(1)-C(3)	102.9(3)
C(13)-C(18)	1.505(4)	C(13)-U(1)-C(3)	114.9(2)
C(14)-C(15)	1.416(4)	C(12)-U(1)-C(3)	144.27(19)
C(14)-C(19)	1.505(4)	C(14)-U(1)-C(3)	97.55(19)
C(15)-C(20)	1.506(4)	C(21)-U(1)-C(11)	114.9(3)
C(11B)-C(15B)	1.411(4)	C(13)-U(1)-C(11)	48.70(16)
C(11B)-C(12B)	1.411(4)	C(12)-U(1)-C(11)	29.41(10)
C(11B)-C(16B)	1.499(4)	C(14)-U(1)-C(11)	48.24(15)
C(12B)-C(13B)	1.411(4)	C(3)-U(1)-C(11)	138.76(19)
C(12B)-C(17B)	1.500(4)	C(21)-U(1)-C(14B)	128.3(3)
C(13B)-C(14B)	1.411(4)	C(4B)-U(1)-C(14B)	86.2(2)
C(13B)-C(18B)	1.500(4)	C(2B)-U(1)-C(14B)	114.62(19)
C(14B)-C(15B)	1.411(4)	C(3B)-U(1)-C(14B)	86.7(2)
C(14B)-C(19B)	1.499(4)	C(5B)-U(1)-C(14B)	116.07(19)
C(15B)-C(20B)	1.499(4)	C(1B)-U(1)-C(14B)	134.90(19)

C(21)-U(1)-C(2)	84.2(3)	C(5B)-U(1)-C(15B)	114.40(19)
C(13)-U(1)-C(2)	139.1(2)	C(1B)-U(1)-C(15B)	142.56(19)
C(12)-U(1)-C(2)	167.3(2)	C(14B)-U(1)-C(15B)	28.84(10)
C(14)-U(1)-C(2)	126.32(19)	C(22)-U(1)-C(15B)	97.1(2)
C(3)-U(1)-C(2)	28.80(9)	C(21)-U(1)-C(13B)	99.8(3)
C(11)-U(1)-C(2)	160.26(18)	C(4B)-U(1)-C(13B)	109.3(2)
C(21)-U(1)-C(4)	130.2(3)	C(2B)-U(1)-C(13B)	116.3(2)
C(13)-U(1)-C(4)	114.20(19)	C(3B)-U(1)-C(13B)	96.8(2)
C(12)-U(1)-C(4)	134.43(19)	C(5B)-U(1)-C(13B)	140.59(19)
C(14)-U(1)-C(4)	87.29(19)	C(1B)-U(1)-C(13B)	145.13(19)
C(3)-U(1)-C(4)	28.82(9)	C(14B)-U(1)-C(13B)	28.82(10)
C(11)-U(1)-C(4)	114.62(19)	C(22)-U(1)-C(13B)	124.6(3)
C(2)-U(1)-C(4)	47.21(14)	C(15B)-U(1)-C(13B)	47.35(15)
C(21)-U(1)-C(15)	138.3(3)	C(21)-U(1)-C(11B)	101.0(3)
C(13)-U(1)-C(15)	48.51(15)	C(4B)-U(1)-C(11B)	121.2(2)
C(12)-U(1)-C(15)	48.34(15)	C(2B)-U(1)-C(11B)	161.61(19)
C(14)-U(1)-C(15)	29.14(10)	C(3B)-U(1)-C(11B)	133.61(19)
C(3)-U(1)-C(15)	109.83(18)	C(5B)-U(1)-C(11B)	136.7(2)
C(11)-U(1)-C(15)	28.99(9)	C(1B)-U(1)-C(11B)	163.89(19)
C(2)-U(1)-C(15)	135.14(18)	C(14B)-U(1)-C(11B)	47.25(15)
C(4)-U(1)-C(15)	87.98(18)	C(22)-U(1)-C(11B)	80.8(2)
C(21)-U(1)-C(22)	68.7(3)	C(15B)-U(1)-C(11B)	28.59(9)
C(4B)-U(1)-C(22)	114.2(3)	C(13B)-U(1)-C(11B)	47.09(15)
C(2B)-U(1)-C(22)	117.4(3)	C(21)-U(1)-C(12B)	84.8(3)
C(3B)-U(1)-C(22)	137.9(3)	C(4B)-U(1)-C(12B)	133.4(2)
C(5B)-U(1)-C(22)	88.0(3)	C(2B)-U(1)-C(12B)	140.6(2)
C(13)-U(1)-C(22)	119.6(3)	C(3B)-U(1)-C(12B)	125.3(2)
C(12)-U(1)-C(22)	90.5(3)	C(5B)-U(1)-C(12B)	161.3(2)
C(1B)-U(1)-C(22)	89.9(3)	C(1B)-U(1)-C(12B)	167.6(2)
C(14)-U(1)-C(22)	133.5(2)	C(14B)-U(1)-C(12B)	47.24(15)
C(3)-U(1)-C(22)	125.2(3)	C(22)-U(1)-C(12B)	96.5(3)
C(11)-U(1)-C(22)	85.4(2)	C(15B)-U(1)-C(12B)	47.10(15)
C(14B)-U(1)-C(22)	125.2(2)	C(13B)-U(1)-C(12B)	28.57(10)
C(2)-U(1)-C(22)	98.0(3)	C(11B)-U(1)-C(12B)	28.45(9)
C(4)-U(1)-C(22)	120.6(3)	C(21)-U(1)-C(1)	97.1(3)
C(15)-U(1)-C(22)	109.4(2)	C(13)-U(1)-C(1)	160.48(19)
C(21)-U(1)-C(15B)	129.0(3)	C(12)-U(1)-C(1)	164.3(2)
C(4B)-U(1)-C(15B)	93.1(2)	C(14)-U(1)-C(1)	133.56(19)
C(2B)-U(1)-C(15B)	137.07(19)	C(3)-U(1)-C(1)	47.02(14)
C(3B)-U(1)-C(15B)	107.5(2)	C(11)-U(1)-C(1)	136.36(19)

C(2)-U(1)-C(1)	28.39(9)	C(21)-Si(1)-C(22)	108.6(4)
C(4)-U(1)-C(1)	46.78(14)	C(24)-Si(1)-C(22)	94.1(8)
C(15)-U(1)-C(1)	124.01(18)	C(23)-Si(1)-C(22)	104.1(5)
C(22)-U(1)-C(1)	79.4(3)	C(21)-Si(1)-C(24B)	108.7(8)
C(21)-U(1)-C(5)	125.3(3)	C(23)-Si(1)-C(24B)	102.3(9)
C(13)-U(1)-C(5)	137.07(19)	C(22)-Si(1)-C(24B)	117.0(9)
C(12)-U(1)-C(5)	142.68(19)	C(21)-Si(1)-U(1)	49.0(2)
C(14)-U(1)-C(5)	107.48(19)	C(24)-Si(1)-U(1)	120.5(7)
C(3)-U(1)-C(5)	47.03(14)	C(23)-Si(1)-U(1)	127.8(4)
C(11)-U(1)-C(5)	113.89(19)	C(22)-Si(1)-U(1)	59.6(3)
C(2)-U(1)-C(5)	46.78(14)	C(24B)-Si(1)-U(1)	129.8(8)
C(4)-U(1)-C(5)	28.39(9)	Si(2)-C(21)-Si(1)	111.1(5)
C(15)-U(1)-C(5)	96.15(19)	Si(1)-C(21)-Si(2B)	128.1(5)
C(22)-U(1)-C(5)	92.3(3)	Si(2)-C(21)-U(1)	151.5(5)
C(1)-U(1)-C(5)	28.17(9)	Si(1)-C(21)-U(1)	97.3(3)
C(21)-U(1)-Si(1)	33.6(2)	Si(2B)-C(21)-U(1)	134.5(5)
C(4B)-U(1)-Si(1)	134.96(15)	Si(1)-C(22)-U(1)	85.3(3)
C(2B)-U(1)-Si(1)	105.79(14)	C(21)-Si(2)-C(26)	118.4(15)
C(3B)-U(1)-Si(1)	135.32(15)	C(21)-Si(2)-C(25)	114.3(11)
C(5B)-U(1)-Si(1)	103.63(14)	C(26)-Si(2)-C(25)	105.7(17)
C(13)-U(1)-Si(1)	109.52(14)	C(21)-Si(2)-C(27)	107.9(12)
C(12)-U(1)-Si(1)	89.88(14)	C(26)-Si(2)-C(27)	107.4(18)
C(1B)-U(1)-Si(1)	89.13(14)	C(25)-Si(2)-C(27)	101.7(14)
C(14)-U(1)-Si(1)	137.67(14)	C(27B)-Si(2B)-C(26B)	109.1(14)
C(3)-U(1)-Si(1)	119.20(14)	C(27B)-Si(2B)-C(21)	117.6(12)
C(11)-U(1)-Si(1)	101.72(14)	C(26B)-Si(2B)-C(21)	111.9(12)
C(14B)-U(1)-Si(1)	135.97(14)	C(27B)-Si(2B)-C(25B)	107.3(16)
C(2)-U(1)-Si(1)	91.75(14)	C(26B)-Si(2B)-C(25B)	101.2(16)
C(4)-U(1)-Si(1)	135.02(14)	C(21)-Si(2B)-C(25B)	108.4(13)
C(15)-U(1)-Si(1)	130.69(14)	C(5)-C(1)-C(2)	108.0
C(22)-U(1)-Si(1)	35.1(2)	C(5)-C(1)-C(6)	126.0
C(15B)-U(1)-Si(1)	116.99(14)	C(2)-C(1)-C(6)	126.0
C(13B)-U(1)-Si(1)	115.78(14)	C(5)-C(1)-U(1)	75.9(2)
C(11B)-U(1)-Si(1)	90.75(14)	C(2)-C(1)-U(1)	73.9(2)
C(12B)-U(1)-Si(1)	90.10(14)	C(6)-C(1)-U(1)	116.3(2)
C(1)-U(1)-Si(1)	88.63(13)	C(3)-C(2)-C(1)	108.0
C(5)-U(1)-Si(1)	112.78(14)	C(3)-C(2)-C(7)	126.0
C(21)-Si(1)-C(24)	120.9(8)	C(1)-C(2)-C(7)	126.0
C(21)-Si(1)-C(23)	116.3(5)	C(3)-C(2)-U(1)	74.4(2)
C(24)-Si(1)-C(23)	109.2(8)	C(1)-C(2)-U(1)	77.7(2)

C(7)-C(2)-U(1)	114.2(2)	C(9B)-C(4B)-U(1)	133.1(2)
C(2)-C(3)-C(4)	108.0	C(5B)-C(4B)-U(1)	76.0(2)
C(2)-C(3)-C(8)	126.0	C(3B)-C(4B)-U(1)	74.5(2)
C(4)-C(3)-C(8)	126.0	C(1B)-C(5B)-C(4B)	112.8
C(2)-C(3)-U(1)	76.8(2)	C(1B)-C(5B)-C(10B)	132.3
C(4)-C(3)-U(1)	76.8(2)	C(4B)-C(5B)-C(10B)	114.9
C(8)-C(3)-U(1)	112.9(2)	C(1B)-C(5B)-U(1)	77.7(2)
C(5)-C(4)-C(3)	108.0	C(4B)-C(5B)-U(1)	72.7(2)
C(5)-C(4)-C(9)	126.0	C(10B)-C(5B)-U(1)	118.6(2)
C(3)-C(4)-C(9)	126.0	C(15)-C(11)-C(12)	108.0
C(5)-C(4)-U(1)	77.7(2)	C(15)-C(11)-C(16)	126.0
C(3)-C(4)-U(1)	74.4(2)	C(12)-C(11)-C(16)	126.0
C(9)-C(4)-U(1)	114.2(2)	C(15)-C(11)-U(1)	76.3(2)
C(4)-C(5)-C(1)	108.0	C(12)-C(11)-U(1)	72.9(2)
C(4)-C(5)-C(10)	126.0	C(16)-C(11)-U(1)	116.9(2)
C(1)-C(5)-C(10)	126.0	C(13)-C(12)-C(11)	108.0
C(4)-C(5)-U(1)	73.9(2)	C(13)-C(12)-C(17)	126.0
C(1)-C(5)-U(1)	75.9(2)	C(11)-C(12)-C(17)	126.0
C(10)-C(5)-U(1)	116.3(2)	C(13)-C(12)-U(1)	74.3(2)
C(5B)-C(1B)-C(2B)	105.7	C(11)-C(12)-U(1)	77.7(2)
C(5B)-C(1B)-C(6B)	123.1	C(17)-C(12)-U(1)	114.3(2)
C(2B)-C(1B)-C(6B)	131.2	C(14)-C(13)-C(12)	108.0
C(5B)-C(1B)-U(1)	73.4(2)	C(14)-C(13)-C(18)	126.0
C(2B)-C(1B)-U(1)	72.1(2)	C(12)-C(13)-C(18)	126.0
C(6B)-C(1B)-U(1)	118.3(2)	C(14)-C(13)-U(1)	77.1(2)
C(1B)-C(2B)-C(3B)	115.0	C(12)-C(13)-U(1)	75.8(2)
C(1B)-C(2B)-C(7B)	127.8	C(18)-C(13)-U(1)	113.5(2)
C(3B)-C(2B)-C(7B)	116.9	C(15)-C(14)-C(13)	108.0
C(1B)-C(2B)-U(1)	78.7(2)	C(15)-C(14)-C(19)	126.0
C(3B)-C(2B)-U(1)	75.8(2)	C(13)-C(14)-C(19)	126.0
C(7B)-C(2B)-U(1)	118.9(2)	C(15)-C(14)-U(1)	77.4(2)
C(2B)-C(3B)-C(8B)	126.6	C(13)-C(14)-U(1)	73.2(2)
C(2B)-C(3B)-C(4B)	104.2	C(19)-C(14)-U(1)	115.6(2)
C(8B)-C(3B)-C(4B)	127.2	C(11)-C(15)-C(14)	108.0
C(2B)-C(3B)-U(1)	74.6(2)	C(11)-C(15)-C(20)	126.0
C(8B)-C(3B)-U(1)	129.8(2)	C(14)-C(15)-C(20)	126.0
C(4B)-C(3B)-U(1)	72.2(2)	C(11)-C(15)-U(1)	74.7(2)
C(9B)-C(4B)-C(5B)	127.1	C(14)-C(15)-U(1)	73.5(2)
C(9B)-C(4B)-C(3B)	125.7	C(20)-C(15)-U(1)	117.7(2)
C(5B)-C(4B)-C(3B)	102.2	C(15B)-C(11B)-C(12B)	108.0

C(15B)-C(11B)-C(16B)	126.0	C(14B)-C(13B)-U(1)	74.8(2)
C(12B)-C(11B)-C(16B)	126.0	C(18B)-C(13B)-U(1)	114.6(2)
C(15B)-C(11B)-U(1)	74.6(2)	C(13B)-C(14B)-C(15B)	108.0
C(12B)-C(11B)-U(1)	75.8(2)	C(13B)-C(14B)-C(19B)	126.0
C(16B)-C(11B)-U(1)	115.8(2)	C(15B)-C(14B)-C(19B)	126.0
C(13B)-C(12B)-C(11B)	108.0	C(13B)-C(14B)-U(1)	76.3(2)
C(13B)-C(12B)-C(17B)	126.0	C(15B)-C(14B)-U(1)	76.3(2)
C(11B)-C(12B)-C(17B)	126.0	C(19B)-C(14B)-U(1)	113.8(2)
C(13B)-C(12B)-U(1)	74.6(2)	C(11B)-C(15B)-C(14B)	108.0
C(11B)-C(12B)-U(1)	75.7(2)	C(11B)-C(15B)-C(20B)	126.0
C(17B)-C(12B)-U(1)	115.8(2)	C(14B)-C(15B)-C(20B)	126.0
C(12B)-C(13B)-C(14B)	108.0	C(11B)-C(15B)-U(1)	76.8(2)
C(12B)-C(13B)-C(18B)	126.0	C(14B)-C(15B)-U(1)	74.9(2)
C(14B)-C(13B)-C(18B)	126.0	C(20B)-C(15B)-U(1)	114.5(2)
C(12B)-C(13B)-U(1)	76.8(2)		

References

(1) Wedal, J. C.; Bekoe, S.; Ziller, J. W.; Furche, F.; Evans, W. J. C–H Bond Activation via U(II) in the Reduction of Heteroleptic Bis(Trimethylsilyl)Amide U(III) Complexes. *Organometallics* **2020**, *39*, 3425–3432, DOI: 10.1021/acs.organomet.0c00496.

(2) Evans, W. J.; Nyce, G. W.; Forrestal, K. J.; Ziller, J. W. Multiple Syntheses of $(C_5Me_5)_3U$. *Organometallics* **2002**, *21*, 1050–1055, DOI: 10.1021/om010831t.

(3) Fagan, P. J.; Manriquez, J. M.; Marks, T. J.; Day, C. S.; Day, V. W.; Vollmer, S. H.; Day, V. W. Synthesis and Properties of a New Class of Highly Reactive Trivalent Actinide Organometallic Compounds. Derivatives of Bis(Pentamethylcyclopentadienyl)-Uranium(III). *Organometallics* **1982**, *1*, 170–180, DOI: 10.1021/om00061a028.

(4) Evans, W. J.; Miller, K. A.; Kozimor, S. A.; Ziller, J. W.; Dipasquale, A. G.; Rheingold, A. L. Actinide Hydride Complexes as Multielectron Reductants : Analogous Reduction Chemistry from $[(C_5Me_5)_2UH]_2$, and $[(C_5Me_5)_2ThH_2]_2$. *Organometallics* **2007**, *26*, 3568–3576, DOI: 10.1021/om7003139.

(5) Graves, C. R.; Scott, B. L.; Morris, D. E.; Kiplinger, J. L. Tetravalent and Pentavalent Uranium Acetylide Complexes Prepared by Oxidative Functionalization with CuC≡CPh. *Organometallics* **2008**, *27*, 3335–3337, DOI: 10.1021/om800466m.

(6) Wedal, J. C.; Windorff, C. J.; Huh, D. N.; Ryan, A. J.; Ziller, J. W.; Evans, W. J. Structural Variations in Cyclopentadienyl Uranium(III) Iodide Complexes. *J. Coord. Chem.* **2021**, *74*, 74–91, DOI: 10.1080/00958972.2020.1856824.

(7) Ward, R. J.; Pividori, D.; Carpentier, A.; Tarlton, M. L.; Kelley, S. P.; Maron, L.; Meyer, K.; Walensky, J. R. Isolation of a $[Fe(CO)_4]^{2-}$-Bridged Diuranium Complex Obtained via Reduction of $Fe(CO)_5$ with Uranium(III). *Organometallics* **2021**, *40*, 1411–1415, DOI: 10.1021/acs.organomet.1c00205.

(8) Webster, C. L.; Ziller, J. W.; Evans, W. J. Reactivity of U^{3+} Metallocene Allyl Complexes Leads to a Nanometer-Sized Uranium Carbonate, $[(C_5Me_5)_2U]_6(\mu\text{-}\kappa^1\text{:}\kappa^2\text{-}CO_3)_6$. *Organometallics* **2013**, *32*, 4820–4827, DOI: 10.1021/om400526h.

(9) Rungthanaphatsophon, P.; Barnes, C. L.; Kelley, S. P.; Walensky, J. R. Four-Electron Reduction Chemistry Using a Uranium(III) Phosphido Complex. *Dalton Trans.* **2018**, *47*, 8189–8192, DOI: 10.1039/C8DT01406J.

(10) Maynadié, J.; Berthet, J.-C.; Thuéry, P.; Ephritikhine, M. From Bent to Linear Uranium Metallocenes: Influence of Counterion, Solvent, and Metal Ion Oxidation State. *Organometallics* **2006**, *25*, 5603–5611, DOI: 10.1021/om060642g.

(11) Webster, C. L.; Bates, J. E.; Fang, M.; Ziller, J. W.; Furche, F.; Evans, W. J. Density Functional Theory and X-Ray Analysis of the Structural Variability in η^5,η^5,η^1-Tris(Ring) Rare Earth/Actinide Tetramethylpyrrolyl Complexes, $(C_5Me_5)_2M(NC_4Me_4)$. *Inorg. Chem.* **2013**, *52*, 3565–3572, DOI: 10.1021/ic300905r.

(12) Guzei, I. A.; Wendt, M. An Improved Method for the Computation of Ligand Steric Effects Based on Solid Angles. *Dalton Trans.* **2006**, No. 33, 3991, DOI: 10.1039/b605102b.

(13) Avens, L. R.; Burns, C. J.; Butcher, R. J.; Clark, D. L.; Gordon, J. C.; Schake, A. R.; Scott, B. L.; Watkin, J. G.; Zwick, B. D. Mono(Pentamethylcyclopentadienyl)Uranium(III) Complexes: Synthesis, Properties, and X-Ray Structures of (η-C_5Me_5)$UI_2(THF)_3$, (η-C_5Me_5)$UI_2(Py)_3$, and (η-C_5Me_5)$U[N(SiMe_3)_2]_2$. *Organometallics* **2000**, *19*, 451–457, DOI: 10.1021/om990718r.

(14) Chamberlain, L. R.; Rothwell, I. P.; Huffman, J. C. Chemistry of Sterically Crowded Aryloxide Ligands. 4. Synthesis and Structure of Mixed Chloro Aryloxides of Tantalum. *Inorg. Chem.* **1984**, *23*, 2575–2578, DOI: 10.1021/ic00185a008.

(15) Coffindaffer, T. W.; Rothwell, I. P.; Huffman, J. C. Dinuclear Arlyoxide Chemistry. 1. A Direct Comparison of Aryloxide and Alkoxide Coordination to a Dimetal Center. Synthesis and Structure of 1,2-Bis(Isopopoxy)Tetrakis(2,6-Dimethylphenoxy)Dimolybdenum (Mo=Mo). *Inorg. Chem.* **1983**, *22*, 2906–2910.

(16) Howard, W. A.; Trnka, T. M.; Parkin, G. Syntheses of the Phenylchalcogenolate Complexes (η^5-$C_5Me_5)_2Zr(EPh)_2$ (E = O, S, Se, Te) and (η^5-$C_5H_5)_2Zr(OPh)_2$: Structural Comparisons within a Series of Complexes Containing Zirconium-Chalcogen Single Bonds. *Inorg. Chem.* **1995**, *34*, 5900–5909, DOI: 10.1021/ic00127a031.

(17) Steffey, B. D.; Fanwick, P. E.; Rothwell, I. P. Solid State Structure of the Tantalum Bis-Aryl Compounds $Ta(OAr\text{-}2,6R_2)_3(C_6H_5)_2$ (R = CH_3, Pr^i; $OAr\text{-}2,6R_2$ = 2,6-Dialkylphenoxide): Observation of a Lack of Correlation of M-OAr Distances and M-O-Ar Angles for Aryloxide Derivatives of Niobium(V) and Tantalum. *Polyhedron* **1990**, *9*, 963–968, DOI: 10.1016/S0277-5387(00)84298-9.

(18) Russo, M. R.; Kaltsoyannis, N.; Sella, A. Are Metal Alkoxides Linear Owing to Electrostatic Repulsion? *Chem. Commun.* **2002**, *2*, 2458–2459, DOI: 10.1039/b207435d.

(19) Hillier, A. C.; Liu, S.-Y.; Sella, A.; Elsegood, M. R. J. Lanthanide Chalcogenolate Complexes: Synthesis and Crystal Structures of the Isoleptic Series [Sm($Tp^{Me,Me}$)$_2$ER] (E = O, S, Se, Te; $Tp^{Me,Me}$= tris-3,5-Dimethylpyrazolylborate). *Inorg. Chem.* **2000**, *39*, 2635–2644, DOI: 10.1021/ic9914793.

(20) Evans, W. J.; Traina, C. A.; Ziller, J. W. Synthesis of Heteroleptic Uranium (μ–η^6:η^6-C_6H_6)$^{2-}$ Sandwich Complexes via Facile Displacement of (η^5-C_5Me_5)$^{1-}$ by Ligands of Lower Hapticity and Their Conversion to Heteroleptic Bis(Imido) Compounds. *J. Am. Chem. Soc.* **2009**, *131*, 17473–17481, DOI: 10.1021/ja9075259.

(21) Castro-Rodriguez, I.; Nakai, H.; Gantzel, P.; Zakharov, L. N.; Rheingold, A. L.; Meyer, K. Evidence for Alkane Coordination to an Electron-Rich Uranium Center. *J. Am. Chem. Soc.* **2003**, *125*, 15734–15735, DOI: 10.1021/ja0379316.

(22) Arnold, P. L.; Farnaby, J. H.; Gardiner, M. G.; Love, J. B. Uranium(III) Coordination Chemistry and Oxidation in a Flexible Small-Cavity Macrocycle. *Organometallics* **2015**, *34*, 2114–2117, DOI: 10.1021/om5012193.

(23) Arnold, P. L.; Mansell, S. M.; Maron, L.; McKay, D. Spontaneous Reduction and C-H Borylation of Arenes Mediated by Uranium(III) Disproportionation. *Nat. Chem.* **2012**, *4*, 668–674, DOI: 10.1038/nchem.1392.

(24) Hoerger, C. J.; La Pierre, H. S.; Maron, L.; Scheurer, A.; Heinemann, F. W.; Meyer, K. Reductive Disproportionation of Nitric Oxide Mediated by Low-Valent Uranium. *Chem. Commun.* **2016**, *52*, 10854–10857, DOI: 10.1039/c6cc06095a.

(25) Mansell, S. M.; Kaltsoyannis, N.; Arnold, P. L. Small Molecule Activation by Uranium

Tris(Aryloxides): Experimental and Computational Studies of Binding of N_2, Coupling of CO, and Deoxygenation Insertion of CO_2 under Ambient Conditions. *J. Am. Chem. Soc.* **2011**, *133*, 9036–9051, DOI: 10.1021/ja2019492.

(26) Schumann, H.; Meese-Marktscheffel, J. A.; Esser, L. Synthesis, Structure, and Reactivity of Organometallic π-Complexes of the Rare Earths in the Oxidation State Ln^{3+} with Aromatic Ligands. *Chem. Rev.* **1995**, *95*, 865–986, DOI: 10.1021/cr00036a004.

(27) Shannon, R. D. Revised Effective Ionic Radii and Systematic Studies of Interatomic Distances in Halides and Chalcogenides. *Acta Crystallogr. Sect. A* **1976**, *32*, 751–767, DOI: 10.1107/S0567739476001551.

(28) Jeske, G.; Lauke, H.; Mauermann, H.; Swepston, P. N.; Schumann, H.; Marks, T. J. Highly Reactive Organolanthanides. Systematic Routes to and Olefin Chemistry of Early and Late Bis(Pentamethylcyclopentadienyl) 4f Hydrocarbyl and Hydride Complexes. *J. Am. Chem. Soc.* **1985**, *107*, 8091–8103, DOI: 10.1021/ja00312a050.

(29) Evans, W. J.; Keyer, R. A.; Ziller, J. W. Investigation of Organolanthanide-Based Carbon-Carbon Bond Formation: Synthesis, Structure, and Coupling Reactivity of Organolanthanide Alkynide Complexes, Including the Unusual Structures of the Trienediyl Complex $[(C_5Me_5)_2Sm]_2[\mu\text{-}\eta^2\text{:}\eta^2\text{-}Ph(CH_2)_2C{=}C{=}C{=}C(CH_2)_2Ph$ and the Unsolvated Alkynide $[(C_5Me_5)_2Sm(C{\equiv}CCMe_3)]_2$. *Organometallics* **1993**, *12*, 2618–2633, DOI: 10.1021/om00031a036.

(30) del Mar Conejo, M.; Parry, J. S.; Carmona, E.; Schultz, M.; Brennann, J. G.; Beshouri, S. M.; Andersen, R. A.; Rogers, R. D.; Coles, S.; Hursthouse, M. B. Carbon Monoxide and Isocyanide Complexes of Trivalent Uranium Metallocenes. *Chem. Eur. J.* **1999**, *5*, 3000–3009, DOI: 10.1002/(SICI)1521-3765(19991001)5:10<3000::AID-

CHEM3000>3.0.CO;2-Q.

(31) Evans, W. J.; Forrestal, K. J.; Ziller, J. W. Activity of [Sm(C_5Me_5)$_3$] in Ethylene Polymerization and Synthesis of [U(C_5Me_5)$_3$], the First Tris(Pentamethylcyclopentadienyl) 5f-Element Complex. *Angew. Chem. Int. Ed.* **1997**, *36*, 774–776, DOI: 10.1002/anie.199707741.

(32) Moehring, S. A.; Beltran-Leiva, M.; Paez-Hernandez, D.; Arratia-Perez, R.; Ziller, J. W.; Evans, W. J. Rare-Earth Metal (II) Aryloxides: Structure, Synthesis, and EPR Spectroscopy of [K(2.2.2-Cryptand)][Sc($OC_6H_2{}^tBu_2$-2,6-Me-4)$_3$]. *Chem. Eur. J.* **2018**, *24*, 18059–18067, DOI: 10.1002/chem.201803807.

(33) Moehring, S. A.; Miehlich, M.; Hoerger, C. J.; Meyer, K.; Ziller, J. W.; Evans, W. J. A Room-Temperature Stable Y(II) Aryloxide: Using Steric Saturation to Kinetically Stabilize Y(II) Complexes. *Inorg. Chem.* **2020**, *59*, 3207–3214, DOI: 10.1021/acs.inorgchem.9b03587.

(34) Evans, W. J.; Ulibarri, T. A. Reactivity of (C_5Me_5)$_2$Sm With Cyclopentadiene and Cyclopentadienide: Isolation of The Mixed-Valent Complex (C_5Me_5)$_2$Sm^{III}(μ-C_5H_5)Sm^{II}(C_5Me_5)$_2$. *J. Am. Chem. Soc.* **1987**, *109*, 4292–4297, DOI: 10.1021/ja00248a025.

(35) Tanner, P. S.; Burkey, D. J.; Hanusa, T. P. Cyclopentadienyl Ring Metathesis with Bis(Pentamethylcyclopentadienyl)Calcium as a Route to Mixed Ring Organolanthanide Complexes; the Crystal Structure of (C_5Me_5)$_2$Nd(C_5H_5). *Polyhedron* **1995**, *14*, 331–333, DOI: 10.1016/0277-5387(94)00316-7.

(36) Demir, S.; Mueller, T. J.; Ziller, J. W.; Evans, W. J. Tris(Polyalkylcyclopentadienyl) Complexes: The Elusive [(η^5-C_5R_5)$_2$M(η^1-C_5R_5)] Structure and Trihapto Cyclopentadienyl

Coordination Involving a Methyl Substituent. *Angew. Chem. Int. Ed.* **2011**, *50*, 515–518, DOI: 10.1002/anie.201005898.

(37) Fieser, M. E.; Bates, J. E.; Ziller, J. W.; Furche, F.; Evans, W. J. Dinitrogen Reduction via Photochemical Activation of Heteroleptic Tris(Cyclopentadienyl) Rare-Earth Complexes. *J. Am. Chem. Soc.* **2013**, *135*, 3804–3807, DOI: 10.1021/ja400664s.

(38) Evans, W. J.; Davis, B. L. Chemistry of Tris (Pentamethylcyclopentadienyl) f-Element Complexes, $(C_5Me_5)_3M$. *Chem. Rev.* **2002**, *102*, 2119–2136, DOI: 10.1021/cr010298r.

(39) Evans, W. J.; Walensky, J. R.; Furche, F.; Ziller, J. W.; DiPasquale, A. G.; Rheingold, A. L. Synthesis of $(C_5Me_5)_2(C_5Me_4H)UMe$, $(C_5Me_5)_2(C_5H_5)UMe$, and $(C_5Me_5)_2UMe[CH(SiMe_3)_2]$ from Cationic Metallocenes for the Evaluation of Sterically Induced Reduction. *Inorg. Chem.* **2008**, *47*, 10169–10176, DOI: 10.1021/ic801232e.

(40) Arduini, A. L.; Takats, J. Reactivity of Dicyclopentadienylbis(Diethylamido)-Uranium(IV). Reactions with Carboxylic and Thiocarboxylic Acids. *Inorg. Chem.* **1981**, *20*, 2480–2485, DOI: 10.1021/ic50222a023.

(41) Evans, W. J.; Seibel, C. A.; Ziller, J. W. Organosamarium-Mediated Transformations of CO_2 and COS: Monoinsertion and Disproportionation Reactions and the Reductive Coupling of CO2 to [O2CCO2]2-. *Inorg. Chem.* **1998**, *37*, 770–776, DOI: 10.1021/ic971381t.

(42) Evans, W. J.; Rego, D. B.; Ziller, J. W.; DiPasquale, A. G.; Rheingold, A. L. Facile Insertion of CO_2 into Tetra- and Pentamethylcyclopentadienyl Lanthanide Moieties To Form $(C_5Me_4RCO_2)^-$ Carboxylate Ligands (R = H, Me). *Organometallics* **2007**, *26*, 4737–4745, DOI: 10.1021/om070223z.

(43) La Pierre, H. S.; Kameo, H.; Halter, D. P.; Heinemann, F. W.; Meyer, K. Coordination and

Redox Isomerization in the Reduction of a Uranium(III) Monoarene Complex. *Angew. Chem. Int. Ed.* **2014**, *53*, 7154–7157, DOI: 10.1002/anie.201402048.

(44) Wedal, J. C.; Barlow, J. M.; Ziller, J. W.; Yang, J. Y.; Evans, W. J. Electrochemical Studies of Tris(Cyclopentadienyl)Thorium and Uranium Complexes in the +2, +3, and +4 Oxidation States. *Chem. Sci.* **2021**, *12*, 8501–8511, DOI: 10.1039/D1SC01906F.

(45) Evans, W. J.; Kozimor, S. A. Expanding the Chemistry of U^{3+} Reducing Agents. *Coord. Chem. Rev.* **2006**, *250*, 911–935, DOI: 10.1016/j.ccr.2006.01.017.

(46) Morris, D. E.; Da Re, R. E.; Jantunen, K. C.; Castro-Rodriguez, I.; Kiplinger, J. L. Trends in Electronic Structure and Redox Energetics for Early-Actinide Pentamethylcyclopentadienyl Complexes. *Organometallics* **2004**, *23*, 5142–5153, DOI: 10.1021/om049634v.

(47) Inman, C. J.; Cloke, F. G. N. The Experimental Determination of Th(IV)/Th(III) Redox Potentials in Organometallic Thorium Complexes. *Dalton Trans.* **2019**, *48*, 10782–10784, DOI: 10.1039/c9dt01553a.

(48) Guo, F. S.; Tsoureas, N.; Huang, G. Z.; Tong, M. L.; Mansikkamäki, A.; Layfield, R. A. Isolation of a Perfectly Linear Uranium(II) Metallocene. *Angew. Chem. Int. Ed.* **2020**, *59*, 2299–2303, DOI: 10.1002/anie.201912663.

(49) Zachmanoglou, C. E.; Docrat, A.; Bridgewater, B. M.; Parkin, G.; Brandow, C. G.; Bercaw, J. E.; Jardine, C. N.; Lyall, M.; Green, J. C.; Keister, J. B. The Electronic Influence of Ring Substituents and Ansa Bridges in Zirconocene Complexes as Probed by Infrared Spectroscopic, Electrochemical, and Computational Studies. *J. Am. Chem. Soc.* **2002**, *124*, 9525–9546, DOI: 10.1021/ja020236y.

(50) MacDonald, M. R.; Fieser, M. E.; Bates, J. E.; Ziller, J. W.; Furche, F.; Evans, W. J.

Identification of the +2 Oxidation State for Uranium in a Crystalline Molecular Complex, [K(2.2.2-Cryptand)][($C_5H_4SiMe_3$)$_3$U]. *J. Am. Chem. Soc.* **2013**, *135*, 13310–13313, DOI: 10.1021/ja406791t.

(51) Windorff, C. J.; MacDonald, M. R.; Meihaus, K. R.; Ziller, J. W.; Long, J. R.; Evans, W. J. Expanding the Chemistry of Molecular U2+ Complexes: Synthesis, Characterization, and Reactivity of the {[C_5H_3($SiMe_3$)$_2$]$_3$U}$^-$ Anion. *Chem. Eur. J.* **2016**, *22*, 772–782, DOI: 10.1002/chem.201503583.

(52) Ryan, A. J.; Angadol, M. A.; Ziller, J. W.; Evans, W. J. Isolation of U(II) Compounds Using Strong Donor Ligands, C_5Me_4H and N($SiMe_3$)$_2$, Including a Three-Coordinate U(II) Complex. *Chem. Commun.* **2019**, *55*, 2325–2327, DOI: 10.1039/C8CC08767A.

(53) Huang, R. H.; Faber, M. K.; Moeggenborg, K. J.; Ward, D. L.; Dye, J. L. Structure of K+(Cryptand[2.2.2]) Electride and Evidence for Trapped Electron Pairs. *Nature* **1988**, *331*, 599–601, DOI: 10.1038/331599a0.

(54) La Pierre, H. S.; Scheurer, A.; Heinemann, F. W.; Hieringer, W.; Meyer, K. Synthesis and Characterization of a Uranium(II) Monoarene Complex Supported by δ Backbonding. *Angew. Chem. Int. Ed.* **2014**, *53*, 7158–7162, DOI: 10.1002/anie.201402050.

(55) Jenkins, T. F.; Woen, D. H.; Mohanam, L. N.; Ziller, J. W.; Furche, F.; Evans, W. J. Tetramethylcyclopentadienyl Ligands Allow Isolation of Ln(II) Ions across the Lanthanide Series in [K(2.2.2-Cryptand)][(C_5Me_4H)$_3$Ln] Complexes. *Organometallics* **2018**, *37*, 3863–3873, DOI: 10.1021/acs.organomet.8b00557.

(56) Jenkins, T. F.; Bekoe, S.; Ziller, J. W.; Furche, F.; Evans, W. J. Synthesis of a Heteroleptic Pentamethylcyclopentadienyl Yttrium(II) Complex, [K(2.2.2-Cryptand)]{(C_5Me_5)$_2$$Y^{II}$[N($SiMe_3$)$_2$]}, and Its C–H Bond Activated Y(III) Derivative.

Organometallics **2021**, *40*, 3917–3925, DOI: 10.1021/acs.organomet.1c00482.

(57) Staroverov, V. N.; Scuseria, G. E.; Tao, J.; Perdew, J. P. Comparative Assessment of a New Nonempirical Density Functional: Molecules and Hydrogen-Bonded Complexes. *J. Chem. Phys.* **2003**, *119*, 12129–12137, DOI: 10.1063/1.1626543.

(58) Schäfer, A.; Klamt, A.; Sattel, D.; Lohrenz, J. C. W.; Eckert, F. COSMO Implementation in TURBOMOLE: Extension of an Efficient Quantum Chemical Code towards Liquid Systems. *Phys. Chem. Chem. Phys.* **2000**, *2*, 2187–2193, DOI: 10.1039/b000184h.

(59) CRC Handbook of Chemistry and Physics. In *CRC Handbook of Chemistry and Physics*; Haynes, W. M., Lide, D. R., Bruno, T. J., Eds.; CRC Press, 2016; pp 943–950.

(60) Bates, J. E.; Furche, F. Harnessing the Meta-Generalized Gradient Approximation for Time-Dependent Density Functional Theory. *J. Chem. Phys.* **2012**, *137*, 164105, DOI: 10.1063/1.4759080.

(61) Ryan, A. J.; Darago, L. E.; Balasubramani, S. G.; Chen, G. P.; Ziller, J. W.; Furche, F.; Long, J. R.; Evans, W. J. Synthesis, Structure, and Magnetism of Tris(Amide) $[Ln\{N(SiMe3)2\}_3]^{1-}$ Complexes of the Non-Traditional +2 Lanthanide Ions. *Chem. Eur. J.* **2018**, *24*, 7702–7709, DOI: 10.1002/chem.201800610.

(62) Balasubramani, S. G.; Chen, G. P.; Coriani, S.; Diedenhofen, M.; Frank, M. S.; Franzke, Y. J.; Furche, F.; Grotjahn, R.; Harding, M. E.; Hättig, C.; Hellweg, A.; Helmich-Paris, B.; Holzer, C.; Huniar, U.; Kaupp, M.; Marefat Khah, A.; Karbalaei Khani, S.; Müller, T.; Mack, F.; Nguyen, B. D.; Parker, S. M.; Perlt, E.; Rappoport, D.; Reiter, K.; Roy, S.; Rückert, M.; Schmitz, G.; Sierka, M.; Tapavicza, E.; Tew, D. P.; van Wüllen, C.; Voora, V. K.; Weigend, F.; Wodyński, A.; Yu, J. M. TURBOMOLE: Modular Program Suite for Ab Initio Quantum-Chemical and Condensed-Matter Simulations. *J. Chem. Phys.* **2020**, *152*,

184107, DOI: 10.1063/5.0004635.

(63) TURBOMOLE V7.4.1. University of Karlsruhe and Forschungszentrum Karlsruhe GmbH.

(64) Wedal, J. C.; Furche, F.; Evans, W. J. Density Functional Theory Analysis of the Importance of Coordination Geometry for $5f^3 6d^1$ versus $5f^4$ Electron Configurations in U(II) Complexes. *Inorg. Chem.* **2021**, *60*, 16316–16325, DOI: 10.1021/acs.inorgchem.1c02161.

(65) Huh, D. N.; Ziller, J. W.; Evans, W. J. Chelate-Free Synthesis of the U(II) Complex, $[(C_5H_3(SiMe_3)_2)_3U]^{1-}$, Using Li and Cs Reductants and Comparative Studies of La(II) and Ce(II) Analogs. *Inorg. Chem.* **2018**, *57*, 11809–11814, DOI: 10.1021/acs.inorgchem.8b01966.

(66) Wedal, J. C.; Bekoe, S.; Ziller, J. W.; Furche, F.; Evans, W. J. In Search of Tris(Trimethylsilylcyclopentadienyl) Thorium. *Dalton Trans.* **2019**, *48*, 16633–16640, DOI: 10.1039/C9DT03674A.

(67) Guzei, I. A.; Wendt, M. Solid-G. Madison, WI 2004.

(68) Modder, D. K.; Palumbo, C. T.; Douair, I.; Fadaei-Tirani, F.; Maron, L.; Mazzanti, M. Delivery of a Masked Uranium(II) by an Oxide-Bridged Diuranium(III) Complex. *Angew. Chem. Int. Ed.* **2021**, *60*, 3737–3744, DOI: 10.1002/anie.202013473.

(69) Hitchcock, P. B.; Lappert, M. F.; Leung, W.-P.; Diansheng, L.; Shun, T. Synthesis and Structures of the Heavier Alkali Metal Alkyls; the X-Ray Structures of $[Na(\mu\text{-}R)]_\infty$ and $[Rb(\mu\text{-}R)(Pmdeta)]_2$ [R = $CH(SiMe_3)_2$, Pmdeta = $(Me_2NCH_2CH_2)_2NMe$]. *J. Chem. Soc., Chem. Commun.* **1993**, No. 18, 1386–1387, DOI: 10.1039/C39930001386.

(70) Davidson, P. J.; Harris, D. H.; Lappert, M. F. Subvalent Group 4B Metal Alkyls and Amides. Part I. The Synthesis and Physical Properties of Kinetically Stable Bis[Bis(Trimethysilyl)Methyl]- Germanium(II), -Tin(II), and -Lead(II). *J. Chem. Soc.,*

Dalton Trans. **1976**, *21*, 2268–2274, DOI: 10.1039/DT9760002268.

(71) Carmichael, C. D.; Jones, N. A.; Arnold, P. L. Low-Valent Uranium Iodides: Straightforward Solution Syntheses of UI_3 and UI_4 Etherates. *Inorg. Chem.* **2008**, *47*, 8577–8579, DOI: 10.1021/ic801138e.

(72) Panda, T. K.; Gamer, M. T.; Roesky, P. W. An Improved Synthesis of Sodium and Potassium Cyclopentadienide. *Organometallics* **2003**, *22*, 877–878, DOI: 10.1021/om0207865.

(73) Evans, W. J.; Kozimor, S. A.; Ziller, J. W.; Fagin, A. A.; Bochkarev, M. N. Facile Syntheses of Unsolvated UI_3 and Tetramethylcyclopentadienyl Uranium Halides. *Inorg. Chem.* **2005**, *44*, 3993–4000, DOI: 10.1021/ic0482685.

(74) Van der Sluys, W. G.; Burns, C. J.; Huffman, J. C.; Sattelberger, A. P. Uranium Alkoxide Chemistry. 1. Synthesis and the Novel Dimeric Structure of the First Homoleptic Uranium(III) Aryloxide Complex. *J. Am. Chem. Soc.* **1988**, *110*, 5924–5925, DOI: 10.1021/ja00225a067.

(75) Bergbreiter, D. E.; Killough, J. M. Reactions of Potassium-Graphite. *J. Am. Chem. Soc.* **1978**, *100*, 2126–2134, DOI: 10.1021/ja00475a025.

(76) Cetinkaya, B.; Gumrukcu, I.; Lappert, M. F.; Atwood, J. L.; Shakir, R. Lithium and Sodium 2,6-Di-Tert-Butylphenoxides and the Crystal and Molecular Structure of $[Li(OC_6H_2Me\text{-}4\text{-}Bu^t_2\text{-}2,6)(OEt_2)]_2$. *J. Am. Chem. Soc.* **1980**, *102*, 2086–2088, DOI: 10.1021/ja00526a053.

(77) Watanabe, T.; Ishida, Y.; Matsuo, T.; Kawaguchi, H. Syntheses and Structures of Zirconium(IV) Complexes Supported by 2,6-Di-Adamantylaryloxide Ligands and Formation of Arene-Bridged Dizirconium Complexes with an Inverse Sandwich Structure. *Dalton Trans.* **2010**, *39*, 484–491, DOI: 10.1039/B911082H.

(78) Grimme, S. Semiempirical GGA-Type Density Functional Constructed with a Long-Range Dispersion Correction. *J. Comput. Chem.* **2006**, *27*, 1787–1799, DOI: 10.1002/jcc.20495.

(79) Weigend, F.; Köhn, A.; Hättig, C. Efficient Use of the Correlation Consistent Basis Sets in Resolution of the Identity MP2 Calculations. *J. Chem. Phys.* **2002**, *116*, 3175–3183, DOI: 10.1063/1.1445115.

(80) Andrae, D.; Häußermann, U.; Dolg, M.; Stoll, H.; Preuß, H. Energy-Adjusted Ab Initio Pseudopotentials for the Second and Third Row Transition Elements. *Theor. Chim. Acta* **1990**, *77*, 123–141, DOI: 10.1007/BF01114537.

(81) Cao, X.; Dolg, M. Segmented Contraction Scheme for Small-Core Actinide Pseudopotential Basis Sets. *J. Mol. Struct.* **2004**, *673*, 203–209, DOI: 10.1016/j.theochem.2003.12.015.

(82) Schäfer, A.; Horn, H.; Ahlrichs, R. Fully Optimized Contracted Gaussian Basis Sets for Atoms Li to Kr. *J. Chem. Phys.* **1992**, *97*, 2571–2577.

(83) Treutler, O.; Ahlrichs, R. Efficient Molecular Numerical Integration Schemes. *J. Chem. Phys.* **1995**, *102*, 346–354, DOI: 10.1063/1.469408.

(84) Deglmann, P.; Furche, F.; Ahlrichs, R. An Efficient Implementation of Second Analytical Derivatives for Density Functional Methods. *Chem. Phys. Lett.* **2002**, *362*, 511–518, DOI: 10.1016/S0009-2614(02)01084-9.

(85) Humphrey, W.; Dalke, A.; Schulten, K. VMD: Visual Molecular Dynamics. *J. Mol. Graph.* **1996**, *14*, 33–38.

(86) APEX2, Version 2014.11-0, Bruker AXS, Inc: Madison, WI 2014.

(87) SAINT, Version 8.34a, Bruker AXS, Inc: Madison, WI 2013.

(88) Sheldrick, G. M. SADABS. Version 2014/5, Bruker AXS, Inc: Madison, WI 2014.

(89) Sheldrick, G. M. SHELXTL. Verison 2014/7, Bruker AXS, Inc: Madison, WI 2014.

(90) *International Tables for Crystallography*; Vol C, Kluwer Academic Publishers: Dordrecht, 1992.

(91) Parsons, S.; Flack, H. D.; Wagner, T. Use of Intensity Quotients and Differences in Absolute Structure Refinement. *Acta Crystallogr. Sect. B Struct. Sci. Cryst. Eng. Mater.* **2013**, *69*, 249–259, DOI: 10.1107/S2052519213010014.

(92) Sheldrick, G. M. CELL_NOW, Vesion 2008/4, Bruker AXS, Inc: Madison, WI 2008.

(93) Sheldrick, G. M. TWINABS, Version 2012/1 Bruker AXS, Inc: Madison, WI 2012.

Chapter 6:

EPR Spectroscopy of $5f^3 6d^1$ U(II) Complexes

Introduction

The use of EPR spectroscopy to analyze the electronic structure of uranium compounds is challenging. U(III) compounds have a $5f^3$ electron configuration which affords an overall ^{4}I ground state ($S = 3/2$, $L = 6$, $J = 9/2$). However, significant spin-orbit coupling mixes other states[1,2] which complicates magnetic analysis.[3] EPR spectra of U(III) compounds have been reported and quite significant differences are observed across different molecular systems. For example, the $U(NHAr^{iPr6})_2I$ complex of Boncella and Odom displays two well-defined peaks at $g = 5.17$ and 4.56,[4] whereas the EPR spectrum of Cp''_3U reported by Lukens has two discernable g values of 2.44 and 2.06.[1]

EPR spectroscopy has also been collected on U(II) compounds. Both [K(crypt)]{[(^{Ad,Me}ArO)$_3$mes]U} and $U(NHAr^{iPr6})_2$ are EPR silent in both perpendicular and parallel modes.[4,5] Both of these compounds have been assigned $5f^4$ electron configurations, and to a simple approximation it can be understood that a diamagnetic ground state is isolated at low temperatures where all four electrons spin-pair. However, EPR studies have not been performed on U(II) compounds that have mixed-principal quantum number $5f^3 6d^1$ electron configurations. It would be useful to have a definitive EPR spectrum of a $5f^3 6d^1$ U(II) compound, as has been done for $6d^1$ Th(III) compounds, so that these compounds can be recognized by EPR and UV-visible spectroscopy before crystallographic confirmation. To this end, this Chapter reports EPR studies of ten U(III) complexes and their analogous U(II) reduction products, along with comparison studies on lanthanide compounds and a discussion of superhyperfine interactions of uranium

compounds with nitrogen-containing ligands. All samples were prepared at UCI. Data were collected either at UC Irvine with the assistance of Meghen Goulet and Professor A. S. Borovik, or at Lawrence Berkeley National Laboratory (LBNL) by Dr. Wayne Lukens, or at UC Davis by David Villareal, Wen Fu, and Professor Dave Britt.

Results

Sample preparation. The homoleptic U(II) compounds $[K(crown)(THF)_2][Cp''_3U]$,[6] $[K(crypt)][Cp'_3U]$,[7] $[K(crypt)][Cp^{tet}_3U]$,[8] and $[K(crypt)][U(NR_2)_3]$[8] ($R = SiMe_3$) were synthesized via literature routes[6–8] and isolated as crystalline material. For solid samples, these crystalline solids were ground in a mortar and pestle and placed in the EPR tube for data collection. For solution measurements, the crystalline solids were dissolved in THF, placed in the EPR tube, and immediately frozen at 77 K. The heteroleptic U(II) compounds $[K(crypt)][(C_5Me_5)_2U(NR_2)]$, $[K(crypt)][(C_5Me_5)U(NR_2)_2]$, $[K(crypt)][(C_5Me_5)_2U(Cp^{tet})]$, $[K(crypt)][(C_5Me_5)_2U(C_5H_5)]$, and $[K(crypt)][(C_5Me_5)_2U(NPh_2)]$ were generated via reduction of the trivalent species with KC_8 and cryptand at low temperature in THF (see Chapter 4 and 5)[9,10] and immediately placed in the EPR sample tube for data collection since the compounds decompose readily. $U(OAr)_3$[11] ($OAr = OC_6H_3{}^tBu_2$-2,6) was reduced similarly with crypt and KC_8 in THF to generate the species "$[K(crypt)][U(OAr)_3]$" and immediately frozen.

U(II) spectra. The EPR spectra of the crystallographically confirmed U(II) compounds and the solutions of the reduction products were collected at 10 K and 77 K at UCI. None of the samples displayed a signal in parallel mode. The perpendicular mode spectra of nine U(II) compounds at 77 K are shown below in Figure 6.1. Individual spectra at 10 K and 77 K are shown in the following Figures 6.2-6.11. The same sample was used to collect the spectra at both temperatures. Interestingly, each compound displays a similar two-line, pseudoaxial spectrum

with *g* values of approximately 2.04 and 2.00, Table 6.1. Many of these spectra were better resolved at 77 K than at 10 K.

Table 6.1: *g* values for U(II) compounds from EPR at 77 K (R = $SiMe_3$, OAr = $OC_6H_3{}^tBu_2$-2,6)

	g values
[K(crypt)][$Cp^{tet}{}_3U$]	3.005, 2.04, 2.01
[K(crown)$(THF)_2$][Cp''_3U]	2.04, 2.01
[K(crypt)][Cp'_3U]	2.04, 2.01
[K(crypt)][$(C_5Me_5)_2UCp^{tet}$]	2.04, 2.00
[K(crypt)][$(C_5Me_5)_2U(NR_2)$]	2.04, 2.00
[K(crypt)][$U(OAr)_3$]	2.04, 2.00
[K(crypt)][$U(NR_2)_3$]	2.04, 2.00
[K(crypt)][$(C_5Me_5)_2U(C_5H_5)$]	2.04, 2.00
[K(crypt)][$(C_5Me_5)_2U(NPh_2)$]	2.04, 2.00
[K(crypt)][$(C_5Me_5)U(NR_2)_2$]	2.04, 2.00

U(III) spectra. Most of the U(III) compounds, the precursors to the U(II) species above, showed no signal at 77 K. This is consistent with literature reports and has been explained due to the rapid spin-lattice relaxation of the f electrons where lower temperatures are needed to observe a spectrum. Indeed at 5 K $Cp^{tet}{}_3U$ displays a weak feature at low field and a strong signal at higher field, Figure 6.12. The data were modelled with *g* values of 2.380, 2.195, and 1.985. This signal is clearly different than the spectrum of [K(crypt)][$Cp^{tet}{}_3U$] in Figure 6.2.

Ln(III) and Ln(II) spectra. For comparison with the uranium spectra, the EPR spectra of $Cp^{tet}{}_3Ln$ and [K(crypt)][$Cp^{tet}{}_3Ln$] (Ln = Ce, Pr, Nd) were collected.[12,13] The Ce(III) compound is a $4f^1$ system, while Pr(III) is $4f^2$ and Nd(III) is $4f^3$. The Ce(II) compound is $4f^15d^1$ and the Pr(II) is $4f^25d^1$. The Nd(II) compound is $4f^35d^1$ and is the congener of the U(II) compound. The lanthanide comparisons can provide more insight into the electronic structure and help determine the influence of the 4f *vs* 5f and 5d *vs* 6d orbitals.[1]

The spectrum of $Cp^{tet}{}_3Ce$ at 5 K, Figure 6.13, is similar to that of $Cp^{tet}{}_3U$, with a single intense feature at $g = 2.15$ in perpendicular mode. However, [K(crypt)][$Cp^{tet}{}_3Ce$] is EPR silent in

both perpendicular and parallel mode, Figure 6.14. The EPR spectrum of Cp^{tet}_3Pr has a single transition at g = 2.54, Figure 6.15. The Pr(II) compound [K(crypt)][Cp^{tet}_3Pr] had a spectrum with two g values very close together, around g = 2.00, Figure 6.16. Similarly, Cp^{tet}_3Nd has a single intense feature at g = 2.15 in perpendicular mode, Figure 6.17, and [K(crypt)][Cp^{tet}_3Nd] is EPR silent in both modes. Signals were observed for [K(crypt)][Cp^{tet}_3Nd], Figures 6.18, but these features are likely due to sample decomposition, as they were not consistent across multiple samples and disappeared as the temperature was raised during data collection. Cp^{tet}_3Nd also showed a signal in parallel mode, but this signal is the same as the perpendicular mode signal as it was so intense.

Table 6.2: Cp^{tet}_3M and [K(crypt)][Cp^{tet}_3M] g values from EPR

	Electron configuration	g values
Cp^{tet}_3Ce	$4f^1$	2.54
[K(crypt)][Cp^{tet}_3Ce]	$4f^15d^1$	silent
Cp^{tet}_3Pr	$4f^2$	2.54
[K(crypt)][Cp^{tet}_3Pr]	$4f^25d^1$	2.00
Cp^{tet}_3Nd	$4f^3$	2.15
[K(crypt)][Cp^{tet}_3Nd]	$4f^35d^1$	silent
Cp^{tet}_3U	$5f^3$	2.380, 2.195, 1.985
[K(crypt)][Cp^{tet}_3U]	$5f^36d^1$	3.005, 2.04, 2.00

Nitrogen-based ligands. Many of the uranium species discussed above had nitrogen-based ligands. Since ^{14}N has a nuclear spin I = 1, the potential for superhyperfine interactions, the coupling of the electronic spin to the nuclear spin, is present. Previous EPR spectra of $U(NR_2)_3$,[14] $U(NHAr^{iPr6})_2$,[4] $U(NHAr^{iPr6})_2I$,[4] and $[U(NHAr^{iPr6})_2][BArF_{24}]$[4] did not observe any nitrogen superhyperfine interactions. Consistent with previous reports, the X-band EPR spectra of $(C_5Me_5)_2U(NR_2)$, Figure 6.19, and $(C_5Me_5)U(NR_2)_2$, Figure 6.20 showed no obvious nitrogen superhyperfine interactions. It was possible that these interactions are so weak that X-band

frequency (9 GHz) may not be able to resolve these features. However, even at Q-band frequency (34 GHz), the spectrum of $(C_5Me_5)U(NR_2)_2$, Figure 6.21, displayed no nitrogen-based interactions.

Table 6.3: X-band EPR *g* values of U(III) compounds with nitrogen ligands (R = $SiMe_3$, $BArF_{24}$ = $B(C_6H_3(CF_3)_2\text{-}3,5)_4$)

	Electronic Configuration	*g* values
$U(NR_2)_3$	$5f^3$	~3 [14]
$(C_5Me_5)_2U(NR_2)$	$5f^3$	4.23
$(C_5Me_5)U(NR_2)_2$	$5f^3$	3.12, 2.11, 0.82 [a]
$[K(crypt)][U(NR_2)_3]$	$5f^36d^1$	2.04, 2.00
$[K(crypt)][(C_5Me_5)_2U(NR_2)]$	$5f^36d^1$	2.04, 2.00
$[K(crypt)][(C_5Me_5)U(NR_2)_2]$	$5f^36d^1$	2.04, 2.00
$[K(crypt)][(C_5Me_5)_2U(NPh_2)]$	$5f^36d^1$	2.04, 2.00
$U(NHAr^{iPr6})_2$	$5f^4$	silent [4]
$U(NHAr^{iPr6})_2I$	$5f^3$	5.17, 4.56 [4]
$[U(NHAr^{iPr6})_2][BArF_{24}]$	$5f^3$	4.3, 3.6, 2.003 [4]

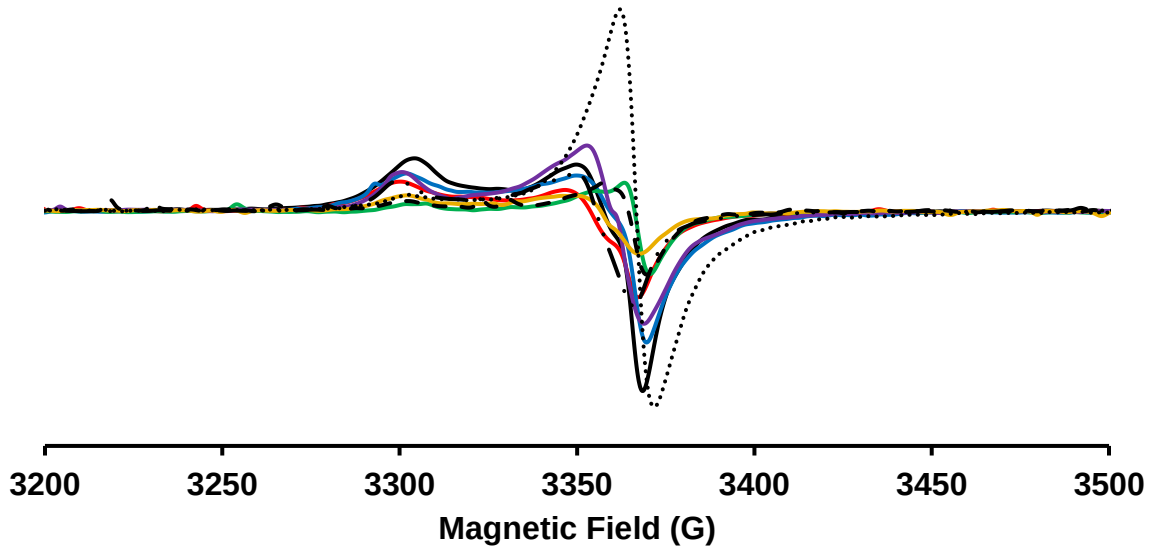

Figure 6.1: X-band, perpendicular mode EPR spectrum of $[K(crown)(THF)_2][Cp''_3U]$ (black), $[K(crypt)][Cp'_3U]$ (red), $[K(crypt)][(C_5Me_5)_2U(C_5Me_4H)]$ (blue), $[K(crypt)][(C_5Me_5)_2U(NR_2)]$ (green), $[K(crypt)][U(OAr)_3]$ (purple), $[K(crypt)][U(NR_2)_3]$ (orange), $[K(crypt)][(C_5Me_5)_2U(C_5H_5)]$ (black, dotted), $[K(crypt)][(C_5Me_5)_2U(NPh_2)]$ (black, dashed), and $[K(crypt)][(C_5Me_5)U(NR_2)_2]$ (black, dashed dot dot) taken as a frozen THF solution at 77 K.

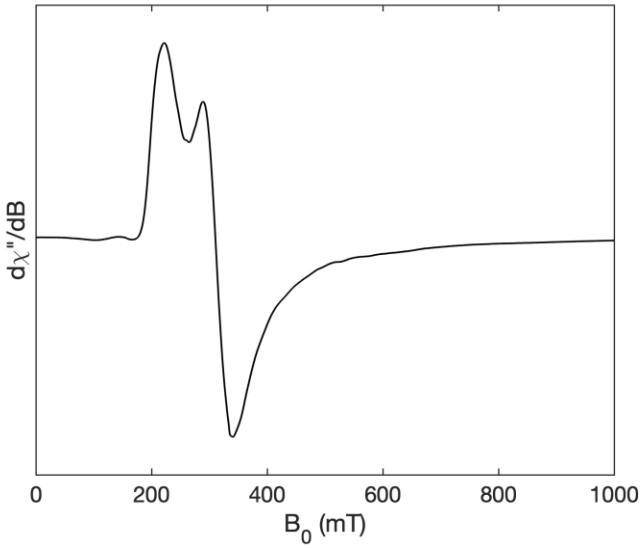

Figure 6.2: X-band, perpendicular mode EPR spectrum of [K(crypt)][Cp^{tet}_3U], taken as powdered sample at 5 K. The U(II) compound was crystallized then ground in a mortar before being loaded into the EPR tube and shipped at −196 °C to UC Davis.

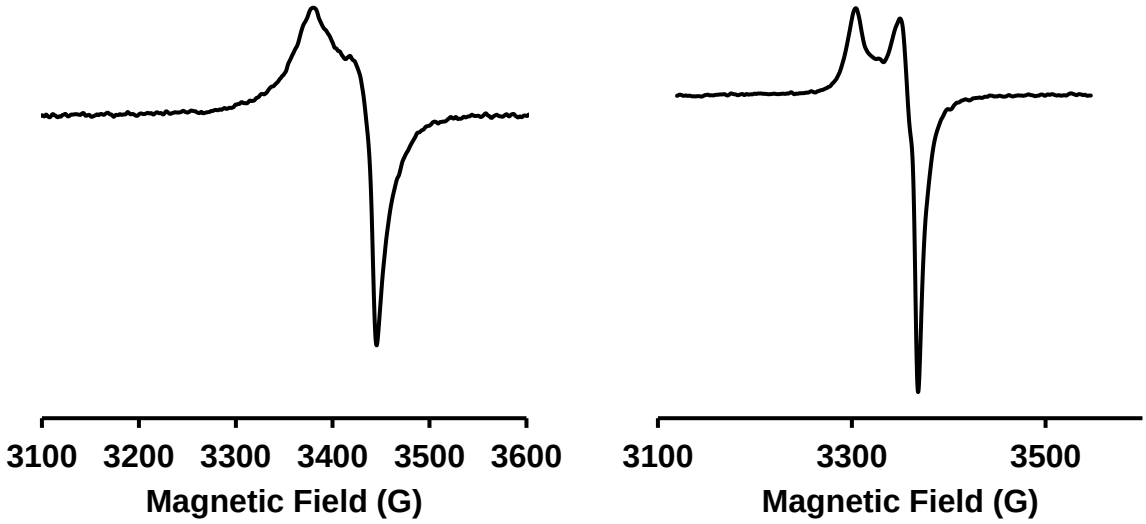

Figure 6.3: X-band, perpendicular mode EPR spectrum of [K(crown)$(THF)_2$][Cp''_3U], taken as a frozen solution in THF at 10 K (left) and at 77 K (right). The U(II) product was crystallized then dissolved in THF and immediately frozen for data collection.

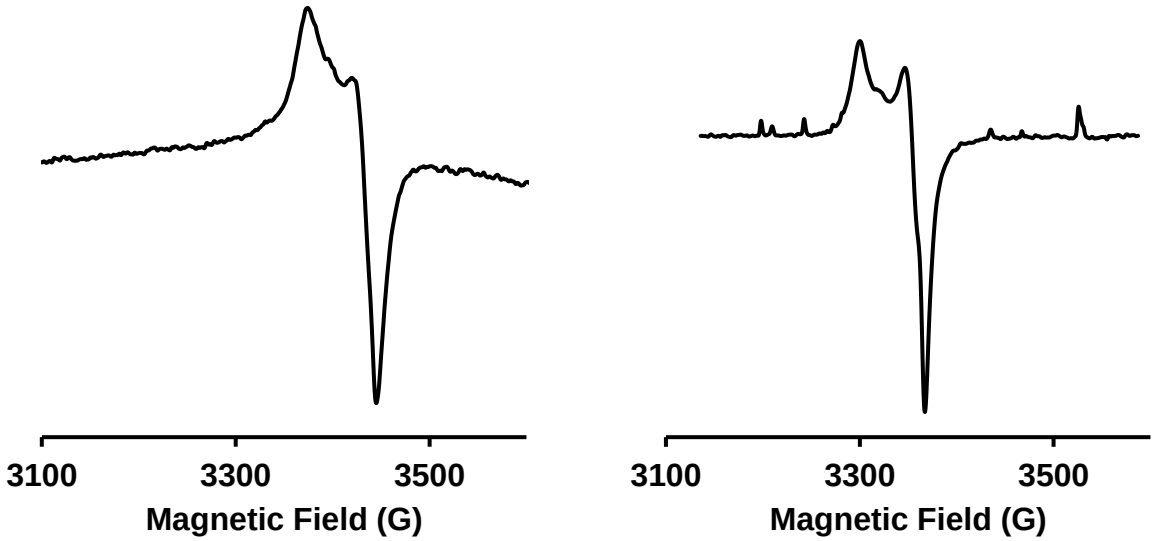

Figure 6.4: X-band, perpendicular mode EPR spectrum of [K(crypt)][Cp′$_3$U], taken as a frozen solution in THF at 10 K (left) and at 77 K (right). The U(II) product was crystallized then dissolved in THF and immediately frozen for data collection.

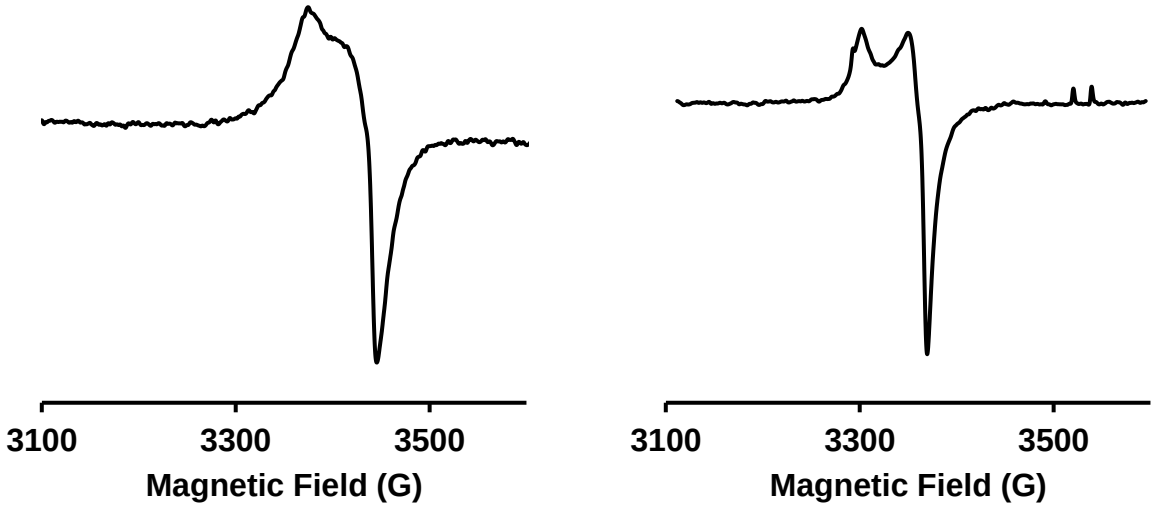

Figure 6.5: X-band, perpendicular mode EPR spectrum of [K(crypt)][$(C_5Me_5)_2UCp^{tet}$], taken as a frozen solution in THF at 10 K (left) and at 77 K (right). The U(II) was freshly prepared via reduction and expressed directly into the EPR tube and frozen for data collection.

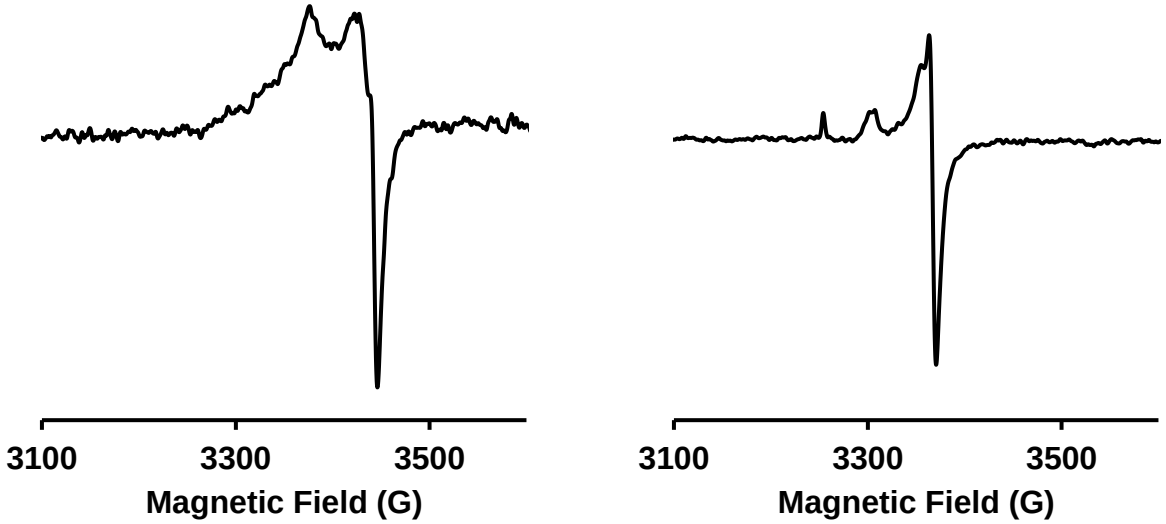

Figure 6.6: X-band, perpendicular mode EPR spectrum of [K(crypt)][$(C_5Me_5)_2U(NR_2)$], taken as a frozen solution in THF at 10 K. The U(II) was freshly prepared via reduction and expressed directly into the EPR tube and frozen for data collection.

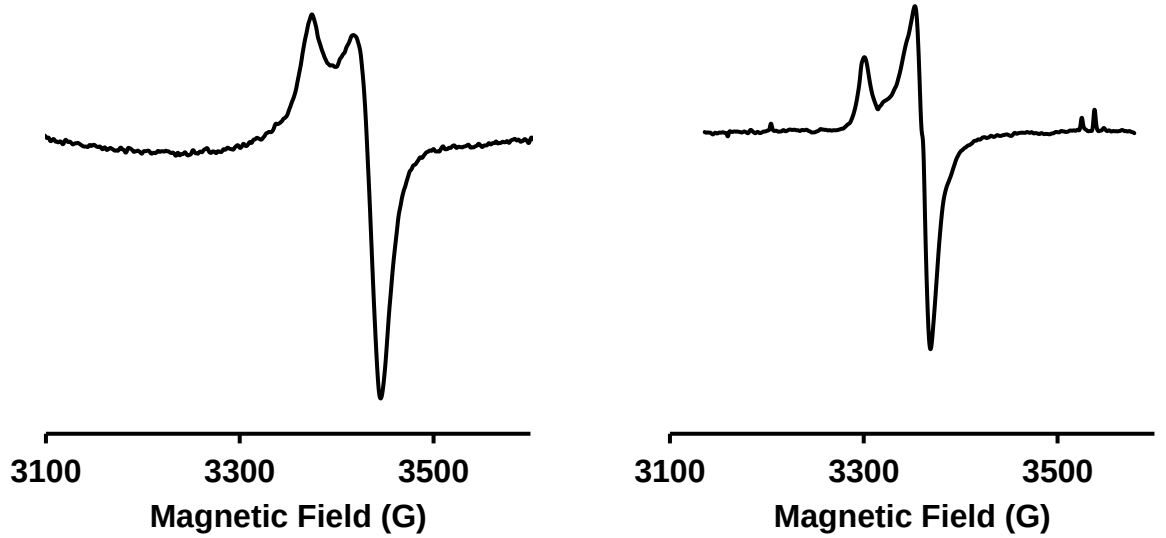

Figure 6.7: X-band, perpendicular mode EPR spectrum of [K(crypt)][$U(OAr)_3$], taken as a frozen solution at 10 K (left) and at 77 K (right). The U(II) was freshly prepared via reduction and expressed directly into the EPR tube and frozen for data collection.

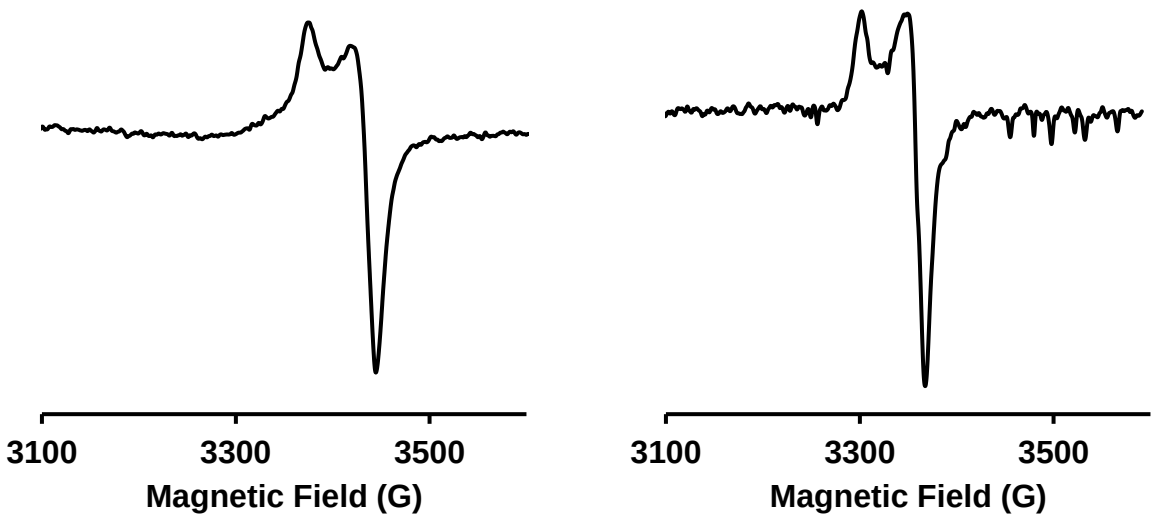

Figure 6.8: X-band, perpendicular mode EPR spectrum of [K(crypt)][$U(NR_2)_3$], taken as a frozen solution at 10 K (left) and at 77 K (right). The U(II) product was crystallized then dissolved in THF and immediately frozen for data collection.

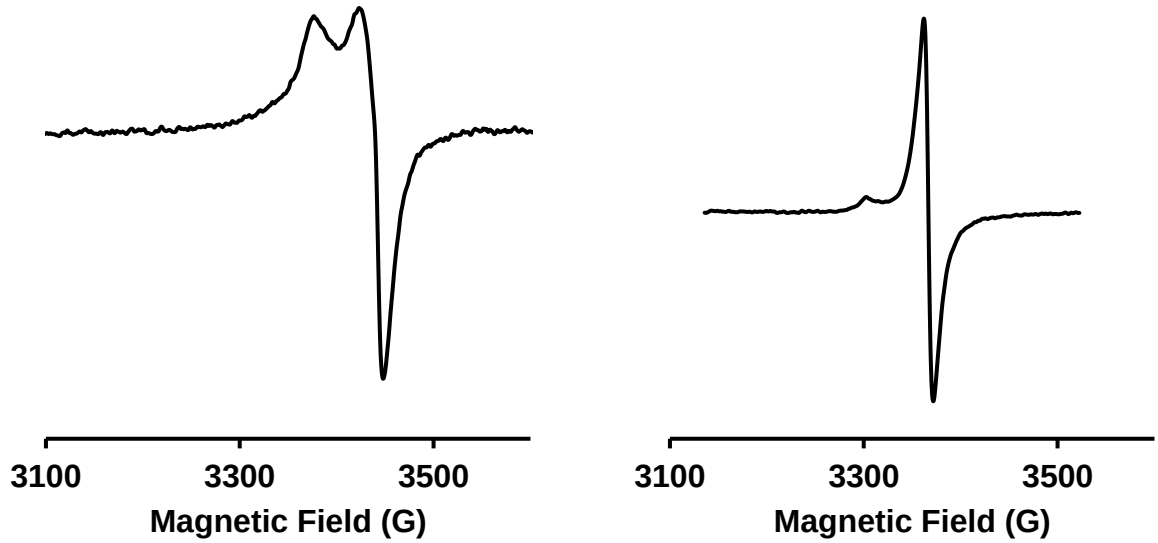

Figure 6.9: X-band, perpendicular mode EPR spectrum of [K(crypt)][$(C_5Me_5)_2U(C_5H_5)$], taken as a frozen solution at 10 K (left) and at 77 K (right). The U(II) was freshly prepared via reduction and expressed directly into the EPR tube and frozen for data collection.

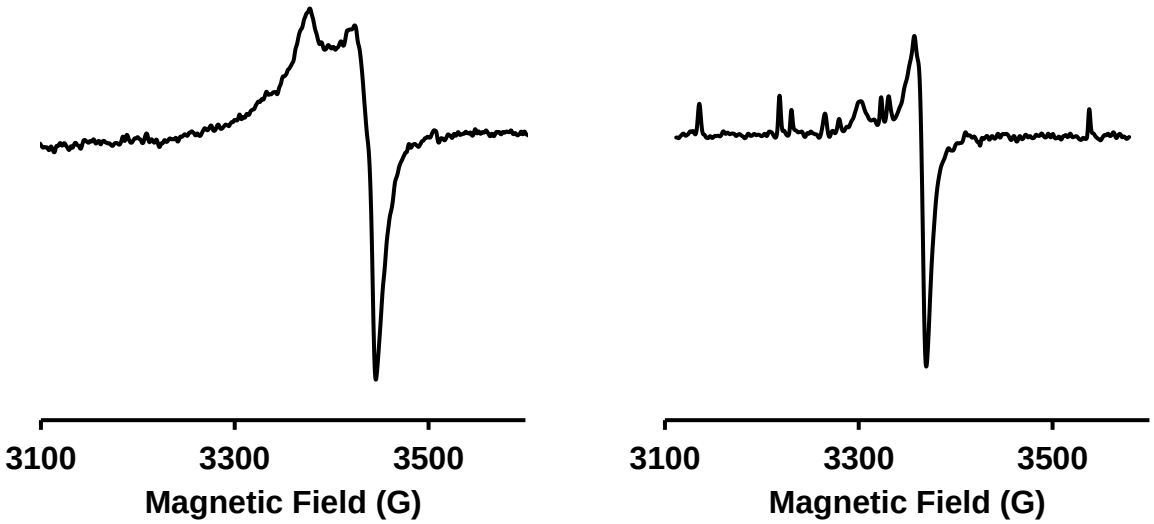

Figure 6.10: X-band, perpendicular mode EPR spectrum of [K(crypt)][$(C_5Me_5)_2U(NPh_2)$], taken as a frozen solution at 10 K (left) and at 77 K (right). The U(II) was freshly prepared via reduction and expressed directly into the EPR tube and frozen for data collection.

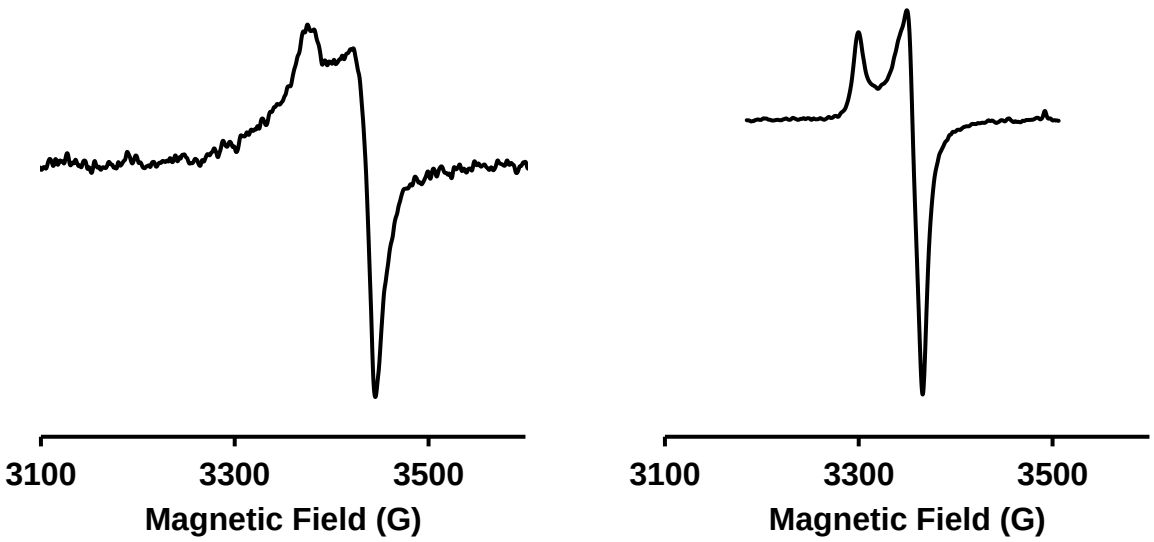

Figure 6.11: X-band, perpendicular mode EPR spectrum of [K(crypt)][$(C_5Me_5)U(NR_2)_2$], taken as a frozen solution at 10 K (left) and at 77 K (right). The U(II) was freshly prepared via reduction and expressed directly into the EPR tube and frozen for data collection.

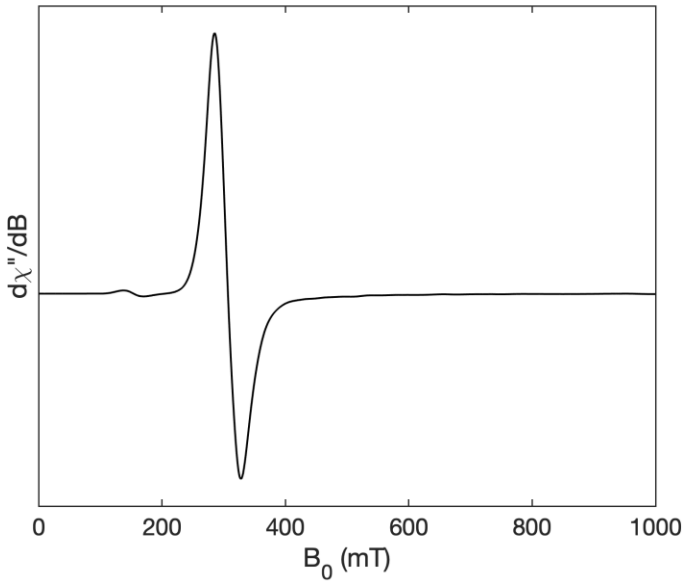

Figure 6.12: X-band, perpendicular mode EPR spectrum of Cp^{tet}_3U, taken as powdered sample at 5 K. The U(III) compound was crystallized then ground in a mortar before being loaded into the EPR tube and shipped at −196 °C to UC Davis.

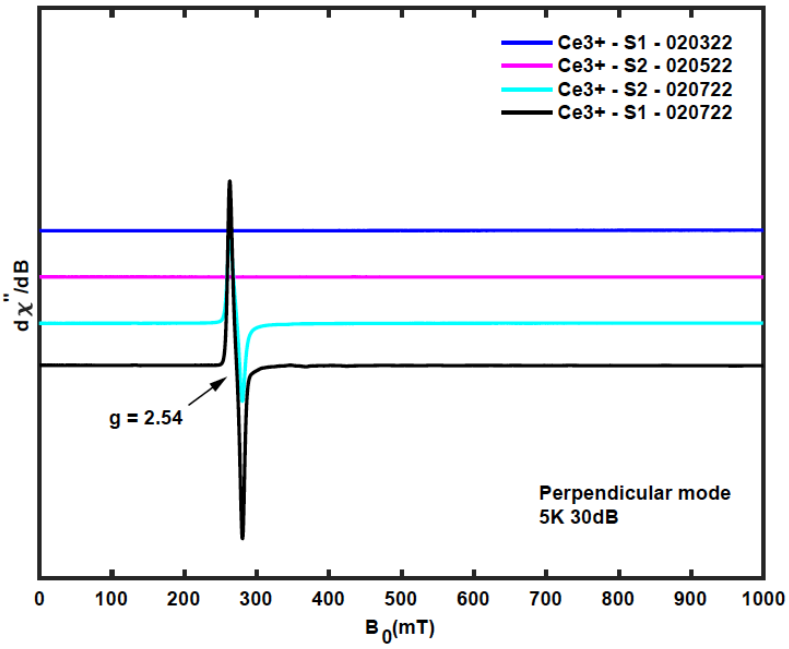

Figure 6.13: X-band, perpendicular mode spectrum of Cp^{tet}_3Ce, taken as a powdered sample at 5 K. The different colored spectra are different samples.

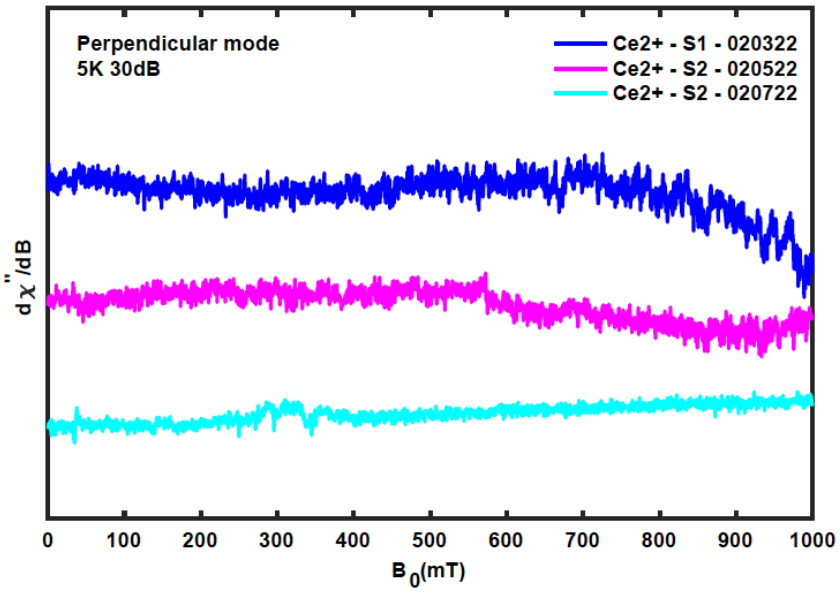

Figure 6.14: X-band, parallel mode spectrum of [K(crypt)][Cp^{tet}_3Ce], taken as a powdered sample at 5 K. The different colored spectra are different samples.

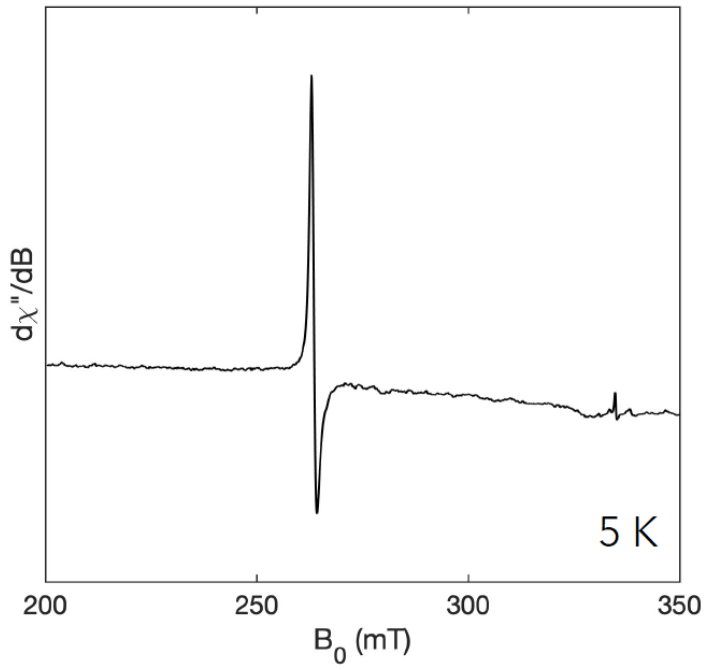

Figure 6.15: X-band, perpendicular mode EPR spectrum of Cp^{tet}_3Pr, taken as a powdered sample at 5 K.

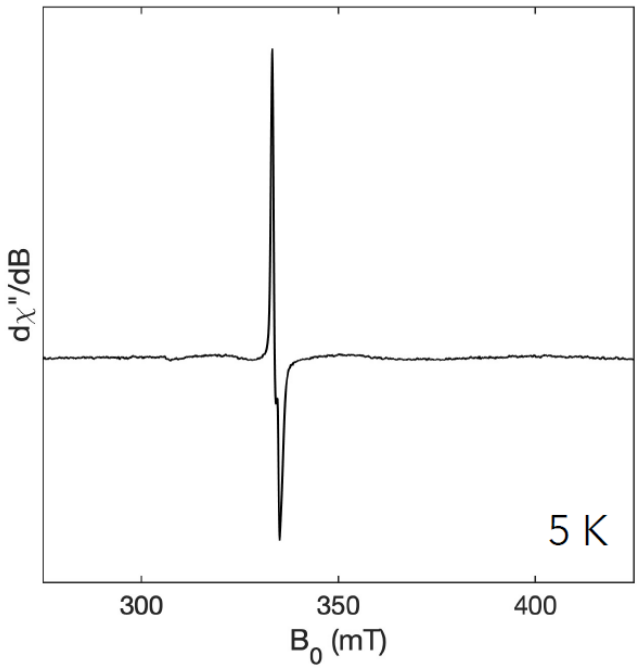

Figure 6.16: X-band, perpendicular mode EPR spectrum of [K(crypt)][Cp^{tet}_3Pr], taken as a powdered sample at 5 K.

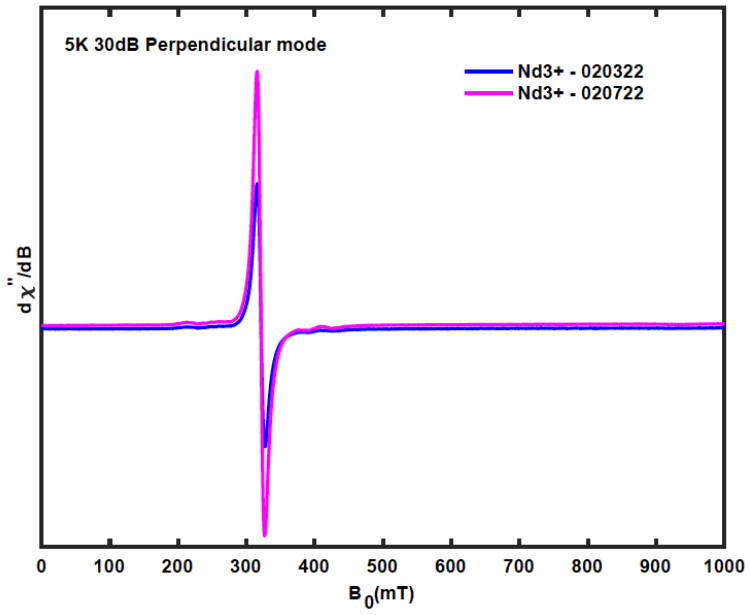

Figure 6.17: X-band, perpendicular mode EPR spectrum of Cp^{tet}_3Nd, taken as a powdered sample at 5 K. The different colored spectra are separate samples.

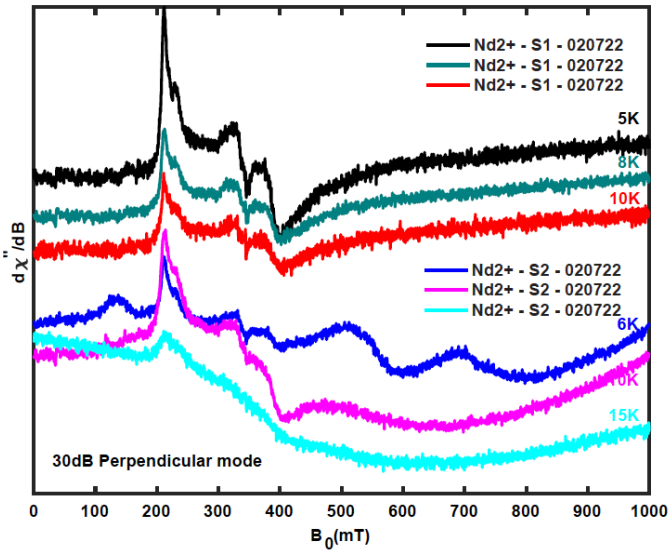

Figure 6.18: X-band, perpendicular mode EPR spectrum of [K(crypt)][Cp^{tet}_3Nd], taken as a powdered sample at ≤10 K. The different colored spectra are different samples. The features are likely due to sample decomposition, as they are not consistent.

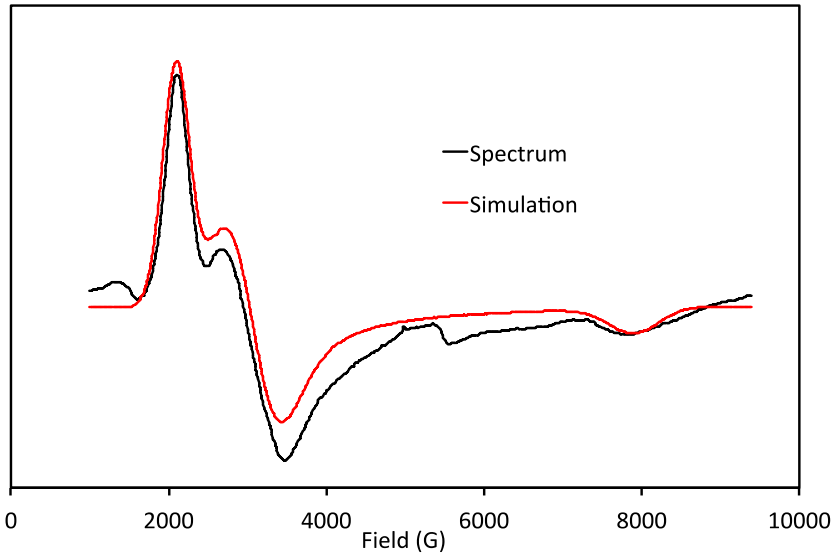

Figure 6.19: X-band, perpendicular mode EPR spectrum of $(C_5Me_5)U(NR_2)_2$, taken as a powdered sample at 3 K.

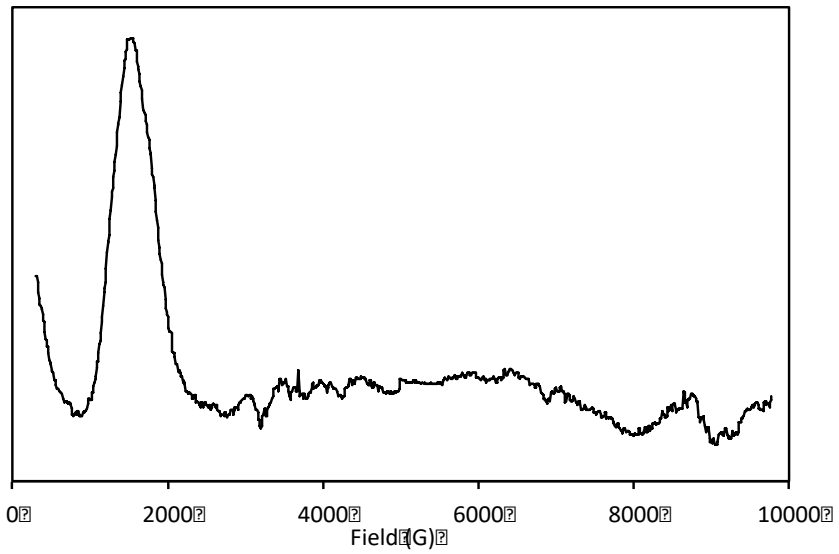

Figure 6.20: X-band, perpendicular mode EPR spectrum of $(C_5Me_5)_2U(NR_2)$, taken as a powdered sample at 3 K.

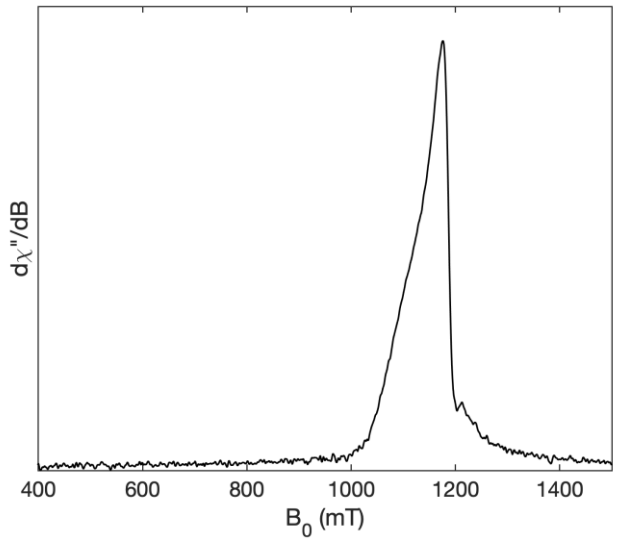

Figure 6.21: Q-band, perpendicular mode EPR spectrum of $(C_5Me_5)U(NR_2)_2$, taken as a powdered sample at 10 K.

Discussion

EPR data collected on U(II) compounds with $5f^36d^1$ electron configurations show very similar two-line spectra with *g* values of 2.04 and 2.00. These spectral features were observed

across ten compounds at both 10 K and 77 K and stand in direct contrast to the EPR-silent, $5f^4$ U(II) compounds [K(crypt)]{[(^{Ad,Me}ArO)$_3$mes]U} and U(NHAr^{iPr6})$_2$. It was interesting to note that the spectra were better resolved at 77 K than at 10 K, but this could simply be due to the inherent sensitivity of the EPR spectrometer at various temperatures. Since both [K(crypt)]{[(^{Ad,Me}ArO)$_3$mes]U} and U(NHAr^{iPr6})$_2$ have been assigned as $5f^4$ electron configurations, a simple interpretation of the silent EPR spectra could be that a diamagnetic ground state is isolated at low temperatures, where all four electrons spin pair in two 5f orbitals. The same situation could be expected to occur for the $5f^36d^1$ U(II) compounds, where a diamagnetic ground state is isolated at low temperatures since the 5f orbitals are lower in energy than the 6d orbitals. Previous magnetic susceptibility measurements on [K(crypt)][Cp′$_3$U] and [K(crypt)][Cp″$_3$U] revealed lower room temperature magnetic moments compared to the trivalent compound Cp′$_3$U, and the magnetic moment for both U(II) compounds trends towards zero at lower temperature.[6] Hence, a more in-depth theoretical analysis is needed to provide an explanation of the magnetic data. Since these are the first EPR spectra measured for mixed principal quantum number molecular compounds, the data are difficult to interpret.

One way to gain further insight is to compare the U(II) spectra with spectra of Ln(II) compounds that also have a mixed principal quantum number $4f^n5d^1$ configuration. Data were collected on Cp$^{tet}_3$M and [K(crypt)][Cp$^{tet}_3$M] for M = U, Ce, Pr, and Nd, where U and Nd are congeners and a direct comparison between the principal quantum number *n*f and *n*d orbitals could be provided. Both $4f^15d^1$ [K(crypt)][Cp$^{tet}_3$Ce] and $4f^35d^1$ [K(crypt)][Cp$^{tet}_3$Nd] are EPR-silent, whereas $4f^25d^1$ [K(crypt)][Cp$^{tet}_3$Pr] and $5f^36d^1$ [K(crypt)][Cp$^{tet}_3$U] has a EPR signal. Theoretical analysis by Wayne Lukens at LBNL suggests that the ground states for [K(crypt)][Cp$^{tet}_3$Ce] and [K(crypt)][Cp$^{tet}_3$Nd] are singlet states, under the assumption that the presence of an electron in the

dz^2 orbital does not alter the f orbital energetic ordering. The same analysis for Nd(II) can be applied to U(II) and would suggest that a singlet state is the energetic ground state for [K(crypt)][Cp^{tet}_3U], but this conclusion is not supported since transitions are observed in the EPR spectrum. The $4f^25d^1$ Pr(II) compound [K(crypt)][Cp^{tet}_3Pr] is predicted to have a doublet ground state by these methods and should have an EPR spectrum.

If the population of the dz^2 orbital altered the energy ordering of the f orbitals, a different ground state could be preferred. Alternatively, if the energy difference between the valence f and d orbitals (due to ligand field effects, for example) are sufficiently small, thermal population of higher energy states could be observed. However, the Ln compounds should have even smaller ligand field splitting effects than U due to the smaller extension of the 4f vs 5f orbitals. Furthermore, the Ce(II) and Nd(II) compounds are EPR-silent, which does not support the orbital energy splitting hypothesis. However, it should be noted that all of these arguments use a simplistic single-electron approximation model. Another option is that the features observed in the EPR spectra of the U(II) compounds are due to U(III) impurities due to decomposition. However, this seems extremely unlikely to occur over ten separate samples.

The observation that the EPR signal is practically unchanged over the different U(II) compounds (g = 2.04, 2.00) is interesting and suggests some consistency across all samples. Since the $5f^36d^1$ U(II) compounds appear to have a diagnostic EPR signal at 77 K, the analogous $5f^3$ U(III) compounds are mostly silent at 77 K, and the $5f^4$ U(II) compounds [K(crypt)]{[(^{Ad,Me}ArO)$_3$mes]U} and U(NHAr^{iPr6})$_2$ are EPR silent, it seems that EPR spectroscopy may be a technique, in addition to UV-visible spectroscopy, to quickly identify the electron configuration of U(II) compounds; $5f^36d^1$ vs $5f^4$. If this is the case, this method would be extremely effective since a compound can be flash-frozen upon formation and decomposition

would be minimal. This is in stark contrast to X-ray crystallography, SQUID magnetometry, and UV-visible spectroscopy that require moderate stability of the compound (see Chapters 4 and 5 for examples of unstable U(II) species that cannot be easily analyzed by these methods).

The axial shape of the EPR spectra of the $5f^3 6d^1$ U(II) compounds is the same as the spectra of other $(dz^2)^1$ $(C_5R_5)_3M$ compounds (M = Y, Zr, La, Th).[12,15–22] While the *g* values differ across metals and ligand systems and hyperfine interactions are possible with ^{89}Y, ^{91}Zr, and ^{138}La, the two-line pattern is apparent. These similarities further suggest that the EPR spectra observed for the $5f^3 6d^1$ U(II) compounds might be due to the $6d^1$ electron.

No superhyperfine interactions were observed for either U(III) or U(II) compounds that had nitrogen ligands bound directly to the uranium center, even at Q-band frequency, which strongly suggests there is little spin density on the nitrogen ligands. This is consistent with the contracted nature of the 5f orbitals and how the U–ligand interactions are mostly ionic in nature. Population of the 6d orbital could allow for covalent metal-ligand interactions, however, all of the $6dz^2$-like HOMOs of the $5f^3 6d^1$ U(II) compounds are calculated to be non-bonding and thus no density resides on the nitrogen atoms that would give rise to superhyperfine interactions observed in the EPR spectrum.

The lack of observed ^{14}N interactions in the U systems is in direct contrast to transition metal species with M–N bonds. For example, the X-band EPR spectrum of [*N*,*N*′-bis(2,6-diisopropylphenyl)-2,6-pyridinedicarboxamide]Cu(NCMe) shows superhyperfine interactions to all three nitrogen atoms bound to the copper center.[23] This difference is likely a result of the covalent nature of the Cu–N bond and the ionic nature of the U–N bond.

Conclusion

X-band EPR spectra of ten $5f^3 6d^1$ U(II) compounds have been collected and show a similar two-line pattern at both 10 K and 77 K. It appears that EPR could be a spectroscopic technique to quickly identify the electron configurations of U(II) compounds, since the $5f^4$ U(II) compounds are EPR silent and the analogous $5f^3$ U(III) compounds are often EPR silent at 77 K. No superhyperfine interactions were observed for U(III) or U(II) compounds that contain nitrogen-bound ligands.

Experimental

All syntheses and manipulations described below were conducted under Ar with rigorous exclusion of air and water using standard glovebox and vacuum line techniques. Solvents were sparged with UHP argon and dried by passage through drying columns prior to use. X-band EPR spectra were recorded on a Bruker EMX spectrometer equipped with an ER041Xg microwave bridge and calibrated with DPPH (g = 2.0036) at UC Irvine, at LBNL by Wayne Lukens, or at UC Davis by David Villareal, Wen Fu, and Dave Britt. Cp^{tet}_3M (M = U, Ce, Pr, Nd),[12,13,24] [K(crypt)][Cp^{tet}_3M] (M = U, Ce, Pr, Nd),[8,12] [K(crown)$(THF)_2$][Cp''_3U],[6] Cp''_3U,[24] [K(crypt)][Cp'_3U],[7] Cp'_3U,[25] $(C_5Me_5)_2UCp^{tet}$,[10] $(C_5Me_5)_2UCp$,[10] $(C_5Me_5)_2UN^*$,[26] $U(OAr)_3$,[18] [K(crypt)][$U(NR_2)_3$],[8] $(C_5Me_5)_2U(NPh_2)(THF)$,[27] and $(C_5Me_5)U(NR_2)_2$[28] were synthesized following literature routes.

EPR samples were prepared as powdered solids or as frozen THF solutions. Powdered samples were prepared from crystalline material, ground with a mortar and pestle, and then transferred to the EPR tube. Solution samples were prepared from crystalline material if possible, otherwise the U(II) species was synthesized via a KC_8 reduction column[29] and the solution was eluted directly into the EPR tube. Samples sent to UC Davis and LBNL were flame-sealed under

vacuum and shipped in a liquid nitrogen dewar. All samples were kept frozen in liquid nitrogen between preparation and data collection to minimize decomposition.

References

(1) Lukens, W. W.; Speldrich, M.; Yang, P.; Duignan, T. J.; Autschbach, J.; Kögerler, P. The Roles of 4f- and 5f-Orbitals in Bonding: A Magnetochemical, Crystal Field, Density Functional Theory, and Multi-Reference Wavefunction Study. *Dalton Trans.* **2016**, *45*, 11508–11521, DOI: 10.1039/C6DT00634E.

(2) Carnall, W. T.; Fields, P. R.; Wybourne, B. G. Spectral Intensities of the Trivalent Lanthanides and Actinides in Solution. I. Pr^{3+}, Nd^{3+}, Er^{3+}, Tm^{3+}, and Yb^{3+}. *J. Chem. Phys.* **1965**, *42*, 3797–3806, DOI: 10.1063/1.1695840.

(3) Kindra, D. R.; Evans, W. J. Magnetic Susceptibility of Uranium Complexes. *Chem. Rev.* **2014**, *114*, 8865–8882, DOI: 10.1021/cr500242w.

(4) Billow, B. S.; Livesay, B. N.; Mokhtarzadeh, C. C.; Mccracken, J.; Shores, M. P.; Boncella, J. M.; Odom, A. L. Synthesis and Characterization of a Neutral U(II) Arene Sandwich Complex. *J. Am. Chem. Soc.* **2018**, *140*, 17369–17373, DOI: 10.1021/jacs.8b10888.

(5) La Pierre, H. S.; Scheurer, A.; Heinemann, F. W.; Hieringer, W.; Meyer, K. Synthesis and Characterization of a Uranium(II) Monoarene Complex Supported by δ Backbonding. *Angew. Chem. Int. Ed.* **2014**, *53*, 7158–7162, DOI: 10.1002/anie.201402050.

(6) Windorff, C. J.; MacDonald, M. R.; Meihaus, K. R.; Ziller, J. W.; Long, J. R.; Evans, W. J. Expanding the Chemistry of Molecular U^{2+} Complexes: Synthesis, Characterization, and Reactivity of the $\{[C_5H_3(SiMe_3)_2]_3U\}^-$ Anion. *Chem. Eur. J.* **2016**, *22*, 772–782, DOI: 10.1002/chem.201503583.

(7) MacDonald, M. R.; Fieser, M. E.; Bates, J. E.; Ziller, J. W.; Furche, F.; Evans, W. J.

Identification of the +2 Oxidation State for Uranium in a Crystalline Molecular Complex, [K(2.2.2-Cryptand)][($C_5H_4SiMe_3$)$_3$U]. *J. Am. Chem. Soc.* **2013**, *135*, 13310–13313, DOI: 10.1021/ja406791t.

(8) Ryan, A. J.; Angadol, M. A.; Ziller, J. W.; Evans, W. J. Isolation of U(II) Compounds Using Strong Donor Ligands, C_5Me_4H and N($SiMe_3$)$_2$, Including a Three-Coordinate U(II) Complex. *Chem. Commun.* **2019**, *55*, 2325–2327, DOI: 10.1039/C8CC08767A.

(9) Wedal, J. C.; Bekoe, S.; Ziller, J. W.; Furche, F.; Evans, W. J. C–H Bond Activation via U(II) in the Reduction of Heteroleptic Bis(Trimethylsilyl)Amide U(III) Complexes. *Organometallics* **2020**, *39*, 3425–3432, DOI: 10.1021/acs.organomet.0c00496.

(10) Wedal, J. C.; Ziller, J. W.; Furche, F.; Evans, W. J. Synthesis and Reduction of Heteroleptic Bis(Cyclopentadienyl) Uranium(III) Complexes. *Inorg. Chem.* **2022**, *in press*, DOI: 10.1021/acs.inorgchem.2c00322.

(11) Van der Sluys, W. G.; Burns, C. J.; Huffman, J. C.; Sattelberger, A. P. Uranium Alkoxide Chemistry. 1. Synthesis and the Novel Dimeric Structure of the First Homoleptic Uranium(III) Aryloxide Complex. *J. Am. Chem. Soc.* **1988**, *110*, 5924–5925, DOI: 10.1021/ja00225a067.

(12) Jenkins, T. F.; Woen, D. H.; Mohanam, L. N.; Ziller, J. W.; Furche, F.; Evans, W. J. Tetramethylcyclopentadienyl Ligands Allow Isolation of Ln(II) Ions across the Lanthanide Series in [K(2.2.2-Cryptand)][(C_5Me_4H)$_3$Ln] Complexes. *Organometallics* **2018**, *37*, 3863–3873, DOI: 10.1021/acs.organomet.8b00557.

(13) Schumann, H.; Glanz, M.; Hemling, H.; Ekkehard Hahn, F. Metallorganische Verbindungen Der Lanthanoide. 93. Tetramethylcyclopentadienyl-Komplexe Ausgewählter 4f-Elemente. *Z. Anorg. Allg. Chem.* **1995**, *621*, 341–345, DOI:

10.1002/zaac.19956210302.

(14) Nakai, H.; Hu, X.; Zakharov, L. N.; Rheingold, A. L.; Meyer, K. Synthesis and Characterization of N-Heterocyclic Carbene Complexes of Uranium(III). *Inorg. Chem.* **2004**, *43*, 855–857, DOI: 10.1021/ic035142j.

(15) Kot, W. K.; Shalimoff, G. V.; Edelstein, N. M.; Edelman, M. A.; Lappert, M. F. [$Th^{III}\{\eta^5$-$C_5H_3(SiMe_3)_2\}_3$], an Actinide Compound with a 6d1 Ground State. *J. Am. Chem. Soc.* **1988**, *110*, 986–987, DOI: 10.1021/ja00211a059.

(16) Hitchcock, P. B.; Lappert, M. F.; Maron, L.; Protchenko, A. V. Lanthanum Does Form Stable Molecular Compounds in the +2 Oxidation State. *Angew. Chem. Int. Ed.* **2008**, *47*, 1488–1491, DOI: 10.1002/anie.200704887.

(17) MacDonald, M. R.; Ziller, J. W.; Evans, W. J. Synthesis of a Crystalline Molecular Complex of Y^{2+}, [(18-Crown-6)K][$(C_5H_4SiMe_3)_3Y$]. *J. Am. Chem. Soc.* **2011**, *133*, 15914–15917, DOI: 10.1021/ja207151y.

(18) Siladke, N. A.; Webster, C. L.; Walensky, J. R.; Takase, M. K.; Ziller, J. W.; Grant, D. J.; Gagliardi, L.; Evans, W. J. Actinide Metallocene Hydride Chemistry: C–H Activation in Tetramethylcyclopentadienyl Ligands to Form [μ-η^5-$C_5Me_3H(CH_2)$-κC]$^{2-}$ Tuck-over Ligands in a Tetrathorium Octahydride Complex. *Organometallics* **2013**, *32*, 6522–6531, DOI: 10.1021/om4008482.

(19) Langeslay, R. R.; Chen, G. P.; Windorff, C. J.; Chan, A. K.; Ziller, J. W.; Furche, F.; Evans, W. J. Synthesis, Structure, and Reactivity of the Sterically Crowded Th^{3+} Complex $(C_5Me_5)_3Th$ Including Formation of the Thorium Carbonyl, [$(C_5Me_5)_3Th(CO)$][BPh_4]. *J. Am. Chem. Soc.* **2017**, *139*, 3387–3398, DOI: 10.1021/jacs.6b10826.

(20) Formanuik, A.; Ariciu, A.-M.; Ortu, F.; Beekmeyer, R.; Kerridge, A.; Tuna, F.; McInnes,

E. J. L.; Mills, D. P. Actinide Covalency Measured by Pulsed Electron Paramagnetic Resonance Spectroscopy. *Nat. Chem.* **2017**, *9*, 578–583, DOI: 10.1038/nchem.2692.

(21) Lukens, W. W.; Andersen, R. A. Synthesis, Structure, and Reactions of $(\eta^5\text{-}C_5H_5)_3Zr$. *Organometallics* **1995**, *14*, 3435–3439, DOI: 10.1021/om00007a050.

(22) Wedal, J. C.; Bekoe, S.; Ziller, J. W.; Furche, F.; Evans, W. J. In Search of Tris(Trimethylsilylcyclopentadienyl) Thorium. *Dalton Trans.* **2019**, *48*, 16633–16640, DOI: 10.1039/C9DT03674A.

(23) Donoghue, P. J.; Gupta, A. K.; Boyce, D. W.; Cramer, C. J.; Tolman, W. B. An Anionic, Tetragonal Copper(II) Superoxide Complex. *J. Am. Chem. Soc.* **2010**, *132*, 15869–15871, DOI: 10.1021/ja106244k.

(24) del Mar Conejo, M.; Parry, J. S.; Carmona, E.; Schultz, M.; Brennann, J. G.; Beshouri, S. M.; Andersen, R. A.; Rogers, R. D.; Coles, S.; Hursthouse, M. B. Carbon Monoxide and Isocyanide Complexes of Trivalent Uranium Metallocenes. *Chem. Eur. J.* **1999**, *5*, 3000–3009, DOI: 10.1002/(SICI)1521-3765(19991001)5:10<3000::AID-CHEM3000>3.0.CO;2-Q.

(25) Brennan, J. G.; Andersen, R. A.; Zalkin, A. Chemistry of Trivalent Uranium Metallocenes: Electron-Transfer Reactions with Carbon Disulfide. Formation of $[(RC_5H_4)_3U]_2[\mu\text{-}\eta^1,\eta^1\text{-}CS_2]$. *Inorg. Chem.* **1986**, *25*, 1756–1760, DOI: 10.1021/ic00231a007.

(26) Fagan, P. J.; Manriquez, J. M.; Marks, T. J.; Day, C. S.; Day, V. W.; Vollmer, S. H.; Day, V. W. Synthesis and Properties of a New Class of Highly Reactive Trivalent Actinide Organometallic Compounds. Derivatives of Bis(Pentamethylcyclopentadienyl)-Uranium(III). *Organometallics* **1982**, *1*, 170–180, DOI: 10.1021/om00061a028.

(27) Graves, C. R.; Scott, B. L.; Morris, D. E.; Kiplinger, J. L. Tetravalent and Pentavalent

Uranium Acetylide Complexes Prepared by Oxidative Functionalization with CuC≡CPh. *Organometallics* **2008**, *27*, 3335–3337, DOI: 10.1021/om800466m.

(28) Avens, L. R.; Burns, C. J.; Butcher, R. J.; Clark, D. L.; Gordon, J. C.; Schake, A. R.; Scott, B. L.; Watkin, J. G.; Zwick, B. D. Mono(Pentamethylcyclopentadienyl)-Uranium(III) Complexes: Synthesis, Properties, and X-Ray Structures of (η-C_5Me_5)$UI_2(THF)_3$, (η-C_5Me_5)$UI_2(Py)_3$, and (η-C_5Me_5)$U[N(SiMe_3)_2]_2$. *Organometallics* **2000**, *19*, 451–457, DOI: 10.1021/om990718r.

(29) MacDonald, M. R.; Bates, J. E.; Ziller, J. W.; Furche, F.; Evans, W. J. Completing the Series of +2 Ions for the Lanthanide Elements: Synthesis of Molecular Complexes of Pr^{2+}, Gd^{2+}, Tb^{2+}, and Lu^{2+}. *J. Am. Chem. Soc.* **2013**, *135*, 9857–9868, DOI: 10.1021/ja403753j.

Chapter 7:

Characterization of the U(V) Complex $(C_5Me_5)_2U^{V}I(=NSiMe_3)$ via Reaction of $(C_5Me_5)_2U^{III}I(THF)$ with N_3SiMe_3

Introduction

Reaction of uranium complexes with azides and oxygen-transfer reagents have been heavily studied due to interest in actinide-ligand multiple bonding.[1–6] Uranium oxo and imido species are of interest for theoretical and reactivity studies.[7–13] To generate uranium-nitrogen multiple bonds, often a uranium complex is reacted with an RN_3 organic azide or PhN=NPh azobenzene reagent to oxidize the metal center and install the imido ligand (=NR).

For example, U(III) compounds within the $[(C_5Me_5)_2U^{III}]^{1+}$ bent metallocene framework will react with azide or azo reagents to generate U(VI) products. This is exemplified by the reaction of $(C_5Me_5)_2U^{III}Cl_2Na$ with adamantyl azide or azobenzene led to the isolation of $(C_5Me_5)_2U^{VI}(=NR)_2$ (R = Ad, Ph),[14] eq 7.1.

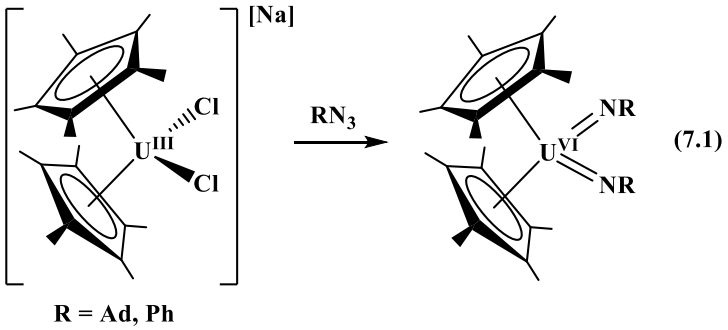

(7.1)

Similarly, $(C_5Me_5)_3U^{III}$ reacts with azobenzene to form $(C_5Me_5)_2U^{VI}(=NR)_2$ with a byproduct of $(C_5Me_5)_2$, eq 7.2.[15]

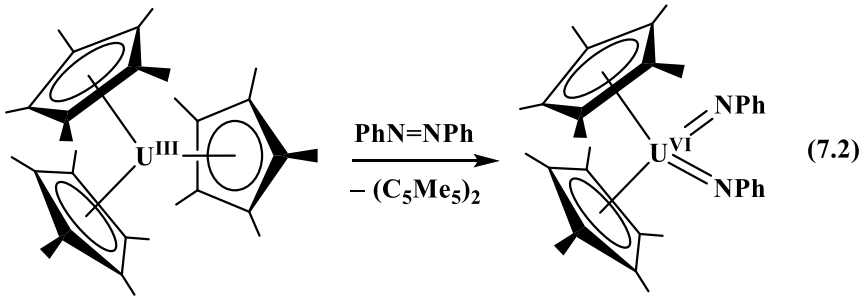

(7.2)

Another example involves reaction of $(C_5Me_5)_2U^{III}[P(SiMe_3)(Mes)](THF)$ (Mes = $C_6H_2Me_3$-2,4,6) with organoazides to form $(C_5Me_5)_2U^{VI}(=NR)_2$ (R = $SiMe_3$, Ad) and dimeric $[P(SiMe_3)(Mes)]_2$,[16] eq 7.3.

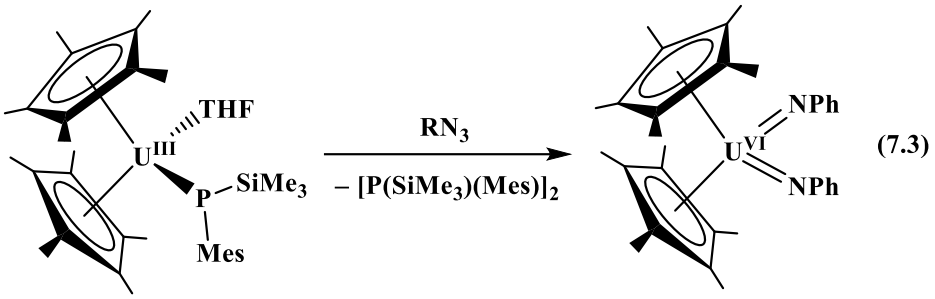

(7.3)

The one exception to these U(III) to U(VI) reactions is the isolation of a U(V) imido species during reaction of $(C_5Me_5)_2U^{III}$(hpp) (hpp = 1,3,4,6,7,8-hexahydro-2H-pyrimido-[1,2-a]pyrimidinato) with N_3SiMe_3 to form $(C_5Me_5)_2U^{V}$(hpp)(=$NSiMe_3$),[17] eq 7.4. The isolation of the U(V) species is likely due to the inability of the hpp ligand to oxidatively dimerize, like the C_5Me_5 and $P(SiMe_3)(Mes)$ ligands in eq 7.2 and 7.3.

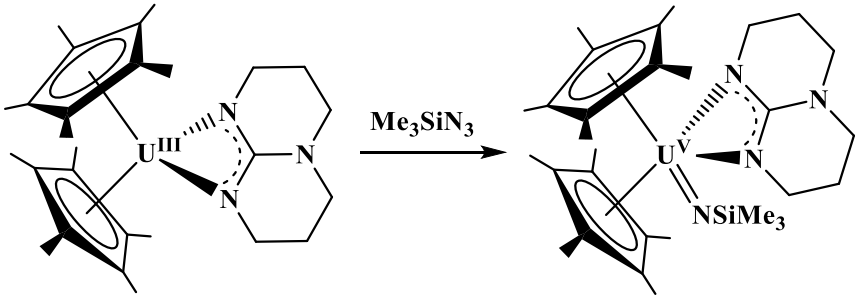

(7.4)

U(V) imido species can be generated in ligand frameworks beyond $[(C_5Me_5)_2U^{III}]^{1+}$, including $Cp''_2U^{V}(=NSiMe_3)Cl$, formed from Cp''_2UCl_2 [$Cp'' = C_5H_3(SiMe_3)_2$] and N_3SiMe_3,[18] $Cp^{ttt}_2U(=NR)$

formed from $Cp^{ttt}_2UMe_2$ and RNH_2 (Cp^{ttt} = $C_5{}^tBu_3H_2$; R = Me, *p*-tolyl, *p*-$MeOC_6H_4$, *p*-$Me_2NC_6H_4$),[19] $Cp^{Me}_3U^V(=NR)$ from $Cp^{Me}_3U^{III}(THF)$ (Cp^{Me} = C_5MeH_4) and RN_3 (R = $SiMe_3$, Ph),[20] $U^V[N(SiMe_3)_2]_3(=NR)$ from $U^{III}[N(SiMe_3)_2]_3$ and N_3R (R = $SiMe_3$, CPh_3, naphthyl),[21,22] $[(^{Ad,tBu}ArO)_3tacn]U^V(=NSiMe_3)$ from $[(^{Ad,tBu}ArO)_3tacn]U^{III}$ and N_3SiMe_3,[23] and [K(18-crown-6)][$U^V(OSiR_3)_4(=NR')$] from [K(18-crown-6)][$U^{III}(OSiR_3)_4$] and N_3R' (R = O^tBu; R′ = $SiMe_3$, Ad).[8]

Furthermore, the U(IV) imido complex $(C_5Me_5)_2U^{IV}(=NAr)(THF)$ reacts with CuX and PhE–EPh to form $(C_5Me_5)_2U^V(=NAr)(X)$ (Ar = 2,6-$^iPr_2C_6H_3$; X = F, Cl, Br, I, OTf, C≡CPh, SPh, SePh, TePh) via oxidation of the uranium center.[24–27] The $(C_5Me_5)_2U^V(=NAr)(X)$ complex can be further derivatized with MX′ (M = Li, K; X′ = NPh_2, OPh, Me, Ph) via salt metathesis reactions to form $(C_5Me_5)_2U^V(=NAr)(X')$.[26]

In the initial report of $(C_5Me_5)_2U^{III}Cl_2Na$ reacting with azide reagents, a mechanism was proposed in which an unobserved U(IV) intermediate $(C_5Me_5)_2U^{IV}(=NR)$ reacts with N_3R to generate the observed U(VI) product $(C_5Me_5)_2U^{VI}(=NR)_2$,[14] Scheme 7.1. Another possible intermediate $(C_5Me_5)_2U^VCl(RN–NR)$ could react with the starting complex $(C_5Me_5)_2U^{III}Cl_2Na$ to form the observed product, Scheme 7.1.

To my knowledge, no U(V) intermediate has been observed in reactions of uranium compounds with organic azides. In this Chapter, the crystal structure of such a U(V) intermediate, $(C_5Me_5)_2U^VI(=NSiMe_3)$, is reported along with the reaction of $(C_5Me_5)_2U^{III}I(THF)$ with N_3SiMe_3 which formed it. This U(V) intermediate appears to be unstable with respect to disproportionation into $(C_5Me_5)_2U^{VI}(=NSiMe_3)_2$ and $(C_5Me_5)_2U^{IV}I_2$ which explains why these intermediates were not observed before. This study provides direct evidence that U(III) reactions with organoazides can form U(VI) bis-imido products via U(V) intermediates.

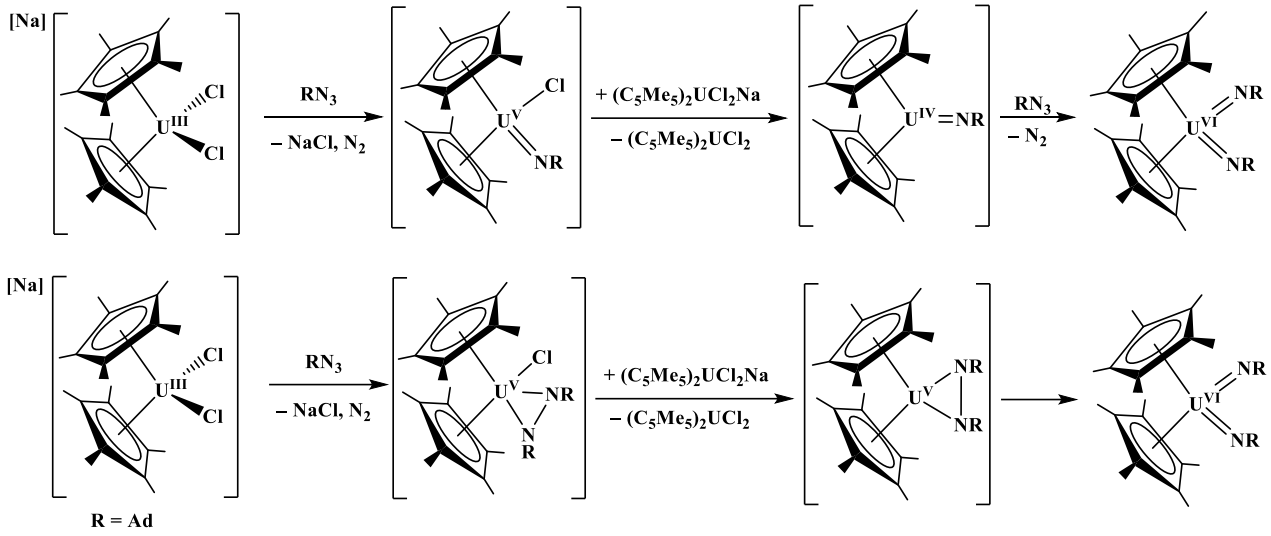

Scheme 7.1: Original proposed mechanisms for the reaction of $(C_5Me_5)_2U^{III}Cl_2Na$ azides.[14]

Results

Initially, the reaction of $(C_5Me_5)_2U^{III}I(THF)$ and Me_3SiN_3 was performed in an attempt to generate $(C_5Me_5)_2U^{III}(N_3)$[28,29] by elimination of Me_3SiI. However, the U(III) reduction of the organic azide took place. The first time this reaction was performed, brown X-ray quality crystals were isolated from hexane upon workup. These were identified as the U(V) mono-imido species $(C_5Me_5)_2U^{V}I(=NSiMe_3)$, **7.1**, by X-ray crystallography, Figure 7.1.

Reduction of the azide by the U(III) center is not surprising, but isolation of the mono-imido species was unexpected given the previous reactions of $[(C_5Me_5)_2U^{III}]^{1+}$ complexes with organic azides that often afford U(VI) bis-imido species, eq 7.1-7.4. Complex **7.1** maintains the bent metallocene motif with the iodide and imido ligand occupying the metallocene wedge positions. The C_5Me_5 rings are crystallographically equivalent by symmetry. The crystal data were not very high quality, so the following metrical discussion should be considered preliminary at best. The U–Cnt distance was 2.496 Å and the U–I distance was 3.1135(12) Å.

$(C_5Me_5)_2U^{VI}(=NSiMe_3)_2$.[16] During these reactions, a second signal was identified in the ^1H NMR spectrum that formed in nearly equal amounts to $(C_5Me_5)_2U^{VI}(=NSiMe_3)_2$. This second species was identified as the U(IV) product, $(C_5Me_5)_2U^{IV}I_2$,[24,34] and its presence can be explained by the disproportionation of **7.1** into $(C_5Me_5)_2U^{VI}(=NSiMe_3)_2$ and $(C_5Me_5)_2U^{IV}I_2$. In other words, compound **7.1** can be an intermediate in the reaction of $(C_5Me_5)_2U^{III}I(THF)$ and Me_3SiN_3, eq 7.5.

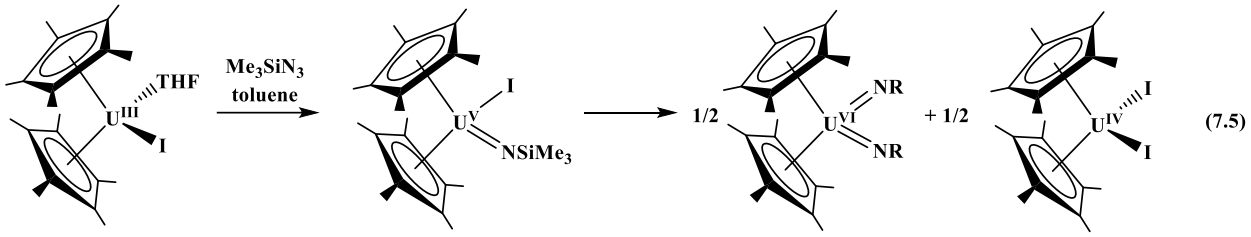

(7.5)

The reaction in eq 7.5 was followed by NMR with excess $(C_5Me_5)_2U^{III}I(THF)$ in hopes of identifying the resonances attributable to **7.1**. Multiple new resonances were observed, more than would be expected for compound **7.1**, and definitive assignment of the spectrum was not possible.

The reactivity of $(C_5Me_5)_2U^{III}I(THF)$ with adamantyl azide was investigated to determine if the reaction above was unique to a trimethylsilyl azide and if an analogous U(V) compound to **7.1** could be identified. However, only $(C_5Me_5)_2U^{VI}(=NAd)_2$[14] and $(C_5Me_5)_2U^{IV}I_2$ were isolated from this reaction, eq 7.6, and no U(V) intermediate could be definitively identified. However, the formation of $(C_5Me_5)_2U^{IV}I_2$ suggests that a disproportionation reaction is active as in eq 7.5.

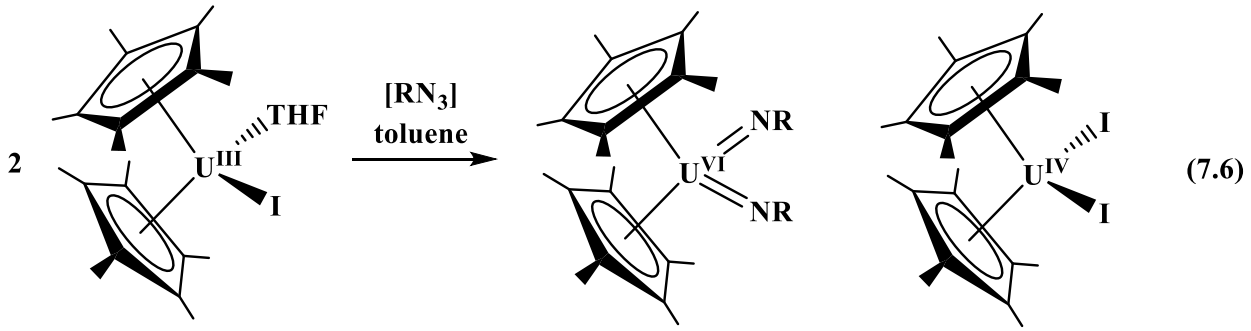

(7.6)

[RN_3] = Me_3SiN_3, AdN_3, PhN=NPh
R = $SiMe_3$, Ad, Ph

$(C_5Me_5)_2U^{VI}(=NSiMe_3)_2$.[16] During these reactions, a second signal was identified in the ^1H NMR spectrum that formed in nearly equal amounts to $(C_5Me_5)_2U^{VI}(=NSiMe_3)_2$. This second species was identified as the U(IV) product, $(C_5Me_5)_2U^{IV}I_2$,[24,34] and its presence can be explained by the disproportionation of **7.1** into $(C_5Me_5)_2U^{VI}(=NSiMe_3)_2$ and $(C_5Me_5)_2U^{IV}I_2$. In other words, compound **7.1** can be an intermediate in the reaction of $(C_5Me_5)_2U^{III}I(THF)$ and Me_3SiN_3, eq 7.5.

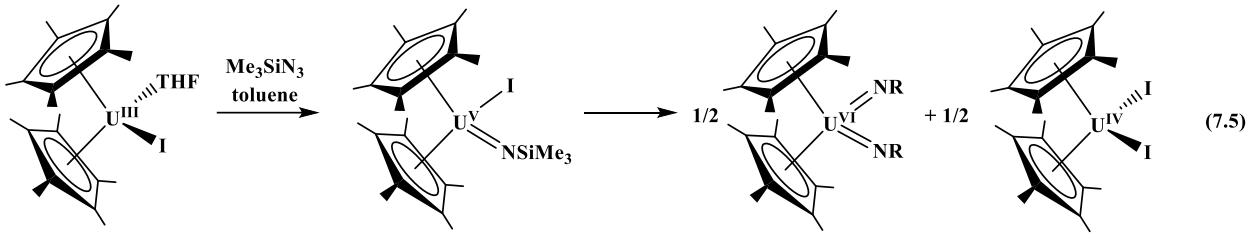

(7.5)

The reaction in eq 7.5 was followed by NMR with excess $(C_5Me_5)_2U^{III}I(THF)$ in hopes of identifying the resonances attributable to **7.1**. Multiple new resonances were observed, more than would be expected for compound **7.1**, and definitive assignment of the spectrum was not possible.

The reactivity of $(C_5Me_5)_2U^{III}I(THF)$ with adamantyl azide was investigated to determine if the reaction above was unique to a trimethylsilyl azide and if an analogous U(V) compound to **7.1** could be identified. However, only $(C_5Me_5)_2U^{VI}(=NAd)_2$[14] and $(C_5Me_5)_2U^{IV}I_2$ were isolated from this reaction, eq 7.6, and no U(V) intermediate could be definitively identified. However, the formation of $(C_5Me_5)_2U^{IV}I_2$ suggests that a disproportionation reaction is active as in eq 7.5.

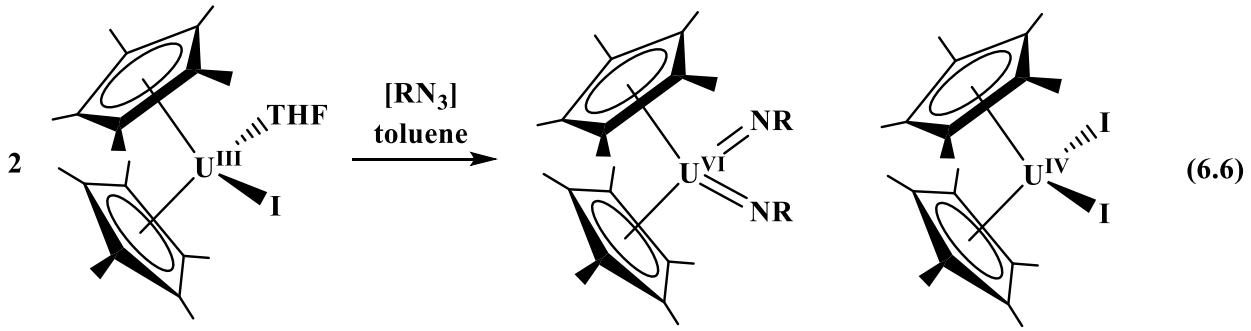

(6.6)

[RN_3] = Me_3SiN_3, AdN_3, PhN=NPh
R = $SiMe_3$, Ad, Ph

Similar results were observed in the reaction of $(C_5Me_5)_2U^{III}I(THF)$ with azobenzene. $(C_5Me_5)_2U^{VI}(=NPh)_2$[14,35] and $(C_5Me_5)_2U^{IV}I_2$ were isolated from the reaction mixture, eq 7.6. Although azobenzene is not formally an azide reagent, the reaction is assumed to again follow a disproportionation mechanism due to the formation of the U(IV) byproduct $(C_5Me_5)_2U^{IV}I_2$.

Discussion

The original mechanisms[14] for the reaction of $(C_5Me_5)_2U^{III}Cl_2Na$ with adamantyl azide, eq 7.1, proposed U(IV) intermediates $(C_5Me_5)_2U^{IV}(=NAd)$ or $(C_5Me_5)_2U^{IV}(RN–NR)$, which could further react to form $(C_5Me_5)_2U^{IV}(=NAd)_2$, Scheme 7.1 The original report does state that $(C_5Me_5)_2U^{IV}Cl_2$ is formed during the reaction, but the authors claimed that this underwent subsequent reduction to the U(III) compound to reenter the proposed reaction cycle.[14] The crystallographic characterization of the U(V) species $(C_5Me_5)_2U^{V}I(=NSiMe_3)$, **7.1**, from the reaction of $(C_5Me_5)_2U^{III}I(THF)$ and N_3SiMe_3 in this Chapter provides insight into the mechanism of the reaction. Further studies on the reaction system showed that the overall reaction proceeds to $(C_5Me_5)_2U^{VI}(=NSiMe_3)_2$ and $(C_5Me_5)_2U^{IV}I_2$, which suggests that **7.1** is an intermediate. Disproportionation of **7.1** would yield the two products $(C_5Me_5)_2U^{VI}(=NSiMe_3)_2$ and $(C_5Me_5)_2U^{IV}I_2$, eq 7.5. Instead of the two reactions proposed in Scheme 7.1, it seems that a disproportionation mechanism is likely active in this reaction with a U(V) intermediate.

Conclusion

Reaction of $(C_5Me_5)_2U^{III}I(THF)$ with azide reagents can form a U(V) intermediate $(C_5Me_5)_2U^{V}I(=NR)$, which was crystallographically identified in the case of $(C_5Me_5)_2U^{V}I(=NSiMe_3)$. It is likely that this intermediate undergoes disproportionation to form a U(IV) product $(C_5Me_5)_2U^{IV}I_2$ and a U(VI) product $(C_5Me_5)_2U^{VI}(=NR)_2$. This study provides a

clear mechanism for the apparent four-electron transformation of a U(III) species into a U(VI) bis-imido product.

Experimental

Crystallization of 7.1. $(C_5Me_5)_2UI(THF)$ (50 mg, 0.071 mmol) was dissolved in toluene (2 mL) to form a dark green solution. N_3SiMe_3 (9 mg, 0.078 mmol) was dissolved in toluene (0.5 mL) and added to the stirring solution. The solution became a brown color. The solution was stirred for two hours then dried under vacuum. Hexane (5 mL) was added to form a brown suspension. The mixture was centrifuged to remove the solids and dried under vacuum. ^{1}H NMR and IR spectroscopy showed the presence of a new paramagnetic compound and suggested the presence of an azide with a stretching frequency of 2114 cm^{-1}. Brown X-ray quality crystals of **7.1** were grown from a concentrated hexane solution at −35 °C.

Reaction of $(C_5Me_5)_2UI(THF)$ and N_3SiMe_3. $(C_5Me_5)_2UI(THF)$ (100 mg, 0.141 mmol) was dissolved in toluene (5 mL) to form a dark green solution. N_3SiMe_3 (18 mg, 0.16 mmol) was dissolved in toluene (0.5 mL) and added to the stirring solution by pipet. The solution became dark brown immediately. The solution was stirred for 30 minutes then dried under vacuum. Hexane (8 mL) was added and the solution was stirred for one hour. Red solids were removed by filtration and the solution was dried to yield brown solids (68 mg, 67%). The ^{1}H NMR spectrum in C_6D_6 showed equal amounts of $(C_5Me_5)_2U(=NSiMe_3)_2$ (δ 4.91 ppm, C_5Me_5)[16] and $(C_5Me_5)_2UI_2$ (δ 17.99 ppm, C_5Me_5).[34]

Reaction of $(C_5Me_5)_2UI(THF)$ and N_3Ad. As above, $(C_5Me_5)_2UI(THF)$ (50 mg, 0.071 mmol) and N_3Ad (13 mg, 0.073 mmol) were combined in toluene (5 mL) to form a brown solution. Slight gas evolution was observed. The solution was dried and the products were extracted into hexane (47 mg, 85%). The ^{1}H NMR spectrum in C_6D_6 showed equal amounts of

$(C_5Me_5)_2U(=NAd)_2$ (δ 4.07 ppm, C_5Me_5)[14] and $(C_5Me_5)_2UI_2$ (δ 18.00 ppm, C_5Me_5).[34] Brown crystals of $(C_5Me_5)_2U(=NAd)_2$ were grown from a concentrated toluene solution at −35 °C and identified by X-ray diffraction.[14]

Reaction of $(C_5Me_5)_2UI(THF)$ and PhN=NPh. As above, $(C_5Me_5)_2UI(THF)$ (50 mg, 0.071 mmol) and PhN=NPh (6.5 mg, 0.036 mmol) were combined in toluene (5 mL) to form a red/brown solution. The solution was stirred for 30 minutes then dried. The products were extracted into hexane, filtered, and dried to yield dark brown solids (39 mg, 76%). The ^{1}H NMR spectrum in C_6D_6 showed equal amounts of $(C_5Me_5)_2U(=NPh)_2$ (δ 4.11 ppm, C_5Me_5)[14] and $(C_5Me_5)_2UI_2$ (δ 17.95 ppm, C_5Me_5).[34]

X-ray Data Collection, Structure Solution and Refinement for 7.1.

A brown crystal of approximate dimensions 0.213 x 0.091 x 0.059 mm was mounted in a cryoloop and transferred to a Bruker SMART APEX II diffractometer system. The APEX2[36] program package was used to determine the unit-cell parameters and for data collection (120 sec/frame scan time). The raw frame data was processed using SAINT[37] and SADABS[38] to yield the reflection data file. Subsequent calculations were carried out using the SHELXTL[39] program package. The diffraction symmetry was 2/*m* and the systematic absences were consistent with the monoclinic space group $P2_1/m$ that was later determined to be correct.

The structure was solved by direct methods and refined on F^2 by full-matrix least-squares techniques. The analytical scattering factors[40] for neutral atoms were used throughout the analysis. Hydrogen atoms were included using a riding model. There were two halves of the molecule in the asymmetric unit. The pentamethylcyclopentadienyl carbons were refined using equivalent anisotropic displacement parameters.

Least-squares analysis yielded wR2 = 0.2141 and Goof = 1.020 for 179 variables refined against 9606 data (0.70 Å), R1 = 0.0766 for those 5680 data with $I > 2.0\sigma(I)$.

Table 7.1: Crystal data and structure refinement for **7.1**.

Identification code	jcw104	
Empirical formula	C_{23} H_{39} I N Si U	
Formula weight	722.57	
Temperature	133(2) K	
Wavelength	0.71073 Å	
Crystal system	Monoclinic	
Space group	$P2_1/m$	
Unit cell dimensions	a = 10.0201(14) Å	α = 90°.
	b = 15.855(2) Å	β = 101.636(2)°.
	c = 19.994(3) Å	γ = 90°.
Volume	3111.2(7) $Å^3$	
Z	4	
Density (calculated)	1.543 mg/m^3	
Absorption coefficient	6.255 mm^{-1}	
F(000)	1372	
Crystal color	brown	
Crystal size	0.213 x 0.091 x 0.059 mm^3	
Theta range for data collection	1.653 to 30.595°	
Index ranges	$-13 \le h \le 14$, $-22 \le k \le 22$, $-28 \le l \le 28$	
Reflections collected	47956	
Independent reflections	9606 [R(int) = 0.0995]	
Completeness to theta = 25.242°	100.0 %	
Absorption correction	Semi-empirical from equivalents	
Max. and min. transmission	0.4330 and 0.3383	
Refinement method	Full-matrix least-squares on F^2	
Data / restraints / parameters	9606 / 0 / 179	
Goodness-of-fit on F^2	1.020	

Final R indices [I>2sigma(I) = 5680 data]	R1 = 0.0766, wR2 = 0.1894
R indices (all data, 0.70 Å)	R1 = 0.1288, wR2 = 0.2141
Largest diff. peak and hole	2.919 and -1.797 e.Å^{-3}

Table 7.2: Bond lengths [Å] and angles [°] for **7.1**.

U(1)-Cnt	2.496	C(5)-C(10)	1.481(5)
U(1)-N(1)	2.060(9)	C(6)-H(6A)	0.9802
U(1)-C(1)#1	2.701(19)	C(6)-H(6B)	0.9802
U(1)-C(1)	2.701(8)	C(6)-H(6C)	0.9802
U(1)-C(2)#1	2.741(7)	C(7)-H(7A)	0.9841
U(1)-C(2)	2.741(7)	C(7)-H(7B)	0.9841
U(1)-C(5)#1	2.75(2)	C(7)-H(7C)	0.9841
U(1)-C(5)	2.746(8)	C(8)-H(8A)	0.9802
U(1)-C(3)	2.810(7)	C(8)-H(8B)	0.9802
U(1)-C(3)#1	2.81(2)	C(8)-H(8C)	0.9802
U(1)-C(4)#1	2.81(2)	C(9)-H(9A)	0.9802
U(1)-C(4)	2.813(7)	C(9)-H(9B)	0.9802
U(1)-I(1)	3.1135(12)	C(9)-H(9C)	0.9802
Si(1)-N(1)	1.668(11)	C(10)-H(10A)	0.9805
Si(1)-C(11)#1	1.81(2)	C(10)-H(10B)	0.9805
Si(1)-C(11)	1.81(2)	C(10)-H(10C)	0.9805
Si(1)-C(12)	1.81(3)	C(11)-H(11A)	0.9801
C(2)-C(3)	1.392(5)	C(11)-H(11B)	0.9801
C(2)-C(1)	1.393(5)	C(11)-H(11C)	0.9801
C(2)-C(7)	1.480(5)	C(12)-H(12A)	1.0157
C(1)-C(5)	1.394(5)	C(12)-H(12B)	1.0158
C(1)-C(6)	1.480(5)	C(12)-H(12C)	1.0159
C(3)-C(4)	1.392(5)	U(2)-N(2)	2.104(12)
C(3)-C(8)	1.480(5)	U(2)-C(14)	2.673(8)
C(4)-C(5)	1.392(5)	U(2)-C(14)#2	2.67(2)
C(4)-C(9)	1.482(5)	U(2)-C(13)	2.719(7)

U(2)-C(13)#2	2.72(2)	C(21)-H(21A)	0.9807
U(2)-C(15)	2.735(8)	C(21)-H(21B)	0.9807
U(2)-C(15)#2	2.74(2)	C(21)-H(21C)	0.9807
U(2)-C(17)#2	2.807(7)	C(22)-H(22A)	0.9799
U(2)-C(17)	2.807(7)	C(22)-H(22B)	0.9799
U(2)-C(16)	2.817(8)	C(22)-H(22C)	0.9799
U(2)-C(16)#2	2.82(2)	C(23)-H(23A)	0.9886
U(2)-I(2)	3.1086(12)	C(23)-H(23B)	0.9886
Si(2)-N(2)	1.615(13)	C(23)-H(23C)	0.9886
Si(2)-C(23)	1.862(18)	C(24)-H(24A)	0.9800
Si(2)-C(24)#2	1.863(18)	C(24)-H(24B)	0.9800
Si(2)-C(24)	1.863(18)	C(24)-H(24C)	0.9800
C(17)-C(16)	1.371(5)		
C(17)-C(13)	1.371(5)	Cnt-U(1)-Cnt	130.77
C(17)-C(18)	1.457(6)	Cnt-U(1)-N(1)	103.83
C(13)-C(14)	1.371(5)	Cnt-U(1)-I(1)	111.68
C(13)-C(19)	1.457(6)	N(1)-U(1)-C(1)#1	90.7(5)
C(14)-C(15)	1.371(5)	N(1)-U(1)-C(1)	90.67(17)
C(14)-C(20)	1.457(6)	C(1)#1-U(1)-C(1)	175.7(5)
C(15)-C(16)	1.371(5)	N(1)-U(1)-C(2)#1	120.29(16)
C(15)-C(21)	1.457(6)	C(1)#1-U(1)-C(2)#1	29.7(5)
C(16)-C(22)	1.457(6)	C(1)-U(1)-C(2)#1	148.9(3)
C(18)-H(18A)	0.9799	N(1)-U(1)-C(2)	120.29(16)
C(18)-H(18B)	0.9799	C(1)#1-U(1)-C(2)	148.9(5)
C(18)-H(18C)	0.9799	C(1)-U(1)-C(2)	29.65(12)
C(19)-H(19A)	1.0037	C(2)#1-U(1)-C(2)	119.4(3)
C(19)-H(19B)	1.0037	N(1)-U(1)-C(5)#1	78.7(5)
C(19)-H(19C)	1.0037	C(1)#1-U(1)-C(5)#1	29.6(3)
C(20)-H(20A)	0.9799	C(1)-U(1)-C(5)#1	154.7(5)
C(20)-H(20B)	0.9799	C(2)#1-U(1)-C(5)#1	48.5(5)
C(20)-H(20C)	0.9799	C(2)-U(1)-C(5)#1	150.4(5)

N(1)-U(1)-C(5)	78.7(2)	C(1)#1-U(1)-C(4)	135.5(5)
C(1)#1-U(1)-C(5)	154.7(5)	C(1)-U(1)-C(4)	48.18(18)
C(1)-U(1)-C(5)	29.63(12)	C(2)#1-U(1)-C(4)	121.4(3)
C(2)#1-U(1)-C(5)	150.4(3)	C(2)-U(1)-C(4)	47.83(18)
C(2)-U(1)-C(5)	48.50(18)	C(5)#1-U(1)-C(4)	110.5(5)
C(5)#1-U(1)-C(5)	125.1(5)	C(5)-U(1)-C(4)	28.97(11)
N(1)-U(1)-C(3)	125.9(2)	C(3)-U(1)-C(4)	28.67(11)
C(1)#1-U(1)-C(3)	133.2(5)	C(3)#1-U(1)-C(4)	93.2(4)
C(1)-U(1)-C(3)	48.23(18)	C(4)#1-U(1)-C(4)	87.4(5)
C(2)#1-U(1)-C(3)	107.0(3)	N(1)-U(1)-I(1)	82.5(3)
C(2)-U(1)-C(3)	29.02(11)	C(1)#1-U(1)-I(1)	88.0(5)
C(5)#1-U(1)-C(3)	121.9(5)	C(1)-U(1)-I(1)	88.04(17)
C(5)-U(1)-C(3)	47.84(18)	C(2)#1-U(1)-I(1)	93.17(17)
N(1)-U(1)-C(3)#1	125.9(4)	C(2)-U(1)-I(1)	93.17(17)
C(1)#1-U(1)-C(3)#1	48.2(5)	C(5)#1-U(1)-I(1)	112.8(5)
C(1)-U(1)-C(3)#1	133.2(3)	C(5)-U(1)-I(1)	112.85(18)
C(2)#1-U(1)-C(3)#1	29.0(4)	C(3)-U(1)-I(1)	121.30(18)
C(2)-U(1)-C(3)#1	107.0(4)	C(3)#1-U(1)-I(1)	121.3(4)
C(5)#1-U(1)-C(3)#1	47.8(5)	C(4)#1-U(1)-I(1)	136.0(4)
C(5)-U(1)-C(3)#1	121.9(4)	C(4)-U(1)-I(1)	136.03(17)
C(3)-U(1)-C(3)#1	85.1(5)	N(1)-Si(1)-C(11)#1	111.3(8)
N(1)-U(1)-C(4)#1	99.4(5)	N(1)-Si(1)-C(11)	111.3(8)
C(1)#1-U(1)-C(4)#1	48.2(5)	C(11)#1-Si(1)-C(11)	112.2(19)
C(1)-U(1)-C(4)#1	135.5(4)	N(1)-Si(1)-C(12)	110.6(10)
C(2)#1-U(1)-C(4)#1	47.8(4)	C(11)#1-Si(1)-C(12)	105.6(8)
C(2)-U(1)-C(4)#1	121.4(4)	C(11)-Si(1)-C(12)	105.6(8)
C(5)#1-U(1)-C(4)#1	29.0(3)	Si(1)-N(1)-U(1)	163.9(7)
C(5)-U(1)-C(4)#1	110.5(4)	C(3)-C(2)-C(1)	108.0
C(3)-U(1)-C(4)#1	93.2(4)	C(3)-C(2)-C(7)	126.0
C(3)#1-U(1)-C(4)#1	28.7(3)	C(1)-C(2)-C(7)	126.0
N(1)-U(1)-C(4)	99.4(3)	C(3)-C(2)-U(1)	78.3(3)

C(1)-C(2)-U(1)	73.6(3)	H(6B)-C(6)-H(6C)	109.5
C(7)-C(2)-U(1)	114.5(3)	C(2)-C(7)-H(7A)	109.9
C(2)-C(1)-C(5)	108.0	C(2)-C(7)-H(7B)	109.9
C(2)-C(1)-C(6)	126.0	H(7A)-C(7)-H(7B)	109.1
C(5)-C(1)-C(6)	126.0	C(2)-C(7)-H(7C)	109.9
C(2)-C(1)-U(1)	76.7(3)	H(7A)-C(7)-H(7C)	109.1
C(5)-C(1)-U(1)	77.0(3)	H(7B)-C(7)-H(7C)	109.1
C(6)-C(1)-U(1)	112.7(3)	C(3)-C(8)-H(8A)	109.5
C(2)-C(3)-C(4)	108.0	C(3)-C(8)-H(8B)	109.5
C(2)-C(3)-C(8)	126.0	H(8A)-C(8)-H(8B)	109.5
C(4)-C(3)-C(8)	126.0	C(3)-C(8)-H(8C)	109.5
C(2)-C(3)-U(1)	72.7(3)	H(8A)-C(8)-H(8C)	109.5
C(4)-C(3)-U(1)	75.8(3)	H(8B)-C(8)-H(8C)	109.5
C(8)-C(3)-U(1)	117.5(3)	C(4)-C(9)-H(9A)	109.5
C(5)-C(4)-C(3)	108.1	C(4)-C(9)-H(9B)	109.5
C(5)-C(4)-C(9)	125.9	H(9A)-C(9)-H(9B)	109.5
C(3)-C(4)-C(9)	126.0	C(4)-C(9)-H(9C)	109.5
C(5)-C(4)-U(1)	72.8(3)	H(9A)-C(9)-H(9C)	109.5
C(3)-C(4)-U(1)	75.5(3)	H(9B)-C(9)-H(9C)	109.5
C(9)-C(4)-U(1)	117.6(3)	C(5)-C(10)-H(10A)	109.5
C(4)-C(5)-C(1)	108.0	C(5)-C(10)-H(10B)	109.5
C(4)-C(5)-C(10)	126.1	H(10A)-C(10)-H(10B)	109.4
C(1)-C(5)-C(10)	126.0	C(5)-C(10)-H(10C)	109.5
C(4)-C(5)-U(1)	78.2(3)	H(10A)-C(10)-H(10C)	109.4
C(1)-C(5)-U(1)	73.4(3)	H(10B)-C(10)-H(10C)	109.4
C(10)-C(5)-U(1)	114.7(3)	Si(1)-C(11)-H(11A)	109.5
C(1)-C(6)-H(6A)	109.5	Si(1)-C(11)-H(11B)	109.5
C(1)-C(6)-H(6B)	109.5	H(11A)-C(11)-H(11B)	109.5
H(6A)-C(6)-H(6B)	109.5	Si(1)-C(11)-H(11C)	109.4
C(1)-C(6)-H(6C)	109.5	H(11A)-C(11)-H(11C)	109.5
H(6A)-C(6)-H(6C)	109.5	H(11B)-C(11)-H(11C)	109.5

Si(1)-C(12)-H(12A)	112.3	C(13)#2-U(2)-C(17)#2	28.7(5)
Si(1)-C(12)-H(12B)	112.3	C(15)-U(2)-C(17)#2	120.1(3)
H(12A)-C(12)-H(12B)	106.5	C(15)#2-U(2)-C(17)#2	47.2(6)
Si(1)-C(12)-H(12C)	112.3	N(2)-U(2)-C(17)	126.3(2)
H(12A)-C(12)-H(12C)	106.5	C(14)-U(2)-C(17)	47.68(19)
H(12B)-C(12)-H(12C)	106.5	C(14)#2-U(2)-C(17)	132.3(5)
N(2)-U(2)-C(14)	90.47(18)	C(13)-U(2)-C(17)	28.67(12)
N(2)-U(2)-C(14)#2	90.5(5)	C(13)#2-U(2)-C(17)	106.8(5)
C(14)-U(2)-C(14)#2	178.5(6)	C(15)-U(2)-C(17)	47.17(19)
N(2)-U(2)-C(13)	119.92(17)	C(15)#2-U(2)-C(17)	120.1(5)
C(14)-U(2)-C(13)	29.45(12)	C(17)#2-U(2)-C(17)	84.6(4)
C(14)#2-U(2)-C(13)	149.6(6)	N(2)-U(2)-C(16)	100.5(3)
N(2)-U(2)-C(13)#2	119.9(4)	C(14)-U(2)-C(16)	47.6(2)
C(14)-U(2)-C(13)#2	149.6(5)	C(14)#2-U(2)-C(16)	133.3(5)
C(14)#2-U(2)-C(13)#2	29.5(3)	C(13)-U(2)-C(16)	47.20(19)
C(13)-U(2)-C(13)#2	120.2(5)	C(13)#2-U(2)-C(16)	120.0(5)
N(2)-U(2)-C(15)	79.5(2)	C(15)-U(2)-C(16)	28.54(12)
C(14)-U(2)-C(15)	29.34(12)	C(15)#2-U(2)-C(16)	108.4(5)
C(14)#2-U(2)-C(15)	152.1(5)	C(17)#2-U(2)-C(16)	92.0(3)
C(13)-U(2)-C(15)	48.00(19)	C(17)-U(2)-C(16)	28.22(12)
C(13)#2-U(2)-C(15)	148.5(5)	N(2)-U(2)-C(16)#2	100.5(5)
N(2)-U(2)-C(15)#2	79.5(5)	C(14)-U(2)-C(16)#2	133.3(4)
C(14)-U(2)-C(15)#2	152.1(5)	C(14)#2-U(2)-C(16)#2	47.6(6)
C(14)#2-U(2)-C(15)#2	29.3(3)	C(13)-U(2)-C(16)#2	120.0(4)
C(13)-U(2)-C(15)#2	148.5(5)	C(13)#2-U(2)-C(16)#2	47.2(5)
C(13)#2-U(2)-C(15)#2	48.0(5)	C(15)-U(2)-C(16)#2	108.4(5)
C(15)-U(2)-C(15)#2	122.8(5)	C(15)#2-U(2)-C(16)#2	28.5(3)
N(2)-U(2)-C(17)#2	126.3(2)	C(17)#2-U(2)-C(16)#2	28.2(4)
C(14)-U(2)-C(17)#2	132.3(3)	C(17)-U(2)-C(16)#2	92.0(5)
C(14)#2-U(2)-C(17)#2	47.7(6)	C(16)-U(2)-C(16)#2	85.8(5)
C(13)-U(2)-C(17)#2	106.8(3)	N(2)-U(2)-I(2)	81.4(3)

C(14)-U(2)-I(2)	89.49(18)	C(13)-C(14)-C(20)	126.0
C(14)#2-U(2)-I(2)	89.5(5)	C(15)-C(14)-U(2)	77.8(3)
C(13)-U(2)-I(2)	94.16(17)	C(13)-C(14)-U(2)	77.1(3)
C(13)#2-U(2)-I(2)	94.2(5)	C(20)-C(14)-U(2)	111.6(3)
C(15)-U(2)-I(2)	114.3(2)	C(16)-C(15)-C(14)	108.0
C(15)#2-U(2)-I(2)	114.3(5)	C(16)-C(15)-C(21)	126.0
C(17)#2-U(2)-I(2)	121.85(18)	C(14)-C(15)-C(21)	126.0
C(17)-U(2)-I(2)	121.85(18)	C(16)-C(15)-U(2)	79.0(3)
C(16)-U(2)-I(2)	136.8(2)	C(14)-C(15)-U(2)	72.8(3)
C(16)#2-U(2)-I(2)	136.8(4)	C(21)-C(15)-U(2)	114.4(3)
N(2)-Si(2)-C(23)	111.4(8)	C(15)-C(16)-C(17)	108.0
N(2)-Si(2)-C(24)#2	112.0(6)	C(15)-C(16)-C(22)	126.0
C(23)-Si(2)-C(24)#2	107.9(7)	C(17)-C(16)-C(22)	126.0
N(2)-Si(2)-C(24)	112.0(6)	C(15)-C(16)-U(2)	72.4(3)
C(23)-Si(2)-C(24)	107.9(7)	C(17)-C(16)-U(2)	75.5(3)
C(24)#2-Si(2)-C(24)	105.4(15)	C(22)-C(16)-U(2)	118.0(3)
Si(2)-N(2)-U(2)	164.2(6)	C(17)-C(18)-H(18A)	109.5
C(16)-C(17)-C(13)	108.0	C(17)-C(18)-H(18B)	109.5
C(16)-C(17)-C(18)	126.0	H(18A)-C(18)-H(18B)	109.5
C(13)-C(17)-C(18)	126.0	C(17)-C(18)-H(18C)	109.5
C(16)-C(17)-U(2)	76.3(3)	H(18A)-C(18)-H(18C)	109.5
C(13)-C(17)-U(2)	72.1(3)	H(18B)-C(18)-H(18C)	109.5
C(18)-C(17)-U(2)	117.6(3)	C(13)-C(19)-H(19A)	112.0
C(17)-C(13)-C(14)	108.0	C(13)-C(19)-H(19B)	112.0
C(17)-C(13)-C(19)	126.0	H(19A)-C(19)-H(19B)	106.9
C(14)-C(13)-C(19)	126.0	C(13)-C(19)-H(19C)	112.0
C(17)-C(13)-U(2)	79.2(3)	H(19A)-C(19)-H(19C)	106.9
C(14)-C(13)-U(2)	73.4(3)	H(19B)-C(19)-H(19C)	106.9
C(19)-C(13)-U(2)	113.6(3)	C(14)-C(20)-H(20A)	109.5
C(15)-C(14)-C(13)	108.0	C(14)-C(20)-H(20B)	109.5
C(15)-C(14)-C(20)	126.0	H(20A)-C(20)-H(20B)	109.5

C(14)-C(20)-H(20C)	109.5	H(22B)-C(22)-H(22C)	109.5
H(20A)-C(20)-H(20C)	109.5	Si(2)-C(23)-H(23A)	110.2
H(20B)-C(20)-H(20C)	109.5	Si(2)-C(23)-H(23B)	110.1
C(15)-C(21)-H(21A)	109.6	H(23A)-C(23)-H(23B)	108.8
C(15)-C(21)-H(21B)	109.6	Si(2)-C(23)-H(23C)	110.1
H(21A)-C(21)-H(21B)	109.4	H(23A)-C(23)-H(23C)	108.8
C(15)-C(21)-H(21C)	109.6	H(23B)-C(23)-H(23C)	108.8
H(21A)-C(21)-H(21C)	109.4	Si(2)-C(24)-H(24A)	109.5
H(21B)-C(21)-H(21C)	109.4	Si(2)-C(24)-H(24B)	109.5
C(16)-C(22)-H(22A)	109.5	H(24A)-C(24)-H(24B)	109.5
C(16)-C(22)-H(22B)	109.5	Si(2)-C(24)-H(24C)	109.5
H(22A)-C(22)-H(22B)	109.5	H(24A)-C(24)-H(24C)	109.5
C(16)-C(22)-H(22C)	109.5	H(24B)-C(24)-H(24C)	109.5
H(22A)-C(22)-H(22C)	109.5		

Symmetry transformations used to generate equivalent atoms:

#1 x,-y+1/2,z #2 x,-y+3/2,z

References

(1) Hayton, T. W.; Boncella, J. M.; Scott, B. L.; Palmer, P. D.; Batista, E. R.; Jeffrey Hay, P. Sythesis of Imido Analogs of the Uranyl Ion. *Science.* **2005**, *310*, 1941–1943, DOI: 10.1126/science.1120069.

(2) Staun, S. L.; Wu, G.; Lukens, W. W.; Hayton, T. W. Synthesis of a Heterobimetallic Actinide Nitride and an Analysis of Its Bonding. *Chem. Sci.* **2021**, *12*, 15519–15527, DOI: 10.1039/d1sc05072a.

(3) Hayton, T. W. Metal–Ligand Multiple Bonding in Uranium: Structure and Reactivity. *Dalton Trans.* **2010**, *39*, 1145–1158, DOI: 10.1039/B909238B.

(4) Du, J.; Seed, J. A.; Berryman, V. E. J.; Kaltsoyannis, N.; Adams, R. W.; Lee, D.; Liddle,

S. T. Exceptional Uranium(VI)-Nitride Triple Bond Covalency from ^{15}N Nuclear Magnetic Resonance Spectroscopy and Quantum Chemical Analysis. *Nat. Commun.* **2021**, *12*, 5649, DOI: 10.1038/s41467-021-25863-2.

(5) King, D. M.; Tuna, F.; McInnes, E. J. L.; McMaster, J.; Lewis, W.; Blake, A. J.; Liddle, S. T. Isolation and Characterization of a Uranium(VI)–Nitride Triple Bond. *Nat. Chem.* **2013**, *5*, 482–488, DOI: 10.1038/nchem.1642.

(6) Hayton, T. W. Recent Developments in Actinide-Ligand Multiple Bonding. *Chem. Commun.* **2013**, *49*, 2956–2973, DOI: 10.1039/c3cc39053e.

(7) Falcone, M.; Chatelain, L.; Scopelliti, R.; Živković, I.; Mazzanti, M. Nitrogen Reduction and Functionalization by a Multimetallic Uranium Nitride Complex. *Nature* **2017**, *547*, 332–335, DOI: 10.1038/nature23279.

(8) Camp, C.; Pécaut, J.; Mazzanti, M. Tuning Uranium–Nitrogen Multiple Bond Formation with Ancillary Siloxide Ligands. *J. Am. Chem. Soc.* **2013**, *135*, 12101–12111, DOI: 10.1021/ja405815b.

(9) Dutkiewicz, M. S.; Goodwin, C. A. P.; Perfetti, M.; Gaunt, A. J.; Griveau, J. C.; Colineau, E.; Kovács, A.; Wooles, A. J.; Caciuffo, R.; Walter, O.; Liddle, S. T. A Terminal Neptunium(V)–Mono(Oxo) Complex. *Nat. Chem.* **2022**, *14*, 342–349, DOI: 10.1038/s41557-021-00858-0.

(10) Arnold, P. L.; Pécharman, A. F.; Hollis, E.; Yahia, A.; Maron, L.; Parsons, S.; Love, J. B. Uranyl Oxo Activation and Functionalization by Metal Cation Coordination. *Nat. Chem.* **2010**, *2*, 1056–1061, DOI: 10.1038/nchem.904.

(11) Ephritikhine, M. The Vitality of Uranium Molecular Chemistry at the Dawn of the XXIst Century. *Dalton Trans.* **2006**, No. 21, 2501–2516, DOI: 10.1039/b603463b.

(12) La Pierre, H. S.; Meyer, K. Activation of Small Molecules by Molecular Uranium Complexes. *Prog. Inorg. Chem.* **2014**, *58*, 303–416, DOI: 10.1002/9781118792797.ch05.

(13) Wedal, J. C.; Evans, W. J. A Rare-Earth Metal Retrospective to Stimulate All Fields. *J. Am. Chem. Soc.* **2021**, *143*, 18354–18367, DOI: 10.1021/jacs.1c08288.

(14) Warner, B. P.; Scott, B. L.; Burns, C. J. A Simple Preparative Route to Bis(Imido)Uranium(VI) Complexes by the Direct Reductions of Diazenes and Azides. *Angew. Chem. Int. Ed.* **1998**, *37*, 959–960, DOI: 10.1002/(SICI)1521-3773(19980420)37:7<959::AID-ANIE959>3.0.CO;2-D.

(15) Evans, W. J.; Kozimor, S. A.; Ziller, J. W. $[(C_5Me_5)_2U][(\mu\text{–}Ph)_2BPh_2]$ as a Four Electron Reductant. *Chem. Commun.* **2005**, No. 37, 4681, DOI: 10.1039/b508612d.

(16) Rungthanaphatsophon, P.; Barnes, C. L.; Kelley, S. P.; Walensky, J. R. Four-Electron Reduction Chemistry Using a Uranium(III) Phosphido Complex. *Dalton Trans.* **2018**, *47*, 8189–8192, DOI: 10.1039/C8DT01406J.

(17) Evans, W. J.; Montalvo, E.; Ziller, J. W.; DiPasquale, A. G.; Rheingold, A. L. Uranium Metallocene Complexes of the 1,3,4,6,7,8-Hexahydro-2H-Pyrimido[1,2-a]Pyrimidinato Ligand, $(Hpp)^{-}$. *Inorg. Chem.* **2010**, *49*, 222–228, DOI: 10.1021/ic901790t.

(18) Blake, P. C.; Lappert, M. F.; Taylor, R. G.; Atwood, J. L.; Zhang, H. Some Aspects of the Coordination and Organometallic Chemistry of Thorium and Uranium (M^{III}, M^{IV}, U^{V}) in +3 and +4 Oxidation States. *Inorg. Chim. Acta* **1987**, *139*, 13–20, DOI: 10.1016/S0020-1693(00)84028-1.

(19) Zi, G.; Blosch, L. L.; Jia, L.; Andersen, R. A. Preparation and Reactions of Base-Free Bis(1,2,4-Tri-Tert -Butylcyclopentadienyl)Uranium Methylimide, $Cp'_2U{=}NMe$, and Related Compounds. *Organometallics* **2005**, *24*, 4602–4612, DOI: 10.1021/om050427k.

(20) Brennan, J. G.; Andersen, R. A. Electron-Transfer Reactions of Trivalent Uranium. Preparation and Structure of the Uranium Metallocene Compounds $(MeC_5H_4)_3U{=}NPh$ and $[(MeC_5H_4)_3U]_2[\mu\text{-}\eta^1,\eta^2\text{-}PhNCO]$. *J. Am. Chem. Soc.* **1985**, *107*, 514–516, DOI: 10.1021/ja00288a047.

(21) Zalkin, A.; Brennan, J. G.; Andersen, R. A. Tris[Bis(Trimethylsilyl)Amido](Trimethylsilylimido)Uranium(V). *Acta Crystallogr. Sect. C Cryst. Struct. Commun.* **1988**, *44*, 1553–1554, DOI: 10.1107/S0108270188005116.

(22) Mullane, K. C.; Carroll, P. J.; Schelter, E. J. Synthesis and Reduction of Uranium(V) Imido Complexes with Redox-Active Substituents. *Chem. – Eur. J.* **2017**, *23*, 5748–5757, DOI: 10.1002/chem.201605758.

(23) Castro-Rodriguez, I.; Olsen, K.; Gantzel, P.; Meyer, K. Uranium Tris-Aryloxide Derivatives Supported by Triazacyclononane: Engendering a Reactive Uranium(III) Center with a Single Pocket for Reactivity. *J. Am. Chem. Soc.* **2003**, *125*, 4565–4571, DOI: 10.1021/ja028342n.

(24) Graves, C. R.; Schelter, E. J.; Cantat, T.; Scott, B. L.; Kiplinger, J. L. A Mild Protocol to Generate Uranium(IV) Mixed-Ligand Metallocene Complexes Using Copper(I) Iodide. *Organometallics* **2008**, *27*, 5371–5378, DOI: 10.1021/om800622g.

(25) Graves, C. R.; Scott, B. L.; Morris, D. E.; Kiplinger, J. L. Tetravalent and Pentavalent Uranium Acetylide Complexes Prepared by Oxidative Functionalization with CuC≡CPh. *Organometallics* **2008**, *27*, 3335–3337, DOI: 10.1021/om800466m.

(26) Graves, C. R.; Vaughn, A. E.; Schelter, E. J.; Scott, B. L.; Thompson, J. D.; Morris, D. E.; Kiplinger, J. L. Probing the Chemistry, Electronic Structure and Redox Energetics in Organometallic Pentavalent Uranium Complexes. *Inorg. Chem.* **2008**, *47*, 11879–11891,

DOI: 10.1021/ic8017375.

(27) Graves, C. R.; Scott, B. L.; Morris, D. E.; Kiplinger, J. L. Selenate and Tellurate Complexes of Pentavalent Uranium. *Chem. Commun.* **2009**, No. 7, 776, DOI: 10.1039/b819097f.

(28) Evans, W. J.; Kozimor, S. A.; Ziller, J. W. Molecular Octa-Uranium Rings with Alternating Nitride and Azide Bridges. *Science.* **2005**, *309*, 1835–1838, DOI: 10.1126/science.1116168.

(29) Boreen, M. A.; Rao, G.; Villarreal, D. G.; Watt, F. A.; Britt, R. D.; Hohloch, S.; Arnold, J. Lewis Acid Capping of a Uranium(V) Nitride: Via a Uranium(III) Azide Molecular Square. *Chem. Commun.* **2020**, *56*, 4535–4538, DOI: 10.1039/d0cc01356k.

(30) Graves, C. R.; Scott, B. L.; Morris, D. E.; Kiplinger, J. L. Facile Access to Pentavalent Uranium Organometallics: One-Electron Oxidation of Uranium(IV) Imido Complexes with Copper(I) Salts. *J. Am. Chem. Soc.* **2007**, *129*, 11914–11915, DOI: 10.1021/ja074889w.

(31) Graves, C. R.; Yang, P.; Kozimor, S. A.; Vaughn, A. E.; Clark, D. L.; Conradson, S. D.; Schelter, E. J.; Scott, B. L.; Thompson, J. D.; Hay, P. J.; Morris, D. E.; Kiplinger, J. L. Organometallic Uranium(V)-Imido Halide Complexes: From Synthesis to Electronic Structure and Bonding. *J. Am. Chem. Soc.* **2008**, *130*, 5272–5285, DOI: 10.1021/ja711010h.

(32) Kaleta, K.; Kessler, M.; Beweries, T.; Arndt, P.; Spannenberg, A.; Rosenthal, U. Different Inertness of Titanocene [Cp_2Ti] and Decamethyltitanocene [Cp^*_2Ti] in Reactions with N,N -Bis(Trimethylsilyl)Sulfurdiimide – Elimination of Tetramethyl-fulvene and Formation of Half-Titanocene Complexes. *Eur. J. Inorg. Chem.* **2012**, *2012*, 3388–3393,

DOI: 10.1002/ejic.201200242.

(33) Jana, A.; Roesky, H. W.; Schulzke, C. Reactivity of Germanium(II) Hydride with Nitrous Oxide, Trimethylsilyl Azide, Ketones, and Alkynes and the Reaction of a Methyl Analogue with Trimethylsilyl Diazomethane. *Dalton Trans.* **2010**, *39*, 132–138, DOI: 10.1039/B914164B.

(34) Maynadié, J.; Berthet, J.-C.; Thuéry, P.; Ephritikhine, M. An Unprecedented Type of Linear Metallocene with an F-Element. *J. Am. Chem. Soc.* **2006**, *128*, 1082–1083, DOI: 10.1021/ja057226s.

(35) Arney, D. S. J.; Burns, C. J.; Smith, D. C. Synthesis and Structure of the First Uranium(VI) Organometallic Complex. *J. Am. Chem. Soc.* **1992**, *114*, 10068–10069, DOI: 10.1021/ja00051a053.

(36) APEX2, Version 2014.11-0, Bruker AXS, Inc: Madison, WI 2014.

(37) SAINT, Version 8.34a, Bruker AXS, Inc: Madison, WI 2013.

(38) Sheldrick, G. M. SADABS, Version 2014/5, Bruker AXS, Inc: Madison, WI 2014.

(39) Sheldrick, G. M. SHELXTL, Version 2014/7, Bruker AXS, Inc: Madison, WI 2014.

(40) *International Tables for Crystallography*; Vol C, Kluwer Academic Publishers: Dordrecht, 1992.

Chapter 8:

Structural Variations in Cyclopentadienyl Uranium(III) Iodide Complexes

Introduction[†]

Investigating the chemistry of U(III) and U(IV) is challenging for many reasons.[1,2] Complexes of U(III) and U(IV) often have brown colors that are not distinctive and their NMR spectra are affected by the paramagnetism of the metal ions. In addition, these two oxidation states have similar room temperature magnetic moments with μ_J values of 3.62 μ_B for U(III) and 3.58 μ_B for U(IV).[3,4] As a consequence, X-ray crystallography plays an important role in the characterization of these complexes.

Crystallographic characterization not only allows a complex to be definitively identified, but it also can reveal unusual bonding modes and minor variations in coordination environments that could not be observed by other methods. These variations provide information on the many structural options that exist in the reactions of these species. To the extent that these variations represent minimum energy structures under some conditions, they also represent possible minimum energy intermediates in subsequent reaction chemistry.[5] This was demonstrated long ago by examining structural variations of ML_5 complexes which followed the trigonal bipyramidal to square pyramidal isomerization trajectory of Berry pseudo-rotation rather than other mechanisms.[5] It is also important to define structural variations crystallographically if a sample is to be characterized by unit cell determination before use.

[†] Portions of this chapter have been published: Wedal, J. C.; Windorff, C. J.; Huh, D. N.; Ryan, A. J.; Ziller, J. W.; Evans, W. J. Structural variations in cyclopentadienyl uranium(III) iodide complexes. *J. Coord. Chem.* **2021**, *74*, 74-91. DOI: 10.1080/00958972.2020.1856824.

This Chapter reports numerous structural options for U(III) iodide complexes with cyclopentadienyl ligands. These data are reported both to help identify these species if they are found in other reaction systems and to show the structural diversity possible with this simple combination of ligands and a single uranium oxidation state.

Results

Synthesis. Complexes $(C_5Me_5)_2UI(THF)$, **8.1**, and $\{[K(OEt_2)_2][(C_5Me_5)_2U(\mu\text{–}I)(\mu_3\text{–}I)]\}_2$, **8.2**, are variations of the possibilities that can crystallize from reactions of two equivalents of KC_5Me_5 and UI_3 in THF and Et_2O, eq 8.1 and 8.2, respectively.

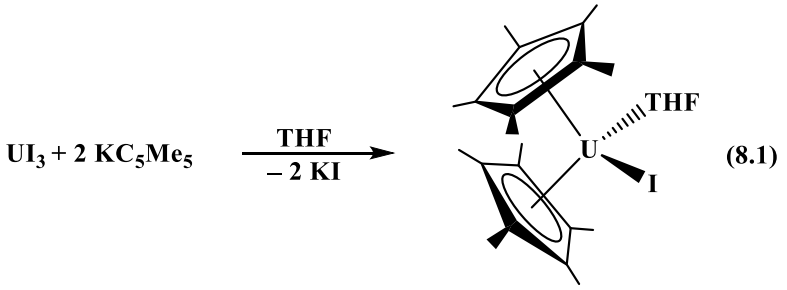

(8.1)

8.1

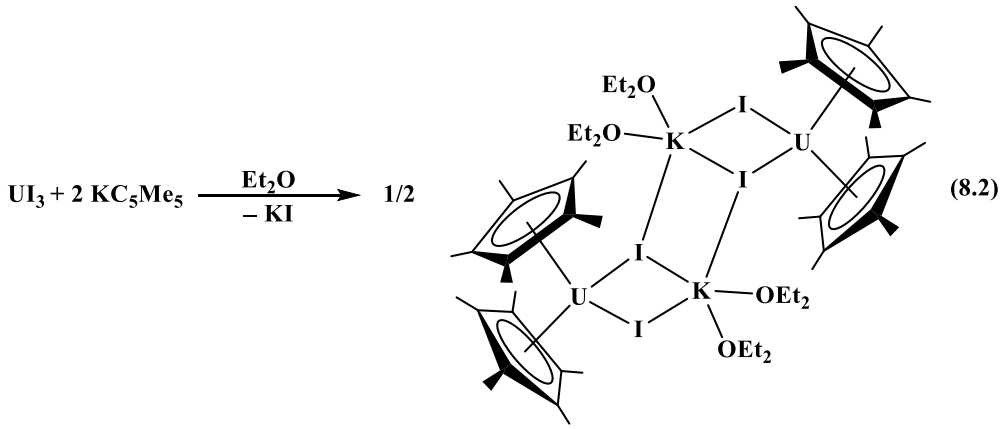

(8.2)

8.2

Complex **8.1**, Figure 8.1, is the product if the ionic metathesis eliminates the KI byproduct cleanly. It is a classic monometallic uranium bent metallocene with two terminal ligands in the wedge formed by the rings. In the absence of THF that coordinates to the uranium center, KI is

incorporated into the final product. Compound **8.2**, Figure 8.2, is much more complicated than compound **8.1** in that it incorporates one equivalent of KI per uranium and crystallizes as a dimer with two metallocene units connected by doubly- and triply-bridging iodide ligands**.** The second half of the molecule is generated by a crystallographic inversion center at the center of the two potassium atoms and the two μ_3–I atoms. Complex **8.2** contains the "$(C_5Me_5)_2U(\mu$–$X)_2M(solvent)_n$" (X = halide, M = alkali metal) "ate-salt" motif that is commonly seen with THF solvating the alkali metal cation,[7–9] but is also observed with Et_2O.[10–14] In this case, the "$(C_5Me_5)_2U(\mu$–$I)_2K(Et_2O)_2$" unit does not crystallize alone, but as a dimer. The ^1H and ^{13}C NMR spectra of **8.2** are consistent with retention of the Et_2O molecules in solution.

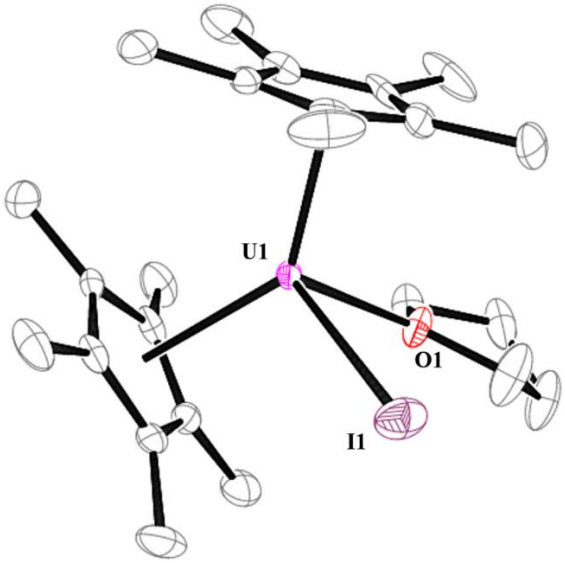

Figure 8.1: Thermal ellipsoid plot of **8.1** with selective atom labelling. Ellipsoids are drawn at 50% probability level. Hydrogen atoms have been omitted for clarity.

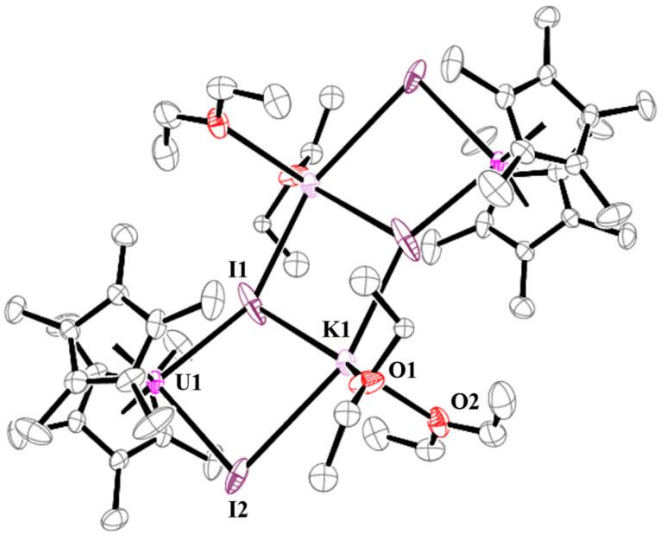

Figure 8.2: Thermal ellipsoid plot of **8.2** with selective atom labelling. Ellipsoids are drawn at 50% probability level. Hydrogen atoms, disorder in the K atom and the ether molecule have been omitted for clarity.

Addition of 18-crown-6 to **8.2** generates yet another variation in which KI is incorporated into the complex, [K(18-crown-6)][$(C_5Me_5)_2U(\mu–I)_2$], **8.3**, eq 8.3, Figure 8.3. In this case, the crown ether is bent back to allow the potassium atom to interact with both bridging iodides. There is one other crystallographically-characterized example that has this "$U(\mu–X)_2M$(18-crown-6)" motif (X = halide; M = alkali metal): the uranyl compound [(18-crown-6)$K(\mu–Br)_2]_2UO_2$ which has two $[K(18\text{-crown-6})]^{1+}$ units that cap bridging bromides.[15] The 18-crown-6 molecules in this uranyl compound are also bent back from the potassium ion as in **8.3**. Compound **8.3** is also similar to dysprosium and neodymium "ate" complexes $[(Cp^{ttt})_2Dy(\mu–Cl)_2K$(18-crown-6)] and $(Cp^{ttt})(C_5H_2{}^tBu_2CMe_2CH_2)Nd(\mu–I)K$(18-crown-6) ($Cp^{ttt} = C_5{}^tBu_3H_2$).[16,17]

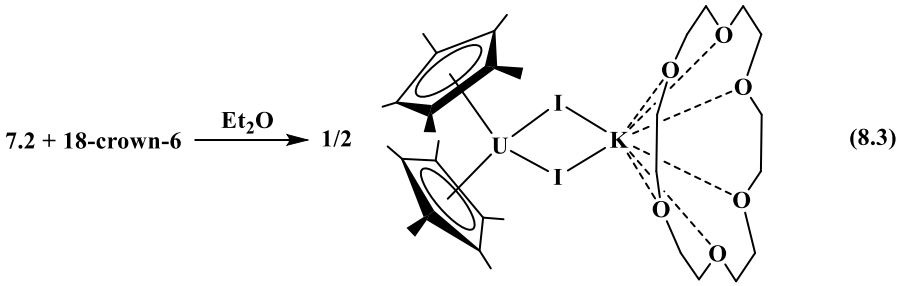

8.3

A fourth type of pentamethylcyclopentadienyl U(III) bent metallocene incorporating iodide was crystallized inadvertently from an attempt to synthesize a U(II) complex from $(C_5Me_5)_2UI(THF)$. The mixture obtained from combining UI_3 and 2 equivalents of KC_5Me_5 in THF was treated with 2.2.2-cryptand and KC_8. The compound that crystallized was not a U(II) complex, but instead the U(III) compound, $[K(2.2.2\text{-cryptand})][(C_5Me_5)_2UI_2]$, **8.4**, eq 8.4. In **8.4**, Figure 8.4, the potassium ion is completely encapsulated by the cryptand and there are no K–I interactions. Complex **8.4** has the classic, formally eight-coordinate structure of bent uranium metallocenes, but with two anionic ligands in the wedge compared to the iodide and THF in complex **8.1**. It is the second example of an anionic $[(C_5Me_5)_2UX_2]^{1-}$ (X = halide) structure after $[(C_5Me_5)_2U(terpy)][(C_5Me_5)_2UI_2]$.[18]

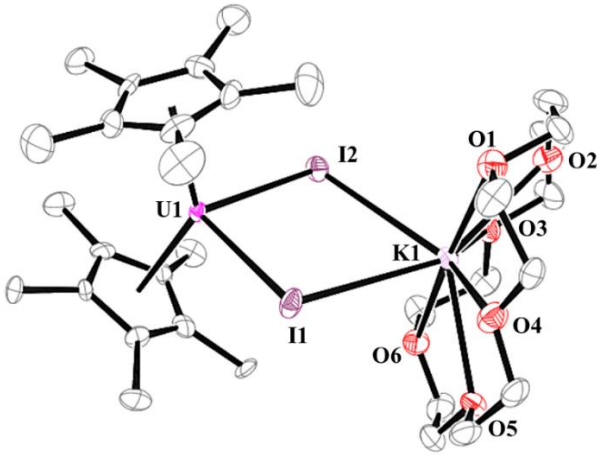

Figure 8.3: Thermal ellipsoid plot of **8.3** with selective atom labelling. Ellipsoids are drawn at 50% probability level and hydrogen atoms have been omitted for clarity.

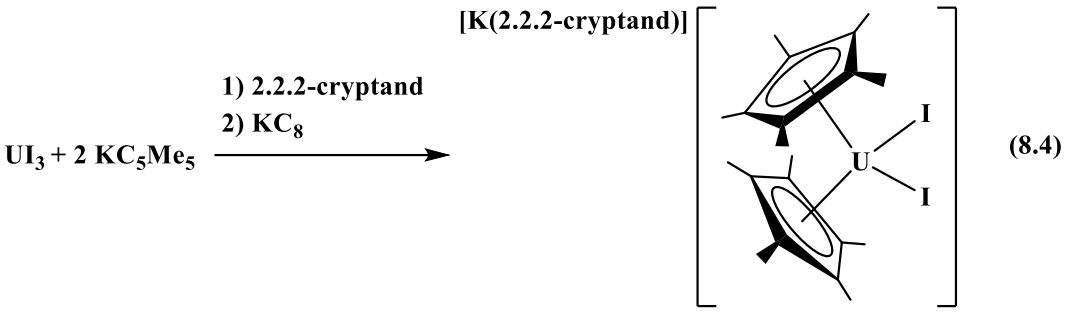

8.4

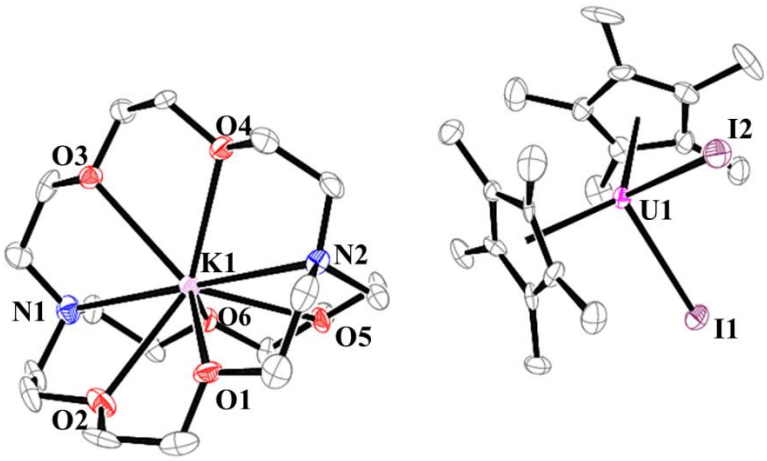

Figure 8.4: Thermal ellipsoid plot of **8.4** with selective atom labelling. Ellipsoids are drawn at 50% probability level. Co-crystallized toluene molecules and hydrogen atoms have been omitted for clarity.

An analog of **8.4** with a different counter-cation, $[Li(THF)_4][(C_5Me_5)_2UI_2]$, **8.5**, was isolated from reactions of $(C_5Me_5)_2UI(THF)$, **8.1**, and $LiCH_2SiMe_3$ or $LiCH(SiMe_3)_2$, eq 8.5, which were attempted for the synthesis of $(C_5Me_5)_2UR$ products. Addition of THF to the reaction mixtures in hexane precipitated bright green solids which were recrystallized to afford **8.5**, Figure 8.5. The anion in **8.5** is identical to that in **8.4**. The $[Li(THF)_4]^{1+}$ cation has been crystallized repeatedly in actinide chemistry.[19–25]

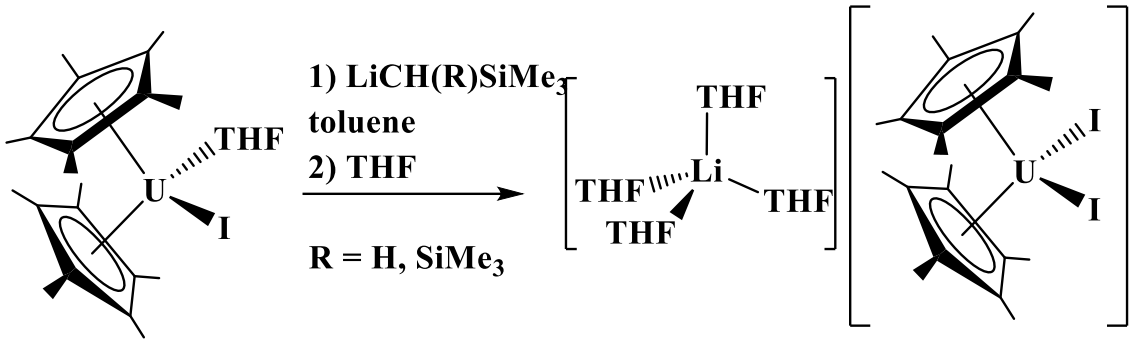

8.1 **8.5**

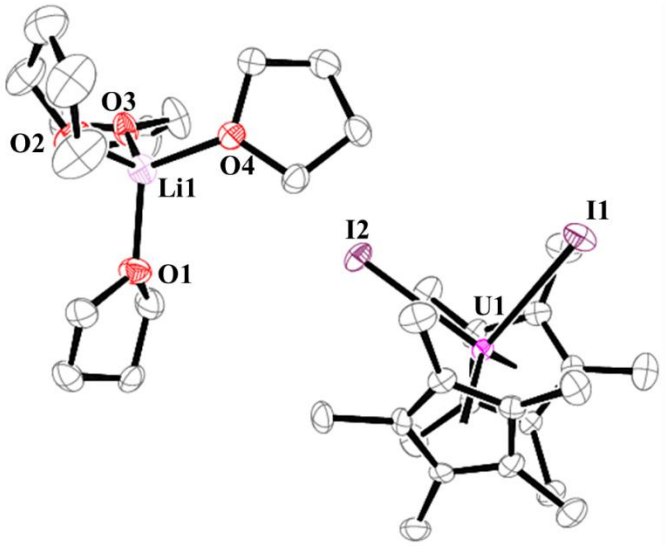

Figure 8.5: Thermal ellipsoid plot of **8.5** with selective atom labelling. Ellipsoids are drawn at 50% probability level and hydrogen atoms have been omitted for clarity.

In one attempt to synthesize $(C_5Me_5)_2U[CH(SiMe_3)_2]$, a crystal of $[Li(THF)_3][(C_5Me_5)_2UI(\mu\text{–}I)]$, **8.6**, Figure 8.6, was isolated. This is a variation of **8.5** in which lithium binds to a bridging iodide and three THF molecules instead of existing as a stand-alone $[Li(THF)_4]^{1+}$ counter-cation. The crystal data on **8.6** were poor, however, and provided only the connectivity of the complex. The desired $(C_5Me_5)_2UR$ products were not formed via this route and these reactions were not pursued further.

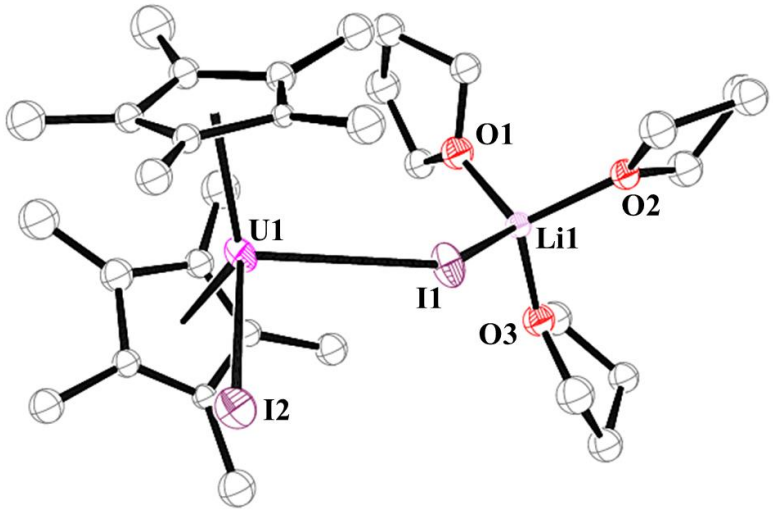

Figure 8.6: Connectivity plot of **8.6** with selective atom labelling.

Equation 8.6 shows the isolation of an analog of [K(18-crown-6)][$(C_5Me_5)_2U(\mu–I)_2$], **8.3**, with the $C_5H_3(SiMe_3)_2$ ligand. The bis(trimethylsilyl)cyclopentadienyl ligand has a size comparable to pentamethylcyclopentadienyl,[26] but with steric bulk on two substituents instead of all five as in C_5Me_5. This complex, {[K(18-crown-6)]$_2(\mu$–toluene)}{[$C_5H_3(SiMe_3)_2]_2UI(\mu–I)\}_2$, **8.7**, Figure 8.7, was made directly from $KC_5H_3(SiMe_3)_2$ and UI_3 in the presence of 18-crown-6 in toluene, eq 8.6, rather than by addition of 18-crown-6 to **8.2**, which formed **8.3**, eq 8.3.

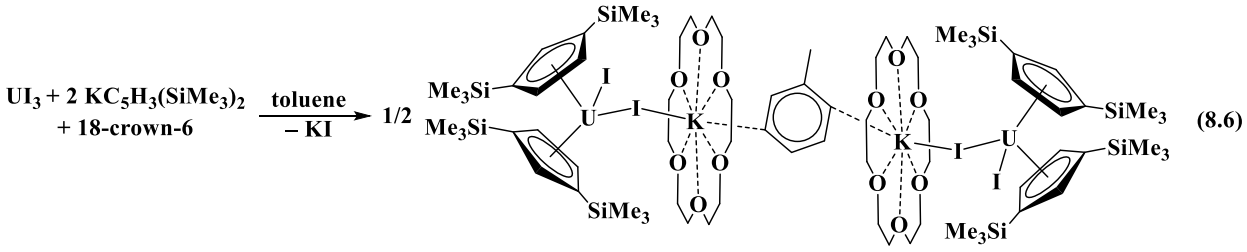

8.7

In contrast to **8.3**, which crystallized with isolated [K(18-crown-6)][$(C_5Me_5)_2U(\mu–I)_2$] units containing two potassium-iodide interactions per uranium, complex **8.7** crystallizes with two [K(18-crown-6)][$C_5H_3(SiMe_3)_2]_2UI(\mu–I)$} units bridged by toluene and each unit has only one potassium-iodide interaction per uranium. Evidently, the potassium is not sterically saturated in

the [K(18-crown-6)](μ–I) unit and coordinates to toluene. Numerous structures with [K(18-crown-6)]$^{1+}$ cations interacting with toluene are in the literature.[27–36] It is possible that the localization of the steric bulk of the $C_5H_3(SiMe_3)_2$ ring in two places allows room for a terminal iodide in **8.6**, but the structure is sufficiently complicated that this feature alone would not generate the structure. It also seems quite possible that a "[K(18-crown-6)]{[$C_5H_3(SiMe_3)_2$]$_2$U(μ–I)$_2$}" direct analog of **8.3** could also crystallize under other conditions.

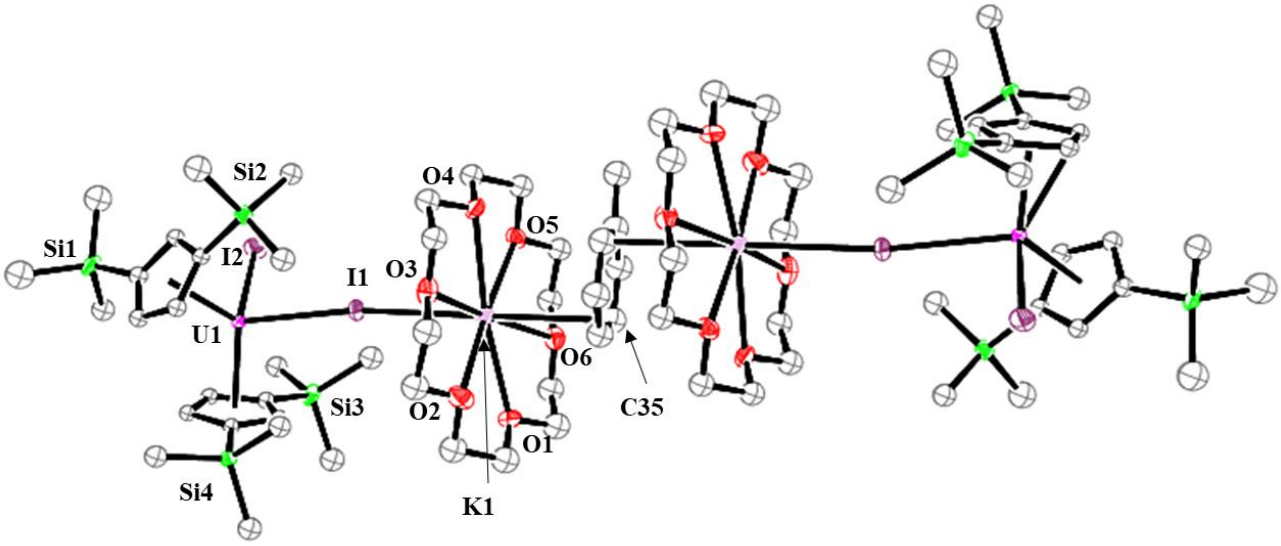

Figure 8.7: Thermal ellipsoid plot of **8.7** with selective atom labelling. Ellipsoids are drawn at 30% probability level. Hydrogen atoms and co-crystallized toluene molecules have been omitted for clarity.

One additional structure is included in this compilation to demonstrate the complexity that can arise if there is a deficiency of C_5Me_5 such that the ratio to iodide is 1:2, eq 8.7. In this case, the trimetallic complex [(C_5Me_5)U]$_3$(μ_3–I)$_2$(μ–I)$_3$I(THF)$_2$, **8.8**, was observed to form, Figure 8.8. Compound **8.8** is isomorphous with the Sm analog [(C_5Me_5)SmI](μ_2–I)$_3$(μ_3–I)$_2$[(C_5Me_5)Sm(THF)$_2$]$_2$.[37]

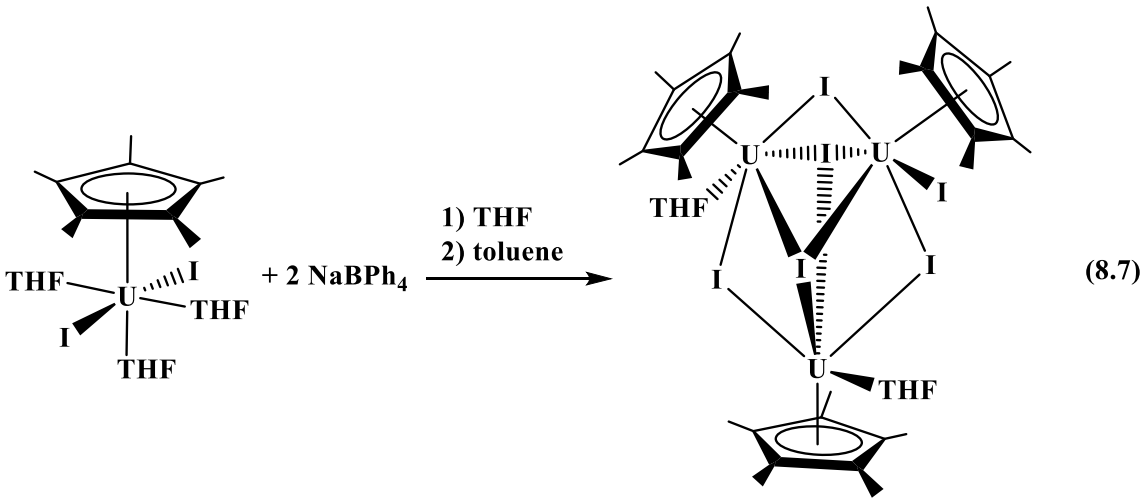

(8.7)

8.8

Compound **8.8** differs from **8.1-8.7** in that it is a mono(cyclopentadienyl) di-iodide instead of a bis(cyclopentadienyl) mono-iodide. Complex **8.8** was isolated from the known monometallic compound of this stoichiometry, $(C_5Me_5)UI_2(THF)_3$,[6] in a reaction with $NaBPh_4$. Monometallic $(C_5Me_5)UI_2(THF)_3$ has been known and structurally characterized since 2001[6] and was crystallized from THF/hexane. In contrast, trimetallic **8.8** crystallized from toluene which emphasizes the importance of crystallization conditions. The formation of compound **8.8** could be viewed as partial desolvation of the starting material $(C_5Me_5)UI_2(THF)_3$.

The three vertices of the triangle in **8.8** are occupied by two $(C_5Me_5)U(THF)$ units and one $(C_5Me_5)UI$ moiety. The U_3I_5 core adopts a distorted hexagonal bipyramidal structure with the five iodide ions defining a trigonal bipyramid. Three iodides are doubly-bridging while two are triply-bridging. The internal $M^{III}_3(\mu\text{–}X)_3(\mu_3\text{–}X)_2$ core has been frequently observed.[38–43] In addition, there is one terminal iodide ligand. The X-ray diffraction data were not of high enough quality to discuss structural parameters.

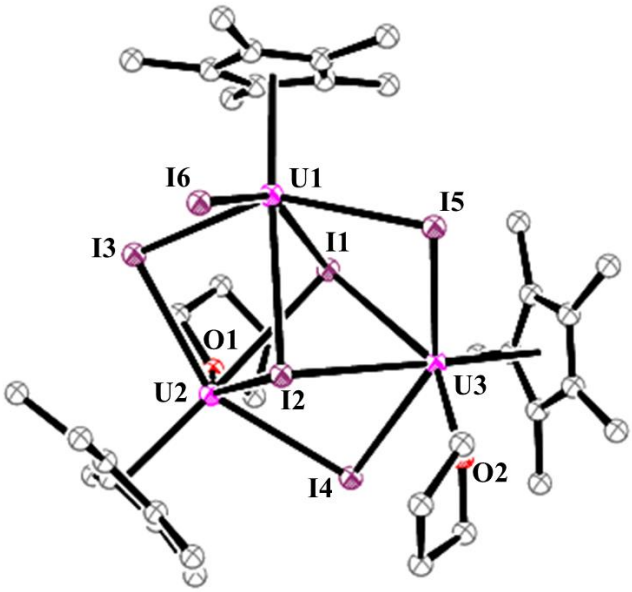

Figure 8.8: Connectivity plot of **8.8** with selective atom labelling.

Structural Comparisons. The metrical parameters of these cyclopentadienyl U(III) iodides are compared in Table 1. The dark green complexes **8.1-8.5** and **8.7**, Figures 8.1-8.7, all have the conventional 8-coordinate bent metallocene structures. The U-(C_5Me_5 ring centroid) and (C_5Me_5 ring centroid)–U–(C_5Me_5 ring centroid) angles are similar in the compounds falling in the narrow ranges 2.486–2.521 Å and 133.4–136.7°, respectively. The (C_5Me_5 ring centroid)–U distances are similar to other crystallographically-characterized U(III) bent metallocenes, e.g. 2.522 Å in $(C_5Me_5)_2U(NPh_2)(THF)$,[44] 2.522 Å in $(C_5Me_5)_2U[(P(Mes)(SiMe_3)](THF)$,[45] 2.523 Å in $(C_5Me_5)_2UI(C_3Me_4N_2)$,[46] 2.461 Å in $[(C_5Me_5)_2U(THF)_2][BPh_4]$,[47] 2.508 Å in $[(C_5Me_5)_2UI_2]^{1-}$,[18] and 2.467 Å in $[Na(18\text{-crown-6})][(C_5Me_5)_2U(S^iPr)_2]$.[48] The U–($C_5Me_5$) centroid and U–I distances and centroid–U–centroid and centroid–U–I angles in **8.4** and **8.5** which both contain $[(C_5Me_5)_2UI_2]^{1-}$ anions, are identical within error.

The uranium center in the $C_5H_3(SiMe_3)_2$ complex, $\{[K(18\text{-crown-6})]_2(\mu\text{–toluene})]\}\{[C_5H_3(SiMe_3)_2]_2UI(\mu\text{–I})\}_2$, **8.7**, has 2.497 and 2.513 Å U–[($C_5H_3(SiMe_3)_2$] ring centroid distances. These are in the range of the U–(C_5Me_5) ring centroid distances of **8.1-8.5**

which reinforces the steric similarity of $C_5H_3(SiMe_3)_2$ and C_5Me_5. However, the 124.5° (ring centroid)–U–(ring centroid) angle is much smaller than the 133.4–136.7° values for **8.1**-**8.5**. Differences between $C_5H_3(SiMe_3)_2$ and C_5Me_5 appear to be typical for these ligands. For example, the (ring centroid)–U–(ring centroid) angle in $[C_5H_3(SiMe_3)_2]_2UMe_2$[49] is 130.77° while the analogous angle in $(C_5Me_5)_2UMe_2$ is 140.53°.[50] The smaller angle is likely possible due to the localization of steric bulk on the cyclopentadienyl substituents in just two sites and not five. The 124.5° (ring centroid)–U–(ring centroid) angle in **8.7** is similar to other bent metallocenes with the $C_5H_3(SiMe_3)_2$ ligand, e.g. 124.11° in $[C_5H_3(SiMe_3)_2]_2U(\mu\text{–}Cl)_2Li(THF)_2$,[51] and 123.37° in $\{[C_5H_3(SiMe_3)_2]_2U(\mu\text{–}O)\}_2$.[52] although it is 130.84° in $\{[C_5H_3(SiMe_3)_2]_2U(\mu\text{–}Cl)\}_2$.[26]

Complex **8.7** has both terminal and bridging iodide ligands which allows a comparison between the two types of iodides to be made in a single compound. As is typical for terminal *vs* bridging, the 3.0711(3) Å terminal U–I distance is shorter than the 3.1206(2) Å bridging U–I distance. However, the two terminal U–I distances in **8.4** differ by similar amounts, 3.0770(9) and 3.1147(9) Å, and the 3.0955(6) Å terminal U–I distance in **8.1** and the 3.0846(6)–3.1096(4) Å bridging U–I distances in **8.2** and **8.3**, are in between. Hence, the U–I distances in these complexes all in a relatively narrow range regardless of their terminal or bridging nature. However, the triply bridging iodide in **8.2** has the longest U–I distance of 3.182(1) Å. The U–terminal iodide distance in **8.7** is longer than the analogous distance of 2.953(2) Å in the tetravalent $[C_5H_3(SiMe_3)_2]_2U^{IV}I_2$ which is consistent with the difference in oxidation state.[53]

$(C_5Me_5)_2UI(THF)$, **8.1**, is the simplest example of a bis(cyclopentadienyl) U(III) iodide which attains the common eight-coordinate environment with the THF solvent so heavily used in this area. The 2.486(4) Å U–O(THF) distance is similar to those in other U(III)–THF complexes,

e.g. 2.573(4) Å in $(C_5Me_5)_2U(NPh_2)(THF)$,[44] 2.516(2) Å in $(C_5Me_5)_2U[(P(Mes)(SiMe_3)](THF)$,[45] and 2.511(8) Å in $[(C_5Me_5)_2U(THF)_2][BPh_4]$.[47]

The potassium ions in **8.2**, **8.3**, **8.4**, and **8.7** exhibit a variety of coordination environments. In $\{[K(OEt_2)_2][(C_5Me_5)_2U(\mu\text{–}I)(\mu_3\text{–}I)]\}_2$, **8.2**, each potassium is five-coordinate and adopts a distorted square pyramidal geometry (τ_5 = 0.15).[54] In **(**$C_5Me_5)_2U(\mu\text{–}I)_2K$(18-crown-6), **8.3**, the potassium is formally eight coordinate with two ligands on the same side of the crown ether ring. The distances are irregular with significantly different K–I distances, 3.666(2) and 3.560(2) Å, for K–I1 and K–I2, respectively, and six K–O distances that span a wide range, 2.780(7)–2.918(7) Å. Two of the shorter distances in this range are for O3 [2.780(7) Å] and O6 [2.820(7) Å] which are across the ring from each other and have an O3–K1–O6 angle of 175.9(2)°. In contrast, the potassium in $\{[C_5H_3(SiMe_3)_2]_2UI(\mu\text{–}I)K$(18-crown-6)$\}_2(\mu$–toluene), **8.7**, is in the center of the crown ether ring with an iodide on one side and a meta-carbon of a toluene ring, C35, oriented toward potassium on the other at a distance of 3.408(4) Å. The other two unique K–C(toluene) distances are longer at 3.672(6) and 3.919(6) Å. The potassium has a hexagonal bipyramidal structure with a 178.4(1)° I1–K–C35 angle. The potassium and the six oxygen atoms of the crown are co-planar to 0.186 Å. The potassium ion in **8.4**, [K(2.2.2-cryptand)]$[(C_5Me_5)_2UI_2]$, is also eight coordinate and has conventional metrical parameters for this entity.[55–57] The 1.90(1)–1.94(1)Å Li–O distances in **8.5** are similar to those of other $Li(THF)_4$ moieties.[19–24]

Table 8.1: Selected distances (Å) and angles (°) for $(C_5Me_5)_2UI(THF)$, **8.1**, $\{[K(OEt_2)_2][(C_5Me_5)_2U(\mu\text{–}I)(\mu_3\text{–}I)]\}_2$, **8.2**, $[K(18\text{-crown-6})][(C_5Me_5)_2U(\mu\text{–}I)_2]$, **8.3**, [K(2.2.2-cryptand)][$(C_5Me_5)_2UI_2$], **8.4**, $[Li(THF)_4][(C_5Me_5)_2UI_2]$, **8.5**, and $\{[K(18\text{-crown-6})]_2(\mu\text{–}toluene)]\}\{[C_5H_3(SiMe_3)_2]_2UI(\mu\text{–}I)\}_2$, **8.7**. Cnt is the cyclopentadienyl ring centroid.

	8.1	**8.2**	**8.3**	**8.4**	**8.5**	**8.7**
U–Cnt	2.491, 2.486	2.508, 2.497	2.517, 2.510	2.518, 2.521	2.515, 2.518	2.497, 2.513
U–$I_{terminal}$	3.0955(6)			3.0770(9), 3.1147(9)	3.1098(7), 3.1242(7)	3.0711(3)
U–(μ–I)		3.1096(4)	3.0846(6), 3.0964(6)			3.1206(2)
U–(μ_3–I)		3.182(1)				
U–O	2.486(4)					
Cnt–U–Cnt	135.7	134.9	136.7	133.4	133.7	124.5
Cnt–U–I	107.7, 105.3	105.9, 104.0, 106.2, 105.2, 104.1, 107.6	101.6, 106.0, 106.5, 104.7	109.0, 104.4, 103.5, 107.4	104.4, 105.4, 105.8, 106.0	104.2, 110.9, 114.7, 103.7
I–U–I		86.32(2), 96.37(2)	93.02(2)	91.11(2)	95.05(2)	94.948(8)
Cnt–U–O	103.9, 103.9					
O–U–I	91.70(9)					

Discussion

The results presented here show how small changes in crystallization conditions can have major effects on the structure of U(III) bent metallocenes. The reaction of UI_3 with two equivalents of KC_5Me_5 in ethereal solvents should ideally eliminate two equivalents of KI and form the classic bent metallocene complex, $(C_5Me_5)_2UI(L)$, where L is the solvent. This occurs in THF and $(C_5Me_5)_2UI(THF)$, **8.1**, Figure 8.1, is isolated. However, in Et_2O a much more complicated

structure can form that retains KI with bridging iodides, $\{[K(OEt_2)_2][(C_5Me_5)_2U(\mu\text{–}I)(\mu_3\text{–}I)]\}_2$, **8.2**, Figure 8.2.

The presence of a chelate like 18-crown-6, would be expected to change the nature of the product and in Et_2O, a mono-uranium complex can be isolated. However, it still has two potassium iodide bridging linkages, $[K(18\text{-crown-6})][(C_5Me_5)_2U(\mu\text{–}I)_2]$, **8.3**, Figure 8.3. A similar reaction with 18-crown-6 but in toluene with the $C_5H_3(SiMe_3)_2$ ligand results in a much more complicated structure, $\{[K(18\text{-crown-6})]_2(\mu\text{–toluene})\}\{[C_5H_3(SiMe_3)_2]_2UI(\mu\text{–}I)\}_2$, **8.7**, Figure 8.7, with bridging and terminal iodide ligands. When the more encapsulating chelate 2.2.2-cryptand is used a simple bent metallocene diiodide anion is formed, $[(C_5Me_5)_2UI_2]^{1-}$ in [K(2.2.2-cryptand)]$[(C_5Me_5)_2UI_2]$, **8.4**, Figure 84. The same anion can form in the absence of chelate when lithium is the alkali metal, $[Li(THF)_4][(C_5Me_5)_2UI_2]$, **8.5**, Figure 8.5. In addition, a variation of **8.5** can crystallize with one less THF in the formula as $[Li(THF)_3][(C_5Me_5)_2UI(\mu\text{–}I)]$, **8.6**, Figure 8.6. This variation of structure in bis(cyclopentadienyl) complexes extends to mono(cyclopentadienyl) species that can crystallize as a monomer in $(C_5Me_5)UI_2(THF)_3$,[6] or as a trimer, $[(C_5Me_5)U]_3(\mu_3\text{–}I)_2(\mu\text{–}I)_3I(THF)_2$, **8.8**, Figure 8.8.

The structural variations identified here would not be readily discernible by ^1H or ^{13}C NMR, UV-visible, or infrared spectroscopy. The compounds are likely to be dynamic in solution and the possibility that these compounds have different structures in solution than in the solid state must also be considered. The presence of lithium could be detected by ^7Li NMR spectroscopy or possibly a flame test, but these methods are not routinely applied to these complexes. Elemental analysis is rarely precise enough to distinguish many of these variations as shown in Table 8.2. All eight compounds have C:H ratios that fall within the small range of 0.5267–0.5909. In some cases, the compounds differ only by one molecule of THF and analytical data is frequently

interpreted in terms of loss of some coordinated solvent. Hence, X-ray crystallography is crucial to identify these variations.

Table 8.2: Analytical Data. Calculated values for compounds **8.1**-**8.8**.

	Calcd C (%)	Calcd H (%)	C:H ratio
8.1	42.34	6.01	0.5909
8.2	36.78	5.76	0.5357
8.3	37.27	5.52	0.5667
8.4	39.77	6.01	0.5556
8.5	41.96	6.30	0.5588
8.6	40.21	5.95	0.5667
8.7	36.80	5.86	0.5267
8.8	23.78	3.41	0.5857

It is worthwhile to consider the existence of these multiple variations since they could well indicate possible reaction pathways in solution as discussed in the introduction. To the extent that these species represent energy minima under some conditions, they could provide mechanistic insight into how reactions occur or why some reactions do not occur.[5] For example, one could expect a metallocene like $(C_5Me_5)_2UI(THF)$, **8.1**, to undergo ionic metatheses with alkyllithium reagents, RLi, to make $(C_5Me_5)_2UR(THF)$ by loss of THF, coordination of the alkyl anion, elimination of LiI, and coordination of THF. However, if the uranium complex has two anionic iodide ligands, i.e. it contains a $[(C_5Me_5)_2UI_2]^{1-}$ unit as in complexes **8.2**–**8.7**, then coordination of the alkyl anion prior to metathesis is much less favorable. Consistent with this idea, the complex $(C_5Me_5)_2U(\mu\text{–}Ph)_2BPh_2$ is an effective precursor in metathesis reactions[58] because the tetraphenylborate anion is weakly coordinating and is easily displaced.[59] The variety of ways in which the $(C_5Me_5)_2UI$ core components of these compounds can interact with solvents and alkali metal iodides could explain why variable yields are sometimes observed for literature preparations. The formation of alkali metal halide adducts depends on experimental details like concentration, temperature, and reaction time. If a coordinating solvent like THF is in high concentration in the

glovebox atmosphere when a reaction is set up, the presence of that solvent could affect which alkali metal halide variation is present in solution.

Conclusion

Eight different coordination modes for uranium(III) complexes containing cyclopentadienyl and iodide ligands have been identified via X-ray crystallography. Slight changes in reaction or crystallization conditions allow for isolation of a variety of coordination modes within the molecule. Changing the solvent from THF to Et_2O affords a dimeric structure with bound Et_2O molecules in $\{[K(OEt_2)_2][(C_5Me_5)_2U(\mu\text{–}I)(\mu_3\text{–}I)]\}_2$, **8.2**, in contrast to a monometallic metallocene in $(C_5Me_5)_2UI(THF)$, **8.1**. The inclusion of 18-crown-6 as a chelating agent to **7.2** led to a simpler, monomeric structure in $[K(18\text{-crown-6})][(C_5Me_5)_2U(\mu\text{–}I)_2]$, **8.3**. The difference in the binding modes of 2.2.2-cryptand and 18-crown-6 is exemplified in compounds **8.3** and $[K(2.2.2\text{-cryptand})][(C_5Me_5)_2UI_2]$, **8.4**; while the potassium ion still interacts with the iodides in **8.3**, the cryptand completely encapsulates the potassium ion in **8.4**. Lithium analogs of **8.3** and **8.4** can form without the need for chelate as shown in $[Li(THF)_4][(C_5Me_5)_2UI_2]$, **8.5**, and $[Li(THF)_3][(C_5Me_5)_2UI(\mu\text{–}I)]$, 8**.6**. Changing the ligand from C_5Me_5 to $C_5H_3(SiMe_3)_2$ allowed for inclusion of a bridging toluene molecule in $\{[K(18\text{-crown-6})]_2(\mu\text{–}toluene)]\}\{[C_5H_3(SiMe_3)_2]_2UI(\mu\text{–}I)\}_2$, **8.7**. A simple change of crystallization solvent altered the composition of mono(cyclopentadienyl)diiodide, $[(C_5Me_5)U]_3(\mu_3\text{–}I)_2(\mu\text{–}I)_3I(THF)_2$, **8.8**, which exists as a trimetallic species in comparison to the known monometallic $(C_5Me_5)UI_2(THF)_3$. All of these structures represent energy minima in a shallow energy surface and could be accessed in solution depending on the local concentrations and components.

Experimental

All syntheses and manipulations described below were conducted under Ar with rigorous exclusion of air and water using standard glovebox techniques. Solvents were sparged with UHP argon and dried by passage through columns containing Q-5 and molecular sieves prior to use. Deuterated NMR solvents were dried over NaK alloy, degassed by three freeze–pump–thaw cycles, and vacuum transferred before use. ^{1}H and ^{13}C{^{1}H} NMR spectra were recorded on an AVANCE600 MHz spectrometer (^{13}C{^{1}H} operating at 150 MHz) at 298 K and referenced to residual protio-solvent resonances. Infrared spectra were recorded as compressed solids on an Agilent Cary 630 ATR-FTIR. Elemental analyses were conducted on a PerkinElmer 2400 Series II CHNS elemental analyzer. 18-Crown-6 (Alfa-Aesar) was sublimed before use. 2.2.2-Cryptand (Aldrich) was dried under 10^{-5} Torr for 12 h before use. UI_3,[60] $KC_5H_3(SiMe_3)_2$,[61] and $(C_5Me_5)UI_2(THF)_3$[6] were synthesized according to literature routes. KC_5Me_5 was prepared from HC_5Me_5 (Strem) and $KN(SiMe_3)_2$ (Sigma) in toluene. $LiCH_2SiMe_3$ (Sigma) was purchased as a solution in hexane and dried to a white solid. $LiCH(SiMe_3)_2$ was synthesized via published procedures.[62]

Synthesis of $(C_5Me_5)_2UI(THF)$, 8.1. $(C_5Me_5)_2UI(THF)$, **8.1**, was synthesized from KC_5Me_5 and UI_3 in THF following literature routes and identified by ^{1}H NMR spectroscopy.[6] Dark green X-ray quality crystals were grown by layering a concentrated THF solution with hexane at −35 °C.

Synthesis of $\{[K(OEt_2)_2][(C_5Me_5)_2U(\mu\text{–}I)(\mu_3\text{–}I)]\}_2$, 8.2. KC_5Me_5 (77 mg, 0.44 mmol) was added to a stirred solution of UI_3 (137 mg, 0.220 mmol) in Et_2O (10 mL). After the forest green solution was stirred overnight, white solids were removed by centrifugation and the supernatant was dried. The product was extracted into Et_2O and dried to yield **8.2** as a dark green

solid (96 mg, 46%). X-ray quality crystals were grown by layering a concentrated Et_2O solution with hexane at −35 °C. ^{1}H NMR (THF-d_8, δ ppm): 3.40 (q, 16H, OCH_2CH$_3$), 1.13 (t, 24H, OCH$_2$CH_3), −0.88 (br s, 60H, C$_5$*Me*$_5$). ^{13}C{^{1}H} NMR (THF-d_8, δ ppm): 66.15 (O*C*H$_2$CH$_3$), 15.50 (OCH$_2$*C*H$_3$). Only the ether resonances were observed between δ 230 and −120 ppm. FT-IR (cm^{-1}): 2965(m), 2891(s), 2852(s), 2721(w), 1489(m), 1441(m), 1382(s), 1284(w), 1148(s), 1091(s), 1043(m), 1020(m), 928(m), 840(m), 798(w). Anal. Calcd. for $C_{20}H_{30}UI_2K$ (%): C 29.98, H 3.77. Found: C, 26.31; H, 3.31. Incomplete combustion was observed across multiple runs, but the experimentally determined C/H ratio, $C_{20}H_{29.98}$, matches expected values.

Synthesis of [K(18-crown-6)][(C$_5$Me$_5$)$_2$U(μ–I)$_2$], 8.3. Complex **8.2** (36 mg, 0.038 mmol) and 18-crown-6 (10 mg, 0.037 mmol) were stirred in Et_2O (10 mL) overnight. The solution was concentrated and layered with hexane at −35 °C. Dark green crystals of **8.3** suitable for X-ray diffraction were grown overnight (39 mg, 99%). ^{1}H NMR (C_6D_6, δ ppm): −0.58 (s, 30H, C$_5$*Me*$_5$). The crown ether resonances were not observed. ^{13}C NMR (C_6D_6, δ ppm): 65.88 (O*C*H$_2$*C*H$_2$O). Only the crown ether resonances were observed between +200 and −200 ppm. FT-IR (cm^{-1}): 2878(m), 2847(m), 1449(m), 1431(m), 1349(s), 1284(w), 1247(m), 1105(s), 1022(w), 959(m), 837(m), 727(w). Anal. Calcd. for $C_{32}H_{34}O_6UI_2K$ (%): C, 36.07; H, 5.11. Found: C, 34.64; H, 4.87. Incomplete combustion and low C values were found across multiple attempts and can be attributed to carbide formation.[63–66] The C:H ratio $C_{32}H_{33.6}$ is close to the expected value.

Synthesis of [K(2.2.2-cryptand)][(C$_5$Me$_5$)$_2$UI$_2$], 8.4. KC_5Me_5 (28 mg, 0.16 mmol) was added to a blue THF (5 mL) solution of UI_3 (50 mg, 0.08 mmol) and was stirred overnight. The resulting green mixture was filtered to remove white solids, presumably KI, and the solvent was removed *in vacuo*. The dried residue (presumably **8.1**) was redissolved in toluene (5 mL) to form a green solution and 2.2.2-cryptand (30 mg, 0.08 mmol) was added. The green solution was then

added to excess KC_8 (15 mg) to form a brown mixture. The brown mixture was then filtered to remove black solids, presumably graphite. The desired U(II) complex was not isolated. Instead, green X-ray quality crystals of the U(III) complex, **8.4**, were grown overnight by layering into hexanes (10 mL) at –35 °C.

Synthesis of $[Li(THF)_4][(C_5Me_5)_2UI_2]$, 8.5, and $[Li(THF)_3][(C_5Me_5)_2UI(\mu–I)]$, 8.6. A toluene solution of $LiCH_2SiMe_3$ (6.6 mg, 0.071 mmol) was added to a green toluene (5 mL) solution of $(C_5Me_5)_2UI(THF)$, **8.1**, (50 mg, 0.071 mmol). The solution was stirred overnight during which time the color had changed to brown. The solvent was removed under vacuum and the solids extracted with hexane (5 mL). The resulting brown solution was centrifuged to remove white solids. THF (1 mL) was added to the supernatant and green solids precipitated. The solvent was removed under vacuum, and the product was dissolved in THF and layered under hexane at −35 °C to afford dark green crystals of **8.5** suitable for X-ray diffraction. Compound **8.5** was also isolated in a similar manner when $LiCH(SiMe_3)_2$ was used instead of $LiCH_2SiMe_3$. In one instance, green crystals of compound **8.6** were isolated instead of compound **8.5** in a reaction with **8.1** and $LiCH(SiMe_3)_2$. The composition of the complex **8.6** was established by X-ray crystallography, but the quality of the data was not high enough to report.

Synthesis of $\{[K(18\text{-crown-}6)]_2(\mu–\text{toluene})\}\{[C_5H_3(SiMe_3)_2]_2UI(\mu–I)\}_2$, 8.7. In a glovebox free of coordinating solvents, $KC_5H_3(SiMe_3)_2$ (49 mg, 0.20 mmol) was added to a stirring slurry of purple UI_3 (75 mg, 0.12 mmol) and 18-crown-6 (32 mg, 0.12 mmol) in toluene (5 mL). The total volume was brought to 10 mL. After about 1 h, the solution began to turn a brown/green color. After the mixture was stirred overnight, the solvent was removed and the residue was extracted with toluene. Solids were removed by centrifugation and the solution was concentrated and placed in the freezer at −35 °C. Overnight, bright green crystals of **8.7** suitable for X-ray

diffraction were grown (111 mg, 73%). Due to the paramagnetism and low solubility of **8.7**, the ^{1}H NMR spectra could not be confidently assigned. ^{13}C NMR (C_6D_6, δ ppm): 68.52 (O*C*H_2*C*H_2O), −0.67 (Si*Me*$_3$). FT-IR (cm^{-1}): 2948(m), 2890(m), 1469(w), 1437(w), 1350(m), 1283(w), 1241(s), 1208(w), 1103(s), 1080(s), 962(m), 920(m), 828(s), 750(m), 688(m). Anal. Calcd. for $C_{75}H_{140}I_4K_2O_{12}Si_8U_2$ (%): C, 35.74; H, 5.60. Found: C, 35.50; H, 5.68.

Synthesis of [(C$_5$Me$_5$)U]$_3$(μ_3–I)$_2$(μ–I)$_3$I(THF)$_2$, 8.8. Compound **8.8** was isolated from a reaction of $(C_5Me_5)UI_2(THF)_3$[6] and $NaBPh_4$ in THF. X-ray quality crystals were grown from a concentrated toluene solution at −35 °C which allowed the compound to be identified by X-ray crystallography. The composition of the complex was established by X-ray crystallography, but the quality of the data was not high enough to report.

X-ray Crystallographic Data

Table 8.3: Crystal data and structure refinement for **8.1-8.5** and **8.7**.

	8.1	**8.2**	**8.3**	**8.5**	**8.6**	**8.7**
Identification code	Jcw24	Cjw13	Cjw22	Jcw37	Dnh93	Cjw16
Empirical formula	$C_{24}H_{38}OIU$	$C_{56}H_{100}I_4K_2O_4U_2$	$C_{32}H_{54}I_2KO_6U$	$C_{36}H_{62}LiO_4I_2U$	$C_{38}H_{66}I_2KN_2O_6U•C_7H_8$	$C_{75}H_{140}I_4K_2O_{12}Si_8U_2•2(C_7H_8)$
Formula weight	707.47	1899.21	1065.68	1057.62	1269.99	2704.71
Temperature (K)	133(2)	88(2)	88(2)	133(2)	133(2)	173(2)
Wavelength (Å)	0.71073	0.71073	0.71073	0.71073	0.71073	0.71073
Crystal system	Triclinic	Monoclinic	Orthorhombic	Monoclinic	Triclinic	Triclinic
Space group	$P\bar{1}$	$P2_1/c$	$Pna2_1$	$P2_1/n$	$P\bar{1}$	$P\bar{1}$
a (Å)	8.6932(14)	12.5367(7)	16.5005(10)	17.753(3)	14.466(3)	13.3143(6)
b (Å)	17.384(3)	17.8717(10)	13.3976(9)	13.278(3)	18.021(3)	13.5434(7)
c (Å)	18.382(3)	15.3300(9)	17.1295(11)	18.919(4)	21.750(4)	17.3810(8)
α (°)	62.278(2)	90	90	90	71.854(3)	103.0980(6)

β (°)	87.126(3)	93.3864(7)	90	114.412(3)	71.994(3)	98.1515(6)
γ (°)	84.556(3)	90	90	90	89.521(3)	106.4164(6)
Volume ($Å^3$)	2448.0(7)	3428.7(3)	3815.0(4)	4061.0(13)	5100.0(15)	2856.2(2)
Z	4	2	4	4	4	1
Calculated density (mg/m^3)	1.920	1.840	1.855	1.730	1.654	1.572
Absorption Coefficient (mm^{-1})	7.902	6.676	6.019	5.550	4.518	4.118
F(000)	1340	1804	2044	2044	2492	1332
Crystal color	Green	Dark green	Green	Green	Green	green
Crystal size (mm^3)	0.274 x 0.231 x 0.219	0.182 x 0.156 x 0.078	0.257 x 0.168 x 0.155	0.241 x 0.131 x 0.082	0.207 x 0.111 x 0.078	0.320 x 0.198 x 0.088
θ range for data collection (°)	1.328 to 29.210	1.627 to 28.319	1.921 to 27.103	1.324 to 25.347	1.195 to 25.347	1.633 to 29.052
Index ranges	$-11 \le h \le 11$, $-20 \le k \le 23$, $0 \le l \le 25$	$-16 \le h \le 16$, $0 \le k \le 23$, $0 \le l \le 20$	$-21 \le h \le 21$, $-17 \le k \le 17$, $-21 \le l \le 21$	$-21 \le h \le 21$, $-15 \le k \le 15$, $-22 \le l \le 22$	$-16 \le h \le 17$, $-20 \le k \le 21$, $0 \le l \le 26$	$-17 \le h \le 17$, $-18 \le k \le 17$, $-23 \le l \le 23$
Reflections collected	13099	48952	40878	43962	19594	35457
Independent Reflections		8321	8414	7433	17733	13992
Completeness	100.0	100.0	100.0	100.0	96.9	99.8
Absorption correction	Semi-empirical from equivalents	Semi-empirical from equivalents	Semi-empirical from equivalents	Semi-empirical from equivalents	Semi-empirical from equivalents	Semi-empirical from equivalents
Max. and min. transmission	0.2638 and 0.1443	0.2627 and 0.2095	0.4318 and 0.2934	0.3343 and 0.1785	0.2602 and 0.1752	0.4318 and 0.3192
Refinement method	Full-matrix least-squares on F^2	Full-matrix least-squares on F^2	Full-matrix least-squares on F^2	Full-matrix least-squares on F^2	Full-matrix least-squares on F^2	Full-matrix least-squares on F^2
Data / restraints / parameters	13099 / 0 / 508	8321 / 0 / 356	8414 / 1 / 390	7433 / 0 / 407	17733 / 3 / 1018	13992 / 20 / 584

Goodness-of-fit on F^2	1.028	1.065	1.025	1.031	1.047	1.045
Final R indices [I>2σ(I)]	R1 = 0.0377, wR2 = 0.0846	R1 = 0.0287, wR2 = 0.0499	R1 = 0.0298, wR2 = 0.0647	R1 = 0.0409, wR2 = 0.0891	R1 = 0.0502, wR2 = 0.0902	R1 = 0.0261, wR2 = 0.0609
R indices (all data)	R1 = 0.0480, wR2 = 0.0895	R1 = 0.0464, wR2 = 0.0548	R1 = 0.0392, wR2 = 0.0685	R1 = 0.0730, wR2 = 0.1033	R1 = 0.0797, wR2 = 0.0999	R1 = 0.0314, wR2 = 0.0631
Data cutoff (Å)	0.73	0.75	0.78	0.83	0.83	0.73
Largest diff. peak and hole (e.A^{-3})	1.658 and -1.856	1.115 and -1.614	2.187 and -0.867	3.452 and -1.426	2.213 and -1.520	1.309 and -1.795

X-ray Data Collection, Structure Solution and Refinement for 8.1.

A green crystal of approximate dimensions 0.219 x 0.231 x 0.274 mm was mounted in a cryoloop and transferred to a Bruker SMART APEX II diffractometer. The APEX2[67] program package and the CELL_NOW[68] were used to determine the unit-cell parameters. Data was collected using a 20 sec/frame scan time for a sphere of diffraction data. The raw frame data was processed using SAINT[69] and TWINABS[70] to yield the reflection data file (HKLF5 format).[70] Subsequent calculations were carried out using the SHELXTL[71] program. There were no systematic absences nor any diffraction symmetry other than the Friedel condition. The centrosymmetric triclinic space group $P\bar{1}$ was assigned and later determined to be correct.

The structure was solved by dual space methods and refined on F^2 by full-matrix least-squares techniques. The analytical scattering factors[72] for neutral atoms were used throughout the analysis. Hydrogen atoms were included using a riding model. There were two molecules of the formula-unit present.

Least-squares analysis yielded wR2 = 0.0895 and Goof = 1.028 for 508 variables refined against 13099 data (0.73 Å), R1 = 0.0377 for those 11492 with I > 2.0σ(I). The structure was refined as a two-component twin.

Table 8.4: Bond lengths [Å] and angles [°] for **8.1.**

U(1)-Cnt1	2.491	C(12)-C(17)	1.507(8)
U(1)-Cnt2	2.486	C(13)-C(14)	1.429(9)
U(1)-O(1)	2.486(4)	C(13)-C(18)	1.500(8)
U(1)-C(13)	2.748(6)	C(14)-C(15)	1.447(9)
U(1)-C(3)	2.749(6)	C(14)-C(19)	1.503(9)
U(1)-C(2)	2.753(5)	C(15)-C(20)	1.500(8)
U(1)-C(11)	2.755(6)	C(21)-C(22)	1.500(9)
U(1)-C(12)	2.761(5)	C(22)-C(23)	1.503(11)
U(1)-C(4)	2.772(6)	C(23)-C(24)	1.512(9)
U(1)-C(1)	2.781(6)	U(2)-Cnt3	2.476
U(1)-C(14)	2.783(6)	U(2)-Cnt4	2.494
U(1)-C(15)	2.785(6)	U(2)-O(2)	2.496(4)
U(1)-C(5)	2.791(5)	U(2)-C(38)	2.739(6)
U(1)-I(1)	3.0955(6)	U(2)-C(25)	2.741(6)
O(1)-C(24)	1.457(7)	U(2)-C(26)	2.742(6)
O(1)-C(21)	1.472(7)	U(2)-C(37)	2.751(6)
C(1)-C(2)	1.425(8)	U(2)-C(29)	2.756(6)
C(1)-C(5)	1.427(8)	U(2)-C(28)	2.759(6)
C(1)-C(6)	1.503(8)	U(2)-C(36)	2.760(6)
C(2)-C(3)	1.415(8)	U(2)-C(27)	2.761(7)
C(2)-C(7)	1.511(8)	U(2)-C(39)	2.791(6)
C(3)-C(4)	1.424(8)	U(2)-C(35)	2.808(6)
C(3)-C(8)	1.492(8)	U(2)-I(2)	3.0636(6)
C(4)-C(5)	1.418(8)	O(2)-C(48)	1.448(8)
C(4)-C(9)	1.501(8)	O(2)-C(45)	1.457(8)
C(5)-C(10)	1.501(8)	C(25)-C(26)	1.400(9)
C(11)-C(15)	1.414(8)	C(25)-C(29)	1.427(10)
C(11)-C(12)	1.433(8)	C(25)-C(30)	1.509(10)
C(11)-C(16)	1.500(9)	C(26)-C(27)	1.425(9)
C(12)-C(13)	1.406(8)	C(26)-C(31)	1.508(8)

C(27)-C(28)	1.405(9)	C(3)-U(1)-C(12)	95.24(17)
C(27)-C(32)	1.491(10)	C(2)-U(1)-C(12)	85.25(16)
C(28)-C(29)	1.402(10)	C(11)-U(1)-C(12)	30.11(17)
C(28)-C(33)	1.500(9)	O(1)-U(1)-C(4)	104.86(15)
C(29)-C(34)	1.497(9)	C(13)-U(1)-C(4)	130.03(17)
C(35)-C(36)	1.402(9)	C(3)-U(1)-C(4)	29.89(16)
C(35)-C(39)	1.412(9)	C(2)-U(1)-C(4)	49.08(16)
C(35)-C(40)	1.519(9)	C(11)-U(1)-C(4)	141.83(17)
C(36)-C(37)	1.411(9)	C(12)-U(1)-C(4)	125.05(17)
C(36)-C(41)	1.527(9)	O(1)-U(1)-C(1)	86.39(15)
C(37)-C(38)	1.442(9)	C(13)-U(1)-C(1)	134.72(17)
C(37)-C(42)	1.487(9)	C(3)-U(1)-C(1)	49.13(18)
C(38)-C(39)	1.411(9)	C(2)-U(1)-C(1)	29.84(17)
C(38)-C(43)	1.504(9)	C(11)-U(1)-C(1)	101.54(17)
C(39)-C(44)	1.496(9)	C(12)-U(1)-C(1)	107.04(17)
C(45)-C(46)	1.491(9)	C(4)-U(1)-C(1)	48.79(18)
C(46)-C(47)	1.494(12)	O(1)-U(1)-C(14)	94.97(16)
C(47)-C(48)	1.491(10)	C(13)-U(1)-C(14)	29.93(18)
		C(3)-U(1)-C(14)	135.62(18)
Cnt1-U(1)-I(1)	107.7	C(2)-U(1)-C(14)	134.27(17)
Cnt1-U(1)-O(1)	103.9	C(11)-U(1)-C(14)	49.31(18)
Cnt2-U(1)-I(1)	105.3	C(12)-U(1)-C(14)	49.03(17)
Cnt2-U(1)-O(1)	103.9	C(4)-U(1)-C(14)	154.36(19)
Cnt1-U(1)-Cnt2	135.7	C(1)-U(1)-C(14)	150.85(18)
O(1)-U(1)-C(13)	124.25(16)	O(1)-U(1)-C(15)	77.92(16)
O(1)-U(1)-C(3)	129.31(16)	C(13)-U(1)-C(15)	49.49(18)
C(13)-U(1)-C(3)	105.87(18)	C(3)-U(1)-C(15)	143.07(18)
O(1)-U(1)-C(2)	115.71(16)	C(2)-U(1)-C(15)	122.14(18)
C(13)-U(1)-C(2)	108.20(17)	C(11)-U(1)-C(15)	29.57(17)
C(3)-U(1)-C(2)	29.81(17)	C(12)-U(1)-C(15)	49.13(17)
O(1)-U(1)-C(11)	94.67(16)	C(4)-U(1)-C(15)	171.20(17)
C(13)-U(1)-C(11)	49.44(18)	C(1)-U(1)-C(15)	123.91(18)
C(3)-U(1)-C(11)	114.56(17)	C(14)-U(1)-C(15)	30.13(18)
C(2)-U(1)-C(11)	92.95(17)	O(1)-U(1)-C(5)	80.18(15)
O(1)-U(1)-C(12)	124.09(16)	C(13)-U(1)-C(5)	154.82(18)
C(13)-U(1)-C(12)	29.57(17)	C(3)-U(1)-C(5)	49.22(17)

C(2)-U(1)-C(5)	49.21(16)	C(2)-C(3)-U(1)	75.3(3)
C(11)-U(1)-C(5)	130.71(18)	C(4)-C(3)-U(1)	76.0(3)
C(12)-U(1)-C(5)	134.14(17)	C(8)-C(3)-U(1)	117.3(4)
C(4)-U(1)-C(5)	29.53(17)	C(5)-C(4)-C(3)	108.5(5)
C(1)-U(1)-C(5)	29.68(16)	C(5)-C(4)-C(9)	124.7(5)
C(14)-U(1)-C(5)	175.15(18)	C(3)-C(4)-C(9)	126.1(6)
C(15)-U(1)-C(5)	146.92(19)	C(5)-C(4)-U(1)	76.0(3)
O(1)-U(1)-I(1)	91.70(9)	C(3)-C(4)-U(1)	74.1(3)
C(13)-U(1)-I(1)	87.52(12)	C(9)-C(4)-U(1)	123.5(4)
C(3)-U(1)-I(1)	97.99(13)	C(4)-C(5)-C(1)	107.5(5)
C(2)-U(1)-I(1)	127.39(12)	C(4)-C(5)-C(10)	124.7(5)
C(11)-U(1)-I(1)	130.58(12)	C(1)-C(5)-C(10)	127.8(6)
C(12)-U(1)-I(1)	116.57(12)	C(4)-C(5)-U(1)	74.5(3)
C(4)-U(1)-I(1)	81.98(12)	C(1)-C(5)-U(1)	74.8(3)
C(1)-U(1)-I(1)	127.78(12)	C(10)-C(5)-U(1)	118.1(4)
C(14)-U(1)-I(1)	81.34(13)	C(15)-C(11)-C(12)	108.2(5)
C(15)-U(1)-I(1)	106.43(13)	C(15)-C(11)-C(16)	123.9(6)
C(5)-U(1)-I(1)	98.67(13)	C(12)-C(11)-C(16)	127.7(5)
C(24)-O(1)-C(21)	109.1(4)	C(15)-C(11)-U(1)	76.4(3)
C(24)-O(1)-U(1)	129.4(3)	C(12)-C(11)-U(1)	75.2(3)
C(21)-O(1)-U(1)	121.5(3)	C(16)-C(11)-U(1)	119.2(4)
C(2)-C(1)-C(5)	108.1(5)	C(13)-C(12)-C(11)	108.3(5)
C(2)-C(1)-C(6)	124.1(5)	C(13)-C(12)-C(17)	123.7(5)
C(5)-C(1)-C(6)	127.2(5)	C(11)-C(12)-C(17)	126.7(5)
C(2)-C(1)-U(1)	74.0(3)	C(13)-C(12)-U(1)	74.7(3)
C(5)-C(1)-U(1)	75.5(3)	C(11)-C(12)-U(1)	74.7(3)
C(6)-C(1)-U(1)	123.8(4)	C(17)-C(12)-U(1)	126.9(4)
C(3)-C(2)-C(1)	108.1(5)	C(12)-C(13)-C(14)	108.5(5)
C(3)-C(2)-C(7)	126.9(6)	C(12)-C(13)-C(18)	126.0(6)
C(1)-C(2)-C(7)	123.6(6)	C(14)-C(13)-C(18)	125.2(6)
C(3)-C(2)-U(1)	74.9(3)	C(12)-C(13)-U(1)	75.7(3)
C(1)-C(2)-U(1)	76.2(3)	C(14)-C(13)-U(1)	76.4(3)
C(7)-C(2)-U(1)	125.9(4)	C(18)-C(13)-U(1)	119.2(4)
C(2)-C(3)-C(4)	107.8(5)	C(13)-C(14)-C(15)	107.3(5)
C(2)-C(3)-C(8)	125.0(5)	C(13)-C(14)-C(19)	126.8(6)
C(4)-C(3)-C(8)	127.1(6)	C(15)-C(14)-C(19)	125.5(6)

C(13)-C(14)-U(1)	73.7(3)	C(26)-U(2)-C(28)	48.79(19)
C(15)-C(14)-U(1)	75.0(3)	C(37)-U(2)-C(28)	116.8(2)
C(19)-C(14)-U(1)	122.8(4)	C(29)-U(2)-C(28)	29.4(2)
C(11)-C(15)-C(14)	107.7(5)	O(2)-U(2)-C(36)	128.31(16)
C(11)-C(15)-C(20)	127.2(6)	C(38)-U(2)-C(36)	49.13(18)
C(14)-C(15)-C(20)	124.7(6)	C(25)-U(2)-C(36)	111.90(19)
C(11)-C(15)-U(1)	74.1(3)	C(26)-U(2)-C(36)	96.19(18)
C(14)-C(15)-U(1)	74.9(3)	C(37)-U(2)-C(36)	29.68(19)
C(20)-C(15)-U(1)	122.8(4)	C(29)-U(2)-C(36)	141.82(19)
O(1)-C(21)-C(22)	104.9(5)	C(28)-U(2)-C(36)	140.0(2)
C(21)-C(22)-C(23)	103.3(6)	O(2)-U(2)-C(27)	103.83(18)
C(22)-C(23)-C(24)	102.7(6)	C(38)-U(2)-C(27)	99.2(2)
O(1)-C(24)-C(23)	105.3(5)	C(25)-U(2)-C(27)	49.3(2)
Cnt3-U(2)-I(2)	105.7	C(26)-U(2)-C(27)	30.01(19)
Cnt3-U(2)-O(2)	105.8	C(37)-U(2)-C(27)	88.99(19)
Cnt4-U(2)-I(2)	107.5	C(29)-U(2)-C(27)	49.1(2)
Cnt4-U(2)-O(2)	104.5	C(28)-U(2)-C(27)	29.5(2)
Cnt3-U(2)-Cnt4	135.6	C(36)-U(2)-C(27)	110.5(2)
O(2)-U(2)-C(38)	88.85(17)	O(2)-U(2)-C(39)	79.96(16)
O(2)-U(2)-C(25)	119.77(18)	C(38)-U(2)-C(39)	29.53(19)
C(38)-U(2)-C(25)	139.5(2)	C(25)-U(2)-C(39)	160.2(2)
O(2)-U(2)-C(26)	130.06(17)	C(26)-U(2)-C(39)	136.27(19)
C(38)-U(2)-C(26)	110.2(2)	C(37)-U(2)-C(39)	49.20(18)
C(25)-U(2)-C(26)	29.6(2)	C(29)-U(2)-C(39)	168.6(2)
O(2)-U(2)-C(37)	119.21(17)	C(28)-U(2)-C(39)	141.9(2)
C(38)-U(2)-C(37)	30.45(19)	C(36)-U(2)-C(39)	48.46(18)
C(25)-U(2)-C(37)	113.3(2)	C(27)-U(2)-C(39)	128.6(2)
C(26)-U(2)-C(37)	87.16(19)	O(2)-U(2)-C(35)	102.51(17)
O(2)-U(2)-C(29)	89.84(18)	C(38)-U(2)-C(35)	48.64(19)
C(38)-U(2)-C(29)	146.6(2)	C(25)-U(2)-C(35)	134.7(2)
C(25)-U(2)-C(29)	30.1(2)	C(26)-U(2)-C(35)	125.06(18)
C(26)-U(2)-C(29)	49.08(19)	C(37)-U(2)-C(35)	48.75(18)
C(37)-U(2)-C(29)	135.19(19)	C(29)-U(2)-C(35)	161.6(2)
O(2)-U(2)-C(28)	81.33(18)	C(28)-U(2)-C(35)	165.1(2)
C(38)-U(2)-C(28)	117.8(2)	C(36)-U(2)-C(35)	29.15(18)
C(25)-U(2)-C(28)	49.0(2)	C(27)-U(2)-C(35)	137.38(19)

C(39)-U(2)-C(35)	29.21(19)	C(29)-C(28)-U(2)	75.2(4)
O(2)-U(2)-I(2)	87.30(11)	C(27)-C(28)-U(2)	75.3(4)
C(38)-U(2)-I(2)	128.36(14)	C(33)-C(28)-U(2)	122.8(5)
C(25)-U(2)-I(2)	84.11(15)	C(28)-C(29)-C(25)	107.4(6)
C(26)-U(2)-I(2)	111.25(15)	C(28)-C(29)-C(34)	126.4(7)
C(37)-U(2)-I(2)	126.45(14)	C(25)-C(29)-C(34)	126.0(7)
C(29)-U(2)-I(2)	84.86(16)	C(28)-C(29)-U(2)	75.4(3)
C(28)-U(2)-I(2)	112.42(16)	C(25)-C(29)-U(2)	74.4(3)
C(36)-U(2)-I(2)	96.93(14)	C(34)-C(29)-U(2)	119.8(5)
C(27)-U(2)-I(2)	131.68(14)	C(36)-C(35)-C(39)	108.1(6)
C(39)-U(2)-I(2)	99.51(14)	C(36)-C(35)-C(40)	125.3(6)
C(35)-U(2)-I(2)	82.25(13)	C(39)-C(35)-C(40)	126.1(6)
C(48)-O(2)-C(45)	108.5(5)	C(36)-C(35)-U(2)	73.5(3)
C(48)-O(2)-U(2)	128.4(4)	C(39)-C(35)-U(2)	74.8(3)
C(45)-O(2)-U(2)	123.0(4)	C(40)-C(35)-U(2)	124.2(4)
C(26)-C(25)-C(29)	107.8(6)	C(35)-C(36)-C(37)	109.3(6)
C(26)-C(25)-C(30)	123.8(7)	C(35)-C(36)-C(41)	124.4(6)
C(29)-C(25)-C(30)	128.2(7)	C(37)-C(36)-C(41)	126.2(6)
C(26)-C(25)-U(2)	75.2(3)	C(35)-C(36)-U(2)	77.3(3)
C(29)-C(25)-U(2)	75.5(4)	C(37)-C(36)-U(2)	74.8(3)
C(30)-C(25)-U(2)	119.8(4)	C(41)-C(36)-U(2)	117.9(4)
C(25)-C(26)-C(27)	108.6(6)	C(36)-C(37)-C(38)	106.5(5)
C(25)-C(26)-C(31)	124.9(7)	C(36)-C(37)-C(42)	127.5(6)
C(27)-C(26)-C(31)	125.7(7)	C(38)-C(37)-C(42)	124.3(7)
C(25)-C(26)-U(2)	75.2(3)	C(36)-C(37)-U(2)	75.5(3)
C(27)-C(26)-U(2)	75.7(4)	C(38)-C(37)-U(2)	74.3(3)
C(31)-C(26)-U(2)	122.8(4)	C(42)-C(37)-U(2)	126.9(4)
C(28)-C(27)-C(26)	106.8(6)	C(39)-C(38)-C(37)	108.0(6)
C(28)-C(27)-C(32)	125.3(7)	C(39)-C(38)-C(43)	127.5(6)
C(26)-C(27)-C(32)	127.2(7)	C(37)-C(38)-C(43)	123.9(6)
C(28)-C(27)-U(2)	75.2(4)	C(39)-C(38)-U(2)	77.3(4)
C(26)-C(27)-U(2)	74.3(4)	C(37)-C(38)-U(2)	75.2(3)
C(32)-C(27)-U(2)	123.2(5)	C(43)-C(38)-U(2)	120.8(4)
C(29)-C(28)-C(27)	109.4(6)	C(38)-C(39)-C(35)	108.1(6)
C(29)-C(28)-C(33)	125.1(7)	C(38)-C(39)-C(44)	127.3(6)
C(27)-C(28)-C(33)	124.9(8)	C(35)-C(39)-C(44)	124.4(6)

C(38)-C(39)-U(2)	73.2(3)	C(45)-C(46)-C(47)	103.7(6)
C(35)-C(39)-U(2)	76.0(3)	C(48)-C(47)-C(46)	102.5(7)
C(44)-C(39)-U(2)	120.6(4)	O(2)-C(48)-C(47)	106.1(6)
O(2)-C(45)-C(46)	105.6(6)		

X-ray Data Collection, Structure Solution and Refinement for 8.2.

A dark green crystal of approximate dimensions 0.078 x 0.156 x 0.182 mm was mounted on a glass fiber and transferred to a Bruker SMART APEX II diffractometer. The APEX2[67] program package and the CELL_NOW[68] were used to determine the unit-cell parameters. Data was collected using a 30 sec/frame scan time for a sphere of diffraction data. The raw frame data was processed using SAINT[69] and TWINABS[70] to yield the reflection data file (HKLF 4/5 format).[70] Subsequent calculations were carried out using the SHELXTL[71] program. The diffraction symmetry was 2/*m* and the systematic absences were consistent with the monoclinic space group $P2_1/c$ that was later determined to be correct.

The structure was solved by direct methods and refined on F^2 by full-matrix least-squares techniques. The analytical scattering factors[72] for neutral atoms were used throughout the analysis. The molecule was located about an inversion center. Hydrogen atoms were included using a riding model. Disordered atoms were included using multiple components with partial site-occupancy-factors.

Least-squares analysis yielded wR2 = 0.0548 and Goof = 1.065 for 356 variables refined against 8321 data (0.75 Å), R1 = 0.0287 for those 7115 with $I > 2.0\sigma(I)$. The structure was refined as a two component twin, $BASF^5 = 0.456$.

Table 8.5: Bond lengths [Å] and angles [°] for **8.2.**

U(1)-Cnt1	2.508	U(1)-C(14)	2.758(5)
U(1)-Cnt2	2.497	U(1)-C(1)	2.762(4)
U(1)-C(13)	2.753(4)	U(1)-C(12)	2.770(4)

U(1)-C(2)	2.771(4)	C(4)-C(9)	1.491(7)
U(1)-C(15)	2.779(5)	C(5)-C(10)	1.500(7)
U(1)-C(3)	2.787(4)	C(11)-C(15)	1.415(7)
U(1)-C(5)	2.792(4)	C(11)-C(12)	1.422(7)
U(1)-C(11)	2.798(4)	C(11)-C(16)	1.517(7)
U(1)-C(4)	2.803(4)	C(12)-C(13)	1.406(7)
U(1)-I(3)	3.0540(15)	C(12)-C(17)	1.501(7)
U(1)-I(1)	3.1096(4)	C(13)-C(14)	1.414(6)
U(1)-I(2)	3.1824(12)	C(13)-C(18)	1.506(6)
I(1)-K(2)	3.384(3)	C(14)-C(15)	1.419(7)
I(1)-K(1)	3.719(3)	C(14)-C(19)	1.501(7)
I(2)-K(1)#1	3.140(3)	C(15)-C(20)	1.522(7)
I(2)-K(1)	3.471(3)	C(21)-C(22)	1.490(9)
I(3)-K(2)	3.510(3)	C(23)-C(24)	1.497(7)
I(3)-K(2)#1	4.083(3)	C(25)-C(26B)	1.382(13)
K(1)-O(2)	2.787(5)	C(25)-C(26)	1.536(11)
K(1)-O(1)	2.843(5)	C(28)-C(27)	1.381(11)
K(1)-I(2)#1	3.140(3)	C(28)-C(27B)	1.562(16)
K(1)-K(1)#1	4.962(6)		
K(2)-O(2)	2.542(5)	Cnt1-U(1)-I(1)	105.9
K(2)-O(1)	2.548(4)	Cnt1-U(1)-I(2)	104.0
K(2)-I(3)#1	4.083(3)	Cnt1-U(1)-I(3)	106.2
O(1)-C(22)	1.426(6)	Cnt2-U(1)-I(1)	105.2
O(1)-C(23)	1.438(6)	Cnt2-U(1)-I(2)	104.1
O(2)-C(27B)	1.223(13)	Cnt2-U(1)-I(3)	107.6
O(2)-C(26)	1.430(10)	Cnt1-U(1)-Cnt2	134.9
O(2)-C(26B)	1.488(12)	C(13)-U(1)-C(14)	29.73(13)
O(2)-C(27)	1.579(10)	C(13)-U(1)-C(1)	113.97(13)
C(1)-C(5)	1.414(7)	C(14)-U(1)-C(1)	142.32(13)
C(1)-C(2)	1.426(6)	C(13)-U(1)-C(12)	29.50(14)
C(1)-C(6)	1.507(7)	C(14)-U(1)-C(12)	49.01(15)
C(2)-C(3)	1.416(7)	C(1)-U(1)-C(12)	106.17(15)
C(2)-C(7)	1.500(6)	C(13)-U(1)-C(2)	87.76(12)
C(3)-C(4)	1.418(7)	C(14)-U(1)-C(2)	113.47(13)
C(3)-C(8)	1.495(7)	C(1)-U(1)-C(2)	29.88(13)
C(4)-C(5)	1.411(7)	C(12)-U(1)-C(2)	90.56(13)

C(13)-U(1)-C(15)	48.70(13)	C(14)-U(1)-I(3)	88.56(10)
C(14)-U(1)-C(15)	29.70(14)	C(1)-U(1)-I(3)	120.81(11)
C(1)-U(1)-C(15)	154.18(15)	C(12)-U(1)-I(3)	133.00(11)
C(12)-U(1)-C(15)	48.71(14)	C(2)-U(1)-I(3)	129.91(10)
C(2)-U(1)-C(15)	135.82(13)	C(15)-U(1)-I(3)	84.64(11)
C(13)-U(1)-C(3)	90.25(14)	C(3)-U(1)-I(3)	103.35(11)
C(14)-U(1)-C(3)	105.15(13)	C(5)-U(1)-I(3)	91.39(10)
C(1)-U(1)-C(3)	48.91(13)	C(11)-U(1)-I(3)	109.82(12)
C(12)-U(1)-C(3)	106.43(15)	C(4)-U(1)-I(3)	81.69(10)
C(2)-U(1)-C(3)	29.52(13)	C(13)-U(1)-I(1)	127.46(9)
C(15)-U(1)-C(3)	134.69(14)	C(14)-U(1)-I(1)	122.63(9)
C(13)-U(1)-C(5)	135.76(13)	C(1)-U(1)-I(1)	85.14(9)
C(14)-U(1)-C(5)	152.90(14)	C(12)-U(1)-I(1)	99.69(11)
C(1)-U(1)-C(5)	29.49(14)	C(2)-U(1)-I(1)	113.09(10)
C(12)-U(1)-C(5)	135.45(14)	C(15)-U(1)-I(1)	92.96(11)
C(2)-U(1)-C(5)	48.80(13)	C(3)-U(1)-I(1)	131.59(9)
C(15)-U(1)-C(5)	175.37(14)	C(5)-U(1)-I(1)	84.38(10)
C(3)-U(1)-C(5)	48.65(13)	C(11)-U(1)-I(1)	79.92(10)
C(13)-U(1)-C(11)	48.65(13)	C(4)-U(1)-I(1)	111.07(11)
C(14)-U(1)-C(11)	48.90(14)	I(3)-U(1)-I(1)	86.32(2)
C(1)-U(1)-C(11)	125.84(16)	C(13)-U(1)-I(2)	109.97(9)
C(12)-U(1)-C(11)	29.59(14)	C(14)-U(1)-I(2)	82.51(10)
C(2)-U(1)-C(11)	118.61(15)	C(1)-U(1)-I(2)	122.41(11)
C(15)-U(1)-C(11)	29.39(15)	C(12)-U(1)-I(2)	129.81(11)
C(3)-U(1)-C(11)	135.69(14)	C(2)-U(1)-I(2)	125.39(10)
C(5)-U(1)-C(11)	152.51(15)	C(15)-U(1)-I(2)	83.40(11)
C(13)-U(1)-C(4)	118.04(15)	C(3)-U(1)-I(2)	97.08(10)
C(14)-U(1)-C(4)	124.56(15)	C(5)-U(1)-I(2)	93.12(11)
C(1)-U(1)-C(4)	48.45(14)	C(11)-U(1)-I(2)	110.87(12)
C(12)-U(1)-C(4)	135.55(15)	C(4)-U(1)-I(2)	78.77(10)
C(2)-U(1)-C(4)	48.47(14)	I(1)-U(1)-I(2)	96.372(19)
C(15)-U(1)-C(4)	151.35(14)	U(1)-I(1)-K(2)	96.95(5)
C(3)-U(1)-C(4)	29.40(14)	U(1)-I(1)-K(1)	86.79(4)
C(5)-U(1)-C(4)	29.22(14)	K(1)#1-I(2)-U(1)	160.59(7)
C(11)-U(1)-C(4)	165.06(15)	K(1)#1-I(2)-K(1)	97.15(7)
C(13)-U(1)-I(3)	117.30(9)	U(1)-I(2)-K(1)	90.08(5)

U(1)-I(3)-K(2)	95.41(6)	C(26B)-O(2)-K(2)	85.9(5)
U(1)-I(3)-K(2)#1	141.01(5)	C(26)-O(2)-K(1)	146.0(5)
K(2)-I(3)-K(2)#1	113.96(6)	C(27)-O(2)-K(1)	107.2(4)
O(2)-K(1)-O(1)	98.30(13)	C(5)-C(1)-C(2)	108.0(4)
O(2)-K(1)-I(2)#1	99.36(12)	C(5)-C(1)-C(6)	126.9(5)
O(1)-K(1)-I(2)#1	90.64(10)	C(2)-C(1)-C(6)	124.8(5)
O(2)-K(1)-I(2)	135.38(13)	C(5)-C(1)-U(1)	76.4(3)
O(1)-K(1)-I(2)	126.30(12)	C(2)-C(1)-U(1)	75.4(3)
I(2)#1-K(1)-I(2)	82.85(7)	C(6)-C(1)-U(1)	118.7(3)
O(2)-K(1)-I(1)	90.63(11)	C(3)-C(2)-C(1)	107.8(4)
O(1)-K(1)-I(1)	100.23(11)	C(3)-C(2)-C(7)	126.0(4)
I(2)#1-K(1)-I(1)	164.07(10)	C(1)-C(2)-C(7)	125.2(5)
I(2)-K(1)-I(1)	81.33(6)	C(3)-C(2)-U(1)	75.9(3)
O(2)-K(1)-K(1)#1	126.93(14)	C(1)-C(2)-U(1)	74.7(2)
O(1)-K(1)-K(1)#1	114.91(13)	C(7)-C(2)-U(1)	124.2(3)
I(2)#1-K(1)-K(1)#1	43.96(5)	C(2)-C(3)-C(4)	107.7(4)
I(2)-K(1)-K(1)#1	38.89(5)	C(2)-C(3)-C(8)	127.3(5)
I(1)-K(1)-K(1)#1	120.20(9)	C(4)-C(3)-C(8)	124.2(5)
O(2)-K(2)-O(1)	113.57(15)	C(2)-C(3)-U(1)	74.6(2)
O(2)-K(2)-I(1)	103.15(13)	C(4)-C(3)-U(1)	75.9(3)
O(1)-K(2)-I(1)	116.62(13)	C(8)-C(3)-U(1)	123.3(3)
O(2)-K(2)-I(3)	125.14(13)	C(5)-C(4)-C(3)	108.6(4)
O(1)-K(2)-I(3)	115.42(13)	C(5)-C(4)-C(9)	125.6(5)
I(1)-K(2)-I(3)	75.39(6)	C(3)-C(4)-C(9)	125.1(5)
O(2)-K(2)-I(3)#1	92.64(12)	C(5)-C(4)-U(1)	75.0(3)
O(1)-K(2)-I(3)#1	88.30(11)	C(3)-C(4)-U(1)	74.7(2)
I(1)-K(2)-I(3)#1	140.53(9)	C(9)-C(4)-U(1)	123.9(3)
I(3)-K(2)-I(3)#1	66.04(6)	C(4)-C(5)-C(1)	107.9(4)
C(22)-O(1)-C(23)	112.4(4)	C(4)-C(5)-C(10)	126.4(5)
C(22)-O(1)-K(2)	125.4(3)	C(1)-C(5)-C(10)	125.6(5)
C(23)-O(1)-K(2)	117.8(3)	C(4)-C(5)-U(1)	75.8(3)
C(22)-O(1)-K(1)	129.4(3)	C(1)-C(5)-U(1)	74.1(2)
C(23)-O(1)-K(1)	117.9(3)	C(10)-C(5)-U(1)	119.6(3)
C(27B)-O(2)-C(26B)	123.1(9)	C(15)-C(11)-C(12)	107.5(4)
C(26)-O(2)-C(27)	104.7(6)	C(15)-C(11)-C(16)	125.9(5)
C(27B)-O(2)-K(2)	151.0(8)	C(12)-C(11)-C(16)	125.7(5)

C(15)-C(11)-U(1)	74.6(3)	C(15)-C(14)-C(19)	127.2(4)
C(12)-C(11)-U(1)	74.1(2)	C(13)-C(14)-U(1)	74.9(3)
C(16)-C(11)-U(1)	125.2(3)	C(15)-C(14)-U(1)	76.0(3)
C(13)-C(12)-C(11)	107.9(4)	C(19)-C(14)-U(1)	118.8(3)
C(13)-C(12)-C(17)	128.1(5)	C(11)-C(15)-C(14)	108.5(4)
C(11)-C(12)-C(17)	123.7(5)	C(11)-C(15)-C(20)	125.1(5)
C(13)-C(12)-U(1)	74.6(3)	C(14)-C(15)-C(20)	126.0(5)
C(11)-C(12)-U(1)	76.3(3)	C(11)-C(15)-U(1)	76.0(3)
C(17)-C(12)-U(1)	120.4(3)	C(14)-C(15)-U(1)	74.3(3)
C(12)-C(13)-C(14)	108.8(4)	C(20)-C(15)-U(1)	121.5(3)
C(12)-C(13)-C(18)	126.7(4)	O(1)-C(22)-C(21)	109.7(5)
C(14)-C(13)-C(18)	123.6(4)	O(1)-C(23)-C(24)	108.8(4)
C(12)-C(13)-U(1)	75.9(3)	O(2)-C(26)-C(25)	108.7(7)
C(14)-C(13)-U(1)	75.3(3)	C(28)-C(27)-O(2)	108.5(6)
C(18)-C(13)-U(1)	123.9(3)	C(25)-C(26B)-O(2)	114.2(8)
C(13)-C(14)-C(15)	107.2(4)	O(2)-C(27B)-C(28)	119.0(11)
C(13)-C(14)-C(19)	125.4(4)		

Symmetry transformations used to generate equivalent atoms:
#1 -x+1,-y,-z+2

X-ray Data Collection, Structure Solution and Refinement for 8.3.

A green crystal of approximate dimensions 0.155 x 0.168 x 0.257 mm was mounted in a cryoloop and transferred to a Bruker SMART APEX II diffractometer. The APEX2[67] program package was used to determine the unit-cell parameters and for data collection (30 sec/frame scan time for a sphere of diffraction data). The raw frame data was processed using SAINT[69] and SADABS[73] to yield the reflection data file. Subsequent calculations were carried out using the SHELXTL[71] program. The diffraction symmetry was *mmm* and the systematic absences were consistent with the orthorhombic space groups *Pnma* and $Pna2_1$. It was later determined that space group $Pna2_1$ was correct.

The structure was solved by direct methods and refined on F^2 by full-matrix least-squares techniques. The analytical scattering factors[72] for neutral atoms were used throughout the analysis. Hydrogen atoms were included using a riding model.

Least-squares analysis yielded wR2 = 0.0685 and Goof = 1.025 for 390 variables refined against 8414 data (0.78 Å), R1 = 0.0298 for those 7412 data with $I > 2.0\sigma(I)$. The structure was refined as a two-component inversion twin.

Table 8.6: Bond lengths [Å] and angles [°] for **8.3.**

U(1)-Cnt1	2.510	C(4)-C(9)	1.488(16)
U(1)-Cnt2	2.517	C(5)-C(10)	1.506(15)
U(1)-C(3)	2.760(10)	C(11)-C(15)	1.401(14)
U(1)-C(4)	2.764(10)	C(11)-C(12)	1.423(13)
U(1)-C(13)	2.782(9)	C(11)-C(16)	1.489(13)
U(1)-C(2)	2.785(11)	C(12)-C(13)	1.426(13)
U(1)-C(15)	2.786(10)	C(12)-C(17)	1.508(13)
U(1)-C(14)	2.788(9)	C(13)-C(14)	1.415(13)
U(1)-C(5)	2.791(9)	C(13)-C(18)	1.516(14)
U(1)-C(11)	2.794(10)	C(14)-C(15)	1.415(14)
U(1)-C(12)	2.801(9)	C(14)-C(19)	1.502(14)
U(1)-C(1)	2.808(9)	C(15)-C(20)	1.517(15)
U(1)-I(2)	3.0846(6)	K(1)-O(3)	2.780(7)
U(1)-I(1)	3.0964(6)	K(1)-O(5)	2.805(7)
I(1)-K(1)	3.6656(18)	K(1)-O(6)	2.820(7)
I(2)-K(1)	3.5600(18)	K(1)-O(1)	2.844(7)
C(1)-C(5)	1.397(15)	K(1)-O(4)	2.858(7)
C(1)-C(2)	1.414(16)	K(1)-O(2)	2.918(7)
C(1)-C(6)	1.511(15)	O(1)-C(21)	1.415(13)
C(2)-C(3)	1.388(16)	O(1)-C(32)	1.420(12)
C(2)-C(7)	1.526(15)	O(2)-C(22)	1.404(11)
C(3)-C(4)	1.448(17)	O(2)-C(23)	1.417(13)
C(3)-C(8)	1.524(15)	O(3)-C(24)	1.422(12)
C(4)-C(5)	1.398(15)	O(3)-C(25)	1.429(12)

O(4)-C(26)	1.402(12)
O(4)-C(27)	1.428(14)
O(5)-C(29)	1.409(13)
O(5)-C(28)	1.414(12)
O(6)-C(31)	1.414(12)
O(6)-C(30)	1.419(12)
C(21)-C(22)	1.498(16)
C(23)-C(24)	1.506(16)
C(25)-C(26)	1.475(16)
C(27)-C(28)	1.479(18)
C(29)-C(30)	1.493(16)
C(31)-C(32)	1.507(15)

Cnt1-U(1)-I(1)	106.0
Cnt1-U(1)-I(2)	101.6
Cnt2-U(1)-I(1)	104.7
Cnt2-U(1)-I(2)	106.5
Cnt1-U(1)-Cnt2	136.7
C(3)-U(1)-C(4)	30.4(4)
C(3)-U(1)-C(13)	127.5(3)
C(4)-U(1)-C(13)	97.6(3)
C(3)-U(1)-C(2)	29.0(3)
C(4)-U(1)-C(2)	48.9(3)
C(13)-U(1)-C(2)	139.1(3)
C(3)-U(1)-C(15)	153.3(3)
C(4)-U(1)-C(15)	137.7(3)
C(13)-U(1)-C(15)	48.3(3)
C(2)-U(1)-C(15)	172.4(3)
C(3)-U(1)-C(14)	156.8(3)
C(4)-U(1)-C(14)	126.6(3)
C(13)-U(1)-C(14)	29.4(3)
C(2)-U(1)-C(14)	154.9(3)
C(15)-U(1)-C(14)	29.4(3)
C(3)-U(1)-C(5)	48.5(3)
C(4)-U(1)-C(5)	29.1(3)
C(13)-U(1)-C(5)	91.1(2)
C(2)-U(1)-C(5)	48.1(3)
C(15)-U(1)-C(5)	139.3(3)
C(14)-U(1)-C(5)	113.9(3)
C(3)-U(1)-C(11)	124.7(3)
C(4)-U(1)-C(11)	111.9(3)
C(13)-U(1)-C(11)	48.6(3)
C(2)-U(1)-C(11)	153.3(3)
C(15)-U(1)-C(11)	29.1(3)
C(14)-U(1)-C(11)	48.6(3)
C(5)-U(1)-C(11)	126.6(3)
C(3)-U(1)-C(12)	113.0(3)
C(4)-U(1)-C(12)	89.6(3)
C(13)-U(1)-C(12)	29.6(3)
C(2)-U(1)-C(12)	138.5(3)
C(15)-U(1)-C(12)	48.2(3)
C(14)-U(1)-C(12)	48.7(3)
C(5)-U(1)-C(12)	97.9(3)
C(11)-U(1)-C(12)	29.5(3)
C(3)-U(1)-C(1)	48.1(3)
C(4)-U(1)-C(1)	48.3(3)
C(13)-U(1)-C(1)	113.1(3)
C(2)-U(1)-C(1)	29.3(3)
C(15)-U(1)-C(1)	155.2(3)
C(14)-U(1)-C(1)	126.0(3)
C(5)-U(1)-C(1)	28.9(3)
C(11)-U(1)-C(1)	155.4(3)
C(12)-U(1)-C(1)	126.2(3)
C(3)-U(1)-I(2)	114.0(3)
C(4)-U(1)-I(2)	126.5(2)
C(13)-U(1)-I(2)	105.0(2)
C(2)-U(1)-I(2)	85.3(2)
C(15)-U(1)-I(2)	90.7(2)
C(14)-U(1)-I(2)	81.99(19)
C(5)-U(1)-I(2)	101.9(2)
C(11)-U(1)-I(2)	119.5(2)
C(12)-U(1)-I(2)	130.6(2)

C(1)-U(1)-I(2)	78.2(2)	C(3)-C(4)-U(1)	74.6(6)
C(3)-U(1)-I(1)	82.5(2)	C(9)-C(4)-U(1)	125.8(7)
C(4)-U(1)-I(1)	108.3(3)	C(1)-C(5)-C(4)	109.4(10)
C(13)-U(1)-I(1)	130.02(19)	C(1)-C(5)-C(10)	124.5(10)
C(2)-U(1)-I(1)	87.6(3)	C(4)-C(5)-C(10)	125.6(11)
C(15)-U(1)-I(1)	86.2(2)	C(1)-C(5)-U(1)	76.2(6)
C(14)-U(1)-I(1)	114.6(2)	C(4)-C(5)-U(1)	74.3(6)
C(5)-U(1)-I(1)	130.7(2)	C(10)-C(5)-U(1)	121.9(6)
C(11)-U(1)-I(1)	81.8(2)	C(15)-C(11)-C(12)	107.7(9)
C(12)-U(1)-I(1)	107.3(2)	C(15)-C(11)-C(16)	126.7(10)
C(1)-U(1)-I(1)	116.1(2)	C(12)-C(11)-C(16)	124.8(10)
I(2)-U(1)-I(1)	93.020(16)	C(15)-C(11)-U(1)	75.1(6)
U(1)-I(1)-K(1)	93.98(3)	C(12)-C(11)-U(1)	75.5(5)
U(1)-I(2)-K(1)	96.30(3)	C(16)-C(11)-U(1)	123.3(7)
C(5)-C(1)-C(2)	107.9(9)	C(11)-C(12)-C(13)	107.5(8)
C(5)-C(1)-C(6)	124.6(11)	C(11)-C(12)-C(17)	124.9(10)
C(2)-C(1)-C(6)	126.9(11)	C(13)-C(12)-C(17)	126.9(9)
C(5)-C(1)-U(1)	74.9(6)	C(11)-C(12)-U(1)	75.0(5)
C(2)-C(1)-U(1)	74.5(6)	C(13)-C(12)-U(1)	74.5(5)
C(6)-C(1)-U(1)	123.7(7)	C(17)-C(12)-U(1)	124.1(7)
C(3)-C(2)-C(1)	108.2(10)	C(14)-C(13)-C(12)	108.3(8)
C(3)-C(2)-C(7)	126.8(12)	C(14)-C(13)-C(18)	124.4(10)
C(1)-C(2)-C(7)	124.9(11)	C(12)-C(13)-C(18)	126.2(10)
C(3)-C(2)-U(1)	74.5(6)	C(14)-C(13)-U(1)	75.5(5)
C(1)-C(2)-U(1)	76.3(6)	C(12)-C(13)-U(1)	75.9(5)
C(7)-C(2)-U(1)	117.8(7)	C(18)-C(13)-U(1)	124.0(6)
C(2)-C(3)-C(4)	108.1(10)	C(13)-C(14)-C(15)	107.2(9)
C(2)-C(3)-C(8)	126.0(12)	C(13)-C(14)-C(19)	125.0(9)
C(4)-C(3)-C(8)	125.2(11)	C(15)-C(14)-C(19)	127.3(9)
C(2)-C(3)-U(1)	76.5(6)	C(13)-C(14)-U(1)	75.0(5)
C(4)-C(3)-U(1)	75.0(6)	C(15)-C(14)-U(1)	75.2(6)
C(8)-C(3)-U(1)	122.5(7)	C(19)-C(14)-U(1)	122.3(6)
C(5)-C(4)-C(3)	106.3(9)	C(11)-C(15)-C(14)	109.3(9)
C(5)-C(4)-C(9)	128.6(12)	C(11)-C(15)-C(20)	126.4(10)
C(3)-C(4)-C(9)	123.4(11)	C(14)-C(15)-C(20)	124.2(9)
C(5)-C(4)-U(1)	76.5(6)	C(11)-C(15)-U(1)	75.8(6)

C(14)-C(15)-U(1)	75.4(6)	C(21)-O(1)-C(32)	111.4(8)
C(20)-C(15)-U(1)	118.0(7)	C(21)-O(1)-K(1)	117.2(6)
O(3)-K(1)-O(5)	119.6(2)	C(32)-O(1)-K(1)	112.4(6)
O(3)-K(1)-O(6)	175.9(2)	C(22)-O(2)-C(23)	113.8(8)
O(5)-K(1)-O(6)	60.6(2)	C(22)-O(2)-K(1)	115.3(6)
O(3)-K(1)-O(1)	116.2(2)	C(23)-O(2)-K(1)	115.6(6)
O(5)-K(1)-O(1)	103.3(2)	C(24)-O(3)-C(25)	112.9(8)
O(6)-K(1)-O(1)	60.3(2)	C(24)-O(3)-K(1)	115.7(6)
O(3)-K(1)-O(4)	60.5(2)	C(25)-O(3)-K(1)	116.0(6)
O(5)-K(1)-O(4)	59.6(2)	C(26)-O(4)-C(27)	113.0(8)
O(6)-K(1)-O(4)	119.0(2)	C(26)-O(4)-K(1)	110.0(6)
O(1)-K(1)-O(4)	124.9(2)	C(27)-O(4)-K(1)	110.8(6)
O(3)-K(1)-O(2)	59.6(2)	C(29)-O(5)-C(28)	114.9(9)
O(5)-K(1)-O(2)	143.94(18)	C(29)-O(5)-K(1)	117.0(6)
O(6)-K(1)-O(2)	117.5(2)	C(28)-O(5)-K(1)	118.7(6)
O(1)-K(1)-O(2)	57.97(19)	C(31)-O(6)-C(30)	112.1(8)
O(4)-K(1)-O(2)	103.6(2)	C(31)-O(6)-K(1)	114.9(6)
O(3)-K(1)-I(2)	79.27(14)	C(30)-O(6)-K(1)	112.3(6)
O(5)-K(1)-I(2)	142.41(14)	O(1)-C(21)-C(22)	108.3(9)
O(6)-K(1)-I(2)	102.94(16)	O(2)-C(22)-C(21)	109.3(8)
O(1)-K(1)-I(2)	94.61(14)	O(2)-C(23)-C(24)	107.5(8)
O(4)-K(1)-I(2)	132.18(15)	O(3)-C(24)-C(23)	112.9(9)
O(2)-K(1)-I(2)	73.26(13)	O(3)-C(25)-C(26)	108.2(9)
O(3)-K(1)-I(1)	95.75(15)	O(4)-C(26)-C(25)	110.8(9)
O(5)-K(1)-I(1)	69.63(13)	O(4)-C(27)-C(28)	110.4(9)
O(6)-K(1)-I(1)	88.16(16)	O(5)-C(28)-C(27)	109.2(8)
O(1)-K(1)-I(1)	144.91(15)	O(5)-C(29)-C(30)	108.1(9)
O(4)-K(1)-I(1)	82.40(14)	O(6)-C(30)-C(29)	113.0(9)
O(2)-K(1)-I(1)	144.00(14)	O(6)-C(31)-C(32)	108.2(9)
I(2)-K(1)-I(1)	76.71(4)	O(1)-C(32)-C(31)	109.3(8)

X-ray Data Collection, Structure Solution and Refinement for 8.4.

A green crystal of approximate dimensions 0.078 x 0.111 x 0.207 mm was mounted in a cryoloop and transferred to a Bruker SMART APEX II diffractometer. The APEX2[67] program

package and the CELL_NOW[68] were used to determine the unit-cell parameters. Data was collected using a 120 sec/frame scan time for a sphere of diffraction data. The raw frame data was processed using SAINT[69] and TWINABS[70] to yield the reflection data file (HKLF5 format).[70] Subsequent calculations were carried out using the SHELXTL[71] program. There were no systematic absences nor any diffraction symmetry other than the Friedel condition The centrosymmetric triclinic space group $P\bar{1}$ was assigned and later determined to be correct.

The structure was solved by direct methods and refined on F^2 by full-matrix least-squares techniques. The analytical scattering factors[72] for neutral atoms were used throughout the analysis. Hydrogen atoms were included using a riding model. There were two molecules of the formula-unit present and two molecules of toluene solvent. One toluene solvent was disordered and included using multiple components, partial site-occupancy-factors, restraints and constraints. It was necessary to assign C(3) and C(4) equivalent anisotropic displacement parameters.

Least-squares analysis yielded wR2 = 0.0999 and Goof = 1.047 for 1018 variables refined against 17733 data (0.83Å), R1 = 0.0502 for those 13835 with $I > 2.0\sigma(I)$. The structure was refined as a two-component twin, BASF[71] = 0.16715.

Table 8.7: Bond lengths [Å] and angles [°] for **8.4.**

U(1)-I(1)	2.518	U(1)-C(2)	2.836(9)
U(1)-I(2)	2.521	U(1)-I(2)	3.0770(9)
U(1)-C(4)	2.743(9)	U(1)-I(1)	3.1147(9)
U(1)-C(5)	2.767(9)	C(1)-C(2)	1.426(13)
U(1)-C(11)	2.769(9)	C(1)-C(5)	1.430(13)
U(1)-C(13)	2.773(9)	C(1)-C(6)	1.495(14)
U(1)-C(12)	2.784(9)	C(2)-C(3)	1.419(14)
U(1)-C(1)	2.806(9)	C(2)-C(7)	1.494(14)
U(1)-C(15)	2.814(9)	C(3)-C(4)	1.423(14)
U(1)-C(3)	2.814(9)	C(3)-C(8)	1.489(13)
U(1)-C(14)	2.816(9)	C(4)-C(5)	1.412(14)

C(4)-C(9)	1.509(14)	C(31)-C(35)	1.398(15)
C(5)-C(10)	1.498(13)	C(31)-C(32)	1.428(14)
C(11)-C(12)	1.395(14)	C(31)-C(36)	1.494(14)
C(11)-C(15)	1.422(14)	C(32)-C(33)	1.406(14)
C(11)-C(16)	1.506(14)	C(32)-C(37)	1.515(15)
C(12)-C(13)	1.391(14)	C(33)-C(34)	1.407(15)
C(12)-C(17)	1.535(14)	C(33)-C(38)	1.511(14)
C(13)-C(14)	1.401(14)	C(34)-C(35)	1.416(15)
C(13)-C(18)	1.512(14)	C(34)-C(39)	1.520(15)
C(14)-C(15)	1.429(14)	C(35)-C(40)	1.508(14)
C(14)-C(19)	1.496(14)	K(1)-O(2)	2.743(7)
C(15)-C(20)	1.487(13)	K(1)-O(4)	2.829(7)
U(2)-I(3)	2.519	K(1)-O(6)	2.833(9)
U(2)-I(4)	2.513	K(1)-O(1)	2.846(8)
U(2)-C(33)	2.750(10)	K(1)-O(3)	2.873(8)
U(2)-C(34)	2.773(10)	K(1)-O(5)	2.890(8)
U(2)-C(32)	2.781(9)	K(1)-N(1)	3.014(10)
U(2)-C(23)	2.782(9)	K(1)-N(2)	3.016(9)
U(2)-C(25)	2.784(9)	O(1)-C(43)	1.410(13)
U(2)-C(24)	2.789(9)	O(1)-C(42)	1.420(15)
U(2)-C(22)	2.804(9)	O(2)-C(45)	1.412(13)
U(2)-C(31)	2.807(10)	O(2)-C(44)	1.439(12)
U(2)-C(21)	2.812(10)	O(3)-C(49)	1.429(13)
U(2)-C(35)	2.812(10)	O(3)-C(48)	1.436(13)
U(2)-I(4)	3.0944(9)	O(4)-C(50)	1.401(12)
U(2)-I(3)	3.1127(9)	O(4)-C(51)	1.409(12)
C(21)-C(22)	1.402(14)	O(5)-C(55)	1.433(15)
C(21)-C(25)	1.418(14)	O(5)-C(54)	1.440(15)
C(21)-C(26)	1.514(14)	O(6)-C(57)	1.409(14)
C(22)-C(23)	1.432(14)	O(6)-C(56)	1.415(13)
C(22)-C(27)	1.506(13)	N(1)-C(47)	1.468(16)
C(23)-C(24)	1.437(13)	N(1)-C(41)	1.484(14)
C(23)-C(28)	1.469(14)	N(1)-C(53)	1.495(15)
C(24)-C(25)	1.413(14)	N(2)-C(46)	1.458(13)
C(24)-C(29)	1.499(14)	N(2)-C(58)	1.479(14)
C(25)-C(30)	1.520(13)	N(2)-C(52)	1.484(13)

C(41)-C(42)	1.515(16)	C(61)-C(62)	1.492(14)
C(43)-C(44)	1.505(16)	C(63)-C(64)	1.506(14)
C(45)-C(46)	1.502(16)	C(65)-C(66)	1.518(14)
C(47)-C(48)	1.507(17)	C(67)-C(68)	1.502(13)
C(49)-C(50)	1.522(15)	C(69)-C(70)	1.486(13)
C(51)-C(52)	1.502(15)	C(71)-C(72)	1.502(14)
C(53)-C(54)	1.47(2)	C(73)-C(74)	1.490(15)
C(55)-C(56)	1.482(17)	C(75)-C(76)	1.496(15)
C(57)-C(58)	1.526(17)	C(77)-C(82)	1.367(18)
K(2)-O(9)	2.793(7)	C(77)-C(78)	1.374(18)
K(2)-O(11)	2.819(7)	C(77)-C(83)	1.459(18)
K(2)-O(8)	2.827(7)	C(78)-C(79)	1.392(19)
K(2)-O(10)	2.840(6)	C(79)-C(80)	1.397(18)
K(2)-O(12)	2.844(7)	C(80)-C(81)	1.345(18)
K(2)-O(7)	2.879(7)	C(81)-C(82)	1.450(19)
K(2)-N(3)	2.992(9)	C(84)-C(85)	1.39(2)
K(2)-N(4)	2.995(8)	C(84)-C(89)	1.44(3)
O(7)-C(61)	1.426(11)	C(84)-C(90)	1.498(10)
O(7)-C(60)	1.437(11)	C(85)-C(86)	1.35(2)
O(8)-C(62)	1.417(11)	C(86)-C(87)	1.33(3)
O(8)-C(63)	1.428(11)	C(87)-C(88)	1.42(3)
O(9)-C(67)	1.426(11)	C(88)-C(89)	1.33(3)
O(9)-C(66)	1.426(11)	C(84B)-C(85B)	1.3900
O(10)-C(68)	1.427(11)	C(84B)-C(89B)	1.3900
O(10)-C(69)	1.439(11)	C(84B)-C(90B)	1.495(10)
O(11)-C(72)	1.429(12)	C(85B)-C(86B)	1.3900
O(11)-C(73)	1.431(12)	C(86B)-C(87B)	1.3900
O(12)-C(74)	1.398(12)	C(87B)-C(88B)	1.3900
O(12)-C(75)	1.420(12)	C(88B)-C(89B)	1.3900
N(3)-C(65)	1.455(12)		
N(3)-C(59)	1.465(13)	Cnt1-U(1)-I(1)	109.0
N(3)-C(71)	1.484(13)	Cnt1-U(1)-I(2)	104.4
N(4)-C(64)	1.456(13)	Cnt2-U(1)-I(1)	103.5
N(4)-C(70)	1.476(12)	Cnt2-U(1)-I(2)	107.4
N(4)-C(76)	1.479(12)	Cnt1-U(1)-Cnt2	133.4
C(59)-C(60)	1.486(15)	C(4)-U(1)-C(5)	29.7(3)

C(4)-U(1)-C(11)	136.9(3)	C(5)-U(1)-C(2)	48.4(3)
C(5)-U(1)-C(11)	114.5(3)	C(11)-U(1)-C(2)	141.3(3)
C(4)-U(1)-C(13)	110.9(3)	C(13)-U(1)-C(2)	159.3(3)
C(5)-U(1)-C(13)	113.0(3)	C(12)-U(1)-C(2)	169.2(3)
C(11)-U(1)-C(13)	48.3(3)	C(1)-U(1)-C(2)	29.3(3)
C(4)-U(1)-C(12)	139.4(3)	C(15)-U(1)-C(2)	127.3(3)
C(5)-U(1)-C(12)	132.8(3)	C(3)-U(1)-C(2)	29.1(3)
C(11)-U(1)-C(12)	29.1(3)	C(14)-U(1)-C(2)	135.1(3)
C(13)-U(1)-C(12)	29.0(3)	C(4)-U(1)-I(2)	128.8(2)
C(4)-U(1)-C(1)	49.1(3)	C(5)-U(1)-I(2)	118.6(2)
C(5)-U(1)-C(1)	29.7(3)	C(11)-U(1)-I(2)	83.1(2)
C(11)-U(1)-C(1)	116.4(3)	C(13)-U(1)-I(2)	120.2(2)
C(13)-U(1)-C(1)	138.6(3)	C(12)-U(1)-I(2)	91.5(2)
C(12)-U(1)-C(1)	144.7(3)	C(1)-U(1)-I(2)	88.9(2)
C(4)-U(1)-C(15)	107.4(3)	C(15)-U(1)-I(2)	106.1(2)
C(5)-U(1)-C(15)	87.0(3)	C(3)-U(1)-I(2)	102.7(2)
C(11)-U(1)-C(15)	29.5(3)	C(14)-U(1)-I(2)	131.3(2)
C(13)-U(1)-C(15)	48.5(3)	C(2)-U(1)-I(2)	80.3(2)
C(12)-U(1)-C(15)	48.2(3)	C(4)-U(1)-I(1)	96.7(2)
C(1)-U(1)-C(15)	98.0(3)	C(5)-U(1)-I(1)	126.4(2)
C(4)-U(1)-C(3)	29.6(3)	C(11)-U(1)-I(1)	112.5(2)
C(5)-U(1)-C(3)	48.5(3)	C(13)-U(1)-I(1)	81.1(2)
C(11)-U(1)-C(3)	162.8(3)	C(12)-U(1)-I(1)	84.6(2)
C(13)-U(1)-C(3)	134.5(3)	C(1)-U(1)-I(1)	130.68(19)
C(12)-U(1)-C(3)	161.8(3)	C(15)-U(1)-I(1)	128.9(2)
C(1)-U(1)-C(3)	48.4(3)	C(3)-U(1)-I(1)	83.8(2)
C(15)-U(1)-C(3)	134.9(3)	C(14)-U(1)-I(1)	106.8(2)
C(4)-U(1)-C(14)	94.4(3)	C(2)-U(1)-I(1)	102.6(2)
C(5)-U(1)-C(14)	86.7(3)	I(2)-U(1)-I(1)	91.11(2)
C(11)-U(1)-C(14)	48.2(3)	C(2)-C(1)-C(5)	107.3(9)
C(13)-U(1)-C(14)	29.0(3)	C(2)-C(1)-C(6)	125.8(9)
C(12)-U(1)-C(14)	47.6(3)	C(5)-C(1)-C(6)	126.8(9)
C(1)-U(1)-C(14)	109.7(3)	C(2)-C(1)-U(1)	76.5(5)
C(15)-U(1)-C(14)	29.4(3)	C(5)-C(1)-U(1)	73.6(5)
C(3)-U(1)-C(14)	123.7(3)	C(6)-C(1)-U(1)	119.3(7)
C(4)-U(1)-C(2)	48.6(3)	C(3)-C(2)-C(1)	108.2(9)

C(3)-C(2)-C(7)	126.1(9)	C(12)-C(13)-C(18)	127.8(9)
C(1)-C(2)-C(7)	124.8(9)	C(14)-C(13)-C(18)	123.5(10)
C(3)-C(2)-U(1)	74.6(5)	C(12)-C(13)-U(1)	75.9(6)
C(1)-C(2)-U(1)	74.2(5)	C(14)-C(13)-U(1)	77.2(5)
C(7)-C(2)-U(1)	125.3(7)	C(18)-C(13)-U(1)	121.1(6)
C(2)-C(3)-C(4)	108.0(9)	C(13)-C(14)-C(15)	108.4(9)
C(2)-C(3)-C(8)	126.1(9)	C(13)-C(14)-C(19)	124.6(10)
C(4)-C(3)-C(8)	125.6(9)	C(15)-C(14)-C(19)	126.3(9)
C(2)-C(3)-U(1)	76.3(5)	C(13)-C(14)-U(1)	73.8(5)
C(4)-C(3)-U(1)	72.4(5)	C(15)-C(14)-U(1)	75.2(5)
C(8)-C(3)-U(1)	121.9(6)	C(19)-C(14)-U(1)	124.5(6)
C(5)-C(4)-C(3)	108.1(9)	C(11)-C(15)-C(14)	106.1(9)
C(5)-C(4)-C(9)	125.9(9)	C(11)-C(15)-C(20)	126.1(9)
C(3)-C(4)-C(9)	126.1(9)	C(14)-C(15)-C(20)	127.3(9)
C(5)-C(4)-U(1)	76.1(5)	C(11)-C(15)-U(1)	73.5(5)
C(3)-C(4)-U(1)	78.0(5)	C(14)-C(15)-U(1)	75.4(5)
C(9)-C(4)-U(1)	112.5(6)	C(20)-C(15)-U(1)	123.0(6)
C(4)-C(5)-C(1)	108.4(9)	Cnt3-U(2)-I(3)	104.7
C(4)-C(5)-C(10)	127.0(9)	Cnt3-U(2)-I(4)	104.6
C(1)-C(5)-C(10)	123.5(9)	Cnt4-U(2)-I(3)	106.3
C(4)-C(5)-U(1)	74.2(5)	Cnt4-U(2)-I(4)	103.9
C(1)-C(5)-U(1)	76.6(5)	Cnt3-U(2)-Cnt4	133.3
C(10)-C(5)-U(1)	125.0(6)	C(33)-U(2)-C(34)	29.5(3)
C(12)-C(11)-C(15)	108.4(9)	C(33)-U(2)-C(32)	29.4(3)
C(12)-C(11)-C(16)	127.8(9)	C(34)-U(2)-C(32)	48.2(3)
C(15)-C(11)-C(16)	122.9(9)	C(33)-U(2)-C(23)	84.2(3)
C(12)-C(11)-U(1)	76.0(5)	C(34)-U(2)-C(23)	94.1(3)
C(15)-C(11)-U(1)	77.0(5)	C(32)-U(2)-C(23)	106.3(3)
C(16)-C(11)-U(1)	121.8(6)	C(33)-U(2)-C(25)	132.6(3)
C(13)-C(12)-C(11)	108.9(9)	C(34)-U(2)-C(25)	138.4(3)
C(13)-C(12)-C(17)	126.3(10)	C(32)-U(2)-C(25)	146.3(3)
C(11)-C(12)-C(17)	124.8(10)	C(23)-U(2)-C(25)	48.8(3)
C(13)-C(12)-U(1)	75.1(5)	C(33)-U(2)-C(24)	110.0(3)
C(11)-C(12)-U(1)	74.8(5)	C(34)-U(2)-C(24)	109.1(3)
C(17)-C(12)-U(1)	116.0(6)	C(32)-U(2)-C(24)	135.6(3)
C(12)-C(13)-C(14)	108.0(9)	C(23)-U(2)-C(24)	29.9(3)

C(25)-U(2)-C(24)	29.4(3)	C(24)-U(2)-I(4)	81.59(19)
C(33)-U(2)-C(22)	88.7(3)	C(22)-U(2)-I(4)	129.8(2)
C(34)-U(2)-C(22)	110.3(3)	C(31)-U(2)-I(4)	100.4(2)
C(32)-U(2)-C(22)	98.3(3)	C(21)-U(2)-I(4)	114.2(2)
C(23)-U(2)-C(22)	29.7(3)	C(35)-U(2)-I(4)	79.4(2)
C(25)-U(2)-C(22)	48.4(3)	C(33)-U(2)-I(3)	119.8(2)
C(24)-U(2)-C(22)	48.8(3)	C(34)-U(2)-I(3)	130.4(2)
C(33)-U(2)-C(31)	48.9(3)	C(32)-U(2)-I(3)	90.6(2)
C(34)-U(2)-C(31)	48.2(3)	C(23)-U(2)-I(3)	127.9(2)
C(32)-U(2)-C(31)	29.6(3)	C(25)-U(2)-I(3)	91.1(2)
C(23)-U(2)-C(31)	133.0(3)	C(24)-U(2)-I(3)	120.4(2)
C(25)-U(2)-C(31)	171.5(3)	C(22)-U(2)-I(3)	100.5(2)
C(24)-U(2)-C(31)	156.9(3)	C(31)-U(2)-I(3)	82.2(2)
C(22)-U(2)-C(31)	127.7(3)	C(21)-U(2)-I(3)	80.0(2)
C(33)-U(2)-C(21)	116.6(3)	C(35)-U(2)-I(3)	104.8(2)
C(34)-U(2)-C(21)	139.0(3)	I(4)-U(2)-I(3)	99.17(2)
C(32)-U(2)-C(21)	118.7(3)	C(22)-C(21)-C(25)	108.6(9)
C(23)-U(2)-C(21)	48.4(3)	C(22)-C(21)-C(26)	124.6(9)
C(25)-U(2)-C(21)	29.4(3)	C(25)-C(21)-C(26)	126.3(9)
C(24)-U(2)-C(21)	48.4(3)	C(22)-C(21)-U(2)	75.2(6)
C(22)-U(2)-C(21)	28.9(3)	C(25)-C(21)-U(2)	74.2(6)
C(31)-U(2)-C(21)	143.0(3)	C(26)-C(21)-U(2)	123.2(6)
C(33)-U(2)-C(35)	48.6(3)	C(21)-C(22)-C(23)	108.2(9)
C(34)-U(2)-C(35)	29.4(3)	C(21)-C(22)-C(27)	124.8(10)
C(32)-U(2)-C(35)	48.0(3)	C(23)-C(22)-C(27)	126.9(9)
C(23)-U(2)-C(35)	123.3(3)	C(21)-C(22)-U(2)	75.8(6)
C(25)-U(2)-C(35)	159.7(3)	C(23)-C(22)-U(2)	74.3(5)
C(24)-U(2)-C(35)	133.0(3)	C(27)-C(22)-U(2)	119.9(6)
C(22)-U(2)-C(35)	137.0(3)	C(22)-C(23)-C(24)	107.2(9)
C(31)-U(2)-C(35)	28.8(3)	C(22)-C(23)-C(28)	129.2(9)
C(21)-U(2)-C(35)	165.0(3)	C(24)-C(23)-C(28)	122.4(10)
C(33)-U(2)-I(4)	119.5(2)	C(22)-C(23)-U(2)	76.0(5)
C(34)-U(2)-I(4)	90.0(2)	C(24)-C(23)-U(2)	75.3(5)
C(32)-U(2)-I(4)	127.1(2)	C(28)-C(23)-U(2)	124.3(7)
C(23)-U(2)-I(4)	107.5(2)	C(25)-C(24)-C(23)	107.7(9)
C(25)-U(2)-I(4)	85.7(2)	C(25)-C(24)-C(29)	127.6(9)

C(23)-C(24)-C(29)	124.4(9)	C(34)-C(35)-C(40)	127.8(11)
C(25)-C(24)-U(2)	75.1(5)	C(31)-C(35)-U(2)	75.4(6)
C(23)-C(24)-U(2)	74.8(5)	C(34)-C(35)-U(2)	73.8(6)
C(29)-C(24)-U(2)	121.0(7)	C(40)-C(35)-U(2)	124.4(7)
C(24)-C(25)-C(21)	108.2(8)	O(2)-K(1)-O(4)	100.3(2)
C(24)-C(25)-C(30)	126.4(9)	O(2)-K(1)-O(6)	92.2(2)
C(21)-C(25)-C(30)	125.1(10)	O(4)-K(1)-O(6)	99.8(2)
C(24)-C(25)-U(2)	75.5(5)	O(2)-K(1)-O(1)	60.6(2)
C(21)-C(25)-U(2)	76.4(5)	O(4)-K(1)-O(1)	136.1(2)
C(30)-C(25)-U(2)	119.2(6)	O(6)-K(1)-O(1)	118.7(2)
C(35)-C(31)-C(32)	107.3(9)	O(2)-K(1)-O(3)	124.6(2)
C(35)-C(31)-C(36)	127.0(10)	O(4)-K(1)-O(3)	60.0(2)
C(32)-C(31)-C(36)	125.3(10)	O(6)-K(1)-O(3)	139.0(2)
C(35)-C(31)-U(2)	75.8(6)	O(1)-K(1)-O(3)	96.9(2)
C(32)-C(31)-U(2)	74.2(5)	O(2)-K(1)-O(5)	127.1(2)
C(36)-C(31)-U(2)	122.1(7)	O(4)-K(1)-O(5)	125.8(2)
C(33)-C(32)-C(31)	108.5(9)	O(6)-K(1)-O(5)	58.7(3)
C(33)-C(32)-C(37)	125.7(9)	O(1)-K(1)-O(5)	93.7(2)
C(31)-C(32)-C(37)	125.7(10)	O(3)-K(1)-O(5)	102.2(2)
C(33)-C(32)-U(2)	74.1(6)	O(2)-K(1)-N(1)	120.4(2)
C(31)-C(32)-U(2)	76.2(5)	O(4)-K(1)-N(1)	119.0(3)
C(37)-C(32)-U(2)	117.3(7)	O(6)-K(1)-N(1)	120.0(3)
C(32)-C(33)-C(34)	107.4(9)	O(1)-K(1)-N(1)	60.0(2)
C(32)-C(33)-C(38)	124.2(10)	O(3)-K(1)-N(1)	59.7(3)
C(34)-C(33)-C(38)	126.3(10)	O(5)-K(1)-N(1)	61.5(3)
C(32)-C(33)-U(2)	76.5(6)	O(2)-K(1)-N(2)	60.3(2)
C(34)-C(33)-U(2)	76.1(6)	O(4)-K(1)-N(2)	61.0(2)
C(38)-C(33)-U(2)	126.4(7)	O(6)-K(1)-N(2)	59.4(2)
C(33)-C(34)-C(35)	108.5(9)	O(1)-K(1)-N(2)	120.7(2)
C(33)-C(34)-C(39)	127.1(10)	O(3)-K(1)-N(2)	120.4(2)
C(35)-C(34)-C(39)	124.2(11)	O(5)-K(1)-N(2)	117.9(3)
C(33)-C(34)-U(2)	74.4(6)	N(1)-K(1)-N(2)	179.2(3)
C(35)-C(34)-U(2)	76.9(6)	C(43)-O(1)-C(42)	110.9(8)
C(39)-C(34)-U(2)	119.1(7)	C(43)-O(1)-K(1)	111.5(6)
C(31)-C(35)-C(34)	108.3(9)	C(42)-O(1)-K(1)	115.0(6)
C(31)-C(35)-C(40)	123.2(10)	C(45)-O(2)-C(44)	112.0(8)

C(45)-O(2)-K(1)	121.2(6)	O(4)-C(51)-C(52)	110.1(8)
C(44)-O(2)-K(1)	118.1(6)	N(2)-C(52)-C(51)	112.9(8)
C(49)-O(3)-C(48)	110.2(8)	C(54)-C(53)-N(1)	114.3(11)
C(49)-O(3)-K(1)	114.0(6)	O(5)-C(54)-C(53)	109.9(11)
C(48)-O(3)-K(1)	114.3(7)	O(5)-C(55)-C(56)	109.5(9)
C(50)-O(4)-C(51)	110.8(8)	O(6)-C(56)-C(55)	108.6(10)
C(50)-O(4)-K(1)	114.2(6)	O(6)-C(57)-C(58)	108.6(9)
C(51)-O(4)-K(1)	115.6(6)	N(2)-C(58)-C(57)	112.4(9)
C(55)-O(5)-C(54)	112.3(10)	O(9)-K(2)-O(11)	94.1(2)
C(55)-O(5)-K(1)	109.2(6)	O(9)-K(2)-O(8)	119.4(2)
C(54)-O(5)-K(1)	112.9(7)	O(11)-K(2)-O(8)	142.5(2)
C(57)-O(6)-C(56)	113.7(9)	O(9)-K(2)-O(10)	60.02(19)
C(57)-O(6)-K(1)	117.5(7)	O(11)-K(2)-O(10)	115.2(2)
C(56)-O(6)-K(1)	119.5(8)	O(8)-K(2)-O(10)	97.07(19)
C(47)-N(1)-C(41)	108.9(10)	O(9)-K(2)-O(12)	130.1(2)
C(47)-N(1)-C(53)	109.9(10)	O(11)-K(2)-O(12)	58.7(2)
C(41)-N(1)-C(53)	109.9(9)	O(8)-K(2)-O(12)	103.6(2)
C(47)-N(1)-K(1)	111.1(6)	O(10)-K(2)-O(12)	92.5(2)
C(41)-N(1)-K(1)	110.1(7)	O(9)-K(2)-O(7)	98.98(19)
C(53)-N(1)-K(1)	106.8(7)	O(11)-K(2)-O(7)	101.5(2)
C(46)-N(2)-C(58)	110.1(8)	O(8)-K(2)-O(7)	59.67(19)
C(46)-N(2)-C(52)	110.8(8)	O(10)-K(2)-O(7)	137.8(2)
C(58)-N(2)-C(52)	108.8(8)	O(12)-K(2)-O(7)	125.4(2)
C(46)-N(2)-K(1)	107.8(6)	O(9)-K(2)-N(3)	61.1(2)
C(58)-N(2)-K(1)	111.5(7)	O(11)-K(2)-N(3)	60.6(2)
C(52)-N(2)-K(1)	107.9(6)	O(8)-K(2)-N(3)	119.4(2)
N(1)-C(41)-C(42)	113.0(9)	O(10)-K(2)-N(3)	120.3(2)
O(1)-C(42)-C(41)	107.5(10)	O(12)-K(2)-N(3)	118.7(2)
O(1)-C(43)-C(44)	110.7(9)	O(7)-K(2)-N(3)	60.8(2)
O(2)-C(44)-C(43)	107.1(9)	O(9)-K(2)-N(4)	120.0(2)
O(2)-C(45)-C(46)	109.7(9)	O(11)-K(2)-N(4)	118.6(2)
N(2)-C(46)-C(45)	113.8(10)	O(8)-K(2)-N(4)	60.5(2)
N(1)-C(47)-C(48)	113.7(10)	O(10)-K(2)-N(4)	60.7(2)
O(3)-C(48)-C(47)	107.6(9)	O(12)-K(2)-N(4)	60.4(2)
O(3)-C(49)-C(50)	108.3(9)	O(7)-K(2)-N(4)	118.9(2)
O(4)-C(50)-C(49)	109.1(9)	N(3)-K(2)-N(4)	178.9(2)

C(61)-O(7)-C(60)	110.7(7)	N(3)-C(65)-C(66)	113.9(8)
C(61)-O(7)-K(2)	111.9(5)	O(9)-C(66)-C(65)	108.6(8)
C(60)-O(7)-K(2)	115.4(6)	O(9)-C(67)-C(68)	108.7(8)
C(62)-O(8)-C(63)	110.5(7)	O(10)-C(68)-C(67)	109.0(8)
C(62)-O(8)-K(2)	116.4(5)	O(10)-C(69)-C(70)	108.5(8)
C(63)-O(8)-K(2)	114.9(5)	N(4)-C(70)-C(69)	114.2(8)
C(67)-O(9)-C(66)	110.6(7)	N(3)-C(71)-C(72)	113.6(8)
C(67)-O(9)-K(2)	116.5(5)	O(11)-C(72)-C(71)	108.4(8)
C(66)-O(9)-K(2)	117.4(5)	O(11)-C(73)-C(74)	108.9(8)
C(68)-O(10)-C(69)	110.8(7)	O(12)-C(74)-C(73)	109.0(8)
C(68)-O(10)-K(2)	113.9(5)	O(12)-C(75)-C(76)	109.7(9)
C(69)-O(10)-K(2)	115.5(5)	N(4)-C(76)-C(75)	114.4(9)
C(72)-O(11)-C(73)	110.9(8)	C(82)-C(77)-C(78)	117.3(14)
C(72)-O(11)-K(2)	115.4(6)	C(82)-C(77)-C(83)	120.8(14)
C(73)-O(11)-K(2)	118.0(6)	C(78)-C(77)-C(83)	121.8(14)
C(74)-O(12)-C(75)	112.3(8)	C(77)-C(78)-C(79)	122.7(14)
C(74)-O(12)-K(2)	115.1(6)	C(78)-C(79)-C(80)	119.8(14)
C(75)-O(12)-K(2)	119.5(6)	C(81)-C(80)-C(79)	119.0(14)
C(65)-N(3)-C(59)	110.4(8)	C(80)-C(81)-C(82)	120.3(14)
C(65)-N(3)-C(71)	110.1(8)	C(77)-C(82)-C(81)	120.8(13)
C(59)-N(3)-C(71)	109.3(8)	C(85)-C(84)-C(89)	116.7(14)
C(65)-N(3)-K(2)	108.2(5)	C(85)-C(84)-C(90)	123.7(16)
C(59)-N(3)-K(2)	109.0(6)	C(89)-C(84)-C(90)	119.5(17)
C(71)-N(3)-K(2)	109.8(6)	C(86)-C(85)-C(84)	123.6(16)
C(64)-N(4)-C(70)	109.2(8)	C(87)-C(86)-C(85)	118(2)
C(64)-N(4)-C(76)	110.2(8)	C(86)-C(87)-C(88)	123(2)
C(70)-N(4)-C(76)	111.1(8)	C(89)-C(88)-C(87)	119(2)
C(64)-N(4)-K(2)	109.7(6)	C(88)-C(89)-C(84)	120(2)
C(70)-N(4)-K(2)	109.0(5)	C(85B)-C(84B)-C(89B)	120.0
C(76)-N(4)-K(2)	107.7(6)	C(85B)-C(84B)-C(90B)	119.9(4)
N(3)-C(59)-C(60)	115.2(9)	C(89B)-C(84B)-C(90B)	120.1(4)
O(7)-C(60)-C(59)	109.8(8)	C(84B)-C(85B)-C(86B)	120.0
O(7)-C(61)-C(62)	108.7(8)	C(87B)-C(86B)-C(85B)	120.0
O(8)-C(62)-C(61)	109.8(8)	C(86B)-C(87B)-C(88B)	120.0
O(8)-C(63)-C(64)	108.6(8)	C(89B)-C(88B)-C(87B)	120.0
N(4)-C(64)-C(63)	113.2(8)	C(88B)-C(89B)-C(84B)	120.0

X-ray Data Collection, Structure Solution and Refinement for 8.5.

A green crystal of approximate dimensions 0.082 x 0.131 x 0.241 mm was mounted in a cryoloop and transferred to a Bruker SMART APEX II diffractometer. The APEX2[67] program package was used to determine the unit-cell parameters and for data collection (90 sec/frame scan time for a sphere of diffraction data). The raw frame data was processed using SAINT[69] and SADABS[73] to yield the reflection data file. Subsequent calculations were carried out using the SHELXTL[71] program. The diffraction symmetry was 2/*m* and the systematic absences were consistent with the monoclinic space group $P2_1/n$ that was later determined to be correct.

The structure was solved by direct methods and refined on F^2 by full-matrix least-squares techniques. The analytical scattering factors[72] for neutral atoms were used throughout the analysis. Hydrogen atoms were included using a riding model.

Least-squares analysis yielded wR2 = 0.1033 and Goof = 1.031 for 407 variables refined against 7433 data (0.83 Å), R1 = 0.0409 for those 5344 data with $I > 2.0\sigma(I)$.

Table 8.8: Bond lengths [Å] and angles [°] for **8.5.**

U(1)-Cnt1	2.518	C(1)-C(5)	1.423(10)
U(1)-Cnt2	2.515	C(1)-C(2)	1.426(10)
U(1)-C(3)	2.764(7)	C(1)-C(6)	1.495(10)
U(1)-C(11)	2.769(7)	C(2)-C(3)	1.388(10)
U(1)-C(12)	2.770(7)	C(2)-C(7)	1.506(11)
U(1)-C(2)	2.777(7)	C(3)-C(4)	1.407(10)
U(1)-C(15)	2.789(7)	C(3)-C(8)	1.545(10)
U(1)-C(13)	2.793(7)	C(4)-C(5)	1.434(11)
U(1)-C(4)	2.797(7)	C(4)-C(9)	1.498(10)
U(1)-C(1)	2.801(7)	C(5)-C(10)	1.505(10)
U(1)-C(5)	2.817(7)	C(11)-C(12)	1.419(10)
U(1)-C(14)	2.830(7)	C(11)-C(15)	1.422(11)
U(1)-I(2)	3.1098(7)	C(11)-C(16)	1.501(11)
U(1)-I(1)	3.1242(7)	C(12)-C(13)	1.410(10)

C(12)-C(17)	1.507(10)	C(3)-U(1)-C(11)	141.6(2)
C(13)-C(14)	1.423(11)	C(3)-U(1)-C(12)	115.0(2)
C(13)-C(18)	1.528(10)	C(11)-U(1)-C(12)	29.7(2)
C(14)-C(15)	1.428(11)	C(3)-U(1)-C(2)	29.0(2)
C(14)-C(19)	1.494(11)	C(11)-U(1)-C(2)	147.0(2)
C(15)-C(20)	1.501(11)	C(12)-U(1)-C(2)	134.0(2)
Li(1)-O(2)	1.899(14)	C(3)-U(1)-C(15)	159.5(2)
Li(1)-O(3)	1.904(14)	C(11)-U(1)-C(15)	29.6(2)
Li(1)-O(4)	1.921(14)	C(12)-U(1)-C(15)	48.9(2)
Li(1)-O(1)	1.939(14)	C(2)-U(1)-C(15)	171.0(2)
O(1)-C(24)	1.440(10)	C(3)-U(1)-C(13)	111.1(2)
O(1)-C(21)	1.456(9)	C(11)-U(1)-C(13)	48.5(2)
O(2)-C(25)	1.437(10)	C(12)-U(1)-C(13)	29.4(2)
O(2)-C(28)	1.441(9)	C(2)-U(1)-C(13)	139.4(2)
O(3)-C(29)	1.437(9)	C(15)-U(1)-C(13)	48.4(2)
O(3)-C(32)	1.447(9)	C(3)-U(1)-C(4)	29.3(2)
O(4)-C(36)	1.411(10)	C(11)-U(1)-C(4)	112.4(2)
O(4)-C(33)	1.446(10)	C(12)-U(1)-C(4)	87.5(2)
C(21)-C(22)	1.527(11)	C(2)-U(1)-C(4)	48.7(2)
C(22)-C(23)	1.506(11)	C(15)-U(1)-C(4)	136.2(2)
C(23)-C(24)	1.500(11)	C(13)-U(1)-C(4)	92.5(2)
C(25)-C(26)	1.484(12)	C(3)-U(1)-C(1)	48.0(2)
C(26)-C(27)	1.500(11)	C(11)-U(1)-C(1)	117.7(2)
C(27)-C(28)	1.526(12)	C(12)-U(1)-C(1)	113.3(2)
C(29)-C(30)	1.513(12)	C(2)-U(1)-C(1)	29.6(2)
C(30)-C(31)	1.522(11)	C(15)-U(1)-C(1)	144.0(2)
C(31)-C(32)	1.500(10)	C(13)-U(1)-C(1)	134.3(2)
C(33)-C(34)	1.484(15)	C(4)-U(1)-C(1)	48.6(2)
C(34)-C(35)	1.530(14)	C(3)-U(1)-C(5)	48.1(2)
C(35)-C(36)	1.495(14)	C(11)-U(1)-C(5)	100.6(2)
		C(12)-U(1)-C(5)	86.7(2)
Cnt1-U(1)-I(1)	105.8	C(2)-U(1)-C(5)	48.7(2)
Cnt1-U(1)-I(2)	104.4	C(15)-U(1)-C(5)	130.2(2)
Cnt2-U(1)-I(1)	105.4	C(13)-U(1)-C(5)	105.0(2)
Cnt2-U(1)-I(2)	106.0	C(4)-U(1)-C(5)	29.6(2)
Cnt1-U(1)-Cnt2	133.7	C(1)-U(1)-C(5)	29.3(2)

C(3)-U(1)-C(14)	132.2(2)	C(3)-C(2)-C(1)	107.0(7)
C(11)-U(1)-C(14)	48.6(2)	C(3)-C(2)-C(7)	127.0(7)
C(12)-U(1)-C(14)	48.7(2)	C(1)-C(2)-C(7)	125.9(7)
C(2)-U(1)-C(14)	159.5(2)	C(3)-C(2)-U(1)	75.0(4)
C(15)-U(1)-C(14)	29.4(2)	C(1)-C(2)-U(1)	76.1(4)
C(13)-U(1)-C(14)	29.3(2)	C(7)-C(2)-U(1)	115.6(5)
C(4)-U(1)-C(14)	120.6(2)	C(2)-C(3)-C(4)	110.7(7)
C(1)-U(1)-C(14)	161.9(2)	C(2)-C(3)-C(8)	125.5(7)
C(5)-U(1)-C(14)	133.5(2)	C(4)-C(3)-C(8)	123.5(7)
C(3)-U(1)-I(2)	117.68(16)	C(2)-C(3)-U(1)	76.0(4)
C(11)-U(1)-I(2)	87.42(15)	C(4)-C(3)-U(1)	76.7(4)
C(12)-U(1)-I(2)	116.23(15)	C(8)-C(3)-U(1)	119.9(5)
C(2)-U(1)-I(2)	88.76(16)	C(3)-C(4)-C(5)	106.5(6)
C(15)-U(1)-I(2)	82.84(16)	C(3)-C(4)-C(9)	125.9(7)
C(13)-U(1)-I(2)	130.95(15)	C(5)-C(4)-C(9)	126.9(7)
C(4)-U(1)-I(2)	128.75(15)	C(3)-C(4)-U(1)	74.0(4)
C(1)-U(1)-I(2)	80.18(15)	C(5)-C(4)-U(1)	76.0(4)
C(5)-U(1)-I(2)	103.10(16)	C(9)-C(4)-U(1)	122.5(5)
C(14)-U(1)-I(2)	108.08(17)	C(1)-C(5)-C(4)	107.5(6)
C(3)-U(1)-I(1)	82.87(15)	C(1)-C(5)-C(10)	123.5(7)
C(11)-U(1)-I(1)	125.88(16)	C(4)-C(5)-C(10)	128.2(7)
C(12)-U(1)-I(1)	124.97(14)	C(1)-C(5)-U(1)	74.7(4)
C(2)-U(1)-I(1)	87.10(15)	C(4)-C(5)-U(1)	74.4(4)
C(15)-U(1)-I(1)	96.95(16)	C(10)-C(5)-U(1)	124.5(5)
C(13)-U(1)-I(1)	95.98(15)	C(12)-C(11)-C(15)	108.2(6)
C(4)-U(1)-I(1)	107.51(15)	C(12)-C(11)-C(16)	125.6(7)
C(1)-U(1)-I(1)	115.94(15)	C(15)-C(11)-C(16)	125.9(7)
C(5)-U(1)-I(1)	130.77(15)	C(12)-C(11)-U(1)	75.2(4)
C(14)-U(1)-I(1)	79.96(15)	C(15)-C(11)-U(1)	75.9(4)
I(2)-U(1)-I(1)	95.05(2)	C(16)-C(11)-U(1)	119.6(5)
C(5)-C(1)-C(2)	108.2(7)	C(13)-C(12)-C(11)	107.6(6)
C(5)-C(1)-C(6)	123.8(7)	C(13)-C(12)-C(17)	125.9(7)
C(2)-C(1)-C(6)	127.2(7)	C(11)-C(12)-C(17)	125.4(7)
C(5)-C(1)-U(1)	76.0(4)	C(13)-C(12)-U(1)	76.2(4)
C(2)-C(1)-U(1)	74.3(4)	C(11)-C(12)-U(1)	75.1(4)
C(6)-C(1)-U(1)	124.0(5)	C(17)-C(12)-U(1)	124.0(5)

C(12)-C(13)-C(14)	109.2(7)	C(21)-O(1)-Li(1)	122.7(6)
C(12)-C(13)-C(18)	126.7(7)	C(25)-O(2)-C(28)	106.3(6)
C(14)-C(13)-C(18)	123.8(7)	C(25)-O(2)-Li(1)	124.7(6)
C(12)-C(13)-U(1)	74.4(4)	C(28)-O(2)-Li(1)	126.9(6)
C(14)-C(13)-U(1)	76.8(4)	C(29)-O(3)-C(32)	108.4(6)
C(18)-C(13)-U(1)	120.9(5)	C(29)-O(3)-Li(1)	122.9(6)
C(13)-C(14)-C(15)	106.9(6)	C(32)-O(3)-Li(1)	125.5(6)
C(13)-C(14)-C(19)	125.9(8)	C(36)-O(4)-C(33)	105.5(7)
C(15)-C(14)-C(19)	126.6(8)	C(36)-O(4)-Li(1)	128.6(6)
C(13)-C(14)-U(1)	73.9(4)	C(33)-O(4)-Li(1)	121.1(7)
C(15)-C(14)-U(1)	73.7(4)	O(1)-C(21)-C(22)	105.4(6)
C(19)-C(14)-U(1)	125.2(5)	C(23)-C(22)-C(21)	104.3(7)
C(11)-C(15)-C(14)	108.1(7)	C(24)-C(23)-C(22)	102.1(7)
C(11)-C(15)-C(20)	126.3(7)	O(1)-C(24)-C(23)	105.5(7)
C(14)-C(15)-C(20)	125.1(7)	O(2)-C(25)-C(26)	107.2(7)
C(11)-C(15)-U(1)	74.4(4)	C(25)-C(26)-C(27)	107.1(8)
C(14)-C(15)-U(1)	76.9(4)	C(26)-C(27)-C(28)	103.1(7)
C(20)-C(15)-U(1)	121.5(5)	O(2)-C(28)-C(27)	105.2(7)
O(2)-Li(1)-O(3)	108.5(7)	O(3)-C(29)-C(30)	104.5(7)
O(2)-Li(1)-O(4)	111.7(7)	C(29)-C(30)-C(31)	102.7(7)
O(3)-Li(1)-O(4)	105.1(6)	C(32)-C(31)-C(30)	103.9(6)
O(2)-Li(1)-O(1)	110.9(7)	O(3)-C(32)-C(31)	107.8(6)
O(3)-Li(1)-O(1)	114.0(7)	O(4)-C(33)-C(34)	106.7(8)
O(4)-Li(1)-O(1)	106.6(7)	C(33)-C(34)-C(35)	105.4(9)
C(24)-O(1)-C(21)	109.2(6)	C(36)-C(35)-C(34)	102.5(8)
C(24)-O(1)-Li(1)	119.9(6)	O(4)-C(36)-C(35)	105.8(8)

X-ray Data Collection, Structure Solution and Refinement for 8.7.

A green crystal of approximate dimensions 0.088 x 0.198 x 0.320 mm was mounted on a glass fiber and transferred to a Bruker SMART APEX II diffractometer. The APEX2[67] program package was used to determine the unit-cell parameters and for data collection (20 sec/frame scan time for a sphere of diffraction data). The raw frame data was processed using SAINT[69] and SADABS[73] to yield the reflection data file. Subsequent calculations were carried out using the

SHELXTL[71] program. There were no systematic absences nor any diffraction symmetry other than the Friedel condition. The centrosymmetric triclinic space group $P\bar{1}$ was assigned and later determined to be correct.

The structure was solved by direct methods and refined on F^2 by full-matrix least-squares techniques. The analytical scattering factors[72] for neutral atoms were used throughout the analysis. Hydrogen atoms were included using a riding model. The molecule was located about an inversion center. C(38) and H(37A) were disordered and included with partial site-occupancy-factors. There were two molecules of toluene solvent present. The toluene solvents were disordered and included using multiple components with partial site occupancy factors.

Least-squares analysis yielded wR2 = 0.0631 and Goof = 1.045 for 584 variables refined against 13992 data (0.73 Å), R1 = 0.0261 for those 12561 data with $I > 2.0\sigma(I)$.

Table 8.9: Bond lengths [Å] and angles [°] for **8.7.**

U(1)-Cnt1	2.497	Si(1)-C(8)	1.870(4)
U(1)-Cnt2	2.513	Si(1)-C(6)	1.871(3)
U(1)-C(5)	2.753(3)	Si(3)-C(12)	1.862(3)
U(1)-C(1)	2.758(3)	Si(3)-C(17)	1.862(4)
U(1)-C(15)	2.767(3)	Si(3)-C(18)	1.865(4)
U(1)-C(2)	2.770(3)	Si(3)-C(19)	1.865(4)
U(1)-C(16)	2.774(3)	Si(2)-C(3)	1.863(3)
U(1)-C(4)	2.779(3)	Si(2)-C(11)	1.865(4)
U(1)-C(14)	2.788(3)	Si(2)-C(9)	1.867(4)
U(1)-C(13)	2.800(3)	Si(2)-C(10)	1.881(4)
U(1)-C(12)	2.810(3)	Si(4)-C(21)	1.858(4)
U(1)-C(3)	2.812(3)	Si(4)-C(22)	1.861(5)
U(1)-I(2)	3.0711(3)	Si(4)-C(14)	1.866(3)
U(1)-I(1)	3.1206(2)	Si(4)-C(20)	1.872(5)
I(1)-K(1)	3.5777(8)	C(1)-C(2)	1.425(4)
Si(1)-C(1)	1.860(3)	C(1)-C(5)	1.429(4)
Si(1)-C(7)	1.870(3)	C(2)-C(3)	1.414(4)

C(3)-C(4)	1.431(4)	C(37)-C(38)	1.405(9)
C(4)-C(5)	1.406(4)	C(39)-C(47)	0.984(11)
C(12)-C(13)	1.416(4)	C(39)-C(48)	1.013(9)
C(12)-C(16)	1.432(4)	C(39)-C(40)	1.3900
C(13)-C(14)	1.426(4)	C(39)-C(44)	1.3900
C(14)-C(15)	1.425(5)	C(39)-C(45)	1.457(7)
C(15)-C(16)	1.404(4)	C(39)-C(46)	1.458(9)
K(1)-O(6)	2.750(3)	C(39)-C(49)	1.498(11)
K(1)-O(2)	2.774(2)	C(39)-C(51)	1.829(9)
K(1)-O(4)	2.781(3)	C(39)-C(50)	1.844(11)
K(1)-O(3)	2.792(2)	C(40)-C(51)	0.791(12)
K(1)-O(5)	2.821(3)	C(40)-C(50)	1.039(11)
K(1)-O(1)	2.833(2)	C(40)-C(41)	1.3900
K(1)-C(35)	3.408(4)	C(40)-C(46)	1.556(10)
O(1)-C(23)	1.414(4)	C(40)-C(49)	1.825(12)
O(1)-C(34)	1.416(4)	C(41)-C(51)	0.919(13)
O(2)-C(25)	1.414(4)	C(41)-C(42)	1.3900
O(2)-C(24)	1.426(5)	C(41)-C(46)	1.505(9)
O(3)-C(27)	1.414(5)	C(42)-C(52)	0.760(13)
O(3)-C(26)	1.442(5)	C(42)-C(46)	1.348(9)
O(4)-C(29)	1.412(6)	C(42)-C(43)	1.3900
O(4)-C(28)	1.431(5)	C(42)-C(51)	1.945(11)
O(5)-C(31)	1.407(6)	C(43)-C(52)	0.822(12)
O(5)-C(30)	1.443(6)	C(43)-C(46)	1.234(10)
O(6)-C(33)	1.399(5)	C(43)-C(44)	1.3900
O(6)-C(32)	1.423(5)	C(43)-C(47)	1.799(11)
C(23)-C(24)	1.490(6)	C(44)-C(47)	0.501(13)
C(25)-C(26)	1.477(6)	C(44)-C(46)	1.295(9)
C(27)-C(28)	1.488(8)	C(44)-C(48)	1.852(12)
C(29)-C(30)	1.471(8)	C(45)-C(48)	0.629(16)
C(31)-C(32)	1.490(7)	C(45)-C(49)	1.144(17)
C(33)-C(34)	1.498(6)	C(45)-C(47)	1.994(14)
C(35)-C(36)	1.354(7)	C(46)-C(47)	1.3900
C(35)-C(37)#1	1.383(7)	C(46)-C(51)	1.3900
C(36)-C(37)	1.385(7)	C(46)-C(52)	1.467(7)
C(37)-C(35)#1	1.383(7)	C(47)-C(48)	1.3900

C(48)-C(49)	1.3900	C(14)-U(1)-C(13)	29.56(8)
C(49)-C(50)	1.3900	C(5)-U(1)-C(12)	120.27(8)
C(50)-C(51)	1.3900	C(1)-U(1)-C(12)	118.18(9)
		C(15)-U(1)-C(12)	48.81(8)
Cnt1-U(1)-I(1)	104.2	C(2)-U(1)-C(12)	141.07(9)
Cnt1-U(1)-I(2)	110.9	C(16)-U(1)-C(12)	29.70(8)
Cnt2-U(1)-I(1)	114.7	C(4)-U(1)-C(12)	144.07(8)
Cnt2-U(1)-I(2)	103.7	C(14)-U(1)-C(12)	49.43(9)
Cnt1-U(1)-Cnt2	124.5	C(13)-U(1)-C(12)	29.25(9)
C(5)-U(1)-C(1)	30.06(8)	C(5)-U(1)-C(3)	49.10(9)
C(5)-U(1)-C(15)	73.67(8)	C(1)-U(1)-C(3)	49.77(9)
C(1)-U(1)-C(15)	85.40(9)	C(15)-U(1)-C(3)	122.32(9)
C(5)-U(1)-C(2)	48.44(8)	C(2)-U(1)-C(3)	29.34(9)
C(1)-U(1)-C(2)	29.86(8)	C(16)-U(1)-C(3)	138.27(9)
C(15)-U(1)-C(2)	115.16(9)	C(4)-U(1)-C(3)	29.66(8)
C(5)-U(1)-C(16)	91.65(9)	C(14)-U(1)-C(3)	128.69(8)
C(1)-U(1)-C(16)	89.61(9)	C(13)-U(1)-C(3)	155.08(9)
C(15)-U(1)-C(16)	29.35(9)	C(12)-U(1)-C(3)	167.83(9)
C(2)-U(1)-C(16)	116.58(9)	C(5)-U(1)-I(2)	118.05(6)
C(5)-U(1)-C(4)	29.45(9)	C(1)-U(1)-I(2)	137.34(6)
C(1)-U(1)-C(4)	49.30(9)	C(15)-U(1)-I(2)	116.85(7)
C(15)-U(1)-C(4)	95.35(9)	C(2)-U(1)-I(2)	114.83(6)
C(2)-U(1)-C(4)	48.09(8)	C(16)-U(1)-I(2)	128.12(7)
C(16)-U(1)-C(4)	118.99(9)	C(4)-U(1)-I(2)	90.68(6)
C(5)-U(1)-C(14)	89.45(8)	C(14)-U(1)-I(2)	87.25(7)
C(1)-U(1)-C(14)	110.39(9)	C(13)-U(1)-I(2)	80.08(7)
C(15)-U(1)-C(14)	29.73(10)	C(12)-U(1)-I(2)	102.96(6)
C(2)-U(1)-C(14)	137.53(9)	C(3)-U(1)-I(2)	88.56(6)
C(16)-U(1)-C(14)	49.10(10)	C(5)-U(1)-I(1)	125.24(6)
C(4)-U(1)-C(14)	99.29(8)	C(1)-U(1)-I(1)	96.36(6)
C(5)-U(1)-C(13)	118.21(8)	C(15)-U(1)-I(1)	130.24(7)
C(1)-U(1)-C(13)	133.07(9)	C(2)-U(1)-I(1)	79.03(6)
C(15)-U(1)-C(13)	48.00(9)	C(16)-U(1)-I(1)	100.92(7)
C(2)-U(1)-C(13)	162.90(9)	C(4)-U(1)-I(1)	123.04(6)
C(16)-U(1)-C(13)	48.04(9)	C(14)-U(1)-I(1)	137.53(6)
C(4)-U(1)-C(13)	127.62(8)	C(13)-U(1)-I(1)	109.15(6)

C(12)-U(1)-I(1)	89.15(6)	C(1)-C(2)-U(1)	74.61(15)
C(3)-U(1)-I(1)	93.78(6)	C(2)-C(3)-C(4)	105.2(3)
I(2)-U(1)-I(1)	94.948(8)	C(2)-C(3)-Si(2)	126.6(2)
U(1)-I(1)-K(1)	167.385(14)	C(4)-C(3)-Si(2)	127.2(2)
C(1)-Si(1)-C(7)	110.24(15)	C(2)-C(3)-U(1)	73.70(15)
C(1)-Si(1)-C(8)	110.75(15)	C(4)-C(3)-U(1)	73.91(15)
C(7)-Si(1)-C(8)	110.72(19)	Si(2)-C(3)-U(1)	125.56(14)
C(1)-Si(1)-C(6)	108.86(16)	C(5)-C(4)-C(3)	109.2(3)
C(7)-Si(1)-C(6)	109.09(17)	C(5)-C(4)-U(1)	74.27(15)
C(8)-Si(1)-C(6)	107.10(17)	C(3)-C(4)-U(1)	76.44(16)
C(12)-Si(3)-C(17)	108.97(16)	C(4)-C(5)-C(1)	109.1(2)
C(12)-Si(3)-C(18)	109.50(15)	C(4)-C(5)-U(1)	76.28(16)
C(17)-Si(3)-C(18)	108.1(2)	C(1)-C(5)-U(1)	75.16(15)
C(12)-Si(3)-C(19)	109.71(16)	C(13)-C(12)-C(16)	105.6(3)
C(17)-Si(3)-C(19)	107.8(2)	C(13)-C(12)-Si(3)	125.0(2)
C(18)-Si(3)-C(19)	112.71(17)	C(16)-C(12)-Si(3)	128.0(2)
C(3)-Si(2)-C(11)	109.81(15)	C(13)-C(12)-U(1)	74.99(16)
C(3)-Si(2)-C(9)	111.44(16)	C(16)-C(12)-U(1)	73.76(16)
C(11)-Si(2)-C(9)	111.2(2)	Si(3)-C(12)-U(1)	126.52(13)
C(3)-Si(2)-C(10)	107.70(17)	C(12)-C(13)-C(14)	110.9(3)
C(11)-Si(2)-C(10)	108.40(18)	C(12)-C(13)-U(1)	75.76(15)
C(9)-Si(2)-C(10)	108.2(2)	C(14)-C(13)-U(1)	74.76(16)
C(21)-Si(4)-C(22)	109.2(2)	C(15)-C(14)-C(13)	105.2(3)
C(21)-Si(4)-C(14)	112.95(15)	C(15)-C(14)-Si(4)	128.0(2)
C(22)-Si(4)-C(14)	108.57(17)	C(13)-C(14)-Si(4)	126.1(2)
C(21)-Si(4)-C(20)	108.4(2)	C(15)-C(14)-U(1)	74.29(16)
C(22)-Si(4)-C(20)	108.9(3)	C(13)-C(14)-U(1)	75.68(16)
C(14)-Si(4)-C(20)	108.7(2)	Si(4)-C(14)-U(1)	122.74(14)
C(2)-C(1)-C(5)	105.1(2)	C(16)-C(15)-C(14)	109.6(3)
C(2)-C(1)-Si(1)	125.0(2)	C(16)-C(15)-U(1)	75.63(16)
C(5)-C(1)-Si(1)	129.3(2)	C(14)-C(15)-U(1)	75.98(17)
C(2)-C(1)-U(1)	75.53(15)	C(15)-C(16)-C(12)	108.7(3)
C(5)-C(1)-U(1)	74.78(15)	C(15)-C(16)-U(1)	75.02(17)
Si(1)-C(1)-U(1)	121.65(13)	C(12)-C(16)-U(1)	76.53(17)
C(3)-C(2)-C(1)	111.3(3)	O(6)-K(1)-O(2)	120.50(8)
C(3)-C(2)-U(1)	76.95(15)	O(6)-K(1)-O(4)	119.76(9)

O(2)-K(1)-O(4)	119.73(9)	C(29)-O(4)-K(1)	118.7(3)
O(6)-K(1)-O(3)	170.85(8)	C(28)-O(4)-K(1)	116.3(2)
O(2)-K(1)-O(3)	60.55(8)	C(31)-O(5)-C(30)	113.3(4)
O(4)-K(1)-O(3)	59.95(9)	C(31)-O(5)-K(1)	113.0(3)
O(6)-K(1)-O(5)	60.25(10)	C(30)-O(5)-K(1)	111.2(3)
O(2)-K(1)-O(5)	175.20(8)	C(33)-O(6)-C(32)	113.7(3)
O(4)-K(1)-O(5)	59.70(10)	C(33)-O(6)-K(1)	116.1(2)
O(3)-K(1)-O(5)	117.85(10)	C(32)-O(6)-K(1)	116.7(3)
O(6)-K(1)-O(1)	61.07(8)	O(1)-C(23)-C(24)	109.4(3)
O(2)-K(1)-O(1)	60.16(7)	O(2)-C(24)-C(23)	108.5(3)
O(4)-K(1)-O(1)	171.05(8)	O(2)-C(25)-C(26)	108.5(3)
O(3)-K(1)-O(1)	117.61(8)	O(3)-C(26)-C(25)	109.0(3)
O(5)-K(1)-O(1)	119.55(9)	O(3)-C(27)-C(28)	108.7(4)
O(6)-K(1)-C(35)	94.56(10)	O(4)-C(28)-C(27)	108.4(4)
O(2)-K(1)-C(35)	92.62(11)	O(4)-C(29)-C(30)	108.7(4)
O(4)-K(1)-C(35)	82.35(10)	O(5)-C(30)-C(29)	109.0(4)
O(3)-K(1)-C(35)	76.29(10)	O(5)-C(31)-C(32)	108.3(4)
O(5)-K(1)-C(35)	82.58(11)	O(6)-C(32)-C(31)	109.1(3)
O(1)-K(1)-C(35)	88.71(10)	O(6)-C(33)-C(34)	109.0(3)
O(6)-K(1)-I(1)	86.67(5)	O(1)-C(34)-C(33)	109.1(3)
O(2)-K(1)-I(1)	85.91(5)	C(36)-C(35)-C(37)#1	118.9(4)
O(4)-K(1)-I(1)	97.88(6)	C(36)-C(35)-K(1)	90.2(3)
O(3)-K(1)-I(1)	102.46(6)	C(37)#1-C(35)-K(1)	101.2(3)
O(5)-K(1)-I(1)	98.88(6)	C(35)-C(36)-C(37)	121.1(5)
O(1)-K(1)-I(1)	91.05(5)	C(35)#1-C(37)-C(36)	120.0(4)
C(35)-K(1)-I(1)	178.43(10)	C(35)#1-C(37)-C(38)	116.7(6)
C(23)-O(1)-C(34)	112.0(3)	C(36)-C(37)-C(38)	123.1(6)
C(23)-O(1)-K(1)	111.7(2)	C(47)-C(39)-C(48)	88.2(8)
C(34)-O(1)-K(1)	109.9(2)	C(47)-C(39)-C(40)	130.3(6)
C(25)-O(2)-C(24)	111.4(3)	C(48)-C(39)-C(40)	140.3(9)
C(25)-O(2)-K(1)	116.6(2)	C(47)-C(39)-C(44)	14.4(7)
C(24)-O(2)-K(1)	117.5(2)	C(48)-C(39)-C(44)	99.6(9)
C(27)-O(3)-C(26)	111.6(3)	C(40)-C(39)-C(44)	120.0
C(27)-O(3)-K(1)	114.9(2)	C(47)-C(39)-C(45)	108.1(7)
C(26)-O(3)-K(1)	112.2(2)	C(48)-C(39)-C(45)	21.1(10)
C(29)-O(4)-C(28)	113.8(4)	C(40)-C(39)-C(45)	119.3(4)

C(44)-C(39)-C(45)	120.3(4)	C(41)-C(40)-C(46)	61.1(3)
C(47)-C(39)-C(46)	66.1(5)	C(51)-C(40)-C(49)	129.6(12)
C(48)-C(39)-C(46)	153.5(11)	C(50)-C(40)-C(49)	49.2(5)
C(40)-C(39)-C(46)	66.2(4)	C(39)-C(40)-C(49)	53.5(5)
C(44)-C(39)-C(46)	54.0(4)	C(41)-C(40)-C(49)	167.0(5)
C(45)-C(39)-C(46)	174.2(6)	C(46)-C(40)-C(49)	110.4(6)
C(47)-C(39)-C(49)	151.3(9)	C(51)-C(41)-C(40)	32.6(8)
C(48)-C(39)-C(49)	63.9(5)	C(51)-C(41)-C(42)	113.2(7)
C(40)-C(39)-C(49)	78.3(6)	C(40)-C(41)-C(42)	120.0
C(44)-C(39)-C(49)	157.9(6)	C(51)-C(41)-C(46)	64.8(5)
C(45)-C(39)-C(49)	45.5(6)	C(40)-C(41)-C(46)	64.9(4)
C(46)-C(39)-C(49)	140.3(8)	C(42)-C(41)-C(46)	55.3(4)
C(47)-C(39)-C(51)	114.4(7)	C(52)-C(42)-C(46)	83.2(9)
C(48)-C(39)-C(51)	155.1(10)	C(52)-C(42)-C(43)	29.7(9)
C(40)-C(39)-C(51)	23.8(4)	C(46)-C(42)-C(43)	53.5(4)
C(44)-C(39)-C(51)	101.4(4)	C(52)-C(42)-C(41)	149.7(9)
C(45)-C(39)-C(51)	137.4(6)	C(46)-C(42)-C(41)	66.7(4)
C(46)-C(39)-C(51)	48.4(3)	C(43)-C(42)-C(41)	120.0
C(49)-C(39)-C(51)	92.2(5)	C(52)-C(42)-C(51)	127.1(11)
C(47)-C(39)-C(50)	157.8(8)	C(46)-C(42)-C(51)	45.6(3)
C(48)-C(39)-C(50)	111.5(8)	C(43)-C(42)-C(51)	98.4(3)
C(40)-C(39)-C(50)	33.9(5)	C(41)-C(42)-C(51)	25.8(4)
C(44)-C(39)-C(50)	143.5(4)	C(52)-C(43)-C(46)	88.7(9)
C(45)-C(39)-C(50)	93.0(6)	C(52)-C(43)-C(44)	147.3(9)
C(46)-C(39)-C(50)	92.9(5)	C(46)-C(43)-C(44)	58.8(4)
C(49)-C(39)-C(50)	47.8(3)	C(52)-C(43)-C(42)	27.3(9)
C(51)-C(39)-C(50)	44.5(2)	C(46)-C(43)-C(42)	61.5(4)
C(51)-C(40)-C(50)	97.9(12)	C(44)-C(43)-C(42)	120.0
C(51)-C(40)-C(39)	111.0(8)	C(52)-C(43)-C(47)	137.8(11)
C(50)-C(40)-C(39)	97.7(8)	C(46)-C(43)-C(47)	50.4(4)
C(51)-C(40)-C(41)	38.8(10)	C(44)-C(43)-C(47)	10.5(5)
C(50)-C(40)-C(41)	128.6(8)	C(42)-C(43)-C(47)	110.7(3)
C(39)-C(40)-C(41)	120.0	C(47)-C(44)-C(46)	90.2(11)
C(51)-C(40)-C(46)	63.1(6)	C(47)-C(44)-C(43)	139.2(15)
C(50)-C(40)-C(46)	135.2(10)	C(46)-C(44)-C(43)	54.6(4)
C(39)-C(40)-C(46)	59.0(3)	C(47)-C(44)-C(39)	29.2(12)

C(46)-C(44)-C(39)	65.7(4)	C(47)-C(46)-C(41)	145.8(6)
C(43)-C(44)-C(39)	120.0	C(51)-C(46)-C(41)	36.8(5)
C(47)-C(44)-C(48)	19.6(15)	C(39)-C(46)-C(41)	108.7(6)
C(46)-C(44)-C(48)	98.3(6)	C(52)-C(46)-C(41)	88.9(6)
C(43)-C(44)-C(48)	152.6(4)	C(43)-C(46)-C(40)	170.5(9)
C(39)-C(44)-C(48)	32.6(4)	C(44)-C(46)-C(40)	114.9(6)
C(48)-C(45)-C(49)	99.2(17)	C(42)-C(46)-C(40)	111.8(6)
C(48)-C(45)-C(39)	35.5(12)	C(47)-C(46)-C(40)	94.2(4)
C(49)-C(45)-C(39)	69.1(7)	C(51)-C(46)-C(40)	30.5(5)
C(48)-C(45)-C(47)	13.2(18)	C(39)-C(46)-C(40)	54.8(3)
C(49)-C(45)-C(47)	96.4(7)	C(52)-C(46)-C(40)	142.4(7)
C(39)-C(45)-C(47)	28.0(3)	C(41)-C(46)-C(40)	54.0(3)
C(43)-C(46)-C(44)	66.6(5)	C(44)-C(47)-C(39)	136.4(19)
C(43)-C(46)-C(42)	65.0(5)	C(44)-C(47)-C(46)	68.7(10)
C(44)-C(46)-C(42)	131.3(8)	C(39)-C(47)-C(46)	73.6(5)
C(43)-C(46)-C(47)	86.4(6)	C(44)-C(47)-C(48)	153(2)
C(44)-C(46)-C(47)	21.1(6)	C(39)-C(47)-C(48)	46.7(5)
C(42)-C(46)-C(47)	148.4(6)	C(46)-C(47)-C(48)	120.0
C(43)-C(46)-C(51)	152.6(6)	C(44)-C(47)-C(43)	30.3(11)
C(44)-C(46)-C(51)	137.9(6)	C(39)-C(47)-C(43)	116.7(7)
C(42)-C(46)-C(51)	90.5(6)	C(46)-C(47)-C(43)	43.2(4)
C(47)-C(46)-C(51)	120.0	C(48)-C(47)-C(43)	162.2(4)
C(43)-C(46)-C(39)	126.7(7)	C(44)-C(47)-C(45)	159(3)
C(44)-C(46)-C(39)	60.3(4)	C(39)-C(47)-C(45)	44.0(5)
C(42)-C(46)-C(39)	164.4(9)	C(46)-C(47)-C(45)	117.5(5)
C(47)-C(46)-C(39)	40.3(4)	C(48)-C(47)-C(45)	5.9(9)
C(51)-C(46)-C(39)	79.8(4)	C(43)-C(47)-C(45)	160.7(6)
C(43)-C(46)-C(52)	34.1(5)	C(45)-C(48)-C(39)	123(2)
C(44)-C(46)-C(52)	100.6(6)	C(45)-C(48)-C(47)	161(3)
C(42)-C(46)-C(52)	31.0(5)	C(39)-C(48)-C(47)	45.0(6)
C(47)-C(46)-C(52)	119.7(4)	C(45)-C(48)-C(49)	54.3(15)
C(51)-C(46)-C(52)	120.3(4)	C(39)-C(48)-C(49)	75.3(6)
C(39)-C(46)-C(52)	159.6(6)	C(47)-C(48)-C(49)	120.0
C(43)-C(46)-C(41)	122.8(7)	C(45)-C(48)-C(44)	168(3)
C(44)-C(46)-C(41)	166.2(8)	C(39)-C(48)-C(44)	47.7(6)
C(42)-C(46)-C(41)	58.0(4)	C(47)-C(48)-C(44)	7.0(6)

C(49)-C(48)-C(44)	121.3(3)	C(41)-C(51)-C(50)	142.9(10)
C(45)-C(49)-C(50)	143.7(8)	C(40)-C(51)-C(46)	86.4(7)
C(45)-C(49)-C(48)	26.5(8)	C(41)-C(51)-C(46)	78.4(7)
C(50)-C(49)-C(48)	120.0	C(50)-C(51)-C(46)	120.0
C(45)-C(49)-C(39)	65.3(7)	C(40)-C(51)-C(39)	45.2(5)
C(50)-C(49)-C(39)	79.3(4)	C(41)-C(51)-C(39)	118.6(8)
C(48)-C(49)-C(39)	40.9(4)	C(50)-C(51)-C(39)	68.4(3)
C(45)-C(49)-C(40)	109.6(9)	C(46)-C(51)-C(39)	51.7(3)
C(50)-C(49)-C(40)	34.5(3)	C(40)-C(51)-C(42)	116.8(10)
C(48)-C(49)-C(40)	88.4(3)	C(41)-C(51)-C(42)	41.1(5)
C(39)-C(49)-C(40)	48.2(3)	C(50)-C(51)-C(42)	162.5(4)
C(40)-C(50)-C(51)	34.3(7)	C(46)-C(51)-C(42)	43.9(3)
C(40)-C(50)-C(49)	96.3(6)	C(39)-C(51)-C(42)	94.9(4)
C(51)-C(50)-C(49)	120.0	C(42)-C(52)-C(43)	123.0(16)
C(40)-C(50)-C(39)	48.3(5)	C(42)-C(52)-C(46)	65.8(9)
C(51)-C(50)-C(39)	67.2(3)	C(43)-C(52)-C(46)	57.2(8)
C(49)-C(50)-C(39)	52.9(3)		
C(40)-C(51)-C(41)	108.5(16)	Symmetry transformations used to generate equivalent atoms: #1 -x+2,-y-1,-z	
C(40)-C(51)-C(50)	47.8(8)		

References

(1) *Organometallic and Coordination Chemistry of the Actinides*; Albrecht-Schmitt, T. E., Ed.; Springer-Verlag Berlin, 2008.

(2) Liddle, S. T. The Renaissance of Non-Aqueous Uranium Chemistry. *Angew. Chem. Int. Ed.* **2015**, *54*, 8604–8641, DOI: 10.1002/anie.201412168.

(3) Kindra, D. R.; Evans, W. J. Magnetic Susceptibility of Uranium Complexes. *Chem. Rev.* **2014**, *114*, 8865–8882, DOI: 10.1021/cr500242w.

(4) Castro-Rodríguez, I.; Meyer, K. Small Molecule Activation at Uranium Coordination Complexes: Control of Reactivity via Molecular Architecture. *Chem. Commun.* **2006**, No. 13, 1353, DOI: 10.1039/b513755c.

(5) Muetterties, E. L. Polytopal Form and Isomerism. *Tetrahedron* **1974**, *30*, 1595–1604, DOI: 10.1016/S0040-4020(01)90682-9.

(6) Avens, L. R.; Burns, C. J.; Butcher, R. J.; Clark, D. L.; Gordon, J. C.; Schake, A. R.; Scott, B. L.; Watkin, J. G.; Zwick, B. D. Mono(Pentamethylcyclopentadienyl)Uranium(III) Complexes: Synthesis, Properties, and X-Ray Structures of (η-C_5Me_5)$UI_2(THF)_3$, (η-C_5Me_5)$UI_2(Py)_3$, and (η-C_5Me_5)$U[N(SiMe_3)_2]_2$. *Organometallics* **2000**, *19*, 451–457, DOI: 10.1021/om990718r.

(7) Evans, W. J.; Peterson, T. T.; Rausch, M. D.; Hunter, W. E.; Zhang, H.; Atwood, J. L. Synthesis and X-Ray Crystallographic Characterization of Asymmetric Organoyttrlum Halide Dimer: $(C_5Me_5)_2Y(\mu\text{-}Cl)YCl(C_5Me_5)_2$. *Organometallics* **1985**, *4*, 554–559, DOI: 10.1021/om00122a022.

(8) Evans, W. J.; Broomhall-dillard, R. N. R.; Foster, S. E.; Ziller, J. W. Synthesis And Structure Of A Pentamethylcyclopentadienyl Thulium Chloride Complex, $[(C_5Me_5)_2Tm(\mu^3\text{-}Cl)_2K(THF)]_n$. *J. Coord. Chem.* **1999**, *46*, 565–572, DOI: 10.1080/00958979908054919.

(9) Evans, W. J.; Keyer, R. A.; Ziller, J. W. Investigation of Organolanthanide-Based Carbon-Carbon Bond Formation: Synthesis, Structure, and Coupling Reactivity of Organolanthanide Alkynide Complexes, Including the Unusual Structures of the Trienediyl Complex [(C5Me5)2Sm]$_2$[μ- η^2: η^2-$Ph(CH_2)_2C{=}C{=}C{=}C\text{-}(CH_2)_2Ph$] and the Unsolvated Aklynide $[(C_5Me_5)_2Sm(C{\equiv}CCMe_3)]_2$. *Organometallics* **1993**, *12*, 2618–2633, DOI: 10.1021/om00031a036.

(10) Korobkov, I.; Gorelsky, S.; Gambarotta, S. Reduced Uranium Complexes: Synthetic and DFT Study of the Role of π Ligation in the Stabilization of Uranium Species in a Formal

Low-Valent State. *J. Am. Chem. Soc.* **2009**, *131*, 10406–10420, DOI: 10.1021/ja9002525.

(11) Hayton, T. W.; Wu, G. Synthesis, Characterization, and Reactivity of a Uranyl β-Diketiminate Complex. *J. Am. Chem. Soc.* **2008**, *130*, 2005–2014, DOI: 10.1021/ja077538q.

(12) Fox, A. R.; Silvia, J. S.; Townsend, E. M.; Cummins, C. C. Six-Coordinate Uranium Complexes Featuring a Bidentate Anilide Ligand. *Comptes Rendus Chim.* **2010**, *13*, 781–789, DOI: 10.1016/j.crci.2010.05.001.

(13) Cooper, O. J.; Mills, D. P.; McMaster, J.; Tuna, F.; McInnes, E. J. L.; Lewis, W.; Blake, A. J.; Liddle, S. T. The Nature of the U=C Double Bond: Pushing the Stability of High-Oxidation-State Uranium Carbenes to the Limit. *Chem. Eur. J.* **2013**, *19*, 7071–7083, DOI: 10.1002/chem.201300071.

(14) Jeske, G.; Lauke, H.; Mauermann, H.; Swepston, P. N.; Schumann, H.; Marks, T. J. Highly Reactive Organolanthanides. Systematic Routes to and Olefin Chemistry of Early and Late Bis(Pentamethylcyclopentadienyl) 4f Hydrocarbyl and Hydride Complexes. *J. Am. Chem. Soc.* **1985**, *107*, 8091–8103, DOI: 10.1021/ja00312a050.

(15) Danis, J. A.; Lin, M. R.; Scott, B. L.; Eichhorn, B. W.; Runde, W. H. Coordination Trends in Alkali Metal Crown Ether Uranyl Halide Complexes: The Series $[A(Crown)]_2[UO_2X_4]$ Where A = Li, Na, K and X = Cl, Br. *Inorg. Chem.* **2001**, *40*, 3389–3394, DOI: 10.1021/ic0011056.

(16) Jaroschik, F.; Nief, F.; Le Goff, X.-F.; Ricard, L. Isolation of Stable Organodysprosium(II) Complexes by Chemical Reduction of Dysprosium(III) Precursors. *Organometallics* **2007**, *26*, 1123–1125, DOI: 10.1021/om0700213.

(17) Jaroschik, F.; Momin, A. A.; Nief, F.; Goff, X. Le; Deacon, G. B.; Junk, P. C.; Le Goff, X.-

F.; Deacon, G. B.; Junk, P. C. Dinitrogen Reduction and C-H Activation by the Divalent Organoneodymium Complex [$(C_5H_2{}^tBu_3)_2$Nd(μ-I)K([18]Crown-6)]. *Angew. Chem. Int. Ed.* **2009**, *48*, 1117–1121, DOI: 10.1002/anie.200804934.

(18) Mehdoui, T.; Berthet, J.-C.; Thuéry, P.; Salmon, L.; Rivière, E.; Ephritikhine, M. Lanthanide(III)/Actinide(III) Differentiation in the Cerium and Uranium Complexes $[M(C_5Me_5)_2(L)]^{0,+}$ (L = 2,2′-Bipyridine, 2,2′:6′,2″-Terpyridine): Structural, Magnetic, and Reactivity Studies. *Chem. Eur. J.* **2005**, *11*, 6994–7006, DOI: 10.1002/chem.200500479.

(19) Huh, D. N.; Roy, S.; Ziller, J. W.; Furche, F.; Evans, W. J. Isolation of a Square-Planar Th(III) Complex: Synthesis and Structure of $[Th(OC_6H_2{}^tBu_2\text{-}2,6\text{-}Me\text{-}4)_4]^{1-}$. *J. Am. Chem. Soc.* **2019**, *141*, 12458–12463, DOI: 10.1021/jacs.9b04399.

(20) Huh, D. N.; Ziller, J. W.; Evans, W. J. Chelate-Free Synthesis of the U(II) Complex, $[(C_5H_3(SiMe_3)_2)_3U]^{1-}$, Using Li and Cs Reductants and Comparative Studies of La(II) and Ce(II) Analogs. *Inorg. Chem.* **2018**, *57*, 11809–11814, DOI: 10.1021/acs.inorgchem.8b01966.

(21) Ayres, A. J.; Wooles, A. J.; Zegke, M.; Tuna, F.; Liddle, S. T. Preparation of Heterobimetallic Ketimido-Actinide-Molybdenum Complexes. *Inorg. Chem.* **2019**, *58*, 13077–13089, DOI: 10.1021/acs.inorgchem.9b01993.

(22) Fronczek, F. R.; Halstead, G. W.; Raymond, K. N. The Synthesis, Crystal Structure, and Reactions of an Actinide Metallocarborane Complex, Bis(η^5-(3)-1,2-Dicarbollyl)Dichlorouranium(IV) Dianion, $[U(C_2B_9H_{11})_2Cl_2]^{2-}$. *J. Am. Chem. Soc.* **1977**, *99*, 1769–1775, DOI: 10.1021/ja00448a015.

(23) Dulong, F.; Thuéry, P.; Ephritikhine, M.; Cantat, T. Synthesis of N -Aryloxy-β-Diketiminate Ligands and Coordination to Zirconium, Ytterbium, Thorium, and Uranium.

Organometallics **2013**, *32*, 1328–1340, DOI: 10.1021/om3010355.

(24) Boronski, J. T.; Doyle, L. R.; Seed, J. A.; Wooles, A. J.; Liddle, S. T. F-Element Half-Sandwich Complexes: A Tetrasilylcyclobutadienyl–Uranium(IV)–Tris(Tetrahydroborate) Anion Pianostool Complex. *Angew. Chem. Int. Ed.* **2020**, *59*, 295–299, DOI: 10.1002/anie.201913640.

(25) Wolford, N. J.; Sergentu, D. C.; Brennessel, W. W.; Autschbach, J.; Neidig, M. L. Homoleptic Aryl Complexes of Uranium(IV). *Angew. Chem. Int. Ed.* **2019**, *58*, 10266–10270, DOI: 10.1002/anie.201905423.

(26) Blake, P. C.; Lappert, M. F.; Taylor, R. G.; Atwood, J. L.; Hunter, W. E.; Zhang, H. A Complete Series of Uranocene(III) Halides [{UCp''_2X}$_n$] [X = F, Cl, Br, or I; Cp″ = η-$C_5H_3(SiMe_3)_2$]; Single-Crystal x-Ray Structure Determinations of the Chloride and Bromide (n = 2 for X^- = μ-Cl^- or μ-Br^-). *J. Chem. Soc. Chem. Commun.* **1986**, *357*, 1394–1395, DOI: 10.1039/C39860001394.

(27) Huang, Y.-L.; Lu, D.-Y.; Yu, H.-C.; Yu, J.-S. K.; Hsu, C.-W.; Kuo, T.-S.; Lee, G.-H.; Wang, Y.; Tsai, Y.-C. Stepwise Construction of the Cr-Cr Quintuple Bond and Its Destruction upon Axial Coordination. *Angew. Chem. Int. Ed.* **2012**, *51*, 7781–7785, DOI: 10.1002/anie.201202337.

(28) McNerney, B.; Whittlesey, B.; Krempner, C. Synthesis and Reactivity of New Pyrazolyl-Functionalized Potassium Silanides. *Eur. J. Inorg. Chem.* **2011**, *2011*, 1699–1702, DOI: 10.1002/ejic.201001291.

(29) Fässler, T. F.; Hoffmann, R.; Hoffmann, S.; Wörle, M. Triple-Decker Type Coordination of a Fullerene Trianion in [K([18]Crown-6)]$_3$[η^6, η^6-C_{60}](η^3-$C_6H_5CH_3$)$^{2-}$-Single Crystal Structure and Magnetic Properties. *Angew. Chem. Int. Ed.* **2000**, *39*, 2091–2094, DOI:

10.1002/1521-3773(20000616)39:12<2091::AID-ANIE2091>3.0.CO;2-8.

(30) McWilliams, S. F.; Bill, E.; Lukat-Rodgers, G.; Rodgers, K. R.; Mercado, B. Q.; Holland, P. L. Effects of N_2 Binding Mode on Iron-Based Functionalization of Dinitrogen to Form an Iron(III) Hydrazido Complex. *J. Am. Chem. Soc.* **2018**, *140*, 8586–8598, DOI: 10.1021/jacs.8b04828.

(31) Zitz, R.; Hlina, J.; Arp, H.; Kinschel, D.; Marschner, C.; Baumgartner, J. Group 4 Metal and Lanthanide Complexes in the Oxidation State +3 with Tris(Trimethylsilyl)Silyl Ligands. *Inorg. Chem.* **2019**, *58*, 7107–7117, DOI: 10.1021/acs.inorgchem.9b00866.

(32) Camp, C.; Pécaut, J.; Mazzanti, M. Tuning Uranium–Nitrogen Multiple Bond Formation with Ancillary Siloxide Ligands. *J. Am. Chem. Soc.* **2013**, *135*, 12101–12111, DOI: 10.1021/ja405815b.

(33) Niu, H.; Mangan, R. J.; Protchenko, A. V.; Phillips, N.; Unkrig, W.; Friedmann, C.; Kolychev, E. L.; Tirfoin, R.; Hicks, J.; Aldridge, S. Experimental and Quantum Chemical Studies of Anionic Analogues of N-Heterocyclic Carbenes. *Dalton Trans.* **2018**, *47*, 7445–7455, DOI: 10.1039/C8DT01661E.

(34) Hitchcock, P. B.; Lappert, M. F.; Protchenko, A. V. The First Crystalline Alkali Metal Salt of a Benzenoid Radical Anion without a Stabilizing Substituent and of a Related Dimer: X-Ray Structures of the Toluene Radical Anion and of the Benzene Radical Anion Dimer Potassium-Crown Ether Salts. *J. Am. Chem. Soc.* **2001**, *123*, 189–190, DOI: 10.1021/ja005580e.

(35) Fang, M.; Bates, J. E.; Lorenz, S. E.; Lee, D. S.; Rego, D. B.; Ziller, J. W.; Furche, F.; Evans, W. J. (N2)3− Radical Chemistry via Trivalent Lanthanide Salt/Alkali Metal Reduction of Dinitrogen: New Syntheses and Examples of $(N_2)^{2-}$ and $(N_2)^{3-}$ Complexes and

Density Functional Theory Comparisons of Closed Shell Sc^{3+}, Y^{3+}, and Lu^{3+} versus $4f^9$ Dy^{3+}. *Inorg. Chem.* **2011**, *50*, 1459–1469, DOI: 10.1021/ic102016k.

(36) Cassani, M. C.; Duncalf, D. J.; Lappert, M. F. The First Example of a Crystalline Subvalent Organolanthanum Complex: $[K([18]Crown\text{-}6)\text{-}(\eta^2\text{-}C_6H_6)_2][(LaCp^{tt}_2)_2(\mu\text{-}\eta^6\text{:}\eta^6\text{-}C_6H_6)]\bullet 2C_6H_6$ ($Cp^{tt} = \eta^5\text{-}C_5H_3Bu^t_2\text{-}1,3$). *J. Am. Chem. Soc.* **1998**, *120*, 12958–12959, DOI: 10.1021/ja980377t.

(37) Bienfait, A. M.; Wolf, B. M.; Törnroos, K. W.; Anwander, R. Donor-Solvent-Dependent Cluster Formation of $(C_5Me_5)SmI_2(THF)_x$-Type Half-Sandwich Complexes. *Organometallics* **2016**, *35*, 3743–3750, DOI: 10.1021/acs.organomet.6b00695.

(38) Evans, W. J.; Boyle, T. J.; Ziller, J. W. Reactivity of $Y_3(OR)_7Cl_2(THF)_2$ with Organoaluminum Reagents: Formation of the Yttrium-Aluminum Complexes $Y(OR)_3(AlMe_3)_3$, $Y(OR)_3(AlMe_3)_2(THF)$, and $Y(OR)_3(AlMe_2)Cl(THF)_2$ and the Halides $YCl_3(DME)_2$ and $YCl_3(THF)_3Y_3(OR)_7O$ ($R = CMe_3$). *J. Am. Chem. Soc.* **1993**, *115*, 5084–5092, DOI: 10.1021/ja00065a020.

(39) Evans, W. J.; Sollberger, M. S. Synthetic and Structural Studies on the Formation of a Tetradecametallic Yttrium Oxide Alkoxide Chloride Complex: An Example of How Molecular Yttrium Oxygen Frameworks Form Extended Arrays. *Inorg. Chem.* **1988**, *27*, 4417–4423, DOI: 10.1021/ic00297a017.

(40) Evans, W. J.; Sollberger, M. S.; Hanusa, T. P. Synthesis and Structure of the Polymetallic Yttrium Alkoxide Complex $Y_3(\mu^3\text{-}OCMe_3)(\mu^3\text{-}Cl)(\mu\text{-}OCMe_3)_3(OCMe_3)_4(THF)_2$ and Related Complexes: $Ln_3(\mu^3\text{-}OR)(\mu^3\text{-}X)(\mu\text{-}OR)_3$ Building Blocks in Yttrium and Lanthanide Alkoxide Chemistry1. *J. Am. Chem. Soc.* **1988**, *110*, 1841–1850, DOI: 10.1021/ja00214a029.

(41) Andersen, R. A.; Templeton, D. H.; Zalkin, A. Synthesis and Crystal Structure of a Neodymium Isopropoxide Chloride, $Nd_6[OCH(CH_3)_2]_{17}Cl$. *Inorg. Chem.* **1978**, *17*, 1962–1965, DOI: 10.1021/ic50185a053.

(42) Coucouvanis, D.; Lester, R. K.; Kanatzidis, M. G.; Kessisoglou, D. First Examples of Polynuclear, Sulfur-Containing, Zirconium Compounds. Synthesis and Structural Characterization of the Trinuclear Zr_3S_3(S-tert-Bu)$_2(BH_4)_4(THF)_2$ and the Hexanuclear Zr_6S_6(S-tert-Bu)$_4(BH_4)_8(THF)_2$ Clusters. *J. Am. Chem. Soc.* **1985**, *107*, 8279–8280, DOI: 10.1021/ja00312a087.

(43) Coucouvanis, D.; Hadjikyriacou, A.; Kanatzidis, M. G. The Synthesis and Structural Characterization of $Zr_3(S)(Bu^tS)_{10}$. A Zr–S Cluster That Contains Thiolate Ligands in Three Different Modes of Co-Ordination. *J. Chem. Soc. Chem. Commun.* **1985**, *3*, 1224–1225, DOI: 10.1039/C39850001224.

(44) Graves, C. R.; Scott, B. L.; Morris, D. E.; Kiplinger, J. L. Tetravalent and Pentavalent Uranium Acetylide Complexes Prepared by Oxidative Functionalization with CuC≡CPh. *Organometallics* **2008**, *27*, 3335–3337, DOI: 10.1021/om800466m.

(45) Rungthanaphatsophon, P.; Barnes, C. L.; Kelley, S. P.; Walensky, J. R. Four-Electron Reduction Chemistry Using a Uranium(III) Phosphido Complex. *Dalton Trans.* **2018**, *47*, 8189–8192, DOI: 10.1039/C8DT01406J.

(46) Mehdoui, T.; Berthet, J.-C.; Thuéry, P.; Ephritikhine, M. The Remarkable Efficiency of N-Heterocyclic Carbenes in Lanthanide(III)/Actinide(III) Differentiation. *Chem. Commun.* **2005**, *80*, 2860, DOI: 10.1039/b503526k.

(47) Boisson, C.; Berthet, J. C.; Ephritikhine, M.; Lance, M.; Nierlich, M. Synthesis and Crystal Structure of $[U(\eta\text{-}C_5Me_5)_2(OC_4H_8)_2][BPh_4]$, the First Cationic Cyclopentadienyl

Compound of Uranium(III). *J. Organomet. Chem.* **1997**, *533*, 7–11, DOI: 10.1016/S0022-328X(96)06807-6.

(48) Arliguie, T.; Lescop, C.; Ventelon, L.; Leverd, P. C.; Thuéry, P.; Nierlich, M.; Ephritikhine, M. C−H and C−S Bond Cleavage in Uranium(III) Thiolato Complexes. *Organometallics* **2001**, *20*, 3698–3703, DOI: 10.1021/om0102551.

(49) Lukens, W. W.; Beshouri, S. M.; Blosch, L. L.; L., S. A.; Andersen, R. A. Preparation, Solution Behavior, and Solid-State Structures of $(1,3\text{-}R_2C_5H_3)_2UX_2$, Where R is CMe_3 or $SiMe_3$ and X is a One-Electron Ligand. *Organometallics* **1999**, *18*, 1235–1246, DOI: 10.1021/om9805988.

(50) Jantunen, K. C.; Burns, C. J.; Castro-Rodriguez, I.; Da Re, R. E.; Golden, J. T.; Morris, D. E.; Scott, B. L.; Taw, F. L.; Kiplinger, J. L. Thorium(IV) and Uranium(IV) Ketimide Complexes Prepared by Nitrile Insertion into Actinide-Alkyl and -Aryl Bonds. *Organometallics* **2004**, *23*, 4682–4692, DOI: 10.1021/om0343824.

(51) Blake, P. C.; Hey, E.; Lappert, M. F.; Atwood, J. L.; Zhang, H. Bis(Trimethylsilyl)Phosphido Complexes II. Bis(Trimethylsilyl)Phosphidobis(Tetrahydrofuran) Lithium as a Reducing Agent; X-Ray Structure of $[UCp''_2(\mu\text{-}Cl)_2Li(THF)_2]$ [Cp″ = $\eta\text{-}C_5H_3(SiMe_3)_2$-1, 3; THF = OC_4H_8]. *J. Organomet. Chem.* **1988**, *353*, 307–314.

(52) Zalkin, A.; Beshouri, S. M. Di-μ-oxo-bis{bis[Bis(Trimethylsilyl)Cyclopentadienyl]Uranium(IV)}. *Acta Crystallogr. Sect. C* **1988**, *44*, 1826–1827, DOI: 10.1107/S0108270188006419.

(53) Shannon, R. D. Revised Effective Ionic Radii and Systematic Studies of Interatomic Distances in Halides and Chalcogenides. *Acta Crystallogr. Sect. A* **1976**, *32*, 751–767, DOI:

10.1107/S0567739476001551.

(54) Addison, A. W.; Rao, T. N.; Reedijk, J.; van Rijn, J.; Verschoor, G. C. Synthesis, Structure, and Spectroscopic Properties of Copper(II) Compounds Containing Nitrogen–Sulphur Donor Ligands; the Crystal and Molecular Structure of Aqua[1,7-Bis(N-Methylbenzimidazol-2′-yl)-2,6-Dithiaheptane]Copper(II) Perchlorate. *J. Chem. Soc.. Dalton Trans.* **1984**, No. 7, 1349–1356, DOI: 10.1039/DT9840001349.

(55) MacDonald, M. R.; Bates, J. E.; Ziller, J. W.; Furche, F.; Evans, W. J. Completing the Series of +2 Ions for the Lanthanide Elements: Synthesis of Molecular Complexes of Pr^{2+}, Gd^{2+}, Tb^{2+}, and Lu^{2+}. *J. Am. Chem. Soc.* **2013**, *135*, 9857–9868, DOI: 10.1021/ja403753j.

(56) MacDonald, M. R.; Fieser, M. E.; Bates, J. E.; Ziller, J. W.; Furche, F.; Evans, W. J. Identification of the +2 Oxidation State for Uranium in a Crystalline Molecular Complex, [K(2.2.2-Cryptand)][$(C_5H_4SiMe_3)_3U$]. *J. Am. Chem. Soc.* **2013**, *135*, 13310–13313, DOI: 10.1021/ja406791t.

(57) Jenkins, T. F.; Woen, D. H.; Mohanam, L. N.; Ziller, J. W.; Furche, F.; Evans, W. J. Tetramethylcyclopentadienyl Ligands Allow Isolation of Ln(II) Ions across the Lanthanide Series in [K(2.2.2-Cryptand)][$(C_5Me_4H)_3Ln$] Complexes. *Organometallics* **2018**, *37*, 3863–3873, DOI: 10.1021/acs.organomet.8b00557.

(58) Evans, W. J.; Nyce, G. W.; Forrestal, K. J.; Ziller, J. W. Multiple Syntheses of $(C_5Me_5)_3U$. *Organometallics* **2002**, *21*, 1050–1055, DOI: 10.1021/om010831t.

(59) Evans, W. J.; Davis, B. L. Chemistry of Tris (Pentamethylcyclopentadienyl) f-Element Complexes, $(C_5Me_5)_3M$. *Chem. Rev.* **2002**, *102*, 2119–2136, DOI: 10.1021/cr010298r.

(60) Carmichael, C. D.; Jones, N. A.; Arnold, P. L. Low-Valent Uranium Iodides: Straightforward Solution Syntheses of UI_3 and UI_4 Etherates. *Inorg. Chem.* **2008**, *47*, 8577–

8579, DOI: 10.1021/ic801138e.

(61) Peterson, J. K.; MacDonald, M. R.; Ziller, J. W.; Evans, W. J. Synthetic Aspects of $(C_5H_4SiMe_3)_3Ln$ Rare-Earth Chemistry: Formation of $(C_5H_4SiMe_3)_3Lu$ via $[(C_5H_4SiMe_3)_2Ln]^+$ Metallocene Precursors. *Organometallics* **2013**, *32*, 2625–2631, DOI: 10.1021/om400116d.

(62) Davidson, P. J.; Harris, D. H.; Lappert, M. F. Subvalent Group 4B Metal Alkyls and Amides. Part I. The Synthesis and Physical Properties of Kinetically Stable Bis[Bis(Trimethysilyl)Methyl]- Germanium(II), -Tin(II), and -Lead(II). *J. Chem. Soc. Dalton*

Trans. **1976**, *21*, 2268–2274, DOI: 10.1039/DT9760002268.

(63) Langeslay, R. R.; Fieser, M. E.; Ziller, J. W.; Furche, F.; Evans, W. J. Synthesis, Structure, and Reactivity of Crystalline Molecular Complexes of the $\{[C_5H_3(SiMe_3)_2]_3Th\}^{1-}$ Anion Containing Thorium in the Formal +2 Oxidation State. *Chem. Sci.* **2015**, *6*, 517–521, DOI: 10.1039/C4SC03033H.

(64) Mansell, S. M.; Kaltsoyannis, N.; Arnold, P. L. Small Molecule Activation by Uranium Tris(Aryloxides): Experimental and Computational Studies of Binding of N_2, Coupling of CO, and Deoxygenation Insertion of CO_2 under Ambient Conditions. *J. Am. Chem. Soc.* **2011**, *133*, 9036–9051, DOI: 10.1021/ja2019492.

(65) Hitchcock, P. B.; Lappert, M. F.; Maron, L.; Protchenko, A. V. Lanthanum Does Form Stable Molecular Compounds in the +2 Oxidation State. *Angew. Chem. Int. Ed.* **2008**, *47*, 1488–1491, DOI: 10.1002/anie.200704887.

(66) Gabbai, F. P.; Chirik, P. J.; Fogg, D. E.; Meyer, K.; Mindiola, D. J.; Schafer, L. L.; You, S.-L. An Editorial About Elemental Analysis. *Organometallics* **2016**, *35*, 3255–3256, DOI:

10.1021/acs.organomet.6b00720.

(67) APEX2 Version 2014.11-0, Bruker AXS, Inc.; Madison, WI 2014.

(68) Sheldrick, G. M. CELL_NOW, Version 2008/4, Bruker AXS, Inc.; Madison, WI 2008.

(69) SAINT Version 8.34a, Bruker AXS, Inc.; Madison, WI 2013.

(70) Sheldrick, G. M. TWINABS, Version 2012/1, Bruker AXS, Inc.; Madison, WI 2012.

(71) Sheldrick, G. M. SHELXTL, Version 2014/7, Bruker AXS, Inc.; Madison, WI 2014.

(72) International Tables for Crystallography 1992, Vol. C., Dordrecht: Kluwer Academic Publishers.

(73) Sheldrick, G. M. SADABS, Version 2014/5, Bruker AXS, Inc.; Madison, WI 2014.

Chapter 9:

Exploring the Use of the Pentaphenylcyclopentadienyl Ligand in Uranium Chemistry: The Crystal Structure of $(C_5Ph_5)UI_2(THF)_2$

Introduction[†]

The largest cyclopentadienyl ligand described in previous Chapters has been the C_5Me_5 ligand, which is ubiquitous in actinide chemistry as it is sterically demanding enough to stabilize a variety of complexes across many oxidation states.[1–6] The larger, penta-substituted ligand, $C_5{}^iPr_5$, has been shown to form the uranium complex $(C_5{}^iPr_5)_2U$, but the use of even larger penta-aryl ligands in actinide chemistry has been limited. There are no uranium examples and only two related $C_5(C_6H_3{}^tBu_2)_5$ thorium complexes[7] are in the literature.

The pentaphenylcyclopentadienyl ligand has been found to form linear complexes of Ca, Ba, Sm, Eu, and Yb.[8–10] As shown in Scheme 9.1, the Deacon group has used the redox-transmetallation/protonolyis (RTP) reaction protocol to make C_5Ph_5 complexes of these metals.[8,9] In some cases, solvent-separated ion pairs (SSIPs) $[M'(THF)_6][C_5Ph_5]_2$ (M′ = Ca, Ba, Yb)[8,9] and $[Yb(diglyme)_3][C_5Ph_5]_2$[10] could be isolated and crystallographically characterized. Reported in this Chapter are synthetic efforts to generate C_5Ph_5 complexes of uranium via conventional ionic metathesis to examine their reduction chemistry[11–16] and the X-ray crystal structures of one uranium complex and two alkali metal complexes that were obtained.

[†] Portions of this Chapter have been published: Wedal, J. C.; Ziller, J. W.; Evans, W. J. Exploring the Use of the Pentaphenylcyclopentadienyl Ligand in Uranium Chemistry: The Crystal Structure of $(C_5Ph_5)UI_2(THF)_2$. *Aust. J. Chem.* **2022**. DOI: 10.1071/CH21318.

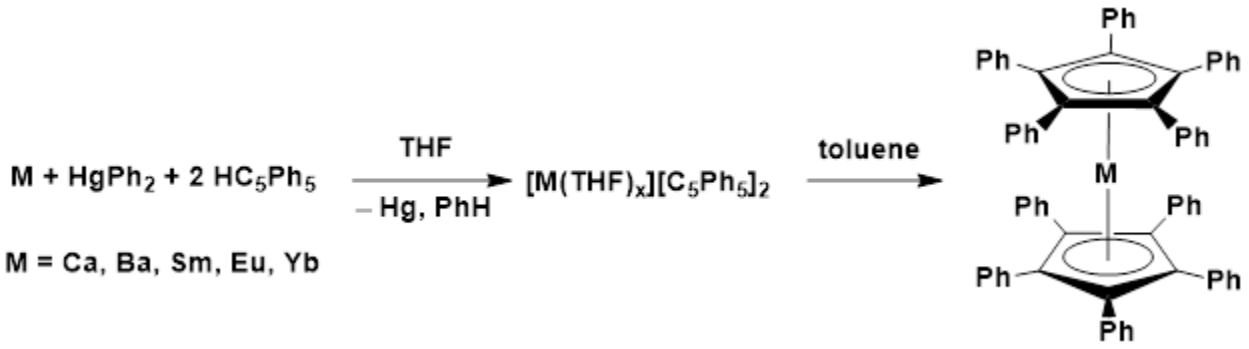

Scheme 9.1: Synthesis of (η^5-$C_5Ph_5)_2M$ via RTP.[8,9]

Results

UI_3 / NaC_5Ph_5 Reactions. Reaction of UI_3 with one equivalent of NaC_5Ph_5 in THF resulted in a deep purple solution. Extraction into toluene and crystallization from THF/hexane resulted in dark purple/brown crystals. The ^{1}H NMR spectra in C_6D_6 and in THF-d_8 displayed multiple broadened resonances due to the paramagnetic U(III) center such that definitive assignments were not possible. However, the crystals could be analyzed by X-ray crystallography and were identified as the four-legged piano stool compound (η^5-$C_5Ph_5)UI_2(THF)_2$, **9.1**, Figure 9.1, which was isolated in 63% yield, eq 9.1.

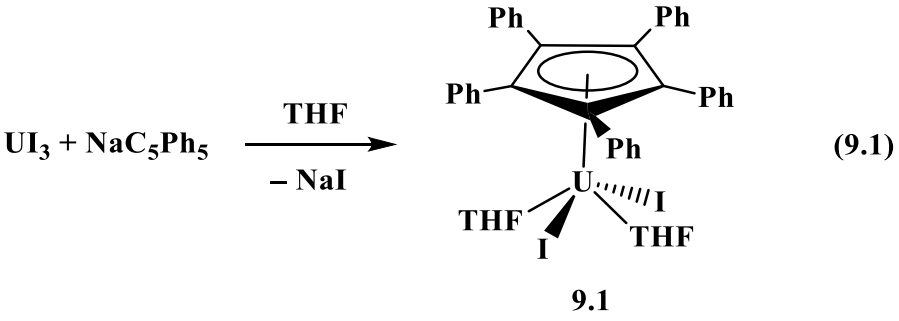

(9.1)

9.1

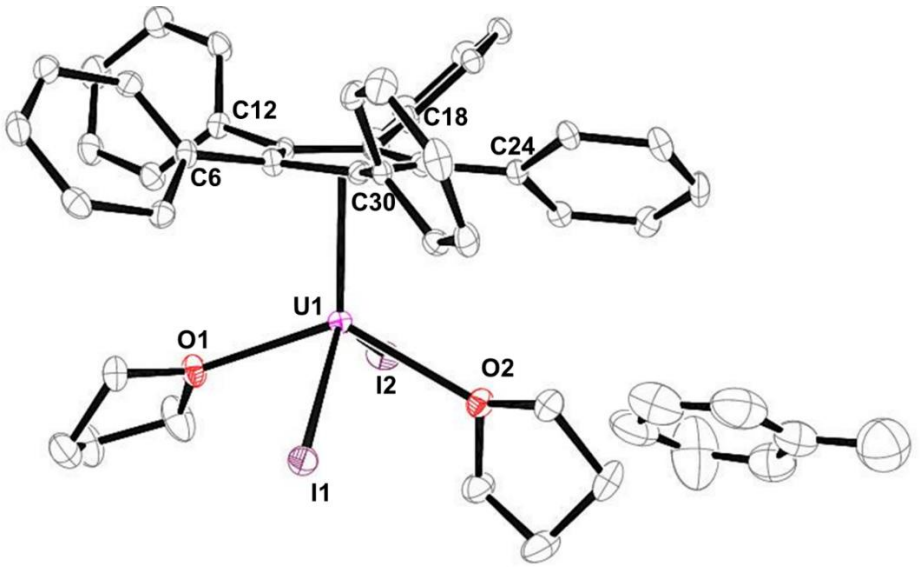

Figure 9.1: Molecular structure of (η^5-C_5Ph_5)$UI_2(THF)_2$·(C_7H_8), **9.1·(C_7H_8)**, with ellipsoids drawn at the 50% probability level and selective atom labelling. Hydrogen atoms have been omitted for clarity.

(η^5-C_5Ph_5)$UI_2(THF)_2$, **9.1**, crystallizes in the $P\bar{1}$ space group with a molecule of toluene. The five phenyl substituents are canted into a propeller shape to minimize the steric interactions. The *ipso*-carbon atoms of the phenyl substituents are bent up out of the C_5 plane, away from the uranium atom, as is typical for penta-substituted cyclopentadienyl f element complexes.[17] The five displacements from the plane, 0.315, 0.039, 0.254, 0.198, and 0.181 Å, for C6, C12, C18, C24, and C30, respectively, do not have a regular pattern. The 2.539 Å U–centroid distance is slightly larger than the 2.504 Å distance in (η^5-C_5Me_5)$UI_2(THF)_3$[18] and the 2.506 Å distance in (η^5-$C_5H_4CMe_2Ph$)$UI_2(THF)_3$,[19] even though the latter two complexes have larger formal coordination numbers. However, the 3.0644(3) Å and 3.1231(3) Å U–iodide distances in **9.1** are shorter than the 3.162 Å and 3.168 Å distances in (η^5-C_5Me_5)$UI_2(THF)_3$, which is consistent with the coordination number difference. The 2.492(3) Å and 2.524(3) Å U–O distances in **9.1** overlap with the range of U–O distances in (η^5-C_5Me_5)$UI_2(THF)_3$: 2.507, 2.533, and 2.569 Å (see Chapter

8). The two pairs of legs in the piano stool complex are arranged in a transoid fashion, but the angles to the cyclopentadienyl ring are not symmetrical: the centroid–U–O angles of **9.1** are 110.7° and 117.4° while the centroid–U–I angles are 109.0° and 121.9°. The O–U–I angles are 74.54(7)°, 78.80(7)°, 79.97(7)° and 86.92(7)°.

Given the facile synthesis of **9.1**, the extension of this chemistry to the synthesis of (η^5-$C_5Ph_5)_2UI$ from two equivalents of NaC_5Ph_5 and UI_3 was attempted. However, this stoichiometry gave complex mixtures of products and no new crystallographically characterizable uranium products. Addition of Lewis bases such as Ph_3PO, pyridine, or *N*,*N*,*N*-trimethyl-1,3,5-triazacyclohexane[20] to potentially increase crystallinity did not aid in product identification. Upon further reaction with $KN(SiMe_3)_2$, white solid precipitated but no uranium-containing products could be identified. In one instance, colorless crystals of [$Na(THF)_3$][η^5-C_5Ph_5], **9.2**, were isolated, Figure 9.2. The structure is discussed below.

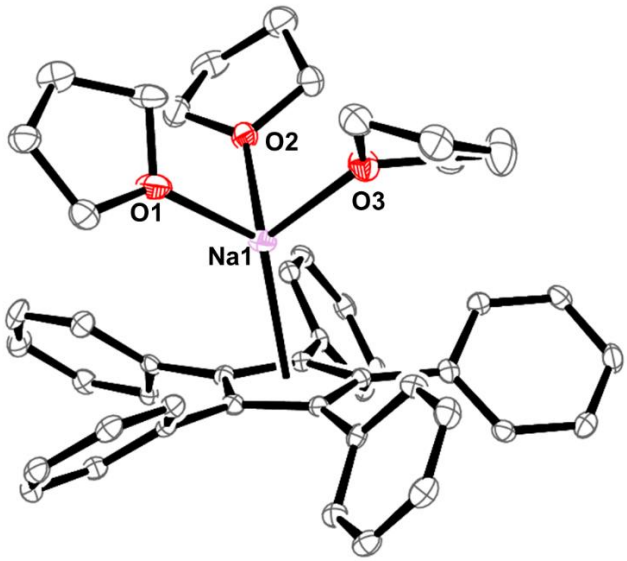

Figure 9.2: Molecular structure of [$Na(THF)_3$][η^5-C_5Ph_5], **9.2**, with ellipsoids drawn at the 50% probability level with selective atom labelling. Hydrogen atoms have been omitted for clarity.

Reduction Reactions. Following the recent studies of reduction of U(III) complexes,[11–16] treatment of the UI_3 / 2 NaC_5Ph_5 product with KC_8 and 18-crown-6 or 2.2.2-cryptand was examined. In both cases, the KC_8 reacts, as evidenced by a color change from bronze to black, but no further evidence for U(II) products could be obtained. Attempts were also made to examine reduction of lanthanide analogs generated *in situ* from LnI_3 and two equivalents of NaC_5Ph_5. When Ln = Nd, the only product that could be definitively characterized was the SSIP[1,2] [K(18-crown-6)$(THF)_2$][C_5Ph_5]. Dark purple crystals of [K(18-crown-6)$(THF)_2$][C_5Ph_5], **9.3**, were grown from THF/hexane and identified by X-ray crystallography, Figure 3.

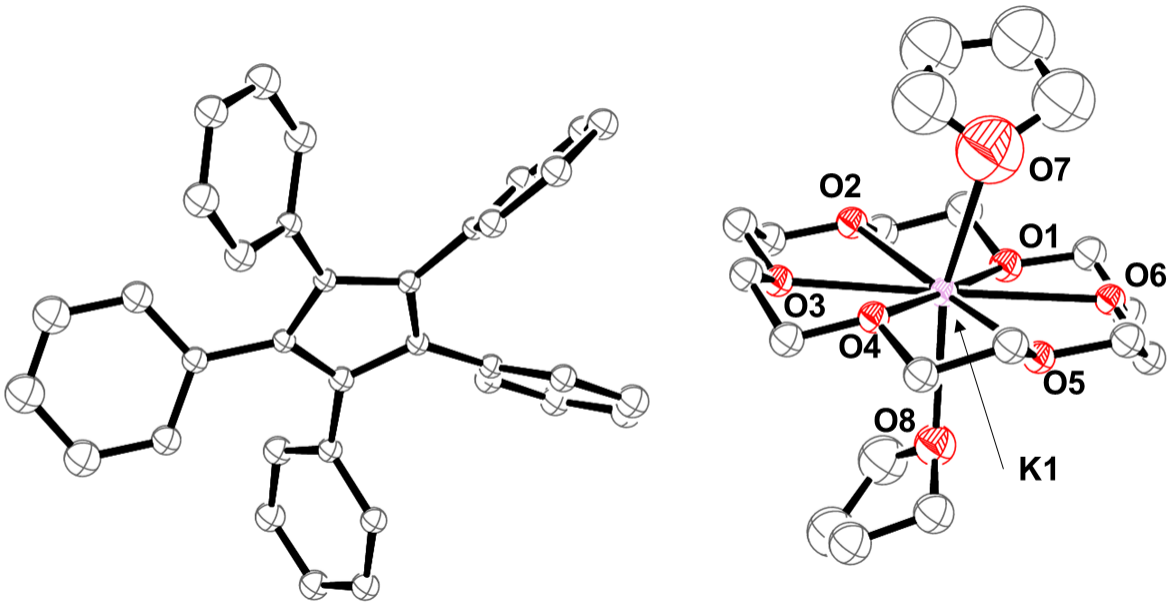

Figure 9.3: Molecular structure of [K(18-crown-6)$(THF)_2$][C_5Ph_5], **9.3**, with ellipsoids drawn at the 50% probability level. Hydrogen atoms have been omitted for clarity.

X-ray Crystal Structures of 9.2 and 9.3. The crystal structures of [Na$(THF)_3$][η^5-C_5Ph_5], **9.2**, and [K(18-crown-6)$(THF)_2$][C_5Ph_5], **9.3**, are the first X-ray crystal structures of alkali metal salts of the pentaphenylcyclopentadienyl ligand without substituted aryl rings. The crystal structures of the Li, K, and Cs salts of M[η^5-$C_5(C_6H_4R)_5$] complexes where R = n-Bu, t-Bu, or i-

Pr,[21,22] and of the Li salt, Li[η^5-$C_5(C_6H_3R_2)_5$] where R = Me and t-Bu,[23] have been reported, but complex **2** is the first Na salt of a [η^5-C_5Ar_5]$^{1-}$ complex of any kind. There are many more examples of crystal structures of these penta-aryl cyclopentadienides with alkaline earth metals, Ae(η^5-C_5Ar_5)$_2$ (Ar = Ph, substituted aryl; Ae = Mg, Ca, Sr, Ba)[8–10,21,22,24,25] and Ba(η^5-C_5Ph_5)$_2$,[9] as well as SSIPs [M′(THF)$_6$][C_5Ph_5]$_2$ (M′ = Ca, Ba, Yb)[8,9] and [Yb(diglyme)$_3$][C_5Ph_5]$_2$.[10]

The metrical parameters in the [C_5Ph_5]$^{1-}$ anions in **9.2** and **9.3** are not unusual, but the displacements of the *ipso*-C atoms from the C5 plane are smaller than those in **9.1**. The *ipso*-C atoms in **9.2** are above the C5 plane, *toward* the Na atom, by 0.014, 0.017, 0.037, 0.061, and 0.129 Å. In the SSIP complex **9.3,** the displacements out of the plane are 0.003, 0.014, 0.018, 0.052, and 0.181 Å.

The 2.563 Å Na–(C_5Ph_5 centroid) distance in **9.2** is slightly longer than the 2.539 Å U–(C_5Ph_5 centroid) distance in **9.1**, even though the U atom in **9.1** is eight-coordinate while the Na atom in **9.2** is six-coordinate. The 1.02 Å six-coordinate ionic radius for Na^{1+} is very close to that of U^{3+}, 1.025 Å.[26] The Na atom is slightly off-center of the C5 ring centroid in **9.2**: the (O3 centroid)–Na–(C5 centroid) angle is 172.47°. There are no supramolecular features in **9.1**-**9.3**.

Discussion

In this Chapter, the synthesis of a mono-cyclopentadienyl uranium C_5Ph_5 complex could be achieved using the conventional ionic metathesis reaction of UI_3 and one equivalent of the cyclopentadienyl salt, NaC_5Ph_5. (η^5-C_5Ph_5)UI_2(THF)$_2$, **9.1**, was isolated in 63% yield and could be structurally characterized by X-ray crystallography. This is the first crystal structure of a C_5Ph_5-ligated uranium compound. However, attempts to introduce two pentaphenylcyclopentadienyl ligands to the metal center via salt metathesis were unsuccessful, in contrast to the RTP method

applicable to Ca, Ba, Sm, Eu, and Yb, Scheme 9.1. Only the alkali metal starting material, $[Na(THF)_3][\eta^5\text{-}C_5Ph_5]$, **9.2**, could be definitively identified.

Attempts to isolate a U(II) complex of C_5Ph_5 by reduction of UI_3 / NaC_5Ph_5 were unsuccessful, but a KC_8 reduction with an analogous NdI_3 / NaC_5Ph_5 system gave a new SSIP, namely, $[K(18\text{-crown-6})(THF)_2][C_5Ph_5]$, **9.3**. The $[C_5Ph_5]^{1-}$ ligand clearly differs from other $(C_5R_5)^{1-}$ ligands in its propensity to crystallize on its own.

Conclusion

UI_3 reacts with NaC_5Ph_5 in THF to form a mono(cyclopentadienyl) complex, $(\eta^5\text{-}C_5Ph_5)UI_2(THF)_2$, in good yield, but efforts to use ionic metathesis to make bis(cyclopentadienyl) complexes were unsuccessful. The $(C_5Ph_5)^{1-}$ ligand readily forms a crystalline mono-cyclopentadienyl complex with sodium, $[Na(THF)_3][\eta^5\text{-}C_5Ph_5]$, but in the presence of potassium and 18-crown-6, a solvent-separated ion pair, $[K(18\text{-crown-6})(THF)_2][C_5Ph_5]$, is isolated.

Experimental Methods

All syntheses and manipulations were conducted under an Ar atmosphere with rigorous exclusion of air and water using standard vacuum line and glovebox techniques. Solvents were sparged with UHP argon and dried by passage through columns containing a copper-based oxygen scavenger and alumina prior to use. Deuterated NMR solvent were dried over NaK alloy, degassed by three freeze-pump-thaw cycles, and vacuum transferred prior to use. Infrared spectra were collected as compressed solids on an Agilent Cary 630 ATR-FTIR. Elemental analyses were conducted on a PerkinElmer 2400 Series II CHNS elemental analyzer. HC_5Ph_5 (Sigma) was dried at 80 °C at 10^{-5} Torr prior to use. 18-Crown-6 (Alfa) was sublimed prior to use. NaH was purchased covered in oil. The oil was removed by washing with copious amounts of hexane and

toluene over a frit, and the NaH was dried under vacuum to yield a free-flowing grey powder. $NdI_3(THF)_{3.5}$,[27] KC_8[28] and UI_3[29] were synthesized following literature routes.

Synthesis of NaC_5Ph_5. This is an alternative route to that previously reported.[30] Inside the glovebox, HC_5Ph_5 (3.40 g, 7.6 mmol) and NaH (0.220 g, 9.2 mmol) were added to a Schlenk flask equipped with a greaseless Teflon stopcock and stir bar. THF (50 mL) was added and the flask was brought out of the glovebox and attached to the Schlenk line. The pale yellow solution was stirred under a positive flow of Ar and gas evolution was observed. After stirring overnight, the solution had turned red. Volatiles were removed under vacuum and the flask was brought into the glovebox. THF (50 mL) was added and grey solids were removed via centrifugation. The deep yellow/orange supernatant was dried to yield off-white solids of NaC_5Ph_5 (3.025 g, 85%).

Synthesis of $(C_5Ph_5)UI_2(THF)_2$, 9.1. Inside the glovebox, UI_3 (72 mg, 0.12 mmol) was dissolved in THF (5 mL) to form a deep blue solution. NaC_5Ph_5 (55 mg, 0.12 mmol) was dissolved in THF (5 mL) and added slowly to the stirred solution of UI_3. The resulting deep-purple solution was stirred overnight. Grey solids (presumably NaI) were removed via centrifugation and the supernatant was filtered and dried. The product was extracted into toluene (10 mL) and black solids were removed via centrifugation. The resulting purple supernatant was dried under vacuum to yield dark purple/brown solids. The solids were redissolved in THF (5 mL) and dried to yield dark purple, almost black solids of $(C_5Ph_5)UI_2(THF)_2$, **9.1** (79 mg, 63%). X-ray quality crystals were grown by layering a concentrated THF solution of $(C_5Ph_5)UI_2(THF)_2$ under hexane at −35 °C. Due to the paramagnetism of the U(III) center, the ^{1}H NMR spectra could not be confidently assigned. IR: 3023m, 2966m, 2875m, 1597m, 1486m, 1441m, 1329w, 1275w, 1156w, 1069m, 1027m, 908m, 834m, 768s, 693s cm^{-1}. Anal. Calcd for $C_{43}H_{41}O_2I_2U$: C, 47.75; H, 3.82. Found: C, 47.15; H, 4.22.

Crystallization of [Na(THF)$_3$][C$_5$Ph$_5$], 9.2. Colorless X-ray quality crystals of [Na(THF)$_3$][C$_5$Ph$_5$] were grown by layering a concentrated THF solution of NaC$_5$Ph$_5$ under hexane at −35 °C. Crystals of **9.2** were also isolated from the reaction of UI$_3$ with two equivalents of NaC$_5$Ph$_5$.

Crystallization of [K(18-crown-6)(THF)$_2$][C$_5$Ph$_5$], 9.3. NdI$_3$ (100 mg, 0.128 mmol) and NaC$_5$Ph$_5$ (121 mg, 0.257 mmol) were stirred in THF overnight, then dried and extracted into toluene. Removal of solvent afforded pale green solids (43 mg). These solids were dissolved in THF along with 18-crown-6 (10 mg, 0.037 mmol), followed by KC$_8$ (12 mg, 0.089 mmol), causing a color change from pale green to purple. Purple X-ray quality crystals of [K(18-crown-6)(THF)$_2$][C$_5$Ph$_5$], **9.3**, were grown from a THF solution layered under hexane at −35 °C.

Crystallography Data.

Table 9.1: X-ray diffraction data for **9.1-9.3**. Data was collected with Mo Kα radiation (0.71073 Å) with a graphite monochromator

	9.1	**9.2**	**9.3**
Internal identifier	jcw25	jcw26	jcw41
Formula	$C_{50}H_{49}I_2O_2U$	$C_{47}H_{49}O_3Na$	$C_{55}H_{65}O_8K$
Formula weight (g/mol)	1173.72	684.85	893.17
Temperature (K)	88(2)	93(2)	133(2)
Crystal system	Triclinic	Orthorhombic	Monoclinic
Space group	$P\bar{1}$	$P2_12_12_1$	$P2_1/n$
Crystal color	Brown	Colorless	Purple
Crystal size (mm^3)	0.138 x 0.214 x 0.532	0.146 x 0.178 x 0.359	0.260 x 0.274 x 0.291
a (Å)	10.8115(7)	9.0566(8)	13.7325(14)
b (Å)	11.5194(7)	19.3468(16)	17.7160(18)
c (Å)	19.1426(12)	21.5360(18)	21.728(2)
α (°)	77.1972(9)	90.0	90.0
β (°)	80.5665(9)	90.0	105.802(2)
γ (°)	71.1332(9)	90.0	90.0
V (Å^3)	2188.9(2)	3773.5(6)	5086.4(9)
Z	2	4	4
ρ_{calcd} (mg/m^3)	1.781	1.205	1.166
μ (mm^{-1})	5.156	0.083	0.156

R1 [$I > 2\sigma$(l)][a]	0.0352	0.0495	0.0701
wR2	0.0839	0.1110	0.2038
Goodness-of-fit on F^2	1.044	1.027	1.039
Range of transmission factors	0.2532–0.4330	0.7833–0.8621	0.6847–0.7454
2θ range (°)	1.899–29.130	1.415–28.311	1.507–25.350
Independent reflections measured	11742	9383	9041
Reflections included refinement	11742	9383	9041

a: $R = \sum|F_o|-|F_c||/\sum F_o|$; $wR2 = \{\sum[w(F_o^2-F_c^2)^2]/\sum[w(F_o^2)^2]\}^{1/2}$

X-ray Data Collection, Structure Solution and Refinement for 9.1.

A brown crystal of approximate dimensions 0.138 x 0.214 x 0.532 mm was mounted in a cryoloop and transferred to a Bruker SMART APEX II diffractometer. The APEX2[1] program package was used to determine the unit-cell parameters. Data was collected using a 15 sec/frame scan. The raw frame data was processed using SAINT[2] and SADABS[3] to yield the reflection data file. Subsequent calculations were carried out using the SHELXTL[4] program. There were no systematic absences nor any diffraction symmetry other than the Friedel condition. The centrosymmetric triclinic space group $P\bar{1}$ was assigned and later determined to be correct.

The structure was solved by dual space methods and refined on F^2 by full-matrix least-squares techniques. The analytical scattering factors[5] for neutral atoms were used throughout the analysis. Hydrogen atoms were included using a riding model. There was one molecule of toluene solvent present.

Least-squares analysis yielded wR2 = 0.0839 and Goof = 1.044 for 492 variables refined against 11742 data (0.73 Å), R1 = 0.0352 for those 9981 data with $I > 2.0\sigma(I)$.

Table 9.2: Bond lengths [Å] and angles [°] for **9.1**.

U(1)-Cnt1	2.539	C(15)-C(16)	1.387(6)
U(1)-O(1)	2.492(3)	C(16)-C(17)	1.377(6)
U(1)-O(2)	2.524(3)	C(18)-C(19)	1.393(5)
U(1)-C(3)	2.744(4)	C(18)-C(23)	1.399(6)
U(1)-C(2)	2.771(4)	C(19)-C(20)	1.392(5)
U(1)-C(4)	2.816(4)	C(20)-C(21)	1.390(6)
U(1)-C(5)	2.875(4)	C(21)-C(22)	1.381(6)
U(1)-C(1)	2.883(4)	C(22)-C(23)	1.388(6)
U(1)-I(2)	3.0644(3)	C(24)-C(25)	1.388(6)
U(1)-I(1)	3.1231(3)	C(24)-C(29)	1.400(6)
O(1)-C(39)	1.456(5)	C(25)-C(26)	1.391(6)
O(1)-C(36)	1.471(5)	C(26)-C(27)	1.388(6)
O(2)-C(43)	1.461(5)	C(27)-C(28)	1.384(6)
O(2)-C(40)	1.477(5)	C(28)-C(29)	1.397(6)
C(1)-C(5)	1.431(5)	C(30)-C(35)	1.391(6)
C(1)-C(2)	1.446(5)	C(30)-C(31)	1.398(6)
C(1)-C(6)	1.480(5)	C(31)-C(32)	1.379(6)
C(2)-C(3)	1.437(5)	C(32)-C(33)	1.385(7)
C(2)-C(12)	1.485(5)	C(33)-C(34)	1.383(7)
C(3)-C(4)	1.440(5)	C(34)-C(35)	1.400(6)
C(3)-C(18)	1.485(5)	C(36)-C(37)	1.515(6)
C(4)-C(5)	1.429(5)	C(37)-C(38)	1.501(7)
C(4)-C(24)	1.483(5)	C(38)-C(39)	1.520(7)
C(5)-C(30)	1.487(5)	C(40)-C(41)	1.514(7)
C(6)-C(7)	1.397(5)	C(41)-C(42)	1.531(7)
C(6)-C(11)	1.406(5)	C(42)-C(43)	1.500(6)
C(7)-C(8)	1.391(6)	C(44)-C(45)	1.291(10)
C(8)-C(9)	1.393(6)	C(44)-C(49)	1.341(11)
C(9)-C(10)	1.386(6)	C(44)-C(50)	1.498(11)
C(10)-C(11)	1.382(6)	C(45)-C(46)	1.419(11)
C(12)-C(13)	1.402(6)	C(46)-C(47)	1.324(11)
C(12)-C(17)	1.411(5)	C(47)-C(48)	1.457(11)
C(13)-C(14)	1.383(6)	C(48)-C(49)	1.418(11)
C(14)-C(15)	1.387(6)		

Cnt1-U(1)-I(1)	121.9	C(4)-U(1)-I(1)	103.45(8)
Cnt1-U(1)-I(2)	109.0	C(5)-U(1)-I(1)	131.36(8)
Cnt1-U(1)-O(1)	110.7	C(1)-U(1)-I(1)	146.14(8)
Cnt1-U(1)-O(2)	117.4	I(2)-U(1)-I(1)	129.011(9)
O(1)-U(1)-O(2)	131.83(10)	C(39)-O(1)-C(36)	108.4(3)
O(1)-U(1)-C(3)	118.56(11)	C(39)-O(1)-U(1)	123.8(3)
O(2)-U(1)-C(3)	104.15(11)	C(36)-O(1)-U(1)	126.3(2)
O(1)-U(1)-C(2)	136.78(11)	C(43)-O(2)-C(40)	108.1(3)
O(2)-U(1)-C(2)	91.40(11)	C(43)-O(2)-U(1)	131.9(2)
C(3)-U(1)-C(2)	30.21(11)	C(40)-O(2)-U(1)	113.7(2)
O(1)-U(1)-C(4)	90.62(11)	C(5)-C(1)-C(2)	107.4(3)
O(2)-U(1)-C(4)	134.13(10)	C(5)-C(1)-C(6)	125.6(3)
C(3)-U(1)-C(4)	29.98(11)	C(2)-C(1)-C(6)	125.7(3)
C(2)-U(1)-C(4)	49.23(11)	C(5)-C(1)-U(1)	75.3(2)
O(1)-U(1)-C(5)	89.04(10)	C(2)-C(1)-U(1)	70.9(2)
O(2)-U(1)-C(5)	138.19(10)	C(6)-C(1)-U(1)	129.6(3)
C(3)-U(1)-C(5)	48.64(11)	C(3)-C(2)-C(1)	108.0(3)
C(2)-U(1)-C(5)	48.45(11)	C(3)-C(2)-C(12)	126.7(4)
C(4)-U(1)-C(5)	29.06(11)	C(1)-C(2)-C(12)	125.4(3)
O(1)-U(1)-C(1)	114.20(11)	C(3)-C(2)-U(1)	73.8(2)
O(2)-U(1)-C(1)	110.27(10)	C(1)-C(2)-U(1)	79.5(2)
C(3)-U(1)-C(1)	48.89(11)	C(12)-C(2)-U(1)	113.0(3)
C(2)-U(1)-C(1)	29.54(11)	C(2)-C(3)-C(4)	108.0(3)
C(4)-U(1)-C(1)	48.19(11)	C(2)-C(3)-C(18)	125.5(3)
C(5)-U(1)-C(1)	28.79(11)	C(4)-C(3)-C(18)	125.4(3)
O(1)-U(1)-I(2)	86.92(7)	C(2)-C(3)-U(1)	75.9(2)
O(2)-U(1)-I(2)	79.97(7)	C(4)-C(3)-U(1)	77.8(2)
C(3)-U(1)-I(2)	131.84(8)	C(18)-C(3)-U(1)	122.2(3)
C(2)-U(1)-I(2)	103.18(8)	C(5)-C(4)-C(3)	107.7(3)
C(4)-U(1)-I(2)	125.60(8)	C(5)-C(4)-C(24)	126.5(3)
C(5)-U(1)-I(2)	96.54(8)	C(3)-C(4)-C(24)	125.2(3)
C(1)-U(1)-I(2)	84.14(8)	C(5)-C(4)-U(1)	77.8(2)
O(1)-U(1)-I(1)	78.80(7)	C(3)-C(4)-U(1)	72.2(2)
O(2)-U(1)-I(1)	74.54(7)	C(24)-C(4)-U(1)	122.7(3)
C(3)-U(1)-I(1)	97.25(8)	C(4)-C(5)-C(1)	108.9(3)
C(2)-U(1)-I(1)	120.61(8)	C(4)-C(5)-C(30)	125.1(3)

C(1)-C(5)-C(30)	125.1(3)	C(29)-C(24)-C(4)	121.3(4)
C(4)-C(5)-U(1)	73.2(2)	C(24)-C(25)-C(26)	121.2(4)
C(1)-C(5)-U(1)	75.9(2)	C(27)-C(26)-C(25)	120.1(4)
C(30)-C(5)-U(1)	126.0(3)	C(28)-C(27)-C(26)	119.6(4)
C(7)-C(6)-C(11)	117.4(4)	C(27)-C(28)-C(29)	120.2(4)
C(7)-C(6)-C(1)	122.8(4)	C(28)-C(29)-C(24)	120.6(4)
C(11)-C(6)-C(1)	119.5(3)	C(35)-C(30)-C(31)	117.6(4)
C(8)-C(7)-C(6)	121.3(4)	C(35)-C(30)-C(5)	122.5(4)
C(7)-C(8)-C(9)	120.2(4)	C(31)-C(30)-C(5)	119.7(4)
C(10)-C(9)-C(8)	119.4(4)	C(32)-C(31)-C(30)	121.7(4)
C(11)-C(10)-C(9)	120.2(4)	C(31)-C(32)-C(33)	120.0(4)
C(10)-C(11)-C(6)	121.5(4)	C(34)-C(33)-C(32)	119.8(4)
C(13)-C(12)-C(17)	118.1(4)	C(33)-C(34)-C(35)	119.8(4)
C(13)-C(12)-C(2)	120.4(3)	C(30)-C(35)-C(34)	121.1(4)
C(17)-C(12)-C(2)	121.5(4)	O(1)-C(36)-C(37)	104.9(4)
C(14)-C(13)-C(12)	120.7(4)	C(38)-C(37)-C(36)	101.9(4)
C(13)-C(14)-C(15)	120.5(4)	C(37)-C(38)-C(39)	103.3(4)
C(16)-C(15)-C(14)	119.5(4)	O(1)-C(39)-C(38)	106.0(4)
C(17)-C(16)-C(15)	120.7(4)	O(2)-C(40)-C(41)	105.6(4)
C(16)-C(17)-C(12)	120.5(4)	C(40)-C(41)-C(42)	102.2(4)
C(19)-C(18)-C(23)	118.1(4)	C(43)-C(42)-C(41)	101.4(4)
C(19)-C(18)-C(3)	122.6(4)	O(2)-C(43)-C(42)	105.3(4)
C(23)-C(18)-C(3)	119.2(4)	C(45)-C(44)-C(49)	117.3(8)
C(20)-C(19)-C(18)	121.5(4)	C(45)-C(44)-C(50)	125.6(8)
C(21)-C(20)-C(19)	119.3(4)	C(49)-C(44)-C(50)	116.9(8)
C(22)-C(21)-C(20)	120.1(4)	C(44)-C(45)-C(46)	124.8(8)
C(21)-C(22)-C(23)	120.4(4)	C(47)-C(46)-C(45)	122.3(8)
C(22)-C(23)-C(18)	120.7(4)	C(46)-C(47)-C(48)	112.8(8)
C(25)-C(24)-C(29)	118.3(4)	C(49)-C(48)-C(47)	122.0(9)
C(25)-C(24)-C(4)	120.3(4)	C(44)-C(49)-C(48)	120.4(8)

X-ray Data Collection, Structure Solution and Refinement for 9.2.

A colorless crystal of approximate dimensions 0.146 x 0.178 x 0.359 mm was mounted in a cryoloop and transferred to a Bruker SMART APEX II diffractometer system. The APEX2[1]

program package was used to determine the unit-cell parameters. Data was collected using a 60 sec/frame scan. The raw frame data was processed using SAINT2 and SADABS[3] to yield the reflection data file. Subsequent calculations were carried out using the SHELXTL[4] program package. The diffraction symmetry was *mmm* and the systematic absences were consistent with the orthorhombic space group $P2_12_12_1$ that was later determined to be correct.

The structure was solved by direct methods and refined on F^2 by full-matrix least-squares techniques. The analytical scattering factors[5] for neutral atoms were used throughout the analysis. Hydrogen atoms were included using a riding model.

Least-squares analysis yielded wR2 = 0.1110 and Goof = 1.027 for 461 variables refined against 9383 data (0.75 Å), R1 = 0.0495 for those 7658 with $I > 2.0\sigma(I)$. The absolute structure could not be assigned by refinement of the Flack parameter.[6] The structure was refined as a two-component inversion twin.

Table 9.3. Bond lengths [Å] and angles [°] for **9.2**.

Na-cnt	2.563	C(2)-C(3)	1.424(3)
Na(1)-O(2)	2.345(2)	C(2)-C(12)	1.486(3)
Na(1)-O(1)	2.362(2)	O(3)-C(44)	1.433(3)
Na(1)-O(3)	2.374(2)	O(3)-C(47)	1.454(3)
Na(1)-C(1)	2.708(3)	C(3)-C(4)	1.419(3)
Na(1)-C(5)	2.749(3)	C(3)-C(18)	1.478(3)
Na(1)-C(2)	2.844(3)	C(4)-C(5)	1.425(3)
Na(1)-C(4)	2.911(3)	C(4)-C(24)	1.486(3)
Na(1)-C(3)	2.960(3)	C(5)-C(30)	1.479(3)
O(1)-C(39)	1.442(3)	C(6)-C(7)	1.398(4)
O(1)-C(36)	1.450(3)	C(6)-C(11)	1.402(4)
C(1)-C(2)	1.428(3)	C(7)-C(8)	1.390(3)
C(1)-C(5)	1.431(3)	C(8)-C(9)	1.391(4)
C(1)-C(6)	1.486(3)	C(9)-C(10)	1.387(4)
O(2)-C(43)	1.431(3)	C(10)-C(11)	1.383(4)
O(2)-C(40)	1.445(4)	C(12)-C(17)	1.399(4)

C(12)-C(13)	1.401(4)	O(2)-Na(1)-C(1)	130.51(8)
C(13)-C(14)	1.387(4)	O(1)-Na(1)-C(1)	104.69(8)
C(14)-C(15)	1.387(4)	O(3)-Na(1)-C(1)	131.95(8)
C(15)-C(16)	1.393(4)	O(2)-Na(1)-C(5)	147.83(8)
C(16)-C(17)	1.382(4)	O(1)-Na(1)-C(5)	115.63(8)
C(18)-C(23)	1.394(4)	O(3)-Na(1)-C(5)	101.89(8)
C(18)-C(19)	1.405(3)	C(1)-Na(1)-C(5)	30.40(7)
C(19)-C(20)	1.388(4)	O(2)-Na(1)-C(2)	103.21(8)
C(20)-C(21)	1.382(4)	O(1)-Na(1)-C(2)	123.15(8)
C(21)-C(22)	1.383(4)	O(3)-Na(1)-C(2)	140.51(8)
C(22)-C(23)	1.390(4)	C(1)-Na(1)-C(2)	29.69(7)
C(24)-C(29)	1.394(4)	C(5)-Na(1)-C(2)	48.78(7)
C(24)-C(25)	1.395(4)	O(2)-Na(1)-C(4)	122.60(8)
C(25)-C(26)	1.390(4)	O(1)-Na(1)-C(4)	144.38(8)
C(26)-C(27)	1.385(4)	O(3)-Na(1)-C(4)	93.97(7)
C(27)-C(28)	1.388(4)	C(1)-Na(1)-C(4)	48.25(7)
C(28)-C(29)	1.390(4)	C(5)-Na(1)-C(4)	28.98(7)
C(30)-C(35)	1.398(4)	C(2)-Na(1)-C(4)	47.07(7)
C(30)-C(31)	1.405(4)	O(2)-Na(1)-C(3)	100.32(8)
C(31)-C(32)	1.381(4)	O(1)-Na(1)-C(3)	150.91(8)
C(32)-C(33)	1.379(4)	O(3)-Na(1)-C(3)	113.79(7)
C(33)-C(34)	1.379(4)	C(1)-Na(1)-C(3)	47.84(7)
C(34)-C(35)	1.391(4)	C(5)-Na(1)-C(3)	47.56(7)
C(36)-C(37)	1.530(4)	C(2)-Na(1)-C(3)	28.32(7)
C(37)-C(38)	1.530(4)	C(4)-Na(1)-C(3)	27.97(7)
C(38)-C(39)	1.512(4)	C(39)-O(1)-C(36)	107.3(2)
C(40)-C(41)	1.510(4)	C(39)-O(1)-Na(1)	112.27(16)
C(41)-C(42)	1.512(5)	C(36)-O(1)-Na(1)	140.31(17)
C(42)-C(43)	1.521(5)	C(2)-C(1)-C(5)	107.9(2)
C(44)-C(45)	1.515(4)	C(2)-C(1)-C(6)	124.6(2)
C(45)-C(46)	1.527(5)	C(5)-C(1)-C(6)	127.6(2)
C(46)-C(47)	1.517(4)	C(2)-C(1)-Na(1)	80.44(14)
		C(5)-C(1)-Na(1)	76.39(14)
O(2)-Na(1)-O(1)	92.20(8)	C(6)-C(1)-Na(1)	108.43(16)
O(2)-Na(1)-O(3)	92.64(8)	C(43)-O(2)-C(40)	106.1(2)
O(1)-Na(1)-O(3)	91.51(8)	C(43)-O(2)-Na(1)	126.16(17)

C(40)-O(2)-Na(1)	127.55(17)	C(17)-C(12)-C(13)	117.6(2)
C(3)-C(2)-C(1)	108.1(2)	C(17)-C(12)-C(2)	121.0(2)
C(3)-C(2)-C(12)	126.9(2)	C(13)-C(12)-C(2)	121.3(2)
C(1)-C(2)-C(12)	125.0(2)	C(14)-C(13)-C(12)	121.0(3)
C(3)-C(2)-Na(1)	80.37(14)	C(15)-C(14)-C(13)	120.7(3)
C(1)-C(2)-Na(1)	69.87(14)	C(14)-C(15)-C(16)	118.8(3)
C(12)-C(2)-Na(1)	117.69(16)	C(17)-C(16)-C(15)	120.6(3)
C(44)-O(3)-C(47)	108.9(2)	C(16)-C(17)-C(12)	121.2(2)
C(44)-O(3)-Na(1)	132.05(17)	C(23)-C(18)-C(19)	117.3(2)
C(47)-O(3)-Na(1)	118.77(16)	C(23)-C(18)-C(3)	122.4(2)
C(4)-C(3)-C(2)	107.9(2)	C(19)-C(18)-C(3)	120.3(2)
C(4)-C(3)-C(18)	123.9(2)	C(20)-C(19)-C(18)	121.5(2)
C(2)-C(3)-C(18)	128.2(2)	C(21)-C(20)-C(19)	119.9(2)
C(4)-C(3)-Na(1)	74.11(14)	C(20)-C(21)-C(22)	119.7(2)
C(2)-C(3)-Na(1)	71.31(14)	C(21)-C(22)-C(23)	120.4(2)
C(18)-C(3)-Na(1)	121.60(16)	C(22)-C(23)-C(18)	121.2(2)
C(3)-C(4)-C(5)	108.6(2)	C(29)-C(24)-C(25)	117.6(2)
C(3)-C(4)-C(24)	125.4(2)	C(29)-C(24)-C(4)	121.9(2)
C(5)-C(4)-C(24)	125.7(2)	C(25)-C(24)-C(4)	120.5(2)
C(3)-C(4)-Na(1)	77.92(14)	C(26)-C(25)-C(24)	121.1(2)
C(5)-C(4)-Na(1)	69.19(13)	C(27)-C(26)-C(25)	120.7(2)
C(24)-C(4)-Na(1)	123.11(16)	C(26)-C(27)-C(28)	118.9(2)
C(4)-C(5)-C(1)	107.6(2)	C(27)-C(28)-C(29)	120.3(2)
C(4)-C(5)-C(30)	123.2(2)	C(28)-C(29)-C(24)	121.4(2)
C(1)-C(5)-C(30)	129.3(2)	C(35)-C(30)-C(31)	116.8(2)
C(4)-C(5)-Na(1)	81.83(14)	C(35)-C(30)-C(5)	123.4(2)
C(1)-C(5)-Na(1)	73.21(14)	C(31)-C(30)-C(5)	119.7(2)
C(30)-C(5)-Na(1)	112.83(16)	C(32)-C(31)-C(30)	121.7(2)
C(7)-C(6)-C(11)	116.9(2)	C(33)-C(32)-C(31)	120.6(3)
C(7)-C(6)-C(1)	122.4(2)	C(32)-C(33)-C(34)	118.8(3)
C(11)-C(6)-C(1)	120.7(2)	C(33)-C(34)-C(35)	121.1(3)
C(8)-C(7)-C(6)	121.5(2)	C(34)-C(35)-C(30)	120.9(3)
C(7)-C(8)-C(9)	120.4(2)	O(1)-C(36)-C(37)	107.2(2)
C(10)-C(9)-C(8)	119.1(2)	C(36)-C(37)-C(38)	103.4(2)
C(11)-C(10)-C(9)	120.2(3)	C(39)-C(38)-C(37)	101.2(2)
C(10)-C(11)-C(6)	121.9(2)	O(1)-C(39)-C(38)	104.9(2)

O(2)-C(40)-C(41)	104.3(2)	O(3)-C(44)-C(45)	105.6(2)
C(40)-C(41)-C(42)	103.4(3)	C(44)-C(45)-C(46)	101.9(2)
C(41)-C(42)-C(43)	105.3(3)	C(47)-C(46)-C(45)	103.3(3)
O(2)-C(43)-C(42)	106.5(2)	O(3)-C(47)-C(46)	106.9(2)

X-ray Data Collection, Structure Solution and Refinement for 9.3.

A purple crystal of approximate dimensions 0.260 x 0.274 x 0.291 mm was mounted in a cryoloop and transferred to a Bruker SMART APEX II diffractometer system. The APEX2[1] program package was used to determine the unit-cell parameters and for data collection (120 sec/frame scan time for 519 frames of data). The raw frame data was processed using SAINT[2] and SADABS[3] to yield the reflection data file. Subsequent calculations were carried out using the SHELXTL[4] program package. The diffraction symmetry was 2/*m* and the systematic absences were consistent with the monoclinic space group $P2_1/n$ that was later determined to be correct.

The structure was solved by direct methods and refined on F^2 by full-matrix least-squares techniques. The analytical scattering factors[5] for neutral atoms were used throughout the analysis. Hydrogen atoms were included using a riding model. One tetrahydrofuran ligand was disordered and included using multiple components, partial site-occupancy-factors, geometric and displacement constraints.

Least-squares analysis yielded wR2 = 0.2038 and Goof = 1.036 for 550 variables refined against 9041 data (0.83Å), R1 = 0.0701 for those 5780 data with $I > 2.0\sigma(I)$. The low bond precision may have been a result of disorder and the incomplete, low multiplicity data set.

There were high residuals present in the final difference-Fourier map. It was probable that additional tetrahydrofuran solvent was present. The SQUEEZE[7a] routine in the PLATON[7b] program package was used to account for the electrons in the solvent accessible voids.

Table 9.4. Bond lengths [Å] and angles [°] for **9.3.**

C(1)-C(5)	1.414(5)	C(30)-C(35)	1.395(5)
C(1)-C(2)	1.424(4)	C(31)-C(32)	1.382(5)
C(1)-C(6)	1.471(5)	C(32)-C(33)	1.382(5)
C(2)-C(3)	1.416(5)	C(33)-C(34)	1.391(5)
C(2)-C(12)	1.475(4)	C(34)-C(35)	1.376(5)
C(3)-C(4)	1.430(5)	K(1)-O(8)	2.659(8)
C(3)-C(18)	1.478(5)	K(1)-O(7)	2.748(3)
C(4)-C(5)	1.414(5)	K(1)-O(4)	2.752(3)
C(4)-C(24)	1.481(5)	K(1)-O(6)	2.783(3)
C(5)-C(30)	1.485(5)	K(1)-O(2)	2.793(3)
C(6)-C(11)	1.390(5)	K(1)-O(1)	2.796(3)
C(6)-C(7)	1.413(5)	K(1)-O(5)	2.811(3)
C(7)-C(8)	1.382(5)	K(1)-O(3)	2.834(3)
C(8)-C(9)	1.374(5)	K(1)-O(8B)	2.901(8)
C(9)-C(10)	1.384(5)	O(1)-C(36)	1.419(4)
C(10)-C(11)	1.389(5)	O(1)-C(47)	1.429(4)
C(12)-C(13)	1.396(5)	O(2)-C(37)	1.421(4)
C(12)-C(17)	1.397(5)	O(2)-C(38)	1.425(4)
C(13)-C(14)	1.380(5)	O(3)-C(39)	1.419(4)
C(14)-C(15)	1.388(5)	O(3)-C(40)	1.427(4)
C(15)-C(16)	1.376(5)	O(4)-C(42)	1.422(4)
C(16)-C(17)	1.378(5)	O(4)-C(41)	1.437(4)
C(18)-C(19)	1.387(5)	O(5)-C(44)	1.419(4)
C(18)-C(23)	1.402(5)	O(5)-C(43)	1.426(5)
C(19)-C(20)	1.383(5)	O(6)-C(45)	1.420(5)
C(20)-C(21)	1.375(5)	O(6)-C(46)	1.433(5)
C(21)-C(22)	1.371(6)	C(36)-C(37)	1.489(5)
C(22)-C(23)	1.393(5)	C(38)-C(39)	1.490(6)
C(24)-C(29)	1.396(5)	C(40)-C(41)	1.491(6)
C(24)-C(25)	1.403(5)	C(42)-C(43)	1.496(6)
C(25)-C(26)	1.380(5)	C(44)-C(45)	1.503(6)
C(26)-C(27)	1.371(7)	C(46)-C(47)	1.488(6)
C(27)-C(28)	1.376(6)	O(7)-C(48)	1.418(5)
C(28)-C(29)	1.388(5)	O(7)-C(51)	1.419(6)
C(30)-C(31)	1.394(5)	C(48)-C(49)	1.478(7)

C(49)-C(50)	1.494(8)	C(13)-C(12)-C(17)	116.7(3)
C(50)-C(51)	1.523(8)	C(13)-C(12)-C(2)	122.2(3)
O(8)-C(55)	1.4100	C(17)-C(12)-C(2)	121.1(3)
O(8)-C(52)	1.4152	C(14)-C(13)-C(12)	121.6(3)
C(52)-C(53)	1.5245	C(13)-C(14)-C(15)	120.6(3)
C(53)-C(54)	1.5149	C(16)-C(15)-C(14)	118.6(3)
C(54)-C(55)	1.5169	C(15)-C(16)-C(17)	120.9(3)
O(8B)-C(52B)	1.4152	C(16)-C(17)-C(12)	121.7(3)
O(8B)-C(55B)	1.5242	C(19)-C(18)-C(23)	116.8(3)
C(52B)-C(53B)	1.4100	C(19)-C(18)-C(3)	122.1(3)
C(53B)-C(54B)	1.5170	C(23)-C(18)-C(3)	121.1(3)
C(54B)-C(55B)	1.5148	C(20)-C(19)-C(18)	121.7(4)
		C(21)-C(20)-C(19)	120.6(4)
C(5)-C(1)-C(2)	107.9(3)	C(22)-C(21)-C(20)	119.3(3)
C(5)-C(1)-C(6)	125.3(3)	C(21)-C(22)-C(23)	120.3(4)
C(2)-C(1)-C(6)	126.8(3)	C(22)-C(23)-C(18)	121.3(4)
C(3)-C(2)-C(1)	107.6(3)	C(29)-C(24)-C(25)	116.8(3)
C(3)-C(2)-C(12)	125.6(3)	C(29)-C(24)-C(4)	121.7(3)
C(1)-C(2)-C(12)	126.8(3)	C(25)-C(24)-C(4)	121.6(3)
C(2)-C(3)-C(4)	108.5(3)	C(26)-C(25)-C(24)	121.5(4)
C(2)-C(3)-C(18)	124.7(3)	C(27)-C(26)-C(25)	120.5(4)
C(4)-C(3)-C(18)	126.8(3)	C(26)-C(27)-C(28)	119.6(4)
C(5)-C(4)-C(3)	107.1(3)	C(27)-C(28)-C(29)	120.3(4)
C(5)-C(4)-C(24)	127.6(3)	C(28)-C(29)-C(24)	121.3(4)
C(3)-C(4)-C(24)	125.3(3)	C(31)-C(30)-C(35)	117.4(3)
C(1)-C(5)-C(4)	108.9(3)	C(31)-C(30)-C(5)	123.0(3)
C(1)-C(5)-C(30)	123.3(3)	C(35)-C(30)-C(5)	119.6(3)
C(4)-C(5)-C(30)	127.4(3)	C(32)-C(31)-C(30)	120.9(3)
C(11)-C(6)-C(7)	116.6(3)	C(33)-C(32)-C(31)	120.9(3)
C(11)-C(6)-C(1)	122.5(3)	C(32)-C(33)-C(34)	119.1(3)
C(7)-C(6)-C(1)	120.9(3)	C(35)-C(34)-C(33)	119.8(3)
C(8)-C(7)-C(6)	121.4(3)	C(34)-C(35)-C(30)	122.0(3)
C(9)-C(8)-C(7)	120.6(3)	O(8)-K(1)-O(7)	164.54(18)
C(8)-C(9)-C(10)	119.4(3)	O(8)-K(1)-O(4)	80.68(18)
C(9)-C(10)-C(11)	120.2(4)	O(7)-K(1)-O(4)	85.20(9)
C(10)-C(11)-C(6)	121.8(3)	O(8)-K(1)-O(6)	99.22(19)

O(7)-K(1)-O(6)	82.63(9)	C(38)-O(2)-K(1)	116.52(19)
O(4)-K(1)-O(6)	120.81(8)	C(39)-O(3)-C(40)	112.8(3)
O(8)-K(1)-O(2)	98.70(18)	C(39)-O(3)-K(1)	113.7(2)
O(7)-K(1)-O(2)	93.63(9)	C(40)-O(3)-K(1)	113.5(2)
O(4)-K(1)-O(2)	119.06(8)	C(42)-O(4)-C(41)	111.9(3)
O(6)-K(1)-O(2)	119.37(8)	C(42)-O(4)-K(1)	114.7(2)
O(8)-K(1)-O(1)	96.22(18)	C(41)-O(4)-K(1)	115.6(2)
O(7)-K(1)-O(1)	97.99(9)	C(44)-O(5)-C(43)	111.8(3)
O(4)-K(1)-O(1)	176.74(8)	C(44)-O(5)-K(1)	112.3(2)
O(6)-K(1)-O(1)	60.54(8)	C(43)-O(5)-K(1)	111.0(2)
O(2)-K(1)-O(1)	60.23(7)	C(45)-O(6)-C(46)	112.4(3)
O(8)-K(1)-O(5)	79.71(17)	C(45)-O(6)-K(1)	116.5(2)
O(7)-K(1)-O(5)	88.08(9)	C(46)-O(6)-K(1)	114.9(2)
O(4)-K(1)-O(5)	61.62(7)	O(1)-C(36)-C(37)	109.2(3)
O(6)-K(1)-O(5)	60.27(8)	O(2)-C(37)-C(36)	109.4(3)
O(2)-K(1)-O(5)	178.20(8)	O(2)-C(38)-C(39)	108.8(3)
O(1)-K(1)-O(5)	118.98(8)	O(3)-C(39)-C(38)	107.9(3)
O(8)-K(1)-O(3)	79.81(19)	O(3)-C(40)-C(41)	108.4(3)
O(7)-K(1)-O(3)	98.67(9)	O(4)-C(41)-C(40)	108.1(3)
O(4)-K(1)-O(3)	60.44(7)	O(4)-C(42)-C(43)	108.5(3)
O(6)-K(1)-O(3)	178.35(8)	O(5)-C(43)-C(42)	109.2(3)
O(2)-K(1)-O(3)	59.61(7)	O(5)-C(44)-C(45)	108.3(3)
O(1)-K(1)-O(3)	118.15(8)	O(6)-C(45)-C(44)	107.9(3)
O(5)-K(1)-O(3)	120.70(7)	O(6)-C(46)-C(47)	109.4(3)
O(7)-K(1)-O(8B)	171.54(15)	O(1)-C(47)-C(46)	108.6(3)
O(4)-K(1)-O(8B)	99.24(19)	C(48)-O(7)-C(51)	108.3(4)
O(6)-K(1)-O(8B)	101.00(18)	C(48)-O(7)-K(1)	118.7(3)
O(2)-K(1)-O(8B)	77.93(14)	C(51)-O(7)-K(1)	118.2(3)
O(1)-K(1)-O(8B)	77.50(19)	O(7)-C(48)-C(49)	105.3(4)
O(5)-K(1)-O(8B)	100.36(14)	C(48)-C(49)-C(50)	102.6(4)
O(3)-K(1)-O(8B)	77.58(18)	C(49)-C(50)-C(51)	103.7(4)
C(36)-O(1)-C(47)	111.6(3)	O(7)-C(51)-C(50)	106.6(4)
C(36)-O(1)-K(1)	115.2(2)	C(55)-O(8)-C(52)	103.7
C(47)-O(1)-K(1)	115.2(2)	C(55)-O(8)-K(1)	129.9(5)
C(37)-O(2)-C(38)	112.2(3)	C(52)-O(8)-K(1)	117.9(5)
C(37)-O(2)-K(1)	115.4(2)	O(8)-C(52)-C(53)	105.4

C(54)-C(53)-C(52)	102.3	C(53B)-C(52B)-O(8B)	103.7
C(53)-C(54)-C(55)	103.7	C(52B)-C(53B)-C(54B)	108.2
O(8)-C(55)-C(54)	108.2	C(55B)-C(54B)-C(53B)	103.7
C(52B)-O(8B)-C(55B)	105.4	C(54B)-C(55B)-O(8B)	102.3
C(52B)-O(8B)-K(1)	127.1(5)	C(54B)-C(55B)-K(1)	102.3(4)
C(55B)-O(8B)-K(1)	94.5(5)	O(8B)-C(55B)-K(1)	58.8(4)

References

(1) Fagan, P. J.; Manriquez, J. M.; Maatta, E. A.; Seyam, A. M.; Marks, T. J. Synthesis and Properties of Bis(Pentamethylcyclopentadienyl) Actinide Hydrocarbyls and Hydrides. A New Class of Highly Reactive f-Element Organometallic Compounds. *J. Am. Chem. Soc.* **1981**, *103*, 6650–6667, DOI: 10.1021/ja00412a021.

(2) Marks, T. J. Actinide Organometallic Chemistry. *Science (80-.).* **1982**, *217*, 989–997.

(3) Wayda, A. L.; Evans, W. J. Synthesis of a Bis(Pentamethylcyclopentadienyl) Derivative of Neodymium. *J. Am. Chem. Soc.* **1980**, *19*, 2190–2191, DOI: 10.1021/ic50209a077.

(4) Watson, P. L.; Whitney, J. F.; Harlow, R. L. (Pentamethylcyclopentadienyl)Ytterbium and -Lutetium Complexes by Metal Oxidation and Metathesis. *Inorg. Chem.* **1981**, *20*, 3271–3278, DOI: 10.1021/ic50224a026.

(5) Tilley, T. D.; Andersen, R. A. Pentamethylcyclopentadienyl Derivatives of the Trivalent Lanthanide Elements Neodymium, Samarium, and Ytterbium. *Inorg. Chem.* **1981**, *20*, 3267–3270, DOI: 10.1021/ic50224a025.

(6) Schumann, H.; Meese-Marktscheffel, J. A.; Esser, L. Synthesis, Structure, and Reactivity of Organometallic .Pi.-Complexes of the Rare Earths in the Oxidation State Ln3+ with Aromatic Ligands. *Chem. Rev.* **1995**, *95*, 865–986, DOI: 10.1021/cr00036a004.

(7) Qin, G.; Wang, Y.; Shi, X.; Del Rosal, I.; Maron, L.; Cheng, J. Monomeric Thorium Dihydrido Complexes: Versatile Precursors to Actinide Metallacycles. *Chem. Commun.*

2019, *55*, 8560–8563, DOI: 10.1039/c9cc04013g.

(8) Kelly, R. P.; Bell, T. D. M.; Cox, R. P.; Daniels, D. P.; Deacon, G. B.; Jaroschik, F.; Junk, P. C.; Le, X. F.; Lemercier, G.; Martinez, A.; Wang, J.; Werner, D.; Le Goff, X. F.; Lemercier, G.; Martinez, A.; Wang, J.; Werner, D. Divalent Tetra- and Penta-Phenylcyclopentadienyl Europium and Samarium Sandwich and Half-Sandwich Complexes: Synthesis, Characterization, and Remarkable Luminescence Properties. *Organometallics* **2015**, *34*, 5624–5636, DOI: 10.1021/acs.organomet.5b00842.

(9) Deacon, G. B.; Forsyth, C. M.; Jaroschik, F.; Junk, P. C.; Kay, D. L.; Maschmeyer, T.; Masters, A. F.; Wang, J.; Field, L. D. Accessing Decaphenylmetallocenes of Ytterbium, Calcium, and Barium by Desolvation of Solvent-Separated Ion Pairs: Overcoming Adverse Solubility Properties. *Organometallics* **2008**, *27*, 4772–4778, DOI: 10.1021/om800501z.

(10) Forsyth, C. M.; Deacon, G. B.; Field, L. D.; Jones, C.; Junk, P. C.; Kay, D. L.; Masters, A. F.; Richards, A. F. Dinuclear Alkynyllanthanoid(II) Dications with Pentaphenylcyclopentadienyl or Tri-Tert-Butyldiphosphacyclopentadienyl Counter Ions. *Chem. Commun.* **2006**, *2*, 1003–1005, DOI: 10.1039/b514358f.

(11) MacDonald, M. R.; Fieser, M. E.; Bates, J. E.; Ziller, J. W.; Furche, F.; Evans, W. J. Identification of the +2 Oxidation State for Uranium in a Crystalline Molecular Complex, [K(2.2.2-Cryptand)][(C5H4SiMe3)3U]. *J. Am. Chem. Soc.* **2013**, *135*, 13310–13313, DOI: 10.1021/ja406791t.

(12) La Pierre, H. S.; Scheurer, A.; Heinemann, F. W.; Hieringer, W.; Meyer, K. Synthesis and Characterization of a Uranium(II) Monoarene Complex Supported by δ Backbonding. *Angew. Chemie Int. Ed.* **2014**, *53*, 7158–7162, DOI: 10.1002/anie.201402050.

(13) Windorff, C. J.; MacDonald, M. R.; Meihaus, K. R.; Ziller, J. W.; Long, J. R.; Evans, W. J.

Expanding the Chemistry of Molecular U2+ Complexes: Synthesis, Characterization, and Reactivity of the {[C5H3(SiMe3)2]3U}− Anion. *Chem. - A Eur. J.* **2016**, *22*, 772–782, DOI: 10.1002/chem.201503583.

(14) Billow, B. S.; Livesay, B. N.; Mokhtarzadeh, C. C.; Mccracken, J.; Shores, M. P.; Boncella, J. M.; Odom, A. L. Synthesis and Characterization of a Neutral U(II) Arene Sandwich Complex. *J. Am. Chem. Soc.* **2018**, *140*, 17369–17373, DOI: 10.1021/jacs.8b10888.

(15) Ryan, A. J.; Angadol, M. A.; Ziller, J. W.; Evans, W. J. Isolation of U(II) Compounds Using Strong Donor Ligands, C5Me4H and N(SiMe3)2, Including a Three-Coordinate U(II) Complex. *Chem. Commun.* **2019**, *55*, 2325–2327, DOI: 10.1039/C8CC08767A.

(16) Wedal, J. C.; Bekoe, S.; Ziller, J. W.; Furche, F.; Evans, W. J. C–H Bond Activation via U(II) in the Reduction of Heteroleptic Bis(Trimethylsilyl)Amide U(III) Complexes. *Organometallics* **2020**, *39*, 3425–3432, DOI: 10.1021/acs.organomet.0c00496.

(17) Evans, W. J.; Kozimor, S. A.; Ziller, J. W. Methyl Displacements from Cyclopentadienyl Ring Planes in Sterically Crowded (C5Me5)3M Complexes. *Inorg. Chem.* **2005**, *44*, 7960–7969, DOI: 10.1021/ic051130h.

(18) Avens, L. R.; Burns, C. J.; Butcher, R. J.; Clark, D. L.; Gordon, J. C.; Schake, A. R.; Scott, B. L.; Watkin, J. G.; Zwick, B. D. Mono(Pentamethylcyclopentadienyl)Uranium(III) Complexes: Synthesis, Properties, and X-Ray Structures of (η-C5Me5)UI2(THF)3, (η-C5Me5)UI2(Py)3, and (η-C5Me5)U[N(SiMe3)2]2. *Organometallics* **2000**, *19*, 451–457, DOI: 10.1021/om990718r.

(19) Kiernicki, J. J.; Newell, B. S.; Matson, E. M.; Anderson, N. H.; Fanwick, P. E.; Shores, M. P.; Bart, S. C. Multielectron C–O Bond Activation Mediated by a Family of Reduced Uranium Complexes. *Inorg. Chem.* **2014**, *53*, 3730–3741, DOI: 10.1021/ic500012x.

(20) Bardonov, D. A.; Komarov, P. D.; Ovchinnikova, V. I.; Puntus, L. N.; Minyaev, M. E.; Nifant'ev, I. E.; Lyssenko, K. A.; Korshunov, V. M.; Taidakov, I. V.; Roitershtein, D. M. Accessing Mononuclear Triphenylcyclopentadienyl Lanthanide Complexes by Using Tridentate Nitrogen Ligands: Synthesis, Structure, Luminescence, and Catalysis. *Organometallics* **2021**, *40*, 1235–1243, DOI: 10.1021/acs.organomet.1c00022.

(21) Orzechowski, L.; Piesik, D. F. J.; Ruspic, C.; Harder, S. Superbulky Metallocene Complexes of the Heavier Alkaline-Earth Metals Strontium and Barium. *J. Chem. Soc. Dalt. Trans.* **2008**, No. 35, 4742–4746, DOI: 10.1039/b809872g.

(22) Ruspic, C.; Moss, J. R.; Schürmann, M.; Harder, S. Remarkable Stability of Metallocenes with Superbulky Ligands: Spontaneous Reduction of SmIII to SmII. *Angew. Chemie Int. Ed.* **2008**, *47*, 2121–2126, DOI: 10.1002/anie.200705001.

(23) Giesbrecht, G. R.; Gordon, J. C.; Clark, D. L.; Scott, B. L. Synthesis, Structure and Solution Dynamics of Lithium Salts of Superbulky Cyclopentadienyl Ligands. *Dalt. Trans.* **2003**, No. 13, 2658–2665, DOI: 10.1039/b302258g.

(24) Shi, X.; Qin, G.; Wang, Y.; Zhao, L.; Liu, Z.; Cheng, J. Super-Bulky Penta-Arylcyclopentadienyl Ligands: Isolation of the Full Range of Half-Sandwich Heavy Alkaline-Earth Metal Hydrides. *Angew. Chemie Int. Ed.* **2019**, *58*, 4356–4360, DOI: 10.1002/anie.201814733.

(25) Schulte, Y.; Weinert, H.; Wölper, C.; Schulz, S. Direct Synthesis of Pentaarylcyclopentadienyl Sandwich and Half-Sandwich Complexes of s-, p-, and d-Block Metals. *Organometallics* **2020**, *39*, 206–216, DOI: 10.1021/acs.organomet.9b00741.

(26) Shannon, R. D. Revised Effective Ionic Radii and Systematic Studies of Interatomic Distances in Halides and Chalcogenides. *Acta Crystallogr. Sect. A* **1976**, *32*, 751–767, DOI:

10.1107/S0567739476001551.

(27) Izod, K.; Liddle, S. T.; Clegg, W. A Convenient Route to Lanthanide Triiodide THF Solvates. Crystal Structures of LnI3(THF)4 [Ln = Pr] and LnI3(THF)3.5 [Ln = Nd , Gd , Y]. *Inorg. Chem.* **2004**, *43*, 214–218, DOI: 10.1021/ic034851u.

(28) Bergbreiter, D. E.; Killough, J. M. Reactions of Potassium-Graphite. *J. Am. Chem. Soc.* **1978**, *100*, 2126–2134, DOI: 10.1021/ja00475a025.

(29) Carmichael, C. D.; Jones, N. A.; Arnold, P. L. Low-Valent Uranium Iodides: Straightforward Solution Syntheses of UI 3 and UI4 Etherates. *Inorg. Chem.* **2008**, *47*, 8577–8579, DOI: 10.1021/ic801138e.

(30) Zhang, R.; Tsutsui, M.; E. Bergbreiter, D. Alkali Metal Salts of Pentaphenylcyclopentadienide. *J. Organomet. Chem.* **1982**, *229*, 109–112, DOI: 10.1016/S0022-328X(00)90273-0.

Chapter 10:

Synthesis of Tris(trimethylsilylcyclopentadienyl) Thorium, Cp'_3Th

Introduction[†]

Complexes of Th(III) ions are difficult to synthesize due to the extremely negative reduction potential of Th(IV)/Th(III), which was originally estimated to be between −3.00 and −3.82 V vs NHE[1–3] (−3.40 and −4.22 V vs Fc^+/Fc),[4] which is in line with the electrochemical results in Chapter 3.[5] Although careful choice of ligand environment and synthetic procedures can allow isolation of Th(III) complexes, only thirteen crystallographically-characterized Th(III) complexes were in the literature as of March 2022.[6–16] There were synthetic reports of $(C_5H_5)_3Th$, $(C_5MeH_4)_3Th$, and $(indenyl)_3Th$ from β-hydride elimination[17] and $\{[(C_5Me_5)_2ThH_2]_2\}^{1-}$ from reduction of $[(C_5Me_5)_2ThH_2)_2$,[12] but these compounds were not characterized by X-ray diffraction. A review of these complexes and the difficulties associated with their syntheses has been published.[18]

Th(III) complexes are of interest not only as strong reductants, but also as precursors to Th(II) compounds. As described in the Introduction, the first molecular example of Th(II) was isolated as $[K(chelate)][Cp''_3Th]$ via reduction of Cp''_3Th [$Cp'' = C_5H_3(SiMe_3)_2$, chelate = 2.2.2-cryptand or (18-crown-6)$(THF)_2$].[19] Previously, the first example of U(II) was isolated with Cp' [$Cp' = C_5H_4(SiMe_3)$] ligands via reduction of Cp'_3U,[20] but this route could not be applied to thorium since Cp'_3Th is not known. In efforts to find additional coordination environments suitable for the synthesis of other Th(II) complexes, the isolation of Cp'_3Th was pursued.

[†] Portions of this Chapter have been published: Wedal, J. C.; Bekoe, S.; Ziller, J. W.; Furche, F.; Evans, W. J. In Search of Tris(trimethylsilylcyclopentadienyl) Thorium. *Dalton Trans.* **2019**, *48*, 16633-16640. DOI: 10.1039/C9DT03674A

Spectroscopic and reactivity evidence for Cp'_3Th is presented in this Chapter. To support these studies, the syntheses of Cp'_3ThI and $Cp'_3Th(C{\equiv}CPh)$ were developed and X-ray crystal structures of Cp'_3ThMe[21,22] and $(Cp'_3Th)_2(\mu\text{-}O)$ were obtained.

Results

Three Cp'_3ThX compounds (X = Cl, Br, I) were synthesized to examine their reduction chemistry. Cp'_3ThCl and Cp'_3ThBr were prepared according to the literature from $ThCl_4(DME)_2$ or $ThBr_4(THF)_4$ and KCp', respectively.[23] Cp'_3ThI was synthesized from Cp'_3ThMe[21,22] and Me_3SiI, which also generated Me_4Si as a product, eq 10.1. The Cp'_3ThMe precursor in eq 10.1 was prepared from Cp'_3ThBr and MeLi and was crystallographically characterized (see below).

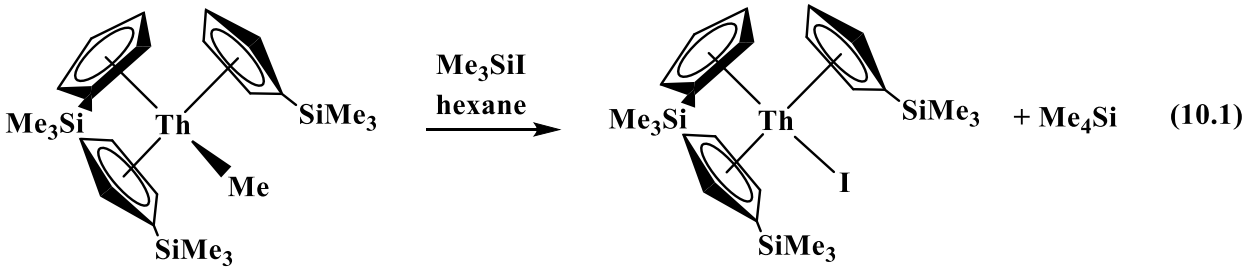

Reaction of Cp'_3ThBr with KC_8 in THF at −35 °C generates a dark blue solution, **A**, and a black precipitate, presumably graphite, eq 10.2. The solution displays an axial EPR signal at 77 K with $g_{\parallel} = 1.98$ and $g_{\perp} = 1.89$, and an isotropic signal at room temperature with $g_{iso} = 1.90$, Figure 10.1. The g values are consistent with all other crystallographically-characterized tris(cyclopentadienyl) Th(III) compounds as shown in Table 10.1.

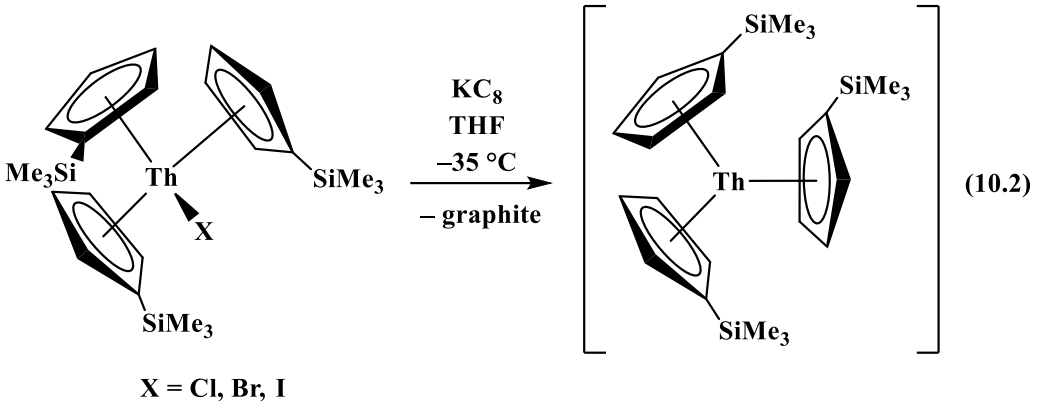

(10.2)

X = Cl, Br, I

The UV-visible absorption spectrum of **A** in THF is very similar to previously characterized Cp''_3Th[9] and has three main features between 490 and 650 nm, Figure 10.2. The measured 100–200 $M^{-1}cm^{-1}$ extinction coefficients are significantly lower than all other crystallographically-characterized tris(cyclopentadienyl) Th(III) species, which have extinction coefficients in the thousands.[9,11,14] The measured values assume complete conversion of Cp'_3ThBr to Cp'_3Th with no decomposition and hence the minimum values. Further studies showed that Cp'_3Th decomposes rapidly, and the measured extinction coefficients are not likely to be accurate.

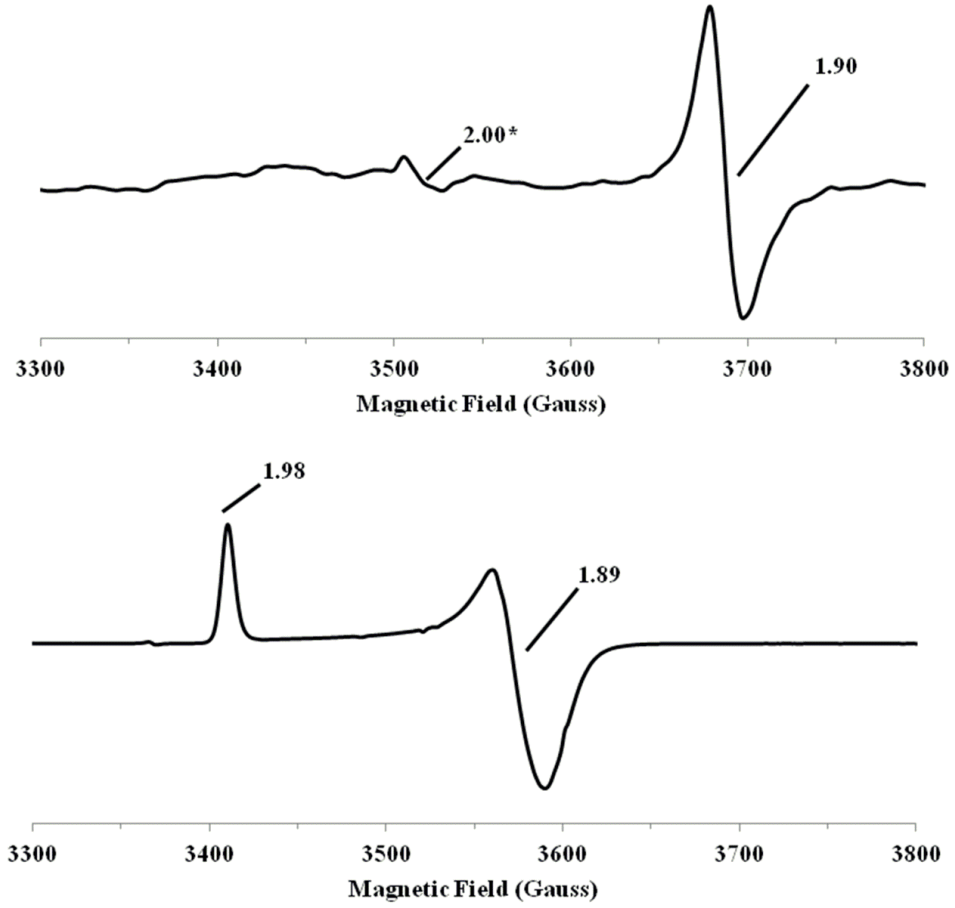

Figure 10.1. X-band EPR of **A** in THF at room temperature (top; mode: perpendicular, v = 9.816566 GHz, P = 2.021, modulation amplitude = 2 mT) and at 77 K (bottom; mode: perpendicular, v = 9.45551 GHz, P = 2.138; modulation amplitude = 2 mT). *The feature at g = 2.00 is attributed to electride.[24]

Table 10.1: Room temperature and 77 K EPR g values of $(C_5R_5)_3Th$ compounds.

	Room temperature g_{iso}	77 K $g_{\|}$, $g_{\perp}$
$[C_5H_3(SiMe_2{}^tBu)_2]_3Th$[9]	1.91	1.98, 1.89[a]
$[C_5H_3(SiMe_3)_2]_3Th$[9]	1.91	1.97, 1.88[a]
$(C_5Me_4H)_3Th$[11]	1.92	1.98, 1.86
$(C_5Me_5)_3Th$[14]	1.88	1.97, 1.85
$(C_5{}^tBu_2H_3)_3Th$[13]	Not reported	1.97, 1.88[a]
A	1.90	1.98, 1.89

[a] Collected at 100 K

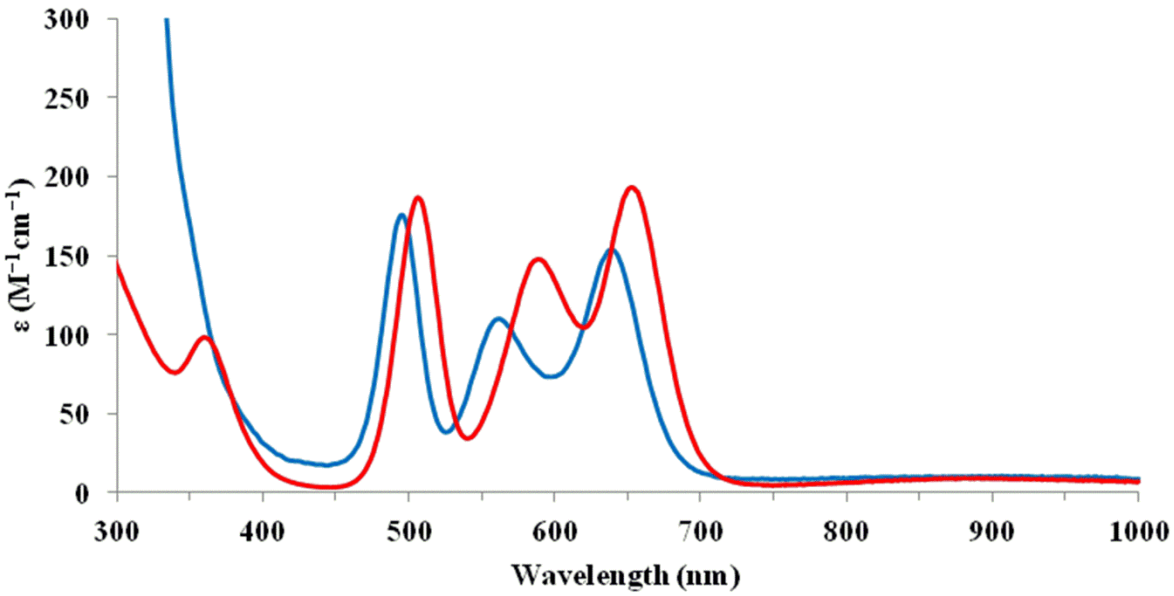

Figure 10.2: UV-visible spectrum of **A** (blue) in THF and Cp''_3Th[9] (red) in THF. The spectrum of Cp''_3Th was scaled down by a factor of 30 to ease comparison.

Reduction of Cp'_3ThCl[17] and Cp'_3ThI with KC_8 in THF also yields dark blue solutions. The EPR spectra at 77 K, as well as the UV-visible spectrum at room temperature, are indistinguishable from the reduction of Cp'_3ThBr, which indicates that this reaction scheme is independent of the halide ligand, eq 10.2. The reduction of Cp'_3ThBr can also be done in Et_2O and toluene with KC_8. However, crystallization attempts at −35 °C immediately following synthesis yield intractable solids and colorless solutions within approximately two hours regardless of the crystallization technique or the toluene, Et_2O, or THF solvent used. When solution **A** in THF was placed under vacuum immediately after synthesis in attempts to isolate solids, the blue color faded to grey within 15 minutes as the mixture was warmed to room temperature from −35 °C. Decomposition of **A** could be monitored by the decrease in absorbance at 496 nm in THF, and a half-life of 5.5 min was estimated for **A** in THF at room temperature, Figure 10.3.

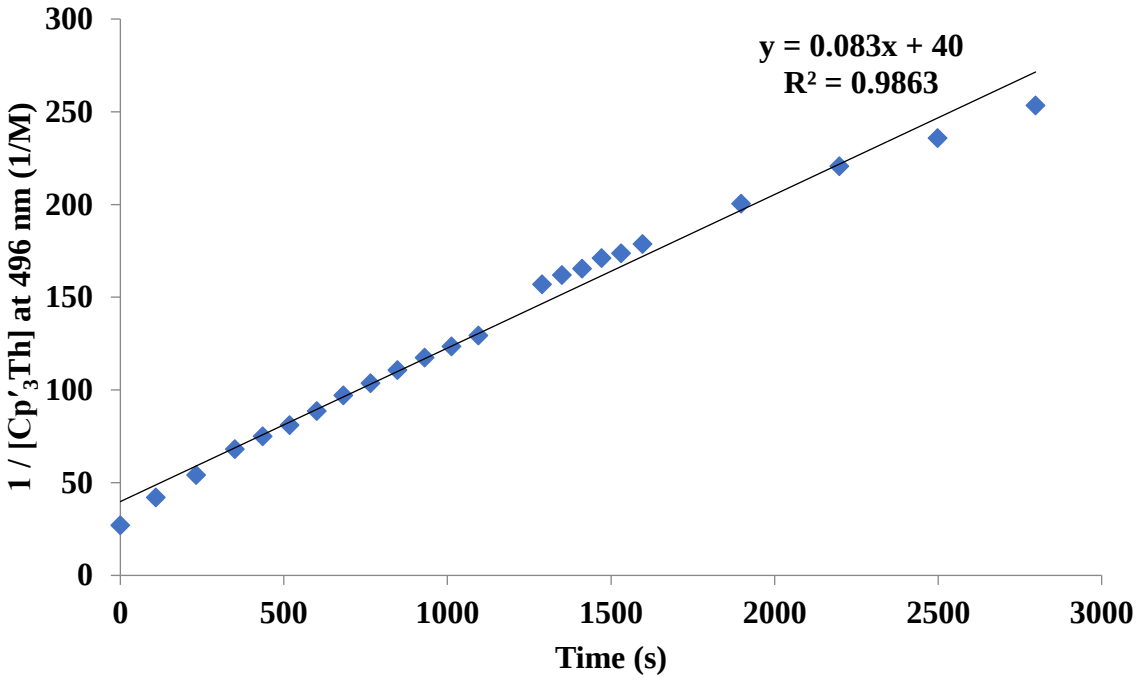

Figure 10.3: Decomposition of **A** by monitoring absorbance at 496 nm in THF.

The cyclic voltammogram of Cp'_3ThCl exhibits a quasi-reversible redox process at – 3.17 V vs Fc^+/Fc, Figure 10.4, using $[^nBu_4N][BPh_4]$ as supporting electrolyte. The process occurs at an identical potential at a scan rate of 200 mV/s, 500 mV/s, and 1000 mV/s, but reversibility is not improved at higher scan rates. The irreversibility of this redox couple might suggest some chemical process occurring once the reduced species is formed, highlighting the highly reactive nature of Th(III) compounds.

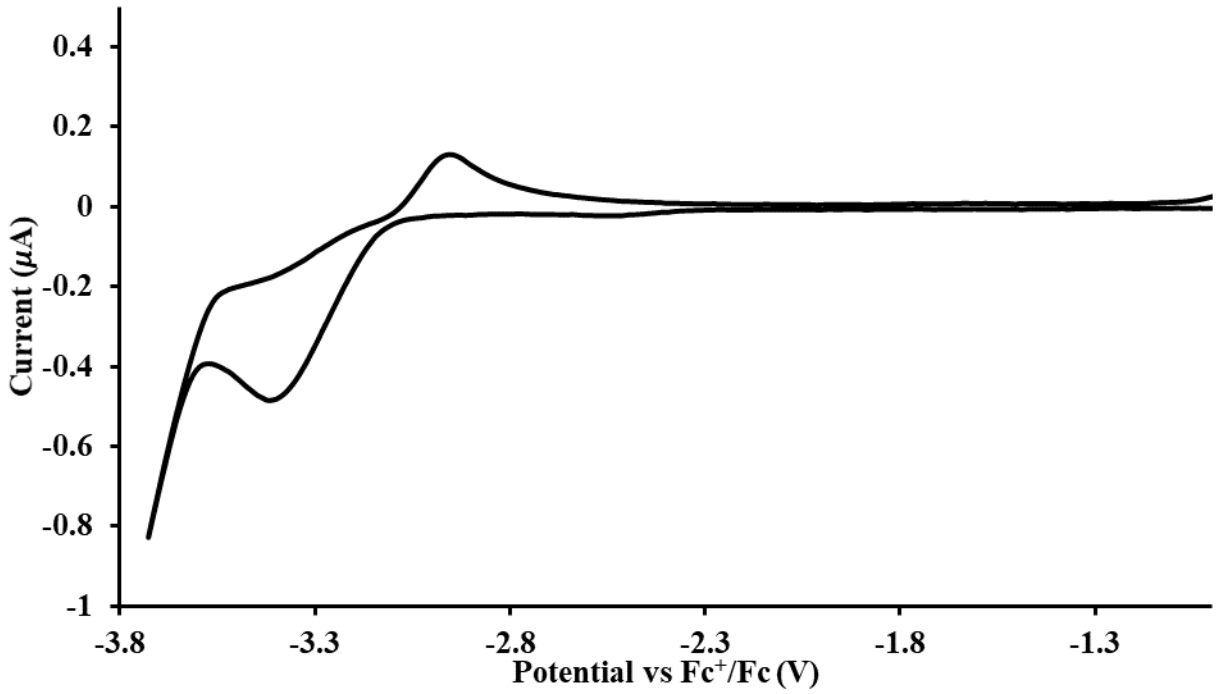

Figure 10.4: Cyclic voltammogram of Cp'_3ThCl in 50 mM [^{n}Bu$_4$N][BPh$_4$] / THF at v = 1000 mV/s. A glassy carbon working electrode, platinum wire counter electrode, and silver wire pseudoreference electrode were used. $(C_5Me_5)_2Fe$ was used as an internal standard.

A common product observed in the reactions with **A** is Cp'_3ThH.[22] Stirring **A** in THF for 90 min at room temperature leads to complete decomposition to a grey solution. The ^{1}H NMR spectrum of this mixture in C_6D_6 displays peaks consistent with Cp'_3ThH as well as at least five other sets of Cp′ resonances suggestive of multiple Cp′ environments. When the same reaction was done in THF-d_8, Cp'_3ThH was still observed in the ^{1}H NMR spectrum and no Th–D resonance was observed in the ^{2}H NMR spectrum, which suggests the hydride does not come from the solvent. Cp'_3ThH also appears as a byproduct in reactions with **A** as described below.

In collaboration with Sam Bekoe and Filipp Furche, geometry optimization calculations on Cp'_3Th, Cp'_3ThBr, and Cp'_3ThBr^{1-} were carried out at the density functional level of theory using

the TPSSh functional.[26] Scalar relativistic effective core potentials (ECPs)[27] with the def-TZVP[28] basis set were used for thorium and polarized split-valence basis sets with diffuse functions def2-SVPD[29] were used for the other atoms. DFT calculations on Cp'_3ThBr matched the known structure within 0.009 Å in bond distances and within degrees in angles. The calculations yielded a Cp'_3Th minimum structure that has a trigonal planar arrangement of the cyclopentadienyl rings as found in crystallographically characterized Cp''_3Th.[5,6] Two $SiMe_3$ substituents point the direction opposite the third, which is consistent with structure of other Cp'_3M complexes (M = Y,[30] La–Nd,[31,32] Sm–Lu,[31–33] U,[20] Np[34]). In order to directly compare the geometry of Cp'_3Th with previously analyzed Cp''_3Th,[12] Cp'_3Th was also optimized with the def2-SV(P) basis set.[29] The average optimized Th–Cp′ ring centroid distance was 0.04 Å shorter than the 2.520 Å distance in Cp''_3Th, as expected for a smaller ligand. For comparison, the average U-ring centroid distances are 2.508 and 2.542 Å in the structures of Cp'_3U[35] and Cp''_3U,[36] respectively.

The highest-occupied molecular orbital (HOMO) calculated for Cp'_3Th had significant $6dz^2$ character, Figure 10.5, which is consistent with the EPR spectra of all other crystallographically-characterized tris(cyclopentadienyl) Th(III) compounds.[9,11,13,14]

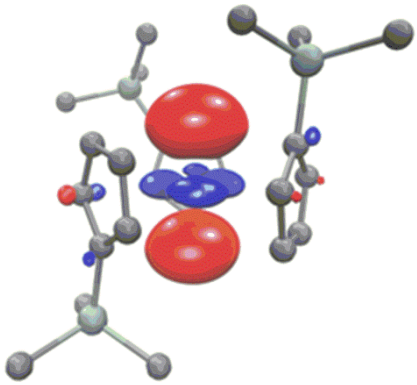

Figure 10.5: Calculated $6dz^2$-like HOMO of Cp'_3Th obtained using DFT with the TPSSh functional, plotted with a contour value of 0.06.

Time dependent DFT (TDDFT) calculations predicted a UV-visible spectrum for Cp'_3Th in good agreement with the experimental spectrum, Figure 10.6. In contrast, the predicted spectrum of the possible reduction product, $[Cp'_3ThBr]^{1-}$, has only a single excitation between 300–800 nm, and an excitation between 900–1000 nm, neither of which are observed in the experimental spectrum. The electronic transitions of Cp'_3Th between 400–1000 nm are predominantly 6d to 5f in character, in agreement with analyses of previous Th(III) complexes.[10,13–16,37]

The optimized structure of $(Cp'_3ThBr)^{1-}$ shows that it is less stable than Cp'_3Th by 2.2 kcal/mol. Further thermochemical calculations indicate that $[Cp'_3ThBr]^{1-}$ is unstable with respect to Cp'_3Th and Br^{1-}. Hence, these calculations are consistent with Cp'_3Th being the product of the reduction of Cp'_3ThBr.

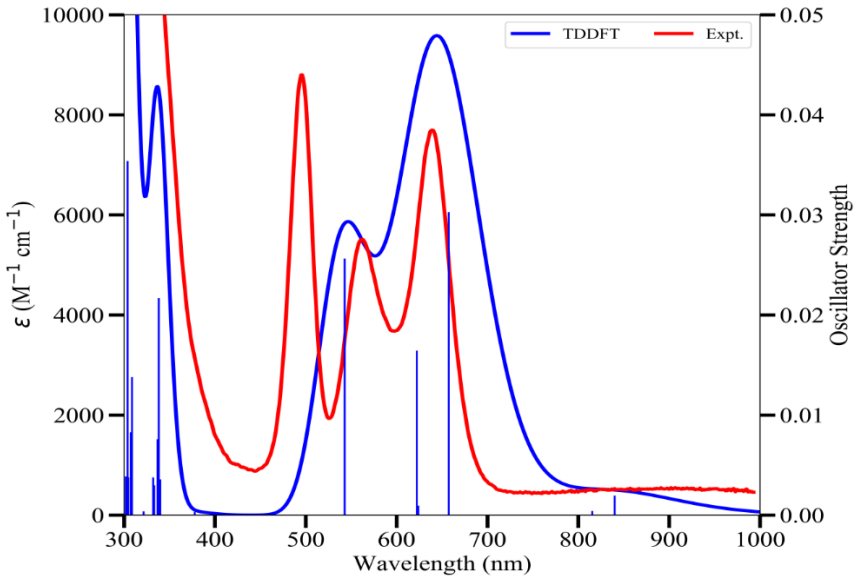

Figure 10.6: Experimental UV-visible spectrum of **A** in THF (red) scaled up by a factor of 50 compared to the simulated TDDFT spectrum of Cp'_3Th (blue). The computed electronic excitation spectrum was empirically blue-shifted by 0.4 eV and broadened using Gaussians with root mean squared width of 0.12 eV.

Further reduction of **A** to Th(II) was attempted. However, no green color was observed in reactions of Cp'_3ThBr with excess KC_8 or K in THF or toluene, or with **A** and another equivalent of KC_8 in THF, which would suggest the formation of Th(II) based on previous studies of $[Cp''_3Th]^{1-}$.[9,19]

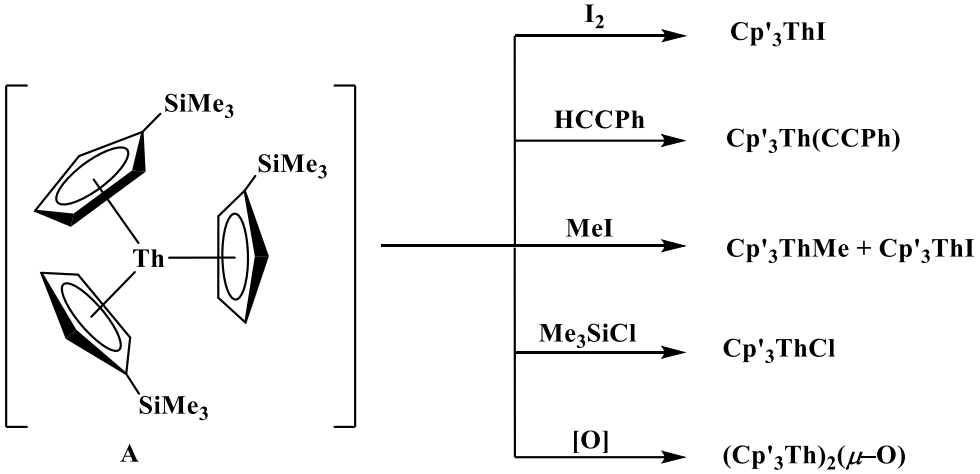

Scheme 10.1: Reactivity of solution **A**.

The reactivity of solution **A** was investigated. Addition of Me_3SiCl to the dark blue solution **A** formed by KC_8 reduction of Cp'_3ThBr gave Cp'_3ThCl as the major product, along with Cp'_3ThH in an 8:1 ratio and at least three other sets of unique Cp′ resonances.

Reaction of **A** with excess I_2[14] gave a color change to orange from which Cp'_3ThI and Cp'_3ThBr were identified by ^1H NMR spectroscopy in a 10:1 ratio, along with at least two other Cp′ environments. No Cp'_3ThH was observed in this reaction.

Addition of HC≡CPh to the dark blue solution **A** gave an immediate color change to orange. $Cp'_3Th(C{\equiv}CPh)$, Cp'_3ThBr, and Cp'_3ThH were identified in approximately 9:8:1 ratio by ^1H NMR spectroscopy. Small signals consistent with other Cp′ environments were also observed.

$Cp'_3Th(C{\equiv}CPh)$ was synthesized independently from Cp'_3ThBr and $LiC{\equiv}CPh$ in Et_2O to allow this characterization.

Addition of 1 drop of neat MeI to **A** immediately formed a colorless solution. The ^1H NMR spectrum contained numerous Cp′ resonances. Cp'_3ThMe, Cp'_3ThI, Cp'_3ThH, and Cp'_3ThBr could be identified in approximately a 4:1.5:1:9 ratio. This differs from the reactivity of $(C_5Me_5)_3Th$ with MeI, which cleanly affords a 2:3 mixture of $(C_5Me_5)_3ThMe$ and $(C_5Me_5)_3ThI$ in an overall yield of 75%.[14] All of these reactions are summarized in Scheme 10.1.

Although Cp'_3ThMe was reported in the literature in 1987,[18] it had not been characterized by X-ray crystallography. The structure was determined as part of this study, Figure 10.7. Cp'_3ThMe crystallizes in the $P\bar{3}$ space group and is another example of a tris(cyclopentadienyl)thorium methyl structure after Cp''_3ThMe[38] and $(C_5Me_5)_3ThMe$.[14] Cp'_3ThMe is isomorphous with Cp'_3ThBr[23] just as Cp''_3ThMe is isomorphous with Cp''_3ThCl.[39] Interestingly, Cp'_3ThCl does not readily crystallize in our hands. In the course of these studies, Cp'_3ThBr was crystallized in the space group $P2_1/c$, a different unit cell from the $P\bar{3}$ space group of the literature.[23]

An interesting structural feature of Cp'_3ThMe and Cp'_3ThBr in both space groups is that the three trimethylsilyl groups in each complex point in the same direction and form a pocket around the fourth ligand, Br or Me, Figure 10.7. The 2.559 Å Th–centroid distance in Cp'_3ThMe is surprisingly similar to the 2.569 Å Th–centroid distance in Cp''_3ThMe. Even more unusual is that the 2.518(3) Å Th–C(Me) distance of Cp'_3ThMe is longer than the 2.477(5) Å Th–C(Me) distance in Cp''_3ThMe, a complex with larger ligands.

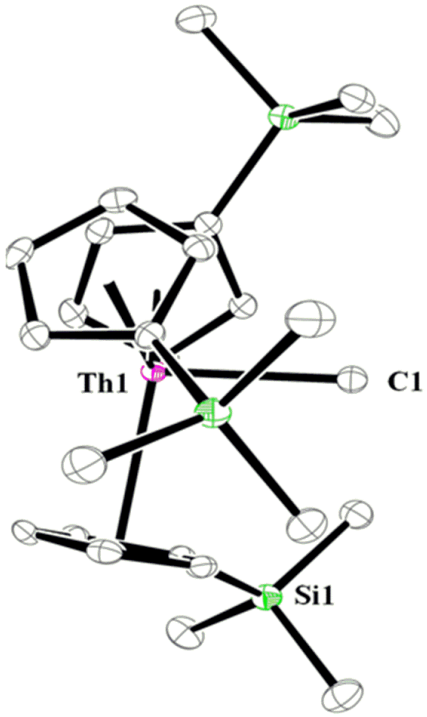

Figure 10.7: Thermal ellipsoid plot of Cp'_3ThMe with selective atom labelling. Ellipsoids are drawn at 50% probability level and hydrogen atoms have been omitted for clarity.

An oxide decomposition product was isolated from the reaction of **A** with C_8H_8. This reaction gave an immediate color change from blue to orange to yellow, but only colorless crystals of $(Cp'_3Th)_2(\mu\text{–}O)$ could be isolated from this reaction, Figure 10.8. The origin of the oxygen is unknown. Attempts to synthesize $(Cp'_3Th)_2(\mu\text{–}O)$ directly from Cp'_3ThMe and H_2O, or from **A** and H_2O,[9,40] TEMPO, pyridine-*N*-oxide,[41,42] and epoxybutane[41,42] were unsuccessful. In the reactions with H_2O or TEMPO, the ^1H NMR spectrum showed peaks consistent with a single Cp′ environment, but these products were not consistent across each reaction. The reactions with pyridine N-oxide and epoxybutane produced a complex mixture of products and were not pursued further.

$(Cp'_3Th)_2(\mu\text{–}O)$ is isomorphous with the uranium analog, $(Cp'_3U)_2(\mu\text{–}O)$.[43] The Th–O–Th angle is rigorously 180°, as the oxygen atom sits at an inversion center of the crystal. The

trimethylsilyl substituents are staggered when observed down the Th–O–Th axis. The Th–O distance in $(Cp'_3Th)_2(\mu–O)$ is approximately 0.04 Å larger than the U analog, while the Th–centroid distances are all approximately 0.06 Å larger than in $(Cp'_3U)_2(\mu–O)$. For comparison, the difference in the six-coordinate radii between Th(IV) and U(IV) is 0.08 Å.[44] The centroid–Th–centroid and centroid–Th–O angles are all similar to $(Cp'_3U)_2(\mu–O)$. Selected bond metrics are given in Table 10.2, while full details are given in Table 10.3 and 10.6.

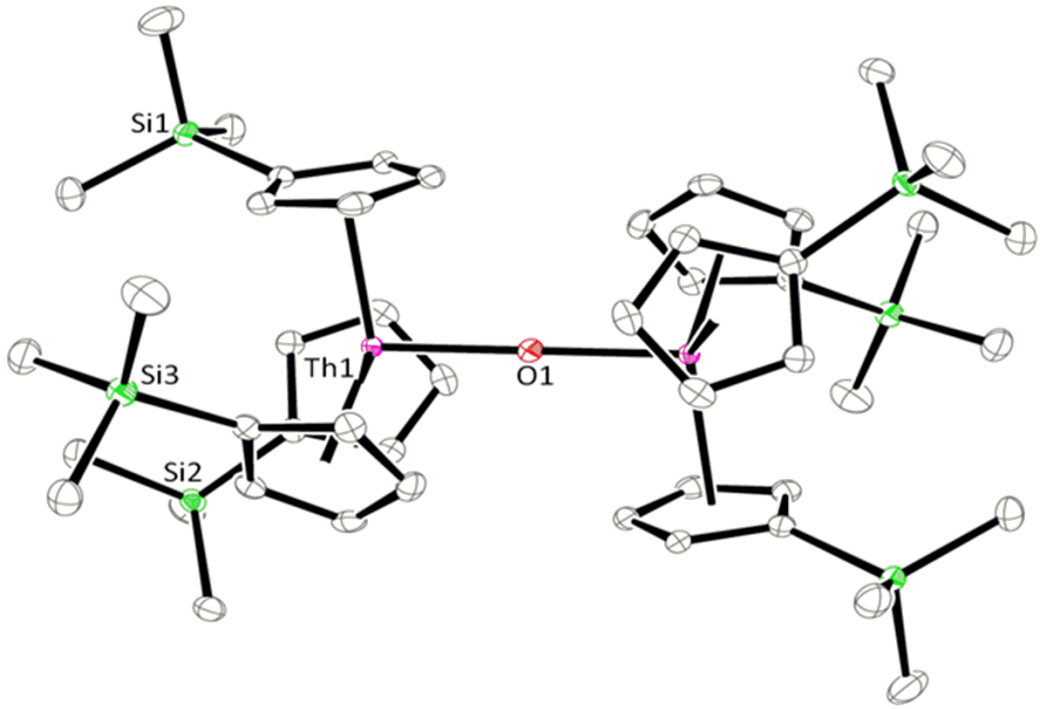

Figure 10.8: Thermal ellipsoid plot of $(Cp'_3Th)_2(\mu–O)$ with selective atom labelling. Ellipsoids are drawn at 50% probability level and hydrogen atoms have been omitted for clarity.

Table 10.2: Selected bond distances and angles of $(Cp'_3Th)_2(\mu\text{–}O)$ and $(Cp'_3U)_2(\mu\text{–}O)$.[36] Cnt is the Cp′ centroid.

	$(Cp'_3Th)_2(\mu\text{–}O)$	$(Cp'_3U)_2(\mu\text{–}O)$
M–O (Å)	2.1460(1)	2.1053(2)
M–cnt (Å)	2.595 2.587 2.594	2.527 2.534 2.536
Cnt–M–cnt (°)	117.6 117.4 117.5	117.2 116.9 117.7
Cnt–M–O (°)	98.6 98.8 100.1	99.4 99.0 100.4

Discussion

Reduction of Cp'_3ThX (X = Cl, Br, or I) with KC_8 yields a dark blue solution, **A**, that has the properties expected for Cp'_3Th. However, the instability of the complex in **A** precludes isolation and full crystallographic characterization. In contrast to other Th(III) complexes which are stable enough to be characterized by single crystal X-ray crystallography or solid-state methods such as elemental analysis, **A** decomposes within two hours at −35 °C with an approximate half-life of 5.5 min at room temperature and was not isolated.

EPR and UV-visible spectroscopy and DFT analysis support the proposed tris-cyclopentadienyl formulation. The EPR spectrum of **A** at 77 K in THF is consistent with a $6d^1$ ground state with g values $g_{\parallel} = 1.98$ and $g_{\perp} = 1.89$. The absorption spectrum of **A** in THF displays three strong features between 490 and 650 nm. TDDFT analysis on Cp'_3Th indicates that these transitions are mainly d-f transitions, consistent with theoretical analyses of other Th(III) complexes.[10,13–16,19,37]

Investigation of the reaction chemistry showed that **A** was not a viable precursor to $(Cp'_3Th)^{1-}$. However, solutions of **A** are extremely reactive. The dark blue solution quickly loses color upon addition of substrate and the reactions produce multiple thorium-containing products. These products were difficult to separate due to the high solubility imparted by the Cp′ ligand. However, NMR evidence was observed for the products expected from reactions of Cp'_3Th with Me_3SiCl, I_2, HC≡CPh, and MeI, Scheme 10.1.

The instability of Cp'_3Th can most likely be explained by the fact that the Cp′ ligands cannot stabilize the highly reactive Th(III) center due to their small size. The analogous actinide complexes Cp'_3U[35] and Cp'_3Np[34] can be isolated and fully characterized. This is presumably because the complexes are more sterically saturated, as U and Np are 0.08 and 0.10 Å smaller than Th, respectively,[44] and also because these An(III) ions are less reducing.

Conclusion

Reduction of Cp'_3ThCl, Cp'_3ThBr, and Cp'_3ThI with KC_8 affords a dark blue solution with properties consistent with the presence of Cp'_3Th as indicated by EPR and UV-visible spectroscopy, DFT calculations, and reactivity studies. Isolation of this complex has not been achieved, in contrast to Cp''_3Th.[5,6] Evidently, the smaller Cp′ ligand does not stabilize the Th(III) center well enough to allow isolation.

Experimental

Unless specifically stated, all syntheses and manipulations described below were conducted under Ar with rigorous exclusion of air and water using standard glovebox techniques. Solvents were sparged with UHP argon and dried by passage through columns containing Q-5 and molecular sieves prior to use. Deuterated NMR solvents were dried over NaK alloy, degassed by three freeze-pump-thaw cycles, and vacuum transferred before use. ^1H and $^{13}C\{^1H\}$ NMR spectra

were recorded on a CRYO500 MHz spectrometer ($^{13}C\{^{1}H\}$ operating at 125 MHz) at 298 K and referenced to residual protio-solvent resonances. UV-visible spectra were collected at 298 K using a Varian Cary 50 Scan UV-visible spectrophotometer in a 1 mm quartz cuvette. X-band EPR spectra were recorded on a Bruker EMX spectrometer equipped with an ER041Xg microwave bridge and calibrated with DPPH (g = 2.0036). Infrared spectra were recorded as compressed solids on an Agilent Cary 630 ATR-FTIR. Elemental analyses were conducted on a PerkinElmer 2400 Series II CHNS elemental analyzer. Electrochemical measurements were recorded with a Princeton Applied Research PARSTAT 2273 Advanced Electrochemical System. MeLi (Sigma) was purchased as a 1.6 M solution in diethyl ether, and solvent was removed to yield MeLi as a bright white solid. Me_3SiCl (Alfa Aesar) was used as received. I_2 was sublimed prior to use. MeI was dried over molecular sieves and vacuum transferred before use. Me_3SiI (Sigma) was dried over molecular sieves, distilled twice under vacuum, and kept under dinitrogen until use. KC_8[45] and Cp'_3ThCl[23] were synthesized following literature procedures. Electrochemical-grade [^{n}Bu$_4$N][BPh$_4$] (99%) was purchased from Sigma and used as received.

Synthesis of Cp'_3ThBr. This complex was prepared according to literature procedures.[23] ^{1}H NMR (toluene-d_8): δ 6.47 (m, 6H, $C_5H_4SiMe_3$), 6.36 (m, 6H, $C_5H_4SiMe_3$), 0.37 ppm (s, 27H, $SiMe_3$). ^{13}C NMR (C_6D_6): δ 128.67 ($C_5H_4SiMe_3$), 128.35 ($C_5H_4SiMe_3$), 121.72 ($C_5H_4SiMe_3$), 0.80 ppm ($SiMe_3$). Colorless X-ray quality crystals grown from a concentrated toluene solution at −35°C crystallized in the space group $P2_1/c$, different from the $P\bar{3}$ space group in the literature.[23]

Synthesis of Cp'_3ThMe.[21,22] A full experimental section is included here since it was not previously reported in the literature. MeLi (15 mg, 0.68 mmol) was tapped into a solution of Cp'_3ThBr (203 mg, 0.280 mmol) in Et_2O (5 mL). The colorless solution was stirred overnight at which point it had turned brown. Brown solids were removed via filtration and the solution was

dried under vacuum. The mixture was extracted into hexane and dried under vacuum to yield white solids of Cp'_3ThMe (130 mg, 70%). This reaction can also be run in toluene with similar yields, but requires 72 h to reach completion. Colorless X-ray-quality crystals were grown from a concentrated hexane solution at −35 °C. ^{1}H NMR (C_6D_6): δ 6.25 (m, 12H, $C_5H_4SiMe_3$), 0.77 (s, 3H, Th-*Me*), 0.34 ppm (s, 27H, Si*Me*$_3$). ^{13}C NMR (C_6D_6): δ 124.9 ($C_5H_4SiMe_3$), 124.2 ($C_5H_4SiMe_3$), 118.9 ($C_5H_4SiMe_3$), 37.0 (Th-*Me*), 0.40 ppm (Si*Me*$_3$). IR: 2949m, 1443m, 1402m, 1310w, 1246s, 1174s, 1086w, 1041s, 901s, 826s, 776s, 744s, 685m cm^{-1}. Anal. Calcd for $C_{25}H_{42}Si_3Th$: C, 45.57; H, 6.43. Found: C, 42.24; H, 5.94. Low combustion analysis was persistent across multiple samples and suggests incomplete combustion, which has been well-documented with some organoactinide complexes.[9,12,19,38,46–48] The C to H ratio in the analytical data gives a formula of $C_{25}H_{41.89}$ which is close to the calculated value of $C_{25}H_{42}$.

Synthesis of Cp'_3ThCl from Cp'_3ThMe and Me_3SiCl. Cp'_3ThMe (38 mg, 0.058 mmol) was dissolved in hexane (3 mL) to yield a colorless solution. Neat Me_3SiCl (3 drops, excess) was added and the colorless solution was stirred for 72 h. Volatiles were removed under vacuum to yield Cp'_3ThCl (35 mg, 89%), which was identified by ^{1}H NMR spectroscopy.[23]

Synthesis of Cp'_3ThI from Cp'_3ThMe and Me_3SiI. Inside the glovebox, Cp'_3ThMe (59 mg, 0.090 mmol) was dissolved in hexane (10 mL) and filtered into a side-arm Schlenk flask to give a pale yellow solution. The flask was brought out of the glovebox and attached to a Schlenk line. Under a flow of nitrogen, doubly-distilled Me_3SiI (15 μL, 0.11 mmol) was added to the stirring solution via microsyringe and the solution immediately became colorless. The solution was stirred for 40 h, at which point a tan precipitate had formed. Volatiles were removed under vacuum and the flask was brought into the glovebox. The solids were extracted with hexane and brown solids were removed via filtration. Removal of solvent yielded Cp'_3ThI as a colorless solid

(31 mg, 45%). ^{1}H NMR (C_6D_6): 6.63 (m, 6H, $C_5H_4SiMe_3$), 6.37 (m, 6H, $C_5H_4SiMe_3$), 0.38 ppm (s, 27H, SiMe_3). ^{1}H NMR (THF-d_8): 6.79 (m, 6H, $C_5H_4SiMe_3$), 6.58 (m, 6H, $C_5H_4SiMe_3$), 0.37 ppm (s, 27H, SiMe_3). ^{13}C NMR (THF-d_8): 130.50 ($C_5H_4SiMe_3$), 128.41 ($C_5H_4SiMe_3$), 122.34 ($C_5H_4SiMe_3$), 1.23 ppm (SiMe_3). IR: 3063w, 2949m, 2922m, 2893m, 2850m, 1442w, 1404w, 1366m, 1310w, 1244s, 1172s, 1117w, 1039s, 900s, 828s, 783s, 748s, 689m cm^{-1}. Anal. Calcd for $C_{24}H_{39}Si_3ThI$: C, 37.40; H, 5.10. Found: C, 37.82; H, 5.36.

Synthesis of Cp′$_3$Th(C≡CPh). LiC≡CPh (22 mg, 0.20 mmol) was tapped into a solution of Cp′$_3$ThBr (126 mg, 0.174 mmol) in Et_2O (5 ml). The colorless solution was stirred overnight. The solution was dried under vacuum, the mixture was extracted into hexane, and insoluble material was removed via filtration before drying under vacuum to yield Cp′$_3$Th(C≡CPh) as a colorless oil, which solidifies at −35 °C (101 mg, 78%). ^{1}H NMR (C_6D_6): δ 7.69 (d, 2H, *o–Ph*), 7.17 (t, 2H, *m–Ph*), 7.03 (t, 1H, *p–Ph*), 6.46 (m, 6H, $C_5H_4SiMe_3$), 6.34 (m, 6H, $C_5H_4SiMe_3$), 0.44 ppm (s, 27H, SiMe_3). ^{13}C NMR (C_6D_6): δ 157.01 (Th–*C*≡CPh), 131.77 ($C_5H_4SiMe_3$), 128.60, 127.64, 127.06, 126.25, 125.17 ($C_5H_4SiMe_3$), 122.24, 120.00 ($C_5H_4SiMe_3$), 0.83 ppm (SiMe_3). IR: 3076w, 2949m, 2891m, 2062m (C≡C), 1591m, 1482s, 1441m, 1404m, 1364s, 1310w, 1241s, 1195m,1173s, 1042s, 902s, 826s, 778s, 749s, 689s cm^{-1}. Anal. Calcd for $C_{32}H_{44}Si_3Th$: C, 51.59; H, 5.95. Found: C, 51.99; H, 6.35.

***In situ* synthesis of Cp′$_3$Th.** Cp′$_3$ThBr (50 mg, 0.069 mmol) was dissolved in THF (1 mL) and chilled to −35 °C. KC_8 (12 mg, 0.089 mmol) was chilled in a separate vial to −35 °C. KC_8 was tapped into the stirring solution of Cp′$_3$ThBr. This immediately generated a dark blue solution, **A**. KC_8 was removed either by filtration or centrifugation after stirring for no longer than 15 min, at which time the solution begins to visibly fade in intensity. Spectroscopic data were collected immediately from these solutions, but rapid decomposition occurs and hence the extinction

coefficients are probably not accurate. UV-visible (THF) λ_{max} nm (approx ε, $M^{-1}cm^{-1}$): 639 (150), 562 (110), 496 (180). EPR (THF, room temperature): g_{iso} = 1.90, (THF, 77 K): $g_{\parallel}$ = 1.98, $g_{\perp}$ = 1.89.

Synthesis of Cp′$_3$ThCl from A and Me$_3$SiCl. Cp′$_3$ThBr (51 mg, 0.070 mmol) in THF (1 mL) and KC_8 (11 mg, 0.081 mmol) were chilled in separate vials at −35 °C for two hours. The KC_8 was tapped into the colorless stirring solution of Cp′$_3$ThBr to form the dark blue solution **A.** Me_3SiCl (3 drops, excess) was added. No immediate color change occurred, so the solution was stirred for 40 min at which point the solution had become colorless. Black solids were removed via centrifugation and the colorless supernatant was dried under vacuum. Extraction into hexane and removal of solvent yielded white solids (36 mg). Cp′$_3$ThCl and Cp′$_3$ThH[22] were identified by ^{1}H NMR spectroscopy in an 8:1 ratio.

Synthesis of Cp′$_3$ThI from A and I$_2$. Following a similar procedure for the synthesis of Cp′$_3$ThClfrom **A**, Cp′$_3$ThBr (48 mg, 0.066 mmol) and KC_8 (11 mg, 0.081 mmol) were combined to form the solution **A**. A solution of I_2 (18 mg, 0.071 mmol) in THF (1 mL) was added dropwise. The mixture immediately turned orange. After stirring for 5 min, the solution was dried and the solids were extracted into hexane. The solvent was removed under vacuum to yield as yellow solids (47 mg), Cp′$_3$ThI and Cp′$_3$ThBr were identified by ^{1}H NMR spectroscopy in a 10:1 ratio, along with a small amount of other unidentifiable peaks.

Synthesis of Cp′$_3$Th(C≡CPh) from A and HC≡CPh. Following a similar procedure for the synthesis of Cp′$_3$ThCl from **A**, Cp′$_3$ThBr (50 mg, 0.069 mmol) and KC_8 (12 mg, 0.089 mmol) were combined to form solution **A**. HC≡CPh (1 drop) was added and the solution immediately became dark orange. After the solution was stirred for 5 min, volatiles were removed under vacuum to yield a dark oil. The oil was extracted into hexane to yield a green-brown solution.

This solution was filtered and dried to yield brown oily solids. $Cp'_3Th(C{\equiv}CPh)$ was identified by ^1H NMR spectroscopy.

Reaction of A and MeI. Following a similar procedure for the synthesis of Cp'_3ThCl from **A**, Cp'_3ThBr (51 mg, 0.070 mmol) and KC_8 (11 mg, 0.081 mmol) were combined to form the solution **A**. MeI (1 drop) was added and the solution immediately turned colorless. After stirring for 5 min, the solution was dried and the solids were extracted into hexane. The solvent was removed under vacuum to yield white solids (44 mg). The mixture contained Cp'_3ThMe and Cp'_3ThI in an approximate 2:3 ratio as determined by ^1H NMR spectroscopy. Cp'_3ThH and Cp'_3ThBr were also observed in the spectrum. Other unidentifiable peaks were also present.

Decomposition of A. Cp'_3ThBr (24 mg, 0.033 mmol) was dissolved in THF (1 mL). KC_8 (excess) was added and the solution immediately became the dark blue color of **A**. The solution was stirred at room temperature for 90 min at which point the solution had become colorless with black solids, presumably graphite. The solids were removed via centrifugation and the grey solution was dried under vacuum. The ^1H NMR spectrum in C_6D_6 displayed multiple unidentifiable peaks, along with Cp'_3ThH.[22] When the same reaction was done in THF-d_8, a similar ^1H NMR spectrum was observed. The ^2H spectrum displayed only THF-d_8 peaks.

Crystallization of $(Cp'_3Th)_2(\mu\text{–}O)$. Cp'_3ThBr (28 mg, 0.039 mmol) was dissolved in THF (1 mL) and chilled to −35 °C. In a separate vial, cyclooctatetrene (8.7 mg, 0.064 mmol) was dissolved in THF (1 mL) and chilled to −35 °C. A pipette was packed with KC_8 (9 mg, 0.064 *m*mol) and chilled to −35 °C. The colorless solution of Cp'_3ThBr was passed through the KC_8 pipette to form **A** and was directly eluted into the yellow stirring solution of C_8H_8. The mixture turned orange briefly before fading to yellow while it stirred. After stirring for 5 min, the solution was dried under vacuum to yield yellow and orange solids. The mixture was washed with hexane

then extracted into THF. Several colorless X-ray-quality crystals were grown from a concentrated THF solution of the mixture at −35 °C, which allowed $(Cp'_3Th)_2(\mu–O)$ to be identified by X-ray crystallography.

X-ray Data Collection, Structure Solution and Refinement for Cp'_3ThBr. A colorless crystal of approximate dimensions 0.194 x 0.199 x 0.258 mm was mounted on a glass fiber and transferred to a Bruker SMART APEX II diffractometer. The APEX2[49] program package was used to determine the unit-cell parameters and for data collection with a 25 sec/frame scan time. The raw frame data was processed using SAINT[50] and SADABS[51] to yield the reflection data file. Subsequent calculations were carried out using the SHELXTL[52] program. The diffraction symmetry was 2/*m* and the systematic absences were consistent with the monoclinic space group $P2_1/c$ that was later determined to be correct.

The structure was solved by direct methods and refined on F^2 by full-matrix least-squares techniques. The analytical scattering factors[53] for neutral atoms were used throughout the analysis. Hydrogen atoms were included using a riding model. There were two molecules of the formula-unit present.

Least-squares analysis yielded wR2 = 0.0687 and Goof = 1.073 for 541 variables refined against 13207 data (0.76 Å), R1 = 0.0286 for those 10983 data with $I > 2.0\sigma(I)$.

Table 10.3: Crystal data and structure refinement for Cp'_3ThBr, Cp'_3ThMe, and $(Cp'_3Th)_2(\mu–O)$.

	Cp'_3ThBr	Cp'_3ThMe	$(Cp'_3Th)_2(\mu–O)$
Identification code	jcw6	jcw4	jcw5
Empirical formula	$C_{24}H_{39}BrSi_3Th$	$C_{25}H_{42}Si_3Th$	$C_{48}H_{78}OSi_6Th_2$
Formula weight	723.77	658.89	1303.72
Temperature (K)	133(2)	88(2)	88(2)
Wavelength (Å)	0.71073	0.71073	0.71073
Crystal system	Monoclinic	Trigonal	Monoclinic

Space group	$P2_1/c$	$P\bar{3}$	$P2_1/c$
a (Å)	21.7256(15)	15.740(2)	9.5444(6)
b (Å)	16.9264(12)	15.740(2)	18.4598(11)
c (Å)	15.1850(10)	6.7581(9)	15.7099(1)
α (°)	90	90	90
β (°)	91.1625(8)	90	103.9575(7)
γ (°)	90	120	90
Volume ($Å^3$)	5582.9(7)	1450.0(4)	2686.2(3)
Z	8	2	2
Calc. Density (mg/m^3)	1.722	1.509	1.612
Absorption coefficient (mm^{-1})	6.911	5.275	5.695
F(000)	2800	648	1276
Crystal color	Colorless	Colorless	Colorless
Crystal size (mm^3)	0.258 x 0.199 x 0.194	0.247 x 0.145 x 0.143	0.329 x 0.205 x 0.112
θ range for data collection (°)	1.525 to 27.894	1.494 to 29.104	1.732 to 29.155
Index ranges	$-28 \leq h \leq 28$, $-21 \leq k \leq 22$, $-19 \leq l \leq 19$	$-21 \leq h \leq 20$, $-20 \leq k \leq 20$, $-8 \leq l \leq 9$	$-13 \leq h \leq 12$, $-24 \leq k \leq 23$, $-20 \leq l \leq 20$
Reflections collected	65691	17774	32844
Independent reflections	13207	2483	6849
Completeness to θ = 25.500°	99.9%	100.0%	100.0%
Absorption correction	Semi-empirical from equivalents	Semi-empirical from equivalents	Semi-empirical from equivalents
Max. and min. transmission	0.4308 and 0.2963	0.4318 and 0.3061	0.4319 and 0.3096
Refinement method	Full-matrix least-squares on F^2	Full-matrix least-squares on F^2	Full-matrix least-squares on F^2
Data / restraints / parameters	13207 / 0 / 541	2483 / 0 / 91	6849 / 0 / 415
Goodness-of-fit on F^2	1.073	1.046	1.037
Final R indices [$I>2\sigma(I)$ = 10983 data]	R1 = 0.0286, wR2 = 0.0656	R1 = 0.0143, wR2 = 0.0298	R1 = 0.0162, wR2 = 0.0320

R indices (all data)	R1 = 0.0372, wR2 = 0.0687	R1 = 0.0162, wR2 = 0.0303	R1 = 0.0201, wR2 = 0.0331
Data cutoff (Å)	0.76	0.73	0.73
Largest diff. peak and hole	3.725 and -1.641 e.Å^{-3}	0.664 and −0.424 e.Å^{-3}	0.565 and −0.498 e.Å^{-3}

Table 9.4: Bond lengths [Å] and angles [°] for Cp'_3ThBr.

Th(1)-Cnt1	2.537	Si(3)-C(24)	1.861(5)
Th(1)-Cnt2	2.539	Si(3)-C(17)	1.868(4)
Th(1)-Cnt3	2.546	C(1)-C(2)	1.425(6)
Th(1)-C(19)	2.775(4)	C(1)-C(5)	1.432(5)
Th(1)-C(3)	2.776(4)	C(2)-C(3)	1.405(6)
Th(1)-C(11)	2.788(4)	C(3)-C(4)	1.414(6)
Th(1)-C(4)	2.792(4)	C(4)-C(5)	1.401(6)
Th(1)-C(20)	2.792(4)	C(9)-C(13)	1.422(5)
Th(1)-C(12)	2.798(4)	C(9)-C(10)	1.423(6)
Th(1)-C(13)	2.803(4)	C(10)-C(11)	1.406(6)
Th(1)-C(5)	2.811(4)	C(11)-C(12)	1.412(6)
Th(1)-C(2)	2.819(4)	C(12)-C(13)	1.391(6)
Th(1)-C(10)	2.819(4)	C(17)-C(21)	1.423(5)
Th(1)-C(21)	2.826(4)	C(17)-C(18)	1.433(6)
Th(1)-C(18)	2.826(4)	C(18)-C(19)	1.408(6)
Th(1)-C(9)	2.834(4)	C(19)-C(20)	1.418(6)
Th(1)-C(1)	2.840(4)	C(20)-C(21)	1.395(6)
Th(1)-Br(1)	2.8515(4)	Th(2)-Cnt4	2.544
Th(1)-C(17)	2.864(4)	Th(2)-Cnt5	2.547
Si(1)-C(7)	1.854(4)	Th(2)-Cnt6	2.544
Si(1)-C(6)	1.858(4)	Th(2)-C(43)	2.772(4)
Si(1)-C(1)	1.874(4)	Th(2)-C(27)	2.776(4)
Si(1)-C(8)	1.874(5)	Th(2)-C(35)	2.784(4)
Si(2)-C(15)	1.853(4)	Th(2)-C(36)	2.798(4)
Si(2)-C(14)	1.864(4)	Th(2)-C(26)	2.803(4)
Si(2)-C(16)	1.867(5)	Th(2)-C(44)	2.808(4)
Si(2)-C(9)	1.884(4)	Th(2)-C(42)	2.817(4)
Si(3)-C(23)	1.853(5)	Th(2)-C(28)	2.822(4)
Si(3)-C(22)	1.859(6)	Th(2)-C(37)	2.823(4)

Th(2)-C(34)	2.827(4)	Cnt2-Th(1)-Br(1)	101.5
Th(2)-C(29)	2.828(4)	Cnt3-Th(1)-Br(1)	100.8
Th(2)-C(45)	2.831(4)	Cnt1-Th(1)-Cnt2	116.2
Th(2)-C(25)	2.839(4)	Cnt1-Th(1)-Cnt3	116.8
Th(2)-Br(2)	2.8450(4)	Cnt2-Th(1)-Cnt3	116.0
Th(2)-C(41)	2.846(4)	C(19)-Th(1)-C(3)	90.66(12)
Th(2)-C(33)	2.853(4)	C(19)-Th(1)-C(11)	88.20(13)
Si(4)-C(31)	1.854(6)	C(3)-Th(1)-C(11)	87.98(13)
Si(4)-C(30)	1.857(5)	C(19)-Th(1)-C(4)	92.41(12)
Si(4)-C(32)	1.858(6)	C(3)-Th(1)-C(4)	29.42(13)
Si(4)-C(25)	1.869(4)	C(11)-Th(1)-C(4)	117.38(12)
Si(5)-C(39)	1.857(5)	C(19)-Th(1)-C(20)	29.51(12)
Si(5)-C(33)	1.865(4)	C(3)-Th(1)-C(20)	120.02(12)
Si(5)-C(40)	1.866(4)	C(11)-Th(1)-C(20)	92.16(13)
Si(5)-C(38)	1.875(5)	C(4)-Th(1)-C(20)	116.11(12)
Si(6)-C(48)	1.858(5)	C(19)-Th(1)-C(12)	117.34(13)
Si(6)-C(46)	1.866(5)	C(3)-Th(1)-C(12)	90.59(13)
Si(6)-C(41)	1.873(4)	C(11)-Th(1)-C(12)	29.29(13)
Si(6)-C(47)	1.874(4)	C(4)-Th(1)-C(12)	115.44(12)
C(25)-C(29)	1.421(6)	C(20)-Th(1)-C(12)	115.74(12)
C(25)-C(26)	1.422(6)	C(19)-Th(1)-C(13)	121.97(12)
C(26)-C(27)	1.411(6)	C(3)-Th(1)-C(13)	117.76(12)
C(27)-C(28)	1.413(6)	C(11)-Th(1)-C(13)	47.88(12)
C(28)-C(29)	1.402(6)	C(4)-Th(1)-C(13)	137.23(12)
C(33)-C(34)	1.422(5)	C(20)-Th(1)-C(13)	105.25(12)
C(33)-C(37)	1.434(6)	C(12)-Th(1)-C(13)	28.76(11)
C(34)-C(35)	1.408(6)	C(19)-Th(1)-C(5)	119.42(12)
C(35)-C(36)	1.409(6)	C(3)-Th(1)-C(5)	47.99(12)
C(36)-C(37)	1.398(6)	C(11)-Th(1)-C(5)	123.74(12)
C(41)-C(45)	1.424(5)	C(4)-Th(1)-C(5)	28.96(11)
C(41)-C(42)	1.428(6)	C(20)-Th(1)-C(5)	136.55(12)
C(42)-C(43)	1.414(6)	C(12)-Th(1)-C(5)	106.61(11)
C(43)-C(44)	1.411(6)	C(13)-Th(1)-C(5)	116.80(11)
C(44)-C(45)	1.400(6)	C(19)-Th(1)-C(2)	116.46(12)
		C(3)-Th(1)-C(2)	29.07(12)
Cnt1-Th(1)-Br(1)	101.2	C(11)-Th(1)-C(2)	76.57(12)

C(4)-Th(1)-C(2)	47.96(12)	C(3)-Th(1)-C(9)	135.62(12)
C(20)-Th(1)-C(2)	145.50(12)	C(11)-Th(1)-C(9)	48.42(11)
C(12)-Th(1)-C(2)	67.51(12)	C(4)-Th(1)-C(9)	163.53(12)
C(13)-Th(1)-C(2)	91.27(12)	C(20)-Th(1)-C(9)	76.05(12)
C(5)-Th(1)-C(2)	47.63(12)	C(12)-Th(1)-C(9)	48.17(11)
C(19)-Th(1)-C(10)	75.31(13)	C(13)-Th(1)-C(9)	29.21(11)
C(3)-Th(1)-C(10)	113.64(13)	C(5)-Th(1)-C(9)	145.34(11)
C(11)-Th(1)-C(10)	29.03(12)	C(2)-Th(1)-C(9)	115.68(12)
C(4)-Th(1)-C(10)	142.12(12)	C(10)-Th(1)-C(9)	29.16(11)
C(20)-Th(1)-C(10)	68.04(12)	C(21)-Th(1)-C(9)	90.61(11)
C(12)-Th(1)-C(10)	47.72(12)	C(18)-Th(1)-C(9)	122.44(12)
C(13)-Th(1)-C(10)	47.54(12)	C(19)-Th(1)-C(1)	138.26(12)
C(5)-Th(1)-C(10)	152.40(12)	C(3)-Th(1)-C(1)	48.52(12)
C(2)-Th(1)-C(10)	105.60(12)	C(11)-Th(1)-C(1)	97.25(12)
C(19)-Th(1)-C(21)	47.91(12)	C(4)-Th(1)-C(1)	48.52(11)
C(3)-Th(1)-C(21)	123.90(12)	C(20)-Th(1)-C(1)	164.54(12)
C(11)-Th(1)-C(21)	119.75(12)	C(12)-Th(1)-C(1)	77.27(11)
C(4)-Th(1)-C(21)	105.24(12)	C(13)-Th(1)-C(1)	90.14(11)
C(20)-Th(1)-C(21)	28.76(12)	C(5)-Th(1)-C(1)	29.36(11)
C(12)-Th(1)-C(21)	137.89(11)	C(2)-Th(1)-C(1)	29.15(11)
C(13)-Th(1)-C(21)	116.53(11)	C(10)-Th(1)-C(1)	124.11(12)
C(5)-Th(1)-C(21)	114.40(12)	C(21)-Th(1)-C(1)	142.82(11)
C(2)-Th(1)-C(21)	152.12(12)	C(18)-Th(1)-C(1)	116.81(11)
C(10)-Th(1)-C(21)	92.89(12)	C(9)-Th(1)-C(1)	119.31(11)
C(19)-Th(1)-C(18)	29.10(12)	C(19)-Th(1)-Br(1)	125.46(9)
C(3)-Th(1)-C(18)	77.66(12)	C(3)-Th(1)-Br(1)	126.24(9)
C(11)-Th(1)-C(18)	113.32(12)	C(11)-Th(1)-Br(1)	126.30(9)
C(4)-Th(1)-C(18)	68.30(12)	C(4)-Th(1)-Br(1)	103.01(9)
C(20)-Th(1)-C(18)	47.84(12)	C(20)-Th(1)-Br(1)	100.68(8)
C(12)-Th(1)-C(18)	142.03(12)	C(12)-Th(1)-Br(1)	102.44(9)
C(13)-Th(1)-C(18)	150.77(12)	C(13)-Th(1)-Br(1)	78.49(8)
C(5)-Th(1)-C(18)	92.12(12)	C(5)-Th(1)-Br(1)	78.45(8)
C(2)-Th(1)-C(18)	106.74(12)	C(2)-Th(1)-Br(1)	112.34(8)
C(10)-Th(1)-C(18)	104.37(12)	C(10)-Th(1)-Br(1)	113.37(8)
C(21)-Th(1)-C(18)	47.33(11)	C(21)-Th(1)-Br(1)	77.55(8)
C(19)-Th(1)-C(9)	95.06(12)	C(18)-Th(1)-Br(1)	113.70(8)

C(9)-Th(1)-Br(1)	84.49(8)	C(2)-C(1)-Si(1)	130.3(3)
C(1)-Th(1)-Br(1)	83.58(8)	C(5)-C(1)-Si(1)	122.8(3)
C(19)-Th(1)-C(17)	48.54(12)	C(2)-C(1)-Th(1)	74.6(2)
C(3)-Th(1)-C(17)	96.91(12)	C(5)-C(1)-Th(1)	74.2(2)
C(11)-Th(1)-C(17)	136.32(12)	Si(1)-C(1)-Th(1)	126.68(17)
C(4)-Th(1)-C(17)	76.28(12)	C(3)-C(2)-C(1)	109.3(4)
C(20)-Th(1)-C(17)	48.18(11)	C(3)-C(2)-Th(1)	73.7(2)
C(12)-Th(1)-C(17)	163.81(12)	C(1)-C(2)-Th(1)	76.2(2)
C(13)-Th(1)-C(17)	145.06(11)	C(2)-C(3)-C(4)	108.0(4)
C(5)-Th(1)-C(17)	88.97(11)	C(2)-C(3)-Th(1)	77.2(2)
C(2)-Th(1)-C(17)	123.54(12)	C(4)-C(3)-Th(1)	75.9(2)
C(10)-Th(1)-C(17)	116.13(12)	C(5)-C(4)-C(3)	107.7(4)
C(21)-Th(1)-C(17)	28.96(11)	C(5)-C(4)-Th(1)	76.3(2)
C(18)-Th(1)-C(17)	29.16(11)	C(3)-C(4)-Th(1)	74.7(2)
C(9)-Th(1)-C(17)	119.41(11)	C(4)-C(5)-C(1)	109.5(4)
C(1)-Th(1)-C(17)	118.30(11)	C(4)-C(5)-Th(1)	74.8(2)
Br(1)-Th(1)-C(17)	84.67(8)	C(1)-C(5)-Th(1)	76.4(2)
C(7)-Si(1)-C(6)	108.1(2)	C(13)-C(9)-C(10)	105.6(3)
C(7)-Si(1)-C(1)	115.99(18)	C(13)-C(9)-Si(2)	123.4(3)
C(6)-Si(1)-C(1)	107.19(19)	C(10)-C(9)-Si(2)	129.2(3)
C(7)-Si(1)-C(8)	108.1(2)	C(13)-C(9)-Th(1)	74.2(2)
C(6)-Si(1)-C(8)	110.2(2)	C(10)-C(9)-Th(1)	74.9(2)
C(1)-Si(1)-C(8)	107.32(19)	Si(2)-C(9)-Th(1)	127.73(18)
C(15)-Si(2)-C(14)	108.6(2)	C(11)-C(10)-C(9)	109.2(4)
C(15)-Si(2)-C(16)	107.5(2)	C(11)-C(10)-Th(1)	74.3(2)
C(14)-Si(2)-C(16)	111.3(2)	C(9)-C(10)-Th(1)	76.0(2)
C(15)-Si(2)-C(9)	115.53(18)	C(10)-C(11)-C(12)	107.5(4)
C(14)-Si(2)-C(9)	107.8(2)	C(10)-C(11)-Th(1)	76.7(2)
C(16)-Si(2)-C(9)	106.14(19)	C(12)-C(11)-Th(1)	75.7(2)
C(23)-Si(3)-C(22)	106.7(3)	C(13)-C(12)-C(11)	108.1(4)
C(23)-Si(3)-C(24)	108.3(3)	C(13)-C(12)-Th(1)	75.8(2)
C(22)-Si(3)-C(24)	109.3(3)	C(11)-C(12)-Th(1)	75.0(2)
C(23)-Si(3)-C(17)	116.1(2)	C(12)-C(13)-C(9)	109.6(4)
C(22)-Si(3)-C(17)	107.8(2)	C(12)-C(13)-Th(1)	75.4(2)
C(24)-Si(3)-C(17)	108.5(2)	C(9)-C(13)-Th(1)	76.6(2)
C(2)-C(1)-C(5)	105.4(3)	C(21)-C(17)-C(18)	105.2(4)

C(21)-C(17)-Si(3)	123.4(3)	C(36)-Th(2)-C(44)	115.68(12)
C(18)-C(17)-Si(3)	129.1(3)	C(26)-Th(2)-C(44)	138.86(12)
C(21)-C(17)-Th(1)	74.0(2)	C(43)-Th(2)-C(42)	29.31(12)
C(18)-C(17)-Th(1)	74.0(2)	C(27)-Th(2)-C(42)	74.52(12)
Si(3)-C(17)-Th(1)	130.13(18)	C(35)-Th(2)-C(42)	116.51(13)
C(19)-C(18)-C(17)	109.4(4)	C(36)-Th(2)-C(42)	144.59(12)
C(19)-C(18)-Th(1)	73.4(2)	C(26)-Th(2)-C(42)	103.80(12)
C(17)-C(18)-Th(1)	76.9(2)	C(44)-Th(2)-C(42)	47.76(12)
C(18)-C(19)-C(20)	107.4(4)	C(43)-Th(2)-C(28)	89.87(13)
C(18)-C(19)-Th(1)	77.5(2)	C(27)-Th(2)-C(28)	29.22(12)
C(20)-C(19)-Th(1)	75.9(2)	C(35)-Th(2)-C(28)	119.97(13)
C(21)-C(20)-C(19)	107.9(4)	C(36)-Th(2)-C(28)	115.54(12)
C(21)-C(20)-Th(1)	77.0(2)	C(26)-Th(2)-C(28)	47.79(12)
C(19)-C(20)-Th(1)	74.6(2)	C(44)-Th(2)-C(28)	114.66(12)
C(20)-C(21)-C(17)	110.1(4)	C(42)-Th(2)-C(28)	66.98(12)
C(20)-C(21)-Th(1)	74.3(2)	C(43)-Th(2)-C(37)	126.82(12)
C(17)-C(21)-Th(1)	77.0(2)	C(27)-Th(2)-C(37)	119.38(12)
Cnt4-Th(2)-Br(2)	102.7	C(35)-Th(2)-C(37)	47.87(12)
Cnt5-Th(2)-Br(2)	100.0	C(36)-Th(2)-C(37)	28.79(11)
Cnt6-Th(2)-Br(2)	100.9	C(26)-Th(2)-C(37)	91.54(12)
Cnt4-Th(1)-Cnt5	116.1	C(44)-Th(2)-C(37)	108.53(12)
Cnt4-Th(1)-Cnt6	115.4	C(42)-Th(2)-C(37)	155.32(12)
Cnt5-Th(1)-Cnt6	117.5	C(28)-Th(2)-C(37)	135.38(12)
C(43)-Th(2)-C(27)	85.37(13)	C(43)-Th(2)-C(34)	79.66(13)
C(43)-Th(2)-C(35)	89.65(13)	C(27)-Th(2)-C(34)	116.97(13)
C(27)-Th(2)-C(35)	91.03(13)	C(35)-Th(2)-C(34)	29.06(13)
C(43)-Th(2)-C(36)	118.89(13)	C(36)-Th(2)-C(34)	47.64(12)
C(27)-Th(2)-C(36)	92.68(12)	C(26)-Th(2)-C(34)	106.03(12)
C(35)-Th(2)-C(36)	29.24(13)	C(44)-Th(2)-C(34)	68.25(12)
C(43)-Th(2)-C(26)	110.62(13)	C(42)-Th(2)-C(34)	108.87(12)
C(27)-Th(2)-C(26)	29.30(12)	C(28)-Th(2)-C(34)	145.95(12)
C(35)-Th(2)-C(26)	76.97(13)	C(37)-Th(2)-C(34)	47.41(12)
C(36)-Th(2)-C(26)	67.84(12)	C(43)-Th(2)-C(29)	117.66(13)
C(43)-Th(2)-C(44)	29.28(13)	C(27)-Th(2)-C(29)	47.79(12)
C(27)-Th(2)-C(44)	114.64(12)	C(35)-Th(2)-C(29)	122.92(13)
C(35)-Th(2)-C(44)	90.21(13)	C(36)-Th(2)-C(29)	104.07(12)

C(26)-Th(2)-C(29)	47.36(12)	C(28)-Th(2)-Br(2)	101.95(9)
C(44)-Th(2)-C(29)	138.00(12)	C(37)-Th(2)-Br(2)	77.70(8)
C(42)-Th(2)-C(29)	91.61(12)	C(34)-Th(2)-Br(2)	110.41(8)
C(28)-Th(2)-C(29)	28.73(12)	C(29)-Th(2)-Br(2)	79.30(9)
C(37)-Th(2)-C(29)	112.89(12)	C(45)-Th(2)-Br(2)	78.65(8)
C(34)-Th(2)-C(29)	150.86(12)	C(25)-Th(2)-Br(2)	86.87(8)
C(43)-Th(2)-C(45)	47.94(12)	C(43)-Th(2)-C(41)	48.72(12)
C(27)-Th(2)-C(45)	121.68(12)	C(27)-Th(2)-C(41)	96.09(12)
C(35)-Th(2)-C(45)	116.55(13)	C(35)-Th(2)-C(41)	136.64(13)
C(36)-Th(2)-C(45)	136.35(12)	C(36)-Th(2)-C(41)	163.81(12)
C(26)-Th(2)-C(45)	150.92(12)	C(26)-Th(2)-C(41)	123.80(12)
C(44)-Th(2)-C(45)	28.75(11)	C(44)-Th(2)-C(41)	48.18(11)
C(42)-Th(2)-C(45)	47.42(12)	C(42)-Th(2)-C(41)	29.21(11)
C(28)-Th(2)-C(45)	106.50(12)	C(28)-Th(2)-C(41)	77.50(12)
C(37)-Th(2)-C(45)	116.84(11)	C(37)-Th(2)-C(41)	144.46(11)
C(34)-Th(2)-C(45)	90.35(12)	C(34)-Th(2)-C(41)	116.18(12)
C(29)-Th(2)-C(45)	118.74(12)	C(29)-Th(2)-C(41)	91.87(12)
C(43)-Th(2)-C(25)	133.67(13)	C(45)-Th(2)-C(41)	29.06(11)
C(27)-Th(2)-C(25)	48.64(12)	C(25)-Th(2)-C(41)	120.79(11)
C(35)-Th(2)-C(25)	95.59(13)	Br(2)-Th(2)-C(41)	82.71(8)
C(36)-Th(2)-C(25)	75.05(12)	C(43)-Th(2)-C(33)	100.79(13)
C(26)-Th(2)-C(25)	29.18(11)	C(27)-Th(2)-C(33)	138.42(12)
C(44)-Th(2)-C(25)	162.22(12)	C(35)-Th(2)-C(33)	48.41(12)
C(42)-Th(2)-C(25)	115.13(12)	C(36)-Th(2)-C(33)	48.21(12)
C(28)-Th(2)-C(25)	48.21(12)	C(26)-Th(2)-C(33)	116.05(12)
C(37)-Th(2)-C(25)	87.61(11)	C(44)-Th(2)-C(33)	79.37(12)
C(34)-Th(2)-C(25)	122.05(12)	C(42)-Th(2)-C(33)	126.87(12)
C(29)-Th(2)-C(25)	29.05(11)	C(28)-Th(2)-C(33)	163.53(12)
C(45)-Th(2)-C(25)	147.51(11)	C(37)-Th(2)-C(33)	29.26(11)
C(43)-Th(2)-Br(2)	126.26(9)	C(34)-Th(2)-C(33)	28.99(11)
C(27)-Th(2)-Br(2)	127.07(9)	C(29)-Th(2)-C(33)	141.25(12)
C(35)-Th(2)-Br(2)	125.19(9)	C(45)-Th(2)-C(33)	89.94(11)
C(36)-Th(2)-Br(2)	102.74(8)	C(25)-Th(2)-C(33)	116.83(11)
C(26)-Th(2)-Br(2)	115.94(8)	Br(2)-Th(2)-C(33)	81.92(8)
C(44)-Th(2)-Br(2)	103.48(9)	C(41)-Th(2)-C(33)	118.96(11)
C(42)-Th(2)-Br(2)	111.36(8)	C(31)-Si(4)-C(30)	109.2(3)

C(31)-Si(4)-C(32)	110.0(3)	C(34)-C(33)-Si(5)	127.6(3)
C(30)-Si(4)-C(32)	107.1(3)	C(37)-C(33)-Si(5)	125.1(3)
C(31)-Si(4)-C(25)	111.5(2)	C(34)-C(33)-Th(2)	74.5(2)
C(30)-Si(4)-C(25)	106.6(2)	C(37)-C(33)-Th(2)	74.2(2)
C(32)-Si(4)-C(25)	112.3(2)	Si(5)-C(33)-Th(2)	128.49(18)
C(39)-Si(5)-C(33)	107.9(2)	C(35)-C(34)-C(33)	109.6(4)
C(39)-Si(5)-C(40)	107.2(2)	C(35)-C(34)-Th(2)	73.8(2)
C(33)-Si(5)-C(40)	115.33(19)	C(33)-C(34)-Th(2)	76.5(2)
C(39)-Si(5)-C(38)	110.1(2)	C(34)-C(35)-C(36)	107.5(4)
C(33)-Si(5)-C(38)	108.2(2)	C(34)-C(35)-Th(2)	77.2(2)
C(40)-Si(5)-C(38)	108.0(2)	C(36)-C(35)-Th(2)	75.9(2)
C(48)-Si(6)-C(46)	109.1(3)	C(37)-C(36)-C(35)	108.3(4)
C(48)-Si(6)-C(41)	115.3(2)	C(37)-C(36)-Th(2)	76.6(2)
C(46)-Si(6)-C(41)	107.0(2)	C(35)-C(36)-Th(2)	74.8(2)
C(48)-Si(6)-C(47)	107.5(2)	C(36)-C(37)-C(33)	109.2(4)
C(46)-Si(6)-C(47)	109.4(3)	C(36)-C(37)-Th(2)	74.6(2)
C(41)-Si(6)-C(47)	108.41(19)	C(33)-C(37)-Th(2)	76.5(2)
C(29)-C(25)-C(26)	105.4(4)	C(45)-C(41)-C(42)	105.5(3)
C(29)-C(25)-Si(4)	122.9(3)	C(45)-C(41)-Si(6)	122.8(3)
C(26)-C(25)-Si(4)	128.5(3)	C(42)-C(41)-Si(6)	129.9(3)
C(29)-C(25)-Th(2)	75.1(2)	C(45)-C(41)-Th(2)	74.9(2)
C(26)-C(25)-Th(2)	74.0(2)	C(42)-C(41)-Th(2)	74.3(2)
Si(4)-C(25)-Th(2)	131.70(18)	Si(6)-C(41)-Th(2)	127.53(18)
C(27)-C(26)-C(25)	109.5(4)	C(43)-C(42)-C(41)	109.2(4)
C(27)-C(26)-Th(2)	74.3(2)	C(43)-C(42)-Th(2)	73.6(2)
C(25)-C(26)-Th(2)	76.8(2)	C(41)-C(42)-Th(2)	76.5(2)
C(26)-C(27)-C(28)	107.6(4)	C(44)-C(43)-C(42)	107.4(4)
C(26)-C(27)-Th(2)	76.4(2)	C(44)-C(43)-Th(2)	76.8(2)
C(28)-C(27)-Th(2)	77.2(2)	C(42)-C(43)-Th(2)	77.1(2)
C(29)-C(28)-C(27)	107.5(4)	C(45)-C(44)-C(43)	108.2(4)
C(29)-C(28)-Th(2)	75.9(2)	C(45)-C(44)-Th(2)	76.5(2)
C(27)-C(28)-Th(2)	73.6(2)	C(43)-C(44)-Th(2)	73.9(2)
C(28)-C(29)-C(25)	109.9(4)	C(44)-C(45)-C(41)	109.6(4)
C(28)-C(29)-Th(2)	75.4(2)	C(44)-C(45)-Th(2)	74.7(2)
C(25)-C(29)-Th(2)	75.9(2)	C(41)-C(45)-Th(2)	76.1(2)
C(34)-C(33)-C(37)	105.4(4)		

X-ray Data Collection, Structure Solution and Refinement for Cp′$_3$ThMe. A colorless crystal of approximate dimensions 0.143 x 0.145 x 0.247 mm was mounted in a cryoloop and transferred to a Bruker SMART APEX II diffractometer. The APEX2[49] program package was used to determine the unit-cell parameters and for data collection with 20 sec/frame scan time. The raw frame data was processed using SAINT[50] and SADABS[51] to yield the reflection data file. The systematic absences were consistent with the trigonal space groups $P3$ and $P\bar{3}$. The centrosymmetric space group $P\bar{3}$ was assigned and later determined to be correct.

The structure was solved by dual space methods and refined on F^2 by full-matrix least-squares techniques. The analytical scattering factors[53] for neutral atoms were used throughout the analysis. Hydrogen atoms were included using a riding model. The molecule was located on a three-fold rotation axis.

Least-squares analysis yielded wR2 = 0.0303 and Goof = 1.046 for 91 variables refined against 2483 data (0.73 Å), R1 = 0.0143 for those 2357 data with $I > 2.0\sigma(I)$.

There were several high residuals present in the final difference-Fourier map. It was not possible to determine the nature of the residuals although it was probable that diethyl ether solvent was present. The SQUEEZE[54] routine in the PLATON[55] program package was used to account for the electrons in the solvent accessible voids.

Table 9.5: Bond lengths [Å] and angles [°] for Cp′$_3$ThMe. Symmetry transformations used to generate equivalent atoms: #1 -y+1,x-y,z #2 -x+y+1,-x+1,z

Th(1)-Cnt	2.559	Th(1)-C(5)#2	2.8081(17)
Th(1)-C(1)	2.518(3)	Th(1)-C(3)#2	2.8307(17)
Th(1)-C(4)	2.7923(16)	Th(1)-C(3)#1	2.8307(17)
Th(1)-C(4)#1	2.7923(17)	Th(1)-C(3)	2.8307(17)
Th(1)-C(4)#2	2.7923(17)	Th(1)-C(6)	2.8409(16)
Th(1)-C(5)	2.8081(17)	Th(1)-C(6)#1	2.8409(16)
Th(1)-C(5)#1	2.8081(17)	Th(1)-C(6)#2	2.8409(16)

Th(1)-C(2)	2.8713(17)
Th(1)-C(2)#1	2.8714(17)
Si(1)-C(7)	1.8667(19)
Si(1)-C(8)	1.868(2)
Si(1)-C(9)	1.8798(19)
Si(1)-C(2)	1.8825(17)
C(2)-C(3)	1.425(2)
C(2)-C(6)	1.429(2)
C(3)-C(4)	1.408(2)
C(4)-C(5)	1.414(2)
C(5)-C(6)	1.407(2)

Cnt-Th(1)-C(1)	97.7
Cnt-Th(1)-Cnt	118.2
C(1)-Th(1)-C(4)	121.64(4)
C(1)-Th(1)-C(4)#1	121.64(4)
C(4)-Th(1)-C(4)#1	95.00(5)
C(1)-Th(1)-C(4)#2	121.64(4)
C(4)-Th(1)-C(4)#2	95.00(5)
C(4)#1-Th(1)-C(4)#2	95.00(5)
C(1)-Th(1)-C(5)	96.51(4)
C(4)-Th(1)-C(5)	29.24(5)
C(4)#1-Th(1)-C(5)	123.30(5)
C(4)#2-Th(1)-C(5)	98.35(5)
C(1)-Th(1)-C(5)#1	96.51(4)
C(4)-Th(1)-C(5)#1	98.35(5)
C(4)#1-Th(1)-C(5)#1	29.24(5)
C(4)#2-Th(1)-C(5)#1	123.30(5)
C(5)-Th(1)-C(5)#1	118.733(15)
C(1)-Th(1)-C(5)#2	96.51(4)
C(4)-Th(1)-C(5)#2	123.29(5)
C(4)#1-Th(1)-C(5)#2	98.35(5)
C(4)#2-Th(1)-C(5)#2	29.24(5)
C(5)-Th(1)-C(5)#2	118.732(15)
C(5)#1-Th(1)-C(5)#2	118.732(14)
C(1)-Th(1)-C(3)#2	112.05(4)
C(4)-Th(1)-C(3)#2	77.99(5)
C(4)#1-Th(1)-C(3)#2	119.47(5)
C(4)#2-Th(1)-C(3)#2	28.99(5)
C(5)-Th(1)-C(3)#2	72.01(5)
C(5)#1-Th(1)-C(3)#2	148.65(5)
C(5)#2-Th(1)-C(3)#2	47.71(5)
C(1)-Th(1)-C(3)#1	112.05(4)
C(4)-Th(1)-C(3)#1	119.47(5)
C(4)#1-Th(1)-C(3)#1	28.99(5)
C(4)#2-Th(1)-C(3)#1	77.99(5)
C(5)-Th(1)-C(3)#1	148.65(5)
C(5)#1-Th(1)-C(3)#1	47.71(5)
C(5)#2-Th(1)-C(3)#1	72.01(5)
C(3)#2-Th(1)-C(3)#1	106.77(4)
C(1)-Th(1)-C(3)	112.05(3)
C(4)-Th(1)-C(3)	29.00(5)
C(4)#1-Th(1)-C(3)	77.99(5)
C(4)#2-Th(1)-C(3)	119.47(5)
C(5)-Th(1)-C(3)	47.71(5)
C(5)#1-Th(1)-C(3)	72.01(5)
C(5)#2-Th(1)-C(3)	148.65(5)
C(3)#2-Th(1)-C(3)	106.77(4)
C(3)#1-Th(1)-C(3)	106.77(4)
C(1)-Th(1)-C(6)	74.01(3)
C(4)-Th(1)-C(6)	47.68(5)
C(4)#1-Th(1)-C(6)	121.74(5)
C(4)#2-Th(1)-C(6)	125.50(5)
C(5)-Th(1)-C(6)	28.83(5)
C(5)#1-Th(1)-C(6)	103.09(5)
C(5)#2-Th(1)-C(6)	138.02(5)
C(3)#2-Th(1)-C(6)	97.19(5)
C(3)#1-Th(1)-C(6)	149.76(5)
C(3)-Th(1)-C(6)	47.24(5)
C(1)-Th(1)-C(6)#1	74.01(3)
C(4)-Th(1)-C(6)#1	125.50(5)
C(4)#1-Th(1)-C(6)#1	47.68(5)

C(4)#2-Th(1)-C(6)#1	121.74(5)	C(4)#2-Th(1)-C(2)#1	93.34(5)
C(5)-Th(1)-C(6)#1	138.02(5)	C(5)-Th(1)-C(2)#1	166.40(5)
C(5)#1-Th(1)-C(6)#1	28.83(5)	C(5)#1-Th(1)-C(2)#1	48.11(5)
C(5)#2-Th(1)-C(6)#1	103.09(5)	C(5)#2-Th(1)-C(2)#1	74.72(5)
C(3)#2-Th(1)-C(6)#1	149.76(5)	C(3)#2-Th(1)-C(2)#1	120.79(5)
C(3)#1-Th(1)-C(6)#1	47.24(5)	C(3)#1-Th(1)-C(2)#1	28.94(5)
C(3)-Th(1)-C(6)#1	97.19(5)	C(3)-Th(1)-C(2)#1	119.88(5)
C(6)-Th(1)-C(6)#1	112.72(3)	C(6)-Th(1)-C(2)#1	141.01(5)
C(1)-Th(1)-C(6)#2	74.01(3)	C(6)#1-Th(1)-C(2)#1	28.97(5)
C(4)-Th(1)-C(6)#2	121.74(5)	C(6)#2-Th(1)-C(2)#1	89.92(5)
C(4)#1-Th(1)-C(6)#2	125.50(5)	C(2)-Th(1)-C(2)#1	118.584(14)
C(4)#2-Th(1)-C(6)#2	47.68(5)	C(7)-Si(1)-C(8)	110.61(10)
C(5)-Th(1)-C(6)#2	103.09(5)	C(7)-Si(1)-C(9)	108.85(9)
C(5)#1-Th(1)-C(6)#2	138.02(5)	C(8)-Si(1)-C(9)	107.00(9)
C(5)#2-Th(1)-C(6)#2	28.83(5)	C(7)-Si(1)-C(2)	107.27(8)
C(3)#2-Th(1)-C(6)#2	47.24(5)	C(8)-Si(1)-C(2)	106.69(8)
C(3)#1-Th(1)-C(6)#2	97.19(5)	C(9)-Si(1)-C(2)	116.40(8)
C(3)-Th(1)-C(6)#2	149.76(5)	C(3)-C(2)-C(6)	105.53(14)
C(6)-Th(1)-C(6)#2	112.72(3)	C(3)-C(2)-Si(1)	126.23(13)
C(6)#1-Th(1)-C(6)#2	112.72(3)	C(6)-C(2)-Si(1)	125.83(13)
C(1)-Th(1)-C(2)	83.12(3)	C(3)-C(2)-Th(1)	73.95(9)
C(4)-Th(1)-C(2)	48.18(5)	C(6)-C(2)-Th(1)	74.33(9)
C(4)#1-Th(1)-C(2)	93.34(5)	Si(1)-C(2)-Th(1)	130.42(7)
C(4)#2-Th(1)-C(2)	142.86(5)	C(4)-C(3)-C(2)	109.44(15)
C(5)-Th(1)-C(2)	48.11(5)	C(4)-C(3)-Th(1)	73.99(9)
C(5)#1-Th(1)-C(2)	74.72(5)	C(2)-C(3)-Th(1)	77.11(9)
C(5)#2-Th(1)-C(2)	166.40(5)	C(3)-C(4)-C(5)	107.84(15)
C(3)#2-Th(1)-C(2)	119.88(5)	C(3)-C(4)-Th(1)	77.02(9)
C(3)#1-Th(1)-C(2)	120.79(5)	C(5)-C(4)-Th(1)	76.00(9)
C(3)-Th(1)-C(2)	28.94(5)	C(6)-C(5)-C(4)	107.69(15)
C(6)-Th(1)-C(2)	28.97(5)	C(6)-C(5)-Th(1)	76.88(9)
C(6)#1-Th(1)-C(2)	89.92(5)	C(4)-C(5)-Th(1)	74.76(9)
C(6)#2-Th(1)-C(2)	141.01(5)	C(5)-C(6)-C(2)	109.49(15)
C(1)-Th(1)-C(2)#1	83.12(3)	C(5)-C(6)-Th(1)	74.29(9)
C(4)-Th(1)-C(2)#1	142.86(5)		
C(4)#1-Th(1)-C(2)#1	48.18(5)		

C(2)-C(6)-Th(1) 76.70(9)

X-ray Data Collection, Structure Solution and Refinement for $(Cp'_3Th)_2(\mu–O)$. A colorless crystal of approximate dimensions 0.112 x 0.205 x 0.329 mm was mounted in a cryoloop and transferred to a Bruker SMART APEX II diffractometer. The APEX2[49] program package was used to determine the unit-cell parameters and for data collection with 15 sec/frame scan time. The raw frame data was processed using SAINT[50] and SADABS[51] to yield the reflection data file. Subsequent calculations were carried out using the SHELXTL[52] program. The diffraction symmetry was 2/*m* and the systematic absences were consistent with the monoclinic space group $P2_1/c$ that was later determined to be correct.

The structure was solved by dual space methods and refined on F^2 by full-matrix least-squares techniques. The analytical scattering factors[53] for neutral atoms were used throughout the analysis. Hydrogen atoms were located from a difference-Fourier map and refined (x,y,z and U_{iso}). The molecule was located on an inversion center.

Least-squares analysis yielded wR2 = 0.0331 and Goof = 1.037 for 415 variables refined against 6849 data (0.73 Å), R1 = 0.0162 for those 6208 data with $I > 2.0\sigma(I)$.

Table 9.6: Bond lengths [Å] and angles [°] for $(Cp'_3Th)_2(\mu–O)$. Symmetry transformations used to generate equivalent atoms: #1 -x+1,-y+1,-z+1

Th(1)-Cnt1	2.594	Th(1)-C(3)	2.842(2)
Th(1)-Cnt2	2.595	Th(1)-C(5)	2.8419(19)
Th(1)-Cnt3	2.587	Th(1)-C(13)	2.8453(19)
Th(1)-O(1)	2.14604(12)	Th(1)-C(18)	2.8752(19)
Th(1)-C(4)	2.803(2)	Th(1)-C(10)	2.884(2)
Th(1)-C(20)	2.8053(19)	Th(1)-C(2)	2.8865(19)
Th(1)-C(12)	2.809(2)	Th(1)-C(17)	2.9034(19)
Th(1)-C(21)	2.8386(19)	Th(1)-C(9)	2.9217(19)
Th(1)-C(19)	2.8401(19)	Th(1)-C(1)	2.9229(18)
Th(1)-C(11)	2.841(2)	Si(1)-C(7)	1.863(2)

Si(1)-C(6)	1.866(2)	C(4)-Th(1)-C(20)	119.96(6)
Si(1)-C(1)	1.867(2)	O(1)-Th(1)-C(12)	92.62(4)
Si(1)-C(8)	1.867(2)	C(4)-Th(1)-C(12)	119.88(6)
Si(2)-C(9)	1.861(2)	C(20)-Th(1)-C(12)	119.50(6)
Si(2)-C(14)	1.864(2)	O(1)-Th(1)-C(21)	119.51(4)
Si(2)-C(16)	1.866(2)	C(4)-Th(1)-C(21)	122.32(6)
Si(2)-C(15)	1.872(2)	C(20)-Th(1)-C(21)	28.91(6)
Si(3)-C(24)	1.861(2)	C(12)-Th(1)-C(21)	105.60(6)
Si(3)-C(23)	1.863(2)	O(1)-Th(1)-C(19)	73.92(4)
Si(3)-C(22)	1.867(3)	C(4)-Th(1)-C(19)	141.11(6)
Si(3)-C(17)	1.869(2)	C(20)-Th(1)-C(19)	28.81(6)
O(1)-Th(1)#1	2.14611(12)	C(12)-Th(1)-C(19)	97.62(6)
C(1)-C(5)	1.422(3)	C(21)-Th(1)-C(19)	47.13(6)
C(1)-C(2)	1.428(3)	O(1)-Th(1)-C(11)	73.80(4)
C(2)-C(3)	1.403(3)	C(4)-Th(1)-C(11)	98.59(6)
C(3)-C(4)	1.406(3)	C(20)-Th(1)-C(11)	139.89(6)
C(4)-C(5)	1.415(3)	C(12)-Th(1)-C(11)	28.83(6)
C(9)-C(13)	1.424(3)	C(21)-Th(1)-C(11)	133.89(6)
C(9)-C(10)	1.429(3)	C(19)-Th(1)-C(11)	111.97(6)
C(10)-C(11)	1.401(3)	O(1)-Th(1)-C(3)	75.23(4)
C(11)-C(12)	1.407(3)	C(4)-Th(1)-C(3)	28.83(6)
C(12)-C(13)	1.410(3)	C(20)-Th(1)-C(3)	97.73(6)
C(17)-C(21)	1.423(3)	C(12)-Th(1)-C(3)	141.47(6)
C(17)-C(18)	1.425(3)	C(21)-Th(1)-C(3)	112.25(6)
C(18)-C(19)	1.403(3)	C(19)-Th(1)-C(3)	113.11(6)
C(19)-C(20)	1.405(3)	C(11)-Th(1)-C(3)	113.86(6)
C(20)-C(21)	1.409(3)	O(1)-Th(1)-C(5)	120.67(4)
		C(4)-Th(1)-C(5)	29.02(6)
Cnt1-Th(1)-O(1)	100.1	C(20)-Th(1)-C(5)	106.21(6)
Cnt2-Th(1)-O(1)	98.6	C(12)-Th(1)-C(5)	121.90(6)
Cnt3-Th(1)-O(1)	98.8	C(21)-Th(1)-C(5)	97.37(6)
Cnt1-Th(1)-Cnt2	117.4	C(19)-Th(1)-C(5)	134.71(6)
Cnt1-Th(1)-Cnt3	117.5	C(11)-Th(1)-C(5)	113.30(6)
Cnt2-Th(1)-Cnt3	117.6	C(3)-Th(1)-C(5)	47.12(6)
O(1)-Th(1)-C(4)	93.17(4)	O(1)-Th(1)-C(13)	119.58(4)
O(1)-Th(1)-C(20)	92.25(4)	C(4)-Th(1)-C(13)	105.04(6)

C(20)-Th(1)-C(13)	123.05(6)	C(5)-Th(1)-C(2)	46.61(6)
C(12)-Th(1)-C(13)	28.86(6)	C(13)-Th(1)-C(2)	142.60(6)
C(21)-Th(1)-C(13)	98.05(6)	C(18)-Th(1)-C(2)	120.18(6)
C(19)-Th(1)-C(13)	113.28(6)	C(10)-Th(1)-C(2)	120.31(6)
C(11)-Th(1)-C(13)	47.05(6)	O(1)-Th(1)-C(17)	116.99(4)
C(3)-Th(1)-C(13)	133.58(6)	C(4)-Th(1)-C(17)	145.58(6)
C(5)-Th(1)-C(13)	96.44(6)	C(20)-Th(1)-C(17)	47.71(6)
O(1)-Th(1)-C(18)	88.77(4)	C(12)-Th(1)-C(17)	77.28(6)
C(4)-Th(1)-C(18)	167.12(6)	C(21)-Th(1)-C(17)	28.68(6)
C(20)-Th(1)-C(18)	47.19(6)	C(19)-Th(1)-C(17)	47.29(6)
C(12)-Th(1)-C(18)	72.69(6)	C(11)-Th(1)-C(17)	105.23(6)
C(21)-Th(1)-C(18)	46.81(6)	C(3)-Th(1)-C(17)	140.90(6)
C(19)-Th(1)-C(18)	28.40(6)	C(5)-Th(1)-C(17)	116.83(6)
C(11)-Th(1)-C(18)	94.18(6)	C(13)-Th(1)-C(17)	75.37(6)
C(3)-Th(1)-C(18)	141.38(6)	C(18)-Th(1)-C(17)	28.55(5)
C(5)-Th(1)-C(18)	143.62(6)	C(10)-Th(1)-C(17)	120.80(6)
C(13)-Th(1)-C(18)	84.92(6)	C(2)-Th(1)-C(17)	112.64(6)
O(1)-Th(1)-C(10)	88.15(4)	O(1)-Th(1)-C(9)	116.39(4)
C(4)-Th(1)-C(10)	73.38(6)	C(4)-Th(1)-C(9)	77.01(6)
C(20)-Th(1)-C(10)	166.58(6)	C(20)-Th(1)-C(9)	146.88(6)
C(12)-Th(1)-C(10)	47.09(6)	C(12)-Th(1)-C(9)	47.62(6)
C(21)-Th(1)-C(10)	144.43(6)	C(21)-Th(1)-C(9)	118.27(6)
C(19)-Th(1)-C(10)	140.24(6)	C(19)-Th(1)-C(9)	141.72(6)
C(11)-Th(1)-C(10)	28.32(6)	C(11)-Th(1)-C(9)	47.22(5)
C(3)-Th(1)-C(10)	95.35(6)	C(3)-Th(1)-C(9)	105.15(6)
C(5)-Th(1)-C(10)	84.98(6)	C(5)-Th(1)-C(9)	74.42(6)
C(13)-Th(1)-C(10)	46.62(6)	C(13)-Th(1)-C(9)	28.55(5)
C(18)-Th(1)-C(10)	119.43(6)	C(18)-Th(1)-C(9)	113.44(6)
O(1)-Th(1)-C(2)	90.26(4)	C(10)-Th(1)-C(9)	28.48(5)
C(4)-Th(1)-C(2)	47.14(6)	C(2)-Th(1)-C(9)	120.04(6)
C(20)-Th(1)-C(2)	73.11(6)	C(17)-Th(1)-C(9)	101.47(5)
C(12)-Th(1)-C(2)	166.89(6)	O(1)-Th(1)-C(1)	118.39(4)
C(21)-Th(1)-C(2)	83.96(6)	C(4)-Th(1)-C(1)	47.71(6)
C(19)-Th(1)-C(2)	95.46(6)	C(20)-Th(1)-C(1)	78.02(6)
C(11)-Th(1)-C(2)	142.08(6)	C(12)-Th(1)-C(1)	144.83(6)
C(3)-Th(1)-C(2)	28.34(6)	C(21)-Th(1)-C(1)	74.63(6)

C(19)-Th(1)-C(1)	106.25(6)	C(3)-C(2)-Th(1)	74.05(11)
C(11)-Th(1)-C(1)	141.79(6)	C(1)-C(2)-Th(1)	77.19(11)
C(3)-Th(1)-C(1)	47.23(6)	C(2)-C(3)-C(4)	108.28(18)
C(5)-Th(1)-C(1)	28.51(5)	C(2)-C(3)-Th(1)	77.61(11)
C(13)-Th(1)-C(1)	116.11(6)	C(4)-C(3)-Th(1)	74.05(11)
C(18)-Th(1)-C(1)	120.70(5)	C(3)-C(4)-C(5)	107.31(18)
C(10)-Th(1)-C(1)	113.48(5)	C(3)-C(4)-Th(1)	77.12(11)
C(2)-Th(1)-C(1)	28.46(5)	C(5)-C(4)-Th(1)	77.02(11)
C(17)-Th(1)-C(1)	100.30(5)	C(4)-C(5)-C(1)	109.62(18)
C(9)-Th(1)-C(1)	100.29(5)	C(4)-C(5)-Th(1)	73.96(11)
C(7)-Si(1)-C(6)	108.11(12)	C(1)-C(5)-Th(1)	78.91(11)
C(7)-Si(1)-C(1)	110.96(11)	C(13)-C(9)-C(10)	105.31(17)
C(6)-Si(1)-C(1)	107.35(10)	C(13)-C(9)-Si(2)	123.93(15)
C(7)-Si(1)-C(8)	111.51(13)	C(10)-C(9)-Si(2)	127.21(15)
C(6)-Si(1)-C(8)	107.16(11)	C(13)-C(9)-Th(1)	72.75(11)
C(1)-Si(1)-C(8)	111.52(10)	C(10)-C(9)-Th(1)	74.31(11)
C(9)-Si(2)-C(14)	106.84(10)	Si(2)-C(9)-Th(1)	134.29(9)
C(9)-Si(2)-C(16)	110.40(10)	C(11)-C(10)-C(9)	109.37(18)
C(14)-Si(2)-C(16)	106.99(12)	C(11)-C(10)-Th(1)	74.13(11)
C(9)-Si(2)-C(15)	112.55(10)	C(9)-C(10)-Th(1)	77.22(11)
C(14)-Si(2)-C(15)	108.42(11)	C(10)-C(11)-C(12)	108.26(18)
C(16)-Si(2)-C(15)	111.36(11)	C(10)-C(11)-Th(1)	77.55(11)
C(24)-Si(3)-C(23)	111.69(11)	C(12)-C(11)-Th(1)	74.33(11)
C(24)-Si(3)-C(22)	108.81(14)	C(11)-C(12)-C(13)	107.39(18)
C(23)-Si(3)-C(22)	107.38(13)	C(11)-C(12)-Th(1)	76.84(12)
C(24)-Si(3)-C(17)	112.43(10)	C(13)-C(12)-Th(1)	76.98(11)
C(23)-Si(3)-C(17)	110.92(10)	C(12)-C(13)-C(9)	109.65(18)
C(22)-Si(3)-C(17)	105.26(11)	C(12)-C(13)-Th(1)	74.16(11)
Th(1)-O(1)-Th(1)#1	180.0	C(9)-C(13)-Th(1)	78.70(11)
C(5)-C(1)-C(2)	105.39(17)	C(21)-C(17)-C(18)	105.66(18)
C(5)-C(1)-Si(1)	124.30(15)	C(21)-C(17)-Si(3)	123.43(15)
C(2)-C(1)-Si(1)	127.08(15)	C(18)-C(17)-Si(3)	127.02(15)
C(5)-C(1)-Th(1)	72.58(10)	C(21)-C(17)-Th(1)	73.13(11)
C(2)-C(1)-Th(1)	74.36(11)	C(18)-C(17)-Th(1)	74.63(11)
Si(1)-C(1)-Th(1)	133.66(9)	Si(3)-C(17)-Th(1)	134.58(9)
C(3)-C(2)-C(1)	109.39(18)	C(19)-C(18)-C(17)	109.17(18)

C(19)-C(18)-Th(1)	74.41(11)	C(19)-C(20)-Th(1)	76.97(11)
C(17)-C(18)-Th(1)	76.82(11)	C(21)-C(20)-Th(1)	76.86(11)
C(18)-C(19)-C(20)	108.25(18)	C(20)-C(21)-C(17)	109.32(18)
C(18)-C(19)-Th(1)	77.19(11)	C(20)-C(21)-Th(1)	74.24(11)
C(20)-C(19)-Th(1)	74.22(11)	C(17)-C(21)-Th(1)	78.19(11)
C(19)-C(20)-C(21)	107.58(18)		

Computational Details. Density functional theory (DFT) using the TPSSh[26] functional with Grimme's D3 dispersion correction[56,57] was employed to study Cp′$_3$ThBr, (Cp′$_3$ThBr)$^{1-}$ and Cp′$_3$Th species. Scalar relativistic effective core potentials (ECPs)[27] with the def-TZVP[28] basis set was used for the thorium and polarized split-valence basis sets with diffuse functions def2-SVPD[29] was used for the other atoms. A grid size of m4 was used. Solvent effects were accounted for using the continuum solvent model (COSMO)[58] with a dielectric constant of THF (ε = 7.52).[59] All structures were computed in the C_1 symmetry with geometry convergence of 10^{-5} a.u and energy convergence of 10^{-7} a.u. Vibrational frequencies were computed for all the optimized structures and were confirmed to be ground state structures with the absence of imaginary frequencies. Free energies and equilibrium constants at 298.15 K were obtained within the rigid rotor-harmonic oscillator approximation. All calculations were carried out with the TURBOMOLE V7.2.1 molecular package.[60,61]

The solvent optimized structure of Cp′$_3$Th shows a 6dz^2-like HOMO orbital, consistent with previous calculations on Cp″$_3$Th.[19] For comparison, Cp′$_3$Th was also optimized with def2-SV(P) basis set[29] for the lighter atoms. The average Th-Cp ring centroid distance was shortened by 0.04 Å for Cp′$_3$Th. The HOMO of (Cp′$_3$ThBr)$^{1-}$ shows 55% 5f-contribution and 45% 6d-contribution while the HOMO of Cp′$_3$ThBr shows little to no 6d-contribution, Figure 10.9.

Time dependent density functional theory (TDDFT) calculations were carried out on the solvent-optimized structures of Cp′$_3$ThBr, (Cp′$_3$ThBr)$^{1-}$, and Cp′$_3$Th using the same functional and

basis sets. TDDFT calculations of the 30 lowest excitations from the spin unrestricted excitations were computed to simulate their UV-visible spectra. To account for the systematic underestimation of excitation energies by semi-local density functionals such as TPSSh,[62] the simulated excitation spectrum was blue-shifted by 0.4 eV. Normalized Gaussian line profiles with a root mean square width of 0.12 eV were centered at the thus obtained excitation energies, scaled by the computed oscillator strength, and superimposed to simulate the experimental absorption spectra. Some notable excitations (in nm) and oscillator strengths in the length gauge (in a.u.) from each band, and dominant single-particle contributions for each transition, are reported in Table 10.7.

Electronic transitions were analyzed with VMD[63] and Mulliken population analysis (MPA). Excitations between 400 and 1000 nm are largely metal-metal transitions with 6d to 5f character for the Cp'_3Th complex. Transitions below 400 nm are mostly 6d to 7p and some 5f to 5f transitions. Excitations in $(Cp'_3ThBr)^{1-}$ are mostly 5f to 5f between 400 and 1000 nm and 5f to 6d below 350 nm. Excitations in Cp'_3ThBr are largely f-f transitions below 400 nm.

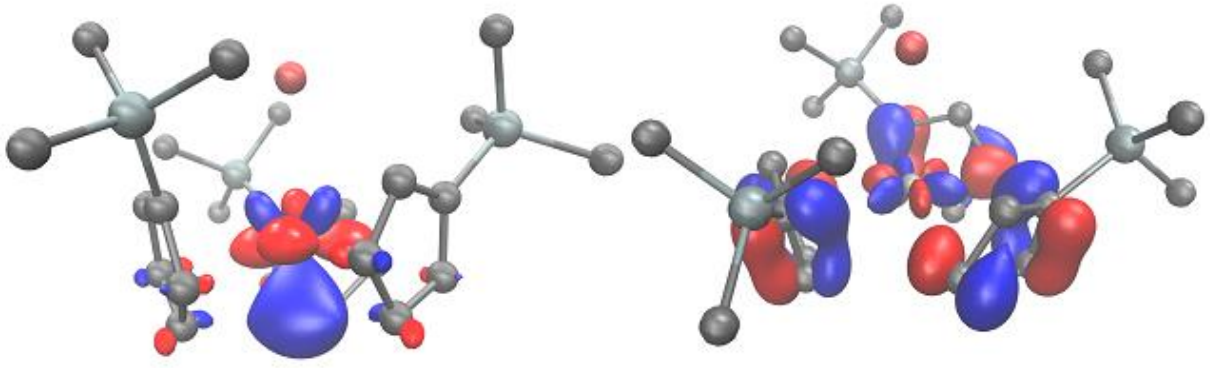

Figure 10.9: Calculated 6d/5f like HOMO of $(Cp'_3ThBr)^{1-}$ (left) and 5f-like HOMO of Cp'_3ThBr (right) plotted with contour values of 0.06.

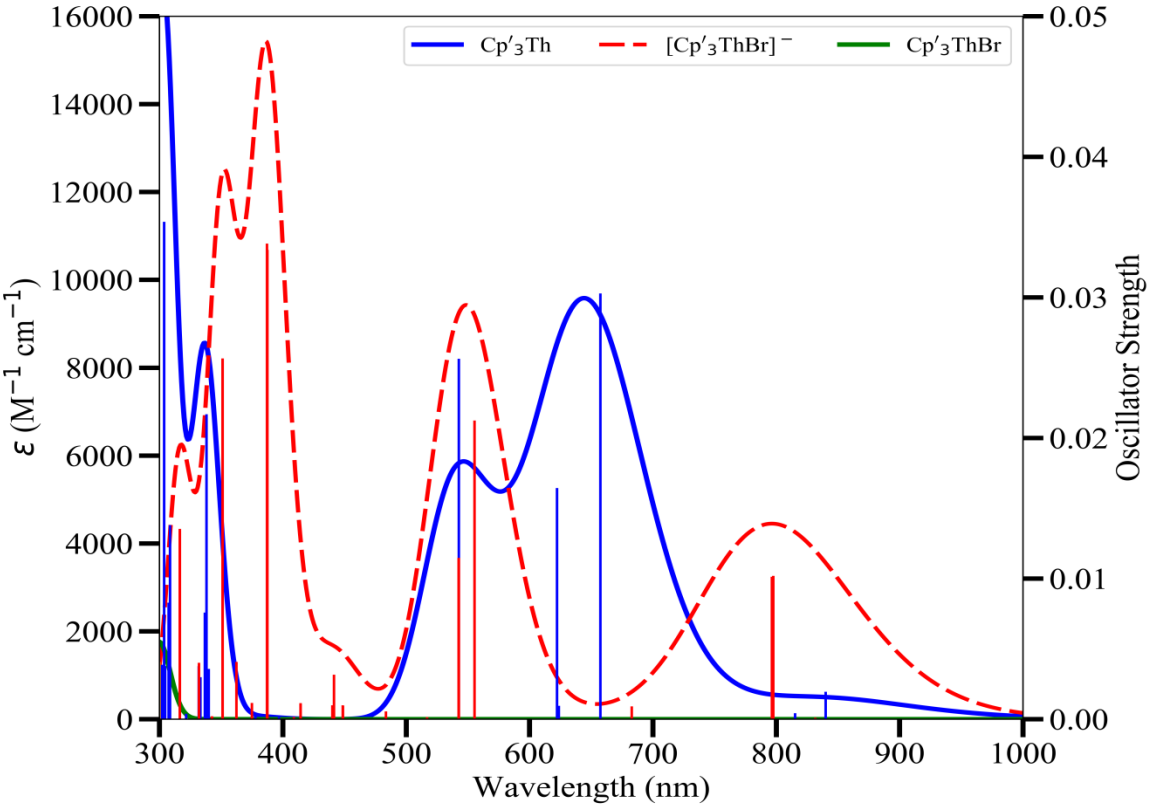

Figure 10.10: Calculated UV-visible spectra of Cp'_3Th (solid blue), $(Cp'_3ThBr)^{1-}$ (dotted red), and Cp'_3ThBr (solid green) with computed TDDFT oscillator strengths shown as vertical lines. The computed excitation energies were empirically blue-shifted by 0.04 eV and a gaussian line broadening of 0.12 eV were applied.

Table 10.7: Electronic excitation summary of Cp'_3Th, $(Cp'_3ThBr)^{1-}$ and Cp'_3ThBr computed using TPSSh functional, def-TZVP/ECPs basis set for thorium and def2-SVPD basis set for lighter atoms. Oscillator strength is reported in the length gauge. The 128a and 146a orbitals are the singly occupied HOMO for Cp'_3Th and $(Cp'_3ThBr)^{1-}$, respectively, and 145a is the doubly occupied HOMO for Cp'_3ThBr.

Compound	Wavelength (nm)	Oscillator Strength (len)	Dominant Contributions			
			occupied	Virtual	% weight	Transition
Cp'_3Th	1152	0.002	128a	129a	98.8	6d-5f
	1106	0.001	128a	130a	99.1	6d-5f
	834.1	0.031	128a	131a	95.2	6d-5f
	778.4	0.016	128a	133a	96.5	6d-5f
	657.9	0.026	128a	134a	96.1	6d-5f
	381.7	0.003	128a	140a	65.1	6d-5f
			128a	137a	10.7	6d-7p
	379.6	0.022	128a	138a	55	6d-7p
			128a	139a	18.9	6d-7p
			128a	141a	11.6	6d-6d
	336.8	0.035	126b	128b	67.6	4f-7s
			128a	143a	7.8	6d-5f/6d-6d
	317.2	0.002	126a	130a	34.7	4f-5f
			126b	130b	31.3	4f-5f
	303.6	0.002	127a	131a	39.4	4f-5f
			127b	131b	8.3	4f-5f
$(Cp'_3ThBr)^{1-}$	1073.8	0.01	146a	151a	89.1	4f-5f
	1071.6	0.01	146a	152a	88.9	4f-5f
	676.6	0.02	146a	153a	91.1	4f-5f
	657.8	0.011	146a	154a	90.3	4f-5f
	478.3	0.011	146a	160a	69.8	4f-5f
			146a	165a	17.9	4f-5f
	442.7	0.033	146a	167a	66.8	4f-5f
	442.4	0.034	146a	168a	67	4f-5f
	396	0.026	146a	171a	70.5	4f-5f

	352.3	0.013	146a	178a	39.9	4f-5f
			146a	182a	19.2	4f-5f
			146a	177a	12.1	4f-5f
			146a	180a	10.5	4f-6d
Cp′$_3$ThBr	332	0.004	145a	147a	94.7	4f-5f
	332	0.004	145a	148a	94.7	4f-5f
	296	0.008	144a	148a	40.8	4f-5f
			143a	147a	39.2	4f-5f
	295.1	0.025	143a	147a	30.6	4f-5f
			144a	148a	29.8	4f-5f
			144a	147a	12.9	4f-5f
			143a	148a	12.5	4f-5f
	295	0.022	143a	148a	30.8	4f-5f
			144a	147a	29.5	4f-5f
			143a	147a	12.8	4f-5f
			144a	148a	12.6	4f-5f
	291.6	0.016	142a	146a	90.9	6p-5f
	284.7	0.02	145a	150a	53.1	4f-5f
			142a	148a	25.1	6p-5f
	249.2	0.076	144a	151a	25.4	4f-5f
			143a	150a	25.4	4f-5f
			140a	148a	16.1	5d-5f
			141a	147a	15.9	5d-5f

References

(1) Nugent, L. J.; Baybarz, R. D.; Burnett, J. L.; Ryan, J. L. Electron-Transfer and f-d Absorption Bands of Some Lanthanide and Actinide Complexes and the Standard (II—III) Oxidation Potential for Each Member of the Lanthanide and Actinide Series. *J. Phys. Chem.* **1973**, *77*, 1528–1539, DOI: 10.1021/j100631a011.

(2) Bratsch, S. G.; Lagowski, J. J. Actinide Thermodynamic Predictions. 3. Thermodynamics of Compounds and Aquo-Ions of the 2+, 3+, and 4+ Oxidation States and Standard Electrode Potentials at 298.15 K. *J. Phys. Chem.* **1986**, *90*, 307–312, DOI: 10.1021/j100274a021.

(3) Ionova, G.; Madic, C.; Guillaumont, R. About the Existence of Th(III) in Aqueous Solution. *Polyhedron* **1991**, *17*, 1991–1995.

(4) Connelly, N. G.; Geiger, W. E. Chemical Redox Agents for Organometallic Chemistry. *Chem. Rev.* **1996**, *96*, 877–910, DOI: 10.1021/cr940053x.

(5) Wedal, J. C.; Barlow, J. M.; Ziller, J. W.; Yang, J. Y.; Evans, W. J. Electrochemical Studies of Tris(Cyclopentadienyl)Thorium and Uranium Complexes in the +2, +3, and +4 Oxidation States. *Chem. Sci.* **2021**, *12*, 8501–8511, DOI: 10.1039/D1SC01906F.

(6) Blake, P. C.; Lappert, M. F.; Atwood, J. L.; Zhang, H. The Synthesis and Characterisation, Including X-Ray Diffraction Study, of [Th{η-$C_5H_3(SiMe_3)_2$}$_3$]; the First Thorium(III) Crystal Structure. *J. Chem. Soc., Chem. Commun.* **1986**, *453*, 1148–1149, DOI: 10.1039/C39860001148.

(7) Parry, J. S.; Cloke, F. G. N.; Coles, S. J.; Hursthouse, M. B. Synthesis and Characterization of the First Sandwich Complex of Trivalent Thorium: A Structural Comparison with the Uranium Analogue. *J. Am. Chem. Soc.* **1999**, *121*, 6867–6871, DOI: 10.1021/ja9903633.

(8) Boronski, J. T.; Seed, J. A.; Hunger, D.; Woodward, A. W.; van Slageren, J.; Wooles, A. J.; Natrajan, L. S.; Kaltsoyannis, N.; Liddle, S. T. A Crystalline Tri-Thorium Cluster with σ-Aromatic Metal–Metal Bonding. *Nature* **2021**, *598*, 72–75, DOI: 10.1038/s41586-021-03888-3.

(9) Blake, P. C.; Edelstein, N. M.; Hitchcock, P. B.; Kot, W. K.; Lappert, M. F.; Shalimoff, G. V.; Tian, S. Synthesis, Properties and Structures of the Tris(Cyclopentadienyl)Thorium(III) Complexes [Th{η^5-$C_5H_3(SiMe_2R)_2$-1,3}$_3$] (R = Me or ^{t}Bu). *J. Organomet. Chem.* **2001**, *636*, 124–129, DOI: 10.1016/S0022-328X(01)00860-9.

(10) Walensky, J. R.; Martin, R. L.; Ziller, J. W.; Evans, W. J. Importance of Energy Level

Matching for Bonding in Th^{3+}–Am^{3+} Actinide Metallocene Amidinates, $(C_5Me_5)_2[^iPrNC(Me)N^iPr]An$. *Inorg. Chem.* **2010**, *49*, 10007–10012, DOI: 10.1021/ic1013285.

(11) Siladke, N. A.; Webster, C. L.; Walensky, J. R.; Takase, M. K.; Ziller, J. W.; Grant, D. J.; Gagliardi, L.; Evans, W. J. Actinide Metallocene Hydride Chemistry: C–H Activation in Tetramethylcyclopentadienyl Ligands to Form $[\mu\text{-}\eta^5\text{-}C_5Me_3H(CH_2)\text{-}\kappa C]^{2-}$ Tuck-over Ligands in a Tetrathorium Octahydride Complex. *Organometallics* **2013**, *32*, 6522–6531, DOI: 10.1021/om4008482.

(12) Langeslay, R. R.; Fieser, M. E.; Ziller, J. W.; Furche, F.; Evans, W. J. Expanding Thorium Hydride Chemistry Through Th^{2+}, Including the Synthesis of a Mixed-Valent Th^{4+}/Th^{3+} Hydride Complex. *J. Am. Chem. Soc.* **2016**, *138*, 4036–4045, DOI: 10.1021/jacs.5b11508.

(13) Formanuik, A.; Ariciu, A.-M.; Ortu, F.; Beekmeyer, R.; Kerridge, A.; Tuna, F.; McInnes, E. J. L.; Mills, D. P. Actinide Covalency Measured by Pulsed Electron Paramagnetic Resonance Spectroscopy. *Nat. Chem.* **2017**, *9*, 578–583, DOI: 10.1038/nchem.2692.

(14) Langeslay, R. R.; Chen, G. P.; Windorff, C. J.; Chan, A. K.; Ziller, J. W.; Furche, F.; Evans, W. J. Synthesis, Structure, and Reactivity of the Sterically Crowded Th^{3+} Complex $(C_5Me_5)_3Th$ Including Formation of the Thorium Carbonyl, $[(C_5Me_5)_3Th(CO)][BPh_4]$. *J. Am. Chem. Soc.* **2017**, *139*, 3387–3398, DOI: 10.1021/jacs.6b10826.

(15) Altman, A. B.; Brown, A. C.; Rao, G.; Lohrey, T. D.; Britt, R. D.; Maron, L.; Minasian, S. G.; Shuh, D. K.; Arnold, J. Chemical Structure and Bonding in a Thorium(III)-Aluminum Heterobimetallic Complex. *Chem. Sci.* **2018**, *9*, 4317–4324, DOI: 10.1039/c8sc01260a.

(16) Huh, D. N.; Roy, S.; Ziller, J. W.; Furche, F.; Evans, W. J. Isolation of a Square-Planar Th(III) Complex: Synthesis and Structure of $[Th(OC_6H_2{}^tBu_2\text{-}2,6\text{-}Me\text{-}4)_4]^{1-}$. *J. Am. Chem.*

Soc. **2019**, *141*, 12458–12463, DOI: 10.1021/jacs.9b04399.

(17) Bruno, J. W.; Kalina, D. G.; Mintz, E. A.; Marks, T. J. Mechanistic Study of Photoinduced β-Hydride Elimination. The Facile Photochemical Synthesis of Low-Valent Thorium and Uranium Organometallics. *J. Am. Chem. Soc.* **1982**, *104*, 1860–1869, DOI: 10.1021/ja00371a014.

(18) Ortu, F.; Formanuik, A.; Innes, J. R.; Mills, D. P. New Vistas in the Molecualr Chemistry of Thorium: Low Oxidation State Complexes. *Dalton Trans.* **2016**, *45*, 7537–7549, DOI: 10.1039/c6dt01111j.

(19) Langeslay, R. R.; Fieser, M. E.; Ziller, J. W.; Furche, F.; Evans, W. J. Synthesis, Structure, and Reactivity of Crystalline Molecular Complexes of the $\{[C_5H_3(SiMe_3)_2]_3Th\}^{1-}$ Anion Containing Thorium in the Formal +2 Oxidation State. *Chem. Sci.* **2015**, *6*, 517–521, DOI: 10.1039/C4SC03033H.

(20) MacDonald, M. R.; Fieser, M. E.; Bates, J. E.; Ziller, J. W.; Furche, F.; Evans, W. J. Identification of the +2 Oxidation State for Uranium in a Crystalline Molecular Complex, $[K(2.2.2\text{-Cryptand})][(C_5H_4SiMe_3)_3U]$. *J. Am. Chem. Soc.* **2013**, *135*, 13310–13313, DOI: 10.1021/ja406791t.

(21) Lin, Z.; Marechal, J. Le; Sabat, M.; Marks, T. J. Models for Organometallic Molecule-Support Complexes. Synthesis and Properties of Cationic Organoactinides. *J. Am. Chem. Soc.* **1987**, *109*, 4127–4129, DOI: 10.1021/ja00247a056.

(22) Weydert, M.; Brennan, J. G.; Andersen, R. A.; Bergman, R. G. Reactions of Uranium(IV) Tertiary Alkyl Bond: Facile Ligand-Assisted Reduction and Insertion of Ethylene and Carbon Monoxide. *Organometallics* **1995**, *14*, 3942–3951, DOI: 10.1021/om00008a046.

(23) Windorff, C. J.; MacDonald, M. R.; Ziller, J. W.; Evans, W. J.

Trimethylsilylcyclopentadienyl (Cp′) Uranium Chemistry: Synthetic and Structural Studies of Cp'_4U and Cp'_3UX (X = Cl, I, Me). *Z. Anorg. Allg. Chem.* **2017**, *643*, 2011–2018, DOI: 10.1002/zaac.201700323.

(24) Jenkins, T. F.; Woen, D. H.; Mohanam, L. N.; Ziller, J. W.; Furche, F.; Evans, W. J. Tetramethylcyclopentadienyl Ligands Allow Isolation of Ln(II) Ions across the Lanthanide Series in [K(2.2.2-Cryptand)][$(C_5Me_4H)_3Ln$] Complexes. *Organometallics* **2018**, *37*, 3863–3873, DOI: 10.1021/acs.organomet.8b00557.

(25) Inman, C. J.; Cloke, F. G. N. The Experimental Determination of Th(IV)/Th(III) Redox Potentials in Organometallic Thorium Complexes. *Dalton Trans.* **2019**, *48*, 10782–10784, DOI: 10.1039/c9dt01553a.

(26) Staroverov, V. N.; Scuseria, G. E.; Tao, J.; Perdew, J. P. Comparative Assessment of a New Nonempirical Density Functional: Molecules and Hydrogen-Bonded Complexes. *J. Chem. Phys.* **2003**, *119*, 12129–12137, DOI: 10.1063/1.1626543.

(27) Küchle, W.; Dolg, M.; Stoll, H.; Preuss, H. Energy-Adjusted Pseudopotentials for the Actinides. Parameter Sets and Test Calculations for Thorium and Thorium Monoxide. *J. Chem. Phys.* **1994**, *100*, 7535–7542, DOI: 10.1063/1.466847.

(28) Cao, X.; Dolg, M. Segmented Contraction Scheme for Small-Core Actinide Pseudopotential Basis Sets. *J. Mol. Struct.* **2004**, *673*, 203–209, DOI: 10.1016/j.theochem.2003.12.015.

(29) Schäfer, A.; Horn, H.; Ahlrichs, R. Fully Optimized Contracted Gaussian Basis Sets for Atoms Li to Kr. *J. Chem. Phys.* **1992**, *97*, 2571–2577.

(30) MacDonald, M. R.; Ziller, J. W.; Evans, W. J. Synthesis of a Crystalline Molecular Complex of Y^{2+}, [(18-Crown-6)K][$(C_5H_4SiMe_3)_3Y$]. *J. Am. Chem. Soc.* **2011**, *133*, 15914–15917, DOI: 10.1021/ja207151y.

(31) Fieser, M. E.; MacDonald, M. R.; Krull, B. T.; Bates, J. E.; Ziller, J. W.; Furche, F.; Evans, W. J. Structural, Spectroscopic, and Theoretical Comparison of Traditional vs Recently Discovered Ln^{2+} Ions in the [K(2.2.2-Cryptand)][$(C_5H_4SiMe_3)_3Ln$] Complexes: The Variable Nature of Dy^{2+} and Nd^{2+}. *J. Am. Chem. Soc.* **2015**, *137*, 369–382, DOI: 10.1021/ja510831n.

(32) MacDonald, M. R.; Bates, J. E.; Ziller, J. W.; Furche, F.; Evans, W. J. Completing the Series of +2 Ions for the Lanthanide Elements: Synthesis of Molecular Complexes of Pr^{2+}, Gd^{2+}, Tb^{2+}, and Lu^{2+}. *J. Am. Chem. Soc.* **2013**, *135*, 9857–9868, DOI: 10.1021/ja403753j.

(33) MacDonald, M. R.; Bates, J. E.; Fieser, M. E.; Ziller, J. W.; Furche, F.; Evans, W. J. Expanding Rare-Earth Oxidation State Chemistry to Molecular Complexes of Holmium(II) and Erbium(II). *J. Am. Chem. Soc.* **2012**, *134*, 8420–8423, DOI: 10.1021/ja303357w.

(34) Dutkiewicz, M. S.; Apostolidis, C.; Walter, O.; Arnold, P. L. Reduction Chemistry of Neptunium Cyclpentadienide Complexes: From Structure to Understanding. *Chem. Sci.* **2017**, *8*, 2553–2561, DOI: 10.1039/c7sc00034k.

(35) Zalkin, A.; Brennan, J. G.; Andersen, R. A. Tris(Trimethylsilylcyclopentadienyl)-Uranium(III). *Acta Crystallogr. Sect. C* **1988**, *C44*, 2104–2106, DOI: 10.1107/S0108270188008327.

(36) del Mar Conejo, M.; Parry, J. S.; Carmona, E.; Schultz, M.; Brennann, J. G.; Beshouri, S. M.; Andersen, R. A.; Rogers, R. D.; Coles, S.; Hursthouse, M. B. Carbon Monoxide and Isocyanide Complexes of Trivalent Uranium Metallocenes. *Chem. Eur. J.* **1999**, *5*, 3000–3009, DOI: 10.1002/(SICI)1521-3765(19991001)5:10<3000::AID-CHEM3000>3.0.CO;2-Q.

(37) Kot, W. K.; Shalimoff, G. V.; Edelstein, N. M.; Edelman, M. A.; Lappert, M. F. [Th^{III}{η^5-

$C_5H_3(SiMe_3)_2\}_3$], an Actinide Compound with a $6d^1$ Ground State. *J. Am. Chem. Soc.* **1988**, *110*, 986–987, DOI: 10.1021/ja00211a059.

(38) Liu, J.; Seed, J. A.; Formanuik, A.; Ortu, F.; Wooles, A. J.; Mills, D. P.; Liddle, S. T. Thorium(IV) Alkyl Synthesis from a Thorium(III) Cyclopentadienyl Complex and an N-Heterocyclic Olefin. *J. Organomet. Chem.* **2018**, *857*, 75–79, DOI: 10.1016/j.jorganchem.2017.08.015.

(39) Blake, P. C.; Edelman, M. A.; Hitchcock, P. B.; Hu, J.; Lappert, M. F.; Tian, S.; Muller, G. Organometallic Chemistry of the Actinides. Part 4. The Chemistry of Some Tris(Cyclopentadienyl) Actinide Complexes. *J. Organomet. Chem.* **1998**, *551*, 261–270.

(40) Blake, P. C.; Lappert, M. F.; Taylor, R. G.; Atwood, J. L.; Zhang, H. Some Aspects of the Coordination and Organometallic Chemistry of Thorium and Uranium (M^{III}, M^{IV}, U^{V}) in +3 and +4 Oxidation States. *Inorg. Chim. Acta* **1987**, *139*, 13–20, DOI: 10.1016/S0020-1693(00)84028-1.

(41) Evans, W. J.; Gonzales, S. L. Formation of a THF Adduct of the Organometallic Samarium Oxide $[(C_5Me_5)_2Sm]_2(\mu\text{-O})$. *J. Organomet. Chem.* **1994**, *480*, 41–44.

(42) Evans, W. J.; Grate, J. W.; Bloom, I.; Hunter, W. E.; Atwood, J. L. Synthesis and X-Ray Crystallographic Characterization of an Oxo-Bridged Bimetallic Organosamarium Complex, $[(C_5Me_5)_2Sm]_2(\mu\text{-O})$. *J. Am. Chem. Soc.* **1985**, *107*, 405–409, DOI: 10.1021/ja00288a021.

(43) Berthet, J.; Le Marechal, J.; Nierlich, M.; Lance, M.; Vigner, J.; Ephritikhine, M. Synthesis and Crystal Structure of the Oxo-Bridged Bimetallic Organouranium Complex $[(Me_3SiC_5H_4)_3U]_2(\mu\text{-O})$. *J. Organomet. Chem.* **1991**, *408*, 335–341.

(44) Shannon, R. D. Revised Effective Ionic Radii and Systematic Studies of Interatomic

Distances in Halides and Chalcogenides. *Acta Crystallogr. Sect. A* **1976**, *32*, 751–767, DOI: 10.1107/S0567739476001551.

(45) Bergbreiter, D. E.; Killough, J. M. Reactions of Potassium-Graphite. *J. Am. Chem. Soc.* **1978**, *100*, 2126–2134, DOI: 10.1021/ja00475a025.

(46) Gaunt, A. J.; Scott, B. L.; Neu, M. P. U(IV) Chalcogenolates Synthesized via Oxidation of Uranium Metal by Dichalcogenides. *Inorg. Chem.* **2006**, *45*, 7401–7407, DOI: 10.1021/ic060560k.

(47) Mansell, S. M.; Kaltsoyannis, N.; Arnold, P. L. Small Molecule Activation by Uranium Tris(Aryloxides): Experimental and Computational Studies of Binding of N_2, Coupling of CO, and Deoxygenation Insertion of CO_2 under Ambient Conditions. *J. Am. Chem. Soc.* **2011**, *133*, 9036–9051, DOI: 10.1021/ja2019492.

(48) Takase, M. K.; Ziller, J. W.; Evans, W. J. The Importance of a Single Methyl Group in Determining the Reaction Chemistry of Pentamethylcyclopentadienyl Cyclooctatetraenyl Uranium Metallocenes. *Chem. Eur. J.* **2011**, *17*, 4871–4878, DOI: 10.1002/chem.201002857.

(49) APEX2. Bruker AXS, Inc: Madison, WI 2014.

(50) SAINT. Bruker AXS, Inc: Madison, WI 2013.

(51) Sheldrick, G. M. SADABS. Bruker AXS, Inc: Madison, WI 2014.

(52) Sheldrick, G. M. SHELXTL. Bruker AXS, Inc: Madison, WI 2014.

(53) *International Tables for Crystallography*; Kluwer Academic Publishers: Dordrecht, 1992.

(54) Spek, A. L. SQUEEZE. *Acta Crystallogr. Sect. C* **2015**, *C71*, 9–19.

(55) Spek, A. L. PLATON. *Acta Crystallogr. Sect. D* **2009**, *D65*, 148–155.

(56) Grimme, S. Semiempirical GGA-Type Density Functional Constructed with a Long-Range

Dispersion Correction. *J. Comput. Chem.* **2006**, *27*, 1787–1799, DOI: 10.1002/jcc.20495.

(57) Grimme, S.; Antony, J.; Ehrlich, S.; Krieg, H. A Consistent and Accurate Ab Initio Parametrization of Density Functional Dispersion Correction (DFT-D) for the 94 Elements H-Pu. *J. Chem. Phys.* **2010**, *132*, 154104, DOI: 10.1063/1.3382344.

(58) Schäfer, A.; Klamt, A.; Sattel, D.; Lohrenz, J. C. W.; Eckert, F. COSMO Implementation in TURBOMOLE: Extension of an Efficient Quantum Chemical Code towards Liquid Systems. *Phys. Chem. Chem. Phys.* **2000**, *2*, 2187–2193, DOI: 10.1039/b000184h.

(59) CRC Handbook of Chemistry and Physics. In *CRC Handbook of Chemistry and Physics*; Haynes, W. M., Lide, D. R., Bruno, T. J., Eds.; CRC Press, 2016; pp 943–950.

(60) TURBOMOLE V7.4.1. University of Karlsruhe and Forschungszentrum Karlsruhe GmbH.

(61) Balasubramani, S. G.; Chen, G. P.; Coriani, S.; Diedenhofen, M.; Frank, M. S.; Franzke, Y. J.; Furche, F.; Grotjahn, R.; Harding, M. E.; Hättig, C.; Hellweg, A.; Helmich-Paris, B.; Holzer, C.; Huniar, U.; Kaupp, M.; Marefat Khah, A.; Karbalaei Khani, S.; Müller, T.; Mack, F.; Nguyen, B. D.; Parker, S. M.; Perlt, E.; Rappoport, D.; Reiter, K.; Roy, S.; Rückert, M.; Schmitz, G.; Sierka, M.; Tapavicza, E.; Tew, D. P.; van Wüllen, C.; Voora, V. K.; Weigend, F.; Wodyński, A.; Yu, J. M. TURBOMOLE: Modular Program Suite for Ab Initio Quantum-Chemical and Condensed-Matter Simulations. *J. Chem. Phys.* **2020**, *152*, 184107, DOI: 10.1063/5.0004635.

(62) Send, R.; Kühn, M.; Furche, F. Assessing Excited State Methods by Adiabatic Excitation Energies. *J. Chem. Theory Comput.* **2011**, *7*, 2376–2386, DOI: 10.1021/ct200272b.

(63) Humphrey, W.; Dalke, A.; Schulten, K. VMD: Visual Molecular Dynamics. *J. Mol. Graph.* **1996**, *14*, 33–38.

Chapter 11:

Anion-Induced Disproportionation of Th(III) Complexes to Form Th(II) and Th(IV) Products

Introduction[†]

The reaction chemistry of organometallic Th(III) and Th(II) complexes is not extensively developed since there are so few crystallographically characterized Th(III) complexes[1–10] and only a single ligand environment for Th(II).[11,12] The electrochemical data in Chapter 3 showed that the Th(IV)/Th(III) and Th(III)/Th(II) redox couples in $Cp''_3Th^{IV}Cl$, Cp''_3Th^{III}, and $[Cp''_3Th^{II}]^{1-}$ are surprisingly similar: −2.96 V vs Fc^+/Fc[12,13] and −2.85 V vs Fc^+/Fc,[12] respectively. This similarity suggested that Th(II) complexes could be synthesized directly from Th(IV) precursors with strong reductants like potassium, and this was confirmed experimentally.[12]

While studying the reaction of Cp''_3Th^{III} [2,11,14] with KH in hopes of synthesizing a new Th(III) complex, such as $[Cp''_3Th^{III}H]^{1-}$, the characteristic green color of the Th(II) anion $[Cp''_3Th^{II}]^{1-}$ was observed instead of the blue-purple of Th(III). Since KH is not a strong enough reductant to affect the Th(III)/Th(II) couple measured electrochemically, this was puzzling. This Chapter reports that not only KH, but also many other alkali metal salts, MX, will react with Cp''_3Th^{III}, to form the Th(II) anion $[Cp''_3Th^{II}]^{1-}$ and the Th(IV) complex, $Cp''_3Th^{IV}X$, as a co-product. Hence, there are many routes to Th(II) complexes by disproportionation which evidently can occur due to the similarity of the Th(IV)/Th(III) and

[†] Portions of this Chapter have been published: Wedal, J. C.; Cajiao, N.; Neidig, M. L.; Evans, W. J. Anion-Induced Disproportionation of Th(III) Complexes to Form Th(II) and Th(IV) Products. *Chem. Commun.* **2022**, *58*, 5289–5291, DOI: 10.1039/d2cc01272c.

Th(III)/Th(II) redox couples. Reported in this Chapter are the details of these reactions and extension of this chemistry to $Cp^{tet}{}_3Th^{III}$ and Cp'_3Th^{III} ($Cp^{tet} = C_5Me_4H$; $Cp' = C_5H_4SiMe_3$).[3,15]

Results and Discussion

A dark blue solution of Cp''_3Th^{III} in THF reacts with KH and 2.2.2-cryptand (crypt) or 18-crown-6 (crown) at room temperature to generate a deep blue/green solution, indicative of the presence of a Th(II) species, over a few hours. From this reaction, crystals of $[K(chelate)][Cp''_3Th^{II}]$[11] can be isolated after workup in addition to $Cp''_3Th^{IV}H$[16] and Cp''_3Th^{III} [2,11,14] as determined by X-ray crystallography and UV-visible and ^1H NMR spectroscopy (Scheme 11.1).

This type of reaction with Cp''_3Th^{III} was found to also occur with other MX salts such as LiMe, NaN_3, and even KCl, generating $[M(chelate)][Cp''_3Th^{II}]$,[11,12] $Cp''_3Th^{IV}X$, and some amount of $Cp''_3Th^{IV}H$, Scheme 11.1. Minimal $Cp''_3Th^{IV}Cl$ was observed in the reaction of Cp''_3Th^{III} with KCl. This is likely because once the reaction occurs to form $[Cp''_3Th^{II}]^{1-}$ and $Cp''_3Th^{IV}Cl$, Scheme 11.2, these then react to reform Cp''_3Th^{III} and KCl in a reaction analogous to the previously observed reaction between $[Na(crown)_2][Cp''_3Th^{II}]$ and $Cp''_3Th^{IV}Br$.[12] The reaction between $[K(crypt)][Cp''_3Th^{II}]$ and $Cp''_3Th^{IV}Cl$ was independently confirmed to form Cp''_3Th^{III} in near quantitative yield. The formation of Th(II) is also observed in reactions with LiMe without the use of a chelate.

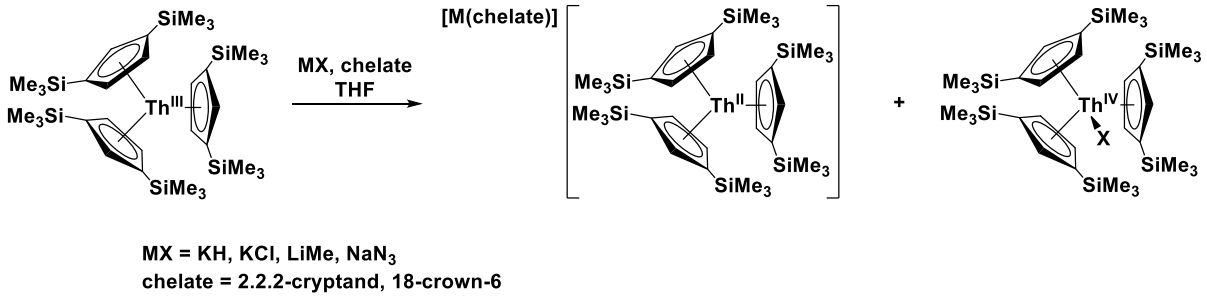

Scheme 11.1: Reaction of Cp''_3Th^{III} with simple MX salts.

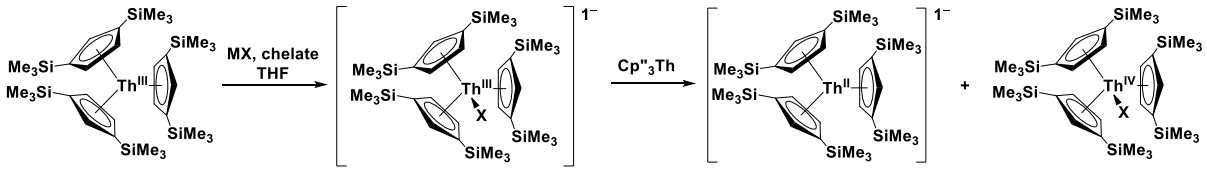

Scheme 11.2: Possible disproportionation mechanism for the reaction of Cp''_3Th^{III} with simple MX salts (M = Li, Na, K; X = H, Cl, Me, N_3).

The reactions with alkyl lithium reagents other than LiMe were also studied. The reaction of Cp''_3Th^{III}, $LiCH_2SiMe_3$, and crypt in THF again formed $[Li(crypt)][Cp''_3Th^{II}]$. In this reaction, $Cp''_3Th^{IV}H$ and Cp''_3Th^{III} were the only other Cp″-containing compounds observable in the ^1H NMR spectrum. Interestingly, the reaction of Cp''_3Th^{III} with ^{n}BuLi formed $[Li(crypt)][Cp''_3Th^{II}]$ in 66% yield, eq 11.1, but neither the expected Th(IV) product, $Cp''_3Th^{IV}(^nBu)$, nor its β–H elimination product, $Cp''_3Th^{IV}H$,[16] were observed in the ^1H NMR spectrum.

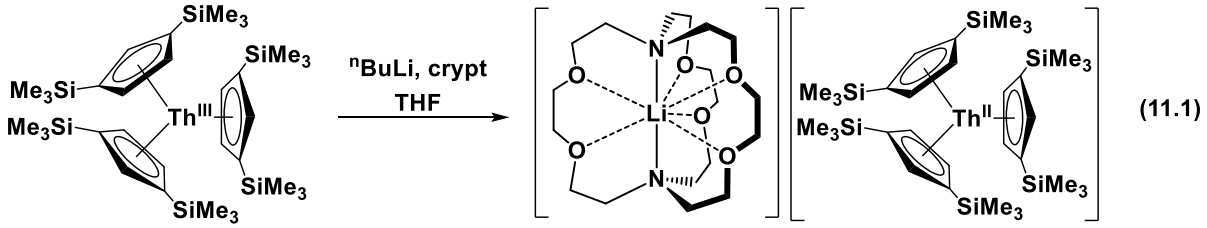

(11.1)

In this case, ^{n}BuLi appeared to act only as a reductant. It is not clear where the hydride product originates in these reactions, but we note that analogous $C_5H_4SiMe_3$ (Cp′) and C_5Me_5 hydrides, $Cp'_3Th^{IV}H$ and $(C_5Me_5)_3Th^{IV}H$, have also been found to be ubiquitous byproducts in reactions with Cp'_3Th^{III} and $(C_5Me_5)_3Th^{III}$.[6,15]

A mechanism can be proposed for the reaction of Cp''_3Th^{III} and MX based on the analogous reactions of Cp'_3U^{III} and Cp''_3U^{III} with KH and chelate, eq 11.2. The uranium reactions form the U(III) anions $[K(crypt)][Cp'_3U^{III}]$ and $[K(crown)(THF)_2][Cp''_3U^{III}]$, respectively, which can be isolated as single crystals.[17,18] The fact that these do not disproportionate is consistent with their electrochemistry.[12]

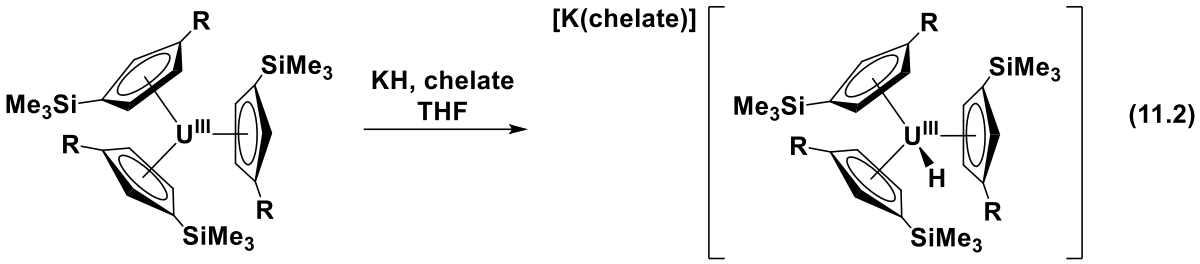

(11.2)

R = H, $SiMe_3$
chelate = 2.2.2-cryptand, 18-crown-6

If a reaction analogous to eq 11.2 occurs between Cp''_3Th^{III} and MX, then $[Cp''_3Th^{III}X]^{1-}$ would form as shown in Scheme 11.2. This species will likely have a reduction potential more negative than the −2.96 V value for Cp''_3Th^{III}.[12] This claim is supported by electrochemical measurements on $Cp''_3Th^{IV}Me$. Only a cathodic event with E_{PC} = −3.48 V vs Fc^+/Fc was observed in the voltammogram for $Cp''_3Th^{IV}Me$, Figure 11.1. For comparison, Cp''_3Th^{III}, $Cp''_3Th^{IV}Br$, and $Cp''_3Th^{IV}Cl$ have cathodic events at E_{PC} = −2.92, −3.00 and −3.04 V, respectively.[12]

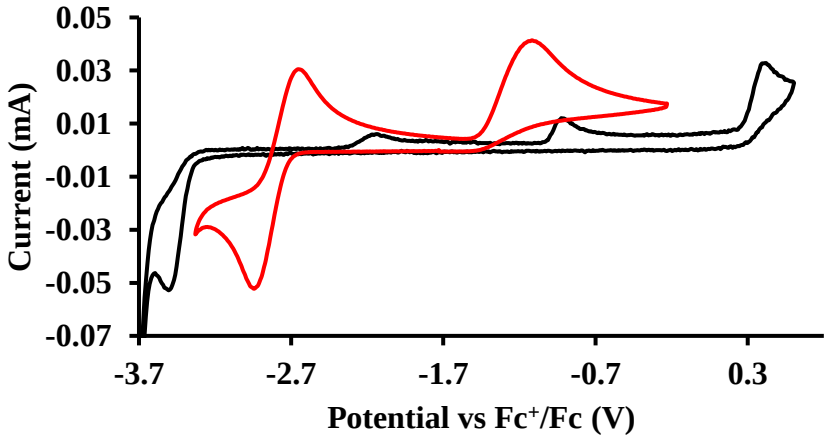

Figure 11.1: Voltammogram of $Cp''_3Th^{IV}Me$ (black) and Cp''_3Th^{III} (red) at v = 200 mV/s in 200 mM $[^nBu_4N][PF_6]$ / THF. The events for $Cp''_3Th^{IV}Me$ occur at −3.48 V [E_{PC}, Th(IV)/Th(III)], −2.045 V (E_{PA1}, related to E_{PC}), −0.90 V (E_{PA2}, likely Cp″ oxidation[12]), and 0.415 V (E_{PA3}). The event at −2.045 V is related to E_{PC} as is it only present after E_{PC} occurs.

The events for Cp''_3Th^{III} occur at −2.94 V (E_{PC}), −2.73 V (E_{PA1}), and −1.09 V (E_{PA2}, Cp″ oxidation).[12]

Thus, electron transfer from $[Cp''_3Th^{III}X]^{1-}$ to Cp''_3Th^{III} would be thermodynamically favorable and could occur to form $Cp''_3Th^{IV}X$ and$[Cp''_3Th^{II}]^{1-}$, which is isolated as the $[M(chelate)]^{1+}$ salt. The formation of Cp''_3Th^{III} in some cases can be explained by the reaction of $Cp''_3Th^{IV}X$ with $[Cp''_3Th^{II}]^{1-}$. The amount of Cp''_3Th^{III} formed likely depends on the relative rate of the reaction between $[Cp''_3Th^{III}X]^{1-}$ and $Cp''_3Th^{IV}X$ versus the disproportionation rate.

Attempts to observe the proposed intermediate $[Cp''_3Th^{III}H]^{1-}$ generated by reaction of Cp''_3Th^{III} and KH via UV-visible spectroscopy were unsuccessful. Due to the large (~5000 $M^{-1}cm^{-1}$) attenuation coefficients of Cp''_3Th^{III},[2,14] UV-visible measurements were performed at roughly 0.15 mM concentrations, in contrast to the bulk reactions which were performed at approximately 15 mM concentrations. Even while stirring the reaction inside the UV-visible cell, no evidence of disproportionation could be observed. Instead, the solution slowly became colorless, indicative of decomposition to Th(IV) products. Control reactions performed inside the glovebox at the same 0.15 mM concentration confirmed that the reaction in Scheme 11.2 does not proceed at low concentrations, possibly because $[Cp''_3Th^{III}H]^{1-}$ reacts with solvent molecules instead of Cp''_3Th^{III}. In collaboration with Nathalia Cajaio and Mike Neidig at the University of Rochester, the reaction with LiMe and Cp''_3Th^{III} was probed at −80 °C and 0.15 mM concentrations to evaluate if an intermediate could be observed at low temperature. However, only new absorption bands attributable to $[Cp''_3Th^{II}]^{1-}$ were observed with concomitant disappearance of the spectrum of Cp''_3Th^{III}, Figure 11.2.

The possibility that the low-valent Th(II) compound $[Cp''_3Th^{II}]^{1-}$ is actually a Th(III)–H species is dispelled by the fact that $[Cp''_3Th^{II}]^{1-}$ has a diamagnetic NMR spectrum and no EPR spectrum.[12] A Th(III)–H species would exhibit a characteristic EPR spectrum and distinct

crystallographic properties as shown for the U(III)–H compounds in eq 11.1 compared to their related U^{II} complexes.[16,17]

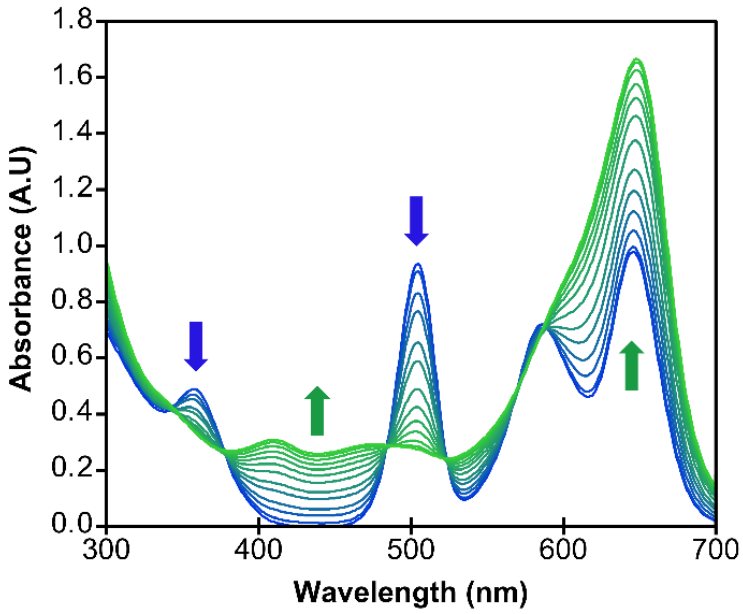

Figure 11.2: UV-visible spectra during the reaction of Cp''_3Th^{III} (blue) and LiMe at −80 °C, showing the appearance of a strong absorption at 650 nm indicative of $[Cp''_3Th^{II}]^{1-}$ (green) with concomitant disappearance of the four bands at 655, 590, 510, and 362 nm. The final spectrum matches that of $[Cp''_3Th^{II}]^{1-}$.[11,12]

Instead of forming the proposed intermediate $[Cp''_3Th^{III}Me]^{1-}$ via reaction with MeLi, the Th(IV) compound $Cp''_3Th^{IV}Me$ could be reduced with KC_8 to form the same product. On one occasion, the reaction of $Cp''_3Th^{IV}Me$ with KC_8 and crown formed a dark red solution from which dark red crystals of $[Cp''_2Th]_2(C_6H_6)$, **11.1**, were identified by X-ray diffraction, Figure 11.3, eq 11.3. [K(crown)][Cp″] was also identified by X-ray crystallography as a coproduct. The benzene in **11.1** likely came from the starting thorium complex $Cp''_3Th^{IV}Me$ from NMR studies.

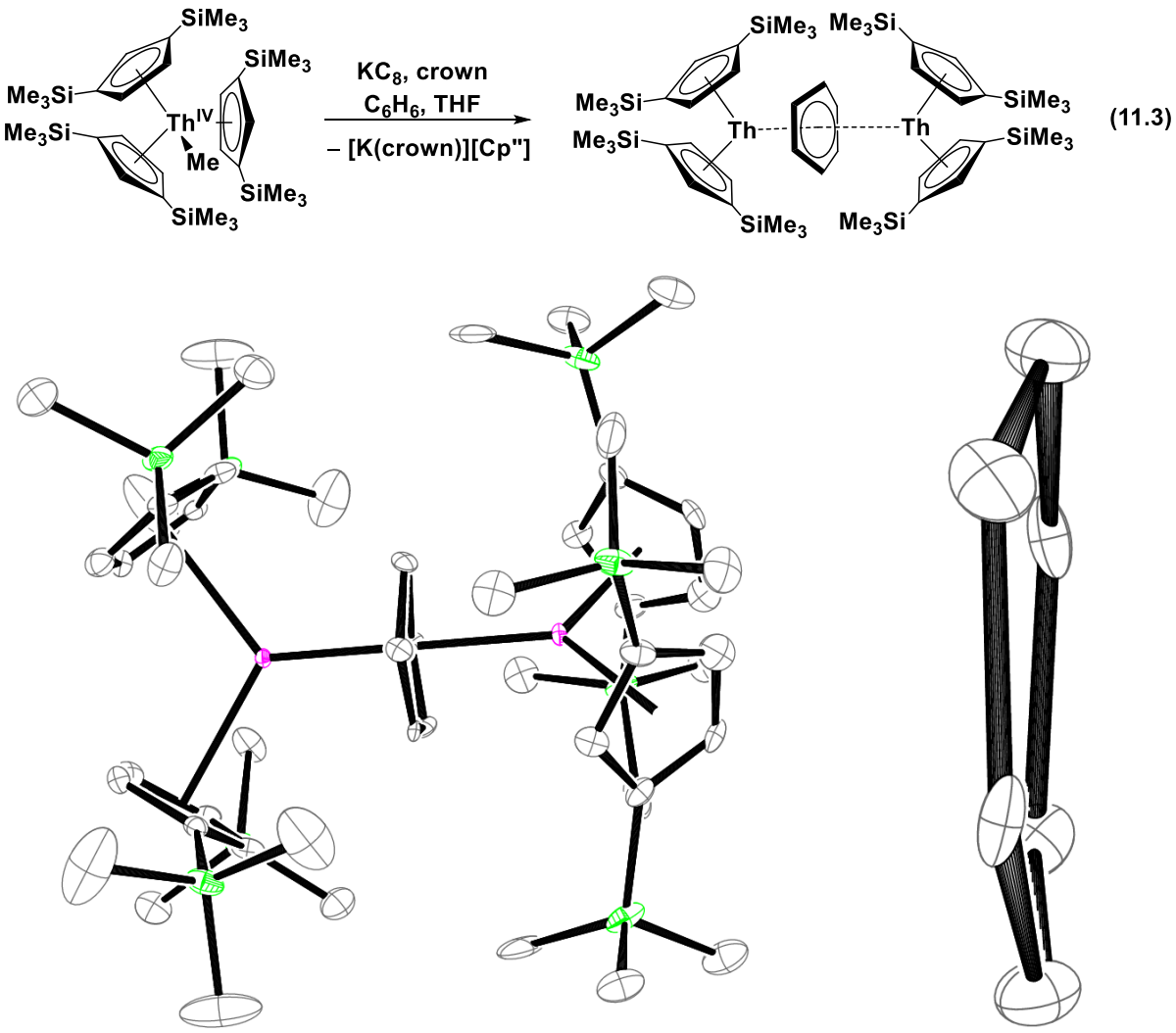

Figure 11.3: Molecular structure of $[Cp''_2Th]_2(C_6H_6)$, **11.1**, (left) and the C_6H_6 unit (right) with ellipsoids drawn at 50% level. Hydrogen atoms have been omitted for clarity.

Compound **11.1** contains two thorium atoms bridged by a non-planar C_6H_6 moiety, where the C_6H_6 ring has a 10° torsion angle. Based on literature precedent[19–22] and the observation that the arene ring is non-planar, this complex likely contains two Th(III) ions and a $(C_6H_6)^{2-}$ ligand. Thorium-arene complexes have been previously reported within the ferrocene (Fc)-substituted amide framework {[Fc(NSi^{t}BuMe$_2$)$_2$]Th}(arene)[20] which were synthesized in one pot from a Th(IV) precursor [Fc(NSi^{t}BuMe$_2$)$_2$]ThCl$_2$(THF), KC_8, and arene in THF (arene = benzene, toluene, naphthalene, biphenyl). Assuming $[Cp''_3ThMe]^{1-}$ is formed during eq 11.3, compound **11.1** is the first example of a Th(III) species reducing arenes.

Typically, Th(III) compounds are not strong enough reductants to form reduced-arene complexes. Indeed, Cp'_3Th^{III}, Cp''_3Th^{III}, $Cp^{tet}_3Th^{III}$, $(C_5Me_5)_3Th^{III}$, and $(C_5Me_5)_2Th^{III}[^iPrNC(Me)N^iPr]$ are soluble in benzene and toluene and do not react. Furthermore, the isolated Th(II) compound $[Kcrypt][Cp''_3Th^{II}]$ does not react with benzene and appears slightly soluble in arenes. Addition of KC_8 to Cp''_3Th^{III} and benzene does not form a red solution. However, once MeLi is added to Cp''_3Th^{III} and benzene a red color develops immediately, suggestive of formation of **11.1**. Clearly, addition of MeLi is modulating this reactivity and could be via the formation of $[Cp''_3Th^{III}Me]^{1-}$.

Further GC-MS and NMR experiments are necessary to determine the fate of the Me^{1-} group in eq 11.3. Compound **11.1** appears paramagnetic in solution and the exact assignment of the thorium and benzene oxidation states can be determined from NMR, UV-visible, and EPR spectroscopies alongside theoretical methods. The expansion of eq 11.3 to other arenes such as toluene, xylene, mesitylene, naphthalene, and biphenyl are of interest. If MeLi can indeed modulate the reactivity of Cp''_3Th^{III}, other substrates should be investigated that do not react with Cp''_3Th^{III}, such as H_2, CO, and ethers like DME and THF.

Since the Th(IV)/Th(III) and Th(III)/Th(II) reduction potentials in complexes of the $(Cp^{tet})_3$ ligand set are also similar,[12] the reaction of KH, $Cp^{tet}_3Th^{III}$, and crypt in THF was examined. The initially purple solution turns orange after 45 minutes and $Cp^{tet}_3Th^{IV}H$, [K(crypt)][Cp^{tet}], and [K(crypt)]{$Cp^{tet}_2Th^{IV}H[\eta^5:\eta^1\text{-}C_5Me_3H(CH_2)]$} were identified from the reaction mixture by ^1H NMR spectroscopy and X-ray crystallography, eq 11.4[5]

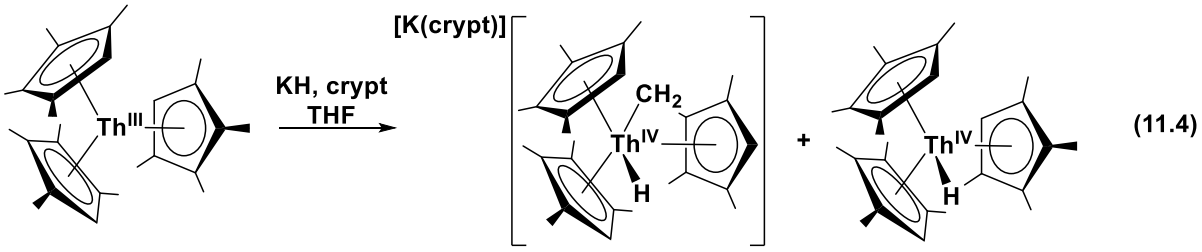

(11.4)

These same products are isolated from the reaction of $Cp^{tet}_3Th^{III}$, KC_8, and crypt in THF, which

forms a dark green solution which may be "[K(crypt)][$Cp^{tet}_3Th^{II}$]" that quickly decomposes.[5] The formation of the C–H bond activation product, [K(crypt)]{$Cp^{tet}_2Th^{IV}H[\eta^5:\eta^1$-$C_5Me_3H(CH_2)]$}, may explain why [K(crypt)][$Cp^{tet}_3Th^{II}$] has proven difficult to isolate. C–H bond activation has been observed before with U(II) complexes[23,24] and may result from Th(II) in this case. These results suggest that $Cp^{tet}_3Th^{III}$ undergoes a similar disproportionation reaction as Cp''_3Th^{III} and a mechanism like Scheme 11.2 may be operative.

Similar results were observed in the reaction of Cp'_3Th^{III} (generated *in situ*, see Chapter 10), KH, and crypt. The dark blue solution of Cp'_3Th^{III} went colorless upon addition of KH and only $Cp'_3Th^{IV}H$ was observed in the ^{1}H NMR spectrum, eq 11.5.

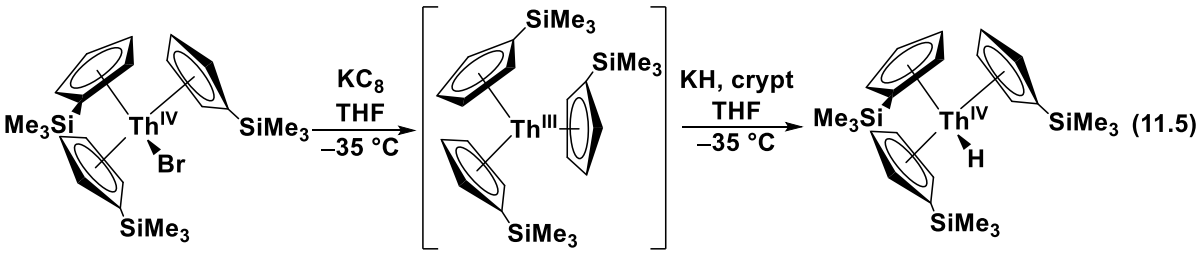

Conclusion

In summary, a new synthetic route to $[Cp''_3Th^{II}]^{1-}$ via the disproportionation of Cp''_3Th^{III} has been discovered. The reaction of Cp''_3Th^{III} with simple MX salts leads to the formation of $Cp''_3Th^{IV}X$ and $[Cp''_3Th^{II}]^{1-}$. A highly reactive "$[Cp''_3Th^{III}X]^{1-}$" complex is a possible intermediate, which can react with benzene to form an arene complex $[Cp''_2Th]_2(C_6H_6)$. The reaction with KH also appears to occur with $Cp^{tet}_3Th^{III}$, which suggests that it can be generalized to other Th(III) and f-element complexes.

Experimental

All syntheses and manipulations described below were conducted under argon with rigorous exclusion of air and water using standard glovebox and vacuum line techniques. Solvents were sparged with UHP argon and dried by passage through columns containing Q-5 and molecular sieves prior to use. Deuterated NMR solvents were dried over NaK alloy,

degassed by three freeze-pump-thaw cycles, and vacuum transferred before use. ^{1}H and ^{13}C NMR spectra were recorded on either a CRYO500 MHz or AVANCE600 MHz at 298 K and referenced to residual protio-solvent resonances. UV-visible spectra were collected at 298 K using a Varian Cary 60 Scan UV-visible spectrophotometer or at −80 °C using a Cary 6000i UV-Vis-NIR spectrometer fitted with a Unisoku cryostat. Infrared spectra were recorded as compressed solids on an Agilent Cary 630 ATR-FTIR. Electrochemical measurements were collected with a Princeton Applied Research PARSTAT 2273 Advanced Electrochemical System. Data were collected with 200 mM $[^{n}Bu_4N][PF_6]$ supporting electrolyte in THF and referenced with internal standard $(C_5Me_5)_2Fe$ following previously reported procedures.[12]

2.2.2-Cryptand (crypt, Aldrich) was used as received. 18-Crown-6 (crown, Alfa) was sublimed before use. KH (Sigma) was washed extensively with hexane and toluene to remove oil and dried under vacuum. ^{n}BuLi (Sigma, 2.5 M solution in hexane) was used as received. LiMe (Sigma) and $LiCH_2SiMe_3$ were purchased as solutions and the solvent was removed to yield both as a bright white powder which were kept at −35 °C until used. NaN_3 and KCl were placed under vacuum at 10^{-5} Torr for 12h before use. KC_8,[25] $Cp''_3Th^{IV}Br$,[11] Cp''_3Th^{III},[11,14,26] $Cp^{tet}_3Th^{III}$,[3] and Cp'_3Th^{III} were synthesized as previously described.

Reaction of Cp''_3Th^{III}, KH, and Crypt. Cp''_3Th^{III} (40 mg, 0.046 mmol) and crypt (18 mg, 0.048 mmol) were dissolved in THF (2 mL). KH (2 mg, 0.050 mmol) was added and the solution was stirred for 5 hours. The solution was dried under vacuum and the products were extracted into hexane to afford a pale blue solution. The solvent was removed under vacuum to yield a blue-grey solid (21 mg). The ^{1}H NMR spectrum in C_6D_6 showed $Cp''_3Th^{IV}H$, Cp''_3Th^{III}, and free crypt. The remaining blue-green solids that did not dissolve in hexane were dissolved in Et_2O, filtered, and dried under vacuum. Crystals were grown from Et_2O/hexane solution at −35 °C and matched the unit cell of $[K(crypt)][Cp''_3Th^{II}]$.[11]

Reaction of Cp''_3Th^{III}, KH, and Crown. Cp''_3Th^{III} (23 mg, 0.027 mmol) and crown (7 mg, 0.027 mmol) were dissolved in THF (2 mL). KH was added and the solution developed a green color as it stirred overnight. The solution was dried under vacuum and extracted into hexane. The remaining blue-green solids were extracted into Et_2O. Both solutions were dried under vacuum. The hexane fraction (16 mg) showed Cp''_3Th^{III} and $Cp''_3Th^{IV}H$ in the ^1H NMR spectrum in a 1:1.1 ratio. $[K(crown)(THF)_2][Cp''_3Th^{II}]$ was identified in the Et_2O fraction (22 mg) by its definitive UV-visible spectrum.[11]

Reaction of Cp''_3Th^{III}, KCl, and Crypt. As described for the KH reaction, Cp''_3Th^{III}, crypt, and KCl were stirred together in THF solution for 2 hours. A dark green color developed. The ^1H NMR spectrum in C_6D_6 of the hexane fraction showed only $Cp''_3Th^{IV}H$. $[K(crypt)][Cp''_3Th^{II}]$ was identified from the Et_2O fraction by UV-visible spectroscopy.

Reaction of Cp''_3Th^{III}, LiMe, and Crypt. Cp''_3Th^{III} (20 mg, 0.023 mmol) and crypt (9 mg, 0.024 mmol) were dissolved in THF (2 mL). LiMe (0.5 mg, 0.023 mmol) was added and the solution turned green after 1 hour. The solution was dried under vacuum. Hexane was added to form a blue solution. This solution was dried under vacuum. The ^1H NMR in C_6D_6 showed $Cp''_3Th^{IV}Me$,[27] Cp''_3Th^{III}, and free crypt. The remaining green solids that did not dissolve in hexane were dissolved in Et_2O, filtered, and dried under vacuum to yield $[Li(crypt)][Cp''_3Th^{II}]$, identified by UV-visible spectroscopy.

Reaction of Cp''_3Th^{III}, NaN_3, and Crypt. Cp''_3Th^{III} (35 mg, 0.041 mmol) and crypt (15 mg, 0.041 mmol) were dissolved in THF (2 mL) and added to NaN_3 (3 mg, 0.046 mmol). The solution developed a green color as it stirred overnight. The solution was dried under vacuum and extracted into hexane. The remaining blue-green solids were extracted in Et_2O. The hexane fraction was dried under vacuum to yield only $Cp''_3Th^{IV}N_3$ (7 mg, 39%) as a colorless oil. ^1H NMR (C_6D_6): δ 6.85 (s, 6H, $C_5H_3(SiMe_3)_2$), 6.81 (s, 3H, $C_5H_3(SiMe_3)_2$), 0.42

(s, 54H, Si*Me*$_3$) ppm. IR: 2952m, 2895w, 2097s, 1440w, 1374w, 1318w, 1247s, 1204w, 1080w, 921sm, 831s, 790m, 753m, 690w cm^{-1}.

Reaction of Cp″$_3$Th^{III}, LiCH$_2$SiMe$_3$, and Crypt. Cp″$_3$Th^{III} (25 mg, 0.029 mmol) and crypt (11 mg, 0.029 mmol) were dissolved in THF (2 mL). LiCH$_2$SiMe$_3$ (3 mg, 0.03 mmol) was added as a solid and the solution quickly turned dark blue-green. The solution was stirred for 2 hours then dried under vacuum. As above, hexane and Et$_2$O fractions were collected. The ^{1}H NMR spectrum in C$_6$D$_6$ of the hexane fraction showed Cp″$_3$Th^{IV}H and Cp″$_3$Th^{III} as the only Cp″-containing compounds present. The Et$_2$O fraction was dried to yield [Li(crypt)][Cp″$_3$Th^{II}] (29 mg, 81%) identified by UV-visible spectroscopy.[12]

Reaction of Cp″$_3$Th^{III}, ^{n}BuLi, and Crypt. Cp″$_3$Th^{III} (45 mg, 0.052 mmol) and crypt (15 mg, 0.040 mmol) were dissolved in THF (2 mL). ^{n}BuLi (0.2 mL of a 2.5 M solution in hexane, 0.5 mmol) was added via syringe to the stirring solution. The solution immediately turned dark green. The solution was stirred for 5 min then dried under vacuum. The solids were washed with hexane then dissolved in Et$_2$O, filtered, and dried under vacuum to yield [Li(crypt)][Cp″$_3$Th^{II}] (41 mg, 66%). The hexane washings were dried under vacuum to yield 21 mg of grey solids. The ^{1}H NMR spectrum in C$_6$D$_6$ showed a single Cp″ environment δ 6.84 (s, 1H, C$_5$*H*$_3$(SiMe$_3$)$_2$), 6.72 (s, 2H, C$_5$*H*$_3$(SiMe$_3$)$_2$), 0.41 ppm (s, 18H, Si*Me*$_3$) that does not match Cp″$_3$ThH. No resonance was observed above 8 ppm indicative of a Th^{IV}–H. The expected product, Cp″$_3$Th^{IV} (^{n}Bu), would likely undergo β–H elimination to form Cp″$_3$Th^{IV}H as was observed with Cp″$_3$Th^{IV}Cl and ^{t}BuLi.[16]

Reaction of Cp$^{tet}_3$Th^{III}, KH, and Crypt. Cp$^{tet}_3$Th^{III} (75 mg, 0.13 mmol) and crypt (47 mg, 0.13 mmol) were dissolved in THF (2 mL). This solution was added to KH (7 mg, 0.2 mmol) and stirred for 1 hour. The color of the solution slowly changed from purple to yellow/orange. The solution was dried under vacuum and the products were extracted into toluene. The ^{1}H NMR spectrum in C$_6$D$_6$ showed Cp$^{tet}_3$Th^{IV}H and free crypt. The remaining

solids were dissolved in THF, filtered, and dried. The ^{1}H NMR spectrum in THF-d_8 showed [K(crypt)][Cp^{tet}] and [K(crypt)][$Cp^{tet}_2Th^{IV}H(\eta^1:\eta^5\text{-}C_5Me_3HCH_2)$].[5] Both compounds were also identified by a unit cell check of single crystals.

Reaction of [K(crown)(THF)$_2$][Cp″$_3$Th^{II}] with Cp″$_3$Th^{IV}Cl. In one vial, [K(crown)(THF)$_2$][Cp″$_3$Th^{II}] (10 mg, 0.008 mmol) was dissolved in THF (1 mL) to form a dark blue/green solution. This solution was added via pipet to a second vial containing a colorless solution of Cp″$_3$Th^{IV}Cl (7 mg, 0.008 mmol) in THF (1 mL). Upon addition, the solution immediately turned deep blue. The solution was stirred for 2 min then dried under vacuum to yield white and blue solids. The solids were redissolved in C_6D_6, filtered, and a ^{1}H NMR spectrum was obtained. The spectrum showed only Cp″$_3$Th^{III}, a small amount of Cp″$_3$Th^{IV}H, and 18-crown-6 with complete disappearance of Cp″$_3$Th^{IV}Cl resonances. The solution was dried under vacuum to yield 11 mg of a dark blue solid (theoretical yield of Cp″$_3$Th^{III} is 14 mg).

***In situ* UV-Visible Spectroscopy of Cp″3Th^{III} with MeLi.** −80 °C electronic absorption studies of the reaction of Cp″$_3$Th^{III} and LiMe were performed using a Cary 6000i UV-Vis-NIR spectrometer fitted with a Unisoku cryostat. An initial absorption spectrum was collected followed by addition of excess LiMe (10 equiv) via syringe to a septum capped 1 cm pathlength quartz cell containing a 0.15 mM solution of Cp″$_3$Th^{III} in THF at -80 ^{o}C. The reaction was then followed through collection of absorption spectra (300-700 nm) every 132 seconds until no further change was observed (~ 28 minutes).

Synthesis of Cp″$_3$Th^{IV}Me from Cp″$_3$Th^{IV}Br. Cp″$_3$Th^{IV}Br (100 mg, 0.106 mmol) was dissolved in Et_2O (5 mL). MeLi was added via syringe (0.07 mL of 1.6M solution in THF, 0.112 mmol) and the colorless solution was stirred overnight. Tan precipitate had formed. The solution was dried under vacuum and hexane was added (10 mL). Solids were removed via

centrifugation and solvent was removed under vacuum to yield off-white solids of $Cp''_3Th^{IV}Me$ (64 mg, 69%), identified by ^1H NMR spectroscopy.[27]

Reaction of $Cp''_3Th^{IV}Me$, KC_8, and Crown to form 11.1. $Cp''_3Th^{IV}Me$ (73 mg, 0.083 mmol) and crown (44 mg, 0.17 mmol) were dissolved in THF (2 mL) to form a colorless solution. To this stirring solution KC_8 (11 mg, 0.081 mmol) was added and the mixture became a deep maroon color. The solution was stirred for five minutes then dried under vacuum. Hexane was added to produce a red solution. This solution was filtered and concentrated under vacuum then placed at −35 °C. Dark red crystals of **11.1** grew overnight. The remaining material that did not dissolve in hexane was extracted into THF and layered with hexane at −35 °C. Colorless crystals of $[K(crown)(THF)_2][Cp''_2Li]$ were identified by X-ray crystallography.

Reaction of Cp'_3Th^{III}, KH, and Crypt. $Cp'_3Th^{IV}Br$ (50 mg, 0.069 mmol) was dissolved in THF (2 mL) and chilled to −35 °C along with KC_8. A second vial was charged with KH (3 mg, 0.075 mmol) and crypt (25 mg, 0.066 mmol) dissolved in THF (1 mL) and chilled to −35 °C. The KC_8 was added to the stirring solution of $Cp'_3Th^{IV}Br$ to generate Cp'_3Th^{III} *in situ*. The solution was quickly centrifuged and the dark blue supernatant was added to the stirring suspension of KH/crypt in THF. The solution immediately turned yellow upon mixing. The solution was stirred for five minutes then dried under vacuum. The products were extracted into hexane and dried under vacuum to yield 28 mg of a mixture of $Cp'_3Th^{IV}H$ and crypt, identified by ^1H NMR spectroscopy. The remaining material that was not soluble in hexane was dissolved in THF, filtered, and dried to yield 34 mg of a yellow solid. Small colorless crystals were grown from THF/hexane at −35 °C but were too small for X-ray crystallography.

Table 11.1: Crystal data and structure refinement for **11.1**.

Identification code	jcw93
Empirical formula	$C_{50}\ H_{90}\ Si_8\ Th_2$
Formula weight	1380.01

Temperature	93(2) K	
Wavelength	0.71073 Å	
Crystal system	Orthorhombic	
Space group	*Fddd*	
Unit cell dimensions	a = 23.587(7) Å	α = 90°.
	b = 23.701(7) Å	β = 90°.
	c = 45.526(14) Å	γ = 90°.
Volume	25450(14) Å^3	
Z	16	
Density (calculated)	1.441 mg/m^3	
Absorption coefficient	4.848 mm^{-1}	
F(000)	10912	
Crystal color	red	
Crystal size	0.217 x 0.170 x 0.162 mm^3	
Theta range for data collection	1.297 to 30.577°	
Index ranges	$-33 \leq h \leq 33$, $-32 \leq k \leq 33$, $-63 \leq l \leq 64$	
Reflections collected	92124	
Independent reflections	9685 [R(int) = 0.0533]	
Completeness to theta = 25.242°	100.0 %	
Absorption correction	Semi-empirical from equivalents	
Max. and min. transmission	0.4330 and 0.3575	
Refinement method	Full-matrix least-squares on F^2	
Data / restraints / parameters	9685 / 0 / 284	
Goodness-of-fit on F^2	1.055	
Final R indices [I>2sigma(I) = 6718 data]	R1 = 0.0504, wR2 = 0.0935	
R indices (all data, 0.70 Å)	R1 = 0.0824, wR2 = 0.1030	
Largest diff. peak and hole	3.509 and -3.497 e.Å^{-3}	

X-ray Data Collection, Structure Solution and Refinement for jcw93.

A red crystal of approximate dimensions 0.217 x 0.170 x 0.12 mm was mounted in a cryoloop and transferred to a Bruker SMART APEX II diffractometer system. The APEX2[28] program package was used to determine the unit-cell parameters and for data collection (60

sec/frame scan time). The raw frame data was processed using SAINT[29] and SADABS[30] to yield the reflection data file. Subsequent calculations were carried out using the SHELXTL[31] program package. The diffraction symmetry was *mmm* and the systematic absences were consistent with the orthorhombic space group *Fddd* that was later determined to be correct.

The structure was solved by dual space methods and refined on F^2 by full-matrix least-squares techniques. The analytical scattering factors[32] for neutral atoms were used throughout the analysis. Hydrogen atoms were included using a riding model.

Least squares analysis yielded wR2 = 0.1030 and Goof = 1.055 for 9685 variables refined against 284 data (0.70 Å), R1 = 0.0504 for those 6718 data with $I > 2.0\sigma(I)$.

There were several high residuals present in the final difference-Fourier map. It was not possible to adequately determine the nature of the residuals although it was probable that hexane solvent was present. The SQUEEZE[33] routine in the PLATON[34] program package was used to account for the electrons in the solvent accessible voids.

Table 11.2: Bond lengths [Å] and angles [°] for **11.1**.

Th(1)-C(1)#1	2.843(7)	Th(2)-C(15)#1	2.824(7)
Th(1)-C(1)	2.843(7)	Th(2)-C(16)	2.816(7)
Th(1)-C(4)#1	2.810(8)	Th(2)-C(16)#1	2.816(7)
Th(1)-C(4)	2.810(8)	Th(2)-C(23)#1	2.701(6)
Th(1)-C(5)	2.796(8)	Th(2)-C(23)	2.701(6)
Th(1)-C(5)#1	2.796(8)	Th(2)-C(24)	2.599(7)
Th(1)-C(23)#1	2.613(6)	Th(2)-C(24)#1	2.599(7)
Th(1)-C(23)	2.613(6)	Th(2)-C(25)#1	2.636(6)
Th(1)-C(24)#1	2.722(7)	Th(2)-C(25)	2.636(6)
Th(1)-C(24)	2.722(7)	Si(1)-C(2)	1.868(8)
Th(1)-C(25)	2.642(6)	Si(1)-C(6)	1.863(10)
Th(1)-C(25)#1	2.643(6)	Si(1)-C(7)	1.905(9)
Th(2)-C(14)	2.856(7)	Si(1)-C(8)	1.848(9)
Th(2)-C(14)#1	2.856(7)	Si(2)-C(5)	1.879(8)
Th(2)-C(15)	2.824(7)	Si(2)-C(9)	1.884(10)

Si(2)-C(10)	1.945(13)	C(11)-H(11A)	0.9800
Si(2)-C(11)	1.850(9)	C(11)-H(11B)	0.9800
Si(3)-C(13)	1.846(7)	C(11)-H(11C)	0.9800
Si(3)-C(17)	1.853(12)	C(12)-H(12)	0.9500
Si(3)-C(18)	1.842(12)	C(12)-C(13)	1.430(9)
Si(3)-C(19)	1.840(11)	C(12)-C(16)	1.410(11)
Si(4)-C(15)	1.894(7)	C(13)-C(14)	1.427(10)
Si(4)-C(20)	1.875(8)	C(14)-H(14)	0.9500
Si(4)-C(21)	1.878(9)	C(14)-C(15)	1.425(10)
Si(4)-C(22)	1.830(9)	C(15)-C(16)	1.416(10)
C(1)-H(1)	0.9500	C(16)-H(16)	0.9500
C(1)-C(2)	1.436(10)	C(17)-H(17A)	0.9800
C(1)-C(5)	1.425(10)	C(17)-H(17B)	0.9800
C(2)-C(3)	1.419(11)	C(17)-H(17C)	0.9800
C(3)-H(3)	0.9500	C(18)-H(18A)	0.9800
C(3)-C(4)	1.407(13)	C(18)-H(18B)	0.9800
C(4)-H(4)	0.9500	C(18)-H(18C)	0.9800
C(4)-C(5)	1.437(11)	C(19)-H(19A)	0.9800
C(6)-H(6A)	0.9800	C(19)-H(19B)	0.9800
C(6)-H(6B)	0.9800	C(19)-H(19C)	0.9800
C(6)-H(6C)	0.9800	C(20)-H(20A)	0.9800
C(7)-H(7A)	0.9800	C(20)-H(20B)	0.9800
C(7)-H(7B)	0.9800	C(20)-H(20C)	0.9800
C(7)-H(7C)	0.9800	C(21)-H(21A)	0.9800
C(8)-H(8A)	0.9800	C(21)-H(21B)	0.9800
C(8)-H(8B)	0.9800	C(21)-H(21C)	0.9800
C(8)-H(8C)	0.9800	C(22)-H(22A)	0.9800
C(9)-H(9A)	0.9800	C(22)-H(22B)	0.9800
C(9)-H(9B)	0.9800	C(22)-H(22C)	0.9800
C(9)-H(9C)	0.9800	C(23)-H(23)	0.9500
C(10)-H(10A)	0.9800	C(23)-C(24)	1.456(9)
C(10)-H(10B)	0.9800	C(23)-C(25)#1	1.465(9)
C(10)-H(10C)	0.9800	C(24)-H(24)	0.9500

C(24)-C(25)	1.429(9)	C(23)-Th(1)-C(24)	31.59(19)
C(25)-C(23)#1	1.465(9)	C(23)-Th(1)-C(24)#1	56.71(19)
C(25)-H(25)	0.9500	C(23)#1-Th(1)-C(24)#1	31.59(19)
		C(23)-Th(1)-C(25)	56.3(2)
C(1)-Th(1)-C(1)#1	165.1(3)	C(23)#1-Th(1)-C(25)	32.4(2)
C(4)-Th(1)-C(1)#1	117.8(2)	C(23)-Th(1)-C(25)#1	32.4(2)
C(4)#1-Th(1)-C(1)#1	47.7(2)	C(23)#1-Th(1)-C(25)#1	56.3(2)
C(4)#1-Th(1)-C(1)	117.8(2)	C(24)#1-Th(1)-C(1)	124.2(2)
C(4)-Th(1)-C(1)	47.7(2)	C(24)-Th(1)-C(1)#1	124.2(2)
C(4)-Th(1)-C(4)#1	74.5(4)	C(24)#1-Th(1)-C(1)#1	70.0(2)
C(5)-Th(1)-C(1)#1	140.2(2)	C(24)-Th(1)-C(1)	70.0(2)
C(5)-Th(1)-C(1)	29.3(2)	C(24)#1-Th(1)-C(4)#1	110.8(2)
C(5)#1-Th(1)-C(1)	140.2(2)	C(24)#1-Th(1)-C(4)	170.9(2)
C(5)#1-Th(1)-C(1)#1	29.3(2)	C(24)-Th(1)-C(4)#1	170.9(2)
C(5)#1-Th(1)-C(4)#1	29.7(2)	C(24)-Th(1)-C(4)	110.8(2)
C(5)-Th(1)-C(4)	29.7(2)	C(24)#1-Th(1)-C(5)#1	81.2(2)
C(5)#1-Th(1)-C(4)	103.4(2)	C(24)#1-Th(1)-C(5)	145.7(2)
C(5)-Th(1)-C(4)#1	103.4(2)	C(24)-Th(1)-C(5)	81.2(2)
C(5)#1-Th(1)-C(5)	132.9(3)	C(24)-Th(1)-C(5)#1	145.7(2)
C(23)-Th(1)-C(1)	97.0(2)	C(24)#1-Th(1)-C(24)	65.0(3)
C(23)#1-Th(1)-C(1)	95.4(2)	C(25)-Th(1)-C(1)	68.6(2)
C(23)-Th(1)-C(1)#1	95.4(2)	C(25)#1-Th(1)-C(1)	125.7(2)
C(23)#1-Th(1)-C(1)#1	97.0(2)	C(25)#1-Th(1)-C(1)#1	68.6(2)
C(23)-Th(1)-C(4)	124.3(2)	C(25)-Th(1)-C(1)#1	125.7(2)
C(23)#1-Th(1)-C(4)	139.4(3)	C(25)#1-Th(1)-C(4)	153.9(2)
C(23)-Th(1)-C(4)#1	139.4(3)	C(25)#1-Th(1)-C(4)#1	116.3(2)
C(23)#1-Th(1)-C(4)#1	124.3(2)	C(25)-Th(1)-C(4)	116.3(2)
C(23)#1-Th(1)-C(5)	122.7(2)	C(25)-Th(1)-C(4)#1	153.9(2)
C(23)-Th(1)-C(5)	97.1(2)	C(25)#1-Th(1)-C(5)	129.4(2)
C(23)-Th(1)-C(5)#1	122.7(2)	C(25)-Th(1)-C(5)	92.2(2)
C(23)#1-Th(1)-C(5)#1	97.1(2)	C(25)#1-Th(1)-C(5)#1	92.2(2)
C(23)-Th(1)-C(23)#1	67.7(3)	C(25)-Th(1)-C(5)#1	129.4(2)
C(23)#1-Th(1)-C(24)	56.70(19)	C(25)-Th(1)-C(24)	30.86(19)

C(25)-Th(1)-C(24)#1	55.8(2)	C(24)-Th(2)-C(14)#1	95.4(2)
C(25)#1-Th(1)-C(24)#1	30.86(19)	C(24)#1-Th(2)-C(14)	95.4(2)
C(25)#1-Th(1)-C(24)	55.8(2)	C(24)-Th(2)-C(14)	99.4(2)
C(25)-Th(1)-C(25)#1	65.2(3)	C(24)-Th(2)-C(15)	98.8(2)
C(14)-Th(2)-C(14)#1	162.2(3)	C(24)#1-Th(2)-C(15)#1	98.8(2)
C(15)#1-Th(2)-C(14)	138.1(2)	C(24)#1-Th(2)-C(15)	122.5(2)
C(15)-Th(2)-C(14)#1	138.1(2)	C(24)-Th(2)-C(15)#1	122.5(2)
C(15)-Th(2)-C(14)	29.1(2)	C(24)#1-Th(2)-C(16)#1	125.1(2)
C(15)#1-Th(2)-C(14)#1	29.1(2)	C(24)-Th(2)-C(16)#1	138.7(2)
C(15)#1-Th(2)-C(15)	130.6(3)	C(24)-Th(2)-C(16)	125.1(2)
C(16)-Th(2)-C(14)	46.9(2)	C(24)#1-Th(2)-C(16)	138.7(2)
C(16)#1-Th(2)-C(14)#1	46.9(2)	C(24)-Th(2)-C(23)#1	57.12(19)
C(16)-Th(2)-C(14)#1	115.7(2)	C(24)#1-Th(2)-C(23)#1	31.8(2)
C(16)#1-Th(2)-C(14)	115.7(2)	C(24)-Th(2)-C(23)	31.8(2)
C(16)-Th(2)-C(15)#1	101.8(2)	C(24)#1-Th(2)-C(23)	57.12(19)
C(16)#1-Th(2)-C(15)	101.8(2)	C(24)-Th(2)-C(24)#1	68.5(3)
C(16)-Th(2)-C(15)	29.1(2)	C(24)#1-Th(2)-C(25)	57.3(2)
C(16)#1-Th(2)-C(15)#1	29.1(2)	C(24)-Th(2)-C(25)#1	57.3(2)
C(16)-Th(2)-C(16)#1	73.4(3)	C(24)#1-Th(2)-C(25)#1	31.68(19)
C(23)-Th(2)-C(14)	71.9(2)	C(24)-Th(2)-C(25)	31.69(19)
C(23)#1-Th(2)-C(14)	124.9(2)	C(25)-Th(2)-C(14)	127.3(2)
C(23)#1-Th(2)-C(14)#1	71.9(2)	C(25)#1-Th(2)-C(14)#1	127.3(2)
C(23)-Th(2)-C(14)#1	124.9(2)	C(25)-Th(2)-C(14)#1	69.9(2)
C(23)-Th(2)-C(15)	82.4(2)	C(25)#1-Th(2)-C(14)	69.9(2)
C(23)#1-Th(2)-C(15)	146.8(2)	C(25)-Th(2)-C(15)#1	93.1(2)
C(23)-Th(2)-C(15)#1	146.8(2)	C(25)-Th(2)-C(15)	130.4(2)
C(23)#1-Th(2)-C(15)#1	82.4(2)	C(25)#1-Th(2)-C(15)#1	130.4(2)
C(23)#1-Th(2)-C(16)#1	111.4(2)	C(25)#1-Th(2)-C(15)	93.1(2)
C(23)-Th(2)-C(16)	111.4(2)	C(25)#1-Th(2)-C(16)#1	154.1(2)
C(23)#1-Th(2)-C(16)	170.5(2)	C(25)-Th(2)-C(16)	154.1(2)
C(23)-Th(2)-C(16)#1	170.5(2)	C(25)#1-Th(2)-C(16)	116.8(2)
C(23)#1-Th(2)-C(23)	65.2(3)	C(25)-Th(2)-C(16)#1	116.8(2)
C(24)#1-Th(2)-C(14)#1	99.4(2)	C(25)-Th(2)-C(23)	55.4(2)

C(25)-Th(2)-C(23)#1	31.8(2)	C(5)-C(1)-C(2)	109.7(7)
C(25)#1-Th(2)-C(23)#1	55.4(2)	Si(1)-C(2)-Th(1)	130.5(3)
C(25)#1-Th(2)-C(23)	31.8(2)	C(1)-C(2)-Th(1)	73.4(4)
C(25)#1-Th(2)-C(25)	65.4(3)	C(1)-C(2)-Si(1)	125.2(6)
C(2)-Si(1)-C(7)	105.4(4)	C(3)-C(2)-Th(1)	74.4(4)
C(6)-Si(1)-C(2)	117.1(4)	C(3)-C(2)-Si(1)	126.5(6)
C(6)-Si(1)-C(7)	106.9(5)	C(3)-C(2)-C(1)	106.1(7)
C(8)-Si(1)-C(2)	109.6(4)	Th(1)-C(3)-H(3)	116.0
C(8)-Si(1)-C(6)	108.9(5)	C(2)-C(3)-Th(1)	77.1(4)
C(8)-Si(1)-C(7)	108.7(4)	C(2)-C(3)-H(3)	125.3
C(5)-Si(2)-C(9)	110.5(4)	C(4)-C(3)-Th(1)	73.6(4)
C(5)-Si(2)-C(10)	107.4(4)	C(4)-C(3)-C(2)	109.4(7)
C(9)-Si(2)-C(10)	112.7(5)	C(4)-C(3)-H(3)	125.3
C(11)-Si(2)-C(5)	107.0(4)	Th(1)-C(4)-H(4)	114.2
C(11)-Si(2)-C(9)	108.6(4)	C(3)-C(4)-Th(1)	77.7(4)
C(11)-Si(2)-C(10)	110.4(4)	C(3)-C(4)-H(4)	125.6
C(13)-Si(3)-C(17)	110.8(4)	C(3)-C(4)-C(5)	108.7(8)
C(18)-Si(3)-C(13)	115.8(4)	C(5)-C(4)-Th(1)	74.6(4)
C(18)-Si(3)-C(17)	106.7(8)	C(5)-C(4)-H(4)	125.6
C(19)-Si(3)-C(13)	105.4(4)	Si(2)-C(5)-Th(1)	122.2(4)
C(19)-Si(3)-C(17)	108.7(8)	C(1)-C(5)-Th(1)	77.2(4)
C(19)-Si(3)-C(18)	109.2(7)	C(1)-C(5)-Si(2)	126.1(6)
C(20)-Si(4)-C(15)	108.7(4)	C(1)-C(5)-C(4)	106.0(7)
C(20)-Si(4)-C(21)	109.5(4)	C(4)-C(5)-Th(1)	75.7(4)
C(21)-Si(4)-C(15)	106.3(4)	C(4)-C(5)-Si(2)	126.7(6)
C(22)-Si(4)-C(15)	109.9(4)	Si(1)-C(6)-H(6A)	109.5
C(22)-Si(4)-C(20)	112.3(4)	Si(1)-C(6)-H(6B)	109.5
C(22)-Si(4)-C(21)	109.9(4)	Si(1)-C(6)-H(6C)	109.5
Th(1)-C(1)-H(1)	115.6	H(6A)-C(6)-H(6B)	109.5
C(2)-C(1)-Th(1)	77.7(4)	H(6A)-C(6)-H(6C)	109.5
C(2)-C(1)-H(1)	125.1	H(6B)-C(6)-H(6C)	109.5
C(5)-C(1)-Th(1)	73.5(4)	Si(1)-C(7)-H(7A)	109.5
C(5)-C(1)-H(1)	125.1	Si(1)-C(7)-H(7B)	109.5

Si(1)-C(7)-H(7C)	109.5	C(16)-C(12)-C(13)	109.7(6)
H(7A)-C(7)-H(7B)	109.5	Si(3)-C(13)-Th(2)	131.7(3)
H(7A)-C(7)-H(7C)	109.5	C(12)-C(13)-Th(2)	73.8(4)
H(7B)-C(7)-H(7C)	109.5	C(12)-C(13)-Si(3)	125.9(5)
Si(1)-C(8)-H(8A)	109.5	C(14)-C(13)-Th(2)	73.7(4)
Si(1)-C(8)-H(8B)	109.5	C(14)-C(13)-Si(3)	126.9(5)
Si(1)-C(8)-H(8C)	109.5	C(14)-C(13)-C(12)	104.3(6)
H(8A)-C(8)-H(8B)	109.5	Th(2)-C(14)-H(14)	115.6
H(8A)-C(8)-H(8C)	109.5	C(13)-C(14)-Th(2)	77.6(4)
H(8B)-C(8)-H(8C)	109.5	C(13)-C(14)-H(14)	124.2
Si(2)-C(9)-H(9A)	109.5	C(15)-C(14)-Th(2)	74.2(4)
Si(2)-C(9)-H(9B)	109.5	C(15)-C(14)-C(13)	111.5(7)
Si(2)-C(9)-H(9C)	109.5	C(15)-C(14)-H(14)	124.2
H(9A)-C(9)-H(9B)	109.5	Si(4)-C(15)-Th(2)	122.1(3)
H(9A)-C(9)-H(9C)	109.5	C(14)-C(15)-Th(2)	76.7(4)
H(9B)-C(9)-H(9C)	109.5	C(14)-C(15)-Si(4)	126.0(5)
Si(2)-C(10)-H(10A)	109.5	C(16)-C(15)-Th(2)	75.2(4)
Si(2)-C(10)-H(10B)	109.5	C(16)-C(15)-Si(4)	127.8(6)
Si(2)-C(10)-H(10C)	109.5	C(16)-C(15)-C(14)	105.3(7)
H(10A)-C(10)-H(10B)	109.5	Th(2)-C(16)-H(16)	113.7
H(10A)-C(10)-H(10C)	109.5	C(12)-C(16)-Th(2)	77.3(4)
H(10B)-C(10)-H(10C)	109.5	C(12)-C(16)-C(15)	109.2(7)
Si(2)-C(11)-H(11A)	109.5	C(12)-C(16)-H(16)	125.4
Si(2)-C(11)-H(11B)	109.5	C(15)-C(16)-Th(2)	75.8(4)
Si(2)-C(11)-H(11C)	109.5	C(15)-C(16)-H(16)	125.4
H(11A)-C(11)-H(11B)	109.5	Si(3)-C(17)-H(17A)	109.5
H(11A)-C(11)-H(11C)	109.5	Si(3)-C(17)-H(17B)	109.5
H(11B)-C(11)-H(11C)	109.5	Si(3)-C(17)-H(17C)	109.5
Th(2)-C(12)-H(12)	115.4	H(17A)-C(17)-H(17B)	109.5
C(13)-C(12)-Th(2)	77.5(4)	H(17A)-C(17)-H(17C)	109.5
C(13)-C(12)-H(12)	125.1	H(17B)-C(17)-H(17C)	109.5
C(16)-C(12)-Th(2)	73.9(4)	Si(3)-C(18)-H(18A)	109.5
C(16)-C(12)-H(12)	125.1	Si(3)-C(18)-H(18B)	109.5

Si(3)-C(18)-H(18C)	109.5	Th(1)-C(23)-H(23)	116.8
H(18A)-C(18)-H(18B)	109.5	Th(2)-C(23)-H(23)	129.7
H(18A)-C(18)-H(18C)	109.5	C(24)-C(23)-Th(1)	78.3(4)
H(18B)-C(18)-H(18C)	109.5	C(24)-C(23)-Th(2)	70.2(4)
Si(3)-C(19)-H(19A)	109.5	C(24)-C(23)-H(23)	120.8
Si(3)-C(19)-H(19B)	109.5	C(24)-C(23)-C(25)#1	118.4(5)
Si(3)-C(19)-H(19C)	109.5	C(25)#1-C(23)-Th(1)	74.9(3)
H(19A)-C(19)-H(19B)	109.5	C(25)#1-C(23)-Th(2)	71.6(3)
H(19A)-C(19)-H(19C)	109.5	C(25)#1-C(23)-H(23)	120.8
H(19B)-C(19)-H(19C)	109.5	Th(1)-C(24)-H(24)	130.2
Si(4)-C(20)-H(20A)	109.5	Th(2)-C(24)-Th(1)	113.3(2)
Si(4)-C(20)-H(20B)	109.5	Th(2)-C(24)-H(24)	116.6
Si(4)-C(20)-H(20C)	109.5	C(23)-C(24)-Th(1)	70.1(4)
H(20A)-C(20)-H(20B)	109.5	C(23)-C(24)-Th(2)	78.0(4)
H(20A)-C(20)-H(20C)	109.5	C(23)-C(24)-H(24)	120.7
H(20B)-C(20)-H(20C)	109.5	C(25)-C(24)-Th(1)	71.5(3)
Si(4)-C(21)-H(21A)	109.5	C(25)-C(24)-Th(2)	75.6(4)
Si(4)-C(21)-H(21B)	109.5	C(25)-C(24)-C(23)	118.6(5)
Si(4)-C(21)-H(21C)	109.5	C(25)-C(24)-H(24)	120.7
H(21A)-C(21)-H(21B)	109.5	Th(1)-C(25)-H(25)	122.0
H(21A)-C(21)-H(21C)	109.5	Th(2)-C(25)-Th(1)	114.7(2)
H(21B)-C(21)-H(21C)	109.5	Th(2)-C(25)-H(25)	123.3
Si(4)-C(22)-H(22A)	109.5	C(23)#1-C(25)-Th(1)	72.7(4)
Si(4)-C(22)-H(22B)	109.5	C(23)#1-C(25)-Th(2)	76.5(3)
Si(4)-C(22)-H(22C)	109.5	C(23)#1-C(25)-H(25)	118.9
H(22A)-C(22)-H(22B)	109.5	C(24)-C(25)-Th(1)	77.6(4)
H(22A)-C(22)-H(22C)	109.5	C(24)-C(25)-Th(2)	72.7(4)
H(22B)-C(22)-H(22C)	109.5	C(24)-C(25)-C(23)#1	122.3(6)
Th(1)-C(23)-Th(2)	113.5(2)	C(24)-C(25)-H(25)	118.9

Symmetry transformations used to generate equivalent atoms:

#1 -x+5/4,-y+5/4,z

References

(1) Parry, J. S.; Cloke, F. G. N.; Coles, S. J.; Hursthouse, M. B. Synthesis and Characterization of the First Sandwich Complex of Trivalent Thorium: A Structural Comparison with the Uranium Analogue. *J. Am. Chem. Soc.* **1999**, *121*, 6867–6871, DOI: 10.1021/ja9903633.

(2) Blake, P. C.; Edelstein, N. M.; Hitchcock, P. B.; Kot, W. K.; Lappert, M. F.; Shalimoff, G. V.; Tian, S. Synthesis, Properties and Structures of the Tris(Cyclopentadienyl)Thorium(III) Complexes [Th{η^5-$C_5H_3(SiMe_2R)_2$-1,3}$_3$] (R = Me or ^{t}Bu). *J. Organomet. Chem.* **2001**, *636*, 124–129, DOI: 10.1016/S0022-328X(01)00860-9.

(3) Siladke, N. A.; Webster, C. L.; Walensky, J. R.; Takase, M. K.; Ziller, J. W.; Grant, D. J.; Gagliardi, L.; Evans, W. J. Actinide Metallocene Hydride Chemistry: C–H Activation in Tetramethylcyclopentadienyl Ligands to Form [μ-η^5-$C_5Me_3H(CH_2)$-κC]$^{2-}$ Tuck-over Ligands in a Tetrathorium Octahydride Complex. *Organometallics* **2013**, *32*, 6522–6531, DOI: 10.1021/om4008482.

(4) Walensky, J. R.; Martin, R. L.; Ziller, J. W.; Evans, W. J. Importance of Energy Level Matching for Bonding in Th^{3+}–Am^{3+} Actinide Metallocene Amidinates, $(C_5Me_5)_2[^iPrNC(Me)N^iPr]An$. *Inorg. Chem.* **2010**, *49*, 10007–10012, DOI: 10.1021/ic1013285.

(5) Langeslay, R. R.; Fieser, M. E.; Ziller, J. W.; Furche, F.; Evans, W. J. Expanding Thorium Hydride Chemistry Through Th^{2+}, Including the Synthesis of a Mixed-Valent Th^{4+}/Th^{3+} Hydride Complex. *J. Am. Chem. Soc.* **2016**, *138*, 4036–4045, DOI: 10.1021/jacs.5b11508.

(6) Langeslay, R. R.; Chen, G. P.; Windorff, C. J.; Chan, A. K.; Ziller, J. W.; Furche, F.;

Evans, W. J. Synthesis, Structure, and Reactivity of the Sterically Crowded Th^{3+} Complex $(C_5Me_5)_3Th$ Including Formation of the Thorium Carbonyl, $[(C_5Me_5)_3Th(CO)][BPh_4]$. *J. Am. Chem. Soc.* **2017**, *139*, 3387–3398, DOI: 10.1021/jacs.6b10826.

(7) Altman, A. B.; Brown, A. C.; Rao, G.; Lohrey, T. D.; Britt, R. D.; Maron, L.; Minasian, S. G.; Shuh, D. K.; Arnold, J. Chemical Structure and Bonding in a Thorium(III)-Aluminum Heterobimetallic Complex. *Chem. Sci.* **2018**, *9*, 4317–4324, DOI: 10.1039/c8sc01260a.

(8) Formanuik, A.; Ariciu, A.-M.; Ortu, F.; Beekmeyer, R.; Kerridge, A.; Tuna, F.; McInnes, E. J. L.; Mills, D. P. Actinide Covalency Measured by Pulsed Electron Paramagnetic Resonance Spectroscopy. *Nat. Chem.* **2017**, *9*, 578–583, DOI: 10.1038/nchem.2692.

(9) Huh, D. N.; Roy, S.; Ziller, J. W.; Furche, F.; Evans, W. J. Isolation of a Square-Planar Th(III) Complex: Synthesis and Structure of $[Th(OC_6H_2{}^tBu_2\text{-}2,6\text{-}Me\text{-}4)_4]^{1-}$. *J. Am. Chem. Soc.* **2019**, *141*, 12458–12463, DOI: 10.1021/jacs.9b04399.

(10) Ortu, F.; Formanuik, A.; Innes, J. R.; Mills, D. P. New Vistas in the Molecualr Chemistry of Thorium: Low Oxidation State Complexes. *Dalton Trans.* **2016**, *45*, 7537–7549, DOI: 10.1039/c6dt01111j.

(11) Langeslay, R. R.; Fieser, M. E.; Ziller, J. W.; Furche, F.; Evans, W. J. Synthesis, Structure, and Reactivity of Crystalline Molecular Complexes of the $\{[C_5H_3(SiMe_3)_2]_3Th\}^{1-}$ Anion Containing Thorium in the Formal +2 Oxidation State. *Chem. Sci.* **2015**, *6*, 517–521, DOI: 10.1039/C4SC03033H.

(12) Wedal, J. C.; Barlow, J. M.; Ziller, J. W.; Yang, J. Y.; Evans, W. J. Electrochemical Studies of Tris(Cyclopentadienyl)Thorium and Uranium Complexes in the +2, +3, and +4 Oxidation States. *Chem. Sci.* **2021**, *12*, 8501–8511, DOI: 10.1039/D1SC01906F.

(13) Inman, C. J.; Cloke, F. G. N. The Experimental Determination of Th(IV)/Th(III) Redox Potentials in Organometallic Thorium Complexes. *Dalton Trans.* **2019**, *48*, 10782–10784, DOI: 10.1039/c9dt01553a.

(14) Blake, P. C.; Lappert, M. F.; Atwood, J. L.; Zhang, H. The Synthesis and Characterisation, Including X-Ray Diffraction Study, of [Th{η-$C_5H_3(SiMe_3)_2$}$_3$]; the First Thorium(III) Crystal Structure. *J. Chem. Soc., Chem. Commun.* **1986**, *453*, 1148–1149, DOI: 10.1039/C39860001148.

(15) Wedal, J. C.; Bekoe, S.; Ziller, J. W.; Furche, F.; Evans, W. J. In Search of Tris(Trimethylsilylcyclopentadienyl) Thorium. *Dalton Trans.* **2019**, *48*, 16633–16640, DOI: 10.1039/C9DT03674A.

(16) Weydert, M.; Brennan, J. G.; Andersen, R. A.; Bergman, R. G. Reactions of Uranium(IV) Tertiary Alkyl Bond: Facile Ligand-Assisted Reduction and Insertion of Ethylene and Carbon Monoxide. *Organometallics* **1995**, *14*, 3942–3951, DOI: 10.1021/om00008a046.

(17) MacDonald, M. R.; Fieser, M. E.; Bates, J. E.; Ziller, J. W.; Furche, F.; Evans, W. J. Identification of the +2 Oxidation State for Uranium in a Crystalline Molecular Complex, [K(2.2.2-Cryptand)][$(C_5H_4SiMe_3)_3$U]. *J. Am. Chem. Soc.* **2013**, *135*, 13310–13313, DOI: 10.1021/ja406791t.

(18) Windorff, C. J.; MacDonald, M. R.; Meihaus, K. R.; Ziller, J. W.; Long, J. R.; Evans, W. J. Expanding the Chemistry of Molecular U^{2+} Complexes: Synthesis, Characterization, and Reactivity of the {$[C_5H_3(SiMe_3)_2]_3U$}$^-$ Anion. *Chem. Eur. J.* **2016**, *22*, 772–782, DOI: 10.1002/chem.201503583.

(19) Kotyk, C. M.; Fieser, M. E.; Palumbo, C. T.; Ziller, J. W.; Darago, L. E.; Long, J. R.; Furche, F.; Evans, W. J. Isolation of +2 Rare Earth Metal Ions with Three Anionic Carbocyclic Rings: Bimetallic Bis(Cyclopentadienyl) Reduced Arene Complexes of

La^{2+} and Ce^{2+} Are Four Electron Reductants. *Chem. Sci.* **2015**, *6*, 7267–7273, DOI: 10.1039/c5sc02486b.

(20) Yu, C.; Liang, J.; Deng, C.; Lefèvre, G.; Cantat, T.; Diaconescu, P. L.; Huang, W. Arene-Bridged Dithorium Complexes: Inverse Sandwiches Supported by a δ bonding Interaction. *J. Am. Chem. Soc.* **2020**, *142*, 21292–21297, DOI: 10.1021/jacs.0c11215.

(21) Kilpatrick, A. F. R.; Green, J. C.; Turner, Z. R.; Buffet, J.-C.; O'Hare, D. Zirconium Arene Triple-Decker Sandwich Complexes: Synthesis, Electronic Structure and Bonding. *Chem. Commun.* **2017**, *53*, 12048–12051, DOI: 10.1039/C7CC07083G.

(22) Kelly, R. P.; Maron, L.; Scopelliti, R.; Mazzanti, M. Reduction of a Cerium(III) Siloxide Complex To Afford a Quadruple-Decker Arene-Bridged Cerium(II) Sandwich. *Angew. Chem. Int. Ed.* **2017**, *56*, 15663–15666, DOI: 10.1002/anie.201709769.

(23) La Pierre, H. S.; Kameo, H.; Halter, D. P.; Heinemann, F. W.; Meyer, K. Coordination and Redox Isomerization in the Reduction of a Uranium(III) Monoarene Complex. *Angew. Chem. Int. Ed.* **2014**, *53*, 7154–7157, DOI: 10.1002/anie.201402048.

(24) Wedal, J. C.; Bekoe, S.; Ziller, J. W.; Furche, F.; Evans, W. J. C–H Bond Activation via U(II) in the Reduction of Heteroleptic Bis(Trimethylsilyl)Amide U(III) Complexes. *Organometallics* **2020**, *39*, 3425–3432, DOI: 10.1021/acs.organomet.0c00496.

(25) Bergbreiter, D. E.; Killough, J. M. Reactions of Potassium-Graphite. *J. Am. Chem. Soc.* **1978**, *100*, 2126–2134, DOI: 10.1021/ja00475a025.

(26) Kot, W. K.; Shalimoff, G. V.; Edelstein, N. M.; Edelman, M. A.; Lappert, M. F. $[Th^{III}\{\eta^5\text{-}C_5H_3(SiMe_3)_2\}_3]$, an Actinide Compound with a $6d^1$ Ground State. *J. Am. Chem. Soc.* **1988**, *110*, 986–987, DOI: 10.1021/ja00211a059.

(27) Liu, J.; Seed, J. A.; Formanuik, A.; Ortu, F.; Wooles, A. J.; Mills, D. P.; Liddle, S. T. Thorium(IV) Alkyl Synthesis from a Thorium(III) Cyclopentadienyl Complex and an N-Heterocyclic Olefin. *J. Organomet. Chem.* **2018**, *857*, 75–79, DOI:

10.1016/j.jorganchem.2017.08.015.

(28) APEX2 Version 2014.11-0, Bruker AXS, Inc.; Madison, WI 2014.

(29) SAINT Version 8.34a, Bruker AXS, Inc.; Madison, WI 2013.

(30) Sheldrick, G. M. SADABS, Version 2014/5, Bruker AXS, Inc.; Madison, WI 2014.

(31) Sheldrick, G. M. SHELXTL, Version 2014/7, Bruker AXS, Inc.; Madison, WI 2014.

(32) International Tables for Crystallography 1992, Vol. C., Dordrecht: Kluwer Academic Publishers.

(33) Spek, A.L. PLATON SQUEEZE: a Tool for the Calculation of the Disordered Solvent Contribution to the Calculated Structure Factors. *Acta Cryst.* **2015**, *C71*, 9-19, DOI: 10.1107/S2053229614024929.

(34) Spek, A. L. Structure Validation in Chemical Crystallography, *Acta. Cryst.* **2009**, *D65*, 148-155, DOI: 10.1107/S090744490804362X.

Chapter 12:

Evaluating Electrochemical Accessibility of $4f^n5d^1$ and $4f^{n+1}$ Ln(II) Ions in $(C_5H_4SiMe_3)_3Ln$ and $(C_5Me_4H)_3Ln$ Complexes

Introduction[†]

As described in Chapter 1, at one time it was assumed that $4f^7$ Eu(II), $4f^{14}$ Yb(II), and $4f^6$ Sm(II) were the only +2 lanthanide ions accessible in solution.[1–3] The availability of these ions was attributed to the quantum mechanical stabilization and symmetric nature of the half-filled and filled-shells and the $4f^6$ configuration that approached a half-filled shell. Chemical[4–6] and electrochemical[7,8] studies were consistent with this idea, with Eu(II) being the most stable, followed by Yb(II) and then Sm(II). Ln(III)/Ln(II) reduction potentials for the $4f^n \rightarrow 4f^{n+1}$ couples, estimated on the basis of thermochemical and electrochemical data were so negative (see Table 12.5 for a compilation) that the Ln(II) ions would react with any solvent.[3,9,10] Tm(II), Dy(II), and Nd(II) were known in the solid state, but were not expected to exist in solution[2,11] until 1997–2001 when Bochkarev and co-workers showed that molecular species of $4f^{13}$ Tm(II), $4f^{10}$ Dy(II), and $4f^4$ Nd(II) could be synthesized.[4,12,13] The $4f^{13}$ Tm(II) ion was the next most likely Ln(II) species since it was approaching a filled shell, but the other two ions did not have electron configurations that could be rationalized by this method. Since no other Ln(II) ions were known even in the solid state, it was believed that Eu(II), Yb(II), Sm(II), Tm(II), Dy(II), and Nd(II) were the only lanthanides that could be isolable in the +2 oxidation state.

[†] Portions of this Chapter have been published: Evaluating Electrochemical Accessibility of $4f^n5d^1$ and $4f^{n+1}$ Ln(II) Ions in $(C_5H_4SiMe_3)_3Ln$ and $(C_5Me_4H)_3Ln$ Complexes. *Dalton Trans.* **2021**, *50*, 14384–14389, DOI: 10.1039/D1DT02427B.

In 2008, Lappert reported La(II) and Ce(II) species via reduction of tris(cyclopentadienyl) complexes[14] and by 2013, Ln(II) were known for all the rest of the lanthanide series (excluding radioactive Pm) and yttrium using this reduction method.[15–21] Lappert reported electrochemical measurements on Cp''_3La and a reversible couple was observed with an $E_{1/2}$ value of −2.80 V vs Fc^+/Fc.[22] However, electrochemical analysis of the other Ln(III)/Ln(II) reduction potentials focused predominantly on the traditional six Ln(II) (Ln = Nd, Sm, Eu, Dy, Tm, and Yb) ions with $4f^{n+1}$ electron configurations[12,13] despite the availability of every lanthanide metal in the +2 oxidation state.

The absence of electrochemical measurements on the non-traditional Ln(III)/Ln(II) redox couples was due in part to the high reactivity of the new $4f^n5d^1$ Ln(II) ions and the very negative reduction potentials needed to form them. The most polar solvent that is inert to these Ln(II) ions[23,24] is THF which, in electrochemical experiments, leads to a large internal resistance and large peak separations.[25,26] In addition, Ln(II) species often react with common supporting electrolytes. Electrochemical studies of low oxidation state actinide complexes in Chapter 3 showed that $[^nBuN_4][BPh_4]$ is suitable for strongly reducing f element systems.[27–31]

In this Chapter, the successful electrochemical determination of the Ln(III)/Ln(II) reduction potential across the entire Cp'_3Ln ($Cp' = C_5H_4SiMe_3$) series using $[^nBu_4N][BPh_4]$ in THF is described. Additionally, the electrochemistry of three Ln(II) complexes, [K(crypt)][Cp'_3Ln] (crypt = 2.2.2-cryptand), is presented to verify the data obtained from Cp'_3Ln studies. Also reported are reduction potentials of nine $Cp^{tet}{}_3Ln$ ($Cp^{tet} = C_5Me_4H$) compounds that were analyzed to investigate the impact of the electron-donation strength of the ligand on the reduction potentials of the lanthanide complexes. A majority of the following data was collected in collaboration with undergraduate student Michael Trinh.

Results

Electrochemical Protocol. Cyclic voltammetry experiments were performed using a glassy carbon disc working electrode, a platinum wire counter electrode, and a silver wire pseudo-reference electrode. Freshly-made 100 mM solutions of [^{n}Bu$_4$N][BPh$_4$] in THF provided the supporting electrolyte. All potentials are reported versus the ferrocenium/ferrocene (Fc^+/Fc) couple, which is reported as −0.40 V vs NHE.[32] Decamethylferrocene, $(C_5Me_5)_2Fe$, which has a reduction potential of −0.495 V vs Fc^+/Fc under the present experimental conditions,[27] was used as an internal standard for all experiments.

$(C_5H_4SiMe_3)_3Ln$. The Cp′$_3$Ln series was chosen for this study since Cp′$_3$Ln can be synthesized for the entire lanthanide series (excluding radioactive promethium), as well as for yttrium.[20] The reduction potentials measured for the Cp′$_3$Ln complexes are given in Table 12.1. The cyclic voltammograms of all the Cp′$_3$Ln complexes, except for Cp′$_3$La and Cp′$_3$Ce, exhibit a quasi-reversible event assigned to the Ln(III)/Ln(II) redox couple. A representative example of Cp′$_3$Tb is shown in Figure 12.1. The ΔE_{pp} varies from 0.18 V to 1.08 V, as was previously found for the actinide and lanthanide electrochemistry in THF using [^{n}Bu$_4$N][BPh$_4$] or [^{n}Bu$_4$N][OTf].[27,33] Variations in scan rate resulted in minimal change to the $E_{1/2}$ value. The cyclic voltammograms for Cp′$_3$La and Cp′$_3$Ce displayed only cathodic events, Figure 12.2. In both cases, the processes are irreversible up to scan rates of v = 800 mV / s.

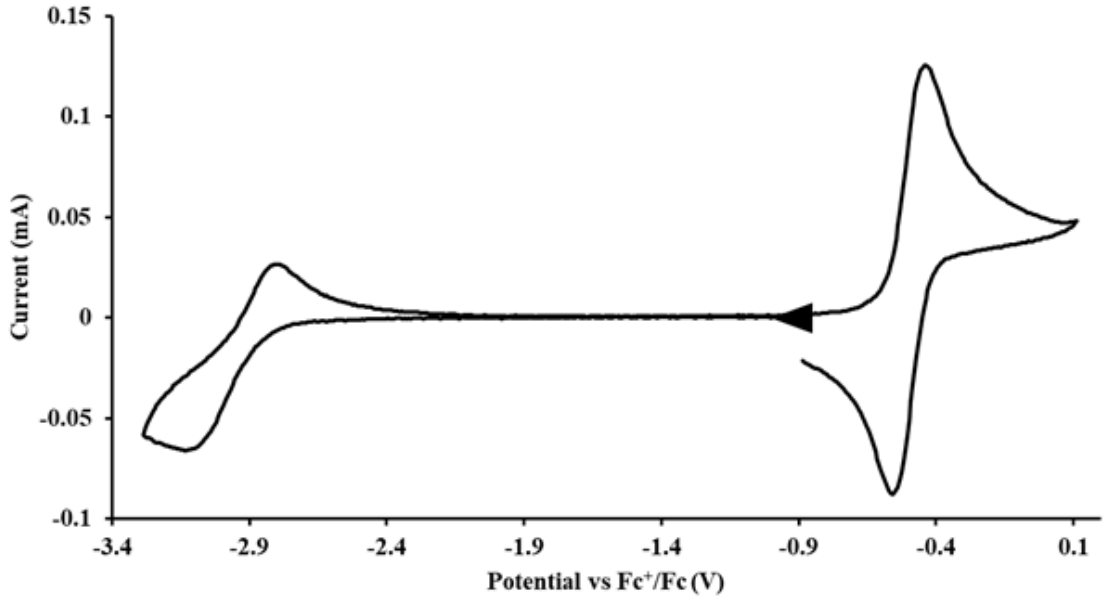

Figure 12.1: Cyclic voltammogram of Cp'_3Tb with the internal standard $(C_5Me_5)_2Fe$ at ν = 200 mV/s. The event assigned to the Tb(III)/Tb(II) couple is centered at −2.95 V. The event at −0.495 V is due to the internal standard.

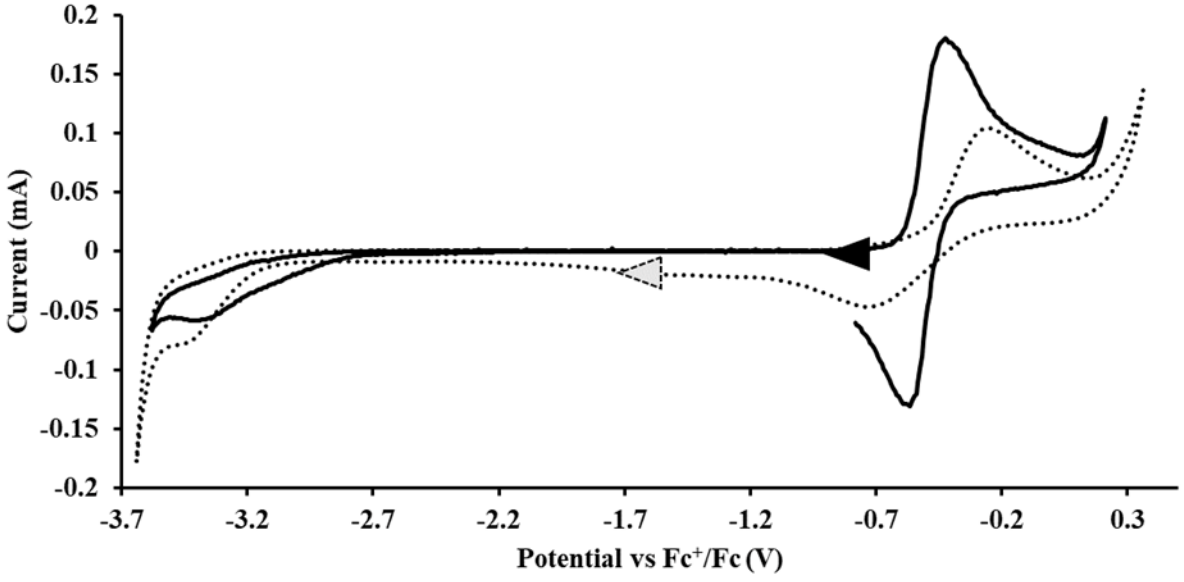

Figure 12.2: Cyclic voltammogram of Cp'_3La (solid) and Cp'_3Ce (dotted) with the internal standard $(C_5Me_5)_2Fe$ at ν = 200 mV/s. The events centered at −0.495 V are due to the internal standard.

To confirm these assignments, Ln(II) complexes [K(crypt)][Cp′$_3$Ln] (Ln = Pr, Sm, Eu) were analyzed, Figure 12.3. The measured $E_{1/2}$ values in Table 12.2 are in good agreement with the values in Table 12.1.

(C$_5$Me$_4$H)$_3$Ln. The Cp$^{tet}_3$Ln compounds were also studied via electrochemistry to determine how the ligand electron-donating strength affects the Ln reduction potential. Ln(II) complexes with the Cp^{tet} ligand set, i.e. [K(crypt)][Cp$^{tet}_3$Ln], have been isolated only for the larger lanthanide metals Ln = La, Ce, Pr, Nd, Sm, Gd, Tb, and Dy. The redox couples observed in the cyclic voltammograms for Cp$^{tet}_3$Ln are summarized in Table 12.3 and Figure 12.4 shows a representative example for Cp$^{tet}_3$Gd. Interestingly, with this ligand set, both E_{PA} and E_{PC} events are observed for Cp$^{tet}_3$La and Cp$^{tet}_3$Ce, the latter of which has the most negative $E_{1/2}$. Overall, the reduction potentials for the Cp$^{tet}_3$Ln series are more negative than the Cp′$_3$Ln series which is consistent with the electron-donating strength of the ligand.[27,34–36]

Table 12.1: Ln(III)/Ln(II) reduction potentials of Cp′$_3$Ln with 100 mM [^{n}Bu$_4$N][BPh$_4$] supporting electrolyte in THF at v = 200 mV / s.

Ln	E_{PC} (V)	E_{PA} (V)	Ln(III)/Ln(II) $E_{1/2}$ (V)
Y	−3.12	−2.94	−3.06
La	−3.36	N/A[a]	N/A
Ce	−3.43	N/A[a]	N/A
Pr	−3.35	−2.93	−3.14
Nd	−3.33	−2.93	−3.14
Sm	−2.76	−2.06	−2.41
Eu	−1.61	−0.53	−1.07
Gd	−3.31	−2.64	−2.98
Tb	−3.10	−2.80	−2.95
Dy	−3.05	−2.86	−2.96
Ho	−3.12	−2.92	−3.02
Er	−3.14	−2.90	−3.02
Tm	−3.04	−2.63	−2.83
Yb	−2.02	−1.27	−1.64
Lu	−3.21	−3.03	−3.12

[a] Denotes the absence of a return oxidation in the cyclic voltammogram.

Table 12.2: Ln(III)/Ln(II) Reduction potentials for Cp'_3Ln and [K(crypt)][Cp'_3Ln] compounds with 100 mM [$^nBu_4N$][BPh_4] supporting electrolyte in THF at ν = 200 mV / s.

	E_{PC} (V)	E_{PA} (V)	Ln(III)/Ln(II) $E_{1/2}$ (V)
Cp'_3Pr	−3.35	−2.93	−3.14
[K(crypt)][Cp'_3Pr]	−3.36	−2.93	−3.15
Cp'_3Sm	−2.76	−2.06	−2.41
[K(crypt)][Cp'_3Sm]	−2.76	−2.06	−2.41
Cp'_3Eu	−1.61	−0.53	−1.07
[K(crypt)][Cp'_3Eu]	−1.48	−1.03	−1.26

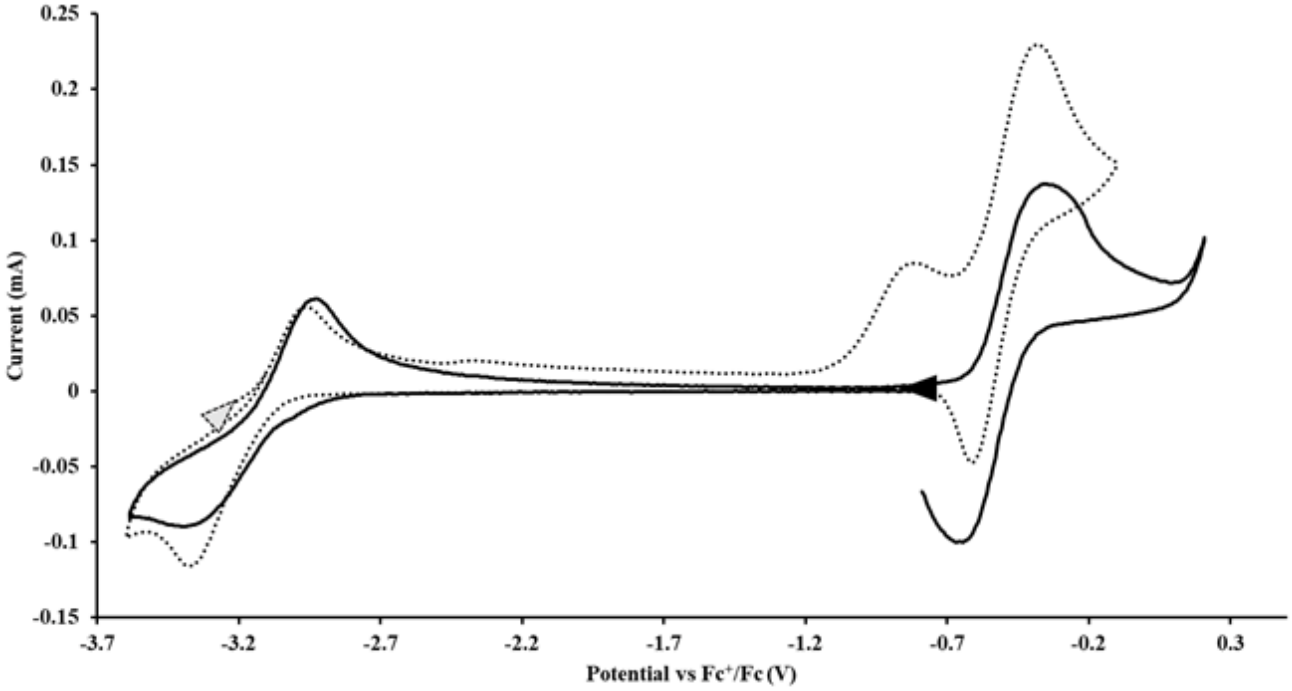

Figure 12.3: Cyclic voltammogram of Cp'_3Pr (solid) and [K(crypt)][Cp'_3Pr] (dashed) with the internal standard $(C_5Me_5)_2Fe$ at ν = 200 mV/s. The events centered at −3.14 V are assigned to the Pr(III)/Pr(II) couple, the anodic event at −0.35 V in the voltammogram of [K(crypt)][Cp'_3Pr] is likely a ligand-based event, and the event centered at −0.495 V is due to the internal standard.

Table 12.3: Ln(III)/Ln(II) reduction potentials of the Cp^{tet}_3Ln compounds with 100 mM [^{n}Bu$_4$N][BPh$_4$] supporting electrolyte in THF at ν = 200 mV / s.

Ln	E_{PC} (V)	E_{PA} (V)	Ln(III)/Ln(II) $E_{1/2}$ (V)
La	−3.48	−3.22	−3.35
Ce	−3.32	−3.22	−3.37
Pr	−3.51	−3.22	−3.27
Nd	−3.27	−3.11	−3.19
Sm	−2.77	−2.43	−2.60
Gd	−3.12	−2.95	−3.04
Tb	−3.19	−3.04	−3.12
Dy	−3.29	−3.10	−3.20
Ho	−3.24	−3.11	−3.18

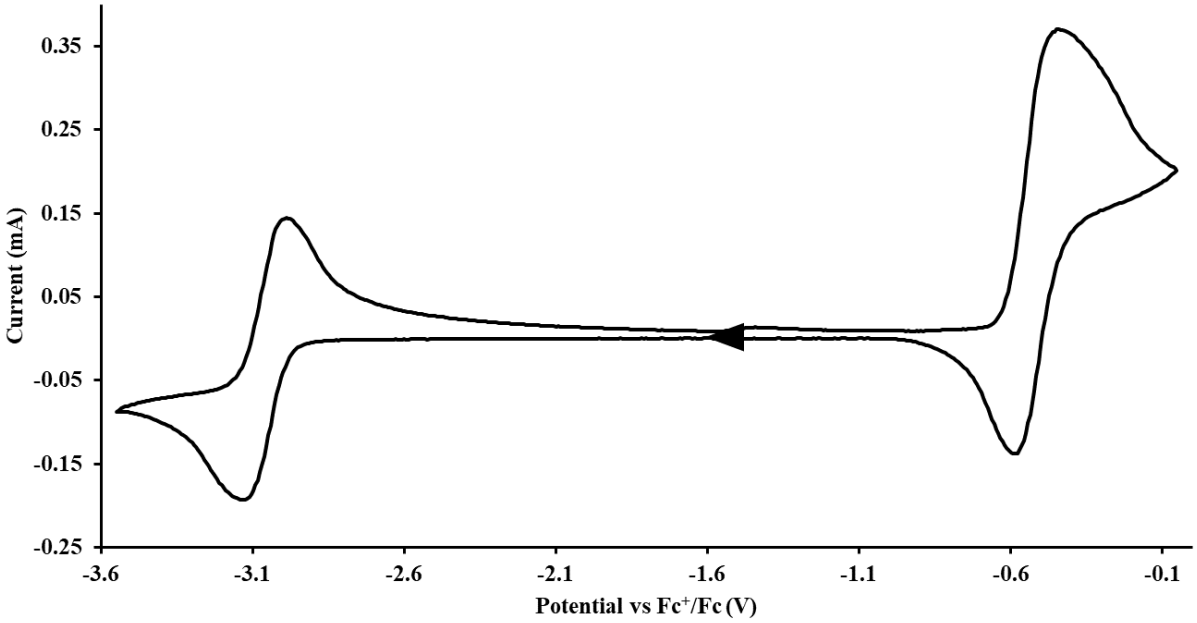

Figure 12.4: Cyclic voltammogram of Cp^{tet}_3Gd with the internal standard $(C_5Me_5)_2Fe$ at ν = 200 mV/s. The event centered at −3.04 V is assigned to the Gd(III)/Gd(II) couple and the event centered at −0.495 V is due to the internal standard.

Discussion

Using [^{n}Bu$_4$N][BPh$_4$] as a supporting electrolyte, it was possible to collect electrochemical data on all the metals in the lanthanide series (except the radioactive Pm). This is because the Cp′$_3$ ligand set is the first to support Ln(II) ions across the series in complexes stable enough for electrochemical analysis.

Except for Cp′$_3$La and Cp′$_3$Ce, quasi-reversible cyclic voltammograms were obtained and the assignment of the redox couple to a Ln(III)/Ln(II) process was confirmed by analyzing the Ln(II) complexes [K(crypt)][Cp′$_3$Ln] for Ln = Pr, Eu, and Sm. For Cp′$_3$La and Cp′$_3$Ce, it is likely that the Ln(II) product participated in a chemical reaction that interfered with the corresponding oxidation in the redox couple.

The [^{n}Bu$_4$N][BPh$_4$] supporting electrolyte also led to successful electrochemical analysis of Cp$^{tet}_3$Ln complexes. Since Cp^{tet} is a more electron-donating ligand than Cp′,[27,34–36] more negative reduction potentials for Cp$^{tet}_3$Ln compared to their Cp′$_3$Ln analogs were observed with shifts of 0.05–0.24 V, depending on the metal. In addition, the electrochemistry of Cp$^{tet}_3$La was more reversible than that of Cp′$_3$La, even though these are some of the most negative potentials measured. Hence, the electrochemical results appear to be quite sensitive to the specific metal and ligand. A plot of the E_{PC} for Cp′$_3$Ln vs E_{PC} for Cp$^{tet}_3$Ln is shown in Figure 12.5. The low R^2 = 0.62 value shows the variability of the data with metal and ligand and the lack of a consistent correlation.

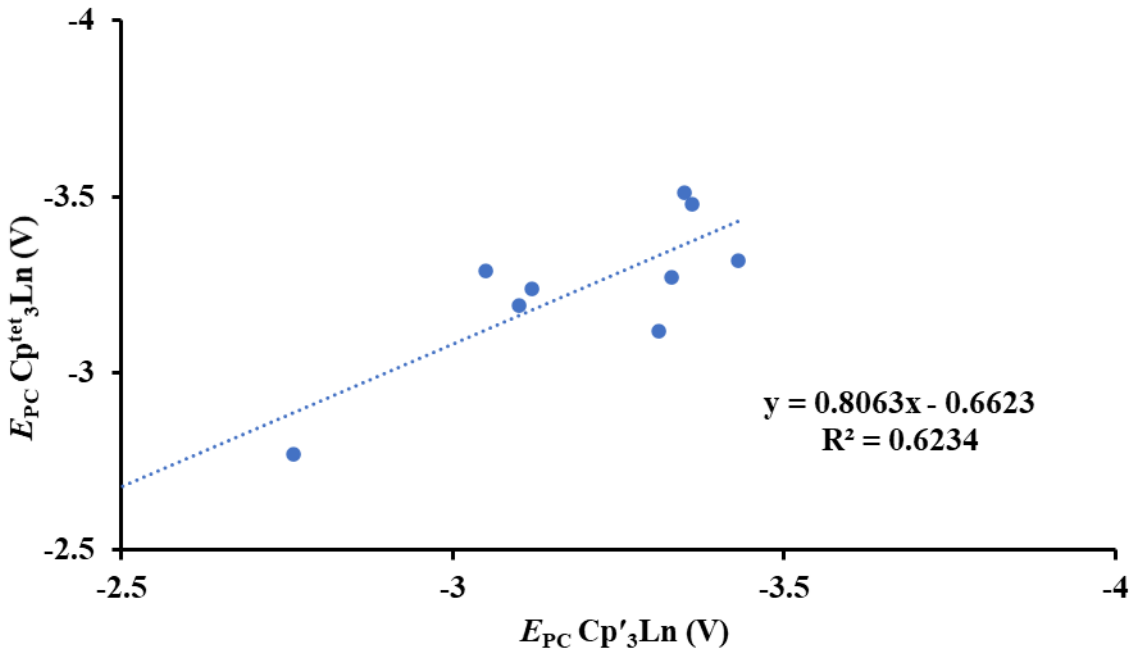

Figure 12.5: E_{PC} for Cp'_3Ln vs E_{PC} for Cp^{tet}_3Ln with "best fit" shown as the dotted line (R^2 = 0.62).

For the traditional $4f^{n+1}$ Ln(II) ions, the Ln(III)/Ln(II) reduction potentials of the Cp'_3Ln complexes follow the order of stability expected based on half-filled shells being more stable than filled shells. Hence, the couple for $4f^7$ Eu(II) (−1.07 V) was less negative than that of $4f^{14}$ Yb(II) (−1.64 V). The Ln(II) ions with electron configurations approaching half-filled and filled subshells are next, $4f^6$ Sm (II) (−2.41 V), and $4f^{13}$ Tm (−2.83 V). These data are valuable since they show consistency with previous studies and match the known reactivity studies in the literature.

The reduction potentials of the non-traditional $4f^n5d^1$ Ln(II) ions were all more negative than those of the traditional ions, a trend that is also consistent with chemical studies in the literature. These $E_{1/2}$ values are plotted against the $4f^{n+1} \rightarrow 4f^n5d^1$ promotion energies for free Ln(II) ions in the gas phase,[37] Figure 12.6. The metals (Ln = Eu, Yb, Sm, Tm) with the largest promotion energy have the least negative reduction potentials and are metals that form $4f^{n+1}$ Ln(II) ions. For all the other entries, the plot shows no correlation with the $4f^n + e^- \rightarrow 4f^n5d^1$ reduction

potential and the $4f^{n+1} \rightarrow 4f^n5d^1$ promotion energy. This lack of correlation and the narrow range

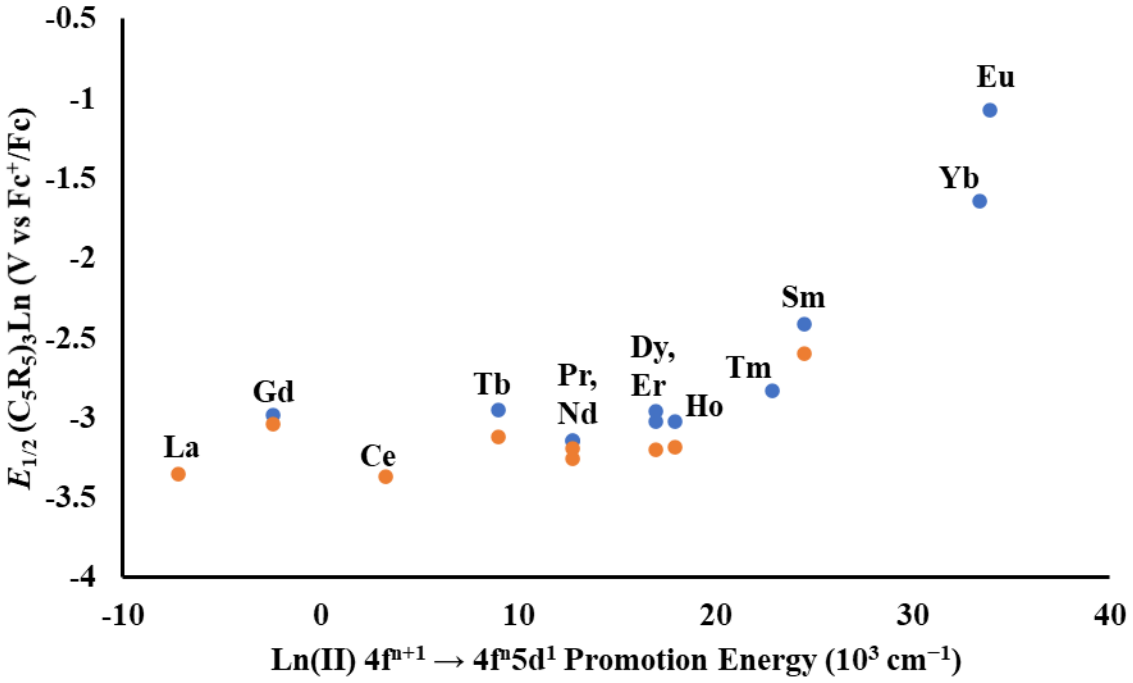

Figure 12.6: $E_{1/2}$ values of Cp'_3Ln (blue) and Cp^{tet}_3Ln (orange) versus $4f^{n+1} \rightarrow 4f^n5d^1$ promotion energies for free Ln^{2+} ions in the gas phase.

of −2.95 V to −3.14 V reduction potentials for the other metals suggests that the electrochemical potential needed to add an electron to a $4f^n$ Ln(III) ion to make the $4f^n5d^1$ Ln(II) ion is similar for all these metals. There is also no obvious correlation between the reduction potentials and the number of 4f electrons in the $4f^n5d^1$ electron configuration, Table 12.4, but it does appear that the Ln(II) ions that have the most unpaired electrons in their electron configurations are the least difficult to reduce. Hence, $4f^75d^1$ Gd(II) with a half-filled 4f shell and $4f^85d^1$ Tb(II) with six formally unpaired 4f electrons have less negative reduction potentials compared to the other ions Table 12.4. Since this analysis is at the single electron approximation level, this should only be noted as an observation that needs further evaluation in the future.

Table 12.4: $E_{1/2}$ and E_{PC} values for Cp'_3Ln in order of increasing reduction potential.

Ln	$E_{1/2}$ (V)	E_{PC} (V)	n in $4f^n5d^1$	Number of unpaired f electrons
Tb	−2.95	−3.10	8	6
Dy	−2.96	−3.05	9	5
Gd	−2.98	−3.31	7	7
Ho	−3.02	−3.12	10	4
Er	−3.02	−3.14	11	4
Lu	−3.12	−3.21	14	0
Nd	−3.14	−3.33	3	3
Pr	−3.14	−3.35	2	2
La		−3.43	0	0
Ce		−3.36	1	1

The reduction potentials of Cp'_3Dy and Cp^{tet}_3Dy are of special interest since Dy(II) is a configurational crossover ion[17,20] that has a $4f^95d^1$ electron configuration in $[K(crypt)][Cp'_3Dy]$[17] and a $4f^{10}$ configuration in $[K(crypt)][Cp^{tet}_3Dy]$.[38] The more negative −3.20 V $E_{1/2}$ for Cp^{tet}_3Dy compared to −2.96 V for Cp'_3Dy is consistent with the large electron-donating power of Cp^{tet}. However, this means that it is easier to populate a 5d orbital in Cp'_3Dy than to add an electron to the 4f valence orbitals of Cp^{tet}_3Dy. Again, this shows the strong dependence of the reduction potentials on ligands.

The determined reduction potentials can also be compared with the values predicted by various methods, Table 12.5. The trends established by the calculated estimates match the values for the Cp'_3Ln series, but it is evident that none of the three methods accurately predict the measured reduction potentials. This further shows the value of electrochemical measurements for these systems.

Table 12.5: Experimental and theoretical calculated Ln(III)/Ln(II) reduction potentials for the lanthanide ions. Values are reported vs Fc^+/Fc (reported as −0.40 V vs NHE).[37]

	Experimental $E_{1/2}$ in Cp'_3Ln	**Thermochemical estimates[3,a]**	**Thermodynamic estimates[9,a]**	**Atomic spectroscopy estimates[10]**
La	N/A	−3.34	−3.4[b]	−2.7
Ce	N/A	−3.36	−3.3[b]	−2.8
Pr	−3.14	−2.63	−2.7	−2.3
Nd	−3.14	−2.22	−2.4	−2.2
Sm	−2.41	−1.17	−1.2	−1.2
Eu	−1.07	0.15	0.1	0.1
Gd	−2.98	−3.42	−3.1[b]	−3.5
Tb	−2.95	−3.07	−3.1[b]	−3.3
Dy	−2.96	−2.02	−2.3	−2.2
Ho	−3.02	−2.40	−2.5	−2.5
Er	−3.02	−2.56	−2.7	−2.7
Tm	−2.83	−1.87	−1.9	−1.9
Yb	−1.64	−0.64	−0.7	−0.7
Lu	−3.12		−4.2[b]	

a: Values are for aqueous ions
b: Ln^{2+} (aq) is predicted to be $4f^n5d^1$

Conclusion

The reduction potentials for all the metals in the lanthanide series except Pm were determined in Cp'_3Ln complexes by electrochemical methods using $[^nBu_4N][BPh_4]$ as a supporting electrolyte in THF. Reactions involving $4f^n \rightarrow 4f^{n+1}$ reductions have the least negative $E_{1/2}$ values, −1.07 V to −2.83 V, and follow patterns for the stability of half-filled and filled-shell electron configurations. Reactions involving $4f^n$ to $4f^n5d^1$ reductions have more negative potentials that fall in the narrower range of −2.95 V to −3.14 V and the correlation with electron configuration is less clear. Cp^{tet}_3Ln complexes are more difficult to reduce which is consistent with the stronger electron-donating character of Cp^{tet} vs Cp′, but there are variations on the Cp^{tet} vs Cp′ data that are dependent on the specific metal.

Experimental Details

All manipulations and syntheses described below were conducted with the rigorous exclusion of air and water using standard Schlenk line and glovebox techniques under an argon atmosphere. Solvents were sparged with UHP argon and dried by passage through columns containing Q-5 and molecular sieves prior to use. Cp'_3Ln,[15–18,39] [K(crypt)][Cp'_3Ln],[17,18] and Cp^{tet}_3Ln[38,40–42] were synthesized according to literature procedures. [^{n}Bu$_4$N][BPh$_4$] (Sigma, electrochemical grade >99%) was recrystallized from acetone three times and dried at 80 °C and 10^{-5} Torr overnight before use. $(C_5Me_5)_2Fe$ (Aldrich) was purified by sublimation before use. Electrochemical measurements were collected with a freshly made THF solution of supporting electrolyte with a glassy carbon working electrode, platinum wire counter electrode, and silver wire pseudo-reference electrode with a Princeton Applied Research PARSTAT 2273 Advanced Electrochemical System and referenced with internal standard $(C_5Me_5)_2Fe$. Internal resistance was measured for each solution and resistance was manually compensated by approximately 90% of the measured value. All scans on Cp'_3Ln and Cp^{tet}_3Ln were in the cathodic direction while scans on [K(crypt)][Cp'_3Ln] were in the anodic direction.

General Electrochemistry Procedure. Inside the glovebox, a stock 100 mM [^{n}Bu$_4$N][BPh$_4$] electrolyte solution was freshly prepared in THF. Between 1–2 mL of this solution were transferred to a 20 mL scintillation vial and a cyclic voltammogram of this solution was collected to verify the electrolyte solution was free of impurities. Roughly 10-20 mg of the Ln compound were dissolved in the same electrolyte solution to yield approximately a 10 mM solution. Electrodes were placed into the vial and the vial was left open to the glovebox atmosphere during data collection. The internal resistance was measured and cyclic voltammetry

experiments were then recorded. $(C_5Me_5)_2Fe$ was added to the solution following all data collection, and a single scan was recorded to measure the internal standard redox event.

References

(1) Nief, F. Molecular Chemistry of the Rare-Earth Elements in Uncommon Low-Valent States. In *Handbook on the Physics and Chemistry of Rare Earths*; Gschneidner, K. A., Bunzil, J.-C. G., Pecharsky, V. K., Eds.; Elsevier Science: Amsterdam, 2010; pp 241–300.

(2) Meyer, G. Reduced Halides of the Rare-Earth Elements. *Chem. Rev.* **1988**, *88*, 93–107, DOI: 10.1021/cr00083a005.

(3) Morss, L. R. Thermochemical Properties of Yttrium, Lanthanum, and the Lanthanide Elements and Ions. *Chem. Rev.* **1976**, *76*, 827–841, DOI: 10.1021/cr60304a007.

(4) Bochkarev, M. N. Molecular Compounds of "New" Divalent Lanthanides. *Coord. Chem. Rev.* **2004**, *248*, 835–851, DOI: 10.1016/j.ccr.2004.04.004.

(5) Evans, W. J. Perspectives in Reductive Lanthanide Chemistry. *Coord. Chem. Rev.* **2000**, *206–207*, 263–283, DOI: 10.1016/S0010-8545(00)00267-8.

(6) Molander, G. A. Application of Lanthanide Reagents in Organic Synthesis. *Chem. Rev.* **1992**, *92*, 29–68, DOI: 10.1021/cr00009a002.

(7) Mikheev, N. B. Lower Oxidation States of Lanthanides and Actinides. *Inorg. Chim. Acta* **1984**, *94*, 241–248, DOI: 10.1016/S0020-1693(00)87451-4.

(8) Bond, A. M.; Deacon, G. B.; Newnham, R. H. Organolanthanoids. 9. Electrochemical Reduction of Tris(Cyclopentadienyl)Samarium(III), -Ytterbium(III), and -Europium(III) Compounds in Tetrahydrofuran. *Organometallics* **1986**, *5*, 2312–2316, DOI: 10.1021/om00142a023.

(9) Bratsch, S. G.; Lagowski, J. J. Lanthanide Thermodynamic Predictions. 7. Thermodynamics of 2+, 3+, and 4+ Aquo Ions and Standard Electrode Potentials at 298.15 K. *J. Phys. Chem.* **1985**, *89*, 3317–3319, DOI: 10.1021/j100261a031.

(10) Nugent, L. J.; Baybarz, R. D.; Burnett, J. L.; Ryan, J. L. Electron-Transfer and f-d Absorption Bands of Some Lanthanide and Actinide Complexes and the Standard (II—III) Oxidation Potential for Each Member of the Lanthanide and Actinide Series. *J. Phys. Chem.* **1973**, *77*, 1528–1539, DOI: 10.1021/j100631a011.

(11) Meyer, G. The Divalent State in Solid Rare-Earth Metal Haldes. In *The Rare Earth Elements: Fundamentals and Applications*; Atwood, D. A., Ed.; Wiley: New York, 2012; pp 241–300.

(12) Bochkarev, M. N.; Fedushkin, I. L.; Fagin, A. A.; Petrovskaya, T. V.; Ziller, J. W.; Broomhall-Dillard, R. N. R.; Evans, W. J. Synthesis and Structure of the First Molecular Thulium(II) Complex: $[TmI_2(MeOCH_2CH_2OMe)_2]$. *Angew. Chem. Int. Ed.* **1997**, *36*, 133–135, DOI: 10.1002/anie.199701331.

(13) Bochkarev, M. N.; Fagin, A. A. A New Route to Neodymium(II) and Dysprosium(II) Iodides. *Chem. Eur. J.* **1999**, *5*, 2990–2992, DOI: 10.1002/(SICI)1521-3765(19991001)5:10<2990::AID-CHEM2990>3.0.CO;2-U.

(14) Hitchcock, P. B.; Lappert, M. F.; Maron, L.; Protchenko, A. V. Lanthanum Does Form Stable Molecular Compounds in the +2 Oxidation State. *Angew. Chem. Int. Ed.* **2008**, *47*, 1488–1491, DOI: 10.1002/anie.200704887.

(15) MacDonald, M. R.; Ziller, J. W.; Evans, W. J. Synthesis of a Crystalline Molecular Complex of Y^{2+}, $[(18\text{-Crown-6})K][(C_5H_4SiMe_3)_3Y]$. *J. Am. Chem. Soc.* **2011**, *133*, 15914–15917, DOI: 10.1021/ja207151y.

(16) MacDonald, M. R.; Bates, J. E.; Fieser, M. E.; Ziller, J. W.; Furche, F.; Evans, W. J. Expanding Rare-Earth Oxidation State Chemistry to Molecular Complexes of Holmium(II) and Erbium(II). *J. Am. Chem. Soc.* **2012**, *134*, 8420–8423, DOI: 10.1021/ja303357w.

(17) Fieser, M. E.; MacDonald, M. R.; Krull, B. T.; Bates, J. E.; Ziller, J. W.; Furche, F.; Evans, W. J. Structural, Spectroscopic, and Theoretical Comparison of Traditional vs Recently Discovered Ln^{2+} Ions in the [K(2.2.2-Cryptand)][$(C_5H_4SiMe_3)_3Ln$] Complexes: The Variable Nature of Dy^{2+} and Nd^{2+}. *J. Am. Chem. Soc.* **2015**, *137*, 369–382, DOI: 10.1021/ja510831n.

(18) MacDonald, M. R.; Bates, J. E.; Ziller, J. W.; Furche, F.; Evans, W. J. Completing the Series of +2 Ions for the Lanthanide Elements: Synthesis of Molecular Complexes of Pr^{2+}, Gd^{2+}, Tb^{2+}, and Lu^{2+}. *J. Am. Chem. Soc.* **2013**, *135*, 9857–9868, DOI: 10.1021/ja403753j.

(19) Palumbo, C. T.; Darago, L. E.; Windor, C. J.; Ziller, J. W.; Evans, W. J.; Windorff, C. J.; Ziller, J. W.; Evans, W. J. Trimethylsilyl versus Bis(Trimethylsilyl) Substitution in Tris(Cyclopentadienyl) Complexes of La, Ce, and Pr: Comparison of Structure, Magnetic Properties, and Reactivity. *Organometallics* **2018**, *37*, 900–905, DOI: 10.1021/acs.organomet.7b00881.

(20) Evans, W. J. Tutorial on the Role of Cyclopentadienyl Ligands in the Discovery of Molecular Complexes of the Rare-Earth and Actinide Metals in New Oxidation States. *Organometallics* **2016**, *35*, 3088–3100, DOI: 10.1021/acs.organomet.6b00466.

(21) Woen, D. H.; Evans, W. J. Expanding the +2 Oxidation State of the Rare-Earth Metals, Uranium, and Thorium in Molecular Complexes. In *Handbook on the Physics and Chemistry of Rare Earths*; Bünzli, J.-C., Pecharsky, V. K., Eds.; Elsevier B.V., 2016; pp 1–57, DOI: 10.1016/bs.hpcre.2016.08.002.

(22) Cassani, M. C.; Lappert, M. F.; Laschi, F. First Identification by EPR Spectra of Lanthanum(II) Organometallic Intermediates (and $E_{1/2}$ for $La^{3+} \rightarrow La^{2+}$) in the C–O Bond Activation of Dimethoxyethane. *Chem. Commun.* **1997**, *2*, 1563–1564, DOI: 10.1039/a702493b.

(23) Huh, D. N.; Ziller, J. W.; Evans, W. J. Isolation of Reactive Ln(II) Complexes with C_5H_4Me Ligands (Cp^{Me}) Using Inverse Sandwich Countercations: Synthesis and Structure of [(18-Crown-6)K(μ-Cp^{Me})K(18-Crown-6)][$Cp^{Me}{}_3Ln^{II}$] (Ln = Tb, Ho). *Dalton Trans.* **2018**, *47*, 17285–17290, DOI: 10.1039/C8DT03890B.

(24) Woen, D. H.; Huh, D. N.; Ziller, J. W.; Evans, W. J. Reactivity of Ln(II) Complexes Supported by $(C_5H_4Me)^{1-}$ Ligands with THF and $PhSiH_3$: Isolation of Ring-Opened, Bridging Alkoxyalkyl, Hydride, and Silyl Products. *Organometallics* **2018**, *37*, 3055–3063, DOI: 10.1021/acs.organomet.8b00419.

(25) Noviandri, I.; Brown, K. N.; Fleming, D. S.; Gulyas, P. T.; Lay, P. A.; Masters, A. F.; Phillips, L. The Decamethylferrocenium/Decamethylferrocene Redox Couple: A Superior Redox Standard to the Ferrocenium/Ferrocene Redox Couple for Studying Solvent Effects on the Thermodynamics of Electron Transfer. *J. Phys. Chem. B* **1999**, *103*, 6713–6722, DOI: 10.1021/jp991381+.

(26) Elgrishi, N.; Rountree, K. J.; McCarthy, B. D.; Rountree, E. S.; Eisenhart, T. T.; Dempsey, J. L. A Practical Beginner's Guide to Cyclic Voltammetry. *J. Chem. Educ.* **2018**, *95*, 197–206, DOI: 10.1021/acs.jchemed.7b00361.

(27) Wedal, J. C.; Barlow, J. M.; Ziller, J. W.; Yang, J. Y.; Evans, W. J. Electrochemical Studies of Tris(Cyclopentadienyl)Thorium and Uranium Complexes in the +2, +3, and +4 Oxidation States. *Chem. Sci.* **2021**, *12*, 8501–8511, DOI: 10.1039/D1SC01906F.

(28) Inman, C. J.; Cloke, F. G. N. The Experimental Determination of Th(IV)/Th(III) Redox Potentials in Organometallic Thorium Complexes. *Dalton Trans.* **2019**, *48*, 10782–10784, DOI: 10.1039/c9dt01553a.

(29) Morris, D. E.; Da Re, R. E.; Jantunen, K. C.; Castro-Rodriguez, I.; Kiplinger, J. L. Trends in Electronic Structure and Redox Energetics for Early-Actinide Pentamethylcyclopentadienyl Complexes. *Organometallics* **2004**, *23*, 5142–5153, DOI: 10.1021/om049634v.

(30) Hlina, J. A.; Pankhurst, J. R.; Kaltsoyannis, N.; Arnold, P. L. Metal-Metal Bonding in Uranium-Group 10 Complexes. *J. Am. Chem. Soc.* **2016**, *138*, 3333–3345, DOI: 10.1021/jacs.5b10698.

(31) Wedal, J. C.; Bekoe, S.; Ziller, J. W.; Furche, F.; Evans, W. J. In Search of Tris(Trimethylsilylcyclopentadienyl) Thorium. *Dalton Trans.* **2019**, *48*, 16633–16640, DOI: 10.1039/C9DT03674A.

(32) Connelly, N. G.; Geiger, W. E. Chemical Redox Agents for Organometallic Chemistry. *Chem. Rev.* **1996**, *96*, 877–910, DOI: 10.1021/cr940053x.

(33) Huh, D. N.; Ciccone, S. R.; Bekoe, S.; Roy, S.; Ziller, J. W.; Furche, F.; Evans, W. J. Synthesis of Ln^{II}-in-Cryptand Complexes by Chemical Reduction of Ln^{III}-in-Cryptand Precursors: Isolation of a Nd^{II}-in-Cryptand Complex. *Angew. Chem. Int. Ed.* **2020**, *59*, 16141–16146, DOI: 10.1002/anie.202006393.

(34) Moehring, S. A.; Evans, W. J. Evaluating Electron Transfer Reactivity of Rare-Earth Metal(II) Complexes Using EPR Spectroscopy. *Organometallics* **2020**, *39*, 1187–1194, DOI: 10.1021/acs.organomet.9b00837.

(35) Moehring, S. A.; Evans, W. J. Evaluating Electron-Transfer Reactivity of Complexes of

Actinides in +2 and +3 Oxidation States by Using EPR Spectroscopy. *Chem. Eur. J.* **2020**, *26*, 1530–1534, DOI: 10.1002/chem.201905581.

(36) Zachmanoglou, C. E.; Docrat, A.; Bridgewater, B. M.; Parkin, G.; Brandow, C. G.; Bercaw, J. E.; Jardine, C. N.; Lyall, M.; Green, J. C.; Keister, J. B. The Electronic Influence of Ring Substituents and Ansa Bridges in Zirconocene Complexes as Probed by Infrared Spectroscopic, Electrochemical, and Computational Studies. *J. Am. Chem. Soc.* **2002**, *124*, 9525–9546, DOI: 10.1021/ja020236y.

(37) Martin, W. C.; Zalubas, R.; Hagan, L. *Atomic Energy Levels-The Rare-Earth Elements*; U.S. Government Printing Office: Washington D.C., 1978.

(38) Jenkins, T. F.; Woen, D. H.; Mohanam, L. N.; Ziller, J. W.; Furche, F.; Evans, W. J. Tetramethylcyclopentadienyl Ligands Allow Isolation of Ln(II) Ions across the Lanthanide Series in [K(2.2.2-Cryptand)][$(C_5Me_4H)_3Ln$] Complexes. *Organometallics* **2018**, *37*, 3863–3873, DOI: 10.1021/acs.organomet.8b00557.

(39) Peterson, J. K.; MacDonald, M. R.; Ziller, J. W.; Evans, W. J. Synthetic Aspects of $(C_5H_4SiMe_3)_3Ln$ Rare-Earth Chemistry: Formation of $(C_5H_4SiMe_3)_3Lu$ via $[(C_5H_4SiMe_3)_2Ln]^+$ Metallocene Precursors. *Organometallics* **2013**, *32*, 2625–2631, DOI: 10.1021/om400116d.

(40) Windorff, C. J.; Dumas, M. T.; Ziller, J. W.; Gaunt, A. J.; Kozimor, S. A.; Evans, W. J. Small-Scale Metal-Based Syntheses of Lanthanide Iodide, Amide, and Cyclopentadienyl Complexes as Analogues for Transuranic Reactions. *Inorg. Chem.* **2017**, *56*, 11981–11989, DOI: 10.1021/acs.inorgchem.7b01968.

(41) Schumann, H.; Glanz, M.; Hemling, H.; Ekkehard Hahn, F. Metallorganische Verbindungen Der Lanthanoide. 93. Tetramethylcyclopentadienyl-Komplexe

Ausgewählter 4f-Elemente. *Z. Anorg. Allg. Chem.* **1995**, *621*, 341–345, DOI: 10.1002/zaac.19956210302.

(42) Evans, W. J.; Rego, D. B.; Ziller, J. W. Synthesis, Structure, and ^{15}N NMR Studies of Paramagnetic Lanthanide Complexes Obtained by Reduction of Dinitrogen. *Inorg. Chem.* **2006**, *45*, 10790–10798, DOI: 10.1021/ic061485g.

Chapter 13:

Rare-Earth Metal Complexes with Trimethyltriazacyclohexane and Trimethyltriazacyclononane Ligands

Introduction

Cyclopentadienyl ligands have been very important in developing the chemistry of the rare-earth metals.[1–3] Three of these anionic, six-electron ligands provide charge balance to the large Ln(III) ions while generating a formally nine-coordinate structure. Neutral chelating six-electron donor ligands like the cyclic, trisubstituted triazacyclohexane, R_3tach, and triazacyclononane, R_3tacn, compounds, Scheme 13.1, have received less attention because they do not provide charge balance. However, there is interest in rare-earth metal compounds containing neutral donors for a variety of applications that are difficult to perform with complexes containing only anionic ligands.[4–8]

Me_3tach **Me_3tacn**

Scheme 13.1: Molecular structures of Me_3tach (left) and Me_3tacn (right).

Rare-earth metal compounds with R_3tach ligands have been reported with Sc (R = Me),[9] Y (R = Me, ^{i}Pr, Cy),[9–12] La (R = Me),[12,13] Ce (R = Me),[14] Pr (R = Me, Et),[13,15] Sm (R = Me, Et, ^{i}Pr, ^{t}Bu, Cy),[12,16,17] and Ho (R = Me).[11] Mitzel and coworkers found subtle changes to the R substituents lead to large changes in the reaction chemistry. For example, reaction of $Sm(AlMe_4)_3$ with ^{i}Pr$_3$tach led to reduction of the samarium center and formation of $(^i\text{Pr}_3\text{tach})_2\text{Sm}(\text{AlMe}_4)_2$,[16] but addition of the same ligand ^{i}Pr$_3$tach to the smaller metal compound $Y(AlMe_4)_3$ led to

deprotonation of a methyl group and formation of the methylidene complex ($^{i}Pr_3$tach)Y($AlMe_4$)($Me_3AlCH_2AlMe_3$).[10] Complexes of R_3tach with third row transition metals W (R = Me, ^{t}Bu)[18–21] and Re (R = Me, Bn)[22] and with main group metals Ge (R = Me),[23] In (R = ^{i}Pr),[24] and Sn (R = Me)[23] have also been reported.

The larger nine-membered triazine Me_3tacn has also been used extensively in transition metal[25–28] and main-group chemistry,[23,29–37] but only a few examples are reported in f-element chemistry, mostly with Sc and Y.[6,9,38] This Chapter reports synthetic, spectroscopic, and crystallographic studies of the coordination chemistry of Me_3tach and Me_3tacn with the rare-earth metals in the +3 oxidation state using LnI_3, $LnCl_3$, and $Ln(OTf)_3$ starting materials. Additionally, the chemistry of Sm(II) was investigated using SmI_2 for comparison with the Sm(III) compounds.

Results

Me_3tach. Addition of two equivalents of Me_3tach to LnI_3 (Ln = La, Ce, Nd) in THF generated (Me_3tach)$_2LnI_3$, **13.1-Ln**, in moderate crystalline yields, eq 13.1. Compound **13.1-La** formed even when one equivalent of Me_3tach was added to the reaction. This has been previously observed, where the reaction of one equivalent of Me_3tach with $Pr(OTf)_3$ formed (Me_3tach)$_2Pr(OTf)_3$.[15]

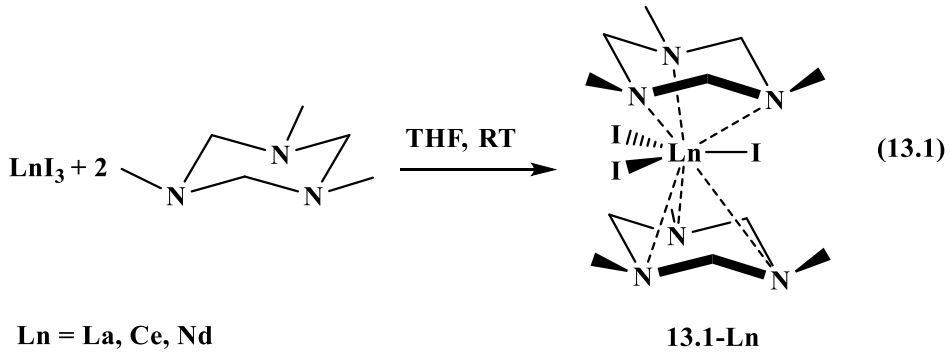

Compounds **13.1-Ln** crystallized in the *Pnma* space group, Figure 13.1. The metal and three iodine atoms resided on a mirror plane, such that only one Me_3tach moiety was observed and

the other was generated by symmetry. The molecule can be described as a tri-capped trigonal prism, where the two Me_3tach rings were eclipsed, and the iodides were staggered with respect to the Me_3tach nitrogen atoms.

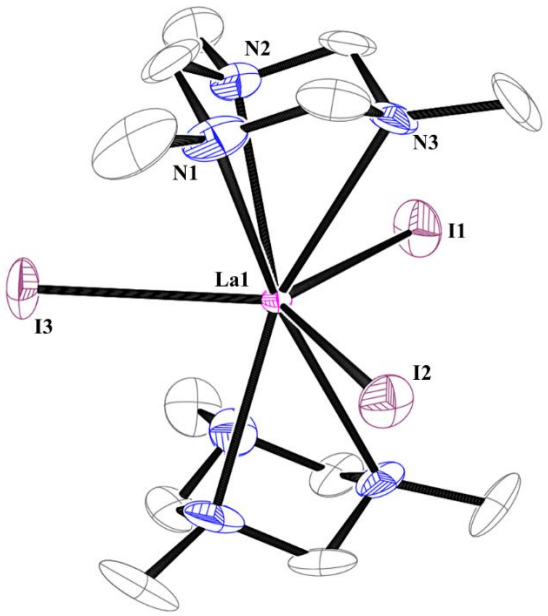

Figure 13.1: Molecular structure of **13.1-La** with selective atom labelling. Ellipsoids are drawn at the 50% probability level and hydrogen atoms have been omitted for clarity. **13.1-Ce** and **13.1-Nd** are isomorphous.

The crystal data on **13.1-Ln** were not high quality, but preliminary metrical parameters could be obtained. These data are summarized in Table 13.1 and highlights are described below. The Ln–Cnt distance decreases from La to Ce to Nd, from 2.467 Å to 2.396 Å, as expected based on the decreasing ionic radii of the metals.[39] The corresponding Ln–N distances also decrease across the series. Although both Me_3tach rings are identical by symmetry, the Cnt–Ln–Cnt angles are slightly less than 180°. The Cnt–Ln–I angles are close to, but not exactly 90°.

Table 13.1: Selected distances (Å) and angles (°) for **13.1-13.4** and **13.6-13.10**. Cnt is the centroid defined by the three nitrogen atoms of the tach or tacn ring, X = Cl, I, O(OTf). Data are preliminary.

	Ln–Cnt	Ln–N	Ln–X	Ln–O(THF)	Cnt–Ln–Cnt	Cnt–Ln–X	Cnt–Ln–O(THF)
13.1-La	2.467	2.803, 2.812, 2.813	3.195, 3.196, 3.213		178.5	89.7, 89.7, 90.7	
13.1-Ce	2.423	2.726, 2.799, 2.808	3.180, 3.199, 3.203		177.9	88.9, 90.5, 90.6	
13.1-Nd	2.396	2.737, 2.754, 2.768	3.153, 3.167, 3.169		177.7	89.4, 89.4, 91.2	
13.2-Nd	2.319, 2.325	2.654, 2.658, 2.681, 2.708 2.711, 2.724	3.183, 3.189		125.6	96.1, 96.8, 98.6, 99.4	
13.2.-Sm	2.221	2.586, 2.604, 2.678	3.011, 3.029		135.2	102.6, 103.5	
13.3-La	2.428	2.776	2.788		180.	90.	
13.4-Y	2.214	2.566, 2.588, 2.614	2.623, 2.636, 2.656	2.421, 2.444		97.1, 98.0, 104.6	105.8, 174.8
13.6-La	2.449, 2.454	2.774, 2.796, 2.825	2.469, 2.524, 2.524, 2.579, 2.777, 2.783, 2.843		163.1	87.0, 96.2, 99.6, 85.5, 86.7, 98.0, 92.5, 83.3	
13.7-Sm	2.313	2.467, 2.667, 2.849	3.417, 3.465	2.581	113.7	97.1, 99.6	123.2
13.8-La	2.129	2.668, 2.744, 2.752	3.134, 3.174, 3.175	2.628		104.1, 105.3, 107.0	171.6
13.9-Y	1.853	2.474, 2.504, 2.512	2.552, 2.560, 2.566			114.5, 117.3, 118.1	

13.10-Sm	2.061	2.699, 2.636, 2.653	3.203, 3.180	2.534		117.6, 119.9	119.7

When reaction 13.1 was examine for Ln = Nd, two different polymorphic crystals were observed under the microscope. One polymorph was found to be **13.1-Nd**, the parallel-ring structure shown above in Figure 13.1. The other polymorph was identified as the bent-ring complex $[(Me_3tach)_2NdI_2][I]$, **13.2-Nd**, Figure 13.2. The two polymorphs could be interchanged by recrystallization from THF/hexane. Compound **13.2-Nd** crystallized in the $P2_1/c$ space group with one outer-sphere iodide. The neodymium center was found to be eight-coordinate and is reminiscent of a bent metallocene structure.

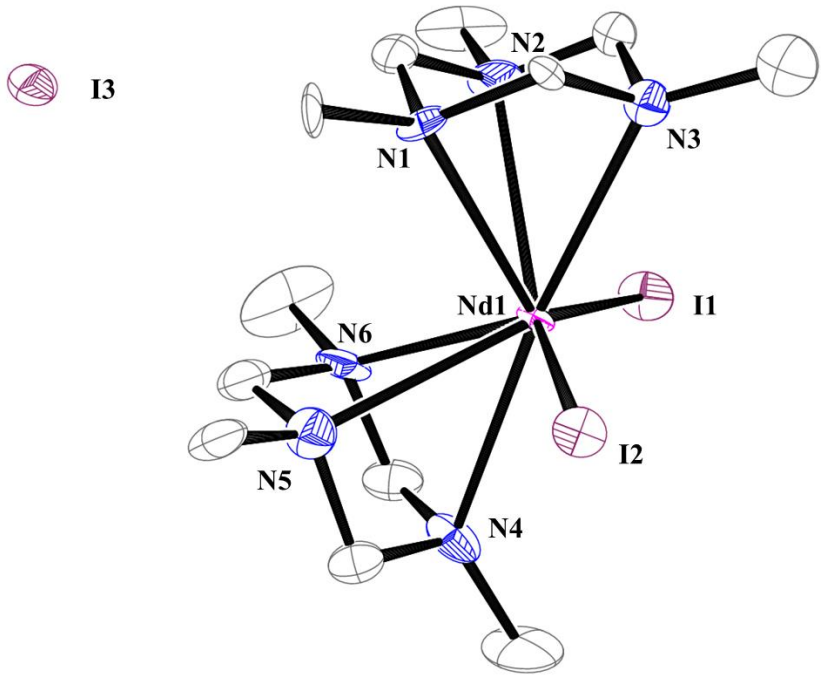

Figure 13.2: Molecular structure of **13.2-Nd** with selective atom labelling. Ellipsoids are drawn at the 50% probability level and hydrogen atoms have been omitted for clarity. **13.2-Sm** is not isomorphous but adopts the same overall structure.

The Nd–Cnt distances in **13.2-Nd** are shorter than the analogous distances in **13.1-Nd**, as expected since **13.2-Nd** has a smaller formal coordination number. The two Me_3tach rings are angled toward each other with a Cnt–Nd–Cnt angle of 125.6°.

Compounds similar to **13.1-Ln** could be made with chloride starting materials. Reaction of Me_3tach with $LaCl_3$ generated $(Me_3tach)_2LaCl_3$, **13.3-La**, eq 13.2.

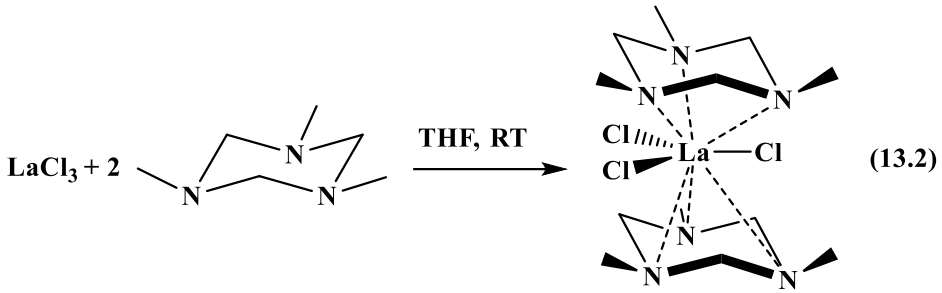

(13.2)

13.3-La

Compound **13.3-La** was significantly less soluble in THF than the iodide analogs, **13.1-Ln**. Compound **13.3-La** crystallized in the $P6_3/m$ space group, Figure 13.3. Analogous to **13.1-Ln**, compound **13.3-La** can be described as a tri-capped trigonal prism with parallel Me_3tach ligands and face-capping chlorides. Only the La, one Cl, one N, and two C atoms were observed in the crystal and the rest of the molecule was generated by symmetry.

Compound **13.3-La** has only one unique value for the La–Cnt, La–N, and La–Cl distances. Due to the space group $P6_3/m$, the Cnt–La–Cnt is exactly 180° and the Cnt–La–Cl angle is exactly 90°. The 2.428 La–Cnt distance in **13.3-La** is slightly shorter than the 2.467 Å La–Cnt distance in **13.1-La**, which could be explained by the presence of smaller chloride ligands in **13.3-La**.

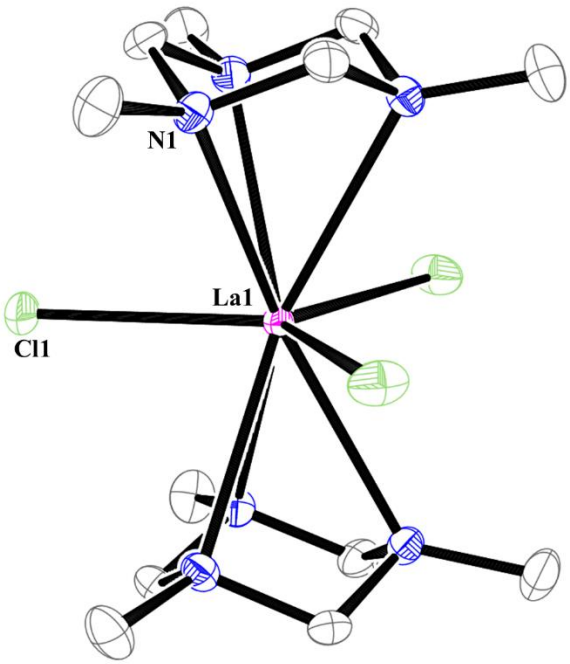

Figure 13.3: Molecular structure of **13.3-La** with selective atom labelling. Ellipsoids are drawn at the 50% probability level and hydrogen atoms have been omitted for clarity.

The smaller rare-earth metal yttrium was investigated to determine if the structural motifs for La–Nd would be similar. However, addition of two equivalents of Me_3tach to YCl_3 generated the mono-Me_3tach complex (Me_3tach)$YCl_3(THF)_2$, **13.4-Y**, after crystallization from THF/hexane, eq 13.3, Figure 13.4.

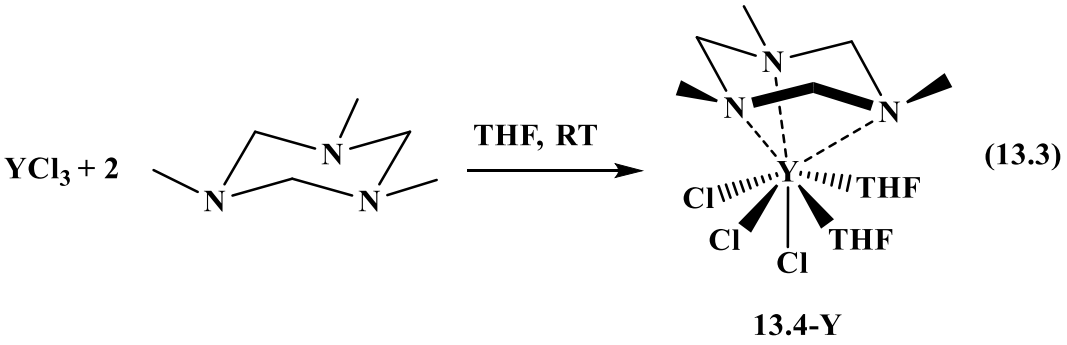

Compound **13.4-Y** crystallized in the $P2_12_12_1$ space group. When considering the Me_3tach centroid formed by the three nitrogen atoms, compound **13.4-Y** can be considered as adopting a distorted octahedral geometry.

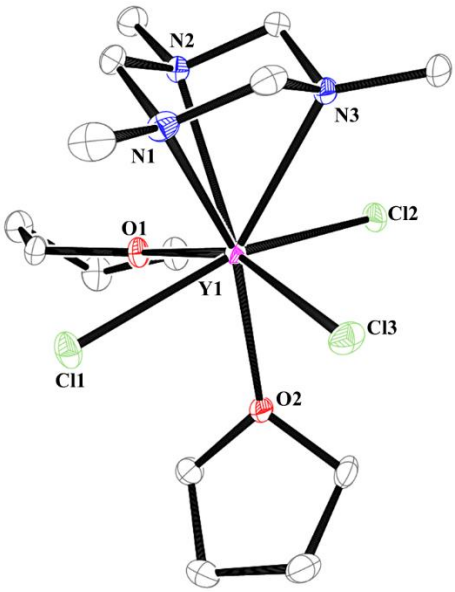

Figure 13.4: Molecular structure of **13.4-Y** with selective atom labelling. Ellipsoids are drawn at the 50% probability level and hydrogen atoms have been omitted for clarity.

The Y–Cnt distance is 2.214 Å, which is shorter than the Ln–Cnt distances in **13.1-Ln** and **13.2-Ln**, although the direct comparison is difficult due to the different geometries and coordination numbers. The yttrium atom lies 0.493 Å above the plane formed by the three chlorine and oxygen atom. The three chlorine atoms and THF molecule in the sample plane are located in an asymmetric manner. The Cnt–Y–Cl angles were 97.1, 98.0, and 104.6° and the Cnt–Y–O(1) angle was 105.8°. The Cnt–Y–O(2) angle involving the other THF molecule was close to linear at 174.8°.

The coordination chemistry of Me_3tach with other rare-earth metal starting materials was also investigated. Reaction of $Pr(OTf)_3$ with Me_3tach was reported to form $(Me_3tach)_2Pr(OTf)_3$.[15] In an attempt to replicate this result with lanthanum to compare with the La compounds **13.1-La**

and **13.3-La** above, $La(OTf)_3$ was reacted with Me_3tach in THF. Instead of forming the expected product, $\{[(Me_3tach)La(\mu\text{–}OH)(\mu\text{–}OTf)]_2(\mu\text{–}OTf)_2\}_2$, **13.5-La**, was identified by X-ray crystallography, eq 13.5.

Compound **13.5-La** is a tetrametallic dimer, Figure 13.5. La(1) and La(2) were bridged by two triflates and two hydroxides, and La(1) and La(1′) were bridged by two triflates. The exact source of the hydroxide is unknown, but the infrared spectrum of the $La(OTf)_3$ starting material showed two broad absorptions around 3300 cm^{-1}, indicating the presence of either H_2O, $[OH]^{1-}$, or residual HOTf.

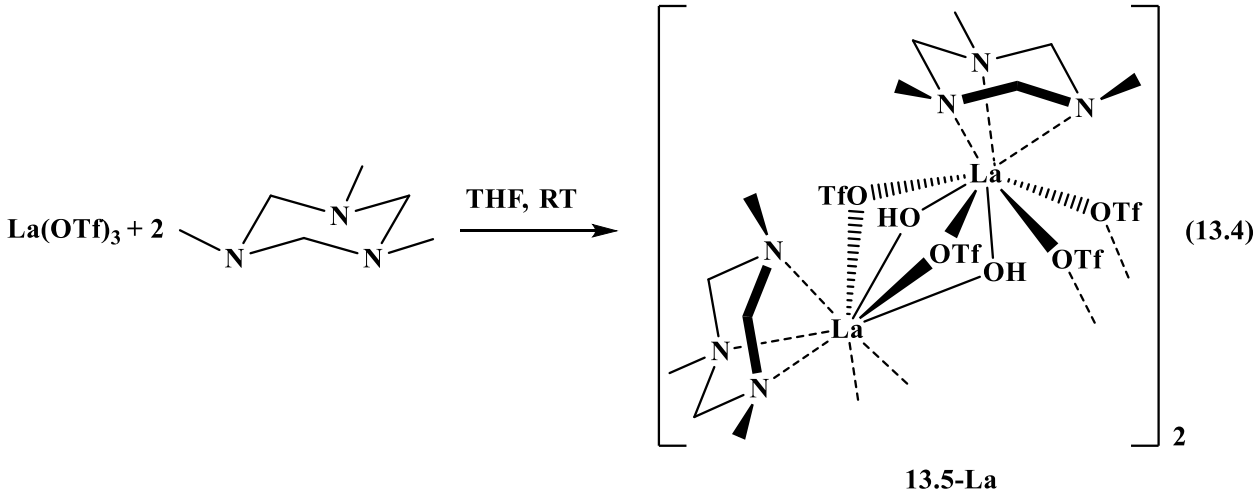

13.5-La

The $La(OTf)_3$ material was placed under 10^{-6} Torr and heated at 100 °C overnight. The free-flowing white powder thus obtained showed no O–H stretches in the infrared spectrum. Subsequent reaction of this $La(OTf)_3$ material with Me_3tach led to the formation of $[HMe_3tach][(Me_3tach)_2La(OTf)_4]$, **13.6-La**, eq 13.5. Compound **13.6-La** was identified by X-ray crystallography, Figure 13.6, in two different unit cells. The only difference between the two cells is that one cell had a toluene molecule present in the lattice, while the other did not. One nitrogen of the Me_3tach moiety that is not bound to the lanthanum center had a methyl group in the axial position which suggests this nitrogen is protonated, this is a countercation to the anionic part of

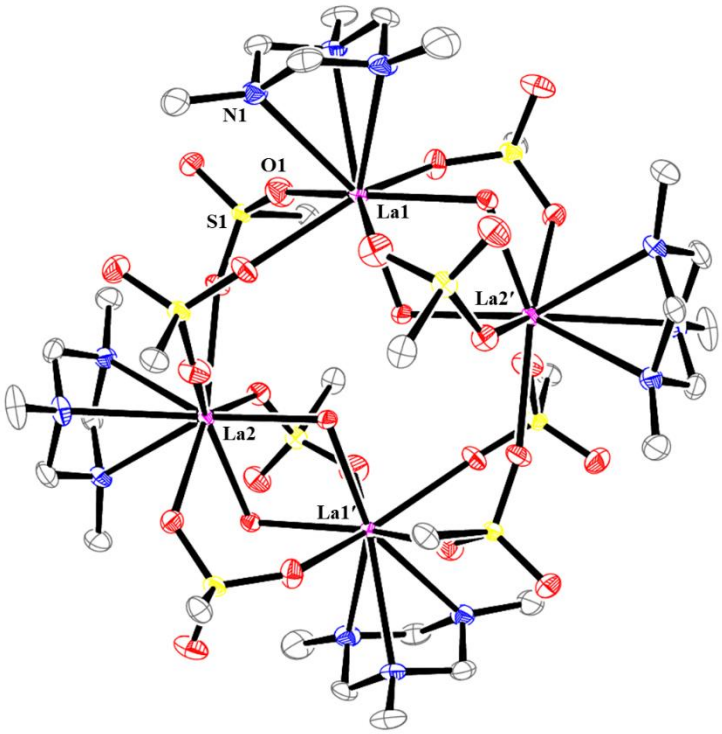

Figure 13.5: Molecular structure of **13.5-La** with selective atom labelling. Ellipsoids are drawn at the 35% probability level. Hydrogen and fluorine atoms have been omitted for clarity.

the compound. In **13.6-La**, the lanthanum center is formally ten coordinate, but it can be considered as having a distorted octahedral geometry when considering the Me_3tach centroids as one position.

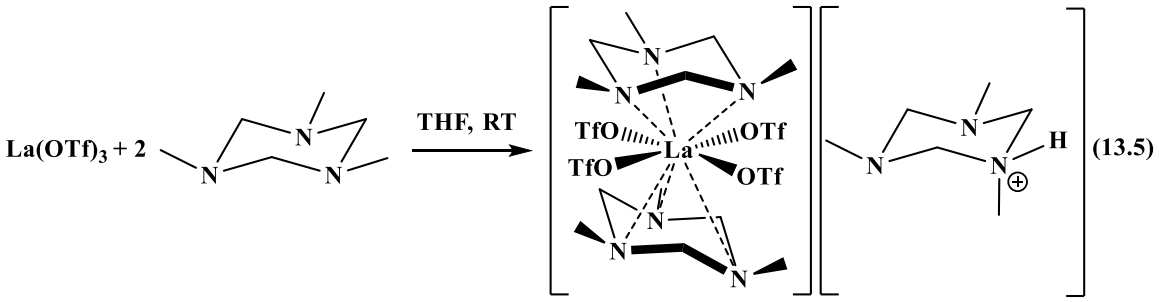

13.6-La

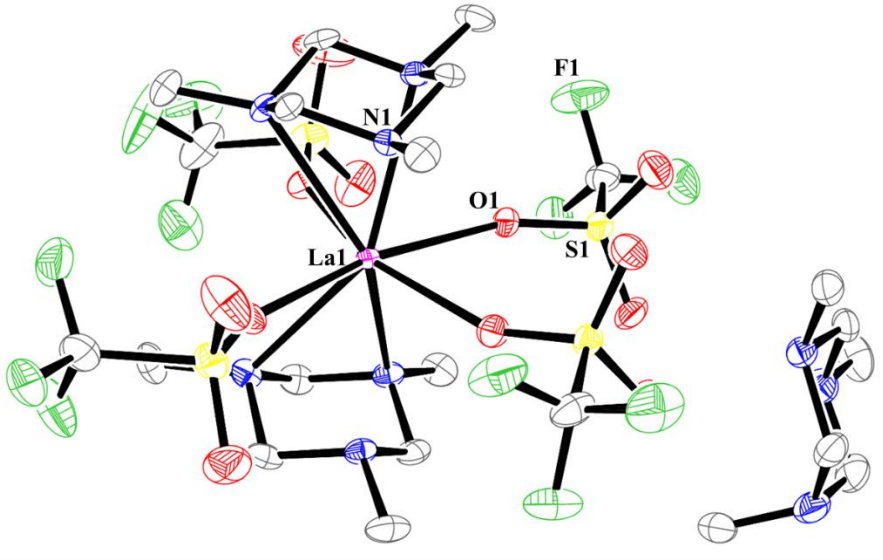

Figure 13.6: Molecular structure of **13.6-La** with selective atom labelling. Ellipsoids are drawn at the 50% probability level and hydrogen atoms have been omitted for clarity.

The La center in **13.6-La** has four anionic ligands coordinated compared to three in **13.1-La**. Even though **13.6-La** has a larger formal coordination number, the La–Cnt and La–N distances are similar to **13.1-La**, Table 13.1. For example, the La–Cnt distances in **13.6-La** were 2.449 and 2.454 Å, while the La–Cnt distance in **13.1-La** was 2.467 Å. The two Me_3tach rings are no longer properly eclipsed as the Cnt–La–Cnt angle is 163.1° and one Me_3tach ring is bent slightly to one side of the molecule. This leads to Cnt–La–O(OTf) angles that deviate, both larger and smaller, from 90°.

Having established some basic Me_3tach coordination chemistry for Ln(III) ions, it was of interest to compare with Ln(II) ions. LnI_2 materials were chosen since they are readily available.[40,41] The reaction of SmI_2[40] with Me_3tach formed a dark green solution from which the red Sm(II) compound $(Me_3tach)_2SmI_2(THF)$, **13.7-Sm**, was isolated, eq 13.6, and identified by X-ray crystallography, Figure 13.7. If the reaction was allowed to stir overnight, the Sm(III) compound, $[(Me_3tach)_2SmI_2][I]$, **13.2-Sm**, was isolated and identified by X-ray diffraction, Figure

13.2. The isolation of the Sm(III) compound **13.2-Sm** is in contrast to the studies with $Sm(AlMe_4)_3$, which formed Sm(II) products in reaction with R_3tach.[13,16,17]

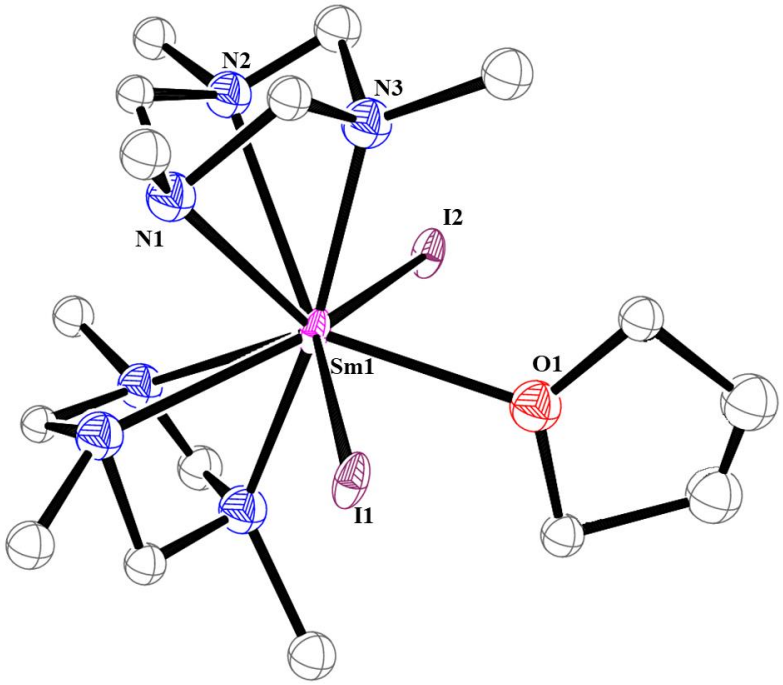

Figure 13.7: Molecular structure of **13.7-Sm** with selective atom labelling. Hydrogen atoms have been omitted for clarity.

Compound **13.7-Sm** crystallized in the *Pnma* space group and only half of the molecule is crystallographically unique. Both Me_3tach rings are crystallographically identical. The crystal data were not high quality, but preliminary data could be obtained. The Sm–Cnt distance of 2.313 Å is similar to the 2.319 and 2.325 Å distances of **13.2-Nd**, even though **13.7-Sm** has a larger coordination number and Sm(II) has a larger six coordinate ionic radius compared to Nd(III) (1.17 vs 0.983 Å). Like **13.2-Ln**, the Me_3tacn rings are canted toward each other, with a 113.7° Cnt–Sm–Cnt angle in **13.7-Sm**.

Compound **13.2-Sm** crystallized in the $P2_1/m$ space group, which is different than **13.2-Nd** which crystallized in the $P2_1/c$ space group. Only one Me_3tach ring is crystallographically unique in **13.2-Sm** which leads to a single set of Sm–N distances and one Sm–Cnt distance. Although the

Sm–Cnt distance of 2.221 Å is shorter than the 2.319 and 2.325 Å distances in **13.2-Nd**, the Cnt–Sm–Cnt angle of 135.2° is larger than the analogous 125.6° angle in **13.2-Nd**. Since the Me_3tach ligands are further from the metal center in **13.2-Nd**, there is more space for them to orient toward each other which can explain the smaller angle.

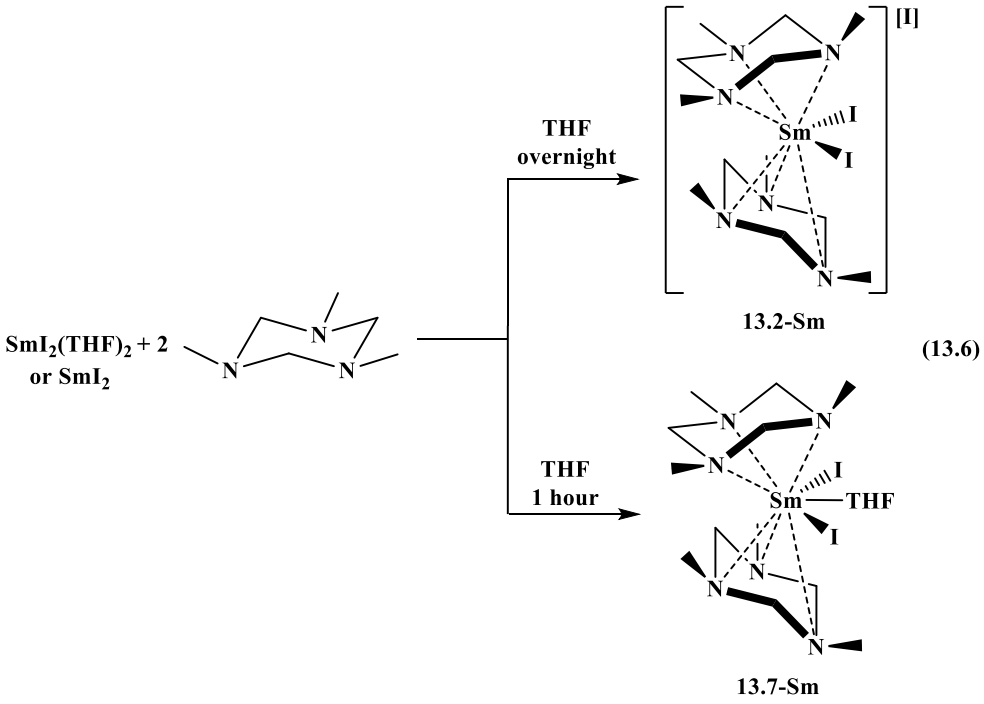

Me_3tacn. The preferential binding of two Me_3tach ligands to the larger rare-earth ions, La, Ce, and Nd is evidenced by the reaction of *one* equivalent of Me_3tach and LaI_3 which forms $(Me_3tach)_2LaI_3$, **13.1-La**. To determine if a complex with a single tridentate donor could be formed, the larger Me_3tacn ligand was investigated with LaI_3. The reaction of LaI_3 with Me_3tacn in THF led to the formation of $(Me_3tacn)LaI_3(THF)$, **13.8-La**, in moderate crystalline yield, eq 13.7.

Compound **13.8-La** crystallized in the *Pna*2_1 space group, Figure 13.8. One THF molecule is coordinated in the solid state and is maintained in solution based on ^{1}H NMR studies. The

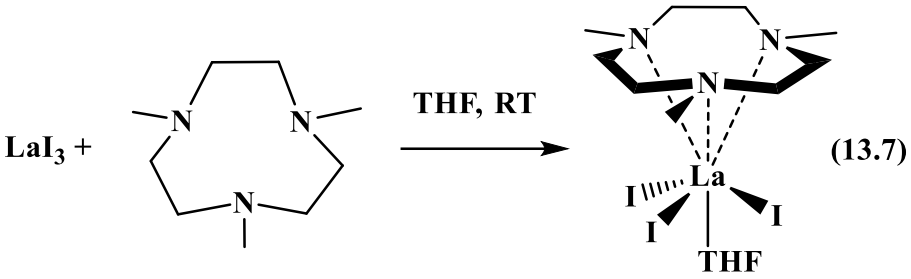

13.8-La

lanthanum center is slightly out of the plane formed by the three iodine atoms. The Cnt–La–O angle is nearly linear at 171.6°. The Cnt–La distance was 2.129 Å, which is significantly shorter than the 2.467 Å Cnt–La distance in **13.1-La** and the 2.449 and 2.454 Å distance in **13.6**. The Me_3tacn ligand is more flexible than Me_3tach due to the ethylene linkers, which likely allows for the chelating ligand to come in closer contact with the metal center.

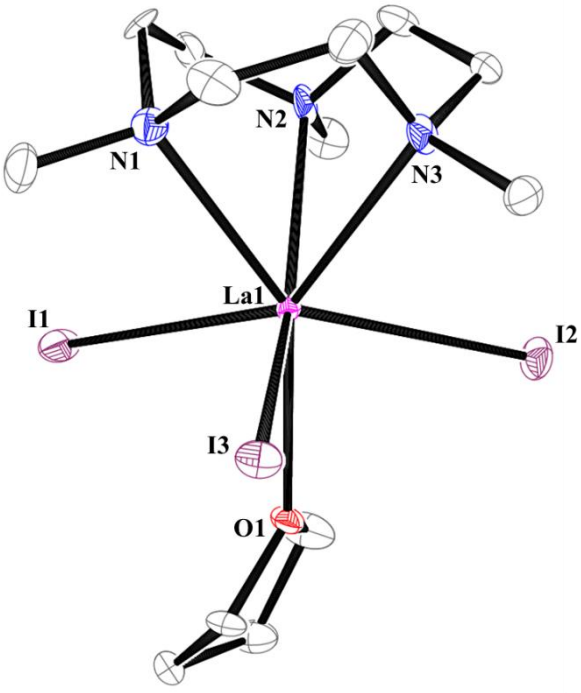

Figure 13.8: Molecular structure of **13.8-La** with selective atom labelling. Ellipsoids are drawn at the 50% probability level and hydrogen atoms have been omitted for clarity.

It is well established in synthetic rare-earth metal chemistry that the compound properties can be tuned based on the ionic radius of the metal. A metal smaller than La was investigated with the Me_3tacn ligand to see how this affected the resulting product. YCl_3 reacted with Me_3tacn in THF to form (Me_3tacn)YCl_3, **13.9-Y**, eq 13.8. Here, the smaller yttrium does not bind a THF molecule as the coordination sphere is evidently saturated at six coordinate. This result was further surprising considering that chloride anions are much smaller than iodide anions in **13.8-La.**

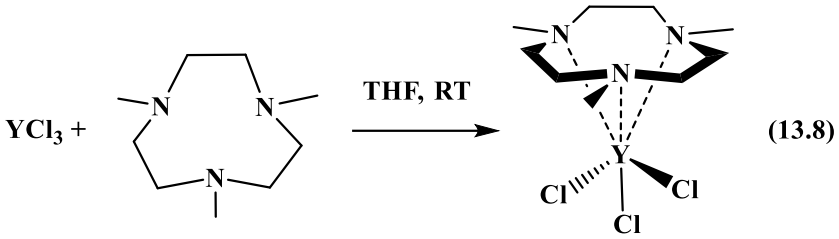

(13.8)

13.9-Y

Compound **13.9-Y** crystallized in the $P2_1/c$ space group, Figure 13.9. The yttrium center is formally six coordinate. If the Me_3tacn ligand is considered as similar to a cyclopentadienyl ligand, compound **13.9-Y** is reminiscent of a three-legged piano stool geometry. The Cnt–Y distance is 1.853 Å, which is shorter than the 2.129 Å Cnt–La distance in **13.8-La** and the 2.214 Å Cnt–Y distance in **13.4-Y**.

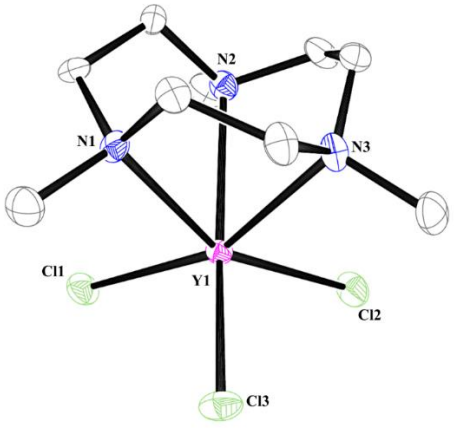

Figure 13.9: Molecular structure of **13.9-Y** with selective atom labelling. Ellipsoids are drawn at the 50% probability level and hydrogen atoms have been omitted for clarity.

The chemistry of Me_3tacn with both large and small rare-earth metals in the 3+ oxidation state was established via eq 13.7 and 13.8. It was of interest to investigate the coordination chemistry with a metal in the 2+ oxidation state. SmI_2 reacts with Me_3tacn in THF to form $(Me_3tacn)SmI_2(THF)$, **13.10**, eq 13.9.

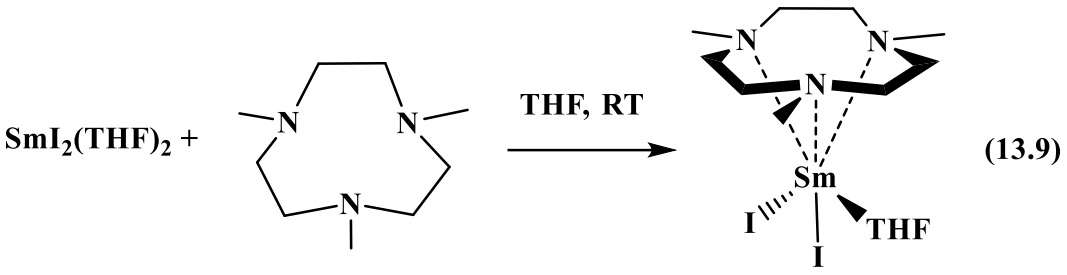

(13.9)

13.10-Sm

Compound **13.10-Sm** crystallizes in the *Pna*2_1 space group, Figure 13.10. Overall, the structure of $(Me_3tacn)SmI_2(THF)$, **13.10-Sm,** is similar to $(Me_3tacn)YCl_3$, **13.9-Y**, where **13.10-Sm** is formally six coordinate and could be considered as having a three-legged piano stool geometry where two iodine atoms and the THF molecule make up the three legs. Complex **13.10-Sm** is significantly different from $(Me_3tach)_2SmI_2(THF)$, **13.7-Sm**, which emphasizes the different coordination chemistry of the triazine rings.

The Cnt–Sm distance in **13.10-Sm** is 2.061 Å, which is shorter than the 2.221 Å Cnt–Sm distance in **13.2-Sm**, the 2.129 Å Cnt–La distance in **13.8-La**, and the 1.853 Å Cnt–Y distance in **13.4-Y**. When subtracting the difference in six-coordinate ionic radii of La^{3+} (1.032), Y^{3+} (0.90), and Sm^{2+} (1.17)[39] from the Ln–Cnt distances, the resulting values of 1.098 (**13.8-La**), 0.953 (**13.4-Y**), and 0.891 Å (**13.10-Sm**) are irregular. Of course, the three compounds have both different geometries and coordinated ligands which complicates the analysis. Regardless, it appears that simple ionic radii arguments are insufficient to explain the observed differences in distances.

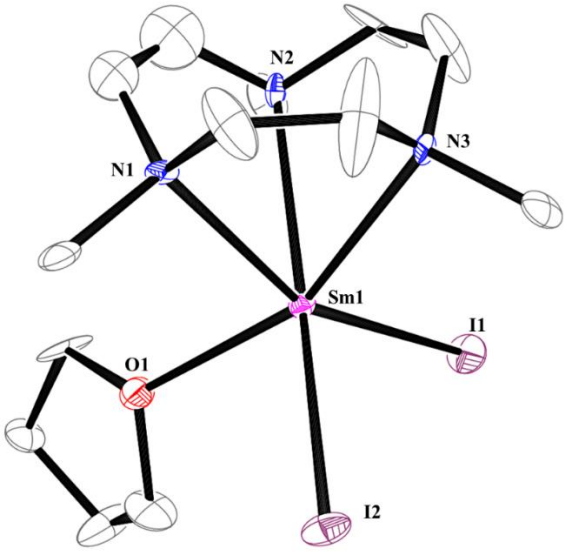

Figure 13.10: Molecular structure of **13.10-Sm** with selective atom labelling. Ellipsoids are drawn at the 50% probability level and hydrogen atoms have been omitted for clarity.

Protonation of Me_3tach and Me_3tacn. Throughout these studies, protonation of the nitrogen cycle was observed. For example, compound **13.6-La** was comprised of a $[HMe_3tach]^{1+}$ cation, eq 13.5. Many times, crystals were obtained of the protonated ligand with the corresponding anion of the starting material. For example, reaction of LnI_3 with Me_3tach inconsistently led to the isolation of [HMe_3tach][I]. In some cases, the oxidation product could be observed in the ^{1}H NMR or infrared spectrum of the crude reaction mixture. The crystal structures of [HMe_3tach][Cl], [HMe_3tach][Br], [HMe_3tach][I], and [HMe_3tacn][OTf] were collected over the course of these studies. All of the structures showed one nitrogen atom with a methyl group in the axial position. The cation and anion were well separated from each other. As an example, the molecular structure of [HMe_3tach][I] is shown in Figure 13.11.

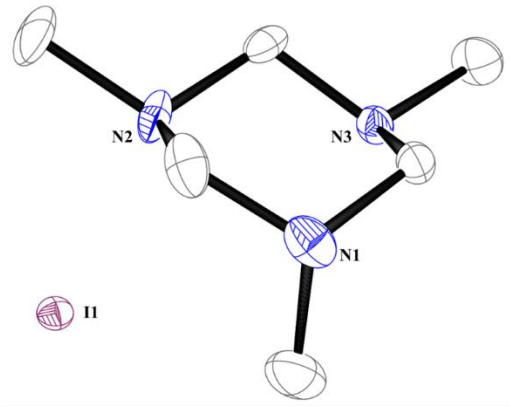

Figure 13.11: Molecular structure of [HMe$_3$tach][I] with selective atom labelling. Ellipsoids are drawn at the 50% probability level and hydrogen atoms have been omitted for clarity.

Discussion

The reaction of LnX_3 and Me$_3$tach in THF leads to the formation of compounds (Me$_3$tach)$_2$LnI$_3$, **13.1-Ln**, and [(Me$_3$tach)$_2$LnI$_2$][I], **13.2** with two Me$_3$tach ligands bound, even when only one equivalent of Me$_3$tach is added to the reaction. The compounds differ in the coordination geometry where **13.1-Ln** has two eclipsed Me$_3$tach ligands and **13.2** have bent rings with one outer-sphere iodide anion. Since the structures of **13.2-Ln** were only obtained for Ln = Nd and Sm, it may suggest that this change in coordination geometry is controlled by the size of the metal ion. However, the structure of **13.1-Nd** was also obtained so Nd may be at the border of the two coordination modes. The Sm(II) compound (Me$_3$tach)$_2$SmI$_2$(THF), **13.7-Sm**, was also identified which has the same bent ring structure of the Ln(III) **13.2-Ln** compounds. The six-coordinate ionic radius of Sm(II) is 1.17 Å, which is larger than the 0.983 Å value of Nd(III),[39] which could explain why compound **13.7-Sm** has a THF bound.

The larger ligand Me$_3$tacn forms compounds with just one Me$_3$tacn ligand, even if excess is added to the reaction. (Me$_3$tacn)LaI$_3$(THF), **13.8-La**, was formed from LaI$_3$ and a four-fold excess of Me$_3$tacn in THF, which suggests a species such as "(Me$_3$tacn)$_2$LaI$_3$," analogous to **13.1-**

La, is too sterically crowded to form. Compounds with Me_3tacn ligands have much shorter Ln–Cnt distances than those with Me_3tach ligands, even when considering the difference in metal radii. This is likely due to the ethylene linkers in the Me_3tacn ligand, which allows the ligand to be more flexible.

The isolation of Me_3tach and Me_3tacn complexes of the rare-earth metals was performed on small scales (<100 mg) and afforded moderate crystalline yields. The fact that the addition of the neutral triaza ligands provides crystalline material could be useful in other systems. Me_3tach could be added to compounds that do not readily crystallize to aid in purification and isolation of these species. Adding Lewis bases to aid in material crystallinity or break up polymeric species into monomers has been performed often with the rare-earth metals with reagents like $R_3P{=}O$, pyridine, and nitriles.[42–47] In fact, Me_3tach has been used for this exact purpose: reaction of $\{[(C_5Ph_3H_2)TbCl_2(THF)]_2(KCl)(THF)\}_4$ with Me_3tach breaks up the tetramer and forms the monometallic compound $(C_5Ph_3H_2)TbCl_2(Me_3tach)$.[48]

The solubility of the Me_3tach and Me_3tacn complexes is of particular interest since compounds **13.1**–**13.4**, and **13.7–13.9** could be considered alternatives to LnX_3 or LnX_2 starting materials. Salt metathesis reactions with a rare-earth metal tri-halide are the prototypical route to form organometallic and inorganic complexes of the rare-earths.[41] These reactions are typically performed in polar solvents such as THF, since the solubility of the LnX_3 compounds is low in non-polar solvents. However, reactions free of THF are often desirable.

The triflate compound $(Me_3tach)_2Pr(OTf)_3$ is soluble in toluene[15] and the $(Me_3tacn)LnCl_3$ complexes (Ln = Sc, Y) are soluble in CH_2Cl_2 and slightly soluble in MeCN.[9,49] The solubilities of **13.1-Ln**, **13.3-La**, and **13.6-La**, **13.7-Sm**, **13.8-La**, **13.9-Y**, and **13.10-Sm** in THF and toluene

are summarized in Table 13.2. Compounds **13.2-Ln**, **13.4-Y**, **13.5-La**, and solvents beyond THF and toluene were not investigated.

Table 13.2: Compound solubility in THF and toluene.

	THF	toluene
$(Me_3tach)_2LnI_3$, **13.1-Ln**	completely	moderately
$(Me_3tach)_2LnCl_3$, **13.3-La**	slightly	insoluble
$[HMe_3tach][(Me_3tach)_2La(OTf)_4]$, **13.6-La**	completely	completely
$(Me_3tach)_2SmI_2(THF)$, **13.7-Sm**	completely	insoluble
$(Me_3tacn)LaI_3(THF)$, **13.8-La**	completely	moderately
$(Me_3tacn)YCl_3$, **13.9-Y**	completely	completely

All of the compounds **13.1**–**13.10** were completely soluble in THF, except for $(Me_3tach)_2LnCl_3$, **13.3-La**, which is only slightly soluble in THF. It was found that **13.3-La**, and $(Me_3tach)_2SmI_2(THF)$, **13.7-Sm**, were insoluble in toluene, and $(Me_3tach)_2LnI_3$, **13.1-Ln**, and $(Me_3tacn)LaI_3(THF)$, **13.8-La**, were moderately soluble in toluene. It was surprising that $(Me_3tacn)YCl_3$, **13.9-Y**, was readily soluble in toluene since **13.3-La** was not and both compounds have chloride ligands. Thus, reactions that are sensitive to ethereal or other strongly coordinating or donating solvents could be synthesized from **13.1-Ln** or another Me_3tach or Me_3tacn compound in toluene.

The Me_3tach and Me_3tacn are apparently quite prone to protonation, evidenced by the crystallographic characterization of $[HMe_3tach][Cl]$, $[Hme_3tach][Br]$, $[Hme_3tach][I]$, and $[Hme_3tacn][Otf]$ from various reactions. It is not evident what the proton source was in the reactions that afforded these crystals, but it is worth noting that these byproducts are often not the major product. In some cases, two species, such as **13.1-La** and what is presumably $[Hme_3tach][I]$, can be observed in the NMR spectra. Despite the seemingly sensitive protonation pathway, complexes with Me_3tach and Me_3tacn can still be isolated in the presence of residual proton sources.

Conclusion

The coordination chemistry of Metach and Me_3tacn ligands with rare-earth metal starting materials such as LnI_3, $LnCl_3$, and $Ln(Otf)_3$ has been explored. For larger metals, compounds with two Me_3tach ligands are preferentially formed and the Me_3tach rings can adopt an eclipsed geometry in $(Me_3tach)_2LnI_3$, **13.1-Ln**, $(Me_3tach)_2LaCl_3$, **13.3-La**, and $[(Me_3tach)_2La(Otf)_4]^{1-}$, **13.6-La**, or a bent conformation in $[(Me_3tach)_2LnI_2][I]$, **13.2-Ln**, and $(Me_3tach)_2SmI_2(THF)$, **13.7-Sm**. For the smaller metal yttrium, a mono-Me_3tach complex $(Me_3tach)Ycl_3(THF)_2$, **13.4-Y**, is formed. The larger ligand Me_3tacn forms 1:1 complexes in $(Me_3tacn)LaI_3(THF)$, **13.8-La**, $(Me_3tacn)Ycl_3$, **13.9-Y**, and $(Me_3tacn)SmI_2(THF)$, **13.10-Sm**. The amine ligands are prone to protonation and compounds $[Hme_3tach][X]$ (X = Cl, Br, I) and $[Hme_3tacn][Otf]$ were crystallographically characterized.

Experimental

All synthesis and manipulations were conducted with rigorous exclusion of air and water using standard vacuum line and glovebox techniques. Solvents were sparged with UHP argon and dried by passage through columns containing water and oxygen scavengers. Deuterated NMR solvents were dried over NaK alloy, degassed by three freeze-pump-thaw cycles, and vacuum transferred before use. ^1H and ^{13}C NMR spectra were recorded on a CRYO500 MHz spectrometer at 298 K. Infrared spectra were recorded as compressed solids on an Agilent Cary 630 ATR-FTIR. Elemental analyses were conducted at the Irvine Materials Research Institute on a ThermoFisher FlashSmart CHNS/O Elemental Analyzer.

Anhydrous $LnCl_3$,[41,50] $La(Otf)_3$,[41] $SmI_2(THF)_2$,[40] and $LnI_3(THF)_4$,[51] were prepared as previously described. Anhydrous, base-free SmI_2 was used as received. Me_3tach and Me_3tacn were purchased under argon and kept over molecular in the glovebox.

Synthesis of $(Me_3tach)_2LaI_3$, 13.1-La. $LaI_3(THF)_4$ (130 mg, 0.161 mmol) was dissolved in THF (5 mL) to form a colorless solution. Me_3tach (48 mg, 0.37 mmol) was dissolved in THF (1 mL) and was slowly added to the stirring solution by pipet. The solution was stirred for two hours and a small amount of precipitate formed. The solids were removed via filtration and the solvent was removed under vacuum to afford a white powder. The solids were redissolved in minimal THF and layered under hexane and placed at −35 °C. Colorless crystals of **13.1-La**, suitable for X-ray diffraction, were grown overnight (9 mg, 14%). ^{1}H NMR (THF-d_8): δ 5.48 (s, 6H, CH_2), 3.12 (s, 6H, CH_2), 2.46 ppm (s, 18H, Me). ^{13}C NMR (THF-d_8): δ 80.1 (CH_2), 38.6 ppm (Me). IR (cm^{-1}): 2954w, 2903w, 2864w, 2801m, 2748w, 2687w, 1686w, 1640w, 1465m, 1384m, 1260s, 1165m, 1104s, 1009m, 935s, 889w, 801w. Anal. Calcd for $C_{12}H_{30}N_6LaI_3$: C, 18.53; H, 3.89; N, 10.80. Found: C, 19.940; H, 4.193; N, 11.679. The values were consistently high and suggest incomplete combustion or decomposition of the sample. The observed ratio $C_{12}H_{30.1}N_{6.0}$ is close to the expected values.

Synthesis of $(Me_3tach)_2CeI_3$, 13.1-Ce. As described above for **13.1-La**, $CeI_3(THF)_4$ (53 mg, 0.065 mmol) and Me_3tach (20 mg, 0.15 mmol) were reacted in THF (3 mL). Colorless crystals of **13.1-Ce** were grown from THF/hexane at −35 °C overnight (33 mg, 65%). ^{1}H NMR (THF-d_8): δ 38.98 (br s, 6H, CH_2), 29.26 (br s, 6H, CH_2), 6.93 ppm (br s, 18H, Me). ^{13}C NMR (THF-d_8): δ 48.6 (CH_2), 30.4 ppm (Me). IR (cm^{-1}): 1984w, 1950w, 2908w, 2860w, 2801m, 2749m, 2686m, 1642m, 1464s, 1384s, 1361m, 1287m, 1259s, 1165m, 1106s, 1075m, 1042w, 1009m, 936s, 866m, 861w, 795w, 727w, 694w. Anal. Calcd for $C_{12}H_{30}N_6CeI_3$: C, 18.50; H, 3.88; N, 10.79. Found: C, 21.03; H, 3.782; N, 9.213.

Synthesis of $(Me_3tach)_2NdI_3$, 13.1-Nd and $[(Me_3tach)_2NdI_2][I]$, 13.2-Nd. As above, $NdI_3(THF)_{3.5}$ (102 mg, 0.131 mmol) was reacted with Me_3tach (34 mg, 0.26 mmol) in THF (5

mL). Pale blue needle-like crystals of **13.1-Nd** suitable for X-ray diffraction were grown from THF/hexane at −35 °C overnight (85 mg, 83%). Pale blue parallelepiped crystals of **13.2-Nd** were grown by recrystallization of **13.1-Nd** from THF/hexane at −35 °C. No resonances in the ^{1}H NMR spectrum were observed between ± 400 ppm. IR (cm^{-1}): 2919m, 2869m, 2804m, 2748m, 2684m, 1642s, 1449s, 1385s, 1288w, 1261s, 1169s, 1104s, 1078m, 1041m, 937s, 888m, 799w, 723w, 693w. Anal. Calcd for $C_{12}H_{30}N_6NdI_3$: C, 18.40; H, 3.86; N, 10.73. Found: C, 17.63; H, 4.261; N, 8.700.

Crystallization of [(Me$_3$tach)$_2$SmI$_2$][I], 13.2-Sm. $SmI_2(THF)_2$ (67 mg, 0.12 mmol) was dissolved in THF (2 mL) to form a deep blue solution. Me_3tach was dissolved in THF and added to the stirring solution via pipet. The solution became dark green. After a few hours, the solution became yellow. The solution was stirred overnight then dried under vacuum. The solids were redissolved in minimal THF and layered under hexane and placed at −35 °C. A few colorless crystals of **13.2-Sm**, suitable for X-ray diffraction, were grown overnight.

Synthesis of (Me$_3$tach)$_2$LaCl$_3$, 13.3. $LaCl_3$ (44 mg, 0.18 mmol) was added to THF (5 mL). Me_3tach (46 mg, 0.36 mmol) was dissolved in THF and added to the stirring suspension by pipet. White solid immediately precipitated. The suspension was stirred for 90 minutes then the mixture was centrifuged. The colorless supernatant was collected and dried under vacuum to yield white solids of **13.3** (7 mg, 8%). Colorless hexagonal prism crystals of **13.3** were grown from THF/hexane at −35 °C overnight. ^{1}H NMR (THF-d_8): δ 2.19 ppm (br s, 18H, Me). Only one resonance was observed due to the low solubility. Due to the low solubility of **13.3** in THF, a ^{13}C spectrum could not be obtained. IR (thin film from THF-d_8, cm^{-1}): 2921s, 2853m, 2806m, 2749w, 2686w, 1644m, 1453s, 1385m, 1263s, 1171m, 1108s, 1079m, 1043m, 1013m, 938s, 889w, 825w.

Synthesis of (Me$_3$tach)Ycl$_3$(THF)$_2$, 13.4. Ycl_3 (50 mg, 0.20 mmol) was stirred in THF (5 mL). Me_3tach was added by pipet to the stirring slurry to form a colorless solution. The solution was stirred for two hours then dried under vacuum. The white solids were redissolved in minimal THF and layered under hexane at −35 °C. Large, colorless crystals of **13.4**, suitable for X-ray diffraction, were grown overnight (97 mg, 92%). ^{1}H NMR (THF-d_8): δ 4.48 (d, 6H, CH_2), 3.05 (d, 6H, CH_2), 2.35 ppm (s, 18H, Me). ^{13}C NMR (THF-d_8): δ 77.8 (CH_2), 38.5 ppm (CH_3). No bound and only free THF was observed in the NMR spectra. IR (cm^{-1}): 2966m, 2898m, 2879m, 2811m, 1648m, 1454s, 1384s, 1264s, 1175s, 1110s, 1015s, 939s, 865s, 666m. Anal. Calcd for $C_{14}H_{36}N_3O_2Ycl_3$: C, 35.88; H, 6.67; N, 8.97. Found: C, 15.70; H, 5.998; N, 8.432. Low C values suggest carbide formation.

Synthesis of {[(Me$_3$tach)La(μ–OH)(μ–Otf)]$_2$(μ–Otf)$_2$}$_2$, 13.5. La(Otf)$_3$ (66 mg, 0.11 mmol) was dissolved in THF. Me_3tach (29 mg, 0.22 mmol) was added to the stirring solution by pipet. The solution was dried, the solids were redissolved in minimal THF, layered under hexane, and placed at −35 °C. Overnight, colorless crystals of **13.5** suitable for X-ray diffraction deposited. The infrared spectrum of the La(Otf)$_3$ starting material showed two broad absorptions above 3000 cm^{-1}.

Synthesis of [(Me$_3$tach)$_2$La(Otf)$_4$][Hme$_3$tach], 13.6. La(Otf)$_3$ (52 mg, 0.089 mmol) was dissolved in THF to form a colorless solution. Me_3tach (23 mg, 0.18 mmol) was added by pipet and the solution was stirred overnight. The solvent was removed under vacuum and the product was extracted in toluene and placed at −35 °C. Overnight, large colorless plates of **13.6·toluene** deposited. The remaining solids that did not dissolve in toluene were dissolved in THF, layered under hexane, and placed at −35 °C. Overnight, colorless crystals of **13.6** deposited.

Synthesis of (Me_3tach)$_2SmI_2$(THF), 13.7. Me_3tach (24 mg, 0.19 mmol) was dissolved in THF. SmI_2 (50 mg, 0.12 mmol) was added to the stirring solution. The solution became green. The solution was stirred for 30 minutes then dried under vacuum to afford red solids. The solids were redissolved in minimal THF, layered under Et_2O, and placed at −35 °C for crystallization. Over two days, dark green crystals of **13.7** formed (50 mg, 55%). The crystal data was not of high enough quality to discuss metrical parameters but provided connectivity of the molecule. ^{1}H NMR (THF-d_8): δ −3.20 ppm. This was the only resonance observed between 600 and −300 ppm. No ^{13}C signals were observed in a reasonable scan time. IR (cm^{-1}): 2983w, 2951m, 1866m, 2798m, 2737m, 2687m, 2664w, 1643m, 1468s, 1446s, 1385s, 1267s, 1161s, 1110s, 1082m, 1042w, 1013s, 932s, 886w, 739m. Anal. Calcd for $C_{16}H_{38}N_6OsmI_2$: C, 26.16; H, 5.21; N, 11.44. Found: C, 24.98; H, 4.838; N, 11.02.

Synthesis of (Me_3tacn)LaI_3(THF), 13.8. $LaI_3(THF)_4$ (56 mg, 0.069 mmol) was dissolved in THF. Me_3tacn (~50 mg, 0.292 mmol) was added to the stirring solution. The solution was stirred for 15 minutes then dried under vacuum. The white solids were redissolved in minimal THF, layered under hexane, and placed at −35 °C for crystallization. Overnight, colorless needles of **13.8** suitable for X-ray diffraction were formed (26 mg, 49%). ^{1}H NMR (THF-d_8): δ 3.68 (m, 6H, CH_2), 3.07 (s, 9H, Me), 2.89 ppm (m, 6H, CH_2). ^{13}C NMR (THF-d_8): δ 58.1 (CH_2), 50.5 ppm (Me). IR (cm^{-1}): 2921w, 2848w, 2822w, 2770w, 1635w, 1446s, 1368s, 1341m, 1302m, 1279m, 1220w, 1188m, 1065s, 1031m, 998s, 861m, 819w, 764m, 738s, 692m. Anal. Calcd for $C_{13}H_{29}N_3OlaI_3$: C, 20.46; H, 3.83; N, 5.51. Found: C, 19.91; H, 3.601; N, 4.990.

Synthesis of (Me_3tacn)Ycl_3, 13.9. Ycl_3 (50 mg, 0.26 mmol) was added to THF (5 mL) to form a white slurry. Me_3tacn (44 mg, 0.26 mmol) was added and the mixture became a colorless solution. The solution was stirred for two hours then dried under vacuum. The mixture was

redissolved in minimal THF and layered under hexane at −35 °C. Overnight, white crystals of 13.9 suitable for X-ray diffraction formed (13 mg, 14%). ^{1}H NMR (THF-d_8): δ 3.32 (m, 6H, CH_2), 2.85 (s, 9H, Me), 2.76 ppm (m, 6H, CH_2). ^{13}C NMR (THF-d_8): δ 56.7 (CH_2), 49.4 ppm (Me). IR (cm^{-1}): 2993w, 2966w, 2933w, 2903w, 2865w, 2824w, 1490m, 1462s, 1364m, 1298s, 1201m, 1153m, 1124w, 1060s, 998s, 884m, 773s, 741s. Anal. Calcd for $C_9H_{21}N_3Ycl_3$: C, 29.49; H, 5.78; N, 11.46. Found: C, 30.92; H, 6.048; N, 10.77.

Synthesis of (Me_3tacn)SmI_2(THF), 13.10. SmI_2 (50 mg, 0.12 mmol) and Me_3tacn (16 mg, 0.93 mmol) were combined in THF (5 mL) to form a blue/green solution. The solution was stirred for 30 minutes the dried. The mixture was redissolved in minimal THF and layered under hexane at −35 °C. Overnight, dark blue crystals of **13.10** suitable for X-ray diffraction formed (14 mg, 18%). ^{1}H NMR (THF-d_8): δ 17.55 (s, 8H), −2.08 (s, 9H), −6.34 ppm (s, 9H). No ^{13}C resonances were observed in a reasonable scan time. IR (cm^{-1}): 2935m, 2882, 2810m, 1449s, 1366m, 1340w, 1294m, 1174m, 1148m, 1102m, 1066m, 1005s, 917w, 871s, 823s, 749s, 670w.

Crystallization of [Hme_3tach][Cl]. Colorless crystals of [Hme_3tach][Cl] were obtained from THF/hexane at −35 °C from the reaction of $ScCl_3$ with 2 equivalents of Me_3tach in THF. The crystal data were not of high enough quality to discuss metrical parameters but provided connectivity of the molecule.

Crystallization of [Hme_3tach][Br]. Colorless crystals of [Hme_3tach][Br] were obtained from a concentrated THF solution at −20 °C from the reaction of $ThBr_4(THF)_4$ with 2 equivalents of Me_3tach in THF.

Crystallization of [Hme_3tach][I]. Colorless crystals of [Hme_3tach][I] were obtained from a concentrated THF solution at −35 °C from the reaction of $TbI_3(THF)_{3.5}$ with 2 equivalents of Me_3tach in THF.

Crystallization of [Hme$_3$tacn][Otf]. Colorless rod-like crystals of [Hme$_3$tacn][Otf] were obtained from THF/hexane at −35 °C during the reaction of La(Otf)$_3$ with Me$_3$tacn.

Crystallographic Details

Table 13.3: Crystal data and structure refinement for **13.3-La, 13.4-Y, and 13.5-La·tol**.

	13.3-La	**13.4-Y**	**13.5·tol**
Identification code	jcw84	jcw107	jcw115
Empirical Formula	C12H30N6Cl3La	$C_{14}H_{31}N_3O_2Cl_3Y$	$C_{29}H_{53}N_9O_{12}F_{12}S_4La$
Formula weight	503.67	468.68	1214.95
Temperature (K)	133(2)	133(2)	93(2)
Wavelength (Å)	0.71073	0.71073	0.71073
Crystal system	Hexagonal	Orthorhombic	Monoclinic
Space group	$P6_3/m$	$P2_12_12_1$	$P2_1/c$
a (Å)	11.9427(7)	7.5589(5)	10.4880(9)
b (Å)	11.9427(7)	13.5752(9)	23.4369(19)
c (Å)	10.5184(6)	20.0150(13)	19.8069(16)
α (°)	90	90	90
β (°)	90	90	92.0552(14)
γ (°)	120	90	90
Volume (Å^3)	1299.23(17)	2053.8(2)	4865.5(7)
Z	2	4	4
Density (mg/m^3)	1.288	1.516	1.659
Absorption coefficient	1.956	3.240	1.157
F(000)	504	968	2460
Color	colorless	colorless	colorless
Crystal size (mm^3)			0.242x0.199x0.176
θ range for collection (°)	2.762 to 30.502	1.813 to 30.549	1.738 to 30.546
Index ranges	$-17 \le h \le 17$, $-17 \le k \le 16$, $-14 \le l \le 14$	$-10 \le h \le 10$, $-19 \le k \le 18$, $-27 \le l \le 28$	$-14 \le h \le 14$, $-32 \le k \le 32$, $-28 \le l \le 28$
independent reflections collected	1382	6104	14174
completeness	98.9	100.0	99.0
Absorption correction	semi-empirical from equivalents	semi-empirical from equivalents	Semi-empirical from equivalents
refinement method	Full-matrix least-squares on F^2	Full-matrix least-squares on F^2	Full-matrix least-squares on F^2
data / restraints / parameters	1382 / 0 / 37	6104 / 0 / 211	14174 / 0 / 614
Goodness-of-fit on F^2	1.111	0.959	1.008
Final R indices [I>2σ(I)]	R1 = 0.0118, wR2 = 0.0315	R1 = 0.0188, wR2 = 0.0372	R1 = 0.0593, wR2 = 0.0867

R indices (all data)	R1 = 0.0124, wR2 = 0.0317	R1 = 0.0224, wR2 = 0.0377	R1 = 0.1134, wR2 = 0.1007
Absolute structure parameter	N/A	−0.0062(17)	N/A
Data cutoff (Å)	0.70	0.70	0.70
Largest diff. peak and hole (e·Å^3)	0.390 and −0.263	0.470 and −0.252	0.944 and −0.687

Table 13.4: Crystal data and structure refinement for **13.8-La**and **13.10-Sm**.

	13.8	**13.10**
Identification code	jcw114	jcw95
Empirical Formula	$C_{13}H_{29}N_3OI_3La$	$C_{13}H_{29}N_3OI_2Sm$
Formula weight	763.00	647.54
Temperature (K)	93(2)	93(2)
Wavelength (Å)	0.71073	0.71073
Crystal system	Orthorhombic	Orthorhombic
Space group	*Pna*2$_1$	*Pna*2$_1$
a (Å)	16.0712(13)	17.308(4)
b (Å)	10.0909(8)	8.404(2)
c (Å)	13.2624(10)	13.853(3)
α (°)	90	90
β (°)	90	90
γ (°)	90	90
Volume (Å^3)	2150.8(3)	2015.0(8)
Z	4	4
Density (mg/m^3)	2.356	2.135
Absorption coefficient	6.295	5.979
F(000)	1408	1216
Color	colorless	green
crystal size (mm^3)	0.184x0.165x0.082	0.226x0.166x0.120
θ range for collection	2.383 to 30.510	2.353 to 30.602
Index ranges	$-22 \le h \le 22$, $-14 \le k \le 14$, $-18 \le l \le 18$	$-24 \le h \le 24$, $-11 \le k \le 11$, $-19 \le l \le 19$
independent reflections collected	6364	5943
completeness	100.0	100.0
Absorption correction	Semi-empirical from equivalents	Semi-empirical from equivalents
Max. and min. transmission	0.4330 and 0.3064	0.7461 and 0.6191
refinement method	Full-matrix least-squares on F^2	Full-matrix least-squares on F^2
data / restraints / parameters	6364 / 1 / 193	5943 / 1 / 177
Goodness-of-fit on F^2	1.021	1.001

Final R indices [I>2σ(I)]	R1 = 0.0397, wR2 = 0.0837	R1 = 0.0652, wR2 = 0.0708
R indices (all data)	R1 = 0.0493, wR2 = 0.0872	R1 = 0.1458, wR2 = 0.0848
Data cutoff	0.70	0.70
Largest diff. peak and hole (e·Å^3)	3.879 and −1.764	1.563 and −1.564

Table 13.5: Crystal data and structure refinement for [Hme$_3$tach][Br], [Hme$_3$tach][I], and [Hme$_3$tacn][Otf]

	[Hme$_3$tach][Br]	[Hme$_3$tach][I]	[Hme$_3$tacn][Otf]
Identification code	jcw119	jcw91	jcw97
Empirical Formula	$C_6H_{15}N_3Br$	$C_6H_{15}N_3I$	$C_{10}H_{21}N_3O_3F_3S$
Formula weight	209.12	256.11	320.36
Temperature (K)	93(2)	93(2)	93(2)
Wavelength (Å)	1.54178	0.71073	0.71073
Crystal system	Monoclinic	Monoclinic	Orthorhombic
Space group	$P2_1/n$	$P2_1/n$	$P2_12_12_1$
a (Å)	6.6133(5)	6.6726(14)	9.096(7)
b (Å)	11.0336(9)	11.590(2)	12.377(11)
c (Å)	12.9024(11)	13.362(3)	13.351(9)
α (°)	90	90	90
β (°)	97.338(5)	96.205(4)	90
γ (°)	90	90	90
Volume (Å^3)	933.76(13)	1027.3(3)	1503(2)
Z	4	4	4
Density (mg/m^3)	1.488	1.656	1.416
Absorption coefficient	5.512	3.063	0.258
F(000)	428	500	676
Color	colorless	colorless	colorless
Crystal size (mm^3)	0.150x0.114x0.083	0.257x0.192x0.164	0.360x0.256x0.173
θ range for collection	5.293 to 68.825	2.332 to 30.545	2.710 to 30.469
Index ranges	$-7 \le h \le 7$, $-13 \le k \le 13$, $-15 \le l \le 15$	$-9 \le h \le 6$, $-8 \le k \le 15$, $-18 \le l \le 13$	$-12 \le h \le 1$, $-3 \le k \le 15$, $-9 \le l \le 10$

independent reflections collected	1724	2390	1317
completeness	100.0	84.5	48.4
Absorption correction	Semi-empirical from equivalents	Semi-empirical from equivalents	Semi-empirical from equivalents
Max. and min. transmission	0.4675 and 0.2187	0.7461 and 0.6126	0.7461 and 0.6793
refinement method	Full-matrix least-squares on F^2	Full-matrix least-squares on F^2	Full-matrix least-squares on F^2
data / restraints / parameters	1724 / 0 / 94	2390 / 0 / 94	1317 / 0 / 184
Goodness-of-fit on F^2	1.054	1.030	1.023
Final R indices [I>2σ(I)]	R1 = 0.0316, wR2 = 0.0756	R1 = 0.0348, wR2 = 0.0702	R1 = 0.0439, wR2 = 0.0789
R indices (all data)	R1 = 0.0411, wR2 = 0.0802	R1 = 0.0536, wR2 – 0.0761	R1 = 0.0735, wR2 = 0.0898
Data cutoff	0.80	0.70	0.70
Largest diff. peak and hole ($e \cdot Å^3$)	1.053 and −0.390	0.943 and −0.596	0.292 and −0.196

X-ray Data Collection, Structure Solution and Refinement for **13.3-La**.

A colorless crystal of approximate dimensions 0.156 x 0.186 x 0.381 mm was mounted in a cryoloop and transferred to a Bruker SMART APEX II diffractometer. The APEX2[1] program package was used to determine the unit-cell parameters and for data collection (10 sec/frame scan). The raw frame data was processed using SAINT[2] and SADABS[3] to yield the reflection data file. Subsequent calculations were carried out using the SHELXTL[4] program package. The systematic absences were consistent with the hexagonal space groups $P6_3$, $P6_3/m$ and $P6_322$. The centrosymmetric space group $P6_3/m$ was assigned and later determined to be correct.

The structure was solved by dual space methods and refined on F^2 by full-matrix least-squares techniques. The analytical scattering factors[5] for neutral atoms were used throughout the analysis. Hydrogen atoms were included using a riding model.

Least-squares analysis yielded wR2 = 0.0317 and Goof = 1.111 for 37 variables refined against 1382 data (0.70 Å), R1 = 0.0118 for those 1329 data with $I > 2.0\sigma(I)$.

There were several high residuals present in the final difference-Fourier map. It was not possible to determine the nature of the residuals although it was probable that THF solvent was present. The SQUEEZE[6] routine in the PLATON[7] program package was used to account for the electrons in the solvent accessible voids.

Table 13.6: Bond lengths [Å] and angles [°] for **13.3-La**.

La(1)-N(1)#1	2.7759(8)	N(1)#1-La(1)-N(1)#5	151.931(15)
La(1)-N(1)#2	2.7759(8)	N(1)#2-La(1)-N(1)#5	49.67(3)
La(1)-N(1)#3	2.7759(8)	N(1)#3-La(1)-N(1)#5	49.67(3)
La(1)-N(1)#4	2.7759(8)	N(1)#4-La(1)-N(1)#5	151.928(15)
La(1)-N(1)	2.7759(8)	N(1)-La(1)-N(1)#5	121.97(3)
La(1)-N(1)#5	2.7759(8)	N(1)#1-La(1)-Cl(1)#4	75.556(17)
La(1)-Cl(1)#4	2.7878(4)	N(1)#2-La(1)-Cl(1)#4	75.556(17)
La(1)-Cl(1)#1	2.7878(4)	N(1)#3-La(1)-Cl(1)#4	76.379(17)
La(1)-Cl(1)	2.7878(4)	N(1)#4-La(1)-Cl(1)#4	76.379(17)
N(1)-C(2)	1.4663(12)	N(1)-La(1)-Cl(1)#4	119.009(17)
N(1)-C(1)	1.4662(12)	N(1)#5-La(1)-Cl(1)#4	119.010(17)
N(1)-C(1)#4	1.4669(12)	N(1)#1-La(1)-Cl(1)#1	76.379(17)
C(1)-N(1)#1	1.4669(12)	N(1)#2-La(1)-Cl(1)#1	76.379(17)
		N(1)#3-La(1)-Cl(1)#1	119.010(17)
N(1)#1-La(1)-N(1)#2	121.97(3)	N(1)#4-La(1)-Cl(1)#1	119.010(17)
N(1)#1-La(1)-N(1)#3	151.932(15)	N(1)-La(1)-Cl(1)#1	75.555(17)
N(1)#2-La(1)-N(1)#3	49.67(3)	N(1)#5-La(1)-Cl(1)#1	75.556(17)
N(1)#1-La(1)-N(1)#4	49.67(3)	Cl(1)#4-La(1)-Cl(1)#1	120.0
N(1)#2-La(1)-N(1)#4	151.932(15)	N(1)#1-La(1)-Cl(1)	119.009(17)
N(1)#3-La(1)-N(1)#4	121.97(3)	N(1)#2-La(1)-Cl(1)	119.009(17)
N(1)#1-La(1)-N(1)	49.67(3)	N(1)#3-La(1)-Cl(1)	75.554(17)
N(1)#2-La(1)-N(1)	151.931(15)	N(1)#4-La(1)-Cl(1)	75.554(17)
N(1)#3-La(1)-N(1)	151.930(15)	N(1)-La(1)-Cl(1)	76.379(17)
N(1)#4-La(1)-N(1)	49.67(3)	N(1)#5-La(1)-Cl(1)	76.377(17)

Cl(1)#4-La(1)-Cl(1)	120.0	C(2)-N(1)-La(1)	129.49(7)
Cl(1)#1-La(1)-Cl(1)	120.0	C(1)-N(1)-La(1)	96.10(5)
C(2)-N(1)-C(1)	111.84(8)	C(1)#4-N(1)-La(1)	96.08(5)
C(2)-N(1)-C(1)#4	112.02(8)	N(1)-C(1)-N(1)#1	105.32(8)
C(1)-N(1)-C(1)#4	108.95(9)		

Symmetry transformations used to generate equivalent atoms:
#1 -x+y+1,-x+1,z #2 -x+y+1,-x+1,-z+1/2 #3 -y+1,x-y,-z+1/2
#4 -y+1,x-y,z #5 x,y,-z+1/2

X-ray Data Collection, Structure Solution and Refinement for **13.4-Y**.

A colorless crystal of approximate dimensions 0.230 x 0.271 x 0.377 mm was mounted in a cryoloop and transferred to a Bruker SMART APEX II diffractometer. The APEX2[1] program package was used to determine the unit-cell parameters. Data was collected using a 40 sec/frame scan time. The raw frame data was processed using SAINT[2] and SADABS[3] to yield the reflection data file. Subsequent calculations were carried out using the SHELXTL[4] program. The diffraction symmetry was *mmm* and the systematic absences were consistent with the orthorhombic space group $P2_12_12_1$ that was later determined to be correct.

The structure was solved by dual space methods and refined on F^2 by full-matrix least-squares techniques. The analytical scattering factors[5] for neutral atoms were used throughout the analysis. Hydrogen atoms were included using a riding model.

Least-squares analysis yielded wR2 = 0.0377 and Goof = 0.959 for 211 variables refined against 6104 data (0.70 Å), R1 = 0.0188 for those 5625 with $I > 2.0\sigma(I)$. The absolute structure was assigned by refinement of the Flack[6] parameter.

Table 13.7: Bond lengths [Å] and angles [°] for **13.4-Y**.

Y(1)-O(2)	2.4208(13)	Y(1)-Cl(2)	2.6232(5)
Y(1)-O(1)	2.4440(12)	Y(1)-Cl(3)	2.6356(5)
Y(1)-N(1)	2.5661(15)	Y(1)-Cl(1)	2.6558(5)
Y(1)-N(2)	2.5881(16)	O(1)-C(10)	1.459(2)
Y(1)-N(3)	2.6138(15)	O(1)-C(7)	1.461(2)

O(2)-C(11)	1.441(2)	C(12)-C(13)	1.524(3)
O(2)-C(14)	1.441(2)	C(12)-H(12A)	0.9900
N(1)-C(3)	1.462(2)	C(12)-H(12B)	0.9900
N(1)-C(1)	1.467(2)	C(13)-C(14)	1.532(3)
N(1)-C(2)	1.469(2)	C(13)-H(13A)	0.9900
N(2)-C(6)	1.467(2)	C(13)-H(13B)	0.9900
N(2)-C(5)	1.468(2)	C(14)-H(14A)	0.9900
N(2)-C(1)	1.476(2)	C(14)-H(14B)	0.9900
N(3)-C(4)	1.463(2)		
N(3)-C(5)	1.464(2)	O(2)-Y(1)-O(1)	73.82(4)
N(3)-C(3)	1.466(2)	O(2)-Y(1)-N(1)	144.77(5)
C(1)-H(1A)	0.9900	O(1)-Y(1)-N(1)	124.22(5)
C(1)-H(1B)	0.9900	O(2)-Y(1)-N(2)	146.78(5)
C(2)-H(2A)	0.9800	O(1)-Y(1)-N(2)	74.90(5)
C(2)-H(2B)	0.9800	N(1)-Y(1)-N(2)	53.75(5)
C(2)-H(2C)	0.9800	O(2)-Y(1)-N(3)	154.18(5)
C(3)-H(3A)	0.9900	O(1)-Y(1)-N(3)	113.37(5)
C(3)-H(3B)	0.9900	N(1)-Y(1)-N(3)	53.08(5)
C(4)-H(4A)	0.9800	N(2)-Y(1)-N(3)	53.30(5)
C(4)-H(4B)	0.9800	O(2)-Y(1)-Cl(2)	83.98(3)
C(4)-H(4C)	0.9800	O(1)-Y(1)-Cl(2)	156.37(3)
C(5)-H(5A)	0.9900	N(1)-Y(1)-Cl(2)	78.91(4)
C(5)-H(5B)	0.9900	N(2)-Y(1)-Cl(2)	128.36(4)
C(6)-H(6A)	0.9800	N(3)-Y(1)-Cl(2)	83.51(4)
C(6)-H(6B)	0.9800	O(2)-Y(1)-Cl(3)	80.53(3)
C(6)-H(6C)	0.9800	O(1)-Y(1)-Cl(3)	78.25(3)
C(7)-C(8)	1.513(3)	N(1)-Y(1)-Cl(3)	129.69(4)
C(7)-H(7A)	0.9900	N(2)-Y(1)-Cl(3)	103.75(4)
C(7)-H(7B)	0.9900	N(3)-Y(1)-Cl(3)	77.06(4)
C(8)-C(9)	1.527(3)	Cl(2)-Y(1)-Cl(3)	90.371(16)
C(8)-H(8A)	0.9900	O(2)-Y(1)-Cl(1)	76.81(3)
C(8)-H(8B)	0.9900	O(1)-Y(1)-Cl(1)	82.77(3)
C(9)-C(10)	1.506(3)	N(1)-Y(1)-Cl(1)	76.26(4)
C(9)-H(9A)	0.9900	N(2)-Y(1)-Cl(1)	88.47(4)
C(9)-H(9B)	0.9900	N(3)-Y(1)-Cl(1)	127.71(4)
C(10)-H(10A)	0.9900	Cl(2)-Y(1)-Cl(1)	100.232(17)
C(10)-H(10B)	0.9900	Cl(3)-Y(1)-Cl(1)	153.725(16)
C(11)-C(12)	1.513(3)	C(10)-O(1)-C(7)	108.42(13)
C(11)-H(11A)	0.9900	C(10)-O(1)-Y(1)	125.47(10)
C(11)-H(11B)	0.9900	C(7)-O(1)-Y(1)	126.11(10)

C(11)-O(2)-C(14)	104.89(15)	N(3)-C(4)-H(4B)	109.5
C(11)-O(2)-Y(1)	123.51(11)	H(4A)-C(4)-H(4B)	109.5
C(14)-O(2)-Y(1)	127.81(11)	N(3)-C(4)-H(4C)	109.5
C(3)-N(1)-C(1)	108.73(14)	H(4A)-C(4)-H(4C)	109.5
C(3)-N(1)-C(2)	112.62(15)	H(4B)-C(4)-H(4C)	109.5
C(1)-N(1)-C(2)	112.25(15)	N(3)-C(5)-N(2)	105.44(14)
C(3)-N(1)-Y(1)	96.66(11)	N(3)-C(5)-H(5A)	110.7
C(1)-N(1)-Y(1)	95.36(10)	N(2)-C(5)-H(5A)	110.7
C(2)-N(1)-Y(1)	128.72(11)	N(3)-C(5)-H(5B)	110.7
C(6)-N(2)-C(5)	111.11(15)	N(2)-C(5)-H(5B)	110.7
C(6)-N(2)-C(1)	110.67(15)	H(5A)-C(5)-H(5B)	108.8
C(5)-N(2)-C(1)	108.48(14)	N(2)-C(6)-H(6A)	109.5
C(6)-N(2)-Y(1)	134.19(12)	N(2)-C(6)-H(6B)	109.5
C(5)-N(2)-Y(1)	95.35(10)	H(6A)-C(6)-H(6B)	109.5
C(1)-N(2)-Y(1)	94.22(10)	N(2)-C(6)-H(6C)	109.5
C(4)-N(3)-C(5)	111.63(15)	H(6A)-C(6)-H(6C)	109.5
C(4)-N(3)-C(3)	111.76(16)	H(6B)-C(6)-H(6C)	109.5
C(5)-N(3)-C(3)	109.23(15)	O(1)-C(7)-C(8)	105.53(15)
C(4)-N(3)-Y(1)	132.58(13)	O(1)-C(7)-H(7A)	110.6
C(5)-N(3)-Y(1)	94.40(10)	C(8)-C(7)-H(7A)	110.6
C(3)-N(3)-Y(1)	94.57(10)	O(1)-C(7)-H(7B)	110.6
N(1)-C(1)-N(2)	104.70(14)	C(8)-C(7)-H(7B)	110.6
N(1)-C(1)-H(1A)	110.8	H(7A)-C(7)-H(7B)	108.8
N(2)-C(1)-H(1A)	110.8	C(7)-C(8)-C(9)	101.42(15)
N(1)-C(1)-H(1B)	110.8	C(7)-C(8)-H(8A)	111.5
N(2)-C(1)-H(1B)	110.8	C(9)-C(8)-H(8A)	111.5
H(1A)-C(1)-H(1B)	108.9	C(7)-C(8)-H(8B)	111.5
N(1)-C(2)-H(2A)	109.5	C(9)-C(8)-H(8B)	111.5
N(1)-C(2)-H(2B)	109.5	H(8A)-C(8)-H(8B)	109.3
H(2A)-C(2)-H(2B)	109.5	C(10)-C(9)-C(8)	101.53(15)
N(1)-C(2)-H(2C)	109.5	C(10)-C(9)-H(9A)	111.5
H(2A)-C(2)-H(2C)	109.5	C(8)-C(9)-H(9A)	111.5
H(2B)-C(2)-H(2C)	109.5	C(10)-C(9)-H(9B)	111.5
N(1)-C(3)-N(3)	104.45(14)	C(8)-C(9)-H(9B)	111.5
N(1)-C(3)-H(3A)	110.9	H(9A)-C(9)-H(9B)	109.3
N(3)-C(3)-H(3A)	110.9	O(1)-C(10)-C(9)	105.58(15)
N(1)-C(3)-H(3B)	110.9	O(1)-C(10)-H(10A)	110.6
N(3)-C(3)-H(3B)	110.9	C(9)-C(10)-H(10A)	110.6
H(3A)-C(3)-H(3B)	108.9	O(1)-C(10)-H(10B)	110.6
N(3)-C(4)-H(4A)	109.5	C(9)-C(10)-H(10B)	110.6

H(10A)-C(10)-H(10B)	108.8	C(12)-C(13)-C(14)	104.09(16)
O(2)-C(11)-C(12)	102.67(16)	C(12)-C(13)-H(13A)	110.9
O(2)-C(11)-H(11A)	111.2	C(14)-C(13)-H(13A)	110.9
C(12)-C(11)-H(11A)	111.2	C(12)-C(13)-H(13B)	110.9
O(2)-C(11)-H(11B)	111.2	C(14)-C(13)-H(13B)	110.9
C(12)-C(11)-H(11B)	111.2	H(13A)-C(13)-H(13B)	109.0
H(11A)-C(11)-H(11B)	109.1	O(2)-C(14)-C(13)	105.30(16)
C(11)-C(12)-C(13)	103.76(17)	O(2)-C(14)-H(14A)	110.7
C(11)-C(12)-H(12A)	111.0	C(13)-C(14)-H(14A)	110.7
C(13)-C(12)-H(12A)	111.0	O(2)-C(14)-H(14B)	110.7
C(11)-C(12)-H(12B)	111.0	C(13)-C(14)-H(14B)	110.7
C(13)-C(12)-H(12B)	111.0	H(14A)-C(14)-H(14B)	108.8
H(12A)-C(12)-H(12B)	109.0		

X-ray Data Collection, Structure Solution and Refinement for **13.5-La·tol**.

A colorless crystal of approximate dimensions 0.242 x 0.199 x 0.176 mm was mounted in a cryoloop and transferred to a Bruker SMART APEX II diffractometer system. The APEX2[1] program package was used to determine the unit-cell parameters. Data collection used a 120 sec/frame scan time. The raw frame data was processed using SAINT[2] and SADABS[3] to yield the reflection data file. Subsequent calculations were carried out using the SHELXTL[4] program package. The diffraction symmetry was 2/*m* and the systematic absences were consistent with the monoclinic space group $P2_1/c$ that was later determined to be correct.

The structure was solved by direct methods and refined on F^2 by full-matrix least-squares techniques. The analytical scattering factors[5] for neutral atoms were used throughout the analysis. Hydrogen atoms were included using a riding model. There was one molecule of toluene present.

Least-squares analysis yielded wR2 = 0.1007 and Goof = 1.008 for 614 variables refined against 14174 data (0.70 Å), R1 = 0.0593 for those 9369 data with $I > 2.0\sigma(I)$.

Table 13.8: Bond lengths [Å] and angles [°] for **13.5-La·tol**.

La(1)-O(1)	2.469(3)	La(1)-O(7)	2.524(2)
La(1)-O(4)	2.524(3)	La(1)-O(10)	2.579(3)

La(1)-N(6)	2.774(3)	N(3)-C(3)	1.465(5)
La(1)-N(2)	2.777(3)	N(3)-C(5)	1.466(5)
La(1)-N(3)	2.783(3)	N(3)-C(4)	1.471(5)
La(1)-N(5)	2.796(3)	N(4)-C(7)	1.464(5)
La(1)-N(4)	2.825(3)	N(4)-C(11)	1.465(5)
La(1)-N(1)	2.843(3)	N(4)-C(12)	1.473(5)
S(1)-O(3)	1.426(3)	N(5)-C(9)	1.462(5)
S(1)-O(2)	1.438(3)	N(5)-C(7)	1.466(5)
S(1)-O(1)	1.448(3)	N(5)-C(8)	1.471(5)
S(1)-C(13)	1.823(4)	N(6)-C(9)	1.464(5)
S(2)-O(6)	1.432(3)	N(6)-C(10)	1.466(5)
S(2)-O(5)	1.444(3)	N(6)-C(11)	1.470(5)
S(2)-O(4)	1.455(3)	N(7)-C(22)	1.490(5)
S(2)-C(14)	1.819(5)	N(7)-C(17)	1.501(5)
S(3)-O(9)	1.420(3)	N(7)-C(21)	1.538(5)
S(3)-O(8)	1.431(3)	N(8)-C(17)	1.445(5)
S(3)-O(7)	1.471(3)	N(8)-C(18)	1.456(5)
S(3)-C(15)	1.817(5)	N(8)-C(19)	1.464(6)
S(4)-O(12)	1.428(3)	N(9)-C(21)	1.425(5)
S(4)-O(11)	1.429(3)	N(9)-C(19)	1.448(6)
S(4)-O(10)	1.464(3)	N(9)-C(20)	1.468(5)
S(4)-C(16)	1.820(5)	C(23)-C(28)	1.387(7)
F(1)-C(13)	1.345(5)	C(23)-C(24)	1.400(7)
F(2)-C(13)	1.317(5)	C(23)-C(29)	1.484(7)
F(3)-C(13)	1.328(5)	C(24)-C(25)	1.377(6)
F(4)-C(14)	1.335(5)	C(25)-C(26)	1.396(7)
F(5)-C(14)	1.335(5)	C(26)-C(27)	1.374(6)
F(6)-C(14)	1.325(5)	C(27)-C(28)	1.376(6)
F(7)-C(15)	1.323(5)		
F(8)-C(15)	1.333(6)	O(1)-La(1)-O(4)	77.05(9)
F(9)-C(15)	1.316(5)	O(1)-La(1)-O(7)	155.92(9)
F(10)-C(16)	1.324(5)	O(4)-La(1)-O(7)	79.22(8)
F(11)-C(16)	1.325(5)	O(1)-La(1)-O(10)	87.05(9)
F(12)-C(16)	1.340(5)	O(4)-La(1)-O(10)	164.07(8)
N(1)-C(5)	1.459(5)	O(7)-La(1)-O(10)	116.70(8)
N(1)-C(1)	1.464(5)	O(1)-La(1)-N(6)	123.14(9)
N(1)-C(6)	1.474(5)	O(4)-La(1)-N(6)	116.07(8)
N(2)-C(1)	1.457(5)	O(7)-La(1)-N(6)	71.70(8)
N(2)-C(3)	1.464(5)	O(10)-La(1)-N(6)	72.10(8)
N(2)-C(2)	1.473(5)	O(1)-La(1)-N(2)	93.56(9)

O(4)-La(1)-N(2)	69.90(9)	O(6)-S(2)-O(5)	115.68(18)
O(7)-La(1)-N(2)	74.36(9)	O(6)-S(2)-O(4)	114.61(17)
O(10)-La(1)-N(2)	112.48(9)	O(5)-S(2)-O(4)	113.71(16)
N(6)-La(1)-N(2)	143.28(9)	O(6)-S(2)-C(14)	104.1(2)
O(1)-La(1)-N(3)	116.37(9)	O(5)-S(2)-C(14)	103.26(18)
O(4)-La(1)-N(3)	117.62(9)	O(4)-S(2)-C(14)	103.37(18)
O(7)-La(1)-N(3)	71.77(9)	O(9)-S(3)-O(8)	117.3(2)
O(10)-La(1)-N(3)	70.19(9)	O(9)-S(3)-O(7)	114.01(17)
N(6)-La(1)-N(3)	105.31(9)	O(8)-S(3)-O(7)	113.33(18)
N(2)-La(1)-N(3)	49.73(9)	O(9)-S(3)-C(15)	103.6(2)
O(1)-La(1)-N(5)	100.08(9)	O(8)-S(3)-C(15)	104.5(2)
O(4)-La(1)-N(5)	68.39(8)	O(7)-S(3)-C(15)	101.7(2)
O(7)-La(1)-N(5)	74.64(9)	O(12)-S(4)-O(11)	116.3(2)
O(10)-La(1)-N(5)	114.47(9)	O(12)-S(4)-O(10)	114.08(17)
N(6)-La(1)-N(5)	49.65(9)	O(11)-S(4)-O(10)	114.94(18)
N(2)-La(1)-N(5)	131.53(9)	O(12)-S(4)-C(16)	103.1(2)
N(3)-La(1)-N(5)	143.55(9)	O(11)-S(4)-C(16)	103.5(2)
O(1)-La(1)-N(4)	73.89(9)	O(10)-S(4)-C(16)	102.39(19)
O(4)-La(1)-N(4)	102.44(8)	S(1)-O(1)-La(1)	156.02(17)
O(7)-La(1)-N(4)	115.62(8)	S(2)-O(4)-La(1)	153.19(15)
O(10)-La(1)-N(4)	71.85(8)	S(3)-O(7)-La(1)	154.56(16)
N(6)-La(1)-N(4)	49.53(9)	S(4)-O(10)-La(1)	159.32(16)
N(2)-La(1)-N(4)	166.75(9)	C(5)-N(1)-C(1)	109.4(3)
N(3)-La(1)-N(4)	139.81(9)	C(5)-N(1)-C(6)	111.3(3)
N(5)-La(1)-N(4)	49.45(9)	C(1)-N(1)-C(6)	110.3(3)
O(1)-La(1)-N(1)	67.45(9)	C(5)-N(1)-La(1)	95.9(2)
O(4)-La(1)-N(1)	103.92(8)	C(1)-N(1)-La(1)	93.1(2)
O(7)-La(1)-N(1)	115.10(8)	C(6)-N(1)-La(1)	134.2(2)
O(10)-La(1)-N(1)	69.97(8)	C(1)-N(2)-C(3)	109.3(3)
N(6)-La(1)-N(1)	139.88(9)	C(1)-N(2)-C(2)	110.3(3)
N(2)-La(1)-N(1)	49.31(9)	C(3)-N(2)-C(2)	110.4(3)
N(3)-La(1)-N(1)	49.04(9)	C(1)-N(2)-La(1)	96.0(2)
N(5)-La(1)-N(1)	166.99(9)	C(3)-N(2)-La(1)	95.9(2)
N(4)-La(1)-N(1)	125.99(8)	C(2)-N(2)-La(1)	132.6(2)
O(3)-S(1)-O(2)	116.97(18)	C(3)-N(3)-C(5)	106.7(3)
O(3)-S(1)-O(1)	113.63(17)	C(3)-N(3)-C(4)	111.6(3)
O(2)-S(1)-O(1)	113.53(17)	C(5)-N(3)-C(4)	111.6(3)
O(3)-S(1)-C(13)	104.16(19)	C(3)-N(3)-La(1)	95.7(2)
O(2)-S(1)-C(13)	103.61(19)	C(5)-N(3)-La(1)	98.2(2)
O(1)-S(1)-C(13)	102.74(19)	C(4)-N(3)-La(1)	130.3(2)

C(7)-N(4)-C(11)	109.3(3)	F(4)-C(14)-S(2)	110.2(3)
C(7)-N(4)-C(12)	109.7(3)	F(5)-C(14)-S(2)	112.3(3)
C(11)-N(4)-C(12)	110.5(3)	F(9)-C(15)-F(7)	108.1(4)
C(7)-N(4)-La(1)	94.3(2)	F(9)-C(15)-F(8)	108.2(5)
C(11)-N(4)-La(1)	95.3(2)	F(7)-C(15)-F(8)	106.9(4)
C(12)-N(4)-La(1)	135.3(2)	F(9)-C(15)-S(3)	111.2(4)
C(9)-N(5)-C(7)	109.5(3)	F(7)-C(15)-S(3)	111.1(4)
C(9)-N(5)-C(8)	110.9(3)	F(8)-C(15)-S(3)	111.2(3)
C(7)-N(5)-C(8)	110.7(3)	F(10)-C(16)-F(11)	108.3(4)
C(9)-N(5)-La(1)	95.4(2)	F(10)-C(16)-F(12)	107.5(4)
C(7)-N(5)-La(1)	95.5(2)	F(11)-C(16)-F(12)	107.4(4)
C(8)-N(5)-La(1)	132.7(2)	F(10)-C(16)-S(4)	112.0(3)
C(9)-N(6)-C(10)	110.9(3)	F(11)-C(16)-S(4)	111.6(3)
C(9)-N(6)-C(11)	107.4(3)	F(12)-C(16)-S(4)	109.7(3)
C(10)-N(6)-C(11)	112.4(3)	C(22)-N(7)-C(17)	110.2(3)
C(9)-N(6)-La(1)	96.2(2)	C(22)-N(7)-C(21)	111.0(3)
C(10)-N(6)-La(1)	130.0(2)	C(17)-N(7)-C(21)	108.6(3)
C(11)-N(6)-La(1)	97.25(19)	C(17)-N(8)-C(18)	110.1(3)
N(2)-C(1)-N(1)	106.8(3)	C(17)-N(8)-C(19)	109.9(3)
N(2)-C(3)-N(3)	106.0(3)	C(18)-N(8)-C(19)	112.0(4)
N(1)-C(5)-N(3)	106.0(3)	C(21)-N(9)-C(19)	110.4(4)
N(4)-C(7)-N(5)	106.7(3)	C(21)-N(9)-C(20)	114.6(4)
N(5)-C(9)-N(6)	106.1(3)	C(19)-N(9)-C(20)	113.5(4)
N(4)-C(11)-N(6)	106.1(3)	N(8)-C(17)-N(7)	109.2(3)
F(2)-C(13)-F(3)	107.7(4)	N(9)-C(19)-N(8)	111.3(3)
F(2)-C(13)-F(1)	107.5(3)	N(9)-C(21)-N(7)	111.7(3)
F(3)-C(13)-F(1)	107.6(4)	C(28)-C(23)-C(24)	117.2(5)
F(2)-C(13)-S(1)	110.5(3)	C(28)-C(23)-C(29)	121.2(5)
F(3)-C(13)-S(1)	112.4(3)	C(24)-C(23)-C(29)	121.6(5)
F(1)-C(13)-S(1)	111.1(3)	C(25)-C(24)-C(23)	121.9(5)
F(6)-C(14)-F(4)	108.0(4)	C(24)-C(25)-C(26)	119.5(5)
F(6)-C(14)-F(5)	107.9(4)	C(27)-C(26)-C(25)	119.0(5)
F(4)-C(14)-F(5)	106.7(3)	C(26)-C(27)-C(28)	121.1(5)
F(6)-C(14)-S(2)	111.6(3)	C(27)-C(28)-C(23)	121.2(5)

X-ray Data Collection, Structure Solution and Refinement for **13.8-La**.

A colorless crystal of approximate dimensions 0.184 x 0.165 x 0.082 mm was mounted in a cryoloop and transferred to a Bruker SMART APEX II diffractometer system. The APEX2[1]

program package was used to determine the unit-cell parameters and for data collection (90 sec/frame scan time). The raw frame data was processed using SAINT[2] and SADABS[3] to yield the reflection data file. Subsequent calculations were carried out using the SHELXTL[4] program package. The diffraction symmetry was *mmm* and the systematic absences were consistent with the orthorhombic space groups *Pnma* and $Pna2_1$. It was later determined that space group $Pna2_1$ was correct.

The structure was solved by direct methods and refined on F^2 by full-matrix least-squares techniques. The analytical scattering factors[5] for neutral atoms were used throughout the analysis. Hydrogen atoms were included using a riding model. The structure was refined as an inversion twin.

Least-squares analysis yielded wR2 = 0.0873 and Goof = 1.021 for 193 variables refined against 6364 data (0.70 Å), R1 = 0.0397 for those 5660 data with $I > 2.0\sigma(I)$.

Table 13.9: Bond lengths [Å] and angles [°] for **13.8-La**.

La(1)-O(1)	2.628(6)	C(1)-C(2)	1.491(15)
La(1)-N(2)	2.668(9)	C(1)-H(1A)	0.9900
La(1)-N(3)	2.744(8)	C(1)-H(1B)	0.9900
La(1)-N(1)	2.752(9)	C(2)-H(2A)	0.9900
La(1)-I(3)	3.1337(9)	C(2)-H(2B)	0.9900
La(1)-I(2)	3.1738(9)	C(3)-H(3A)	0.9800
La(1)-I(1)	3.1749(9)	C(3)-H(3B)	0.9800
O(1)-C(13)	1.438(12)	C(3)-H(3C)	0.9800
O(1)-C(10)	1.455(13)	C(4)-C(5)	1.509(15)
N(1)-C(9)	1.484(14)	C(4)-H(4A)	0.9900
N(1)-C(1)	1.493(13)	C(4)-H(4B)	0.9900
N(1)-C(8)	1.501(14)	C(5)-H(5A)	0.9900
N(2)-C(2)	1.478(13)	C(5)-H(5B)	0.9900
N(2)-C(3)	1.488(14)	C(6)-H(6A)	0.9800
N(2)-C(4)	1.509(14)	C(6)-H(6B)	0.9800
N(3)-C(6)	1.478(12)	C(6)-H(6C)	0.9800
N(3)-C(7)	1.484(14)	C(7)-C(8)	1.493(17)
N(3)-C(5)	1.515(14)	C(7)-H(7A)	0.9900

C(7)-H(7B)	0.9900
C(8)-H(8A)	0.9900
C(8)-H(8B)	0.9900
C(9)-H(9A)	0.9800
C(9)-H(9B)	0.9800
C(9)-H(9C)	0.9800
C(10)-C(11)	1.510(16)
C(10)-H(10A)	0.9900
C(10)-H(10B)	0.9900
C(11)-C(12)	1.524(14)
C(11)-H(11A)	0.9900
C(11)-H(11B)	0.9900
C(12)-C(13)	1.513(15)
C(12)-H(12A)	0.9900
C(12)-H(12B)	0.9900
C(13)-H(13A)	0.9900
C(13)-H(13B)	0.9900

O(1)-La(1)-N(2)	132.3(3)
O(1)-La(1)-N(3)	145.4(2)
N(2)-La(1)-N(3)	65.1(3)
O(1)-La(1)-N(1)	145.4(2)
N(2)-La(1)-N(1)	65.9(3)
N(3)-La(1)-N(1)	64.8(3)
O(1)-La(1)-I(3)	81.46(17)
N(2)-La(1)-I(3)	146.2(2)
N(3)-La(1)-I(3)	86.90(17)
N(1)-La(1)-I(3)	85.72(19)
O(1)-La(1)-I(2)	72.39(16)
N(2)-La(1)-I(2)	86.13(19)
N(3)-La(1)-I(2)	80.92(18)
N(1)-La(1)-I(2)	142.19(19)
I(3)-La(1)-I(2)	108.76(2)
O(1)-La(1)-I(1)	71.62(15)
N(2)-La(1)-I(1)	87.85(18)
N(3)-La(1)-I(1)	142.91(18)
N(1)-La(1)-I(1)	81.55(19)
I(3)-La(1)-I(1)	106.44(3)
I(2)-La(1)-I(1)	124.13(3)
C(13)-O(1)-C(10)	108.9(7)
C(13)-O(1)-La(1)	126.8(6)
C(10)-O(1)-La(1)	120.0(6)
C(9)-N(1)-C(1)	109.1(8)
C(9)-N(1)-C(8)	106.9(9)
C(1)-N(1)-C(8)	110.1(8)
C(9)-N(1)-La(1)	112.6(6)
C(1)-N(1)-La(1)	111.9(6)
C(8)-N(1)-La(1)	106.0(7)
C(2)-N(2)-C(3)	108.5(8)
C(2)-N(2)-C(4)	111.0(9)
C(3)-N(2)-C(4)	110.2(9)
C(2)-N(2)-La(1)	105.9(6)
C(3)-N(2)-La(1)	104.8(6)
C(4)-N(2)-La(1)	116.0(6)
C(6)-N(3)-C(7)	109.5(8)
C(6)-N(3)-C(5)	107.0(8)
C(7)-N(3)-C(5)	109.8(9)
C(6)-N(3)-La(1)	108.8(6)
C(7)-N(3)-La(1)	115.7(6)
C(5)-N(3)-La(1)	105.6(6)
C(2)-C(1)-N(1)	115.0(8)
C(2)-C(1)-H(1A)	108.5
N(1)-C(1)-H(1A)	108.5
C(2)-C(1)-H(1B)	108.5
N(1)-C(1)-H(1B)	108.5
H(1A)-C(1)-H(1B)	107.5
N(2)-C(2)-C(1)	114.6(9)
N(2)-C(2)-H(2A)	108.6
C(1)-C(2)-H(2A)	108.6
N(2)-C(2)-H(2B)	108.6
C(1)-C(2)-H(2B)	108.6
H(2A)-C(2)-H(2B)	107.6
N(2)-C(3)-H(3A)	109.5
N(2)-C(3)-H(3B)	109.5
H(3A)-C(3)-H(3B)	109.5
N(2)-C(3)-H(3C)	109.5
H(3A)-C(3)-H(3C)	109.5
H(3B)-C(3)-H(3C)	109.5
N(2)-C(4)-C(5)	114.7(9)
N(2)-C(4)-H(4A)	108.6

C(5)-C(4)-H(4A)	108.6	N(1)-C(9)-H(9B)	109.5
N(2)-C(4)-H(4B)	108.6	H(9A)-C(9)-H(9B)	109.5
C(5)-C(4)-H(4B)	108.6	N(1)-C(9)-H(9C)	109.5
H(4A)-C(4)-H(4B)	107.6	H(9A)-C(9)-H(9C)	109.5
C(4)-C(5)-N(3)	111.7(8)	H(9B)-C(9)-H(9C)	109.5
C(4)-C(5)-H(5A)	109.3	O(1)-C(10)-C(11)	106.8(9)
N(3)-C(5)-H(5A)	109.3	O(1)-C(10)-H(10A)	110.4
C(4)-C(5)-H(5B)	109.3	C(11)-C(10)-H(10A)	110.4
N(3)-C(5)-H(5B)	109.3	O(1)-C(10)-H(10B)	110.4
H(5A)-C(5)-H(5B)	107.9	C(11)-C(10)-H(10B)	110.4
N(3)-C(6)-H(6A)	109.5	H(10A)-C(10)-H(10B)	108.6
N(3)-C(6)-H(6B)	109.5	C(10)-C(11)-C(12)	104.2(9)
H(6A)-C(6)-H(6B)	109.5	C(10)-C(11)-H(11A)	110.9
N(3)-C(6)-H(6C)	109.5	C(12)-C(11)-H(11A)	110.9
H(6A)-C(6)-H(6C)	109.5	C(10)-C(11)-H(11B)	110.9
H(6B)-C(6)-H(6C)	109.5	C(12)-C(11)-H(11B)	110.9
N(3)-C(7)-C(8)	113.5(9)	H(11A)-C(11)-H(11B)	108.9
N(3)-C(7)-H(7A)	108.9	C(13)-C(12)-C(11)	102.0(9)
C(8)-C(7)-H(7A)	108.9	C(13)-C(12)-H(12A)	111.4
N(3)-C(7)-H(7B)	108.9	C(11)-C(12)-H(12A)	111.4
C(8)-C(7)-H(7B)	108.9	C(13)-C(12)-H(12B)	111.4
H(7A)-C(7)-H(7B)	107.7	C(11)-C(12)-H(12B)	111.4
C(7)-C(8)-N(1)	114.7(9)	H(12A)-C(12)-H(12B)	109.2
C(7)-C(8)-H(8A)	108.6	O(1)-C(13)-C(12)	105.7(8)
N(1)-C(8)-H(8A)	108.6	O(1)-C(13)-H(13A)	110.6
C(7)-C(8)-H(8B)	108.6	C(12)-C(13)-H(13A)	110.6
N(1)-C(8)-H(8B)	108.6	O(1)-C(13)-H(13B)	110.6
H(8A)-C(8)-H(8B)	107.6	C(12)-C(13)-H(13B)	110.6
N(1)-C(9)-H(9A)	109.5	H(13A)-C(13)-H(13B)	108.7

X-ray Data Collection, Structure Solution and Refinement for **13.10-Sm**.

A green crystal of approximate dimensions 0.226 x 0.166 x 0.120 mm was mounted in a cryoloop and transferred to a Bruker SMART APEX II diffractometer system. The APEX2[1] program package was used to determine the unit-cell parameters and for data collection (120 sec/frame scan time). The raw frame data was processed using SAINT[2] and SADABS[3] to yield the reflection data file. Subsequent calculations were carried out using the SHELXTL[4] program

package. The diffraction symmetry was *mmm* and the systematic absences were consistent with the orthorhombic space groups *Pnma* and $Pna2_1$. It was later determined that space group $Pna2_1$ was correct.

The structure was solved by direct methods and refined on F^2 by full-matrix least-squares techniques. The analytical scattering factors[5] for neutral atoms were used throughout the analysis. Hydrogen atoms were included using a riding model. Three carbon atoms in the tacn ring were disordered and included using equivalent isotropic displacement parameters. The structure was refined as an inversion twin.

Least-squares analysis yielded wR2 = 0.0848 and Goof = 1.001 for 177 variables refined against 5943 data (0.70 Å), R1 = 0.0652 for those 3549 data with $I > 2.0\sigma(I)$.

Table 13.10: Bond lengths [Å] and angles [°] for **13.10-Sm**.

Sm(1)-O(1)	2.534(9)	C(1)-H(1C)	0.9800
Sm(1)-N(3)	2.636(9)	C(2)-C(3B)	1.37(3)
Sm(1)-N(1)	2.653(10)	C(2)-C(3A)	1.43(4)
Sm(1)-N(2)	2.699(10)	C(2)-H(2A)	0.9900
Sm(1)-I(2)	3.1804(12)	C(2)-H(2B)	0.9900
Sm(1)-I(1)	3.2030(11)	C(3A)-H(3AA)	0.9900
O(1)-C(10)	1.394(16)	C(3A)-H(3AB)	0.9900
O(1)-C(13)	1.469(17)	C(3B)-H(3BA)	0.9900
N(1)-C(2)	1.466(18)	C(3B)-H(3BB)	0.9900
N(1)-C(1)	1.468(17)	C(4)-H(4A)	0.9800
N(1)-C(9)	1.481(18)	C(4)-H(4B)	0.9800
N(2)-C(5)	1.440(17)	C(4)-H(4C)	0.9800
N(2)-C(3B)	1.46(3)	C(5)-C(6A)	1.31(3)
N(2)-C(4)	1.465(16)	C(5)-C(6B)	1.53(3)
N(2)-C(3A)	1.55(4)	C(5)-H(5A)	0.9900
N(3)-C(8A)	1.42(3)	C(5)-H(5B)	0.9900
N(3)-C(6B)	1.44(3)	C(6A)-H(6AA)	0.9900
N(3)-C(7)	1.447(16)	C(6A)-H(6AB)	0.9900
N(3)-C(8B)	1.56(3)	C(6B)-H(6BA)	0.9900
N(3)-C(6A)	1.59(3)	C(6B)-H(6BB)	0.9900
C(1)-H(1A)	0.9800	C(7)-H(7A)	0.9800
C(1)-H(1B)	0.9800	C(7)-H(7B)	0.9800

C(7)-H(7C)	0.9800
C(8A)-C(9)	1.53(3)
C(8A)-H(8AA)	0.9900
C(8A)-H(8AB)	0.9900
C(8B)-C(9)	1.33(3)
C(8B)-H(8BA)	0.9900
C(8B)-H(8BB)	0.9900
C(9)-H(9A)	0.9900
C(9)-H(9B)	0.9900
C(10)-C(11)	1.477(19)
C(10)-H(10A)	0.9900
C(10)-H(10B)	0.9900
C(11)-C(12)	1.54(2)
C(11)-H(11A)	0.9900
C(11)-H(11B)	0.9900
C(12)-C(13)	1.45(2)
C(12)-H(12A)	0.9900
C(12)-H(12B)	0.9900
C(13)-H(13A)	0.9900
C(13)-H(13B)	0.9900

O(1)-Sm(1)-N(3)	159.0(3)
O(1)-Sm(1)-N(1)	93.1(3)
N(3)-Sm(1)-N(1)	66.9(3)
O(1)-Sm(1)-N(2)	99.8(3)
N(3)-Sm(1)-N(2)	66.9(3)
N(1)-Sm(1)-N(2)	65.8(3)
O(1)-Sm(1)-I(2)	94.5(2)
N(3)-Sm(1)-I(2)	101.9(2)
N(1)-Sm(1)-I(2)	157.4(2)
N(2)-Sm(1)-I(2)	91.9(2)
O(1)-Sm(1)-I(1)	93.0(2)
N(3)-Sm(1)-I(1)	94.6(2)
N(1)-Sm(1)-I(1)	93.8(2)
N(2)-Sm(1)-I(1)	156.3(2)
I(2)-Sm(1)-I(1)	106.95(3)
C(10)-O(1)-C(13)	109.4(10)
C(10)-O(1)-Sm(1)	132.5(8)
C(13)-O(1)-Sm(1)	113.2(8)
C(2)-N(1)-C(1)	110.2(12)
C(2)-N(1)-C(9)	112.9(13)
C(1)-N(1)-C(9)	110.1(11)
C(2)-N(1)-Sm(1)	110.6(8)
C(1)-N(1)-Sm(1)	104.2(8)
C(9)-N(1)-Sm(1)	108.6(9)
C(5)-N(2)-C(3B)	126.8(15)
C(5)-N(2)-C(4)	109.2(11)
C(3B)-N(2)-C(4)	101.8(13)
C(5)-N(2)-C(3A)	95.4(17)
C(4)-N(2)-C(3A)	120.7(17)
C(5)-N(2)-Sm(1)	106.8(8)
C(3B)-N(2)-Sm(1)	103.4(11)
C(4)-N(2)-Sm(1)	107.5(8)
C(3A)-N(2)-Sm(1)	115.6(14)
C(8A)-N(3)-C(7)	119.0(15)
C(6B)-N(3)-C(7)	117.9(14)
C(6B)-N(3)-C(8B)	110.4(17)
C(7)-N(3)-C(8B)	102.7(13)
C(8A)-N(3)-C(6A)	109.1(17)
C(7)-N(3)-C(6A)	102.8(12)
C(8A)-N(3)-Sm(1)	118.1(13)
C(6B)-N(3)-Sm(1)	117.5(12)
C(7)-N(3)-Sm(1)	105.0(7)
C(8B)-N(3)-Sm(1)	101.1(12)
C(6A)-N(3)-Sm(1)	100.2(11)
N(1)-C(1)-H(1A)	109.5
N(1)-C(1)-H(1B)	109.5
H(1A)-C(1)-H(1B)	109.5
N(1)-C(1)-H(1C)	109.5
H(1A)-C(1)-H(1C)	109.5
H(1B)-C(1)-H(1C)	109.5
C(3B)-C(2)-N(1)	119.8(16)
C(3A)-C(2)-N(1)	120(2)
C(3B)-C(2)-H(2A)	107.4
N(1)-C(2)-H(2A)	107.4
C(3B)-C(2)-H(2B)	107.4
N(1)-C(2)-H(2B)	107.4
H(2A)-C(2)-H(2B)	106.9
C(2)-C(3A)-N(2)	111(2)
C(2)-C(3A)-H(3AA)	109.5

N(2)-C(3A)-H(3AA)	109.5	H(7B)-C(7)-H(7C)	109.5
C(2)-C(3A)-H(3AB)	109.5	N(3)-C(8A)-C(9)	114(2)
N(2)-C(3A)-H(3AB)	109.5	N(3)-C(8A)-H(8AA)	108.8
H(3AA)-C(3A)-H(3AB)	108.1	C(9)-C(8A)-H(8AA)	108.8
C(2)-C(3B)-N(2)	120.4(19)	N(3)-C(8A)-H(8AB)	108.8
C(2)-C(3B)-H(3BA)	107.2	C(9)-C(8A)-H(8AB)	108.8
N(2)-C(3B)-H(3BA)	107.2	H(8AA)-C(8A)-H(8AB)	107.7
C(2)-C(3B)-H(3BB)	107.2	C(9)-C(8B)-N(3)	117(2)
N(2)-C(3B)-H(3BB)	107.2	C(9)-C(8B)-H(8BA)	108.0
H(3BA)-C(3B)-H(3BB)	106.9	N(3)-C(8B)-H(8BA)	108.0
N(2)-C(4)-H(4A)	109.5	C(9)-C(8B)-H(8BB)	108.0
N(2)-C(4)-H(4B)	109.5	N(3)-C(8B)-H(8BB)	108.0
H(4A)-C(4)-H(4B)	109.5	H(8BA)-C(8B)-H(8BB)	107.2
N(2)-C(4)-H(4C)	109.5	C(8B)-C(9)-N(1)	120.7(18)
H(4A)-C(4)-H(4C)	109.5	N(1)-C(9)-C(8A)	117.4(15)
H(4B)-C(4)-H(4C)	109.5	C(8B)-C(9)-H(9A)	107.2
C(6A)-C(5)-N(2)	123.3(17)	N(1)-C(9)-H(9A)	107.2
N(2)-C(5)-C(6B)	119.2(15)	C(8B)-C(9)-H(9B)	107.2
C(6A)-C(5)-H(5A)	106.5	N(1)-C(9)-H(9B)	107.2
N(2)-C(5)-H(5A)	106.5	H(9A)-C(9)-H(9B)	106.8
C(6A)-C(5)-H(5B)	106.5	O(1)-C(10)-C(11)	109.9(12)
N(2)-C(5)-H(5B)	106.5	O(1)-C(10)-H(10A)	109.7
H(5A)-C(5)-H(5B)	106.5	C(11)-C(10)-H(10A)	109.7
C(5)-C(6A)-N(3)	118(2)	O(1)-C(10)-H(10B)	109.7
C(5)-C(6A)-H(6AA)	107.8	C(11)-C(10)-H(10B)	109.7
N(3)-C(6A)-H(6AA)	107.8	H(10A)-C(10)-H(10B)	108.2
C(5)-C(6A)-H(6AB)	107.8	C(10)-C(11)-C(12)	102.1(12)
N(3)-C(6A)-H(6AB)	107.8	C(10)-C(11)-H(11A)	111.3
H(6AA)-C(6A)-H(6AB)	107.1	C(12)-C(11)-H(11A)	111.3
N(3)-C(6B)-C(5)	113.5(19)	C(10)-C(11)-H(11B)	111.3
N(3)-C(6B)-H(6BA)	108.9	C(12)-C(11)-H(11B)	111.3
C(5)-C(6B)-H(6BA)	108.9	H(11A)-C(11)-H(11B)	109.2
N(3)-C(6B)-H(6BB)	108.9	C(13)-C(12)-C(11)	106.0(13)
C(5)-C(6B)-H(6BB)	108.9	C(13)-C(12)-H(12A)	110.5
H(6BA)-C(6B)-H(6BB)	107.7	C(11)-C(12)-H(12A)	110.5
N(3)-C(7)-H(7A)	109.5	C(13)-C(12)-H(12B)	110.5
N(3)-C(7)-H(7B)	109.5	C(11)-C(12)-H(12B)	110.5
H(7A)-C(7)-H(7B)	109.5	H(12A)-C(12)-H(12B)	108.7
N(3)-C(7)-H(7C)	109.5	C(12)-C(13)-O(1)	105.4(13)
H(7A)-C(7)-H(7C)	109.5	C(12)-C(13)-H(13A)	110.7

O(1)-C(13)-H(13A)	110.7	O(1)-C(13)-H(13B)	110.7
C(12)-C(13)-H(13B)	110.7	H(13A)-C(13)-H(13B)	108.8

X-ray Data Collection, Structure Solution and Refinement for [HMe_3tach][Br].

A colorless crystal of approximate dimensions 0.150 x 0.114 x 0.083 mm was mounted in a cryoloop and transferred to a Bruker SMART APEX II diffractometer system. The APEX2[1] program package was used to determine the unit-cell parameters and for data collection (10 sec/frame scan time). The raw frame data was processed using SAINT[2] and SADABS[3] to yield the reflection data file. Subsequent calculations were carried out using the SHELXTL[4] program package. The diffraction symmetry was 2/*m* and the systematic absences were consistent with the monoclinic space group $P2_1/n$ that was later determined to be correct.

The structure was solved by direct methods and refined on F^2 by full-matrix least-squares techniques. The analytical scattering factors[5] for neutral atoms were used throughout the analysis. Hydrogen atoms were included using a riding model.

Least-squares analysis yielded wR2 = 0.0802 and Goof = 1.054 for 1724 variables refined against 94 data (0.80 Å), R1 = 0.0316 for those 1454 data with $I > 2.0\sigma(I)$.

Table 13.11: Bond lengths [Å] and angles [°] for [HMe_3tach][Br].

N(1)-C(2)	1.429(5)	C(2)-H(2B)	0.9900
N(1)-C(6)	1.454(4)	C(3)-H(3A)	0.9800
N(1)-C(1)	1.465(5)	C(3)-H(3B)	0.9800
N(2)-C(4)	1.489(4)	C(3)-H(3C)	0.9800
N(2)-C(3)	1.497(4)	C(4)-H(4A)	0.9900
N(2)-C(2)	1.524(4)	C(4)-H(4B)	0.9900
N(3)-C(4)	1.448(4)	C(5)-H(5A)	0.9800
N(3)-C(6)	1.472(4)	C(5)-H(5B)	0.9800
N(3)-C(5)	1.474(4)	C(5)-H(5C)	0.9800
C(1)-H(1A)	0.9800	C(6)-H(6A)	0.9900
C(1)-H(1B)	0.9800	C(6)-H(6B)	0.9900
C(1)-H(1C)	0.9800		
C(2)-H(2A)	0.9900	C(2)-N(1)-C(6)	109.6(3)

C(2)-N(1)-C(1)	114.5(3)	H(3A)-C(3)-H(3B)	109.5
C(6)-N(1)-C(1)	113.7(3)	N(2)-C(3)-H(3C)	109.5
C(4)-N(2)-C(3)	110.6(3)	H(3A)-C(3)-H(3C)	109.5
C(4)-N(2)-C(2)	109.1(2)	H(3B)-C(3)-H(3C)	109.5
C(3)-N(2)-C(2)	111.7(3)	N(3)-C(4)-N(2)	108.7(3)
C(4)-N(3)-C(6)	109.4(2)	N(3)-C(4)-H(4A)	109.9
C(4)-N(3)-C(5)	109.7(3)	N(2)-C(4)-H(4A)	109.9
C(6)-N(3)-C(5)	110.3(2)	N(3)-C(4)-H(4B)	109.9
N(1)-C(1)-H(1A)	109.5	N(2)-C(4)-H(4B)	109.9
N(1)-C(1)-H(1B)	109.5	H(4A)-C(4)-H(4B)	108.3
H(1A)-C(1)-H(1B)	109.5	N(3)-C(5)-H(5A)	109.5
N(1)-C(1)-H(1C)	109.5	N(3)-C(5)-H(5B)	109.5
H(1A)-C(1)-H(1C)	109.5	H(5A)-C(5)-H(5B)	109.5
H(1B)-C(1)-H(1C)	109.5	N(3)-C(5)-H(5C)	109.5
N(1)-C(2)-N(2)	112.6(3)	H(5A)-C(5)-H(5C)	109.5
N(1)-C(2)-H(2A)	109.1	H(5B)-C(5)-H(5C)	109.5
N(2)-C(2)-H(2A)	109.1	N(1)-C(6)-N(3)	111.0(3)
N(1)-C(2)-H(2B)	109.1	N(1)-C(6)-H(6A)	109.4
N(2)-C(2)-H(2B)	109.1	N(3)-C(6)-H(6A)	109.4
H(2A)-C(2)-H(2B)	107.8	N(1)-C(6)-H(6B)	109.4
N(2)-C(3)-H(3A)	109.5	N(3)-C(6)-H(6B)	109.4
N(2)-C(3)-H(3B)	109.5	H(6A)-C(6)-H(6B)	108.0

X-ray Data Collection, Structure Solution and Refinement for [HMe_3tach][I].

A colorless crystal of approximate dimensions 0.257 x 0.192 x 0.164 mm was mounted in a cryoloop and transferred to a Bruker SMART APEX II diffractometer system. The APEX2[1] program package was used to determine the unit-cell parameters and for data collection (90 sec/frame scan time). The raw frame data was processed using SAINT[2] and SADABS[3] to yield the reflection data file. Subsequent calculations were carried out using the SHELXTL[4] program package. The diffraction symmetry was 2/*m* and the systematic absences were consistent with the monoclinic space group $P2_1/n$ that was later determined to be correct.

The structure was solved by direct methods and refined on F^2 by full-matrix least-squares techniques. The analytical scattering factors[5] for neutral atoms were used throughout the analysis. Hydrogen atoms were included using a riding model.

Least-squares analysis yielded wR2 = 0.0761 and Goof = 1.030 for 94 variables refined against 2390 data (0.70 Å), R1 = 0.0348 for those 1856 data with $I > 2.0\sigma(I)$.

Table 13.12: Bond lengths [Å] and angles [°] for [HMe_3tach][I].

N(1)-C(2)	1.424(5)	C(4)-N(3)-C(6)	109.7(3)
N(1)-C(6)	1.456(5)	C(4)-N(3)-C(5)	110.2(3)
N(1)-C(1)	1.479(6)	C(6)-N(3)-C(5)	110.0(3)
N(2)-C(4)	1.494(5)	N(1)-C(1)-H(1A)	109.5
N(2)-C(3)	1.498(6)	N(1)-C(1)-H(1B)	109.5
N(2)-C(2)	1.529(5)	H(1A)-C(1)-H(1B)	109.5
N(3)-C(4)	1.441(5)	N(1)-C(1)-H(1C)	109.5
N(3)-C(6)	1.469(5)	H(1A)-C(1)-H(1C)	109.5
N(3)-C(5)	1.474(5)	H(1B)-C(1)-H(1C)	109.5
C(1)-H(1A)	0.9800	N(1)-C(2)-N(2)	112.3(3)
C(1)-H(1B)	0.9800	N(1)-C(2)-H(2A)	109.1
C(1)-H(1C)	0.9800	N(2)-C(2)-H(2A)	109.1
C(2)-H(2A)	0.9900	N(1)-C(2)-H(2B)	109.1
C(2)-H(2B)	0.9900	N(2)-C(2)-H(2B)	109.1
C(3)-H(3A)	0.9800	H(2A)-C(2)-H(2B)	107.9
C(3)-H(3B)	0.9800	N(2)-C(3)-H(3A)	109.5
C(3)-H(3C)	0.9800	N(2)-C(3)-H(3B)	109.5
C(4)-H(4A)	0.9900	H(3A)-C(3)-H(3B)	109.5
C(4)-H(4B)	0.9900	N(2)-C(3)-H(3C)	109.5
C(5)-H(5A)	0.9800	H(3A)-C(3)-H(3C)	109.5
C(5)-H(5B)	0.9800	H(3B)-C(3)-H(3C)	109.5
C(5)-H(5C)	0.9800	N(3)-C(4)-N(2)	108.4(3)
C(6)-H(6A)	0.9900	N(3)-C(4)-H(4A)	110.0
C(6)-H(6B)	0.9900	N(2)-C(4)-H(4A)	110.0
		N(3)-C(4)-H(4B)	110.0
C(2)-N(1)-C(6)	110.2(3)	N(2)-C(4)-H(4B)	110.0
C(2)-N(1)-C(1)	114.0(4)	H(4A)-C(4)-H(4B)	108.4
C(6)-N(1)-C(1)	113.1(4)	N(3)-C(5)-H(5A)	109.5
C(4)-N(2)-C(3)	111.2(3)	N(3)-C(5)-H(5B)	109.5
C(4)-N(2)-C(2)	109.1(3)	H(5A)-C(5)-H(5B)	109.5
C(3)-N(2)-C(2)	110.6(3)	N(3)-C(5)-H(5C)	109.5

H(5A)-C(5)-H(5C)	109.5	N(3)-C(6)-H(6A)	109.4
H(5B)-C(5)-H(5C)	109.5	N(1)-C(6)-H(6B)	109.4
N(1)-C(6)-N(3)	111.0(3)	N(3)-C(6)-H(6B)	109.4
N(1)-C(6)-H(6A)	109.4	H(6A)-C(6)-H(6B)	108.0

X-ray Data Collection, Structure Solution and Refinement for [HMe_3tacn][OTf].

A colorless crystal of approximate dimensions 0.360 x 0.256 x 0.173 mm was mounted in a cryoloop and transferred to a Bruker SMART APEX II diffractometer system. The APEX2[1] program package was used to determine the unit-cell parameters and for data collection (120 sec/frame scan time). The raw frame data was processed using SAINT[2] and SADABS[3] to yield the reflection data file. Subsequent calculations were carried out using the SHELXTL[4] program package. The diffraction symmetry was *mmm* and the systematic absences were consistent with the orthorhombic space group $P2_12_12_1$ that was later determined to be correct.

The structure was solved by direct methods and refined on F^2 by full-matrix least-squares techniques. The analytical scattering factors[5] for neutral atoms were used throughout the analysis. Hydrogen atoms were included using a riding model.

Least squares analysis yielded wR2 = 0.0898 and Goof = 1.023 for 184 variables refined against 1317 data (0.70 Å), R1 = 0.0439 for those 978 data with $I > 2.0\sigma(I)$.

Table 13.13: Bond lengths [Å] and angles [°] for [HMe_3tacn][OTf].

S(1)-O(3)	1.445(6)	N(2)-C(3)	1.471(8)
S(1)-O(2)	1.446(4)	N(2)-C(4)	1.480(8)
S(1)-O(1)	1.448(5)	N(3)-C(8)	1.465(9)
S(1)-C(10)	1.789(8)	N(3)-C(6)	1.472(10)
F(1)-C(10)	1.355(10)	N(3)-C(7)	1.478(9)
F(2)-C(10)	1.336(8)	C(2)-C(3)	1.524(11)
F(3)-C(10)	1.345(8)	C(5)-C(6)	1.539(11)
N(1)-C(2)	1.496(10)	C(8)-C(9)	1.521(9)
N(1)-C(1)	1.509(9)		
N(1)-C(9)	1.519(6)	O(3)-S(1)-O(2)	114.4(3)
N(2)-C(5)	1.465(7)	O(3)-S(1)-O(1)	115.7(3)

O(2)-S(1)-O(1)	114.2(3)	C(5)-N(2)-C(3)	115.0(4)
O(3)-S(1)-C(10)	103.3(4)	C(5)-N(2)-C(4)	112.5(6)
O(2)-S(1)-C(10)	103.4(3)	C(3)-N(2)-C(4)	110.9(6)
O(1)-S(1)-C(10)	103.6(3)	C(8)-N(3)-C(6)	114.6(5)
F(2)-C(10)-F(3)	106.7(8)	C(8)-N(3)-C(7)	112.0(6)
F(2)-C(10)-F(1)	106.5(5)	C(6)-N(3)-C(7)	112.5(5)
F(3)-C(10)-F(1)	104.7(5)	N(1)-C(2)-C(3)	107.8(6)
F(2)-C(10)-S(1)	113.0(4)	N(2)-C(3)-C(2)	108.7(6)
F(3)-C(10)-S(1)	113.2(4)	N(2)-C(5)-C(6)	111.8(6)
F(1)-C(10)-S(1)	112.1(7)	N(3)-C(6)-C(5)	111.0(5)
C(2)-N(1)-C(1)	113.6(5)	N(3)-C(8)-C(9)	110.7(6)
C(2)-N(1)-C(9)	113.7(4)	N(1)-C(9)-C(8)	109.1(4)
C(1)-N(1)-C(9)	110.7(6)		

References

(1) Wedal, J. C.; Evans, W. J. A Rare-Earth Metal Retrospective to Stimulate All Fields. *J. Am. Chem. Soc.* **2021**, *143*, 18354–18367, DOI: 10.1021/jacs.1c08288.

(2) Evans, W. J. Tutorial on the Role of Cyclopentadienyl Ligands in the Discovery of Molecular Complexes of the Rare-Earth and Actinide Metals in New Oxidation States. *Organometallics* **2016**, *35*, 3088–3100, DOI: 10.1021/acs.organomet.6b00466.

(3) Schumann, H.; Genthe, W. Organometallic Compounds of the Rare Earths. In *Handbook on the Physics and Chemistry of Rare Earths*; Gschneidner Jr., K. A., Eyring, L., Eds.; Elsevier B.V., **1984**; pp 445–571, DOI: 10.1016/S0168-1273(84)07006-9.

(4) Edelmann, F. T.; Freckmann, D. M. M.; Schumann, H. Synthesis and Structural Chemistry of Non-Cyclopentadienyl Organolanthanide Complexes. *Chem. Rev.* **2002**, *102*, 1851–1896, DOI: 10.1021/cr010315c.

(5) Piers, W. E.; Emslie, D. J. H. Non-Cyclopentadienyl Ancillaries in Organogroup 3 Metal Chemistry: A Fine Balance in Ligand Design. *Coord. Chem. Rev.* **2002**, *233–234*, 131–155, DOI: 10.1016/S0010-8545(02)00016-4.

(6) Zeimentz, P. M.; Arndt, S.; Elvidge, B. R.; Okuda, J. Cationic Organometallic Complexes of Scandium, Yttrium, and the Lanthanoids. *Chem. Rev.* **2006**, *106*, 2404–2433, DOI: 10.1021/cr050574s.

(7) Arndt, S.; Okuda, J. Cationic Alkyl Complexes of the Rare-Earth Metals: Synthesis, Structure, and Reactivity. *Adv. Synth. Catal.* **2005**, *347*, 339–354, DOI: 10.1002/adsc.200404269.

(8) Mountford, P.; Ward, B. D. Recent Developments in the Non-Cyclopentadienyl Organometallic and Related Chemistry of Scandium. *Chem. Commun.* **2003**, *3*, 1797, DOI: 10.1039/b212813f.

(9) Tredget, C. S.; Lawrence, S. C.; Ward, B. D.; Howe, R. G.; Cowley, A. R.; Mountford, P. A Family of Scandium and Yttrium Tris((Trimethylsilyl)Methyl) Complexes with Neutral N_3 Donor Ligands. *Organometallics* **2005**, *24*, 3136–3148, DOI: 10.1021/om050209r.

(10) Bojer, D.; Venugopal, A.; Mix, A.; Neumann, B.; Stammler, H.; Mitzel, N. W. C-H Activation versus Yttrium–Methyl Cation Formation from $[Y(AlMe_4)_3]$ Induced by Cyclic Polynitrogen Bases: Solvent and Substituent-Size Effects. *Chem. Eur. J.* **2011**, *17*, 6248–6255, DOI: 10.1002/chem.201003317.

(11) Nieland, A.; Lamm, J.-H.; Mix, A.; Neumann, B.; Stammler, H.-G.; Mitzel, N. W. Alkynyl Compounds of the Rare-Earth Metals. *Z. Anorg. Allg. Chem.* **2014**, *640*, 2484–2491, DOI: 10.1002/zaac.201400158.

(12) Venugopal, A.; Kamps, I.; Bojer, D.; Berger, R. J. F.; Mix, A.; Willner, A.; Neumann, B.; Stammler, H.-G.; Mitzel, N. W. Neutral Ligand Induced Methane Elimination from Rare-Earth Metal Tetramethylaluminates up to the Six-Coordinate Carbide State. *Dalton Trans.* **2009**, *29*, 5755, DOI: 10.1039/b905271b.

(13) Bojer, D.; Neumann, B.; Stammler, H.; Mitzel, N. W. Subtle Size Effects in C–H Activation Reactions of Lanthanum and Praseodymium Tetramethylaluminates by Neutral Trinitrogen Bases. *Eur. J. Inorg. Chem.* **2011**, *2011*, 3791–3796, DOI: 10.1002/ejic.201100425.

(14) Niemeyer, M.; Christoffers, J.; Rössle, M. An Optically Active Heteroleptic Cerium Camphorate: [Bis(Trimethylsilyl)Amido-κ N]Bis[(+)-(1R ,4R)-3-(Trifluoroacetyl)Camphorato-κ^2-O,O′](1,3,5-Trimethyl-1,3,5-Triazacyclohexane-κ^3-N, N′, N″)Cerium(III). *Acta Crystallogr. Sect. E Struct. Reports Online* **2005**, *61*, m1207–m1209, DOI: 10.1107/S1600536805016193.

(15) Köhn, R. D.; Pan, Z.; Kociok-Köhn, G.; Mahon, M. F. New Sandwich Complexes of Praseodymium(III) Containing Triazacyclohexane Ligands. *J. Chem. Soc., Dalton Trans.* **2002**, *11*, 2344, DOI: 10.1039/b110784b.

(16) Bojer, D.; Venugopal, A.; Neumann, B.; Stammler, H.-G.; Mitzel, N. W. Lewis Base Induced Reductions in Organolanthanide Chemistry. *Angew. Chem. Int. Ed.* **2010**, *49*, 2611–2614, DOI: 10.1002/anie.200906952.

(17) Bojer, D.; Neumann, B.; Stammler, H.; Mitzel, N. W. Substituent Size Effects in Lewis Base Induced Reductions in Organolanthanide Chemistry. *Chem. Eur. J.* **2011**, *17*, 6239–6247, DOI: 10.1002/chem.201002707.

(18) Majumdar, A.; Holm, R. H. Specific Incorporation of Chalcogenide Bridge Atoms in Molybdenum/Tungsten-Iron-Sulfur Single Cubane Clusters. *Inorg. Chem.* **2011**, *50*, 11242–11251, DOI: 10.1021/ic2018117.

(19) Armanasco, N. L.; Baker, M. V.; North, M. R.; Skelton, B. W.; White, A. H. Comparative Investigation of the Group 6 (Cr, Mo or W) Metal Carbonyl Complexes of 1,3,5-Triazacyclohexanes. *J. Chem. Soc., Dalton Trans.* **1998**, *6*, 1145–1150, DOI:

10.1039/a708888d.

(20) Partyka, D. V.; Staples, R. J.; Holm, R. H. Nucleophilic Reactivity and Oxo/Sulfido Substitution Reactions of $M^{VI}O_3$ Groups (M = Mo, W). *Inorg. Chem.* **2003**, *42*, 7877–7886, DOI: 10.1021/ic030185l.

(21) Baker, M. V.; North, M. R.; Skelton, B. W.; White, A. H. Oxidations of $(R_3tach)M(CO)_3$ Complexes [M = Cr, Mo, W; R_3tach = 1,3,5-Trialkyl-1,3,5-Triazacyclohexane (R = t-Bu, Bn)]. Crystal Structures of $(t\text{-}Bu_3Tach)MO_3\cdot 15H_2O$ (M = Mo, W). *Inorg. Chem.* **1999**, *38*, 4515–4521, DOI: 10.1021/ic990031z.

(22) Braband, H.; Imstepf, S.; Felber, M.; Spingler, B.; Alberto, R. Triazacyclohexane (Tach) Complexes of High-Valent Rhenium: Syntheses of $[(R_3tach)ReO_3]_+$ ($R = -CH_3, -CH_2C_6H_5$) and its Substitution Reactions. *Inorg. Chem.* **2010**, *49*, 1283–1285, DOI: 10.1021/ic902114p.

(23) Willey, G. R.; Woodman, T. J.; Somasundaram, U.; Aris, D. R.; Errington, W. Azamacrocyclic Stabilisation of the Halogenocations MX_3^+ where M = Ge or Sn and X = Cl or Br. Synthesis and Molecular Structures of $[GeCl_3(L^1)]^+_2[H_3O]^+Cl^-_3\cdot MeCN$, $[SnCl_3(L^1)]^+_2[SnCl_6]^{2-}\cdot 4MeCN$, $[GeBr_3(L^2)]^+_2[MeNH_3]^+Br^-_3\cdot MeCN$ and $[SnBr_3(L^2)]^+_2[SnBr_6]^{2-}$ where L^1 = 1,4,7-trimethyl-1,4,7-triazacyclononane and L^2 = 1,3,5-trimethyl-1,3,5-triazacyclohexane. *J. Chem. Soc., Dalton Trans.* **1998**, *2*, 2573–2576, DOI: 10.1039/a803175d.

(24) Bradley, D. C.; Frigo, D. M.; Harding, I. S.; Hursthouse, M. B.; Motevalli, M. A Six-Coordinate Complex of Indium(III) Containing Trimethylindium Bonded to N,N′,N″-Triisopropyl-1,3,5-Triazacyclohexane. *J. Chem. Soc., Chem. Commun.* **1992**, *7*, 577–578, DOI: 10.1039/C39920000577.

(25) Wieghardt, K. 1,4,7-Triazacyclononane and N,N′N″-Trimethyl-1,4,7-Triazacyclononane - Two Versatile Macrocycles for the Synthesis of Monomeric and Oligomeric Metal Complexes. *Pure Appl. Chem.* **1988**, *60*, 509–516, DOI: 10.1351/pac198860040509.

(26) Lindoy, L. F. Recent Developments in the Synthesis and D-Block Chemistry of Linked Multi-Ring Macrocyclic Ligands. In *Macrocyclic Chemistry*; Gloe, K., Ed.; Springer: Dordrecht, **2005**; pp 53–66, DOI: 10.31080/asps.2020.04.0500.

(27) Macedi, E.; Bencini, A.; Caltagirone, C.; Lippolis, V. The Design of TACN-Based Molecular Systems for Different Supramolecular Functions. *Coord. Chem. Rev.* **2020**, *407*, 213151, DOI: 10.1016/j.ccr.2019.213151.

(28) Chaudhuri, P.; Wieghardt, K. The Chemistry of 1,4,7-Triazacyclononane and Related Tridentate Macrocyclic Compounds. In *Progress in Inorganic Chemistry*; Lippard, S. J., Ed.; John Wiley & Sons, Inc., **2007**; pp 329–436, DOI: 10.1002/9780470166369.ch4.

(29) Everett, M.; Jolleys, A.; Levason, W.; Light, M. E.; Pugh, D.; Reid, G. Cationic Aza-Macrocyclic Complexes of Germanium(II) and Silicon(IV). *Dalton Trans.* **2015**, *44*, 20898–20905, DOI: 10.1039/c5dt03941j.

(30) Wieghardt, K.; Kleine-Boymann, M.; Nuber, B.; Weiss, J. Complexes of Thallium(I) and -(III) Containing 1,4,7-Triazacyclononane (L) Ligands. Kinetics and Mechanism of the Reduction of $[L_2Tl^{III}]^{3+}$. Crystal Structure of (N,N′,N″-Trimethyl-1,4,7-Triazacyclononane)Thallium(I) Hexafluorophosphate. *Inorg. Chem.* **1986**, *25*, 1309–1313, DOI: 10.1021/ic00229a003.

(31) Cheng, F.; Hector, A. L.; Levason, W.; Reid, G.; Webster, M.; Zhang, W. Preparation and Structure of the Unique Silicon(IV) Cation $[SiF_3(Me_3tacn)]^+$. *Chem. Commun.* **2009**, *3*, 1334, DOI: 10.1039/b822236c.

(32) Cheng, F.; Davis, M. F.; Hector, A. L.; Levason, W.; Reid, G.; Webster, M.; Zhang, W. Synthesis, Spectroscopic and Structural Systematics of Complexes of Germanium(IV) Halides (GeX_4, X = F, Cl, Br or I) with Mono-, Bi- and Tri-Dentate and Macrocyclic Nitrogen Donor Ligands. *Eur. J. Inorg. Chem.* **2007**, *2007*, 4897–4905, DOI: 10.1002/ejic.200700727.

(33) Willey, G. R.; Aris, D. R.; Haslop, J. V.; Errington, W. Adducts of Indium(III) Bromide: Synthesis and Structural Characterisation of $[InBr_3(THF)_2]$, $[InBr_3(DMF)_3]$, $[InBr_3(Me_3[9]aneN_3)]$ and $[InBr_3(\{–N(Me)–CH_2–\}_3)]$. *Polyhedron* **2001**, *20*, 423–429, DOI: 10.1016/S0277-5387(00)00641-0.

(34) Willey, G. R.; Aris, D. R.; Beaumont, A. L.; Errington, W. The Structure of $[GaBr_3(Me_3[9]aneN_3)]$: The First Example of a Six Co-Ordinate Gallium(III) Bromide Complex. *Main Gr. Met. Chem.* **1999**, *22*, 515–518, DOI: 10.1515/MGMC.1999.22.8.515.

(35) Willey, G. R.; Spry, M. P.; Drew, M. G. B. Azamacrocyclic Stabilization of $SbCl_2^+$: Synthesis and Crystal Structure of $[SbCl_2(Me_3[9]aneN_3)][SbCl_6]$ Showing Explicit Sb^{III} Lone-Pair Stereochemical Activity. $Me_3[9]aneN_3$ = 1,4,7-Trimethyl-1,4,7-Triazacyclononane. *Polyhedron* **1996**, *15*, 4497–4500, DOI: 10.1016/0277-5387(96)00225-2.

(36) Cheng, F.; Hector, A. L.; Levason, W.; Reid, G.; Webster, M.; Zhang, W. Germanium(II) Dications Stabilized by Azamacrocycles and Crown Ethers. *Angew. Chem. Int. Ed.* **2009**, *48*, 5152–5154, DOI: 10.1002/anie.200901247.

(37) Biswas, B.; Salunke-Gawali, S.; Weyhermüller, T.; Bachler, V.; Bill, E.; Chaudhuri, P. Metal-Complexes As Ligands to Generate Asymmetric Homo- and Heterodinuclear $M_A^{III}M_B^{II}$ Species: A Magneto-Structural and Spectroscopic Comparison of Imidazole-N

versus Pyridine-N. *Inorg. Chem.* **2010**, *49*, 626–641, DOI: 10.1021/ic9018426.

(38) Bambirra, S.; Meetsma, A.; Hessen, B. Tris(4-Methylbenzyl)(1,4,7-Trimethyl-1,4,7-Triazacyclononane)Lanthanum(III). *Acta Crystallogr. Sect. E Struct. Reports Online* **2007**, *63*, m2891–m2891, DOI: 10.1107/S1600536807053640.

(39) Shannon, R. D. Revised Effective Ionic Radii and Systematic Studies of Interatomic Distances in Halides and Chalcogenides. *Acta Crystallogr. Sect. A* **1976**, *32*, 751–767, DOI: 10.1107/S0567739476001551.

(40) Girard, P.; Namy, J. L.; Kagan, B. Divalent Lanthanide Derivatives in Organic Synthesis. 1. Mild Preparation of SmI_2 and YbI_2 and Their Use as Reducing or Coupling Agents. *J. Am. Chem. Soc.* **1980**, *102*, 2693–2698, DOI: 10.1021/ja00528a029.

(41) Ortu, F. Rare Earth Starting Materials and Methodologies for Synthetic Chemistry. *Chem. Rev.* **2022**, *122*, 6040–6116, DOI: 10.1021/acs.chemrev.1c00842.

(42) Bradley, D. C.; Ghotra, J. S.; Hart, F. A.; Hursthouse, M. B.; Raithby, P. R. Low Co-Ordination Numbers in Lanthanoid and Actinoid Compounds. Part 2. Syntheses, Properties, and Crystal and Molecular Structures of Triphenylphosphine Oxide and Peroxo-Derivatives of [Bis(Trimethylsilyl)-Amido]Lanthanoids. *J. Chem. Soc., Dalton Trans.* **1977**, *12*, 1166, DOI: 10.1039/dt9770001166.

(43) Allen, M.; Aspinall, H. C.; Moore, S. R.; Hursthouse, M. B.; Karvalov, A. I. Benzophenone Complexes of the Lanthanides: Synthesis of $[Ln\{N(SiMe_3)_2\}_3(Ph_2CO)]$ (L = La, Eu, Tb, Yb or Y) and X-Ray Crystal Structure of the Terbium Complex. *Polyhedron* **1992**, *11*, 409–413, DOI: 10.1016/S0277-5387(00)83194-0.

(44) Crozier, A. R.; Törnroos, K. W.; Maichle-Mössmer, C.; Anwander, R. Trivalent Cerium and Praseodymium Aromatic Ketone Adducts. *Eur. J. Inorg. Chem.* **2013**, *2013*, 409–414,

DOI: 10.1002/ejic.201201171.

(45) Li, Y.; Chen, X.; Gong, Y. Synthesis of a Dinuclear Europium(III) Complex through Deprotonation and Oxygen-Atom Transfer of Trimethylamine N-Oxide. *Dalton Trans.* **2019**, *48*, 17158–17162, DOI: 10.1039/C9DT04234B.

(46) Schumann, H.; Meese-Marktscheffel, J. A.; Esser, L. Synthesis, Structure, and Reactivity of Organometallic π-Complexes of the Rare Earths in the Oxidation State Ln^{3+} with Aromatic Ligands. *Chem. Rev.* **1995**, *95*, 865–986, DOI: 10.1021/cr00036a004.

(47) Mehdoui, T.; Berthet, J.; Thuéry, P.; Ephritikhine, M. Lanthanide(III)/Actinide(III) Differentiation in Coordination of Azine Molecules to Tris(Cyclopentadienyl) Complexes of Cerium and Uranium. *Dalton Trans.* **2004**, *4*, 579–590, DOI: 10.1039/B313992A.

(48) Bardonov, D. A.; Komarov, P. D.; Ovchinnikova, V. I.; Puntus, L. N.; Minyaev, M. E.; Nifant'ev, I. E.; Lyssenko, K. A.; Korshunov, V. M.; Taidakov, I. V.; Roitershtein, D. M. Accessing Mononuclear Triphenylcyclopentadienyl Lanthanide Complexes by Using Tridentate Nitrogen Ligands: Synthesis, Structure, Luminescence, and Catalysis. *Organometallics* **2021**, *40*, 1235–1243, DOI: 10.1021/acs.organomet.1c00022.

(49) Hajela, S.; Schaefer, W. P.; Bercaw, J. E. Highly Electron Deficient Group 3 Organometallic Complexes Based on the 1,4,7-Trimethyl-1,4,7-Triazacyclononane Ligand System. *J. Organomet. Chem.* **1997**, *532*, 45–53, DOI: 10.1016/S0022-328X(96)06768-X.

(50) Taylor, M. D. Preparation of Anhydrous Lanthanon Halides. *Chem. Rev.* **1962**, *62*, 503–511, DOI: 10.1021/cr60220a001.

(51) Windorff, C. J.; Dumas, M. T.; Ziller, J. W.; Gaunt, A. J.; Kozimor, S. A.; Evans, W. J. Small-Scale Metal-Based Syntheses of Lanthanide Iodide, Amide, and Cyclopentadienyl

Complexes as Analogues for Transuranic Reactions. *Inorg. Chem.* **2017**, *56*, 11981–11989, DOI: 10.1021/acs.inorgchem.7b01968.

(52) APEX2 Version 2014.11-0, Bruker AXS, Inc.; Madison, WI 2014.

(53) SAINT Version 8.34a, Bruker AXS, Inc.; Madison, WI 2013.

(54) Sheldrick, G. M. SADABS, Version 2014/5, Bruker AXS, Inc.; Madison, WI 2014.

(55) Sheldrick, G. M. SHELXTL, Version 2014/7, Bruker AXS, Inc.; Madison, WI 2014.

(56) International Tables for Crystallography **1992**, Vol. C., Dordrecht: Kluwer Academic Publishers.

(57) (a) Spek, A.L. SQUEEZE, *Acta Cryst*. **2015**, *C71*, 9-19. (b) Spek, A. L. PLATON, *Acta. Cryst.* **2009**, *D65*, 148-155.

(58) Spek, A. L. PLATON, *Acta. Cryst.*, **2009**, *D65*, 148-155.

Chapter 14:

Uranium Triiodide Complexes of Trimethyltriazacyclohexane and Trimethyltriazacyclononane

Introduction

Fundamental insight into the properties of actinide elements can be derived from well-defined molecular compounds that can be studied in detail in a laboratory setting. These studies can provide information on redox chemistry,[1–5] electronic structure,[6,7] covalency,[8,9] multiple bonding,[10–12] and the reactivity[13–18] of actinide elements, which in turn can lead to better methodology for recycling and nuclear waste remediation.[19–23]

Although this information is commonly obtained with the less radioactive elements thorium and uranium, it is more challenging to accomplish the syntheses and characterizations with the transuranic metals. The transuranic elements are often only available on milligram scales and must be handled with special precautions due to their high radioactivity. However, knowledge of the transuranic chemistry is most valuable for addressing problems of nuclear energy. To optimize transuranic chemistry, reaction optimizations and scale-downs are often performed with lanthanides of similar size or with thorium and uranium[1,24–28] using compounds that can be handled with significantly fewer safety precautions. Finding systems with thorium and uranium that can be extended to the transuranic elements is of particular interest for direct comparisons of the properties of early versus late actinides.

This Chapter reports a rare example of the synthesis of a new class of actinide complexes that can be made simply from uranium halides and extended to neptunium and plutonium. Coordination chemistry studies with the 1,3,5-trimethyl-1,3,5-triazacyclohexane (Me_3tach) and 1,4,7-trimethyl-1,4,7-triazacyclononane (Me_3tacn) ligands, Scheme 13.1, with uranium led to

discovery of simple, high-yielding reactions that could be extended to transuranic elements. Me_3tach has been employed with transition metals[29] and rare-earth metals[30–35] and Me_3tacn has been used with transition metals[36–39] and rare-earth metals,[40,41] but there are no reports of studies of either compound with actinides. This Chapter reports the synthesis, spectroscopic studies, and X-ray crystal structures of $(Me_3tach)_2UI_3$, $(Me_3tach)UI_3(py)_2$, and $(Me_3tacn)UI_3(THF)$ and the use of $(Me_3tach)_2UI_3$ as a UI_3 synthon.

Results

Synthesis. $(Me_3tach)_2UI_3$, **14.1**, was initially identified by X-ray crystallography during the reaction of UI_3, NaC_5Ph_5, and Me_3tach in an attempt to isolate a monometallic C_5Ph_5-ligated uranium complex (see Chapter 8).[42,43] Complex **14.1** can be synthesized directly from UI_3 and two equivalents of Me_3tach in THF, eq 14.1. The reaction occurs upon mixing and the product can be crystallized within 12 h. These are good parameters for extension to the transuranic metals.

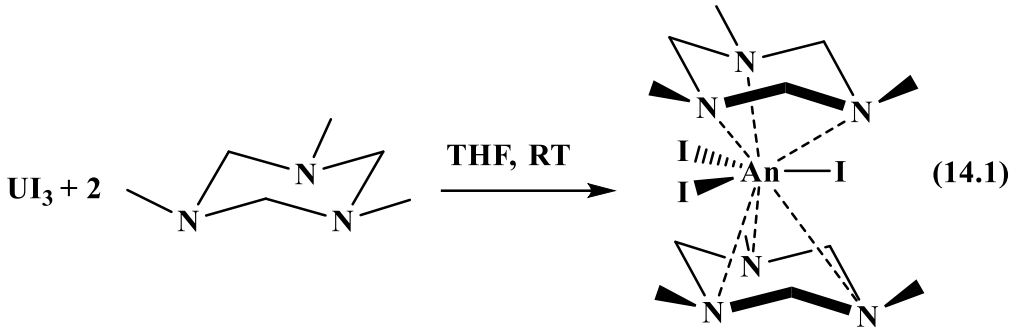

14.1

Compound **14.1** was also the only product formed when one equivalent of Me_3tach is added to the reaction. Similar results were observed with Me_3tach and $Pr(OTf)_3$, forming $(Me_3tach)_2Pr(OTf)_3$ no matter the equivalents of Me_3tach added.[35]

Complex **14.1** is a brown solid and is soluble in THF, Et_2O, toluene, and benzene. When dissolved in THF or Et_2O, **14.1** formed a green solution, but a red/brown solution is generated in

benzene or toluene. The ^{1}H NMR spectrum of **14.1** in THF-d_8 displayed multiple resonances that could not be definitively assigned. However, in C_6D_6 there were only three resonances at 37.01, 33.94, and 11.06 ppm that are assigned to CH_2, CH_2, and CH_3 groups, respectively. The two protons in the methylene fragment likely resonate at different frequencies since the Me_3tach ring is locked in a single conformation due to binding to the metal center.

While investigating the solubility of **14.1**, it was found that dissolving the complex in pyridine led to the formation of a new uranium-containing product. Recrystallization from pyridine/Et_2O at −35 °C afforded black crystals of $(Me_3tach)UI_3(py)_2$, **14.2**, eq 14.2.

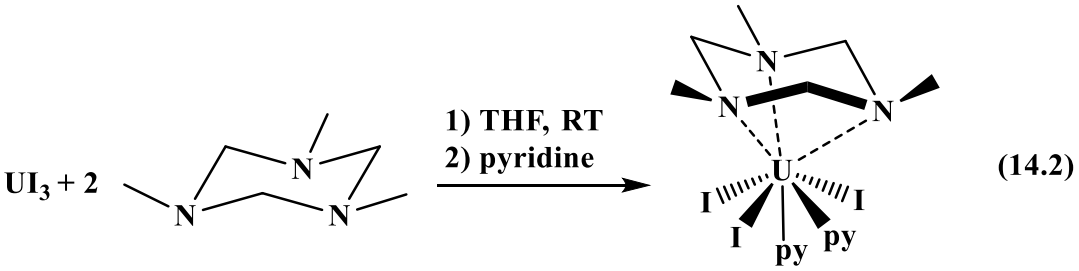

(14.2)

14.2

Compound **14.2** could also be synthesized directly from UI_3 and Me_3tach in pyridine. Compound **14.2** was formed regardless of how many excess equivalents of Me_3tach per uranium are added to the reaction. Despite the crude reaction mixture being completely soluble in pyridine, compound **14.2** required significant mixing to redissolve in pyridine. However, it dissolved readily in THF, forming a green solution. The ^{1}H NMR spectrum of **14.2** in THF-d_8 showed two discernable resonances at 13.66 and 9.42 ppm, assigned to the CH_2 and CH_3 groups of the Me_3tach ligand, respectively. This spectrum is different from that of **14.1**.

It was intriguing that compound **14.1** is formed even with only one equivalent of Me_3tach is added to the solution. In efforts to generate a complex with just one tridentate ligand, the larger nine-membered ring, Me_3tacn, was investigated. Reaction of UI_3 with Me_3tacn and subsequent

crystallization from THF/hexane at −35 °C afforded dark blue X-ray quality crystals of (Me_3tacn)UI_3(THF), **14.3**, eq 14.3. Compound **14.3** formed a dark purple solution in THF, but dried to a green solid, suggesting lability of THF. Compound **14.3** was significantly less soluble in THF than **14.1** and **14.2**. The ^{1}H NMR spectrum in THF-d_8 showed three resonances at 40.96, 13.95, and −34.16 ppm with roughly identical integration values which made conclusive assignment difficult. Variable temperature NMR studies could aid in the assignment and should be performed.

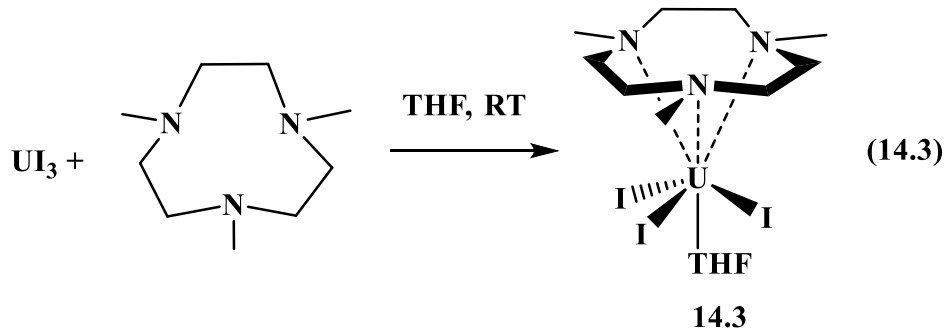

(14.3)

14.3

X-ray Crystallography. The X-ray crystal structure of **14.1** was obtained in two different unit cells; *Pnma* from THF/hexane at −35 °C and $P2_1/n$ from a concentrated toluene solution at −35 °C, Figure 14.1. Both structures contain eclipsed Me_3tach rings, with the three iodide ligands residing between the nitrogen atoms such that the uranium center can be described as a tri-capped trigonal prism. In the *Pnma* cell the uranium and iodine atoms reside on a mirror plane so only one Me_3tach ligand is observed and the second is generated by symmetry. This structure is discussed in detail below.

To aid in the structural discussion, a centroid, Cnt, will be defined for the Me_3tach ligand as the center of the three nitrogen atoms. The U–Cnt distance is 2.431 Å, while the U–N distances are 2.773(6), 2.780(7), and 2.782(7) Å and the U–I distances are 3.1738(8), 3.1770(9), and 3.1874(9) Å. These values are in line with other U(III)–N and U(III)–I distances.[44–47] The Cnt–

U–I angles are 89.28, 90.27, and 90.47°. The Cnt–U–Cnt angle is almost linear at 178.54°. The three iodide ligands are almost evenly distributed around the uranium center with I–U–I angles of 117.91, 120.79, and 121.29°.

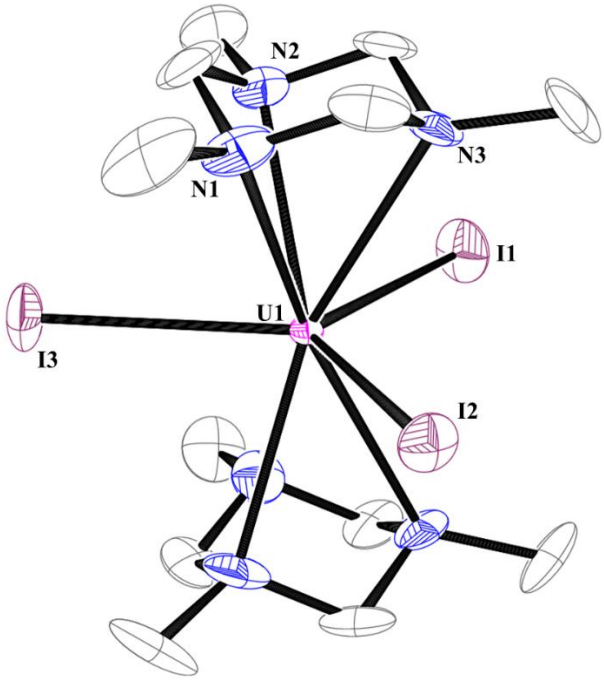

Figure 14.1: Molecular structure of **14.1** with selective atom labelling. Ellipsoids are drawn at the 50% probability level. Hydrogen atoms have been omitted for clarity.

Compound **14.2** crystallized from py/Et_2O in the $P2_1/n$ space group, Figure 14.2. One half molecule of pyridine is present in the asymmetric unit. The three iodides are staggered with respect to the three Me_3tacn nitrogen atoms, as in **14.1** above, while the N(5) atom in pyridine eclipses the N(3) atom in Me_3tacn. The uranium center is formally eight coordinate, but when considering the Cnt, three iodides, and two pyridine molecules, the uranium can be described as having a distorted octahedral geometry. The U sits 0.568 Å out of the plane formed by the three iodine and N(4) atoms. The U–Cnt distance is 2.338 Å, which is shorter than the 2.431 Å U–Cnt distance in **14.1**, which can be explained by the smaller coordination number of **14.2**. The U–N(tach) distances are

2.665(10), 2.715(10), and 2.719(9) Å. The U–N(4) distance of 2.673(9) Å, which is *trans* to the Me_3tach ring, is within error of the 2.724(11) Å U–N(5) distance. The U–I distances of 3.1464(10), 3.1483(10), and 3.1636(10) Å are similar to each other and slightly shorter than the U–I distances in **14.1**.

The Cnt–U–N(4) angle is almost linear at 176.52°. The three iodine atoms and N(5) are not located about the uranium in a symmetric manner. The Cnt–U–I angles are 97.20, 100.13, and 102.84° and the Cnt–U–N(4) angle is 103.07°. Likewise, the I–U–I angles are 88.88, 92.81 and 156.56°. The N(4)–U–I angles are 84.61, 85.77, and 159.62°. The N(4)–U–N(5) angle of 75.66° is more acute than the N(4)–U–I angles of 76.60, 80.33, and 84.22°, which shows that the two pyridine molecules are canted slightly toward each other.

Compound **14.3** crystallized from THF/hexane in the *Pna*2_1 space group, Figure 14.3. Like compound **14.1** and **14.2** above, the three iodide ligands are staggered with respect to the three nitrogen atoms. The uranium atom is seven coordinate and sits 0.835 Å out of the plane created by the three iodide atoms. The oxygen atom of the THF molecule is 1.744 Å below the plane of the three iodides. The U–Cnt distance was 2.109 Å, which is shorter than the 2.431 and 2.338 Å distances of **14.1** and **14.2**. The U–N distances are 2.656(7), 2.724(7), and 2.732(7) Å while the U–I distances are 3.1001(6), 3.1440(7), and 3.1481(6) Å and the U–O distance is 2.601(5) Å.

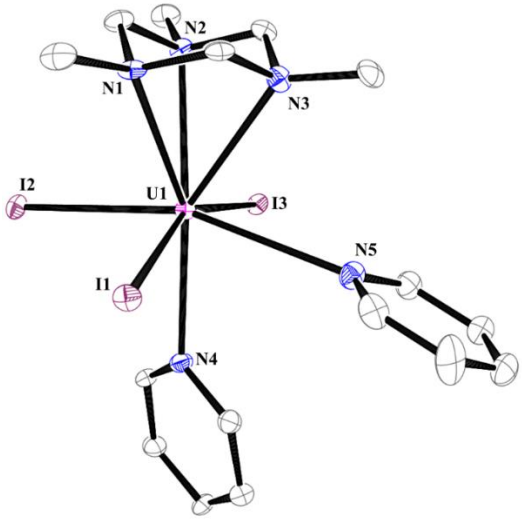

Figure 14.2: Molecular structure of **14.2** with selective atom labelling. Ellipsoids are drawn at the 50% probability level. Hydrogen atoms and cocrystallized pyridine have been omitted for clarity.

The Cnt–U–O angle is almost linear at 170.82°. The Cnt–U–I angles are 104.16, 105.29, and 107.28°. Since the uranium atom is above the plane of the three iodides, the O–U–I angles of 71.50, 71.95, and 81.89° are much more acute. Finally, the I–U–I angles are asymmetrical at 106.49, 108.39, and 124.19°.

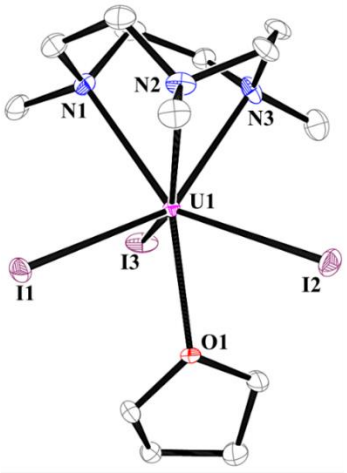

Figure 14.3: Molecular structure of **14.3** with selective atom labelling. Ellipsoids are drawn at the 50% probability level. Hydrogen atoms have been omitted for clarity.

UV-Visible Absorption Spectroscopy. The UV-visible spectra of **14.1**, **14.2**, and **14.3** are shown in Figure 14.4. All compounds displayed weak electronic transitions at low energy that are likely 5f-5f and 5f-6f in character. At higher energy, stronger transitions were observed and likely involve ligand character. The spectrum of **14.1** in toluene (Figure 14.14, black) was similar to the spectrum of **14.1** in THF (Figure 14.4, red) although there were more intense transitions around 600 nm when dissolved in THF. This could account for the visible color difference of the two solutions. Compound **14.2** dissolved in THF also had similar absorptions around 600 nm, but the spectrum lacked the fine structure that is observed for **14.1**. Compound **14.3** had more intense transitions around 600 nm than **14.1** and **14.2** and the spectrum also lacked fine structure. Compound **14.2** was not soluble enough to collect an absorption spectrum in pyridine.

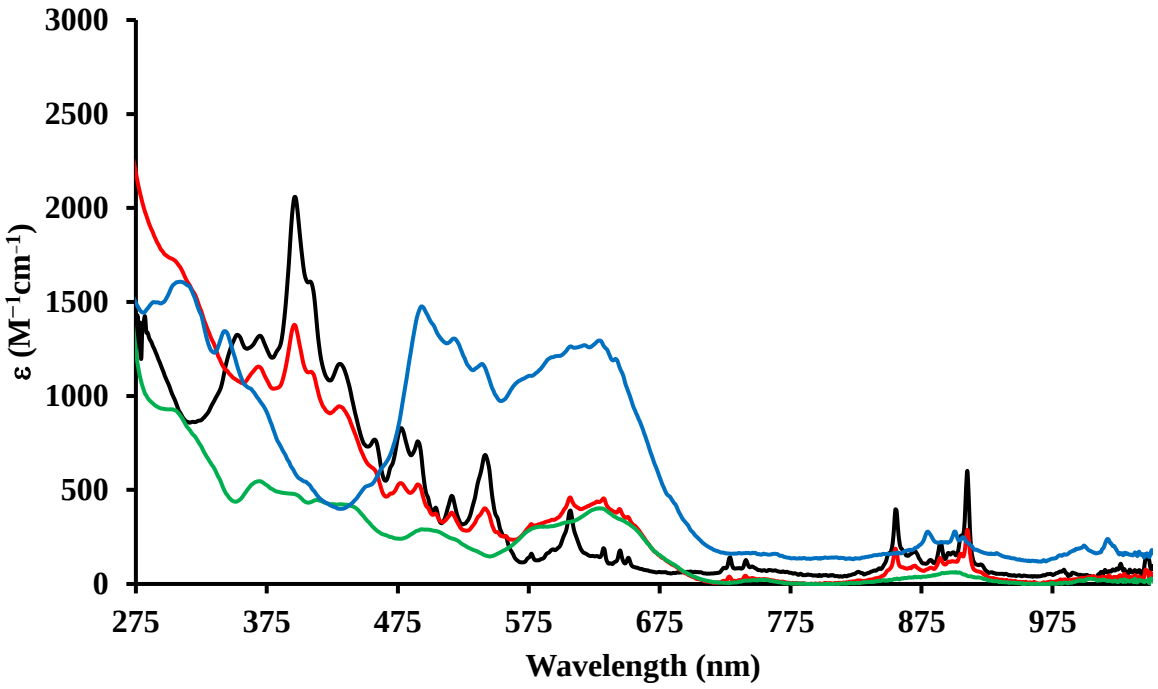

Figure 14.4: UV-visible spectra of **14.1** in toluene (black), **14.1** in THF (red), **14.2** in THF (blue), and **14.3** in THF (green).

$(Me_3tach)_2UI_3$, 14.1, as a U(III) Synthon. It was of interest to determine if compound **14.1** could act as a UI_3 starting material. Following the literature routes to $(C_5Me_4H)_3U$,[48] $U(NR_2)_3$,[49] and Cp''_3U[50] (R = $SiMe_3$, Cp″ = $C_5H_3R_2$) using **14.1** in place of UI_3 afforded the desired U(III) compounds in moderate crystalline yield, Scheme 14.1.

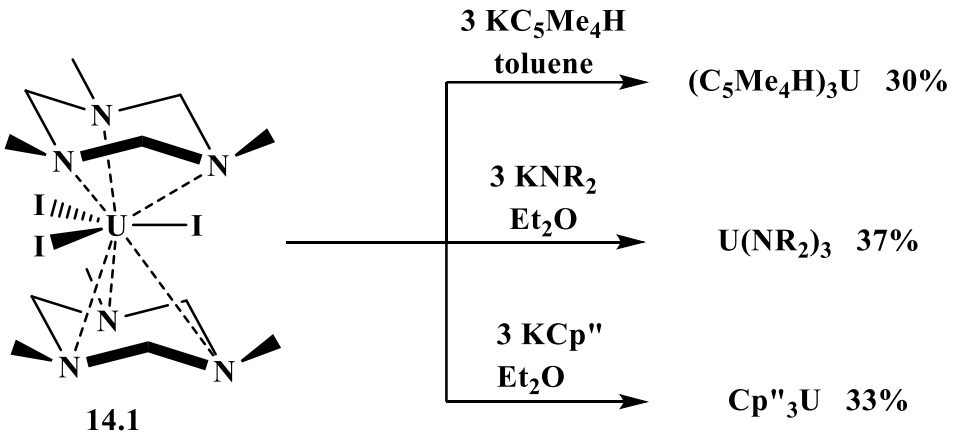

Scheme 14.1: Synthesis of U(III) complexes from **14.1** (R = $SiMe_3$, Cp″ = $C_5H_3R_2$).

Hence, compound **14.1** is a viable precursor to U(III) complexes. In fact, **14.1** offers the possible advantage of being soluble in arenes if ethereal or strongly coordinating solvents like THF and pyridine are to be avoided.

Discussion

Simply expanding the coordination chemistry of the Me_3tach and Me_3tacn ligands, which have been used extensively in transition metal, rare-earth metal, and main group chemistry, to the actinide metals led to the formation of a new class of uranium compounds. The reactions above to form **14.1**, **14.2**, and **14.3** occurred almost immediately upon mixing and afforded high yields of X-ray quality crystals of the actinide-containing compounds in roughly 12 hours (overnight), even when performed at 10 mg scale. These reaction protocols are excellent for extension to the transuranic elements, such as Np, Pu, and Am. In fact, in a collaboration with Drs. Jesse Murillo

and Andrew Gaunt at Los Alamos National Laboratory (LANL), Np and Pu analogs of **14.1** have been made. The binding of two Me_3tach ligands increases the molecular weight of AnI_3 by approximately 33%, which could be advantageous when working with small amounts of transuranic starting materials.

X-ray crystallography studies showed that the UI_3 moiety can bind two Me_3tach ligands in **14.1** and a single Me_3tach ligand in **14.2**. Evidently, pyridine will displace a Me_3tach ligand and bind to the uranium center as dissolution of **14.1** in pyridine leads to the formation of **14.2**. Only one of the larger Me_3tacn ligand binds to uranium in **14.3**, which coordinates one THF to fulfill the coordination sphere. The Me_3tacn ligand is more flexible which leads to shorter U–N and U–Cnt distances than Me_3tach complexes.

Compound **14.1** proved to be a useful surrogate for UI_3, although the yields of the homoleptic U(III) compounds $(C_5Me_4H)_3U$, $U(NR_2)_3$, and Cp''_3U were much lower when using **14.1** instead of UI_3 or $UI_3(THF)_4$. This is likely because the Me_3tach binds tightly to the uranium center in THF, Et_2O, and toluene that it is difficult to displace, even by an anionic ligand. The chelating nature of the Me_3tach ligand is also likely to contribute to the low yields. However, **14.1** is soluble in arenes while UI_3 and $UI_3(THF)_4$ are not, which could provide synthetic routes to compounds that are sensitive to strong donor solvents. Cp^{tet}_3U will form a THF adduct, $Cp^{tet}_3U(THF)$, when crystallized from THF, but the use of **14.1** allows access to Lewis-base free compounds such as Cp^{tet}_3U, Scheme 14.1, and can likely be extended to other systems.

Conclusion

Me_3tach and Me_3tacn have been used to expand the coordination chemistry of UI_3, a common U(III) starting material. Three new U(III) compounds have been fully characterized by spectroscopic and crystallographic techniques. The formation of these compounds is sensitive to

solvent conditions, but can be performed on 10 mg scale, which allows extension of this chemistry to the highly radioactive transuranic elements. The toluene solubility of $(Me_3tach)_2UI_3$, **14.1**, makes it an attractive new U(III) synthon.

Experimental

All manipulations and syntheses described below were conducted with the rigorous exclusion of air and water using standard Schlenk line and glovebox techniques under an argon atmosphere. THF, Et_2O, and hexane were sparged with UHP argon and dried by passage through columns containing a copper-based drying agent, alumina, and/or molecular sieves prior to use. Pyridine was vacuum distilled and kept over molecular sieves. Deuterated NMR solvents were dried over NaK alloy or molecular sieves, degassed by three freeze–pump–thaw cycles, and vacuum transferred before use. ^1H were recorded on a CRYO500 MHz spectrometer at 298 K and referenced to residual protio-solvent resonances. UV-visible spectra were collected at 298 K using a Varian Cary 50 Scan UV-visible spectrophotometer in a 1 mm or 1 cm quartz cuvette. Infrared spectra were recorded as compressed solids on an Agilent Cary 630 ATR-FTIR. Elemental analyses samples were prepared inside a nitrogen-filled glovebox and analyses were conducted on a Thermo Scientific FlashSmart CHNS/O Elemental Analyzer at the Irvine Materials Research Institute.

UI_3 was synthesized according to published routes.[51] Me_3tach (Fisher) and Me_3tacn (stabilized with $NaHCO_3$, Fisher) were purchased under argon, immediately placed in the glovebox upon being received, and kept over molecular sieves.

Synthesis of $(Me_3tach)_2UI_3$, 14.1. UI_3 (82 mg, 0.13 mmol) was dissolved in THF (5 mL) to form a deep blue solution. Me_3tach (34 mg, 0.26 mmol) was dissolved in THF (1 mL) and added to the stirring solution by pipet. The solution immediately became red/brown and was

stirred for 30 minutes then dried under vacuum. The resulting red/brown solids were redissolved in minimal THF and layered under hexane and placed at −35 °C. Dark brown crystals of **14.1** suitable for X-ray diffraction were grown overnight (80 mg, 69%). ^{1}H NMR (C_6D_6): δ 37.01 (br s, 6H, CH_2), 33.94 (br s, 6H, CH_2), and 11.06 ppm (br s, 18H, Me). ^{1}H NMR (THF-d_8): δ 13.87 (br s, 1H), 11.28 (vbr s, 4H), 10.42 (br s, 2H), 9.54 (s, 1H) ppm. UV-visible (THF) λ (ε, $M^{-1}cm^{-1}$): 911 (288), 906 (151), 890 (131), 871 (91), 855 (188), 742 (33), 729 (33), 645 (395), 633 (451), 608 (442), 579 (311), 543 (392), 518 (363), 492 (521), 479 (529), 458sh (601), 434 (926), 410sh (1121), 3967 (1371), 371 (1144), 307sh (1711). UV-visible (toluene) λ (ε, $M^{-1}cm^{-1}$): 910 (602), 890 (219), 884 (113), 871 (166), 856 (388), 741 (127), 729 (141), 652 (129), 645 (178), 633 (182), 606 (381), 578 (149), 543 (668), 515 (448), 505 (388), 491 (753), 479 (814), 458 (765), 433 (1167), 409sh (1602), 397 (2057), 371 (1314), 354 (1318). IR (cm^{-1}): 2961w, 2869w, 2807m, 2749w, 1686w, 1593s, 1436s, 1383m, 1261s, 1215s, 1173m, 1099s, 1063m, 997m, 935s, 751s, 692s. Anal. Calcd for $C_{12}H_{30}N_6I_3U$: C, 16.43; H, 3.45; N, 9.58. Found: C, 15.21; H, 3.156; N, 9.403. Low carbon values were found across multiple runs and are suggestive of carbide formation.[15,45,52–55]

Small scale synthesis of 14.1. As above, UI_3 (15 mg, 0.024 mmol) and Me_3tach (6 mg, 0.046 mmol) were combined in THF (2 mL). The reaction was stirred for 2 hours then dried and setup for crystallization at −35 °C. Dark brown crystals of **14.1**, suitable for X-ray diffraction, formed overnight (14 mg, 66%).

Synthesis of (Me_3tach)$UI_3(py)_2$, 14.2. UI_3 (47 mg, 0.074 mmol) and Me_3tach (21 mg, 0.16 mmol) were combined in THF (5 mL) to presumably form **14.1**. The solution was dried and the red/brown residue was dissolved in pyridine (2 mL) to form a black solution. The solution was layered under Et_2O and placed at −35 °C. Overnight, black crystals of **14.2·½py** suitable for X-

ray diffraction were grown (47 mg, 67%). ^{1}H NMR (THF-d_8): δ 13.66 (br s, 6H, CH_2), 9.42 ppm (s, 9H, Me). UV-visible (THF) λ (ε, $M^{-1}cm^{-1}$): 906 (54), 752 (20), 651sh (321), 633 (397), 604sh (327), 586 (304), 521sh (229), 502 (284), 440sh (414), 416 (442), 398 (473), 372 (540), 305 (923), 234, (7936). IR (cm^{-1}): 2961w, 2869w, 2807m, 2749w, 1686w, 1593s, 1436s, 1383m, 1261s, 1215s, 1173m, 1099s, 1063m, 997m, 835s, 751m, 692s. Anal. Calcd for $C_{18.5}H_{27.5}N_{5.5}I_3U$: C, 23.50; H, 2.93; N, 8.15. Found: C, 17.80; H, 3.039; N, 8.144. Low carbon values were found across multiple runs and are suggestive of carbide formation.[15,45,52–55]

Synthesis of (Me$_3$tacn)UI$_3$(THF), 14.3. UI_3 (66 mg, 0.11 mmol) and Me_3tacn (18 mg, 0.11 mmol) were combined in THF to form a purple solution. The solution was stirred for 2 hours then dried to afford dark blue solids. The solids were redissolved in minimal THF, filtered, and layered under hexane at −35 °C. Black rod-like crystals suitable for X-ray diffraction grew overnight (49 mg, 53%). ^{1}H NMR (THF-d_8): δ 40.96 (br s, 1H), 13.95 (br s, 1.4H), −34.16 ppm (br s, 1H). UV-visible (THF) λ (ε, $M^{-1}cm^{-1}$): 1019 (218), 1001 (192), 908 (240), 902 (254), 881 (270), 643 (1182), 631 (1284), 920 (1261), 608 (1261), 594sh (1207), 577sh (1107), 541 (1158), 520 (1294), 495 (1466), 407sh (530), 365sh (1020), 345 (1331), 312 (1600), 291 (1498). IR (cm^{-1}): 2924w, 2851w, 2816w, 1448s, 1368m, 1336w, 1295m, 1067s, 1021m, 996s, 919w, 861m, 764s, 741s. Anal. Calcd for $C_{13}H_{29}N_3OI_3U$: C, 18.11; H, 3.39; N, 4.87. Found: C, 17.84; H, 3.43; N, 5.475. Low carbon values were found across multiple runs and are suggestive of carbide formation.[15,45,52–55]

Table 14.1: Crystal data and structure refinement for **14.1-14.3**.

	14.1	**14.2**	**14.3**
Identification Code	jcw80	jcw124	jcw108
Empirical Formula	$C_{12}H_{30}I_3N_6U$	$C_{16}H_{25}I_3N_5U{\cdot}½(C_5H_5N)$	$C_{13}H_{29}N_3OI_3U$
Formula Weight	877.15	947.70	862.12
Temperature (K)	93(2)	133(2)	93(2)
Wavelength (Å)	0.71073	0.71073	0.71073

Crystal system	Orthorhombic	Monoclinic	Orthorhombic
Space group	*Pnma*	$P2_1/n$	$Pna2_1$
a (Å)	23.4671(14)	8.645(2)	16.0444(12)
b (Å)	10.6688(7)	19.159(5)	10.0683(7)
c (Å)	12.1413(7)	16.072(4)	13.1963(10)
Alpha (°)	90	90	90
beta (°)	90	105.189(4)	90
Gamma (°)	90	90	90
Volume ($Å^3$)	3039.8(3)	2569.1(11)	2131.7(3)
Z	4	4	4
Density (mg/m^3)	1.917	2.450	2.686
Absorption Correction	8.391	9.938	11.962
F(000)	1580	1720	1548
Color	red	black	purple
Size (mm^3)	0.435x0.227x0.114	0.314x0.302x0.286	0.172x0.157x0.133
Theta range	1.736 to 31.451	1.689 to 30.576	2.388 to 29.596
Index ranges	$-33 \leq h \leq 34$, $-14 \leq k \leq 15$, $-16 \leq l \leq 17$	$-12 \leq h \leq 12$, $-26 \leq k \leq 26$, $-22 \leq l \leq 22$	$-22 \leq h \leq 21$, $-13 \leq k \leq 13$, $-18 \leq l \leq 18$
Reflections collected	44476	60443	24279
Independent reflections	5060	7742	5910
Completeness (%)	100.0	99.8	100.0
Absorption correction	Semi-empirical from equivalents	Semi-empirical from equivalents	Semi-empirical from equivalents
Refinement method	Full-matrix least-squares on F^2	Full-matrix least-squares on F^2	Full-matrix least-squares on F^2
Data / restraints / parameters	5060 / 0 / 109	7742 / 0 / 256	5910 / 1 / 194
Goodness-of-fit on F^2	1.097	1.080	1.045
Final R indices [$I>2\sigma(I)$]	R1 = 0.0554, wR2 = 0.1207	R1 = 0.0628, wR2 = 0.1427	R1 = 0.0261, wR2 = 0.0573
R indices (all data)	R1 = 0.0624, wR2 = 0.1233	R1 = 0.0833, wR2 = 0.1505	R1 = 0.0284, wR2 = 0.0581
Data cutoff (Å)	0.70	0.70	0.72
Largest diff peak and hole ($e \cdot A^{-3}$)	3.885 and −3.234	5.317 and −2.436	2.472 and −1.201

X-ray Data Collection, Structure Solution and Refinement for **14.1**.

A red crystal of approximate dimensions 0.435 x 0.227 x 0.114 mm was mounted in a cryoloop and transferred to a Bruker SMART APEX II diffractometer system. The APEX2[56] program package was used to determine the unit-cell parameters and for data collection (15

sec/frame scan time). The raw frame data was processed using SAINT[57] and SADABS[58] to yield the reflection data file. Subsequent calculations were carried out using the SHELXTL[59] program package. The diffraction symmetry was *mmm* and the systematic absences were consistent with the orthorhombic space groups *Pnma* and $Pna2_1$. It was later determined that space group *Pnma* was correct.

The structure was solved by direct methods and refined on F^2 by full-matrix least-squares techniques. The analytical scattering factors[60] for neutral atoms were used throughout the analysis. Hydrogen atoms were included using a riding model.

Least-squares analysis yielded wR2 = 0.1233 and Goof = 1.097 for 109 variables refined against 5060 data (0.70 Å), R1 = 0.0554 for those 4492 data with $I > 2.0\sigma(I)$.

There were several high residuals present in the final difference-Fourier map. It was not possible to determine the nature of the residuals although it was probable that THF and or hexane solvent was present. The SQUEEZE[61] routine in the PLATON[62] program package was used to account for the electrons in the solvent accessible voids.

Table 14.2: Bond lengths [Å] and angles [°] for **14.1**.

U(1)-N(1)	2.773(6)	N(1)-C(1)	1.481(12)
U(1)-N(1)#1	2.773(6)	N(2)-C(2)	1.462(14)
U(1)-N(3)#1	2.780(7)	N(2)-C(4)	1.470(13)
U(1)-N(3)	2.780(7)	N(2)-C(3)	1.478(13)
U(1)-N(2)#1	2.782(7)	N(3)-C(4)	1.445(13)
U(1)-N(2)	2.782(7)	N(3)-C(5)	1.474(13)
U(1)-I(1)	3.1738(8)	N(3)-C(6)	1.485(12)
U(1)-I(2)	3.1770(9)	C(1)-H(1A)	0.9800
U(1)-I(3)	3.1874(9)	C(1)-H(1B)	0.9800
N(1)-C(6)	1.452(11)	C(1)-H(1C)	0.9800
N(1)-C(2)	1.458(13)	C(2)-H(2A)	0.9900

C(2)-H(2B)	0.9900
C(3)-H(3A)	0.9800
C(3)-H(3B)	0.9800
C(3)-H(3C)	0.9800
C(4)-H(4A)	0.9900
C(4)-H(4B)	0.9900
C(5)-H(5A)	0.9800
C(5)-H(5B)	0.9800
C(5)-H(5C)	0.9800
C(6)-H(6A)	0.9900
C(6)-H(6B)	0.9900

N(1)-U(1)-N(1)#1	121.2(3)
N(1)-U(1)-N(3)#1	150.8(2)
N(1)#1-U(1)-N(3)#1	49.8(2)
N(1)-U(1)-N(3)	49.8(2)
N(1)#1-U(1)-N(3)	150.8(2)
N(3)#1-U(1)-N(3)	121.2(4)
N(1)-U(1)-N(2)#1	152.2(2)
N(1)#1-U(1)-N(2)#1	49.3(3)
N(3)#1-U(1)-N(2)#1	49.7(3)
N(3)-U(1)-N(2)#1	152.9(3)
N(1)-U(1)-N(2)	49.3(3)
N(1)#1-U(1)-N(2)	152.2(2)
N(3)#1-U(1)-N(2)	152.9(3)
N(3)-U(1)-N(2)	49.7(3)
N(2)#1-U(1)-N(2)	123.8(4)
N(1)-U(1)-I(1)	76.96(16)
N(1)#1-U(1)-I(1)	76.96(16)
N(3)#1-U(1)-I(1)	119.38(18)
N(3)-U(1)-I(1)	119.39(18)
N(2)#1-U(1)-I(1)	75.35(18)
N(2)-U(1)-I(1)	75.35(18)
N(1)-U(1)-I(2)	119.40(16)
N(1)#1-U(1)-I(2)	119.40(16)
N(3)#1-U(1)-I(2)	76.39(18)
N(3)-U(1)-I(2)	76.39(18)
N(2)#1-U(1)-I(2)	76.54(19)
N(2)-U(1)-I(2)	76.54(19)
I(1)-U(1)-I(2)	117.91(3)
N(1)-U(1)-I(3)	74.99(16)
N(1)#1-U(1)-I(3)	74.99(16)
N(3)#1-U(1)-I(3)	75.78(17)
N(3)-U(1)-I(3)	75.77(17)
N(2)#1-U(1)-I(3)	118.09(18)
N(2)-U(1)-I(3)	118.09(18)
I(1)-U(1)-I(3)	120.79(3)
I(2)-U(1)-I(3)	121.29(3)
C(6)-N(1)-C(2)	108.6(8)
C(6)-N(1)-C(1)	111.6(7)
C(2)-N(1)-C(1)	111.0(8)
C(6)-N(1)-U(1)	96.9(5)
C(2)-N(1)-U(1)	96.7(5)
C(1)-N(1)-U(1)	129.8(6)
C(2)-N(2)-C(4)	107.8(9)
C(2)-N(2)-C(3)	112.3(9)
C(4)-N(2)-C(3)	111.3(9)
C(2)-N(2)-U(1)	96.3(5)
C(4)-N(2)-U(1)	95.8(5)
C(3)-N(2)-U(1)	130.6(7)
C(4)-N(3)-C(5)	113.5(8)
C(4)-N(3)-C(6)	106.5(9)

C(5)-N(3)-C(6)	111.6(8)	H(3A)-C(3)-H(3C)	109.5
C(4)-N(3)-U(1)	96.5(5)	H(3B)-C(3)-H(3C)	109.5
C(5)-N(3)-U(1)	129.8(7)	N(3)-C(4)-N(2)	106.6(7)
C(6)-N(3)-U(1)	95.7(5)	N(3)-C(4)-H(4A)	110.4
N(1)-C(1)-H(1A)	109.5	N(2)-C(4)-H(4A)	110.4
N(1)-C(1)-H(1B)	109.5	N(3)-C(4)-H(4B)	110.4
H(1A)-C(1)-H(1B)	109.5	N(2)-C(4)-H(4B)	110.4
N(1)-C(1)-H(1C)	109.5	H(4A)-C(4)-H(4B)	108.6
H(1A)-C(1)-H(1C)	109.5	N(3)-C(5)-H(5A)	109.5
H(1B)-C(1)-H(1C)	109.5	N(3)-C(5)-H(5B)	109.5
N(1)-C(2)-N(2)	105.0(7)	H(5A)-C(5)-H(5B)	109.5
N(1)-C(2)-H(2A)	110.7	N(3)-C(5)-H(5C)	109.5
N(2)-C(2)-H(2A)	110.7	H(5A)-C(5)-H(5C)	109.5
N(1)-C(2)-H(2B)	110.7	H(5B)-C(5)-H(5C)	109.5
N(2)-C(2)-H(2B)	110.7	N(1)-C(6)-N(3)	105.5(7)
H(2A)-C(2)-H(2B)	108.8	N(1)-C(6)-H(6A)	110.6
N(2)-C(3)-H(3A)	109.5	N(3)-C(6)-H(6A)	110.6
N(2)-C(3)-H(3B)	109.5	N(1)-C(6)-H(6B)	110.6
H(3A)-C(3)-H(3B)	109.5	N(3)-C(6)-H(6B)	110.6
N(2)-C(3)-H(3C)	109.5	H(6A)-C(6)-H(6B)	108.8

Symmetry transformations used to generate equivalent atoms:
#1 x,-y+3/2,z

X-ray Data Collection, Structure Solution and Refinement for **14.2**.

A black crystal of approximate dimensions 0.314 x 0.302 x 0.286 mm was mounted in a cryoloop and transferred to a Bruker SMART APEX II diffractometer system. The APEX2[56] program package was used to determine the unit-cell parameters and for data collection (90 sec/frame scan time). The raw frame data was processed using SAINT[57] and SADABS[58] to yield the reflection data file. Subsequent calculations were carried out using the SHELXTL[59] program

package. The diffraction symmetry was 2/*m* and the systematic absences were consistent with the monoclinic space group $P2_1/n$ that was later determined to be correct.

The structure was solved by direct methods and refined on F^2 by full-matrix least-squares techniques. The analytical scattering factors[60] for neutral atoms were used throughout the analysis. Hydrogen atoms were included using a riding model. There was one half pyridine solvent molecule present. The solvent was located about an inversion center. One position was modeled as a 50:50 mixed occupancy of nitrogen and carbon.

Least-squares analysis yielded wR2 = 0.1505 and Goof = 1.080 for 256 variables refined against 7742 data (0.70 Å), R1 = 0.0628 for those 6165 data with $I > 2.0\sigma(I)$.

Table 14.3: Bond lengths [Å] and angles [°] for **14.2**.

U(1)-N(3)	2.665(10)	N(4)-C(11)	1.333(15)
U(1)-N(4)	2.673(9)	N(5)-C(16)	1.332(16)
U(1)-N(1)	2.715(10)	N(5)-C(12)	1.335(18)
U(1)-N(2)	2.719(9)	C(1)-H(1A)	0.9800
U(1)-N(5)	2.724(11)	C(1)-H(1B)	0.9800
U(1)-I(1)	3.1464(10)	C(1)-H(1C)	0.9800
U(1)-I(2)	3.1483(10)	C(2)-H(2A)	0.9900
U(1)-I(3)	3.1636(10)	C(2)-H(2B)	0.9900
N(1)-C(2)	1.449(15)	C(3)-H(3A)	0.9800
N(1)-C(1)	1.469(16)	C(3)-H(3B)	0.9800
N(1)-C(6)	1.488(17)	C(3)-H(3C)	0.9800
N(2)-C(3)	1.459(15)	C(4)-H(4A)	0.9900
N(2)-C(4)	1.463(16)	C(4)-H(4B)	0.9900
N(2)-C(2)	1.474(15)	C(5)-H(5A)	0.9800
N(3)-C(5)	1.467(18)	C(5)-H(5B)	0.9800
N(3)-C(4)	1.467(15)	C(5)-H(5C)	0.9800
N(3)-C(6)	1.474(16)	C(6)-H(6A)	0.9900
N(4)-C(7)	1.316(15)	C(6)-H(6B)	0.9900

C(7)-C(8)	1.385(16)	N(3)-U(1)-N(4)	147.9(3)
C(7)-H(7)	0.9500	N(3)-U(1)-N(1)	51.7(3)
C(8)-C(9)	1.391(19)	N(4)-U(1)-N(1)	153.6(3)
C(8)-H(8)	0.9500	N(3)-U(1)-N(2)	51.5(3)
C(9)-C(10)	1.37(2)	N(4)-U(1)-N(2)	148.1(3)
C(9)-H(9)	0.9500	N(1)-U(1)-N(2)	50.9(3)
C(10)-C(11)	1.370(19)	N(3)-U(1)-N(5)	72.5(3)
C(10)-H(10)	0.9500	N(4)-U(1)-N(5)	75.7(3)
C(11)-H(11)	0.9500	N(1)-U(1)-N(5)	115.4(3)
C(12)-C(13)	1.39(2)	N(2)-U(1)-N(5)	116.6(3)
C(12)-H(12)	0.9500	N(3)-U(1)-I(1)	100.5(2)
C(13)-C(14)	1.40(2)	N(4)-U(1)-I(1)	80.3(2)
C(13)-H(13)	0.9500	N(1)-U(1)-I(1)	77.2(2)
C(14)-C(15)	1.38(2)	N(2)-U(1)-I(1)	128.0(2)
C(14)-H(14)	0.9500	N(5)-U(1)-I(1)	84.6(2)
C(15)-C(16)	1.398(18)	N(3)-U(1)-I(2)	127.7(2)
C(15)-H(15)	0.9500	N(4)-U(1)-I(2)	84.2(2)
C(16)-H(16)	0.9500	N(1)-U(1)-I(2)	81.7(2)
N(6)-C(19)#1	1.27(4)	N(2)-U(1)-I(2)	82.4(2)
N(6)-C(18)	1.36(4)	N(5)-U(1)-I(2)	159.6(2)
C(18)-C(19)	1.36(4)	I(1)-U(1)-I(2)	88.88(3)
C(18)-C(17)	1.36(4)	N(3)-U(1)-I(3)	96.9(2)
C(18)-H(18)	0.9500	N(4)-U(1)-I(3)	76.6(2)
C(18)-H(18A)	0.9500	N(1)-U(1)-I(3)	126.2(2)
C(19)-C(17)#1	1.27(4)	N(2)-U(1)-I(3)	75.3(2)
C(19)-N(6)#1	1.27(4)	N(5)-U(1)-I(3)	85.8(2)
C(19)-H(19)	0.9500	I(1)-U(1)-I(3)	156.56(2)
C(19)-H(19A)	0.9500	I(2)-U(1)-I(3)	92.81(3)
C(17)-C(19)#1	1.27(4)	C(2)-N(1)-C(1)	110.2(10)
C(17)-H(17)	0.9500	C(2)-N(1)-C(6)	108.6(10)
		C(1)-N(1)-C(6)	111.4(10)

C(2)-N(1)-U(1)	96.6(6)	N(2)-C(2)-H(2B)	110.5
C(1)-N(1)-U(1)	133.4(8)	H(2A)-C(2)-H(2B)	108.7
C(6)-N(1)-U(1)	94.1(7)	N(2)-C(3)-H(3A)	109.5
C(3)-N(2)-C(4)	111.2(10)	N(2)-C(3)-H(3B)	109.5
C(3)-N(2)-C(2)	110.9(10)	H(3A)-C(3)-H(3B)	109.5
C(4)-N(2)-C(2)	108.9(9)	N(2)-C(3)-H(3C)	109.5
C(3)-N(2)-U(1)	133.7(8)	H(3A)-C(3)-H(3C)	109.5
C(4)-N(2)-U(1)	93.6(6)	H(3B)-C(3)-H(3C)	109.5
C(2)-N(2)-U(1)	95.8(6)	N(2)-C(4)-N(3)	106.0(9)
C(5)-N(3)-C(4)	110.5(10)	N(2)-C(4)-H(4A)	110.5
C(5)-N(3)-C(6)	110.6(10)	N(3)-C(4)-H(4A)	110.5
C(4)-N(3)-C(6)	109.0(10)	N(2)-C(4)-H(4B)	110.5
C(5)-N(3)-U(1)	132.2(8)	N(3)-C(4)-H(4B)	110.5
C(4)-N(3)-U(1)	95.8(7)	H(4A)-C(4)-H(4B)	108.7
C(6)-N(3)-U(1)	96.5(7)	N(3)-C(5)-H(5A)	109.5
C(7)-N(4)-C(11)	115.8(10)	N(3)-C(5)-H(5B)	109.5
C(7)-N(4)-U(1)	120.1(7)	H(5A)-C(5)-H(5B)	109.5
C(11)-N(4)-U(1)	123.6(8)	N(3)-C(5)-H(5C)	109.5
C(16)-N(5)-C(12)	116.3(12)	H(5A)-C(5)-H(5C)	109.5
C(16)-N(5)-U(1)	123.1(8)	H(5B)-C(5)-H(5C)	109.5
C(12)-N(5)-U(1)	120.2(9)	N(3)-C(6)-N(1)	104.8(9)
N(1)-C(1)-H(1A)	109.5	N(3)-C(6)-H(6A)	110.8
N(1)-C(1)-H(1B)	109.5	N(1)-C(6)-H(6A)	110.8
H(1A)-C(1)-H(1B)	109.5	N(3)-C(6)-H(6B)	110.8
N(1)-C(1)-H(1C)	109.5	N(1)-C(6)-H(6B)	110.8
H(1A)-C(1)-H(1C)	109.5	H(6A)-C(6)-H(6B)	108.9
H(1B)-C(1)-H(1C)	109.5	N(4)-C(7)-C(8)	125.2(12)
N(1)-C(2)-N(2)	106.0(9)	N(4)-C(7)-H(7)	117.4
N(1)-C(2)-H(2A)	110.5	C(8)-C(7)-H(7)	117.4
N(2)-C(2)-H(2A)	110.5	C(7)-C(8)-C(9)	116.8(12)
N(1)-C(2)-H(2B)	110.5	C(7)-C(8)-H(8)	121.6

C(9)-C(8)-H(8)	121.6	C(16)-C(15)-H(15)	121.0
C(10)-C(9)-C(8)	119.2(12)	N(5)-C(16)-C(15)	125.1(12)
C(10)-C(9)-H(9)	120.4	N(5)-C(16)-H(16)	117.4
C(8)-C(9)-H(9)	120.4	C(15)-C(16)-H(16)	117.4
C(9)-C(10)-C(11)	118.5(12)	C(19)#1-N(6)-C(18)	116(3)
C(9)-C(10)-H(10)	120.8	C(19)-C(18)-C(17)	127(3)
C(11)-C(10)-H(10)	120.8	C(19)-C(18)-N(6)	127(3)
N(4)-C(11)-C(10)	124.5(12)	C(19)-C(18)-H(18)	116.6
N(4)-C(11)-H(11)	117.8	N(6)-C(18)-H(18)	116.6
C(10)-C(11)-H(11)	117.8	C(19)-C(18)-H(18A)	116.6
N(5)-C(12)-C(13)	123.1(14)	C(17)-C(18)-H(18A)	116.6
N(5)-C(12)-H(12)	118.4	C(17)#1-C(19)-C(18)	117(3)
C(13)-C(12)-H(12)	118.4	N(6)#1-C(19)-C(18)	117(3)
C(12)-C(13)-C(14)	120.0(14)	N(6)#1-C(19)-H(19)	121.6
C(12)-C(13)-H(13)	120.0	C(18)-C(19)-H(19)	121.6
C(14)-C(13)-H(13)	120.0	C(17)#1-C(19)-H(19A)	121.6
C(15)-C(14)-C(13)	117.3(14)	C(18)-C(19)-H(19A)	121.6
C(15)-C(14)-H(14)	121.3	C(19)#1-C(17)-C(18)	116(3)
C(13)-C(14)-H(14)	121.3	C(19)#1-C(17)-H(17)	121.9
C(14)-C(15)-C(16)	118.0(13)	C(18)-C(17)-H(17)	121.9
C(14)-C(15)-H(15)	121.0		

Symmetry transformations used to generate equivalent atoms:
#1 -x+2,-y+1,-z+1

X-ray Data Collection, Structure Solution and Refinement for **14.3**.

A purple crystal of approximate dimensions 0.133 x 0.157 x 0.172 mm was mounted in a cryoloop and transferred to a Bruker SMART APEX II diffractometer system. The APEX2[56] program package was used to determine the unit-cell parameters and for data collection (30

sec/frame scan time). The raw frame data was processed using SAINT[57] and SADABS[58] to yield the reflection data file. Subsequent calculations were carried out using the SHELXTL[59] program package. The diffraction symmetry was *mmm* and the systematic absences were consistent with the orthorhombic space groups *Pnma* and *Pna*2_1. It was later determined that space group *Pna*2_1 was correct.

The structure was solved by direct methods and refined on F^2 by full-matrix least-squares techniques. The analytical scattering factors[60] for neutral atoms were used throughout the analysis. Hydrogen atoms were included using a riding model.

Least-squares analysis yielded wR2 = 0.0581 and Goof = 1.045 for 194 variables refined against 5910 data (0.72Å), R1 = 0.0261 for those 5640 data with $I > 2.0\sigma(I)$. The structure was refined as a two-component inversion twin.

Table 14.4: Bond lengths [Å] and angles [°] for **14.3**.

U(1)-O(1)	2.601(5)	C(8)-C(9)	1.494(13)
U(1)-N(3)	2.656(7)	C(10)-C(11)	1.503(13)
U(1)-N(2)	2.724(7)	C(11)-C(12)	1.523(12)
U(1)-N(1)	2.732(7)	C(12)-C(13)	1.529(12)
U(1)-I(1)	3.1001(6)		
U(1)-I(2)	3.1440(7)	O(1)-U(1)-N(3)	131.4(2)
U(1)-I(3)	3.1481(6)	O(1)-U(1)-N(2)	145.22(19)
O(1)-C(13)	1.448(10)	N(3)-U(1)-N(2)	65.5(2)
O(1)-C(10)	1.472(11)	O(1)-U(1)-N(1)	145.5(2)
N(1)-C(1)	1.492(11)	N(3)-U(1)-N(1)	66.3(2)
N(1)-C(9)	1.506(11)	N(2)-U(1)-N(1)	65.2(2)
N(1)-C(2)	1.508(11)	O(1)-U(1)-I(1)	81.89(14)
N(2)-C(4)	1.488(10)	N(3)-U(1)-I(1)	146.72(17)
N(2)-C(3)	1.494(12)	N(2)-U(1)-I(1)	87.02(15)
N(2)-C(5)	1.510(11)	N(1)-U(1)-I(1)	85.82(16)
N(3)-C(8)	1.473(11)	O(1)-U(1)-I(2)	71.95(14)
N(3)-C(7)	1.481(12)	N(3)-U(1)-I(2)	86.18(16)
N(3)-C(6)	1.507(11)	N(2)-U(1)-I(2)	80.64(15)
C(2)-C(3)	1.503(13)	N(1)-U(1)-I(2)	142.48(15)
C(5)-C(6)	1.503(12)	I(1)-U(1)-I(2)	108.393(18)

O(1)-U(1)-I(3)	71.50(12)	C(3)-N(2)-U(1)	115.8(5)
N(3)-U(1)-I(3)	87.70(15)	C(5)-N(2)-U(1)	106.0(5)
N(2)-U(1)-I(3)	143.19(15)	C(8)-N(3)-C(7)	108.3(7)
N(1)-U(1)-I(3)	81.45(15)	C(8)-N(3)-C(6)	111.5(7)
I(1)-U(1)-I(3)	106.489(19)	C(7)-N(3)-C(6)	110.8(7)
I(2)-U(1)-I(3)	124.195(19)	C(8)-N(3)-U(1)	105.3(5)
C(13)-O(1)-C(10)	108.2(6)	C(7)-N(3)-U(1)	104.6(6)
C(13)-O(1)-U(1)	126.2(5)	C(6)-N(3)-U(1)	115.9(5)
C(10)-O(1)-U(1)	121.1(5)	C(3)-C(2)-N(1)	114.0(7)
C(1)-N(1)-C(9)	109.5(7)	N(2)-C(3)-C(2)	112.6(7)
C(1)-N(1)-C(2)	106.9(7)	C(6)-C(5)-N(2)	112.1(7)
C(9)-N(1)-C(2)	110.3(7)	C(5)-C(6)-N(3)	114.6(7)
C(1)-N(1)-U(1)	112.3(5)	N(3)-C(8)-C(9)	114.6(7)
C(9)-N(1)-U(1)	111.9(5)	C(8)-C(9)-N(1)	114.0(7)
C(2)-N(1)-U(1)	105.8(5)	O(1)-C(10)-C(11)	106.5(7)
C(4)-N(2)-C(3)	109.3(7)	C(10)-C(11)-C(12)	105.0(8)
C(4)-N(2)-C(5)	107.4(7)	C(11)-C(12)-C(13)	100.7(8)
C(3)-N(2)-C(5)	108.5(7)	O(1)-C(13)-C(12)	106.2(7)
C(4)-N(2)-U(1)	109.5(5)		

References

(1) Windorff, C. J.; Chen, G. P.; Cross, J. N.; Evans, W. J.; Furche, F.; Gaunt, A. J.; Janicke, M. T.; Kozimor, S. A.; Scott, B. L. Identification of the Formal +2 Oxidation State of Plutonium: Synthesis and Characterization of $\{Pu^{II}[C_5H_3(SiMe_3)_2]_3\}^-$. *J. Am. Chem. Soc.* **2017**, *139*, 3970–3973, DOI: 10.1021/jacs.7b00706.

(2) Su, J.; Windorff, C. J.; Batista, E. R.; Evans, W. J.; Gaunt, A. J.; Janicke, M. T.; Kozimor, S. A.; Scott, B. L.; Woen, D. H.; Yang, P. Identification of the Formal +2 Oxidation State of Neptunium: Synthesis and Structural Characterization of $\{Np^{II}[C_5H_3(SiMe_3)_2]_3\}^{1-}$. *J. Am. Chem. Soc.* **2018**, *140*, 7425–7428, DOI: 10.1021/jacs.8b03907.

(3) Blake, P. C.; Lappert, M. F.; Atwood, J. L.; Zhang, H. The Synthesis and Characterisation, Including X-Ray Diffraction Study, of $[Th\{\eta\text{-}C_5H_3(SiMe_3)_2\}_3]$; the First Thorium(III) Crystal Structure. *J. Chem. Soc., Chem. Commun.* **1986**, *453*, 1148–1149, DOI:

10.1039/C39860001148.

(4) Langeslay, R. R.; Fieser, M. E.; Ziller, J. W.; Furche, F.; Evans, W. J. Synthesis, Structure, and Reactivity of Crystalline Molecular Complexes of the $\{[C_5H_3(SiMe_3)_2]_3Th\}^{1-}$ Anion Containing Thorium in the Formal +2 Oxidation State. *Chem. Sci.* **2015**, *6*, 517–521, DOI: 10.1039/C4SC03033H.

(5) Dutkiewicz, M. S.; Farnaby, J. H.; Apostolidis, C.; Colineau, E.; Walter, O.; Magnani, N.; Gardiner, M. G.; Love, J. B.; Kaltsoyannis, N.; Caciuffo, R.; Arnold, P. L. Organometallic Neptunium(III) Complexes. *Nat. Chem.* **2016**, *8*, 797–802, DOI: 10.1038/nchem.2520.

(6) Pepper, M.; Bursten, B. E. The Electronic Structure of Actinide-Containing Molecules: A Challenge to Applied Quantum Chemistry. *Chem. Rev.* **1991**, *91*, 719–741, DOI: 10.1021/cr00005a005.

(7) Boronski, J. T.; Seed, J. A.; Hunger, D.; Woodward, A. W.; van Slageren, J.; Wooles, A. J.; Natrajan, L. S.; Kaltsoyannis, N.; Liddle, S. T. A Crystalline Tri-Thorium Cluster with σ-Aromatic Metal–Metal Bonding. *Nature* **2021**, *598*, 72–75, DOI: 10.1038/s41586-021-03888-3.

(8) Lu, E.; Sajjad, S.; Berryman, V. E. J.; Wooles, A. J.; Kaltsoyannis, N.; Liddle, S. T. Emergence of the Structure-Directing Role of f-Orbital Overlap-Driven Covalency. *Nat. Commun.* **2019**, *10*, 634, DOI: 10.1038/s41467-019-08553-y.

(9) Minasian, S. G.; Krinsky, J. L.; Arnold, J. Evaluating F-Element Bonding from Structure and Thermodynamics. *Chem. Eur. J.* **2011**, *17*, 12234–12245, DOI: 10.1002/chem.201101447.

(10) Staun, S. L.; Wu, G.; Lukens, W. W.; Hayton, T. W. Synthesis of a Heterobimetallic Actinide Nitride and an Analysis of Its Bonding. *Chem. Sci.* **2021**, *12*, 15519–15527, DOI:

10.1039/d1sc05072a.

(11) Camp, C.; Pécaut, J.; Mazzanti, M. Tuning Uranium–Nitrogen Multiple Bond Formation with Ancillary Siloxide Ligands. *J. Am. Chem. Soc.* **2013**, *135*, 12101–12111, DOI: 10.1021/ja405815b.

(12) Hayton, T. W.; Boncella, J. M.; Scott, B. L.; Palmer, P. D.; Batista, E. R.; Jeffrey Hay, P. Sythesis of Imido Analogs of the Uranyl Ion. *Science* **2005**, *310*, 1941–1943, DOI: 10.1126/science.1120069.

(13) Summerscales, O. T.; Cloke, F. G. N.; Hitchcock, P. B.; Green, J. C.; Hazari, N. Reductive Cyclotrimerization of Carbon Monoxide to the Deltate Dianion by an Organometallic Uranium Complex. *Science* **2006**, *311*, 829–831, DOI: 10.1126/science.1121784.

(14) Castro-Rodriguez, I.; Nakai, H.; Zakharov, L. N.; Rheingold, A. L.; Meyer, K. A Linear, O-Coordinated η^1-CO_2 Bound to Uranium. *Science* **2004**, *305*, 1757–1759, DOI: 10.1126/science.1102602.

(15) Mansell, S. M.; Kaltsoyannis, N.; Arnold, P. L. Small Molecule Activation by Uranium Tris(Aryloxides): Experimental and Computational Studies of Binding of N_2, Coupling of CO, and Deoxygenation Insertion of CO_2 under Ambient Conditions. *J. Am. Chem. Soc.* **2011**, *133*, 9036–9051, DOI: 10.1021/ja2019492.

(16) Halter, D. P.; Heinemann, F. W.; Bachmann, J.; Meyer, K. Uranium-Mediated Electrocatalytic Dihydrogen Production from Water. *Nature* **2016**, *530*, 317–321, DOI: 10.1038/nature16530.

(17) Modder, D. K.; Palumbo, C. T.; Douair, I.; Fadaei-Tirani, F.; Maron, L.; Mazzanti, M. Delivery of a Masked Uranium(II) by an Oxide-Bridged Diuranium(III) Complex. *Angew. Chem. Int. Ed.* **2021**, *60*, 3737–3744, DOI: 10.1002/anie.202013473.

(18) Gardner, B. M.; Kefalidis, C. E.; Lu, E.; Patel, D.; McInnes, E. J. L.; Tuna, F.; Wooles, A. J.; Maron, L.; Liddle, S. T. Evidence for Single Metal Two Electron Oxidative Addition and Reductive Elimination at Uranium. *Nat. Commun.* **2017**, *8*, 1898, DOI: 10.1038/s41467-017-01363-0.

(19) Runde, W. H.; Mincher, B. J. Higher Oxidation States of Americium: Preparation, Characterization and Use for Separations. *Chem. Rev.* **2011**, *111*, 5723–5741, DOI: 10.1021/cr100181f.

(20) Dares, C. J.; Lapides, A. M.; Mincher, B. J.; Meyer, T. J. Electrochemical Oxidation of ^{243}Am(III) in Nitric Acid by a Terpyridyl-Derivatized Electrode. *Science* **2015**, *350*, 652–655, DOI: 10.1126/science.aac9217.

(21) Burns, J. D.; Moyer, B. A. Group Hexavalent Actinide Separations: A New Approach to Used Nuclear Fuel Recycling. *Inorg. Chem.* **2016**, *55*, 8913–8919, DOI: 10.1021/acs.inorgchem.6b01430.

(22) Zhang, J. Electrochemistry of Actinides and Fission Products in Molten Salts—Data Review. *J. Nucl. Mater.* **2014**, *447*, 271–284, DOI: 10.1016/j.jnucmat.2013.12.017.

(23) Sun, X.; Luo, H.; Dai, S. Ionic Liquids-Based Extraction: A Promising Strategy for the Advanced Nuclear Fuel Cycle. *Chem. Rev.* **2012**, *112*, 2100–2128, DOI: 10.1021/cr200193x.

(24) Windorff, C. J.; Dumas, M. T.; Ziller, J. W.; Gaunt, A. J.; Kozimor, S. A.; Evans, W. J. Small-Scale Metal-Based Syntheses of Lanthanide Iodide, Amide, and Cyclopentadienyl Complexes as Analogues for Transuranic Reactions. *Inorg. Chem.* **2017**, *56*, 11981–11989, DOI: 10.1021/acs.inorgchem.7b01968.

(25) Goodwin, C. A. P.; Su, J.; Stevens, L. M.; White, F. D.; Anderson, N. H.; Auxier, J. D.;

Albrecht-Schönzart, T. E.; Batista, E. R.; Briscoe, S. F.; Cross, J. N.; Evans, W. J.; Gaiser, A. N.; Gaunt, A. J.; James, M. R.; Janicke, M. T.; Jenkins, T. F.; Jones, Z. R.; Kozimor, S. A.; Scott, B. L.; Sperling, J. M.; Wedal, J. C.; Windorff, C. J.; Yang, P.; Ziller, J. W. Isolation and Characterization of a Californium Metallocene. *Nature* **2021**, *599*, 421–424, DOI: 10.1038/s41586-021-04027-8.

(26) Goodwin, C. A. P.; Ciccone, S. R.; Bekoe, S.; Majumdar, S.; Scott, B. L.; Ziller, J. W.; Gaunt, A. J.; Furche, F.; Evans, W. J. 2.2.2-Cryptand Complexes of Neptunium(III) and Plutonium(III). *Chem. Commun.* **2022**, *58*, 997–1000, DOI: 10.1039/D1CC05904A.

(27) Goodwin, C. A. P.; Su, J.; Albrecht-Schmitt, T. E.; Blake, A. V.; Batista, E. R.; Daly, S. R.; Dehnen, S.; Evans, W. J.; Gaunt, A. J.; Kozimor, S. A.; Lichtenberger, N.; Scott, B. L.; Yang, P. [Am($C_5Me_4H)_3$]: An Organometallic Americium Complex. *Angew. Chem. Int. Ed.* **2019**, *58*, 11695–11699, DOI: 10.1002/anie.201905225.

(28) Carter, K. P.; Shield, K. M.; Smith, K. F.; Jones, Z. R.; Wacker, J. N.; Arnedo-Sanchez, L.; Mattox, T. M.; Moreau, L. M.; Knope, K. E.; Kozimor, S. A.; Booth, C. H.; Abergel, R. J. Structural and Spectroscopic Characterization of an Einsteinium Complex. *Nature* **2021**, *590*, 85–88, DOI: 10.1038/s41586-020-03179-3.

(29) Braband, H.; Imstepf, S.; Felber, M.; Spingler, B.; Alberto, R. Triazacyclohexane (Tach) Complexes of High-Valent Rhenium: Syntheses of $[(R_3tach)ReO_3]^+$ (R = −CH3, $-CH_2C_6H_5$) and Its Substitution Reactions. *Inorg. Chem.* **2010**, *49*, 1283–1285, DOI: 10.1021/ic902114p.

(30) Tredget, C. S.; Lawrence, S. C.; Ward, B. D.; Howe, R. G.; Cowley, A. R.; Mountford, P. A Family of Scandium and Yttrium Tris((Trimethylsilyl)Methyl) Complexes with Neutral N_3 Donor Ligands. *Organometallics* **2005**, *24*, 3136–3148, DOI: 10.1021/om050209r.

(31) Nieland, A.; Lamm, J.-H.; Mix, A.; Neumann, B.; Stammler, H.-G.; Mitzel, N. W. Alkynyl Compounds of the Rare-Earth Metals. *Z. Anorg. Allg. Chem.* **2014**, *640*, 2484–2491, DOI: 10.1002/zaac.201400158.

(32) Venugopal, A.; Kamps, I.; Bojer, D.; Berger, R. J. F.; Mix, A.; Willner, A.; Neumann, B.; Stammler, H.-G.; Mitzel, N. W. Neutral Ligand Induced Methane Elimination from Rare-Earth Metal Tetramethylaluminates up to the Six-Coordinate Carbide State. *Dalton Trans.* **2009**, No. 29, 5755, DOI: 10.1039/b905271b.

(33) Bojer, D.; Neumann, B.; Stammler, H.; Mitzel, N. W. Subtle Size Effects in C–H Activation Reactions of Lanthanum and Praseodymium Tetramethylaluminates by Neutral Trinitrogen Bases. *Eur. J. Inorg. Chem.* **2011**, *2011*, 3791–3796, DOI: 10.1002/ejic.201100425.

(34) Niemeyer, M.; Christoffers, J.; Rössle, M. An Optically Active Heteroleptic Cerium Camphorate: [Bis(Trimethylsilyl)Amido-κN]Bis[(+)-(1R,4R)-3-(Trifluoroacetyl)-Camphorato-κ^2-O,O′](1,3,5-Trimethyl-1,3,5-Triazacyclohexane-κ^3-N, N′, N″)Cerium(III). *Acta Crystallogr. Sect. E Struct. Reports Online* **2005**, *61*, m1207–m1209, DOI: 10.1107/S1600536805016193.

(35) Köhn, R. D.; Pan, Z.; Kociok-Köhn, G.; Mahon, M. F. New Sandwich Complexes of Praseodymium(III) Containing Triazacyclohexane Ligands. *J. Chem. Soc., Dalton Trans.* **2002**, No. 11, 2344, DOI: 10.1039/b110784b.

(36) Wieghardt, K. 1,4,7-Triazacyclononane and N,N'N''-Trimethyl-1,4,7-Triazacyclononane - Two Versatile Macrocycles for the Synthesis of Monomeric and Oligomeric Metal Complexes. *Pure Appl. Chem.* **1988**, *60*, 509–516, DOI: 10.1351/pac198860040509.

(37) Lindoy, L. F. Recent Developments in the Synthesis and D-Block Chemistry of Linked Multi-Ring Macrocyclic Ligands. In *Macrocyclic Chemistry*; Gloe, K., Ed.; Springer:

Dordrecht, 2005; pp 53–66, DOI: 10.31080/asps.2020.04.0500.

(38) Macedi, E.; Bencini, A.; Caltagirone, C.; Lippolis, V. The Design of TACN-Based Molecular Systems for Different Supramolecular Functions. *Coord. Chem. Rev.* **2020**, *407*, 213151, DOI: 10.1016/j.ccr.2019.213151.

(39) Chaudhuri, P.; Wieghardt, K. The Chemistry of 1,4,7-Triazacyclononane and Related Tridentate Macrocyclic Compounds. In *Progress in Inorganic Chemistry*; Lippard, S. J., Ed.; John Wiley & Sons, Inc., 2007; pp 329–436, DOI: 10.1002/9780470166369.ch4.

(40) Zeimentz, P. M.; Arndt, S.; Elvidge, B. R.; Okuda, J. Cationic Organometallic Complexes of Scandium, Yttrium, and the Lanthanoids. *Chem. Rev.* **2006**, *106*, 2404–2433, DOI: 10.1021/cr050574s.

(41) Bambirra, S.; Meetsma, A.; Hessen, B. Tris(4-Methylbenzyl)(1,4,7-Trimethyl-1,4,7-Triazacyclononane)Lanthanum(III). *Acta Crystallogr. Sect. E Struct. Reports Online* **2007**, *63*, m2891–m2891, DOI: 10.1107/S1600536807053640.

(42) Wedal, J. C.; Ziller, J. W.; Evans, W. J. Exploring the Use of the Pentaphenylcyclopentadienyl Ligand in Uranium Chemistry: The Crystal Structure of $(C_5Ph_5)UI_2(THF)_2$. *Aust. J. Chemsitry* **2022**, DOI: 10.1071/CH21318.

(43) Bardonov, D. A.; Komarov, P. D.; Ovchinnikova, V. I.; Puntus, L. N.; Minyaev, M. E.; Nifant'ev, I. E.; Lyssenko, K. A.; Korshunov, V. M.; Taidakov, I. V.; Roitershtein, D. M. Accessing Mononuclear Triphenylcyclopentadienyl Lanthanide Complexes by Using Tridentate Nitrogen Ligands: Synthesis, Structure, Luminescence, and Catalysis. *Organometallics* **2021**, *40*, 1235–1243, DOI: 10.1021/acs.organomet.1c00022.

(44) Wedal, J. C.; Windorff, C. J.; Huh, D. N.; Ryan, A. J.; Ziller, J. W.; Evans, W. J. Structural Variations in Cyclopentadienyl Uranium(III) Iodide Complexes. *J. Coord. Chem.* **2021**, *74*,

74–91, DOI: 10.1080/00958972.2020.1856824.

(45) Wedal, J. C.; Bekoe, S.; Ziller, J. W.; Furche, F.; Evans, W. J. C–H Bond Activation via U(II) in the Reduction of Heteroleptic Bis(Trimethylsilyl)Amide U(III) Complexes. *Organometallics* **2020**, *39*, 3425–3432, DOI: 10.1021/acs.organomet.0c00496.

(46) Zalkin, A.; Brennan, J. G.; Andersen, R. A. Tris(Trimethylsilylcyclopentadienyl)-Uranium(III). *Acta Crystallogr. Sect. C* **1988**, *C44*, 2104–2106, DOI: 10.1107/S0108270188008327.

(47) La Pierre, H. S.; Meyer, K. Activation of Small Molecules by Molecular Uranium Complexes. *Prog. Inorg. Chem.* **2014**, *58*, 303–416, DOI: 10.1002/9781118792797.ch05.

(48) Evans, W. J.; Kozimor, S. A.; Ziller, J. W.; Fagin, A. A.; Bochkarev, M. N. Facile Syntheses of Unsolvated UI_3 and Tetramethylcyclopentadienyl Uranium Halides. *Inorg. Chem.* **2005**, *44*, 3993–4000, DOI: 10.1021/ic0482685.

(49) Avens, L. R.; Clark, D. L.; Sattelberger, A. P.; Watkin, J. G.; Zwick, B. D. A Convenient Entry into Trivalent Actinide Chemistry: Synthesis and Characterization of $AnI_3(THF)_4$ and $An[N(SiMe_3)_2]_3$ (An = U, Np, Pu). *Inorg. Chem.* **1994**, *33*, 2248–2256, DOI: 10.1021/ic00088a030.

(50) Windorff, C. J.; Evans, W. J. ^{29}Si NMR Spectra of Silicon-Containing Uranium Complexes. *Organometallics* **2014**, *33*, 3786–3791, DOI: 10.1021/om500512q.

(51) Carmichael, C. D.; Jones, N. A.; Arnold, P. L. Low-Valent Uranium Iodides: Straightforward Solution Syntheses of UI_3 and UI_4 Etherates. *Inorg. Chem.* **2008**, *47*, 8577–8579, DOI: 10.1021/ic801138e.

(52) Takase, M. K.; Ziller, J. W.; Evans, W. J. The Importance of a Single Methyl Group in Determining the Reaction Chemistry of Pentamethylcyclopentadienyl Cyclooctatetraenyl

Uranium Metallocenes. *Chem. Eur. J.* **2011**, *17*, 4871–4878, DOI: 10.1002/chem.201002857.

(53) Liu, J.; Seed, J. A.; Formanuik, A.; Ortu, F.; Wooles, A. J.; Mills, D. P.; Liddle, S. T. Thorium(IV) Alkyl Synthesis from a Thorium(III) Cyclopentadienyl Complex and an N-Heterocyclic Olefin. *J. Organomet. Chem.* **2018**, *857*, 75–79, DOI: 10.1016/j.jorganchem.2017.08.015.

(54) Gaunt, A. J.; Scott, B. L.; Neu, M. P. U(IV) Chalcogenolates Synthesized via Oxidation of Uranium Metal by Dichalcogenides. *Inorg. Chem.* **2006**, *45*, 7401–7407, DOI: 10.1021/ic060560k.

(55) Gabbai, F. P.; Chirik, P. J.; Fogg, D. E.; Meyer, K.; Mindiola, D. J.; Schafer, L. L.; You, S.-L. An Editorial About Elemental Analysis. *Organometallics* **2016**, *35*, 3255–3256, DOI: 10.1021/acs.organomet.6b00720.

(56) APEX2 Version 2014.11-0, Bruker AXS, Inc: Madison, WI 2014.

(57) SAINT Version 8.34a, Bruker AXS, Inc: Madison, WI 2013.

(58) Sheldrick, G. M. SADABS, Version 2014/5, Bruker AXS, Inc: Madison, WI 2014.

(59) Sheldrick, G. M. SHELXTL, Version 2014/7, Bruker AXS, Inc: Madison, WI 2014.

(60) *International Tables for Crystallography*; Vol. C, Kluwer Academic Publishers: Dordrecht, **1992**.

(61) Spek, A. L. PLATON SQUEEZE: A Tool for the Calculation of the Disordered Solvent Contribution to the Calculated Structure Factors. *Acta Crystallogr. Sect. C Struct. Chem.* **2015**, *71*, 9–18, DOI: 10.1107/S2053229614024929.

(62) Spek, A. L. Structure Validation in Chemical Crystallography. *Acta Crystallogr. Sect. D Biol. Crystallogr.* **2009**, *65*, 148–155, DOI: 10.1107/S090744490804362X.

Chapter 15:

Expanding Bismuth Trihalide Coordination Chemistry with Trimethyltriazacyclohexane and Trimethyltriazacyclononane

Introduction

The previous Chapters have described chemistry with the rare-earth metals and actinides, but this Chapter focuses on bismuth coordination chemistry. There are several connections between bismuth and the f elements that make these studies worthwhile. Bismuth has traditionally been considered an uninteresting element, much like the rare-earth metals.[1] While Bi^{3+} has a nearly identical ionic radius to La^{3+},[2] bismuth is much more electronegative (2.02 on the Pauling scale) than La^{3+} (1.10) which could greatly affect the chemistry. At present, bismuth also has more available oxidation states than the rare-earth metals. The oxidation states of bismuth are between 0 to +5, while the rare-earth metals typically are found in the +3, with the +2 and +4 state being accessible under select conditions.[1,3,4] Hence, the following study was performed to compare with the results in Chapters 13 and 14, but also to explore bismuth coordination chemistry in general.

The coordination chemistry of bismuth trihalides, BiX_3, with neutral donors, L, was extensively examined in the 1980s and 1990s through a series of studies which identified several common structural types. These included BiX_3L_3, $[X_2L_2Bi(\mu\text{–}X)]_2$, $[(X_3L_2Bi)_3(\mu^3\text{–}X)]^{1-}$, $\{[X_2LBi(\mu^3\text{–}X)(\mu\text{–}X)][BiXL(\mu\text{–}X)]\}_2$ and $[X_2L_2Bi(\mu\text{–}X)]_n$, as shown by the representative examples in Scheme 15.1.[5–11]

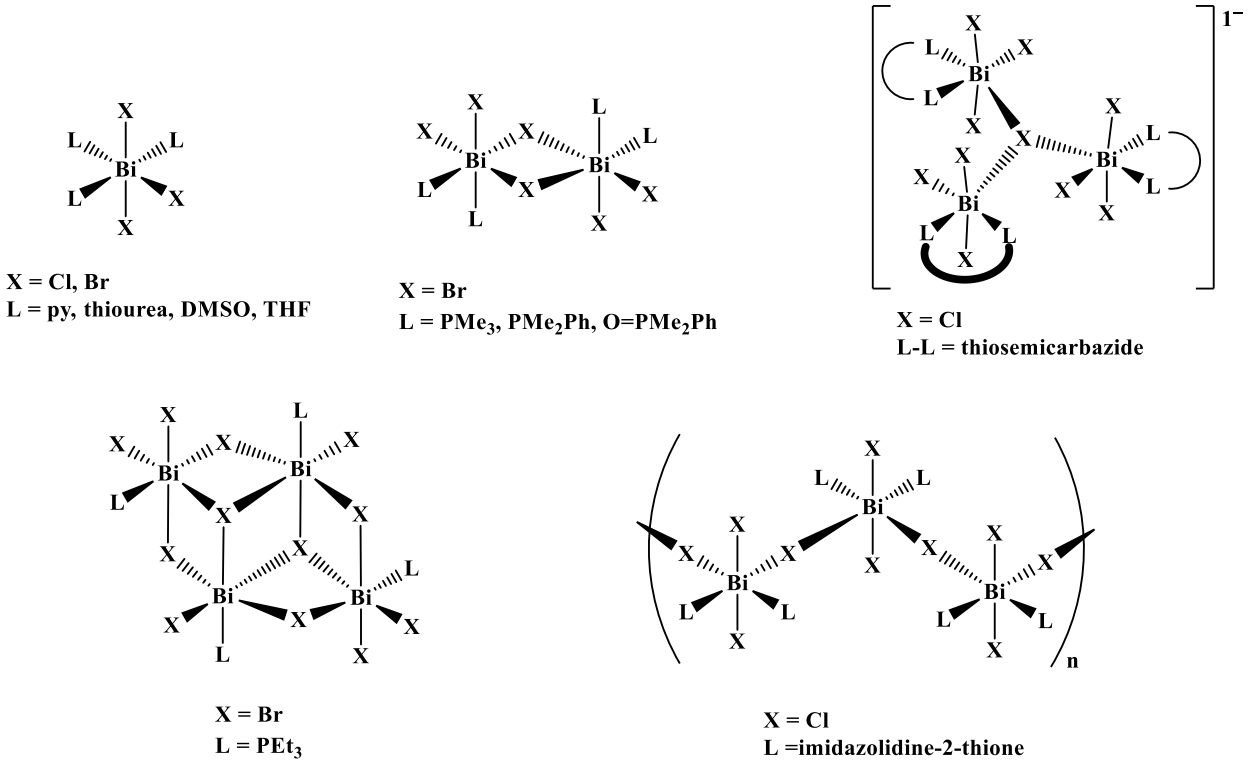

Scheme 15.1: Representative structural examples of bismuth-halide complexes with neutral donors.

As part of an investigation of the coordination capacity of 1,3,5-trimethyltriazacyclohexane, Me_3tach, with large metals (see Chapters 13 and 14), the coordination chemistry of some bismuth trihalides with this nitrogen chelate was examined. Tri-substituted triazacyclohexanes R_3tach have been employed with rare-earth metals (see Chapter 13 for a summary), with third row transition metals W[12–15] and Re,[16] and with main group metals Ge,[17] In,[18] and Sn,[17] R_3tach ligands have not been used with bismuth. The closest example involves a complex of the larger nine-membered triamine, 1,4,7-trimethyltriazacyclononane, Me_3tacn, namely (Me_3tacn)$BiCl_3$.[19] The related {[1-carboxymethyl-4,7-bis(1-methylimidazol-2-ylmethyl)-tacn]BiCl}[BPh_4][20] and the arsenic chloride structure, [(Me_3tacn)$AsCl_2$][($AsCl_2$)$_2$(μ–Cl)(μ-O)],[21]

are also in the literature. Me_3tacn has been used extensively in transition metal,[22–25] f-element,[26,27] and main-group chemistry,[17,28–36] but only these two examples are known for bismuth.

This Chapter reports the synthetic, spectroscopic, and crystallographic data on the coordination chemistry of Me_3tach with bismuth trihalides. The studies showed that bismuth can coordinate to one or two Me_3tach ligands and that the product formed in THF is quite different than that formed in pyridine. In addition, a comparative structure with the larger Me_3tacn ligand is described. During these studies, we obtained the first crystal structure of a THF adduct of BiI_3, which is a common bismuth starting material used in THF. The data reflect the diverse coordination chemistry of bismuth and the utility of Me_3tach in expanding it.

Results and Discussion

$[BiI(THF)(\mu\text{–}I)_2]_n$, 15.1. At the start of this project, it was of interest to characterize the THF coordination chemistry of BiI_3. Although the molecular structures of $BiX_3(THF)_3$ were known for X = Cl[7,8] and Br,[8] the analogous iodide structure had never been reported. Previous studies of BiI_3 in THF afforded orange crystals that lose solvent and only unsolvated BiI_3 was obtained.[8] Consistent with this work, crystallization of BiI_3 from THF gave dark red crystals. These crystals dry to an orange powder and eventually revert to the grey color of unsolvated BiI_3 if kept under vacuum. The infrared spectrum of this grey material shows no absorptions characteristic of THF. The dark red crystals were analyzed by X-ray diffraction and the polymeric species $[BiI(THF)(\mu\text{–}I)_2]_n$, **15.1**, was identified, eq 15.1.

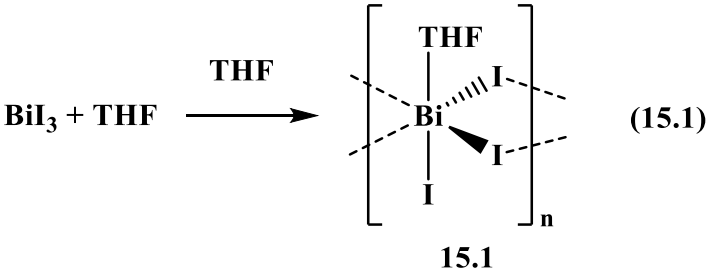

(15.1)

15.1

The X-ray crystal structure of $[BiI(THF)(\mu\text{–}I)_2]_n$, **15.1**, is shown in Figure 151. The bismuth atom, one terminal iodide, one bridging iodide, and the THF molecule are the crystallographically unique components of the structure and the rest is generated by symmetry. Each bismuth center adopts a distorted octahedral geometry. The O–Bi–I(2) angle is almost linear at 178.1(2)° and the I(2)–Bi–I(1) and I(2)–Bi–I(1′) angles are 95.55(2) and 94.96(2)°, respectively. However, the 80.38(2)° I(1)–Bi–I(1) angle differs from the 94.15(2)° I(1)–Bi–I(1′) angle of adjacent iodides and the trans I(1)–Bi–I(1′) angle is 167.44(2)°. The bridging iodide ligands are not situated symmetrically between the bismuth atoms: the 3.2607(7) Å Bi–I(1) distance is quite different from the 2.9628(6) Å Bi–I(1′) distance. These bridging distances are longer than the 2.8801(9) Å Bi–I(2) distance involving of terminal iodide, as expected for bridging versus terminal ligands. The Bi–O distance is 2.618(10) Å. The Bi….Bi distance is 4.337 Å and the Bi–I(1)–Bi angle is 88.23(2)°, which is the same as the Bi–I(1′)–Bi angle.

In contrast to **15.1**, both $BiCl_3(THF)_3$ and $BiBr_3(THF)_3$ exist as monomers in the solid state. All three adopt distorted octahedral geometries. The Bi–O distances of 2.63(2), 2.65(2), and 2.67(2) Å in $BiCl_3(THF)_3$, 2.600(8), 2.635(7), and 2.700(7) Å in $BiBr_3(THF)_3$, and 2.618(10) Å in **15.1** are all similar within the error limits. The Bi–X distances increase with increasing size of terminal halide, from an average of 2.488 Å for X = Cl, to 2.658 Å for X = Br, and to the single value of 2.8801(9) Å for X = I. The related bis(THF) structures of $[BiCl(THF)_2(\mu\text{–}Cl)_2]_n$[8] and $[YCl(THF)_2(\mu\text{–}Cl)_2]_n$[37] are polymeric in the solid state and have two terminally bound THF molecules, one terminal chloride, and two bridging chlorides, similar to **15.1** with one additional THF bound to the metal center. $[BiCl(THF)_2(\mu\text{–}Cl)_2]_n$[8] has asymmetric Bi–bridging chloride distances like is found for Bi–I(1) and Bi–(I1′) in **15.1**, but the Y–bridging chloride distances in $[YCl(THF)_2(\mu\text{–}Cl)_2]_n$[37] are similar.

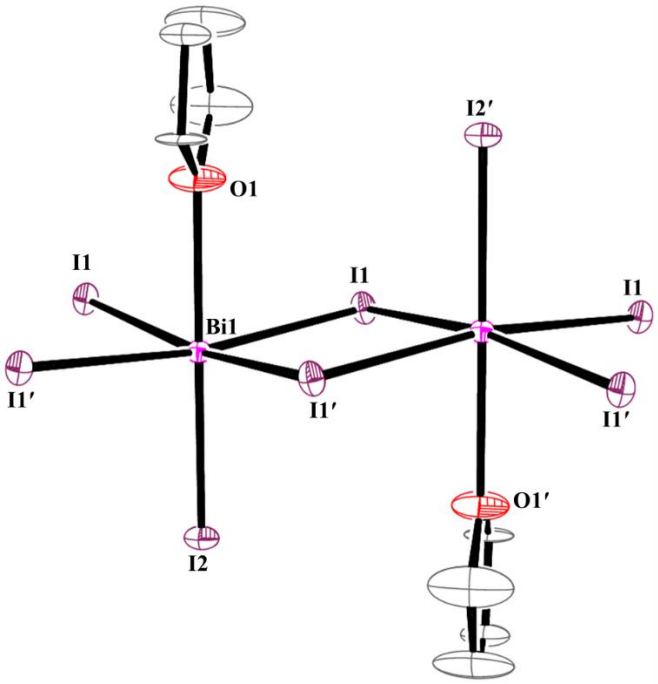

Figure 15.1: Molecular structure of $[BiI(THF)_2(\mu\text{–}I)_2]_n$, **15.1**, with selective atom labelling. Ellipsoids are drawn at the 50% probability level. Hydrogen atoms have been omitted for clarity.

Me_3tach complexes. $(Me_3tach)_2BiI_3$, 15.2. Addition of two equivalents of Me_3tach to a yellow solution of BiI_3 in THF generated a red-orange solution. Recrystallization from THF/hexane at −35 °C afforded a red compound that analyzed as $(Me_3tach)_2BiI_3$, **15.2**, in 67% yield, eq 15.2. The ^{1}H NMR spectrum of **15.2** displayed resonances at δ 4.44 and 2.61 ppm, that can be assigned to the CH_2 and CH_3 groups of the Me_3tach ligand, Table 15.1. However, X-ray quality crystals could not be obtained.

Table 15.1: ^{1}H NMR shifts of **15.2**, **15.3**, and **15.5-15.7** in THF-d_8 (δ, ppm).

	CH_2	Me
$(Me_3tach)_2BiI_3$, **15.2**	4.44	2.61
$[(Me_3tach)_2BiI_2][(Me_3tach)BiI_2]$, **15.3**	4.26	2.60
$(Me_3tach)BiI_3(py)_2$, **15.5**	4.80	2.81
$(Me_3tach)BiCl_3(py)_2$, **15.6**	*not observed*	2.58
$(Me_3tacn)BiI_3$, **15.7**	3.29	3.38

[(Me$_3$tach)$_2$BiI$_2$][(Me$_3$tach)BiI$_4$], 15.3. Although single crystals suitable for X-ray diffraction of **15.2** were not obtained, information on the coordination of Me_3tach to iodide-ligated bismuth was obtained in other ways. Addition of *one* equivalent of Me_3tach to BiI_3 in THF and subsequent recrystallization from THF/hexane at −35 °C afforded an orange powder which was sparingly soluble in THF and practically insoluble in Et_2O, CH_2Cl_2, and arenes. Broad signals were observed in the ^{1}H NMR spectrum in THF-d_8 at δ 4.26 and 2.60 ppm, that can be assigned to a single Me_3tach environment or an equilibrium of multiple different environments. No resonances attributable to bound THF were observed. Combustion analysis data on the orange powder were consistent with a formula containing three Me_3tach and two BiI_3 units, i.e. $(Me_3tach)_3(BiI_3)_2$. Recrystallization of the orange powder from THF/hexane at −35 °C gave red X-ray quality crystals which were found by X-ray diffraction to match that analysis in that this was the ion-pair $[(Me_3tach)_2BiI_2][(Me_3tach)BiI_4]$, **15.3**, eq 15.3, Figure 15.2.

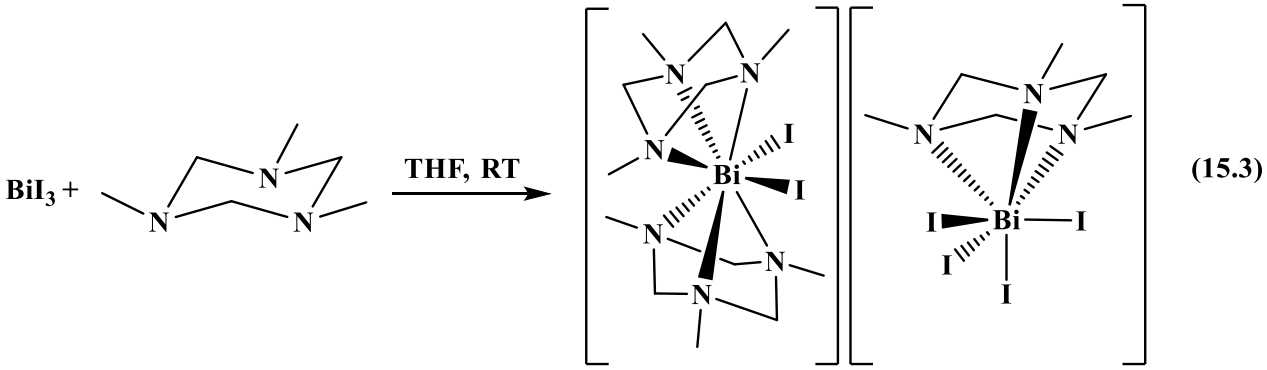

(15.3)

15.3

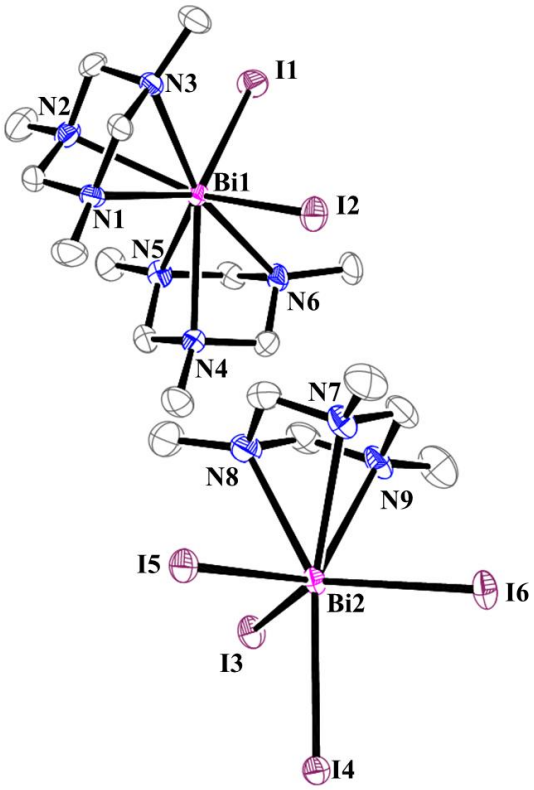

Figure 15.2: Molecular structure of $[(Me_3tach)_2BiI_2][(Me_3tach)BiI_4]$, **15.3**, with selective atom labelling. Ellipsoids are drawn at the 50% probability level. Hydrogen atoms and cocrystallized THF molecules have been omitted for clarity.

The ion pair provides crystallographic confirmation of both 1:1 and 1:2 Bi:Me_3tach coordination. The cation has an eight-coordinate bismuth with two Me_3tach ligands and the anion is seven-coordinate with only one Me_3tach ligand. The crystals contain 2.5 molecules of THF per formula unit. A related bismuth iodide ion-pair, $[BiI_2(tpy)_2][Bi_2I_7(tpy)]$ (tpy = 2,2′:6′,2″-terpyridine), has been structurally characterized in which the bismuth atom in the cation is coordinated to three nitrogen donor atoms and two iodides like the cationic unit in **15.3**.[38]

In the metrical analysis of the Me_3tach complexes, it was instructive to calculate the centroid of the three nitrogen atoms in the Me_3tach ligand which is denoted Cnt. When considering the two centroids and iodides, the Bi(1) center in the cation of **15.3** adopts a geometry reminiscent

of a $(C_5R_5)_2MX_2$ bent metallocene (R = H, alkyl; X = halide or pseudohalide). The 135.6° Cnt–Bi(1)–Cnt angle is similar to analogous angles in $(C_5R_5)_2MX_2$ bent metallocenes.[1,39–47] In the anion, Bi(2) has a trigonal bipyramidal coordination by this metric, with the Me_3tach centroid occupying an axial position opposite one iodide with a 174.2° Cnt–Bi(2)–I(4) angle. The Cnt–Bi(2)–equatorial iodide angles are 94.8, 95.8, and 97.8°. The three equatorial iodides around Bi(2) are staggered with respect to the three nitrogen atoms in the Me_3tach ring. The wide range of six Bi(1)–N_{ring} distances in the cation, 2.595(4)–2.740(4) Å, overlaps with the 2.702(5)–2.742(4) Å Bi(2)–N_{ring} distances in the anion.

Based on the formal coordination number difference, it could be expected that distances involving Bi(1) in the cation would be longer than those involving Bi(2) in the anion. However, the Bi(1)–Cnt distances were 2.284 and 2.339 Å, while the Bi(2)–Cnt distance was 2.372 Å. This observation is likely a result of chelation of the nitrogen donor atoms versus the monodentate nature of the iodide ligands. The Bi(1)–I distances of 2.9606(4) and 2.9701(4) Å are at the low end of the range of Bi(2)–I distances in the anion, 2.9670(4), 3.0533(4), 3.0832(4), and 3.1551(4) Å. The latter, longest Bi–I distance is that of the axial Bi(2)–I(4) bound *trans* to the Me_3tach ring.

The $[(Me_3tach)_2BiI_2]^{1+}$ cation in **15.3** is unusual in that there are no structurally characterized main group complexes that have two Me_3tach ligands coordinated in the metallocene-like environment of Bi(1) in compound **15.3**. The closest structure is the mono-Me_3tach complex, $[(Me_3tach)SnBr_3][SnBr_6]$,[17] which has a Sn–Cnt distance of 1.891. Complexes with two Me_3tach ligands coordinated to alkaline-earth and rare-earth metals are known, however, e.g. $(Me_3tach)_2CaR_2$ (R = $AlEt_4$, $P(SiMe_3)_2$, benzyl),[48–50] $[(R_3tach)_2YR'_2][AlMe_2R'_2]$ (R = Me, cyclohexyl; R′ = Me, C≡CPh),[51,52] and $(R_3tach)_2Sm(AlMe_4)_2$ (R = cyclohexyl, ^{i}Pr, Et).[53,54] The

Table 15.2: Selected metrical parameters for the Me_3tach and Me_3tacn complexes **15.3** and **15.5-15.7**. N_{ring} refers to the nitrogen atoms in the Me_3tach and Me_3tacn ligands, N_{py} refers to the pyridine nitrogen, X is the halide (I, Cl), and Cnt is the centroid of the three nitrogen atoms of the Me_3tach and Me_3tacn rings.

	[(Me_3tach)$_2$BiI_2]-[(Me_3tach)BiI_4], 15.3	**(Me_3tach)BiI_3(py)$_2$, 15.5**	**(Me_3tach)BiCl_3(py)$_2$, 15.6**	**(Me_3tacn)BiI_3, 15.7**
Bi–N_{ring}	2.595(4), 2.644(4), 2.668(4), 2.691(4), 2.721(4), 2.740(4), 2.702(5), 2.740(5), 2.742(4)	2.721(6), 2.734(6), 2.755(6)	2.6563(18), 2.6737(19), 2.7199(17)	2.536(7), 2.549(8), 2.580(7)
Bi–I	2.9606(4), 2.9701(4), 2.9670(4), 3.0533(4), 3.0832(4), 3.1551(4)	2.9577(6), 3.0777(6), 3.0942(5)		3.0106(8), 3.0594(8), 3.0671(8)
Bi–Cl			2.6556(6), 2.7024(6), 2.7377(6)	
Bi–N_{py}		2.644(6), 2.945(7)	2.6682(19), 2.7724(17)	
N_{ring}–Bi–N_{ring}	51.0(1), 51.4(1), 51.7(1), 51.7(1), 52.2(1), 52.6(1), 83.3(1), 88.6(1), 91.7(1), 111.3(1), 113.1(1), 139.4(1), 140.7(1), 143.0(1), 143.4(1), 162.5(1),	50.6(2), 50.54(17), 50.83(18)	51.26(5), 51.59(5), 51.91(6)	70.1(2), 70.2(3), 70.5(2)
X–Bi–X	82.31(1), 82.75(1), 87.93(1), 105.08(1), 110.53(1), 113.06(1), 133.09(1),	91.415(16), 94.957(16), 156.102(16)	97.196(18), 95.057(18), 157.178(16)	97.56(2), 101.07(3), 102.01(2)
Bi–Cnt	2.284, 2.339, 2.372	2.380	2.320	1.909
Cnt–Bi–X	94.8, 95.8, 97.8, 102.6, 103.2, 103.4, 104.0, 174.2	98.23, 99.69, 102.15	95.26, 98.62, 99.34	117.15, 117.16, 118.56
Cnt–Bi–N_{py}		101.35, 176.10	105.60, 176.36	

M–cnt distances of **15.3** and the previously reported compounds span the range of 1.11–1.27 Å and are quite similar when the difference in ionic radius[2] and R_3tach substituent size isconsidered,

Table 15.3. This is reminiscent of the metal-ligand bond distance similarity noted by Raymond for cyclopentadienyl and cyclooctatetraenyl f element complexes.[55]

Table 15.3: M–Cnt distances (Å) in eight coordinate $(R_3tach)_2ML_2$ complexes.

	M–Cnt	Eight-coordinate ionic radius	M-Cnt distance – radius
$[(Me_3tach)_2BiI_2]^{1+}$, **15.3**	2.284, 2.339	1.170	1.114, 1.169
$(Me_3tach)_2Ca(AlEt_4)_2$[50]	2.236	1.120	1.116
$(Me_3tach)_2Ca[P(SiMe_3)_2]$[49]	2.272	1.120	1.152
$(Me_3tach)_2Ca(benzyl)_2$[48]	2.304, 2.319	1.120	1.184, 1.199
$(Me_3tach)_2Y(C{\equiv}CPh)_2][AlMe_2(C{\equiv}CPh)_2]$[52]	2.160, 2.171	1.019	1.141, 1.152
$[(Me_3tach)_2YMe_2][AlMe_4]$[51]	2.223, 2.229	1.019	1.204, 1.210
$(^iPr_3tach)_2Sm(AlMe_4)_2$[53]	2.409	1.270	1.139
$(Et_3tach)_2Sm(AlMe_4)_2$[53]	2.416	1.270	1.146
$(cyclohexyl_3tach)_2Sm(AlMe_4)_2$[54]	2.447, 2.455	1.270	1.177, 1.185
$[(cyclohexyl_3tach)_2YMe_2][AlMe_4]$[51]	2.281, 2.291	1.019	1.262, 1.272

The $[(Me_3tach)BiI_4]^{1-}$ anion in **15.3** is also unusual in that there are no known structures of the type $(R_3tach)MX_4$ where X = halide. The closest examples are the seven-coordinate complexes, $(R_3tach)Ln[\eta^4\text{-}Me_3AlCH_2AlMe_2CH_2AlMe_3]$, $(R_3tach)Ln[CH(AlMe_3)_3]$ (R = Me, cyclohexyl, ^{t}Bu, ^{i}Pr; Ln = La, Pr, Sm)[56,57] and $(^iPr_3tach)Y(AlMe_4)(\eta^3\text{-}Me_3AlCH_2AlMe_3)$.[51] The M–Cnt distance range in these Me_3tach complexes is small, 1.24–1.27 Å, Table 15.4, when adjusted for the difference in ionic radii. It is likely that these seven coordinate distances fall in the higher range of the eight coordinate distances in Table 15.3, because the presence of two chelating R_3tach ligands leads to shorter M–Cnt distances.

$[(Me_3tach)_2BiI_2]_3[Bi_2I_9][I][HMe_3tach]\cdot THF$, 15.4. On one occasion, recrystallization of **15.2** yielded red crystals of $[(Me_3tach)_2BiI_2]_3[Bi_2I_9][I][HMe_3tach]\cdot THF$, **15.4**, which was identified by X-ray crystallography, Figure 15.3. While the X-ray data were not of high enough quality to report metrical data, the connectivity of the structure was confirmed. This structural variant is very complicated in that it contains *three* $[(Me_3tach)_2BiI_2]^{1+}$ cations like those in **15.3**, one $[I_3Bi(\mu\text{–}I)_3BiI_3]^{3-}$ trianion, one free $[I]^{1-}$ anion, one molecule of THF, and one $[HMe_3tach]^{1+}$

Table 15.4: M–Cnt distances in seven coordinate $(R_3tach)ML_4$ complexes.

	M–Cnt (Å)	Seven-coordinate ionic radius (Å)[a,b]	M–Cnt distance – radius (Å)
$(Me_3tach)Sm[\eta^4\text{-}Me_3AlCH_2AlMe_2\text{-}CH_2AlMe_3]$[57]	2.262, 2.270	1.020	1.242, 1.250
$[(Me_3tach)BiI_4]^{1-}$, **15.3**	2.372	1.110	1.272
$(Me_3tach)Pr[CH(AlMe_3)_3]$[56]	2.322, 2.398	1.053	1.269, 1.345
$(^iPr_3tach)Y(AlMe_4)(\eta^3\text{-}Me_3AlCH_2AlMe_3)$[51]	2.220	0.960	1.260
$(^iPr_3tach)Sm[\eta^4\text{-}Me_3AlCH_2AlMe_2\text{-}CH_2AlMe_3]$[53]	2.315	1.020	1.295
$(^iPr_3tach)La[\eta^4\text{-}Me_3AlCH_2AlMe_2\text{-}CH_2AlMe_3]$[56]	2.405	1.100	1.305
$(cyclohexyl_3tach)Sm[CH(AlMe_3)_3]$[54]	2.351	1.020	1.331
$(^tBu_3tach)Pr[\eta^4\text{-}Me_3AlCH_2AlMe_2\text{-}CH_2AlMe_3]$[56]	2.411	1.053	1.358
$(^tBu_3tach)La[\eta^4\text{-}Me_3AlCH_2AlMe_2\text{-}CH_2AlMe_3]$[56]	2.469	1.100	1.369

a: A 1.10 Å seven coordinate radius was used for Bi^{3+} and 1.053 Å for Pr^{3+} based on extrapolation from the other values in the Shannon compilation.[2]

cation. The $[HMe_3tach]^{1+}$ cation was identified by the unique displacement of the Me group from the chair conformation of the Me_3tach ligand which suggests that N(19) is the protonated nitrogen. A search of the Cambridge Structural Database of $[Bi_2I_9]^{n-}$ anions found 56 citations of which 37 had n = 1 and the other 19 had n = 3 as found in complex **15.4**.[58] Examples include $[Bi_2I_9]^{n-}$ mono-

and trianions with an additional $[I]^{1-}$ or $[I_3]^{1-}$ anion in the same molecule[59–62] as found for **15.4**. Numerous structures have been investigated due to the interest of BiI_3 as a photovoltaic.[58,63–66]

$(Me_3tach)BiI_3(py)_2$, 15.5. Although the solubility of **15.2** and **15.3** in ethers was limited, these solids were completely soluble in pyridine (py) and generated orange solutions. Recrystallization of **15.2** from py/Et_2O at −35 °C afforded gold crystals of $(Me_3tach)BiI_3(py)_2$, **15.5**, which was isolated in 81% yield, eq 15.4, and identified by X-ray crystallography, Figure 15.4. Compound **15.5** can be synthesized directly from BiI_3 and Me_3tach in pyridine no matter how many extra equivalents of Me_3tach are added and the yield is not drastically affected by the variable stoichiometry. Although the crude reaction mixture of BiI_3 and Me_3tach is completely

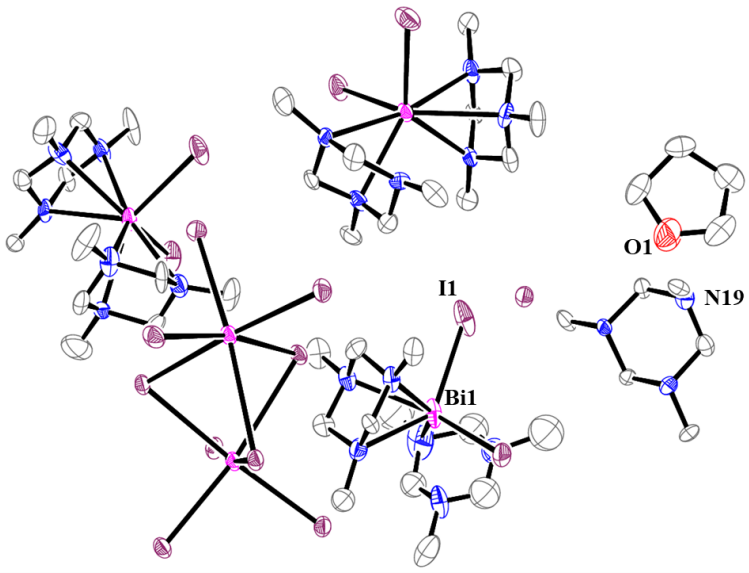

Figure 15.3: Connectivity structure of $[(Me_3tach)_2BiI_2]_3[Bi_2I_9][I][HMe_3tach]\cdot THF$, **15.4**, with selective atom labelling. Hydrogen atoms have been omitted for clarity.

soluble in pyridine, crystalline **15.5** is practically insoluble in pyridine and NMR spectroscopy was performed in THF-d_8. Resonances in the ^1H NMR spectrum at 4.80 and 2.81 ppm are assigned to the Me_3tach ligand, Table 15.1. These two resonances are similar to the 4.85 and 2.77 ppm shifts

for **15.3**, Table 15.1. The two pyridine molecules of **15.5** are displaced in THF-d_8, and exactly two equivalents of free pyridine per one Me_3tach are observed in the NMR spectrum. No bound THF was observed.

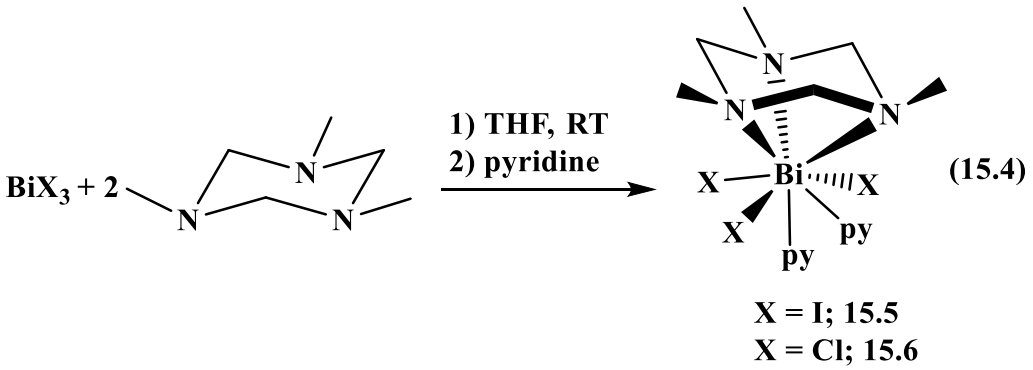

(15.4)

$(Me_3tach)BiX_3(py)_2$, **15.5**, crystallizes with one half molecule of pyridine in the asymmetric unit. Selected metrical parameters are summarized in Table 15.2. The bismuth center is formally eight coordinate, but when considering the Me_3tach ring centroid as occupying just one position, the compound has a distorted octahedral geometry with a pyridine trans to the Me_3tach centroid and a 176.10° Cnt–Bi–N_{py} angle. The four other ligands in the complex are bent away from the Me_3tach centroid with Cnt–Bi–I angles of 98.23, 99.69, and 102.15° and a Cnt–Bi–N_{py} angle of 101.35°. The bismuth center is out of the plane formed by the three iodides and the N5 atom by 0.571 Å. The Bi–I distances vary with lengths of 2.9577(6), 3.0777(6), and 3.0942(5) Å. The Bi-pyridine distances are also different. The 2.945(7) Å Bi–N(5) distance of the pyridine *cis* to the Me_3tach ring is significantly longer than the 2.644(6) Å Bi–N(4) distance for the pyridine in the *trans* position. This differs from the $[(Me_3tach)BiI_4]^{1-}$ anion in **15.3** in which the iodide trans to Me_3tach has the longest distance. The Bi–N_{ring} distances in **15.5** are equivalent within error at 2.721(6), 2.734(6), and 2.755(6) Å and this leads to a Bi–Cnt distance of 2.380 Å, which is similar to the 2.372 Å analog in the seven coordinate $[(Me_3tach)BiI_4]^{1-}$ anion in **15.3**. The similarity may

arise since the Bi–N(5) distance is so long in **15.5** that it is more appropriately described as seven coordinate.

$(Me_3tach)BiCl_3(py)_2$, 15.6. The chloride analog of **15.5**, namely $(Me_3tach)BiCl_3(py)_2$, **15.6**, was synthesized in 34% yield in an identical manner to **15.5**, eq 15.**4**, and characterized by X-ray crystallography. In contrast to **15.5**, solutions of **15.6** in pyridine and the crystals of **15.6** are colorless. This is similar to the situation of BiI_3 vs $BiCl_3$ in THF. Complex **15.6** is less soluble than **15.5** in general and only one broad resonance at 2.58 ppm (ω 165 Hz) could be observed in the ^{1}H NMR spectrum collected in THF-d_8.

Complex **15.6** is not isomorphous with **15.5** because **15.6** does not contain a pyridine molecule in the lattice. Otherwise, the two compounds are structurally similar. The Cnt–Bi–N_{py} angle is 176.36° and the four other ligands are bent away from the Me_3tach with Cnt–Bi–Cl angles of 95.26, 98.62, and 99.34° and Cnt–Bi–N_{py} angle of 105.60°. The bismuth atom lies 0.404 Å out of the plane formed by the three chlorides and the N5 atom. The 2.6563(18), 2.6737(19), 2.7199(17) Å Bi–N_{ring} distances and the 2.320 Å Bi–Cnt distance are slightly shorter than those in **15.5,** consistent with the presence of smaller chloride ligands versus iodide. The Bi–Cl distances were 2.6556(6), 2.7024(6), and 2.7376(6) Å. The 2.6682(19) and 2.7724(17) Å Bi–N_{py} distances are not as different in **15.6** as in **15.5**. The longer Bi–N_{py} distance is for the pyridine *cis* to the Me_3tach ring.

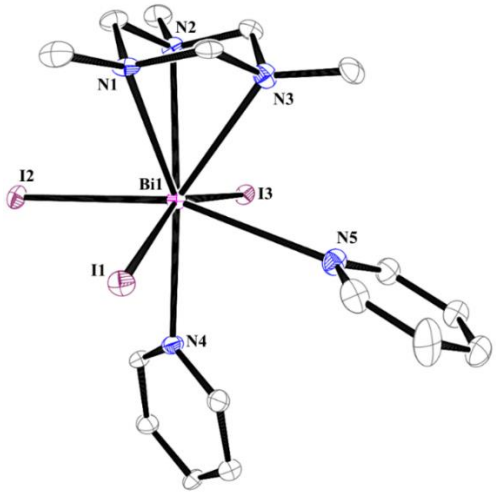

Figure 15.4: Molecular structure of [(Me_3tach)BiI_3($py)_2$], **15.5**, with selective atom labelling. Ellipsoids are drawn at the 50% probability level. Hydrogen atoms and the cocrystallized pyridine molecule have been omitted for clarity.

(Me_3tacn)BiI_3, 15.7. The bismuth iodide chemistry described above with Me_3tach was compared with the chemistry of BiI_3 with the larger, nine-membered triamine, Me_3tacn. Reaction of Me_3tacn with BiI_3 in THF formed a bright orange solution. Following workup, dark red crystals were grown from THF/hexane at −35 °C and (Me_3tacn)BiI_3, **15.7**, was identified by X-ray diffraction, eq 15.5, Figure 15.5. Compound **15.7** was sparingly soluble in THF, but completely soluble in pyridine. The ^{1}H NMR spectrum in THF-d_8 displayed two resonances at 3.38 and 3.29 ppm, assigned to the CH_2 and Me groups of the Me_3tacn ligand, respectively, Table 15.1. No evidence of bound THF was observed in the NMR spectrum. The ^{1}H NMR spectrum in py-d_5 had two resonances at 3.46 and 3.37 ppm with no evidence for bound THF or pyridine. These values for **15.7** are similar to the two resonances observed at 3.50 and 3.03 ppm for (Me_3tacn)$BiCl_3$,[19] likely measured in CD_3CN.

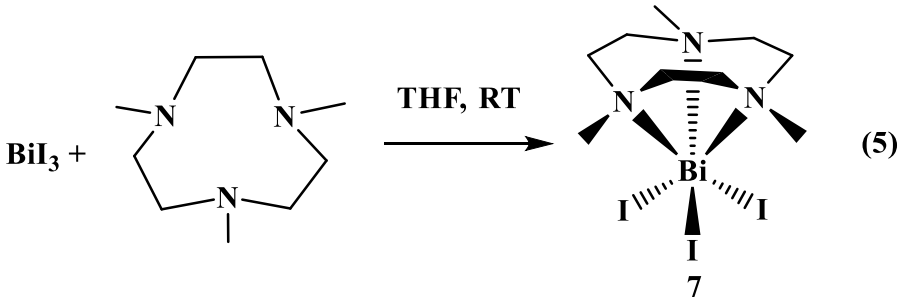

The molecular structure of **15.7** is shown in Figure 15.5. The bismuth atom is six coordinate and adopts a distorted octahedral geometry. The structure of **15.7** is reminiscent of three-legged piano-stool cyclopentadienyl complexes, $(C_5R_5)MX_3$, following the analogy described earlier involving the similarity of these tridentate amine ligands and cyclopentadienyl ligands. The iodide ligands are staggered with respect to the nitrogen atoms in the Me_3tacn ligand as was found for the anion in **15.3**, $[(Me_3tach)BiI_4]^{1-}$, above. The 22.536(7), 2.549(8), and 2.580(7) Å Bi–N_{ring} distances in **15.7** are longer than the analogous distances of 2.44(3), 2.45(2), and 2.47(2) Å in $(Me_3tacn)BiCl_3$, likely due to the larger size of iodide in **15.7**. However, the Bi–N_{ring} distances in **15.7** are shorter than those in **15.3** and **15.5**, Table 15.2. This can be seen in the 1.909 Å Bi–Cnt distance in **15.7** which is significantly shorter than the Bi–Cnt distances of 2.284, 2.339, and 2.372 Å in **15.3** and 2.380 Å in **15.5**. The shorter distances are consistent with the smaller coordination number of **15.7**. However, the 3.0106(8), 3.0594(8), and 3.0671(8) Å Bi–I distances in **15.7** fall within the 2.9577(6)–3.1551(4) Å distances in **15.3** and **15.5**, so the difference in bond distances cannot be explained by coordination number alone. Evidently, the ethylene bridges in Me_3tacn allow the nitrogen donor atoms to get closer to bismuth, giving the larger Me_3tacn ligand the tighter coordination and shorter distances.

The structural motif in **15.7** is also observed in Me_3tacn complexes of main group and transition metals. Related Me_3tacn structures have M–Cnt distances in the range of 0.76–0.92 Å, Table 15.5. Clearly, the M–Cnt distances with Me_3tacn ligands are much shorter than the M–Cnt

distances with Me_3tach ligands found in Tables 15.3 and 15.4. Additional metrical parameters are summarized in Table 15.2.

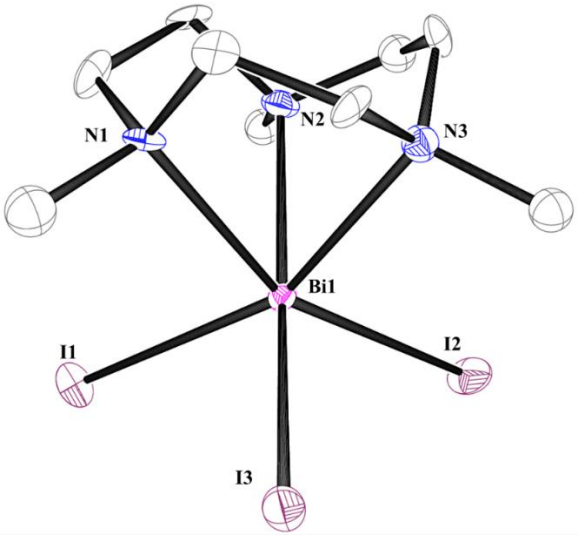

Figure 15.5: Molecular structure of (Me_3tacn)BiI_3, **15.7**, with selective atom labelling. Ellipsoids are drawn at the 50% probability level. Hydrogen atoms have been omitted for clarity.

Table 15.5: M–Cnt distances in selected six coordinate (Me_3tacn)MX_3 complexes.

	M–Cnt (Å)	Six-coordinate ionic radius (Å)	M–Cnt distance – radius (Å)
(Me_3tacn)InF_3[67]	1.560	0.80	0.760
(Me_3tacn)$BiCl_3$[19]	1.816	1.03	0.786
[(Me_3tacn)$MoBr_3$]$^{1+}$ [68]	1.550	0.72[a]	0.830
[(Me_3tacn)$SnCl_3$]$^{1+}$ [17]	1.525, 1.513	0.69	0.835, 0.823
(Me_3tacn)$InBr_3$[67]	1.645	0.80	0.845
(Me_3tacn)BiI_3, **15.7**	1.909	1.03	0.879
(Me_3tacn)$ScCl_3$[69]	1.655	0.745	0.910
(Me_3tacn)YI_3[70]	1.820	0.90	0.920

a: A 0.72 Å six-coordinate radius was used for Mo^{2+} based on extrapolation from the other values in the Shannon compilation.[2]

UV-visible Spectroscopy. UV-visible spectra were collected of BiI_3, (Me_3tach)$_2BiI_3$, **15.2**, [(Me_3tach)$_2BiI_2$][(Me_3tach)BiI_4], **15.3,** (Me_3tach)BiI_3(py)$_2$, **15.5**, and (Me_3tacn)BiI_3, **15.7** in THF, Figure 15.6, and of BiI_3, **15.5**, and **15.7** in pyridine, Figure 15.7. Compounds **15.2**, **15.3**,

15.5, and **15.7** in THF have four features that occur at similar wavelengths with large attenuation coefficients ε that are consistent with allowed transitions. These occur around 475 nm, 300 nm, 270 nm, and 230 nm, Table 15.6. BiI_3 without a nitrogen chelate also displays multiple strong absorptions although the pattern is different. Complexes **15.5**, **15.7,** and BiI_3 in pyridine also display strong absorptions, but with fewer distinct bands, Table 15.7. Since $BiCl_3(THF)_2$ and $BiBr_3(THF)_3$ are colorless and pale yellow, respectively,[8] the electronic absorptions seen for BiI_3, **15.2**, **15.3**, **15.5**, and **15.7** likely involve orbitals with significant iodine character. Transitions of the type in Tables 15.6 and 15.7 have been previously observed for BiI_3 coordination complexes with porphyrins and thioamides.[71–73]

Table 15.6: UV-visible data for BiI_3, **15.2**, **15.3, 15.5**, and **15.7** in THF (sh = shoulder).

	λ (nm)	ε ($M^{-1}cm^{-1}$ x 1000)
$BiI_3(THF)_x$	430 (sh), 396, 331, 245, 228 (sh)	13, 19, 21, 69, 61
$(Me_3tach)_2BiI_3$, **15.2**	474, 338 (sh), 317, 275, 228	11, 13, 21, 19, 24
$[(Me_3tach)_2BiI_2][(Me_3tach)BiI_4]$, **15.3**	470, 341 (sh), 316, 274, 227	25, 26, 47, 43, 56
$(Me_3tach)BiI_3(py)_2$, **15.5**	475, 339 (sh), 318, 269, 228	16, 18, 31, 31, 38
$(Me_3tacn)BiI_3$, **15.7**	487, 321, 287, 240, 218	7.1, 15, 14, 20, 24

Table 15.7: UV-visible data for BiI_3, **15.5**, and **15.7** in pyridine (sh = shoulder).

	λ (nm)	ε ($M^{-1}cm^{-1}$ x 1000)
$BiI_3(py)_x$	444, 360, 324	2.6, 3.3, 3.8
$(Me_3tach)BiI_3(py)_2$, **15.5**	445, 342 (sh), 317	6.9, 9.4, 11
$(Me_3tacn)BiI_3$, **15.7**	483, 320	15, 33

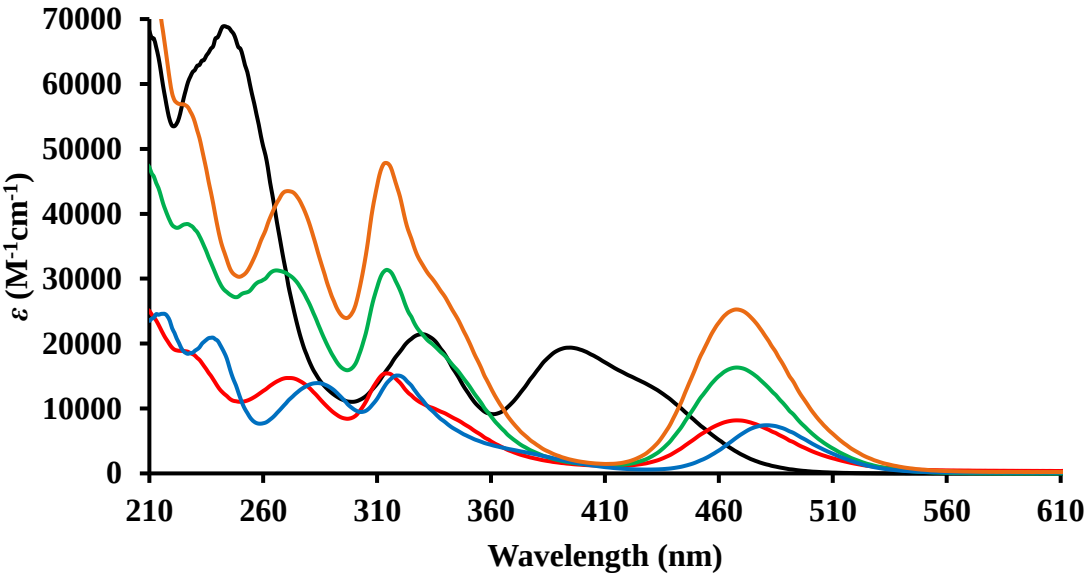

Figure 15.6: UV-visible spectroscopy of BiI_3 (black), **15.2** (red), **15.3** (orange), **15.5** (green), and **15.7** (blue) in THF.

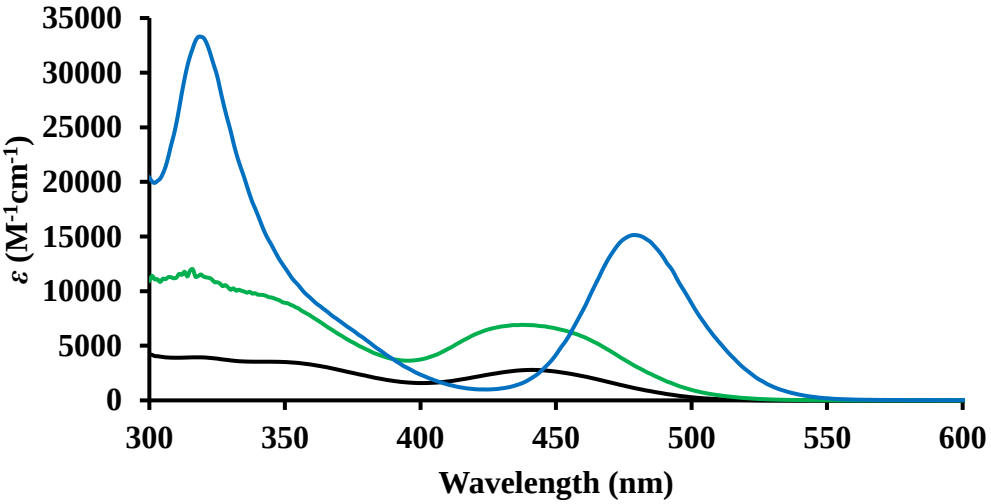

Figure 15.7: UV-visible spectroscopy of BiI_3 (black), **15.5** (green), and **15.7** (blue) in pyridine.

Conclusion

Me_3tach readily binds to bismuth trihalides with both 1:1 and 1:2 Bi:Me_3tach ratios. A variety of structures are accessible including coordination environments reminiscent of organometallic metallocene and piano stool geometries. This is consistent with the compact six

electron tridentate coordination motif provided by Me_3tach which is like that of a cyclopentadienide ligand. The observation of multiple structural variations demonstrates the flexibility in coordination of the Me_3tach ligand with bismuth and highlights the unusual, underexplored coordination chemistry of bismuth halides with simple donor ligands. Compounds **15.3** and **15.4** constitute the first crystal structures of a main-group metal with two R_3tach ligands. In contrast to the Me_3tach complexes, the related, more commonly used nine-member ring Me_3tacn binds to BiI_3 without any additional ligands. This emphasizes the advantage of the smaller Me_3tach ligand when a less sterically demanding tridentate nitrogen chelate is desirable.

Experimental Details

All manipulations and syntheses described below were con- ducted with the rigorous exclusion of air and water using standard Schlenk line and glovebox techniques under an argon atmosphere. THF, Et_2O, and hexane were sparged with UHP argon and dried by passage through columns containing a copper-based drying agent, alumina, and/or molecular sieves prior to use. Pyridine was vacuum distilled and kept over molecular sieves. Deuterated NMR solvents were dried over NaK alloy or molecular sieves, degassed by three freeze–pump–thaw cycles, and vacuum transferred before use. ^{1}H and $^{13}C\{^{1}H\}$ NMR spectra were recorded on a CRYO500 or AVANCE600 MHz spectrometer at 298 K and referenced to residual protio-solvent resonances. UV-visible spectra were collected at 298 K using a Varian Cary 50 Scan UV-visible spectrophotometer in a 1 mm or 1 cm quartz cuvette. Infrared spectra were recorded as compressed solids on an Agilent Cary 630 ATR-FTIR. Elemental analyses samples were prepared inside a nitrogen-filled glovebox and analyses were conducted on a Thermo Scientific FlashSmart CHNS/O Elemental Analyzer at the Irvine Materials Research Institute.

$BiCl_3$ (Aldrich) and BiI_3 (Aldrich) were used as received. Me_3tach (stabilized with $NaHCO_3$, Fisher) and Me_3tacn (Fisher) were purchased under argon, immediately placed in the glovebox upon being received, and kept over molecular sieves. 18-crown-6 (Alfa Aesar) was sublimed prior to use.

Crystallization of [BiI(THF)(μ–I)$_2$]$_n$, 15.1. BiI_3 was dissolved in minimal THF to form a yellow solution. Red crystals of **15.1** suitable for X-ray diffraction were grown from THF/hexane at −35 °C. Extended exposure of the red crystals to vacuum resulted in the formation of a grey powder of BiI_3. The infrared spectrum of the grey powder thus obtained showed no absorptions for THF. The ^{1}H and ^{13}C NMR of BiI_3 in THF-d_8 displayed no resonances other than protio-THF, suggesting rapid exchange on the NMR timescale or that THF is not bound in solution. UV-visible (THF) λ, ε ($mM^{-1}cm^{-1}$): 430sh (13), 396 (19), 33 (21), 245 (69), 228sh (61). UV-visible (py) λ, ε ($mM^{-1}cm^{-1}$): 444 (2.6), 360 (3.3), 324 (3.8).

Synthesis of (Me_3tach)$_2$$BiI_3$, 15.2. BiI_3 (70 mg, 0.12 mmol) was dissolved in THF (5 mL) to form a yellow solution. While stirring, a solution of Me_3tach (31 mg, 0.24 mmol) in THF (1 mL) was added via pipet. The solution immediately turned bright orange. The solution was stirred for two hours and then dried under vacuum to afford red/orange solids. The solids were redissolved in minimal THF and layered under hexane and placed at −35 °C overnight. The yellow solution was decanted, leaving an orange powder which was dried under vacuum to afford **15.2** (67 mg, 67%). ^{1}H NMR (THF-d_8): δ 4.44 (br s, 6H, CH_2), 2.61 ppm (br s, 9H, Me). ^{13}C (THF-d_8): δ 76.6 (CH_2), 38.6 ppm (Me). IR: 2907w, 2863w, 2801m, 2745m, 1684w, 1453s, 1411m, 1383w, 1264s, 1164m, 1105s, 1075m, 1004m, 829s, 866m cm^{-1}. UV-visible (THF) λ, ε ($mM^{-1}cm^{-1}$): 474 (11), 338sh (13), 317 (21), 275 (19), 228 (24). Anal. Calcd for $C_{12}H_{30}N_6Bi_1I_3$: C, 16.99; H, 3.57; N, 9.91. Found: C, 16.83; H, 2.992; N, 9.811.

Synthesis of [(Me$_3$tach)$_2$BiI$_2$][(Me$_3$tach)BiI$_4$], 15.3. As described above for **15.2**, BiI_3 (50 mg, 0.085 mmol) and Me_3tach (11 mg, 0.085 mmol) were combined in THF (5 mL) to form a red solution. The solution was stirred for two hours then dried under vacuum to afford red solids. Recrystallization from THF/hexane at −35 °C afforded an orange powder of **15.3** (49 mg, 80%). Red X-ray quality crystals of **15.3·2.5THF** were grown from THF/hexane at −35 °C. ^{1}H NMR (THF-d_8): δ 4.26 (br s, 12H, CH_2), 2.60 ppm (s, 18H, Me). A ^{13}C NMR spectrum could not be obtained due to the low solubility of **15.3**. IR: 2916w, 2863w, 2800m, 2741w, 1685w, 1592w, 1459m, 1441m, 1414w, 1380m, 1263s, 1158s, 1103s, 1074m, 1038w, 1004m, 926s, 865m cm^{-1}. UV-visible (THF) λ, ε (mM^{-1}cm^{-1}): 470 (25), 341sh (26), 316 (47), 274 (43), 227 (56). Anal. Calcd for $C_{18}H_{45}N_9Bi_2I_6$: C, 13.80; H, 2.89; N, 8.04. Found: C, 13.99; H, 2.735; N, 8.169.

Crystallization of [(Me$_3$tach)$_2$BiI$_2$]$_3$[Bi$_2$I$_9$][I][HMe$_3$tach]·THF, 15.4. On one occasion during the synthesis of **15.2** described above, dark red crystals were formed from a concentrated THF solution at −35 °C. These were identified by X-ray crystallography as [(Me$_3$tach)$_2$BiI$_2$]$_3$[Bi$_2$I$_9$][I][HMe$_3$tach]·THF, **15.4**.

Synthesis of (Me$_3$tach)BiI$_3$(py)$_2$, 15.5. BiI_3 (50 mg, 0.085 mmol) and Me_3tach (22 mg, 0.17 mmol) were combined as described above for compound **15.2**. The crude red/orange powder from the reaction mixture was dissolved in minimal pyridine and layered under Et_2O at −35 °C. After two days, gold crystals of **15.5·½py** suitable for X-ray diffraction had formed. The mother liquor was decanted and the crystals were dried under vacuum to afford **15.5**. A second crop of gold crystals of **15.5** was isolated in the same way from pyridine / Et_2O (55 mg, 81%). ^{1}H NMR (py-d_5): δ 4.57 (br s, 6H, CH_2), 2.51 ppm (br s, 9H, Me). ^{1}H NMR (THF-d_8): δ 4.80 (d, 6H, CH_2), 2.81 ppm (br s, 9H, Me). Exactly two equivalents of free pyridine (δ 8.55, 7.66, 7.25 ppm) per (Me$_3$tach)BI_3 were observed in the ^{1}H NMR spectrum suggesting dissociation. No resonances

attributable to bound THF were observed. ^{13}C (THF-d_8): δ 76.0 (CH2), 37.8 ppm (Me). IR (cm^{-1}): 2955w, 2859w, 2800m, 2748w, 1591s, 1434s, 1271m, 1210m, 1161w, 1108s, 1062m, 1001s, 931s, 874w, 746s, 690s. UV-visible (THF) λ, ε (mM^{-1}cm^{-1}): 475 (16), 339sh (18), 318 (31), 269 (31), 228 (38). UV-visible (py) λ, ε (M^{-1}cm^{-1}): 445 (6.0), 342sh (9.4), 317 (11). Anal. Calcd for $C_{18.5}H_{27.5}N_{5.5}Bi_1I_3$: C, 24.24; H, 3.02; N, 8.40. Found: C, 25.58; H, 2.853; N, 7.73.

Synthesis of (Me$_3$tach)BiCl$_3$, 15.6. $BiCl_3$ (113 mg, 0.358 mmol) was dissolved in THF (5 mL) to form a colorless solution. While stirring, Me_3tach (93 mg, 0.72 mmol) as a solution in THF was added. White precipitate formed immediately upon addition. The slurry was stirred for two hours then dried under vacuum. Pyridine (3 mL) was added and the solution was filtered and layered under Et_2O and placed at −35 °C for crystallization. Colorless crystals of **15.6** suitable for X-ray diffraction formed over two days. The mother liquor was decanted and the crystals were dried to afford white solid **15.6** (74 mg, 34%). ^{1}H NMR (THF-d_8): δ 2.58 ppm (br s, 9H, Me). A ^{13}C spectrum was not obtained due to the insolubility of compound **15.6** in THF and pyridine. IR (cm^{-1}): 2987w, 2807m, 1588s, 1438s, 1681m, 1270m, 1213s, 1152w, 1114s, 1066m, 996m, 931s, 768m, 712m, 692s. Anal. Calcd For $C_{16}H_{25}N_5Bi_1Cl_3$: C, 31.88; H, 4.18; N, 11.62. Found: C, 31.82; H, 4.004; N, 11.98.

Synthesis of (Me$_3$tacn)BiI$_3$, 15.7. BiI_3 (50 mg, 0.85 mmol) and Me_3tacn (15 mg, 0.0.088 mmol) were combined in THF (5 mL) to form a red solution with red precipitate. The slurry was stirred overnight then dried under vacuum. The solids were redissolved in pyridine, filtered, and dried under vacuum to afford a red/orange powder of **15.7** (45 mg, 70%). Red X-ray quality crystals were grown from THF/hexane at −35 °C. ^{1}H NMR (py-d_5): δ 3.46 (s, 9H, Me), 3.37 ppm (dd, 12H, CH_2). ^{13}C (py-d_5): δ 57.7 (CH_2), 52.9 ppm (Me). ^{1}H NMR (THF-d_8): δ 3.38 (s, 9H, Me), 3.29 ppm (dd, 12H, CH_2). No resonances attributable to bound THF or pyridine were

observed. ^{13}C (THF-d_8): δ 76.0 (CH_2), 37.8 ppm (Me). IR (cm^{-1}): 2854w, 2815w, 1454m, 1376w, 1298s, 1224w, 1149m, 1061s, 1001s, 883m, 734s. UV-visible (THF) λ, ε ($mM^{-1}cm^{-1}$): 487 (7.1), 321 (15), 287 (14), 240 (20), 218 (24). UV-visible (py) λ (nm), ε ($mM^{-1}cm^{-1}$): 483 (15), 320 (33). Anal. Calcd For $C_9H_{21}N_3Bi_1I_3$: C, 14.21; H, 2.78; N, 5.52. Found: C, 14.51; H, 2.735; N, 6.57. The nitrogen content was consistently high across multiple samples.

Crystallographic Details

Table 15.8: Crystal data and structure refinements for $[BiI(THF)(\mu\text{–}I)_2]_n$, **15.1,** $[(Me_3tach)_2BiI_2][(Me_3tach)BiI_4]\cdot 2.5(THF)$, **15.3·2.5(THF)**, and $[(Me_3tach)BiI_3(py)_2]$, **15.5**.

	15.1	**15.3·2.5(THF)**	**15.5**
Identification code	jcw105	jcw109	jcw106
Empirical formula	$[C_4H_8BiI_3O]_\infty$	$(C_{12}H_{30}BiI_2N_6)(C_6H_{15}BiI_4N_3)\bullet 2.5(C_4H_8O)$	$C_{16}H_{25}BiI_3N_5\cdot ½(C_5H_5N)$
Formula weight	661.78	1747.25	916.64
Temperature (K)	133(2)	133(2)	93(2)
Wavelength (Å)	0.71073	0.71073	0.71073
Crystal system	Monoclinic	Monoclinic	Monoclinic
Space group	$P2_1/n$	$C2/c$	$P2_1/c$
a (Å)	7.4002(6)	31.3434(18)	8.5783(9)
b (Å)	8.5475(7)	13.3984(8)	19.2132(19)
c (Å)	9.0433(8)	25.1713(15)	15.9499(4)
α (°)	90	90	90
β (°)	90.2111(13)	110.8376(9)	105.424(16)
γ (°)	90	90	90
Volume ($Å^3$)	572.01(8)	9879.3(10)	2534.1(4)
Z	2	8	4
Density (mg/m^3)	3.842	2.349	2.403
Absorption coefficient (mm^{-1})	23.452	10.900	10.627
F(000)	564	6400	1676
Crystal color	red	red	gold

Crystal size (mm^3)	0.173 x 0.162 x 0.146	0.326 x 0.140 x 0.132	0.190 x 0.166 x 0.117
θ range for data collection (°)	2.252 to 30.635	1.390 to 28.699	1.696 to 31.468
Index ranges	$-10 \leq h \leq 10$, $0 \leq k \leq 12$, $0 \leq l \leq 12$	$-42 \leq h \leq 42$, $-18 \leq k \leq 18$, $-34 \leq l \leq 34$	$-11 \leq h \leq 12$, $-27 \leq k \leq 28$, $-23 \leq l \leq 23$
Independent reflections	1930	12760	7859
Completeness to θ = 25.500°	99.7	100.0	99.9
Absorption correction	Semi-empirical from equivalents	Semi-empirical from equivalents	Semi-empirical from equivalents
Max. and min. transmission	0.4330 and 0.1664	0.2125 and 0.0935	0.3379 and 0.2363
Refinement method	Full-matrix least-squares on F^2	Full-matrix least-squares on F^2	Full-matrix least-squares on F^2
Data / restraints / parameters	1930 / 0 / 47	12760 / 0 / 427	7859 / 0 / 256
Goodness-of-fit on F^2	1.112	1.059	1.441
Final R indices [$I>2\sigma(I)$]	R1 = 0.0386, wR2 = 0.0901	R1 = 0.0296, wR2 = 0.0576	R1 = 0.0443, wR2 = 0.0900
R indices (all data)	R1 = 0.0424, wR2 = 0.0915	R1 = 0.0424, wR2 = 0.0613	R1 = 0.0487, wR2 = 0.0910
Data cutoff (Å)	0.70	0.74	0.68
Largest diff. peak and hole ($e.Å^3$)	2.640 and -2.471	1.501 and -0.999	1.893 and -2.377

Table 15.9: Crystal data and structure refinements for [$(Me_3tach)BiCl_3(py)_2$], **15.6,** and $(Me_3tacn)BiI_3$, **15.7**.

	15.6	**15.7**
Identification code	jcw121	jcw94
Empirical formula	$C_{16}H_{25}BiCl_3N_5$	$C_9H_{21}BiI_3N_3$
Formula weight	602.74	760.97
Temperature (K)	93(2)	133.15
Wavelength (Å)	0.71073	0.71073
Crystal system	Monoclinic	Monoclinic

Space group	$P2_1/n$	$P2_1/n$
a (Å)	9.3693(13)	8.43456(17)
b (Å)	16.691(2)	14.042(3)
c (Å)	13.4828(19)	15.206(3)
α (°)	90	90
β (°)	93.843(3)	101.109(4)
γ (°)	90	90
Volume ($Å^3$)	2103.8(5)	1767.5(6)
Z	4	4
Density (mg/m^3)	1.903	2.860
Absorption coefficient (mm^{-1})	8.771	15.200
F(000)	1160	1352
Crystal color	colorless	red
Crystal size (mm^3)	0.272 x 0.218 x 0.148	0.110 x 0.108 x 0.096
θ range for data collection (°)	1.944 to 30.554	1.991 to 27.133°
Index ranges	$-13 \leq h \leq 13$, $-23 \leq k \leq 21$, $-19 \leq l \leq 18$	$-10 \leq h \leq 10$, $0 \leq k \leq 18$, $0 \leq l \leq 19$
Independent reflections	6341	4174
Completeness to θ = 25.500°	100.0	99.9
Absorption correction	Semi-empirical from equivalents	Semi-empirical from equivalents
Max. and min. transmission	0.4330 and 0.3009	0.2075 and 0.1371
Refinement method	Full-matrix least-squares on F^2	Full-matrix least-squares on F^2
Data / restraints / parameters	6341 / 0 / 229	4174 / 0 / 149
Goodness-of-fit on F^2	1.039	1.123
Final R indices [$I>2\sigma(I)$]	R1 = 0.0179, wR2 = 0.0371	R1 = 0.0388, wR2 = 0.0583
R indices (all data)	R1 = 0.0218, wR2 = 0.0380	R1 = 0.0517, wR2 = 0.0611
Data cutoff (Å)	0.70	0.78
Largest diff. peak and hole ($e.Å^3$)	1.331 and −0.666	1.277 and −1.024

X-ray Data Collection, Structure Solution and Refinement for **$[BiI(THF)(\mu\text{–}I)_2]_n$, 15.1**.

A red crystal of approximate dimensions 0.146 x 0.162 x 0.173 mm was mounted in a cryoloop and transferred to a Bruker SMART APEX II diffractometer system. The APEX2[74]

program package and the CELL_NOW[75] were used to determine the unit-cell parameters. Data was collected using a 30 sec/frame scan time. The raw frame data was processed using SAINT[76] and TWINABS[77] to yield the reflection data file (HKLF 5 format). Subsequent calculations were carried out using the SHELXTL[78] program package. The diffraction symmetry was 2/*m* and the systematic absences were consistent with the monoclinic space groups $P2_1$ and $P2_1/m$. It was later determined that space group $P2_1/m$ was correct.

The structure was solved by direct methods and refined on F^2 by full-matrix least-squares techniques. The analytical scattering factors[79] for neutral atoms were used throughout the analysis. Hydrogen atoms were included using a riding model. The molecule was located on a mirror plane and was polymeric, repeating about inversion centers. The tetrahydrofuran ligand was disordered. Carbon atoms were included using equivalent anisotropic displacement parameters.

Least-squares analysis yielded wR2 = 0.0915 and Goof = 1.112 for 47 variables refined against 1930 data (0.70 Å), R1 = 0.0386 for those 1792 with $I > 2.0\sigma(I)$. The structure was refined as a three-component twin.

Table 15.10: Bond lengths [Å] and angles [°] for **15.1**.

Bi(1)-O(1)	2.618(10)		
Bi(1)-I(2)	2.8801(9)	O(1)-Bi(1)-I(2)	178.1(2)
Bi(1)-I(1)#1	2.9628(6)	O(1)-Bi(1)-I(1)#1	83.78(16)
Bi(1)-I(1)	2.9628(6)	I(2)-Bi(1)-I(1)#1	94.96(2)
Bi(1)-I(1)#2	3.2606(7)	O(1)-Bi(1)-I(1)	83.78(15)
Bi(1)-I(1)#3	3.2606(7)	I(2)-Bi(1)-I(1)	94.96(2)
I(1)-Bi(1)#2	3.2607(7)	I(1)#1-Bi(1)-I(1)	94.15(2)
O(1)-C(1)	1.345(19)	O(1)-Bi(1)-I(1)#2	85.87(17)
O(1)-C(4)	1.467(19)	I(2)-Bi(1)-I(1)#2	95.55(2)
C(1)-C(2)	1.51(2)	I(1)#1-Bi(1)-I(1)#2	167.439(17)
C(2)-C(3)	1.43(2)	I(1)-Bi(1)-I(1)#2	91.774(15)
C(3)-C(4)	1.49(3)	O(1)-Bi(1)-I(1)#3	85.87(17)

I(2)-Bi(1)-I(1)#3	95.55(2)	C(1)-O(1)-Bi(1)	124.6(8)
I(1)#1-Bi(1)-I(1)#3	91.773(15)	C(4)-O(1)-Bi(1)	127.4(10)
I(1)-Bi(1)-I(1)#3	167.439(17)	O(1)-C(1)-C(2)	110.3(13)
I(1)#2-Bi(1)-I(1)#3	80.38(2)	C(3)-C(2)-C(1)	103.3(13)
Bi(1)-I(1)-Bi(1)#2	88.226(15)	C(2)-C(3)-C(4)	106.4(16)
C(1)-O(1)-C(4)	106.6(12)	O(1)-C(4)-C(3)	102.5(15)

Symmetry transformations used to generate equivalent atoms:
#1 x,-y+3/2,z #2 -x+1,-y+1,-z+1 #3 -x+1,y+1/2,-z+1

X-ray Data Collection, Structure Solution and Refinement for **[(Me$_3$tach)$_2$BiI$_2$][(Me$_3$tach)BiI$_4$]·2.5(THF), 15.3·2.5THF.**

A red crystal of approximate dimensions 0.132 x 0.140 x 0.326 mm was mounted in a cryoloop and transferred to a Bruker SMART APEX II diffractometer. The APEX2[74] program package was used to determine the unit-cell parameters. Data were collected using a 60 sec/frame scan time. The raw frame data was processed using SAINT[76] and SADABS[80] to yield the reflection data file. Subsequent calculations were carried out using the SHELXTL[78] program. The diffraction symmetry was 2/*m* and the systematic absences were consistent with the monoclinic space groups *Cc*, and *C*2/*c*. It was later determined that space group *C*2*c* was correct.

The structure was solved by direct methods and refined on F^2 by full-matrix least-squares techniques. The analytical scattering factors[79] for neutral atoms were used throughout the analysis. Hydrogen atoms were included using a riding model. There were two different independent molecules and 2.5 molecules of tetrahydrofuran solvent present. One solvent molecule was disordered and refined using multiple components, partial site-occupancy-factors, and equivalent anisotropic displacement parameters for the carbon atoms. The half-molecule of solvent was

located about an inversion center and refined as a rigid group with partial site-occupancy-factors and equivalent anisotropic displacement parameters for all atoms.

Least-squares analysis yielded wR2 = 0.0613 and Goof = 1.0595 for 427 variables refined against 12760 data (0.74 Å), R1 = 0.0296 for those 10702 data with I > 2.0σ(I).

Table 15.11: Bond lengths [Å] and angles [°] for **15.3·2.5THF**.

Bi(1)-N(3)	2.595(4)	N(6)-C(11)	1.464(7)
Bi(1)-N(6)	2.644(4)	N(6)-C(10)	1.472(6)
Bi(1)-N(2)	2.668(4)	Bi(2)-N(8)	2.702(5)
Bi(1)-N(1)	2.691(4)	Bi(2)-N(7)	2.740(5)
Bi(1)-N(5)	2.721(4)	Bi(2)-N(9)	2.742(4)
Bi(1)-N(4)	2.740(4)	Bi(2)-I(5)	2.9670(4)
Bi(1)-I(1)	2.9606(4)	Bi(2)-I(6)	3.0533(4)
Bi(1)-I(2)	2.9701(4)	Bi(2)-I(3)	3.0832(4)
N(1)-C(1)	1.452(7)	Bi(2)-I(4)	3.1551(4)
N(1)-C(5)	1.458(6)	N(7)-C(18)	1.456(7)
N(1)-C(6)	1.472(7)	N(7)-C(13)	1.457(7)
N(2)-C(2)	1.455(7)	N(7)-C(17)	1.459(7)
N(2)-C(3)	1.468(7)	N(8)-C(13)	1.455(7)
N(2)-C(1)	1.472(7)	N(8)-C(14)	1.459(7)
N(3)-C(5)	1.461(6)	N(8)-C(15)	1.472(8)
N(3)-C(3)	1.463(7)	N(9)-C(15)	1.450(7)
N(3)-C(4)	1.464(6)	N(9)-C(17)	1.453(7)
N(4)-C(11)	1.456(6)	N(9)-C(16)	1.478(7)
N(4)-C(7)	1.461(6)	O(1)-C(19)	1.388(9)
N(4)-C(12)	1.462(7)	O(1)-C(22)	1.410(9)
N(5)-C(7)	1.464(7)	C(19)-C(20)	1.483(10)
N(5)-C(8)	1.468(7)	C(20)-C(21)	1.531(11)
N(5)-C(9)	1.473(6)	C(21)-C(22)	1.495(11)
N(6)-C(9)	1.458(7)	O(2)-C(23B)	1.30(3)

O(2)-C(26)	1.319(16)	N(6)-Bi(1)-I(1)	83.34(10)
O(2)-C(23)	1.44(2)	N(2)-Bi(1)-I(1)	90.44(10)
O(2)-C(26B)	1.64(3)	N(1)-Bi(1)-I(1)	133.11(9)
C(23)-C(24)	1.54(3)	N(5)-Bi(1)-I(1)	91.29(9)
C(24)-C(25)	1.48(2)	N(4)-Bi(1)-I(1)	132.30(9)
C(25)-C(26)	1.52(2)	N(3)-Bi(1)-I(2)	86.01(9)
C(23B)-C(24B)	1.44(4)	N(6)-Bi(1)-I(2)	85.70(10)
C(24B)-C(25B)	1.52(3)	N(2)-Bi(1)-I(2)	134.30(9)
C(25B)-C(26B)	1.47(3)	N(1)-Bi(1)-I(2)	89.51(10)
O(3)-C(30)	1.4101	N(5)-Bi(1)-I(2)	132.46(9)
O(3)-C(27)	1.4152	N(4)-Bi(1)-I(2)	87.78(9)
C(27)-C(28)	1.5244	I(1)-Bi(1)-I(2)	105.083(12)
C(28)-C(29)	1.5147	C(1)-N(1)-C(5)	110.0(4)
C(29)-C(30)	1.5170	C(1)-N(1)-C(6)	112.4(4)
		C(5)-N(1)-C(6)	111.6(4)
N(3)-Bi(1)-N(6)	162.54(12)	C(1)-N(1)-Bi(1)	95.4(3)
N(3)-Bi(1)-N(2)	52.58(13)	C(5)-N(1)-Bi(1)	92.5(3)
N(6)-Bi(1)-N(2)	139.42(13)	C(6)-N(1)-Bi(1)	132.3(3)
N(3)-Bi(1)-N(1)	52.22(12)	C(2)-N(2)-C(3)	113.0(4)
N(6)-Bi(1)-N(1)	142.95(13)	C(2)-N(2)-C(1)	112.8(5)
N(2)-Bi(1)-N(1)	51.67(14)	C(3)-N(2)-C(1)	109.0(4)
N(3)-Bi(1)-N(5)	140.73(13)	C(2)-N(2)-Bi(1)	130.3(3)
N(6)-Bi(1)-N(5)	51.68(13)	C(3)-N(2)-Bi(1)	92.8(3)
N(2)-Bi(1)-N(5)	88.63(13)	C(1)-N(2)-Bi(1)	95.9(3)
N(1)-Bi(1)-N(5)	111.30(13)	C(5)-N(3)-C(3)	109.7(4)
N(3)-Bi(1)-N(4)	143.38(12)	C(5)-N(3)-C(4)	112.8(4)
N(6)-Bi(1)-N(4)	51.44(12)	C(3)-N(3)-C(4)	113.0(4)
N(2)-Bi(1)-N(4)	113.09(13)	C(5)-N(3)-Bi(1)	96.3(3)
N(1)-Bi(1)-N(4)	91.72(12)	C(3)-N(3)-Bi(1)	95.9(3)
N(5)-Bi(1)-N(4)	51.01(13)	C(4)-N(3)-Bi(1)	126.8(3)
N(3)-Bi(1)-I(1)	84.03(9)	C(11)-N(4)-C(7)	109.4(4)

C(11)-N(4)-C(12)	111.9(4)	N(9)-Bi(2)-I(6)	84.31(9)
C(7)-N(4)-C(12)	111.8(4)	I(5)-Bi(2)-I(6)	110.532(11)
C(11)-N(4)-Bi(1)	92.6(3)	N(8)-Bi(2)-I(3)	77.07(10)
C(7)-N(4)-Bi(1)	95.0(3)	N(7)-Bi(2)-I(3)	123.92(9)
C(12)-N(4)-Bi(1)	133.3(3)	N(9)-Bi(2)-I(3)	82.98(9)
C(7)-N(5)-C(8)	111.2(4)	I(5)-Bi(2)-I(3)	113.055(11)
C(7)-N(5)-C(9)	109.3(4)	I(6)-Bi(2)-I(3)	133.089(11)
C(8)-N(5)-C(9)	111.4(4)	N(8)-Bi(2)-I(4)	151.84(9)
C(7)-N(5)-Bi(1)	95.7(3)	N(7)-Bi(2)-I(4)	153.76(9)
C(8)-N(5)-Bi(1)	134.0(3)	N(9)-Bi(2)-I(4)	144.79(10)
C(9)-N(5)-Bi(1)	92.5(3)	I(5)-Bi(2)-I(4)	87.933(10)
C(9)-N(6)-C(11)	109.9(4)	I(6)-Bi(2)-I(4)	82.758(11)
C(9)-N(6)-C(10)	112.1(4)	I(3)-Bi(2)-I(4)	82.305(10)
C(11)-N(6)-C(10)	111.8(4)	C(18)-N(7)-C(13)	113.0(5)
C(9)-N(6)-Bi(1)	96.0(3)	C(18)-N(7)-C(17)	112.3(4)
C(11)-N(6)-Bi(1)	96.4(3)	C(13)-N(7)-C(17)	109.9(4)
C(10)-N(6)-Bi(1)	128.6(3)	C(18)-N(7)-Bi(2)	129.8(4)
N(1)-C(1)-N(2)	106.0(4)	C(13)-N(7)-Bi(2)	94.1(3)
N(3)-C(3)-N(2)	105.4(4)	C(17)-N(7)-Bi(2)	95.1(3)
N(1)-C(5)-N(3)	105.7(4)	C(13)-N(8)-C(14)	112.8(5)
N(4)-C(7)-N(5)	107.0(4)	C(13)-N(8)-C(15)	109.3(4)
N(6)-C(9)-N(5)	105.9(4)	C(14)-N(8)-C(15)	112.9(5)
N(4)-C(11)-N(6)	106.4(4)	C(13)-N(8)-Bi(2)	95.8(3)
N(8)-Bi(2)-N(7)	50.70(13)	C(14)-N(8)-Bi(2)	128.3(4)
N(8)-Bi(2)-N(9)	50.88(14)	C(15)-N(8)-Bi(2)	95.2(3)
N(7)-Bi(2)-N(9)	50.38(14)	C(15)-N(9)-C(17)	110.2(5)
N(8)-Bi(2)-I(5)	82.80(11)	C(15)-N(9)-C(16)	112.9(5)
N(7)-Bi(2)-I(5)	82.51(9)	C(17)-N(9)-C(16)	112.0(4)
N(9)-Bi(2)-I(5)	127.28(10)	C(15)-N(9)-Bi(2)	94.1(3)
N(8)-Bi(2)-I(6)	125.39(9)	C(17)-N(9)-Bi(2)	95.2(3)
N(7)-Bi(2)-I(6)	77.89(9)	C(16)-N(9)-Bi(2)	130.1(4)

N(8)-C(13)-N(7)	106.3(4)	C(24)-C(25)-C(26)	99.9(13)
N(9)-C(15)-N(8)	106.3(4)	O(2)-C(26)-C(25)	104.0(12)
N(9)-C(17)-N(7)	106.5(4)	O(2)-C(23B)-C(24B)	117(2)
C(19)-O(1)-C(22)	106.1(6)	C(23B)-C(24B)-C(25B)	99(2)
O(1)-C(19)-C(20)	110.7(6)	C(26B)-C(25B)-C(24B)	106(2)
C(19)-C(20)-C(21)	101.6(6)	C(25B)-C(26B)-O(2)	103.9(17)
C(22)-C(21)-C(20)	99.4(6)	C(30)-O(3)-C(27)	103.7
O(1)-C(22)-C(21)	106.6(6)	O(3)-C(27)-C(28)	105.4
C(26)-O(2)-C(23)	112.4(11)	C(29)-C(28)-C(27)	102.3
C(23B)-O(2)-C(26B)	101.4(16)	C(28)-C(29)-C(30)	103.7
O(2)-C(23)-C(24)	99.0(14)	O(3)-C(30)-C(29)	108.2
C(25)-C(24)-C(23)	108.6(17)		

X-ray Data Collection, Structure Solution and Refinement for **15.5**.

A gold crystal of approximate dimensions 0.190 x 0.166 x 0.117 mm was mounted in a cryoloop and transferred to a Bruker SMART APEX II diffractometer system. The APEX2[74] program package was used to determine the unit-cell parameters. Data collection used a 30 sec/frame scan time. The raw frame data was processed using SAINT[76] and SADABS[80] to yield the reflection data file. Subsequent calculations were carried out using the SHELXTL[78] program package. The diffraction symmetry was 2/*m* and the systematic absences were consistent with the monoclinic space group $P2_1/c$ that was later determined to be correct.

The structure was solved by direct methods and refined on F^2 by full-matrix least-squares techniques. The analytical scattering factors[79] for neutral atoms were used throughout the analysis. Hydrogen atoms were included using a riding model.

There was one half pyridine solvent molecule present. The solvent was located about an inversion center. One position was modeled as a 50:50 mixed occupancy of nitrogen and carbon.

Least-squares analysis yielded wR2 = 0.0910 and Goof = 1.441 for 256 variables refined against 7859 data (0.68 Å), R1 = 0.0443 for those 7262 data with $I > 2.0\sigma(I)$.

Table 15.12: Bond lengths [Å] and angles [°] for **15.5**.

Bi(1)-N(4)	2.644(6)
Bi(1)-N(3)	2.721(6)
Bi(1)-N(2)	2.734(6)
Bi(1)-N(1)	2.755(6)
Bi(1)-N(5)	2.945(7)
Bi(1)-I(2)	2.9577(6)
Bi(1)-I(3)	3.0777(6)
Bi(1)-I(1)	3.0942(5)
N(1)-C(3)	1.454(9)
N(1)-C(2)	1.462(9)
N(1)-C(1)	1.464(10)
N(2)-C(5)	1.450(9)
N(2)-C(3)	1.467(9)
N(2)-C(4)	1.468(9)
N(3)-C(1)	1.447(10)
N(3)-C(5)	1.468(9)
N(3)-C(6)	1.473(10)
N(4)-C(7)	1.339(9)
N(4)-C(11)	1.345(9)
C(7)-C(8)	1.381(10)
C(8)-C(9)	1.387(11)
C(9)-C(10)	1.374(12)
C(10)-C(11)	1.389(11)
N(6)-C(18)	1.350(15)
N(6)-C(17)#1	1.384(15)
C(17)-C(18)	1.373(16)
C(17)-C(19)#1	1.384(15)
C(17)-N(6)#1	1.384(15)
N(5)-C(12)	1.349(10)
N(5)-C(16)	1.351(10)
C(12)-C(13)	1.385(13)
C(13)-C(14)	1.372(13)
C(14)-C(15)	1.364(11)
C(15)-C(16)	1.376(11)

N(4)-Bi(1)-N(3)	147.7(2)
N(4)-Bi(1)-N(2)	148.73(18)
N(3)-Bi(1)-N(2)	50.83(18)
N(4)-Bi(1)-N(1)	154.47(19)
N(3)-Bi(1)-N(1)	50.6(2)
N(2)-Bi(1)-N(1)	50.54(17)
N(4)-Bi(1)-N(5)	76.34(19)
N(3)-Bi(1)-N(5)	71.62(19)
N(2)-Bi(1)-N(5)	115.31(18)
N(1)-Bi(1)-N(5)	113.41(19)
N(4)-Bi(1)-I(2)	84.21(14)
N(3)-Bi(1)-I(2)	127.98(14)
N(2)-Bi(1)-I(2)	83.11(13)
N(1)-Bi(1)-I(2)	83.24(14)
N(5)-Bi(1)-I(2)	160.32(13)
N(4)-Bi(1)-I(3)	80.76(14)
N(3)-Bi(1)-I(3)	98.90(13)
N(2)-Bi(1)-I(3)	127.96(12)
N(1)-Bi(1)-I(3)	77.43(12)
N(5)-Bi(1)-I(3)	82.61(13)
I(2)-Bi(1)-I(3)	91.415(16)
N(4)-Bi(1)-I(1)	77.02(14)
N(3)-Bi(1)-I(1)	95.24(13)
N(2)-Bi(1)-I(1)	75.75(12)
N(1)-Bi(1)-I(1)	126.17(12)
N(5)-Bi(1)-I(1)	83.71(13)
I(2)-Bi(1)-I(1)	94.957(16)

I(3)-Bi(1)-I(1)	156.102(16)	N(1)-C(3)-N(2)	106.7(6)
C(3)-N(1)-C(2)	111.5(6)	N(2)-C(5)-N(3)	106.7(6)
C(3)-N(1)-C(1)	109.8(6)	N(4)-C(7)-C(8)	123.5(7)
C(2)-N(1)-C(1)	113.3(6)	C(7)-C(8)-C(9)	118.5(7)
C(3)-N(1)-Bi(1)	94.8(4)	C(10)-C(9)-C(8)	118.8(7)
C(2)-N(1)-Bi(1)	131.1(5)	C(9)-C(10)-C(11)	119.2(7)
C(1)-N(1)-Bi(1)	93.8(4)	N(4)-C(11)-C(10)	122.6(7)
C(5)-N(2)-C(3)	110.1(6)	C(18)-N(6)-C(17)#1	120.9(11)
C(5)-N(2)-C(4)	112.3(6)	C(18)-C(17)-C(19)#1	122.1(11)
C(3)-N(2)-C(4)	111.2(6)	C(18)-C(17)-N(6)#1	122.1(11)
C(5)-N(2)-Bi(1)	94.1(4)	C(19)#1-C(17)-N(6)#1	0.0
C(3)-N(2)-Bi(1)	95.3(4)	N(6)-C(18)-C(17)	117.0(10)
C(4)-N(2)-Bi(1)	131.5(5)	C(12)-N(5)-C(16)	116.3(7)
C(1)-N(3)-C(5)	110.3(6)	C(12)-N(5)-Bi(1)	121.4(5)
C(1)-N(3)-C(6)	112.0(6)	C(16)-N(5)-Bi(1)	121.5(5)
C(5)-N(3)-C(6)	111.5(6)	N(5)-C(12)-C(13)	123.3(8)
C(1)-N(3)-Bi(1)	95.6(4)	C(14)-C(13)-C(12)	119.1(8)
C(5)-N(3)-Bi(1)	94.2(4)	C(15)-C(14)-C(13)	118.2(8)
C(6)-N(3)-Bi(1)	131.0(5)	C(14)-C(15)-C(16)	120.5(8)
C(7)-N(4)-C(11)	117.3(7)	N(5)-C(16)-C(15)	122.6(7)
C(7)-N(4)-Bi(1)	120.2(5)		
C(11)-N(4)-Bi(1)	121.2(5)	Symmetry transformations used to generate	
N(3)-C(1)-N(1)	106.9(6)	equivalent atoms: #1 -x,-y,-z+1	

X-ray Data Collection, Structure Solution and Refinement for **15.6**.

A colorless crystal of approximate dimensions 0.272 x 0.218 x 0.148 mm was mounted in a cryoloop and transferred to a Bruker SMART APEX II diffractometer system. The APEX2[74] program package was used to determine the unit-cell parameters. Data was collected using a 20 sec/frame scan time. The raw frame data was processed using SAINT[76] and SADABS[80] to yield the reflection data file. Subsequent calculations were carried out using the SHELXTL[78] program package. The diffraction symmetry was 2/*m* and the systematic absences were consistent with the monoclinic space group $P2_1/n$ that was later determined to be correct.

The structure was solved by direct methods and refined on F^2 by full-matrix least-squares techniques. The analytical scattering factors[79] for neutral atoms were used throughout the analysis. Hydrogen atoms were included using a riding model.

Least-squares analysis yielded wR2 = 0.0380 and Goof = 1.039 for 229 variables refined against 6341 data (0.70 Å), R1 = 0.0179 for those 5732 data with $I > 2.0\sigma(I)$.

Table 15.13: Bond lengths [Å] and angles [°] for **15.6**.

Bi(1)-Cl(3)	2.6556(6)	Cl(3)-Bi(1)-N(2)	79.75(4)
Bi(1)-N(2)	2.6563(18)	Cl(3)-Bi(1)-N(5)	82.14(4)
Bi(1)-N(5)	2.6682(19)	N(2)-Bi(1)-N(5)	146.15(6)
Bi(1)-N(1)	2.6737(19)	Cl(3)-Bi(1)-N(1)	125.67(4)
Bi(1)-Cl(2)	2.7024(6)	N(2)-Bi(1)-N(1)	51.91(6)
Bi(1)-N(3)	2.7199(17)	N(5)-Bi(1)-N(1)	152.05(6)
Bi(1)-Cl(1)	2.7376(6)	Cl(3)-Bi(1)-Cl(2)	97.196(18)
Bi(1)-N(4)	2.7724(17)	N(2)-Bi(1)-Cl(2)	75.68(4)
N(1)-C(2)	1.467(3)	N(5)-Bi(1)-Cl(2)	78.54(4)
N(1)-C(1)	1.468(3)	N(1)-Bi(1)-Cl(2)	93.53(4)
N(1)-C(6)	1.473(2)	Cl(3)-Bi(1)-N(3)	80.50(4)
N(2)-C(2)	1.463(3)	N(2)-Bi(1)-N(3)	51.26(5)
N(2)-C(3)	1.467(3)	N(5)-Bi(1)-N(3)	150.98(5)
N(2)-C(4)	1.469(2)	N(1)-Bi(1)-N(3)	51.59(5)
N(3)-C(4)	1.460(3)	Cl(2)-Bi(1)-N(3)	126.61(4)
N(3)-C(6)	1.461(3)	Cl(3)-Bi(1)-Cl(1)	95.057(18)
N(3)-C(5)	1.465(3)	N(2)-Bi(1)-Cl(1)	125.63(4)
N(4)-C(11)	1.345(3)	N(5)-Bi(1)-Cl(1)	84.18(4)
N(4)-C(7)	1.348(3)	N(1)-Bi(1)-Cl(1)	94.86(4)
N(5)-C(16)	1.336(3)	Cl(2)-Bi(1)-Cl(1)	157.178(16)
N(5)-C(12)	1.339(3)	N(3)-Bi(1)-Cl(1)	74.42(4)
C(7)-C(8)	1.384(3)	Cl(3)-Bi(1)-N(4)	159.09(4)
C(8)-C(9)	1.387(3)	N(2)-Bi(1)-N(4)	119.47(5)
C(9)-C(10)	1.385(3)	N(5)-Bi(1)-N(4)	77.09(5)
C(10)-C(11)	1.386(3)	N(1)-Bi(1)-N(4)	75.21(5)
C(12)-C(13)	1.388(3)	Cl(2)-Bi(1)-N(4)	81.16(4)
C(13)-C(14)	1.374(4)	N(3)-Bi(1)-N(4)	117.31(5)
C(14)-C(15)	1.379(3)	Cl(1)-Bi(1)-N(4)	80.54(4)
C(15)-C(16)	1.388(3)	C(2)-N(1)-C(1)	112.04(17)
		C(2)-N(1)-C(6)	109.68(17)

C(1)-N(1)-C(6)	111.77(17)	C(7)-N(4)-Bi(1)	121.38(14)
C(2)-N(1)-Bi(1)	94.17(12)	C(16)-N(5)-C(12)	117.4(2)
C(1)-N(1)-Bi(1)	131.32(14)	C(16)-N(5)-Bi(1)	119.25(14)
C(6)-N(1)-Bi(1)	95.36(12)	C(12)-N(5)-Bi(1)	123.06(15)
C(2)-N(2)-C(3)	113.09(17)	N(2)-C(2)-N(1)	105.55(16)
C(2)-N(2)-C(4)	109.73(17)	N(3)-C(4)-N(2)	105.16(16)
C(3)-N(2)-C(4)	112.87(17)	N(3)-C(6)-N(1)	106.26(16)
C(2)-N(2)-Bi(1)	94.99(12)	N(4)-C(7)-C(8)	123.2(2)
C(3)-N(2)-Bi(1)	126.95(14)	C(7)-C(8)-C(9)	118.84(19)
C(4)-N(2)-Bi(1)	96.85(11)	C(10)-C(9)-C(8)	118.7(2)
C(4)-N(3)-C(6)	110.48(16)	C(9)-C(10)-C(11)	118.8(2)
C(4)-N(3)-C(5)	112.31(16)	N(4)-C(11)-C(10)	123.20(19)
C(6)-N(3)-C(5)	111.90(16)	N(5)-C(12)-C(13)	122.9(2)
C(4)-N(3)-Bi(1)	94.46(11)	C(14)-C(13)-C(12)	118.9(2)
C(6)-N(3)-Bi(1)	93.79(11)	C(13)-C(14)-C(15)	118.9(2)
C(5)-N(3)-Bi(1)	131.45(13)	C(14)-C(15)-C(16)	118.7(2)
C(11)-N(4)-C(7)	117.23(18)	N(5)-C(16)-C(15)	123.1(2)
C(11)-N(4)-Bi(1)	121.23(13)		

X-ray Data Collection, Structure Solution and Refinement for **15.7**.

A red crystal of approximate dimensions 0.110 x 0.108 x 0.096 mm was mounted in a cryoloop and transferred to a Bruker SMART APEX II diffractometer system. The APEX2[74] program package and the CELL_NOW[75] were used to determine the unit-cell parameters. Data was collected using a 60 sec/frame scan time. The raw frame data was processed using SAINT[76] and TWINABS[77] to yield the reflection data file (HKLF 5 format). Subsequent calculations were carried out using the SHELXTL[78] program package. The diffraction symmetry was 2/*m* and the systematic absences were consistent with the monoclinic space group $P2_1/n$ that was later determined to be correct.

The structure was solved by direct methods and refined on F^2 by full-matrix least-squares techniques. The analytical scattering factors[79] for neutral atoms were used throughout the analysis. Hydrogen atoms were included using a riding model.

Least-squares analysis yielded wR2 = 0.0611 and Goof = 1.123 for 149 variables refined against 4174 data (0.78 Å), R1 = 0.0388 for those 3641 with I > 2.0σ(I). The structure was refined as a two-component twin, BASF[78] = 0.2818(7).

Table 15.14: Bond lengths [Å] and angles [°] for **15.7**.

Bi(1)-N(3)	2.536(7)	N(2)-Bi(1)-I(2)	94.23(17)
Bi(1)-N(1)	2.549(8)	I(1)-Bi(1)-I(2)	102.01(2)
Bi(1)-N(2)	2.580(7)	N(3)-Bi(1)-I(3)	94.50(16)
Bi(1)-I(1)	3.0106(8)	N(1)-Bi(1)-I(3)	158.70(17)
Bi(1)-I(2)	3.0594(8)	N(2)-Bi(1)-I(3)	90.91(17)
Bi(1)-I(3)	3.0671(8)	I(1)-Bi(1)-I(3)	101.07(3)
N(1)-C(1)	1.470(11)	I(2)-Bi(1)-I(3)	97.56(2)
N(1)-C(2)	1.476(11)	C(1)-N(1)-C(2)	109.0(7)
N(1)-C(9)	1.500(11)	C(1)-N(1)-C(9)	110.2(7)
N(2)-C(3)	1.481(12)	C(2)-N(1)-C(9)	112.7(7)
N(2)-C(4)	1.482(11)	C(1)-N(1)-Bi(1)	109.2(6)
N(2)-C(5)	1.492(12)	C(2)-N(1)-Bi(1)	103.3(5)
N(3)-C(7)	1.490(11)	C(9)-N(1)-Bi(1)	112.1(5)
N(3)-C(6)	1.493(11)	C(3)-N(2)-C(4)	111.0(7)
N(3)-C(8)	1.500(11)	C(3)-N(2)-C(5)	113.6(7)
C(2)-C(3)	1.527(13)	C(4)-N(2)-C(5)	110.5(8)
C(5)-C(6)	1.516(12)	C(3)-N(2)-Bi(1)	111.8(5)
C(8)-C(9)	1.492(13)	C(4)-N(2)-Bi(1)	107.4(5)
N(3)-Bi(1)-N(1)	70.5(2)	C(5)-N(2)-Bi(1)	102.0(5)
N(3)-Bi(1)-N(2)	70.2(2)	C(7)-N(3)-C(6)	110.8(7)
N(1)-Bi(1)-N(2)	70.1(2)	C(7)-N(3)-C(8)	109.4(7)
N(3)-Bi(1)-I(1)	90.60(16)	C(6)-N(3)-C(8)	112.9(7)
N(1)-Bi(1)-I(1)	94.28(17)	C(7)-N(3)-Bi(1)	107.7(5)
N(2)-Bi(1)-I(1)	158.25(16)	C(6)-N(3)-Bi(1)	112.6(5)
N(3)-Bi(1)-I(2)	160.49(16)	C(8)-N(3)-Bi(1)	103.0(5)
N(1)-Bi(1)-I(2)	93.56(17)	N(1)-C(2)-C(3)	113.1(7)

N(2)-C(3)-C(2)	112.7(7)	C(9)-C(8)-N(3)	113.6(7)
N(2)-C(5)-C(6)	112.6(8)	C(8)-C(9)-N(1)	112.7(7)
N(3)-C(6)-C(5)	113.2(7)		

References

(1) Wedal, J. C.; Evans, W. J. A Rare-Earth Metal Retrospective to Stimulate All Fields. *J. Am. Chem. Soc.* **2021**, *143*, 18354–18367, DOI: 10.1021/jacs.1c08288.

(2) Shannon, R. D. Revised Effective Ionic Radii and Systematic Studies of Interatomic Distances in Halides and Chalcogenides. *Acta Crystallogr. Sect. A* **1976**, *32*, 751–767, DOI: 10.1107/S0567739476001551.

(3) Evans, W. J. Tutorial on the Role of Cyclopentadienyl Ligands in the Discovery of Molecular Complexes of the Rare-Earth and Actinide Metals in New Oxidation States. *Organometallics* **2016**, *35*, 3088–3100, DOI: 10.1021/acs.organomet.6b00466.

(4) Woen, D. H.; Evans, W. J. Expanding the +2 Oxidation State of the Rare-Earth Metals, Uranium, and Thorium in Molecular Complexes. In *Handbook on the Physics and Chemistry of Rare Earths*; Bünzli, J.-C., Pecharsky, V. K., Eds.; Elsevier B.V., 2016; pp 1–57, DOI: 10.1016/bs.hpcre.2016.08.002.

(5) Battaglia, L. Pietro; Corradi, A. B.; Pelizzi, G.; Tani, M. E. V. Cationic and Anionic Bismuth(III) in Chloro-Thiourea Complexes: Crystal Structure of $[Bi(tu)_6][Bi\{(tu)_{1.5}Cl_{1.5}\}Cl_3]_2$ (tu = thiourea). *J. Chem. Soc. Dalton Trans.* **1977**, No. 12, 1141, DOI: 10.1039/dt9770001141.

(6) Jones, P. G.; Henschel, D.; Weitze, A.; Blaschette, A. Kristall- und Molekülstruktur von fac-Trichloro-Tris(Dimethylsulfoxid)Bismut(III) $BiCl_3(DMSO)_3$. *Z. Anorg. Allg. Chem.* **1994**, *620*, 1037–1040, DOI: 10.1002/zaac.19946200615.

(7) Eveland, J. R.; Whitmire, K. H. Complexes of Bismuth(III) Chloride with Oxygen Donor

Ligands. Structural Characterization of $BiCl_3$·3THF, $BiCl_3$·diglyme and $BiCl_3$·diethylcarbitol. *Inorg. Chim. Acta* **1996**, *249*, 41–46, DOI: 10.1016/0020-1693(96)05024-4.

(8) Carmalt, C. J.; Clegg, W.; Elsegood, M. R. J.; Errington, R. J.; Havelock, J.; Lightfoot, P.; Norman, N. C.; Scott, A. J. Tetrahydrofuran Adducts of Bismuth Trichloride and Bismuth Tribromide. *Inorg. Chem.* **1996**, *35*, 3709–3712, DOI: 10.1021/ic951635f.

(9) Clegg, W.; Errington, R. J.; Flynn, R. J.; Green, M. E.; Hockless, D. C. R.; Norman, N. C.; Gibson, V. C.; Tavakkoli, K. Edge-Shared, Bioctahedral, Bismuth Phosphine Complexes. *J. Chem. Soc. Dalton Trans.* **1992**, No. 10, 1753, DOI: 10.1039/dt9920001753.

(10) Clegg, W.; Elsegood, M. R. J.; Graham, V.; Norman, N. C.; Pickett, N. L.; Tavakkoli, K. Neutral Phosphine Complexes of Antimony(III) and Bismuth(III) Halides. *J. Chem. Soc. Dalton Trans.* **1994**, No. 12, 1743, DOI: 10.1039/dt9940001743.

(11) Battaglia, L. P.; Corradi, A. B.; Nardelli, M.; Tani, M. E. V. X-Ray Crystal Structures of μ 4 -Chloro-{tris[Trichloro(Thiosemicarbazide)-Bismuth(III)]}[Tris(Thiosemicarbazide)Bismuth(III)] Hexachlorobismuthate(III) Chloride and Catena-μ-Chloro-Dichlorobis(Ethylenethiourea)-Bismuth(III). *J. Chem. Soc., Dalton Trans.* **1978**, No. 6, 583–587, DOI: 10.1039/DT9780000583.

(12) Majumdar, A.; Holm, R. H. Specific Incorporation of Chalcogenide Bridge Atoms in Molybdenum/Tungsten-Iron-Sulfur Single Cubane Clusters. *Inorg. Chem.* **2011**, *50*, 11242–11251, DOI: 10.1021/ic2018117.

(13) Armanasco, N. L.; Baker, M. V.; North, M. R.; Skelton, B. W.; White, A. H. Comparative Investigation of the Group 6 (Cr, Mo or W) Metal Carbonyl Complexes of 1,3,5-Triazacyclohexanes. *J. Chem. Soc. Dalton Trans.* **1998**, *6*, 1145–1150, DOI:

10.1039/a708888d.

(14) Partyka, D. V.; Staples, R. J.; Holm, R. H. Nucleophilic Reactivity and Oxo/Sulfido Substitution Reactions of $M^{VI}O_3$ Groups (M = Mo, W). *Inorg. Chem.* **2003**, *42*, 7877–7886, DOI: 10.1021/ic030185l.

(15) Baker, M. V.; North, M. R.; Skelton, B. W.; White, A. H. Oxidations of (R3tach)M(CO)3 Complexes [M = Cr, Mo, W; R_3tach = 1,3,5-Trialkyl-1,3,5-Triazacyclohexane (R = t-Bu, Bn)]. Crystal Structures of (t-Bu_3Tach)$MO_3 \cdot 15H_2O$ (M = Mo, W). *Inorg. Chem.* **1999**, *38*, 4515–4521, DOI: 10.1021/ic990031z.

(16) Braband, H.; Imstepf, S.; Felber, M.; Spingler, B.; Alberto, R. Triazacyclohexane (Tach) Complexes of High-Valent Rhenium: Syntheses of $[(R_3tach)ReO_3]^+$ ($R = -CH_3, -CH_2C_6H_5$) and Its Substitution Reactions. *Inorg. Chem.* **2010**, *49*, 1283–1285, DOI: 10.1021/ic902114p.

(17) Willey, G. R.; Woodman, T. J.; Somasundaram, U.; Aris, D. R.; Errington, W. Azamacrocyclic Stabilisation of the Halogenocations MX_3^+ Where M = Ge or Sn and X = Cl or Br. Synthesis and Molecular Structures of $[GeCl_3(L^1)]^+_2[H_3O]^+Cl^-_3 \cdot MeCN$, $[SnCl_3(L^1)]^+_2[SnCl_6]^{2-} \cdot 4MeCN$, $[GeBr_3(L^2)]^+_2[MeNH_3]^+Br^-_3 \cdot MeCN$ and $[SnBr_3(L^2)]^+_2[SnBr_6]^{2-}$ Where. *J. Chem. Soc. Dalton Trans.* **1998**, *2*, 2573–2576, DOI: 10.1039/a803175d.

(18) Bradley, D. C.; Frigo, D. M.; Harding, I. S.; Hursthouse, M. B.; Motevalli, M. A Six-Coordinate Complex of Indium(III) Containing Trimethylindium Bonded to N,N′,N″-Triisopropyl-1,3,5-Triazacyclohexane. *J. Chem. Soc. Chem. Commun.* **1992**, No. 7, 577–578, DOI: 10.1039/C39920000577.

(19) Willey, G. R.; Daly, L. T.; Rudd, M. D.; Drew, M. G. B. Azamacrocyclic Complexation of

Bismuth(III): Formation and Structure of fac-($BiCl_3 \cdot Me_3[9]aneN_3$) Where $Me_3[9]aneN_3$ = 1,4,7-Trimethyl-1,4,7-Triazacyclononane. *Polyhedron* **1995**, *14*, 315–318, DOI: 10.1016/0277-5387(94)00348-I.

(20) Di Vaira, M.; Mani, F.; Stoppioni, P. Lead(II) and Bismuth(III) Complexes with Macrocyclic Ligands. *Eur. J. Inorg. Chem.* **1999**, *1999*, 833–837, DOI: 10.1002/(SICI)1099-0682(199905)1999:5<833::AID-EJIC833>3.0.CO;2-1.

(21) Willey, G. R.; Daly, L. T.; Meehan, P. R.; Drew, M. G. B. Controlled Hydrolysis Reactions of the Group 15 Element–Azamacrocyclic Complexes MCl_3L (M = As, Sb or Bi; L = 1,4,7-Trimethyl-1,4,7-Triazacyclononane). Formation and Crystal Structures of $[AsCl_2L][As_2OCl_5]$, $[H_2L]_2[Sb_2OCl_6]Cl_2$, [HL]I and $[H_2L]_2[Sb_2Cl_9]Cl$. *J. Chem. Soc. Dalton Trans.* **1996**, No. 21, 4045–4053, DOI: 10.1039/DT9960004045.

(22) Wieghardt, K. 1,4,7-Triazacyclononane and N,N'N''-Trimethyl-1,4,7-Triazacyclononane - Two Versatile Macrocycles for the Synthesis of Monomeric and Oligomeric Metal Complexes. *Pure Appl. Chem.* **1988**, *60*, 509–516, DOI: 10.1351/pac198860040509.

(23) Lindoy, L. F. Recent Developments in the Synthesis and D-Block Chemistry of Linked Multi-Ring Macrocyclic Ligands. In *Macrocyclic Chemistry*; Gloe, K., Ed.; Springer: Dordrecht, 2005; pp 53–66, DOI: 10.31080/asps.2020.04.0500.

(24) Macedi, E.; Bencini, A.; Caltagirone, C.; Lippolis, V. The Design of TACN-Based Molecular Systems for Different Supramolecular Functions. *Coord. Chem. Rev.* **2020**, *407*, 213151, DOI: 10.1016/j.ccr.2019.213151.

(25) Chaudhuri, P.; Wieghardt, K. The Chemistry of 1,4,7-Triazacyclononane and Related Tridentate Macrocyclic Compounds. In *Progress in Inorganic Chemistry*; Lippard, S. J., Ed.; John Wiley & Sons, Inc., 2007; pp 329–436, DOI: 10.1002/9780470166369.ch4.

(26) Zeimentz, P. M.; Arndt, S.; Elvidge, B. R.; Okuda, J. Cationic Organometallic Complexes of Scandium, Yttrium, and the Lanthanoids. *Chem. Rev.* **2006**, *106*, 2404–2433, DOI: 10.1021/cr050574s.

(27) Bambirra, S.; Meetsma, A.; Hessen, B. Tris(4-Methylbenzyl)(1,4,7-Trimethyl-1,4,7-Triazacyclononane)Lanthanum(III). *Acta Crystallogr. Sect. E Struct. Reports Online* **2007**, *63*, m2891–m2891, DOI: 10.1107/S1600536807053640.

(28) Everett, M.; Jolleys, A.; Levason, W.; Light, M. E.; Pugh, D.; Reid, G. Cationic Aza-Macrocyclic Complexes of Germanium(II) and Silicon(IV). *Dalton Trans.* **2015**, *44*, 20898–20905, DOI: 10.1039/c5dt03941j.

(29) Wieghardt, K.; Kleine-Boymann, M.; Nuber, B.; Weiss, J. Complexes of Thallium(I) and -(III) Containing 1,4,7-Triazacyclononane (L) Ligands. Kinetics and Mechanism of the Reduction of $[L_2Tl^{III}]^{3+}$. Crystal Structure of (N,N',N"-Trimethyl-1,4,7-Triazacyclononane)Thallium(I) Hexafluorophosphate. *Inorg. Chem.* **1986**, *25*, 1309–1313, DOI: 10.1021/ic00229a003.

(30) Cheng, F.; Hector, A. L.; Levason, W.; Reid, G.; Webster, M.; Zhang, W. Preparation and Structure of the Unique Silicon(Iv) Cation $[SiF_3(Me_3tacn)]^+$. *Chem. Commun.* **2009**, *3*, 1334, DOI: 10.1039/b822236c.

(31) Cheng, F.; Davis, M. F.; Hector, A. L.; Levason, W.; Reid, G.; Webster, M.; Zhang, W. Synthesis, Spectroscopic and Structural Systematics of Complexes of Germanium(IV) Halides (GeX_4, X = F, Cl, Br or I) with Mono-, Bi- and Tri-Dentate and Macrocyclic Nitrogen Donor Ligands. *Eur. J. Inorg. Chem.* **2007**, *2007*, 4897–4905, DOI: 10.1002/ejic.200700727.

(32) Willey, G. R.; Aris, D. R.; Haslop, J. V.; Errington, W. Adducts of Indium(III) Bromide:

Synthesis and Structural Characterisation of [$InBr_3(THF)_2$], [$InBr_3(DMF)_3$], [$InBr_3(Me_3[9]aneN3)$] and [$InBr_3(\{–N(Me)–CH_2–\}_3)$]. *Polyhedron* **2001**, *20*, 423–429, DOI: 10.1016/S0277-5387(00)00641-0.

(33) Willey, G. R.; Aris, D. R.; Beaumont, A. L.; Errington, W. The Structure of [$GaBr_3(Me_3[9]aneN_3)$]: The First Example of a Six Co-ordinate Gallium(III) Bromide Complex. *Main Gr. Met. Chem.* **1999**, *22*, 515–518, DOI: 10.1515/MGMC.1999.22.8.515.

(34) Willey, G. R.; Spry, M. P.; Drew, M. G. B. Azamacrocyclic Stabilization of $SbCl^{2+}$: Synthesis and Crystal Structure of [$SbCl_2(Me_3[9]aneN_3)][SbCl_6$] Showing Explicit Sb^{III} Lone-Pair Stereochemical Activity. $Me_3[9]aneN_3$ = 1,4,7-Trimethyl-1,4,7-Triazacyclononane. *Polyhedron* **1996**, *15*, 4497–4500, DOI: 10.1016/0277-5387(96)00225-2.

(35) Cheng, F.; Hector, A. L.; Levason, W.; Reid, G.; Webster, M.; Zhang, W. Germanium(II) Dications Stabilized by Azamacrocycles and Crown Ethers. *Angew. Chem. Int. Ed.* **2009**, *48*, 5152–5154, DOI: 10.1002/anie.200901247.

(36) Biswas, B.; Salunke-Gawali, S.; Weyhermüller, T.; Bachler, V.; Bill, E.; Chaudhuri, P. Metal-Complexes As Ligands to Generate Asymmetric Homo- and Heterodinuclear $M_A^{III}M_B^{II}$ Species: A Magneto-Structural and Spectroscopic Comparison of Imidazole-N versus Pyridine-N. *Inorg. Chem.* **2010**, *49*, 626–641, DOI: 10.1021/ic9018426.

(37) Sobota, P.; Utko, J.; Szafert, S. Ionization of YCl_3 in Tetrahydrofuran. Crystal Structures of the [*trans*-$YCl_2(THF)_5$][*trans*-$YCl_4(THF)_2$] Salt and Polymeric $[YCl_3.2THF]_\infty$ Compounds. *Inorg. Chem.* **1994**, *33*, 5203–5206, DOI: 10.1021/ic00101a011.

(38) Tershansy, M. A.; Goforth, A. M.; Smith, M. D.; zur Loye, H.-C. The Synthesis and Crystal Structure of [$BiI_2(tpy)_2$][$Bi_2I_7(tpy)$]: A New Metal Halide Material. *J. Chem. Crystallogr.*

2008, *38*, 453–459, DOI: 10.1007/s10870-008-9342-x.

(39) Wedal, J. C.; Bekoe, S.; Ziller, J. W.; Furche, F.; Evans, W. J. C–H Bond Activation via U(II) in the Reduction of Heteroleptic Bis(Trimethylsilyl)Amide U(III) Complexes. *Organometallics* **2020**, *39*, 3425–3432, DOI: 10.1021/acs.organomet.0c00496.

(40) Wedal, J. C.; Windorff, C. J.; Huh, D. N.; Ryan, A. J.; Ziller, J. W.; Evans, W. J. Structural Variations in Cyclopentadienyl Uranium(III) Iodide Complexes. *J. Coord. Chem.* **2021**, *74*, 74–91, DOI: 10.1080/00958972.2020.1856824.

(41) Schumann, H.; Meese-Marktscheffel, J. A.; Esser, L. Synthesis, Structure, and Reactivity of Organometallic .Pi.-Complexes of the Rare Earths in the Oxidation State Ln^{3+} with Aromatic Ligands. *Chem. Rev.* **1995**, *95*, 865–986, DOI: 10.1021/cr00036a004.

(42) Manriquez, J. M.; Fagan, P. J.; Marks, T. J. Bis(Pentamethylcyclopentadienyl)Actinide Chemistry: Properties of Stable Thorium and Uranium Dialkyls and Hydrides. *J. Am. Chem. Soc.* **1978**, *100*, 3939–3941, DOI: 10.1021/ja00480a053.

(43) Fagan, P. J.; Manriquez, J. M.; Maatta, E. A.; Seyam, A. M.; Marks, T. J. Synthesis and Properties of Bis(Pentamethylcyclopentadienyl) Actinide Hydrocarbyls and Hydrides. A New Class of Highly Reactive f-Element Organometallic Compounds. *J. Am. Chem. Soc.* **1981**, *103*, 6650–6667, DOI: 10.1021/ja00412a021.

(44) Edelmann, F. T. Scandium, Yttrium, and the Lanthanide and Actinide Elements, Excluding Zero Oxidation State Complexes. In *Comprehensive Organometallic Chemistry II*; Abel, E. W., Stone, F. G. A., Wilkinson, G., Eds.; Elsevier B.V., 1995; pp 11–212, DOI: 10.1016/B978-008046519-7.00026-5.

(45) Ortu, F. Rare Earth Starting Materials and Methodologies for Synthetic Chemistry. *Chem. Rev.* **2022**, *122*, 6040–6116, DOI: 10.1021/acs.chemrev.1c00842.

(46) Poli, R. Open-Shell Organometallics as a Bridge between Werner-Type and Low-Valent Organometallic Complexes. The Effect of the Spin State on the Stability, Reactivity, and Structure. *Chem. Rev.* **1996**, *96*, 2135–2204, DOI: 10.1021/cr9500343.

(47) Hey-Hawkins, E. Bis(Cyclopentadienyl)Zirconium(IV) or Hafnium-(IV) Compounds with Si-, Ge-, Sn-, N-, P-, As-, Sb-, O-, S-, Se-, Te-, or Transition Metal-Centered Anionic Ligands. *Chem. Rev.* **1994**, *94*, 1661–1717, DOI: 10.1021/cr00030a009.

(48) Krieck, S.; Görls, H.; Westerhausen, M. Mechanistic Elucidation of the Formation of the Inverse Ca(I) Sandwich Complex $[(THF)_3Ca(\mu\text{-}C_6H_3\text{-}1,3,5\text{-}Ph_3)Ca(THF)_3]$ and Stability of Aryl-Substituted Phenylcalcium Complexes. *J. Am. Chem. Soc.* **2010**, *132*, 12492–12501, DOI: 10.1021/ja105534w.

(49) Westerhausen, M.; Schwarz, W. Synthese Und Spekroskopische Charakterisierung von Erdalkalimetallbis[Bis(Trimethylsilyl Phosphaniden]—Molekülstrukturen von $Ca[P(SiMe_3)_2]_2{\cdot}_2$TMTA Und $Ba[P(SiMe_3])_2]_2{\cdot}4$THF. *J. Organomet. Chem.* **1993**, *463*, 51–63, DOI: 10.1016/0022-328X(93)83398-F.

(50) Hülsmann, M.; Neumann, B.; Stammler, H.; Mitzel, N. W. Complex Formation of Calcium Bis(Tetraethylaluminate) with N-Donor Ligands. *Eur. J. Inorg. Chem.* **2012**, *2012*, 4200–4209, DOI: 10.1002/ejic.201200453.

(51) Bojer, D.; Venugopal, A.; Mix, A.; Neumann, B.; Stammler, H.; Mitzel, N. W. C-H Activation versus Yttrium–Methyl Cation Formation from $[Y(AlMe_4)_3]$ Induced by Cyclic Polynitrogen Bases: Solvent and Substituent-Size Effects. *Chem. Eur. J.* **2011**, *17*, 6248–6255, DOI: 10.1002/chem.201003317.

(52) Nieland, A.; Lamm, J.-H.; Mix, A.; Neumann, B.; Stammler, H.-G.; Mitzel, N. W. Alkynyl Compounds of the Rare-Earth Metals. *Z. Anorg. Allg. Chem.* **2014**, *640*, 2484–2491, DOI:

10.1002/zaac.201400158.

(53) Bojer, D.; Neumann, B.; Stammler, H.; Mitzel, N. W. Substituent Size Effects in Lewis Base Induced Reductions in Organolanthanide Chemistry. *Chem. Eur. J.* **2011**, *17*, 6239–6247, DOI: 10.1002/chem.201002707.

(54) Bojer, D.; Venugopal, A.; Neumann, B.; Stammler, H.-G.; Mitzel, N. W. Lewis Base Induced Reductions in Organolanthanide Chemistry. *Angew. Chem. Int. Ed.* **2010**, *49*, 2611–2614, DOI: 10.1002/anie.200906952.

(55) Raymond, K. N.; Eigenbrot, C. W. Structural Criteria for the Mode of Bonding of Organoactinides and -Lanthanides and Related Compounds. *Acc. Chem. Res.* **1980**, *13*, 276–283, DOI: 10.1021/ar50152a005.

(56) Bojer, D.; Neumann, B.; Stammler, H.; Mitzel, N. W. Subtle Size Effects in C–H Activation Reactions of Lanthanum and Praseodymium Tetramethylaluminates by Neutral Trinitrogen Bases. *Eur. J. Inorg. Chem.* **2011**, *2011*, 3791–3796, DOI: 10.1002/ejic.201100425.

(57) Venugopal, A.; Kamps, I.; Bojer, D.; Berger, R. J. F.; Mix, A.; Willner, A.; Neumann, B.; Stammler, H.-G.; Mitzel, N. W. Neutral Ligand Induced Methane Elimination from Rare-Earth Metal Tetramethylaluminates up to the Six-Coordinate Carbide State. *Dalton Trans.* **2009**, No. 29, 5755, DOI: 10.1039/b905271b.

(58) Wu, L. M.; Wu, X. T.; Chen, L. Structural Overview and Structure-Property Relationships of Iodoplumbate and Iodobismuthate. *Coord. Chem. Rev.* **2009**, *253*, 2787–2804, DOI: 10.1016/j.ccr.2009.08.003.

(59) Kotov, V. Y.; Ilyukhin, A. B.; Buikin, P. A.; Yorov, K. E. Mixed Halide Hybrid Halobismuthates and Their in Situ Transformations. *Mendeleev Commun.* **2019**, *29*, 537–540, DOI: 10.1016/j.mencom.2019.09.020.

(60) Oswald, I. W. H.; Ahn, H.; Neilson, J. R. Influence of Organic Cation Planarity on Structural Templating in Hybrid Metal-Halides. *Dalton Trans.* **2019**, *48*, 16340–16349, DOI: 10.1039/c9dt03207j.

(61) Kou, B.; Zhang, W.; Ji, C.; Wu, Z.; Zhang, S.; Liu, X.; Luo, J. Tunable Optical Absorption in Lead-Free Perovskite-like Hybrids by Iodide Management. *Chem. Commun.* **2019**, *55*, 14174–14177, DOI: 10.1039/c9cc05365d.

(62) Goforth, A. M.; Tershansy, M. A.; Smith, M. D.; Peterson, L. R.; Kelley, J. G.; DeBenedetti, W. J. I.; Zur Loye, H. C. Structural Diversity and Thermochromic Properties of Iodobismuthate Materials Containing D-Metal Coordination Cations: Observation of a High Symmetry $[Bi_3I_{11}]^{2-}$ Anion and of Isolated I-Anions. *J. Am. Chem. Soc.* **2011**, *133*, 603–612, DOI: 10.1021/ja108278j.

(63) Mehring, M. From Molecules to Bismuth Oxide-Based Materials : Potential Homo- and Heterometallic Precursors and Model Compounds. *Coord. Chem. Rev.* **2007**, *251*, 974–1006, DOI: 10.1016/j.ccr.2006.06.005.

(64) Mitzi, D. B.; Brock, P. Structure and Optical Properties of Several Organic-Inorganic Hybrids Containing Corner-Sharing Chains of Bismuth Iodide Octahedra. *Inorg. Chem.* **2001**, *40*, 2096–2104, DOI: 10.1021/ic000622l.

(65) Zhu, X. H.; Mercier, N.; Frère, P.; Blanchard, P.; Roncali, J.; Allain, M.; Pasquier, C.; Riou, A. Effect of Mono- versus Di-Ammonium Cation of 2,2′-Bithiophene Derivatives on the Structure of Organic-Inorganic Hybrid Materials Based on Iodo Metallates. *Inorg. Chem.* **2003**, *42*, 5330–5339, DOI: 10.1021/ic034235y.

(66) Fisher, G. A.; Norman, N. C. The Structures of the Group 15 Element(III) Halides and Halogenoanions. In *Advances in Inorganic Chemistry*; Skyes, A. G., Ed.; Academic Press,

1994; pp 233–271, DOI: 10.1016/S0898-8838(08)60173-7.

(67) Bhalla, R.; Darby, C.; Levason, W.; Luthra, S. K.; McRobbie, G.; Reid, G.; Sanderson, G.; Zhang, W. Triaza-Macrocyclic Complexes of Aluminium, Gallium and Indium Halides: Fast ^{18}F and ^{19}F Incorporation via Halide Exchange under Mild Conditions in Aqueous Solution. *Chem. Sci.* **2014**, *5*, 381–391, DOI: 10.1039/c3sc52104d.

(68) Backes-Dahmann, G.; Herrmann, W.; Wieghardt, K.; Weiss, J. Preparation and Electrochemical Investigation of Monomeric Complexes of Molybdenum(0-VI) with the Ligand 1,4,7-Trimethyl-1,4,7-Triazacyclononane (L). Crystal Structure of $[Mo^{IV}LBr_3](PF_6)$. *Inorg. Chem.* **1985**, *24*, 485–491, DOI: 10.1021/ic00198a011.

(69) Hajela, S.; Schaefer, W. P.; Bercaw, J. E. Highly Electron Deficient Group 3 Organometallic Complexes Based on the 1,4,7-Trimethyl-1,4,7-Triazacyclononane Ligand System. *J. Organomet. Chem.* **1997**, *532*, 45–53, DOI: 10.1016/S0022-328X(96)06768-X.

(70) Curnock, E.; Levason, W.; Light, M. E.; Luthra, S. K.; McRobbie, G.; Monzittu, F. M.; Reid, G.; Williams, R. N. Group 3 Metal Trihalide Complexes with Neutral N-Donor Ligands – Exploring Their Affinity towards Fluoride. *Dalton Trans.* **2018**, *47*, 6059–6068, DOI: 10.1039/C8DT00480C.

(71) Petroff, Y.; Yu, P. Y.; Shen, Y. R. Absorption, Photoluminescence, and Resonant Raman Scattering in BiI_3. *Phys. Status Solidi* **1974**, *61*, 419–427, DOI: 10.1002/pssb.2220610206.

(72) Ageeva, T. A.; Golubev, D. V.; Gorshkova, A. S.; Ionov, A. M.; Koifman, O. I.; Mozhchil, R. N.; Rumyantseva, V. D.; Sigov, A. S.; Fomichev, V. V. Synthesis and Spectroscopic Studies of Bismuth(III) Iodide Porphyrins. *Macroheterocycles* **2018**, *11*, 155–161, DOI: 10.6060/mhc180171.

(73) Ozturk, I. I.; Banti, C. N.; Hadjikakou, S. K.; Panagiotou, N.; Tasiopoulos, A. J. Structural Architectures and Biological Properties of Main Group Bismuth(III) Iodide Complexes with Heterocyclic Thioamides. *Inorganica Chim. Acta* **2019**, *497*, 119094, DOI: 10.1016/j.ica.2019.119094.

(74) APEX2, Version 2014.11-0, Bruker AXS, Inc: Madison, WI 2014.

(75) Sheldrick, G. M. CELL_NOW, Version 2008/4, Bruker AXS, Inc: Madison, WI 2008.

(76) SAINT, Version 8.34a, Bruker AXS, Inc: Madison, WI 2013.

(77) Sheldrick, G. M. TWINABS, Version 2012/1, Bruker AXS, Inc: Madison, WI 2012.

(78) Sheldrick, G. M. SHELXTL, Version 2014/7, Bruker AXS, Inc: Madison, WI 2014.

(79) *International Tables for Crystallography*; Vol C, Kluwer Academic Publishers: Dordrecht, 1992.

(80) Sheldrick, G. M. SADABS, Version 2014/5, Bruker AXS, Inc: Madison, WI 2014.

Appendix A:

Reduction of Cp^{tet}_3Th and Synthesis of Cp^{tet}_2ThOAr'

Introduction

Currently, there is only a single ligand environment that supports the Th(II) ion in molecular species, namely in $[Cp''_3Th]^{1-}$.[1,2] It would be of interest to expand from this single example and find other ligand frameworks that could support the Th(II) ion to gain a better understanding of its reaction chemistry and how to manipulate the thorium redox processes. The recent electrochemical study (see Chapter 3) showed the Th(III)/Th(II) couple for Cp^{tet}_3Th at −3.28 V vs Fc^+/Fc in THF.[2] This is more negative than the −2.85 V for Cp''_3Th, as expected for a stronger electron donating ligand. Previous studies with Cp^{tet}_3Th, KC_8, and H_2 reported formation a green solution that may be a Th(II) species.[3] Based on this work, the reduction of Cp^{tet}_3Th under an argon atmosphere was attempted and reported in this Appendix.

Another ligand system that could provide a possible route to Th(II) complexes is the heteroleptic Cp^{tet}_2ThOAr', the analogs of the uranium complexes described in Chapter 5. This class of Th(III) complexes has not been explored, where the closest analogs are the amidinate and aluminate compounds $Cp^*_2Th[^iPrNC(Me)N^iPr]$ and $Cp^{tt}_2Th(\mu\text{–}H)_3AlC(SiMe_3)_3$.[4,5] A route to Cp^{tet}_2ThOAr' was envisioned via protonolysis from Cp^{tet}_3Th and $HOAr'$ and the results are reported in this Appendix.

Results and Discussion

Reduction of Cp^{tet}_3Th. Reaction of purple Cp^{tet}_3Th, crypt, and KC_8 in THF at −35°C leads to the formation of a dark green solution, Scheme A.1.

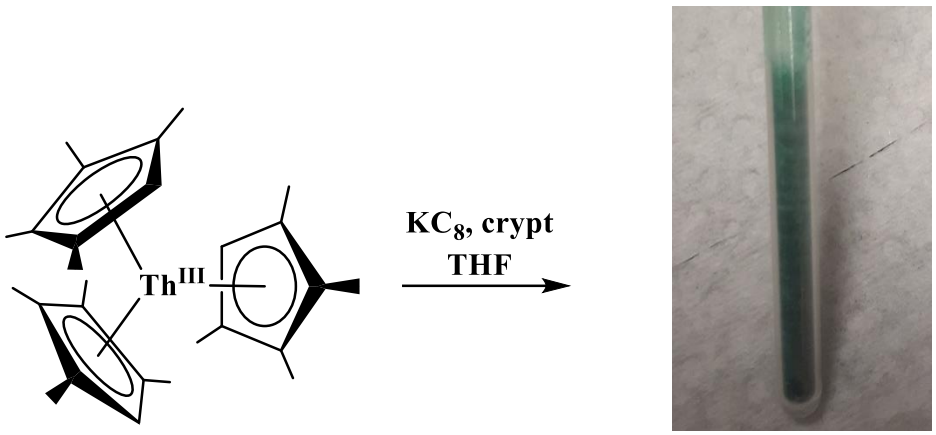

Scheme A.1: Reduction of Cp^{tet}_3Th and formation of a dark green solution, shown as a frozen THF solution inside an EPR tube.

The green species is unstable and decomposes to an orange solution at −35 °C over a few hours. From this mixture, $Cp^{tet}_2Th(H)(\eta^5:\eta^1\text{-}C_5HMe_3CH_2)$, Cp^{tet}_3ThH, and [K(crypt)][Cp^{tet}] could be identified by ^{1}H NMR and X-ray crystallography.[3] These are the same three products that result from the reduction of Cp^{tet}_3Th with KC_8 under an H_2 atmosphere,[3] although other species were also present. In the reaction in Scheme A.1, there were only the three products.

The EPR spectrum of the green product in Scheme A.1 was collected immediately after reduction. The spectrum in THF at 77 K in perpendicular mode is silent. The green compound is not stable enough for an EPR spectrum to be collected at room temperature as it decomposes readily. The lack of EPR signal in perpendicular mode suggests an integer spin system. If the green product is indeed a Th(II) species, this could either be a diamagnetic $6d^2$ Th(II) ion like what is observed for $[Cp''_3Th]^{1-}$,[6] or a triplet state having either a $5f^16d^1$ or $6d^2$ configuration. Based on the results for $[Cp''_3Th]^{1-}$, the DFT studies described in Chapter 2, and previous studies on $(C_5R_5)_3M$ complexes, the diamagnetic $6d^2$ configuration is expected to be favored for a Th(II) species like $[Cp^{tet}_3Th]^{1-}$.

To verify this hypothesis, DFT calculations were performed on $[Cp^{tet}_3Th]^{1-}$. The singlet state ($6d^2$ configuration) is favored over the triplet state ($5f^16d^1$ configuration) by 10.3 kcal/mol. The highest occupied molecular orbital is a doubly-occupied $6dz^2$-like orbital, Figure A.1. This orbital comprised of 43% 6d and 30% 7s character, as judged by Mulliken population analysis which systematically overestimates the amount of *n*s character. Minimal electron density resides in the π system the Cp^{tet} rings. Thus, $[Cp^{tet}_3Th]^{1-}$ can be best described as a diamagnetic Th(II) compound with a $6d^2$ electron configuration, much like $[Cp''_3Th]^{1-}$.

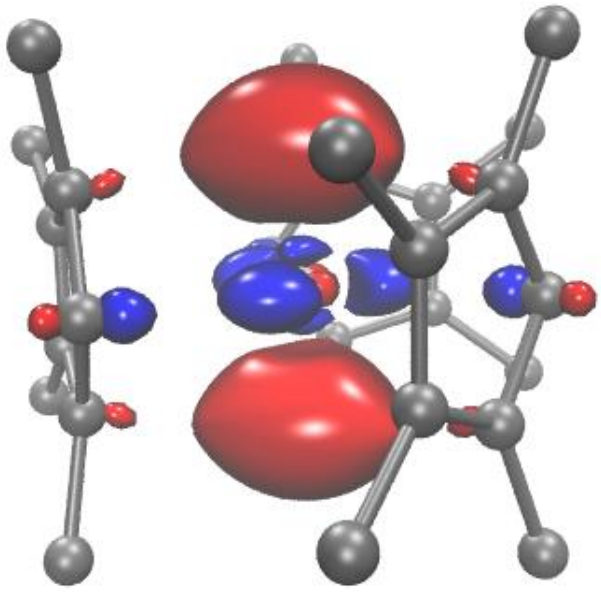

Figure A.1: Calculated $6dz^2$-like HOMO of $[Cp^{tet}_3Th]^{1-}$, plotted with contour value of 0.05.

Collection of the electronic absorption spectrum was attempted, but each attempt resulted in decomposition and the resulting UV-visible spectrum was collected of the yellow solution. The same results occurred when the UV-visible cell was kept chilled at −78 °C in a dry ice/isopropanol bath during transport from the glovebox to the spectrophotometer. Once the cell was removed from the cold bath and placed in the spectrometer, it quickly changed color. A different spectroscopy setup could be useful for collecting the low-temperature UV-visible spectrum of this green species. Likewise, crystallization to determine the exact identity of this compound must be

performed at low temperatures, likely below −78 °C. This was attempted in the cold well of the glovebox at −78 °C, but decomposition occurred before anything crystallized. The related $[Cp^{tet}_3U]^{1-}$ and $(C_5Me_5)_3Th$ complexes[7,8] can be synthesized and crystallographically characterized, which suggests that neither electronic or steric factors alone can explain the high reactivity and instability of "$[Cp^{tet}_3Th]^{1-}$.".

Time-dependent DFT was used to simulate the absorption spectrum of $[Cp^{tet}_3Th]^{1-}$. The computed spectrum is shown below in Figure A.2. The transitions at wavelengths longer than 480 nm (lower energy) are dominated by 6d to 5f and 6d to 7p transitions. Electronic transitions at higher energy are mainly 6d to 5f and 6d to ligand π (MLCT) in character, Table A.1. These transitions are predicted to be more intense than the related 6d to 5f and MLCT transitions observed for Cp^{tet}_3Th,[9] consistent with the intensity difference between Cp''_3Th and $[Cp''_3Th]^{1-}$.[1]

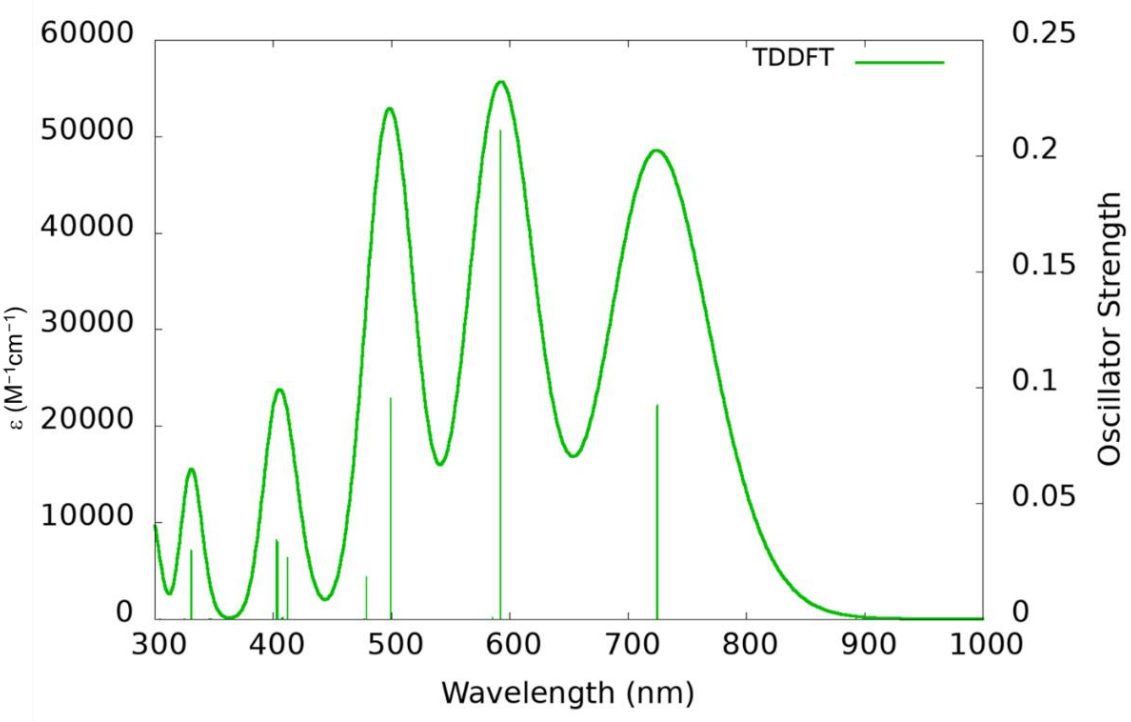

Figure A.2: Theoretical UV-visible spectrum with computed TDDFT oscillator strengths shown as vertical lines. A Gaussian line broadening of 0.15 eV was applied.

Table A.1: Electronic excitation summary for $[Cp^{tet}_3Th]^{1-}$. Only the dominant contribution to the transition is reported. 116a is the 6dz2-like HOMO. "Ligand" assignments denote the Cp^{tet} π system.

Wavelength (nm)	Oscillator Strength (len)	Occupied	Virtual	% Contribution	Assignment
725	0.092	116	120	92.7	6d-->5f
724	0.092	116	121	92.7	6d-->5f
593	0.211	116	122	97.5	6d-->7p
500	0.095	116	125	95.2	6d-->7p
500	0.095	116	124	95.3	6d-->7p
479	0.018	116	126	94.7	6d-->5f
412	0.026	116	128	93.9	6d-->ligand
408	0.001	116	131	88.7	6d-->5f/ligand
404	0.033	116	129	93.2	6d-->5f/ligand
403	0.034	116	130	94.4	6d-->5f/ligand
331	0.029	116	135	98.5	6d-->ligand
331	0.030	116	136	98.5	6d-->ligand
297	0.019	116	140	90.9	6d-->ligand
292	0.002	116	141	77.7	6d-->ligand
292	0.001	116	117	31.2	6d-->5f

Synthesis of Heteroleptic Cp^{tet}_2ThOAr'. Another potential candidate for reduction studies were heteroleptic Th(III) complexes. Chapter 5 described uranium complexes of the type $Cp^*_2UOAr^x$, where OAr^x = OAr′ and OAr*. It was of interest to determine if analogous thorium compound could be synthesized and subsequently reduced to make Th(II) compounds. These experiments have the added benefit of forming new Th(III) species, which are rare in general as described in Chapters 1, 3, 10, and 11.

Cp^{tet}_3Th appeared to react with both HOAr′ in toluene, eq A.1, forming a deep blue solution different from the purple solution of the starting material. Attempts to extract the products into hexane led to almost immediate discoloration of the solution, indicative of decomposition to Th(IV) products: the purple color would fade within seconds after hexane addition.

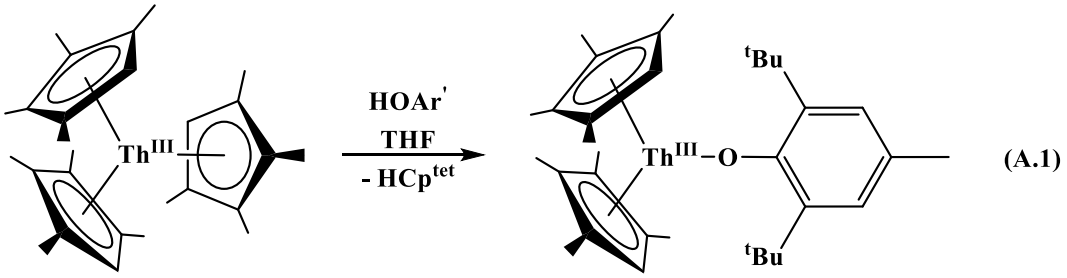

(A.1)

The dark blue/purple solids that were isolated from these reactions could be dissolved in toluene or THF without discoloration. The EPR spectrum at 77 K in toluene of the reaction mixture of Cp^{tet}_3Th and HOAr′ displayed an axial signal with *g* values of 1.98 and 1.86, and at room temperature an isotropic signal with *g* value of 1.89, Figure A.3. The signal at 77 K is practically identical to that of Cp^{tet}_3Th, which has *g* values of 1.98 and 1.86, but at room temperature the g value for Cp^{tet}_3Th is 1.92.[9] Based on previous EPR studies of $Cp^{tt}_2Th(\mu\text{–}H)_3AlCR_3$ (Cp^{tt} = $C_5{}^tBu_2H_3$; R = $SiMe_3$)[5] and $[(C_5Me_5)_2Y(NR_2)]^{1-}$,[10] the EPR spectrum of Cp^{tet}_2ThOAr' was predicted to exhibit a rhombic signal. However, $(C_5Me_5)_2Th[^iPrNC(Me)N^iPr]$ displays an axial EPR signal and adopts a pseudotetrahedral geometry[4] so this analysis must go beyond the simple geometric approximation. From the EPR spectrum, it was not clear whether the heteroleptic Th(III) compounds did indeed form and crystallization should be attempted to verify the composition. ^1H NMR studies could also be useful to compare with the NMR spectra of Cp^{tet}_3Th as an initial method to determine if a reaction did indeed occur.

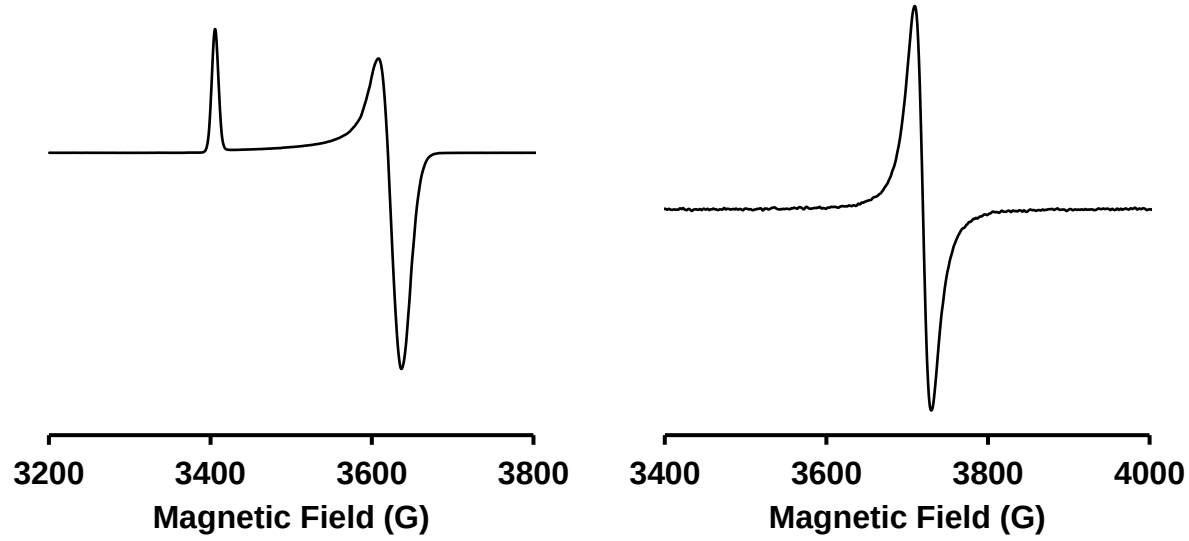

Figure A.3: X-band EPR spectrum of the reaction of Cp^{tet}_3Th with HOAr′, taken as a toluene solution at 77 K (left) and at room temperature (right).

Conclusion

The reduction of Cp^{tet}_3Th to form a Th(II) species such as [K(crypt)][Cp^{tet}_3Th] was attempted, forming a dark green solution which is EPR silent. DFT suggests the formation of a diamagnetic, $6d^2$ Th(II) compound like what was observed for $[Cp''_3Th]^{1-}$. The putative Cp^{tet}-ligated Th(II) species is extremely unstable and other ligand environments are likely necessary to form a stable Th(II) compounds. The synthesis of a heteroleptic compound such as Cp^{tet}_2ThOAr' was attempted, but definitive characterization of the product was elusive.

Experimental

All syntheses and manipulations were conducted under an Ar atmosphere with rigorous exclusion of air and water using standard glovebox techniques. Solvents were sparged with UHP argon and dried by passage through columns containing Q-5 and molecular sieves prior to use. EPR spectra were collected at X-band frequency on a Bruker EMX spectrometer equipped with an ER041Xg microwave bridge. Cp^{tet}_3Th[9] and KC_8[11] were synthesized via literature routes.

HOAr′ (Aldrich) was sublimed prior to use. 2.2.2-cryptand (crypt, Aldrich) was dried under 10^{-5} Torr for 12 h before use.

Reaction of Cp^{tet}_3Th with KC_8 and crypt. Cp^{tet}_3Th (20 mg, 0.034 mmol) and crypt (13 mg, 0.035 mmol) were dissolved in THF (2 mL) and chilled to −78 °C in the glovebox cold well. A separate vial of KC_8 was similarly chilled along with multiple pipets and an EPR tube. The KC8 was packed into a pipet to form a reduction column and the purple thorium solution was filtered through, causing a color change to bright green. An aliquot of this solution was immediately placed in the EPR tube and frozen for data collection. The green color persisted for a few hours at −78 °C but no crystals formed before decomposition occurred.

Reaction of Cp^{tet}_3Th with HOAr′. Cp^{tet}_3Th (21 mg, 0.035 mmol) was dissolved in toluene (5 mL). HOAr′ (19 mg, 0.086 mmol) was added to the stirring purple solution. The solution was stirred for two hours then dried under vacuum. Extraction into hexane led to the formation of a colorless solution. The solids were extracted into toluene, filtered, and dried to yield blue/purple and white solids (31 mg). EPR spectra were collected of the mixture as a frozen toluene solution.

Computational Details. Theoretical calculations on $[Cp^{tet}_3Th]^{1-}$ were carried out at the density functional level of theory using the TPSSh[12] functional with Grimme's D3 dispersion correction[13,14] in C_1 symmetry. Scalar relativistic effective core potentials (ECPs)[15] with the def-TZVP[16] basis set were used for Th and polarized split-valence basis sets with diffuse functions def2-SV(P)[17] were used for the other atoms. Quadrature grids of size 4 were used throughout.[18] The continuum solvation model COSMO[19] was included to model solvent effects with a dielectric constant of 7.52 and a refractive index of 1.41 for THF. [20] Geometry optimizations were computed starting from X-ray structure of Cp^{tet}_3Th with geometry convergence thresholds of 10^{-4} a.u. and

energy convergence of 10^{-8} a.u. Ground state geometries were confirmed by the lack of imaginary frequencies in the vibrational spectrum. Time-dependent DFT studies were performed with the same parameters as described above. Molecular orbitals were analyzed with VMD[21] and Mulliken population analysis. All computations were completed using the TURBOMOLE program suite, Version V7.4.1.[22,23]

References

(1) Langeslay, R. R.; Fieser, M. E.; Ziller, J. W.; Furche, F.; Evans, W. J. Synthesis, Structure, and Reactivity of Crystalline Molecular Complexes of the $\{[C_5H_3(SiMe_3)_2]_3Th\}^{1-}$ Anion Containing Thorium in the Formal +2 Oxidation State. *Chem. Sci.* **2015**, *6*, 517–521, DOI: 10.1039/C4SC03033H.

(2) Wedal, J. C.; Barlow, J. M.; Ziller, J. W.; Yang, J. Y.; Evans, W. J. Electrochemical Studies of Tris(Cyclopentadienyl)Thorium and Uranium Complexes in the +2, +3, and +4 Oxidation States. *Chem. Sci.* **2021**, *12*, 8501–8511, DOI: 10.1039/D1SC01906F.

(3) Langeslay, R. R.; Fieser, M. E.; Ziller, J. W.; Furche, F.; Evans, W. J. Expanding Thorium Hydride Chemistry Through Th^{2+}, Including the Synthesis of a Mixed-Valent Th^{4+}/Th^{3+} Hydride Complex. *J. Am. Chem. Soc.* **2016**, *138*, 4036–4045, DOI: 10.1021/jacs.5b11508.

(4) Walensky, J. R.; Martin, R. L.; Ziller, J. W.; Evans, W. J. Importance of Energy Level Matching for Bonding in Th^{3+}–Am^{3+} Actinide Metallocene Amidinates, $(C_5Me_5)_2[^iPrNC(Me)N^iPr]An$. *Inorg. Chem.* **2010**, *49*, 10007–10012, DOI: 10.1021/ic1013285.

(5) Altman, A. B.; Brown, A. C.; Rao, G.; Lohrey, T. D.; Britt, R. D.; Maron, L.; Minasian, S. G.; Shuh, D. K.; Arnold, J. Chemical Structure and Bonding in a Thorium(III)-Aluminum Heterobimetallic Complex. *Chem. Sci.* **2018**, *9*, 4317–4324, DOI: 10.1039/c8sc01260a.

(6) Kot, W. K.; Shalimoff, G. V.; Edelstein, N. M.; Edelman, M. A.; Lappert, M. F. [$Th^{III}\{\eta^5$-$C_5H_3(SiMe_3)_2\}_3$], an Actinide Compound with a $6d^1$ Ground State. *J. Am. Chem. Soc.* **1988**, *110*, 986–987, DOI: 10.1021/ja00211a059.

(7) Ryan, A. J.; Angadol, M. A.; Ziller, J. W.; Evans, W. J. Isolation of U(II) Compounds Using Strong Donor Ligands, C_5Me_4H and $N(SiMe_3)_2$, Including a Three-Coordinate U(II) Complex. *Chem. Commun.* **2019**, *55*, 2325–2327, DOI: 10.1039/C8CC08767A.

(8) Langeslay, R. R.; Chen, G. P.; Windorff, C. J.; Chan, A. K.; Ziller, J. W.; Furche, F.; Evans, W. J. Synthesis, Structure, and Reactivity of the Sterically Crowded Th^{3+} Complex $(C_5Me_5)_3Th$ Including Formation of the Thorium Carbonyl, $[(C_5Me_5)_3Th(CO)][BPh_4]$. *J. Am. Chem. Soc.* **2017**, *139*, 3387–3398, DOI: 10.1021/jacs.6b10826.

(9) Siladke, N. A.; Webster, C. L.; Walensky, J. R.; Takase, M. K.; Ziller, J. W.; Grant, D. J.; Gagliardi, L.; Evans, W. J. Actinide Metallocene Hydride Chemistry: C–H Activation in Tetramethylcyclopentadienyl Ligands to Form $[\mu$-η^5-$C_5Me_3H(CH_2)$-$\kappa C]^{2-}$ Tuck-over Ligands in a Tetrathorium Octahydride Complex. *Organometallics* **2013**, *32*, 6522–6531, DOI: 10.1021/om4008482.

(10) Jenkins, T. F.; Bekoe, S.; Ziller, J. W.; Furche, F.; Evans, W. J. Synthesis of a Heteroleptic Pentamethylcyclopentadienyl Yttrium(II) Complex, [K(2.2.2-Cryptand)]$\{(C_5Me_5)_2Y^{II}[N(SiMe_3)_2]\}$, and Its C–H Bond Activated Y(III) Derivative. *Organometallics* **2021**, *40*, 3917–3925, DOI: 10.1021/acs.organomet.1c00482.

(11) Bergbreiter, D. E.; Killough, J. M. Reactions of Potassium-Graphite. *J. Am. Chem. Soc.* **1978**, *100*, 2126–2134, DOI: 10.1021/ja00475a025.

(12) Staroverov, V. N.; Scuseria, G. E.; Tao, J.; Perdew, J. P. Comparative Assessment of a New Nonempirical Density Functional: Molecules and Hydrogen-Bonded Complexes. *J. Chem.*

Phys. **2003**, *119*, 12129–12137, DOI: 10.1063/1.1626543.

(13) Grimme, S. Semiempirical GGA-Type Density Functional Constructed with a Long-Range Dispersion Correction. *J. Comput. Chem.* **2006**, *27*, 1787–1799, DOI: 10.1002/jcc.20495.

(14) Grimme, S.; Antony, J.; Ehrlich, S.; Krieg, H. A Consistent and Accurate Ab Initio Parametrization of Density Functional Dispersion Correction (DFT-D) for the 94 Elements H-Pu. *J. Chem. Phys.* **2010**, *132*, 154104, DOI: 10.1063/1.3382344.

(15) Küchle, W.; Dolg, M.; Stoll, H.; Preuss, H. Energy-Adjusted Pseudopotentials for the Actinides. Parameter Sets and Test Calculations for Thorium and Thorium Monoxide. *J. Chem. Phys.* **1994**, *100*, 7535–7542, DOI: 10.1063/1.466847.

(16) Weigend, F.; Ahlrichs, R. Balanced Basis Sets of Split Valence, Triple Zeta Valence and Quadruple Zeta Valence Quality for H to Rn: Design and Assessment of Accuracy. *Phys. Chem. Chem. Phys.* **2005**, *7*, 3297–3305, DOI: 10.1039/b508541a.

(17) Schäfer, A.; Horn, H.; Ahlrichs, R. Fully Optimized Contracted Gaussian Basis Sets for Atoms Li to Kr. *J. Chem. Phys.* **1992**, *97*, 2571–2577.

(18) Treutler, O.; Ahlrichs, R. Efficient Molecular Numerical Integration Schemes. *J. Chem. Phys.* **1995**, *102*, 346–354, DOI: 10.1063/1.469408.

(19) Schäfer, A.; Klamt, A.; Sattel, D.; Lohrenz, J. C. W.; Eckert, F. COSMO Implementation in TURBOMOLE: Extension of an Efficient Quantum Chemical Code towards Liquid Systems. *Phys. Chem. Chem. Phys.* **2000**, *2*, 2187–2193, DOI: 10.1039/b000184h.

(20) CRC Handbook of Chemistry and Physics. In *CRC Handbook of Chemistry and Physics*; Haynes, W. M., Lide, D. R., Bruno, T. J., Eds.; CRC Press, 2016; pp 943–950.

(21) Humphrey, W.; Dalke, A.; Schulten, K. VMD: Visual Molecular Dynamics. *J. Mol. Graph.* **1996**, *14*, 33–38.

(22) TURBOMOLE V7.4.1. University of Karlsruhe and Forschungszentrum Karlsruhe GmbH.

(23) Balasubramani, S. G.; Chen, G. P.; Coriani, S.; Diedenhofen, M.; Frank, M. S.; Franzke, Y. J.; Furche, F.; Grotjahn, R.; Harding, M. E.; Hättig, C.; Hellweg, A.; Helmich-Paris, B.; Holzer, C.; Huniar, U.; Kaupp, M.; Marefat Khah, A.; Karbalaei Khani, S.; Müller, T.; Mack, F.; Nguyen, B. D.; Parker, S. M.; Perlt, E.; Rappoport, D.; Reiter, K.; Roy, S.; Rückert, M.; Schmitz, G.; Sierka, M.; Tapavicza, E.; Tew, D. P.; van Wüllen, C.; Voora, V. K.; Weigend, F.; Wodyński, A.; Yu, J. M. TURBOMOLE: Modular Program Suite for Ab Initio Quantum-Chemical and Condensed-Matter Simulations. *J. Chem. Phys.* **2020**, *152*, 184107, DOI: 10.1063/5.0004635.

Appendix B:

DFT Analysis of an Yttrium Complex Synthesized from the Ring-Opening of Benzoxazole

Results[†]

This Appendix describes DFT analysis on an yttrium complex synthesized via deprotonation and ring-opening of benzoxazole, C_7H_5NO, Figure B.1, and the mono-reduced product that results from reaction with KC_8.

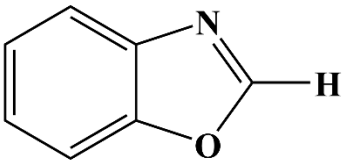

Figure B.1: Structure of benzoxazole.

The dark red compound $[(C_5Me_5)_2Y(\mu\text{-}2\text{-}CNC_6H_4O\text{-}\kappa C\text{:}\kappa O)]_2$, **B.1**, was synthesized by Megan Dumas from the allyl complex $(C_5Me_5)_2Y(C_3H_5)$ and benzoxazole in hexane, eq B.1. The Dy and Tb compounds were also synthesized by this same route.

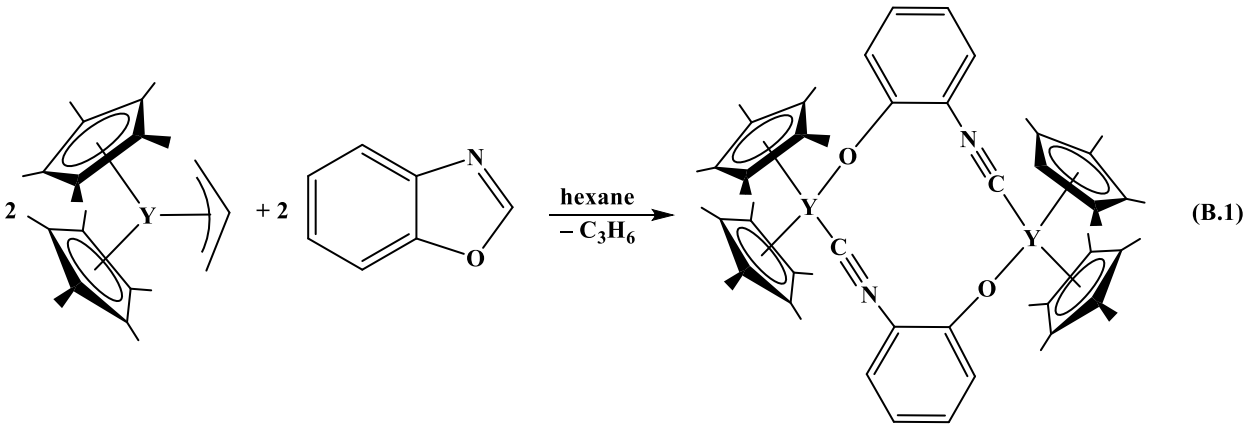

(B.1)

B.1

[†] Portions of this Appendix have been published: Dumas, M. T.; Jenkins, T. J.; Wedal, J. C.; Ziller, J. W.; Furche, F.; Evans, W. J. Synthesis of a 2-Isocyanophenolate Ligand, $(2\text{-}CNC_6H_4O)^{1-}$, by Ring-Opening of Benzoxazole with Rare Earth Metal Complexes, *Organometallics*, **2021**, *40*, 735-741, DOI: 10.1021/acs.organomet.1c00002.

The compound has a planar, 12-membered ring, comprised of two yttrium centers and the ring-opened benzoxazole moiety. **B.1** has overlapping, broad absorbance peaks between 350 and 550 nm responsible for the dark red color, Figure B.2. Intensely colored complexes are not common for trivalent rare earth metals and the large extinction coefficients observed are consistent with Laporte allowed charge transfer transitions involving the C_5Me_5 and 2-isocyanophenolate ligands.

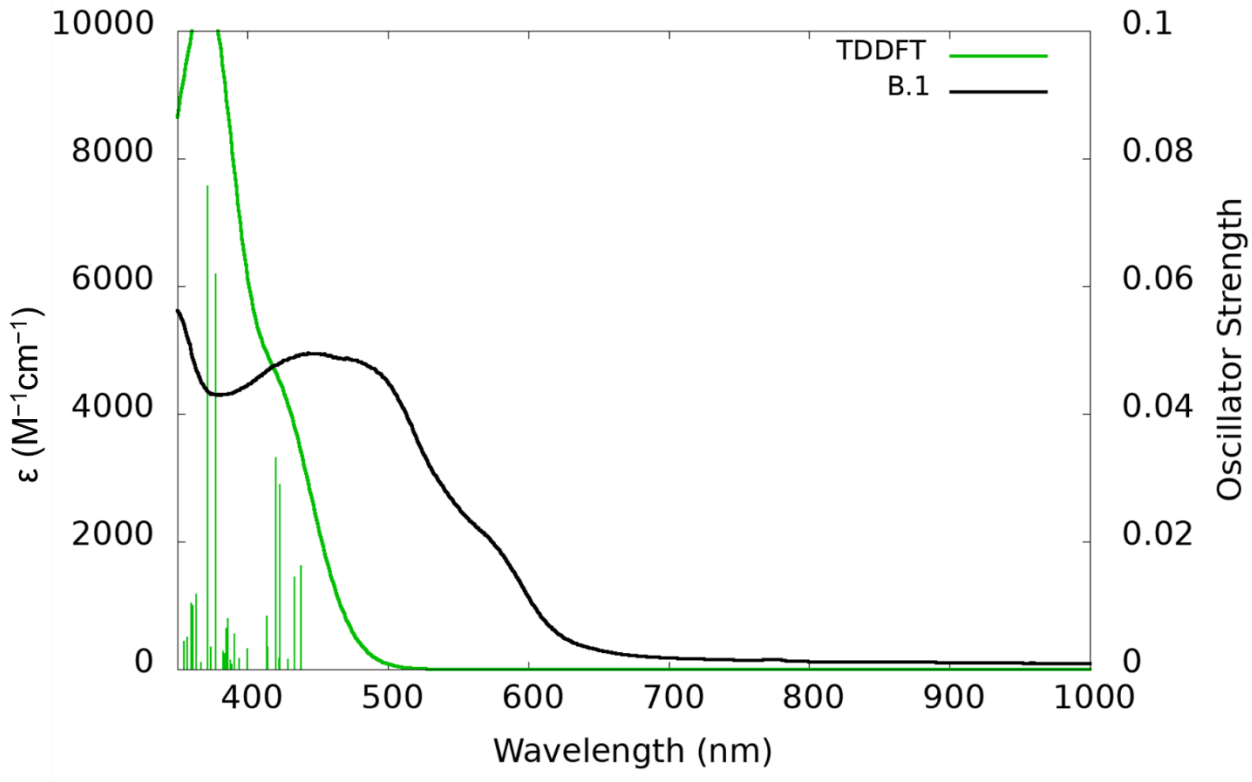

Figure B.2: UV-visible spectra **B.1** (black) and the simulated spectrum of **B.1** with TDDFT oscillator strengths shown as vertical lines (green). A Gaussian line broadening of 0.15 eV was applied and the computed excitation energies were empirically red shifted by 0.1 eV. To ease comparison, the computed intensities were scaled by a factor of 0.5.

To gain further insight into the electronic structure of the ring-opened product, geometry optimization calculations on **B.1** were completed using the TPSSh hybrid meta-generalized gradient density functional approximation.[1] Effective core potentials (ECPs)[2] with polarized

triple-ζ (def2-TZVP) basis sets[3] were used for Y and split-valence basis sets with polarization for non-hydrogen atoms (def2-SV(P)) were used elsewhere.[4] All calculations were performed with TURBOMOLE V7.4.1.[5,6] In the optimized ground state structure, the highest occupied molecular orbital (HOMO) resides in the π system of the C_5Me_5 rings, Figure B.3. The first lowest unoccupied molecular orbital (LUMO) is a π^* orbital on the $(CNC_6H_4O)^{1-}$ ligand, Figure B.3.

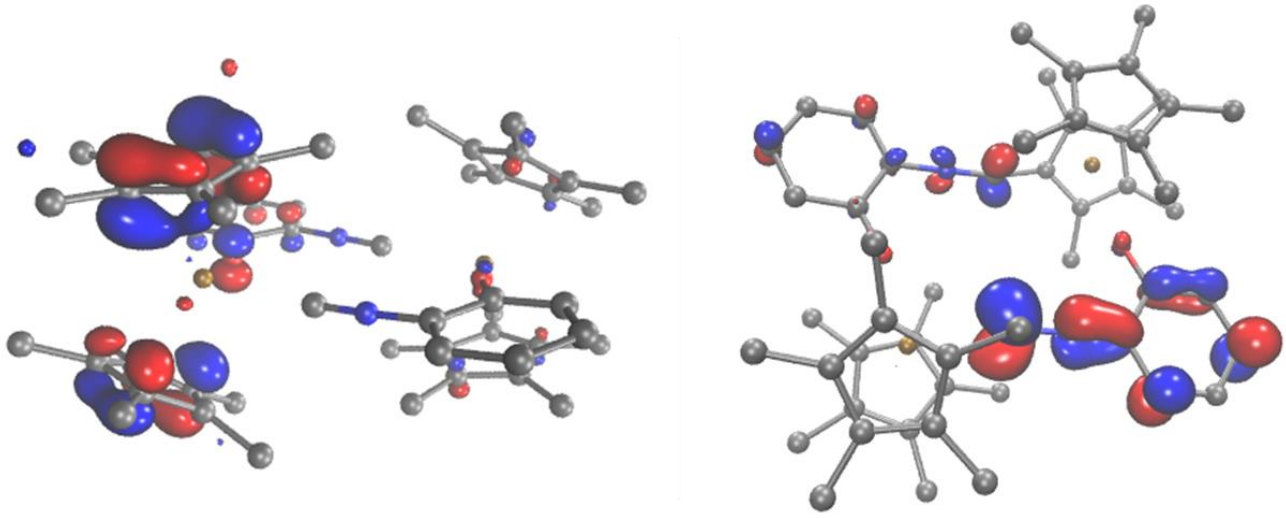

Figure B.3: HOMO (left) and LUMO (right) of **B.1**, plotted with contour value 0.05.

Time-dependent density functional theory (TDDFT) calculations were performed to analyze the experimental spectrum, Figure B.2. All the computed absorptions are $\pi \rightarrow \pi^*$ transitions, from the occupied C_5Me_5 π system to the unoccupied (CNC_6H_4O) π^* system and do not involve any significant metal character. While TDDFT using semi-local functionals notoriously underestimates the energy of long-range charge transfer states,[7] the HOMO-LUMO transition responsible for the visible absorption of **B.1** is optically bright, indicating short to intermediate range charge transfer.

DFT calculations were also carried out on the product of reducing **B.2** to investigate if the mono-reduced species, labelled **B.2**, would contain Y(II) or a radical in the bimetallic ring. To

this end, the vertical electron affinity of **B.1** was computed using spin-unrestricted Kohn-Sham DFT theory. To account for solvation of this radical anion species, the polarizable continuum model COSMO[8] for THF ($\varepsilon = 7.52$) was used.[9] The α-spin HOMO of **B.2** is purely ligand-based and is a π^* orbital on the CNC_6H_4O ligand, Figure B.4, similar to the LUMO of **B.1**. The α-spin LUMO of **B.2** is also a π^* orbital on the CNC_6H_4O ligand. The lowest α-spin unoccupied orbital for **B.1** with significant metal character was LUMO +3 and exhibits π bonding character between the empty 4d orbitals on Y and the isocyanide moiety of the CNC_6H_4O ligand, Figure B.4.

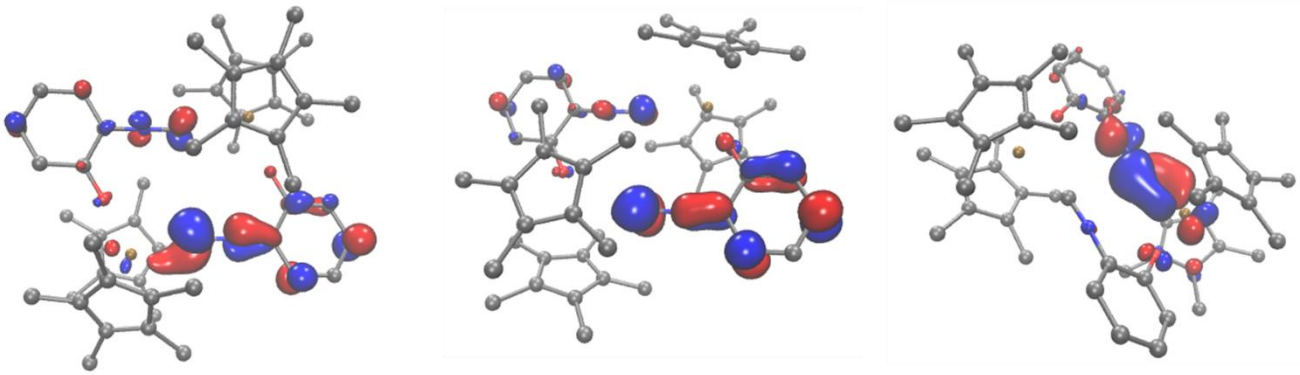

Figure B.4: HOMO (left), LUMO (middle), and LUMO +3 (right) of **B.2**, plotted with contour value 0.05. Hydrogen atoms have been omitted for clarity.

TDDFT calculations on **B.2** show a new absorption band compared to **B.1**, Figure B.5. This new band is comprised of transitions from the occupied HOMO of **B.2** into unoccupied π/π^* orbitals and do not have any significant metal character. Further details can be found in the Supporting Information. The electronic structure calculations support the experimental observations described below that reduction of **B.** is ligand-based and not yttrium-based.

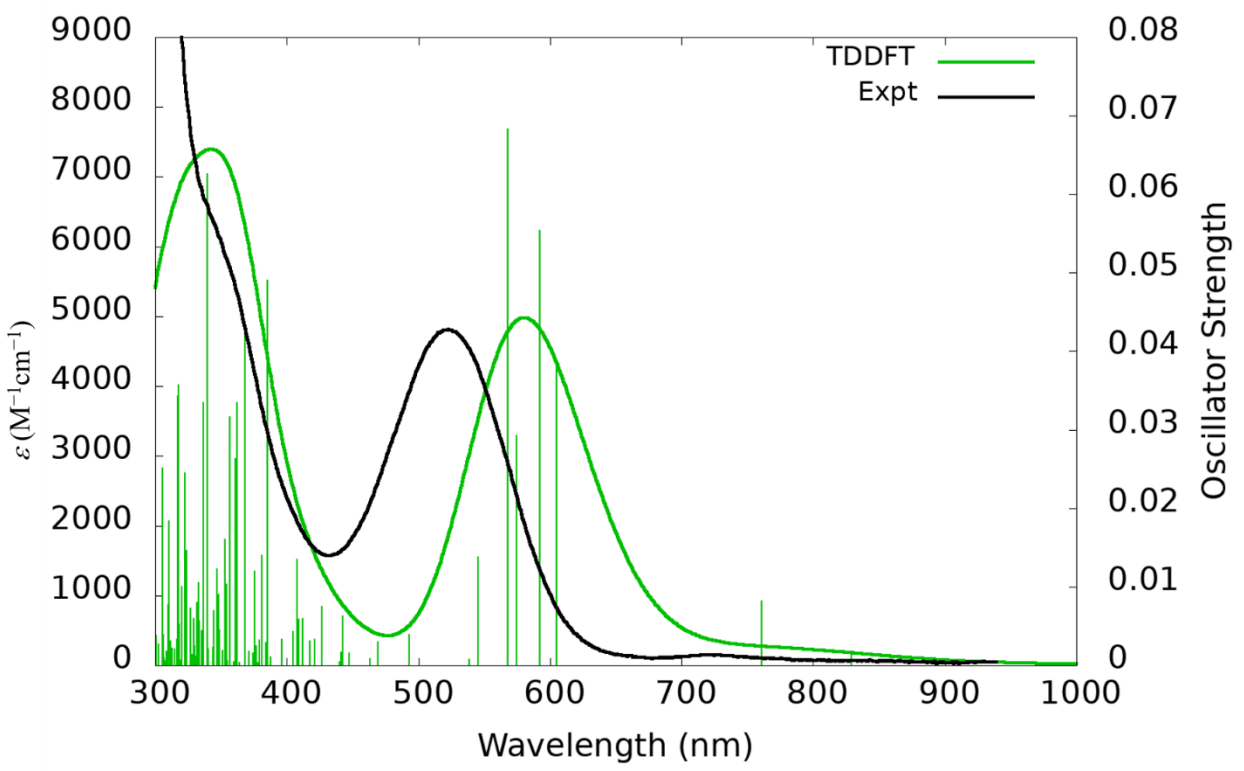

Figure B.5: Experimental UV-visible spectrum of **B.2** (black) (λ = 524 nm, ε = 4800 $M^{-1}cm^{-1}$) and the simulated spectrum of **B.2** with TDDFT oscillator strengths shown as vertical lines (green). A Gaussian line broadening of 0.15 eV was applied and the computed intensities were scaled by a factor of 0.5 to ease comparison.

The reduction of **B.1**, performed by Megan Dumas and Tener Jenkins, did not generate an isolable crystalline complex nor did it result in an obvious color change. However, the UV-visible spectrum of the product, **B.2**, differed from that of **B.1** and matched that calculated by TDDFT, Figure B.5, for a complex with the twelve-membered ring reduced by one electron. EPR spectra of **B.2** were obtained that also substantiated the results of the DFT calculations.

Computational Details. Electronic structure calculations on **B.1** and **B.2** were carried out at the density functional level of theory using the TPSSh functional[1] with Grimme's D3 dispersion

correction[10] and the resolution of the identity (RI-J) approximation.[11] No symmetry constraints were applied. Effective core potentials (ECPs)[2] with the def2-TZVP[3] basis set were used for Y and polarized split-valence basis sets with diffuse functions def2-SV(P)[4] were used for the light atoms C, H, N, and O. Quadrature grids of size m4 were used throughout.[12] The continuum solvation model COSMO[8] was included in the calculations on **B.2** to model solvent effects with a dielectric constant $\varepsilon = 7.52$ for THF.[9] Geometry optimizations were computed starting from the X-ray structures of **B.1** with geometry convergence threshold 10^{-4} a.u. and energy converge of at least 10^{-7} a.u. Ground state geometries were confirmed by the lack of imaginary frequencies in the vibrational spectra.[13] Time dependent DFT calculations of vertical excitations and oscillator strengths[14] were carried out on the optimized structures of **B.1** and **B.2** with identical basis sets as described above. UV-Visible spectra were simulated using Gaussian line profiles with a root mean-square width of 0.15 eV. Molecular orbitals and electronic transition states were analyzed with VMD[15] and Mulliken population analysis. All computations were completed using the TURBOMOLE program suite V7.4.1.

Electronic Structure Calculations on B.1. Ground state structure optimizations on **B.1** were performed starting with the crystal structure coordinates. The optimized geometry resulted in a C_1-symmetric singlet ground state. Molecular orbital plots and Mulliken population analyses revealed no significant metal-based character in the valence orbitals for **B.1**. The LUMO+3 orbital had electron density on the Y center (24% Y) that could interact with the π system on the OC_6H_4CN moiety.

The computed TDDFT spectrum had electronic transitions that were based almost entirely in the C_5Me_5 and OC_6H_4CN ligand π systems and did not contain any significant metal-based orbital character. The computed spectrum is in qualitative agreement with the experimental

spectrum, although the strongest transition is computed to be ~100 nm blue-shifted compared to the experimental spectrum. This could be a result of the relatively small basis set used for the light atoms, def2-SV(P). The addition of the solvent model COSMO with hexane (ε = 0.16) did not appreciably affect the energy of the computed transitions.

Geometry optimizations were performed on the first excited state with the PBE0 functional.[16] The optimized structure was observed to no longer have a coplanar $(Y–OC_6H_4CN)_2$ core as was found for the ground state and crystal structure. The phenyl ring is canted out of the Y–O–CN plane which could affect the conjugation and should thus blue-shift the computed excitations relative to what was originally calculated for **B.1**.

Table B.1. Electronic excitation summary for **B.1** using the TPSSh functional with def2-TZVP on Y and def2-SV(P) on light atoms. Oscillator strengths are reported in the length gauge. Only the dominant contribution to the overall excitation are reported. All excitations are $\pi \rightarrow \pi^*$ transitions, from the occupied C_5Me_5 π system to the unoccupied (CNC_6H_4O) π^* system. 222a is the HOMO while 223a is the LUMO.

Wavelength (nm)	Oscillator Strength	Dominant contribution		
		Occupied	Virtual	% weight
423	0.016	222a	223a	72.2
418	0.014	221a	223a	39.3
415	0.002	221a	223a	47.0
409	0.029	219a	223a	65.5
408	0.002	220a	223a	79.3
406	0.033	221a	224a	61.6

401	0.003	219a	224a	55.4
400	0.008	220a	224a	60.8
387	0.003	222a	225a	92.7
382	0.002	221a	225a	82.0
379	0.005	218a	223a	75.2
376	0.001	217a	223a	69.2
374	0.008	219a	225a	27.8
373	0.006	220a	225a	39.6
372	0.002	218a	224a	46.3
371	0.003	216a	224a	57.9
366	0.062	222a	226a	35.6
366	0.057	222a	226a	41.9
363	0.003	221a	226a	84.6
361	0.076	215a	223a	77.5
356	0.001	215a	224a	78.4
353	0.012	220a	226a	53.7
351	0.010	219a	226a	53.4
350	0.010	218a	225a	77.9
347	0.005	217a	225a	57.9
345	0.004	216a	225a	57.4
336	0.126	215a	225a	58.1
329	0.002	217a	226a	44.7

Electronic Structure Calculations on B.2. Geometry optimizations were completed starting with the optimized structure of **B.1**. The optimized structure resulted in a C1-symmetric doublet ground state. The HOMO of **B.2** was similar to the LUMO of **B.1**, which was located in the π system of the OC_6H_4CN ring. The computed TDDFT spectrum of **B.1** using the COSMO model with THF as solvent showed a new band located around 500 nm that involved transitions from the newly occupied OC_6H_4CN ring (HOMO of **B.2**) to empty π orbitals on the C_5Me_5 and OC_6H_4CN moieties.

Table B.2. Electronic excitation summary for **B.2** using the TPSSh functional with def2-TZVP on Y and def2-SV(P) on light atoms. Oscillator strengths are reported in the length gauge. Only the dominant contribution to the overall transitions are reported. 223a is the HOMO while 224a is the LUMO.

Wavelength (nm)	Oscillator Strength	Dominant contribution		
		Occupied	Virtual	% weight
829	0.001	223a	227a	97.8
761	0.008	223a	228a	97.1
605	0.039	223a	229a	92.8
592	0.055	223a	230a	78.9
574	0.029	223a	231a	79.3
568	0.068	223a	232a	70.9
545	0.014	223a	234a	81.5
493	0.004	233a	235a	96.4
469	0.003	233a	237a	61.7

463	0.001	223a	236a	65.1
447	0.004	221a	224a	55.8
442	0.003	223a	239a	86.9
441	0.001	222a	224a	79.7
427	0.007	223a	240a	78.6
421	0.003	223a	241a	49.5
418	0.003	223a	242a	46.5
412	0.006	220a	224a	93.3
409	0.006	222b	223b	90.7
408	0.013	221b	223b	35.4
405	0.004	219a	224a	93.0
396	0.003	218a	224a	46.6
388	0.001	223a	243a	91.4
385	0.049	223a	245a	25.0
384	0.003	220b	223b	94.7
381	0.014	219b	223b	66.4
379	0.003	217a	224a	76.1
376	0.002	222a	225a	25.8
375	0.012	223a	244a	38.7
374	0.002	216a	224a	30.3
371	0.002	215a	224a	40.7
368	0.042	222a	225a	20.9
362	0.033	218b	223b	32.3

361	0.026	222b	225b	19.8
357	0.032	221a	225a	34.6
354	0.010	223a	246a	35.9
354	0.003	223a	246a	41.9
353	0.016	220b	224b	65.6
351	0.002	215b	223b	42.2
348	0.004	221b	225b	53.9
348	0.009	215b	223b	26.6
347	0.012	222b	228b	7.4
344	0.007	214a	224a	24.7
344	0.001	220a	225a	55.1
344	0.002	223a	247a	78.9
340	0.002	218a	225a	21.3
340	0.063	219b	224b	41.4
337	0.033	214b	223b	36.6
336	0.002	220b	225b	53.7
335	0.004	214b	223b	26.2
334	0.006	221a	226a	48.8
333	0.010	220b	225b	19.9

References

(1) Staroverov, V. N.; Scuseria, G. E.; Tao, J.; Perdew, J. P. Comparative Assessment of a New Nonempirical Density Functional: Molecules and Hydrogen-Bonded Complexes. *J. Chem.*

Phys. **2003**, *119*, 12129–12137, DOI: 10.1063/1.1626543.

(2) Andrae, D.; Häußermann, U.; Dolg, M.; Stoll, H.; Preuß, H. Energy-Adjusted Ab Initio Pseudopotentials for the Second and Third Row Transition Elements. *Theor. Chim. Acta* **1990**, *77*, 123–141, DOI: 10.1007/BF01114537.

(3) Weigend, F.; Ahlrichs, R. Balanced Basis Sets of Split Valence, Triple Zeta Valence and Quadruple Zeta Valence Quality for H to Rn: Design and Assessment of Accuracy. *Phys. Chem. Chem. Phys.* **2005**, *7*, 3297–3305, DOI: 10.1039/b508541a.

(4) Schäfer, A.; Horn, H.; Ahlrichs, R. Fully Optimized Contracted Gaussian Basis Sets for Atoms Li to Kr. *J. Chem. Phys.* **1992**, *97*, 2571–2577.

(5) TURBOMOLE V7.4.1. University of Karlsruhe and Forschungszentrum Karlsruhe GmbH.

(6) Balasubramani, S. G.; Chen, G. P.; Coriani, S.; Diedenhofen, M.; Frank, M. S.; Franzke, Y. J.; Furche, F.; Grotjahn, R.; Harding, M. E.; Hättig, C.; Hellweg, A.; Helmich-Paris, B.; Holzer, C.; Huniar, U.; Kaupp, M.; Marefat Khah, A.; Karbalaei Khani, S.; Müller, T.; Mack, F.; Nguyen, B. D.; Parker, S. M.; Perlt, E.; Rappoport, D.; Reiter, K.; Roy, S.; Rückert, M.; Schmitz, G.; Sierka, M.; Tapavicza, E.; Tew, D. P.; van Wüllen, C.; Voora, V. K.; Weigend, F.; Wodyński, A.; Yu, J. M. TURBOMOLE: Modular Program Suite for Ab Initio Quantum-Chemical and Condensed-Matter Simulations. *J. Chem. Phys.* **2020**, *152*, 184107, DOI: 10.1063/5.0004635.

(7) Dreuw, A.; Weisman, J. L.; Head-Gordon, M. Long-Range Charge-Transfer Excited States in Time-Dependent Density Functional Theory Require Non-Local Exchange. *J. Chem. Phys.* **2003**, *119*, 2943–2946, DOI: 10.1063/1.1590951.

(8) Schäfer, A.; Klamt, A.; Sattel, D.; Lohrenz, J. C. W.; Eckert, F. COSMO Implementation in TURBOMOLE: Extension of an Efficient Quantum Chemical Code towards Liquid

Systems. *Phys. Chem. Chem. Phys.* **2000**, *2*, 2187–2193, DOI: 10.1039/b000184h.

(9) CRC Handbook of Chemistry and Physics. In *CRC Handbook of Chemistry and Physics*; Haynes, W. M., Lide, D. R., Bruno, T. J., Eds.; CRC Press, 2016; pp 943–950.

(10) Grimme, S.; Antony, J.; Ehrlich, S.; Krieg, H. A Consistent and Accurate Ab Initio Parametrization of Density Functional Dispersion Correction (DFT-D) for the 94 Elements H-Pu. *J. Chem. Phys.* **2010**, *132*, 154104, DOI: 10.1063/1.3382344.

(11) Weigend, F.; Köhn, A.; Hättig, C. Efficient Use of the Correlation Consistent Basis Sets in Resolution of the Identity MP2 Calculations. *J. Chem. Phys.* **2002**, *116*, 3175–3183, DOI: 10.1063/1.1445115.

(12) Treutler, O.; Ahlrichs, R. Efficient Molecular Numerical Integration Schemes. *J. Chem. Phys.* **1995**, *102*, 346–354, DOI: 10.1063/1.469408.

(13) Deglmann, P.; Furche, F.; Ahlrichs, R. An Efficient Implementation of Second Analytical Derivatives for Density Functional Methods. *Chem. Phys. Lett.* **2002**, *362*, 511–518, DOI: 10.1016/S0009-2614(02)01084-9.

(14) Bates, J. E.; Furche, F. Harnessing the Meta-Generalized Gradient Approximation for Time-Dependent Density Functional Theory. *J. Chem. Phys.* **2012**, *137*, 164105, DOI: 10.1063/1.4759080.

(15) Humphrey, W.; Dalke, A.; Schulten, K. VMD: Visual Molecular Dynamics. *J. Mol. Graph.* **1996**, *14*, 33–38.

(16) Perdew, J. P.; Ernzerhof, M.; Burke, K. Rationale for Mixing Exact Exchange with Density Functional Approximations. *J. Chem. Phys.* **1996**, *105*, 9982–9985, DOI: 10.1063/1.472933.

Appendix C:

Improved Synthesis and Spectroscopic Characterization of a Reduced Bimetallic Yttrium *Ansa*-Metallocene Hydride Complex, [K(crypt)][(μ–Cp^{An})Y(μ–H)]$_2$

Introduction

As described in Chapter 1, the discovery that the +2 oxidation state was available in crystallographically-characterizable complexes of all the rare-earth metals opened new opportunities in rare-earth reduction chemistry.[1–6] The structural, spectroscopic, and magnetic data along with theoretical calculations indicated that the non-traditional lanthanides formed $4f^n5d^1$ Ln(II) ions rather than the traditional $4f^{n+1}$ Ln(II) ions of Eu, Yb, Sm, Tm, Dy, and Nd.[5–8] The data on new Y(II) complexes were consistent with $4d^1$ ions.[2]

Bimetallic complexes with metal-metal bonds have been elusive with the rare-earth metals due to the limited radial extension of the 4f orbitals[9,10] and Y–Y bonds have not been possible with Y(III) because it is a $4d^0$ ion. Metal-metal bonding does occur in the elemental metals in the solid state and bonds between rare-earth metals have been reported within the special environment of fullerenes.[11–18] The use of $4f^n5d^1$ electron configurations to form Ln-Ln bonds have been realized in an iodide bridged bimetallic system, [($C_5{}^iPr_5$)Ln]$_2$(μ–I)$_3$ (Ln = Y, Gd, Tb, Dy).[19]

Density functional theory calculations on bridged bimetallic yttrium complexes such as [Cp′$_2$Y(μ–Cl)]$_2$ and [Cp′$_2$Y(μ–H)(THF)]$_2$ suggested that reduction of these species could possibly lead to Y–Y bonds[20] where the bridging hydride and methyl complexes could engage in electron-deficient three-center two-electron bonding.[21,22] Potassium graphite reductions of [Cp′$_2$Y(μ–Cl)]$_2$,[20] [Cp′$_2$Y(μ–CH$_3$)]$_2$,[23] and [Cp′$_2$Y(μ–H)(THF)]$_2$[20] formed dark colored solutions and both UV-visible data and EPR spectra suggested Y(II) was present, but crystallographic evidence was

not obtained.[20,23] In the case of the $[Cp'_2Y(\mu\text{–}H)(THF)]_2$ reduction reactions, the only product identified by X-ray crystallography was the Y(III) trimetallic tetrahydride, [K(2.2.2-cryptand)]{$[Cp'_2Y(\mu\text{–}H)]_3(\mu_3\text{–}H)$}.[20]

To reduce the tendency of the metallocene hydrides to form trimetallic species, yttrium hydride complexes of the *ansa*-cyclopentadienyl ligand $Me_2Si[C_5H_3(SiMe_3)]_2$, Cp^{An}, were pursued. A bimetallic Cp^{An} hydride complex of Sm had been synthesized and crystallographically characterized in 2000, eq C.1.[24] In this complex, the Cp^{An} ligands bridge across two samarium

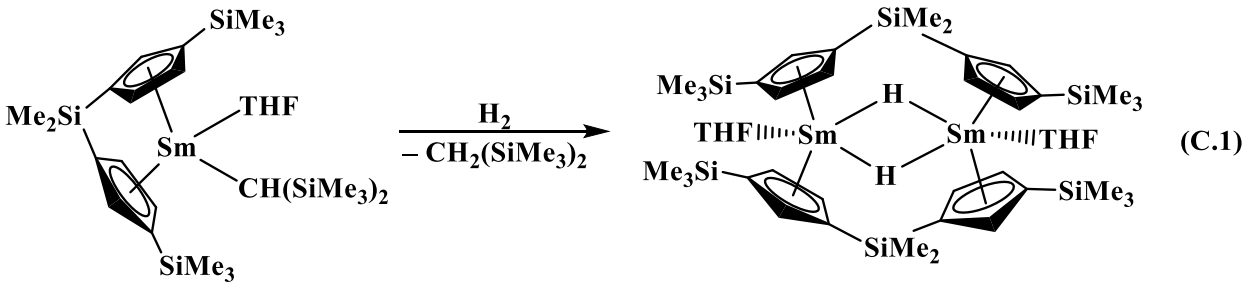

(C.1)

ions in a structure referred to as a "flyover" complex. Such a bonding mode would not be expected to favor a trimetallic species, as was observed in the reduction of $[Cp'_2Y(\mu\text{–}H)]_2$ which formed [K(2.2.2-cryptand)]{$[Cp'_2Y(\mu\text{–}H)]_3(\mu_3\text{–}H)$}. Indeed, Dr. Megan Dumas had succeeded in the crystallographic characterization of a reduced bimetallic yttrium hydride complex, **C.6**, via the route in Scheme C.1, but the spectroscopic data were difficult to interpret. Analysis of the compound was further difficult because it could be accessed across multiple steps in low yields.

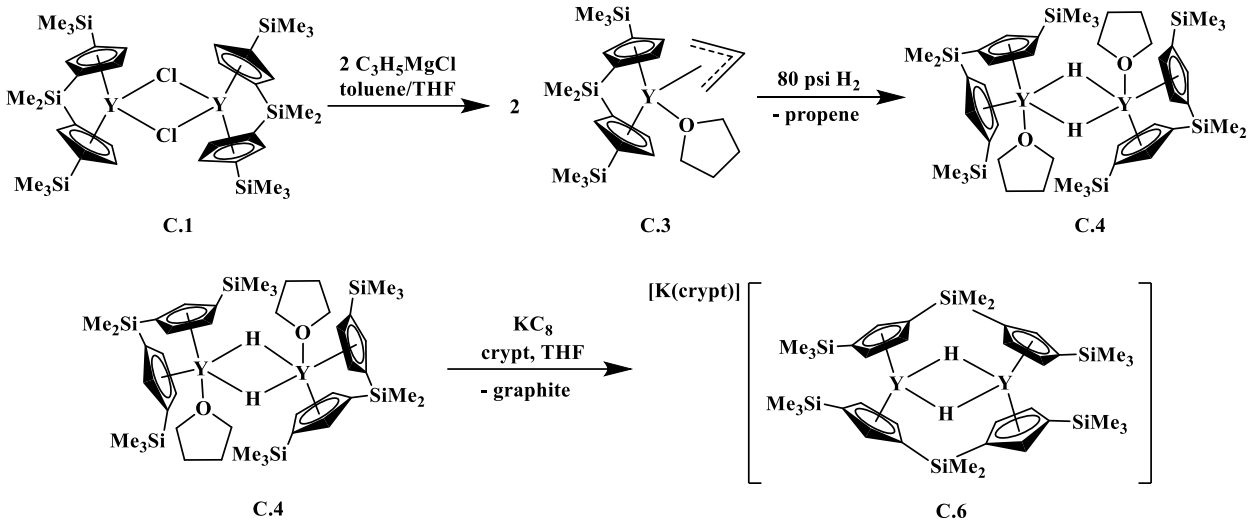

Scheme C.1: Synthesis of **C.6** from the previously reported **C.1**.[25]

In this Appendix, improvements to the synthetic route to the reduced bimetallic species are reported along with solid-state UV-visible and EPR spectroscopic characterization of the reduced species which supports the assignment of an yttrium-yttrium bonding interaction. Additionally, a neutral bimetallic yttrium complex, $[(\mu\text{–}Cp^{An})Y(\mu\text{–}H)]_2$, was crystallographically characterized which can be compared with the reduced species.

Results and Discussion

Improved Synthesis of $[Cp^{An}Y(\mu\text{-}H)(THF)]_2$, C.4. The initial synthesis of the bimetallic, bridging hydride complex **C.4** was accomplished via the route in Scheme C.1. The chloride species $[Cp^{An}Y(\mu\text{–}Cl)]_2$, **C.1**, was previously reported by Molander and coworkers in 20% yield in refluxing THF.[25] This result was reproducible, generating a large amount of brown oily solids that could be removed by washing with pentane. Further study has revealed that one of the byproducts was the monometallic complex $Cp^{An}YCl(THF)$, **C.2**, which is in equilibrium with **C.1** in THF solution. Many other reaction conditions were investigated in collaboration with Lauren Anderson-Sanchez, Table C.1, and it was found that the reaction of two equivalents of YCl_3 and

one equivalent of K_2Cp^{An} in refluxing toluene for 48 hours afforded compound **C.1** in 39% yield (entry 3), and avoided THF entirely.

Table C.1: Improvement on the synthesis of **C.1**.

Entry	Conditions	Yield of **C.1**
1[25]	YCl_3 + K_2Cp^{An} THF, 6h, −78 °C to reflux	20%
2	YCl_3 + K_2Cp^{An} THF, 12h, 65° toluene, 12h, 100 °C	40%
3	YCl_3 + K_2Cp^{An} toluene, 48h, 100 °C	39%
4	2 YCl_3 + K_2Cp^{An} toluene, 48h, 100 °C	24%
5	2 YCl_3 + K_2Cp^{An} THF, 12h, 65° toluene, 12h, 100 °C	31%
6	1.2 YCl_3 + K_2Cp^{An} THF, 12h, 65° toluene, 12h, 100 °C	34%

Compound **C.1** reacted with $LiHBEt_3$ and $PhSiH_3$, but neither reaction formed the desired bridging hydride product **C.4**. To obtain the hydride, hydrogenolysis of an allyl complex was necessary. Both bimetallic **C.1** and monometallic **C.2** react with (allyl)MgCl in toluene to generate $Cp^{An}Y(C_3H_5)(THF)$, **C.3**, as a bright yellow solid, Scheme C.1.

Treatment of bright yellow **C.3** with 60 psi of H_2 gas in the absence of solvent generated a colorless solid within 1 hour. The solids were washed with pentane to remove unreacted **C.3**, dissolved in toluene, and recrystallized to yield the yttrium hydride complex $[Cp^{An}Y(\mu\text{–}H)(THF)]_2$, **C.4**. This procedure is similar to the route developed by Megan Dumas.[42] However it was found that dissolution of the reaction mixture in toluene was necessary for the isolation of **C.4** and it did not appear that **C.4** could be isolated directly from the hydrogen reaction vessel.

Crystallization of [(μ–Cp^{An})Y(μ–H)]$_2$, C.5. In one instance during the attempted synthesis of **C.6**, crystals were obtained of unsolvated [(μ–Cp^{An})Y(μ–H)]$_2$, **C.5**, Figure C.1, that cocrystallized with [K(crypt)][Cp^{An}Y(C$_3$H$_5$)(H)]. Presumably, some remnant amount of **C.3** was carried over during the reaction of **C.4** with KC$_8$ and crypt. The isolation of the base-free bimetallic bridging hydride species with a "flyover" Cp^{An} ligand **C.5** is of particular interest for comparison with compound **C.4** and **C.6** (vide infra). The Y…Y distance of 3.478 Å in **C.5** is significantly smaller than the 3.6311(5) Å Y…Y distance in **C.4**, which could be explained by the smaller coordination number or changes in the binding mode of the Cp^{An} ligand.

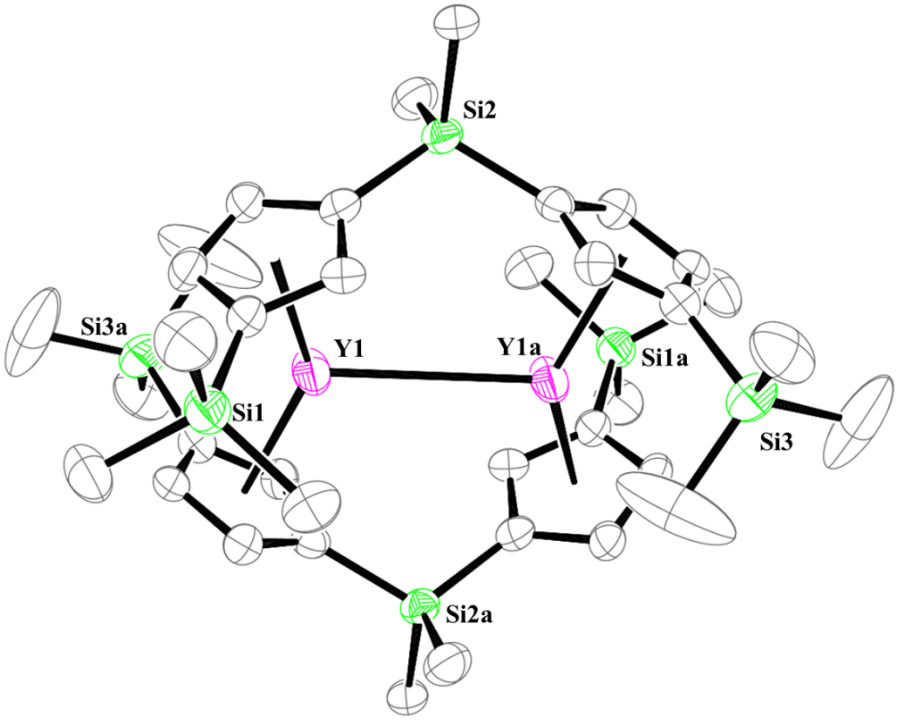

Figure C.1: Molecular structure of [(μ–Cp^{An})Y(μ–H)]$_2$, **C.5**, with thermal ellipsoids drawn at the 35% probability level and selective atom labelling. Cocrystallized [K(crypt)][Cp^{An}Y(C$_3$H$_5$)(H)], THF, and hydrogen atoms have been omitted for clarity.

Synthesis of [K(crypt)][(μ–CpAn)Y(μ–H)]$_2$, C.6. The reaction of colorless **C.4** with excess KC$_8$ and 1 equivalent of 2.2.2-cryptand (crypt) in THF at –30 °C produced an intensely-

colored red-brown solution from which [K(crypt)][(μ–Cp^{An})Y(μ–H)]$_2$, **C.6**, was isolated, Scheme C.1.

Interestingly, the binding mode of the Cp^{An} ligand in **C.5** and **C.6** is found to be a "flyover" structure, as was observed for [(μ–Cp^{An})Sm(μ–H)(THF)]$_2$.[24] These are different from **C.1**–**C.4**, which complicates the direct comparison between the structures of **C.4** and **C.6**. For example, the Cnt–Y–Cnt angles are widely different, 119.9° and 135.4° in **C.4** and **C.6**, respectively, Table C.2. Fortunately, **C.5** was isolated and can be compared to **C.6**.

The 3.3992(6) Å and 3.4022(7) Å Y…Y distances in **C.6** are the smallest Y…Y distance in the literature so far. The distances in **C.6** are approximately 0.08 Å shorter than the Y…Y distance in **C.5**, consistent with a strong Y…Y interaction due to the added electron. The distances in **C.6** are also significantly shorter than the 3.635(4) Å and 3.596(2) Å distances reported for a fullerene complex that is described as having Y–Y bonds.[11] The Y…Y distance in **C.6** is also shorter than the 3.727(1) Å distance in the metal-metal bonded [($C_5{}^iPr_5$)Y]$_2$(μ–I)$_3$.[19]

Table C.2: Comparison of Distances (Å) and Angles (°) between **C.4, C.5, C.6**, [(C_5Me_5)Y]$_2$(μ–I)$_3$, and {[(C_5H_4)$_2$SiMe$_2$]Y(μ–H)(THF)}$_2$. **C.6** has two independent molecules in the unit cell.

	C.4	**C.5**	**C.6**	**{[(C_5H_4)$_2$SiMe$_2$]Y(μ–H)(THF)}$_2$**	**[($C_5{}^iPr_5$)Y]$_2$(μ–I)$_3$**
Y–Cnt1	2.392	2.371	2.358, 2.362	2.315	2.337
Y–Cnt2	2.457	2.373	2.358, 2.367	2.357	
Cnt1–Y–Cnt2	119.9		135.4, 137.5	129.5	
Y…Y	3.6311(5)	3.479	3.3992(6), 3.4022(7)	3.514(3)	3.727(1)

EPR Spectroscopy. Initial solution phase EPR spectra of the crude red-brown reaction mixture formed from reduction of $[Cp^{An}Y(\mu\text{–}H)]_2$, presumably containing **C.6**, were obtained at 77 K and room temperature. The room temperature EPR spectrum contains a two-line pattern at g_{iso} = 1.99 with a hyperfine coupling constant of 40 G. The spectra are similar to the EPR spectra obtained from KC_8 reductions of monometallic Cp'_3Y (g_{iso} = 1.991, 36.6 G)[2] and Cp''_3Y (g_{iso} = 1.9908, 36.1 G)[33] except that the A value is slightly higher. Compound **C.6** is bimetallic in the solid state, but the solution-phase EPR spectra suggest that the unpaired electron is coupled to a single yttrium center and not to either bridging hydride atom. The deuterium analog of **C.6**, $[K(crypt)][(\mu\text{–}Cp^{An})Y(\mu\text{–}D)]_2$, prepared analogously to **C.6** except with D_2, gave identical EPR spectra. This can be explained if the unpaired electron resides on a single metal center (Robin Day Class I, completely localized),[34] or that the complex is monomeric in solution. A species such as "$[K(crypt)][Cp^{An}YH]$" has no precedent in rare-earth metal chemistry but could explain the observed EPR spectrum. Similar phenomena in bimetallic mixed valence Cu^I/Cu^{II} complexes have been observed, and it was postulated that the unpaired electron is localized on just one metal center on the EPR timescale.[35–37]

UV-Visible Spectroscopy. The initial UV-visible spectrum of **C.6** in THF, collected by Dr. Megan Dumas, displayed a broad absorbance at 410 nm with a minimum attenuation coefficient of approximately 1680 $M^{-1}cm^{-1}$. The spectrum was similar to those of $[K(crown)][Cp'_3Y]$ and $[K(crypt)][Cp'_3Y]$ which have absorptions at 530 nm (ε = 2500 $M^{-1}cm^{-1}$)[2] and 520 nm (ε = 4500 $M^{-1}cm^{-1}$),[4,7] respectively. This is in contrast to $[(C_5{}^iPr_5)Y]_2(\mu\text{–}I)_3$ which had an intense IVCT band around 700 nm.[19] However, IVCT bands are often located in the near IR region. Accordingly, the UV-Vis/NIR of **C.6** was recorded in THF and a broad absorption was observed around 1200 nm, which is assigned as an IVCT transition. Other sharper transitions were

observed in the NIR region, but these are likely overtones due to C–H stretching vibrations in the molecule.

Conclusion

An improved synthesis to the reduced, bimetallic complex $[Cp^{An}Y(\mu\text{–}H)(THF)]_2$, **C.4**, was developed. New crystallographic and spectroscopic data were collected to support the previous data to assign **C.6** as a reduced bimetallic complex with a strong Y…Y interaction, likely due to the presence of an electron in an orbital with Y-Y bonding character. The singly-occupied orbital does not have significant bridging hydrogen character since no coupling is observed to either the ^{1}H or ^{2}H nucleus in EPR spectroscopy. An intervalence charge transfer transition was observed in the near-infrared spectrum which supports the Y-Y bonding interaction.

Experimental Details

All manipulations and syntheses described below were conducted with the rigorous exclusion of air and water using standard Schlenk line and glovebox techniques under an argon atmosphere. Solvents were sparged with UHP argon and dried by passage through columns containing water and oxygen scavengers prior to use. Deuterated NMR solvents were dried over NaK alloy, degassed by three freeze-pump-thaw cycles, and vacuum transferred before use. ^{1}H NMR spectra and $^{13}C\{^{1}H\}$ NMR spectra were recorded on Bruker CRYO500 MHz spectrometer operating at 125 MHz for ^{13}C at 298 K unless otherwise stated and referenced internally to residual protio-solvent resonances. Infrared spectra were collected as compressed solids on an Agilent Cary 630 ATR-FTIR. Elemental analyses were conducted on a Perkin-Elmer 2400 Series II CHNS elemental analyzer. UV-visible/Near-IR spectra were collected at 298 K using a Jasco V-670UV/Vis/NIR spectrometer. EPR spectra were collected using X-band frequency on a Bruker

EMX spectrometer equipped with an ER041XG microwave bridge, and the magnetic field was calibrated with DPPH (g = 2.0036).

Potassium bis(trimethylsilyl)amide (Sigma-Aldrich) was purified by dissolving in toluene, centrifuging to remove insoluble material, and removing solvent from the supernatant. Allylmagnesium chloride (2.0 M solution in THF, Sigma-Aldrich), 1,4-dioxane (Sigma-Aldrich), and trimethylsilyl chloride (Alfa Aesar) were used as received. 2.2.2-cryptand (Sigma-Aldrich) was placed under vacuum (10^{-3} Torr) before use. H_2 (Praxair) and D_2 (Sigma) gas were used as received. Anhydrous YCl_3,[38] KC_8,[39] and KCp′[40] were prepared according to the literature.

K_2Cp^{An}. In the glovebox, KCp′ (2.382 g, 0.01351 mol) was dissolved in Et_2O (50 mL) to form a tan solution. Me_2SiCl_2 (0.871 g, 0.00675 mol) was slowly added to the stirring solution via pipet. A white precipitate quickly formed. The solution was stirred for 2 days then filtered to remove a tan solid. The solids were washed with Et_2O (3 x 15 mL) and hexane (3 x 15 mL) and the washings were combined with the filtrate and transferred to a new round bottom flask. To this peach-colored stirring solution was added $KN(SiMe_3)_2$ (2.673 g, 0.01340 mol) and the solution was stirred overnight. The solution was dried and hexane (50 mL) was added to form a suspension and stirred overnight. The solids were filtered, washed with hexane (3 x 15 mL), toluene (3 x 15 mL), and hexane (3 x 15 mL) to afford white solids of K_2Cp^{An}. These solids were sometimes contaminated with starting material and stirring in toluene overnight, followed by centrifugation to collect the solids, resulted in pure K_2CpAn (2.50 g, 91% based on KCp′). ^{1}H NMR (500 MHz, THF-d_8): δ 6.04 (m, 2H, $[C_5H_3SiMe_3]_2SiMe_2$), 6.03 (m, 2H, $[C_5H_3SiMe_3]_2SiMe_2$), 5.92 (m, 2H, $[C_5H_3SiMe_3]_2SiMe_2$), 0.57 (s, 6H, $SiMe_2$), 0.01 ppm (s, 18H, $SiMe_3$). ^{13}C NMR (500 MHz, THF-d_8): δ 120.52($[C_5H_3SiMe_3]_2SiMe_2$), 119.03 ($[C_5H_3SiMe_3]_2SiMe_2$), 115.40 ($[C_5H_3SiMe_3]_2SiMe_2$),

114.94 [$C_5H_3SiMe_3]_2SiMe_2$), 114.36 [$C_5H_3SiMe_3]_2SiMe_2$), 1.37 (SiMe_3), −0.56 (SiMe_2), −2.53 (SiMe_2) ppm.

[Cp^{An}Y(μ–Cl)]$_2$, C.1. This is an adaptation from literature.[41] Inside the glovebox, K_2Cp^{An} (0.523 g, 1.28 mmol), YCl_3 (250 mg, 1.28 mmol), and a stir bar were transferred to a Schlenk flask equipped with a greaseless Teflon stopcock. Toluene (40 mL) was added to form a pale suspension. The flask was brought out of the glovebox, attached to a Schlenk line, and stirred at 100 °C for two days. After a few hours, the mixture had turned into a yellow solution which faded in color as the reaction progressed. The solution was removed from heat, dried under vacuum, and the flask was brought inside a glovebox. The mixture was extracted into toluene (20 mL), centrifuged to remove solids, and the supernatant was filtered. The tan solution was dried under vacuum to yield orange and off-white solids. The solids were washed with pentane until the orange washing were colorless and dried to yield white solids of **C.1**, (230 mg, 39%), confirmed by ^{1}H and ^{13}C NMR spectroscopy.[41]

Crystallization of Cp^{An}YCl(THF), C.2. The crude mixture from the above reaction to form **C.1** was stirred in THF overnight. The solvent was removed under vacuum and the solids were extracted into toluene, filtered, and dried under vacuum. ^{1}H NMR spectroscopy showed the presence of **C.1** and another Cp^{An} environment. The solids were washed with pentane to afford white solids. Hexane was added to form a suspension. The hexane-soluble fraction contained **C.1**, identified by ^{1}H NMR spectroscopy. The remaining solids were dissolved in minimal toluene and placed in the freezer at −35 °C. Colorless blocks of **C.2**, suitable for X-ray diffraction, were grown overnight. ^{1}H NMR (C_6D_6): δ 6.38 (m, 2H, $C_5H_3SiMe_3$), 6.30 (m, 2H, $C_5H_3SiMe_3$), 5.94 (m, 2H, $C_5H_3SiMe_3$), 3.46 (s, 4H, THF), 1.25 (s, 4H, THF), 0.77 (s, 3H, SiMe_2), 0.71 (s, 3H, SiMe_2), 0.51 ppm (s, 18H, SiMe_3). ^{13}C NMR (C_6D_6): δ 130.4 ($C_5H_3SiMe_3$), 123.8($C_5H_3SiMe_3$), 121.9

($C_5H_3SiMe_3$), 120.9 ($C_5H_3SiMe_3$), 116.2 ($C_5H_3SiMe_3$), 25.4 (THF), 0.2 (SiMe_3), −3.5 (SiMe_2), −4.8 ppm (SiMe_2). IR (cm^{-1}): 3076w, 3054w, 2951m, 2894m, 1438m, 1404w, 1243s, 1200m, 1078s, 920s, 822s, 782s, 750s, 684m. Anal. Calcd for $C_{22}H_{38}O_1Si_3Cl_1Y_1$: C, 50.13; H, 7.27. Found: C, 45.69; H, 6.622. Low combustion values were found across multiple samples as has been previously observed for high silicon-containing organometallic compounds. The calculated ratio of $C_{22}H_{38.0}$ matches the expected value.

$Cp^{An}Y(\eta^3–C_3H_5)(THF)$, C.3. In a nitrogen-filled glovebox, $[Cp^{An}Y(\mu–Cl)]_2$, **C.1**, (528 mg, 0.584 mmol) was dissolved in toluene (150 mL) to yield a clear, colorless solution. Allylmagnesium chloride (2.0 M solution in THF, 0.48 mL, 0.966 mmol) was added dropwise via a syringe to the stirred solution. The resulting bright yellow solution was stirred overnight. After volatiles were removed under vacuum, hexane (150 mL) and 1,4-dioxane (7 mL) were added. The resulting cloudy yellow mixture was stirred overnight. The cloudy yellow solution was centrifuged to remove colorless solids. The yellow supernatant was filtered and isolated. Additional product was extracted from the colorless solids by centrifugation with hexane (40 mL) twice. The yellow supernatants were combined, and the solvent was removed under vacuum to yield **C.3** as a crude yellow powder (0.478 g, 0.899 mmol, 80%). The crude yellow powder was crystallized from a concentrated hexane solution at –35 °C to yield **C.3** (186 g, 0.350 mmol, 32%). ^{1}H NMR (600 MHz, C_6D_6) are consistent with previous data:[42] δ 6.46 (t, J_{HH} = 2.5 Hz, 1 H, {$Me_2Si[C_5H_3(Me_3Si)]_2$}), 6.30 (t, J_{HH} = 2.5 Hz, 1 H, {$Me_2Si[C_5H_3(Me_3Si)]_2$}), 5.93 (t, J_{HH} = 2.5 Hz, 1 H, {$Me_2Si[C_5H_3(Me_3Si)]_2$}), 5.72 (quint, J_{HH} = 5 Hz, 1 H, $[CH_2]_2CH$), 3.44 (br s, 4H, THF), 2.97 (d, J_{HH} = 15 Hz, 4 H, $[CH_2]_2CH$), 1.26 (t, J_{HH} = 7.5 Hz, 4 H, THF), 0.89 (s, 3 H, {$Me_2Si[C_5H_3(Me_3Si)]_2$}), 0.28 (s, 3 H, {$Me_2Si[C_5H_3(Me_3Si)]_2$}), 0.26 ppm (s, 18 H, {$Me_2Si[C_5H_3(Me_3Si)]_2$}).

[Cp^{An}Y(μ–H)(THF)]$_2$, C.4. In a nitrogen-filled glove box, a Fischer-Porter high pressure apparatus was charged with crystalline yellow **C.3** (150 mg, 0.326 mmol), sealed, and attached to a high-pressure gas line. The pressure in the vessel was reduced and slowly charged with H_2 (60 psi) before being sealed and left overnight. The sample changed from yellow to colorless after 1 hour. After 24 h, residual hydrogen was removed under vacuum. The vessel was recharged with 60 psi H_2 and left overnight. The vessel was evacuated and transferred to an argon-filled glovebox. The resulting brown solids were washed with pentane (2 mL) twice, dissolved in toluene, filtered, and dried under vacuum to afford **C.4** as a colorless/beige solid (136 mg, 0.138 mmol, 85%).[42]

[Cp^{An}Y(μ–*D*)(THF)]$_2$. As described above, **C.3** (85 mg, 0.16 mmol) was reacted with D_2 at 80 psi to yield white solids of [Cp^{An}Y(μ–*D*)(THF)]$_2$.

[K(crypt)][(μ–Cp^{An})Y(μ–H)]$_2$, C.6. Compound **C.6** was synthesized according to the previous report.[42] **C.4** was reacted with KC_8 in the presence of 2.2.2-cryptand at –35 °C and crystallized from THF/pentane at –35 °C to afford dark brown crystals of **C.6**.

Crystallization of C.5. During one attempted synthesis of **C.6**, the solution turned orange instead of dark brown. Colorless crystals were grown from THF/pentane at −35 °C and identified by X-ray diffraction as **C.5**·[K(crypt)][Cp^{An}Y(C_3H_5)(H)]·THF.

References

(1) Hitchcock, P. B.; Lappert, M. F.; Maron, L.; Protchenko, A. V. Lanthanum Does Form Stable Molecular Compounds in the +2 Oxidation State. *Angew. Chem. Int. Ed.* **2008**, *47*, 1488–1491, DOI: 10.1002/anie.200704887.

(2) MacDonald, M. R.; Ziller, J. W.; Evans, W. J. Synthesis of a Crystalline Molecular Complex of Y^{2+}, [(18-Crown-6)K][($C_5H_4SiMe_3$)$_3$Y]. *J. Am. Chem. Soc.* **2011**, *133*, 15914–15917, DOI: 10.1021/ja207151y.

(3) MacDonald, M. R.; Bates, J. E.; Fieser, M. E.; Ziller, J. W.; Furche, F.; Evans, W. J. Expanding Rare-Earth Oxidation State Chemistry to Molecular Complexes of Holmium(II) and Erbium(II). *J. Am. Chem. Soc.* **2012**, *134*, 8420–8423, DOI: 10.1021/ja303357w.

(4) MacDonald, M. R.; Bates, J. E.; Ziller, J. W.; Furche, F.; Evans, W. J. Completing the Series of +2 Ions for the Lanthanide Elements: Synthesis of Molecular Complexes of Pr^{2+}, Gd^{2+}, Tb^{2+}, and Lu^{2+}. *J. Am. Chem. Soc.* **2013**, *135*, 9857–9868, DOI: 10.1021/ja403753j.

(5) Meyer, G. Reduced Halides of the Rare-Earth Elements. *Chem. Rev.* **1988**, *88*, 93–107, DOI: 10.1021/cr00083a005.

(6) Seitz, M.; Oliver, A. G.; Raymond, K. N. The Lanthanide Contraction Revisited. *J. Am. Chem. Soc.* **2007**, *129*, 11153–11160, DOI: 10.1021/ja072750f.

(7) Fieser, M. E.; MacDonald, M. R.; Krull, B. T.; Bates, J. E.; Ziller, J. W.; Furche, F.; Evans, W. J. Structural, Spectroscopic, and Theoretical Comparison of Traditional vs Recently Discovered Ln^{2+} Ions in the [K(2.2.2-Cryptand)][$(C_5H_4SiMe_3)_3Ln$] Complexes: The Variable Nature of Dy^{2+} and Nd^{2+}. *J. Am. Chem. Soc.* **2015**, *137*, 369–382, DOI: 10.1021/ja510831n.

(8) Meihaus, K. R.; Fieser, M. E.; Corbey, J. F.; Evans, W. J.; Long, J. R. Record High Single-Ion Magnetic Moments Through $4f^n5d^1$ Electron Configurations in the Divalent Lanthanide Complexes $[(C_5H_4SiMe_3)_3Ln]^-$. *J. Am. Chem. Soc.* **2015**, *137*, 9855–9860, DOI: 10.1021/jacs.5b03710.

(9) Crosswhite, H. M.; Crosswhite, H.; Carnall, W. T.; Paszek, A. P. Spectrum Analysis of U^{3+}:$LaCl_3$. *J. Chem. Phys.* **1980**, *72*, 5103–5117.

(10) Atwood, D. *The Rare Earths: Fundamentals and Applications*; **2012**.

(11) Pan, C.; Shen, W.; Yang, L.; Bao, L.; Wei, Z.; Jin, P.; Fang, H.; Xie, Y.; Akasaka, T.; Lu,

X. Crystallographic Characterization of Y_2C_{2n} (2n = 82, 88–94): Direct Y–Y Bonding and Cage-Dependent Cluster Evolution. *Chem. Sci.* **2019**, *10*, 4707–4713, DOI: 10.1039/C9SC00941H.

(12) Yang, T.; Zhao, X.; Osawa, E. Can a Metal-Metal Bond Hop in the Fullerene Cage? *Chem. Eur. J.* **2011**, *17*, 10230–10234, DOI: 10.1002/chem.201101233.

(13) Popov, A. A.; Avdoshenko, S. M.; Pendás, A. M.; Dunsch, L. Bonding between Strongly Repulsive Metal Atoms: An Oxymoron Made Real in a Confined Space of Endohedral Metallofullerenes. *Chem. Commun.* **2012**, *48*, 8031, DOI: 10.1039/c2cc32568c.

(14) Zuo, T.; Xu, L.; Beavers, C. M.; Olmstead, M. M.; Fu, W.; Crawford, T. D.; Balch, A. L.; Dorn, H. C. $M_2@C_{79}N$ (M = Y, Tb): Isolation and Characterization of Stable Endohedral Metallofullerenes Exhibiting M−M Bonding Interactions inside Aza[80]Fullerene Cages. *J. Am. Chem. Soc.* **2008**, *130*, 12992–12997, DOI: 10.1021/ja802417d.

(15) Bao, L.; Chen, M.; Pan, C.; Yamaguchi, T.; Kato, T.; Olmstead, M. M.; Balch, A. L.; Akasaka, T.; Lu, X. Crystallographic Evidence for Direct Metal-Metal Bonding in a Stable Open-Shell $La_2@I_h$-C_{80} Derivative. *Angew. Chem. Int. Ed.* **2016**, *55*, 4242–4246, DOI: 10.1002/anie.201511930.

(16) Yamada, M.; Kurihara, H.; Suzuki, M.; Saito, M.; Slanina, Z.; Uhlik, F.; Aizawa, T.; Kato, T.; Olmstead, M. M.; Balch, A. L.; Maeda, Y.; Nagase, S.; Lu, X.; Akasaka, T. Hiding and Recovering Electrons in a Dimetallic Endohedral Fullerene: Air-Stable Products from Radical Additions. *J. Am. Chem. Soc.* **2015**, *137*, 232–238, DOI: 10.1021/ja509956y.

(17) Liu, F.; Krylov, D. S.; Spree, L.; Avdoshenko, S. M.; Samoylova, N. A.; Rosenkranz, M.; Kostanyan, A.; Greber, T.; Wolter, A. U. B.; Büchner, B.; Popov, A. A. Single Molecule Magnet with an Unpaired Electron Trapped between Two Lanthanide Ions inside a

Fullerene. *Nat. Commun.* **2017**, *8*, 16098, DOI: 10.1038/ncomms16098.

(18) Shen, W.; Bao, L.; Wu, Y.; Pan, C.; Zhao, S.; Fang, H.; Xie, Y.; Jin, P.; Peng, P.; Li, F.-F.; Lu, X. $Lu_2@C_{2n}$ (2n = 82, 84, 86): Crystallographic Evidence of Direct Lu–Lu Bonding between Two Divalent Lutetium Ions Inside Fullerene Cages. *J. Am. Chem. Soc.* **2017**, *139*, 9979–9984, DOI: 10.1021/jacs.7b04421.

(19) Gould, C. A.; McClain, K. R.; Reta, D.; Kragskow, J. G. C.; Marchiori, D. A.; Lachman, E.; Choi, E.; Analytis, J. G.; Britt, R. D.; Chilton, N. F.; Harvey, B. G.; Long, J. R. Ultrahard Magnetism from Mixed-Valence Dilanthanide Complexes with Metal–Metal Bonding. *Science* **2022**, *375*, 198–202, DOI: 10.1126/science.abl5470.

(20) Dumas, M. T.; Chen, G. P.; Hu, J. Y.; Nascimento, M. A.; Rawson, J. M.; Ziller, J. W.; Furche, F.; Evans, W. J. Synthesis and Reductive Chemistry of Bimetallic and Trimetallic Rare-Earth Metallocene Hydrides with $(C_5H_4SiMe_3)^{1-}$ Ligands. *J. Organomet. Chem.* **2017**, *849–850*, 38–47, DOI: 10.1016/j.jorganchem.2017.05.057.

(21) Ortiz, J. V.; Hoffmann, R. Hydride Bridges between $LnCp_2$ Centers. *Inorg. Chem.* **1985**, *24*, 2095–2104, DOI: 10.1021/ic00207a027.

(22) Venanzi, L. M. Transition Metal Complexes with Bridging Hydride Ligands. *Coord. Chem. Rev.* **1982**, *43*, 251–274.

(23) Dumas, M. T.; Ziller, J. W.; Evans, W. J. Synthesis and Reduction of Bimetallic Methyl-Bridged Rare-Earth Metal Complexes, $[(C_5H_4SiMe_3)_2Ln(\mu\text{-}CH_3)]_2$ (Ln = Y, Tb, Dy). *ACS Omega* **2019**, *4*, 398–402, DOI: 10.1021/acsomega.8b02665.

(24) Desurmont, G.; Li, Y.; Yasuda, H.; Maruo, T.; Kanehisa, N.; Kai, Y. Reaction Pathway for the Formation of Binuclear Samarocene Hydride from Monomeric Alkyl Samarocene Derivative and the Effective Catalysis of Samarocene Hydride for the Block

Copolymerization of Ethylene with Polar Monomers. *Organometallics* **2000**, *19*, 1811–1813, DOI: 10.1021/om990952h.

(25) Molander, G. A.; Dowdy, E. D.; Schumann, H. Catalytic Cyclization/Silylation of Dienes Containing 1,1-Disubstituted Olefins Using Organolanthanide and Group 3 Organometallic Complexes. *J. Org. Chem.* **1998**, *63*, 3386–3396, DOI: 10.1021/jo972359k.

(26) Zhang, J.; Yi, W.; Zhang, Z.; Chen, Z.; Zhou, X. Facile Synthesis of Organolanthanide Hydrides with Metallic Potassium: Crystal Structures and Reactivity. *Organometallics* **2011**, *30*, 4320–4324, DOI: 10.1021/om2003877.

(27) Arndt, S.; Kramer, M. U.; Fegler, W.; Nakajima, Y.; Del Rosal, I.; Poteau, R.; Spaniol, T. P.; Maron, L.; Okuda, J. Yttrium Dihydride Cation $[YH_2(THF)_2]^+_n$: Aggregate Formation and Reaction with (NNNN)-Type Macrocycles. *Organometallics* **2015**, *34*, 3739–3747, DOI: 10.1021/acs.organomet.5b00422.

(28) Evans, W. J.; Meadows, J. H.; Wayda, A. L.; Hunter, W. E.; Atwood, J. L. Organolanthanide Hydride Chemistry. 1. Synthesis and x-Ray Crystallographic Characterization of Dimeric Organolanthanide and Organoyttrium Hydride Complexes. *J. Am. Chem. Soc.* **1982**, *104*, 2008–2014, DOI: 10.1021/ja00371a035.

(29) Gountchev, T. I.; Tilley, T. D. Yttrium Complexes of the Chelating, C_2-Symmetric, Bis(Silylamido)Biphenyl Ligand $[DADMB]^{2-}$ (=$\{[6,6'\text{-}Me_2\text{-}(C_6H_3)_2](2,2'\text{-}NSiMe_2{}^tBu)_2\}^{2-}$). *Organometallics* **1999**, *18*, 2896–2905, DOI: 10.1021/om9901170.

(30) Hultzsch, K. C.; Spaniol, T. P.; Okuda, J. Half-Sandwich Alkyl and Hydrido Complexes of Yttrium: Convenient Synthesis and Polymerization Catalysis of Polar Monomers. *Angew. Chem. Int. Ed.* **1999**, *38*, 227–230, DOI: 10.1002/(SICI)1521-3773(19990115)38:1/2<227::AID-ANIE227>3.0.CO;2-M.

(31) Evans, W. J.; Drummond, D. K.; Hanusa, T. P.; Doedens, R. J. Organolanthanide and Organoyttrium Hydride Chemistry. 9. Bis(1,3-Dimethylcyclopentadienyl)Yttrium Complexes. Synthesis and x-Ray Crystallographic Characterization of [(1,3-$Me_2C_5H_3)_2Y(\alpha\text{-}Me)]_2$, $[(1,3\text{-}Me_2C_5H_3)_2Y(\mu\text{-}H)]_3$, and $[(1,3\text{-}Me_2C_5H_3)_2(THF)Y(\mu\text{-}H)]_2$. *Organometallics* **1987**, *6*, 2279–2285, DOI: 10.1021/om00154a002.

(32) Trifonov, A. A.; Skvortsov, G. G.; Lyubov, D. M.; Skorodumova, N. A.; Fukin, G. K.; Baranov, E. V.; Glushakova, V. N. Postmetallocene Lanthanide–Hydrido Chemistry: A New Family of Complexes $[\{Ln\{(Me_3Si)_2NC(N^iPr)_2\}_2(\mu\text{-}H)\}_2]$ (Ln=Y, Nd, Sm, Gd, Yb) Supported by Guanidinate Ligands—Synthesis, Structure, and Catalytic Activity in Olefin Polymerization. *Chem. Eur. J.* **2006**, *12*, 5320–5327, DOI: 10.1002/chem.200600058.

(33) Corbey, J. F.; Woen, D. H.; Palumbo, C. T.; Fieser, M. E.; Ziller, J. W.; Furche, F.; Evans, W. J. Ligand Effects in the Synthesis of Ln2+ Complexes by Reduction of Tris(Cyclopentadienyl) Precursors Including C–H Bond Activation of an Indenyl Anion. *Organometallics* **2015**, *34*, 3909–3921, DOI: 10.1021/acs.organomet.5b00500.

(34) Robin, M. B.; Day, P. Mixed-Valent Chemistry - A Survey and Classification. In *Advances in Inorganic Chemistry and Radiochemistry*; Elsevier, 1968; pp 247–422, DOI: 10.1016/S0065-2792(08)60179-X.

(35) Long, R. C.; Hendrickson, D. N. Intramolecular Electron Transfer in a Series of Mixed-Valence Copper(II)-Copper(I) Complexes. *J. Am. Chem. Soc.* **1983**, *105*, 1513–1521, DOI: 10.1021/ja00344a018.

(36) Gagne, R. R.; Koval, C. A.; Smith, T. J. Binuclear Complexes of Macrocyclic Ligands. A Mixed-Valence Copper(II)-Copper(I) Complex Which Exhibits Unusual Temperature-Dependent Behavior. *J. Am. Chem. Soc.* **1977**, *99*, 8367–8368, DOI: 10.1021/ja00467a067.

(37) Gagne, R. R.; Koval, C. A.; Smith, T. J.; Cimolino, M. C. Binuclear Complexes of Macrocyclic Ligands. Electrochemical and Spectral Properties of Homobinuclear $Cu^{II}Cu^{II}$, $Cu^{II}Cu^{I}$, and $Cu^{I}Cu^{I}$ Species Including an Estimated Intramolecular Electron Transfer Rate. *J. Am. Chem. Soc.* **1979**, *101*, 4571–4580, DOI: 10.1021/ja00510a023.

(38) Taylor, M. D. Preparation of Anhydrous Lanthanon Halides. *Chem. Rev.* **1962**, *62*, 503–511, DOI: 10.1021/cr60220a001.

(39) Bergbreiter, D. E.; Killough, J. M. Reactions of Potassium-Graphite. *J. Am. Chem. Soc.* **1978**, *100*, 2126–2134, DOI: 10.1021/ja00475a025.

(40) Peterson, J. K.; MacDonald, M. R.; Ziller, J. W.; Evans, W. J. Synthetic Aspects of $(C_5H_4SiMe_3)_3Ln$ Rare-Earth Chemistry: Formation of $(C_5H_4SiMe_3)_3Lu$ via $[(C_5H_4SiMe_3)_2Ln]^+$ Metallocene Precursors. *Organometallics* **2013**, *32*, 2625–2631, DOI: 10.1021/om400116d.

(41) Molander, G. A.; Dowdy, E. D.; Schumann, H. Catalytic Cyclization / Silylation of Dienes Containing 1,1-Disubstituted Olefins Using Organolanthanide and Group 3 Organometallic Complexes The Catalytic Cyclization / Silylation Reaction of Hindered Dienes Has Been Investigated Using The. *J. Org. Chem.* **1998**, *63*, 3386–3396.

(42) Dumas, M. T. Synthesis and Reductive Chemistry of Bimetallic Complexes of the Rare-Earth Metals. Ph.D. Dissertation, University of California, Irvine, Irvine, CA 92697, **2019**.

Appendix D:

Uranium Borohydride Coordination Chemistry and Hydroboration of $Me_2C=CMe_2$

Introduction

Uranium(IV) borohydride, $U(BH_4)_4$, was studied during the Manhattan Project due to its high volatility as a way to separate uranium isotopes and enrich uranium materials for use in nuclear fuel and other applications.[1–7] Beyond these early reports, little work had been done involving the coordination chemistry of uranium borohydride compounds until a report in 2014 from Polly Arnold and coworkers that developed a facile[8,9] solution phase synthesis of the U(III) borohydride $U(BH_4)_3(THF)_2$, eq D.1.[10] This new synthetic route allowed for studies utilizing $U(BH_4)_3$ as a starting material for further derivatization.[4,5,11–17]

$$UI_3 + 3\ NaBH_4 \xrightarrow[-\ 3\ NaI]{THF} U(BH_4)_3(THF)_2 \quad \textbf{(D.1)}$$

D.1

Using $U(BH_4)_4$, Ephritikhine and coworkers found that reaction with $Me_2C=CMe_2$ led to the formation of $U(H_3BCMe_2CHMe_2)_4$, a new borohydride derivative.[18] This study was not developed further,[19,20] but stands in contrast to transition metal-mediated hydroboration of unsaturated substrates, such as alkenes,[21–25] where the transition-metal catalyzed reactivity was described as a Lewis acid effect. Rarely has the resulting alkylborohydride been trapped at the transition metal center. Reports of alkene hydroboration using $LiBH_4$ and $NaBH_4$[26] and polymerization of isoprene, butadiene, styrene, and methyl methacrylate using Nd borohydride compounds[27] have also been published. It should be noted that substituted alkali-metal borohydrides MBH_3R, (M = Li, Na, K) can be synthesized from the alkyl borane and alkali-metal hydride[28] and these are likely active for alkene hydroboration.[26] This Appendix reports on the

coordination chemistry of U(III) with BH_4 ligands and some preliminary reactions with $Me_2C{=}CMe_2$.

Results and Discussion

Synthesis of Uranium Borohydride Compounds. $U(BH_4)_3(THF)_2$, **D.1**, was synthesized via the reported route of eq D.1. The previous study did not report the X-ray structure. Crystallization of **D.1** from THF/hexane at −35 °C afforded dark red plates and $U(BH_4)_3(THF)_4$ was identified by X-ray diffraction, Figure D.1. In the solid state, **D.1** crystallizes with four bound THF molecules, but the bulk powder material has only two THF molecules, which might suggest some BH_4 ligands bridge multiple uranium centers.

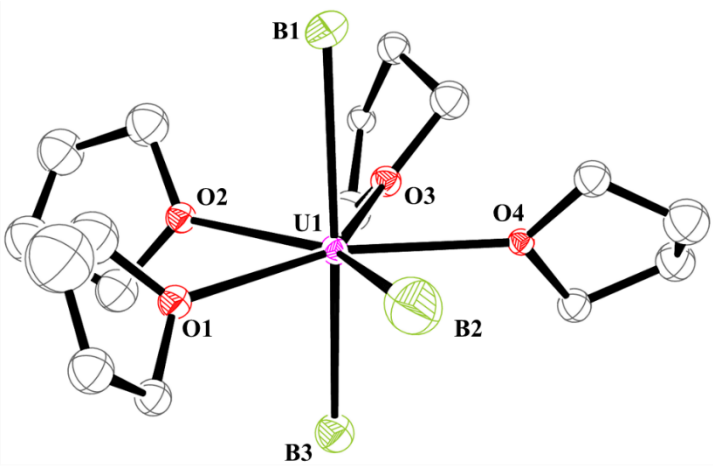

Figure D.1: Molecular structure of $U(BH_4)_3(THF)_4$. Ellipsoids are drawn at the 50% probability level and hydrogen atoms have been omitted for clarity.

$U(BH_4)_3(THF)_4$ crystallized in the $P\bar{1}$ space group and was isomorphous with $La(BH_4)_3(THF)_4$.[29] The uranium center can be described as a distorted pentagonal bipyramidal with a 168.6° B(1)–U(1)–B(3) angle.

When a reaction analogous to **D.1** was performed with two equivalents of $NaBH_4$, a new compound **D.2**, was isolated, eq D.2. The infrared spectrum of **D.2** shows B–H stretching

frequencies at 2430 and 2213 cm^{-1}, which are different from the 2446, 2205, and 2147 cm^{-1} B–H stretching frequencies of **D.1**, Table D.1. The number and energy of the B–H stretching frequencies in the infrared spectrum of metal borohydride compounds can be used to determine the hapticity of the BH_4 ligand.[4] However, this analysis can be complicated if two BH_4 ligands are inequivalent. If the BH_4 ligands in **D.2** are identical, the two frequencies around 2400 and 2200 cm^{-1} suggest that the BH_4 units are bound through three bridging hydrides, i.e. $M(\mu\text{–}H)_3BH$.

$$\mathbf{UI_3 + 2\ NaBH_4 \xrightarrow[-\ 2\ NaI]{THF} U(BH_4)_2I(THF)_2} \quad \textbf{(D.2)}$$

Table D.1: Some spectroscopic data for compounds **D.1**, **D.2**, **D.4**-**D.6**, and $NaBH_4$.

	B–H stretching frequencies (cm^{-1})	^1H NMR (THF-d_8, δ, ppm)
$U(BH_4)_3(THF)_2$, **D.1**[10]	2446, 2205, 2147, 1162	85 (BH_4)
$U(BH_4)_2I(THF)_2$, **D.2**	2430, 2213	
$[U(H_3BCMe_2CHMe_2)_2(THF)_2(u\text{–}I)]_2$, **D.4**		168 (H_3BR), 5.45 (CH), −1.06 (Me), −2.39 (Me)
$(C_5Me_5)_2U(BH_4)(THF)$, **D.5**	2414, 2273	−2.43 (C_5Me_5), −14.87 (THF), −42.46 (THF)
$(C_5Me_5)U(BH_4)_2(THF)_2$, **D.6**	2473, 2231, 2111	12.41 (BH_4), −2.36 (C_5Me_5), −14.84 (THF), −42.35 (THF)
$NaBH_4$	2936, 2284, 2216, 1107	

Crystallization of **D.2** from THF/hexane at −35 °C afforded dark red plates suitable for X-ray diffraction. $U(BH_4)_2I(THF)_4$ was identified by X-ray diffraction and crystallized in the $P\bar{1}$ space group and was isomorphous with $U(BH_4)_3(THF)_4$. Since $U(BH_4)_3(THF)_4$, $U(BH_4)_2I(THF)_4$, and $UI_3(THF)_4$[30] have practically identical cell dimensions, a simple check of the unit cell cannot determine the number of BH_4 and iodide groups ligated to uranium. However, both the IR and

NMR spectra of these compounds are unique, Table 5.1. Interestingly, the $LnBr_3(THF)_4$ complexes (Ln = Ce, Pr, Nd, Sm, Pu, Am)[31–35] share the same unit cell as $U(BH_4)_3(THF)_4$, $U(BH_4)_2I(THF)_4$, and $UI_3(THF)_4$.

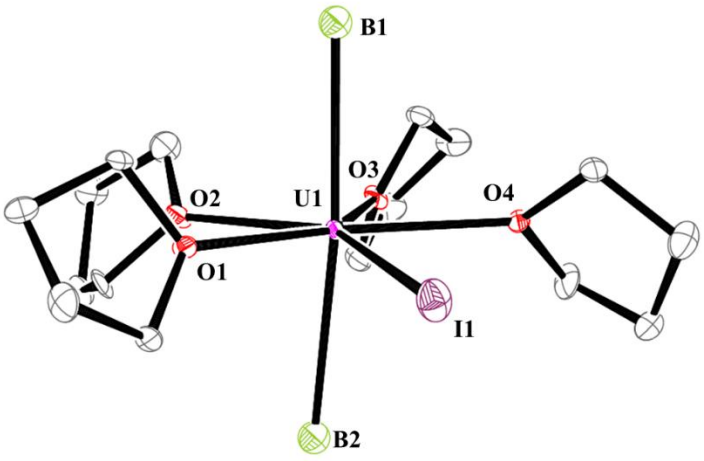

Figure D.2: Molecular structure of $U(BH_4)_2I(THF)_2$. Ellipsoids are drawn at the 50% probability level and hydrogen atoms have been omitted for clarity.

During these studies, a crystal structure of $U(BH_4)I_2(THF)_4$ was obtained, Figure D.3. $U(BH_4)I_2(THF)_4$ again has the same unit cell as $U(BH_4)_3(THF)_4$, $U(BH_4)_2I(THF)_4$, and $UI_3(THF)_4$.

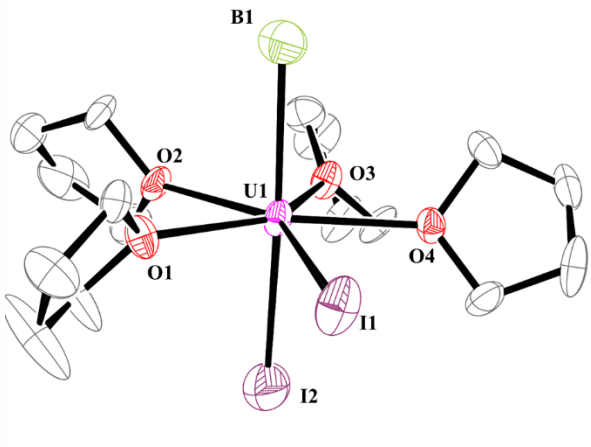

Figure D.3: Molecular structure of $U(BH_4)I_2(THF)_4$. Ellipsoids are drawn at the 50% probability level and hydrogen atoms have been omitted for clarity.

Alkene Reactivity. With both **D.1** and **D.2** available, the reactivity with alkenes was investigated. Initially, tetramethylethylene, $Me_2C{=}CMe_2$, was investigated since Ephritikhine had shown reaction of $U(BH_4)_4$ with $Me_2C{=}CMe_2$ led to the formation of $U(H_3BCMe_2CHMe_2)_4$.[18] In addition, the Nd complex $Nd(H_3BCMe_2CHMe_2)_3(THF)_3$ was previously synthesized from $NdCl_3$ and $Na(H_3BCMe_2CHMe_2)$ in THF.[27]

Analogous results were observed with **D.1** and **D.2**. Reaction of **D.1** with three equivalents of $Me_2C{=}CMe_2$ in THF led to the formation of a new complex, **D.3**. Based on the stoichiometry and previous reports, compound **D.3** was expected to be a species such as "$U(H_3BCMe_2CHMe_2)_3(THF)_x$," but characterization data were inconclusive. Compound **D.3** is soluble in hexane while **D.1** is not, which allows for facile workup and purification. Crystallization of **D.3** from concentrated THF or hexane at −35 °C afforded dark red crystals of **D.3**, but X-ray crystal data were not obtained.

In a similar reaction, **D.2** reacted with $Me_2C{=}CMe_2$ in THF and $[U(H_3BCMe_2CHMe_2)_2(THF)_2(\mu\text{–}I)]_2$, **D.4**, was identified by X-ray diffraction, eq D.3, Figure D.4.

$$\mathbf{U(BH_4)_2I(THF)_2 + 2\ Me_2C{=}CMe_2 \xrightarrow{THF} \underset{\mathbf{D.4}}{1/2\ [U(H_3BCMe_2CHMe_2)_2(THF)_2(\mu\text{–}I)]_2}} \quad \mathbf{(D.3)}$$

Compound **D.4** crystallized in the $P2_1$ space group and was found to be dimeric. The monomeric unit is crystallographically unique such that the other half is generated by symmetry. The ^1H NMR spectrum of **D.4** in THF-d_8 showed four resonances consistent with the solid-state structure. Resonances at −1.06 and −2.39 ppm are assigned to two sets of methyl groups and a broad resonance at 168 ppm was assigned to the BH_3 unit. A small, broad peak was found at 5.45 ppm and integrates correctly for the CH group.

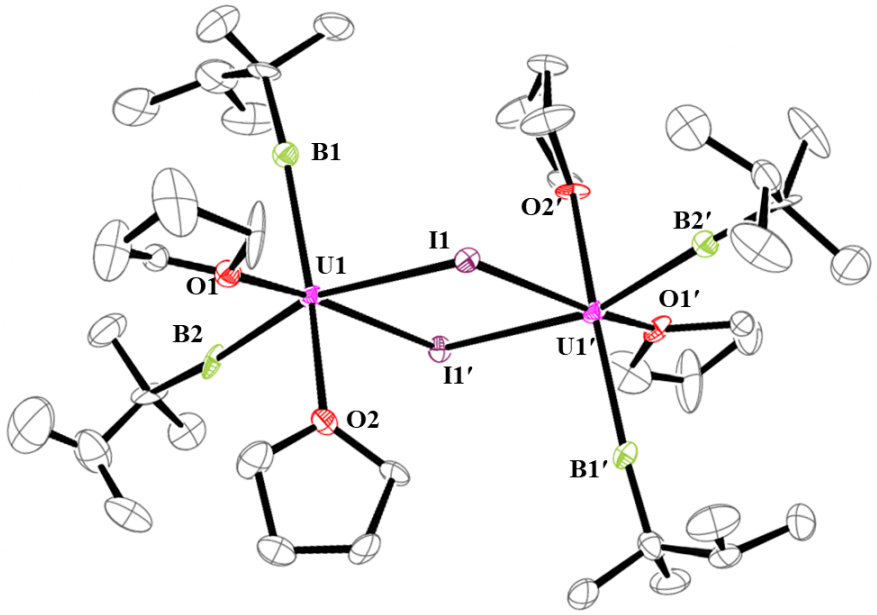

Figure D.4: Molecular structure of **D.4**. Ellipsoids are drawn at the 35% probability level and hydrogen atoms have been omitted for clarity.

Synthesis of Pentamethylcyclopentadienyl Uranium Borohydride Complexes. It was of interest to examine uranium borohydride compounds within heteroleptic ligand environments similar to the studies described in Chapter 5. Accordingly, $(C_5Me_5)_2U(BH_4)(THF)$, **D.5**, was synthesized from $(C_5Me_5)_2UI(THF)$ and $NaBH_4$ in THF, eq D.4. Compound **D.5** could also be synthesized from **D.1** and two equivalents of KC_5Me_5 in THF, eq D.4.

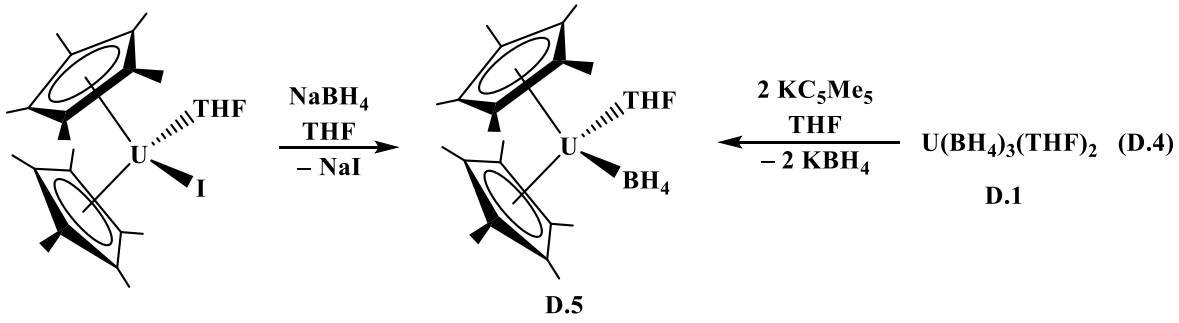

The ^1H NMR spectrum of **D.5** in C_6D_6 displayed a resonance at −2.43 ppm assigned to the C_5Me_5 ligands and two peaks at −14.87 and −42.46 ppm that are assigned to the THF ligand. All

three of these resonances are consistent with the U(III) bent metallocene environment, but the BH_4 resonance could not be conclusively identified. The infrared spectrum displayed two absorptions at 2414 and 2273 cm^{-1}, indicating a BH_4 group was present.

Crystallization of **D.5** from a concentrated hexane solution at −35 °C afforded dark green crystals that confirmed the structure, Figure D.5. Compound **D.5** crystallized in the $P\bar{1}$ space group with two independent formula units in the unit cell. The structure is isomorphous with the yttrium analog $(C_5Me_5)_2Y(BH_4)(THF)$.[36]

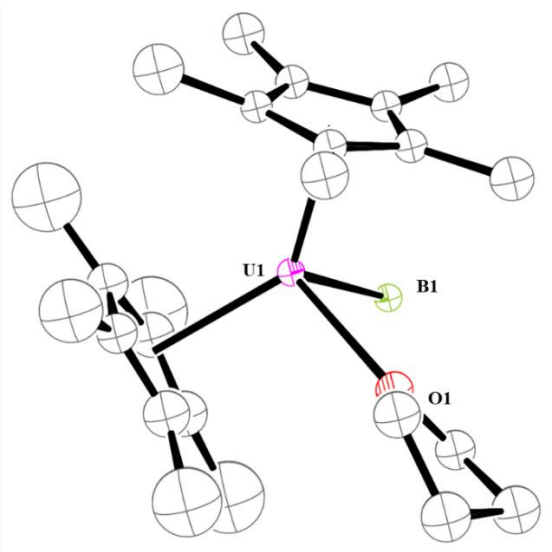

Figure D.5: Molecular structure of **D.5**. Ellipsoids are drawn at the 50% probability level and hydrogen atoms have been omitted for clarity.

Attempts to synthesize a mono-cyclopentadienyl complex were also made. Compound **D.2** reacted with KC_5Me_5 in THF to form a brown solid, **D.6**. The IR spectrum of **D.6** displayed three B–H stretching frequencies at 2473, 2231, and 2111 cm^{-1} which suggests the BH_4 units are bound in an asymmetric manner and could be either mono-, bi- or tridentate. The ^1H NMR spectrum in C_6D_6 displayed peaks at 12.41 and −2.36 ppm that integrate in an 8:15 ratio, assigned to two BH_4 ligands and one C_5Me_5 ligand, respectively. Two additional peaks at −14.84 and −42.35 ppm are

assigned to bound THF and the integration suggests that two THF molecules are bound in solution. The spectroscopic data support the formulation of **D.6** as $(C_5Me_5)U(BH_4)_2(THF)_2$, eq D.5.

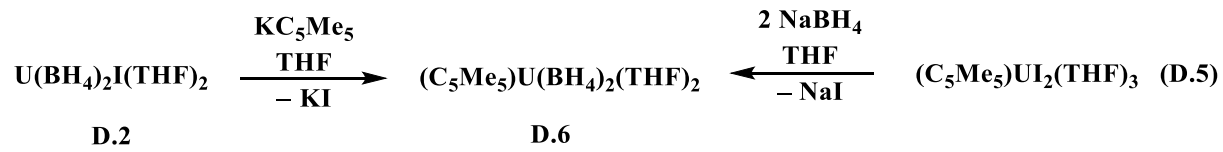

Compound **D.6** could also be synthesized from $(C_5Me_5)UI_2(THF)_3$ and $NaBH_4$ in THF, eq D.5.

$Me_2C{=}CMe_2$ was added to a solution of **D.5** in THF to investigate whether **D.5** was capable of the hydroboration reactivity observed in eq D.3. No reaction was observed after 24 hours. The same result was observed when the reaction was performed in hexane, which suggested that the presence of bound THF was not the determining factor for the observed reactivity results. The overall lack of reactivity is attributed to the steric size of the C_5Me_5 ligands. The mechanism for the hydroboration of uranium borohydride compounds has not been studied and it is interesting to consider an intermediate where the alkene must bind to the uranium center before reacting with the B–H bond, in which case the large C_5Me_5 ligands may prevent this from occurring.

The reduction of **D.5** was investigated to determine if a heteroleptic U(II) species could be formed with BH_4 ligands, similar to the results presented in Chapters 2 and 5. The reaction of **D.5** with KC_8 in the presence of crypt in THF at −35 °C led to a color change from green to dark blue, suggestive of a U(II) species, but the solution changed to red within seconds. If a U(II) compound was formed, it was extremely short lived. Crystallization from THF/hexane at −35 °C afforded dichroic green/brown crystals of $[K(crypt)][(C_5Me_5)_2U(BH_4)_2]$, **D.7**, which was identified by X-ray diffraction, eq D.6, Figure D.6.

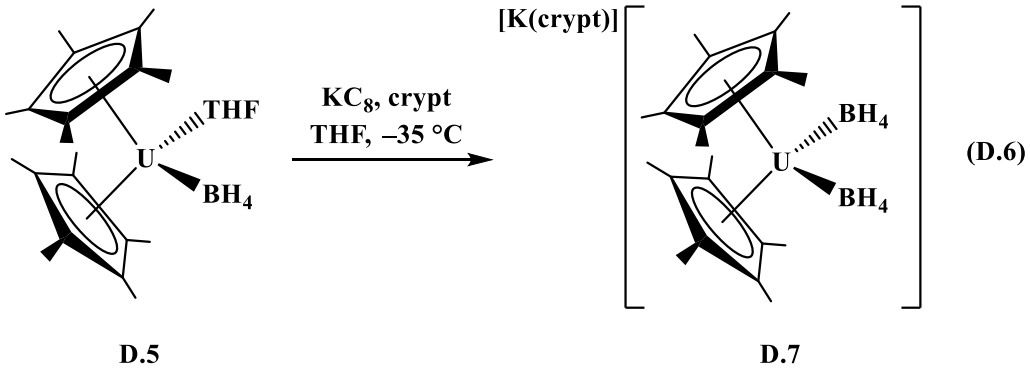

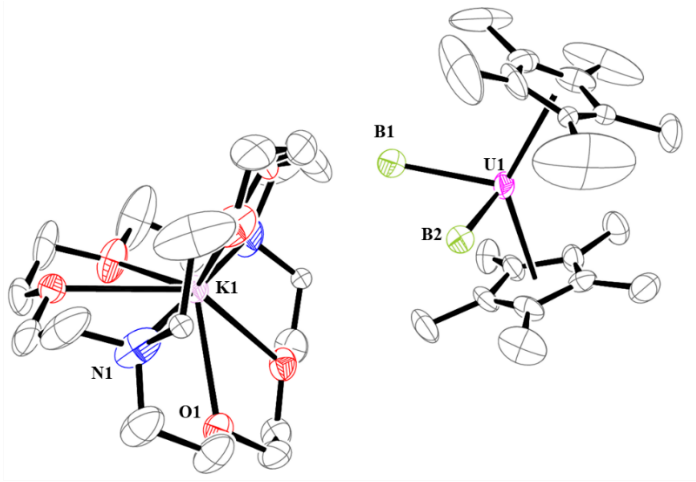

Figure D.6: Molecular structure of **D.7**. Ellipsoids are drawn at the 50% probability level and hydrogen atoms have been omitted for clarity.

Conclusion

The coordination chemistry of U(III) with borohydride ligands has been expanded to include heteroleptic complexes with C_5Me_5, BH_4, and I ligands. $U(BH_4)_3(THF)_2$ and $U(BH_4)_2I(THF)_3$ could be synthesized from UI_3 and the appropriate amount of $NaBH_4$ and were crystallographically characterized. The mono-borohydride complex $U(BH_4)I_2(THF)_4$ was also crystallographically characterized. Hydroboration of tetramethylethylene with $U(BH_4)_3(THF)_2$ and $U(BH_4)_2I(THF)_3$ led to the formation of substituted alkylborohydride ligands, which suggests that other unsaturated substrates should be investigated for similar reactivity.\

Experimental

All manipulations and syntheses described below were conducted with the rigorous exclusion of air and water using standard Schlenk line and glovebox techniques under an argon atmosphere. Solvents were sparged with UHP argon and dried by passage through columns containing a copper-based drying agent, alumina, and/or molecular sieves prior to use. Deuterated NMR solvents were dried over NaK alloy or molecular sieves, degassed by three freeze–pump–thaw cycles, and vacuum transferred before use. ^{1}H were recorded on a CRYO500 MHz spectrometer at 298 K and referenced to residual protio-solvent resonances. Infrared spectra were recorded as compressed solids on an Agilent Cary 630 ATR-FTIR.

$U(BH_4)_3(THF)_2$,[10] UI_3,[37] $(C_5Me_5)_2UI(THF)$,[38] $(C_5Me_5)UI_2(THF)_3$,[38] and KC_8[39] were prepared according to literature procedures. KC_5Me_5 was prepared from HC_5Me_5 and $KN(SiMe_3)_2$ in toluene. $NaBH_4$ and 2.2.2-cryptand (crypt) were used as received. $Me_2C{=}CMe_2$ was degassed by three freeze-pump-thaw cycles before use.

Synthesis of $U(BH_4)_3(THF)_2$, D.1. Compound **D.1** was prepared are previously described[10] and confirmed by infrared spectroscopy. Red X-ray quality crystals of $U(BH_4)_3(THF)_4$ were grown by layering a concentrated THF solution of **D.1** under hexane at −35 °C.

Synthesis of $U(BH_4)_2I(THF)_2$, D.2. Compound **D.2** was made in an analogous manner to **D.1**.[10] UI_3 (100 mg, 0.162 mmol) and $NaBH_4$ (12 mg, 0.32 mmol) were combined in THF (10 mL) to form a dark red solution. The solution was stirred overnight then dried under vacuum. The solids were redissolved in minimal THF and placed in the freezer at −35 °C. Overnight, dark red crystals of **D.2** formed. Red X-ray quality crystals of $U(BH_4)_2I(THF)_4$ were grown by layering a concentrated THF solution of **D.2** under hexane at −35 °C. IR (cm^{-1}): 2978m, 2889m, 2430s, 2213s, 1445m, 1340m, 1293w, 1243w, 1146s, 1087w, 1006s, 916m, 833s, 667s.

Synthesis of $U(H_3BCMe_2CHMe_2)_3(THF)_2$, D.3. **D.1** (50 mg, 0.12 mmol) was dissolved in THF (3 mL) to form a red solution. $Me_2C{=}CMe_2$ (31 mg, 0.37 mmol) was added slowly via pipet. The solution was stirred overnight then dried and extracted into toluene, filtered, and dried under vacuum to afford a red oil of **D.3**.

Synthesis of $[U(H_3BCMe_2CHMe_2)_2(THF)_2(\mu\text{–}I)]_2$, D.4. **D.2** (55 mg, 0.10 mmol) was dissolved in THF to form a red solution. $Me_2C{=}CMe_2$ (33 mg, 0.39 mmol) was added and the red color of the solution faded slightly in intensity. The solution was stirred overnight then dried under vacuum. The product was extracted into hexane, filtered, and dried to afford a red oil (57 mg, 81%). Dark red crystals of **D.4** suitable for X-ray diffraction were grown from a concentrated hexane solution at −35 °C after two days.

Synthesis of $(C_5Me_5)_2U(BH_4)(THF)$, D.5, from $(C_5Me_5)_2UI(THF)$. $(C_5Me_5)_2UI(THF)$ (80 mg, 0.11 mmol) and $NaBH_4$ (4 mg, 0.1 mmol) were combined in THF to form a green solution. The solution was stirred overnight and white solids were removed via centrifugation. The solution was dried and the product was extracted into hexane. The solution was filtered and dried to afford a green solid of **D.5** (53 mg, 79%). ^{1}H NMR (C_6D_6): δ −2.43 (s, 30H, C_5Me_5), −14.87 (s, 4H, THF), −42.46 ppm (s, 4H, THF). IR (cm^{-1}): 2955w, 2877m, 2846m, 2403m, 2118m, 1476m, 1442m, 1354s, 1295m, 1258m, 1132m, 1101s, 948s, 830m, 752m.

Synthesis of D.5, from D.1. **D.1** (81 mg, 0.18 mmol) and KC_5Me_5 (107 mg, 0.366 mmol) were combined in THF to form a dark green solution. The solution was stirred overnight. White solids were removed via centrifugation. The solution was dried then the product was extracted into toluene, filtered, and dried. The tacky solids were triturated with hexane and dried to afford a dark green powder of **D.5** (78 mg, 72%).

Synthesis of $(C_5Me_5)U(BH_4)_2(THF)_2$, D.6, from $(C_5Me_5)UI_2(THF)_3$. $(C_5Me_5)UI_2(THF)_3$ (76 mg, 0.090 mmol) and $NaBH_4$ (7 mg, 0.18 mmol) were combined in THF to form a red solution. The solution was stirred overnight then dried under vacuum. The product was extracted into toluene, filtered, and dried to afford a brown solid of **D.6**. ^{1}H NMR (C_6D_6): δ 12.41 (s, 8H, BH_4), −2.36 (s, 15H, C_5Me_5), −14.86 (s, 8H, THF), −42.40 ppm (s, 8H, THF). IR (cm^{-1}): 2895m, 2852m, 2473s, 2231s, 2111s, 1487w, 1432m, 1377m, 1162s, 1095w, 1063w, 1020m, 946m, 890m, 801m, 752m, 694w.

Synthesis of D.6 from D.2. D.2 (110 mg, 0.204 mmol) and KC_5Me_5 (28 mg, 0.16 mmol) were combined in THF. The initially red solution turned green/brown after a few hours. The solution was stirred overnight. White solids were removed via centrifugation and solvent was removed under vacuum. The product was extracted into toluene, the green solution was filtered, and dried to afford **D.5** as a green solid (47 mg, 54% based on KC_5Me_5).

Synthesis of [K(crypt)][$(C_5Me_5)_2U(BH_4)_2$], D.7, from D.5. D.5 (53 mg, 0.089 mmol) and crypt (23 mg, 0.061 mmol) were dissolved in THF (2 mL) to form a green solution and chilled to −35 °C. KC_8 (excess) was packed into a pipet column and placed in the freezer. A vial of hexane and multiple pipets were also placed in the freezer. After allowing the equipment to cool, the green solution was passed over the KC_8, forming a dark green solution, and eluted directly under the hexane for crystallization. Overnight, dark green/brown dichroic crystals of **D.7**, suitable for X-ray diffraction, formed.

References

(1) Schlesinger, H. I.; Brown, H. C.; Abraham, B.; Bond, A. C.; Davidson, N.; Finholt, A. E.; Gilbreath, J. R.; Hoekstra, H.; Horvitz, L.; Hyde, E. K.; Katz, J. J.; Knight, J.; Lad, R. A.; Mayfield, D. L.; Rapp, L.; Ritter, D. M.; Schwartz, A. M.; Sheft, I.; Tuck, L. D.; Walker,

A. O. New Developments in the Chemistry of Diborane and the Borohydrides. I. General Summary. *J. Am. Chem. Soc.* **1953**, *75*, 186–190, DOI: 10.1021/ja01097a049.

(2) Schlesinger, H. I.; Brown, H. C. Uranium(IV) Borohydride. *J. Am. Chem. Soc.* **1953**, *75*, 219–221, DOI: 10.1021/ja01097a058.

(3) Schlesinger, H. I.; Brown, H. C.; Horvitz, L.; Bond, A. C.; Tuck, L. D.; Walker, A. O. The Methyl Derivatives of Uranium(IV) Borohydride. *J. Am. Chem. Soc.* **1953**, *75*, 222–224, DOI: 10.1021/ja01097a059.

(4) Marks, T. J.; Kolb, J. R. Covalent Transition Metal, Lanthanide, and Actinide Tetrahydroborate Complexes. *Chem. Rev.* **1977**, *77*, 263–293, DOI: 10.1021/cr60306a004.

(5) Ephritikhine, M. Synthesis, Structure, and Reactions of Hydride, Borohydride, and Aluminohydride Compounds of the f-Elements. *Chem. Rev.* **1997**, *97*, 2193–2242, DOI: 10.1021/cr960366n.

(6) Volkov, V. V.; Myakishev, K. G. *Radiokhim* **1980**, 745.

(7) Paskevicius, M.; Jepsen, L. H.; Schouwink, P.; Černý, R.; Ravnsbæk, D. B.; Filinchuk, Y.; Dornheim, M.; Besenbacher, F.; Jensen, T. R. Metal Borohydrides and Derivatives – Synthesis, Structure and Properties. *Chem. Soc. Rev.* **2017**, *46*, 1565–1634, DOI: 10.1039/C6CS00705H.

(8) Mannig, D.; Noth, H. Metal Boranates and Boranatometallates. 13. Preparation and Molecular Structure of Uranium(III) Tetrahydridoborate-3-Tetrahydrofuran. *Z. Anorg. Allg. Chem.* **1986**, *543*, 66, DOI: 10.1002/zaac.19865431208.

(9) Moody, D. C.; Odom, J. D. The Chemistry of Trivalent Uranium. *J. Inorg. Nucl. Chem.* **1979**, *41*, 533–535, DOI: 10.1016/0022-1902(79)80439-x.

(10) Arnold, P. L.; Stevens, C. J.; Farnaby, J. H.; Gardiner, M. G.; Nichol, G. S.; Love, J. B.

New Chemistry from an Old Reagent: Mono- and Dinuclear Macrocyclic Uranium(III) Complexes from $[U(BH_4)_3(THF)_2]$. *J. Am. Chem. Soc.* **2014**, *136*, 10218–10221, DOI: 10.1021/ja504835a.

(11) Daly, S. R.; Girolami, G. S. Synthesis, Characterization, and Structures of Uranium(III) N, N-Dimethylaminodiboranates. *Inorg. Chem.* **2010**, *49*, 5157–5166, DOI: 10.1021/ic100290j.

(12) Baudry, D.; Bulot, E.; Charpin, P.; Ephritikhine, M.; Lance, M.; Nierlich, M.; Vigner, J. Arene Uranium Borohydrides: Synthesis and Crystal Structure of $(\eta\text{-}C_6Me_6)U(BH_4)_3$. *J. Organomet. Chem.* **1989**, *371*, 155–162, DOI: 10.1016/0022-328X(89)88022-2.

(13) Arliguie, T.; Belkhiri, L.; Bouaoud, S. E.; Thuéry, P.; Villiers, C.; Boucekkine, A.; Ephritikhine, M. Lanthanide(Lll) and Actinide(Lll) Complexes $[M(BH_4)_2(THF)_5][BPh_4]$ and $[M(BH_4)_2(18\text{-Crown-6})][BPh_4]$ (M = Nd, Ce, U): Synthesis, Crystal Structure, and Density Functional Theory Investigation of the Covalent Contribution to Metal-Borohydride Bonding. *Inorg. Chem.* **2009**, *48*, 221–230, DOI: 10.1021/ic801685v.

(14) Arliguie, T.; Lance, M.; Nierlich, M.; Vigner, J.; Ephritikhine, M. Inverse Cycloheptatrienyl Sandwich Complexes. Crystal structure of $[U(BH_4)_2(OC_4H_8)_5][(BH_4)_3U(\mu\text{-}\eta^7,\eta^7\text{-}C_7H_7)U(BH_4)_3]$ *J. Chem. Soc. Chem. Commun.* **1994**, *179*, 847–848.

(15) Boronski, J. T.; Doyle, L. R.; Seed, J. A.; Wooles, A. J.; Liddle, S. T. F-Element Half-Sandwich Complexes: A Tetrasilylcyclobutadienyl–Uranium(IV)–Tris(Tetrahydroborate) Anion Pianostool Complex. *Angew. Chemie Int. Ed.* **2020**, *59*, 295–299, DOI: 10.1002/anie.201913640.

(16) Fetrow, T. V.; Grabow, J. P.; Leddy, J.; Daly, S. R. Convenient Syntheses of Trivalent Uranium Halide Starting Materials without Uranium Metal. *Inorg. Chem.* **2021**, *60*, 7593–

7601, DOI: 10.1021/acs.inorgchem.1c00598.

(17) Arnold, P. L.; Farnaby, J. H.; Gardiner, M. G.; Love, J. B. Uranium(III) Coordination Chemistry and Oxidation in a Flexible Small-Cavity Macrocycle. *Organometallics* **2015**, *34*, 2114–2117, DOI: 10.1021/om5012193.

(18) Villiers, C.; Ephritikhine, M. Novel Hydroboration of Highly Substituted Alkenes Catalysed by Borohydride Complexes of Uranium, Neodymium and Zirconium. *J. Chem. Soc. Chem. Commun.* **1995**, No. 9, 979, DOI: 10.1039/c39950000979.

(19) Torrent, M.; Solà, M.; Frenking, G. Theoretical Studies of Some Transition-Metal-Mediated Reactions of Industrial and Synthetic Importance. *Chem. Rev.* **2000**, *100*, 439–494, DOI: 10.1021/cr980452i.

(20) Beletskaya, I.; Pelter, A. Hydroborations Catalysed by Transition Metal Complexes. *Tetrahedron* **1997**, *53*, 4957–5026, DOI: 10.1016/S0040-4020(97)00001-X.

(21) Lee, H. S.; Isagawa, K.; Toyoda, H.; Otsuji, Y. Regio- And Stereo-Selectivities In the Titanium Complex Catalyzed Hydroboration of Carbon–Carbon Double Bonds In Various Unsaturated Compounds. *Chem. Lett.* **1984**, *13*, 673–676, DOI: 10.1246/cl.1984.673.

(22) Lee, H. S.; Isagawa, K.; Otsuji, Y. Hydroboration of Alkenes and Alkynes with Sodium Borohydride Catalyzed by Titanium Complex. *Chem. Lett.* **1984**, *13*, 363–366, DOI: 10.1246/cl.1984.363.

(23) Kumar, K. S. R.; Baskaran, S.; Chandrasekaran, S. An Unusual Anti-Markovnikov Hydration of Alkenes with Titanium(III) Tetrahydroborates. *Tetrahedron Lett.* **1993**, *34*, 171–174, DOI: 10.1016/S0040-4039(00)60086-2.

(24) Periasamy, M.; Thirumalaikumar, M. Methods of Enhancement of Reactivity and Selectivity of Sodium Borohydride for Applications in Organic Synthesis. *J. Organomet.*

Chem. **2000**, *609*, 137–151, DOI: 10.1016/S0022-328X(00)00210-2.

(25) Isagawa, K.; Sano, H.; Hattori, M.; Otsuji, Y. Catalytic Hydroboration of Olefins by use of Titanium Complex As Catalyst. *Chem. Lett.* **1979**, *8*, 1069–1072, DOI: 10.1246/cl.1979.1069.

(26) Villiers, C.; Ephritikhine, M. Borane-Catalyzed Hydroboration of Substituted Alkenes by Lithium Borohydride or Sodium Borohydride. *Tetrahedron Lett.* **2003**, *44*, 8077–8079, DOI: 10.1016/j.tetlet.2003.09.055.

(27) Tanaka, R.; Shinto, Y.; Matsuzaki, R.; Nakayama, Y.; Shiono, T. Stereospecific Polymerization of Conjugated Dienes Using Neodymium Alkylborohydride Complexes. *Dalton Trans.* **2019**, *48*, 7267–7273, DOI: 10.1039/C8DT04220A.

(28) Brown, H. C.; Singaram, B.; Punnoose Mathew, C. Addition Compounds of Alkali Metal Hydrides. 20. Reaction of Representative Mono- and Dialkylboranes with Saline Hydrides To Form the Corresponding Alkylborohydrides. *J. Org. Chem.* **1981**, *46*, 2712–2717, DOI: 10.1021/jo00326a022.

(29) Ortu, F.; Packer, D.; Liu, J.; Burton, M.; Formanuik, A.; Mills, D. P. Synthesis and Structural Characterization of Lanthanum and Cerium Substituted Cyclopentadienyl Borohydride Complexes. *J. Organomet. Chem.* **2018**, *857*, 45–51, DOI: 10.1016/j.jorganchem.2017.09.010.

(30) Heinemann, F. W.; Löffler, S.; Meyer, K. Experimental Crystal Structure Determination. *CSD Commun.* **2018**, DOI: 10.5517/ccdc.csd.cc20zc8n.

(31) Hitchcock, P. B.; Hulkes, A. G.; Lappert, M. F. Oxidation in Nonclassical Organolanthanide Chemistry: Synthesis, Characterization, and X-Ray Crystal Structures of Cerium(III) and -(IV) Amides. *Inorg. Chem.* **2004**, *43*, 1031–1038, DOI: 10.1021/ic035100v.

(32) Petriček, S. Syntheses of Lanthanide Bromide Complexes from Oxides and the Crystal Structures of $[LnBr_3(DME)_2]$ (Ln = Pr, Nd, Sm, Eu), $[LnBr_3(THF)_4]$ (Ln = Pr, Sm) and $[EuBr_2(THF)_5][EuBr_4(THF)_2]$. *Polyhedron* **2004**, *23*, 2293–2301, DOI: 10.1016/j.poly.2004.07.009.

(33) Boyle, T. J.; Ottley, L. A. M.; Alam, T. M.; Rodriguez, M. A.; Yang, P.; Mcintyre, S. K. Structural Characterization of Methanol Substituted Lanthanum Halides. *Polyhedron* **2010**, *29*, 1784–1795, DOI: 10.1016/j.poly.2010.02.027.

(34) Galley, S. S.; Sperling, J. M.; Windorff, C. J.; Zeller, M.; Albrecht-Schmitt, T. E.; Bart, S. C. Conversion of Americia to Anhydrous Trivalent Americium Halides. *Organometallics* **2019**, *38*, 606–609, DOI: 10.1021/acs.organomet.8b00840.

(35) Gaunt, A. J.; Reilly, S. D.; Enriquez, A. E.; Hayton, T. W.; Boncella, J. M.; Scott, B. L.; Neu, M. P. Low-Valent Molecular Plutonium Halide Complexes. *Inorg. Chem.* **2008**, *47*, 8412–8419, DOI: 10.1021/ic8009139.

(36) Demir, S.; Siladke, N. A.; Ziller, J. W.; Evans, W. J. Scandium and Yttrium Metallocene Borohydride Complexes: Comparisons of $(BH_4)^{1-}$ vs. $(BPh_4)^{1-}$ Coordination and Reactivity. *Dalton Trans.* **2012**, *41*, 9659–9666, DOI: 10.1039/c2dt30861d.

(37) Carmichael, C. D.; Jones, N. A.; Arnold, P. L. Low-Valent Uranium Iodides: Straightforward Solution Syntheses of UI_3 and UI_4 Etherates. *Inorg. Chem.* **2008**, *47*, 8577–8579, DOI: 10.1021/ic801138e.

(38) Avens, L. R.; Burns, C. J.; Butcher, R. J.; Clark, D. L.; Gordon, J. C.; Schake, A. R.; Scott, B. L.; Watkin, J. G.; Zwick, B. D. Mono(Pentamethylcyclopentadienyl)Uranium(III) Complexes: Synthesis, Properties, and X-Ray Structures of $(\eta\text{-}C_5Me_5)UI_2(THF)_3$, $(\eta\text{-}C_5Me_5)UI_2(Py)_3$, and $(\eta\text{-}C_5Me_5)U[N(SiMe_3)_2]_2$. *Organometallics* **2000**, *19*, 451–457, DOI:

10.1021/om990718r.

(39) Bergbreiter, D. E.; Killough, J. M. Reactions of Potassium-Graphite. *J. Am. Chem. Soc.* **1978**, *100*, 2126–2134, DOI: 10.1021/ja00475a025.

Appendix E:

DFT Studies of f-Block Complexes

Introduction

Previous Chapters (2, 4, 5, and 10) and Appendices (A and B) have reported DFT studies on various rare-earth metal and actinide complexes. Beyond those already discussed, many other species have been investigated by DFT methods. This Appendix summarizes these studies. Most studies were aimed at understanding the ground state electronic structure in various coordination environments much like what was described in Chapter 2. A few compounds were investigated computationally to support synthetic and spectroscopic studies by the Evans group. As a result, the electronic structures of these compounds are discussed in more detail than others.

Computational Details

Electronic structure calculations were carried out at the density functional level of theory using the TPSSh functional[1] with Grimme's D3 dispersion correction[2,3] and the resolution of the identity (RI-J) approximation.[4] No symmetry constraints were applied. Effective core potentials (ECPs)[5] with the def-TZVP[6] or def2-TZVP[6] (when available) basis set were used for the central metal atom and polarized split-valence basis sets with diffuse functions def2-SV(P)[7] were used for the light atoms. Quadrature grids of size 4 or m4 were used throughout.[8] For anionic species, the continuum solvation model COSMO[9] was included in the calculations to model solvent effects with a dielectric constant ε = 7.52 for THF.[10] Geometry optimizations were computed starting from the X-ray structures when available with geometry convergence threshold 10^{-4} a.u. and energy converge of at least 10^{-7} a.u. Ground state geometries were confirmed by the lack of imaginary frequencies in the vibrational spectra.[11] Time dependent DFT calculations of vertical excitations and oscillator strengths[12] were carried out on the optimized structures with identical

basis sets as described above. UV-Visible spectra were simulated using Gaussian line profiles with a root mean-square width of 0.15 eV. Molecular orbitals and electronic transition states were analyzed with VMD[13] and Mulliken population analysis. All computations were completed using the TURBOMOLE program suite V7.4.1.[14,15]

Results and Discussion

Table E.1 summarizes the DFT studies with the calculated ground states, if time-dependent DFT (TDDFT) was performed to simulate the UV-Visible spectrum, and any additional comments on the species.

Table E.1: Summary of calculated electronic ground states. Cp* = C_5Me_5; Cp = C_5H_5; acac = acetylacetonate; Cp^{tet} = C_5Me_4H; Ar = $–C_6H_3{}^tBu_2$-2,6; TMP = NC_4Me_4; R = $SiMe_3$.

Compound	Ground State	TDDFT	Comments
$\{Cp^*_2Th[^iPrNC(Me)N^iPr]\}^{1-}$	$6d^2$, singlet favored	yes	a
Cp_3Th	$6d^1$	yes	a
$[Cp_3ThCl]^{1-}$	$5f^1$	yes	a
$Cp^*_2Th[CyNC(Me)NCy]$	$6d^1$	yes	a
$\{Cp^*_2Th[CyNC(Me)NCy]\}^{1-}$	$6d^2$, singlet favored	yes	a
$(C_6{}^tBu_3H_3)_2Y$	$4d^3$, singlet and triplet close in energy	no	see ref 16,17
$[(C_6{}^tBu_3H_3)_2Y]^{1+}$	$4d^2$	no	
$Cp^*_2Th(acac)$	$6d^0$, acac radical	no	
$Cp^*_2ThCp^{tet}$	$6d^1$	yes	
$[Cp^*_2ThCp^{tet}]^{1-}$	$6d^2$	yes	
$[Cp_4Th]^{1-}$	$5f^1$	yes	a
$Th(OCPh_3)_3$	$6d^1$, significant 7s character	no	structure is pyramidalized
$[Lu(crypt)]^{2+}$	$4f^{14}5d^1$	no	C_2 ground state. See ref 18
$[U(SAr)_4]^{2-}$	$5f^36d^1$	no	C_4 ground state. Structure is pyramidalized
$[Th(OAr)_4]^{1-}$	$6d^1$	yes (done in C_1 at D_4 geometry)	D_4 ground state
$[(TMP)_3Y]^{1-}$	4d1	no	all three rings are η^5

$[Sc(Si^tBu_2Me)_3]^{1-}$	$3d^1$	no	a
$[Y(Si^tBu_2Me)_3]^{1-}$	$4d^1$	no	a, structure is pyramidalized
$[La(NR_2)_3]^{1-}$	$5d^1$	yes (additional p primitive, did in C_1 at C_3 geom)	a, C_3 ground state

a: To support synthetic studies

Cp_3Th, $[Cp_4Th]^{1-}$, and $[Cp_3ThCl]^{1-}$ were analyzed to aid in the chemical reduction studies of Cp_3ThCl. Experimentally, KC_8 reduction of Cp_3ThCl formed a blue/green solution which had a rhombic EPR signal suggestive of a metal-based radical, Figure E.1.

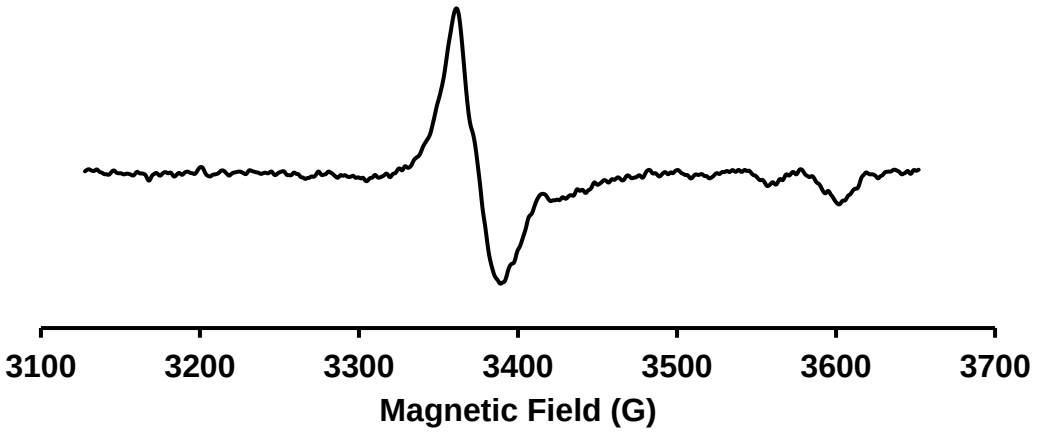

Figure E.1: X-band EPR of the reaction product of Cp_3ThCl and KC_8 collected as a frozen THF solution at 77 K. g = 2.00, 1.99, 1.87.

This solution also had a broad absorption in the UV-visible spectrum around 900 nm, Figure E.2. TDDFT studies on Cp_3Th and $[Cp_3ThCl]^{1-}$ both showed broad transitions around this energy, but the computed transitions for Cp_3Th were higher in energy than the experimental spectrum and computed transitions for $[Cp_3ThCl]^{1-}$ were lower in energy, Figure E.2.

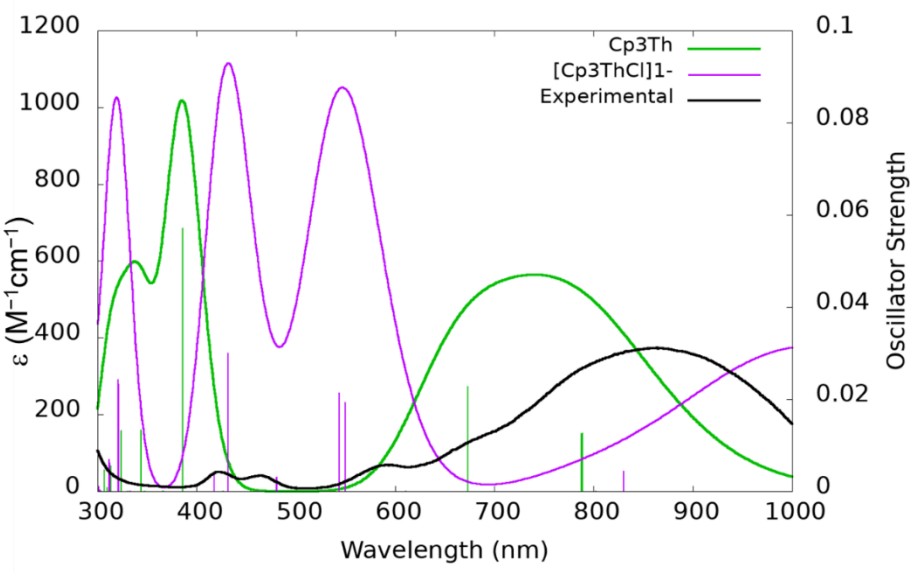

Figure E.2: Experimental UV-visible spectrum of the KC_8 reaction product of Cp_3ThCl (black), and the computed UV-visible spectrum of Cp_3Th (green) and $[Cp_3ThCl]^{1-}$ (purple) with oscillator strengths shown as vertical lines. A Gaussian broadening of 0.15 eV was applied and both computed spectra were scaled by a factor of 0.10 to ease comparison.

The thorium amidinate species $Cp^*_2Th[^iPrNC(Me)N^iPr]$, $\{Cp^*_2Th[^iPrNC(Me)N^iPr]\}^{1-}$, $Cp^*_2Th[CyNC(Me)NCy]$, and $\{Cp^*_2Th[CyNC(Me)NCy]\}^{1-}$ were studied computationally to support synthetic experiments in attempts to form new Th(II) species. $Cp^*_2Th[^iPrNC(Me)N^iPr]$ was previously reported and was shown to be a $6d^1$ Th(III) compound.[19] Computationally, both amidinate complexes were predicted to form $6d^1$ Th(III) and $6d^2$ Th(II) compounds. TDDFT studies on $Cp^*_2Th[^iPrNC(Me)N^iPr]$ and $Cp^*_2Th[CyNC(Me)NCy]$ showed electronic transitions at similar energies which suggested the nature of the substituents on the amidinate ligands did not drastically affect the electronic structure of the thorium center.

$[Th(OAr)_4]^{1-}$ was also studied computationally to support synthetic studies. The OAr′ complex $[Th(OAr')_4]^{1-}$ (OAr′ = $-OC_6H_2{}^tBu_2$-2,6-Me-4) was previously reported and was shown to form a square planar, $6d^1$ Th(III) complex.[20] The $[Th(OAr)_4]^{1-}$ complex, without the methyl

substituent in the *para* position of the aryloxide ligand, was also calculated to adopt a square planar geometry. TDDFT studies of $[Th(OAr)_4]^{1-}$ showed minimal changes from the spectrum of $[Th(OAr')_4]^{1-}$, which suggested that the methyl substituent had little effect on the electronic structure, much like what was observed for the amidinate systems above.

Other thorium compounds $Th(OCPh_3)_3$, $Cp^*_2ThCp^{tet}$, $[Cp^*_2ThCp^{tet}]^{1-}$, and $Cp^*_2Th(acac)$ were studied. Both $Th(OCPh_3)_3$ and $Cp^*_2ThCp^{tet}$ were calculated to be $6d^1$ Th(III) compounds. The ground state structure of $Th(OCPh_3)_3$ was significantly pyramidalized. The HOMO was a $6dz^2$-like orbital, but Mulliken population analysis revealed that this orbital had 44% 7s character and 37% 6d character. While Mulliken population analysis usually overestimates the amount of *n*s character, to my knowledge such a drastic difference has not been previously observed. This might suggest that the pyramidalization of the compound has an effect on the orbital mixing. If this is generalizable to other f-element systems, it could be useful for designing compounds with high *n*s character which has been shown to be an important property for qubit systems.[21]

$[Cp^*_2ThCp^{tet}]^{1-}$ was calculated to be a diamagnetic, $6d^2$ Th(II) species, with the $5f^16d^1$ triplet state being higher in energy by 17.6 kcal/mol. This result is analogous to the U(II) compound $[Cp^*_2UCp^{tet}]^{1-}$ in Chapter 5. Interestingly, the thorium acac compound $Cp^*_2Th(acac)$ was calculated to be a Th(IV) compound, with a radical residing on the acac ligand. The ground state structure of $Cp^*_2Th(acac)$ was pseudo tetrahedral and based on the results from Chapter 2, might suggest that there is no low-lying 6d orbital in this geometry. However, the amidinate compound $Cp^*_2Th[^iPrNC(Me)N^iPr]$ also adopts a pseudo tetrahedral geometry so it is more likely that the acac ligand orbitals are lower in energy than the valence orbitals on thorium, such that the acac is reduced before the thorium center.

A uranium thiophenolate compound was studied, where $[U(SAr)_4]^{2-}$ is the thiophenol analog to $[Th(OAr)_4]^{1-}$. While it was found that $[Th(OAr)_4]^{1-}$ adopted a square planar geometry, $[U(SAr)_4]^{2-}$ was found to adopt a slightly pyramidalized geometry. However, a $5f^36d^1$ U(II) configuration was still preferred with a $6dz^2$-like HOMO. Ligands with second- and third-row donor atoms are rare for f element compounds,[22–24] and there are no Th(III), Th(II), or U(II) compounds known.

Rare-earth metal compounds were also studied to find other ligand environments that may be suitable for forming non-traditional compounds. The TMP ligand (TMP = tetramethylpyrrolyl, NC_4Me_4) can be considered to be a heteroatom-substituted analog for Cp^{tet} and has been studied in f element chemistry and forms η^1-NC^4Me^4 complexes binding through the nitrogen atom.[25] Computationally, a tris-η^5 ring system was studied although this has not yet been observed synthetically. Replacing the three CH moieties with a nitrogen atom in Cp^{tet}_3Y, then reoptimizing the structure, led to a ground state geometry of $(TMP)_3Y$ with all three TMP ligand bound η^5. The ground state of the reduced $[(TMP)_3Y]^{1-}$ also had all three rings bound η5 and was consistent with a $4d^1$ configuration of Y(II). These results suggest that other heteroatom-substituted rings may be able to stabilize the highly reducing nd^1 systems of the rare-earth metals.

A different ligand system that has been successful in stabilizing traditional Ln(II) ions is the crypt system.[18] 2.2.2-Cryptand has also been found to encapsulate Ln(III) and An(III) ions.[26–29] However, the crypt ligand environment has not yet been found to stabilize non-traditional Ln(II) ions. In Chapter 5 it was found that $[U(crypt)]^{2+}$ had a U(II) ion that was best described as having a $5f^36d^1$ electron configuration. It was of interest to determine if a non-traditional Ln(II) ion would be stabilized by crypt. Accordingly, $[Lu(crypt)]^{2+}$ was studied since Lu(III) has a $4f^{14}$ configuration and the added electron to form Lu(II) cannot occupy a 4f orbital. Calculations on

$[Lu(crypt)]^{2+}$ in C_2 symmetry are consistent with a $4f^{14}5d^1$ configuration with $5dz^2$-like HOMO. A species such as $[Lu(crypt)]^{2+}$ or $[Lu(crypt)][X]_2$ seems like a reasonable synthetic target.

The bis-arene compounds $(C_6{}^tBu_3H_3)_2Ln$ are the only formally zero-valent rare-earth metal complexes known. These were made by vaporizing the rare-earth metal into a solution of tri-*tert*-butylbenzene. Spectroscopic and magnetic data support $4f^n6s^2$ configurations for Pr, Nd, Sm, Eu, Gd, Tb, Dy, Ho, Er, Tm, and Yb, while Sc, Y, La, and Lu have nd^1 configurations. Since zero-valent compounds could be isolated, a natural progression is to examine the possibility of Ln(I) and Ln(−I) compounds, although this has no precedent in f element chemistry. To begin, calculations on $(C_6{}^tBu_3H_3)_2Y$ were performed which converged to a $4d^3$ ground state in C_i symmetry, where the triplet and singlet states were practically identical in energy. Other symmetry restraints were applied but the $4d^3$ configuration was always found to be lowest in energy. The calculation with a $5s^24d^1$ configuration would not readily converge, but suggested that this configuration was well over 4 eV / 92 kca/mol higher in energy than the $4d^3$ configuration. These results suggest some systematic error in the calculation or the need for additional parameters, since the results do not match the experimental data.

Nevertheless, the cationic species $[(C_6{}^tBu_3H_3)_2Y]^{1+}$ was investigated and a $4d^2$ configuration was found, which suggests that oxidation of $(C_6{}^tBu_3H_3)_2Y$ might form a Y(I) compound. The anionic species $[(C_6{}^tBu_3H_3)_2Y]^{1-}$ was also investigated and preliminary results suggest the reduction of the arene instead of forming a Y(−I) compound.

As mentioned above, compounds of non-traditional rare-earth metals with second- and third-row donors have not been reported. However, complexes of traditional Sm(II) and Yb(II) of the type $Ln(Si^tBu_2Me)_2(THF)_2$ have been reported.[30] To support synthetic studies, the tris(silanide) species $[Ln(Si^tBu_2Me)_3]^{1-}$ were investigated computationally for Sc and Y. Both

species were found to be pyramidalized like what was observed for the tris(alkyl) and tris(amide species) $Ln[CH(SiMe_3)_2]_3$ and $Ln(NR_2)_3$.[31–33] The Ln(II) species $[Ln(Si^tBu_2Me)_3]^{1-}$ (Ln = Y, Sc) were found to have an nd^1 configuration like what was observed for $[Ln(NR_2)_3]^{1-}$.[31,34] If the homoleptic Ln(III) species $Ln(Si^tBu_2Me)_3$ can be formed, it seems reasonable that the Ln(II) can be synthesized and will have nd^1 configurations.

The tris(amide) species $[Ln(NR_2)_3]^{1-}$ (R = $SiMe_3$) have been isolated for all the rare-earth metals besides La, Ce, and Pm.[31,34,35] For some reason, the La and Ce compounds appear to be significantly more reactive than the other analogs. To determine if there was an electronic explanation for the observed reactivity, $[La(NR_2)_3]^{1-}$ was investigated computationally. The ground state was consistent with a $5d^1$ La(II) species with a $5dz^2$-like HOMO. These results are consistent with the other Ln compounds previously reported. The computed UV-Visible spectrum of $[La(NR_2)_3]^{1-}$, calculated with an additional diffuse p primitive added by downward extrapolation, showed an intense 5d-6p transition around 800 nm, Figure E.3. Again, this is consistent with the experimental data on the other $[Ln(NR_2)_3]^{1-}$ complexes. It does not appear there is an electronic reasoning for the instability of the La(II) compound.

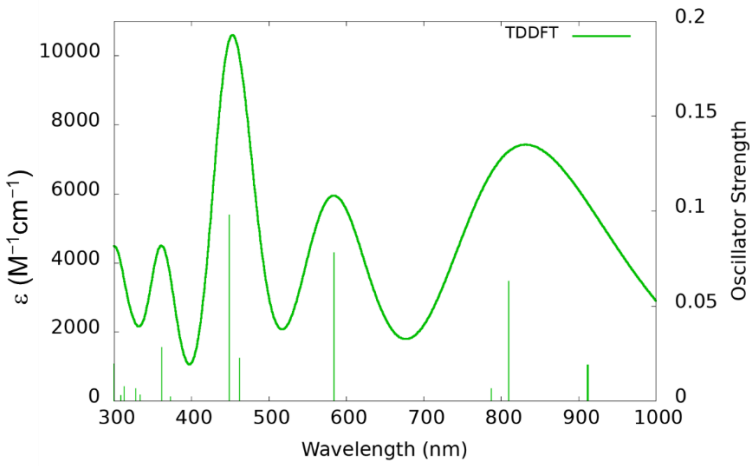

Figure E.3: Computed UV-visible spectrum of $[La(NR_2)_3]^{1-}$ with oscillator strengths shown as vertical lines. A Gaussian broadening of 0.15 eV was applied.

References

(1) Staroverov, V. N.; Scuseria, G. E.; Tao, J.; Perdew, J. P. Comparative Assessment of a New Nonempirical Density Functional: Molecules and Hydrogen-Bonded Complexes. *J. Chem. Phys.* **2003**, *119*, 12129–12137, DOI: 10.1063/1.1626543.

(2) Grimme, S.; Antony, J.; Ehrlich, S.; Krieg, H. A Consistent and Accurate Ab Initio Parametrization of Density Functional Dispersion Correction (DFT-D) for the 94 Elements H-Pu. *J. Chem. Phys.* **2010**, *132*, 154104, DOI: 10.1063/1.3382344.

(3) Grimme, S. Semiempirical GGA-Type Density Functional Constructed with a Long-Range Dispersion Correction. *J. Comput. Chem.* **2006**, *27*, 1787–1799, DOI: 10.1002/jcc.20495.

(4) Weigend, F.; Köhn, A.; Hättig, C. Efficient Use of the Correlation Consistent Basis Sets in Resolution of the Identity MP2 Calculations. *J. Chem. Phys.* **2002**, *116*, 3175–3183, DOI: 10.1063/1.1445115.

(5) Andrae, D.; Häußermann, U.; Dolg, M.; Stoll, H.; Preuß, H. Energy-Adjusted Ab Initio Pseudopotentials for the Second and Third Row Transition Elements. *Theor. Chim. Acta* **1990**, *77*, 123–141, DOI: 10.1007/BF01114537.

(6) Weigend, F.; Ahlrichs, R. Balanced Basis Sets of Split Valence, Triple Zeta Valence and Quadruple Zeta Valence Quality for H to Rn: Design and Assessment of Accuracy. *Phys. Chem. Chem. Phys.* **2005**, *7*, 3297–3305, DOI: 10.1039/b508541a.

(7) Schäfer, A.; Horn, H.; Ahlrichs, R. Fully Optimized Contracted Gaussian Basis Sets for Atoms Li to Kr. *J. Chem. Phys.* **1992**, *97*, 2571–2577.

(8) Treutler, O.; Ahlrichs, R. Efficient Molecular Numerical Integration Schemes. *J. Chem. Phys.* **1995**, *102*, 346–354, DOI: 10.1063/1.469408.

(9) Schäfer, A.; Klamt, A.; Sattel, D.; Lohrenz, J. C. W.; Eckert, F. COSMO Implementation

in TURBOMOLE: Extension of an Efficient Quantum Chemical Code towards Liquid Systems. *Phys. Chem. Chem. Phys.* **2000**, *2*, 2187–2193, DOI: 10.1039/b000184h.

(10) In *CRC Handbook of Chemistry and Physics*; Haynes, W. M., Lide, D. R., Bruno, T. J., Eds.; CRC Press, 2016; pp 943–950.

(11) Deglmann, P.; Furche, F.; Ahlrichs, R. An Efficient Implementation of Second Analytical Derivatives for Density Functional Methods. *Chem. Phys. Lett.* **2002**, *362*, 511–518, DOI: 10.1016/S0009-2614(02)01084-9.

(12) Bates, J. E.; Furche, F. Harnessing the Meta-Generalized Gradient Approximation for Time-Dependent Density Functional Theory. *J. Chem. Phys.* **2012**, *137*, 164105, DOI: 10.1063/1.4759080.

(13) Humphrey, W.; Dalke, A.; Schulten, K. VMD: Visual Molecular Dynamics. *J. Mol. Graph.* **1996**, *14*, 33–38.

(14) Balasubramani, S. G.; Chen, G. P.; Coriani, S.; Diedenhofen, M.; Frank, M. S.; Franzke, Y. J.; Furche, F.; Grotjahn, R.; Harding, M. E.; Hättig, C.; Hellweg, A.; Helmich-Paris, B.; Holzer, C.; Huniar, U.; Kaupp, M.; Marefat Khah, A.; Karbalaei Khani, S.; Müller, T.; Mack, F.; Nguyen, B. D.; Parker, S. M.; Perlt, E.; Rappoport, D.; Reiter, K.; Roy, S.; Rückert, M.; Schmitz, G.; Sierka, M.; Tapavicza, E.; Tew, D. P.; van Wüllen, C.; Voora, V. K.; Weigend, F.; Wodyński, A.; Yu, J. M. TURBOMOLE: Modular Program Suite for Ab Initio Quantum-Chemical and Condensed-Matter Simulations. *J. Chem. Phys.* **2020**, *152*, 184107, DOI: 10.1063/5.0004635.

(15) TURBOMOLE V7.4.1, a development of University of Karlsruhe and Forschungszentrum Karlsruhe GmbH, 1989–2007, TURBOMOLE GmbH, since 2007; available from https://turbomole.com.

(16) Brennan, J. G.; Cloke, F. G. N.; Sameh, A. A.; Zalkin, A. Synthesis of Bis(η-1,3,5-tri-*t*-Butylbenzene) Sandwich Complexes of Yttrium(0) and Gadolinium(0); the X-Ray Crystal Structure of the First Authentic Lanthanide(0) Complex, [Gd(η-$Bu^t_3C_6H_3)_2$]. *J. Chem. Soc., Chem. Commun.* **1987**, No. 21, 1668–1669, DOI: 10.1039/C39870001668.

(17) Cloke, F. G. N. Zero Oxidation State Compounds of Scandium, Yttrium, and the Lanthanides. *Chem. Soc. Rev.* **1993**, *22*, 17–24, DOI: 10.1039/CS9932200017.

(18) Huh, D. N.; Ciccone, S. R.; Bekoe, S.; Roy, S.; Ziller, J. W.; Furche, F.; Evans, W. J. Synthesis of Ln^{II}-in-Cryptand Complexes by Chemical Reduction of Ln^{III}-in-Cryptand Precursors: Isolation of a Nd^{II}-in-Cryptand Complex. *Angew. Chem. Int. Ed.* **2020**, *59*, 16141–16146, DOI: 10.1002/anie.202006393.

(19) Walensky, J. R.; Martin, R. L.; Ziller, J. W.; Evans, W. J. Importance of Energy Level Matching for Bonding in Th^{3+}–Am^{3+} Actinide Metallocene Amidinates, $(C_5Me_5)_2[^iPrNC(Me)N^iPr]An$. *Inorg. Chem.* **2010**, *49*, 10007–10012, DOI: 10.1021/ic1013285.

(20) Huh, D. N.; Roy, S.; Ziller, J. W.; Furche, F.; Evans, W. J. Isolation of a Square-Planar Th(III) Complex: Synthesis and Structure of $[Th(OC_6H_2{}^tBu_2\text{-}2,6\text{-}Me\text{-}4)_4]^{1-}$. *J. Am. Chem. Soc.* **2019**, *141*, 12458–12463, DOI: 10.1021/jacs.9b04399.

(21) Kundu, K.; White, J. R. K.; Moehring, S. A.; Yu, J. M.; Ziller, J. W.; Furche, F.; Evans, W. J.; Hill, S. A 9.2-GHz Clock Transition in a Lu(II) Molecular Spin Qubit Arising from a 3,467-MHz Hyperfine Interaction. *Nat. Chem.* **2022**, *14*, 392–397, DOI: 10.1038/s41557-022-00894-4.

(22) Pividori, D.; Miehlich, M. E.; Kestel, B.; Heinemann, F. W.; Scheurer, A.; Patzschke, M.; Meyer, K. Uranium Going the Soft Way: Low-Valent Uranium(III) Coordinated to an

Arene-Anchored Tris-Thiophenolate Ligand. *Inorg. Chem.* **2021**, *60*, 16455–16465, DOI: 10.1021/acs.inorgchem.1c02310.

(23) Rookes, T. M.; Wildman, E. P.; Balázs, G.; Gardner, B. M.; Wooles, A. J.; Gregson, M.; Tuna, F.; Scheer, M.; Liddle, S. T. Actinide–Pnictide (An−Pn) Bonds Spanning Non-Metal, Metalloid, and Metal Combinations (An = U, Th; Pn = P, As, Sb, Bi). *Angew. Chem. Int. Ed.* **2018**, *57*, 1332–1336, DOI: 10.1002/anie.201711824.

(24) Reánt, B. L. L.; Liddle, S. T.; Mills, D. P. F-Element Silicon and Heavy Tetrel Chemistry. *Chem. Sci.* **2020**, *11*, 10871–10886, DOI: 10.1039/d0sc04655h.

(25) Webster, C. L.; Bates, J. E.; Fang, M.; Ziller, J. W.; Furche, F.; Evans, W. J. Density Functional Theory and X-Ray Analysis of the Structural Variability in η^5,η^5,η^1-Tris(Ring) Rare Earth/Actinide Tetramethylpyrrolyl Complexes, $(C_5Me_5)_2M(NC_4Me_4)$. *Inorg. Chem.* **2013**, *52*, 3565–3572, DOI: 10.1021/ic300905r.

(26) Goodwin, C. A. P.; Ciccone, S. R.; Bekoe, S.; Majumdar, S.; Scott, B. L.; Ziller, J. W.; Gaunt, A. J.; Furche, F.; Evans, W. J. 2.2.2-Cryptand Complexes of Neptunium(III) and Plutonium(III). *Chem. Commun.* **2022**, *58*, 997–1000, DOI: 10.1039/D1CC05904A.

(27) Huh, D. N.; Barlow, J. M.; Ciccone, S. R.; Ziller, J. W.; Yang, J. Y.; Evans, W. J. Stabilization of U(III) to Oxidation and Hydrolysis by Encapsulation Using 2.2.2-Cryptand. *Inorg. Chem.* **2020**, *59*, 17077–17083, DOI: 10.1021/acs.inorgchem.0c02286.

(28) Huh, D. N.; Windorff, C. J.; Ziller, J. W.; Evans, W. J. Synthesis of Uranium-in-Cryptand Complexes. *Chem. Commun.* **2018**, *54*, 10272–10275, DOI: 10.1039/C8CC05341C.

(29) Huh, D. N.; Ziller, J. W.; Evans, W. J. Facile Encapsulation of Ln(II) Ions into Cryptate Complexes from $LnI_2(THF)_2$ Precursors (Ln = Sm, Eu, Yb). *Inorg. Chem.* **2019**, *58*, 9613–9617, DOI: 10.1021/acs.inorgchem.9b01049.

(30) Réant, B. L. L.; Berryman, V. E. J.; Basford, A. R.; Nodaraki, L. E.; Wooles, A. J.; Tuna, F.; Kaltsoyannis, N.; Mills, D. P.; Liddle, S. T. ^{29}Si NMR Spectroscopy as a Probe of s- And f-Block Metal(II)-Silanide Bond Covalency. *J. Am. Chem. Soc.* **2021**, *143*, 9813–9824, DOI: 10.1021/jacs.1c03236.

(31) Ryan, A. J.; Darago, L. E.; Balasubramani, S. G.; Chen, G. P.; Ziller, J. W.; Furche, F.; Long, J. R.; Evans, W. J. Synthesis , Structure , and Magnetism of Tris(Amide) $[Ln\{N(SiMe_3)_2\}_3]^{1-}$ Complexes of the Non-Traditional +2 Lanthanide Ions. *Chem. Eur. J.* **2018**, *24*, 7702–7709, DOI: 10.1002/chem.201800610.

(32) Bradley, D. C.; Ghotra, J. S.; Hart, F. A. Low Co-Ordination Numbers in Lanthanide and Actinide Compounds. Part I. The Preparation and Characterization of Tris{bis(Trimethylsilyl)-Amido}lanthanides. *J. Chem. Soc., Dalton Trans.* **1973**, No. 10, 1021, DOI: 10.1039/dt9730001021.

(33) Hitchcock, P. B.; Lappert, M. F.; Smith, R. G.; Bartlett, R. A.; Power, P. P. Synthesis and Structural Characterisation of the First Neutral Homoleptic Lanthanide Metal(III) Alkyls: $[LnR_3]$ [Ln = La or Sm, R = $CH(SiMe_3)_2$]. *J. Chem. Soc., Chem. Commun.* **1988**, *3*, 1007, DOI: 10.1039/c39880001007.

(34) Ryan, A. J.; Ziller, J. W.; Evans, W. J. The Importance of the Counter-Cation in Reductive Rare-Earth Metal Chemistry: 18-Crown-6 Instead of 2,2,2-Cryptand Allows Isolation of $[Y^{II}(NR_2)_3]^{1-}$ and Ynediolate and Enediolate Complexes from CO Reactions. *Chem. Sci.* **2020**, *11*, 2006–2014, DOI: 10.1039/C9SC05794C.

(35) Woen, D. H.; Chen, G. P.; Ziller, J. W.; Boyle, T. J.; Furche, F.; Evans, W. J. End-On Bridging Dinitrogen Complex of Scandium. *J. Am. Chem. Soc.* **2017**, *139*, 14861–14864.

Appendix F:

List of Crystal Structures

Abbreviations: $Cp^N = C_5Me_4SiMe_3$; 18c6 = crown = 18-crown-6; Cp′ = $C_5H_4SiMe_3$; Pc = phthalocyanine; N* = $N(SiMe_3)_2$; crypt = 2.2.2-cryptand; $Cp^{tet} = C_5Me_4H$; Cp* = C_5Me_5; R* = $CH(SiMe_3)_2$; Cp = C_5H_5; OAr′ = $OC_6H_2{}^tBu_2$-2,6-Me-4; OAr = $OC_6H_3{}^tBu_2$-2,6; Cp″ = $C_5H_3(SiMe_3)_2$; OAr* = $OC_6H_2Ad_2$-2,6-^{t}Bu-4; $Cp^{An} = (C_5H_3SiMe_3)_2SiMe_2$; poat = $N[CH_2CH_2NP(O)Ph_2]_3$; Me_3tach = 1,3,5-trimethyl-1,3,5-triazacyclohexane; Me_3tacn = 1,4,7-trimethyl-1,4,7-triazacyclononane; OTf = $–O_3SCF_3$; pyr = pyridine; pmdta = $Me_2NCH_2CH_2N(Me)CH_2CH_2NMe_2$; thexyl = $–CMe_2CHMe_2$; Ad = 1-adamantyl.

Table F.1: List of crystal structures ordered by number.

JCW	Formula	Page #	Notes
1	$[HNEt_3][BPh_4]$	1032	
2	$Cp^N{}_2YCl(thf)$	1038	
3	$(18c6)BiCl_3$	1069	see VEPREN
4	Cp'_3ThMe	1092	
5	$[Cp'_3Th]_2(\mu\text{-}O)$	2011	
6	Cp'_3ThBr	2046	
7	???	2076	
8	$[Li(THF)_4][PcLi]$	3005	
9	$[K(crypt)][BPh_4]$	3015	
10	$[K(crypt)][Cp^{tet}]$	3016	xtl was black. from THF/ether
11	(N*$_2$La(THF))2(u-O)	3006	
12	$[K(crypt)][(Cp^{tet}{}_3U)_2(\mu\text{-}I)]$	3051	
13	$Cp^{Tet}{}_3U$ + KI + crypt	3062	data good but cannot solve
14	$[N^*{}_2(THF)La(\mu\text{-}Cl)]_2$	3075	
15	$Cp^{tet}{}_3Th$ + KI + crypt	3092	twinned? Data good but cannot solve
16	$[Cp^{tet}{}_3U]^{1-}$ + NO	3102	too poor resolution, from tol
17	$[K(crypt)][Cp^{tet}]$	3122	xtl was red, from THF/hex
18	[K18c6][azobenzene]	3077	
19	Al_2O_3	3142	
20	$[Cp^{tet}{}_3U]^{1-}$ + NO	3133	from THF
21	HC_5Ph_5	3126	
22	$Cp^{tet}{}_3Th$	3145	c = 1/2 of lit reference
23	looks like $[Kcrypt][Cp^{tet}{}_3UI]$	3160	
24	Cp*$_2$UI(THF)	3165	

25	$(C_5Ph_5)UI_2(THF)_2$	3181	
26	$NaC_5Ph_5(THF)_3$	3191	
27	$[K(Crypt)][Cp^*_2U(CH_2SiMe_2NSiMe_3)]$	3200	
28	$Cp^*_2UCp^{tet}$	3178	looks like tris-Cp but can't define all the Cp substituents
29	reaction Cp^*_2UI/KC_8/crown	3216	
30	$[Kcrypt][Cp^*N^*U(CH_2SiMe_2NSiMe_3)]$	3225	
31	[Kcrypt][PhN=NPh]	3222	
32	$UN^*_3 + KC_8$ + crypt -- cyclometallate?	3235	
33	$UN^*_3 + KC_8$ + crypt -- cyclometallate?	3235	
34	(KcryptTHF)(UN^*_4)	3256	see GAGLIK, UWECUW, WIKGAA
35	$[Na(crown)_2][Cp"_3Th]$	3295	
36	$[Kcrypt][Cp^*_2U(BH_4)_2]$	4020	
37	$[Li(THF)_4][Cp^*_2UI_2]$	4025	
38	$U(BH_4)_3(MeCN)_x$	4030	couldn't solve
39	$[Li(crypt)][Cp"_3Th]$	4031	Cannot solve
40	$R^*_2U(u\text{-}I)_2(u^3\text{-}I)[Li(OEt_2)_2]_2$	4025	first An with 2 R*
41	$[Na(crown)THF_2][C_5Ph_5]$	4045	was purple
42	$Cp^*_2U(I)(THF)$	4040	see jcw24
43	$Cp^*_2UI(u\text{-}I)LiTHF_3$	4025	
44	$[Kcrypt][Cp^*_2U(NPh_2)_2]$	4089	
45	$[Kcrypt][Cp^*_2UBH_4]$ decomp		
46	$Cp_2ThClTHF_3$	4099	see BIXVOT
47	$[Kcrypt][Cp^*_2UCpI]$	4123	
48	$[Cscrypt][Cp"_3Th]$	4117	iso with SOQXON
49	$[Kcrypt][UOAr]_4$	4128	
50	$Cp^*_2UR^*$	4025	
51	Cp^*_2UOAr'	4146	
52	$Cp^*_2U(BH_4)(THF)$		twinned
53	$[Kcrypt][Cp^*_2UH(BH_4)]$	4172	
54	[Kcrypt][Cp*2UIBH4]	4183	disorder in I, BH4
55	$[Cp"_2UI]_2$	4190	might be bridge oxide as well
56	$[Kcrypt][Cp^*_2UIH]$	4205	
57	$[K(crypt)][Cp^*_2U(BH_4)_2]$	4213	disorder in H, BH4 like jcw54 or two BH4 groups
58	$\{[(Me_2CHCMe_2)BH_3]_2(THF)_2U(u\text{-}I)\}_2$	4224	poor data quality
59	$[Kcrown(THF)][Kcrown(THF)_2][Cp"UOAr_2'X]_2$	4234	
60	$[Cp"_2U(u\text{-}X)]_2$	4225	
61	$[Kcrypt][Cp^*_2UX_2]$. THF (X = BH_4? OH, etc)	4250	
62	Cp^*_2UI + MeLi + tol	4257	dont bother
63	$(Cp^{tet})_2UI(THF)$	4262	
64	$U(BH_4)_2I(THF)_4$	4260	matches $La(BH_4)_3THF_4$ cell
65	HOAr* THF		see LAS4. No count
66	$Cp"UOAr'_2(THF)$	5019	3 component twin but should be ok
67	Cp^*_2CeOAr'	5018	isomorphous with jcw51
68	$U(BH_4)_3(THF)_4$	5030	disordered I with BH4? same cell as jcw64

69	$[Cp''_2U(u\text{-}OH)]_2$	5033	not isomorphous with µ-O
70	$Cp^{tet}_2UOAr^*$	5028	from hex/tol
71	[Kcrypt][$Cp^*_2UOAr'I$]	5044	
72	$Cp^{An}Y(allyl)(THF)$		see mtd54
73	$NaBH_4$	5051	from MeCN/Et2O
74	Cp^{tet}_2UOAr' $Cp^{tet}_2UOAr'THF$	5069	
75	K(crown)(THF)OAr'	5083	
76	$[Cp'_2U(u\text{-}O)]_3$. 2hexane	5105	
77	$(poat)_2Y_3OCl$	5093	Tb is isomorphous
78	$[K(crown)THF_2][UOAr_4]$	5123	
79	$[KcrownTHF_2][Cp''_3UH]$	5151	
80	$(Me_3tach)UI_3(Me_3tach)$	5150	from THF/hex
81	Cp'_2ZrCl_2	5163	iso with Ti JUCTIK
82	$(Me_3tach)UI_3(Me_3tach)$	5158	from toluene
83	$[(Me_3tach)_2NdI_2][I]$	5169	
84	$(Me_3tach)_2LaCl_3$	5168	not iso with U, but does form sandwich
85	$[(Me_3tach)_2BiI_2]_3[I][Bi_2I_9][Me_3tachH][THF]$	5173	
86	$[K(crypt)][Cp^{tet}]$	5185	new cell
87	$(Me_3tach)_2LaI_3$	5189	iso with jcw80
88	$(Me_3tach)_2UI_2X$	5193	cannot resolve X, is on 2-fold
89	$[(Me_3tach)La]_4(u\text{-}OH)_4(u^2{:}k^2\text{-}OTf)_8$	5192	
90	$(Me_3tach)_2CeI_3$	5190	iso with La, U I think. Can solve in Pnma
91	$[HMe_3tach][I]$	5191	
92	$[K(crown)(THF)_2][Cp''_2Li]$	5235	
93	$(Cp''_2Th)_2(C_6H_6)$	5235	
94	$(Me_3tacn)BiI_3$	5229	
95	$(Me_3tacn)SmI_2(THF)$	5239	
96	$(Me_3tach)_2NdI_3$	5234	iso with U, La, Ce eclipsed rings
97	$[HMe_3tacn][OTf]$	5230	
98	Cp^*_2UCp		
99	$(Me_3tacn)TbI_3$	5231	
100	$[Me_3tachSmI_2][I]$	5247	
101	K(crown)N*	5205	
102	K(crown)N*	5205	
103	K(crown)N*	5205	identical to 102
104	$Cp^*_2UI(=NSiMe_3)$	5224	
105	$BiI_3(THF)$	5255	
106	$(Me_3tach)BiI_3(pyr)_2.pyr$	5254	
107	$(Me_3tach)YCl_3(THF)_2$	5259	
108	$(Me_3tacn)UI_3(THF)$	5256	
109	$[(Me_3tach)_2BiI_2][Me_3tachBiI_4]\cdot 2.5THF$	5254	
110	$[Me_3tach][Cl]$	5253	
111	$(Me_3tach)BiI_3(pyr)_2$	5265	same as jcw106
112	[Kcrypt][Cp'']	5252	new cell
113	$(Me_3tach)_2SmI_2$	5264	
114	$(Me_3tacn)LaI_3(THF)$	5262	iso w 108
115	$[tach_2LaOTf_4][HMe_3tach].tol$	5269	

116	$(Me_3tacn)YCl_3$	5263	
117	$[(Me_3tach)_2LaOTf_4][HMe_3tach]$	5269	
118	$(Me_3tach)_2SmI_2THF$	5270	
119	$[Me_3tach][Br]$	5261	
120	$(Me_3tach)BiCl_3(pyr)_2$	5275	
121	$(Me_3tach)BiCl_3(pyr)_2$	5276	
122	$(pmdta)UI_3$	5278	ligands sit on mirror, cant resolve
123	$[U(H_3Bthexyl)_2(THF_2)(u\text{-}I)]_2$	GG1012	diff cell than jcw58
124	$(Me_3tach)UI_3(pyr)_2 \cdot Pyr$	5279	iso with jcw106
125	$U(BH_4)_2I(THF)_4$	GG1010	also named gg1
126	$Cp^*_2U(Cp^{tet})$	5299	see jcw28
127	$[Kcrypt][Cp^{An}Y(allyl)(H)] \cdot [(u\text{-}Cp^{An})Y(u\text{-}Cl)]_2 \cdot$ THF	6030	
128	$Cp^{An}YCl(THF)$	6017	
129	$Cp^*_2U(NAd)_2$	6039	